



# Effects of Oil and Gas Exploration and Development at Selected Continental Slope Sites in the Gulf of Mexico

## Volume II: Technical Report



# **Effects of Oil and Gas Exploration and Development at Selected Continental Slope Sites in the Gulf of Mexico**

## **Volume II: Technical Report**

Author

Continental Shelf Associates, Inc.

Prepared under MMS Contract  
1435-01-00-CT-31034  
by  
Continental Shelf Associates, Inc.  
759 Parkway Street  
Jupiter, Florida 33477-9596

Published by

**U.S. Department of the Interior  
Minerals Management Service  
Gulf of Mexico OCS Region**

**New Orleans  
July 2006**

## **Disclaimer**

This report was prepared under contract between the Minerals Management Service (MMS) and Continental Shelf Associates, Inc. This report has been technically reviewed by the MMS and has been approved for publication. Approval does not signify that the contents necessarily reflect the views or policies of the MMS, nor does mention of trade names or commercial products constitute endorsement or recommendation for use. It is, however, exempt from review and compliance with MMS editorial standards.

## **Report Availability**

Extra copies of this report may be obtained from the Public Information Office at the following address:

U.S. Department of the Interior  
Minerals Management Service  
Gulf of Mexico OCS Region  
Public Information Office (MS 5034)  
1201 Elmwood Park Boulevard  
New Orleans, LA 70123-2394

Telephone: (504) 736-2519 or  
1-800-200-GULF

## **Citation**

Suggested citation:

Continental Shelf Associates, Inc. 2006. Effects of Oil and Gas Exploration and Development at Selected Continental Slope Sites in the Gulf of Mexico. Volume II: Technical Report. U.S. Department of the Interior, Minerals Management Service, Gulf of Mexico OCS Region, New Orleans, LA. OCS Study MMS 2006-045. 636 pp.

## Acknowledgments

The program was conducted by a large, multidisciplinary team under the direction of Continental Shelf Associates, Inc. (CSA). David Gettleson was the program manager and Alan Hart served as deputy program manager and data manager. Neal Phillips was the scientific editor for the final report. Principal investigators are acknowledged at the head of each report chapter.

We appreciate the assistance of MMS staff including Greg Boland (Contracting Officer's Technical Representative), Mary Boatman (Technical Performance Evaluation Committee), Debra Bridge (Contracting Officer), and Tom Ahlfeld. Jill Leale with the MMS Mapping & Automation Unit provided historical well data and georeferenced maps of well locations based on the MMS Technical Information Management System.

Drilling discharge data were kindly provided by Vince Cottone (ChevronTexaco) and Kent Satterlee, Ellen Polanski, and Jane Chady (Shell). Joe Smith (ExxonMobil) sent unpublished reports that were helpful in drilling discharge calculations.

The Scientific Review Board consisted of Andy Glickman (ChevronTexaco), Donald Harper (Texas A&M University at Galveston), and Jim Ray (Oceanic Environmental Solutions). Additional input in the study design was provided by Peter Arnold (independent consultant), Maynard Brandsma (Brandsma Engineering), and Woollcott Smith (Temple University).

We wish to recognize the following individuals for their roles in the field surveys:

- Jay Northcutt (C&C Technologies) – Project manager, geophysical cruises
- Tony George (C&C Technologies) – Manager, geophysical interpretation
- Scott Melancon – Party chief, geophysical Cruises 2A and 3A
- Tim MacEwan – Senior operator, geophysical Cruise 2A
- Scott McBay, David Aucoin, and Paige Melancon – Party chiefs, geophysical Cruise 1A
- Roger Fay (TDI-Brooks International, Inc.) – Chief scientist, chemical/biological cruises
- Lynwood Powell (CSA) – Field operations manager, chemical/biological Cruises 1B and 2B; navigation/post-plotting and geographic information system development
- Frank Johnson (CSA) – Field operations manager, chemical/biological Cruise 3B

Other cruise participants including staff from Continental Shelf Associates, Inc., C&C Technologies, TDI-Brooks International, Inc., Florida Institute of Technology, and Louisiana State University are too numerous to list individually, but their contributions are sincerely appreciated. We also wish to acknowledge Wayne Ispording (University of South Alabama) for conducting laboratory sediment grain size analyses.

The CSA document production team included Melody Powell (document production coordinator and technical editor), Heidi Glick (technical editor), Suzanne Short (graphics), and Debbie Raffel, Karen Stokesbury, Lynanne Rockhill, and Debbie Cannon (word processing).

# Contents

	Page
<b>LIST OF FIGURES.....</b>	<b>xv</b>
<b>LIST OF TABLES.....</b>	<b>xliii</b>
<b>LIST OF ACRONYMS AND ABBREVIATIONS.....</b>	<b>li</b>
<b>1. INTRODUCTION.....</b>	<b>1</b>
1.1 Background.....	1
1.2 Study Objectives.....	3
1.3 Report Organization .....	3
<b>2. STUDY DESIGN AND GENERAL METHODS.....</b>	<b>5</b>
2.1 Site Selection.....	5
2.2 Far-field Sites (Reference Areas) .....	7
2.3 Sampling Cruises.....	8
2.3.1 Geophysical Cruises .....	8
2.3.2 Chemical/Biological Cruises .....	14
2.4 Sampling Design .....	14
2.4.1 Geophysical Characterization.....	15
2.4.2 Chemical/Biological Sampling.....	15
2.5 Sampling Methodology .....	16
2.5.1 Box Cores .....	16
2.5.2 Sediment Profile Imaging.....	20
2.5.3 Seafloor Photographs.....	20
2.5.4 Baited Traps.....	23
2.6 Sampling Locations and Data Collected.....	23
<b>3. DRILLING ACTIVITIES.....</b>	<b>31</b>
3.1 Near-field Sites .....	32
3.1.1 Viosca Knoll Block 916 (Exploration Site).....	32
3.1.2 Garden Banks Block 516 (Exploration/Development Site).....	34
3.1.3 Garden Banks Block 602 (Post-Development Site) .....	39
3.1.4 Mississippi Canyon Block 292 (Post-Development Site) .....	42
3.1.5 Summary .....	45
3.2 Far-field Sites .....	48
3.2.1 Viosca Knoll Block 916 .....	54
3.2.2 Garden Banks Block 516.....	54
3.2.3 Garden Banks Block 602.....	54
3.2.4 Mississippi Canyon Block 292 .....	55
3.2.5 Summary and Preliminary Evaluation.....	55
<b>4. GEOPHYSICAL CHARACTERIZATION OF STUDY SITES.....</b>	<b>57</b>
4.1 Introduction and Geologic Framework.....	57
4.2 Data Collection Schedule and Instrumentation .....	59
4.3 Viosca Knoll Block 916 – Exploration Site .....	62
4.3.1 Introduction .....	62
4.3.2 Data Quality for the Pre-Drilling Survey .....	62
4.3.3 Site Characterization: Pre-Drilling .....	64

**Contents**  
(continued)

	<b>Page</b>
4.3.4 Data Quality for the Post-Drilling Survey .....	64
4.3.5 Site Characterization: Post-Drilling.....	69
4.4 Mississippi Canyon Block 292 – Post-Development Site .....	69
4.4.1 Introduction .....	69
4.4.2 Data Quality.....	72
4.4.3 Site Characterization .....	72
4.5 Garden Banks Block 602 – Post-Development Site .....	79
4.5.1 Introduction .....	79
4.5.2 Data Quality.....	79
4.5.3 Site Characterization .....	79
4.6 Garden Banks Block 516 – Exploration/Development Site .....	85
4.6.1 Introduction .....	85
4.6.2 Data Quality.....	85
4.6.3 Site Characterization .....	88
4.7 Conclusions .....	93
<b>5. SEDIMENT GRAIN SIZE.....</b>	<b>95</b>
5.1 Introduction .....	95
5.2 Laboratory Methods .....	95
5.3 Results .....	95
5.3.1 Viosca Knoll Block 916 .....	97
5.3.2 Garden Banks Block 516.....	102
5.3.3 Garden Banks Block 602.....	109
5.3.4 Mississippi Canyon Block 292.....	117
5.4 Discussion.....	124
<b>6. SEDIMENT PROFILE IMAGING AT EXPLORATION AND EXPLORATION/DEVELOPMENT SITES .....</b>	<b>131</b>
6.1 Introduction .....	131
6.2 Methods .....	131
6.3 Garden Banks Block 516 – Cruise 1B.....	132
6.3.1 Survey Design and Location .....	132
6.3.2 Sediment Fabric, Texture, Color, and Small-Scale Stratigraphy.....	133
6.3.3 Depth of the Apparent Redox Potential Discontinuity .....	138
6.3.4 Infaunal Successional Stages.....	141
6.3.5 Organism-Sediment Index (OSI).....	146
6.4 Viosca Knoll Block 916 – Cruise 1B (Pre-Drilling) .....	150
6.4.1 Survey Design and Location .....	150
6.4.2 Sediment Fabric, Texture, Color, and Small-Scale Stratigraphy.....	157
6.4.3 Depth of the Apparent Redox Potential Discontinuity .....	158
6.4.4 Infaunal Successional Stages.....	160
6.4.5 Organism-Sediment Index.....	164

**Contents**  
(continued)

	<b>Page</b>
6.5 Garden Banks Block 516 – Cruise 2B .....	173
6.5.1 Survey Design and Location .....	173
6.5.2 Sediment Fabric, Texture, Color, and Small-Scale Stratigraphy .....	174
6.5.3 Depth of the Apparent Redox Potential Discontinuity .....	177
6.5.4 Infaunal Successional Stage .....	179
6.5.5 Organism-Sediment Index .....	186
6.6 Viosca Knoll Block 916 – Cruise 3B (Post-Drilling) .....	191
6.6.1 Survey Design and Location .....	191
6.6.2 Sediment Fabric, Texture, Color, and Small-Scale Stratigraphy .....	191
6.6.3 Depth of the Apparent Redox Potential Discontinuity .....	193
6.6.4 Infaunal Successional Stages .....	193
6.6.5 Organism-Sediment Index .....	196
6.7 Summary and Conclusions .....	200
6.7.1 Garden Banks Block 516 .....	200
6.7.2 Viosca Knoll Block 916 .....	205
6.8 Plates .....	207
<b>7. SEDIMENT PROFILE IMAGING AT POST-DEVELOPMENT SITES .....</b>	<b>215</b>
7.1 Introduction .....	215
7.2 Methods .....	215
7.2.1 Survey Design and Transect Location .....	215
7.2.2 Camera Operation and Field Sampling .....	218
7.2.3 Image Analysis .....	222
7.3 Results .....	225
7.3.1 Garden Banks Block 602 .....	225
7.3.2 Mississippi Canyon Block 292 .....	232
7.4 Discussion .....	239
7.4.1 Garden Banks Block 602 .....	239
7.4.2 Mississippi Canyon Block 292 .....	240
7.5 Conclusions .....	240
7.5.1 Garden Banks Block 602 .....	240
7.5.2 Mississippi Canyon Block 292 .....	241
<b>8. METALS, TOTAL ORGANIC CARBON, AND REDOX CONDITIONS IN SEDIMENTS .....</b>	<b>243</b>
8.1 Introduction .....	243
8.2 Methods .....	245
8.2.1 Sampling and Field Measurements .....	245
8.2.2 Interstitial Water Collection and Analysis .....	247
8.2.3 Laboratory Analysis .....	247
8.2.4 Quality Control and Quality Assurance .....	251
8.3 Viosca Knoll Block 916 – Exploration Site .....	252
8.3.1 Metals and Total Organic Carbon .....	252
8.3.2 Sediment Geochronology .....	258
8.3.3 Sediment Oxygen Levels and Redox Conditions .....	258
8.3.4 Interstitial Water Composition .....	264

**Contents**  
(continued)

	<b>Page</b>
8.4 Garden Banks Block 516 – Exploration/Development Site .....	271
8.4.1 Metals and Total Organic Carbon .....	271
8.4.2 Sediment Geochronology .....	281
8.4.3 Sediment Oxygen Levels and Redox Conditions .....	281
8.4.4 Interstitial Water Composition .....	286
8.5 Garden Banks Block 602 And Mississippi Canyon Block 292 – Post-Development Sites.....	289
8.5.1 Metals and Total Organic Carbon .....	289
8.5.2 Sediment Geochronology .....	299
8.5.3 Sediment Oxygen Levels and Redox Conditions .....	301
8.5.4 Interstitial Water Composition .....	303
8.5.5 Metals in Isopods and Crabs.....	309
8.6 Discussion of Sediment Trace Metals .....	314
8.7 Conclusions .....	325
<b>9. SEDIMENT AND TISSUE HYDROCARBONS .....</b>	<b>327</b>
9.1 Introduction .....	327
9.2 Analytical Methods .....	329
9.2.1 Extraction of Sediments for Aromatic and Saturated Hydrocarbons .....	329
9.2.2 Extraction of Tissues for Aromatic Hydrocarbons.....	329
9.2.3 Determination of Aromatic Hydrocarbons .....	329
9.2.4 Determination of Aliphatic Hydrocarbons .....	330
9.2.5 Quality Assurance/Quality Control .....	330
9.3 Results – Sediments.....	331
9.3.1 Viosca Knoll Block 916 – Exploration Site .....	331
9.3.2 Garden Banks Block 516 – Exploration/Development Site .....	334
9.3.3 Garden Banks Block 602 – Post-Development Site .....	337
9.3.4 Mississippi Canyon Block 292 – Post-Development Site .....	340
9.4 Results – Tissue Samples .....	343
9.5 Discussion.....	344
<b>10. SEDIMENT MICROBES.....</b>	<b>345</b>
10.1 Introduction .....	345
10.2 Materials and Methods .....	347
10.2.1 ATP Assay.....	348
10.2.2 Microbial Respiration .....	350
10.2.3 Sediment DNA Extraction, Quantification, and Amplification.....	351
10.2.4 Toxicity Bioassay .....	351
10.3 Results .....	351
10.3.1 ATP Analysis.....	351
10.3.2 Toxicity Bioassay .....	353
10.3.3 DNA Assay.....	356
10.3.4 Respiration.....	356
10.4 Discussion.....	357



**Contents**  
(continued)

	<b>Page</b>
<b>11. MEIOFAUNA AND MACROINFAUNA.....</b>	<b>361</b>
11.1 Introduction .....	361
11.2 Materials and Methods .....	361
11.3 Meiofaunal Results and Discussion.....	362
11.3.1 Viosca Knoll Block 916 .....	362
11.3.2 Garden Banks Block 516.....	363
11.3.3 Garden Banks Block 602.....	370
11.3.4 Mississippi Canyon Block 292.....	373
11.3.5 Individual Groups and Environmental Correlations.....	373
11.3.6 Nematode Feeding Groups and Harpacticoid Reproductive Status.....	376
11.3.7 Discussion .....	376
11.4 Macroinfaunal Results and Discussion.....	380
11.4.1 Viosca Knoll Block 916 .....	380
11.4.2 Garden Banks Block 516.....	385
11.4.3 Garden Banks Block 602.....	388
11.4.4 Mississippi Canyon Block 292.....	388
11.4.5 Individual Groups and Environmental Correlations.....	392
11.4.6 Detailed Macroinfaunal Taxonomic Analysis.....	401
11.4.7 Discussion .....	410
11.5 Conclusions .....	412
11.5.1 Meiofauna.....	412
11.5.2 Macroinfauna.....	412
<b>12. MEGAFUNA AND IMAGE ANALYSIS .....</b>	<b>415</b>
12.1 Introduction: Image-Based Sampling.....	415
12.2 Methods .....	416
12.2.1 Field Sampling.....	416
12.2.2 Image Processing.....	416
12.2.3 Color Analysis .....	421
12.2.4 Color Models.....	421
12.3 Results .....	422
12.3.1 Texture Analysis.....	422
12.3.2 Color Analysis .....	422
12.4 Faunal Analysis .....	430
12.5 Discussion.....	439
12.5.1 Faunal Results .....	439
12.5.2 Color Analysis .....	439
12.5.3 Consideration of Size .....	439
<b>13. GENETIC DIVERSITY OF HARPACTICOID COPEPODS .....</b>	<b>441</b>
13.1 Introduction .....	441
13.2 Methods .....	443
13.2.1 Collection and Processing of Samples.....	443
13.2.2 Genetic Methods.....	443
13.2.3 Data Analysis.....	444
13.3 Results .....	445

**Contents**  
(continued)

	<b>Page</b>
13.3.1 Numerical Response to Disturbance by <i>Bathycleptopsyllus</i> sp. ....	445
13.3.2 Genetic Divergence .....	445
13.3.3 Population Structure .....	447
13.3.4 Genetic Diversity .....	450
13.4 Discussion.....	450
13.4.1 Numerical Response to Disturbance by <i>Bathycleptopsyllus</i> sp. ....	450
13.4.2 Genetic Divergence .....	453
13.4.3 Population Structure .....	454
13.4.4 Genetic Diversity .....	455
13.5 Conclusions .....	457
<b>14. SEDIMENT TOXICITY .....</b>	<b>459</b>
14.1 Introduction .....	459
14.2 Materials and Methods .....	459
14.2.1 Sediment Sampling Locations .....	459
14.2.2 Test Organism Collection.....	459
14.2.3 Sediment Sample Preparation.....	460
14.2.4 Toxicity Test.....	460
14.3 Results .....	461
14.3.1 Mississippi Canyon Block 292 .....	461
14.3.2 Garden Banks Block 602.....	463
14.4 Discussion.....	464
14.4.1 Mississippi Canyon Block 292 .....	464
14.4.2 Garden Banks 602 .....	466
14.5 Conclusions .....	469
<b>15. SYNTHESIS .....</b>	<b>471</b>
15.1 Introduction .....	471
15.1.1 Baseline Conditions.....	471
15.1.2 Drilling Activities.....	474
15.2 Nature and Extent of Impacts .....	476
15.2.1 Physical .....	476
15.2.2 Chemical.....	489
15.2.3 Biological .....	505
15.3 Site Comparisons.....	522
15.3.1 Areal Extent of Impacts .....	522
15.3.2 Severity of Impacts.....	523
15.3.3 Duration of Impacts .....	526
15.4 Methodology Evaluation .....	531
15.4.1 Selection of Far-Field Sites .....	531
15.4.2 Geophysical Surveys .....	532
15.4.3 Seafloor Photography .....	532
15.4.4 Detecting Benthic Community Impacts .....	533
15.5 Conclusions .....	533

**Contents**  
(continued)

	<b>Page</b>
<b>16. ECOLOGICAL RISK ASSESSMENT.....</b>	<b>535</b>
16.1 Introduction .....	535
16.2 Problem Formulation.....	536
16.2.1 Deepwater Drilling in the Gulf of Mexico .....	536
16.2.2 Drilling Practices and Discharge Histories.....	537
16.2.3 The Benthic Environment of the Study Area .....	539
16.2.4 Conceptual Model .....	542
16.3 Exposure Assessment .....	549
16.3.1 Physical Disturbance of Sediments .....	549
16.3.2 Chemical Alteration of Sediments.....	551
16.3.3 Metals in Sediments .....	556
16.3.4 Polycyclic Aromatic Hydrocarbons and Metals in Tissues of Benthic Megafauna.....	559
16.3.5 Summary of Exposure .....	562
16.4 Effects Assessment.....	563
16.4.1 Sediment Toxicity .....	563
16.4.2 Sediment Microbial Activity .....	564
16.4.3 Meiofaunal and Macrofaunal Communities .....	569
16.4.4 Demersal/Benthic Megafauna .....	573
16.4.5 Summary of Injury .....	573
16.5 Risk Characterization .....	575
16.5.1 Causes of Sediment Toxicity.....	575
16.5.2 Causes of Organic Enrichment.....	575
16.5.3 Changes in Benthic Communities .....	576
16.5.4 Summary .....	577
<b>17. LITERATURE CITED .....</b>	<b>579</b>

## List of Figures

Figure	Page
1.1 Study sites .....	1
1.2 Number of wells drilled in the deepwater Gulf of Mexico over the past decade (From: Richardson et al. 2004) .....	2
2.1 Location of near-field (NF) and far-field (FF) sites for Viosca Knoll Block 916 .....	9
2.2 Location of near-field (NF) and far-field (FF) sites for Garden Banks Block 516 .....	10
2.3 Location of near-field (NF) and far-field (FF) sites for Garden Banks Block 602 .....	11
2.4 Location of near-field (NF) and far-field (FF) sites for Mississippi Canyon Block 292 .....	12
2.5 Schedule including sampling cruises and wells drilled during this study .....	13
2.6 Idealized sampling plans for study sites .....	17
2.7 Deployment of box core .....	18
2.8 Schematic of box core subsampling .....	19
2.9 Schematic diagram of the sediment profile camera and its operation .....	21
2.10 Configuration of dragged sled for seafloor photography .....	22
2.11 Schematic diagram of baited traps used to obtain organisms for tissue analyses .....	24
2.12 Near-field sampling locations at Viosca Knoll Block 916 .....	26
2.13 Near-field sampling locations at Garden Banks Block 516 .....	27
2.14 Near-field sampling locations at Garden Banks Block 602 .....	28
2.15 Near-field sampling locations at Mississippi Canyon Block 292 .....	29
3.1 Well locations in and near the Viosca Knoll Block 916 near-field site .....	33
3.2 Well locations in and near the Garden Banks Block 516 near-field site .....	36
3.3 Diagram of subsea wellheads, manifold, and flowlines at the Garden Banks Block 516 site .....	38

## List of Figures

(continued)

Figure	Page
3.4	Well locations in and near the Garden Banks Block 602 near-field site ..... 40
3.5	Diagram of subsea wellheads, manifold, and flowlines at the Garden Banks Block 602 site ..... 43
3.6	Well locations in and near the Mississippi Canyon Block 292 near-field site ..... 44
3.7	Diagram of subsea wellheads, manifold, and flowlines at the Mississippi Canyon Block 292 site ..... 46
3.8	Timeline showing drilling activities at the four near-field sites ..... 47
3.9	Location of blocks with previous wells in relation to Viosca Knoll Block 916 near-field (NF) and far-field (FF) sites ..... 50
3.10	Location of previous wells in relation to Garden Banks Block 516 near-field (NF) and far-field (FF) sites ..... 51
3.11	Location of blocks with previous wells in relation to Garden Banks Block 602 near-field (NF) and far-field (FF) sites ..... 52
3.12	Location of blocks with previous wells in relation to Mississippi Canyon Block 292 near-field (NF) and far-field (FF) sites ..... 53
4.1	A computer enhanced shaded relief map of the northern Gulf of Mexico continental slope ..... 58
4.2	Working configuration of the HUGIN 3000 autonomous underwater vehicle showing the “free-swimming” HUGIN collecting data from a predetermined height above the seafloor ..... 61
4.3	Location map of Viosca Knoll (VK) Block 916 ..... 63
4.4	Chirp sonar subbottom profile collected during Cruise 1A (pre-drilling) on Survey Line 1011 approximately 50 m west of the proposed wellsite in Viosca Knoll (VK) Block 916 ..... 65
4.5	A shaded relief image of the Viosca Knoll (VK) 916 study area showing the location of the wellsite for VK 916 Well No. 1 with regard to the distinct channel-levee feature trending roughly northwest-southeast through the eastern part of the block ..... 66
4.6	A sector of the side-scan sonar mosaic produced for the Viosca Knoll (VK) Block 916 area of interest ..... 67

## List of Figures

(continued)

Figure		Page
4.7	A section of a chirp sonar subbottom profile acquired along Line 136, which trends north-south across the Viosca Knoll (VK) Block 916 wellsite.....	68
4.8	Map of cuttings and anchor scars around the Viosca Knoll (VK) Block 916 site based on the Cruise 3A geophysical survey (August 2002).....	70
4.9	A portion of side-scan sonar Line 104 showing debris that appears to be pipe on the seafloor within the Viosca Knoll Block 916 study area.....	71
4.10	A shaded relief image of the Mississippi Canyon (MC) Block 292 study area showing the approximate location of the study site on the southeastern flank of a distinct dome-like feature produced by a salt mass in the shallow subsurface.....	73
4.11	Chirp sonar subbottom profile (Line 319) illustrating an area of seafloor erosion that in plan-view trends northeast-southwest just south of the Mississippi Canyon Block 292 wellsites.....	74
4.12	Image of a portion of a 120-kHz side-scan sonar survey line (Line 316) that trends north-south a short distance to the west of the Mississippi Canyon Block 292 well cluster.....	75
4.13	Map of drilling mud, cuttings, and anchor scars around the Mississippi Canyon (MC) Block 292 site based on the Cruise 2A geophysical survey (June-July 2001) .....	77
4.14	A sector of the side-scan sonar mosaic for the Mississippi Canyon (MC) Block 292 area.....	78
4.15	A shaded relief image of the Garden Banks (GB) 602 and GB 516 areas.....	80
4.16	A section of side-scan sonar Line 116 showing the well cluster in Garden Banks (GB) Block 602 and radial pattern of high reflectance (dark streaks and patches, interpreted as possible cuttings from rig discharges).....	82
4.17	A section of side-scan sonar Line 112 illustrating the man-made scars in the hemipelagic surface sediments of the Garden Banks Block 602 study area.....	83

## List of Figures

(continued)

Figure		Page
4.18	Map of drilling mud, cuttings, and anchor scars around the Garden Banks (GB) 602 site based on the Cruise 2A geophysical survey (June-July 2001).....	84
4.19	This reduced version of the side-scan sonar mosaic illustrates the seafloor complexity to the southeast of the Garden Banks Block 516 wellsite.....	86
4.20	This section of chirp sonar subbottom profile (Line 212) crosses a prominent fault that trends east-west along the flank of the salt-supported ridge to the south of the drilling site in Garden Banks Block 516 .....	87
4.21	This section of side-scan sonar data from Garden Banks Block 516, Survey Line 227, illustrates the complexity of the seafloor in the transition area between the salt-supported high ground to the southeast of the wellsite and the basin floor where the wellsite is located .....	89
4.22	This portion of chirp sonar subbottom profile (Garden Banks Block 516, Line 227) shows a hemipelagic sediment drape over a chaotic and largely acoustically opaque submarine landslide deposit.....	90
4.23	Section of side-scan sonar record from Garden Banks Block 516, Line 216 showing the wellsite area with high-reflectance (dark) areas interpreted as possible cuttings from rig discharges and low-reflectance (light) areas interpreted as possible mud/cuttings from well jetting.....	91
4.24	Map of drilling mud, cuttings, and anchor scars around the Garden Banks Block 516 site based on the Cruise 2A geophysical survey (June-July 2001).....	92
5.1	Ternary plots summarizing grain size data for Viosca Knoll Block 916 .....	99
5.2	Percentages of sand, silt, and clay in relation to proximity to drilling at Viosca Knoll Block 916 .....	100
5.3	Grain size distribution at Viosca Knoll Block 916 on the post-drilling survey (Cruise 3B).....	101
5.4	Percentages of sand and sediments >0.5 mm (coarse sand, very coarse sand, and gravel) on Cruise 3B at Viosca Knoll Block 916 in relation to geophysically mapped cuttings.....	103

## List of Figures

(continued)

Figure		Page
5.5	Relationships between sand percentages and concentrations of drilling indicators (barium and synthetic-based fluid [SBF] concentrations) at Viosca Knoll Block 916 on the post-drilling survey (Cruise 3B) .....	104
5.6	Depth profiles from discretionary stations (DS) at Viosca Knoll Block 916 on the post-drilling survey (Cruise 3B) .....	105
5.7	Ternary plots summarizing grain size data for Garden Banks Block 516 .....	107
5.8	Percentages of sand, silt, and clay in relation to proximity to drilling at Garden Banks Block 516 .....	108
5.9	Grain size distribution at Garden Banks Block 516 on Cruise 2B .....	110
5.10	Percentages of sand on Cruise 1B and Cruise 2B at Garden Banks Block 516 in relation to geophysically mapped cuttings .....	111
5.11	Relationships between sand percentages and concentrations of drilling indicators (barium and synthetic-based fluids [SBF] at Garden Banks Block 516 on Cruised 1B and 2B) .....	112
5.12	Depth profiles from discretionary stations (DS) at Garden Banks Block 516 on Cruise 2B (post-development) .....	113
5.13	Ternary plot summarizing grain size data for Garden Banks Block 602 .....	115
5.14	Percentages of sand, silt, and clay in relation to proximity to drilling at Garden Banks Block 602 .....	116
5.15	Grain size distribution at Garden Banks Block 602 on Cruise 2B .....	118
5.16	Sand percentages on Cruise 2B at Garden Banks Block 602 in relation to geophysically mapped cuttings .....	119
5.17	Relationships between sand, silt, and clay percentages and concentrations of barium (drilling fluid indicator) at Garden Banks Block 602 on Cruise 2B .....	120
5.18	Depth profiles from discretionary stations (DS) at Garden Banks Block 602 on Cruise 2B (post-development) .....	121
5.19	Ternary plot summarizing grain size data for Mississippi Canyon Block 292 .....	123



## List of Figures

(continued)

Figure		Page
5.20	Percentages of coarse and very coarse sand (>0.5 mm), sand, silt, and clay in relation to proximity to drilling at Mississippi Canyon Block 292 .....	125
5.21	Sand percentages on Cruise 2B at Mississippi Canyon Block 292 in relation to geophysically mapped cuttings .....	126
5.22	Relationships between sand, silt, and clay percentages and concentrations of barium (drilling fluid indicator) at Mississippi Canyon Block 292 on Cruise 2B .....	127
5.23	Grain size distribution at Mississippi Canyon Block 292 on Cruise 2B .....	128
5.24	Depth profiles from discretionary stations (DS) at Mississippi Canyon Block 292 on Cruise 2B (post-development) .....	129
6.1	Location of Garden Banks Block 516 exploration/development site and associated reference areas where sediment profile imaging (SPI) transects were surveyed.....	134
6.2	Garden Banks Block 516 near-field (NF) station map, showing positions of sediment profile imaging transects and stations sampled during Cruise 1B (October-November 2000).....	135
6.3	Garden Banks Block 516 Far-field 2 (FF2) station map, showing positions of sediment profile imaging transect and stations sampled during Cruise 1B (October-November 2000).....	135
6.4	Garden Banks Block 516 Far-field 4 (FF4) station map, showing positions of sediment profile imaging transect and stations sampled during Cruise 1B (October-November 2000).....	136
6.5	Garden Banks Block 516 Far-field 6 (FF6) station map, showing positions of sediment profile imaging transect and stations sampled during Cruise 1B (October-November 2000).....	136
6.6	Mapped distribution of mean apparent redox potential discontinuity (RPD) depths along the three near-field transects sampled at Garden Banks Block 516 during Cruise 1B (October-November 2000) .....	139
6.7	Redox potential discontinuity (RPD) depth-frequency distributions at three near-field transects in Garden Banks Block 516 during Cruise 1B (October-November 2000) .....	140

## List of Figures

(continued)

Figure		Page
6.8	Mapped distribution of mean apparent redox potential discontinuity (RPD) depths along Transect FF2 at Garden Banks Block 516 during Cruise 1B (October-November 2000) .....	142
6.9	Mapped distribution of mean apparent redox potential discontinuity (RPD) depths along Transect FF4 at Garden Banks Block 516 during Cruise 1B (October-November 2000) .....	142
6.10	Mapped distribution of mean apparent redox potential discontinuity (RPD) depths along Transect FF6 at Garden Banks Block 516 during Cruise 1B (October-November 2000) .....	143
6.11	Redox potential discontinuity (RPD) depth-frequency distributions at three far-field transects at Garden Banks Block 516 during Cruise 1B (October-November 2000) .....	144
6.12	Mapped distribution of infaunal successional stages along all three near-field transects at Garden Banks Block 516 during Cruise 1B (October-November 2000) .....	145
6.13	Mapped distribution of infaunal successional stages along Transect FF2 at Garden Banks Block 516 during Cruise 1B (October-November 2000) .....	147
6.14	Mapped distribution of infaunal successional stages along Transect FF4 at Garden Banks Block 516 during Cruise 1B (October-November 2000) .....	147
6.15	Mapped distribution of infaunal successional stages along Transect FF6 at Garden Banks Block 516 during Cruise 1B (October-November 2000).....	147
6.16	Mapped distribution of the Organism-Sediment Index (OSI) along all three near-field transects at Garden Banks Block 516 during Cruise 1B (October-November 2000) .....	148
6.17	Organism-Sediment Index (OSI) class-frequency distributions at all three near-field transects sampled at Garden Banks Block 516 during Cruise 1B (October-November 2000) .....	149
6.18	Mapped distribution of the Organism-Sediment Index (OSI) along Transect FF2 at Garden Banks Block 516 during Cruise 1B (October-November 2000) .....	151

## List of Figures

(continued)

Figure		Page
6.19	Mapped distribution of the Organism-Sediment Index (OSI) along Transect FF4 at Garden Banks Block 516 during Cruise 1B (October-November 2000) .....	151
6.20	Mapped distribution of the Organism-Sediment Index (OSI) along Transect FF6 at Garden Banks Block 516 during Cruise 1B (October-November 2000) .....	151
6.21	Organism-Sediment Index (OSI) class-frequency distributions at all three far-field transects at Garden Banks Block 516 during Cruise 1B (October-November 2000) .....	152
6.22	Organism-Sediment Index (OSI) class-frequency distributions at all near-field and far-field transects at Garden Banks Block 516 during Cruise 1B (October-November 2000) .....	153
6.23	Location of Viosca Knoll Block 916 exploration site and associated reference areas where sediment profile imaging (SPI) transects were surveyed on Cruise 1B.....	154
6.24	Viosca Knoll Block 916 near-field (NF) station map, showing positions of sediment profile imaging transects and stations.....	155
6.25	Viosca Knoll Block 916 Far-field 2 (FF2) station map, showing positions of sediment profile imaging transects and stations .....	155
6.26	Viosca Knoll Block 916 Far-field 4 (FF4) station map, showing positions of sediment profile imaging transect and stations.....	156
6.27	Viosca Knoll Block 916 Far-field 6 (FF6) station map, showing positions of sediment profile imaging transect and stations.....	156
6.28	Mapped distribution of apparent redox potential discontinuity (RPD) depth, in centimeters, along the two near-field transects in Viosca Knoll Block 916 during pre-drilling Cruise 1B (October-November 2000) .....	159
6.29	Redox potential discontinuity (RPD) depth-frequency distributions at two near-field transects in Viosca Knoll Block 916 during pre-drilling Cruise 1B (October-November 2000) .....	160
6.30	Redox potential discontinuity (RPD) depth-frequency distributions along Transect FF2 at Viosca Knoll Block 916 during pre-drilling Cruise 1B (October-November 2000) .....	161

## List of Figures

(continued)

Figure		Page
6.31	Redox potential discontinuity (RPD) depth-frequency distributions at three far-field transects sampled at Viosca Knoll Block 916 during pre-drilling Cruise 1B (October-November 2000) .....	162
6.32	Redox potential discontinuity (RPD) depth-frequency distributions along Transect FF4 at Viosca Knoll Block 916 during pre-drilling Cruise 1B (October-November 2000) .....	163
6.33	Redox potential discontinuity (RPD) depth-frequency distributions along Transect FF6 at Viosca Knoll Block 916 during pre-drilling Cruise 1B (October-November 2000) .....	163
6.34	Mapped distribution of infaunal successional stages along Transects NF-1 and NF-2 at Viosca Knoll Block 916 during pre-drilling Cruise 1B (October-November 2000) .....	165
6.35	Mapped distribution of successional stages along Transect FF2 at Viosca Knoll Block 916 during pre-drilling Cruise 1B (October-November 2000) .....	166
6.36	Mapped distribution of successional stages along Transect FF4 at Viosca Knoll Block 916 during pre-drilling Cruise 1B (October-November 2000) .....	166
6.37	Mapped distribution of successional stages along Transect FF6 at Viosca Knoll Block 916 during pre-drilling Cruise 1B (October-November 2000) .....	167
6.38	Mapped distribution of the Organism-Sediment Index (OSI) along the two near-field transects taken at Viosca Knoll Block 916 during pre-drilling Cruise 1B (October-November 2000) .....	168
6.39	Organism-Sediment Index (OSI) class-frequency distributions at two near-field transects in Viosca Knoll Block 916 during pre-drilling Cruise 1B (October-November 2000) .....	169
6.40	Mapped distribution of the Organism-Sediment Index (OSI) along the Transect FF2 at Viosca Knoll Block 916 during pre-drilling Cruise 1B (October-November 2000) .....	170
6.41	Organism-Sediment Index (OSI) class-frequency distributions at three far-field transects in Viosca Knoll Block 916 during pre-drilling Cruise 1B (October-November 2000) .....	171

## List of Figures

(continued)

Figure		Page
6.42	Mapped distribution of the Organism-Sediment Index (OSI) along Transect FF4 at Viosca Knoll Block 916 during pre-drilling Cruise 1B (October-November 2000) .....	172
6.43	Mapped distribution of the Organism-Sediment Index (OSI) along Transect FF6 at Viosca Knoll Block 916 during pre-drilling Cruise 1B (October-November 2000) .....	172
6.44	Organism-Sediment Index (OSI) class-frequency distributions at all near-field and far-field transects sampled at Viosca Knoll Block 916 during pre-drilling Cruise 1B (October-November 2000).....	173
6.45	Garden Banks Block 516 near-field (NF) map showing transects and stations sampled during Cruise 2B (July 2001).....	175
6.46	Garden Banks Block 516 Far-field 3 (FF3) station map, showing transects and stations sampled during Cruise 2B (July 2001) .....	175
6.47	Garden Banks Block 516 Far-field 4 (FF4) station map, showing transects and stations sampled during Cruise 2B (July 2001).....	176
6.48	Garden Banks Block 516 Far-field 5 (FF5) station map, showing transects and stations sampled during Cruise 2B (July 2001).....	176
6.49	Mapped distribution of apparent redox potential discontinuity (RPD) depth, in centimeters, along the three near-field transects taken at Garden Banks Block 516 during Cruise 2B (July 2001).....	178
6.50	Redox potential discontinuity (RPD) depth-frequency distributions at three near-field transects sampled at Garden Banks Block 516 during Cruise 2B (July 2001).....	180
6.51	Mapped distribution of apparent redox potential discontinuity (RPD) depth, in centimeters, along the two transects surveyed at Far-field 3 (FF3) during Cruise 2B (July 2001) .....	181
6.52	Mapped distribution of apparent redox potential discontinuity (RPD) depth, in centimeters, along Transect FF4 at Garden Banks Block 516 during Cruise 2B (July 2001) .....	181
6.53	Mapped distribution of apparent redox potential discontinuity (RPD) depth, in centimeters, along Transect FF5 at Garden Banks Block 516 during Cruise 2B (July 2001) .....	181

## List of Figures

(continued)

Figure		Page
6.54	Redox potential discontinuity (RPD) depth-frequency distributions at three far-field transects sampled at Garden Banks Block 516 during Cruise 2B (July 2001).....	182
6.55	Mapped distribution of infaunal successional stages along all three near-field transects at Garden Banks Block 516 during Cruise 2B (July 2001).....	184
6.56	Mapped distribution of infaunal successional stages along the two transects at Garden Banks Block 516, Far-field 3 (FF3) during Cruise 2B (July 2001).....	185
6.57	Mapped distribution of infaunal successional stages along Transect FF4 at Garden Banks Block 516 during Cruise 2B (July 2001) .....	185
6.58	Mapped distribution of infaunal successional stages along Transect FF5 at Garden Banks Block 516 during Cruise 2B (July 2001) .....	185
6.59	Mapped distribution of the Organism-Sediment Index (OSI) along all three near-field transects at Garden Banks Block 516 during Cruise 2B (July 2001).....	187
6.60	Organism-Sediment Index (OSI) class-frequency distribution for all stations belonging to all three near-field transects surveyed at Garden Banks Block 516 during Cruise 2B (July 2001).....	188
6.61	Mapped distribution of the Organism-Sediment Index (OSI) along far-field transects at FF3 at Garden Banks Block 516 during Cruise 2B (July 2001).....	188
6.62	Organism-Sediment Index (OSI) frequency distributions at the three far-field transects at Garden Banks Block 516 during Cruise 2B (July 2001).....	189
6.63	Mapped distribution of the Organism-Sediment Index (OSI) along Transect FF4 at Garden Banks Block 516 during Cruise 2B (July 2001).....	190
6.64	Mapped distribution of the Organism-Sediment Index (OSI) along Transect FF5 at Garden Banks Block 516 during Cruise 2B (July 2001).....	190
6.65	Viosca Knoll Block 916 near-field station map showing positions of sediment profile imaging transects and stations surveyed during post-drilling Cruise 3B (August 2002).....	192

## List of Figures

(continued)

Figure		Page
6.66	Mapped distribution of apparent redox potential discontinuity depth in centimeters, along the three near-field transects at Viosca Knoll Block 916 during post-drilling Cruise 3B (August 2002).....	194
6.67	Apparent redox potential discontinuity (RPD) depth-frequency distributions at the three near-field transects at Viosca Knoll Block 916 during post-drilling Cruise 3B (August 2002).....	195
6.68	Mapped distribution of infaunal successional stages along all three near-field transects surveyed at Viosca Knoll Block 916 during post-drilling Cruise 3B (August 2002).....	197
6.69	Mapped distribution of the Organism-Sediment Index (OSI) along the three near-field transects at Viosca Knoll Block 916 during post-drilling Cruise 3B (August 2002).....	198
6.70	Organism-Sediment Index (OSI) class-frequency distributions at the three near-field transects at Viosca Knoll Block 916 during post-drilling Cruise 3B (August 2002).....	199
7.1	Location of Garden Banks Block 602 post-development site and associated reference areas where sediment profile imaging (SPI) transects were surveyed.....	216
7.2	Location of Mississippi Canyon Block 292 post-development site and associated reference areas where sediment profile imaging (SPI) transects were surveyed.....	217
7.3	Locations of sediment profile imaging (SPI) transects at Garden Banks Block 602 near-field site on Cruise 2B (July 2001).....	219
7.4	Locations of sediment profile imaging (SPI) transects at Mississippi Canyon Block 292 near-field site on Cruise 2B (July 2001).....	219
7.5	Locations of sediment profile imaging (SPI) transects at Garden Banks Block 602 far-field sites on Cruise 2B (July 2001).....	220
7.6	Locations of sediment profile imaging (SPI) transects at Mississippi Canyon Block 292 far-field sites on Cruise 2B (July 2001).....	221
7.7	Number and appearance of color sediment layers at stations along Garden Banks Block 602 near-field transects .....	226

## List of Figures

(continued)

Figure		Page
7.8	Histogram showing the distribution of apparent color redox potential discontinuity (RPD) layer depth for Garden Banks Block 602 near-field (NF) and far-field (FF) transects .....	227
7.9	Appearance of color sediment layers at stations along Garden Banks Block 602 far-field transects .....	229
7.10	Average thickness of color layers (cm) at Garden Banks Block 602 sites.....	231
7.11	Average depth of apparent color redox potential discontinuity (RPD) layer (cm) at Garden Banks Block 602 far-field (FF) and near-field (NF) transects .....	231
7.12	Appearance of color sediment layers at stations along Mississippi Canyon Block 292 near-field transects.....	233
7.13	Histogram showing the distribution of apparent color redox potential discontinuity (RPD) layer depth for Mississippi Canyon Block 292 near-field (NF) and far-field (FF) transects.....	234
7.14	Sediment profile imaging image from Mississippi Canyon Block 292, Station NF-1.08, showing a large burrow structure near the center and extending down from sediment-water interface to bottom of image.....	235
7.15	Appearance of color sediment layers at stations along Mississippi Canyon Block 292 far-field transects .....	237
7.16	Average thickness of color layers (cm) at Mississippi Canyon Block 292 sites .....	238
7.17	Fauna from Mississippi Canyon Block 292 .....	238
7.18	Average depth of apparent color redox potential discontinuity (RPD) layer (cm) at Mississippi Canyon Block 292 far-field (FF) and near-field (NF) transects.....	239
8.1	Photographs showing (a) oxygen probe inserted in top of sediment core and close-up of electrode and electronic control box, (b) redox potential (Eh) electrode inserted in sediment core, and (c) whole-core squeezer .....	246



## List of Figures

(continued)

Figure		Page
8.2	Concentrations of barium (Ba) with markers and numbers showing means and lines showing standard deviations in sediment from near-field (NF) and far-field (FF) stations at Viosca Knoll (VK) 916 during pre-exploration drilling Cruise 1B and post-exploration drilling Cruise 3B.....	255
8.3	Concentrations of barium (Ba) at Viosca Knoll (VK) 916 near-field (NF) stations during post-drilling Cruise 3B.....	255
8.4	Vertical profiles for concentrations of barium (Ba) in sediment from discretionary (DS) stations during post-exploration Cruise 3B to Viosca Knoll (VK) 916 .....	256
8.5	Concentrations of barium (Ba) versus mercury (Hg) for sediments from far-field (FF) and near-field (NF) stations from Viosca Knoll (VK) 916 collected during pre-exploration Cruise 1B and post-exploration Cruise 3B.....	257
8.6	Vertical profiles for concentrations of mercury (Hg) in sediment from discretionary (DS) stations during post-exploration Cruise 3B to Viosca Knoll (VK) 916 .....	257
8.7	Concentrations of total organic carbon (TOC) with circles and numbers showing means and lines showing standard deviations in sediment from near-field (NF) and far-field (FF) stations from Viosca Knoll (VK) 916 during pre-exploration drilling Cruise 1B and post-exploration drilling Cruise 3B.....	259
8.8	Concentrations of barium (Ba) versus total organic carbon (TOC) for sediments from far-field (FF) and near-field (NF) stations from Viosca Knoll (VK) 916 collected during pre-exploration Cruise 1B and post-exploration Cruise 3B.....	259
8.9	Vertical profiles for concentrations of total organic carbon (TOC) in sediment from discretionary (DS) stations for post-exploration Cruise 3B to Viosca Knoll (VK) 916 .....	260
8.10	Vertical profiles for activities of excess $^{210}\text{Pb}$ in sediment from far-field (FF) and near-field (NF) stations at Viosca Knoll (VK) 916 for Cruise 1B.....	261
8.11	Approximate redox potential (Eh) values at which various redox reactions occur in water (after Drever 1997).....	262

## List of Figures

(continued)

Figure		Page
8.12	Vertical profiles for dissolved oxygen, redox potential (Eh), and pH in sediment from representative near-field (NF), far-field (FF), and discretionary (DS) stations from Viosca Knoll (VK) 916 (note different depth scales for oxygen versus Eh) .....	263
8.13	Integrated amounts of oxygen in the sediment column at near-field (NF), far-field (FF), and discretionary (DS) stations at Viosca Knoll (VK) 916 for pre-exploration Cruise 1B and post-exploration Cruise 3B .....	265
8.14	Vertical profiles for dissolved oxygen, Eh, nitrate, sulfate, manganese, and iron from interstitial water from Station FF-B02, Viosca Knoll (VK) 916, for pre-exploration Cruise 1B .....	266
8.15	Vertical profiles for dissolved oxygen, Eh, nitrate, sulfate, manganese, and iron from interstitial water from Station NF-B02, Viosca Knoll (VK) 916, for pre-exploration Cruise 1B .....	267
8.16	Vertical profiles for dissolved oxygen, Eh, sulfate, ammonia, manganese, and iron from interstitial water at Station FF-B03, Viosca Knoll (VK) 916, for post-exploration Cruise 3B.....	269
8.17	Vertical profiles for dissolved oxygen, Eh, sulfate, ammonia, manganese, and iron from interstitial water at Station DS-2, Viosca Knoll (VK) 916, for post-exploration Cruise 3B.....	270
8.18	Vertical profiles for concentrations of manganese (Mn) in sediment from discretionary (DS) stations for post-exploration Cruise 3B to Viosca Knoll (VK) 916 .....	271
8.19	Concentrations of aluminum (Al) versus (a) iron (Fe) and (b) barium (Ba) for sediments from far-field (FF), near-field (NF), and discretionary (DS) stations from Garden Banks (GB) 516 collected during Cruises 1B and 2B.....	273
8.20	Concentrations of barium (Ba) with markers and numbers showing means and lines showing standard deviations in sediment from near-field (NF) and far-field (FF) stations at Garden Banks (GB) 516 during Cruises 1B and 2B.....	274
8.21	Concentrations of barium (Ba) at Garden Banks (GB) 516 near-field (NF) stations during Cruises 1B and 2B.....	275

## List of Figures

(continued)

Figure		Page
8.22	Vertical profiles for concentrations of barium (Ba) and aluminum (Al) in sediment from discretionary (DS) stations at Garden Banks (GB) 516 for Cruise 2B .....	277
8.23	Concentrations of aluminum (Al) versus manganese (Mn) for sediments from far-field (FF), and near-field (NF), and discretionary (DS) stations from Garden Banks (GB) 516 collected during Cruises 1B and 2B .....	277
8.24	Concentrations of barium (Ba) versus (a) mercury (Hg) and (b) lead (Pb) for sediments from far-field (FF) and near-field (NF) stations from Garden Banks (GB) 516 collected during Cruises 1B and 2B .....	278
8.25	Vertical profiles for concentrations of mercury (Hg) in sediment from discretionary (DS) stations for Cruise 2B at Garden Banks (GB) 516.....	279
8.26	Concentrations of total organic carbon (TOC) with markers and numbers showing means and lines showing standard deviations in sediment from near-field (NF) and far-field (FF) stations from Garden Banks (GB) 516 during Cruises 1B and 2B .....	279
8.27	Concentrations of barium (Ba) versus total organic carbon (TOC) for sediments from far-field (FF), near-field (NF), and discretionary (DS) stations from Garden Banks (GB) 516 collected during Cruises 1B and 2B .....	280
8.28	Vertical profiles for concentrations of total organic carbon (TOC) in sediment from discretionary (DS) stations for Cruise 2B at Garden Banks (GB) 516.....	280
8.29	Vertical profiles for activities of excess $^{210}\text{Pb}$ in sediment from Garden Banks (GB) 516 for Station FF6 during Cruise 2B and Station NF-B02 for Cruise 2B .....	282
8.30	Vertical profiles for dissolved oxygen, redox potential (Eh), and pH in sediment from representative near-field (NF) and far-field (FF) stations at Garden Banks (GB) 516 from Cruise 1B .....	283
8.31	Vertical profiles for dissolved oxygen, redox potential (Eh), and pH in sediment from representative near-field (NF), far-field (FF), and discretionary (DS) stations from Garden Banks (GB) 516 from Cruise 2B .....	284

## List of Figures

(continued)

Figure		Page
8.32	Integrated amounts of oxygen in the sediment column at near-field (NF), far-field (FF), and discretionary (DS) stations at Garden Banks (GB) 516 for Cruises 1B and 2B .....	286
8.33	Vertical profiles for dissolved oxygen, Eh, nitrate, sulfate, manganese, and iron from interstitial water from Station FF-B02 at Garden Banks (GB) 516 during Cruise 1B .....	287
8.34	Vertical profiles for dissolved oxygen, Eh, ammonia, sulfate, manganese, and iron from interstitial water from Station NF-B01 at Garden Banks (GB) 516 during Cruise 1B.....	288
8.35	Vertical profiles for dissolved oxygen, Eh, ammonia, sulfate, manganese, and iron from interstitial water from Station FF-B06 at Garden Banks (GB) 516 during Cruise 2B.....	290
8.36	Vertical profiles for concentrations of manganese (Mn) in sediment from discretionary (DS) stations at Garden Banks (GB) 516 for Cruise 2B .....	291
8.37	Concentrations of barium (Ba) with markers and numbers showing means and lines showing standard deviations in sediment from near-field (NF) and far-field (FF) stations at Garden Banks (GB) 602 and Mississippi Canyon (MC) 292 during post-development Cruise 2B.....	293
8.38	Concentrations of barium (Ba) at Garden Banks (GB) 602 and Mississippi Canyon (MC) 292 near-field (NF) stations during post-development Cruise 2B .....	294
8.39	Vertical profiles for concentrations of barium (Ba) in sediment from discretionary (DS) stations at Garden Banks (GB) 602 and Mississippi Canyon (MC) 292.....	295
8.40	Concentrations of barium (Ba) versus (a) lead (Pb) and (b) mercury (Hg) for sediments from far-field (FF) and near-field (NF) stations from Garden Banks (GB) 602 and Mississippi Canyon (MC) 292 collected during Cruise 2B .....	296
8.41	Concentrations of mercury (Hg) with markers and numbers bars showing means and lines showing standard deviations in sediment from near-field (NF) and far-field (FF) stations at Garden Banks (GB) 602 and Mississippi Canyon (MC) 292 during Cruise 2B .....	297

## List of Figures

(continued)

Figure		Page
8.42	Vertical profiles for concentrations of mercury (Hg) in sediment from discretionary (DS) stations at Garden Banks (GB) 602 and Mississippi Canyon (MC) 292.....	298
8.43	Concentrations of total organic carbon (TOC) with markers and numbers showing means and lines showing standard deviations in sediment from near-field (NF) and far-field (FF) stations at Garden Banks (GB) 602 and Mississippi Canyon (MC) 292 during post-development Cruise 2B .....	298
8.44	Vertical profiles for concentrations of total organic carbon (TOC) in sediment from discretionary (DS) stations at Garden Banks (GB) 602 and Mississippi Canyon (MC) 292.....	299
8.45	Vertical profiles for activities of excess $^{210}\text{Pb}$ in sediment from Garden Banks (GB) 602 Station FF-B05 and excess $^{210}\text{Pb}$ and $^{137}\text{Cs}$ from Mississippi Canyon (MC) 292 Station FF-B02.....	300
8.46	Vertical profiles for dissolved oxygen, redox potential (Eh), and pH in sediment from representative near-field (NF), far-field (FF), and discretionary (DS) stations at Garden Banks (GB) 602 .....	302
8.47	Integrated amounts of oxygen in the sediment column at near-field (NF), far-field (FF), and discretionary (DS) stations at Garden Banks (GB) 602 and Mississippi Canyon (MC) 292.....	303
8.48	Vertical profiles for dissolved oxygen, redox potential (Eh), and pH in sediment from representative near-field (NF), far-field (FF), and discretionary (DS) stations at Mississippi Canyon (MC) 292.....	304
8.49	Vertical profiles for dissolved oxygen, Eh, nitrate, ammonia, manganese, and sulfate from interstitial water from Station FF-B05 at site Garden Banks (GB) 602 during post-development Cruise 2B.....	305
8.50	Vertical profiles for dissolved oxygen, Eh, nitrate, ammonia, manganese, and sulfate from interstitial water from discretionary station DS-2 at Garden Banks (GB) 602 during post-development Cruise 2B.....	306
8.51	Vertical profiles for dissolved oxygen, Eh, nitrate, ammonia, and sulfate from interstitial water from Station FF-B02 at Mississippi Canyon (MC) 292 during post-development Cruise 2B.....	307

## List of Figures

(continued)

Figure		Page
8.52	Vertical profiles for dissolved oxygen, Eh, nitrate, ammonia, manganese, and sulfate from interstitial water from discretionary station DS-2 at Mississippi Canyon (MC) 292 during post-development Cruise 2B .....	308
8.53	Vertical profiles for concentrations of manganese (Mn) in sediment from discretionary (DS) stations at Garden Banks (GB) 602 and Mississippi Canyon (MC) 292 for post-development Cruise 2B .....	309
8.54	Photograph of giant amphipod <i>Bathynomus giganteus</i> from the Gulf of Mexico .....	310
8.55	Photograph of red crab <i>Chaceon quinquegens</i> from the Gulf of Mexico.....	310
8.56	Water content and concentrations of arsenic (As), barium (Ba), cadmium (Cd), chromium (Cr), and copper (Cu) in soft tissue from the isopod <i>Bathynomus giganteus</i> from near-field (NF) and far-field (FF) stations from post-development sites Garden Banks (GB) 602 and Mississippi Canyon (MC) 292.....	312
8.57	Concentrations of iron (Fe), mercury (Hg), nickel (Ni), lead (Pb), vanadium (V), and zinc (Zn) in soft tissue from the isopod <i>Bathynomus giganteus</i> from near-field (NF) and far-field (FF) stations from post-development sites Garden Banks (GB) 602 and Mississippi Canyon (MC) 292.....	313
8.58	Water content and concentrations of arsenic (As), barium (Ba), cadmium (Cd), chromium (Cr), and copper (Cu) in soft tissue from the crab <i>Chaceon</i> from near-field (NF) and far-field (FF) stations from post-development sites Garden Banks (GB) 602 and Mississippi Canyon (MC) 292.....	315
8.59	Concentrations of iron (Fe), mercury (Hg), nickel (Ni), lead (Pb), vanadium (V), and zinc (Zn) in soft tissue from the crab <i>Chaceon</i> from near-field (NF) and far-field (FF) stations from post-development sites Garden Banks (GB) 602 and Mississippi Canyon (MC) 292.....	316
8.60	Concentrations of aluminum (Al) versus iron (Fe) for sediments from all stations.....	317
8.61	Concentrations of aluminum (Al) versus vanadium (V) for all sediments collected during the project .....	317

## List of Figures

(continued)

Figure	Page
8.62	Concentrations of aluminum (Al) versus zinc (Zn) for sediments from (a) far-field (FF) stations and (b) all stations (FF and near-field [NF], including discretionary [DS] stations)..... 319
8.63	Concentrations of aluminum (Al) versus lead (Pb) for sediments from far-field (FF) and near-field (NF) stations (data for discretionary [DS] stations are plotted as NF samples) ..... 320
8.64	Concentrations of aluminum (Al) versus arsenic (As) for sediments from far-field (FF) and near-field (NF) stations (data for discretionary [DS] stations are plotted as NF samples)..... 321
8.65	Concentrations of (a) aluminum (Al) versus mercury (Hg) and (b) barium (Ba) versus Hg for sediments from far-field (FF) and near-field (NF) stations (data for discretionary [DS] stations are plotted as NF samples) ..... 322
8.66	Concentrations of aluminum (Al) versus (a) cadmium (Cd) and (b) copper (Cu) for sediments from far-field (FF) and near-field (NF) stations (data for discretionary stations are plotted as NF samples)..... 323
8.67	Concentrations of aluminum (Al) versus (a) nickel (Ni) and (b) chromium (Cr) for sediments from far-field (FF) and near-field (NF) stations (data for discretionary stations are plotted as NF samples)..... 324
9.1	Typical background hydrocarbon distribution in deep sea sediment ..... 328
9.2	A sediment hydrocarbon pattern that displays a synthetic based fluid pattern..... 328
9.3	Spatial distribution of synthetic-based fluid (SBF) concentrations at Viosca Knoll (VK) Block 916 on Cruise 1B (pre-drilling) and Cruise 3B (post-drilling)..... 333
9.4	Spatial distribution of synthetic-based fluid (SBF) concentrations at Garden Banks (GB) Block 516 on Cruise 1B and Cruise 2B..... 336
9.5	Spatial distribution of synthetic-based fluid (SBF) concentrations at Garden Banks (GB) Block 602 on Cruise 2B..... 339
9.6	Spatial distribution of synthetic-based fluid (SBF) concentrations at Mississippi Canyon (MC) Block 292 on Cruise 2B ..... 342

## List of Figures

(continued)

Figure		Page
10.1	A comparison between the recovery of a stable internal adenosine triphosphate (ATP) standard to the recovery of the <sup>14</sup> C ATP adsorption standard .....	349
10.2	The effect of sediment grain size on the recovery of the <sup>14</sup> C ATP extraction standard.....	350
10.3	Microbial adenosine triphosphate (ATP) concentrations at the four study sites.....	354
10.4	The relative toxicity of sediment extracts for selected sampling sites at VK 916 before and after drilling .....	355
10.5	The relative toxicity of sediment extracts for selected sampling sites at GB 516 before and after drilling .....	355
10.6	The relative toxicity of sediment extracts for selected sampling sites at a) GB 602 and b) MC 292 .....	356
10.7	Respired carbon dioxide from acetate in sediments from GB 516, Cruise 1B .....	357
11.1	Total meiofaunal densities at the four study sites.....	365
11.2	Taxonomic composition of meiofauna at Viosca Knoll Block 916 .....	366
11.3	Taxonomic composition of meiofauna at Garden Banks Block 516.....	369
11.4	Taxonomic composition of meiofauna at Garden Banks Block 602 and Mississippi Canyon Block 292.....	372
11.5	Comparison of near-field and far-field abundances of meiofaunal nematodes, harpacticoids, and annelids in post-drilling samples.....	375
11.6	Total macroinfaunal densities at the four study sites .....	382
11.7	Taxonomic composition of macroinfauna at Viosca Knoll Block 916 .....	383
11.8	Taxonomic composition of macroinfauna at Garden Banks Block 516.....	387
11.9	Taxonomic composition of macroinfauna at Garden Banks Block 602 and Mississippi Canyon Block 292 .....	390
11.10	Comparison of near-field and far-field abundances of macroinfaunal annelids, gastropods, and bivalves in post-drilling samples.....	393



## List of Figures

(continued)

Figure	Page
11.11 Comparison of near-field and far-field abundances of macroinfaunal amphipods, aplacophorans, and ostracods in post-drilling samples .....	394
11.12 Annelid (predominantly polychaete) densities vs. barium concentrations on post-drilling cruises .....	396
11.13 Annelid (predominantly polychaete) densities vs. synthetic-based fluid (SBF) concentrations on post-drilling cruises .....	397
11.14 Gastropod densities vs. sediment barium, synthetic-based fluid (SBF), and total organic carbon concentrations at near-field (NF), post-drilling stations .....	398
11.15 Amphipod densities vs. sediment barium concentrations on post-drilling cruises .....	399
11.16 Ostracod densities vs. sediment barium concentrations on post-drilling cruises .....	400
11.17 Macroinfaunal community characteristics for the detailed, 24-station analysis .....	405
11.18 Station/cruise groups resolved by multidimensional scaling of macroinfaunal data from the 24-station dataset .....	406
11.19 Comparison of sediment barium, synthetic-based fluid (SBF), and total organic carbon concentrations at station groups identified from multidimensional scaling ordination .....	408
12.1 Locations of camera sled transects at Viosca Knoll (VK) Block 916 near-field (NF) site .....	417
12.2 Locations of camera sled transects at Garden Banks (GB) Block 516 near-field (NF) site .....	418
12.3 Locations of camera sled transects at Garden Banks (GB) Block 602 near-field (NF) site .....	419
12.4 Locations of camera sled transects at Mississippi Canyon (MC) Block 292 near-field (NF) site .....	420
12.5 Image analysis results for Viosca Knoll (VK) Block 916, Cruise 1B, near-field transects .....	423

## List of Figures

(continued)

Figure		Page
12.6	Image analysis results for Viosca Knoll (VK) Block 916, Cruise 3B, Near-field Transect 1 .....	424
12.7	Image analysis results for Viosca Knoll (VK) Block 916, Cruise 3B, Near-field Transect 2 .....	425
12.8	Locations of example photographs in relation to geophysically mapped cuttings deposits at Viosca Knoll (VK) Block 916 on Cruise 3B .....	426
12.9	Image analysis results for Garden Banks (GB) Block 516, Cruise 1B, Near-field Transect 1 .....	427
12.10	Image analysis results for Garden Banks (GB) Block 516, Cruise 2B, Near-field Transect 1 .....	428
12.11	Image analysis results for Garden Banks (GB) Block 516, Cruise 1B, far-field transects .....	429
12.12	Image analysis results for Garden Banks (GB) Block 602, Cruise 2B, Near-field Transect 3 .....	431
12.13	Image analysis results for Garden Banks (GB) Block 602, Cruise 2B, far-field transects .....	432
12.14	Image analysis results for Mississippi Canyon (MC) Block 292, Cruise 2B, Near-field Transect 3 .....	433
12.15	Image analysis results for Mississippi Canyon (MC) Block 292, Cruise 2B, far-field transects .....	434
13.1	Relationship between synthetic based fluid (SBF) concentrations and the number of <i>Bathyletopsyllus</i> sp. per box core at the near-field sites .....	446
13.2	Haplotype network of 15 unique cytochrome c oxidase subunit I COX I sequences .....	448
13.3	Relationship between haplotype diversity and nucleotide diversity of COX I sequences for five species of harpacticoid copepods including <i>Bathyletopsyllus</i> sp. ....	451
13.4	Mismatch distributions for pairwise haplotype distances between <i>Bathyletopsyllus</i> sp. individuals collected at Garden Banks (GB) Block 602 and Mississippi Canyon (MC) Block 292 .....	452
14.1	Sediment toxicity test system .....	461

## List of Figures

(continued)

Figure	Page
14.2	Regression of barium concentration against fraction of amphipods surviving in a 10-day sediment toxicity test with near-field and far-field sediments from Mississippi Canyon Block 292 ..... 465
14.3	Regression of synthetic based fluid (SBF) concentration against fraction of amphipods surviving in a 10-day sediment toxicity test with near-field and far-field sediments from Mississippi Canyon Block 292..... 466
14.4	Regression of barium concentration against fraction of amphipods surviving in a 10-day sediment toxicity test in near-field and far-field sediments at Garden Banks Block 602..... 467
14.5	Regression of synthetic based fluid (SBF) concentration against fraction of amphipods surviving in a 10-day sediment toxicity test with near-field and far-field sediments from Garden Banks Block 602..... 468
14.6	Regression of polycyclic aromatic hydrocarbon (PAH) concentration against fraction of amphipods surviving in a 10-day sediment toxicity test with near-field and far-field sediments from Garden Banks Block 602 ..... 469
15.1	Microbial biomass and meiofaunal and macroinfaunal densities at far-field sites..... 473
15.2	Extent of geophysically mapped drilling mud and cuttings deposits around (a) Viosca Knoll 916 on Cruise 3A; (b) Garden Banks 516 on Cruise 2A; (c) Garden Banks 602 on Cruise 2A; and (d) Mississippi Canyon 292 on Cruise 2A ..... 481
15.3	Side-scan sonar mosaic showing highly reflective seafloor (dark areas, presumed rig discharge deposits) at Viosca Knoll 916 on Cruise 3A (post-exploration) ..... 484
15.4	Distribution of highly reflective seafloor (dark areas, presumed rig discharge deposits) at Garden Banks 516 on Cruise 2A (post-development)..... 485
15.5	Isopach (thickness) plot of geophysically mapped drilling deposits at Viosca Knoll 916..... 486
15.6	Sediment percentages of sand, silt, and clay in relation to proximity to drilling ..... 487
15.7	Far-field concentrations of barium and synthetic-based fluids ..... 490

## List of Figures

(continued)

Figure	Page
15.8 Barium and synthetic-based fluid (SBF) concentrations on Cruise 3B at Viosca Knoll 916 site in relation to geophysically mapped rig discharge deposits.....	492
15.9 Barium and synthetic-based fluid (SBF) concentrations on Cruise 2B at Garden Banks 516 in relation to geophysically mapped mud and cuttings deposits .....	493
15.10 Barium and synthetic-based fluid (SBF) concentrations on Cruise 2B at Garden Banks 602 in relation to geophysically mapped mud and cuttings deposits.....	494
15.11 Barium and synthetic-based fluid (SBF) concentrations on Cruise 2B at Mississippi Canyon 292 site in relation to geophysically mapped mud and cuttings deposits .....	495
15.12 Sediment concentrations of barium, synthetic-based fluids (SBF), and polycyclic aromatic hydrocarbons (PAHs) in relation to proximity to drilling.....	496
15.13 Relationship between total organic carbon (TOC) and synthetic-based fluid (SBF) concentrations in near-field sediments at the four sites .....	500
15.14 Integrated amounts of oxygen in the sediment column at near-field (NF), far-field (FF), and discretionary (DS) stations at all four sites.....	501
15.15 Redox potential (Eh) values at 1 to 3 cm depth in the sediment column at Viosca Knoll 916 and Garden Banks 516 on post-exploration cruises in relation to geophysically mapped mud and cuttings deposits.....	503
15.16 Redox potential (Eh) values at 1 to 3 cm depth in the sediment column at Garden Banks 516, Garden Banks 602, and Mississippi Canyon 292 on post-development cruises in relation to geophysically mapped mud and cuttings deposits .....	504
15.17 Microbial adenosine triphosphate (ATP) concentrations at the four study sites.....	508
15.18 Microbial adenosine triphosphate (ATP) concentrations at Viosca Knoll 916 and Garden Banks 516 on post-drilling cruises in relation to sediment synthetic-based fluid (SBF) concentrations.....	510
15.19 Microbial adenosine triphosphate (ATP) concentrations at Garden Banks 602 and Mississippi Canyon 292 on Cruise 2B (post-drilling) in relation to sediment synthetic-based fluid (SBF) concentrations.....	511

## List of Figures

(continued)

Figure		Page
15.20	Meiofaunal and macrofaunal densities in relation to proximity to drilling.....	513
15.21	Annelid (predominantly polychaete) densities vs. synthetic-based fluid (SBF) concentrations on post-drilling cruises.....	514
15.22	Gastropod densities vs. sediment barium, synthetic-based fluid (SBF), and total organic carbon concentrations at near-field (NF), post-drilling stations .....	515
15.23	Amphipod densities vs. sediment barium concentrations on post-drilling cruises.....	517
15.24	Macrofaunal community characteristics for the detailed, 24-station analysis.....	518
15.25	Fish abundance along camera sled transects at each site .....	519
15.26	Ophiuroid abundance along camera sled transects at each site.....	520
15.27	Geophysically mapped areal extent of drilling discharge deposits in relation to (a) number of wells drilled and (b) estimated synthetic-based mud (SBM) cuttings discharges .....	524
15.28	Areal extent of cuttings deposits (number of near-field stations with very high barium or synthetic-based fluid [SBF] concentrations) in relation to estimated synthetic-based mud (SBM) and water-based mud (WBM) cuttings discharges.....	525
15.29	Relationship between post-drilling sediment barium and synthetic-based fluid (SBF) concentrations within near-field sites and estimated volumes of SBF cuttings discharges.....	527
15.30	Difference between mean near-field and far-field sediment oxygen levels in relation to sediment synthetic-based fluid (SBF) concentrations and estimated SBF cuttings discharges.....	528
15.31	Plots of (a) geometric mean synthetic-based fluid (SBF) concentration and (b) geophysically mapped areal extent of drilling discharge deposits in relation to estimated synthetic-based mud (SBM) cuttings discharges.....	529
16.1	Facilities from which offshore wells are drilled change with water depth.....	537

**List of Figures**  
(continued)

<b>Figure</b>		<b>Page</b>
16.2	Dispersion and fates of drilling muds and cuttings following discharge to the ocean.....	547
16.3	Total meiofaunal densities in near-field (NF) and far-field (FF) sediments from the four study sites.....	570
16.4	Total macroinfaunal densities in near-field (NF) and far-field (FF) sediments from the four study sites.....	570

## List of Tables

Table	Page
2.1	Coordinates of near-field and far-field sites ..... 6
2.2	Sampling cruises..... 8
2.3	Numbers of samples collected and transects completed during chemical/biological cruises..... 25
2.4	Numbers of animals collected from baited trap sets during Cruise 2B ..... 25
3.1	Wells drilled within 10 km of the Viosca Knoll (VK) Block 916 near-field (NF) site..... 32
3.2	Discharge summary for Viosca Knoll Block 916 Well No. 1 (27 November to 18 December 2001) ..... 34
3.3	Wells drilled within 10 km of the Garden Banks (GB) Block 516 near-field (NF) site..... 35
3.4	Discharge summary for Garden Banks Block 516 wells within the near-field site ..... 37
3.5	Wells drilled within 10 km of the Garden Banks (GB) Block 602 near-field (NF) site center ..... 39
3.6	Discharge summary for Garden Banks Block 602 wells within the near-field site ..... 41
3.7	Wells drilled within 10 km of the Mississippi Canyon (MC) Block 292 near-field (NF) site..... 42
3.8	Discharge summary for Mississippi Canyon Block 292 wells within the near-field site ..... 45
3.9	Drilling summary for wells within each near-field site ..... 48
3.10	Previous wells near far-field (FF) sites..... 49
4.1	Geophysical surveys..... 60
5.1	Summary of baseline grain size characteristics for sites based on far-field data..... 96
5.2	Analysis of variance (ANOVA) results for sediment grain size ..... 96
5.3	Sediment grain size results for Viosca Knoll Block 916..... 98

## List of Tables

(continued)

Table		Page
5.4	Sediment grain size results for Garden Banks Block 516 .....	106
5.5	Sediment grain size results for Garden Banks Block 602 .....	114
5.6	Sediment grain size results for Mississippi Canyon Block 292 .....	122
6.1	Comparison between Cruise 1B and Cruise 2B sediment profile imaging (SPI) survey results for Garden Banks Block 516 near-field stations .....	201
6.2	Comparison between Cruise 1B (pre-drilling) and Cruise 3B (post-drilling) sediment profile imaging (SPI) survey results for Viosca Knoll Block 916 near-field stations .....	202
7.1	Phi scale sizes and sediment descriptors .....	224
8.1	Number of samples collected and analyzed for various parameters at each site .....	244
8.2	Summary of instrumental methods and method detection limits (MDLs) for metal analysis of sediment and organisms .....	249
8.3	Data quality objectives and criteria .....	249
8.4	Means $\pm$ standard deviations with ranges in parentheses for metals, and total organic carbon (TOC) for Viosca Knoll 916 for pre- and post-exploration cruises .....	253
8.5	Results of statistical comparisons (t-tests) for concentrations of metals among cruises (1B for pre-exploration and 3B for post-exploration) and zones for Viosca Knoll 916.....	254
8.6	Summary data for dissolved oxygen, redox potential (Eh), and pH for sediment from Viosca Knoll (VK) 916 at near-field (NF), far-field (FF), and discretionary (DS) stations during pre-exploration Cruise 1B and post-exploration Cruise 3B .....	260
8.7	Selected reactions showing the decomposition of organic matter by various oxidation agents (after Froelich et al. 1979) .....	265
8.8	Means $\pm$ standard deviations with ranges in parentheses for metals, and total organic carbon (TOC) for Garden Banks 516 for Cruises 1B and 2B.....	272



## List of Tables

(continued)

Table		Page
8.9	Results of statistical comparisons (t-tests) for concentrations of metals among cruises (1B and 2B) and zones (NF and FF) for Garden Banks 516 .....	274
8.10	Summary data for dissolved oxygen, redox potential (Eh), and pH for sediment from Garden Banks (GB) 516 at near-field (NF), far-field (FF), and discretionary (DS) stations during Cruises 1B and 2B .....	285
8.11	Means, standard deviations, and ranges for metals and total organic carbon (TOC) for Garden Banks (GB) 602 and Mississippi Canyon (MC) 292 during post-development Cruise 2B .....	292
8.12	Results of statistical comparisons (t-tests) for post-development Garden Banks (GB) 602 and Mississippi Canyon (MC) 292 during Cruise 2B.....	293
8.13	Summary data for dissolved oxygen, redox potential (Eh), and pH for sediment from Garden Banks (GB) 602 and Mississippi Canyon (MC) 292 at near-field (NF), far-field (FF), and discretionary (DS) stations during post-development Cruise 2B .....	301
8.14	Means $\pm$ standard deviations for samples of the giant amphipod <i>Bathynomus giganteus</i> from far-field (FF) and near-field (NF) stations from post-development sites Garden Banks (GB) 602 and Mississippi Canyon (MC) 292 .....	311
8.15	Means $\pm$ standard deviations for samples of the red crab <i>Chaceon quinquegens</i> from far-field (FF) and near-field (NF) stations from post-development sites Garden Banks (GB) 602 and Mississippi Canyon (MC) 292 .....	311
9.1	Sediment synthetic based fluid (SBF) and total polycyclic aromatic hydrocarbon (PAH) concentrations at Viosca Knoll Block 916.....	331
9.2	Synthetic based fluid (SBF) and total polycyclic aromatic hydrocarbon (PAH) sediment concentrations in the Viosca Knoll Block 916 discretionary box core samples from Cruise 3B (August 2002).....	332
9.3	Sediment synthetic based fluid (SBF) and total polycyclic aromatic hydrocarbon (PAH) concentrations at Garden Banks Block 516 .....	334
9.4	Synthetic based fluid (SBF) and total polycyclic aromatic hydrocarbon (PAH) sediment concentrations in the Garden Banks Block 516 discretionary box core samples from Cruise 2B (July 2001).....	335

## List of Tables

(continued)

Table		Page
9.5	Sediment synthetic based fluid (SBF) and total polycyclic aromatic hydrocarbon (PAH) concentrations at Garden Banks Block 602 on Cruise 2B (July 2001).....	337
9.6	Synthetic based fluid (SBF) and total polycyclic aromatic hydrocarbon (PAH) sediment concentrations in the Garden Banks Block 602 discretionary box core samples from Cruise 2B (July 2001).....	338
9.7	Sediment synthetic based fluid (SBF) and total polycyclic aromatic hydrocarbon (PAH) concentrations at Mississippi Canyon Block 292 on Cruise 2B (July 2001).....	340
9.8	Synthetic based fluid (SBF) and total polycyclic aromatic hydrocarbon (PAH) sediment concentrations in the Mississippi Canyon Block 292 discretionary box core samples from Cruise 2B (July 2001).....	341
9.9	Summary of polycyclic aromatic hydrocarbons (PAH) in tissue samples from Garden Banks Block 602 (GB 602) and Mississippi Canyon Block 292 (MC 292).....	343
10.1	Numbers of microbial subsamples collected from box cores.....	347
10.2	Sediment adenosine triphosphate (ATP) concentrations (ng g <sup>-1</sup> dry wt) for all near-field and far-field sites .....	352
11.1	Meiofaunal community statistics for Viosca Knoll Block 916 .....	364
11.2	ANOVA results for meiofaunal groups.....	367
11.3	Meiofaunal community statistics for Garden Banks Block 516.....	368
11.4	Meiofaunal community statistics for Garden Banks Block 602, Cruise 2B (July 2001).....	371
11.5	Meiofaunal community statistics for Mississippi Canyon Block 292, Cruise 2B (July 2001).....	374
11.6	Rank correlation coefficients (Spearman's rho) between meiofaunal densities and environmental variables within areas exposed to drilling discharges (near-field sites on post-drilling cruises) .....	377
11.7	Additional meiofaunal analyses from Cruise 2B: nematode trophic groups and harpacticoid copepod reproductive condition .....	377
11.8	Macroinfaunal community statistics for Viosca Knoll Block 916 .....	381

## List of Tables

(continued)

Table	Page
11.9 ANOVA results for macroinfaunal groups.....	384
11.10 Macroinfaunal community statistics for Garden Banks Block 516.....	386
11.11 Macroinfaunal community statistics for Garden Banks Block 602, Cruise 2B (July 2001).....	389
11.12 Macroinfaunal community statistics for Mississippi Canyon Block 292, Cruise 2B (July 2001).....	391
11.13 Rank correlation coefficients (Spearman's rho) between macroinfaunal densities and environmental variables within areas exposed to drilling discharges (near-field sites on post-drilling cruises) .....	395
11.14 Samples included in the 24-station analysis of macroinfauna.....	402
11.15 Ten most abundant macroinfaunal taxa for the 24-station analysis .....	403
11.16 Macroinfauna community statistics for the 24-station analysis .....	403
11.17 Station groups (A through D) resolved by multi-dimensional scaling (MDS).....	407
11.18 Average abundance of infaunal species accounting for at least 50% of the within-group similarity in station (sample) groups A through D.....	409
12.1 Results of photographic faunal survey .....	435
12.2 Results of comparisons between near-field and far-field tows.....	438
13.1 Number of <i>Bathycleptopsyllus</i> sp. collected from box cores at the near-field sites of Garden Banks (GB) Block 602 and Mississippi Canyon (MC) Block 292.....	447
13.2 Distribution of <i>Bathycleptopsyllus</i> sp. haplotypes at each sampled location in Garden Banks Block 602 and Mississippi Canyon Block 292.....	449
13.3 Analysis of molecular variance across the populations from the Garden Banks 602 and Mississippi Canyon 292 sites.....	449
14.1 Characteristics of the two development drilling sites from which sediments for solid phase toxicity testing were collected.....	459
14.2 Toxicity test conditions .....	461

## List of Tables

(continued)

Table	Page
14.3	Stocking density for test chambers found at test completion to have more than 20 amphipods..... 462
14.4	Amphipod survival in the toxicity tests with sediments from Mississippi Canyon Block 292, performed 7 to 17 August 2001 ..... 462
14.5	Amphipod survival in the toxicity tests with sediments from Garden Banks Block 602, performed 20 to 30 August 2001..... 464
15.1	Comparison of baseline environmental characteristics based on data from far-field sites..... 472
15.2	Drilling summary for wells within each near-field site..... 475
15.3	Impact summary..... 477
15.4	Geophysically estimated areal extent of drilling mud and cuttings deposits at each near-field site ..... 480
15.5	Confidence intervals for far-field barium and synthetic-based fluid (SBF) concentrations..... 491
15.6	Organism-sediment index (OSI) and successional stage for Viosca Knoll 916 (VK 916) and Garden Banks 516 (GB 516)..... 506
15.7	Presence of microbial mats as recorded in sediment profile images..... 509
15.8	Comparison of sites with respect to areal extent of mud and cuttings deposits..... 522
15.9	Comparison of near-field sites with respect to impact severity ..... 523
15.10	Timing of drilling vs. cruise dates..... 526
15.11	Impacts observed at various time intervals after drilling, including wells in blocks adjacent to the study sites..... 530
16.1	Summary of drilling activities within 500 m of the four drillsites before and during this study ..... 538
16.2	Names and chemical structures of synthetic chemicals used most frequently in the Gulf of Mexico for SBM (From Neff et al., 2000) ..... 543
16.3	Concentration ranges of several metals in water based muds (WBM) from different sources and in typical soils and marine sediments ..... 544

## List of Tables

(continued)

Table	Page
16.4	Concentrations of synthetic based fluid (SBF) chemical in near-field, far-field, and discretionary box core sediments from the four sites monitored in this investigation..... 552
16.5	Concentrations of hydrocarbons in composite samples of water based mud (WBM) and drill cuttings (in parentheses) from three drilling depths in a well in the Point Arguello Field, California..... 553
16.6	Concentrations of total polycyclic aromatic hydrocarbons (PAH) in near-field, far-field, and discretionary box core sediments from the four sites..... 554
16.7	Mean ( $\pm$ standard deviation) and range of concentrations of total organic carbon in sediments from the four study sites..... 555
16.8	Mean ( $\pm$ standard deviation) and range of concentrations of barium in sediments from the four study sites..... 556
16.9	Mean ( $\pm$ standard deviation) and range of concentrations of mercury in sediments from the four study sites..... 557
16.10	Mean ( $\pm$ standard deviation) and range of concentrations of lead in sediments from the four study sites..... 558
16.11	Mean ( $\pm$ standard deviation) and range of concentrations of zinc in sediments from the four study sites..... 559
16.12	Concentrations of total polycyclic aromatic hydrocarbons (PAH) ( $\mu\text{g/g}$ dry wt) in whole soft tissues of giant isopods <i>Bathynomus giganteus</i> and red crabs <i>Chaceon quinquedens</i> collected in July 2001 from MC 292 and GB 602 ..... 560
16.13	Mean ( $\pm$ standard deviation) concentrations of 11 metals in whole soft tissues of giant isopods <i>Bathynomus giganteus</i> and red crabs <i>Chaceon quinquedens</i> collected in July 2001 from MC 292 and GB 602 ..... 561
16.14	Summary of evidence of physical disturbance to or chemical exposure of the near-field benthic environment at the four study sites ..... 562
16.15	Survival of amphipods <i>Leptocheirus plumulosus</i> in 10-day sediment toxicity tests with 12 replicate sediment samples each from near-field and far-field stations at MC 292 and GB 602 ..... 564

## List of Tables

(continued)

<b>Table</b>		<b>Page</b>
16.16	Ranges of redox potential discontinuity (RPD) depths and Eh at 1 cm in sediments from near-field (NF), discretionary (DS), and far-field (FF) zones at the four study sites .....	567
16.17	Sediment adenosine triphosphate (ATP) concentrations (ng/g dry wt) in surface sediments collected at 12 near-field and 6 far-field stations at the four study sites .....	568
16.18	Benthic macrofaunal community parameters for near-field (NF) and far-field (FF) sediments at the four study sites .....	571
16.19	Summary of evidence of biological injury to the near-field benthic environment at the four study sites .....	574

## List of Acronyms and Abbreviations

AAS	atomic absorption spectrometry	GC-FID	gas chromatography-flame ionization detection
ACL	Acoustic Command Link	GFAAS	graphite furnace atomic absorption spectrometry
ADL	Acoustic Data Link	GIS	geographic information system
Al	aluminum	GOOMEX	Gulf of Mexico Offshore Operations Monitoring Experiment
AMOVA	analysis of molecular variance	H <sub>2</sub> O <sub>2</sub>	hydrogen peroxide
ANOVA	analysis of variance	HCl	hydrochloric acid
AODC	acridine orange direct count	Hg	mercury
API	American Petroleum Institute	HiPAP	High Precision Acoustic Positioning
As	arsenic	HSD	Honest Significant Difference
ASTM	American Society for Testing and Materials	IAPSO	International Association for the Physical Sciences of the Ocean
ATP	adenosine triphosphate	IC	ion chromatography
AUV	autonomous underwater vehicle	ICP-MS	inductively coupled plasma – mass spectrometry
Ba	barium	ID	internal diameter
BaSO <sub>4</sub>	barite (barium sulfate)	IO	internal olefin
bbf	barrel	IS	internal standard
Bp	base pair	kHz	kilohertz
Cd	cadmium	LAO	linear-alpha-olefin
COX I	cytochrome c oxidase subunit I	LPIL	Lowest Practical Identification Level
Cr	chromium	MAFLA	Mississippi-Alabama-Florida
CRM	certified reference material	MC 292	Mississippi Canyon Block 292
Cu	copper	MDL	method detection limit
CVAAS	cold vapor atomic absorption spectrometry	MDS	multidimensional scaling
DGPS	differential global positioning system	MMS	Minerals Management Service
DIW	deionized water	Mn	manganese
DNA	deoxyribonucleic acid	mtDNA	mitochondrial deoxyribonucleic acid
DOC	dissolved organic carbon	NF	near-field
DS	discretionary station	NH <sub>4</sub> <sup>+</sup>	ammonium
EDTA	ethylenediaminetetraacetic acid	Ni	nickel
Eh	redox potential	NIST	National Institute of Standards and Technology
FAAS	flame atomic absorption spectrometry	NO <sub>3</sub> <sup>-</sup>	nitrate
Fe	iron	NOAA	National Oceanic and Atmospheric Administration
FF	far-field	NRC	National Research Council
FIT	Florida Institute of Technology	NTIS	National Technical Information Service
FOV	field of view		
GB 516	Garden Banks Block 516		
GB 602	Garden Banks Block 602		
GC/MS	gas chromatography-mass spectrometry		

## List of Acronyms and Abbreviations

(continued)

OSI	organism-sediment index
PAH	polycyclic aromatic hydrocarbon
PAO	poly-alpha-olefin
Pb	lead
PCR	polymerase chain reaction
PO <sub>4</sub> <sup>3-</sup>	phosphate
REMOTS	remote ecological monitoring of the seafloor
RGB	red, green, and blue
RPD	redox potential discontinuity
RRF	relative response factor
rRNA	ribosomal ribonucleic acid
RSD	relative standard deviation
SBF	synthetic-based fluid
SBM	synthetic-based mud
SD	standard deviation
SDS	sodium dodecyl sulfate
SIMPER	similarity percentage breakdown
SO <sub>4</sub> <sup>2-</sup>	sulfate
SOP	standard operating procedure
SPI	sediment profile imaging
ST	sidetrack
TOC	total organic carbon
UCM	unresolved complex mixture
USEPA	United States Environmental Protection Agency
V	vanadium
VK 916	Viosca Knoll Block 916
WBM	water-based mud
Zn	zinc



# Chapter 1 Introduction

*Neal W. Phillips and Alan D. Hart  
Continental Shelf Associates, Inc.*

This is the final report of a field study to assess the impacts of oil and gas exploration and development at four sites on the Gulf of Mexico continental slope (**Figure 1.1**). The study was conducted for the Minerals Management Service (MMS) by a team of scientists under the management of Continental Shelf Associates, Inc. Key participants are listed in the Acknowledgments, and authors/principal investigators are listed at the head of each chapter.

## 1.1 BACKGROUND

The deepwater Gulf of Mexico (water depths greater than or equal to 305 m) has seen a remarkable increase in oil and gas exploration, development, and production in recent years (Cranswick and Regg 1997; Baud et al. 2000; Richardson et al. 2004; French et al. 2005). Favorable economics, the development of innovative technologies, the announcement of large deepwater discoveries, the passage of the Deep Water Royalty Relief Act, and the opportunity to lease new prospects have all contributed to the revitalization of exploration and development in the Gulf of Mexico (Ward 2000; Richardson et al. 2004). As of March 2005, more than 900 exploration wells had been drilled in the deepwater Gulf, at least 115 deepwater discoveries had been announced, and there were 107 deepwater production projects (French et al. 2005). The number of wells drilled in the deepwater Gulf has increased dramatically in the past decade, with much of the activity in water depths of 450 to 1,500 m (**Figure 1.2**).



**Figure 1.1.** Study sites.

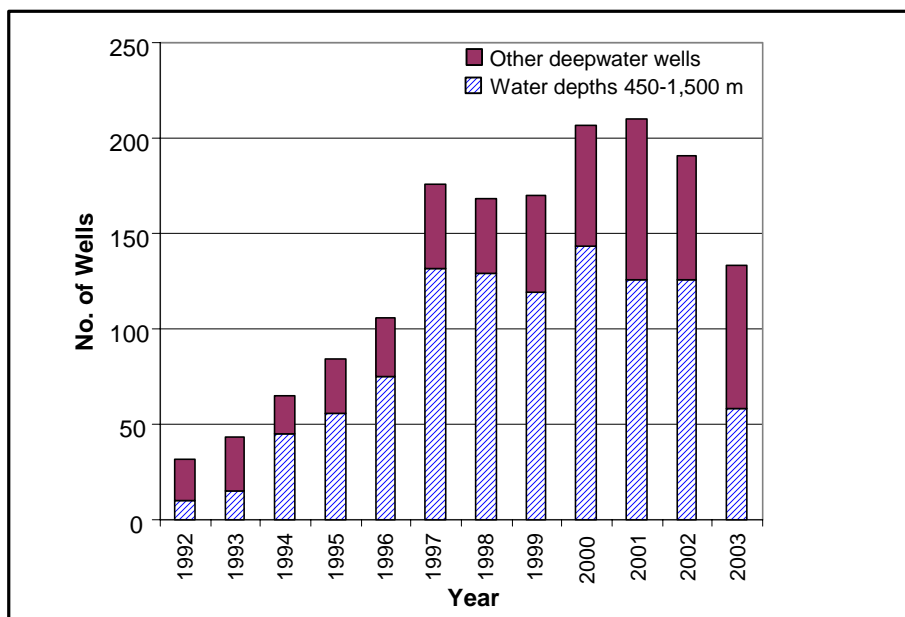


**Figure 1.2.** Number of wells drilled in the deepwater Gulf of Mexico over the past decade (From: Richardson et al. 2004).

Deepwater operations are significantly different from conventional operations on the continental shelf, which have been studied for decades. They are farther from shore, encounter different environmental conditions, are technologically more sophisticated, and may involve much higher production rates. These differences present many technical and regulatory challenges (MMS 2000a, 2004a). MMS has responded by conducting environmental workshops (Carney 1998; MMS 2003), preparing environmental impact assessments (MMS 2000a,b), sponsoring scientific literature reviews (Continental Shelf Associates, Inc. 2000; Gallaway et al. 2001; Nowlin et al. 2001), initiating new field studies of deepwater benthic communities (MacDonald 2002; Rowe and Kennicutt 2002), and requiring additional environmental information from deepwater operators (MMS 2004b).

This study addresses one aspect of deepwater operations: the impacts of drilling activities on the benthic environment around wellsites. Studies on the continental shelf have documented impacts of water-based drilling fluids and cuttings on benthic organisms near wellsites (National Research Council 1983; Neff 1987; Neff et al. 1989a; Hinwood et al. 1994; Hyland et al. 1994). However, because of the environmental and technological differences, the applicability of this knowledge to deepwater benthic communities is unknown (Carney 1998, 2001). For example, the increased use of synthetic-based drilling muds (SBMs) may result in volumes and characteristics of discharged material quite different from those used for decades in shallower water (Neff et al. 2000; Boehm et al. 2001). However, other than opportunistic studies (Gallaway et al. 1997), there have been few field measurements and observations around deepwater drillsites in the Gulf of Mexico. One other benthic study that included some deepwater sites (the Gulf of Mexico Comprehensive Synthetic Based Muds Monitoring Program) was conducted by a consortium of offshore operators, mud companies, chemical companies, the MMS, and the Department of Energy (Continental Shelf Associates, Inc. 2004).

## 1.2 STUDY OBJECTIVES

The objectives of this study were to assess the physical, chemical, and biological impacts of oil and gas development at selected exploration and development wellsites on the Gulf of Mexico continental slope. The findings from this study will assist the MMS in conducting environmental analyses, as well as in developing mitigative measures and regulations specifically tailored to deepwater operations.

Specific objectives were to document (1) drilling mud and cuttings accumulations; (2) physical modification/disturbance of the seabed due to anchors and their mooring systems; (3) debris accumulations; (4) physical/chemical modification of sediments; and (5) effects on benthic organisms.

## 1.3 REPORT ORGANIZATION

Study design and general sampling methodology are discussed in *Chapter 2*. This includes site selection, statistical design, cruise scheduling, sampling patterns at each site, and general methodology for collecting samples and data. The drilling history of each study site is discussed in *Chapter 3*. Subsequent chapters describe the methods and results for each individual discipline:

- *Chapter 4* – Geophysical Characterization
- *Chapter 5* – Sediment Grain Size
- *Chapters 6 and 7* – Sediment Profile Imaging
- *Chapter 8* – Metals, Total Organic Carbon, and Redox Conditions
- *Chapter 9* – Sediment and Tissue Hydrocarbons
- *Chapter 10* – Sediment Microbes
- *Chapter 11* – Meiofauna and Macroinfauna
- *Chapter 12* – Megafauna and Image Analysis
- *Chapter 13* – Genetic Diversity of Harpacticoid Copepods
- *Chapter 14* – Sediment Toxicity

The report culminates in a Synthesis (*Chapter 15*) and an Ecological Risk Assessment (*Chapter 16*). Additional supporting data are presented in the Appendices.

## Chapter 2 Study Design and General Methods

*Neal W. Phillips and Alan D. Hart  
Continental Shelf Associates, Inc.*

This chapter describes site selection, sampling design and general methodology, cruise scheduling, and numbers and locations of samples collected at each site. Detailed methodology for individual tasks is discussed in subsequent chapters.

### 2.1 SITE SELECTION

Four study sites were selected (**Figure 1.1**). Coordinates are listed in **Table 2.1**. The sites were as follows:

- Viosca Knoll Block 916 (VK 916) was an exploration site sampled before and after drilling of a single exploration well.
- Garden Banks Block 516 (GB 516) was an exploration/development site that was sampled once after exploration drilling and again after several development wells were drilled.
- Garden Banks Block 602 (GB 602) and Mississippi Canyon Block 292 (MC 292) were post-development sites sampled once after several exploration and development wells had been drilled.

#### Program Overview

- Four “near-field” study sites
- Six “far-field” (reference) areas for each site (10 to 25 km away)
- Water depths about 1,000 to 1,150 m
- VK 916 exploration site sampled before and after drilling of a single exploration well
- GB 516 exploration/development site sampled after exploration drilling and again after several development wells were drilled
- GB 602 and MC 292 post-development sites sampled once after drilling of several exploration and development wells
- Six cruises (three geophysical, three chemical/biological)
- Geophysical mapping included bathymetry, side-scan sonar, and subbottom profiling
- Chemical/biological surveys included box coring, sediment profile imaging, seafloor photographs, and baited traps (for tissue samples)

Site selection was based on MMS requirements and operators’ drilling schedules rather than any attempt to select geographically or bathymetrically representative sites. The MMS requested that two exploration sites and three post-development sites be selected on the northern Gulf of Mexico continental slope (the number of post-development sites was ultimately reduced to two). The general requirements were as follows:

- Sites should be located in water depths greater than 1,000 m.
- Sites should be located at a similar water depth and be biologically and geologically similar.
- At least one exploration site and one post-development site must be located as far east as possible in the Central Planning Area (e.g., near DeSoto Canyon). Ideally, the other sites should be selected to represent the central Gulf and western Gulf.
- Sites drilled with an anchored drilling unit were preferred so that physical effects of anchoring could be studied.

For exploration sites, it was preferred that no previous drilling had occurred in the block. For post-development sites, all drilling activities were to have been completed prior to the first cruise.

**Table 2.1.** Coordinates of near-field and far-field sites. Each site is defined as a circle (see text); center coordinates are listed.

Site	Water Depth (m)	X/Y Coordinates <sup>a</sup>		Latitude/Longitude	
		X (ft)	Y (ft)	Latitude	Longitude
<b>Viosca Knoll Block 916</b>					
Near-Field	1,125	1,356,696.75	10,564,161.84	29° 06' 24.31"N	87° 53' 19.48"W
Far-Field 1	1,120	1,307,060.85	10,546,095.85	29° 03' 21.38"N	88° 02' 37.34"W
Far-Field 2	1,110	1,326,067.53	10,552,404.38	29° 04' 25.47"N	87° 59' 03.73"W
Far-Field 3	1,100	1,386,058.05	10,578,800.84	29° 08' 51.37"N	87° 47' 49.52"W
Far-Field 4	1,035	1,392,675.95	10,584,517.89	29° 09' 48.42"N	87° 46' 35.29"W
Far-Field 5	1,020	1,400,341.89	10,589,614.93	29° 10' 39.39"N	87° 45' 09.17"W
Far-Field 6	1,015	1,406,544.02	10,592,651.90	29° 11' 09.86"N	87° 43' 59.40"W
<b>Garden Banks Block 516</b>					
Near-Field	1,033	1,839,531.91	9,975,977.93	27° 29' 23.81"N	92° 23' 08.26"W
Far-Field 1	1,000	1,807,547.80	9,961,278.59	27° 26' 59.64"N	92° 29' 04.20"W
Far-Field 2	1,025	1,874,369.31	9,983,961.58	27° 30' 41.04"N	92° 16' 40.80"W
Far-Field 3	1,000	1,879,644.10	9,985,191.94	27° 30' 52.92"N	92° 15' 42.12"W
Far-Field 4	1,015	1,887,623.85	9,989,128.90	27° 31' 31.44"N	92° 14' 13.20"W
Far-Field 5	1,015	1,889,749.42	9,991,213.58	27° 31' 51.96"N	92° 13' 49.44"W
Far-Field 6	1,020	1,895,561.98	9,989,178.54	27° 31' 31.44"N	92° 12' 45.00"W
<b>Garden Banks Block 602</b>					
Near-Field	1,125	1,815,625.00	9,934,903.00	27° 22' 38.02"N	92° 27' 35.79"W
Far-Field 1	1,125	1,767,744.00	9,934,848.00	27° 22' 39.25"N	92° 36' 27.09"W
Far-Field 2	1,100	1,765,104.00	9,902,640.00	27° 17' 20.26"N	92° 36' 57.49"W
Far-Field 3	1,175	1,768,272.00	9,876,768.00	27° 13' 03.85"N	92° 36' 23.26"W
Far-Field 4	1,175	1,795,200.00	9,875,184.00	27° 12' 47.23"N	92° 31' 24.95"W
Far-Field 5	1,100	1,813,152.00	9,891,552.00	27° 15' 28.67"N	92° 28' 05.28"W
Far-Field 6	1,125	1,872,816.00	9,935,904.00	27° 22' 45.08"N	92° 17' 01.13"W
<b>Mississippi Canyon Block 292</b>					
Near-Field	1,034	1,129,042.00	10,419,990.00	28° 42' 13.08"N	88° 35' 44.19"W
Far-Field 1	1,120	1,062,336.00	10,421,136.00	28° 42' 15.01"N	88° 48' 13.39"W
Far-Field 2	1,030	1,067,088.00	10,430,640.00	28° 43' 49.81"N	88° 47' 21.64"W
Far-Field 3	1,025	1,107,216.00	10,459,152.00	28° 48' 37.85"N	88° 39' 55.42"W
Far-Field 4	1,050	1,107,744.00	10,450,704.00	28° 47' 14.29"N	88° 39' 48.16"W
Far-Field 5	1,025	1,139,424.00	10,455,984.00	28° 48' 10.82"N	88° 33' 52.92"W
Far-Field 6	1,035	1,143,648.00	10,459,680.00	28° 48' 47.96"N	88° 33' 05.98"W

<sup>a</sup> X/Y coordinates are for Universal Transverse Mercator, North American Datum 1927, Zone 15 (Garden Banks Block 516 and Garden Banks Block 602) and Zone 16 (Mississippi Canyon Block 292 and Viosca Knoll Block 916).

**Exploration Sites.** To select potential exploration sites, the team worked with the MMS and operators to identify Exploration Plans for wells in water depths of 1,000 to 1,500 m with a projected starting date in the fourth quarter of 2000. This range of water depths was selected because anchoring impacts were of interest and anchored rigs are infrequently used in deeper water. It also was assumed that the geology and biology of sites within this depth range in the Central and Western Planning Areas would be generally similar. This process ultimately resulted in the selection of VK 916, which fulfills the requirement for a site near the eastern edge of the Central Planning Area. No previous wells had been drilled in VK 916.

Although a second exploration site with no previous drilling was sought, none was available where an operator was planning to drill within the time frame for the pre- and post-drilling cruises. Therefore, GB 516 in the Western Planning Area was selected as the best available site, even though previous exploration wells had been drilled in the block. This was essentially an exploration/development site that was sampled after exploration drilling and again after additional development wells were drilled during this study. See *Chapter 3* for further discussion of previous drilling.

**Post-Development Sites.** To select potential post-development sites, the team worked with the MMS and operators to identify development/production sites in water depths greater than 1,000 m where drilling (with an anchored drilling rig) would be completed by September 2000. Five potential sites met these requirements:

- Garden Banks Block 602
- Mississippi Canyon Block 292
- Mississippi Canyon Block 934
- Mississippi Canyon Block 687
- East Breaks Block 945

The first three sites were selected due to their similar water depths (approximately 1,000 to 1,150 m). Mississippi Canyon Block 934 was ultimately dropped from the program for budgetary reasons before any surveys were conducted there. The final post-development sites were GB 602 and MC 292. The former is in the Western Planning Area, and the latter fulfills the requirement for a site near the eastern edge of the Central Planning Area.

## **2.2 FAR-FIELD SITES (REFERENCE AREAS)**

For chemical/biological sampling, each study site was defined as a circle 500 m in radius around the drilling location (rationale is discussed later in this chapter). Six circular far-field sites (or “reference areas”) also were designated for each site. These were chosen to be at about the same depth as the near-field site and 10 to 25 km away. Each far-field site was a circle 204 m in radius, such that the total area of six far-field sites combined was equal to that of the near-field site, and the number of samples was allocated so that the sampling intensity was the same.

Far-field sites were located using bathymetric maps provided by the MMS showing locations of previous wells in the vicinity of each near-field site. These maps were used to plot numerous potential far-field sites that met the criteria (distance of 10 to 25 km from the corresponding near-field site and similar water depths). From these possibilities, six far-field sites were randomly chosen for each site. Although previous wellsites were avoided to the extent practicable, most far-field sites had at least one previous well drilled within 10 km (see *Chapter 3*). **Table 2.1** lists the latitude/longitude coordinates and water depths of far-field sites. Locations are shown on **Figures 2.1** through **2.4**.

## 2.3 SAMPLING CRUISES

**Figure 2.5** shows the program schedule, including the timing of the six cruises (**Table 2.2**) and drilling activities that occurred at GB 516 and VK 916 during this study. Previous drilling at the two post-development sites (GB 602 and MC 292) as well as at GB 516 occurred at various times before this study began, as discussed under drilling history in *Chapter 3*.

**Table 2.2.** Sampling cruises.

Site	Cruise					
	1A	1B	2A	2B	3A	3B
<i>Cruise Type:</i>	<i>Geophysical</i>	<i>Chem/Biol</i>	<i>Geophysical</i>	<i>Chem/Biol</i>	<i>Geophysical</i>	<i>Chem/Biol</i>
<i>Cruise Start:</i>	<i>11/10/2000</i>	<i>10/23/2000</i>	<i>6/24/2001</i>	<i>7/8/2001</i>	<i>8/7/2002</i>	<i>8/4/2002</i>
<i>Cruise End:</i>	<i>1/1/2001</i>	<i>11/17/2000</i>	<i>7/7/2001</i>	<i>7/25/2001</i>	<i>8/12/2002</i>	<i>8/14/2002</i>
VK 916	pre-drilling	pre-drilling	--	--	post-drilling	post-drilling
GB 516	--	post-drilling <sup>a</sup>	post-drilling	post-drilling	--	--
GB 602	--	--	post-drilling	post-drilling	--	--
MC 292	--	--	post-drilling	post-drilling	--	--

<sup>a</sup> Cruise 1B at GB 516 preceded drilling of several development wells; however, exploration wells had been drilled previously (see *Chapter 3*).

GB = Garden Banks; MC = Mississippi Canyon; VK = Viosca Knoll.

### 2.3.1 Geophysical Cruises

Cruise 1A was conducted using a high resolution deep-tow system aboard the R/V OCEAN SURVEYOR, a geophysical survey vessel. Cruises 2A and 3A were conducted aboard the M/V RIG SUPPORTER using the C&C Technologies autonomous underwater vehicle (AUV), the HUGIN 3000. A differential global positioning system (DGPS) was used for navigation on all cruises.

- Cruise 1A was conducted from 10 November 2000 to 1 January 2001. This cruise was originally intended to survey all of the sites. However, due to extended weather delays, as well as equipment, software, and vessel problems, VK 916 was the only site surveyed.

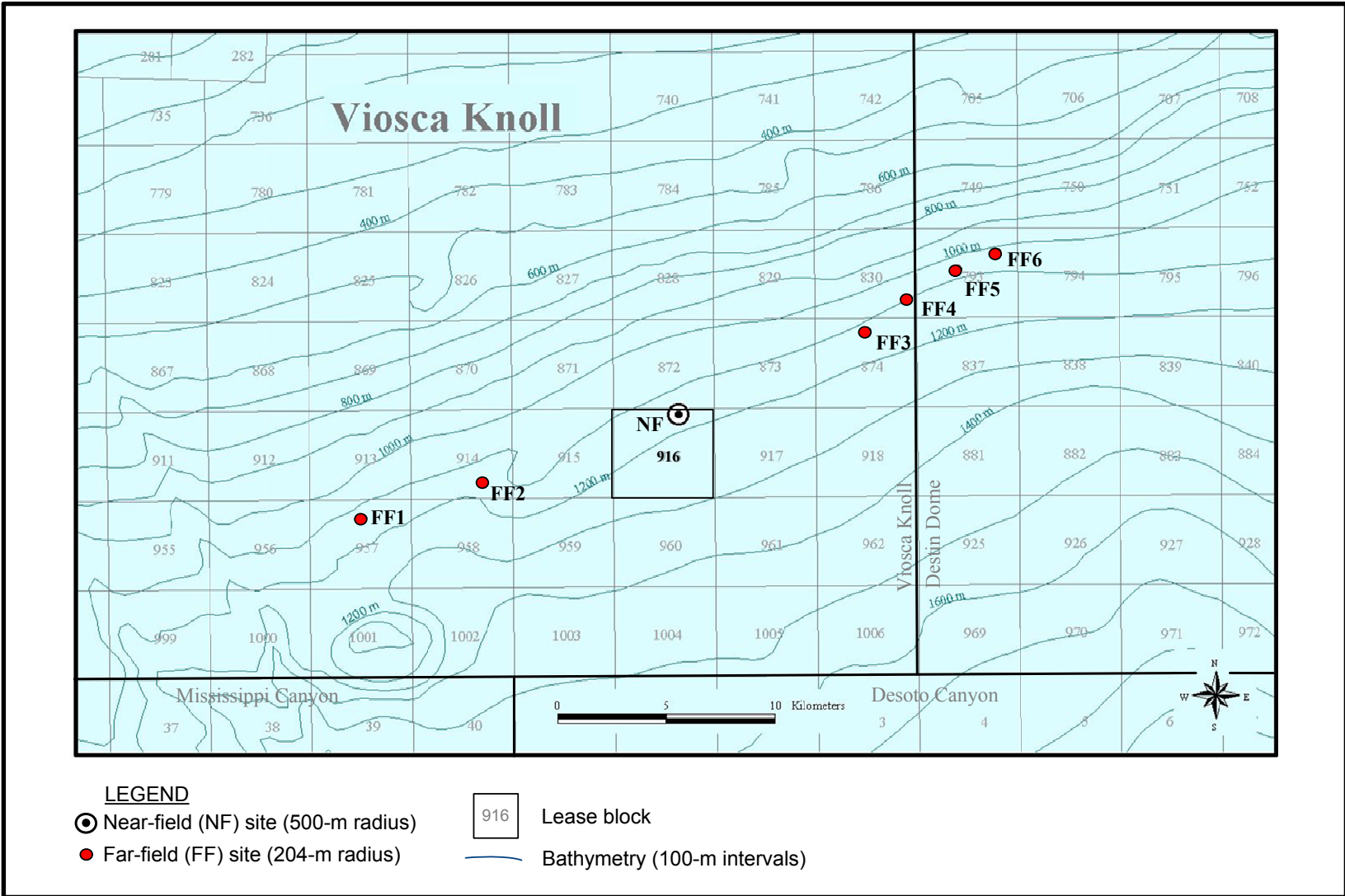
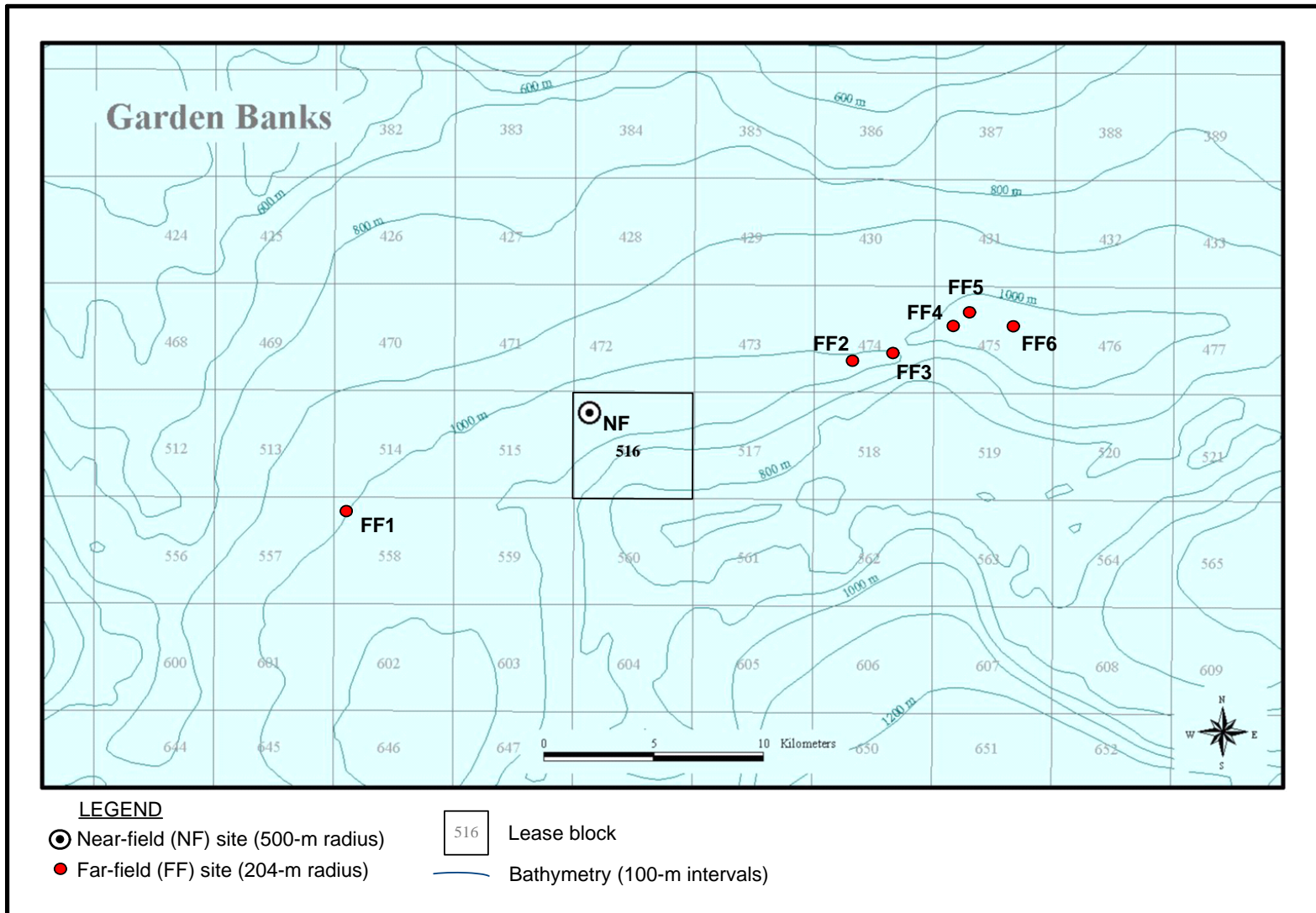
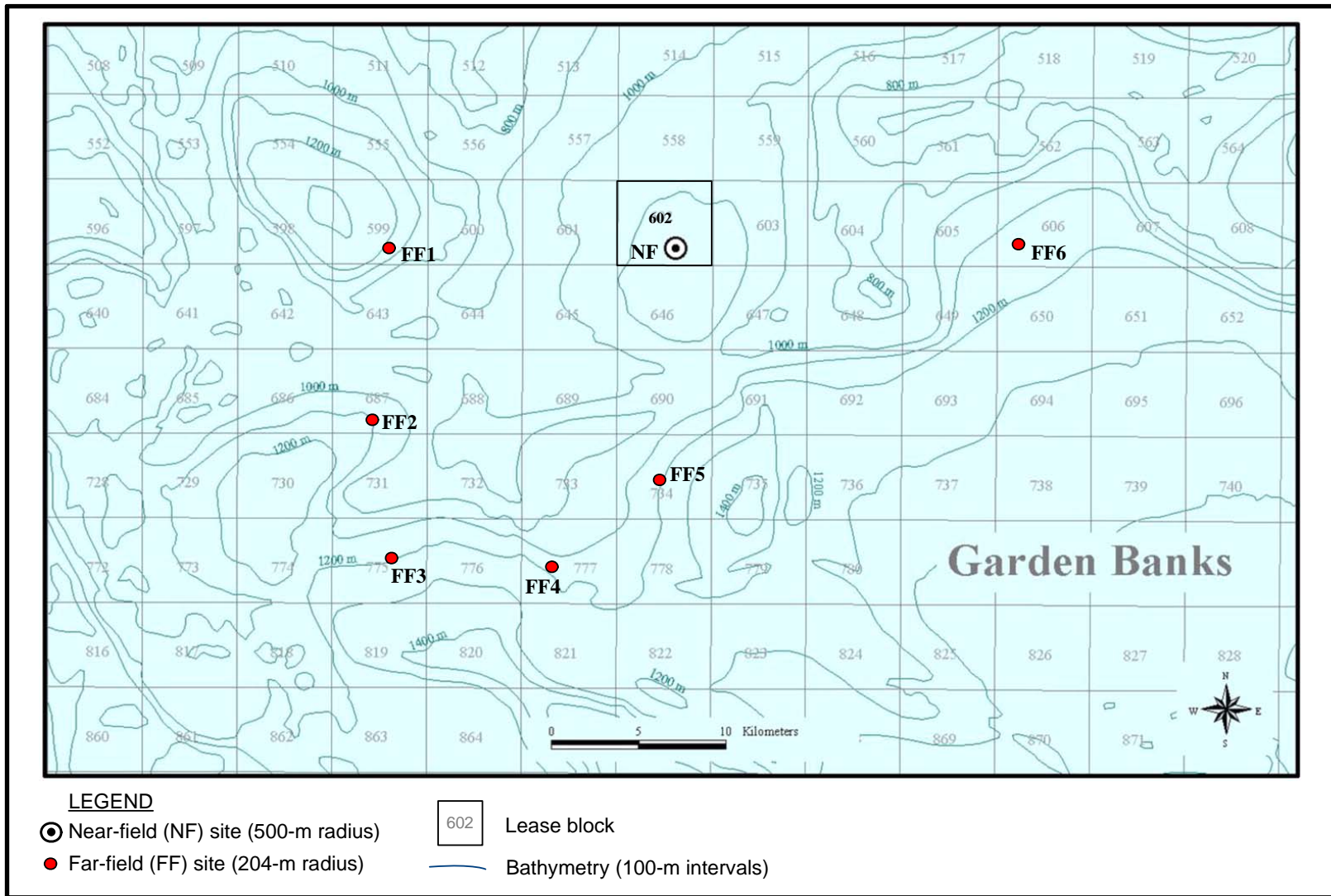


Figure 2.1. Location of near-field (NF) and far-field (FF) sites for Viosca Knoll Block 916.





**Figure 2.2.** Location of near-field (NF) and far-field (FF) sites for Garden Banks Block 516.



**Figure 2.3.** Location of near-field (NF) and far-field (FF) sites for Garden Banks Block 602.

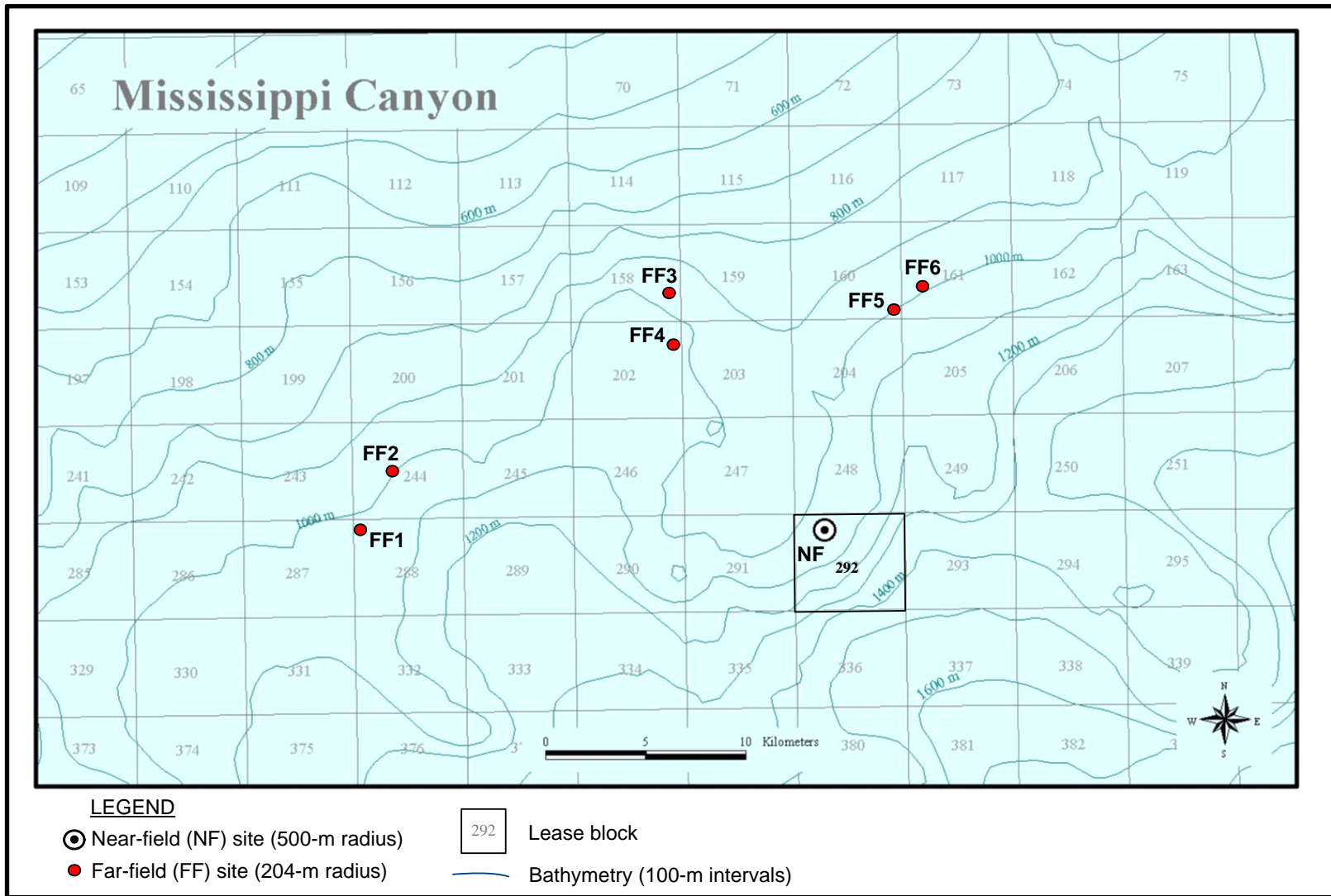


**Figure 2.4.** Location of near-field (NF) and far-field (FF) sites for Mississippi Canyon Block 292.

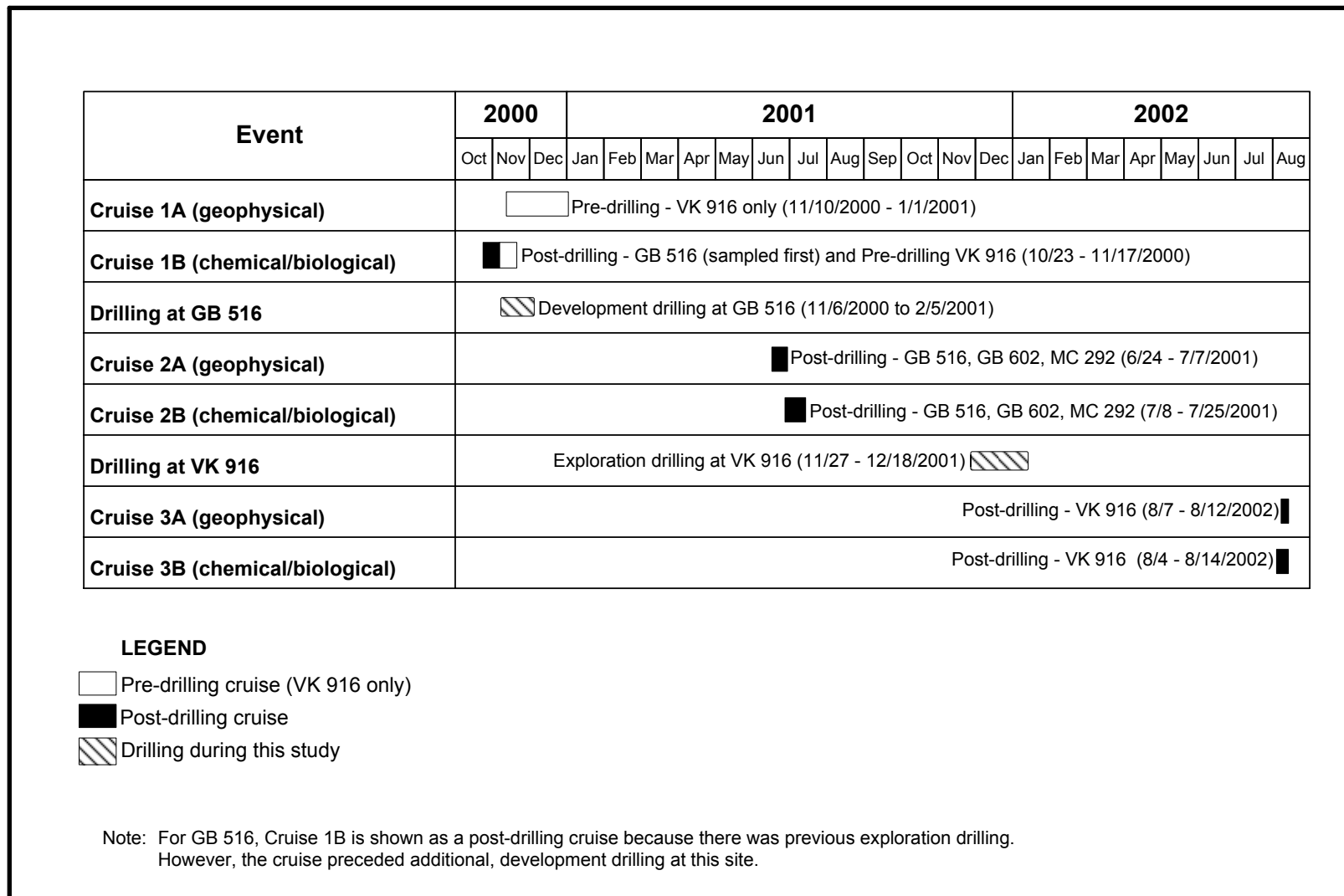


**Figure 2.5.** Schedule including sampling cruises and wells drilled during this study. Previous drilling at GB 516, GB 602, and MC 292 occurred at various times before this study, and dates are not shown (see *Chapter 3*).

- Cruise 2A was conducted from 24 June to 7 July 2001 using the same vessel and navigation. Surveys were conducted at both post-development sites (GB 602 and MC 292), and a post-drilling survey was conducted at GB 516 following the completion of development drilling there. Due to a delay in the drilling schedule at VK 916, the post-drilling cruise at that site was postponed.
- Cruise 3A was conducted from 7 to 12 August 2002. This was a post-drilling survey of the VK 916 site following the completion of exploration drilling there.

### 2.3.2 Chemical/Biological Cruises

Chemical/Biological Cruises 1B and 2B were conducted aboard the R/V GLORITA, which was mobilized out of Freeport, Texas. Cruise 3B was conducted aboard the R/V J.W. POWELL, which was mobilized out of Houma, Louisiana. Both ships were equipped with DGPS navigation.

- Cruise 1B was conducted from 23 October to 17 November 2000. During this cruise, samples and photographs were collected at both GB 516 and VK 916.
- Cruise 2B was conducted from 8 to 25 July 2001. During this survey, samples and photographs were collected at both post-development sites (GB 602 and MC 292) and at the GB 516 site after the completion of development drilling there. Due to a delay in the drilling schedule at VK 916, the post-drilling cruise at that site was postponed.
- Cruise 3B was conducted from 4 to 14 August 2002. This cruise was a post-drilling survey of the VK 916 site following the completion of exploration drilling there.

## 2.4 SAMPLING DESIGN

The VK 916 exploration site was sampled before and after drilling. Sampling at this site conforms to the “optimal impact study design” (Green 1979) in which pre-drilling baseline data are collected at near-field sites and corresponding reference areas. Hypotheses can be tested concerning both temporal (before and after) and spatial differences (near-field versus far-field). The experimental design supports using analysis of variance/covariance for statistical testing.

The two post-development sites, MC 292 and GB 602, were sampled only *after* drilling of several previous wells. Sampling at these sites was intended to provide a “snapshot” of impacts after the completion of development operations, similar to the Gulf of Mexico Offshore Operations Monitoring Experiment (GOOMEX) study (Kennicutt et al. 1996a). At these sites, impact must be inferred from spatial differences alone – i.e., comparisons with reference areas. Comparisons of the near-field area to the far-field areas can be used to directly examine potential impacts.

The situation at GB 516 presents the most difficulties for interpretation. Although surveys were conducted before and after development drilling, the site had already been exposed to previous exploration drilling. The two surveys at this site essentially provide two snapshots of drilling impacts – one after exploration drilling and the second after development drilling. As with the two post-development sites, impact can be inferred from spatial differences – i.e., comparisons with reference areas. In addition, temporal comparisons between surveys may provide some indication of development drilling impacts.

The two broad categories of data collection were geophysical characterization and chemical/biological sampling. The sampling design for each type is explained below.

#### **2.4.1 Geophysical Characterization**

Geophysical characterization was intended to determine (1) the areal extent and accumulation of muds and cuttings; (2) the physical modification or disturbance of the sea bed due to impacts from anchors and their mooring systems including chains or wire ropes; and (3) the accumulation of debris attributable to oil and gas development activity.

To address these objectives, bathymetric, side-scan sonar, and subbottom profile data were collected at each site. These data were used to construct broad-scale images of the seafloor, which were interpreted to map possible anchor scars and accumulations of cuttings and drilling fluids. An area approximately 3,000 m in radius was surveyed at each site, to encompass the anchor patterns for typical moored drilling units in this water depth. Further information on the areal coverage and detailed methods for the geophysical surveys are provided in *Chapter 4*.

The design of this part of the study allows a non-statistical evaluation of physical impacts through interpretation of spatial patterns within sites, as well as comparisons of before-and-after surveys at the exploration sites. Since far-field sites were not surveyed, there are no spatial comparisons with “unaffected” areas. Information from the operators, including wellsite and anchor locations and reports from previous geophysical surveys, aided in the interpretation.

#### **2.4.2 Chemical/Biological Sampling**

Chemical/biological sampling was intended to document (1) physical and chemical modification of sediments; and (2) effects on benthic organisms. Samples and data were collected with four types of equipment:

- Box core sampler (to obtain samples of sediment, microbiota, meiofauna, and macroinfauna)
- Sediment profile imaging (SPI) camera (to obtain cross-sectional images of the upper sediment column)
- Still camera on a towed/dragged sled (to obtain photographs of the seafloor and megafauna)
- Baited traps (to obtain animals for tissue analyses)

For chemical/biological sampling, each study site was defined as a circle 500 m in radius around the drilling location. The 500-m radius was chosen in order to sample intensively where SBM cuttings are most likely to accumulate at concentrations sufficient to produce biological effects. Because the distribution of SBM cuttings typically is patchy (Neff et al. 2000), a higher sampling density near the drillsite increases the chances of sampling where the cuttings are deposited. Preliminary calculations and discussions with industry representatives indicated that (1) concentrations of synthetic based fluids (SBFs) most likely would not be detectable beyond 500 m from the discharge point; and (2) SBF concentrations exceeding 1 ppm (an apparent threshold for biological effects; Neff et al. 2000) are most likely to occur within 300 m of the discharge point. Therefore, the project team and MMS agreed that a radius of 500 m would be used to define a near-field site, and that 8 of the 12 box cores at each site would be collected within 300 m of the wellsite.

**Figure 2.6** shows the idealized sampling pattern for chemical/biological sampling. Box cores were to be collected at 12 randomly selected locations within the 500-m radius at each study site (8 samples within 300 m and 4 samples between 300 and 500 m radii). Box cores also were to be collected at 12 far-field locations (two locations selected randomly within each of six far-field sites). Sediment profile photographs were to be collected along three drift transects in the near-field and along one transect at each of three far-field sites, with approximately 36 images per transect. Still photographs of the seafloor and megafauna were collected along three transects at each near-field site and along one transect at each of three far-field sites (approximately 375 photographs per transect). Baited traps were to be deployed at the two post-development sites to collect organisms for tissue analyses. For each site, eight traps were deployed in the near-field, and four traps were placed at each of two corresponding far-field sites. The actual number of samples and transects differed from the planned number in some cases, as summarized later in **Tables 2.3** and **2.4**. For example, during Cruise 3B, far-field SPI transects were attempted at VK 916 FF2 and FF4; however, due to problems with the camera, no usable data were collected. Also, one of the baited traps at MC 292 did not capture any animals because high current and inadequate weight on the ground line kept it off the bottom.

Box core locations were determined randomly within each site on each cruise. For this purpose, the 500-m circle was divided into quadrants to ensure that box cores were distributed in all directions around the site center. Precise placement of box cores is very difficult in this water depth, so a couple of samples at GB 516 that were pre-plotted just inside the 500-m radius actually fell outside it. In addition to the regular box core samples, subsurface sediment samples for chemistry analyses also were collected from three non-random “discretionary” stations within the near-field zone during Cruise 2B (GB 516, GB 602, and MC 292) and Cruise 3B (VK 916). The “discretionary” stations were chosen within areas identified from geophysical surveys as likely mud and cuttings deposits.

Camera sled and SPI transects were not randomized; the transects were conducted so as to drift across each site based on prevailing currents. The still camera was programmed to take photographs at regular intervals (every 5 seconds). The SPI system was repeatedly lowered to take as many profiles as possible during each transect (not explicitly random or regular intervals).

As discussed in *Chapter 3*, three of the sites (GB 516, GB 602, and MC 292) had well-related structures on the bottom including subsea wellheads, manifolds, flowlines, and umbilicals. Sampling locations were adjusted where necessary to avoid contacting these structures.

## **2.5 SAMPLING METHODOLOGY**

### **2.5.1 Box Cores**

Sediment samples were collected with a 0.25-m<sup>2</sup> Gray-O’Hara box core (**Figure 2.7**). Procedures for operation of this box core were patterned after Hessler and Jumars (1974) as modified by Blake et al. (1985, 1987) and Blake and Grassle (1994). The box was partitioned into subcores for various sample types (**Figure 2.8**). Subcores with a total surface area of 0.1 m<sup>2</sup> were taken for macrofauna; other subcores were obtained for meiofauna, microbiota, chemistry, and other parameters as required. Thus, both the chemical/sediment samples and the biology samples were taken from each deployment. A Sonardyne positioning system was used during the box coring. A transponder was attached to the side of the box corer, giving its position and height off the bottom. Precision was 0.2% of slant range, or about 2 m for box coring in this depth.

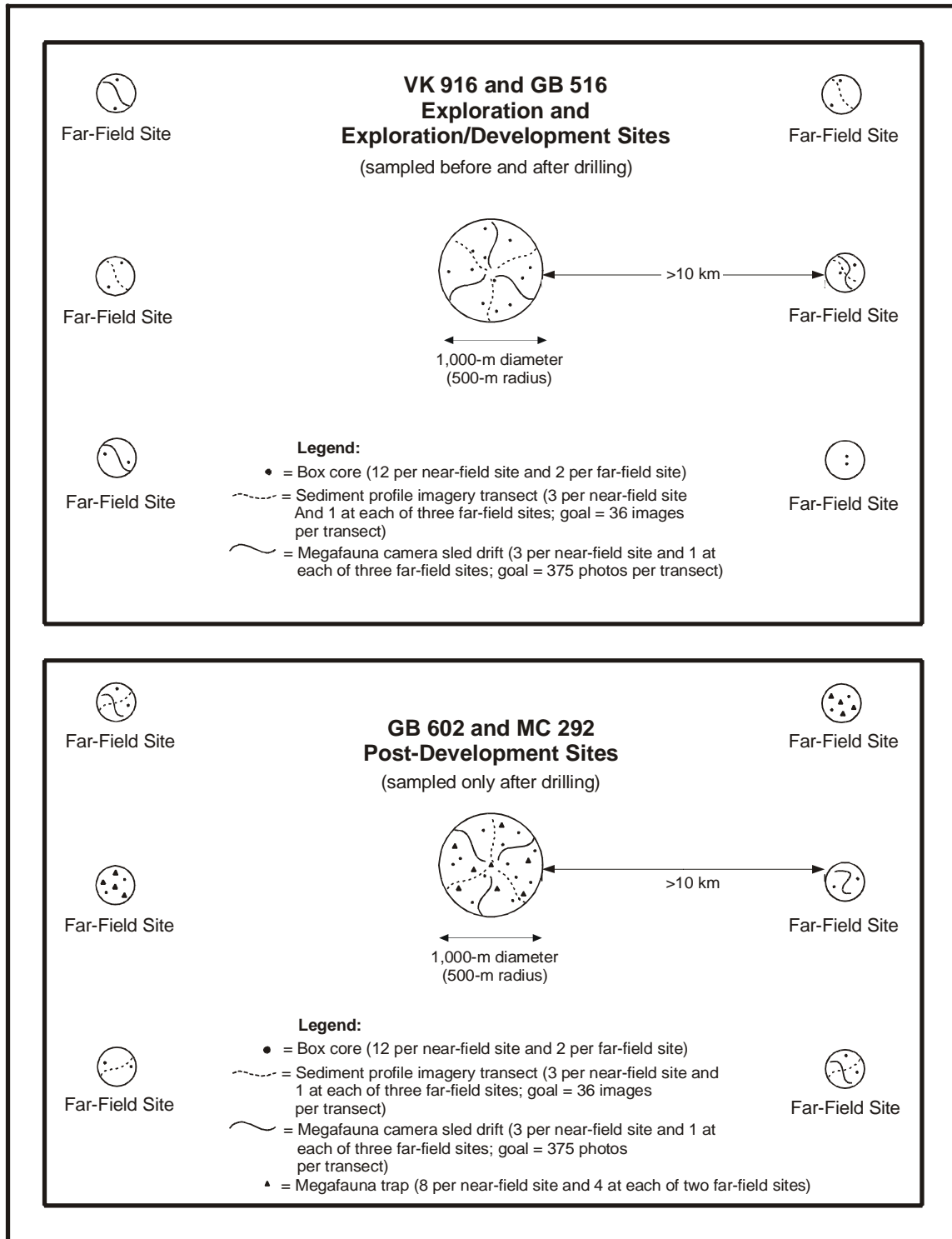


**Figure 2.6.** Idealized sampling plans for study sites.





**Figure 2.7.** Deployment of box core.

After retrieval of the box core, the entire surface of the sample was examined. Sediment color, evidence of disturbance, and any interesting or unusual biological or physical features were noted. During the processing of biology, sediment, and chemistry subcores, care was taken to avoid disturbing or otherwise contaminating the samples before they were processed. If a subcore was considered to be disturbed, or exhibited evidence of leakage, it was replaced with an alternate subcore.

Subsamples were removed from each box core for analysis of

- Sediment grain size and clay mineralogy (*Chapter 5*)
- Sediment metals and total organic carbon (*Chapter 8*)
- Sediment redox chemistry (direct Eh and pH measurements) (*Chapter 8*)
- Sediment hydrocarbons (*Chapter 9*)
- Microbiota (*Chapter 10*)
- Meiofauna (*Chapter 11*)
- Macroinfauna (*Chapter 11*)
- Harpacticoid genetic diversity (*Chapter 13*)
- Sediment toxicity testing (GB 602 and MC 292 only; *Chapter 14*)

In addition, sediment samples for radionuclide analysis and interstitial water for interstitial water chemistry were removed from selected box cores at each site (*Chapter 8*).

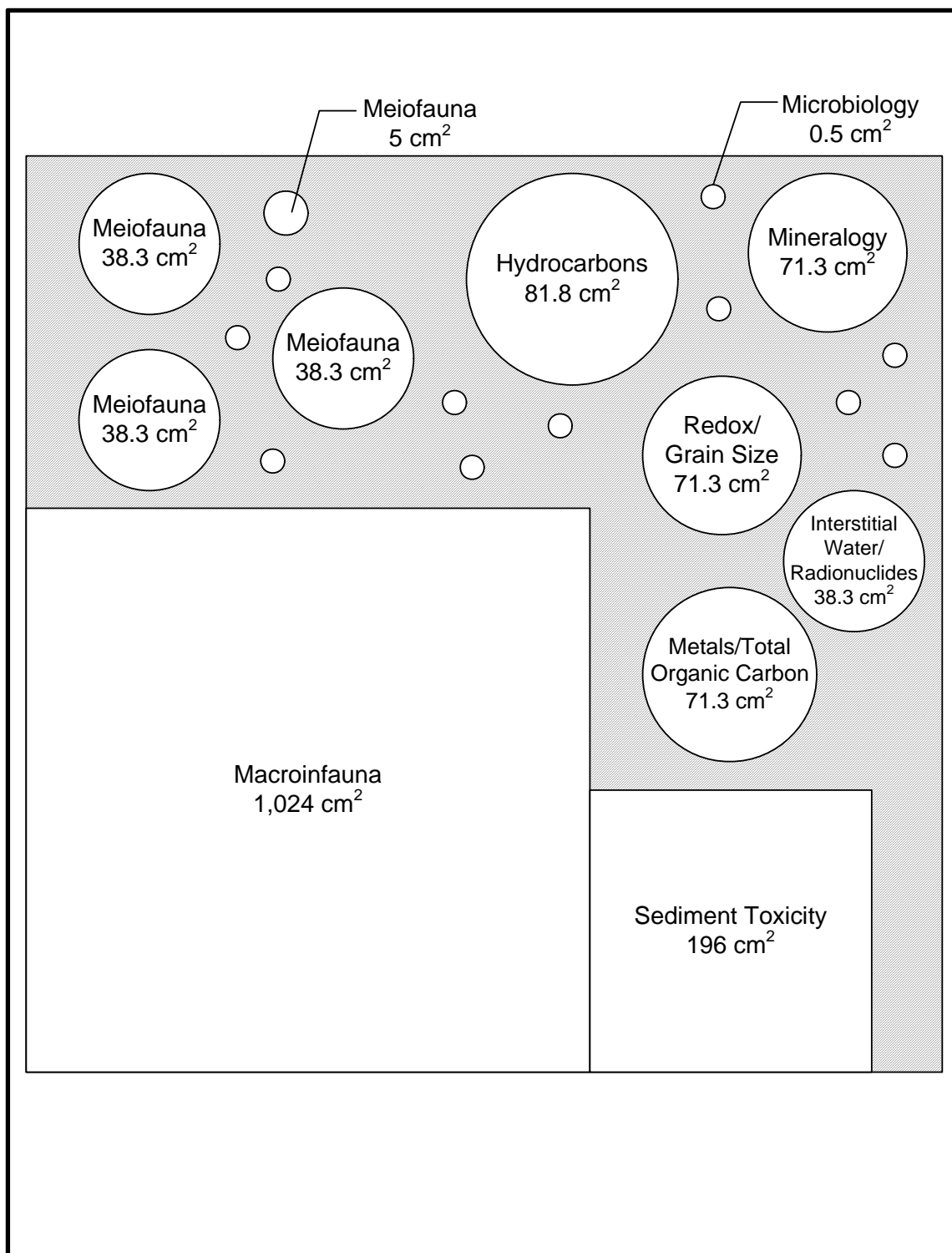


**Figure 2.8.** Schematic of box core subsampling. The box is 50 cm on a side (0.25 m<sup>2</sup>).

### 2.5.2 Sediment Profile Imaging

At each site, SPI photographs were collected along three drift transects in the near-field and at three of the six far-field sites (**Figure 2.6**). Although the plan was to take 36 images along each drift transect, the actual number of usable images per transect varied, as discussed in *Chapters 6* and *7*.

SPI photographs were taken with a Benthos Model 3731 sediment profile camera (Ocean Imaging Systems, North Falmouth, Massachusetts) (**Figure 2.9**). The profile camera works like an inverted periscope with a deep-sea 35-mm camera mechanism mounted horizontally inside a water-tight housing on top of a wedge-shaped prism. The camera provides images of up to 20 cm of the upper sediment column in profile. During each SPI camera transect, the camera array was regularly lowered to the bottom. A transponder was attached to the side of the SPI camera, giving its position and height off the bottom. As the frame reached the bottom, the sliding prism device would penetrate the seafloor sediment and automatically trigger the camera's shutter. The photograph, taken through the prism, shows a vertical swath of sediment in front of the prism's glass face. When the camera was raised between photographs, a wiper blade cleaned the faceplate. Detailed methods are provided in *Chapters 6* and *7*.

### 2.5.3 Seafloor Photographs

A camera on a dragged sled was used to collect still photographs of the seafloor and benthic organisms. These photographs were used for visual analyses of sediment appearance and megafauna (*Chapter 12*).

The seafloor photographs were collected using a camera and flash unit that was housed in an aluminum sled dragged behind the survey vessel (**Figure 2.10**). The camera was a Benthos Model 372 deep-sea 35-mm camera, which takes 800 exposures per loading. The camera system was deployed with a pre-programmed time delay of 90 minutes before acquiring images and a set time interval of 5 seconds between photographs.

The drag sled was connected to a 272-kg weight by a 30-m length of wire rope (**Figure 2.10**). The weight was connected to the main winch cable of the survey vessel. A transponder was mounted on the weight to aid in determining when the sled was approaching the seafloor.

Once deployed on the bottom, the sled was in constant contact with the seafloor. This method ensured a constant camera-to-seafloor distance. The drag sled was able to traverse seafloor changes of up to 1 m due to wide "runners" extending horizontally from the back and vertically from the front of the sled.

While the drag sled was being deployed, the survey vessel maintained a slight forward motion into the surface current, approximately 0.25 to 0.5 knots. Once the sled was on the bottom, the survey vessel increased speed to 0.5 to 1 knot. Global positioning system navigational positions were recorded. Times corresponding to beginning of deployment, sled on bottom, sled off bottom, and end of recovery also were recorded. After the sled was retrieved, the still camera was removed, and two lengths of film ("tails") were processed to check for proper photographic area and data chamber exposure settings.

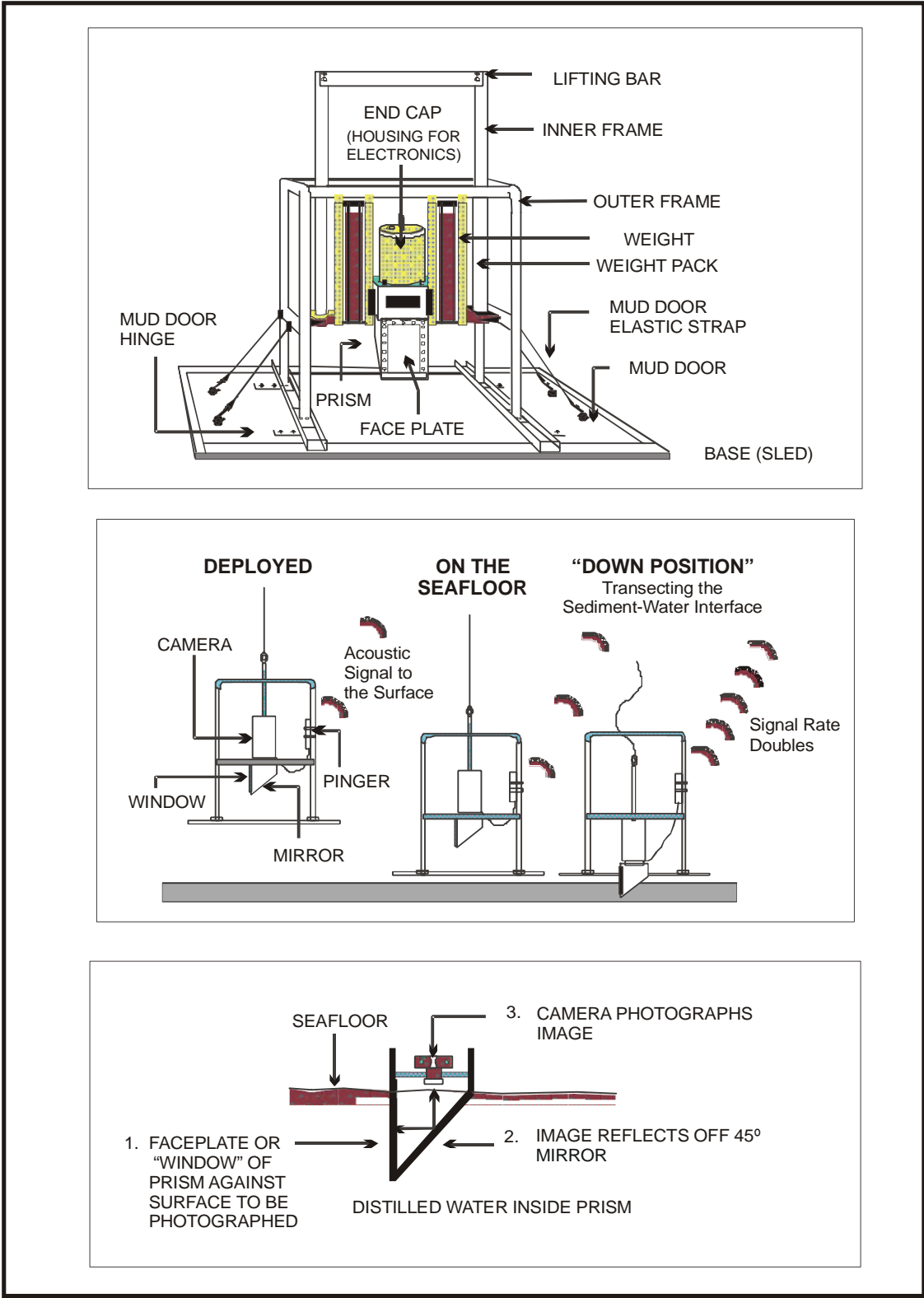


**Figure 2.9.** Schematic diagram of the sediment profile camera and its operation.

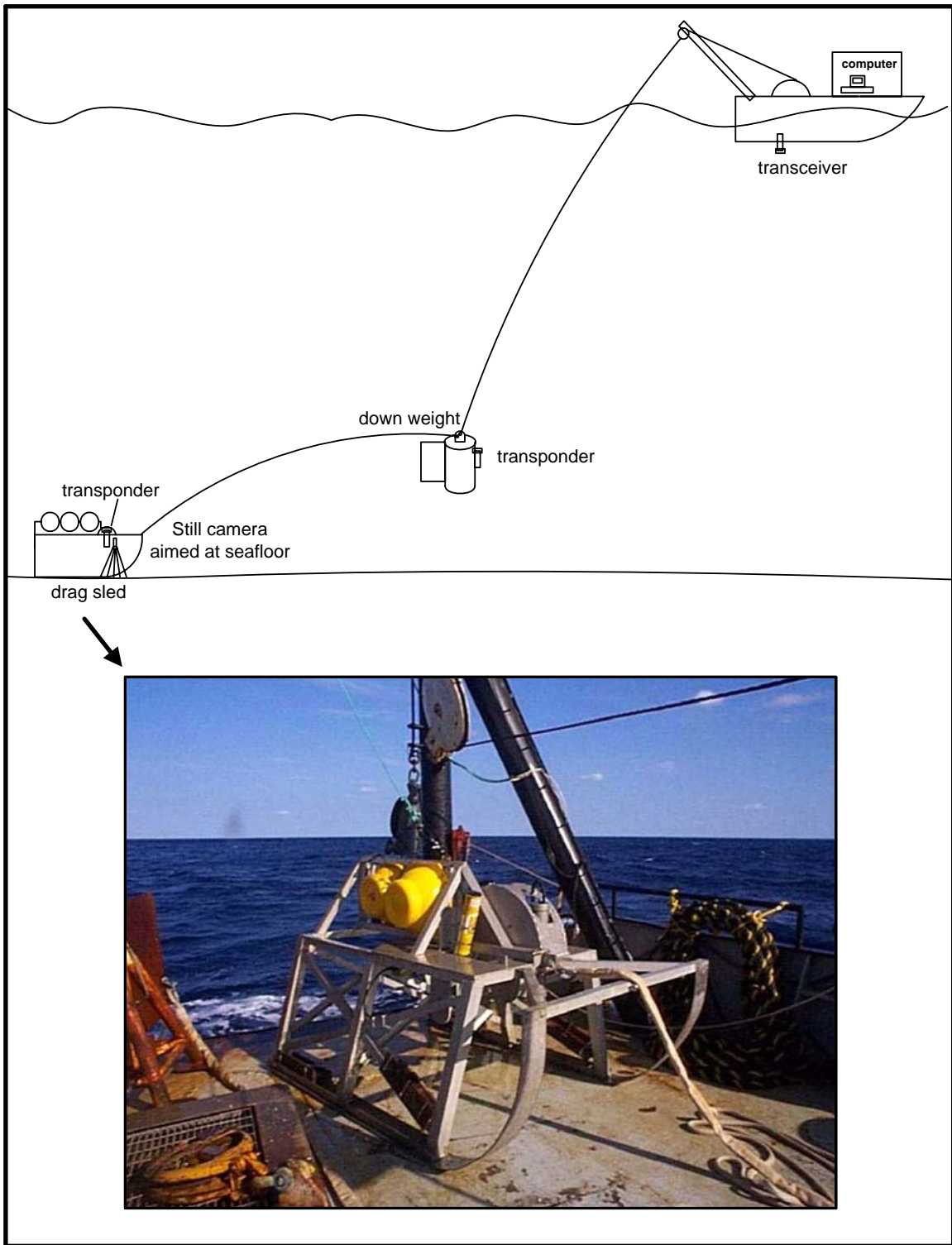


**Figure 2.10.** Configuration of dragged sled for seafloor photography.

#### 2.5.4 Baited Traps

Baited traps were used during Cruise 2B to collect animals for tissue analyses at the two post-development sites (GB 602 and MC 292) and corresponding far-field sites. A diagrammatic representation of a typical trap set is shown in **Figure 2.11**. The traps were similar in design to those used in the U.S. Pacific Northwest in the commercial dungeness crab fishery. The traps are 2 m in length by 1.5 m wide, with two openings for fish to enter.

At each trap station, a set of four baited traps was deployed along a common, weighted line, with each trap separated by a distance of 46 m. One end of the ground line was connected to a separate line that extended to the surface and was supported there by a pair of inflatable buoys and a single spar buoy marker. After deployment, each trap set was allowed to “fish” for a period of 18 to 24 hours, after which the traps were retrieved and any organisms captured were removed.

### 2.6 SAMPLING LOCATIONS AND DATA COLLECTED

**Table 2.3** summarizes numbers of samples collected and transects completed during each cruise. Detailed listings are provided in *Appendix A1*. **Table 2.4** lists numbers of animals captured in the baited traps.

**Figures 2.12** through **2.15** show the sampling locations for each near-field site on each cruise. Far-field sampling locations are shown in *Appendix A2*.

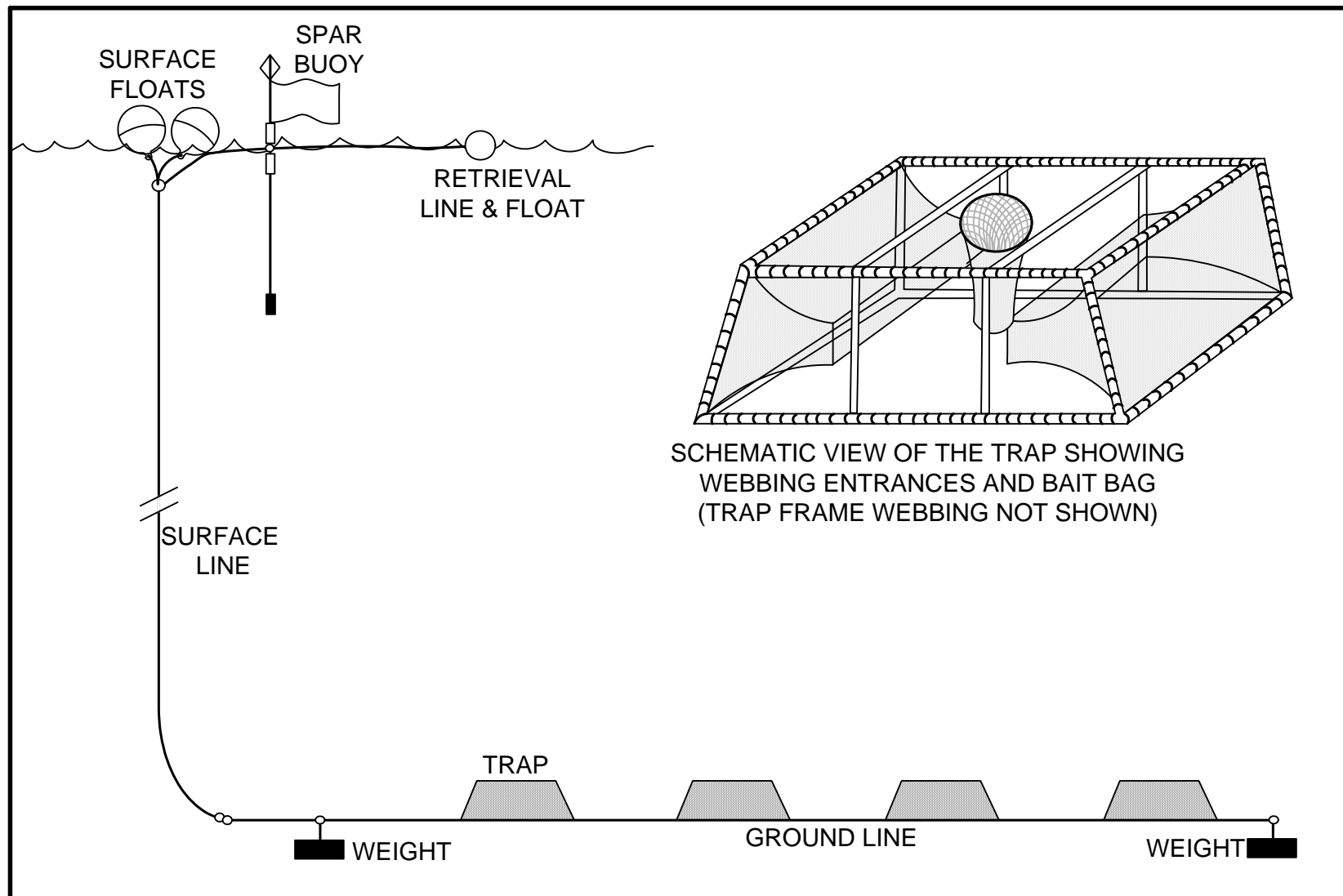


**Figure 2.11.** Schematic diagram of baited traps used to obtain organisms for tissue analyses.

**Table 2.3.** Numbers of samples collected and transects completed during chemical/biological cruises.

Cruise and Site	Box Cores		SPI Transects		Sled Transects		Trap Sets <sup>a</sup>	
	NF	FF	NF	FF	NF	FF	NF	FF
Cruise 1B								
VK 916	12	10	2	3	3	4	--	--
GB 516	12	12	3	3	3	5	--	--
Cruise 2B								
GB 516	12+3 <sup>b</sup>	12	3	3	3	3	--	--
GB 602	12+3 <sup>b</sup>	12	3	3	3	3	2	1
MC 292	12+3 <sup>b</sup>	12	2	3	3	3	2	2
Cruise 3B								
VK 916	12+3 <sup>b</sup>	12	3	0 <sup>c</sup>	3	2	--	--

NF = near-field; FF = far-field; SPI = sediment profile imaging.

<sup>a</sup> Each trap set included four traps.

<sup>b</sup> Three additional “discretionary” box cores samples for subsurface sediment analyses were taken at near-field sites during Cruises 2B and 3B.

<sup>c</sup> During Cruise 3B, far-field transects were attempted at VK 916 FF2 and FF4; however, due to problems with the SPI camera, no usable data were collected.

**Table 2.4.** Numbers of animals collected from baited trap sets during Cruise 2B.

Station	Species	Type	Number Captured				Total	TPH Samples	Metals Samples
			Trap 1	Trap 2	Trap 3	Trap 4			
Garden Banks 602									
NF-Trap1	<i>Bathynomus giganteus</i>	Isopod	4	4	3	7	18	4	4
	<i>Chaceon quinque-dens</i>	Crab	24	24	24	21	93	4	4
NF-Trap2	<i>Bathynomus giganteus</i>	Isopod	12	8	10	5	35	4	4
	<i>Chaceon quinque-dens</i>	Crab	11	5	6	8	30	4	4
FF5-Trap	<i>Bathynomus giganteus</i>	Isopod	11	17	12	21	61	8	8
	<i>Chaceon quinque-dens</i>	Crab	5	0	1	2	8	4	4
Mississippi Canyon 292									
NF-Trap1	<i>Bathynomus giganteus</i>	Isopod	0 <sup>a</sup>	3	2	3	8	4	4
	<i>Chaceon quinque-dens</i>	Crab	0 <sup>a</sup>	1	4	1	6	3	3
NF-Trap2	<i>Bathynomus giganteus</i>	Isopod	1	5	0	4	10	8	8
	<i>Chaceon quinque-dens</i>	Crab	15	17	1	30	63	0	0
FF3-Trap	<i>Bathynomus giganteus</i>	Isopod	5	7	2	2	16	8	8
	<i>Chaceon quinque-dens</i>	Crab	13	15	6	21	55	8	8
	<i>Centrophorus uyato?</i> <sup>b</sup>	Fish	0	0	0	1	1	5	5
FF4-Trap	<i>Bathynomus giganteus</i>	Isopod	5	2	3	6	16	8	8
	<i>Chaceon quinque-dens</i>	Crab	3	9	5	16	33	8	8
	<i>Centrophorus uyato?</i> <sup>b</sup>	Fish	0	0	0	1	1	0	0

TPH = total petroleum hydrocarbons.

<sup>a</sup> Lead (#1) trap did not rest on bottom due to high current and inadequate weight on ground line.

<sup>b</sup> Single specimens were frozen and donated to Texas A&M University museum.



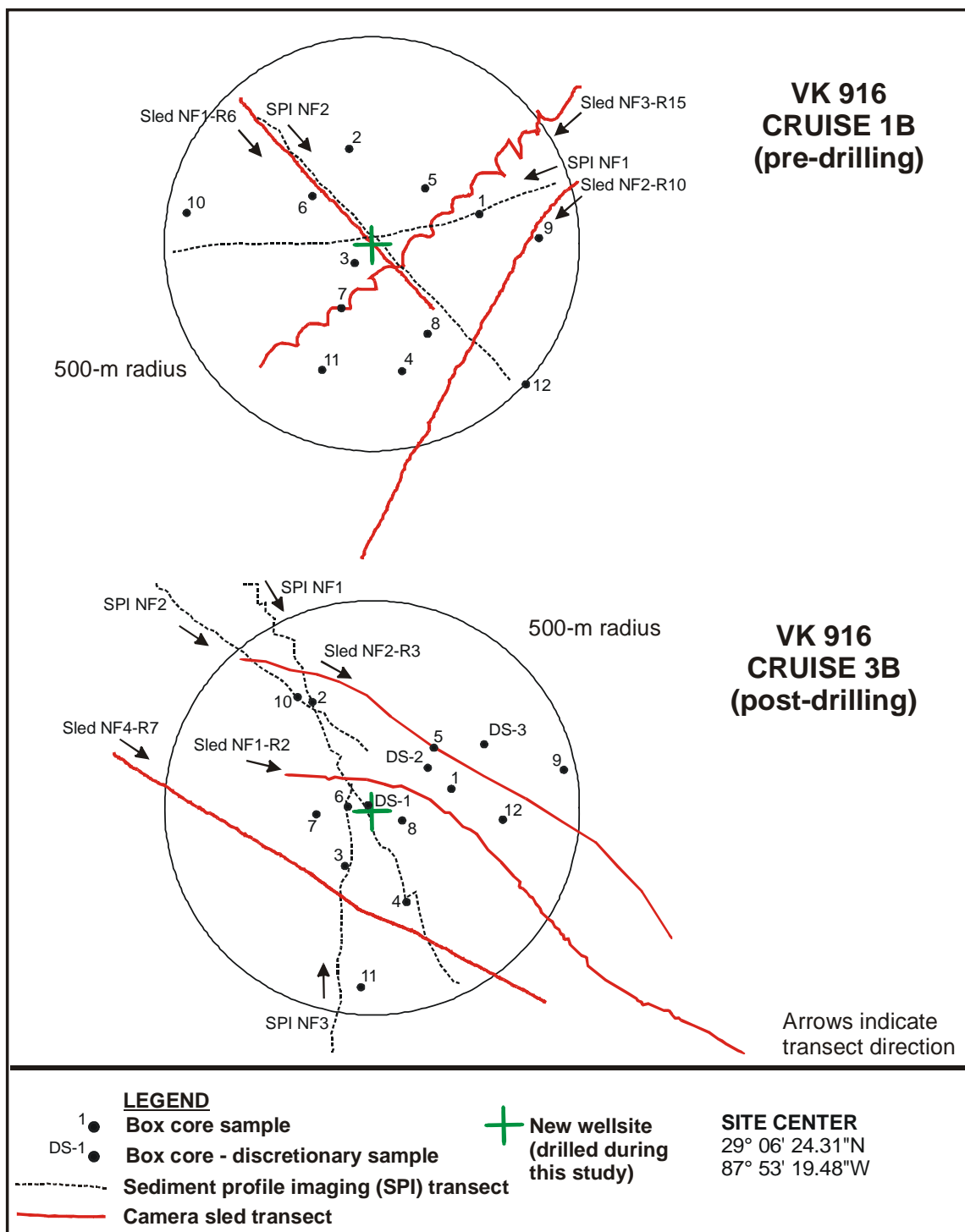


Figure 2.12. Near-field sampling locations at Viosca Knoll Block 916.

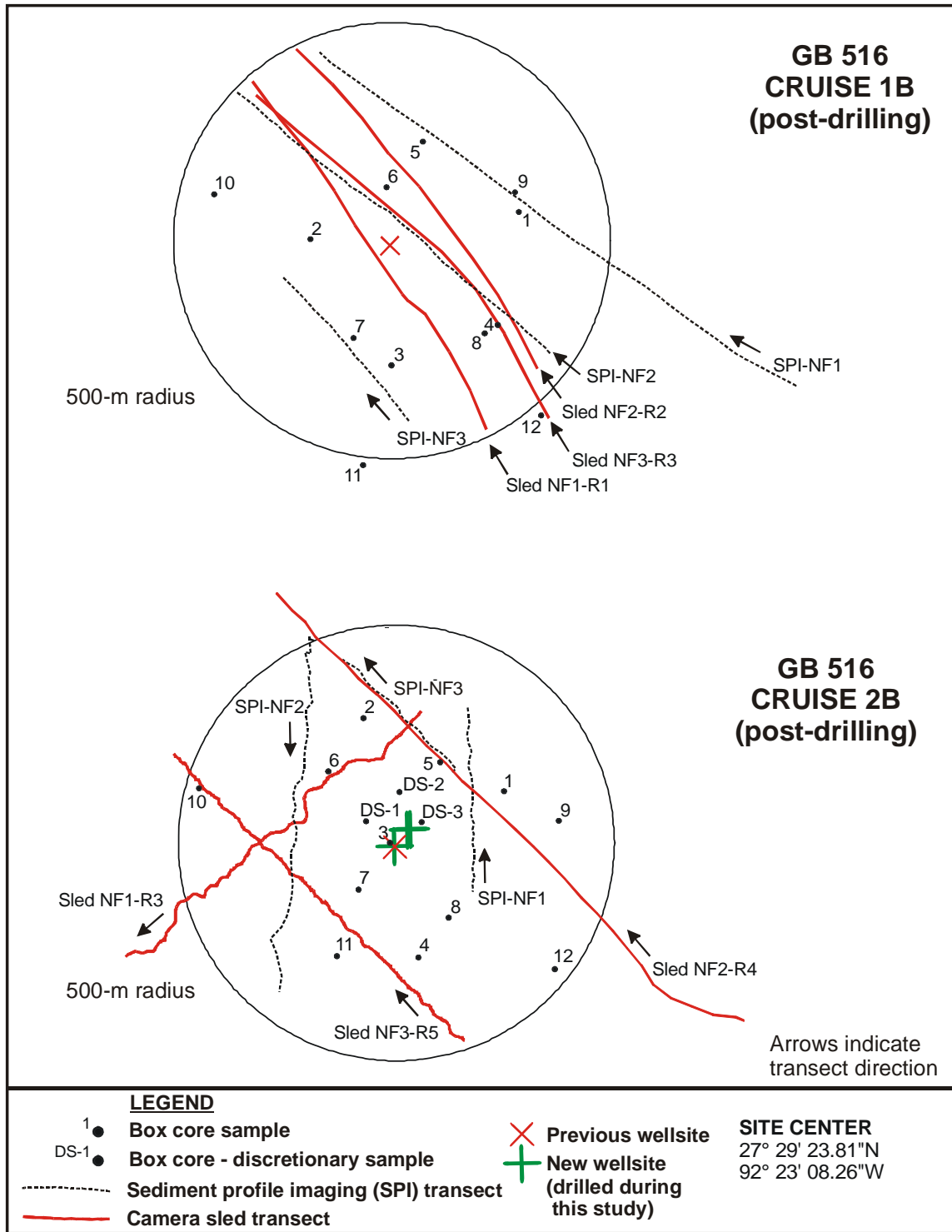


Figure 2.13. Near-field sampling locations at Garden Banks Block 516.

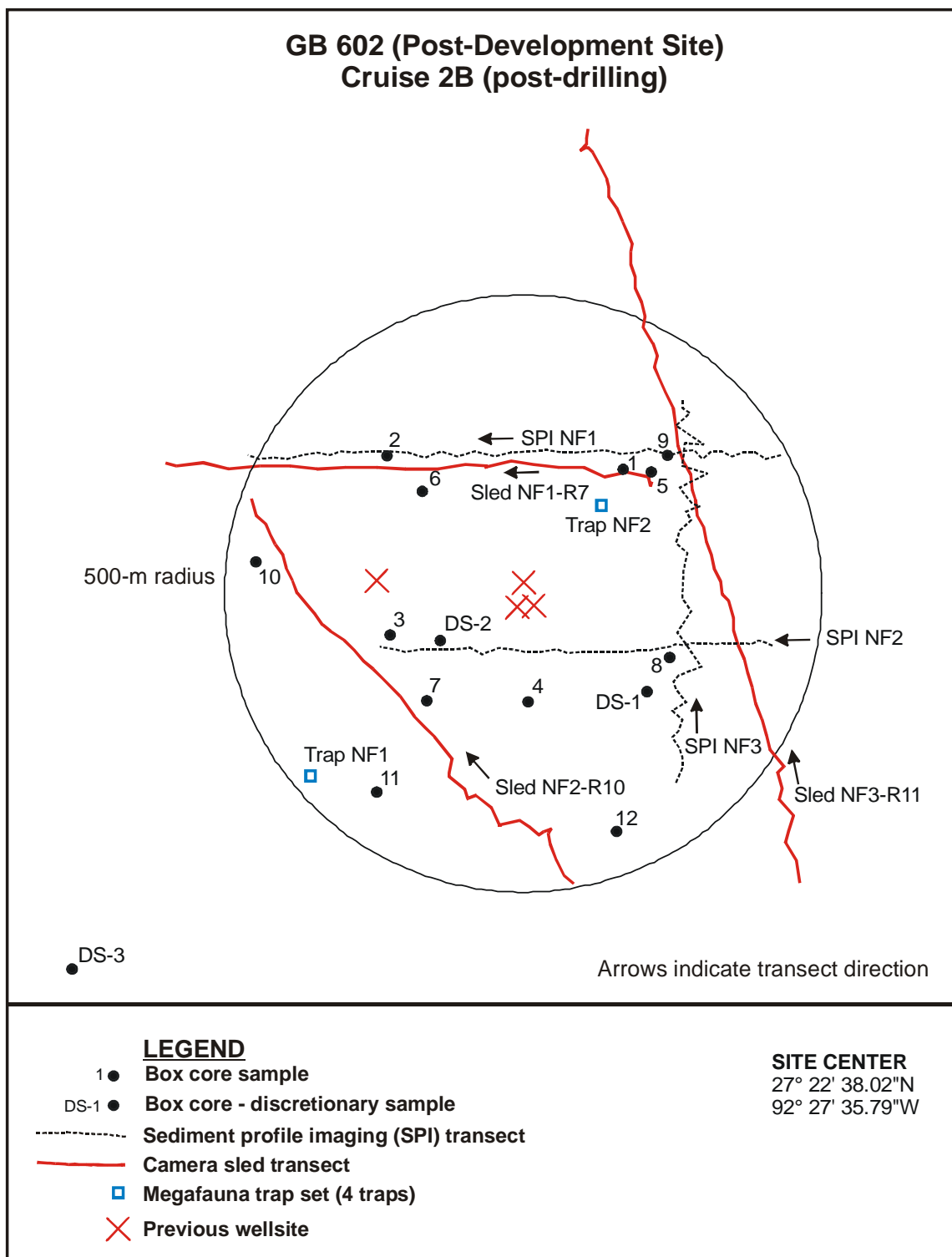


Figure 2.14. Near-field sampling locations at Garden Banks Block 602.

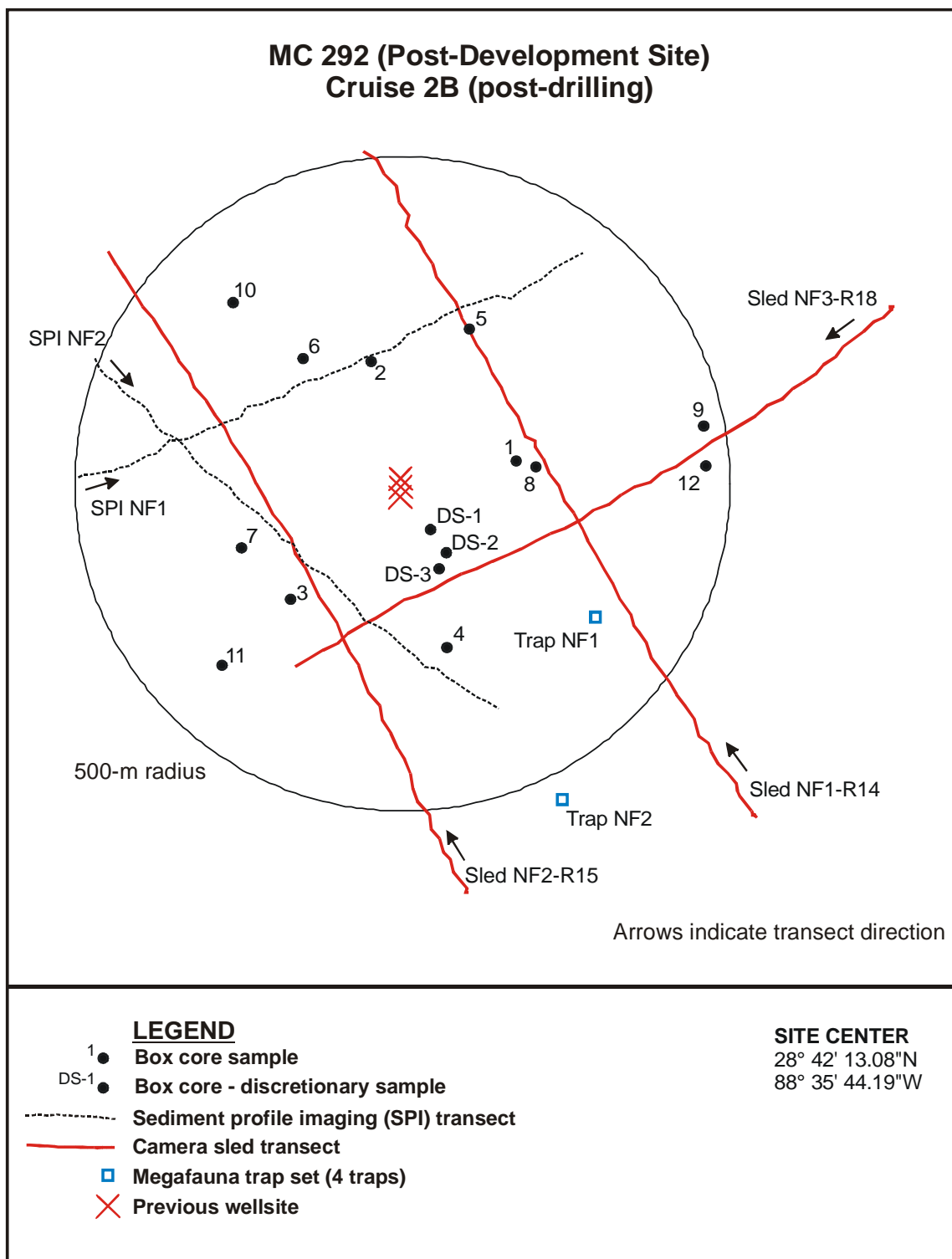


Figure 2.15. Near-field sampling locations at Mississippi Canyon Block 292.

## Chapter 3 Drilling Activities

Neal W. Phillips  
Continental Shelf Associates, Inc.

---

This section summarizes drilling activities at and near the study sites, including

- Wellsite, anchor locations, and drilling discharge information for each near-field site
- Other wells drilled within 10 km of each near-field site
- Wells drilled within 10 km of far-field (reference) sites

Well locations were plotted by the MMS based on data from their Technical Information Management System. Detailed listings of well locations within 10 km of each site are presented in *Appendix B1*. All wellsites plotted here refer to surface (seafloor) locations. Sidetracks (directionally drilled wells branching off an existing borehole) are listed in the MMS database as separate wells from the same surface location. Exploration and development plans for each of the four blocks were downloaded from the MMS website. Drilling discharge information was obtained from operators and the MMS.

Both water-based muds (WBM) and synthetic-based muds (SBMs)<sup>1</sup> were used for drilling at the near-field sites. The general sequence of events was similar for most wells. The initial well interval was drilled “open hole” using the drill bit and twisting pipe. The flow of spud mud and water through the drill bit jetted the cuttings out of the way and up along the pipe to the seabed surface, where they accumulated around the hole in a small pile. Spud muds consisting primarily of water and bentonite clay were used for this jetting process. At this point, the drill bit and drill pipe were removed. A surface casing was inserted in the hole, and cement was pumped down the casing pipe, where it emerged from the hole and flowed up along the outside of the casing pipe. Once the cement hardened, appropriate wellhead equipment was attached to the surface of the casing (at the seafloor). The wellhead was connected to a marine riser system that returned muds and cuttings to the drilling rig during the remainder of the drilling process. Typically, one or more well intervals were drilled using WBM, with WBM cuttings and muds discharged from the rig. Finally, the mud system was switched to SBM for drilling of remaining well intervals. In some cases, there were bulk discharges of remaining WBM prior to switching to SBM. During SBM intervals, SBM cuttings were discharged, but muds were retained, except for those adhering to cuttings (see *Chapter 16* for information on effluent limitation guidelines for drilling discharges). In addition, mud inventory reports indicate that some quantities of SBMs were lost to the formation, lost during casing/cementing operations, or left in the wellbore for future sidetracks.

Because they branch off an existing borehole, sidetracks do not involve the initial release of water-based mud and cuttings at the seafloor. In addition, sidetracks are usually shorter in duration than straight wells and have smaller hole sizes, resulting in lower discharge volumes per well. Sidetracks at these sites were drilled primarily using SBMs.

SBMs used in the Gulf of Mexico are almost exclusively internal olefins or linear- $\alpha$ -olefins (Neff et al. 2000). Internal olefins such as Novaplus, Novadril, or Syn-Teq were used at one or more of

---

<sup>1</sup> The terms synthetic-based mud (SBM) and synthetic-based fluid (SBF) are often used interchangeably. However, in this report, SBF refers to chemical measurements of the base fluid in sediment, whereas SBM refers to the drilling muds and cuttings *per se*.

the study sites. Petrofree LE, a linear- $\alpha$ -olefin, may have been used at GB 516 and GB 602. Petrofree ester may also have been used in one well at GB 602.

Discharge volumes were estimated using hole sizes (diameters and lengths for well intervals) provided by the operators. In some cases, actual well intervals were available; in others, planned well intervals from Exploration Plans were used. To allow consistent comparisons among wells, cuttings volume was always estimated in this report as 1.5 times hole volume (operators used multipliers ranging from 1.05 to 4.0). Drilling fluid volume (for WBM intervals) was estimated as 11 times hole volume (Walk, Haydel and Associates 1989). Detailed calculations for each well are presented in *Appendix B2*.

### 3.1 NEAR-FIELD SITES

#### 3.1.1 Viosca Knoll Block 916 (Exploration Site)

Viosca Knoll Block 916 is located about 170 km SSE of Mobile, Alabama. Water depth at the wellsite is approximately 1,125 m.

##### 3.1.1.1 Overview

**Table 3.1** lists all wells drilled within 10 km of the VK 916 near-field site through the end of Cruise 3B (14 August 2002). There were no previous wells in this block. However, several wells had been drilled within 10 km. The nearest wells were located about 2.3 km NNW in VK 872 and were drilled approximately 2 years before the start of this study (**Figure 3.1**).

**Table 3.1.** Wells drilled within 10 km of the Viosca Knoll (VK) Block 916 near-field (NF) site.

Distance from NF Site Center	Block	Number of Wells	Dates	Timing	
				Prior to This Study	During This Study (between Cruises 1B and 3B)
0	VK 916	1	Nov-Dec 2001	--	•
2.3 km	VK 872	2	Nov-Dec 1998	•	--
3.5 km	VK 873	1	Feb-Mar 1988	•	--
4.6 -7.4 km	VK 915	8	Jan 2001-June 2002	--	•
5.3 km	VK 915	9	Apr 1993-Apr 1998	•	--
6.4 km	VK 871	1	May-July 1994	•	--
7.2 km	VK 917	1	Nov-Dec 2001	--	•
7.6 km	VK 827	2	Sep-Oct 1998; June 2000	•	--

During this study, Shell drilled a single exploration well in VK 916. Details are provided below. Other drilling that occurred within 10 km of the near-field site during the program included 8 wells in VK 915 between January 2001 and June 2002, with distances ranging from 4.6 to 7.4 km; and 1 well 7.2 km away in VK 917, drilled in November-December 2001 (**Table 3.1**). Due to the distances from these other wells, any effects are assumed to be negligible in comparison with the single well drilled in VK 916 during this study.

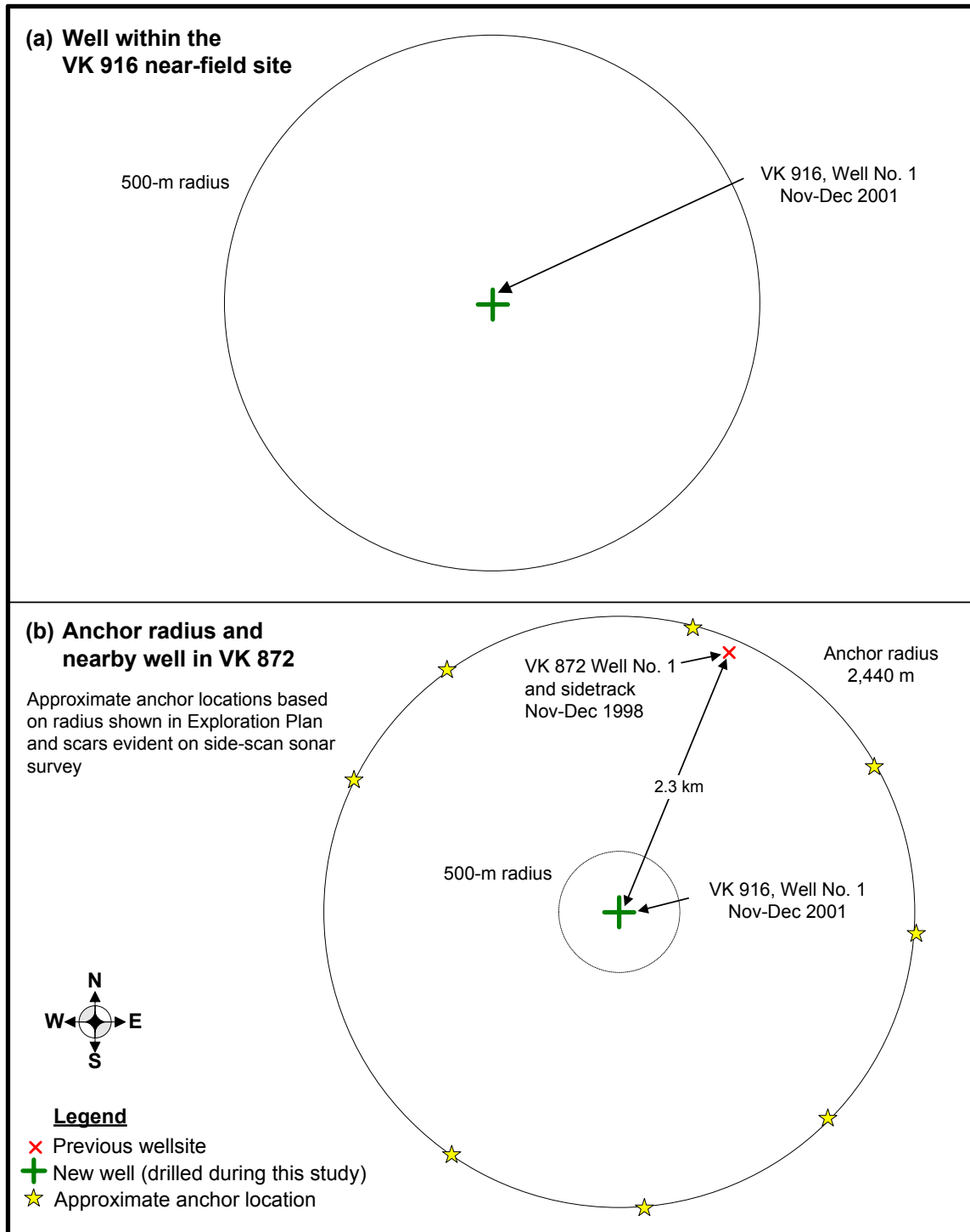


**Figure 3.1.** Well locations in and near the Viosca Knoll Block 916 near-field site.

### 3.1.1.2 Drilling Program

A single exploration well (No. 1) was spudded on 27 November 2001 and reached total depth on 18 December 2001, when it was plugged and abandoned. The wellsite was at the center of the VK 916 near-field site in a water depth of approximately 1,125 m.

The drilling rig was the NOBLE JIM THOMPSON, a semisubmersible. Anchor patterns shown in the Exploration Plan indicate eight anchors would be deployed radially at distances of 2,440 m from the wellsite, with approximately 450 m of anchor chain on the seafloor near each anchor location. The anchor locations were revised after the initial Exploration Plan was submitted, and therefore the anchor radius is shown with presumed anchor locations based on scars from the side-scan sonar survey (**Figure 3.1**).

Both WBM and SBM were used during drilling (**Table 3.2**). The first well interval was jetted using seawater and a seawater-based bentonite gel mud. During this first interval, all of the mud and cuttings were released at the seafloor. The second interval also used seawater and gel mud, with mud and cuttings discharged from the drilling rig. There was a bulk discharge of WBM at the end of the second interval. The remaining well intervals were drilled using the SBM Syn-Teq, an internal olefin isomer. Cuttings were discharged during these intervals, but SBM was recirculated and retained. The drilling mud contractor's inventory indicates there were some losses of SBM to the formation and during casing and cementing operations.

**Table 3.2.** Discharge summary for Viosca Knoll Block 916 Well No. 1 (27 November to 18 December 2001).

Well Interval	Hole Size (inches)	Estimated Seafloor Discharges (bbl)		Estimated Drilling Rig Discharges (bbl)			SBM Name
		WBM	WBM Cuttings	WBM	WBM Cuttings	SBM Cuttings	
IA	36	3,074	419		--	--	--
IB	26	--	--	12,807 <sup>a</sup>	1,746	--	--
II	20	--	--	--	--	950	Syn-Teq
III	14.75	--	--	--	--	951	Syn-Teq
IV	10.63	--	--	--	--	609	Syn-Teq
<b>Total:</b>		<b>3,074</b>	<b>419</b>	<b>12,807</b>	<b>1,746</b>	<b>2,510</b>	

SBM = synthetic-based mud; WBM = water-based mud.

Source: Spud date and total depth date as listed in Minerals Management Service Technical Information Management System. Well intervals and hole sizes were provided by Shell, and discharge volumes were estimated using hole volume times 11 for drilling fluids, hole volume times 1.5 for cuttings. Synthetic drilling fluids were not discharged (other than those adhering to cuttings), but the inventory indicates SBM losses including 256 bbl lost and 141 bbl left behind the liner during interval II, 1,634 bbl lost during casing and cementing operations during interval III, and 160 bbl lost to the formation during interval IV.

<sup>a</sup> Water-based mud was dumped at end of this interval to prepare for SBM system.

### 3.1.2 Garden Banks Block 516 (Exploration/Development Site)

Garden Banks Block 516 is located in the Western Planning Area, about 275 km SSE of Cameron, Louisiana. The center of the site has a water depth of 1,033 m. The prospect is named Serrano.



### 3.1.2.1 Overview

Three exploration wells had been drilled in GB 516 prior to this study, and five development wells were drilled during the study. **Figure 3.2** shows the well locations, and **Table 3.3** lists all wells drilled within 10 km through the end of Cruise 2B (25 July 2001).

**Table 3.3.** Wells drilled within 10 km of the Garden Banks (GB) Block 516 near-field (NF) site.

Distance from NF Site Center	Block	Number of Wells	Dates	Timing	
				Prior to This Study	During This Study (between Cruises 1B and 2B)
0	GB 516	2	July-Aug 1999	•	--
0-50 m	GB 516	5	Nov 2000-Feb 2001	--	•
1.15 km	GB 516	1	Sep 1995-July 1996	•	--
3.9 km	GB 515	1	June 1999	•	--
8.2 km	GB 559	6	Feb 1999-Oct 2000	•	• <sup>a</sup>
7.5-9.1 km	GB 426/471	40	Feb 1987-June 2000	•	--
8.4 km	GB 426	1	May 2001	--	•

<sup>a</sup> Two of these wells overlapped a few days with the start of Cruise 1B.

Two of the previous wells (a straight well and one sidetrack) were at the center of the near-field site and were drilled in July-August 1999. The other was 1,150 m to the southeast and was drilled between September 1995 and July 1996. The five new wells included two additional sidetracks of the 1999 well at the center of the GB 516 near-field site, and one straight well and two sidetracks at a location about 50 m to the northeast of the site center.

Several other wells had been drilled within 10 km of the GB 516 site (**Table 3.3**). The nearest was a single well 3.9 km southwest in GB 515 (drilled in June 1999). Six previous wells were drilled about 8.2 km to the southwest in GB 559 (February 1999 to October 2000). Two of these were ongoing at the end of October 2000 during the first few days of Cruise 1B. Also, 40 wells were drilled at locations 7.5 to 9.1 km away in the southeast corner of GB 426 and the adjacent corner of GB 471 between February 1987 and June 2000, with one additional well in GB 426 during this program (May 2001). These were associated with Shell's Auger facility in GB 426. Due to the distance, any effects are assumed to be negligible in comparison with the wells drilled within the GB 516 near-field site before and during this study.

### 3.1.2.2 Drilling Program

Exploration Well No. 1 was drilled in GB 516 between September 1995 and July 1996. Discharge data were not obtained for this well, which is 1,150 m southeast of the near-field site center. The Exploration Plan indicates that WBM and SBM (Novadril or Petrofree ester) were planned to be used.

Between 13 July and 21 August 1999, Well No. SE001 and one sidetrack were drilled at the center of the near-field site. These two exploration wells were drilled about 14 to 15 months prior to Cruises 1A and 1B.

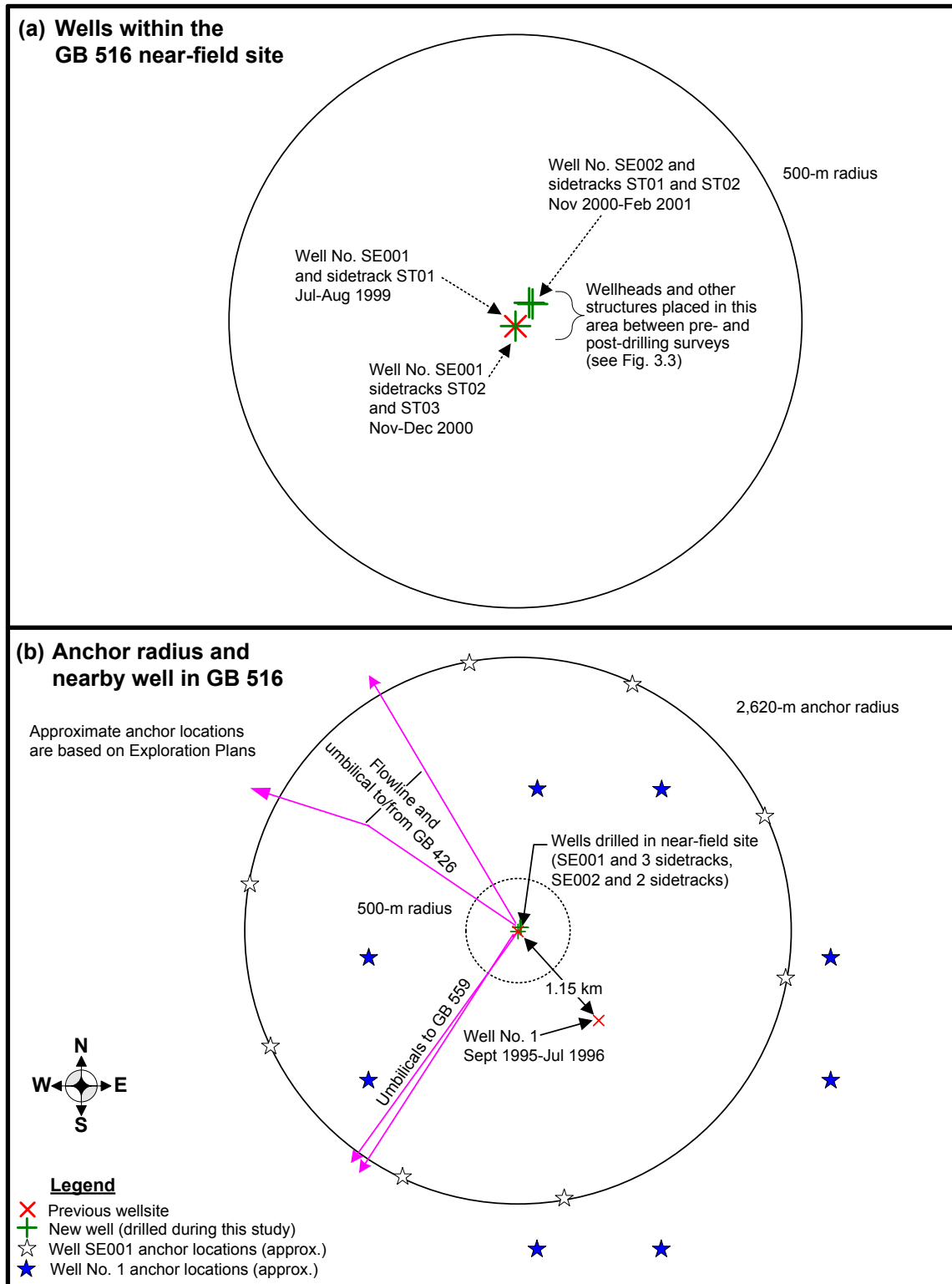


**Figure 3.2.** Well locations in and near the Garden Banks Block 516 near-field site.

In 2000, Shell filed a development plan for GB 516, and subsequently five development wells were drilled between 6 November 2000 and 5 February 2001. These included two additional sidetracks of Well No. SE001 at the center of the GB 516 near-field site, and Well No. SE002 and two sidetracks at a surface location about 50 m to the northeast of the site center. At the same time, a flowline and an umbilical were placed on the seafloor, connecting to processing facilities on the Auger platform in GB 426, approximately 10 km to the north (**Figure 3.3**). Two umbilicals also connect to the nearby Oregano prospect in GB 559. In addition to the flowline and umbilicals, structures on the seafloor in GB 516 include two subsea wellheads, a flowline sled, and an umbilical distribution module.

Both water-based muds and associated cuttings, as well as SBM cuttings, were discharged during drilling. Exploration and development plans included the option of using either of two SBMs, Novaplus (an internal olefin) or Petrofree LE (a linear- $\alpha$ -olefin). Novaplus was the only SBM used for the wells and sidetracks drilled in 2000-2001; it is not known which SBM was used on the 1999 wells. **Table 3.4** summarizes the discharge data.

**Table 3.4.** Discharge summary for Garden Banks Block 516 wells within the near-field site.

Well No.	Dates	Estimated Seafloor Discharges (bbl)		Estimated Drilling Rig Discharges (bbl)			SBM Name
		WBM	WBM Cuttings	WBM	WBM Cuttings	SBM Cuttings	
SE001 & SE001 ST 1	7/13/99-8/15/99 8/20/99-8/21/99	6,501 <sup>a</sup>	887 <sup>a</sup>	14,731 <sup>a</sup>	2,009 <sup>a</sup>	1,904 <sup>a</sup>	Novaplus or Petrofree LE
SE001-ST 2	11/29/00-12/15/00	--	--	--	--	2,031	Novaplus
SE001-ST 3	12/24/00-12/29/00	--	--	--	--	672	Novaplus
SE002 & SE002-ST 1	11/06/00-11/21/00 11/24/00-11/25/00	6,501	887	14,731	2,009	1,904	Novaplus
SE002-ST 2	1/30/01-2/05/01	--	--	--	--	802	Novaplus
<b>Total:</b>		<b>13,002</b>	<b>1,774</b>	<b>29,462</b>	<b>4,018</b>	<b>7,313</b>	

SBM = synthetic-based mud; ST = sidetrack; WBM = water-based mud.

Source: Spud date and total depth date as listed in Minerals Management Service Technical Information Management System. Well intervals and hole sizes were provided by Shell, and discharge volumes were estimated using hole volume times 11 for drilling fluids, hole volume times 1.5 for cuttings.

<sup>a</sup> Actual well intervals not available; assumed identical to Well Nos. SE002 and SE002-ST 1.

Semisubmersible drilling rigs were used for all of the wells. Well No. SE001 and Sidetrack 1 were drilled by the TRANSOCEAN MARIANUS. The Exploration Plan indicates an anchor radius of 2,620 m with 550 m of anchor chain on the bottom at each location. Sidetracks 2 and 3 of Well No. SE001, as well as Well No. SE002 and Sidetracks 1 and 2, were drilled by the DIAMOND OCEAN WORKER. Anchor locations are not known, but the radius is assumed to be similar. Approximate anchor locations are plotted on **Figure 3.2**.

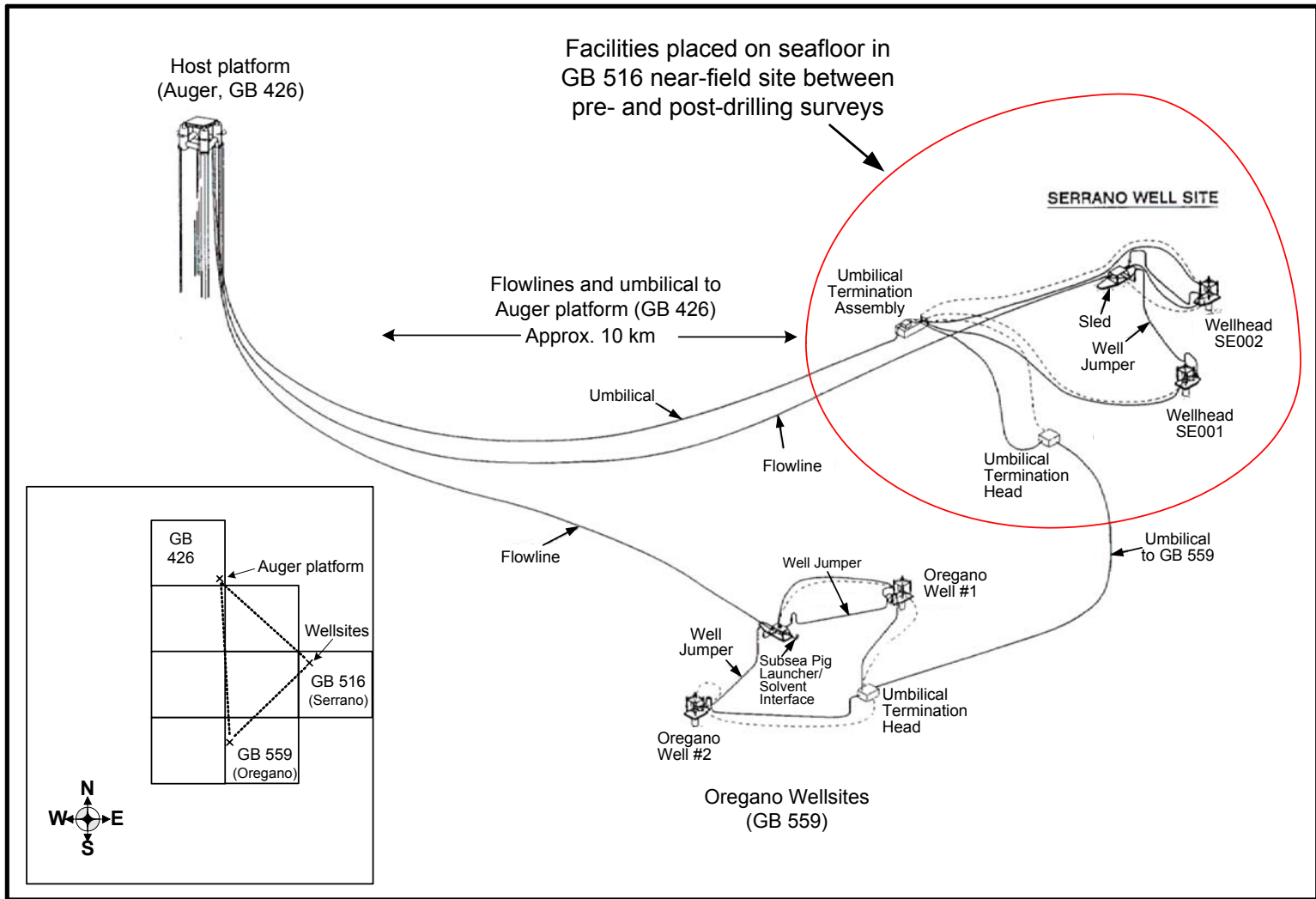


Figure 3.3. Diagram of subsea wellheads, manifold, and flowlines at the Garden Banks Block 516 site.

### 3.1.3 Garden Banks Block 602 (Post-Development Site)

Garden Banks Block 602 is located in a water depth of 1,125 m, about 280 km SSE of Cameron, Louisiana. The block is leased by Shell, and the prospect has been named Macaroni.

#### 3.1.3.1 Overview

Seven wells were drilled within the GB 602 near-field site between September 1995 and January 2001 (**Figure 3.4**). All of these were prior to the only sampling at this site (Cruises 2A and 2B). Three other exploration/development wells were drilled in GB 602 approximately 2.3 km NNE of the site center (**Table 3.5**). The only other wells within a 10-km radius were 6 wells in GB 559 and 1 well in GB 600, the latter of which was being drilled at the time of Cruise 2B.

**Table 3.5.** Wells drilled within 10 km of the Garden Banks (GB) Block 602 near-field (NF) site center.

Distance from NF Site Center	Block	Number of Wells	Dates	Timing		Notes
				Prior to Cruise 2B	During Cruise 2B	
22 m	GB 602	6	Sep 1995-Jan 2001	•	--	Well Nos. 2, 4, and 5, each with a straight well and a single sidetrack
247 m	GB 602	1	Sep 1995	•	--	Well No. 1, lost to shallow water flow
1.3 km	GB 602	1	Feb 1996	•	--	Geotechnical borehole (9 days)
2.3 km	GB 602	3	Apr-Aug 1996	•	--	Well No. 3 and two sidetracks
6.6-6.7 km	GB 559	6	Feb 1999-Oct 2000	•	--	
8.3 km	GB 600	1	June-Aug 2001	--	•	Drilling ongoing during Cruise 2B (8 to 25 July 2001)

In addition to the exploration and development wells, in February 1996, one geotechnical borehole was drilled in GB 602, about 1.3 km northeast of the near-field site center (**Figure 3.4**). The Exploration Plan indicates that a dynamically positioned survey vessel would be used, and therefore no anchoring was involved. Because there was no anchoring and only small quantities of mud and cuttings were discharged at the seafloor, any effects are assumed to be negligible in comparison with the wells drilled within the near-field site.

#### 3.1.3.2 Drilling Program

**Figure 3.4** shows a diagram of the GB 602 site. Exploration Well No. 1, located 247 m west of the site center, was drilled in September 1995 and permanently abandoned (“junked”) after it was lost to shallow water flow. Six other wells (three straight wells with corresponding sidetracks) were drilled at three surface locations near the site center (which is between the three wellsites and about 22 m from each). Exploration Well No. 2 was drilled between September 1995 and January 1996, and a sidetrack was drilled in February-March 1997. Development Wells No. 4 (and sidetrack) and No. 5 (and sidetrack) were drilled between December 1998 and January 2001.

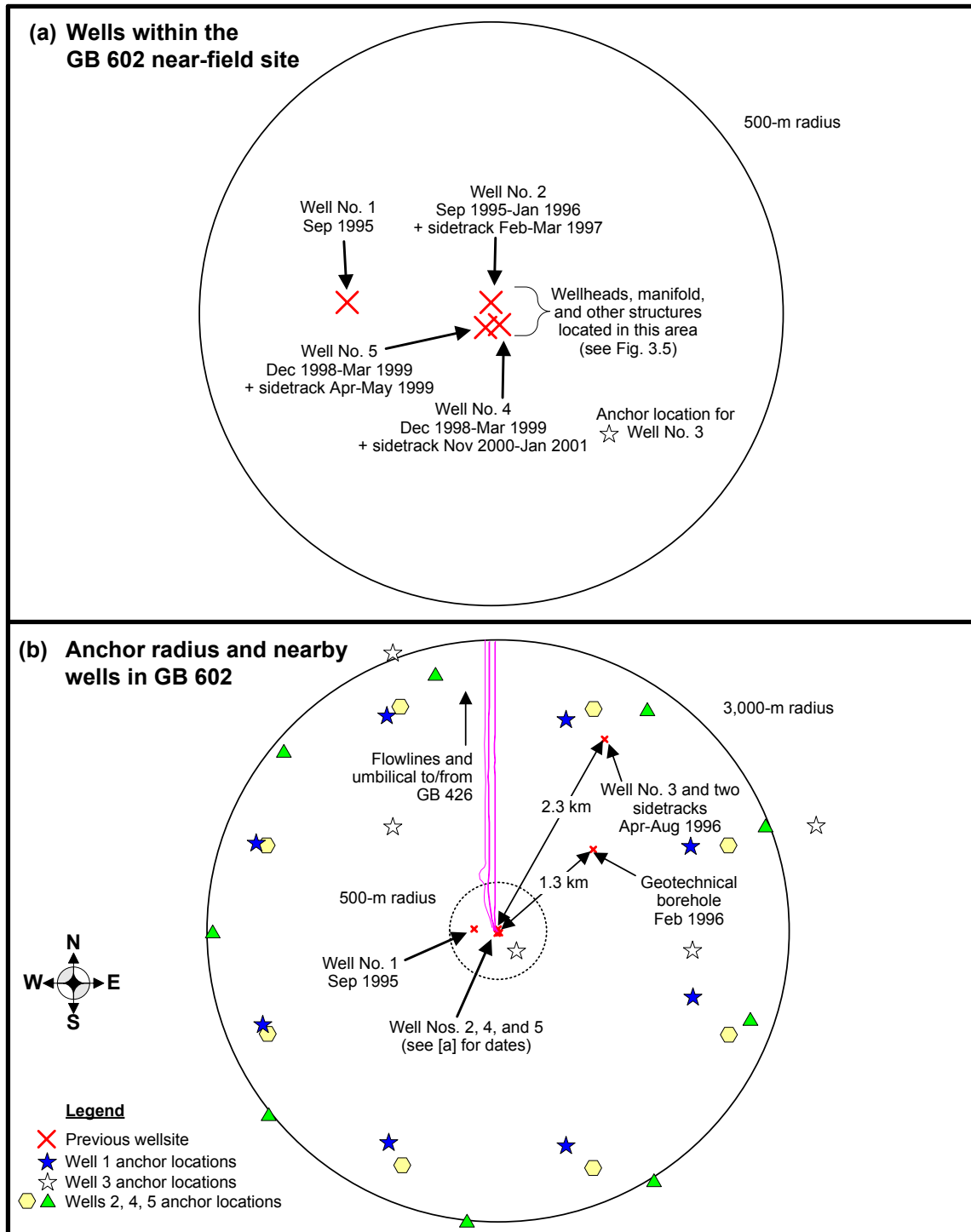


Figure 3.4. Well locations in and near the Garden Banks Block 602 near-field site.

**Table 3.6** summarizes estimated drilling discharges from wells within the near-field site. Well interval data were provided by Shell. Both WBM and SBM were used during drilling. After the initial jetting, during which WBM and associated cuttings were released at the seafloor, each well had four or five intervals of drilling with WBM, with mud and cuttings discharges from the drilling rig. Subsequent intervals were drilled using SBM, with discharge of SBM cuttings.

**Table 3.6.** Discharge summary for Garden Banks Block 602 wells within the near-field site.

Well No.	Dates	Estimated Seafloor Discharges (bbl)		Estimated Drilling Rig Discharges (bbl)			SBM Name
		WBM	WBM Cuttings	WBM	WBM Cuttings	SBM Cuttings	
1	9/13/95-9/21/95	2,770	378	30,447	4,152	5,098	Novadril or Petrofree ester
2	9/25/95-1/21/96	2,770	378	14,938	2,037	5,589	Novaplus or Petrofree LE
2-ST1	2/25/97-3/24/97	2,714	370	9,198	1,254	3,839	Novaplus or Petrofree LE
4	12/10/98-9/27/99	4,760	649	9,055	1,235	3,079	Novaplus or Petrofree LE
4-ST1	11/29/00-1/3/01	2,714 <sup>a</sup>	370 <sup>a</sup>	9,198 <sup>a</sup>	1,254 <sup>a</sup>	3,839 <sup>a</sup>	Novaplus or Petrofree LE
5	12/11/98-3/7/99	5,504	751	9,267	1,264	3,056	Novaplus or Petrofree LE
5-ST1	4/26/99-5/29/99	2,714 <sup>a</sup>	370 <sup>a</sup>	9,198 <sup>a</sup>	1,254 <sup>a</sup>	3,839 <sup>a</sup>	Novaplus or Petrofree LE
<b>Total:</b>		<b>23,946</b>	<b>3,266</b>	<b>91,301</b>	<b>12,450</b>	<b>28,339</b>	

SBM = synthetic-based mud; ST = sidetrack; WBM = water-based mud.

Source: Spud date and total depth date as listed in Minerals Management Service Technical Information Management System. Well intervals and hole sizes were provided by Shell, and discharge volumes were estimated using hole volume times 11 for drilling fluids, hole volume times 1.5 for cuttings.

<sup>a</sup> Well intervals not available; assumed same as No. 2 sidetrack based on similar duration of drilling.

The Exploration Plan for Well No. 1 included the option of two SBMs, Novadril (an internal olefin) or Petrofree ester. The Development Plan (for Well Nos. 2, 4, and 5) included Novaplus (an internal olefin) and Petrofree LE (a linear- $\alpha$ -olefin). It is not known which SBM was actually used.

Anchored semi-submersible rigs were used to drill the wells. The proposed drilling rig for Well Nos. 1 and 2 was the SONAT RATHER. The NOBLE PAUL ROMANO was the rig for Well No. 4 and a sidetrack as well as the sidetrack of Well No. 5. For Well No. 5, the rig was the TRANSOCEAN RICHARDSON. The Exploration Plan for Well Nos. 1 and 2 shows an anchor radius of 2,377 m with 914 m of anchor chain contacting the bottom at each location. The development plan for Well Nos. 4 and 5 shows an anchor radius of 2,540 m with approximately 650 m of chain on the bottom at each location. The anchor radii are shown on **Figure 3.4**.

In addition to the drilling activities, several structures were installed on the seafloor (**Figure 3.5**). These included a four-well manifold, an umbilical distribution module, and flowlines. Typically, a subsea well manifold is about 5 to 10 m square and 5 m or more in height. Most of the structures are within a radius of about 75 m. Two insulated flowlines were connected to processing facilities located on the Auger platform in GB 426, approximately 19 km to the north.

### 3.1.4 Mississippi Canyon Block 292 (Post-Development Site)

Mississippi Canyon Block 292 is located in a water depth of approximately 1,034 m and is approximately 200 km southeast of New Orleans. The block is leased by Texaco, and the prospect has been named Gemini.

#### 3.1.4.1 Overview

**Figure 3.6** shows a diagram of wellsite locations at the MC 292 near-field site. Five wells were drilled at three closely-spaced locations near the center of the site between May 1995 and July 1999. From south to north, these are Well Nos. 1, 3 (and sidetrack), and 4 (and sidetrack). These are producing wells with a subsea manifold and flow lines carrying gas to VK 900, about 44 km to the north.

The nearest other wells are 2.5 km to the north in MC 248 (three wells, January to March 2000) (**Table 3.7**). Five other wells were drilled in MC 292 between September 1996 and March 1997 (Well No. 2 and several sidetracks), but these were more than 3 km SSE of the near-field site center. A total of six additional wells had been drilled within MC 247, 248, and 291 at distances ranging from 2.5 to 4.0 km (**Table 3.7**). Due to the distances, any effects are assumed to be negligible in comparison with the wells drilled within the MC 292 near-field site.

**Table 3.7.** Wells drilled within 10 km of the Mississippi Canyon (MC) Block 292 near-field (NF) site.

Distance from NF Site Center	Block	Number of Wells	Dates	Timing	
				Prior to This Study	During This Study
0 m	MC 292	2	Feb-June 1999	•	--
15 m	MC 292	3	May 1995-July 1999	•	--
2.5 km	MC 248	3	Jan-Mar 2000	•	--
2.9 km	MC 291	1	Aug-Oct 1997	•	--
3.2 km	MC 292	5	Sep 1996-Mar 1997	•	--
4.0 km	MC 247	2	Nov 1997-Feb 1998	•	--

#### 3.1.4.2 Drilling Program

Well No. 1 was drilled from May to September 1995 and was subsequently completed in 1999 as part of development operations. Development Well Nos. 3 and 4 and their respective sidetracks were drilled and completed from February to July 1999. The surface locations of Well Nos. 3 and 4 were 15 m and 30 m, respectively, north of Well No. 1. The MC 292 near-field site is centered on the middle (Well No. 3) location.



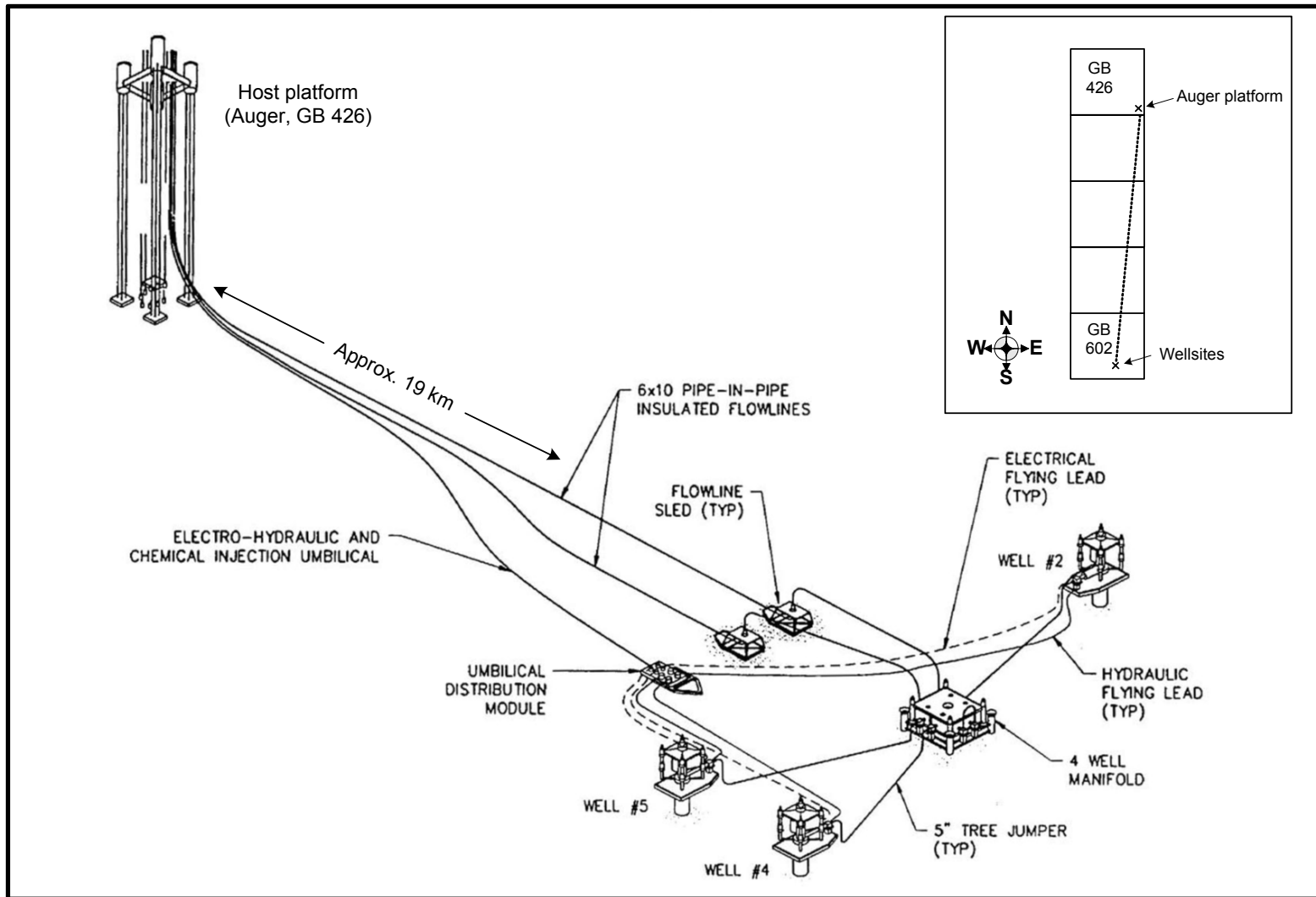


**Figure 3.5.** Diagram of subsea wellheads, manifold, and flowlines at the Garden Banks Block 602 site.

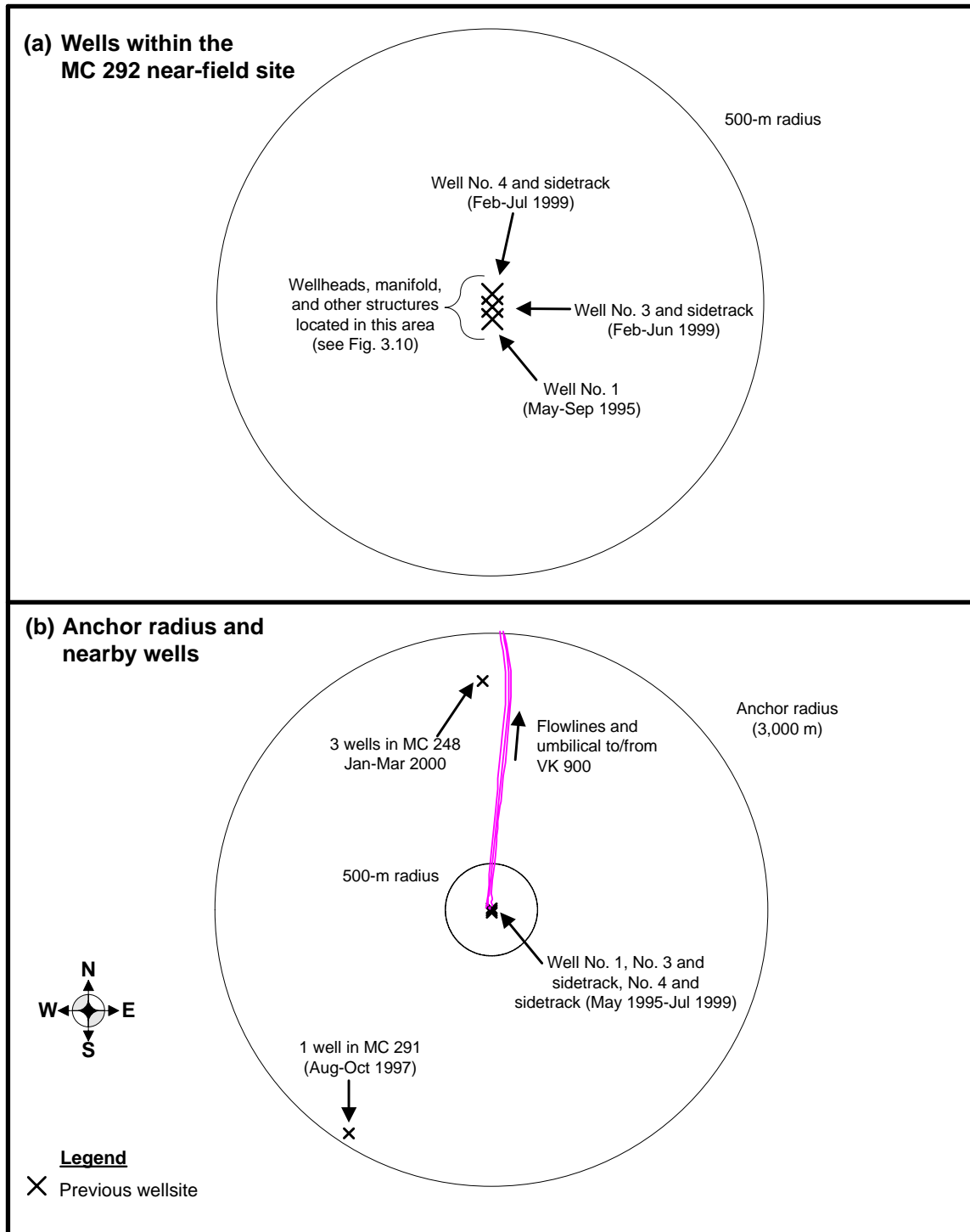


**Figure 3.6.** Well locations in and near the Mississippi Canyon Block 292 near-field site.

Well Nos. 1, 3, and 4 were drilled with WBM, which were discharged along with cuttings (**Table 3.8**). These included initial discharges at the seafloor during jetting, and subsequent discharges from the drilling rig. The two sidetracks (3-ST1 and 4-ST1) were drilled using Novaplus, an internal olefin SBM. Due to the short duration of drilling (11 days and 8 days for 3-ST1 and 4-ST1, respectively), relatively small quantities of SBM cuttings were discharged from the drilling rig.

**Table 3.8.** Discharge summary for Mississippi Canyon Block 292 wells within the near-field site.

Well No.	Dates	Estimated Seafloor Discharges (bbl)		Estimated Drilling Rig Discharges (bbl)			SBM Name
		WBM	WBM Cuttings	WBM	WBM Cuttings	SBM Cuttings	
1	5/7/95 -9/7/95	3,351	457	35,648	4,861	--	--
3	2/11/99-4/15/99	3,490	476	29,156	3,976	--	--
3-ST1	6/10/99-6/21/99	--	--	--	--	462	Novaplus
4	2/4/99-3/13/99	3,490	476	29,156	3,976	--	--
4-ST1	7/8/99-7/16/99	--	--	--	--	1,028	Novaplus
<b>Total:</b>		<b>10,331</b>	<b>1,409</b>	<b>93,960</b>	<b>12,813</b>	<b>1,490</b>	

SBM = synthetic-based mud; ST = sidetrack; WBM = water-based mud.

Source: Spud date and total depth date as listed in Minerals Management Service Technical Information Management System. Well intervals and hole sizes were provided by Texaco, and discharge volumes were estimated using hole volume times 11 for drilling fluids, hole volume times 1.5 for cuttings.

All three wells and sidetracks were drilled using a semisubmersible rig, the OCEAN STAR. The Exploration Plan indicates an anchor radius of approximately 3,000 m. Exact anchor locations could not be plotted based on the available information.

In addition to drilling the wells, a four-well manifold, two flowlines, and a hydraulic/electric control umbilical with chemical injection capability were installed (**Figure 3.7**). The flowlines extend north from the manifold to Platform "A" in VK 900.

### 3.1.5 Summary

The four near-field sites represent a range of drilling activities. **Table 3.9** summarizes the number of wells drilled in the near-field sites before and during this study, as well as the discharge data. **Figure 3.8** shows the timing of drilling activities at each of the sites in relation to sampling cruises during this study.

VK 916 is the simplest case, with no previous drilling in the near-field site and a single exploration well drilled during this study. A semisubmersible drilling rig was used, and one set of anchors was deployed. Both WBM and SBM were used during drilling. This site was sampled before and after drilling.

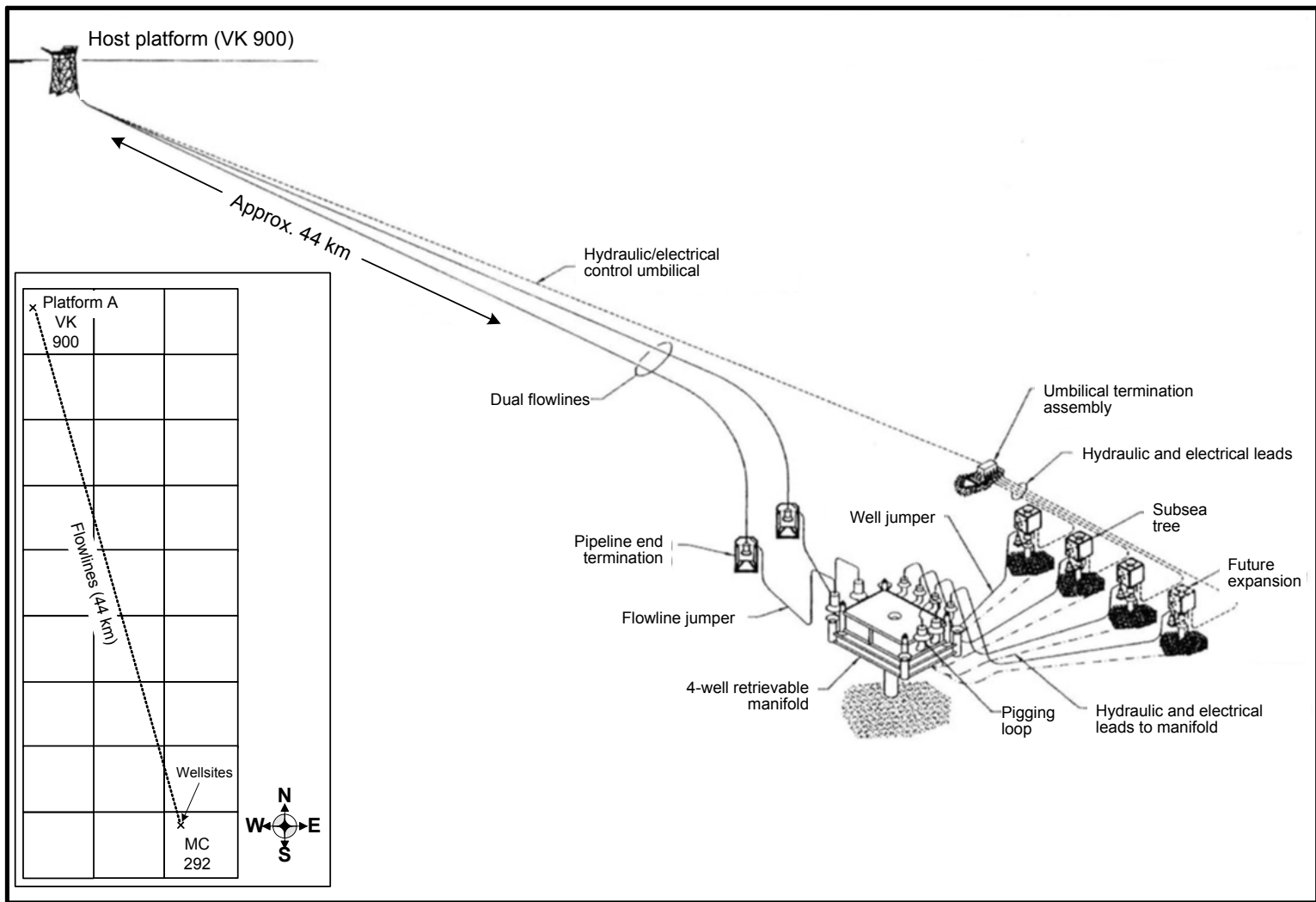
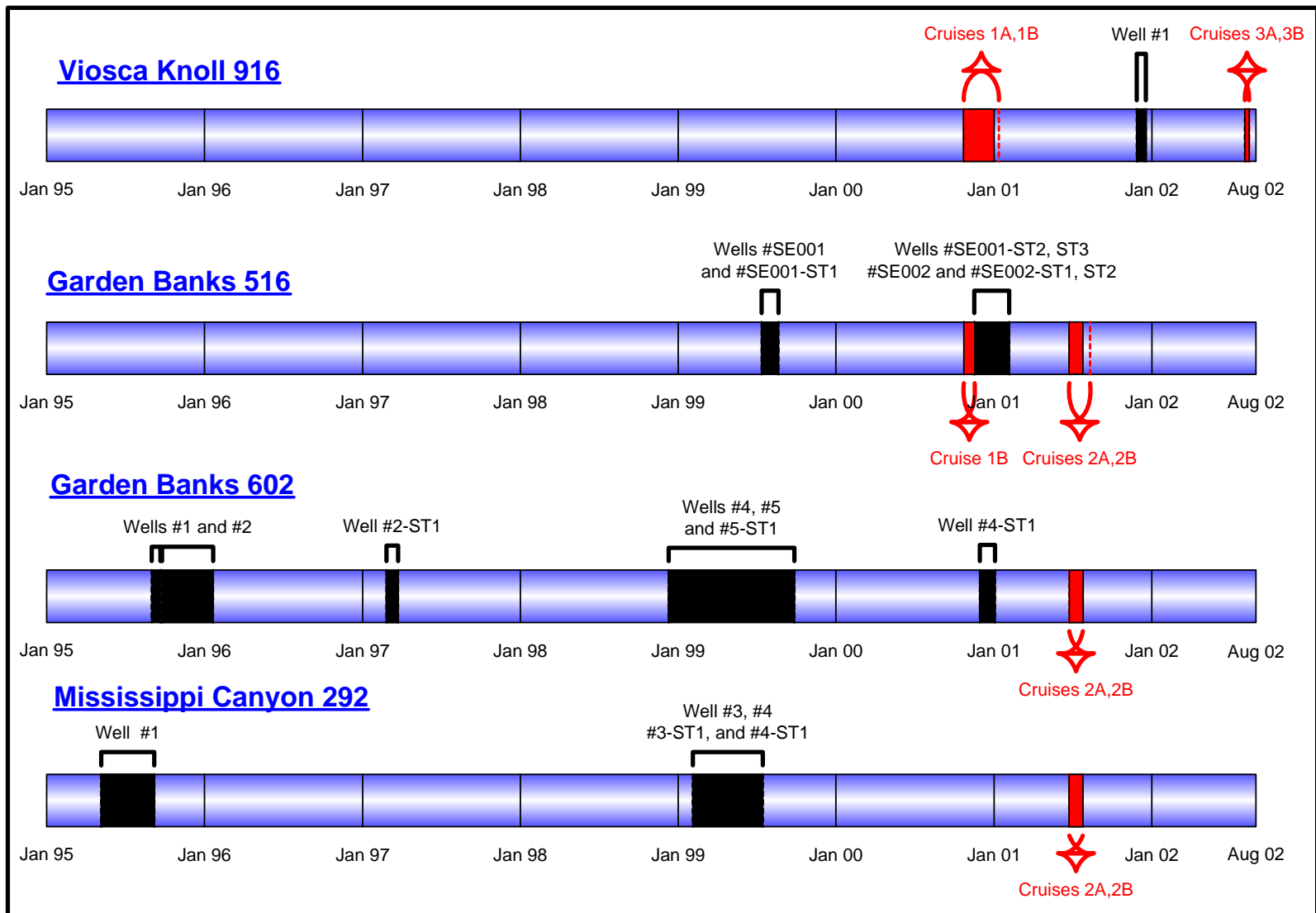


Figure 3.7. Diagram of subsea wellheads, manifold, and flowlines at the Mississippi Canyon Block 292 site.



**Figure 3.8.** Timeline showing drilling activities at the four near-field sites.

**Table 3.9.** Drilling summary for wells within each near-field site.

Site	Number of Wells Within 500-m Radius		Estimated Seafloor Discharges (bbl)		Estimated Drilling Rig Discharges (bbl)			SBM Type
	Prior to this Study	During this Study	WBM	WBM Cuttings	WBM	WBM Cuttings	SBM Cuttings	
VK 916	0	1	3,074	419	12,807	1,746	2,510	Syn-Teq (IO)
GB 516	2	5	13,002	1,774	29,462	4,018	7,313	Novaplus (IO); possibly Petrofree LE (LAO) (1 well)
GB 602	7	0	23,946	3,266	91,301	12,450	28,339	Novadril (IO) or Petrofree ester (1 well); Novaplus (IO) or Petrofree LE (LAO) (all others)
MC 292	5	0	10,331	1,409	93,960	12,813	1,490	Novaplus (IO)

IO = internal olefin; LAO = linear- $\alpha$ -olefin; SBM = synthetic-based mud; WBM = water-based mud. GB = Garden Banks; MC = Mississippi Canyon; VK = Viosca Knoll.

GB 602 and MC 292 are development sites with several previous wells and no new drilling during this study. Drilling occurred at various times over several years, so there are multiple anchor deployments and sets of drilling discharges. An important difference is that most of the drilling at MC 292 was done with WBM, with SBM used only for two sidetracks. Therefore, the total quantity of SBM cuttings discharged at MC 292 was the smallest among the four sites. These sites were sampled once during Cruises 2A/2B to provide a snapshot of post-drilling status.

GB 516 is the most complex case, with two previous wells and five new wells drilled during this study. Overall, activities were similar to those at the other development sites (GB 602 and MC 292) in that multiple wells were drilled over time, with multiple anchor deployments and drilling discharges; and subsea wellheads, manifolds, and flowlines were installed connecting to a remote platform. The difference is that two “snapshots” were obtained – once during Cruise 1B after the two exploration wells had been drilled and again on Cruises 2A/2B after the five additional development wells had been drilled.

### 3.2 FAR-FIELD SITES

For each of the four near-field sites, six far-field sites (or “reference areas”) were designated. These were chosen to be at about the same depth as the near-field site and 10 to 25 km away. The intention was also to locate these sites away from other previous wellsites, to the extent possible. However, due to the large number of wellsites in the Gulf of Mexico, it was difficult to find far-field sites at similar water depths that were not within 10 km of previous drilling.

**Table 3.10** summarizes the number of wells within 10 km of each far-field site. Well locations are shown on **Figures 3.9** through **3.12**. Each site is discussed individually below, followed by a summary and preliminary evaluation.

**Table 3.10.** Previous wells near far-field (FF) sites.

Site	No. of Previous Wellsites		Distance to Nearest Well(s)	Block of Nearest Well(s)	Dates of Nearest Well(s)	Rating of FF Site <sup>b</sup>
	Within 10 km	Within 3 km				
<b>Viosca Knoll Block 916 (exploration site)</b>						
FF1	63	4	1.9 km	VK 957 (4 wells)	Jan-July 1989	Fair
FF2	41	4	2.6 km	VK 915 (4 wells)	Mar-May 2002	Fair
FF3	30	0	5.5 km	VK 829 (1 well)	June-Aug 1994	Good
FF4	26	0	5.7 km	VK 829 (1 well)	June-Aug 1994	Good
FF5	25	0	6.3 km	VK 786 (24 wells)	June 1995-June 2002	Good
FF6	25	0	6.7 km	VK 786 (24 wells)	June 1995-June 2002	Good
<b>Garden Banks Block 516 (exploration/development site)</b>						
FF1	19	0	4.6 km	GB 559 (6 wells)	Feb 1999-Oct 2000	Good
FF2	6	0	8.6-8.9 km	GB 386 (6 wells)	June 1997-Mar 1999	Good
FF3	6	0	8.5-8.6 km	GB 386 (6 wells)	June 1997-Mar 1999	Good
FF4	7	0	7.8 km	GB 386 (2 wells)	Nov 1998-Mar 1999	Good
FF5	12	0	7.5 km	GB 386 (2 wells)	Nov 1998-Mar 1999	Good
FF6	3	0	8.4-8.9 km	GB 386-387 (3 wells)	Apr 1990-Mar 1999	Good
<b>Garden Banks Block 602 (post-development site)</b>						
FF1	1	0	6.5 km	GB 600 (1 well) <sup>a</sup>	June-Aug 2001	Good
FF2	0	0	>10 km	--	--	Excellent
FF3	0	0	>10 km	--	--	Excellent
FF4	0	0	>10 km	--	--	Excellent
FF5	0	0	>10 km	--	--	Excellent
FF6	1	0	6.3 km	GB 562 (1 well)	Aug-Sep 2000	Good
<b>Mississippi Canyon Block 292 (post-development site)</b>						
FF1	12	2	1.1 km 2.7 km	MC 243 (1 well) MC 243 (1 well)	Sep-Oct 1994 Aug-Sep 1999	Poor
FF2	13	1	2.0 km	MC 243 (1 well)	Aug-Sep 1999	Fair
FF3	2	0	7.4 km 7.5 km	MC 201 (1 well) MC 160 (1 well)	Jan 1988 Sep-Nov 1989	Good
FF4	7	0	7.1 km	MC 201 (1 well)	Jan 1988	Good
FF5	9	0	4.6 km	MC 160 (1 well)	Sep-Nov 1989	Good
FF6	6	0	4.8 km	MC 160 (1 well)	Sep-Nov 1989	Good

<sup>a</sup> Drilling of this well was ongoing during Cruise 2B (8 to 25 July 2001).

<sup>b</sup> Excellent – no previous wells within 10 km; Good – no previous wells within 3 km, but one or more between 3 km and 10 km away; Fair – previous well(s) between 1.5 km and 3 km away; and Poor – previous well(s) within 1.5 km.

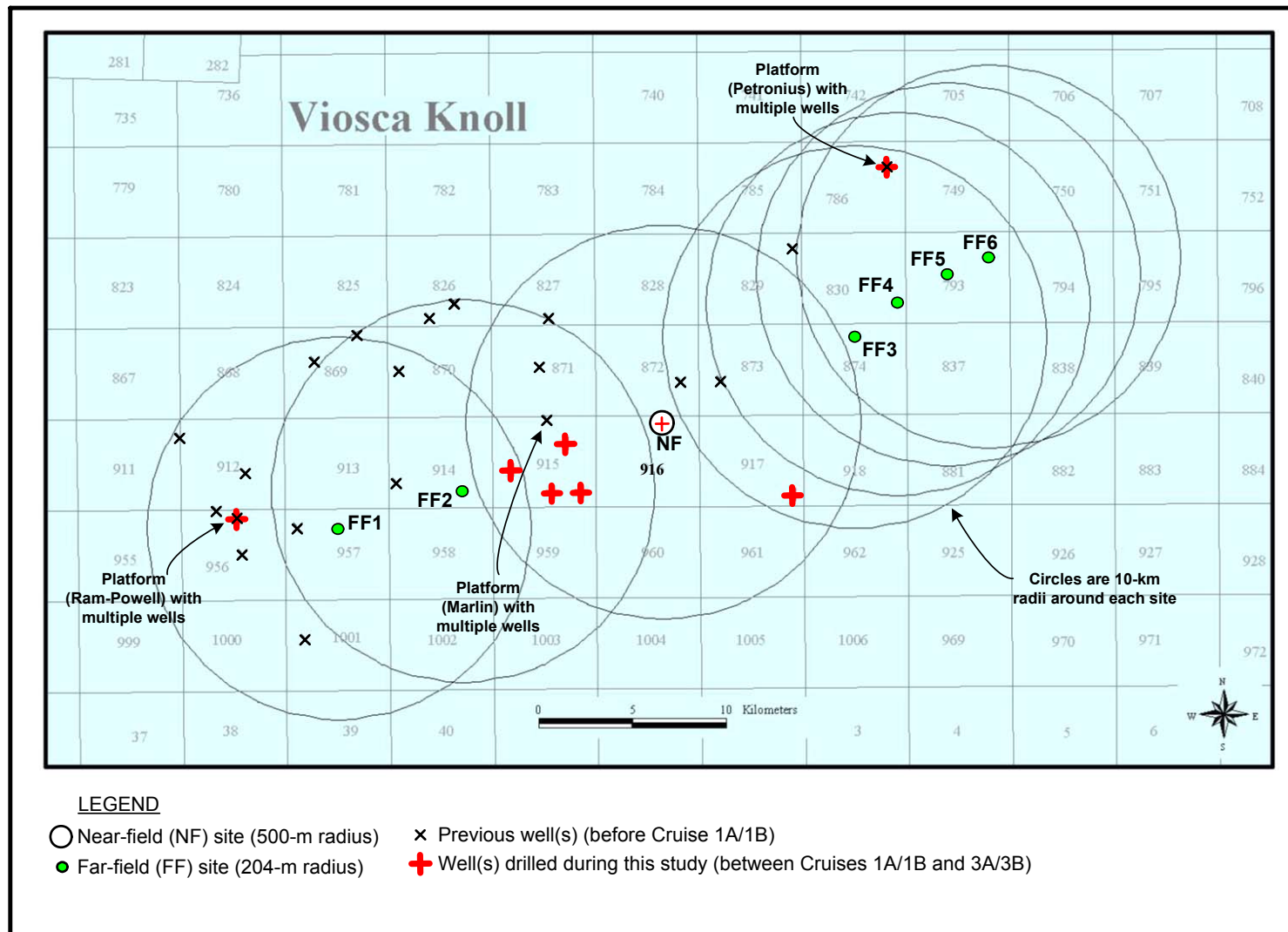


**Figure 3.9.** Location of blocks with previous wells in relation to Viosca Knoll Block 916 near-field (NF) and far-field (FF) sites.



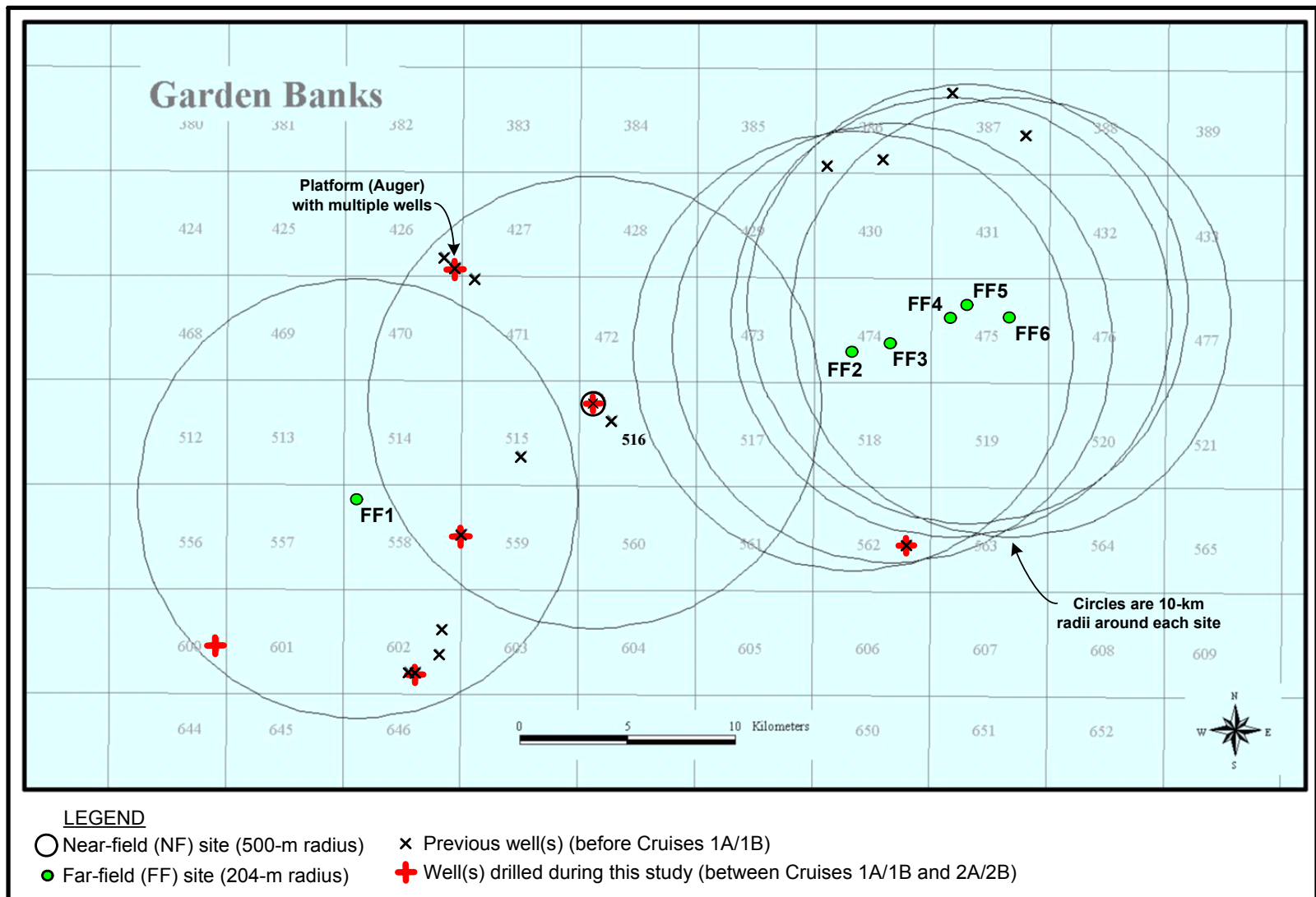


**Figure 3.10.** Location of previous wells in relation to Garden Banks Block 516 near-field (NF) and far-field (FF) sites.

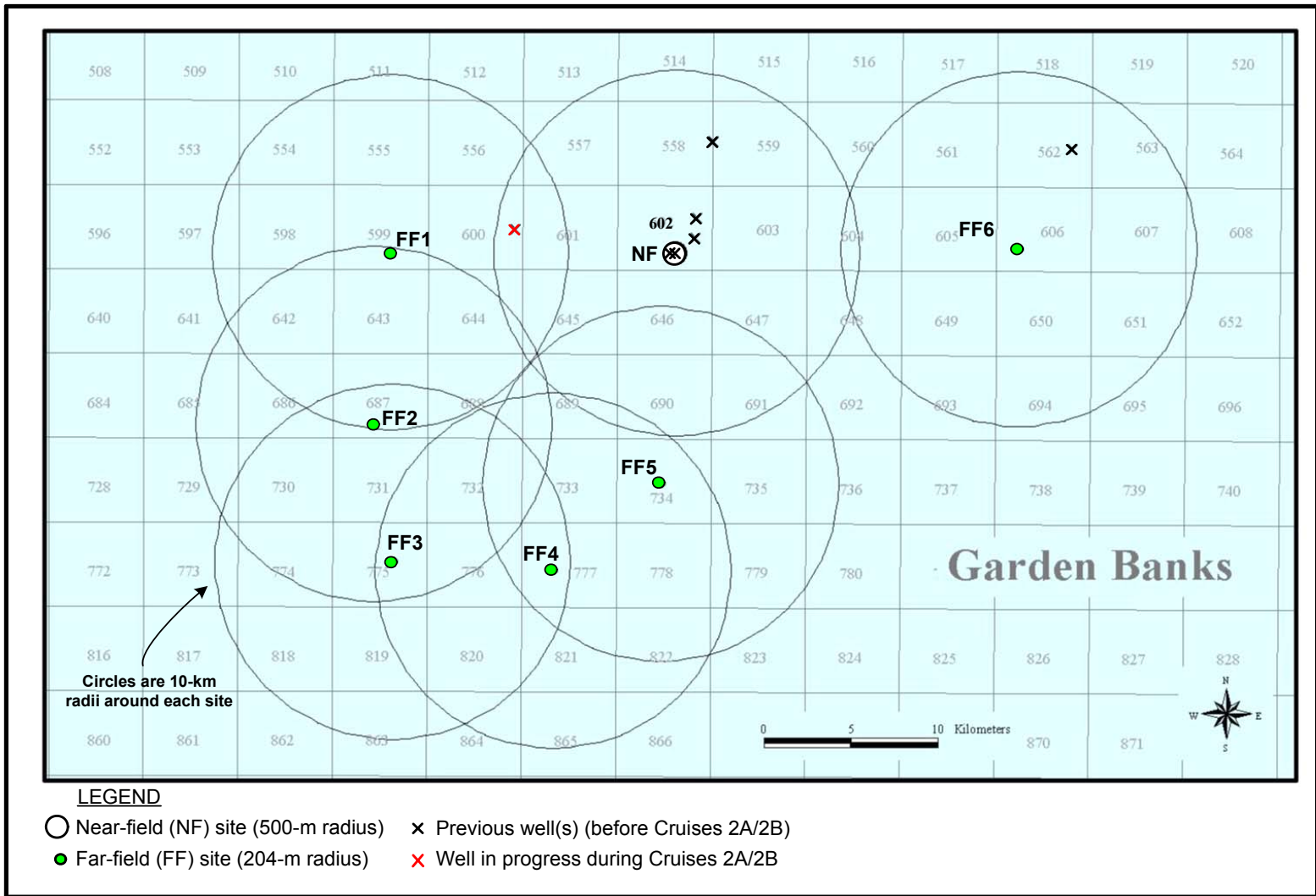


**Figure 3.11.** Location of blocks with previous wells in relation to Garden Banks Block 602 near-field (NF) and far-field (FF) sites.

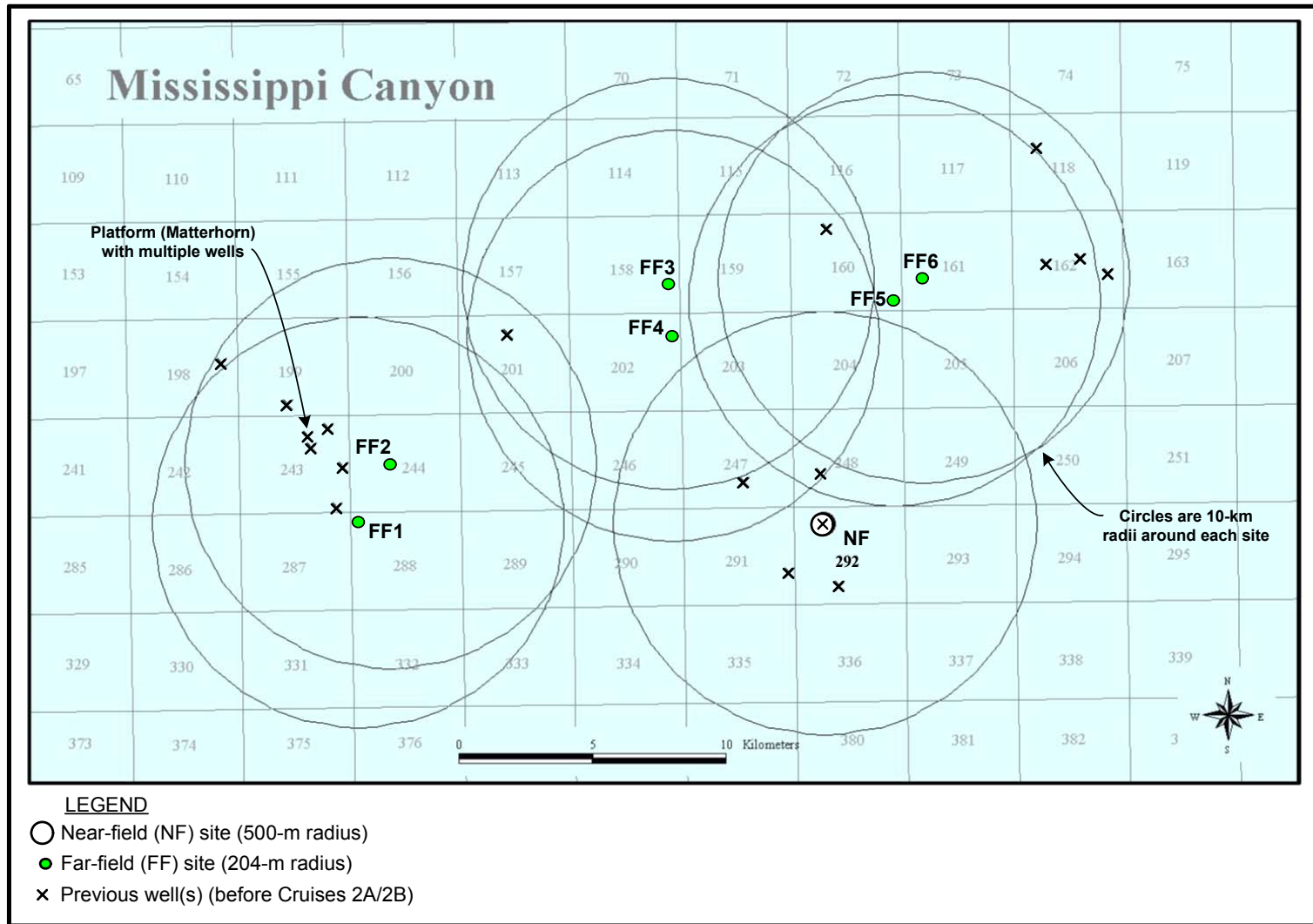


Figure 3.12. Location of blocks with previous wells in relation to Mississippi Canyon Block 292 near-field (NF) and far-field (FF) sites.

### 3.2.1 Viosca Knoll Block 916

All VK 916, far-field sites had previous drilling within 10 km, and two of them (FF1 and FF2) had previous wells in the same block (**Figure 3.9**).

Site FF1 had the largest number of previous wells, 63 within 10 km and 4 wells within 3 km. The nearest wells were about 1.9 km to the west in the same lease block (VK 957); these four wells were drilled between January and July 1989. There also were 40 wells drilled between February 1987 and December 2001 at the Ram-Powell location in adjacent block VK 956, about 4.7 km west of FF1.

Site FF2 had 41 previous wells within 10 km and 4 wells within 3 km. The nearest were four wells approximately 2.6 km away in VK 915. These were drilled between March and May 2002, just before Cruises 3A and 3B.

Sites FF3, FF4, FF5, and FF6 had no previous wells within 3 km. However, there were numerous previous wells between 5 and 10 km away, most of these at a single location (Petronius platform) in VK 786.

### 3.2.2 Garden Banks Block 516

At the time of the post-drilling survey (Cruise 2B, July 2001), no previous wells had been drilled in any of the blocks where GB 516 far-field sites were located. However, all of the far-field sites had one or more previous wells within 10 km (**Figure 3.10**).

Three blocks adjacent to FF1 had previous wells. The closest was about 4.6 km ESE in GB 559, where six wells were drilled between February 1999 and October 2000. In June 1999, one well was drilled in GB 515, about 7.1 km to the ENE. Also, 11 wells were drilled between September 1995 and January 2001 in GB 602, approximately 7 to 8.5 km SSE of FF1. In addition, drilling was ongoing during Cruise 2B at a single wellsite GB 600, about 8.8 km SW of FF1. Drilling occurred between 24 June and 13 August 2001 (Cruise 2B was conducted from 8 to 25 July 2001).

For sites FF2 through FF6, there were no previous wells in adjacent blocks. However, each site was within 10 km of at least one previous well in GB 386, 387, or 562. The nearest wells were generally 7.5 to 8.9 km away and were drilled between June 1997 and March 1999.

### 3.2.3 Garden Banks Block 602

At the time of Cruise 2B (July 2001), no previous wells had been drilled in any of the blocks where GB 602 far-field sites were located (**Figure 3.11**). There were no previous wells within 10 km of FF2, FF3, FF4, or FF5.

There was one well being drilled within 10 km of the FF1 site at the time of Cruise 2B. This exploration well in GB 600 is about 6.5 km ENE of FF1. Drilling occurred between 24 June and 13 August 2001 (Cruise 2B was conducted from 8 to 25 July 2001).

There was one previous well within 10 km of the FF6 site. This exploration well was drilled between 14 August and 19 September 2000 in Block 562, about 6.3 km NNE of FF6.

### **3.2.4 Mississippi Canyon Block 292**

All of the MC 292 far-field sites had previous wells within 10 km (**Figure 3.12**). FF1 and FF2 had the largest number of previous wells, with 12 or 13 within 10 km. The closest to FF1 was a single well 1.1 km away in MC 243, drilled in September-October 1994. The closest to FF2 was a single well 2 km away in MC 243, drilled in August-September 1999.

For FF3 and FF4, the nearest well was over 7 km away. For FF5 and FF6, the nearest previous well was nearly 5 km away. The nearest wells to each of these sites were drilled in the late 1980's (January 1988-November 1989).

### **3.2.5 Summary and Preliminary Evaluation**

To avoid impacts of previous drilling, two factors to consider are anchor radius and areal extent of drilling mud and cuttings deposits. In this water depth, anchoring (including dragging of chains and cables) can affect specific locations within about 3 km around each drilling site. Planned anchoring locations usually are presented in exploration plans or development plans submitted to MMS, but actual locations may vary. Although the chances of randomly collecting a sample (e.g., box core) within an anchor scar are small, it would be wise to place reference sites at least 3 km from any previous drillsite.

With respect to drilling discharges, the main concern is to avoid cuttings deposits from previous wells. In this water depth, drilling mud discharges (except for those released at the wellbore during jetting) are likely to be thinly dispersed over many kilometers or tens of kilometers (Brandsma 1990). While it is impossible to avoid potential exposure to mud particles, accumulations beyond a few hundred meters from the wellsite presumably would be miniscule and undetectable by the most sensitive measures.

In contrast, because of the hydrophobic nature of the base fluid, SBM cuttings tend to clump together and settle rapidly to the seafloor (Brandsma 1996; Neff et al. 2000). Previous observations indicate that most SBM cuttings are deposited within about 250 m of the drillsite, both on the continental shelf and upper slope (Continental Shelf Associates, Inc. 2004). During this study, SBF concentrations at most stations near the 500-m near-field radius were low, but one discretionary station approximately 1 km from the GB 602 wellsites showed elevated SBF concentrations (see *Chapter 15*).

WBM cuttings have a wider range of settling velocities, and in theory, some particles may be carried tens of kilometers before settling to the bottom (Brandsma 1990). Observations during this study indicate geophysically mappable deposits (interpreted as cuttings) extended for several hundred meters to about 1 km from the site center (see *Chapter 4*).

Far-field sites located at least 3 km from previous wellsites are likely to avoid previous anchoring impacts. With respect to avoiding cuttings and drilling mud deposits, farther is better, but

certainly a far-field site within (or close to) 1 km of any previous wellsite would be suspect. Based on this discussion, the far-field sites are rated as follows in **Table 3.10**:

- Excellent – no previous wells within 10 km
- Good – no previous wells within 3 km, but one or more between 3 km and 10 km away
- Fair – previous well(s) between 1.5 km and 3 km away
- Poor – previous well(s) within 1.5 km

Based on this rating system, all of the far-field sites were rated as “excellent” or “good” with the following exceptions (**Table 3.10**):

- VK 916, FF1 – rated fair; 4 wells were drilled only 1.9 km away, but the drilling occurred more than 10 years ago. This site also had a very large number of wells within 10 km (63).
- VK 916, FF2 – rated fair, with 4 recent wells (March-May 2002) located 2.6 km away and a total of 41 wells within 10 km.
- MC 292, FF1 – rated poor, with one well 1.1 km away (September-October 1994) and another 2.7 km away (August-September 1999).
- MC 292, FF2 – rated fair, with the nearest well 2 km away (August-September 1999).

The adequacy of far-field sites is discussed further in *Chapter 15*, which includes a statistical evaluation of barium and SBF concentrations. Briefly, the analysis indicates there are some differences among far-field sites, some of which may reflect the effects of previous drilling. However, barium and SBF concentrations at the far-field sites are orders of magnitude lower than most values measured in the near-field, and differences among far-field sites are small relative to the variations in the near-field. For this reason, all far-field sites are retained for analysis in subsequent chapters.

## Chapter 4 Geophysical Characterization of Study Sites

*Harry H. Roberts  
Louisiana State University*

---

### 4.1 INTRODUCTION AND GEOLOGIC FRAMEWORK

This study focuses on the effects of oil and gas exploration and development at four selected sites on the continental slope of the northern Gulf of Mexico. The study sites are located in the world's most mature deepwater hydrocarbon exploration-production province. The continental slope offshore of the northern Gulf states is also perhaps the most geologically complex continental slope in today's oceans. The shaded relief map of **Figure 4.1** reflects the complexity of the slope's surface topography, a reflection of an equally complex subsurface geology.

Our present knowledge base for both the surface and subsurface geology of the northern Gulf's continental slope is largely a product of the search for and production of oil and gas. Since the late 1970's, when the exploration front moved to the upper continental slope, an enormous database of 3D-seismic, bathymetry, high resolution geohazard-scale acoustic and sediment core data have been compiled for deep water. These data sets confirm the geologic complexity of this province and support the idea that the slope's geologic configuration derives from the interdependency of terrigenous clastic sedimentation and salt tectonics (Humphries 1978). Research conducted in the early and mid-1990's emphasizes that variations in sedimentation rate affect the growth of salt bodies. Salt deformation, in turn, exerts a strong control on the locations and orientations of intraslope minibasins and associated fault networks (Talbot 1993; Vendeville and Jackson 1993; Weimer et al. 1994; Diegel et al. 1995; Rowan 1995; Rowan et al. 1995).

The northern Gulf of Mexico continental slope covers an area of over 193,000 mi<sup>2</sup> and is defined by the shelf edge at roughly the 200-m isobath to the upper limit of the continental rise at an approximate depth of 2,600 to 2,750 m (Bouma and Roberts 1990). The most complex part of the basin's continental slope occurs opposite east Texas and Louisiana. In this province, regional topography is dominated by domes or knolls associated with salt in the shallow subsurface and intervening basins, as discussed above and is illustrated by **Figure 4.1**. Seafloor slopes associated with these regional-scale features range from less than 1° on the dome tops and along the basin floors to over 20° on the side of domes and on basin flanks. Observable on this regional topography of domes and basins are smaller-scale geologic features that are associated with high variability in sediment type and local relief. Near-surface geology and topography of the upper continental slope in the northern Gulf of Mexico is highly influenced by cyclic episodes of shelf edge progradation and sediment input to deep water. In addition to filling mini-basins and mobilizing salt, sediment loading during periods of lowered sea level activates faults. Faulting creates abrupt relief and steep slopes (some near vertical) on the modern ocean floor of the slope. Faults function as avenues of transport for fluids and gases to or near the modern seafloor. The process of fluid and gas expulsion has an important impact on the present surficial geology of the slope. Expulsion of large volumes of fluidized sediment results in the formation of mud volcanoes and mud flows (Neurauter and Roberts 1992; Kohl and Roberts 1994). Seepage and venting results in the development of highly populated communities of chemosynthetic organisms (Kennicutt et al. 1985), creation of brine pools and pockmarks (MacDonald et al. 1990), gas hydrate mound formation (Brooks et al. 1985), and precipitation of carbonates and other exotic minerals to form hardgrounds, chimneys, and mound-like buildups (Roberts and Aharon 1994).

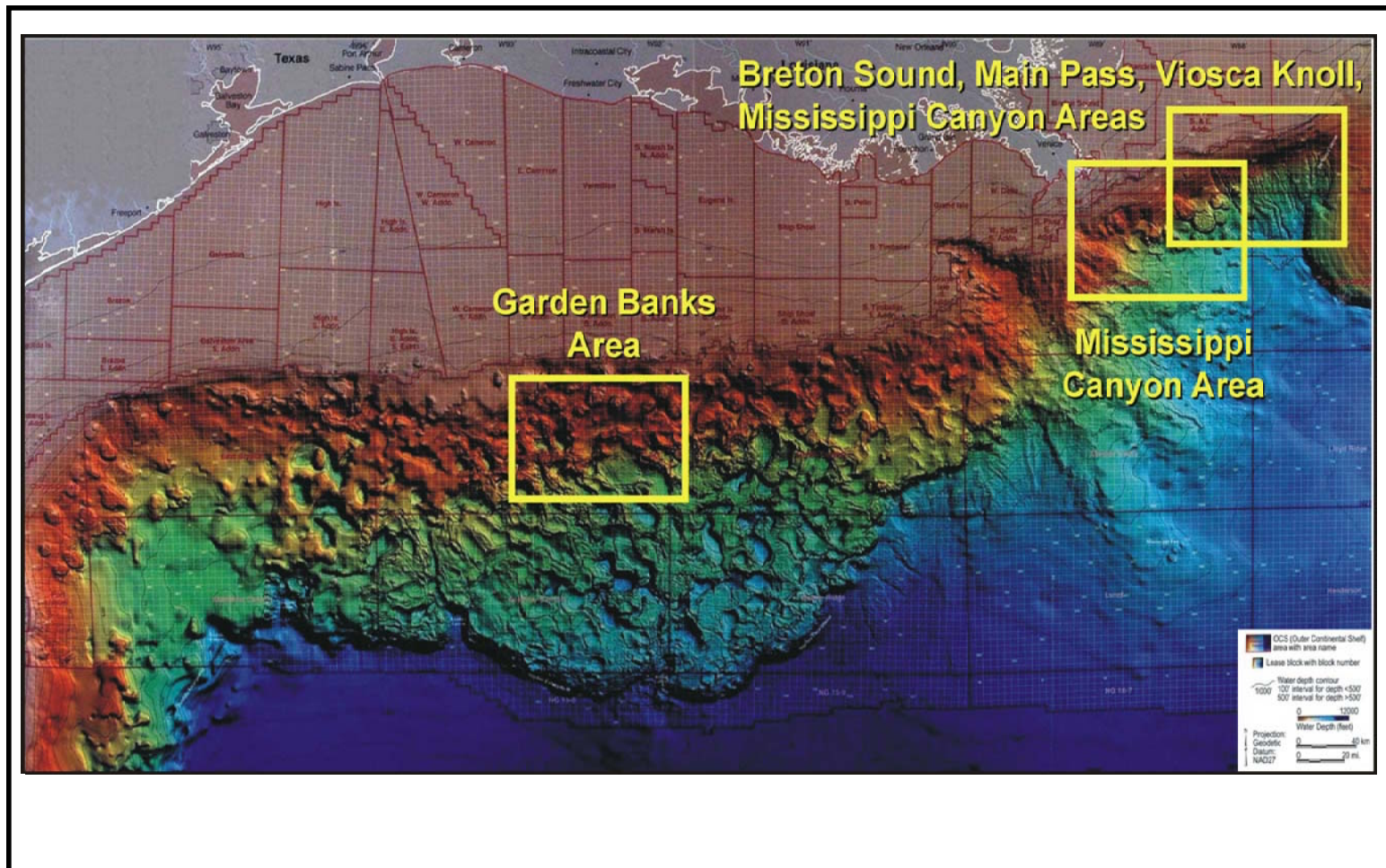


**Figure 4.1.** A computer enhanced shaded relief map of the northern Gulf of Mexico continental slope. Multibeam bathymetry data were the primary input data for generating this view of the slope's complex surface topography. Over time, this complexity is a product of the interaction of massive volumes of sediment input to the slope during periods of lowered sea level and associated modification of underlying salt masses. The three general areas of data collection for this study are shown.



These various seafloor responses are all products of vertical flux of hydrocarbon gases, crude oil, and other formation fluids migrating to the ocean floor along faults.

The Mississippi River, which feeds a delta that has nearly prograded to the shelf edge, makes a comparatively small impact on modern slope sedimentation. In response to a lack of siliciclastic sediment input during the present highstand of sea level, a thin hemipelagic sediment unit drapes slope topography. These sediments are composed of numerous calcareous pelagic foraminifera tests in a matrix of hemipelagic clay. When studied carefully using X-ray radiography, sediments of the hemipelagic drape have a massive character, rarely display bedding, are highly bioturbated, and frequently show the effects of early diagenesis.

On the upper continental slope, the hemipelagic drape is frequently missing from the tops of regional domes and knolls. Sedimentologists with experience in the Gulf of Mexico consider this relationship a product of dome top erosion by Loop Current intrusions directly on the slope or the impact of Loop Current eddies that transit from east to west along the shelf-slope break. The Loop Current can impact the seafloor to depths of nearly 1,000 m (Hamilton 1990). Dome tops on the upper continental slope within this depth range frequently exhibit seafloor erosion exposing older sediments and frequently deformed sediments. Both slumping due to oversteepening on salt dome flanks and faulting associated with salt movement frequently cause dome flank and dome top sediment deformation.

In contrast to seafloor covered with a hemipelagic drape deposit, there are vast areas of slope impacted by fluid and gas expulsion. These areas appear much more complex both visually and on geophysical records.

## 4.2 DATA COLLECTION SCHEDULE AND INSTRUMENTATION

The data collection plan as originally drafted included the acquisition of geophysical data (side-scan sonar, subbottom profiles, and bathymetry) from four sites within the upper continental slope province of the northern Gulf of Mexico. As initially planned, these data sets were to be collected with a high resolution deep-tow system. Delays associated with weather and instrumentation problems mandated a rethinking of the data collection schedule and equipment to be focused on the data collection program. Ultimately, one exploration site, VK 916, was completed with the deep-tow system between November 2000 and January 2001 (Cruise 1A) and resurveyed with different instrumentation in May 2002 (Cruise 3A). The other three sites – MC 292, GB 602, and GB 516 were surveyed in June-July 2001 (Cruise 2A). **Table 4.1** summarizes the dates of data collection, locations, and types of data collection systems used. **Figure 4.1** illustrates the general areas of the continental slope where specific sites were surveyed.

The pre-drilling survey at VK 916 (Cruise 1A) was the only one conducted for this project with the deep-tow system, which involved two boats. The data collection systems in the deep-tow fish included (1) a dual frequency EdgeTech side-scan sonar that operated at center frequencies of 120 kHz and 420 kHz, (2) an EdgeTech chirp subbottom profiler with a frequency bandwidth of 2 to 10 kHz, and (3) a deepwater precision depth sensor. An electro-hydraulic winch with approximately 6,400 m of cable controlled the depth of the fish above the bottom.

**Table 4.1.** Geophysical surveys.

Cruise	Dates	Location	Survey Timing	Equipment <sup>a</sup>
1A	11-12 Nov. 2000	VK 916	Pre-drilling	Deep-tow
	29-30 Nov. 2000	VK 916	Pre-drilling	Deep-tow
	6 Dec. 2000	VK 916	Pre-drilling	Deep-tow
	9-10 Dec. 2000	VK 916	Pre-drilling	Deep-tow
	30 Dec. 2000	VK 916	Pre-drilling	Deep-tow (fathometer only)
	1 Jan. 2001	VK 916	Pre-drilling	Deep-tow
2A	25-29 June 2001	MC 292	Post-drilling	AUV
	2-4 July 2001	GB 602	Post-drilling	AUV
	5-7 July 2001	GB 516	Post-drilling	AUV
3A	16-18 May 2002	VK 916	Post-drilling	AUV

<sup>a</sup> Deep-tow (two boats): EdgeTech side-scan sonar, EdgeTech chirp subbottom profiler, Odom Hydrographic Systems, Inc. deep-water echotrac (single-beam), and cesium magnetometer. AUV (HUGIN 3000): EdgeTech side-scan sonar, EdgeTech chirp subbottom profiler, and Simrad EM2000 swath bathymetry.

AUV = autonomous underwater vehicle; GB = Garden Banks; MC = Mississippi Canyon; VK = Viosca Knoll.

The initial deep-tow survey at VK 916 was plagued by rough weather and sea state conditions, equipment failure, and persistent electronic problems with the towfish, resulting in lengthy, costly delays (see *Appendix C1* for details). Therefore, it was decided that data quality would be better and data collection schedules could be met more efficiently for other sites using the C&C Technologies AUV, the HUGIN 3000. The post-exploration survey of VK 916 (Cruise 3A) also used the AUV (**Table 4.1**).

**Figure 4.2** illustrates the working configuration of the HUGIN 3000 AUV with the M/V RIG SUPPORTER. The HUGIN is an untethered survey vehicle designed to collect high resolution geophysical data in deep water (to about 2,700 m). Data collection systems include (1) a Simrad EM 2000 swath bathymetry system, (2) an EdgeTech side-scan sonar, and (3) an EdgeTech chirp subbottom profiler. The swath bathymetry system collects soundings under the AUV in a 200-m swath composed of up to 111 individual beams. A precision depth sensor on the AUV provides an accurate depth of the fish above the bottom. Once the data are downloaded from the AUV data storage drives, bathymetric data are processed using C&C Technologies software, and maps are produced. The EdgeTech side-scan sonar has proved to be a reliable and high resolution source of seafloor data. This side-scan simultaneously transmits two linearly swept frequency modulated pulses centered at two frequencies, 120 kHz and 410 kHz. In this project, survey lines were set up so that at 120-kHz frequency, swaths would overlap approximately 20%. This configuration resulted in continuous coverage of the study area. Mosaics of the seafloor were constructed. The limited high resolution lines were processed at the 410-kHz frequency. Data processing and production of hard copy products can be carried out aboard the mother ship. Subbottom data were acquired with the EdgeTech chirp sonar subbottom profiler, which transmits pulses that are generated in the frequency range of 2 to 8 kHz. This system provides extremely high resolution data on near seafloor stratigraphy and is very reliable. For this project, the chirp subbottom profiler provided valuable subsurface information when used in conjunction with side-scan sonar data for interpretation of seafloor features and sediment distribution patterns.

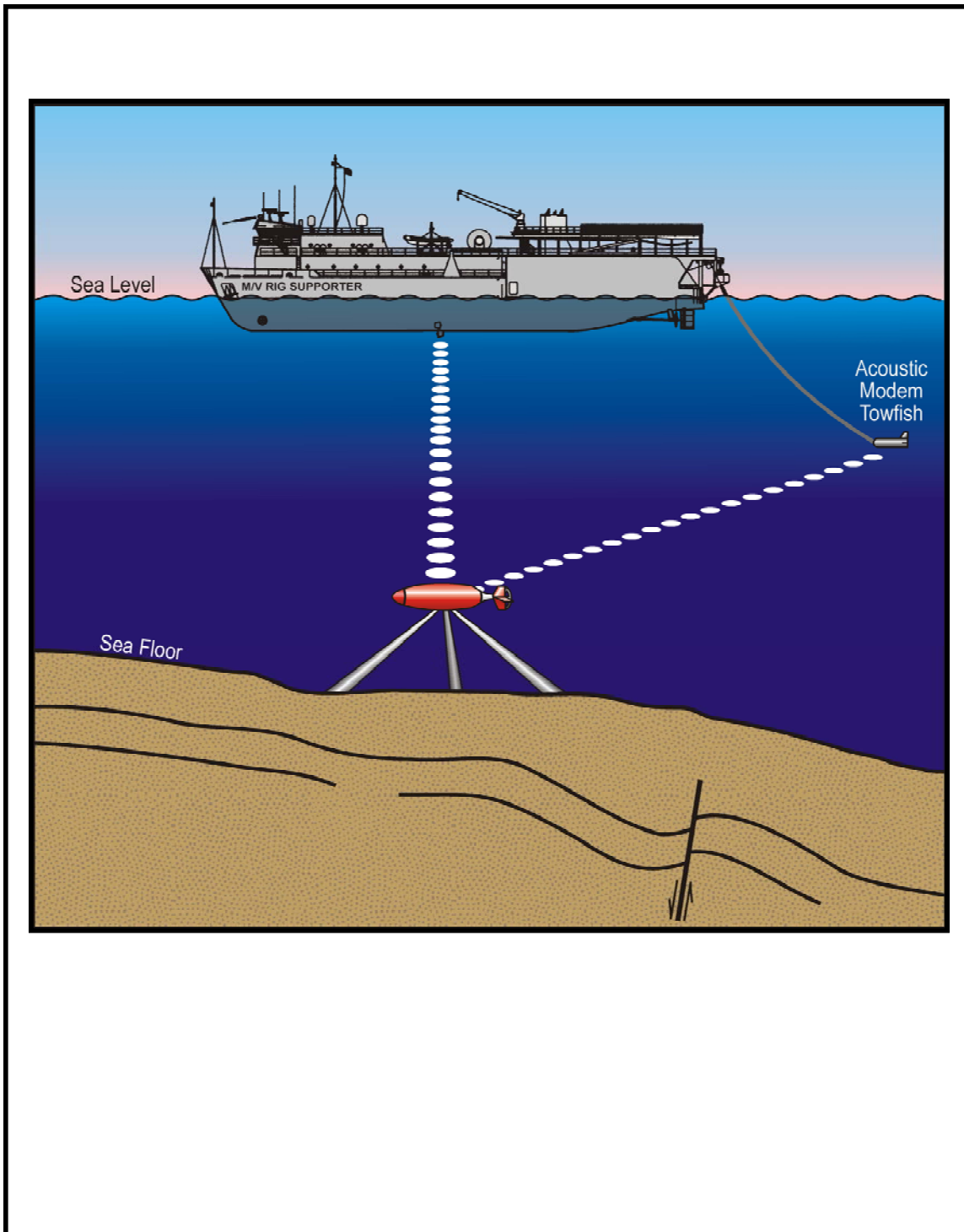


**Figure 4.2.** Working configuration of the HUGIN 3000 autonomous underwater vehicle showing the “free-swimming” HUGIN collecting data from a predetermined height above the seafloor. The HUGIN remains in constant communication with the mother ship through acoustic links.

Data transmission is accomplished by using three transponders: (1) HiPAP (High Precision Acoustic Positioning), (2) ACL (Acoustic Command Link), and (3) ADL (Acoustic Data Link). The AUV is powered by an aluminum-oxygen fuel cell that sustains continuous operation for nearly 2 days before a fuel cell change.

The AUV is computer-controlled. Two titanium spheres house three computers, which control navigation, data collection/processing, and system status. Dual 50-gigabyte data storage drives manage the high rate of digital data collection. The mother ship is in constant contact with the AUV through three top-side computers. All sensors are constantly monitored, and quality control of data acquisition is accomplished through transmission of limited data sets by way of an acoustic link. A DGPS provides the mother ship positions while AUV positions are calculated using ultra short baseline acoustics, inertial navigation, and Doppler velocity log. Other instruments used to help operate the AUV are (1) a precision depth sensor, (2) an altimeter, (3) an acoustic Doppler log, and (4) a salinity/temperature probe to generate data for calculating sound velocity in the water column. The vehicle is capable of transmitting data to the mother ship for quality control purposes through an acoustic link.

### **4.3 VIOSCA KNOLL BLOCK 916 – EXPLORATION SITE**

#### **4.3.1 Introduction**

The Viosca Knoll lease area is located east of the modern lobe of the Mississippi River delta (**Figure 4.1**). The shelf edge forms the upper boundary of this area. Most of the Viosca Knoll lease blocks fall within upper continental slope water depths. However, the southeast corner of the lease area extends into mid-slope depths. **Figure 4.3** shows the approximate location of the wellsite in the northeast corner of VK 916. This area of the slope is dominated by updip lobate protrusions at the shelf edge and distinct channel-levee systems that originate near the shelf edge and cross the entire slope, where they terminate on the deep Gulf of Mexico basin floor at a water depth of approximately 2,450 m. These channel-levee systems represent conduits for bypassing sediment from the shelf edge at periods of lowered sea level during the Pleistocene. The channel-levee systems can be linked to shelf edge deltas, which form the compensationally stacked protrusions that occur at the shelf-slope break east of the modern Mississippi delta to the head of DeSoto Canyon.

The VK 916 site is located on the western flank of a well-defined channel-levee system. In addition to these sediment by-pass conduits, the Viosca Knoll lease area, as well as the adjacent northern part of the Mississippi Canyon lease area, are regions of the slope that display distinct surface topography related to the occurrence of salt masses in the shallow subsurface.

#### **4.3.2 Data Quality for the Pre-Drilling Survey**

As **Table 4.1** documents, data collection at VK 916 started in November 2000 using a deep-tow system for collecting high resolution acoustic data (bathymetry, side-scan sonar, and chirp sonar). The pre-drilling site survey at VK 916 (Cruise 1A) was accomplished between November 2000 and January 2001. Data products for the pre-drilling survey are given in *Appendix C1*.

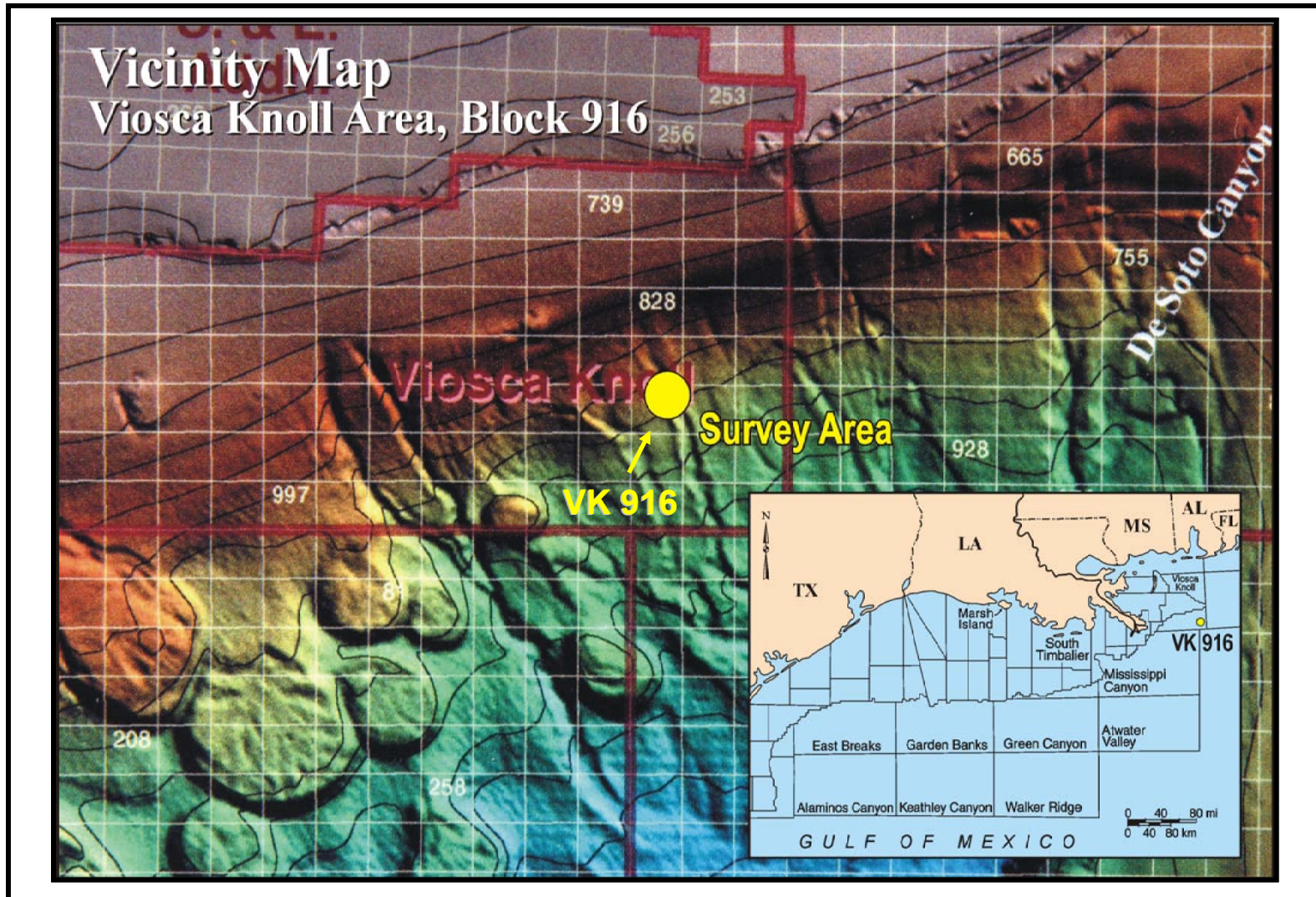


**Figure 4.3.** Location map of Viosca Knoll (VK) Block 916. Note that on the computer enhanced multibeam bathymetry map, VK 916 occurs on the western flank of a channel-levee system that starts just below the shelf-slope break.

Weather and instrumentation problems, including loss of major instrumentation components, affected the deep-tow survey throughout the November 2000 to January 2001 data collection period. Despite substantial difficulties, useable data sets were generated. Two data sets are very important to the objectives and goals of this research program: side-scan sonar mosaics and high resolution chirp sonar subbottom profiles. The side-scan data were considered to be fair. A problem that manifested itself as banding appeared on the record up to 50 m from the nadir, or survey track line. The records were still useable, and some of the banding was removed during processing.

**Figure 4.4** is an example of the chirp sonar subbottom data acquired near the proposed wellsite in VK 916. Chirp sonar subbottom profiles were considered of good quality even though some of the first records collected were noisy. The noise problem was found to be in an electronic circuit and was eventually corrected. Another problem resulted from flying the deep-tow fish less than 25 m over the bottom. When closer to the bottom, part of the record was eliminated. So, the fish was kept above this critical height.

#### 4.3.3 Site Characterization: Pre-Drilling

Data products from the pre-drilling survey (Cruise 1A) are provided in *Appendix C1*. The bathymetry of the study area clearly shows the channel-like feature that trends roughly northwest-southeast through the eastern sector of VK 916. At the proposed wellsite in the northeastern part of the block, water depths are approximately 1,128 m, shallowing to the north and deepening to the south. The side-scan sonar data indicate no disturbances on the seafloor in the vicinity of the proposed wellsite, and as discussed previously, subbottom profiles near the wellsite and across the study area in general describe a hemipelagic sediment drape over the seafloor throughout the area of interest. These surficial sediments exhibit no surface irregularity or significant amplitude changes within the area around the proposed wellsite. Undisturbed seafloor is the interpretation of this region of VK 916 as determined from evaluation of the geophysical data sets.

#### 4.3.4 Data Quality for the Post-Drilling Survey

The post-drilling survey of VK 916 (Cruise 3A) was conducted 16-18 May 2002 using the AUV. The data collection sensors associated with the AUV and its basic operations are discussed in a previous section of this chapter. All data products from the post-exploration AUV survey are provided in *Appendix C2*.

Quality of side-scan sonar, chirp sonar subbottom profiles, and multibeam bathymetry from the AUV survey of the VK 916 study site was excellent. The high resolution multibeam bathymetry (see bathymetry map in *Appendix C2*) provides the necessary data to construct shaded relief images of the study area (**Figure 4.5**). Side-scan sonar data were collected over the entire study area (defined by a circle of 3,050-m radius from the wellsite) using the low frequency 120-kHz setting. A higher resolution data set was collected around the wellsite using the high frequency 410-kHz setting. Mosaics from both frequencies are included in *Appendix C2*. Both the 120-kHz and 410-kHz side-scan sonar records were of excellent quality. **Figure 4.6** illustrates a portion of the 410-kHz side-scan sonar mosaic centered on the wellsite. The chirp sonar subbottom profile records (e.g., **Figure 4.7**) also were of very high quality and were important in identifying areas of probable deposition of drilling mud and well cuttings on the modern seafloor.

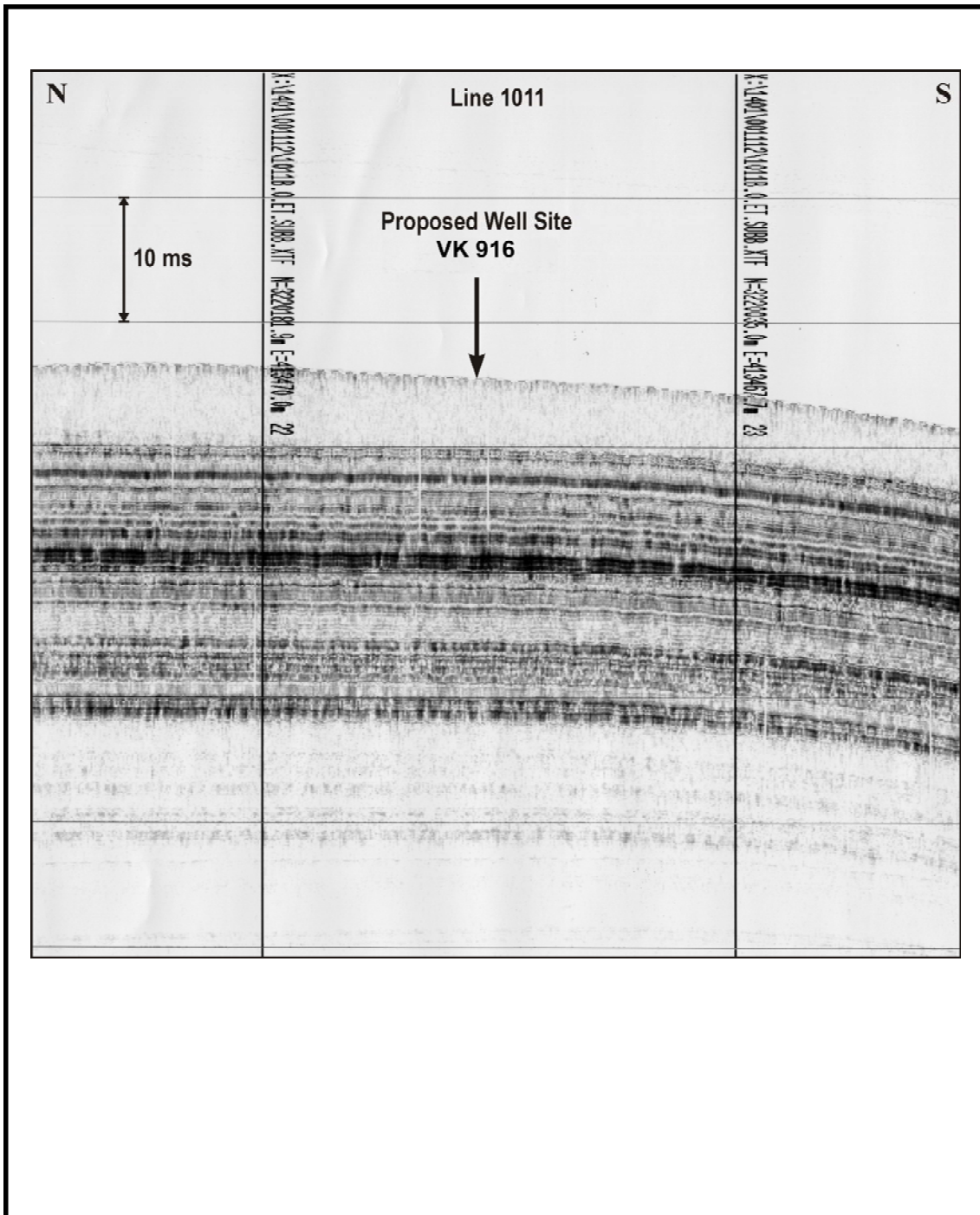


**Figure 4.4.** Chirp sonar subbottom profile collected during Cruise 1A (pre-drilling) on Survey Line 1011 approximately 50 m west of the proposed wellsite in Viosca Knoll (VK) Block 916. Note the well-defined hemipelagic drape (acoustically opaque surface unit) overlying closely spaced reflectors. Also, the uniform character of the seafloor reflector suggests no disturbance or foreign material in the area.

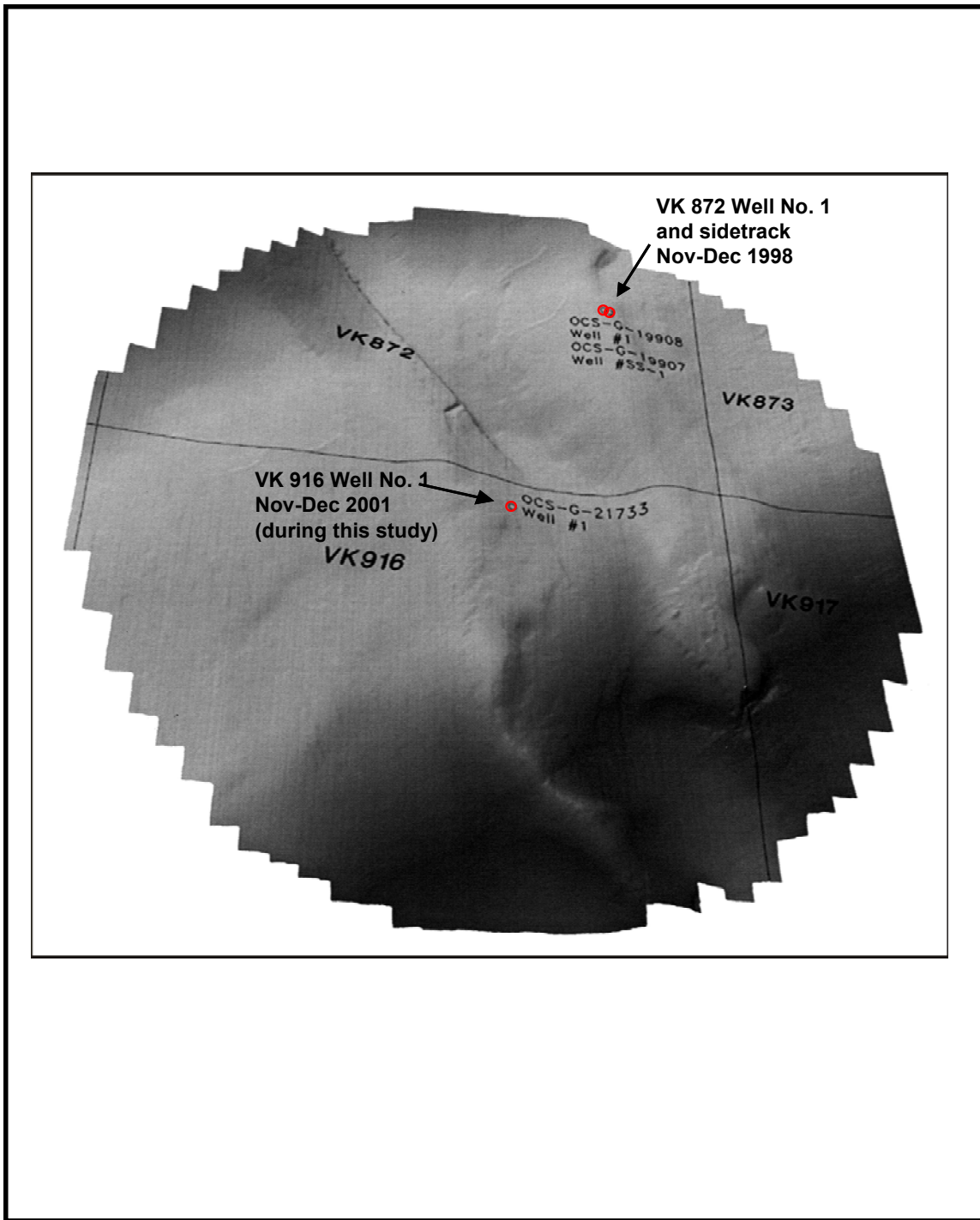


**Figure 4.5.** A shaded relief image of the Viosca Knoll (VK) 916 study area showing the location of the wellsite for VK 916 Well No. 1 with regard to the distinct channel-levee feature trending roughly northwest-southeast through the eastern part of the block. Note the previous wellsite about 2.3 km away in VK 872.



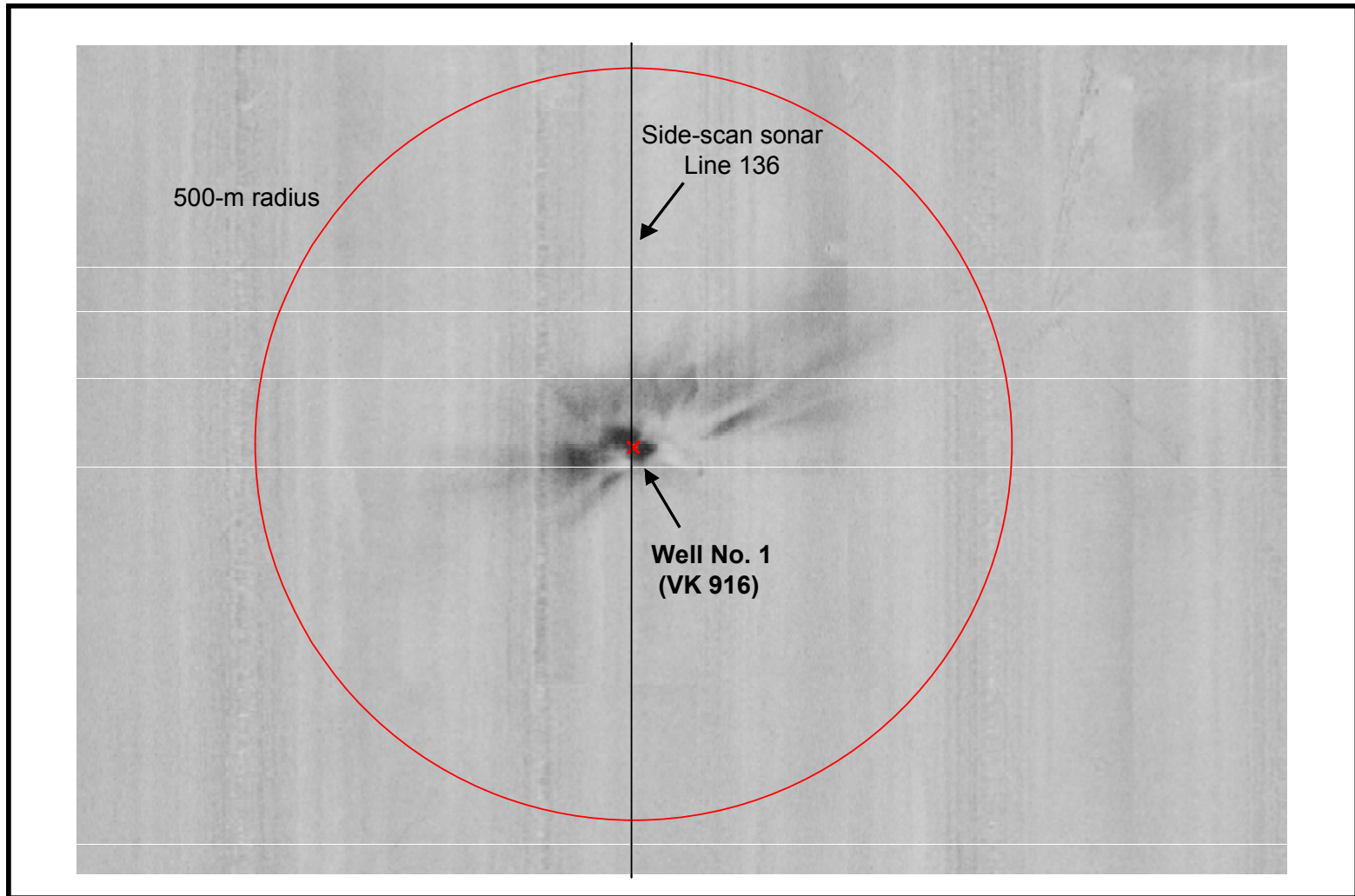


**Figure 4.6.** A sector of the side-scan sonar mosaic produced for the Viosca Knoll (VK) Block 916 area of interest. Note the highly reflective seafloor areas roughly radiating from the wellsite. See Figure 4.7 for a chirp subbottom profile along Line 136.

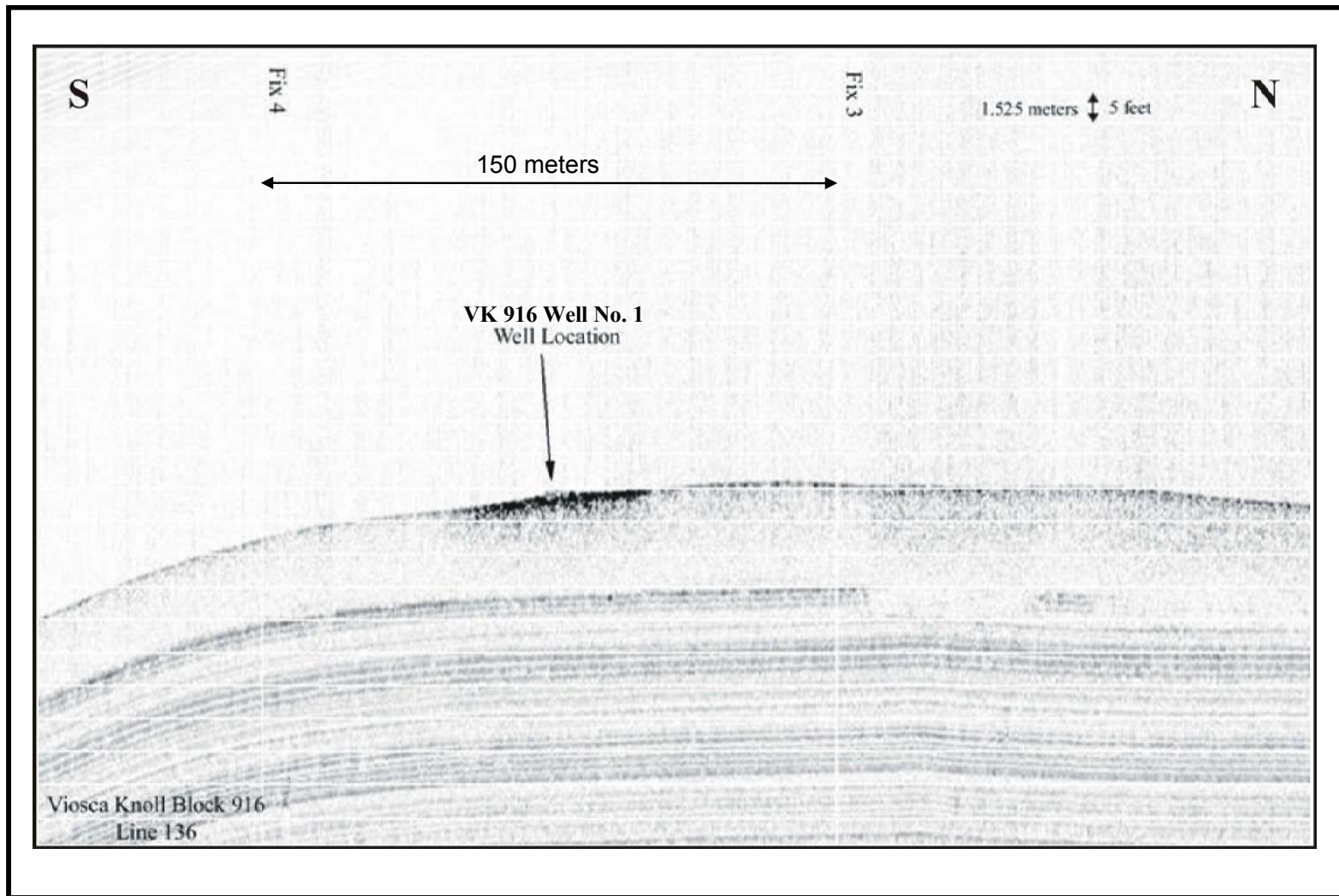


**Figure 4.7.** A section of a chirp sonar subbottom profile acquired along Line 136, which trends north-south across the Viosca Knoll (VK) Block 916 wellsite. Note the high surface reflectivity around the wellsite. This high amplitude response of the seafloor reflector is interpreted as high density drilling mud and cuttings from seafloor releases during well jetting.

#### 4.3.5 Site Characterization: Post-Drilling

On the post-drilling survey, the seafloor around the wellsite was considerably different on high resolution acoustic records than most of the surrounding seafloor (**Figures 4.6** and **4.7**). The chirp sonar subbottom profiles proved very important for identifying areas interpreted as having been impacted by drilling mud and well cuttings, both of which have a higher specific gravity than the surficial hemipelagic muds. Barite, a common component of drilling mud, has a specific gravity that ranges between 4.3 to 4.6, while calcite and aragonite, the many microfossil tests that comprise the hemipelagic sediment, have a specific gravity of 2.6 to 2.7. In addition, cuttings are derived from subsurface sediments that are much more compacted and therefore are denser than surface hemipelagic sediments that drape most of the northern Gulf continental slope. Consequently, these denser sediments, when deposited over hemipelagic sediments, create an acoustic impedance difference that translates into a higher amplitude reflection on subbottom profiler records, as can be clearly seen on **Figure 4.7**. When mapped from both surface reflectance on side-scan sonar and chirp sonar subbottom records, the zone of high amplitude surface response describes a northeast-southwest trending area shown in **Figure 4.8**. This zone is about 610 m in its longest dimension and averages about 250 m wide. The thickness of deposition was estimated to range from about 0 to 45 cm (see the Isopach Map in *Appendix C2*). The side-scan data also define two pockmarks on the seafloor near the drilling site and a number of drag marks related primarily to anchoring during the drilling operation. Subbottom data clearly define the channel of the channel-levee system discussed previously. On the Seafloor Investigation Map of *Appendix C2*, this channel-like feature is defined by mass movement and debris flow deposits because these types of deposits fill the channel.

**Figure 4.8** also shows that possible cuttings and anchor scars were evident from two previous wells in VK 872, about 8 km to the north/northeast of the VK 916 wellsite. These wells were drilled in November-December 1998, about 3.5 years prior to Cruise 3A. The side-scan sonar records also showed anchor scars associated with an older wellsite in VK 873 (drilled in March 1988, 14 years before Cruise 3A).

**Figure 4.9** shows an area of debris on the seafloor west-northwest of the drilling site. These sonar targets appear elongated and are probably pipes. These targets were not present in the data sets collected for the pre-drilling survey. In fact, the only targets on the side-scan sonar records of the pre-drilling survey were the pockmarks near the drilling site.

### 4.4 MISSISSIPPI CANYON BLOCK 292 – POST-DEVELOPMENT SITE

#### 4.4.1 Introduction

The MC 292 site is located on the upper continental slope east of Mississippi Canyon and southeast of the modern lobe of the Mississippi River delta (**Figure 4.1**). Water depths in the area of interest range from about 1,280 m in the southeastern part of the area to approximately 920 m in the northwestern sector (see bathymetry map in *Appendix C3*). The area around the wellsite has a water depth of approximately 1,034 m.

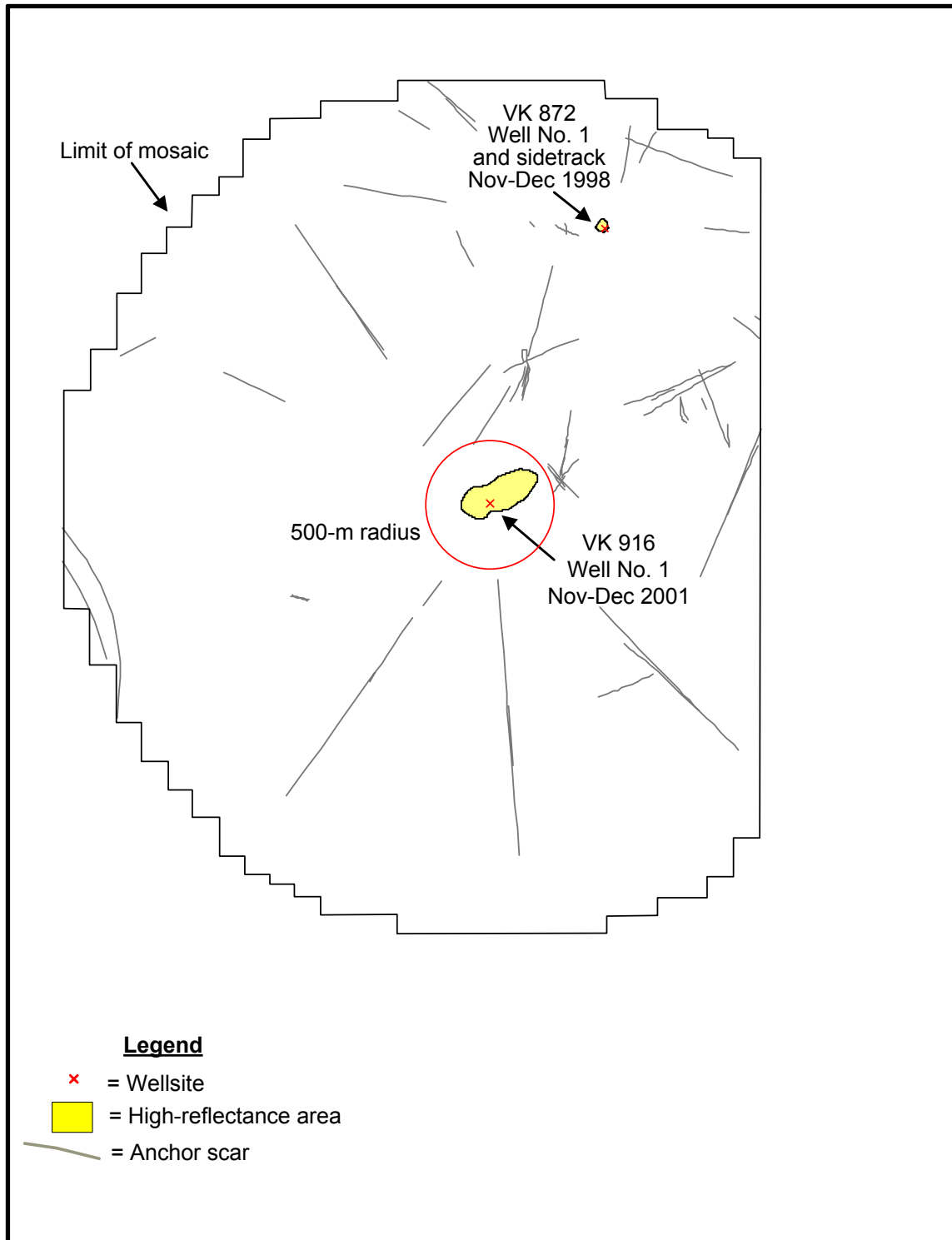


**Figure 4.8.** Map of cuttings and anchor scars around the Viosca Knoll (VK) Block 916 site based on the Cruise 3A geophysical survey (August 2002). High-reflectance areas are interpreted as possible cuttings.

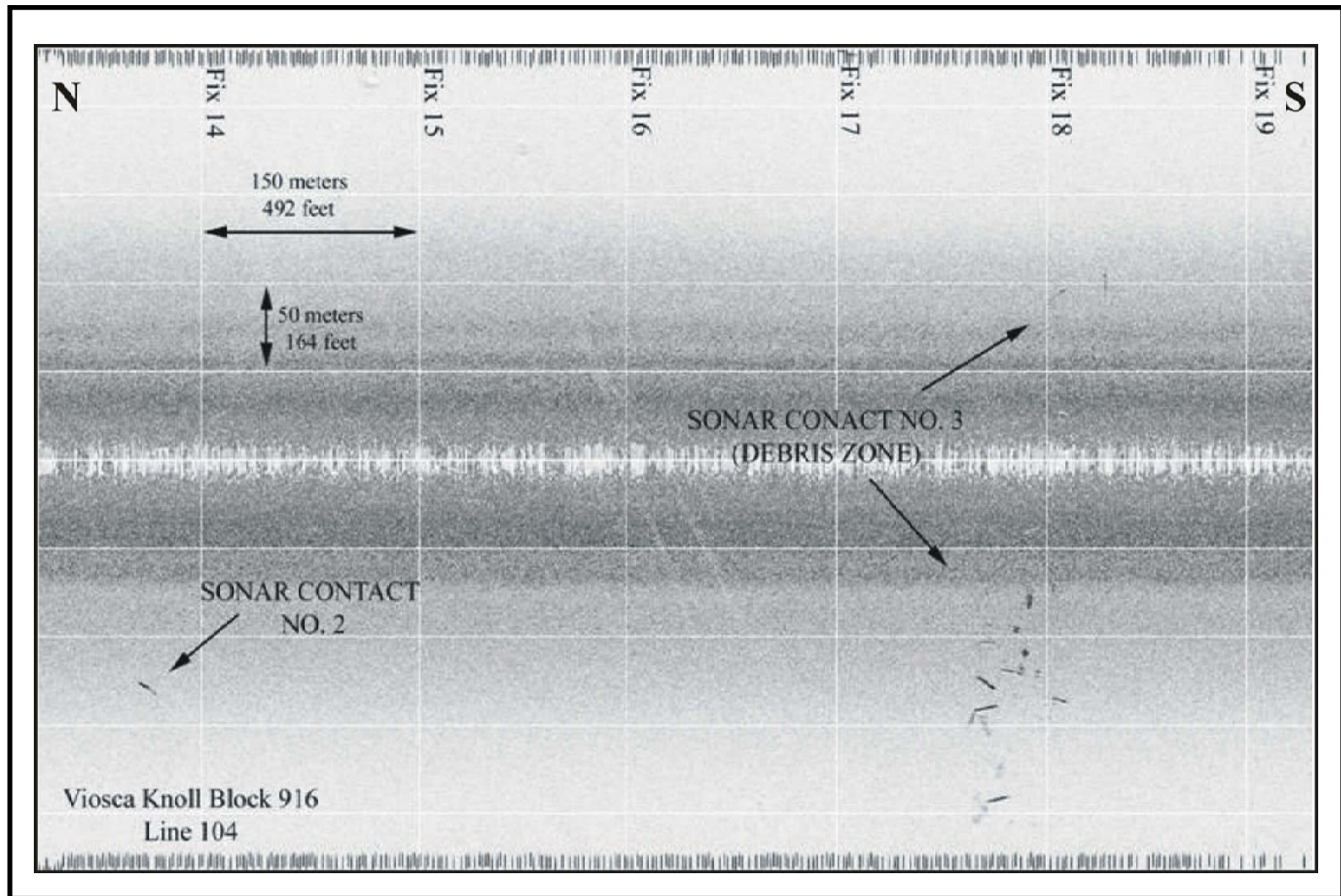


**Figure 4.9.** A portion of side-scan sonar Line 104 showing debris that appears to be pipe on the seafloor within the Viosca Knoll Block 916 study area.

The MC 292 site is located on the southeastern flank of a regional dome-like feature supported by a shallow subsurface salt mass (**Figure 4.10**). The slope gradient increases significantly on the flank and to the south of this structure. A canyon-like feature trending northwest-southeast along the eastern side of the dome may have functioned as a conduit (channel-levee system) for transporting shallow-water shelf edge sediments to deepwater depositional sites at some time in the past. However, subsequent salt movement appears to have blocked part of the channel, unlike more continuous counterparts to the east. This blockage probably resulted from the late Pleistocene sediment loading of the slope by updip shelf edge deltas derived from the Mobile and perhaps the Pascagoula rivers causing movement of shallow salt across the downslope trend of the channel-levee system.

Because of the dominant east-to-west surface currents in this part of the northern Gulf of Mexico, suspended sediments from the Mississippi River rarely impact the area of interest. Therefore, a persistent unit of hemipelagic sediments is draped across the topographic features of this part of the continental slope. However, because the Loop Current frequently impacts the shelf edge and upper slope east of the modern lobe of the Mississippi River delta, this hemipelagic drape is sometimes eroded on the tops and flanks of salt supported domes and knolls. **Figure 4.11** shows a high resolution chirp sonar subbottom profile segment (Line 319) south of the wellsites illustrating seafloor erosion along the southeastern flank of the salt-supported feature. The entire area of seafloor erosion mapped in MC 292 can be found on the Seafloor Investigation Map of *Appendix C3*. Trending in the same direction as the area of seafloor erosion (southwest-northeast) are a series of surface and near-surface faults mapped from the chirp sonar subbottom records. These faults are slightly to the south of the main zone of erosion and clearly follow the perimeter of the subsurface salt mass. No fluid and gas expulsion features could be found in association with the faulting.

#### **4.4.2 Data Quality**

The high resolution acoustic data collected by the AUV in support of the post-development survey of the MC 292 well area were of excellent quality. The multibeam bathymetric data produced a high quality map that details the dominant features of the seafloor. Combined with the high quality side-scan sonar images of the seafloor and the very high resolution chirp sonar subbottom profiles, these state-of-the-art data sets provided unmatched insight into the surface and near-surface geologic conditions of the study area. Map products are provided in *Appendix C3*.

#### **4.4.3 Site Characterization**

Both the low frequency (120 kHz) and high frequency (410 kHz) side-scan sonar images of the wellsites and surrounding areas show variations in surface backscatter strength and definable patterns of seafloor reflectance. **Figure 4.12** is a 120-kHz side-scan sonar image of the wellsite vicinity. Note the radial pattern of high backscatter reflectance (darker areas) and the zone of no or minimal reflectance (white area) that occurs southeast of the well cluster. These two areas are very different with regard to surface reflectivity and are interpreted to represent two types of drilling-related deposition.

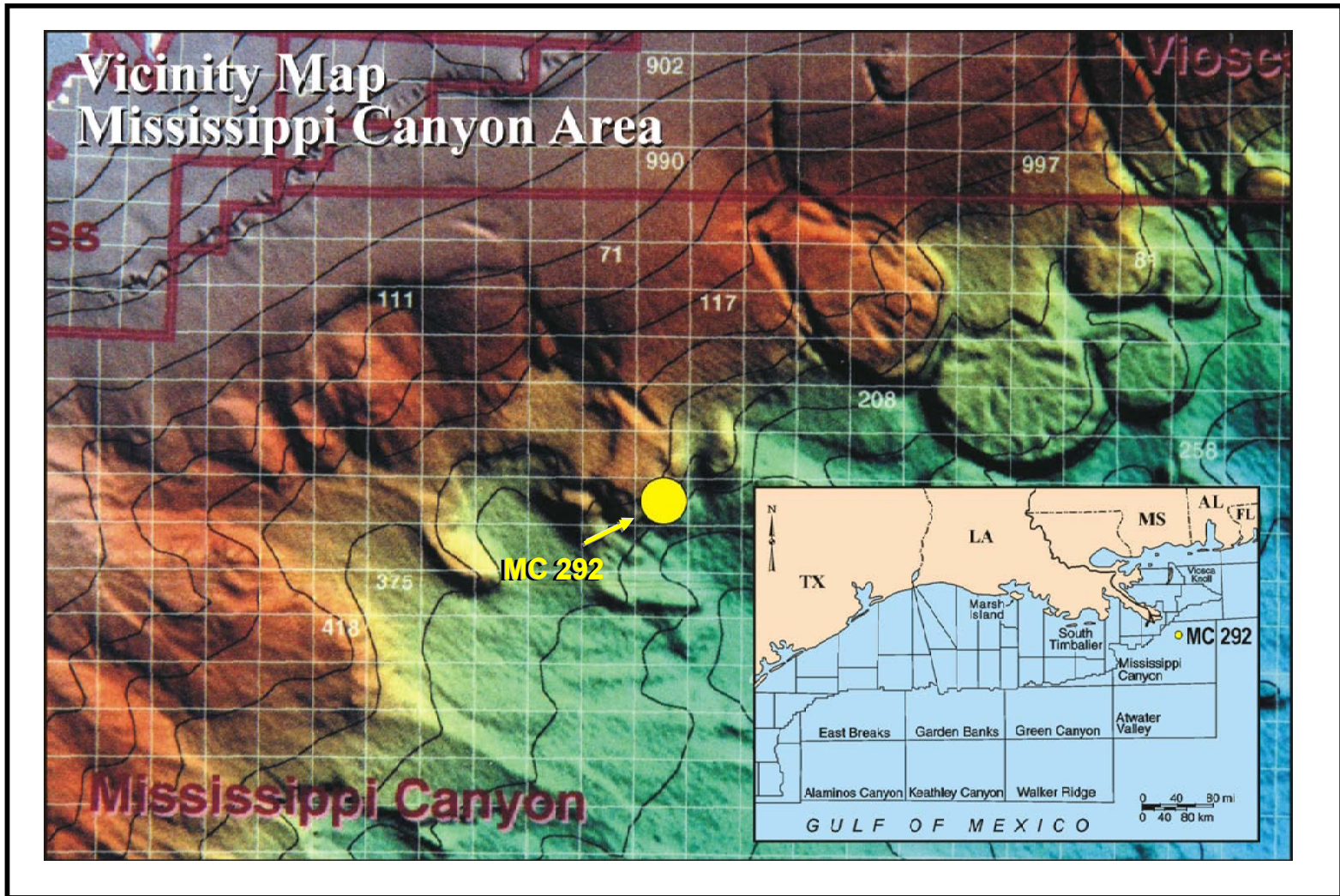


**Figure 4.10.** A shaded relief image of the Mississippi Canyon (MC) Block 292 study area showing the approximate location of the study site on the southeastern flank of a distinct dome-like feature produced by a salt mass in the shallow subsurface. Note the channel-like feature along the eastern side of this dome.

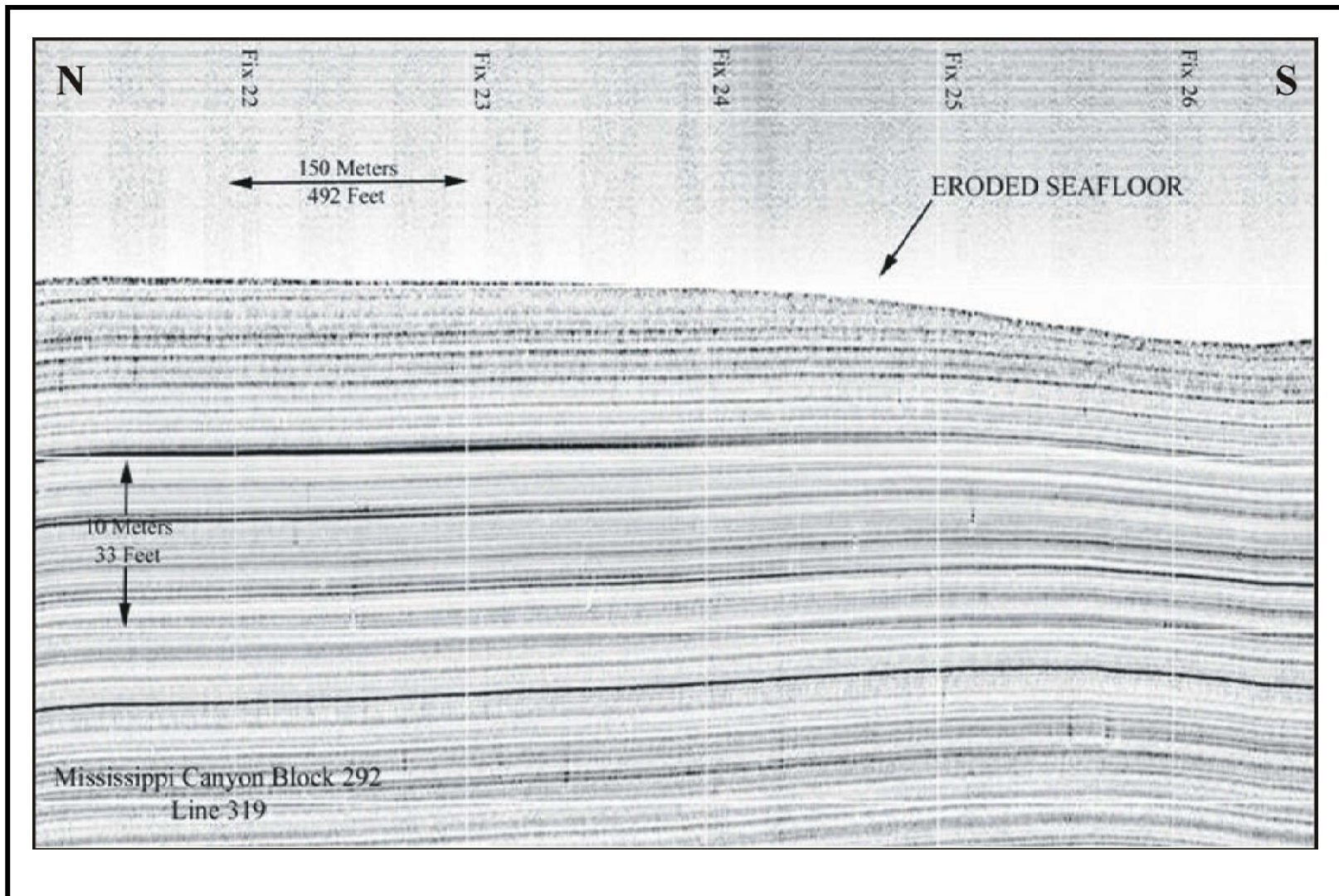


**Figure 4.11.** Chirp sonar subbottom profile (Line 319) illustrating an area of seafloor erosion that in plan-view trends northeast-southwest just south of the Mississippi Canyon Block 292 wellsites.



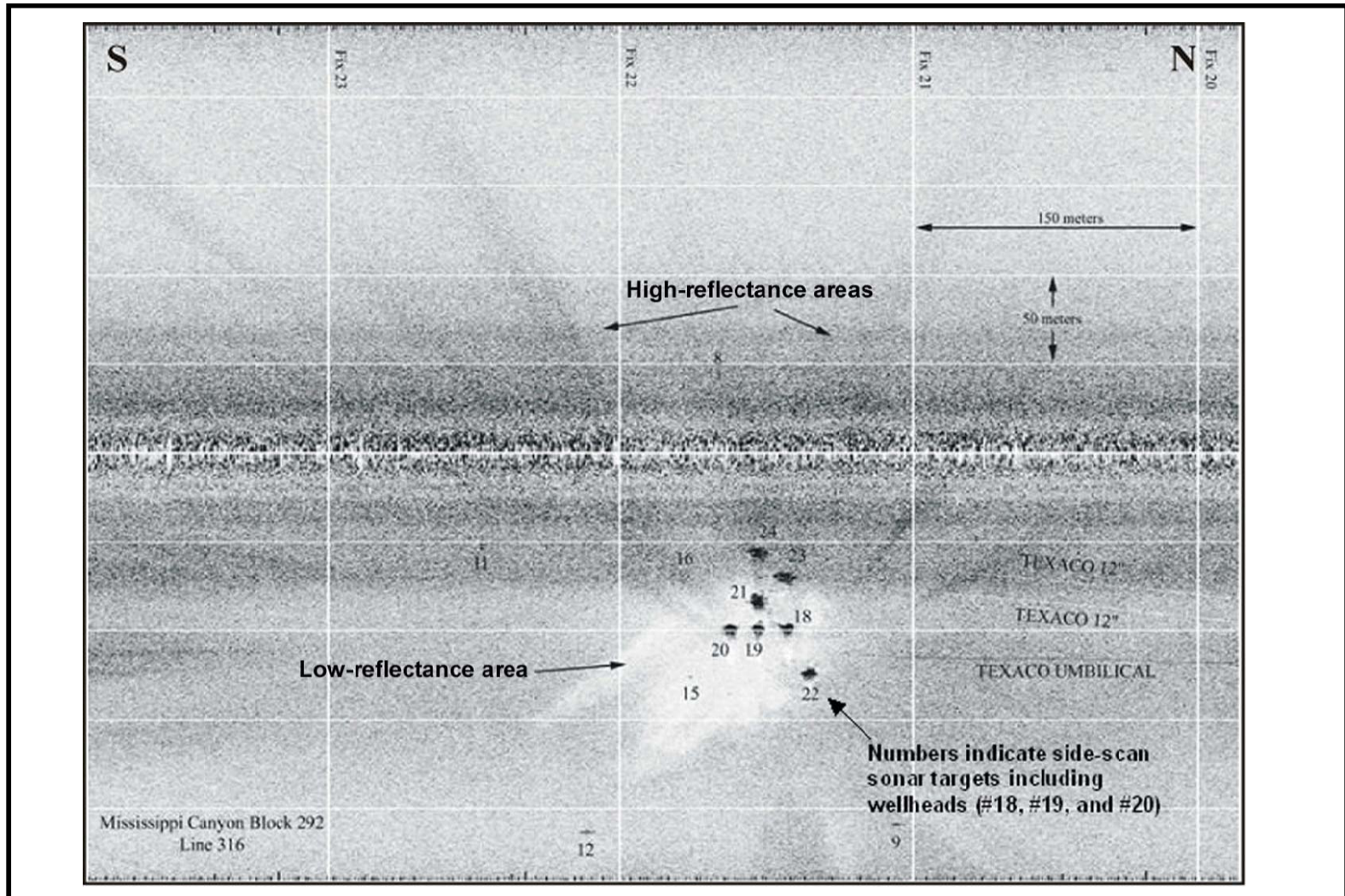


**Figure 4.12.** Image of a portion of a 120-kHz side-scan sonar survey line (Line 316) that trends north-south a short distance to the west of the Mississippi Canyon Block 292 well cluster. Note the radial pattern of high-reflectance (dark) areas (interpreted as possible cuttings from rig discharges) and the low-reflectance (white) area near the wells (interpreted as possible mud/cuttings from well jetting).

The combination of a smooth seafloor (little backscatter on side-scan sonar records) and a high amplitude response at the seafloor on high resolution subbottom profiles identifies areas of probable drilling mud and cuttings deposition from initial discharges during jetting of wells. **Figure 4.13** illustrates this area around the well cluster in MC 292, which is approximately 75 m wide and slightly over 150 m in length.

Outside of the low reflectance area near the wellsites, the high reflectance star-like pattern radiating from the wellsites is a little more difficult to interpret. The high reflectivity on side-scan sonar records means a higher “surface roughness” than surrounding areas of undisturbed seafloor. This surface roughness can develop from a variety of processes including: (1) deposition of well cuttings that are coarser-grained than typical hemipelagic sediments, (2) disturbances of the bottom (producing grooves, furrows, etc.) caused by the process of setting the anchors for drilling operations, (3) the dropping of sediment clumps to the seafloor from the anchor cables as they are pulled into place, and (4) a combination of some or all of the above. Even though the maps in *Appendix C3* identify these areas as well cuttings, all of the aforementioned processes could produce the reflectance patterns observed on side-scan sonar records. The Seafloor Investigation Map (*Appendix C3*) shows that the radial high reflectance patterns roughly align themselves with the linear and radial anchor cable scars on the seafloor in the far-field away from the well cluster.

Twenty-six side-scan sonar targets were identified within the study area. These sonar targets are identified in the Survey Report of *Appendix C3*. The wellheads and manifolds are clearly visible on the side-scan image shown in **Figure 4.12**. The subbottom profiles clearly identified a series of northeast-southwest trending faults in the southeastern and eastern sectors of the study area. The seafloor was offset by as much as 0.6 m by some of the faults. However, fluid and gas expulsion features were not identified. The fault trend is interpreted to mark the approximate edge of the salt mass in the subsurface.

Within the MC 292 survey area, anchor scars and possible drilling mud and cuttings were evident from other nearby wells in MC 291, MC 292, and MC 248 (**Figure 4.13**). **Figure 4.14** shows a portion of the side-scan sonar mosaic focusing on the wellsite in MC 248 where three wells were drilled between January and March 2000. The low reflectance areas near the wellsite are interpreted to be drilling mud and cuttings released at the seafloor during the initial jetting of the well, and the bands radiating from the wellsite are interpreted to be rig-discharged cuttings that settled to the seafloor.

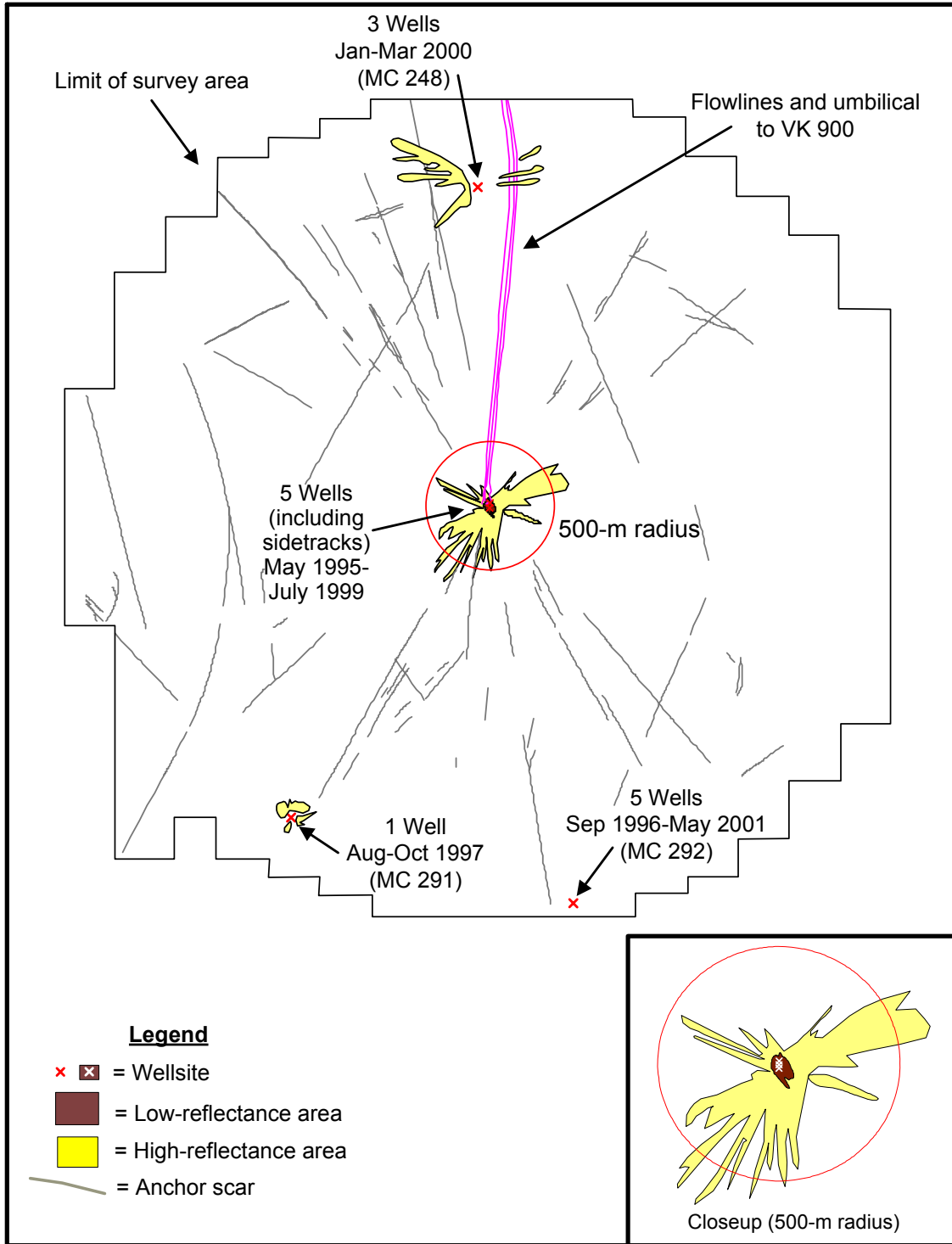


**Figure 4.13.** Map of drilling mud, cuttings, and anchor scars around the Mississippi Canyon (MC) Block 292 site based on the Cruise 2A geophysical survey (June-July 2001). Low-reflectance areas are interpreted as possible mud/cuttings from seafloor releases during well jetting. High-reflectance areas are interpreted as possible cuttings from rig discharges.

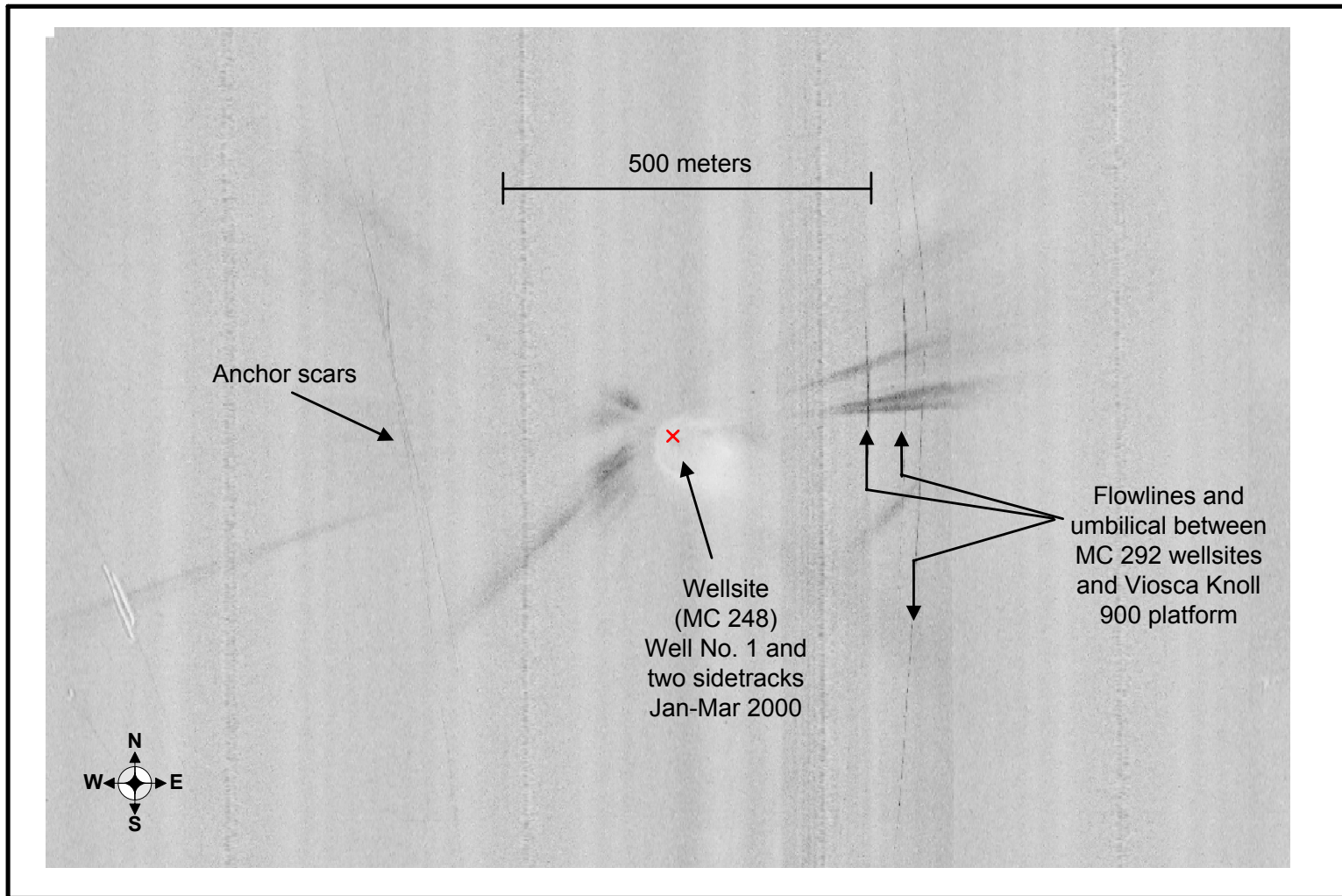


**Figure 4.14.** A sector of the side-scan sonar mosaic for the Mississippi Canyon (MC) Block 292 area. This closeup shows a wellsite in the adjacent block (MC 248) where three wells were drilled from January to March 2000, about 1.5 years before the Cruise 2A survey. See Figure 4.13 for location relative to the MC 292 wellsite. Note the high-reflectance areas (possible cuttings) radiating from the wellsite and the low-reflectance area immediately around the wellsite (possible mud/cuttings from well jetting).

## 4.5 GARDEN BANKS BLOCK 602 – POST-DEVELOPMENT SITE

### 4.5.1 Introduction

The study site in GB 602 is located in an intraslope basin directly south of the chenier plain coast of western Louisiana. Water depths in the area of interest range from about 1,067 m in the northwest to 1,130 m at the center of the basin just south of the wellsite area. **Figure 4.1** shows the general area of the continental slope in which the two Garden Banks sites are located. **Figure 4.15** is a shaded relief map showing both the GB 602 and GB 516 locations.

The GB 602 site is located near the center of an intraslope basin on the upper continental slope. This basin is downslope of a shelf edge that has been impacted by the deposition of shelf margin deltas during late Pleistocene periods of lowered sea level (Suter and Berryhill 1985). These deltas and their fluvial systems were the sources of sediment for filling intraslope basins in this general area. At the same time, this sedimentary loading caused adjustment of subsurface salt, which activated faults and caused vertical migration of fluids and gas. The basin is surrounded by high and irregular topographic features related to salt in the shallow subsurface. These basin margins are the originating points for submarine landslides, faulting, and fluid/gas expulsion. North of the GB 602 study site is Shell's Auger Field. In this area, large submarine landslides followed by fluid and gas expulsion have impacted both the latest sedimentary fill in the basin and the character of the seafloor on basin-flanking domes. However, for most of the area of interest in GB 602, the seafloor sediments are composed of a well-developed hemipelagic drape. In chirp sonar subbottom profiler records, this area is represented by uniform and parallel subbottom reflectors.

### 4.5.2 Data Quality

The high resolution acoustic data collected by the AUV in support of the post-development survey of the GB 602 well area were of excellent quality. The multibeam bathymetric data produced a high quality map that details the dominant features of the seafloor. Combined with the high quality side-scan sonar images of the seafloor and the very high resolution chirp sonar subbottom profiles, these state-of-the-art data sets provided unmatched insight into the surface and near-surface geology conditions of the study area. Map products are provided in *Appendix C3*.

### 4.5.3 Site Characterization

The side-scan data from the study area describe a very uniform reflectance except for the man-made features and disturbances of surficial sediment. As might be expected from the seafloor in intraslope basins, the hemipelagic drape deposited over the slope as sea level rose from the latest Pleistocene glacial maximum (approximately 18 thousand years before present) is very uniform. Unless submarine landslides and/or fluid/gas expulsion from adjacent high relief areas disrupt the hemipelagic drape deposits, basin floors tend to be essentially featureless. The GB 602 site is no exception. On both side-scan sonar and chirp sonar subbottom profiler records, the basin fill is uniform and without evidence of natural disruptions. However, data from the AUV identified 43 sonar targets related to human activity in the area, as shown on the Seafloor Investigation Map, which along with bathymetry maps and side-scan sonar mosaics are presented in *Appendix C3*.

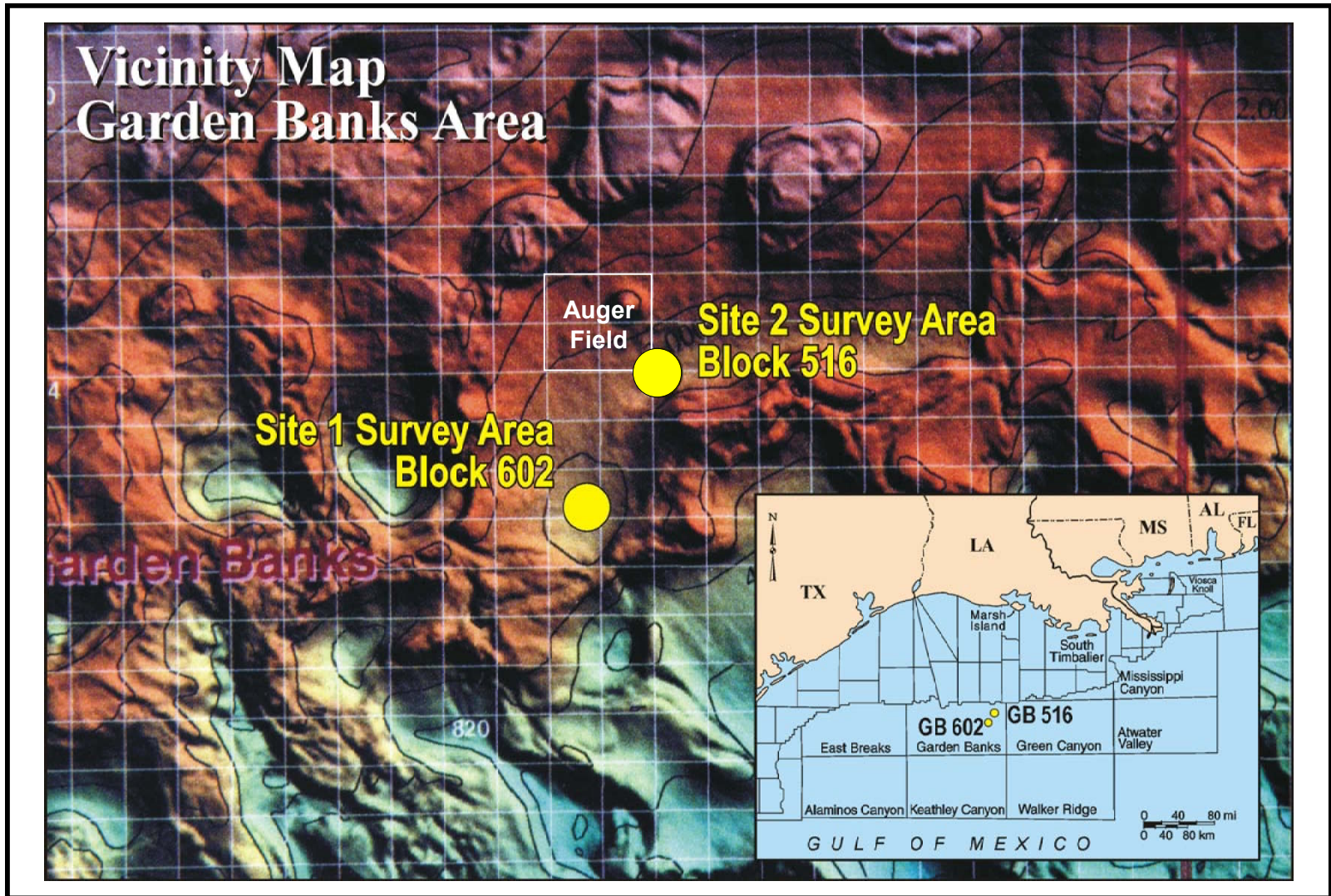


**Figure 4.15.** A shaded relief image of the Garden Banks (GB) 602 and GB 516 areas. The yellow dots represent the approximate location of study sites within GB 602 and GB 516.

**Figure 4.16** illustrates seafloor characteristics of the well cluster area in GB 602 as imaged acoustically using side-scan sonar. Dominant features in this image are the areas of high reflectance (dark) that are arranged as linear features radiating from the wellsite zone, a low reflectance area around the wells, and a mound-like feature to the west of the well cluster. The Seafloor Investigation Map of *Appendix C3*, compiled from features on the side-scan sonar mosaic, shows that within the 3,050-m radius circle around the drill site, there are numerous linear scars on the seabed. An example of these scars is illustrated in **Figure 4.17**. These scars are associated with anchoring in preparation for drilling activities. The radial patterns of these impressions in the bottom sediments roughly align themselves with the radial high reflectance zones on side-scan records that radiate from the well cluster. On the map of **Figure 4.18**, these radial high reflectance patterns are interpreted as well cuttings. However, as explained in a previous section of this chapter, clumps of sediment dropped from the anchoring cables also can contribute to the high backscatter (reflectance) on side-scan sonar records since the host hemipelagic sediments are typically uniformly fine-grained, and except for burrowing, the surface is relatively smooth.

The zone of low reflectivity around the well cluster is interpreted as drilling mud and cuttings released at the seafloor during the initial jetting of wells. In this case, the area is small, approximately 75 m wide and 213 m in its longest dimension. A small mound of possible drilling mud and cuttings also is interpreted to be located approximately 200 m west of the main well cluster. This low-relief mound is a little over 30 m in its north-south (longest) dimension and is located next to an earlier wellsite (well no. 1, see *Chapter 3*).

Other seafloor features of the area include two flowlines and an umbilical trending north from the well cluster site (**Figure 4.18**).

Within the GB 602 survey area, anchor scars and mud/cuttings were evident from other nearby wells in the same block (**Figure 4.18**). In particular, drilling mud and cuttings were mapped around a wellsite approximately 2.3 km north/northeast of the main GB 602 site; three wells were drilled there between April and August 1996, about 5 years prior to Cruise 2A (see *Chapter 3*). The low reflectance areas near the wellsite are interpreted to be drilling mud and cuttings from initial well jetting, and the bands radiating from the wellsite are interpreted to be rig-discharged cuttings, as explained previously.

A geotechnical borehole was drilled in February 1996 about 1.3 km northeast of the main site, but no mud or cuttings deposits are apparent around this wellsite.

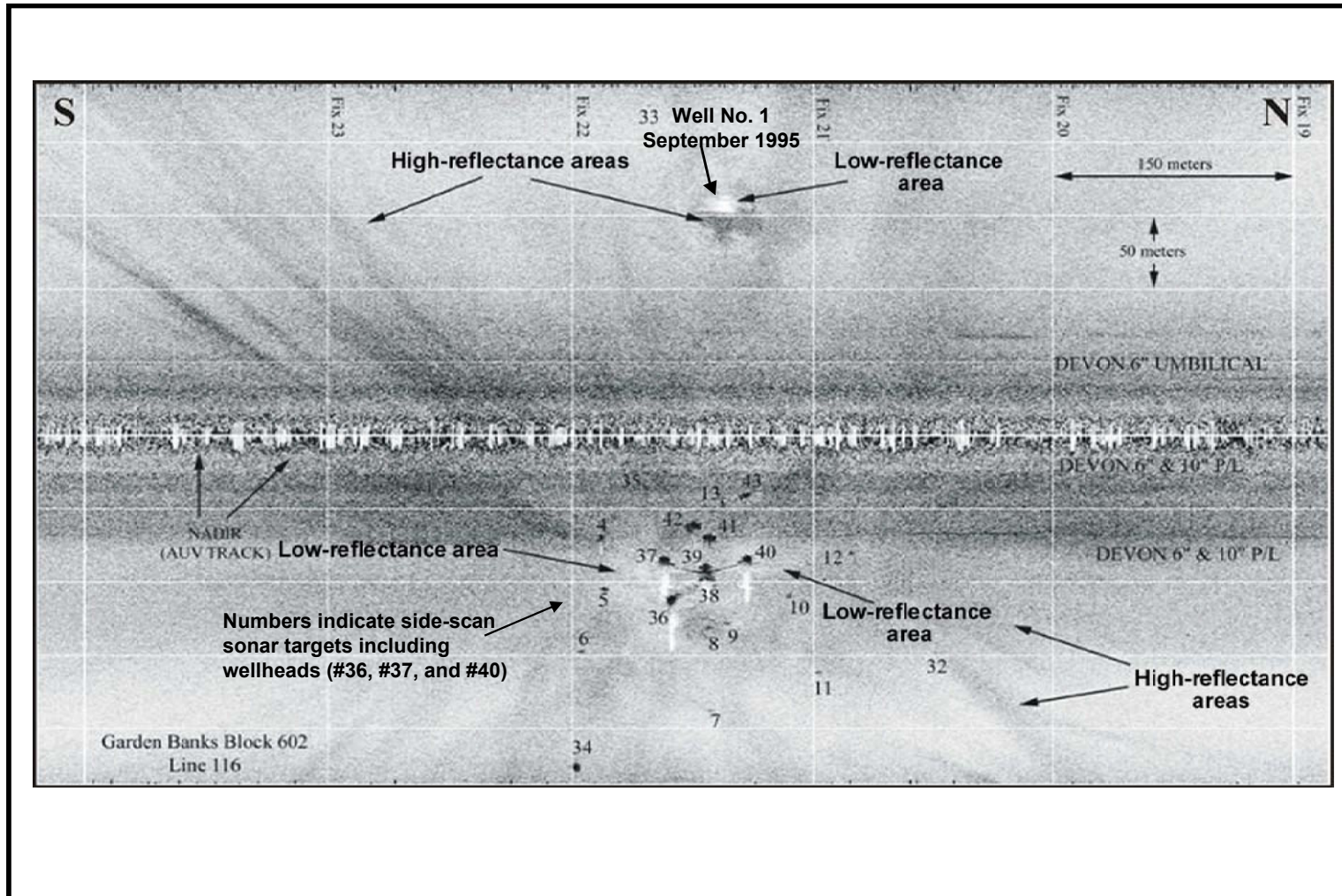


**Figure 4.16.** A section of side-scan sonar Line 116 showing the well cluster in Garden Banks (GB) Block 602 and radial pattern of high reflectance (dark streaks and patches, interpreted as possible cuttings from rig discharges). Note the region of low reflectance in the vicinity of the wells (interpreted as possible mud/cuttings from well jetting). Well Nos. 2, 4, and 5 (and sidetracks) are in the well cluster, and Well No. 1 was drilled about 250 m to the west.



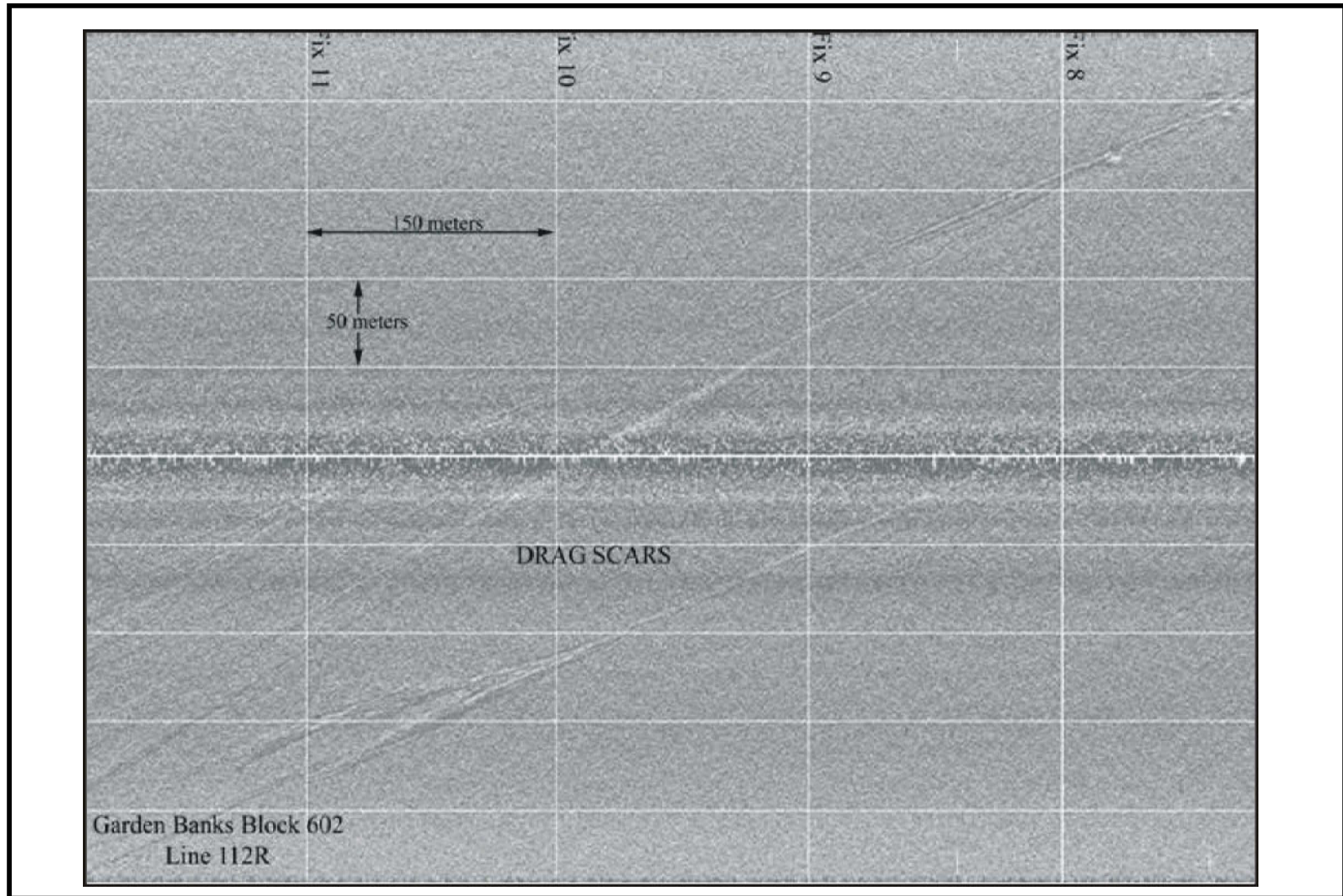


**Figure 4.17.** A section of side-scan sonar Line 112 illustrating the man-made scars in the hemipelagic surface sediments of the Garden Banks Block 602 study area. These scars were made during anchoring for drilling activities.

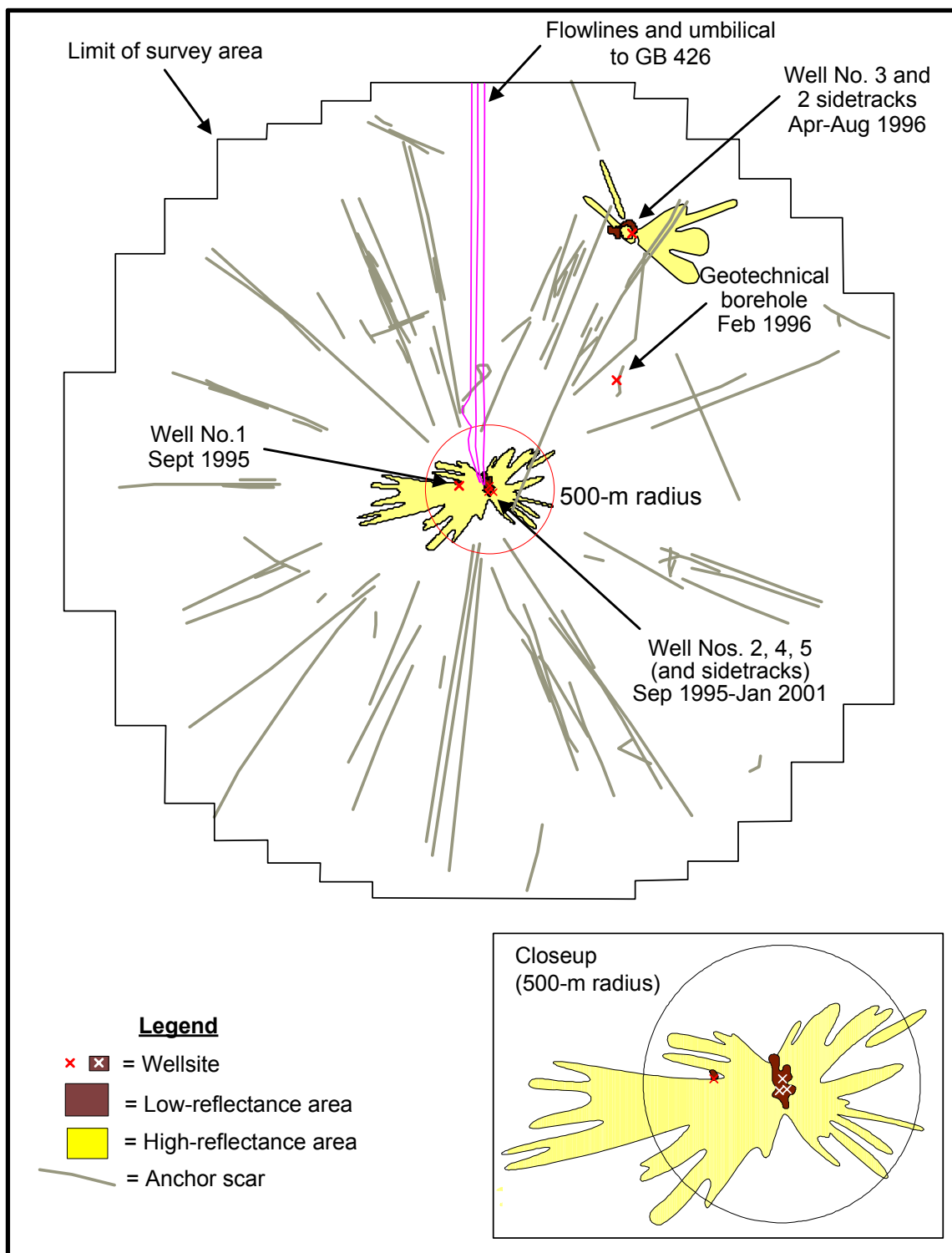


**Figure 4.18.** Map of drilling mud, cuttings, and anchor scars around the Garden Banks (GB) 602 site based on the Cruise 2A geophysical survey (June-July 2001). Low-reflectance areas are interpreted as possible mud/cuttings from seafloor releases during well jetting. High-reflectance areas are interpreted as possible cuttings from rig discharges.

## 4.6 GARDEN BANKS BLOCK 516 – EXPLORATION/DEVELOPMENT SITE

### 4.6.1 Introduction

The GB 516 site is located on the upper continental slope southwest of the distinct mound-shaped “diapiric hill” in the basin containing Shell’s Auger Field (**Figure 4.15**). The area of interest is located on the northern flank of an east-west trending salt-supported ridge that exhibits extremely complex seafloor topography and geology. The bathymetric map of the region provided in *Appendix C3* illustrates the complexity of this area to the south of the wellsite. Within the 3,050-m radius circle around the well location, water depths vary from 790 m on the ridge top to slightly over 1,035 m immediately north of the wellsite. Even though bathymetry of the wellsite area describes a rather smooth seafloor, it is clear from the side-scan sonar mosaic and chirp sonar subbottom profile data that large areas of the basin fill to the south and east of the wellsite have been impacted by faulting, sediment gravity flows, and other mass movement events; fluid/gas expulsion; and seafloor lithification. This site is clearly the most geologically diverse and complex of all the sites investigated in this research project.

The complex seafloor area is identified on the reduced side-scan sonar mosaic of the area **Figure 4.19**. The full-scale map is included in *Appendix C3*. As explained above, this area of complicated seafloor is associated with a salt-supported ridge that rises over 244 m above the basin floor near the wellsite. Salt movement related to sedimentary loading during periods of falling sea level to early rise of sea level during the Pleistocene is largely responsible for the faulting that is prevalent in GB 516 south of the wellsite. In addition to offsetting the seafloor, as can be observed in data sets from this area, e.g., **Figure 4.20**, the faults function as conduits for vertical migration of fluids (including fluidized sediment and crude oil) and gases to the present day seafloor. As discussed in the introductory section of this chapter, the flux rate of hydrocarbon-carrying fluids and gases to the seafloor has an important impact on geologic and biologic response. The response can be quite variable from depositional features that form from expulsion of fluidized sediment to lithification of seafloor sediments. The acoustic data collected in the GB 516 area indicate that this region probably has all of these responses.

### 4.6.2 Data Quality

The high resolution acoustic data collected by the AUV in support of the post-development survey of the GB 516 well area were of excellent quality. The multibeam bathymetric data produced a high quality map that details the dominant features of the seafloor. Combined with the high quality side-scan sonar images of the seafloor and the very high resolution chirp sonar subbottom profiles, these state-of-the-art data sets provided unmatched insight into the surface and near-surface geologic conditions of the study area. Map products are provided in *Appendix C3*.

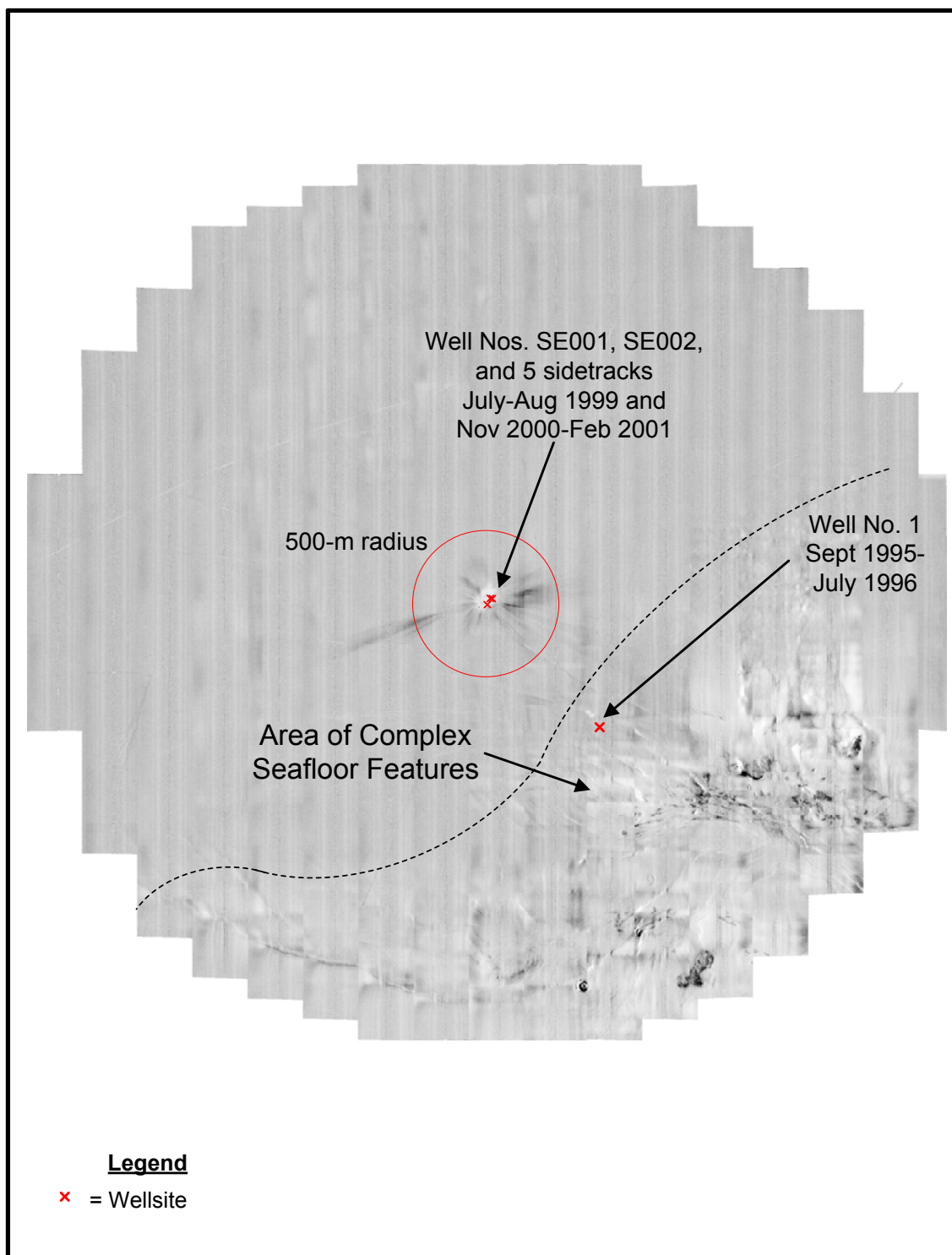


**Figure 4.19.** This reduced version of the side-scan sonar mosaic illustrates the seafloor complexity to the southeast of the Garden Banks Block 516 wellsite. The variability of backscatter reflectance in this area is produced by a variety of features including faults, submarine landslides, fluid/gas expulsion vents, and zones of seafloor lithification.

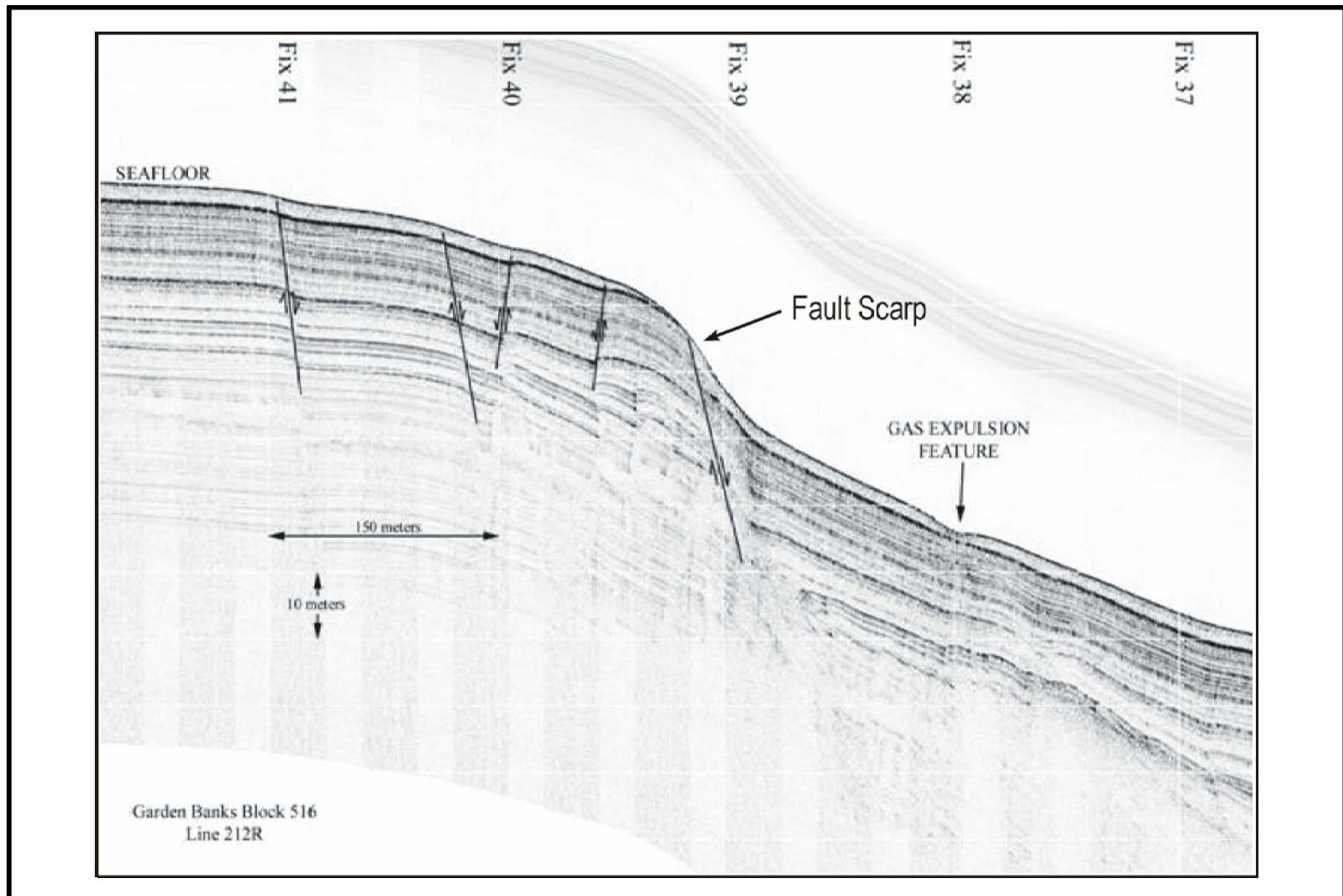


**Figure 4.20.** This section of chirp sonar subbottom profile (Line 212) crosses a prominent fault that trends east-west along the flank of the salt-supported ridge to the south of the drilling site in Garden Banks Block 516. Note the numerous small faults and the gas expulsion feature (pockmark).

### 4.6.3 Site Characterization

High backscatter (reflectance) areas to the southeast of the wellsite (**Figure 4.19**) are probably related to zones of seafloor lithification. The numerous fluid/gas expulsion features scattered throughout this region of GB 516 (e.g., **Figure 4.20**, *Appendix C3*) suggest that hydrocarbon gases and probably crude oil are reaching the modern seafloor. Microbial utilization of hydrocarbons produces carbonates that bind surficial sediments to create cemented pavements, crusts, and mounds. These features usually occur in areas that are impacted by faulting such as this region of the block, which borders the salt-supported high ground. They produce a strong reflectance, or backscatter, on side-scan sonar records.

In addition to the faulting and fluid and gas expulsion features, the high slopes coupled with periodic salt in the southern part of the area of interest promote sediment instability. As a result, mass movement is common, and in this area, there is abundant evidence of slope failure and transport of sediment northward into the adjacent basin. **Figure 4.21** clearly shows that the surface reflects the underlying blocks and irregular depositional surface of debris from a buried submarine landslide. The subbottom data of **Figure 4.22** illustrate the irregular top surface and acoustic transparency of the submarine landslide deposits. Because these deposits are draped with both hemipelagic deposits and stratified units beneath, the landslide probably occurred at or before the latest Pleistocene glacial maximum (approximately 18 thousand years before present). Toward the wellsite, the surface geology becomes more undisturbed, and subsurface stratigraphy is composed of uniform parallel reflectors.

**Figures 4.23** and **4.24** illustrate the wellsite area and the interpreted backscatter reflectance patterns. As in the other study sites, the dark reflectance patterns radiating from the wellsite are interpreted as the products of well cuttings and clumps of sediment/sediment disturbances caused by the process of anchoring prior to drilling operations. When these patterns are compared with cable scars on the bottom (Seafloor Interpretation Map, *Appendix C3*), there is a favorable alignment. The zone of low backscatter in the immediate vicinity of the drilling site is interpreted as an area of drilling mud and cuttings from the initial jetting of wells. The fine-grained nature of drilling mud and lack of bioturbation features as compared to the older surrounding seafloor account for the lack of reflectance. These areas typically have a high amplitude response (high acoustic impedance) on subbottom records because of the high specific gravity minerals used in drilling mud.

In addition to the mud and cuttings around the study site, the mapping showed deposits around a previous wellsite about 1.2 km to the southeast (**Figure 4.24**). This well was drilled between September 1995 and July 1996, about 5 years prior to Cruise 2A.

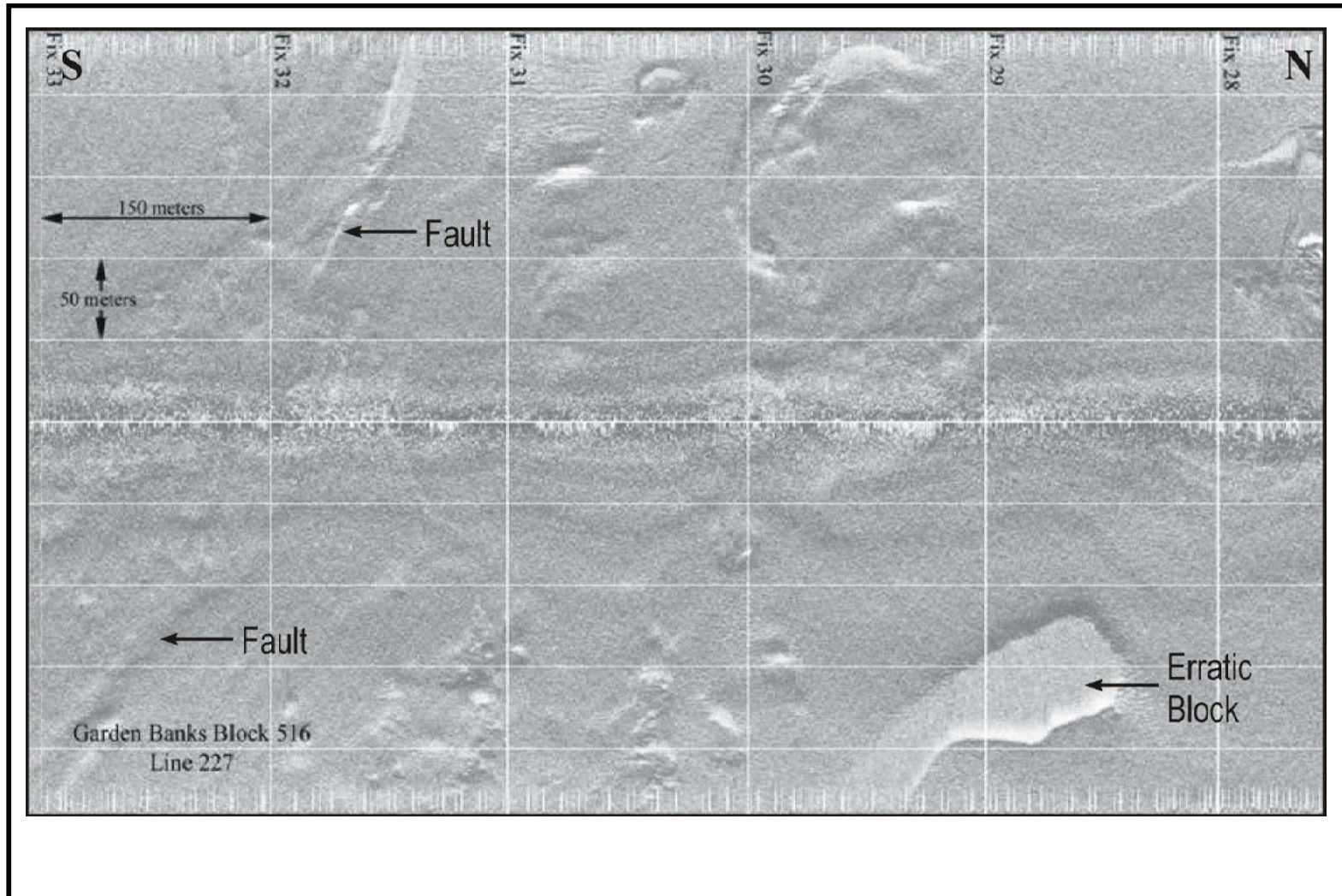


**Figure 4.21.** This section of side-scan sonar data from Garden Banks Block 516, Survey Line 227, illustrates the complexity of the seafloor in the transition area between the salt-supported high ground to the southeast of the wellsite and the basin floor where the wellsite is located. This complexity is associated with both faulting and submarine landslide deposits. Note the erratic block of sediment.

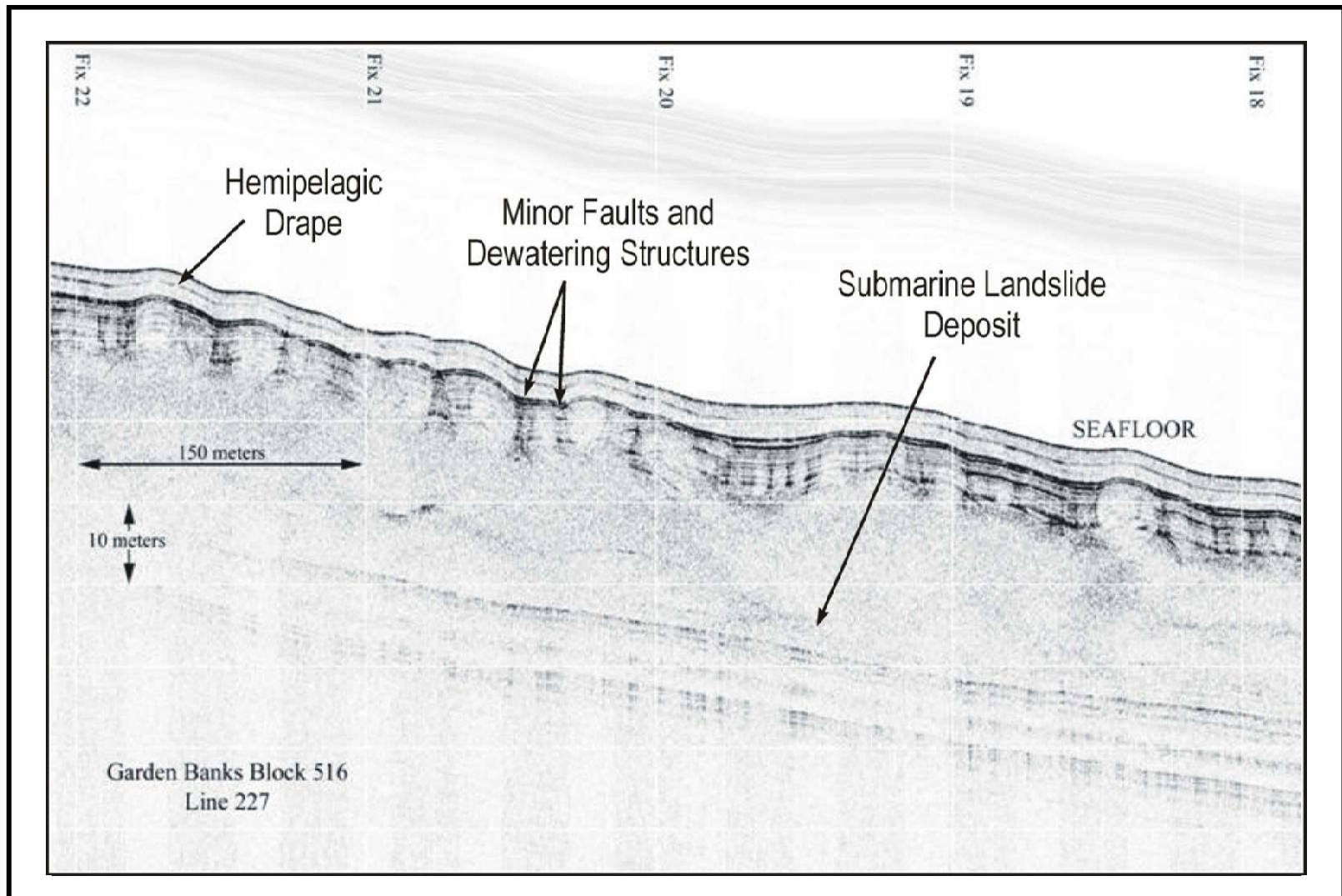


**Figure 4.22.** This portion of chirp sonar subbottom profile (Garden Banks Block 516, Line 227) shows a hemipelagic sediment drape over a chaotic and largely acoustically opaque submarine landslide deposit.



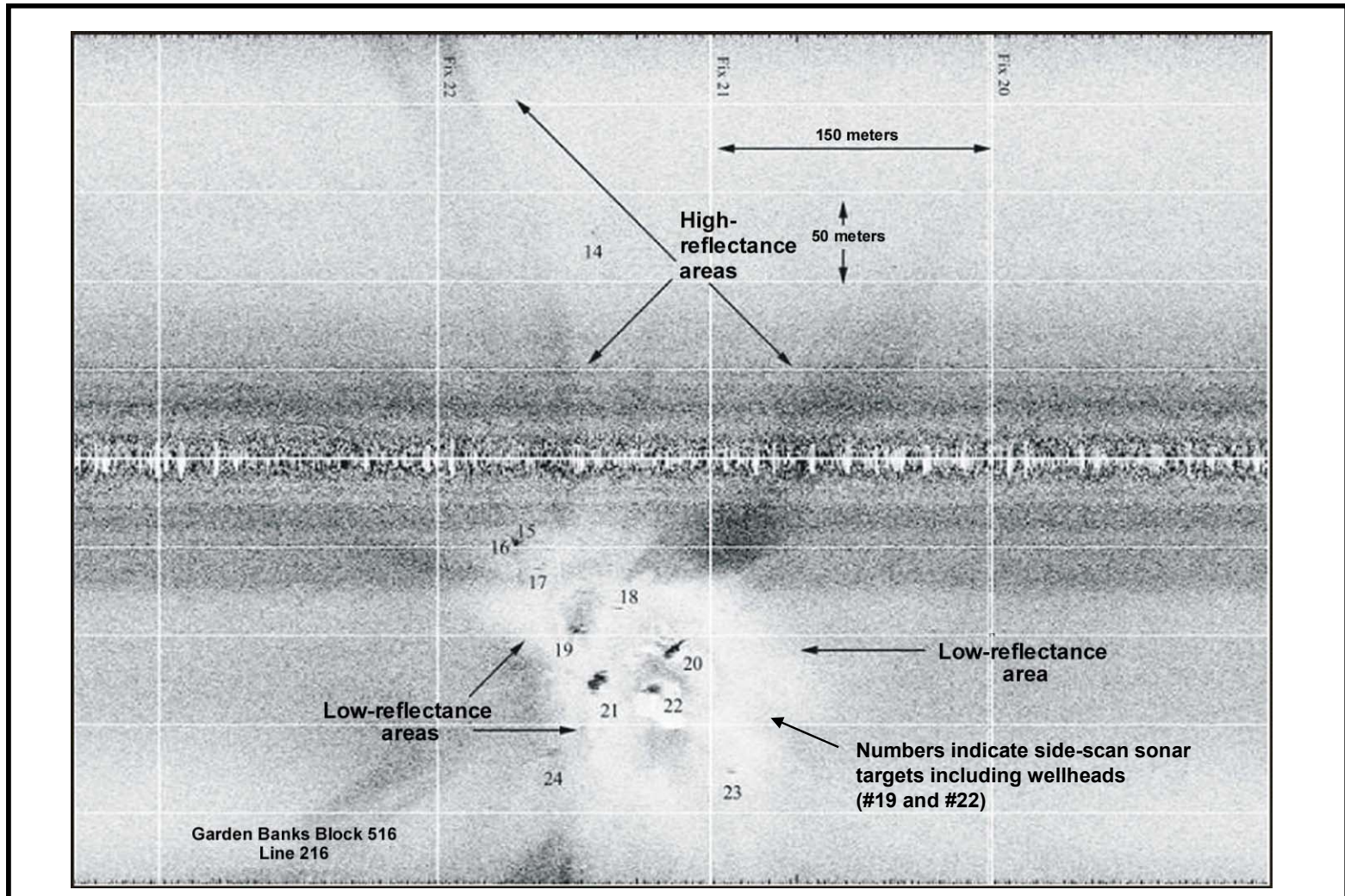


**Figure 4.23.** Section of side-scan sonar record from Garden Banks Block 516, Line 216 showing the wellsite area with high-reflectance (dark) areas interpreted as possible cuttings from rig discharges and low-reflectance (light) areas interpreted as possible mud/cuttings from well jetting.

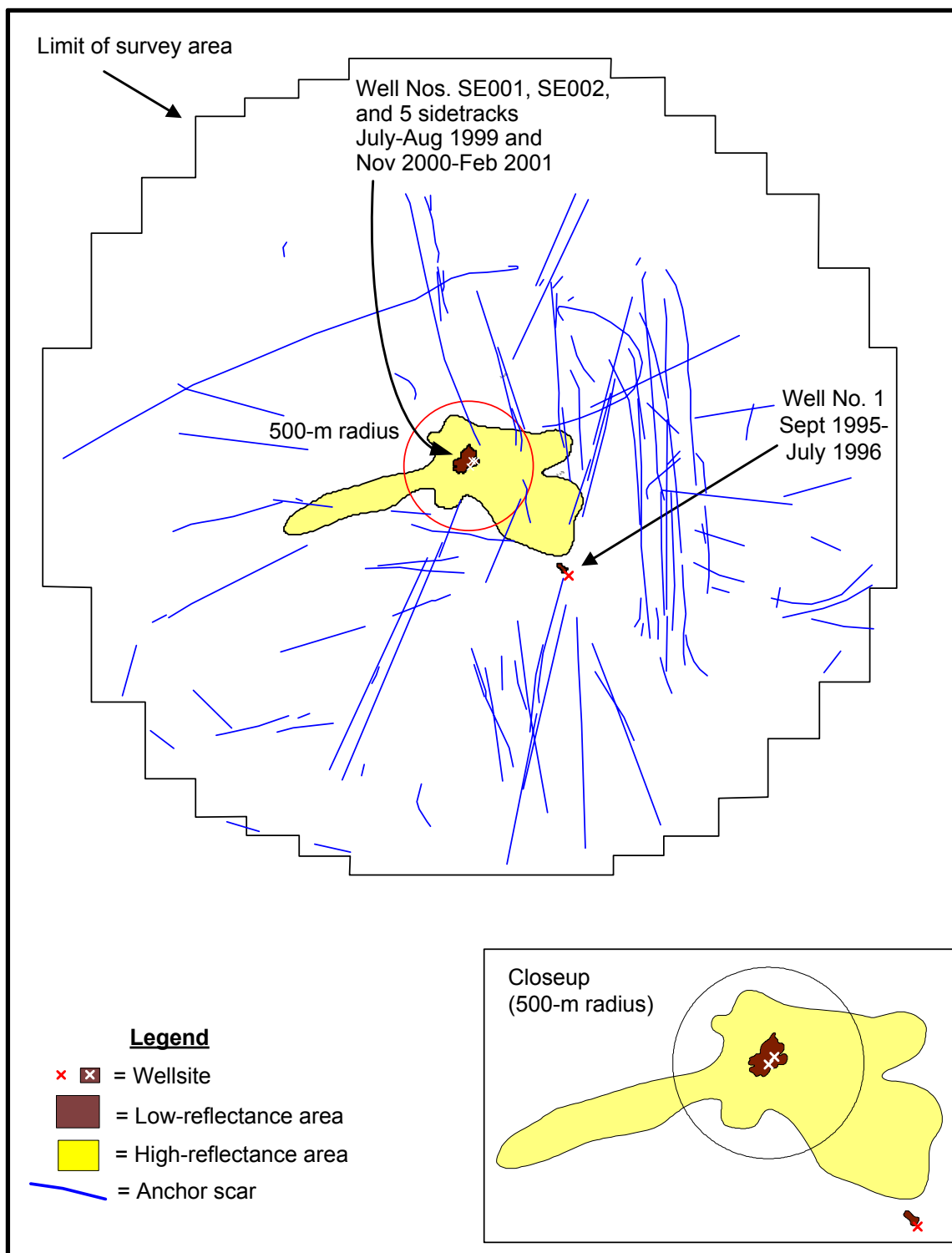


**Figure 4.24.** Map of drilling mud, cuttings, and anchor scars around the Garden Banks Block 516 site based on the Cruise 2A geophysical survey (June-July 2001). Low-reflectance areas are interpreted as possible mud/cuttings from seafloor releases during well jetting. High-reflectance areas are interpreted as possible cuttings from rig discharges.

## 4.7 CONCLUSIONS

Side-scan sonar and chirp sonar subbottom profiler records were useful, though not definitive, in mapping deposits of suspected drilling mud and cuttings. In the immediate vicinity of wellsites, some areas showed a combination of a smooth seafloor (little backscatter on side-scan sonar records) and a high amplitude response at the seafloor on subbottom profiles. These were interpreted as zones where muds and cuttings were released at the seafloor during the initial jetting of each well (see *Chapter 3*). Typically, these initial deposits create a shallow, compact mound around the wellbore. Generally, these areas were mapped within about 100 m of wellsites. Other activities including installation of seafloor equipment (see *Chapter 3*) may also have contributed to the observed low-reflectance pattern around the wellsites.

More extensive areas where side-scan sonar showed high reflectivity extending in a radial pattern around the wellsites were interpreted as possible cuttings discharged from the drilling rig. These areas typically extended several hundred meters from wellsites, with the greatest extent (about 1 km from the wellsite) observed at GB 602 and GB 516. Cuttings are derived from subsurface sediments that are much more compacted and therefore denser than surface hemipelagic sediments that drape most of the northern Gulf continental slope. When scattered across the seafloor by surface discharges, these cuttings create an acoustic impedance difference that translates into a higher amplitude reflection on side-scan sonar and subbottom profiler records. Although the maps identify these areas as cuttings, other processes could produce the reflectance patterns, including seafloor disturbances (grooves, furrows, etc.) caused by the process of setting anchors and the dropping of sediment clumps to the seafloor from the anchor cables as they are pulled into place.

The geophysical surveys also detected anchor scars ranging from less than 100 m to over 3 km in length, extending to the limit of the surveyed area around the wellsites. VK 916 had only one set of anchor scars associated with the exploratory drilling at this site. The other three sites, surveyed post-development, had several sets of anchor scars, reflecting the use of different drilling rigs to drill various wells over time.

Persistent cuttings and/or anchor scars from previous activities at nearby wellsites also were evident. At VK 916, possible cuttings and anchor scars were present from two previous wells drilled in nearby VK 872 in November to December 1998, about 3.5 years prior to Cruise 3A. The VK 916 survey also showed anchor scars associated with an older wellsite in VK 873 (drilled 14 years before Cruise 3A). At the MC 292 site, suspected cuttings deposits and anchor scars were evident around a wellsite in the adjacent block MC 291 from drilling between August and October 1997. Within the GB 602 survey area, anchor scars and mud/cuttings were evident from three wells drilled between April and August 1996, about 5 years prior to Cruise 2A. In the GB 516 area, the mapping showed drilling deposits around a previous wellsite drilled between September 1995 and July 1996, about 5 years prior to Cruise 2A. Taken together, these observations suggest that physically detectable impacts of drilling activities can persist for several years in the deepwater environment.

**Editor's Note:** In subsequent chapters, the high-reflectivity areas extending radially around wellsites are identified as “possible cuttings” or “rig discharge deposits” and the low-reflectance areas in the immediate vicinity of wellsites are identified as “well jetting deposits.” No ground-truthing was conducted to verify that these designations are accurate. This issue is discussed further in *Chapter 15* where other lines of evidence including sediment chemistry can be brought to bear.

## Chapter 5 Sediment Grain Size

Neal W. Phillips and Robert B. Cady  
Continental Shelf Associates, Inc.

---

### 5.1 INTRODUCTION

On each cruise, sediment samples were collected using a box core at random stations within near-field and far-field sites (see *Chapter 2*). From each box core, a subsample of the top 2 cm was obtained for grain size analysis. Additional box cores were collected from three non-random discretionary stations placed in geophysically mapped cuttings/mud zones within each near-field site during Cruises 2B and 3B. Subsamples from these box cores were sectioned in 2-cm intervals to a depth of 10 cm. Raw grain size data are presented in *Appendices D1, D2, and D3*.

### 5.2 LABORATORY METHODS

Sediment grain size was analyzed by Dr. Wayne Isphording (University of South Alabama/Tierra Consulting). Standard sieve and hydrometer methodologies were used, as specified in American Society for Testing and Materials (ASTM) D-422. Statistical measures of central tendency and dispersion (mean diameter, sorting, skewness, and kurtosis) were generated. Additional information produced by these analyses includes descriptive properties of each sample based upon sediment classification procedures (Folk 1974).

The text refers to phi intervals and percentages of gravel, sand, silt, and clay. These are defined as follows:

- $\Phi = -\log_2(D)$  where  $D$  = particle diameter in mm
- Gravel = particles with diameters  $> 2$  mm ( $< \Phi - 1$ )
- Sand = particles with diameters between 2 mm and 62.5  $\mu\text{m}$  ( $\Phi - 1$  to 4.0)
- Silt = particle diameters between 62.5  $\mu\text{m}$  and 3.9  $\mu\text{m}$  ( $\Phi$  4.0 to 8.0)
- Clay = particle diameters  $< 3.9$   $\mu\text{m}$  ( $> \Phi$  8.0)

### 5.3 RESULTS

At the far-field sites away from drilling influences, sediments were predominantly clay (~60% to 75%) and silt (~20% to 30%) at all four locations (**Table 5.1**). Mean grain sizes generally were in the 1 to 3  $\mu\text{m}$  range. Sediments at the two western sites (Garden Banks Blocks 516 and 602) had slightly higher sand percentages (e.g., some values greater than 10%) compared with the two sites closer to the Mississippi River (Viosca Knoll Block 916 and Mississippi Canyon Block 292) (generally less than 5% sand). Small percentages of gravel were present at only three stations (including both near- and far-field samples).

**Table 5.2** provides analysis of variance (ANOVA) results for mean grain size and sand, silt, and clay percentages at each site. Individual sites are discussed in the following sections.

**Table 5.1.** Summary of baseline grain size characteristics for sites based on far-field data. Values are means of all far-field stations, with ranges in parentheses.

Site	Cruise	Mean Grain Size ( $\mu\text{m}$ )	Mean Percentages		
			Sand	Silt	Clay
VK 916	1B	2.44 (1.34 – 4.41)	3.49 (2.09 – 5.40)	29.14 (23.82 – 43.64)	67.25 (50.96 – 73.22)
	3B	1.75 (1.19 – 2.34)	3.12 (1.69 – 4.77)	21.13 (16.08 – 27.18)	75.75 (69.03 – 81.45)
GB 516	1B	2.95 (1.88 – 5.63)	5.28 (3.03 – 12.04)	31.69 (19.76 – 60.15)	63.03 (34.53 – 77.21)
	2B	2.40 (0.66 – 10.00)	6.16 (4.18 – 10.38)	32.07 (15.96 – 54.43)	61.78 (40.09 – 76.93)
GB 602	2B	2.03 (0.27 – 13.23)	10.28 (5.22 – 16.50)	21.47 (11.92 – 61.82)	68.26 (29.16 – 78.62)
MC 292	2B	1.61 (0.18 – 7.42)	1.93 (0.65 – 3.07)	28.37 (16.30 – 64.13)	69.70 (34.25 – 81.50)

**Table 5.2.** Analysis of variance (ANOVA) results for sediment grain size. Statistically significant differences ( $p < 0.05$ ) are indicated by bold type and an asterisk. Where the overall ANOVA was not significant, probabilities for cruise, site, and interaction are not listed. Multiple comparison results (Tukey's honest significant difference) are provided for significant ANOVAs. For testing, mean grain size in microns (rather than phi units) was used. Sand, silt, and clay percentages were arcsin-transformed.

Site	Parameter	ANOVA Result (probability > F)				Comparisons
		Overall	Cruise	NF vs. FF	Interaction	
VK 916	Mean	0.0710	--	--	--	--
	Sand	<b>0.0224*</b>	0.0957	0.3353	<b>0.0127*</b>	Cr3 NF > Cr1 NF
	Silt	<b>0.0055*</b>	<b>0.0015*</b>	0.1270	0.4330	Cr1 NF > Cr3 FF Cr1 FF > Cr3 FF
	Clay	<b>0.0164*</b>	<b>0.0093*</b>	0.1147	0.2337	Cr3 FF > Cr1 NF Cr3 FF > Cr1 FF
GB 516	Mean	0.7491	--	--	--	--
	Sand	<b>&lt;0.0001*</b>	<b>&lt;0.0001*</b>	<b>0.0032*</b>	<b>0.0113*</b>	Cr2 NF > all others
	Silt	0.3766	--	--	--	--
	Clay	0.8643	--	--	--	--
GB 602	Mean	0.2151	N/A	--	N/A	--
	Sand	0.4477	N/A	--	N/A	--
	Silt	0.1102	N/A	--	N/A	--
	Clay	0.0813	N/A	--	N/A	--
MC 292	Mean	0.8159	N/A	--	--	--
	Sand	<b>0.0013*</b>	N/A	<b>0.0013*</b>	N/A	NF > FF
	Silt	0.8082	N/A	--	N/A	--
	Clay	0.6716	N/A	--	N/A	--

Cr = cruise; NF = near-field; FF = far-field; N/A = not applicable (there was only one cruise at GB 602 and MC 292).

### 5.3.1 Viosca Knoll Block 916

Viosca Knoll Block 916 (VK 916) was sampled on Cruise 1B (October/November 2000) and Cruise 3B (August 2002). The two cruises served as pre- and post-drilling surveys for this exploration site. Basic statistics are summarized in **Table 5.3**. Ternary plots are shown in **Figure 5.1**.

Mean grain size ranged from 1.02 to 6.40  $\mu\text{m}$ , with most stations being in the 2 to 3  $\mu\text{m}$  range. Based on the grain size statistics, sediments can be characterized as poorly or very poorly sorted and the size distribution was coarse-skewed. The Folk's textural description was primarily "clay" or "mud" on Cruise 1B and "clay" on Cruise 3B. On Cruise 1B, sediments averaged about 67% clay and 30% silt at both near-field and far-field sites. Cruise 3B sediments on average had more clay (73%) and less silt (23%). Small percentages of gravel were present at two stations (FF4-B02 on Cruise 1B and NF-B01 on Cruise 3B).

On Cruise 1B, there was considerable variation in the relative proportions of silt and clay, particularly at the near-field site. Clay ranged from about 41% to 84% at near-field stations as compared with 51% to 73% at far-field stations. The range was much narrower on Cruise 3B (63% to 78% near-field, 69% to 81% far-field).

On the post-drilling survey, several near-field stations had slightly elevated sand percentages compared with the far-field (**Figure 5.1**). This pattern is more easily seen on **Figure 5.2**, which shows sand, silt, and clay percentages for post-drilling stations grouped into three categories:

- Far-field stations (>10 km from drillsite)
- Near-field stations 300 to 500 m from site center
- Near-field stations within 300 m of site center

Most stations had less than 5% sand, with the exception of a few near-field, post-drilling stations. Among random near-field stations, the highest post-drilling sand percentage was 7.70% at station NF-B01. However, one discretionary station (NF-DS3) had 17.14% sand. Near-field sand percentages were significantly higher on Cruise 3B than on Cruise 1B (**Table 5.2**).

Significant differences were also detected for silt and clay (**Table 5.2**), but some of these appear to be temporal (cruise-to-cruise) variations unrelated to drilling. For example, Cruise 3B far-field sites had significantly less silt and more clay than both near-field and far-field sites sampled on Cruise 1B. Although **Figure 5.2** suggests that post-drilling, near-field stations tended to have more silt and less clay than far-field stations, these differences were not significant.

Differences in sand/silt/clay percentages are part of a larger pattern in which the post-drilling grain size distribution in the near-field was shifted toward coarser particles. **Figure 5.3** compares the post-drilling grain size distribution for average near-field and far-field sediments and for near-field station NF-DS3. This station is used as an example because it had high barium (73,000  $\mu\text{g/g}$ ) and synthetic-based fluid (SBF) (27,319  $\mu\text{g/g}$ ) concentrations, indicating the presence of drilling fluids and cuttings (see *Chapters 8 and 9*). The grain size distribution was coarse-skewed at both near-field and far-field stations, but more so in the near-field. Elevated percentages in the sand and coarse silt phi intervals at Station NF-DS3 are evident on **Figure 5.3**.

**Table 5.3.** Sediment grain size results for Viosca Knoll Block 916.

Station	Gravel (%)	Sand (%)	Silt (%)	Clay (%)	Mean Grain Size (µm)	Folk's Textural Description
<b>CRUISE 1B (Pre-Drilling)</b>						
<b>Near-Field</b>						
NF-B01	0.00	4.24	35.64	60.12	2.91	Mud
NF-B02	0.00	2.47	27.28	70.25	2.23	Clay
NF-B03	0.00	1.30	28.31	70.40	2.28	Clay
NF-B04	0.00	2.48	56.40	41.11	6.40	Mud
NF-B05	0.00	3.82	37.84	58.34	3.67	Mud
NF-B06	0.00	2.33	19.77	77.90	1.30	Clay
NF-B07	0.00	4.53	40.40	55.07	3.68	Mud
NF-B08	0.00	3.80	29.96	66.23	2.46	Clay
NF-B09	0.00	3.46	27.70	68.84	2.32	Clay
NF-B10	0.00	2.55	26.23	71.23	1.89	Clay
NF-B11	0.00	2.51	26.35	71.14	2.30	Clay
NF-B12	0.00	1.23	14.59	84.18	1.02	Clay
<b>Far-Field</b>						
FF2-B01	0.00	3.30	26.23	70.47	2.26	Clay
FF2-B02	0.00	3.16	29.95	66.89	2.27	Clay
FF3-B01	0.00	4.90	39.25	55.85	3.59	Mud
FF3-B02	0.00	3.69	25.62	70.69	2.24	Clay
FF4-B01	0.00	5.40	43.64	50.96	4.41	Mud
FF4-B02	1.20	3.10	24.93	70.77	1.34	Slightly gravelly mud
FF5-B01	0.00	2.96	23.82	73.22	1.86	Clay
FF5-B02	0.00	3.10	25.77	71.13	2.20	Clay
FF6-B01	0.00	3.22	24.91	71.87	2.10	Clay
FF6-B02	0.00	2.09	27.24	70.67	2.15	Clay
<b>CRUISE 3B (Post-Exploration)</b>						
<b>Near-Field</b>						
NF-B01	0.74	7.70	28.91	62.65	2.69	Slightly gravelly mud
NF-B02	0.00	3.41	22.39	74.21	1.86	Clay
NF-B03	0.00	5.48	26.76	67.77	2.36	Clay
NF-B04	0.00	2.73	24.59	72.68	2.20	Clay
NF-B05	0.00	6.83	26.43	66.74	2.27	Clay
NF-B06	0.00	6.54	23.23	70.23	2.09	Clay
NF-B07	0.00	7.61	29.50	62.89	2.86	Clay
NF-B08	0.00	3.18	28.53	68.28	2.32	Clay
NF-B09	0.00	2.25	24.04	73.71	2.01	Clay
NF-B10	0.00	2.16	19.94	77.91	1.35	Clay
NF-B11	0.00	5.01	24.28	70.72	2.25	Clay
NF-B12	0.00	3.05	25.92	71.03	2.24	Clay
<b>Far-Field</b>						
FF1-B01	0.00	3.96	26.05	69.99	2.20	Clay
FF1-B02	0.00	3.40	25.02	71.58	2.32	Clay
FF2-B01	0.00	2.54	17.68	79.78	1.45	Clay
FF2-B02	0.00	2.27	16.66	81.07	1.37	Clay
FF3-B01	0.00	3.02	17.70	79.28	1.46	Clay
FF3-B02	0.00	3.34	23.78	72.88	1.91	Clay
FF4-B01	0.00	2.47	16.08	81.45	1.19	Clay
FF4-B02	0.00	2.87	27.18	69.95	2.12	Clay
FF5-B01	0.00	1.69	17.16	81.15	1.43	Clay
FF5-B02	0.00	2.98	17.56	79.46	1.32	Clay
FF6-B01	0.00	4.18	22.45	73.38	1.89	Clay
FF6-B02	0.00	4.77	26.20	69.03	2.34	Clay



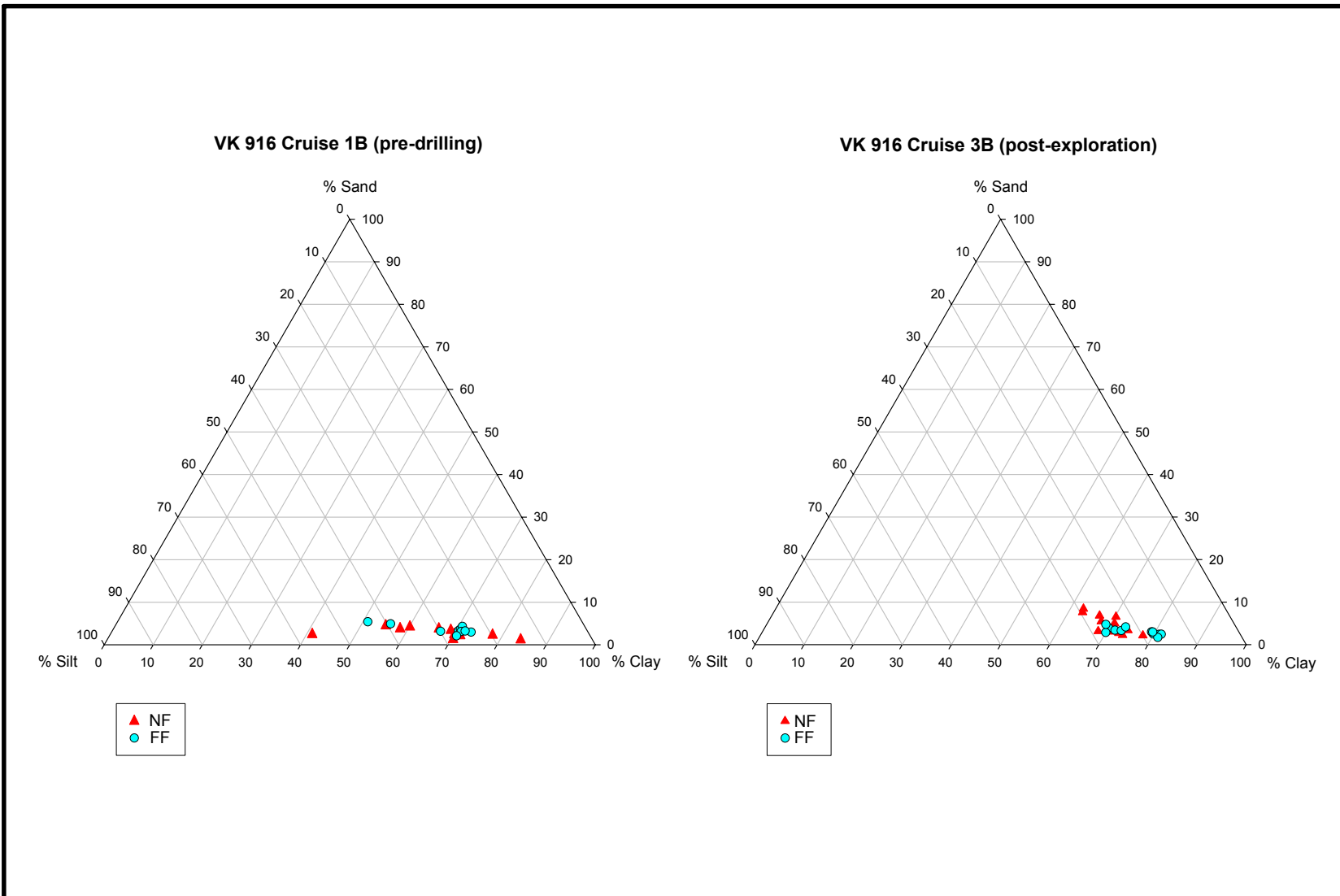
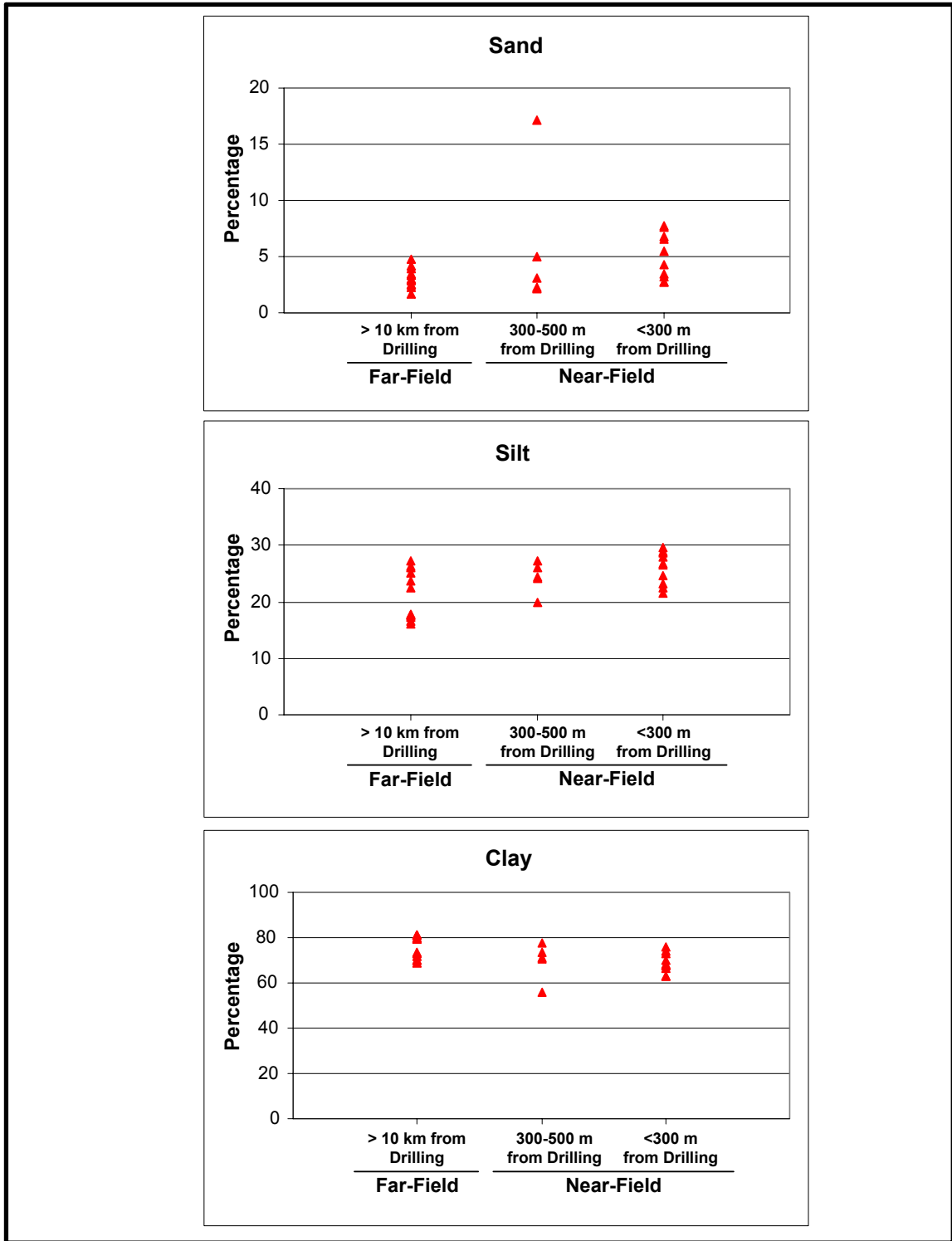
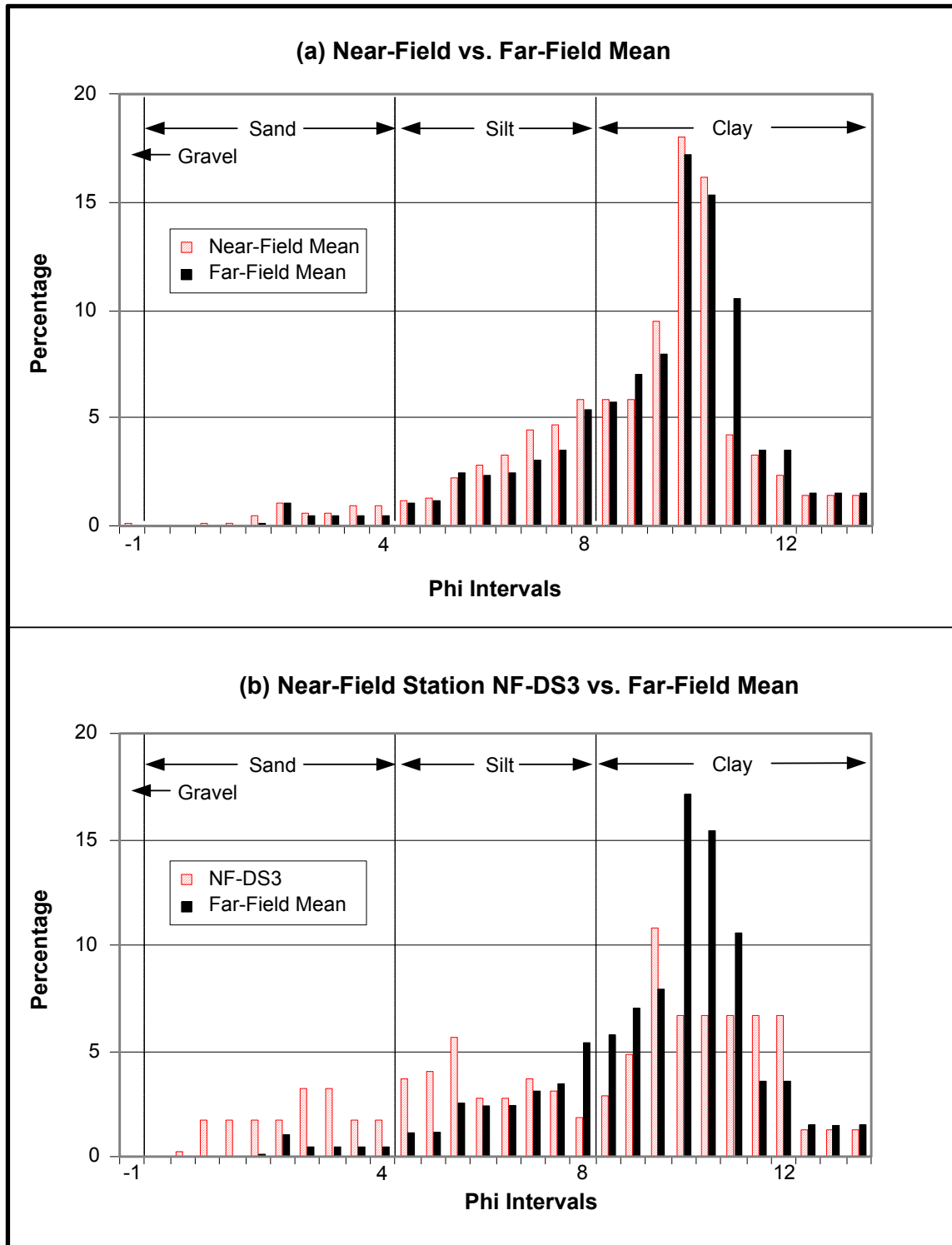


Figure 5.1. Ternary plots summarizing grain size data for Viosca Knoll Block 916.



**Figure 5.2.** Percentages of sand, silt, and clay in relation to proximity to drilling at Viosca Knoll Block 916. Points are individual stations including non-random "discretionary" stations. Only data from the post-drilling survey (Cruise 3B) are included. Note the elevated sand percentages at some near-field stations.



**Figure 5.3.** Grain size distribution at Viosca Knoll Block 916 on the post-drilling survey (Cruise 3B). (a) Comparison of near-field and far-field averages. (b) Comparison of near-field station NF-DS3 and far-field average. Note the shift toward coarser sediments in the near-field.

Within the near-field site, areas geophysically mapped as cuttings (see *Chapter 4*) tended to have relatively high percentages of sand (**Figure 5.4**). In the near-field, sand percentage was positively correlated with sediment barium ( $r = 0.76$ ,  $n = 12$ ,  $p < 0.01$ ) and SBF ( $r = 0.68$ ,  $n = 12$ ,  $p < 0.02$ ) (calculated using random stations only) (**Figure 5.5**) suggesting that the presence of drilling discharges increased the percentage of sand. However, some near-field stations with elevated barium and/or SBF had sand percentages similar to those seen in the far-field.

Subsamples from the three discretionary stations on Cruise 3B were sectioned in 2-cm intervals to a depth of 10 cm. Generally, sediments in the top two intervals (0 to 4 cm) had more sand and silt and less clay than deeper intervals (**Figure 5.6**). Station NF-DS3 was most strongly affected, with the sand percentage declining from 17.14% at the surface to less than 2% at depths greater than 4 cm. Only a slight trend (if any) was present at Station NF-DS1. The apparent depth of the mud/cuttings layer at this site (about 4 cm) is consistent with estimates presented in *Chapter 8* based on barium and total organic carbon data.

### 5.3.2 Garden Banks Block 516

Garden Banks Block 516 (GB 516) was sampled on Cruise 1B (October/November 2000) and Cruise 2B (July 2001). The first cruise was post-exploration, as two previous wells had been drilled at this site in 1999 (see *Chapter 3*). The second cruise was post-development, following the drilling of five new wells. Basic grain size statistics are summarized in **Table 5.4**. Ternary plots are shown in **Figure 5.7**.

Mean grain size ranged from 0.55 to 10.0  $\mu\text{m}$ , with most stations being in the 2 to 4  $\mu\text{m}$  range. Sediments can be characterized as poorly or very poorly sorted and the size distribution was coarse-skewed. The Folk's textural description was primarily "clay" or "mud" on both cruises, but several near-field stations on Cruise 2B were classified as "sandy clay" or "sandy mud." On Cruise 1B, sediments averaged about 64% clay and 31% silt at both near-field and far-field sites. Cruise 2B sediments on average had more sand (8%) and slightly less silt (29%) and clay (62%). Gravel-sized particles ( $>2$  mm) were not present in any samples.

On both cruises, the range of silt and clay concentrations was greater in the far-field than in the near-field. One station on Cruise 1B (FF4-B01) and two on Cruise 2B (FF1-B02 and FF2-B02) had noticeably more silt and less clay than the other far-field stations (**Figure 5.7**).

On Cruise 1B, sand percentages were similar at near-field and far-field stations. However, on Cruise 2B, several near-field stations had elevated sand percentages (**Figure 5.7**). This trend is more easily seen on **Figure 5.8**, which shows sand, silt, and clay percentages for post-drilling stations grouped into the same three categories mentioned previously (far-field, near-field 300 to 500 m, and near-field within 300 m). ANOVA indicated that near-field sand percentages on Cruise 2B were higher than far-field percentages, and also higher than both near- and far-field percentages from Cruise 1B (**Table 5.2**).

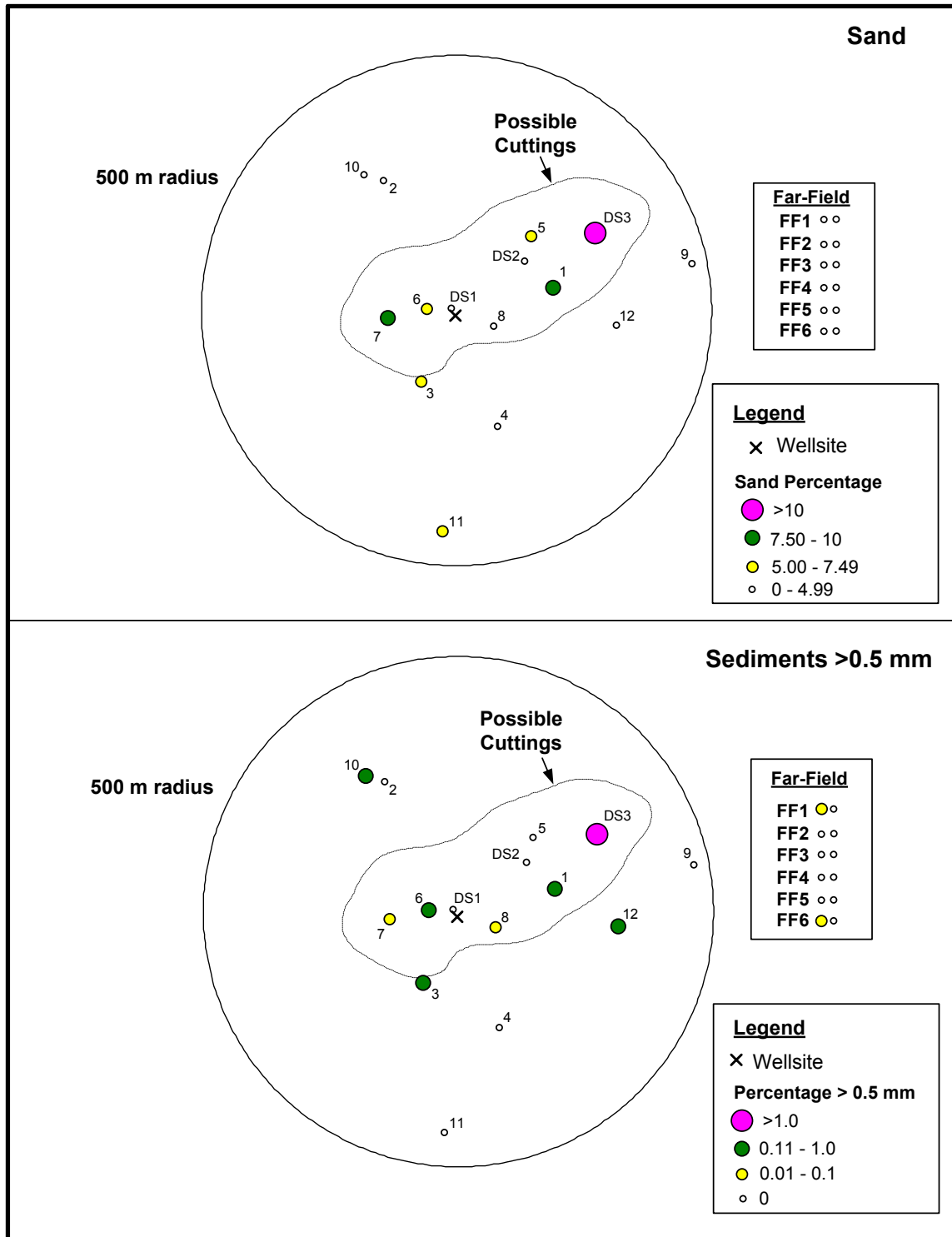


**Figure 5.4.** Percentages of sand and sediments >0.5 mm (coarse sand, very coarse sand, and gravel) on Cruise 3B at Viosca Knoll Block 916 in relation to geophysically mapped cuttings. Replicate values for far-field stations are shown in a separate box.

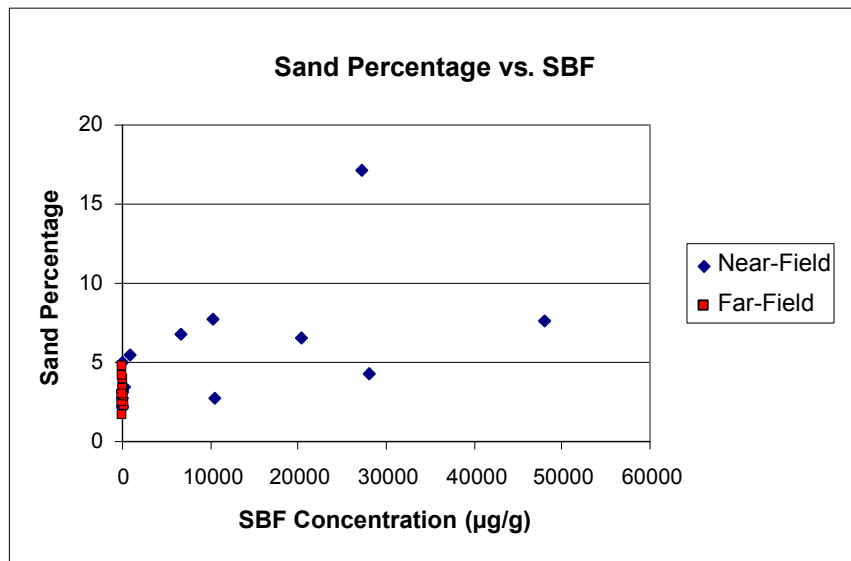
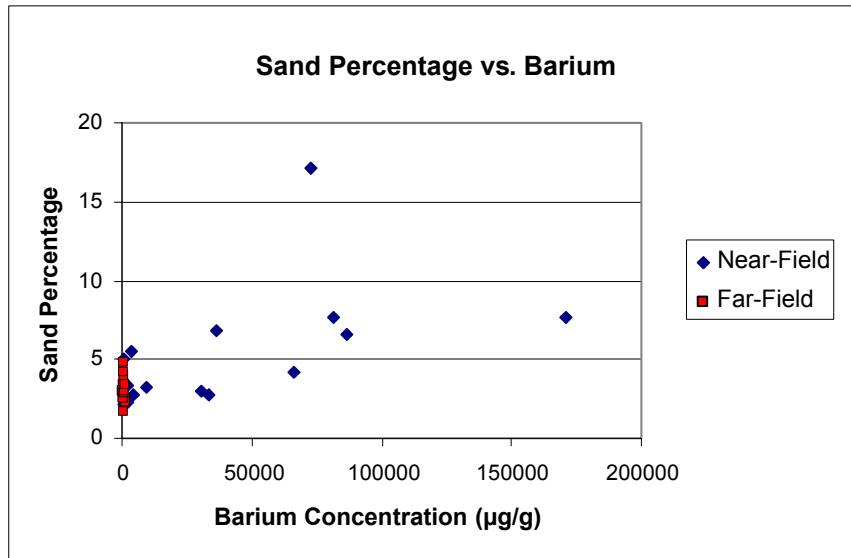


**Figure 5.5.** Relationships between sand percentages and concentrations of drilling indicators (barium and synthetic-based fluid [SBF] concentrations) at Viosca Knoll Block 916 on the post-drilling survey (Cruise 3B). Within the near-field, sand percentage was positively correlated with barium and SBF concentrations.

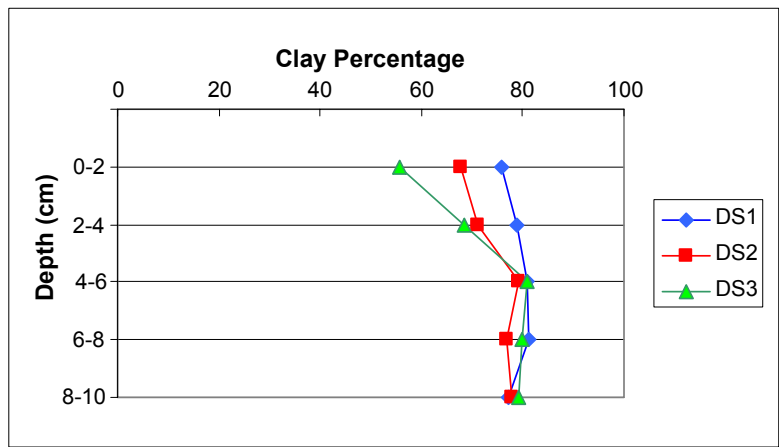
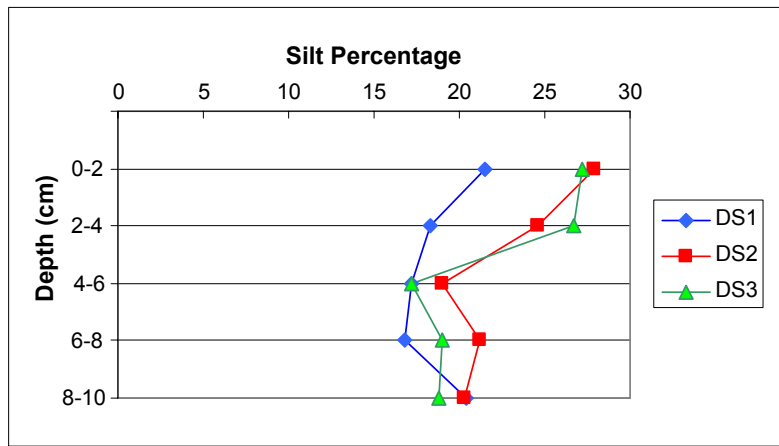
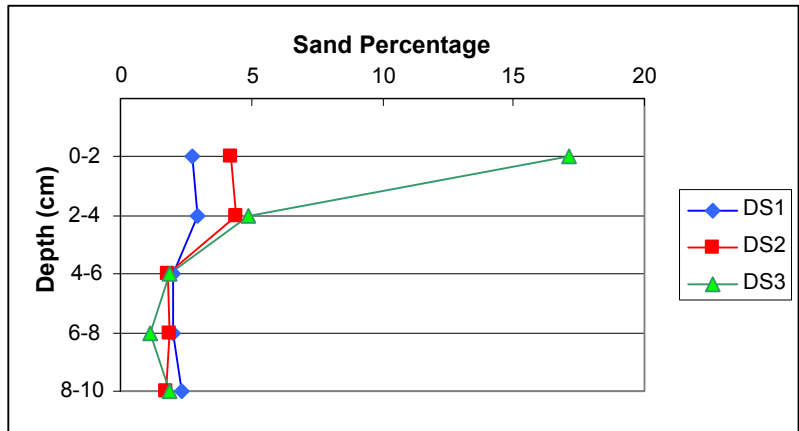


**Figure 5.6.** Depth profiles from discretionary stations (DS) at Viosca Knoll Block 916 on the post-drilling survey (Cruise 3B).

**Table 5.4.** Sediment grain size results for Garden Banks Block 516.

Station	Gravel (%)	Sand (%)	Silt (%)	Clay (%)	Mean Grain Size (μm)	Folk's Textural Description
<b>CRUISE 1B (post-exploration)</b>						
<b>Near-Field</b>						
NF-B01	0.00	4.50	33.31	62.19	3.18	Mud
NF-B02	0.00	6.80	37.61	55.59	3.84	Mud
NF-B03	0.00	4.68	22.30	73.02	1.80	Clay
NF-B04	0.00	5.11	36.17	58.71	3.52	Mud
NF-B05	0.00	4.70	32.36	62.94	2.76	Mud
NF-B06	0.00	5.09	30.58	64.33	3.11	Clay
NF-B07	0.00	4.85	21.72	73.43	1.96	Clay
NF-B08	0.00	5.37	29.10	65.52	2.43	Clay
NF-B09	0.00	6.53	23.12	70.35	2.20	Clay
NF-B10	0.00	4.42	33.89	61.69	2.77	Mud
NF-B11	0.00	5.37	32.42	62.21	2.81	Mud
NF-B12	0.00	7.25	24.77	67.99	2.35	Clay
<b>Far-Field</b>						
FF1-B01	0.00	5.84	34.58	59.58	3.43	Mud
FF1-B02	0.00	4.35	33.81	61.84	3.05	Mud
FF2-B01	0.00	3.03	19.76	77.21	1.88	Clay
FF2-B02	0.00	12.04	27.48	60.48	3.40	Sandy clay
FF3-B01	0.00	6.09	32.59	61.32	2.99	Mud
FF3-B02	0.00	4.74	27.09	68.17	2.52	Clay
FF4-B01	0.00	5.33	60.15	34.53	5.63	Mud
FF4-B02	0.00	6.61	27.31	66.08	2.70	Clay
FF5-B01	0.00	3.32	27.99	68.68	2.32	Clay
FF5-B02	0.00	4.56	30.26	65.18	2.98	Clay
FF6-B01	0.00	4.06	30.77	65.17	2.30	Clay
FF6-B02	0.00	3.37	28.54	68.10	2.22	Clay
<b>CRUISE 2B (post-development)</b>						
<b>Near-Field</b>						
NF-B01	0.00	5.18	23.71	71.12	2.60	Clay
NF-B02	0.00	8.95	31.25	59.80	1.23	Mud
NF-B03	0.00	11.25	37.16	51.58	4.95	Sandy mud
NF-B04	0.00	9.21	31.14	59.65	1.69	Mud
NF-B05	0.00	15.16	18.76	66.08	1.89	Sandy clay
NF-B06	0.00	18.23	36.18	45.59	6.80	Sandy mud
NF-B07	0.00	9.80	25.22	64.97	0.94	Clay
NF-B08	0.00	5.83	32.08	62.09	2.41	Mud
NF-B09	0.00	8.12	22.36	69.51	2.26	Clay
NF-B10	0.00	12.86	23.46	63.67	2.90	Sandy clay
NF-B11	0.00	7.98	14.77	77.25	0.55	Clay
NF-B12	0.00	9.74	25.58	64.68	0.75	Clay
<b>Far-Field</b>						
FF1-B01	0.00	6.60	31.58	61.82	1.60	Mud
FF1-B02	0.00	6.46	46.42	47.12	4.54	Mud
FF2-B01	0.00	5.29	29.69	65.02	2.93	Clay
FF2-B02	0.00	5.48	54.43	40.09	7.46	Mud
FF3-B01	0.00	5.03	32.85	62.13	1.01	Mud
FF3-B02	0.00	10.38	25.53	64.10	2.65	Sandy clay
FF4-B01	0.00	6.93	30.13	62.94	1.15	Clay
FF4-B02	0.00	7.11	15.96	76.93	2.01	Clay
FF5-B01	0.00	4.18	33.63	62.19	0.66	Mud
FF5-B02	0.00	5.39	30.76	63.85	1.28	Clay
FF6-B01	0.00	5.25	27.95	66.80	10.00	Clay
FF6-B02	0.00	5.76	25.91	68.33	8.62	Clay



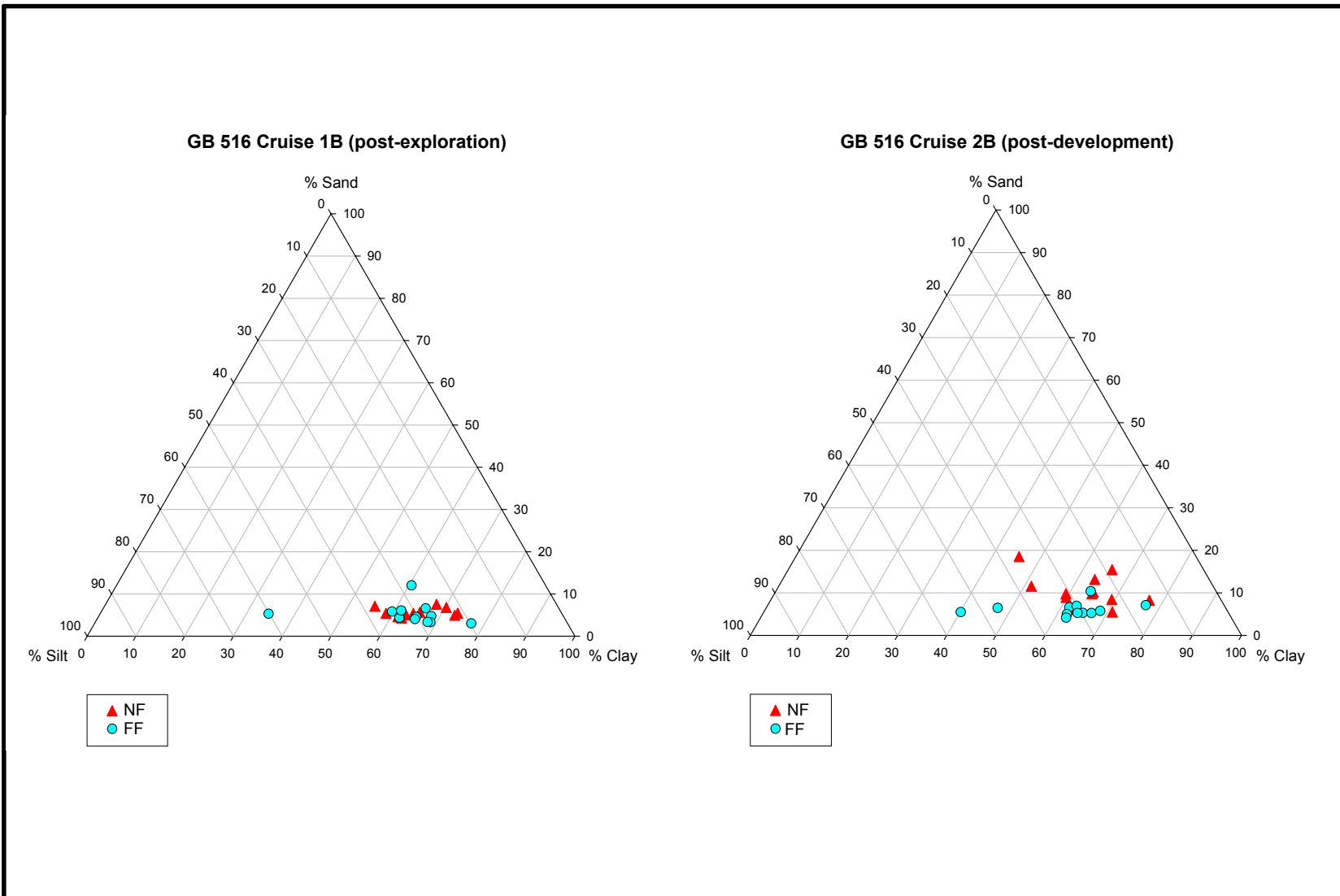
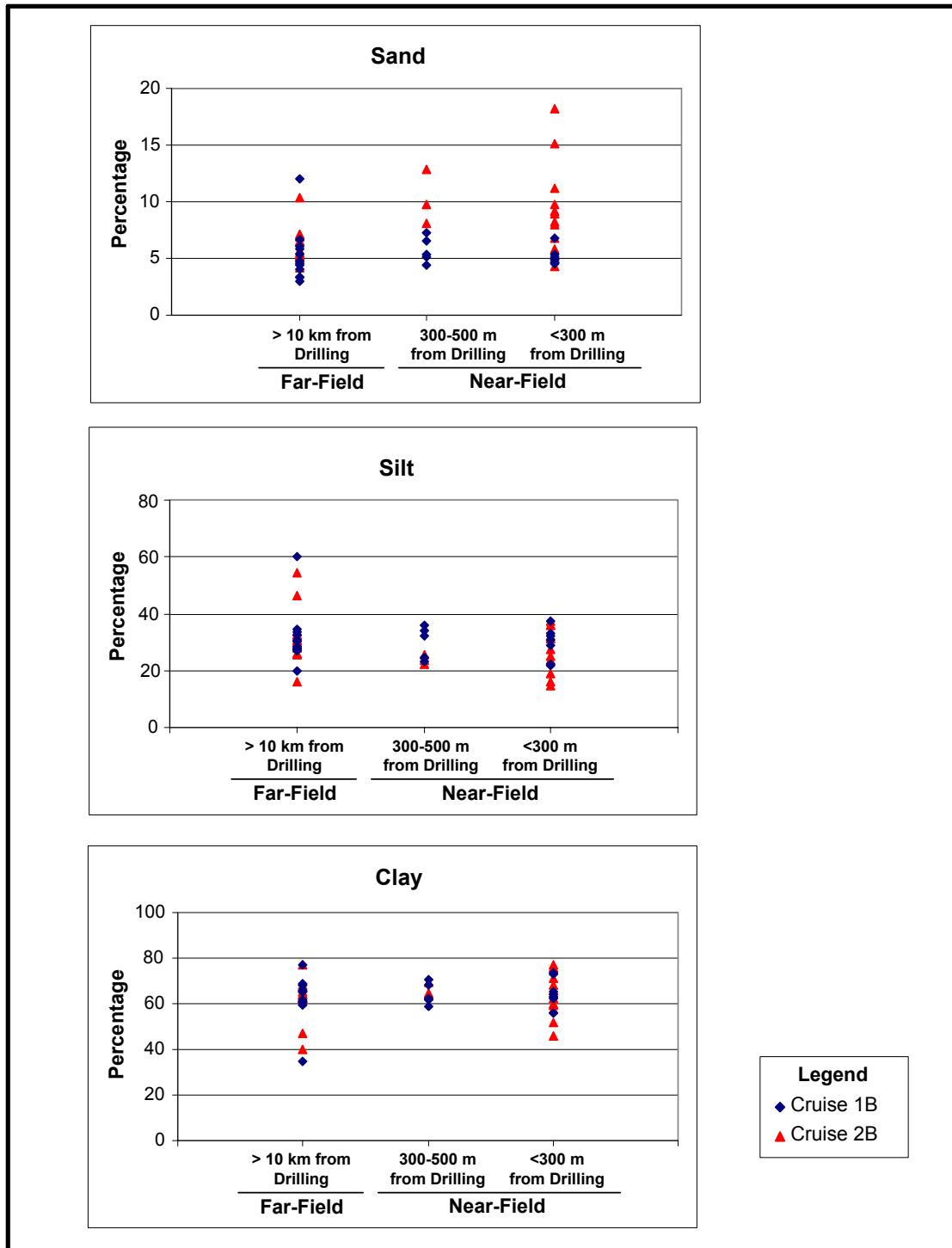


Figure 5.7. Ternary plots summarizing grain size data for Garden Banks Block 516.



**Figure 5.8.** Percentages of sand, silt, and clay in relation to proximity to drilling at Garden Banks Block 516. Points are individual stations including non-random "discretionary" stations. Note the elevated sand percentages at some near-field stations and elevated silt at some far-field stations.

The grain size distribution at GB 516 was bimodal at both near-field and far-field stations, with peaks around phi 4.5 to 5.0 (coarse silt) and phi 10 (clay) (**Figure 5.9**). On average, near-field stations had higher percentages in the coarser phi classes (sand) and lower percentages in the coarse silt range when compared with the far-field stations. **Figure 5.9(b)** shows that one discretionary station (NF-DS2) had elevated percentages in several clay size categories, possibly due to drilling fluid particles. This station had very high concentrations of barium (198,000  $\mu\text{g/g}$ ) and SBF (117,280  $\mu\text{g/g}$ ), indicating the presence of drilling fluids and cuttings (see *Chapters 8 and 9*).

On Cruise 2B, most near-field stations were within geophysically mapped cuttings zones (see *Chapter 4*) and had higher sand percentages than most far-field stations (**Figure 5.10**). However, one near-field station (NF-B10) outside the cuttings zone had >10% sand. On Cruise 1B, there was little or no difference between sand percentages at near-field vs. far-field stations (there was no geophysical map for this cruise, so the location of stations in relation to cuttings zones is unknown). There was no consistent relationship between sand percentages and sediment barium and SBF concentrations on either cruise (**Figure 5.11**).

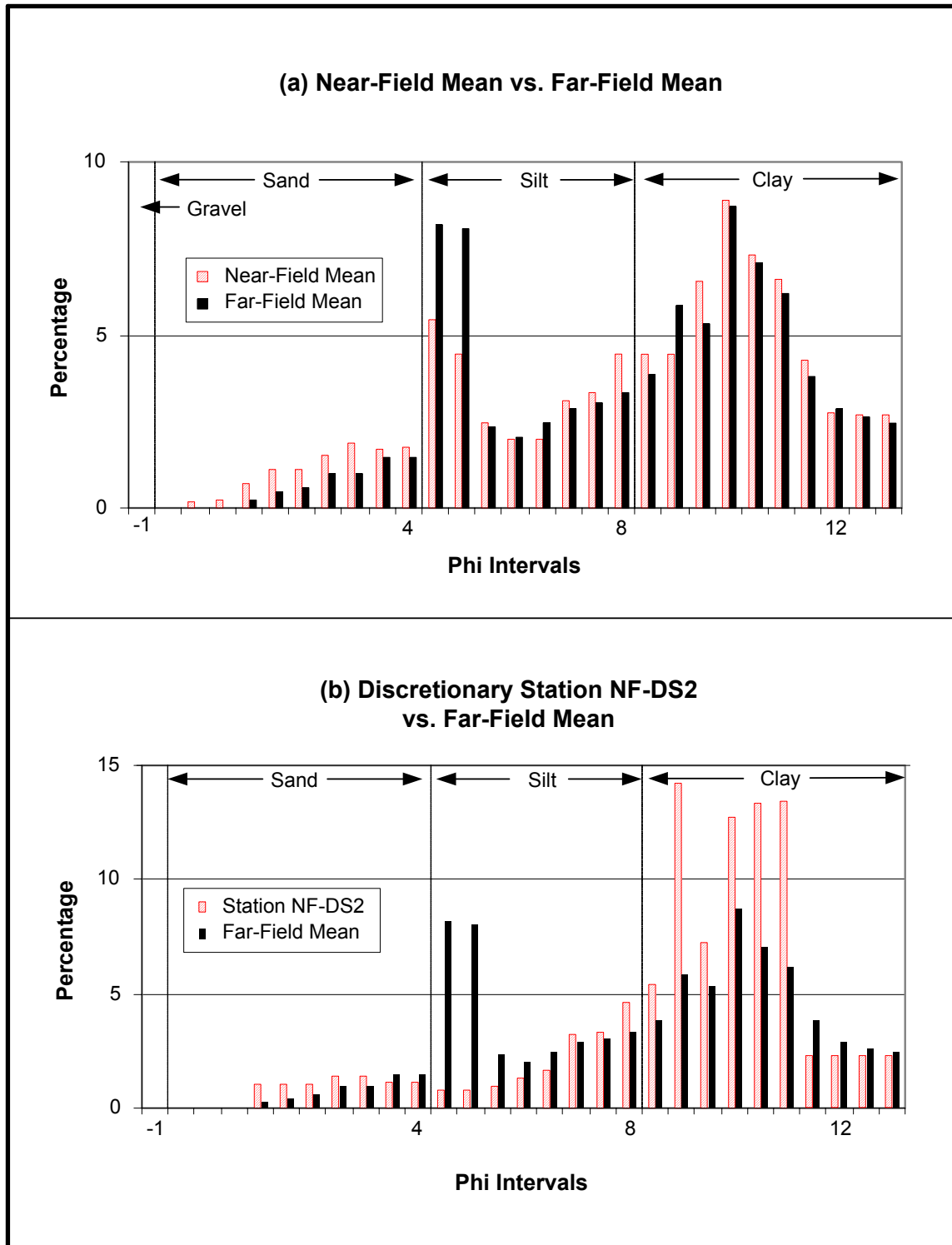
Subsamples from the three discretionary stations on Cruise 2B were sectioned in 2-cm intervals to a depth of 10 cm. While all of the stations had higher sand percentages at the surface than at 10 cm depth, there was also a subsurface maximum for Stations DS1 and DS2 (**Figure 5.12**). Based on sand percentages, the thickness of mud and cuttings at this site may extend to a depth of 6 to 8 cm. Station DS2 was quite different from the other two stations, in particular having more silt and less clay at all depths below 2 cm. It is not known whether this represents an impact or natural variation.

### 5.3.3 Garden Banks Block 602

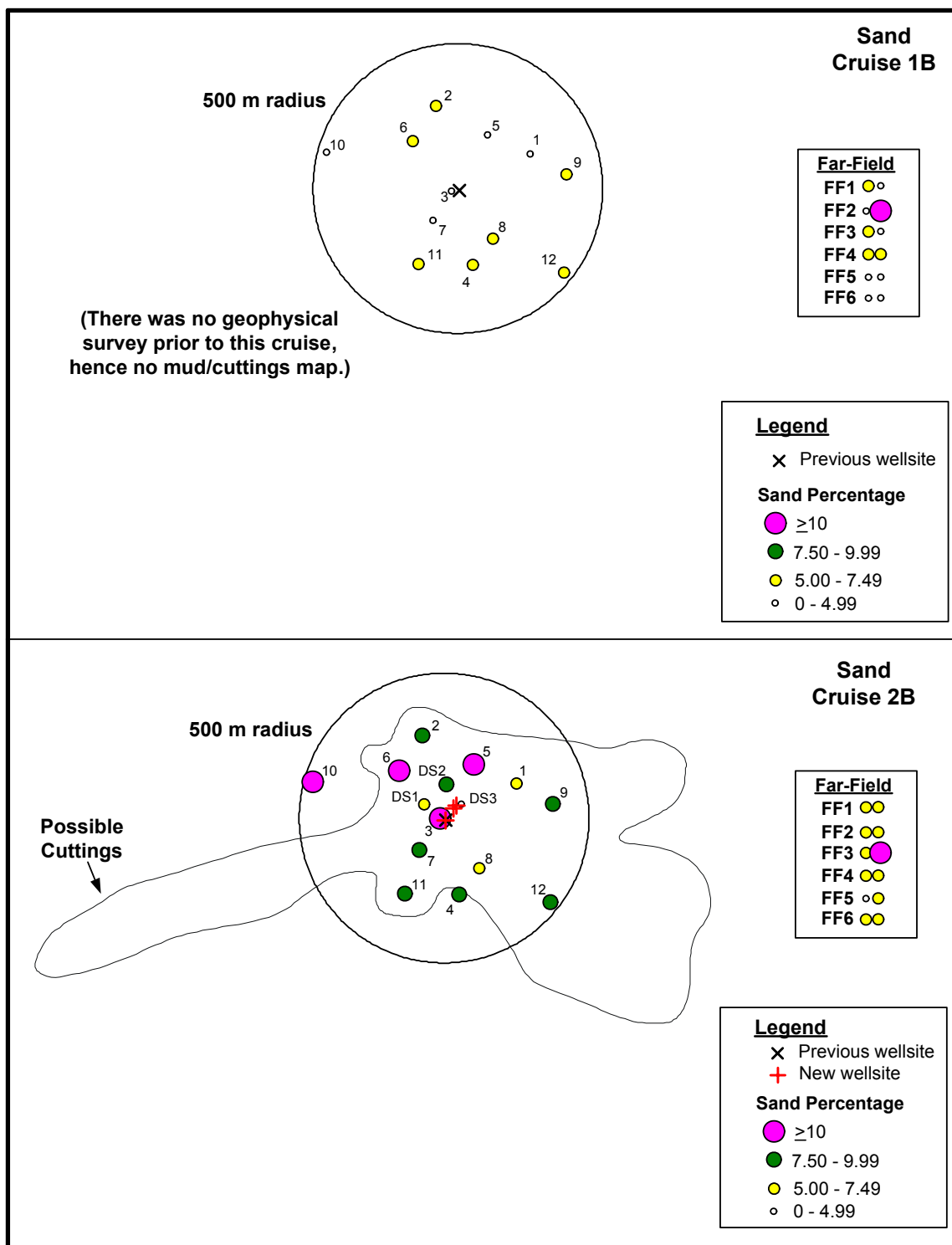
Garden Banks Block 602 (GB 602) was sampled on Cruise 2B (July 2001). This was a post-development survey; seven wells had been drilled within the near-field site between September 1995 and January 2001 (see *Chapter 3*). Basic grain size statistics are summarized in **Table 5.5**. Ternary plots are shown in **Figure 5.13**.

Mean grain size ranged from 0.27 to 13.23  $\mu\text{m}$ . Mean grain size was generally  $<2 \mu\text{m}$  at far-field stations and in the 2 to 4  $\mu\text{m}$  range at near-field stations. Sediments can be characterized as very poorly or extremely poorly sorted and the size distribution was strongly coarse-skewed. The Folk's textural description was primarily "sandy mud" or "sandy clay" in the near-field and "clay" or "sandy clay" in the far-field. Gravel-sized particles were not present in any samples.

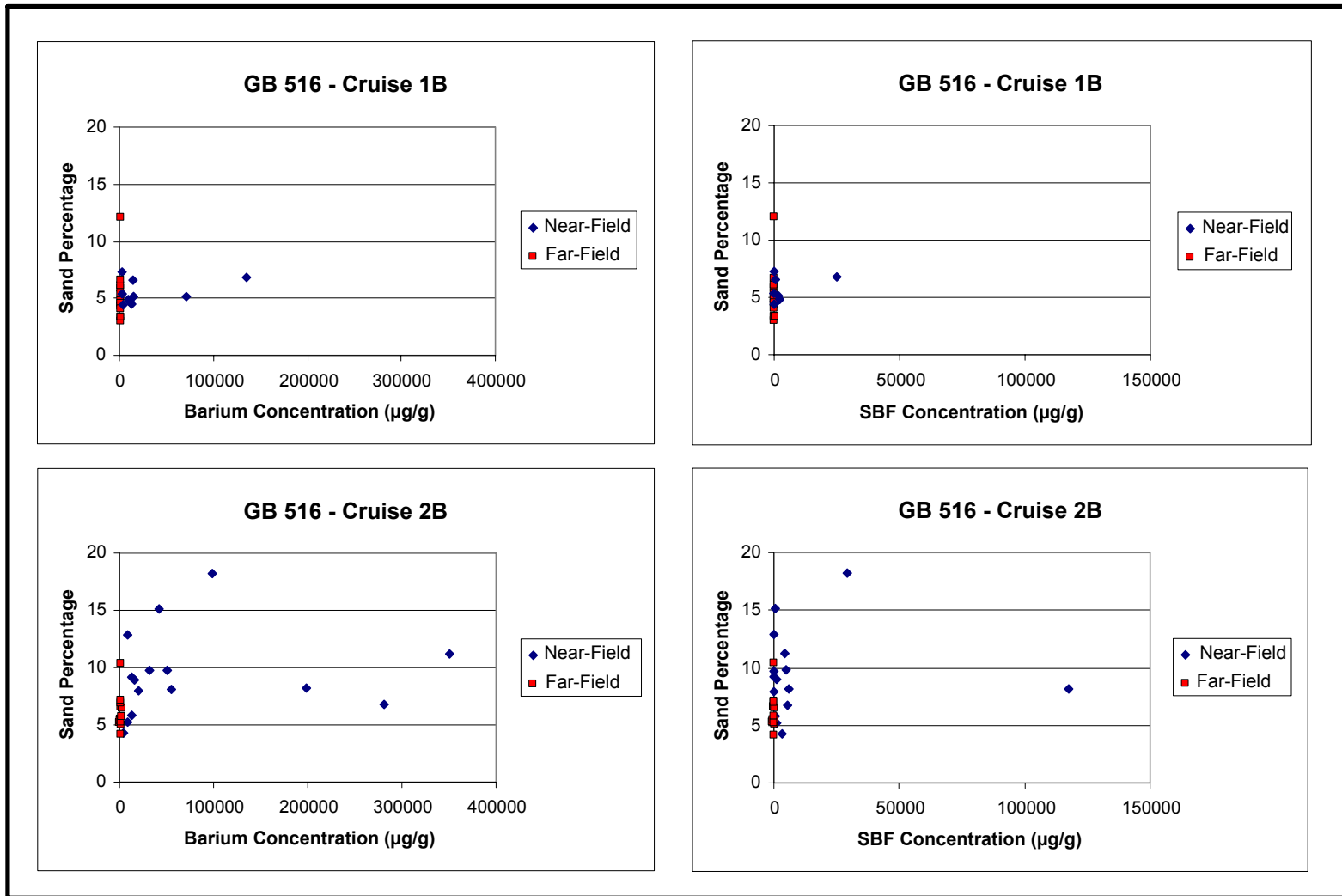
At both near-field and far-field sites, there was one station with much more silt and less clay than the other stations (**Figure 5.13**). Aside from these samples, the near-field stations generally had a greater range of silt and clay content than the far-field stations. The same pattern is evident on **Figure 5.14**, which shows sand, silt, and clay percentages for stations grouped into the same three categories mentioned previously (far-field, near-field 300 to 500 m, and near-field within 300 m). Generally, there is a pattern of increasing silt and decreasing clay near drilling. However, the ANOVAs for silt and clay are not significant (**Table 5.2**).



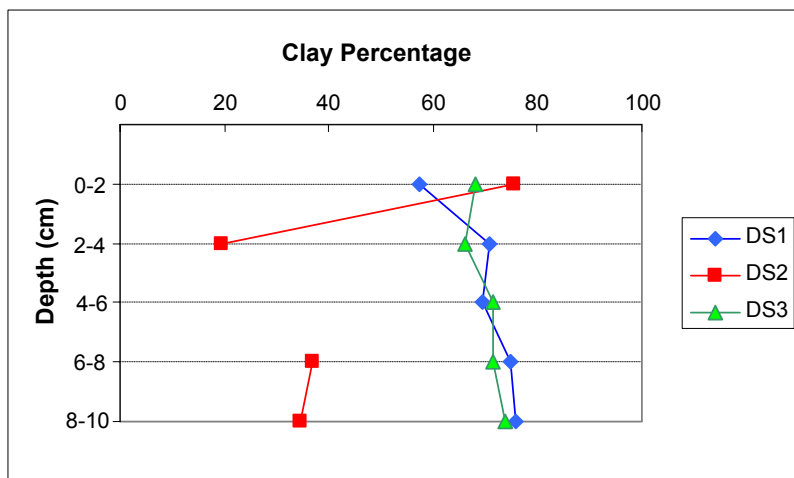
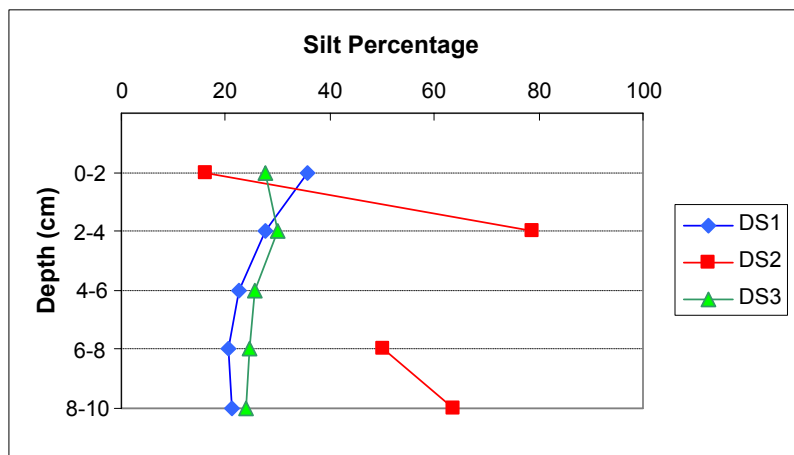
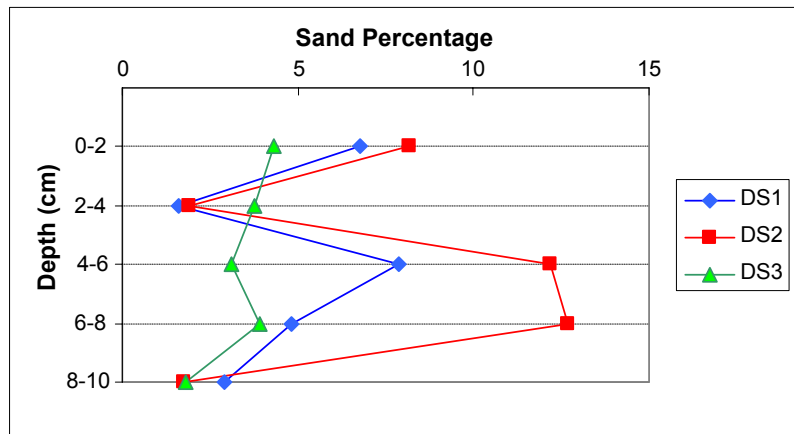
**Figure 5.9.** Grain size distribution at Garden Banks Block 516 on Cruise 2B. (a) Near-field mean vs. far-field mean; (b) discretionary station NF-DS2 vs. far-field mean.



**Figure 5.10.** Percentages of sand on Cruise 1B and Cruise 2B at Garden Banks Block 516 in relation to geophysically mapped cuttings. There was no geophysical map for Cruise 1B. Replicate values for far-field stations are shown in a separate box.



**Figure 5.11.** Relationships between sand percentages and concentrations of drilling indicators (barium and synthetic-based fluids [SBF]) at Garden Banks Block 516 on Cruises 1B and 2B. There were no significant correlations between sand percentages and barium or SBF concentrations.



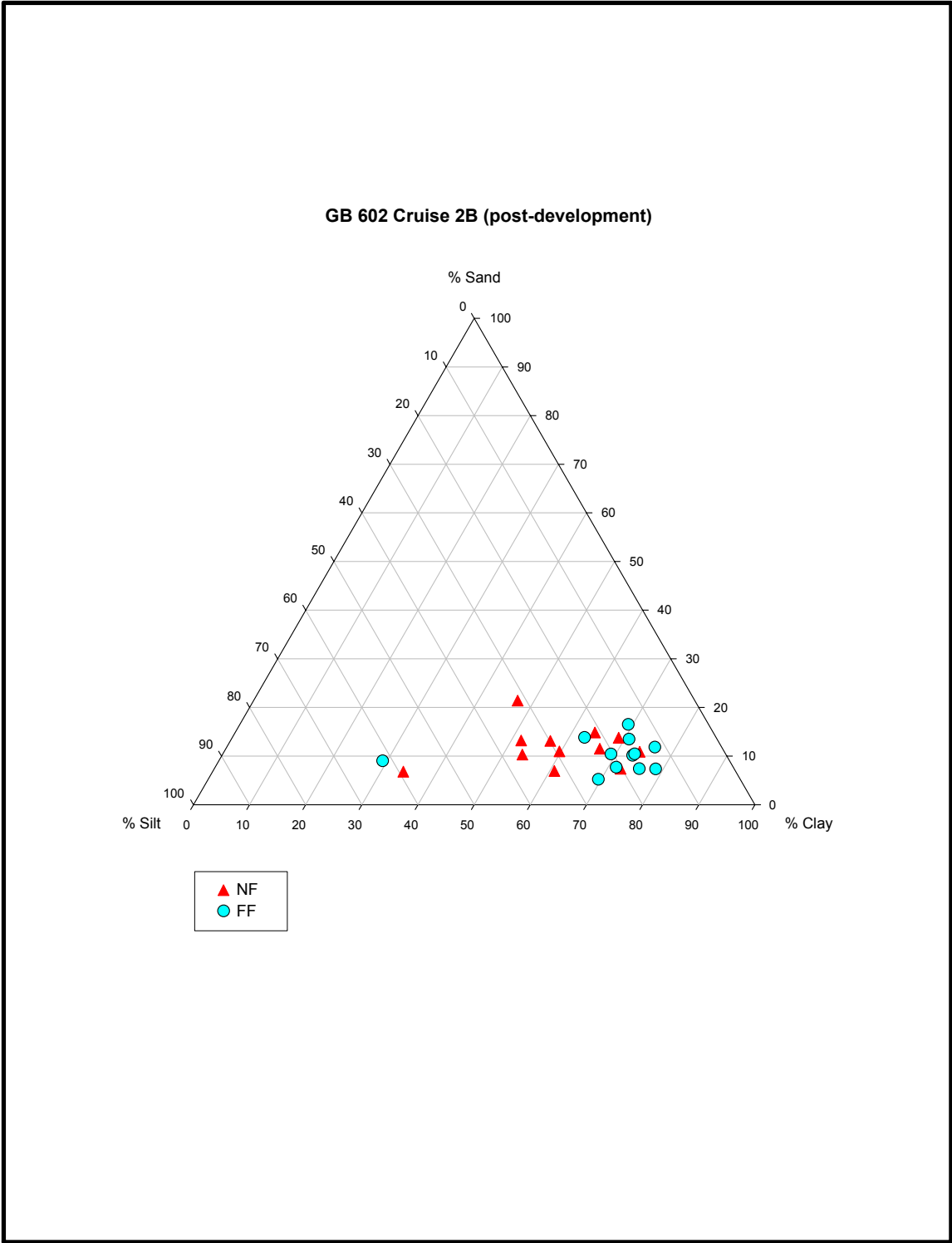
Note: Separate silt and clay values were not obtained for the 4-6 cm interval of DS2.

Figure 5.12. Depth profiles from discretionary stations (DS) at Garden Banks Block 516 on Cruise 2B (post-development).

**Table 5.5.** Sediment grain size results for Garden Banks Block 602.

Station	Gravel (%)	Sand (%)	Silt (%)	Clay (%)	Mean Grain Size ( $\mu\text{m}$ )	Folk's Textural Description
<b>Near-Field</b>						
NF-B01	0.00	6.50	59.38	34.12	4.36	Mud
NF-B02	0.00	10.59	15.25	74.17	2.62	Sandy clay
NF-B03	0.00	21.12	31.70	47.18	7.10	Sandy mud
NF-B04	0.00	7.11	20.37	72.52	2.66	Clay
NF-B05	0.00	10.67	29.49	59.85	2.39	Sandy clay
NF-B06	0.00	12.83	30.03	57.14	3.25	Sandy mud
NF-B07	0.00	12.93	35.19	51.87	3.78	Sandy mud
NF-B08	0.00	11.22	22.03	66.76	3.41	Sandy clay
NF-B09	0.00	6.64	32.41	60.95	3.25	Mud
NF-B10	0.00	10.02	36.41	53.57	3.86	Sandy mud
NF-B11	0.00	14.55	21.23	64.22	2.31	Sandy clay
NF-B12	0.00	13.48	17.55	68.98	2.16	Sandy clay
<b>Far-Field</b>						
FF1-B01	0.00	7.70	20.87	71.43	1.95	Clay
FF1-B02	0.00	10.42	20.45	69.13	0.51	Sandy clay
FF2-B01	0.00	13.48	15.70	70.82	0.97	Sandy clay
FF2-B02	0.00	7.40	16.92	75.68	1.10	Clay
FF3-B01	0.00	5.22	25.29	69.50	0.67	Clay
FF3-B02	0.00	13.84	23.44	62.72	0.56	Sandy clay
FF4-B01	0.00	10.14	16.52	73.34	0.88	Sandy clay
FF4-B02	0.00	11.84	11.92	76.25	1.16	Sandy clay
FF5-B01	0.00	7.36	14.02	78.62	0.27	Clay
FF5-B02	0.00	9.02	61.82	29.16	13.23	Silt
FF6-B01	0.00	10.44	16.31	73.26	1.67	Sandy clay
FF6-B02	0.00	16.50	14.33	69.17	1.35	Sandy clay





**Figure 5.13.** Ternary plot summarizing grain size data for Garden Banks Block 602.

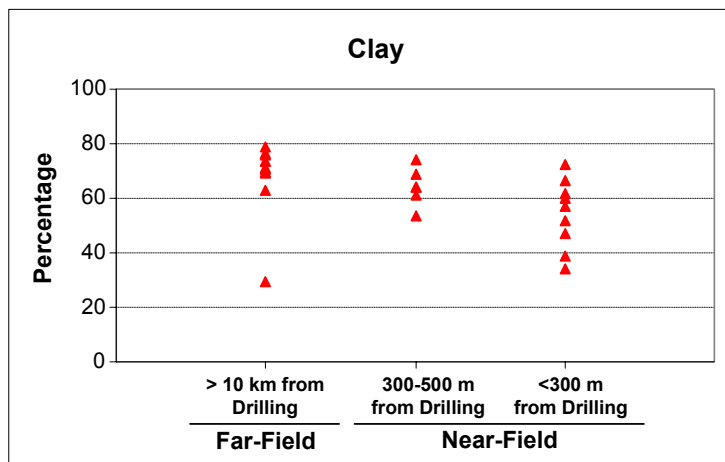
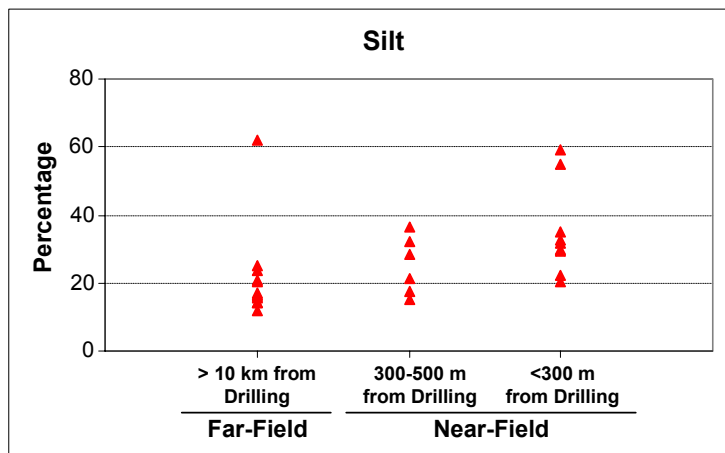
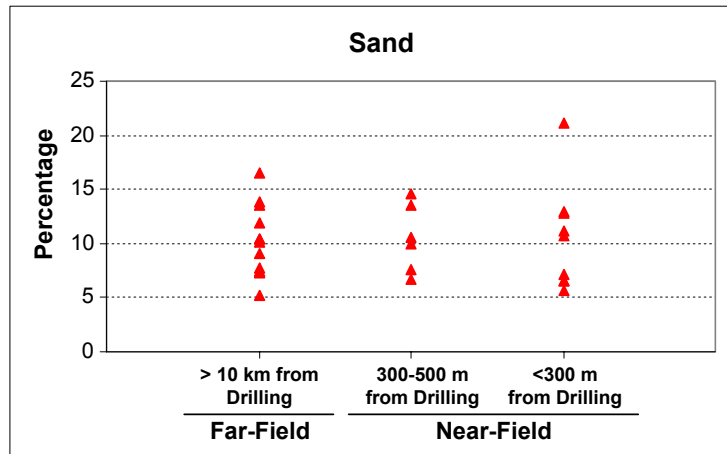


**Figure 5.14.** Percentages of sand, silt, and clay in relation to proximity to drilling at Garden Banks Block 602. Points are individual stations including non-random "discretionary" stations.

Sand percentages were similar at near-field and far-field stations with the exception of one near-field station with the highest value (NF-B03, 21.12%). The ANOVA for sand was not significant (**Table 5.2**).

The grain size distribution at GB 602 was bimodal at both near-field and far-field stations, with peaks around phi 3.5 to 4.0 (very fine sand) and phi 9.0 (clay) (**Figure 5.15a**). On average, near-field stations had higher percentages in the coarser phi classes (phi <3.0) and lower percentages in the 3.5 and 4.0 phi intervals when compared with the far-field stations.

**Figure 5.15b** shows the grain size distribution at Station NF-B03, which had high concentrations of drilling fluid indicators (barium: 111,000 µg/g and SBF: 8,446 µg/g) (see *Chapters 8 and 9*). The increase in the medium to coarse sand fraction is particularly evident at this station.

Most of the near-field stations at GB 602 were within zones geophysically mapped as cuttings (see *Chapter 4*). There was little or no difference in sand percentage among near-field stations within vs. outside the cuttings zones (**Figure 5.16**). Generally, near-field and far-field stations had similar sand percentages. There was no consistent relationship between sand, silt, and clay percentages vs. sediment barium concentrations (**Figure 5.17**).

Subsamples from the three discretionary stations were sectioned in 2-cm intervals to a depth of 10 cm. Sand percentages show a subsurface maximum for all three stations in the 4 to 6 cm range (**Figure 5.18**). This may reflect layering from previous drilling discharges. Silt percentages for DS1, which had the highest barium and SBF concentration (see *Chapters 8 and 9*), declined from the surface to a depth of 6 to 8 cm. The thickness of mud and cuttings layers at this site may extend to a depth of 6 to 8 cm.

#### **5.3.4 Mississippi Canyon Block 292**

Mississippi Canyon Block 292 (MC 292) was sampled on Cruise 2B (July 2001). This was a post-development survey; five wells were drilled near the center of the site between May 1995 and July 1999 (see *Chapter 3*). Basic grain size statistics are summarized in **Table 5.6**. A ternary plot is shown in **Figure 5.19**.

Mean grain size ranged from 0.18 to 7.42 µm. Mean grain size was generally <3 µm at both far-field and near-field stations. Generally, sediments can be characterized as very poorly or extremely poorly sorted and the size distribution was strongly coarse-skewed. The Folk's textural description was primarily "clay" or "mud" at both far-field and near-field stations. Gravel-sized particles (>2 mm) were not present in any samples.

At the far-field site, there was one station (FF5-B02) with much more silt and less clay than the other stations (**Figure 5.19**). The silt and clay content of near-field and far-field stations did not differ significantly according to the ANOVA (**Table 5.2**).

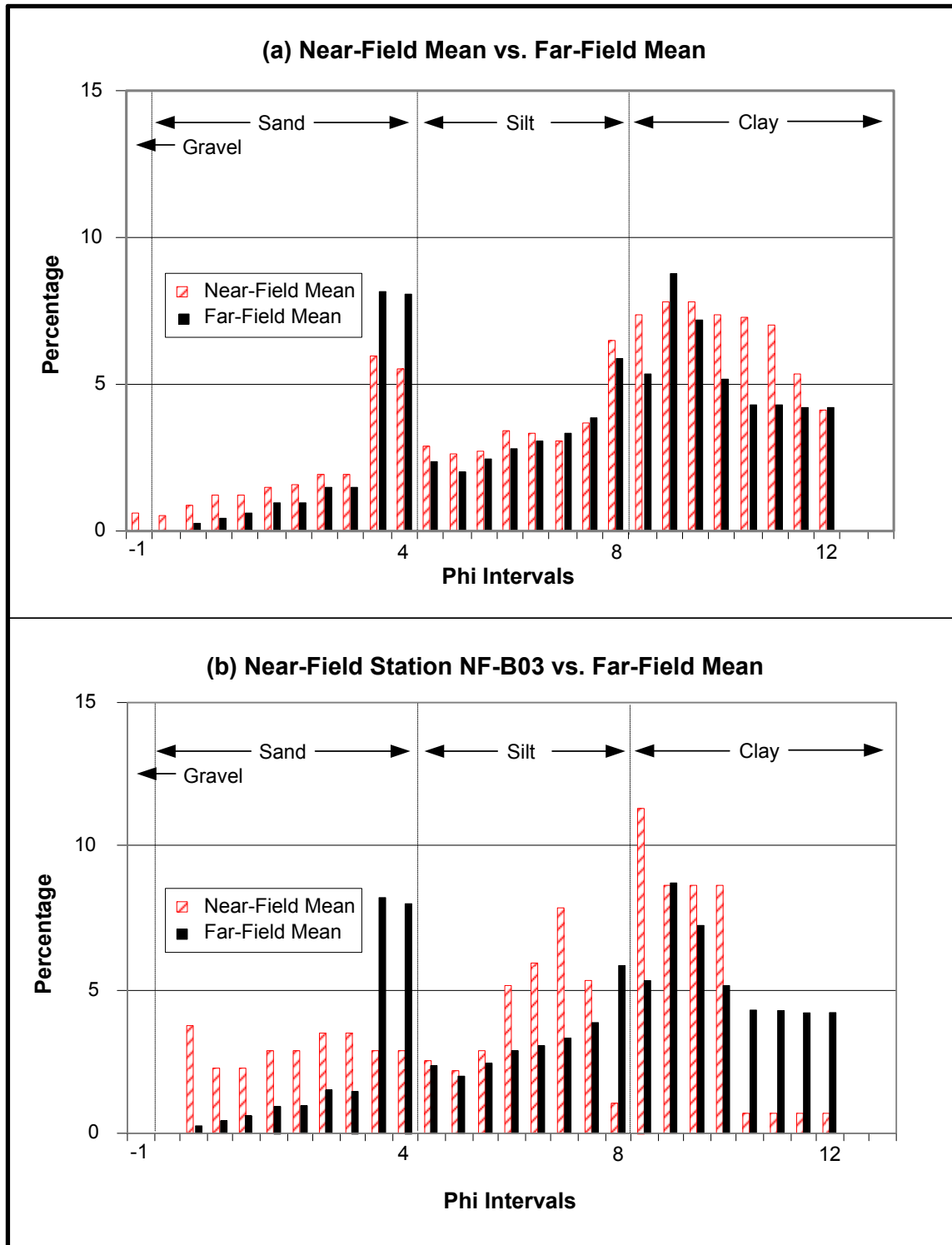
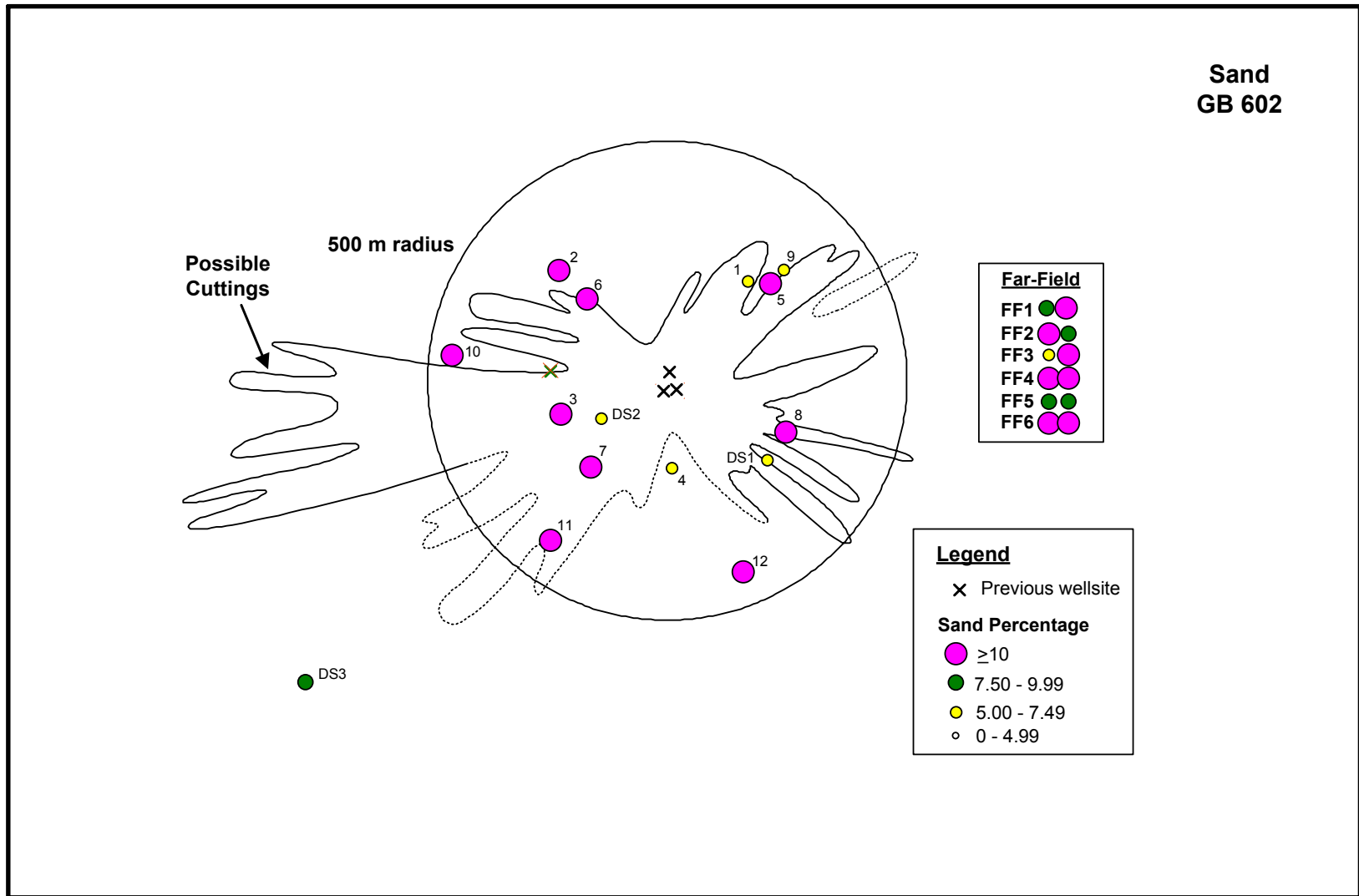
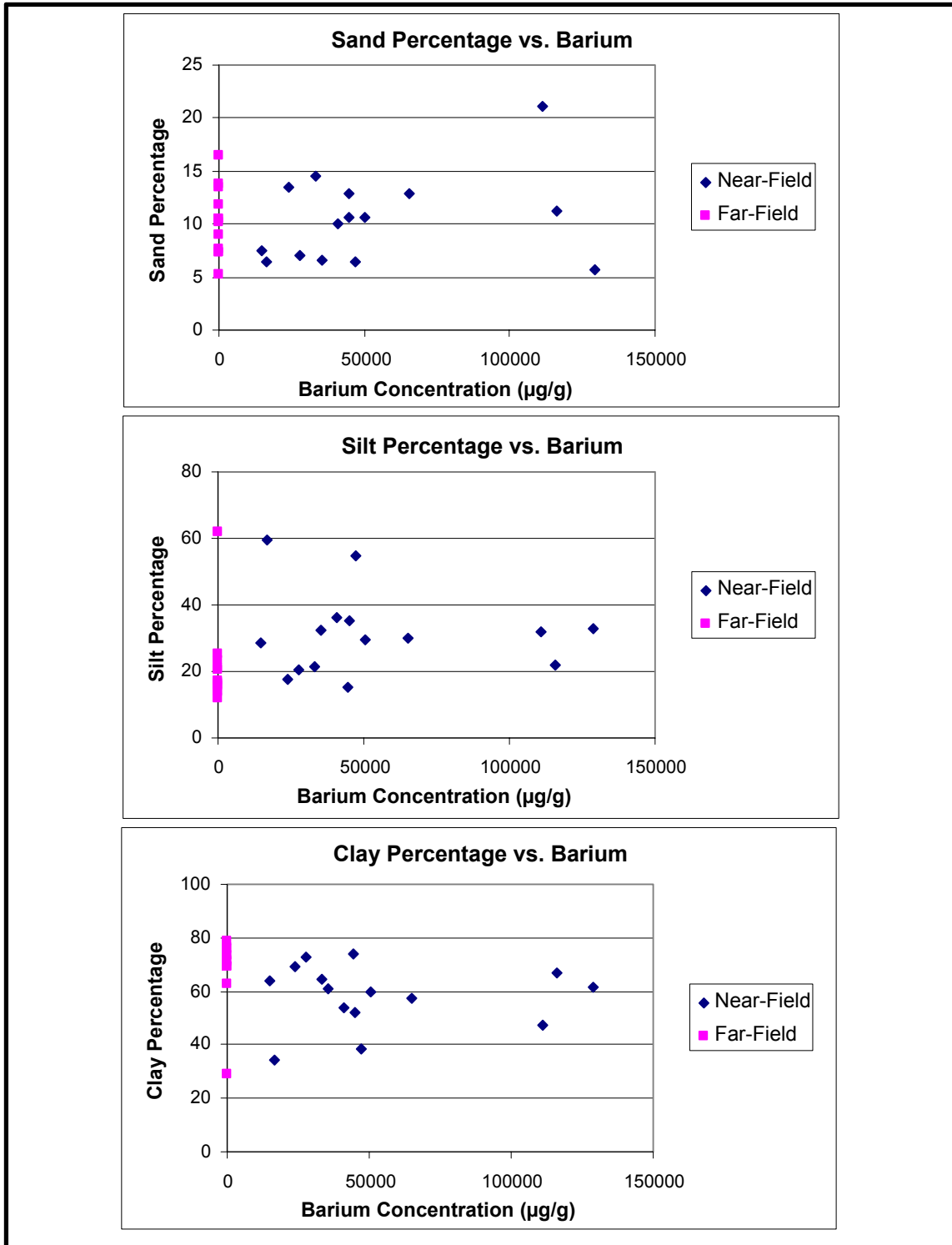


Figure 5.15. Grain size distribution at Garden Banks Block 602 on Cruise 2B. (a) Near-field mean vs. far-field mean; (b) near-field Station NF-B03 vs. far-field mean.



**Figure 5.16.** Sand percentages on Cruise 2B at Garden Banks Block 602 in relation to geophysically mapped cuttings. Replicate values for far-field stations are shown in a separate box.



**Figure 5.17.** Relationships between sand, silt, and clay percentages and concentrations of barium (drilling fluid indicator) at Garden Banks Block 602 on Cruise 2B. There were no significant correlations between barium concentrations and sand, silt, or clay percentages.

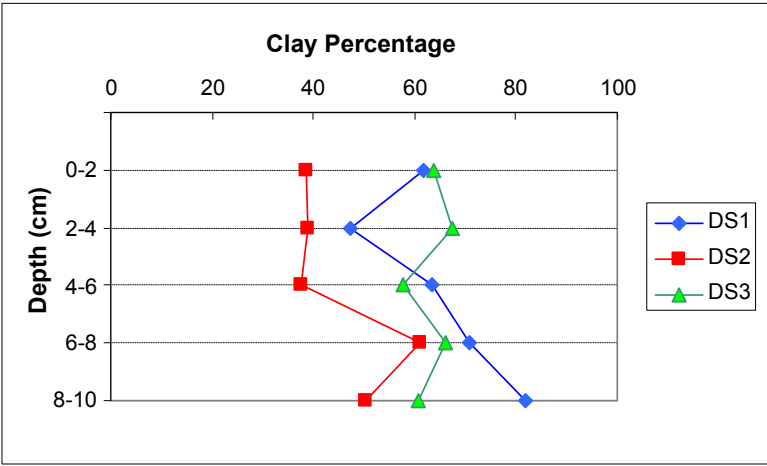
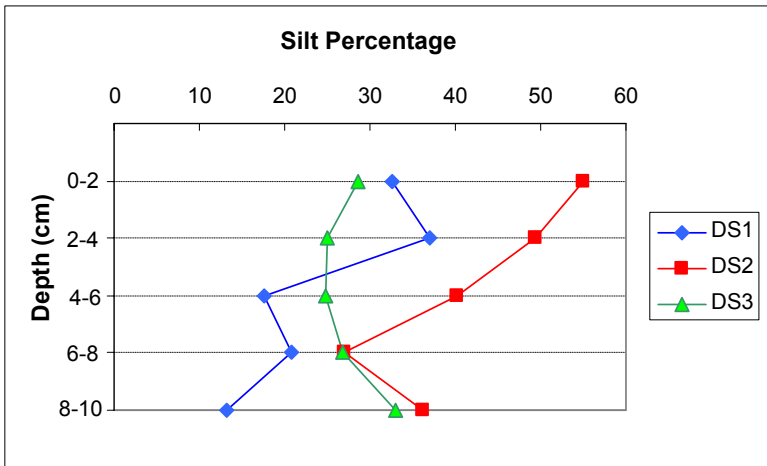
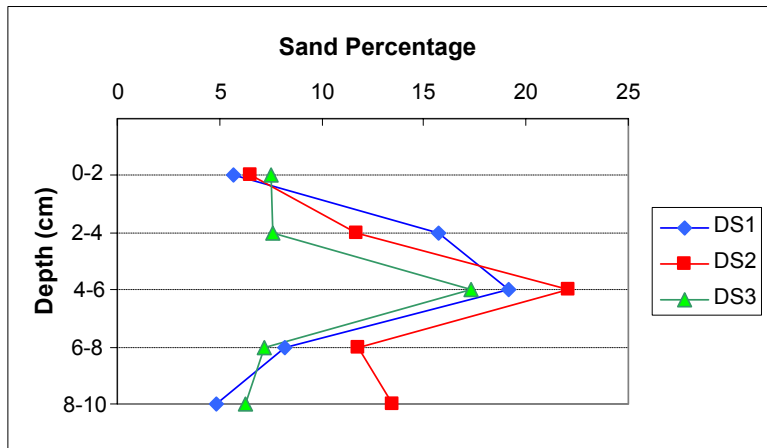


**Figure 5.18.** Depth profiles from discretionary stations (DS) at Garden Banks Block 602 on Cruise 2B (post-development).

**Table 5.6.** Sediment grain size results for Mississippi Canyon Block 292.

Station	Gravel (%)	Sand (%)	Silt (%)	Clay (%)	Mean Grain Size ( $\mu\text{m}$ )	Folk's Textural Description
<b>Near-Field</b>						
NF-B01	0.00	3.34	19.04	77.62	1.26	Clay
NF-B02	0.00	2.78	26.28	70.94	2.08	Clay
NF-B03	0.00	7.14	22.20	70.66	0.77	Clay
NF-B04	0.00	4.04	30.55	65.41	0.69	Clay
NF-B05	0.00	5.79	40.98	53.23	1.95	Mud
NF-B06	0.00	3.04	18.27	78.69	0.99	Clay
NF-B07	0.00	3.14	43.53	53.33	2.95	Mud
NF-B08	0.00	8.51	35.30	56.19	0.87	Mud
NF-B09	0.00	1.46	19.39	79.15	1.41	Clay
NF-B10	0.00	13.83	23.02	63.14	2.07	Sandy clay
NF-B11	0.00	3.72	24.96	71.32	0.82	Clay
NF-B12	0.00	3.59	21.75	74.66	1.74	Clay
<b>Far-Field</b>						
FF1-B01	0.00	1.79	17.70	80.51	1.17	Clay
FF1-B02	0.00	1.89	23.29	74.82	1.75	Clay
FF2-B01	0.00	3.07	23.62	73.31	1.93	Clay
FF2-B02	0.00	2.50	25.16	72.34	2.20	Clay
FF3-B01	0.00	1.15	19.80	79.06	0.31	Clay
FF3-B02	0.00	0.65	29.99	69.36	0.41	Clay
FF4-B01	0.00	2.78	38.53	58.70	1.02	Mud
FF4-B02	0.00	1.75	27.86	70.40	0.59	Clay
FF5-B01	0.00	2.19	16.30	81.50	1.06	Clay
FF5-B02	0.00	1.62	64.13	34.25	7.42	Mud
FF6-B01	0.00	2.65	19.82	77.53	1.24	Clay
FF6-B02	0.00	1.14	34.24	64.62	0.18	Mud



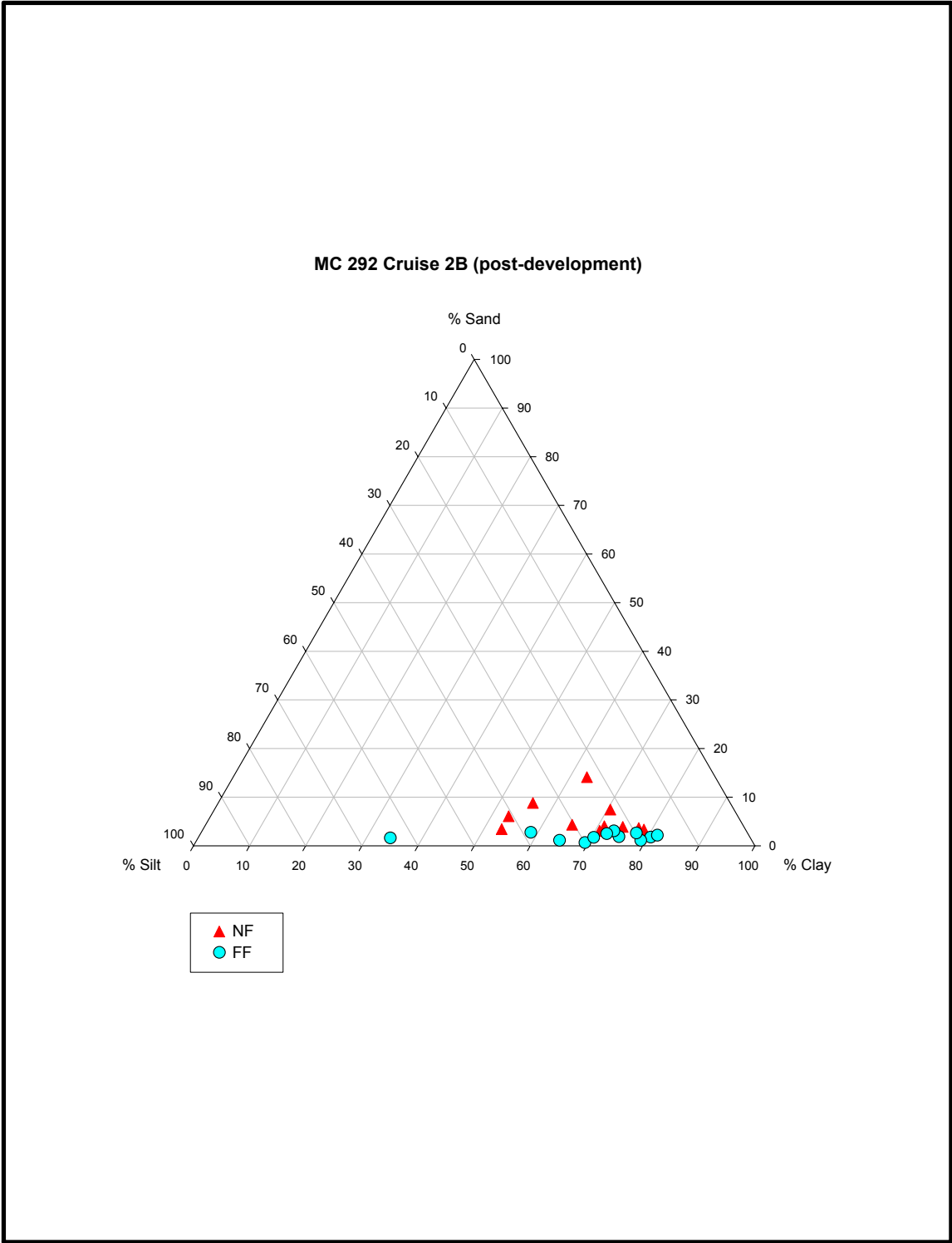


**Figure 5.19.** Ternary plot summarizing grain size data for Mississippi Canyon 292.

**Figure 5.20** shows sand, silt, and clay percentages for stations grouped into the same three categories mentioned previously (far-field, near-field 300 to 500 m, and near-field within 300 m). Also shown is the percentage of particles > 0.5 mm in diameter (coarse and very coarse sand). While silt and clay percentages in the near-field were within the far-field range, sand and coarse/very coarse sand percentages were elevated at some near-field stations. For example, sand percentages at far-field stations were all less than 3.1%, but those in the near-field ranged as high as 13.83% (NF-B10). The ANOVA indicates that sand percentages were significantly higher in the near-field (**Table 5.2**).

However, the pattern of elevated sand percentages did not correspond with geophysically mapped cuttings zones (**Figure 5.21**). Also, there was no consistent relationship between sand, silt, and clay percentages vs. sediment barium concentrations (**Figure 5.22**) or SBF concentrations (not shown).

The grain size distribution at MC 292 was bimodal at both near-field and far-field stations, with peaks around phi 4.5 to 5.0 (coarse silt) and phi 9.5 to 11 (clay) (**Figure 5.23a**). On average, near-field stations had higher percentages in the coarser phi classes (sand) and slightly lower percentages in several silt and clay phi intervals when compared with the far-field stations. **Figure 5.23b** shows the grain size distribution at Station NF-B01, which had the highest concentrations of drilling fluid indicators (barium: 39,700 µg/g and SBF: 2,408 µg/g) (see *Chapters 8 and 9*). The elevated clay percentages may reflect the presence of drilling fluid particles.

Subsamples from the three discretionary stations were sectioned in 2-cm intervals to a depth of 10 cm. At all three stations, sediments were predominantly clay at all depths, with most of the variation in the top 4 cm (**Figure 5.24**). At Station DS1, the sand percentage was elevated in the top 6 cm. Station DS3 had slightly elevated sand and silt in the top 2 cm. Station DS2 had a subsurface peak in sand and silt percentages at 2 to 4 cm depth and relatively high sand percentages all the way to 10 cm depth.

## 5.4 DISCUSSION

Drilling discharges have been shown to affect sediment grain size and mineralogy around wellsites in shallow water (National Research Council 1983; Neff 1987; Continental Shelf Associates, Inc. 1989; Hinwood et al. 1994). The solid components of drilling fluids (muds) consist of clay-size particles (e.g., bentonite, barite). Cuttings are particles of crushed rock produced by the grinding action of the drill bit as it penetrates into subsurface formations (Neff 1987). They can range in size from clay-sized particles to coarse gravel and have an angular configuration. While very coarse (gravel-sized) particles were noted near some drillsites in another deepwater monitoring program (Continental Shelf Associates, Inc. 2004), in the present study, apparently the cuttings were mostly within the size range of particles present in surficial sediments. Alternatively, the coarsest deposits may not have been sampled because our stations were not close enough to the wellsites.

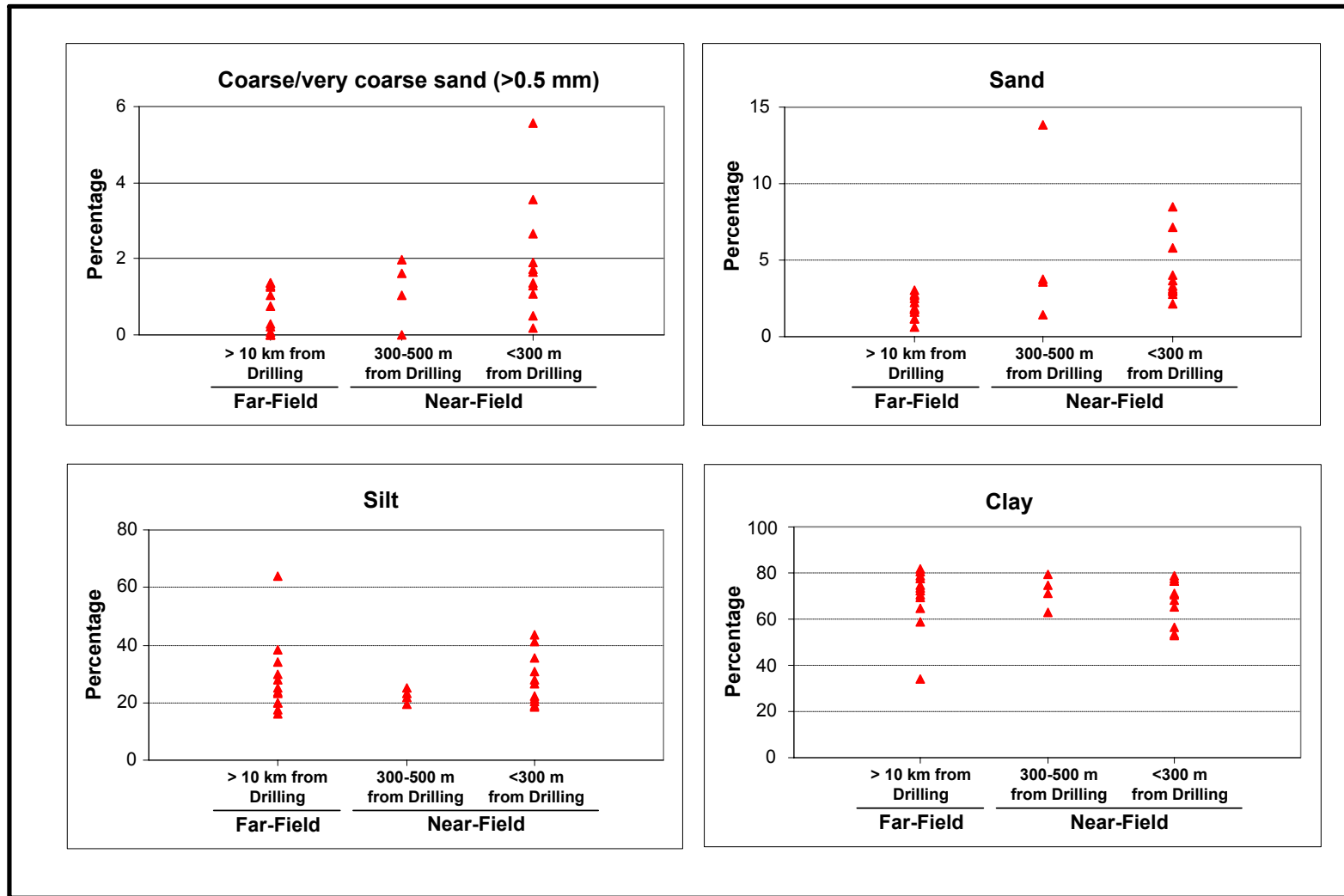


**Figure 5.20.** Percentages of coarse and very coarse sand (>0.5 mm), sand, silt, and clay in relation to proximity to drilling at Mississippi Canyon Block 292. Points are individual stations including non-random "discretionary" stations. Note the elevated percentages of sand and coarse/very coarse sand at some near-field stations.

**Sand  
MC 292**

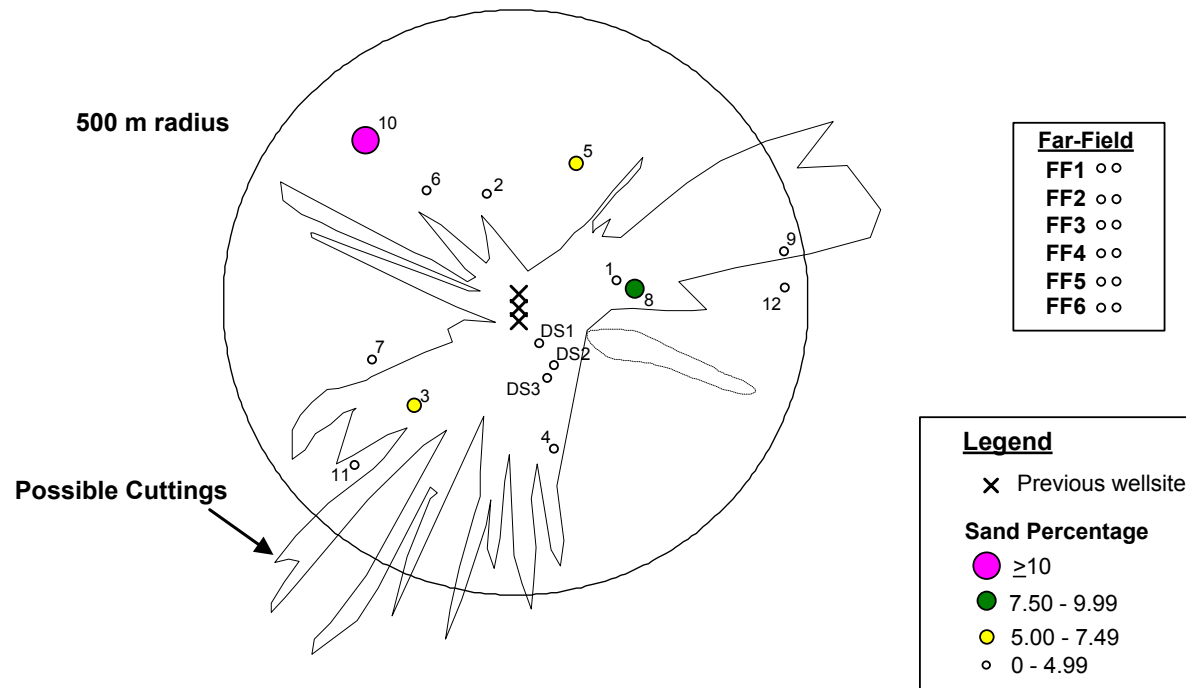


**Figure 5.21.** Sand percentages on Cruise 2B at Mississippi Canyon Block 292 in relation to geophysically mapped cuttings.

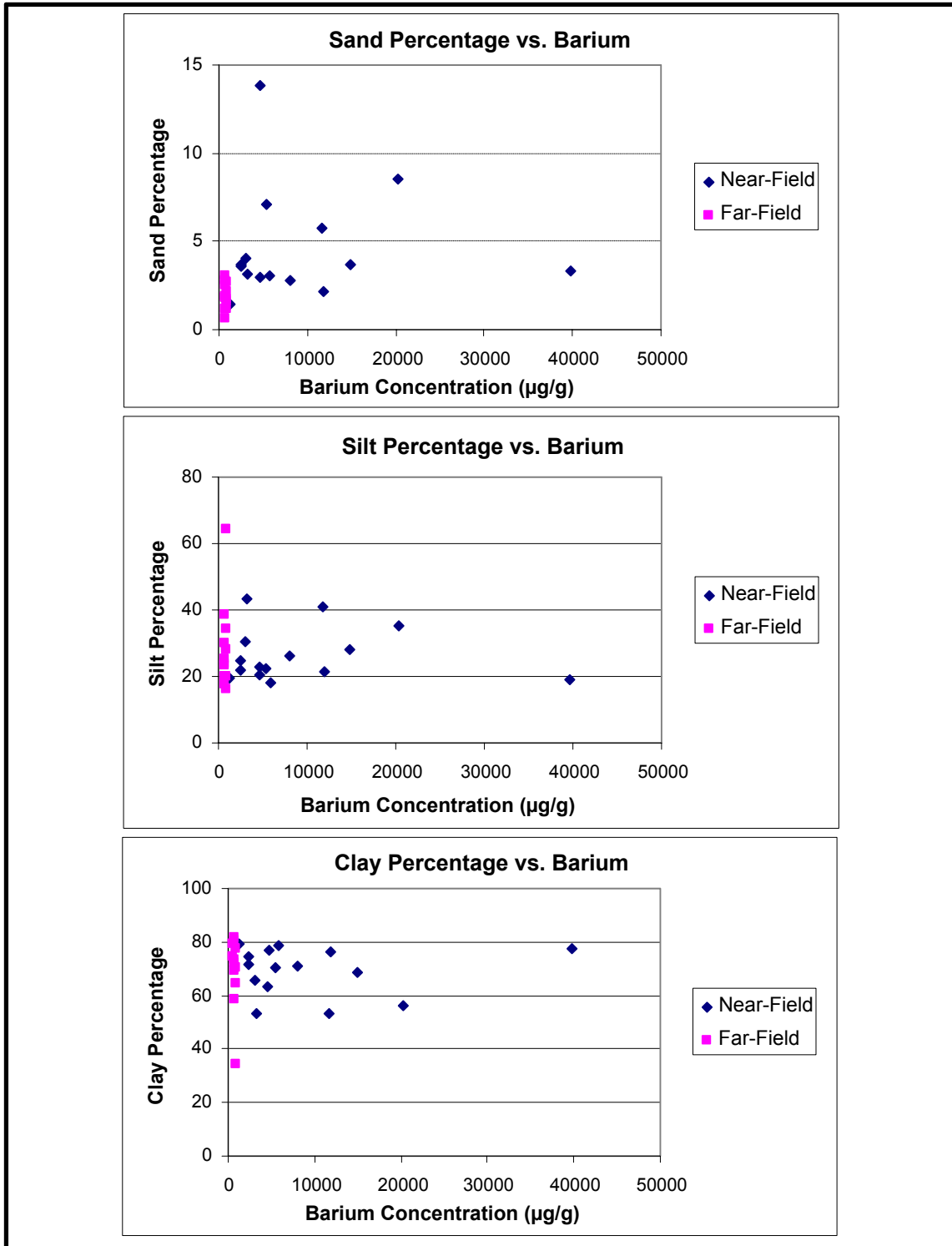
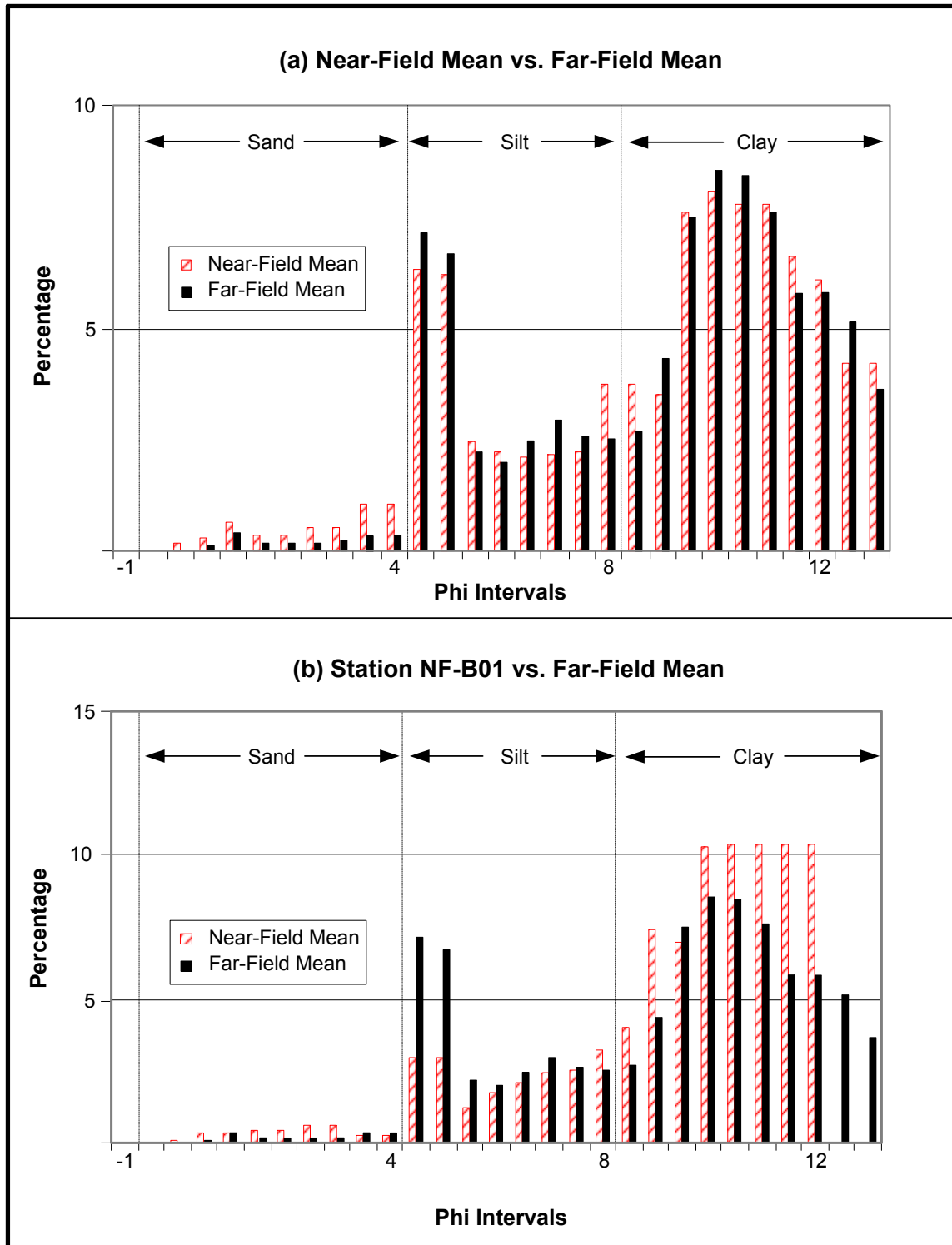
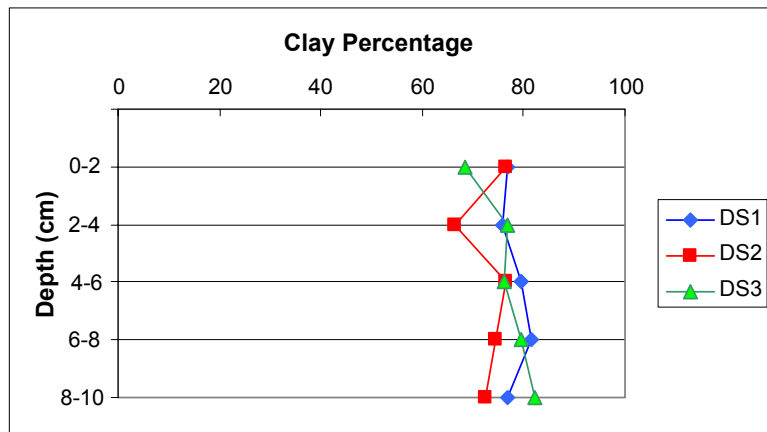
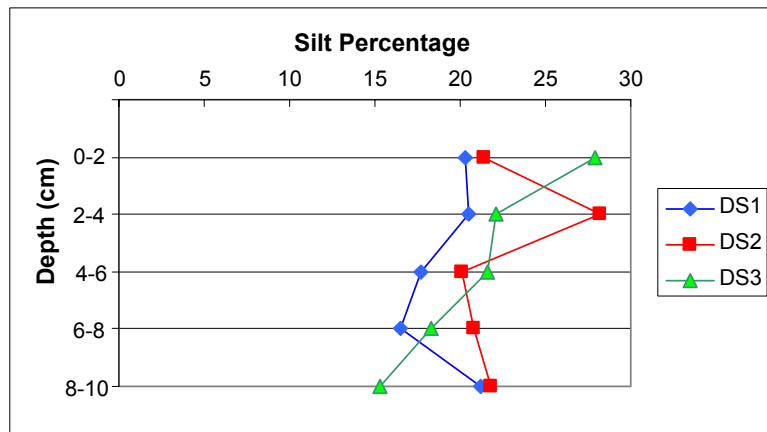
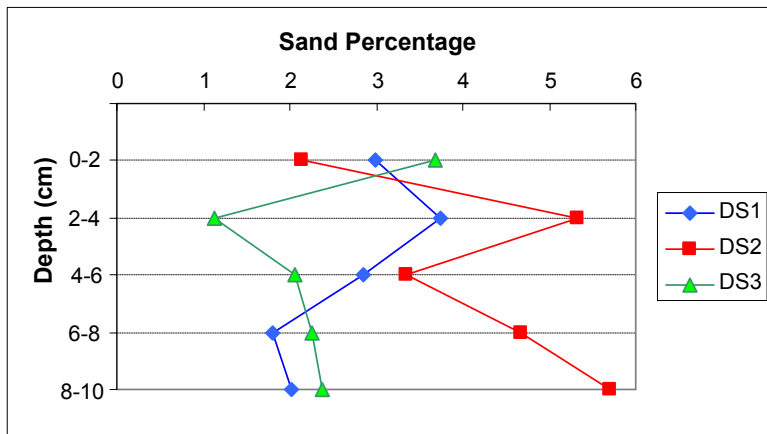


Figure 5.22. Relationships between sand, silt, and clay percentages and concentrations of barium (drilling fluid indicator) at Mississippi Canyon Block 292 on Cruise 2B.



**Figure 5.23.** Grain size distribution at Mississippi Canyon Block 292 on Cruise 2B. (a) Near-field mean vs. far-field mean; (b) Station NF-B01 vs. far-field mean.



**Figure 5.24.** Depth profiles from discretionary stations (DS) at Mississippi Canyon Block 292 on Cruise 2B (post-development).

Cuttings with adhering SBMs tend to clump together when discharged and settle rapidly to the seafloor (Brandsma 1996; Neff et al. 2000). Once deposited, these clumps are eventually broken up due to microbiological activity and physical disturbance. Time intervals of 5 months to nearly 2 years elapsed prior to post-drilling surveys, depending on the site. If loosely adhering clumps were present after this time, they would have been disaggregated during sampling and grain size analysis.

Drilling discharges deposited within the near-field sites presumably consist mainly of (1) cuttings and water-based muds released at the seafloor during the early stage of drilling; and (2) surface-discharged cuttings with small percentages of adhering drilling fluids. The latter is probably the main contributor at our stations. Also, water-based drilling fluids discharged at the surface would likely have been widely dispersed while settling to the bottom in a water depth of 1,000 m or more and probably would not appreciably affect grain size of bottom sediments.

In this study, there were no major, gross changes in sediment grain size distribution around the wellsites due to drilling. Sediments at post-drilling, near-field stations remained predominantly clay and silt. Only three samples had small percentages of gravel-sized particles and these included both near- and far-field stations. The main impact appears to be patchy areas of elevated sand percentages in the near-field. Near-field, post-drilling elevations in sand percentages were detected statistically at VK 916, GB 516 (Cruise 2B), and MC 292, but not at GB 602 nor at GB 516 on Cruise 1B. Elevated sand percentages are consistent with results of another deepwater monitoring program (Continental Shelf Associates, Inc. 2004).

Large variations in the relative percentages of silt and clay were evident at all four sites (e.g., see ternary diagrams). Some of these variations were observed at both near- and far-field sites (including pre-drilling samples at VK 916) and are assumed due to natural processes rather than drilling discharges. However, there was increased clay content in some samples with high concentrations of drilling fluid indicators (e.g., GB 516 Station NF-DS2, **Figure 5.9**; GB 602 Station NF-B03, **Figure 5.15**). Also, at GB 602 (and to a lesser extent, VK 916), there was generally more silt and less clay near drilling.

Grain size variations were patchy within near-field sites and the spatial pattern did not necessarily correspond to the cuttings or mud zones mapped in *Chapter 4*. Also, except for VK 916, there were no strong correlations between percentages of sand, silt, or clay and concentrations of drilling indicators such as barium and SBF. These findings suggest that grain size distribution *per se* is not a very good indicator of drilling discharge impacts. Other physical measures have been determined to be more definitive in identifying cuttings, such as visual analysis for angular or tabular particles (Continental Shelf Associates, Inc. 2004).

Due to the relatively subtle nature of grain size changes, the vertical profiles at discretionary stations were not very helpful in identifying the depths of impacts. The most clearcut results were seen at the exploration site (VK 916) where only a single well was drilled; here, impacts were evident to a depth of about 4 cm. The other three sites, all of which had multiple wells drilled over several years, provide some evidence of possible effects at greater depths, approaching 10 cm. However, other variables such as barium or SBF concentration are undoubtedly better indicators of the depth of mud and cuttings deposits.



## Chapter 6 Sediment Profile Imaging at Exploration and Exploration/Development Sites

*Isabelle P. Williams, Donald C. Rhoads, James A. Blake, and Pamela L. Neubert  
ENSR International, Marine and Coastal Center*

---

### 6.1 INTRODUCTION

ENSR International, Marine and Coastal Center was responsible for analyzing the sediment profile images collected at GB 516 and VK 916. Sediment profile imaging (SPI) surveys were conducted at both sites in October-November 2000 (Cruise 1B). A second survey was conducted at GB 516 in July 2001 (Cruise 2B) and at VK 916 in August 2002 (Cruise 3B). GB 516 was an exploration/development site that was sampled once after exploration drilling and again after development drilling. VK 916 was an exploration site that was sampled before and after drilling of a single exploration well (see *Chapter 3*).

Detailed data summaries are provided in *Appendix E1* (Cruise 1B), *Appendix E2* (Cruise 2B), and *Appendix E3* (Cruise 3B). Reduced versions of the images (plates) are presented at the end of the chapter, and larger versions are provided in *Appendix E4*.

### 6.2 METHODS

For the Cruise 1B surveys at GB 516 and VK 916, as well as the Cruise 2B survey at GB 516, sediment profile images were provided as photographic slides. These were digitized and stored on CD-ROM as Kodak® .pcd files by Boston Photo Imaging. All of the Cruise 1B slides were digitized. During Cruise 2B at GB 516, two pictures were taken at each station. From these two images, the second (showing deeper camera penetration) image was chosen for digitization, unless the camera had penetrated so deeply that no sediment-water interface was visible. For the VK 916 post-drilling survey (Cruise 3B), a digital camera system was used so that the sediment profile images were provided directly on CD-ROMs; the best image for each station was chosen for analysis.

The digitized images were analyzed with ImagePro Plus 4.5 software. Each digitized image was analyzed for penetration depth, surface roughness, apparent redox potential discontinuity (RPD) depth, grain size major mode, infaunal successional stage, the presence of methane bubbles, anoxia of the water overlying the sediment surface, and biogenic features, such as burrows and tubes. Any additional observations were entered into a comment field. A specialized Microsoft Access™ database program, written at ENSR International, automatically calculates the organism-sediment index (OSI) from the entries recorded for RPD, successional stage, presence/absence of methane, and presence/absence of apparent anoxia at the sediment surface (Rhoads and Germano 1982). The data are compiled onto separate data sheets for ease in re-examination, which is performed for quality control purposes. In addition, the Microsoft Access™ program generates a Microsoft Excel™ spreadsheet containing all of the recorded data. Edited versions of these spreadsheets are given in *Appendices E1, E2, and E3*.

The following is a description of each of the SPI parameters that were measured:

1. *Penetration depth* is measured from the sediment-water interface to the bottom of the image (20-cm maximum) and is a measure of substratum softness, which depends on characteristics such as water content and sediment grain size.
2. *Surface roughness* is the difference between the least and greatest penetration depth across the sediment-water interface depicted on the image (the width is 15 cm). It may be a measure for physical disturbance, natural or anthropogenic, or of biological activity such as burrowing.
3. The *apparent RPD depth* is measured from the sediment-water interface to the depth in the sediment at which there is a change in sediment color from tan or brownish (ferric hydroxides) in the well-oxygenated surface layer to grayish (ferric hydroxides being reduced) or black (presence of sulfide, anoxic conditions) at a few millimeters to several centimeters in depth where there is a lack or absence of oxygen. The RPD depth depends on physical and biological mechanisms such as currents, organic loading, and bioturbation by infaunal organisms, and is commonly used as a first approximation measure of the health of a benthic habitat.
4. *Methane bubbles*, discernable by their strong reflectance (silvery color), form only under severely oxygen-depleted sediment conditions as a result of anaerobic bacterial metabolism.
5. The *grain size major mode* is the dominant particle size in an image, measured visually by comparing the slide with a photograph of phi size classes.
6. *Infaunal successional stages* (seres) are derived from a paradigm describing recolonization of disturbed shallow water habitats. Application of this paradigm to our study sites is an extrapolation, as detailed knowledge about infaunal successional stages is not available for these sites. Stage I organisms live very close to the sediment-water interface and are pioneers, as they require little oxidized sediment. By their feeding and burrowing activities, these Stage I animals, often small annelids, deepen the RPD, preparing the sediment for colonization by somewhat larger animals such as amphipods (Stage II). Stage III organisms are large, deep-burrowing, head-down deposit feeders, usually polychaetes and echinoderms, which aerate the sediment to several centimeters in depth. Their presence indicates an equilibrium community and a healthy environment. The term “azoic” is used here to describe retrograde areas where there are apparently no macrofauna present (no Stage I tubes visible at the sediment surface and no Stage III feeding voids observed at depth). Of course, these areas are not truly azoic because mats of filamentous sulphate-reducing bacteria may be present, as well as meiofauna and possibly macroinfauna that did not leave any visible traces.

### **6.3 GARDEN BANKS BLOCK 516 – CRUISE 1B**

#### **6.3.1 Survey Design and Location**

GB 516 was an exploration/development site that was sampled once after exploration drilling and again after several development wells were drilled (see *Chapter 3*). The first SPI survey was conducted from 28 October until 1 November 2000 (Cruise 1B). This block is approximately 130 nm from the Mississippi Delta, encompasses depths of 800 to 1,100 m, and contains wellsites

in the northwest quadrant. All near-field SPI images were taken in depths of about 1,000 to 1,100 m (**Figure 6.1**). Most stations in the near-field were located within a 1,000-m diameter circle roughly centered on a wellsite where two exploratory wells were drilled in 1999 (see *Chapter 3*). Three sub-parallel near-field transects were sampled in a southeast to northwest direction, generally oriented normal to the local bathymetric contours. Each station was treated separately in this analysis; no pair of stations was considered as true replicates, as the ship was not repositioned between samples.

In addition, samples were collected along three control transects in the far-field. These transects were located 10 to 20 km east of the near-field site and were selected to represent ambient or reference bottom conditions (**Figure 6.1**).

#### *6.3.1.1 Near-Field Stations*

Transect NF-1 consisted of 28 stations. Usable SPI photographs (i.e., image quality that allowed analysis) were obtained from 27 stations. Transect NF-2 consisted of 36 stations, and 30 of these yielded usable SPI images. Transect NF-3 consisted of 20 stations, of which 18 were usable. Most near-field stations were positioned within the near-field site. The exceptions were Stations NF-1.01 to NF-1.10, located on a portion of Transect NF-1 that extended beyond the near-field site to the southeast. **Figure 6.2** shows near-field transects.

#### *6.3.1.2 Far-Field Stations*

The three far-field transects are shown in **Figures 6.3, 6.4, and 6.5**. Transect FF2 had 22 stations, and all images were usable. Transect FF4 consisted of 17 stations, and all images were usable. Transect FF6 consisted of 20 stations, with usable data from 18 stations.

### **6.3.2 Sediment Fabric, Texture, Color, and Small-Scale Stratigraphy**

Sediment profile images provide information about small-scale vertical gradients in sediment structure, as recorded within the photographs. Features observed include changes in sediment fabric (spatial arrangement of grains or grain aggregates), texture, color, and microstratigraphy (laminations, graded bedding, homogeneous layers, burrow-mottled intervals, etc.). This information is used, in conjunction with other SPI parameters, to infer sedimentation processes.

#### *6.3.2.1 Near-Field Stations*

The texture (grain size) at most stations sampled at GB 516 during Cruise 1B varies with depth below the sediment-water interface. The upper few centimeters of sediment consist of sand-sized aggregates in the range of 2-1 to 3-2 phi (fine to medium sand). The component particles of these sand-sized aggregates consist only of silt and clay-sized particles. Deeper layers consist of very fine silt to clay particles (greater than 4 phi). Near-surface aggregates are interpreted as accumulated fecal pellets, pseudofeces, or parcels of sediment that were broken up by the process of bioturbation (foraging and/or burrowing). Below the depth of active bioturbation, sand-sized aggregates are compacted (coalesced) and therefore have lost their sand-sized appearance.

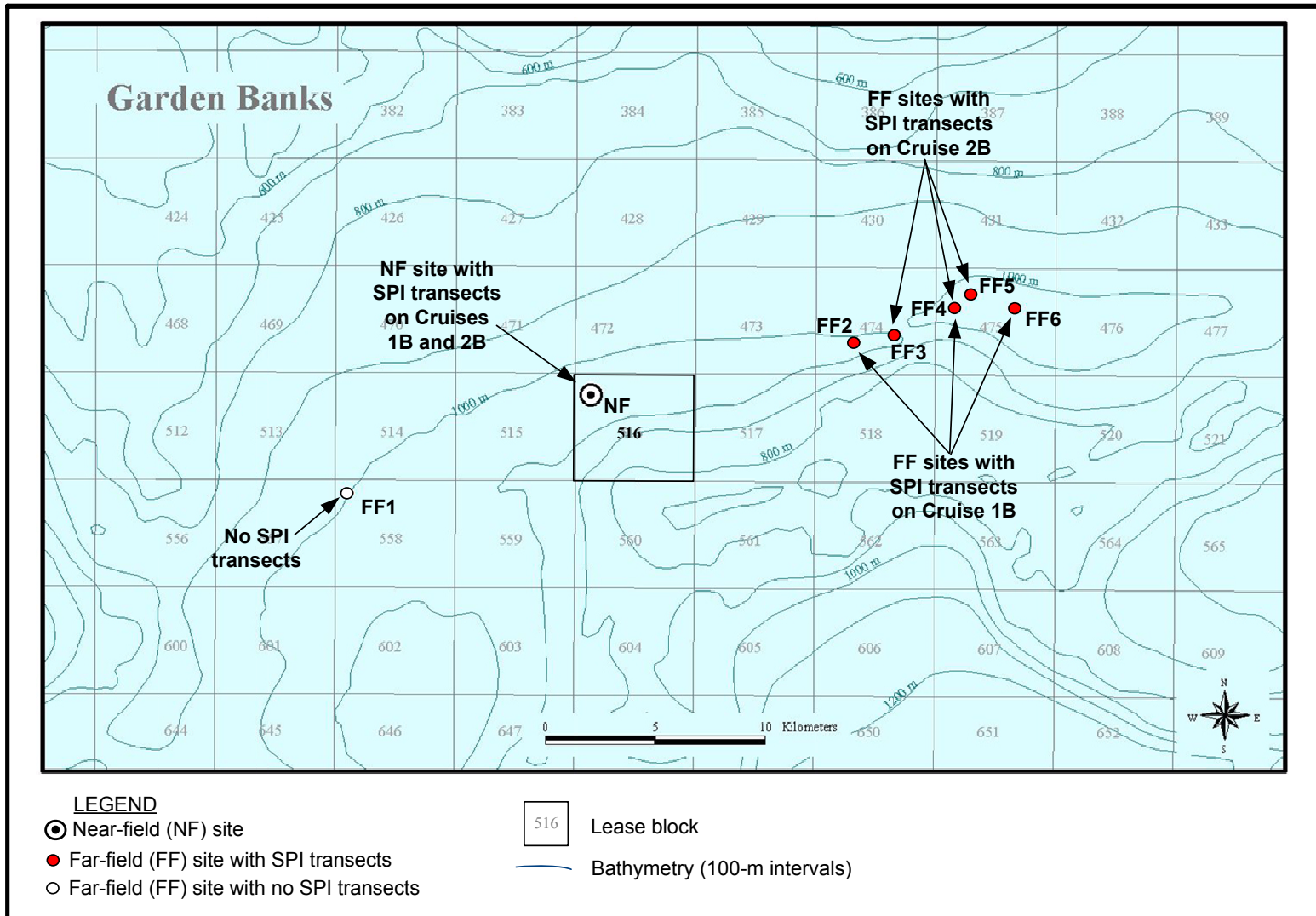


**Figure 6.1.** Location of Garden Banks Block 516 exploration/development site and associated reference areas where sediment profile imaging (SPI) transects were surveyed.

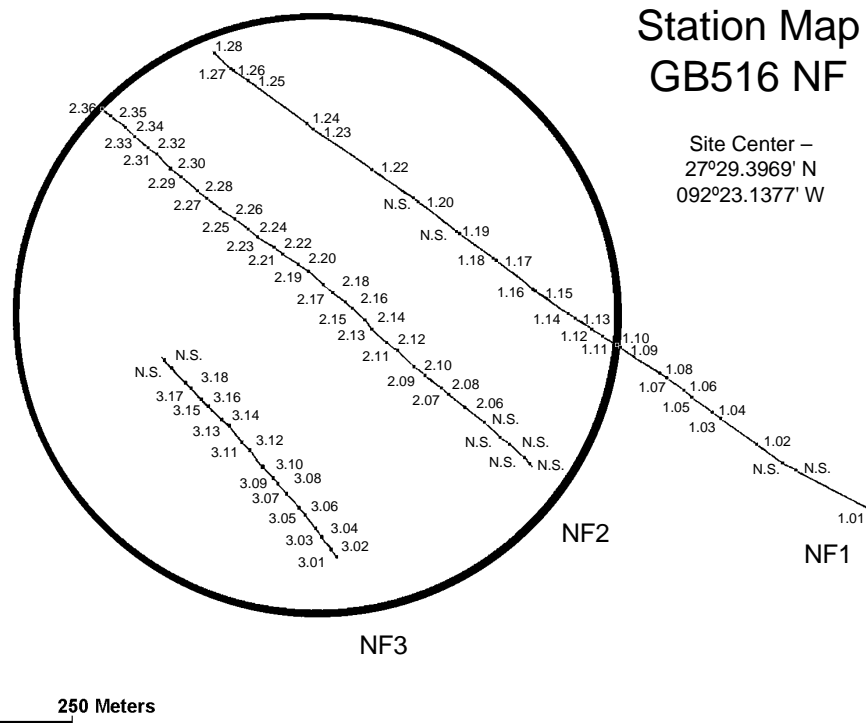


**Figure 6.2.** Garden Banks Block 516 near-field (NF) station map, showing positions of sediment profile imaging transects and stations sampled during Cruise 1B (October-November 2000). The NF site radius is 500 m.

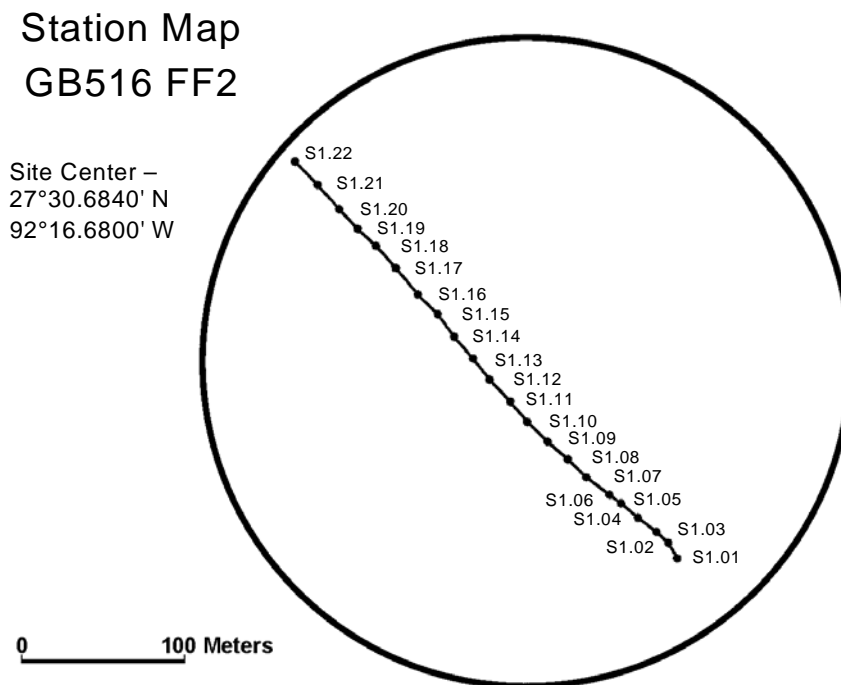
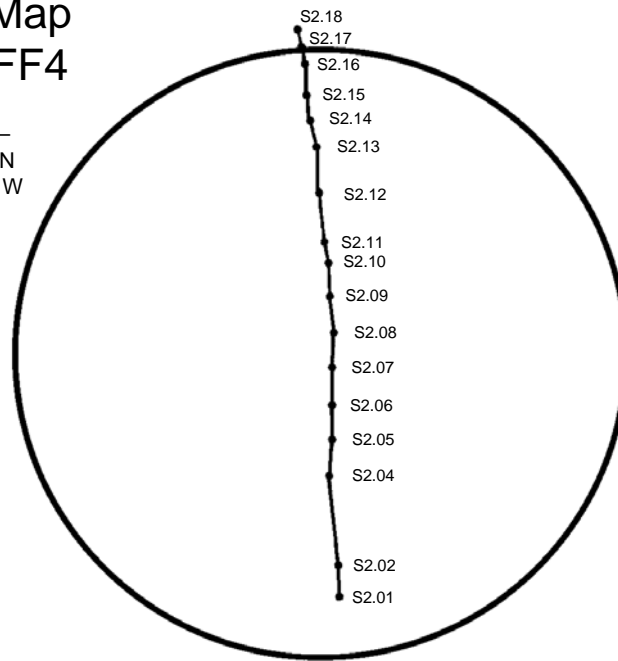


**Figure 6.3.** Garden Banks Block 516 Far-field 2 (FF2) station map, showing positions of sediment profile imaging transect and stations sampled during Cruise 1B (October-November 2000). The FF site radius is 204 m.

### Station Map GB516 FF4

Site Center –  
27°31.5240' N  
092°14.2200' W

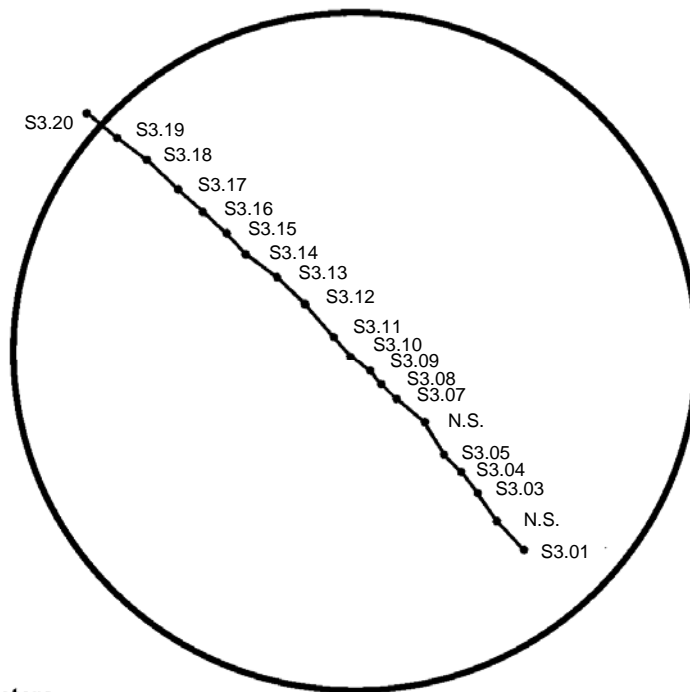


0 100 Meters

**Figure 6.4.** Garden Banks Block 516 Far-field 4 (FF4) station map, showing positions of sediment profile imaging transect and stations sampled during Cruise 1B (October-November 2000). The FF site radius is 204 m.

### Station Map GB516 FF6

Site Center –  
27°31.5240' N  
092°12.7500' W



0 100 Meters

**Figure 6.5.** Garden Banks Block 516 Far-field 6 (FF6) station map, showing positions of sediment profile imaging transect and stations sampled during Cruise 1B (October-November 2000). The FF site radius is 204 m.

Overall, sediment color, fabric, and microstratigraphy at stations sampled along Transects NF-1 and NF-2 differ from those sampled along Transect NF-3. For example, the sediment profile image from Station NF-1.19 (*Plate 1*) on Transect NF-1 shows a granular surface layer of pink to reddish-tan sediment underlain by a dark gray to black sulfidic layer. Deeper in the deposit there are three to four gray to black layers interposed within this pink to reddish-tan sediment. The pink to reddish-tan color is imparted to the sediment by the presence of mineral particles coated with ferric hydroxide ("rust") and/or manganese carbonate. Manganese is present in very high concentrations in Mississippi Delta sediments (Trefry and Presley 1982), and the oxidized form, manganese carbonate, can be brown or pink (R. Aller, pers. comm., 2003). At some previous time, these particles were exposed to high oxygen tensions so that the iron present was precipitated as surface coatings. Once oxidized, these ferric hydroxide coatings tend to be metastable and remain oxidized even when surrounded by anoxic interstitial waters. The gray-to-black layers are reduced sediments associated with the anaerobic decay of organic matter and accumulation of iron sulfides. The layering of oxidized and reduced sediments strongly suggests a recent history of changing inputs into the upper sediment column. Although this stratigraphy was common to both Transects NF-1 and NF-2, it also was observed (but not as well developed) at the far-field stations (see below).

Color, fabric, and stratigraphy at several stations along Transects NF-1 and NF-2 are distinctive in that they represent environments that are extremely enriched organically (*Plates 2 to 5*). Station NF-2.12 is representative of areas where a white microbial mat at the sediment surface overlies a sulfidic gray layer, which in turn overlies a mottled light gray to tan sediment (*Plate 2*). No apparent RPD is observed; i.e., there is no oxidized surface layer. This is consistent with measured oxygen penetration depths as small as 0.3 cm (*Chapter 8*). The image (*Plate 3*) taken at Station NF-2.21 also shows the presence of a white surface microbial mat (on the right). Filaments of these microbial colonies are seen suspended above the sediment-water interface. Some tan-colored sedimentary intervals are present under the mat, along with buried gray sulfidic sediment at the SPI camera penetration depth. Station NF-2.22 has a microbial mat and a gray mottled sediment column at SPI camera penetration depth (*Plate 4*). A microbial mat is also present at Station NF-2.23 (*Plate 5*), but the sediment column below the mat is completely gray to black; no ferric hydroxide (yellow to tan color) is observed. The sequence of stations going from NF-2.21 to NF-2.22 then to NF-2.23 is presumed to represent a spatial gradient of decreasing benthic habitat quality (i.e., increasing organic enrichment over time).

Near-field Transect NF-3 does not have any microbial mats on the sediment surface, and most of the sediment is pink to reddish-tan. For example, the image taken at Station NF-3.17 shows burrow-mottled oxidized sediment with only a hint of gray layering at the penetration depth of the camera (*Plate 6*). A feeding void is present. The general fabric and color of stations on Transect NF-3 are more similar to the reference (ambient) far-field stations than they are to stations on Transects NF-1 and NF-2 (see below) and suggest that Transect NF-3 is in an area with less organic input than that covered by Transects NF-1 and NF-2.

### 6.3.2.2 Far-Field Stations

All of the images taken at far-field transect stations show surface sediments consisting of sand-sized organic-mineral aggregates (2-1 phi or medium sand). At depth, the sand-sized texture is lost due to compaction, and most of the deeper sediment column is silt-clay in texture

(greater than 4 phi). As reported in *Chapter 5*, samples of the top 2 cm indicate mean grain sizes of about 9 to 8 phi, finer than the sandy surface sediments but consistent with silt-clay seen at depth. Sediment color is predominantly pink to reddish-tan with most stations showing gray to black sulfidic layers at depth. For example, Station FF6-3.13 (*Plate 7*) has pink to tan mottled surface sediments underlain by a thin layer of sulfidic gray to black sediment, which, in turn, overlies a homogeneous light gray layer. Far-field Station FF2-1.4 (*Plate 8*) also shows a near-surface layer of mottled pink to tan sediment overlying faint gray layers at depth. This color and fabric is similar to that observed at stations imaged on Transect NF-3 (e.g., compare with SPI Station NF-3.17 [*Plate 6*]).

### 6.3.3 Depth of the Apparent Redox Potential Discontinuity

The near-surface zone of intensive particle mixing and interstitial water exchange is recognized in SPI images by a difference in color between the mixed zone (light tan or pink) and underlying sediment (darker red, gray, or black). With the relative absence of reduced compounds such as hydrogen sulfide and/or iron sulfides, the light tan color in the mixed zone results from the oxidation of particulate iron coatings on sediment particles (ferric hydroxide) while the light pink color can be imparted by manganese carbonate (Dr. Robert Aller, Stony Brook University, NY, pers. comm.). The zone of intensive mixing can be related to physical processes such as sediment resuspension or bed-load transport, but in most cases mixing is related to bioturbation by resident infauna. Vertical gradients in sediment color, as described above, are related to the oxidation state of the sediment. However, because we are inferring the oxidation state from sediment color, this parameter is called the “apparent” RPD. The true RPD (as measured by polarographic electrodes) is usually shallower than the apparent RPD. Deeply oxidized surface sediment (i.e., a deep apparent RPD) is usually indicative of a well-developed and active bioturbating infaunal community with oxygenated overlying water. Surface mixed zones that are shallow or absent usually are associated with ecologically stressed benthic systems, such as recently disturbed seabeds devoid of infauna or early successional stages, or bottom areas overlain by hypoxic or anoxic water.

#### 6.3.3.1 Near-Field Stations

**Figure 6.6** shows the mapped distribution of mean apparent RPD depths for the three near-field transects. Areas of moderate to deep surface-mixed zones ( $\geq 0.5$  cm), are distinguished by diagonal lines. The area of thin RPD depths, even zero thickness at many stations, encompasses most of that part of Transect NF-1 lying within the 1-km diameter circle as well as most of Transect NF-2. Most stations on Transect NF-3 (82%) have apparent RPD depths greater than 0.5 cm in thickness. For all near-field stations where apparent RPD depths could be determined ( $n = 74$ ), the mean RPD depth was 0.83 cm.

Apparent RPD depth-frequency histograms are shown in **Figure 6.7**. Apparent RPD depths are skewed toward the 0.0 to 0.99-cm class on all three transects, but Transect NF-2 has fewer stations with deeper RPD depths than either Transects NF-1 or NF-3. The four stations with RPD depths greater than 3 cm on Transect NF-1 are all on that portion of the transect outside of the target circle, and the four stations with RPD depths greater than 2 cm on Transect NF-2 are all clustered on the southernmost end of the line.



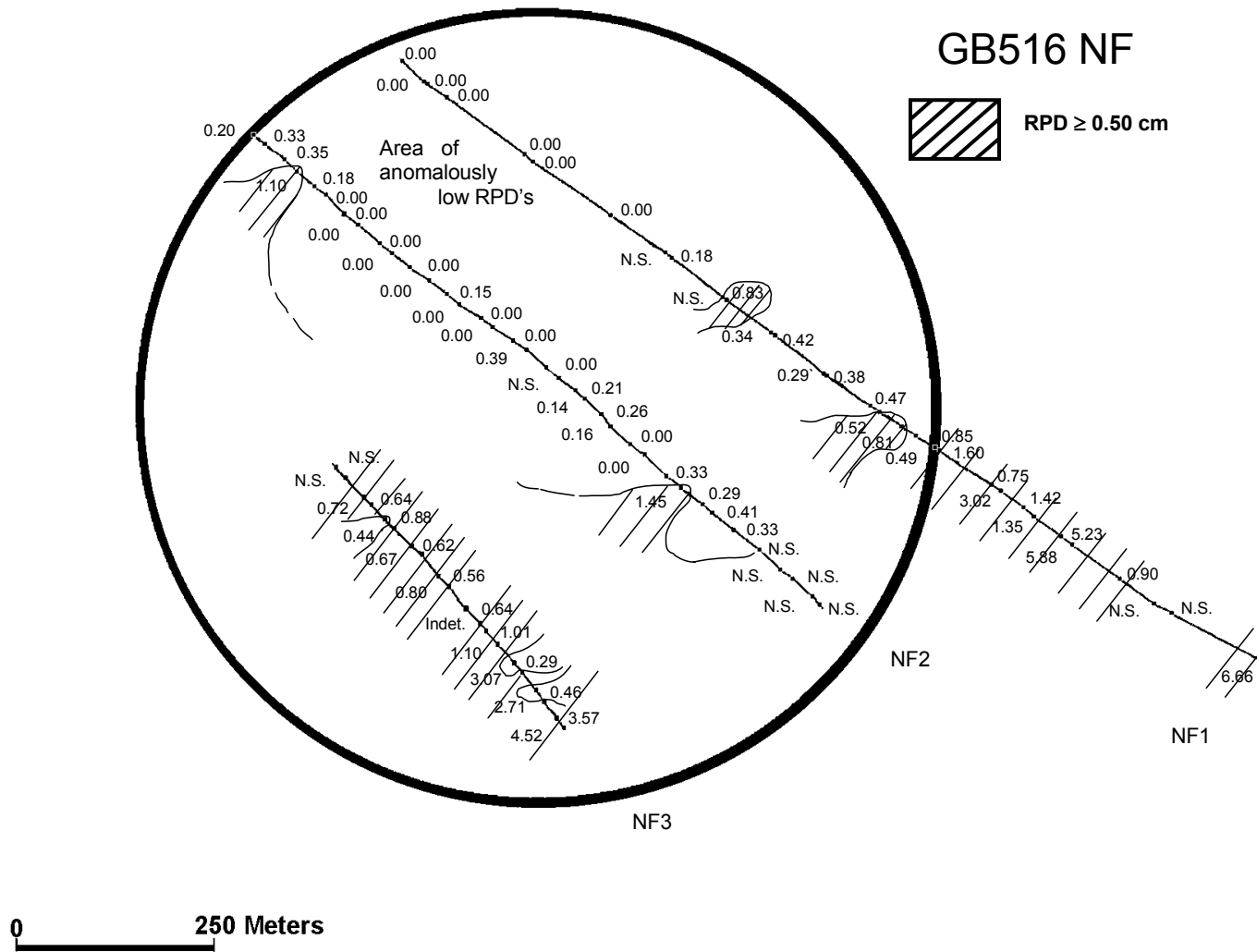


**Figure 6.6.** Mapped distribution of mean apparent redox potential discontinuity (RPD) depths along the three near-field transects sampled at Garden Banks Block 516 during Cruise 1B (October-November 2000). The NF site radius is 500 m.

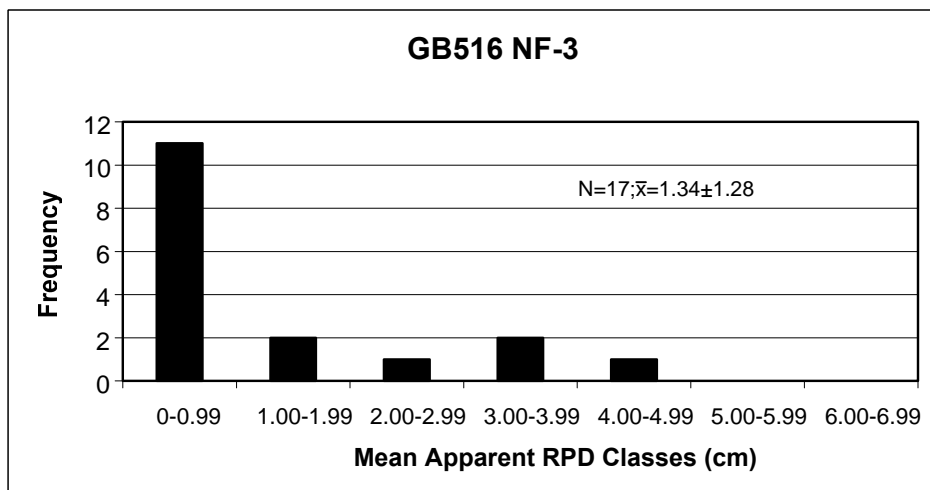
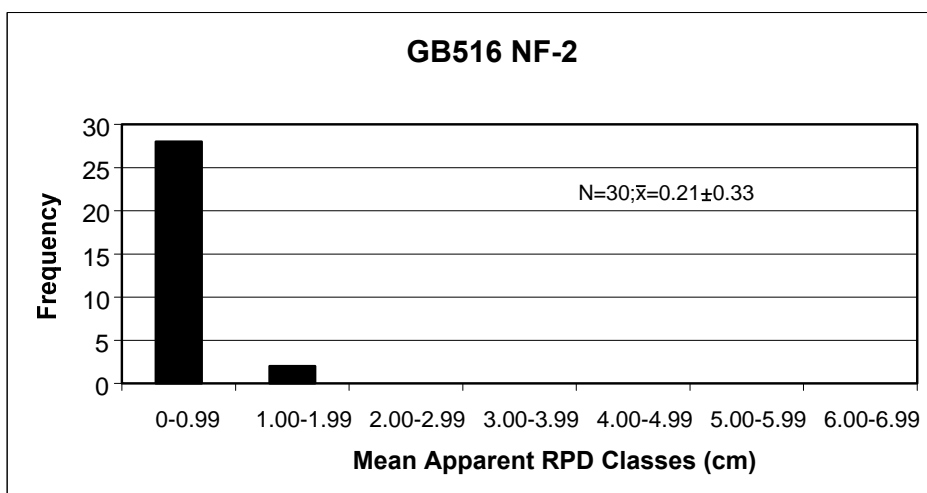
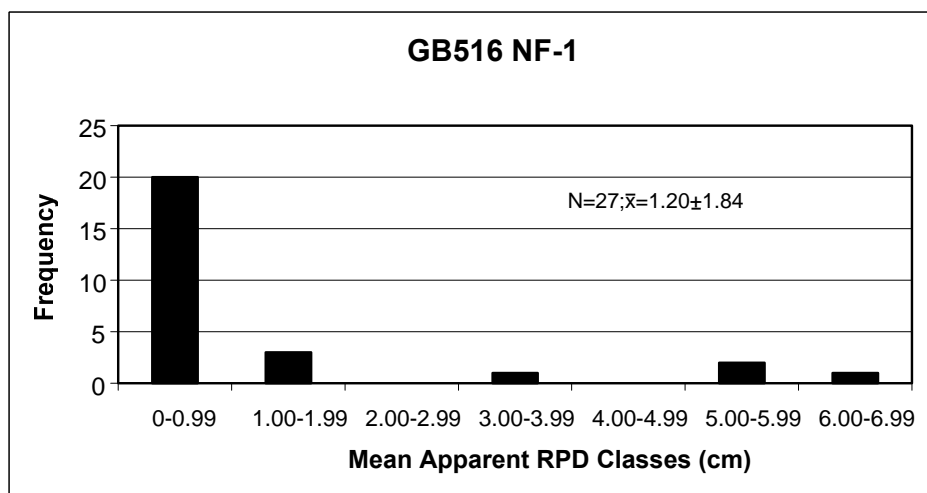


**Figure 6.7.** Redox potential discontinuity (RPD) depth-frequency distributions at three near-field transects in Garden Banks Block 516 during Cruise 1B (October-November 2000).

### 6.3.3.2 Far-Field Stations

All stations but one on Transect FF2 have mean apparent RPD depths equal to or greater than 0.5 cm (**Figure 6.8**). Far-field Transects FF4 (**Figure 6.9**) and FF6 (**Figure 6.10**) both show patchy distributions of mean apparent RPD depths with approximately 38% and 20%, respectively, of the RPD values equal to, or less than, 0.5 cm in thickness. No zero values were measured along any of the three far-field transects. For all far-field stations where the apparent RPD depth could be determined ( $n = 53$ ), the mean RPD depth was 1.04 cm.

The RPD depth-frequency distribution at all three far-field transects show that most values fall below 1.0 cm in thickness (**Figure 6.11**). However, Transect FF2 has the greatest proportion of stations (41%) with values equal to or greater than 1.0 cm in thickness. Transects FF4 and FF6 have similar RPD depth-frequency distributions with 25% and 20%, respectively, of stations with RPD depths equal to or greater than 1.0 cm.

### 6.3.4 Infaunal Successional Stages

Macroinfaunal colonization of soft granular substrata proceeds from the sediment-water interface downward. Following a physical or chemical benthic disturbance, small opportunistic or pioneering species tend to be first colonizers, particularly in a primary succession. These Stage I species usually are dominated by small polychaetes that live near the sediment-water interface, and many build dense fields of tubes. Over time, the deeper sediment column is invaded by later colonizing species, particularly head-down deposit-feeders that form distinctive feeding voids within the sediment column that are visible in SPI images (Stage III species). Stage I and Stage III species often coexist, and these associations are identified as Stage I-III seres. It is sometimes possible to identify transitional seres (Stage II) that involve species that “fill-in” between Stage I and Stage III, but this requires detailed knowledge about the successional dynamics at the study site. As this knowledge is lacking for the sites mapped here, no Stage II seres are identified.

In this survey, we have identified three successional bottom types:

1. Bottom sediments that are retrograde areas where there are apparently no macrofauna present (no Stage I tubes visible at the sediment surface and no Stage III feeding voids observed at depth). These heavily impacted stations are called "azoic" even though mats of filamentous sulphate-reducing bacteria may be present (see *Plates 2-5*).
2. Bottom sediments that exhibit only Stage I pioneers (Stage I seres).
3. Bottom sediments that show evidence of subsurface feeding voids (with, or without, Stage I species at the surface). These are mapped as Stage I-III or Stage III seres. This sequence of seres is presumed to represent a gradient from heavily impacted (azoic) benthic sediments to those that are least impacted (Stage III seres).

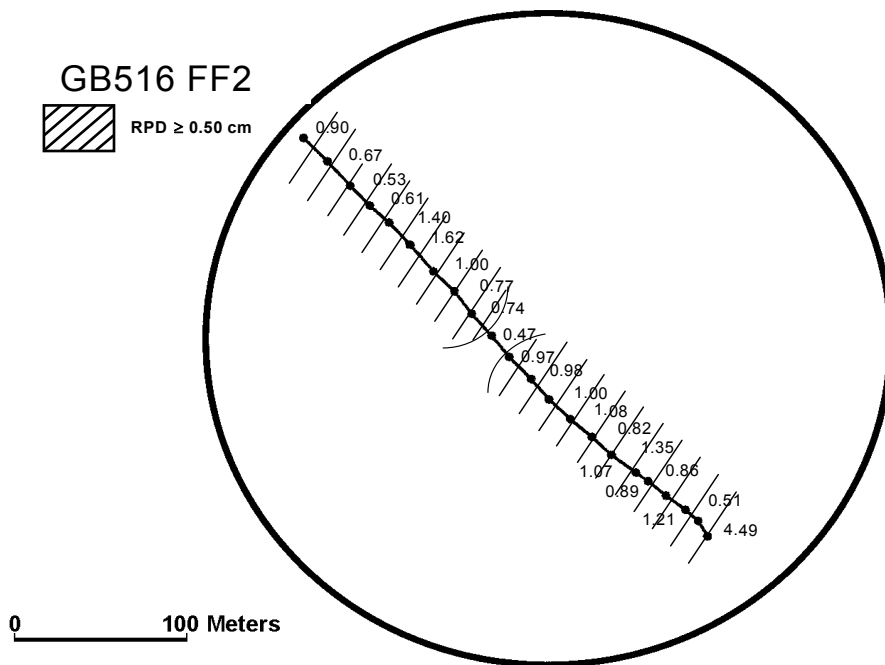


**Figure 6.8.** Mapped distribution of mean apparent redox potential discontinuity (RPD) depths along Transect FF2 at Garden Banks Block 516 during Cruise 1B (October-November 2000). The FF site radius is 204 m.

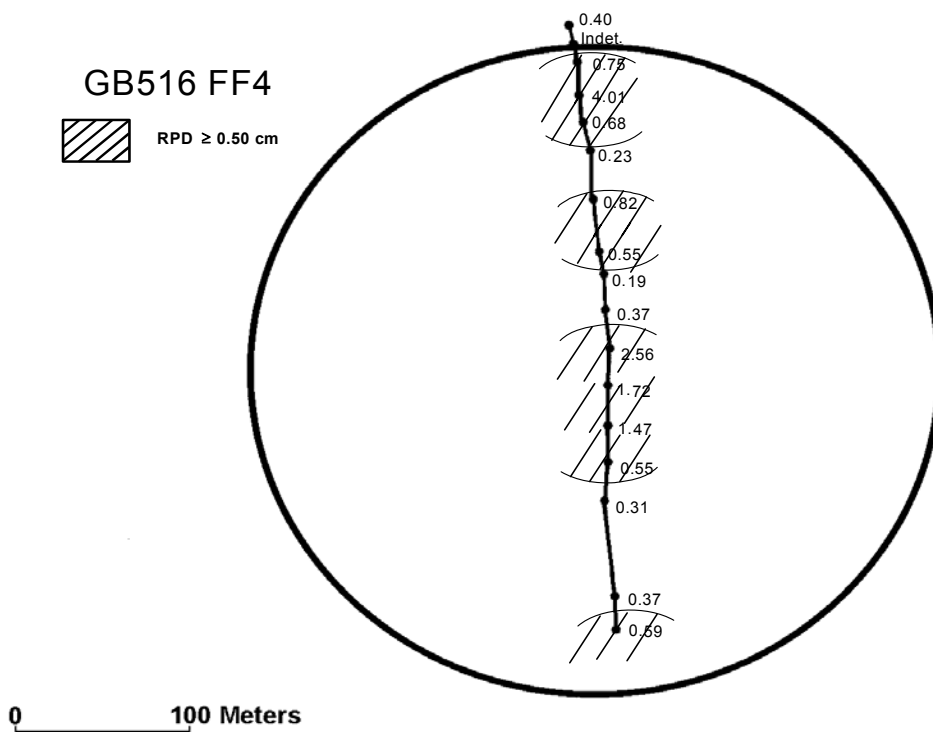


**Figure 6.9.** Mapped distribution of mean apparent redox potential discontinuity (RPD) depths along Transect FF4 at Garden Banks Block 516 during Cruise 1B (October-November 2000). The FF site radius is 204 m.

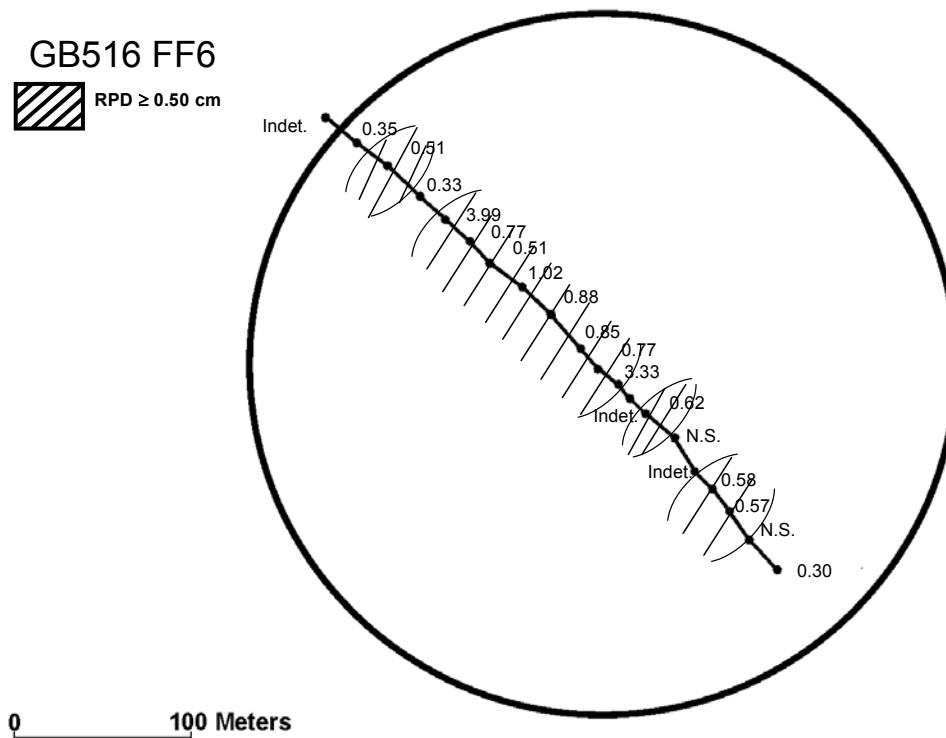


**Figure 6.10.** Mapped distribution of mean apparent redox potential discontinuity (RPD) depths along Transect FF6 at Garden Banks Block 516 during Cruise 1B (October-November 2000). The FF site radius is 204 m.

#### 6.3.4.1 Near-Field Stations

**Figure 6.12** shows the mapped distribution of successional seres as inferred from SPI data. Transect NF-2 has the lowest overall successional status, with almost half of the stations being azoic (43%) and 87% of the stations being either azoic or in a pioneering (Stage I) sere. Transect NF-1 has only four azoic stations (16%), and 76% are in either an azoic or pioneering (Stage I) status. Transect NF-3 stands in marked contrast to Transects NF-1 and NF-2 as over half (56%) of the stations along Transect NF-3 showed evidence (subsurface feeding voids) of Stage III species. No azoic stations were found along Transect NF-3 (**Figure 6.12**). Comparison of the near-field successional sere map (**Figure 6.12**) with the near-field map of the depth of the apparent RPD (**Figure 6.6**) shows that all of the azoic stations fall within the area of anomalously thin apparent RPD depths (zero or less than 0.5 cm in thickness). The location of this area northwest of the site center is generally consistent with the zone of relatively high barium and SBF concentrations (see *Chapters 8 and 9*).

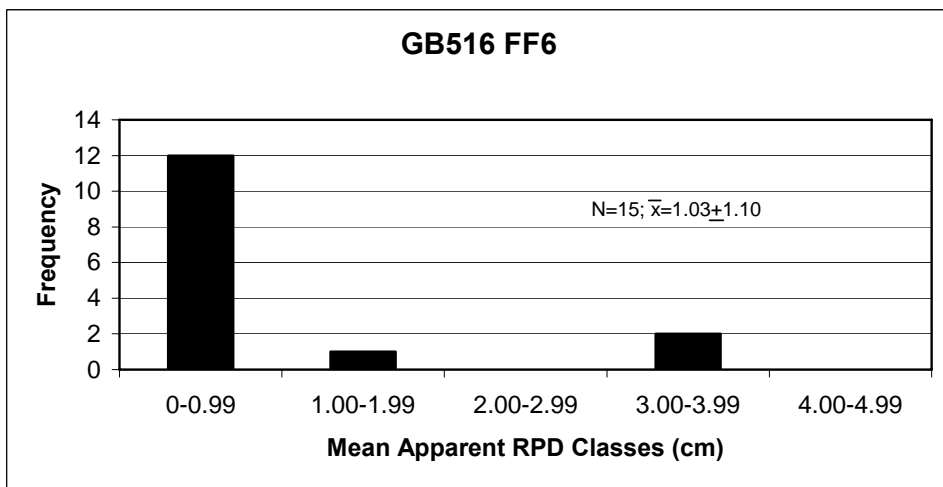
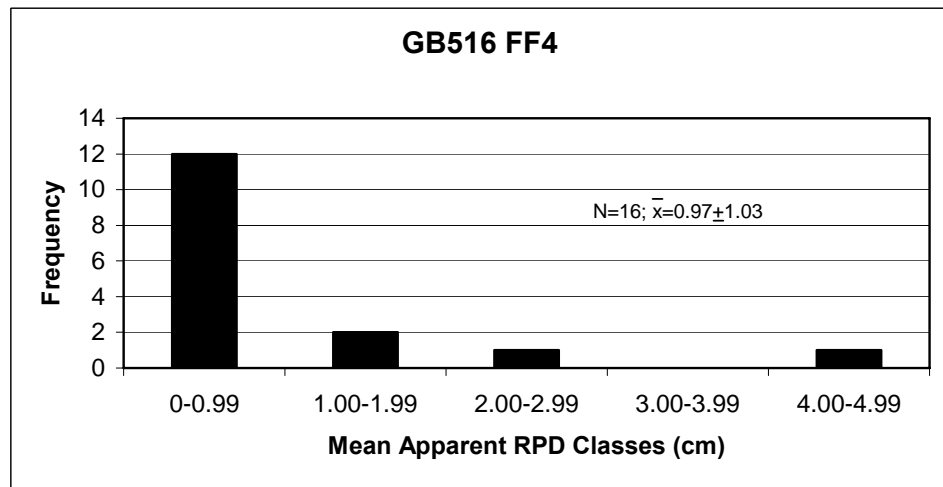
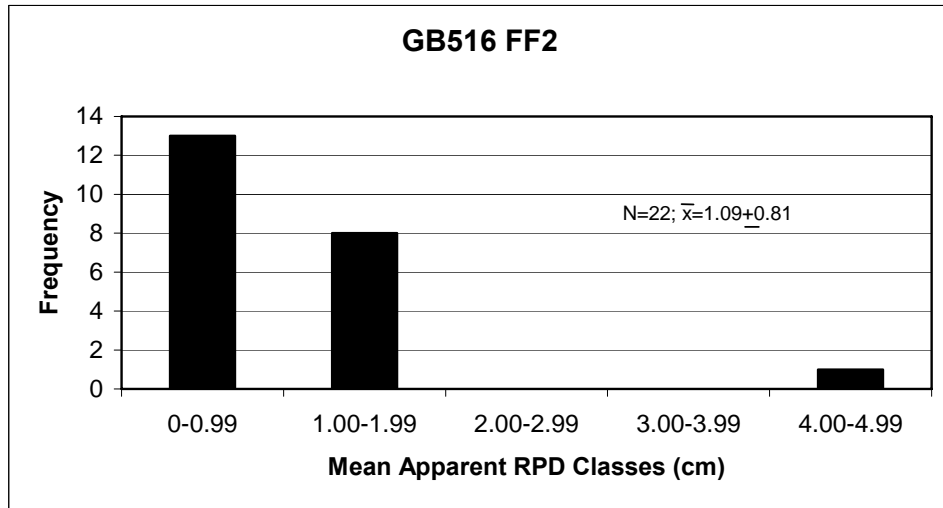


**Figure 6.11.** Redox potential discontinuity (RPD) depth-frequency distributions at three far-field transects at Garden Banks Block 516 during Cruise 1B (October-November 2000).

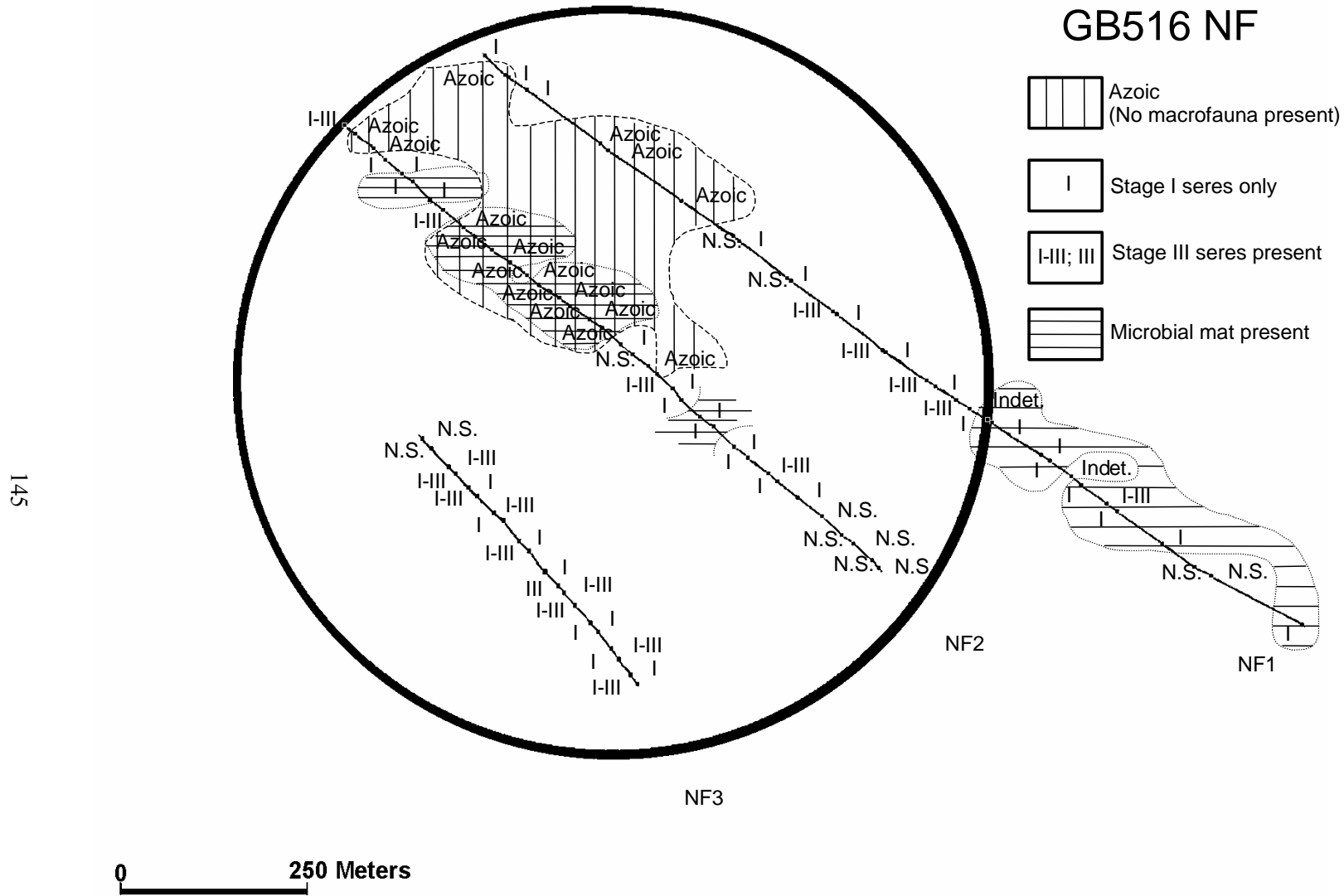


**Figure 6.12.** Mapped distribution of infaunal successional stages along all three near-field transects at Garden Banks Block 516 during Cruise 1B (October-November 2000). The NF site radius is 500 m.

#### 6.3.4.2 Far-Field Stations

Far-field Transect FF2 shows a mixture of Stage I and III seres, with over half (59%) of the stations dominated by Stage I seres. These Stage I areas (Stations FF2.8 to FF2.16) are located predominantly in the center of this transect (**Figure 6.13**). Stations along Transect FF4 are divided evenly between Stage I and III seres, but there is no spatial gradient apparent along the transect (**Figure 6.14**). Finally, Transect FF6 also is a patchy mixture of Stage I and III seres, with slightly more than half of the stations (56%) dominated by Stage III species (**Figure 6.15**). The northwestern end of this transect (Stations FF6.17 through FF6.20) is dominated by Stage I seres. No azoic stations were observed along any of the three far-field transects.

#### 6.3.5 Organism-Sediment Index (OSI)

The OSI is a parameter that describes overall benthic habitat quality (Rhoads and Germano 1986). The index takes into account the depth of the apparent RPD, successional stage, presence or absence of sediment methane bubbles, and presence or absence of reduced sediment near the sediment-water interface. The value of the index can range from +11 (best habitat value) to -10 (worst habitat value). Application of this paradigm to our study sites is an extrapolation, as detailed knowledge about infaunal successional stages is not available for these sites. However, past experience in mapping this index in a variety of shallow and deep water environments around the world has shown that indices of +6 or greater represent benthic habitats with minimal chemical or physical disturbance. Values of the OSI below +6 tend to be associated with disturbed benthic habitats. Negative OSI values reflect a highly disturbed benthos, such as bottom areas impacted by dredging, dumping, chemical contamination, or seafloor areas overlain by anoxic or hypoxic water. The GB 516 data set includes OSI values ranging from the highest value (+11) to a low of -8.

##### 6.3.5.1 Near-Field Stations

The worst benthic habitat quality (negative OSI values) of the GB 516 survey was at 7 stations along Transect NF-1 (Stations NF-1.22-1.28) and at 19 stations (Stations NF-2.11-2.12; 2.16-2.17; 2.19-2.28; 2.30-2.32; 2.34-2.35) along Transect NF-2 (**Figure 6.16**). This area of the seafloor appears to have experienced organic enrichment and high inventories of sedimentary sulfides at some earlier time. The benthic macroinfaunal community is depauperate, and filamentous anaerobic bacteria dominate. These lowest OSI values occur at the northwestern end of Transects NF-1 and NF-2 in the deeper end of the transects. The stations with the best benthic habitat quality (OSI equal to, or greater than +6) are found at 8 stations (1, 3, 4, 7, 12, 14, 16, and 18) located at the southeastern end of Transect NF-1; four of these are outside of the 1-km diameter circle. Transect NF-3 has 11 stations with mean OSI values equal to, or greater than +6. **Figure 6.17** shows the frequency distributions of OSI values at the three near-field transects. Using these distributions, transects are ranked on overall benthic habitat quality, from high to low, as NF-3 > NF-1 > NF-2.



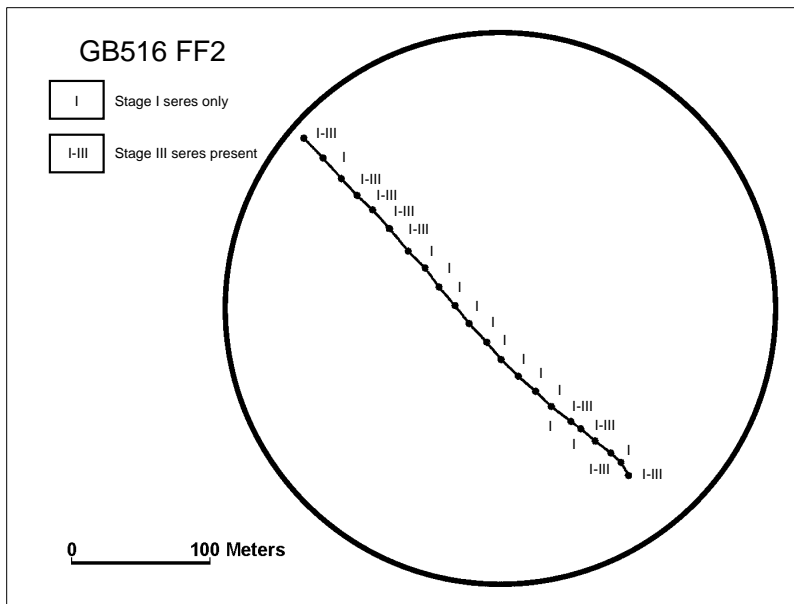


**Figure 6.13.** Mapped distribution of infaunal successional stages along Transect FF2 at Garden Banks Block 516 during Cruise 1B (October-November 2000). The FF site radius is 204 m.

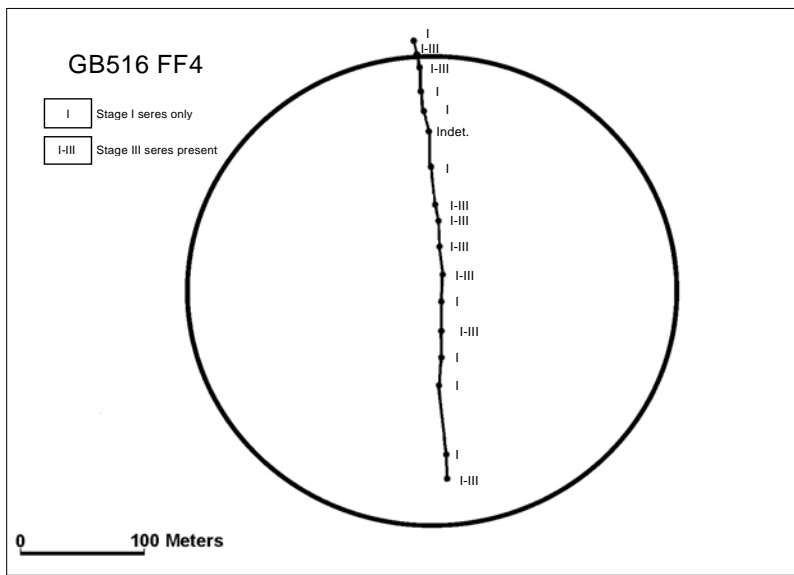


**Figure 6.14.** Mapped distribution of infaunal successional stages along Transect FF4 at Garden Banks Block 516 during Cruise 1B (October-November 2000). The FF site radius is 204 m.

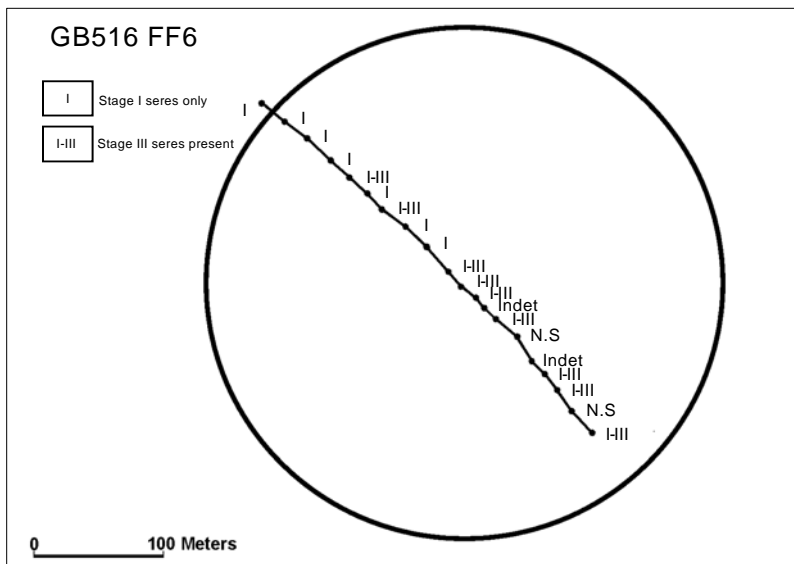


**Figure 6.15.** Mapped distribution of infaunal successional stages along Transect FF6 at Garden Banks Block 516 during Cruise 1B (October-November 2000). The FF site radius is 204 m.

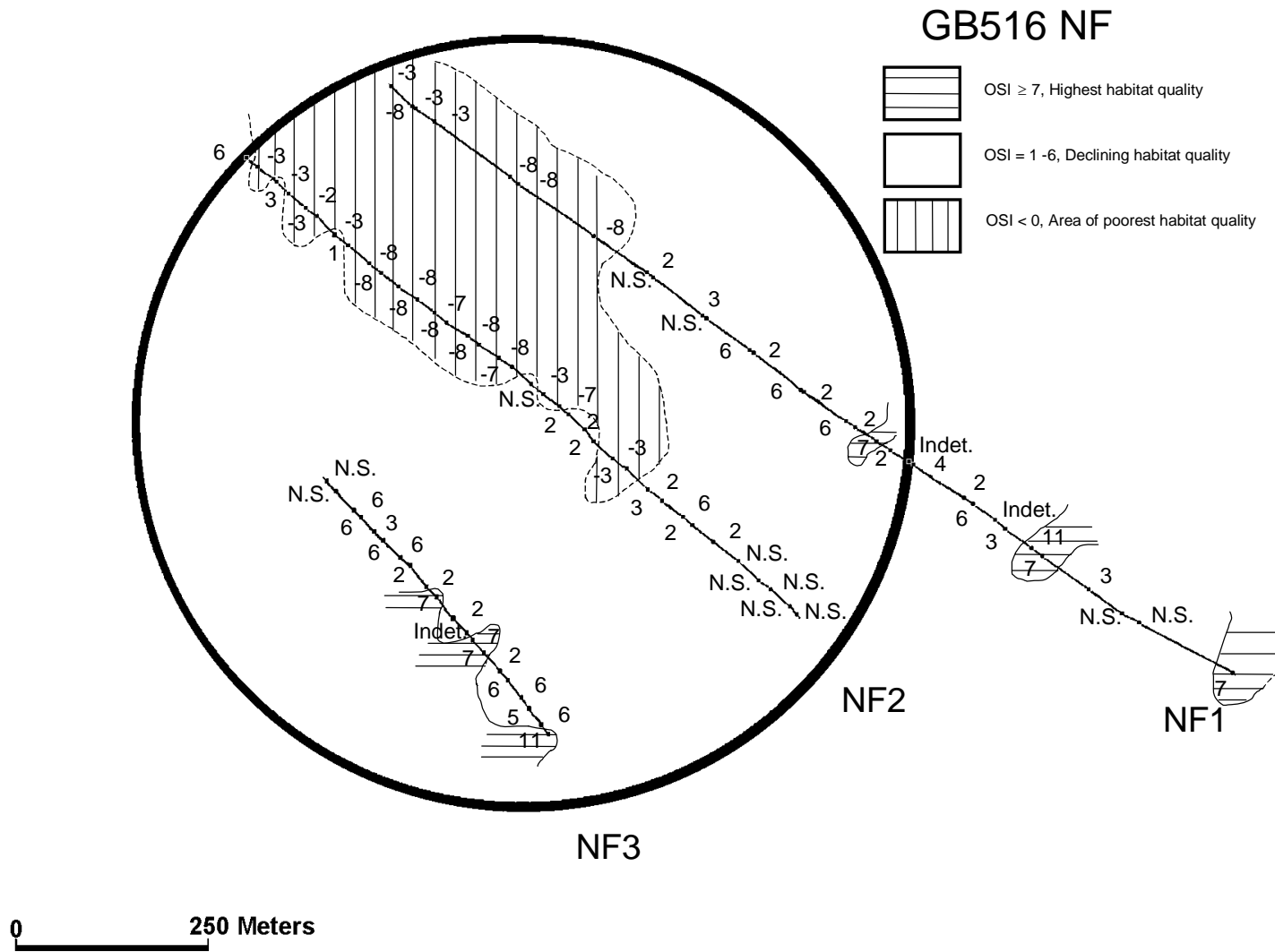


**Figure 6.16.** Mapped distribution of the Organism-Sediment Index (OSI) along all three near-field transects at Garden Banks Block 516 during Cruise 1B (October-November 2000). The NF site radius is 500 m.

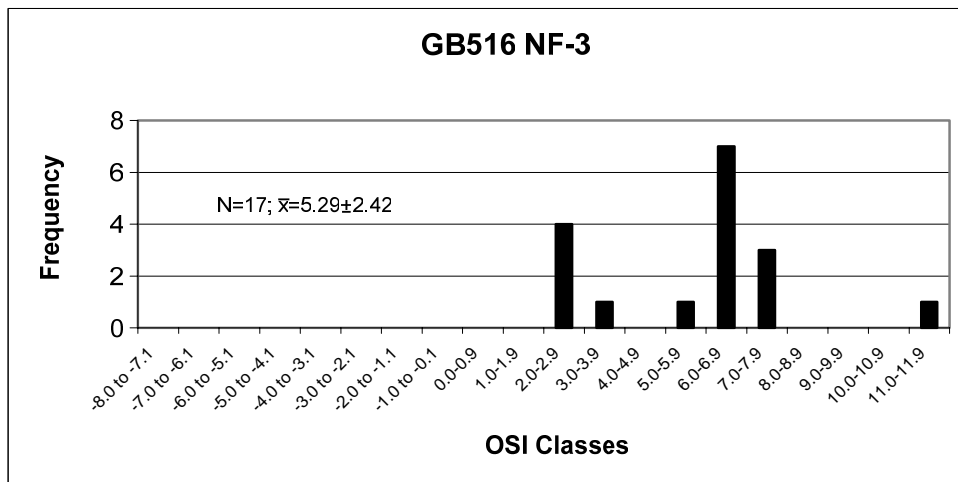
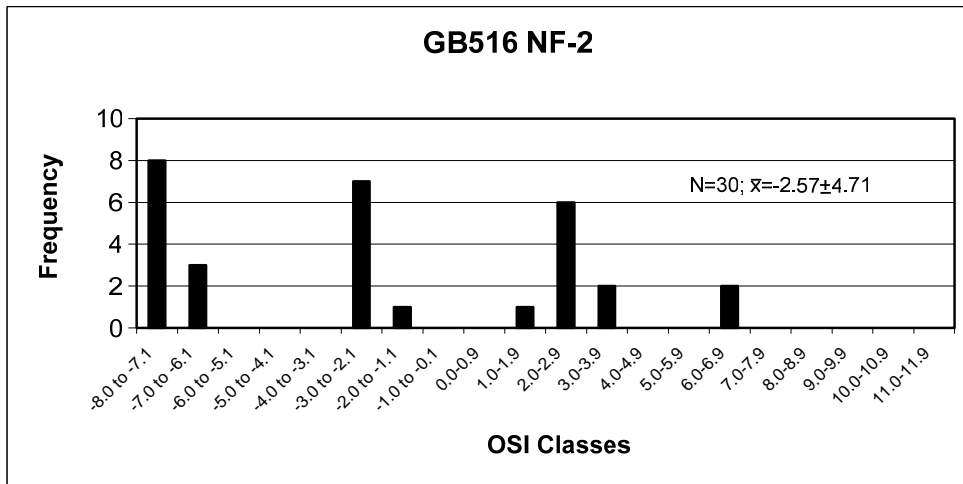
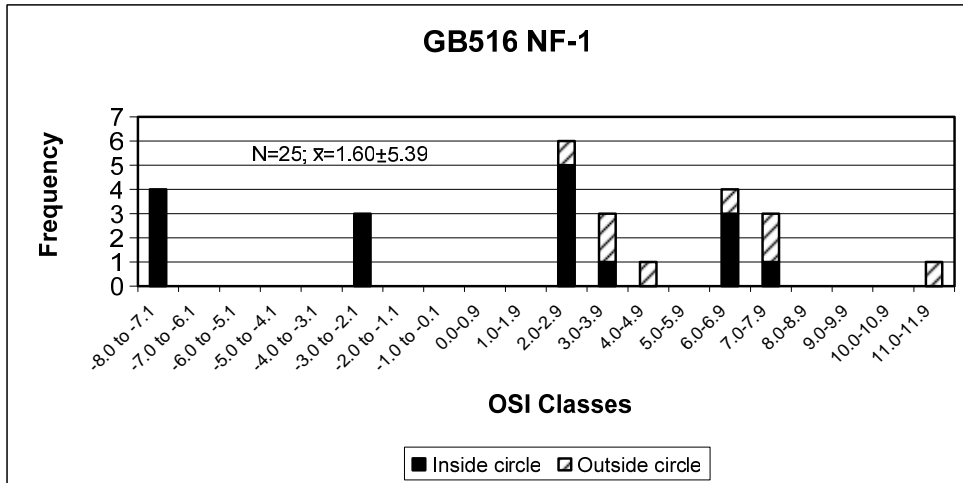


**Figure 6.17.** Organism-Sediment Index (OSI) class-frequency distributions at all three near-field transects sampled at Garden Banks Block 516 during Cruise 1B (October-November 2000).

#### 6.3.5.2 Far-Field Stations

The spatial pattern of OSI values along the three far-field transects was patchy. Segments of each of the three transects contained stations with relatively high OSI values (equal to, or greater than +6) alternating with those having lower values. However, no far-field stations (**Figures 6.18, 6.19, and 6.20**) were found with zero or negative OSI values. The frequency histograms show this bimodality (**Figure 6.21**). The overall distribution of OSI values at the three transects appeared to be similar. If one compares the far-field OSI distributions with all near-field stations falling within the reference circle, the distributions are similar for values of OSI equal to or higher than 1. However, the near-field sampling sites show a unique signature, with 26 stations falling within the poor habitat (or negative OSI) category (**Figure 6.22**), suggesting that habitat quality within the GB 516 near-field site was lower than that within far-field sites.

### 6.4 VIOSCA KNOLL BLOCK 916 – CRUISE 1B (PRE-DRILLING)

#### 6.4.1 Survey Design and Location

A pre-drilling SPI survey was conducted at VK 916 in October-November 2000 (Cruise 1B). This block lies within a depth range of about 1,000 to 1,300 m (**Figure 6.23**) and is approximately 50 nm east of the mouth of the Mississippi Delta. All of the near-field SPI images were taken near the 1,200-m depth contour, within a 1,000-m diameter circle, about 0.5 nm NNE of the block center. Two intersecting transects were sampled at the near-field site. The first transect (NF-1) was sampled in a northwest to southeast direction, oriented normal to the bathymetric contour. The second transect (NF-2) was sampled from east to west tangentially to the local bathymetry. One image per station was acquired in this reconnaissance mapping survey to rapidly delineate spatial gradients in benthic habitat quality. No attempt was made to replicate stations along the two VK 916 near-field transects (**Figure 6.24**).

In addition, samples were collected along three control transects at far-field sites. Two of these sites were situated approximately 12 to 15 km northeast of the near-field site, while the third was located 10 km to the southwest (**Figure 6.23**). Far-field transects were selected with the assumption that they represented ambient or reference bottom conditions. This survey was intended to establish a pre-drilling baseline in order to evaluate potential changes in seafloor conditions related to subsequent drilling activities.

##### 6.4.1.1 Near-Field Stations

All near-field stations on the two transects were located inside the 1,000-m diameter circle within the VK 916 Block. Usable SPI photographs (i.e., image quality that allowed analysis) were obtained from all but one station along both near-field transects, for a total of 78 analyzable images, 45 from Transect NF-1 and 33 from Transect NF-2. **Figure 6.24** shows these near-field transects along with the site center latitude and longitude.

##### 6.4.1.2 Far-Field Stations

The three far-field transects are shown in **Figures 6.25, 6.26, and 6.27**. Each far-field site consists of a single transect lying largely within the perimeter of a 408-m diameter circle. Transect FF2 had 20 stations (**Figure 6.25**). Transect FF4 consisted of 18 stations (**Figure 6.26**), and Transect FF6 consisted of 20 stations (**Figure 6.27**). Analyzable images were obtained from 55 stations out of a total of 58 stations sampled.

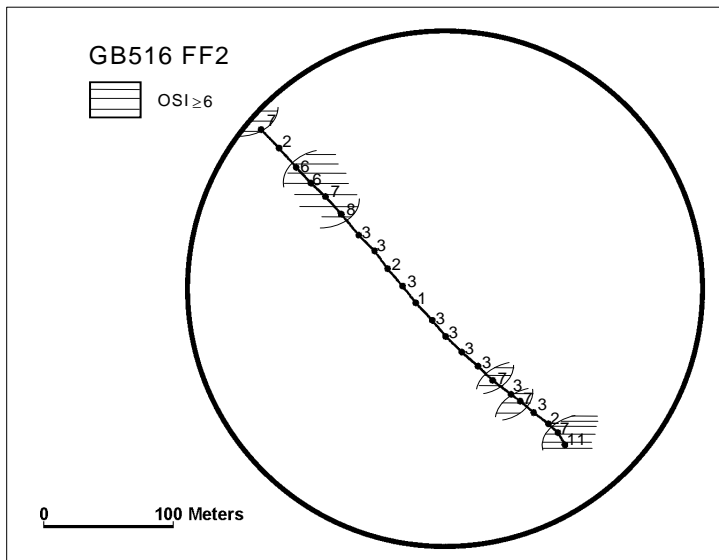


**Figure 6.18.** Mapped distribution of the Organism-Sediment Index (OSI) along Transect FF2 at Garden Banks Block 516 during Cruise 1B (October-November 2000). The FF site radius is 204 m.

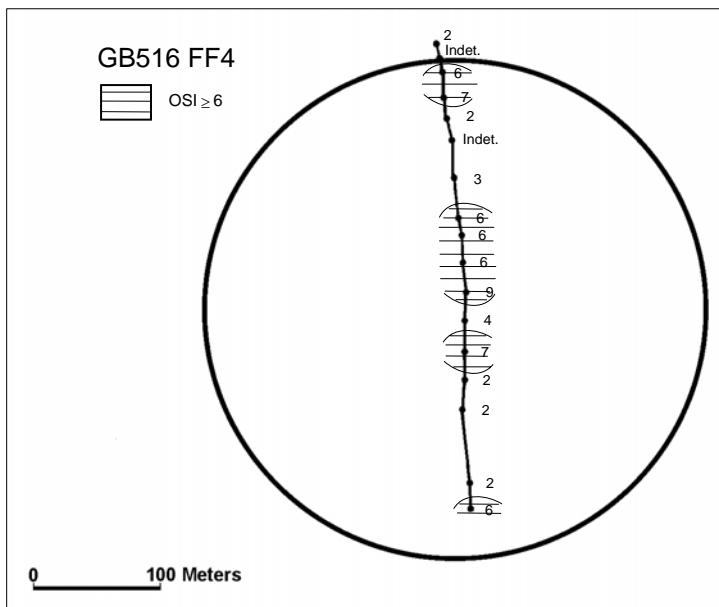


**Figure 6.19.** Mapped distribution of the Organism-Sediment Index (OSI) along Transect FF4 at Garden Banks Block 516 during Cruise 1B (October-November 2000). The FF site radius is 204 m.

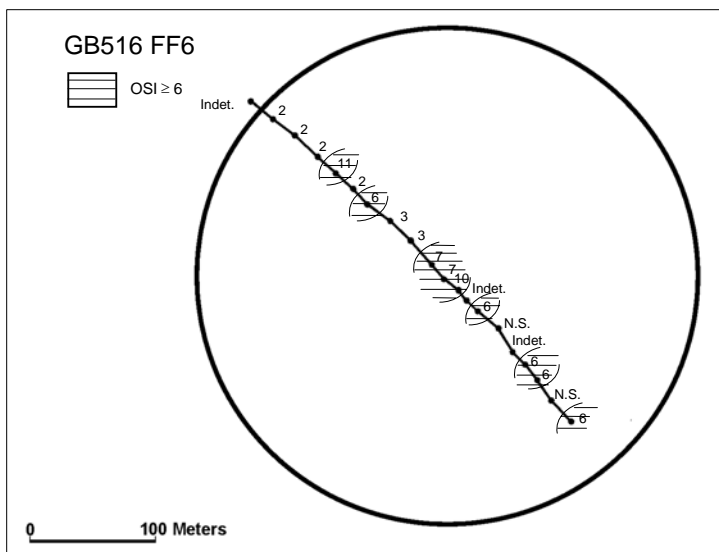


**Figure 6.20.** Mapped distribution of the Organism-Sediment Index (OSI) along Transect FF6 at Garden Banks Block 516 during Cruise 1B (October-November 2000). The FF site radius is 204 m.

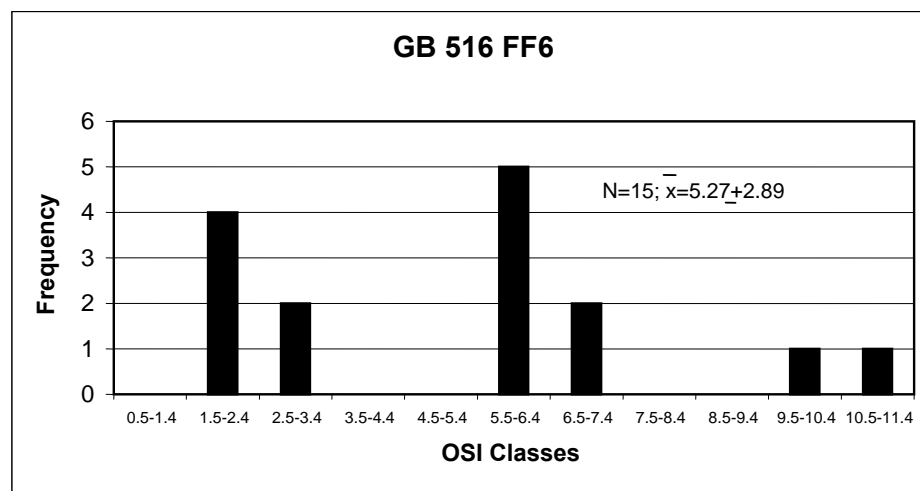
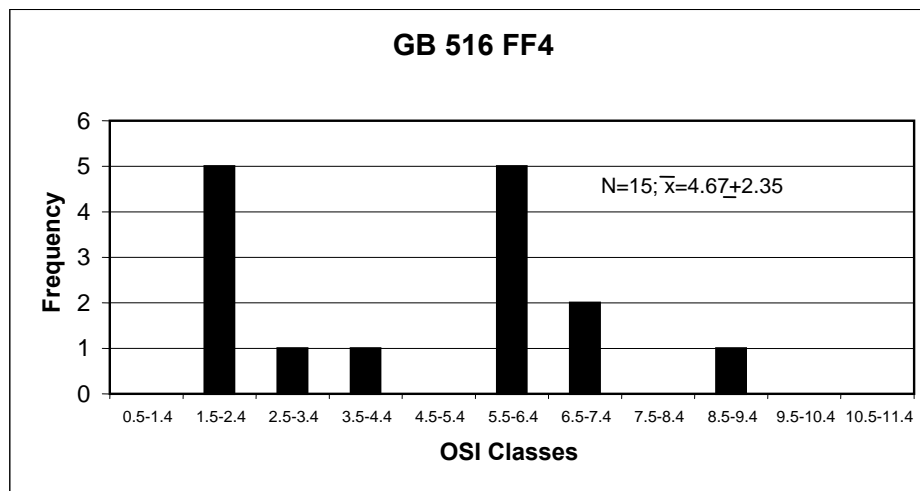
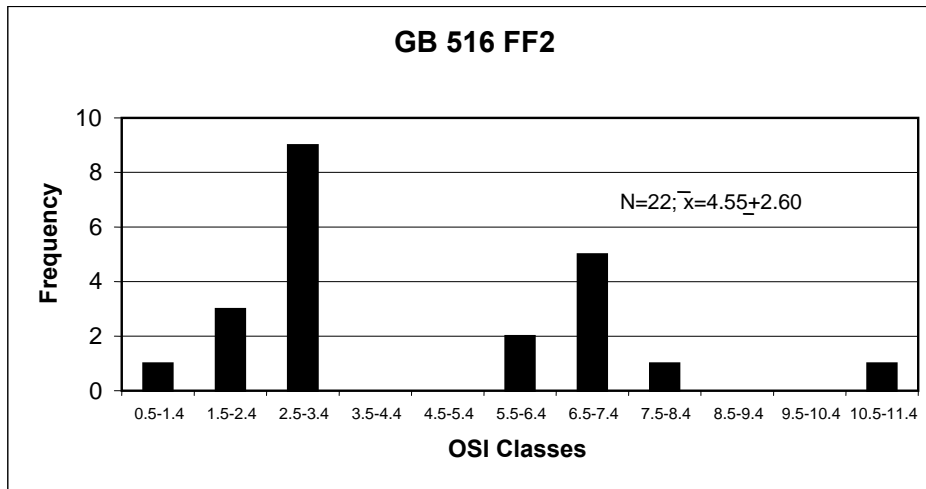


**Figure 6.21.** Organism-Sediment Index (OSI) class-frequency distributions at all three far-field transects at Garden Banks Block 516 during Cruise 1B (October-November 2000).

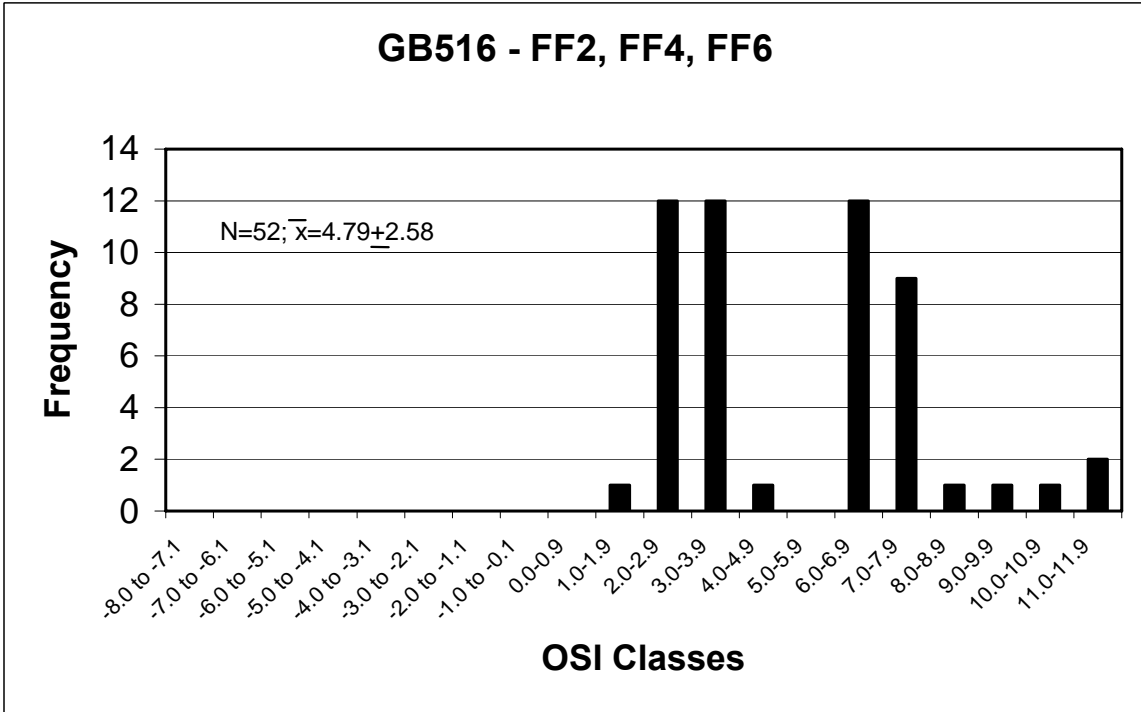
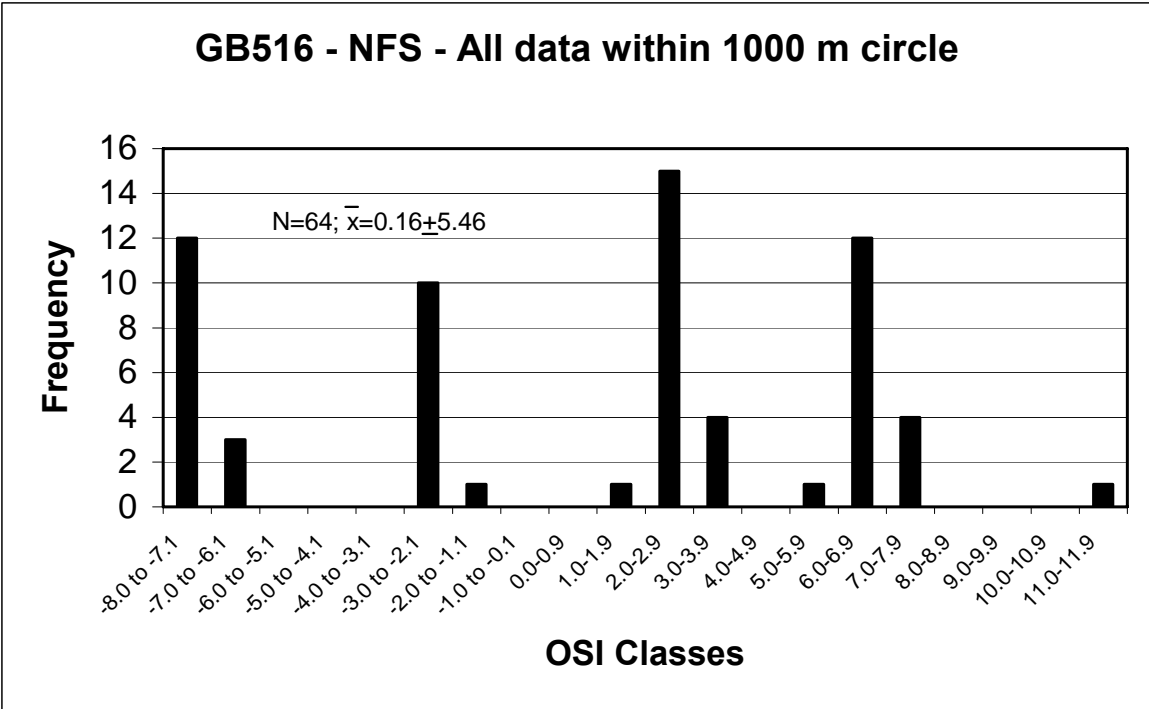


**Figure 6.22.** Organism-Sediment Index (OSI) class-frequency distributions at all near-field and far-field transects at Garden Banks Block 516 during Cruise 1B (October-November 2000).

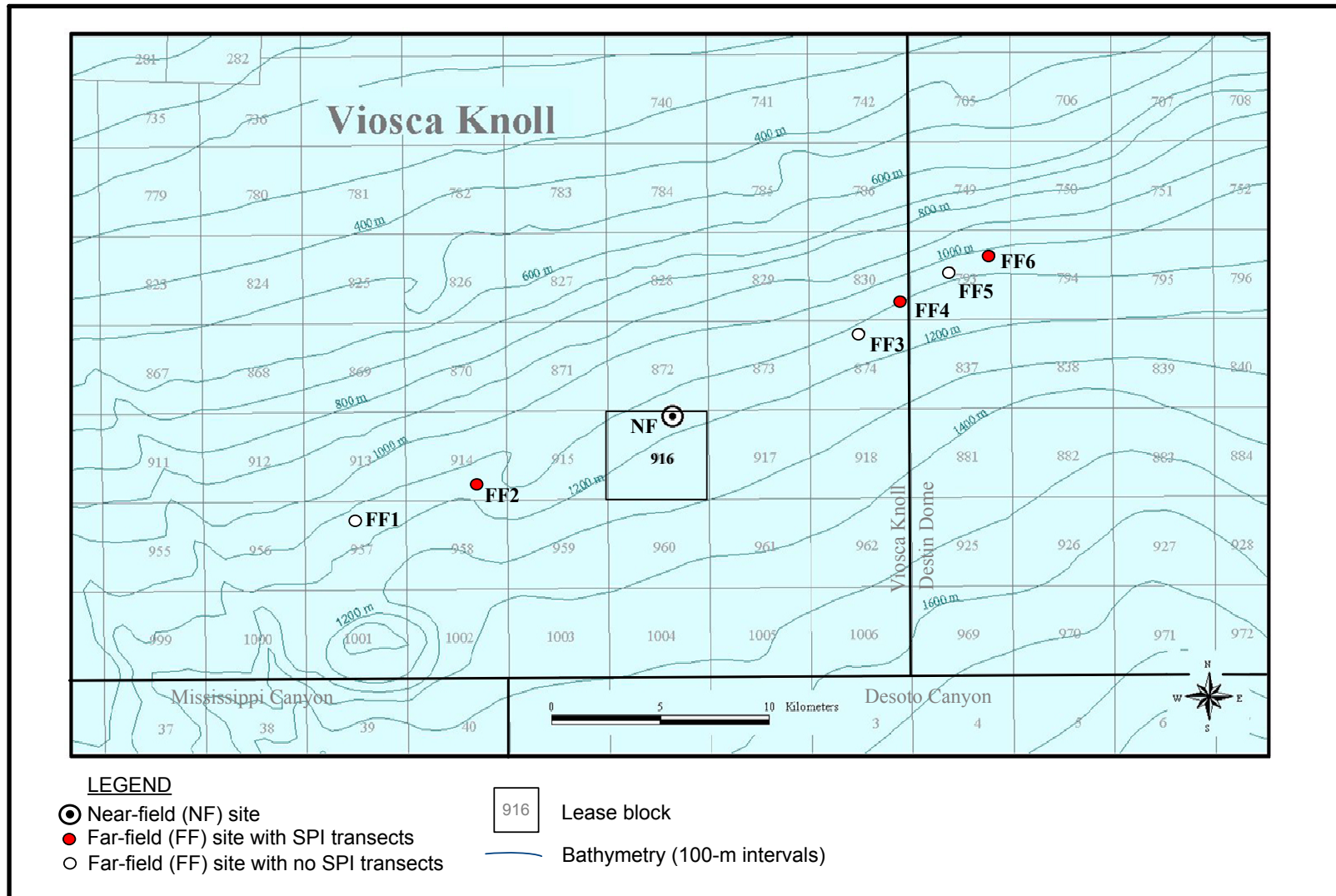


**Figure 6.23.** Location of Viosca Knoll Block 916 exploration site and associated reference areas where sediment profile imaging (SPI) transects were surveyed on Cruise 1B.



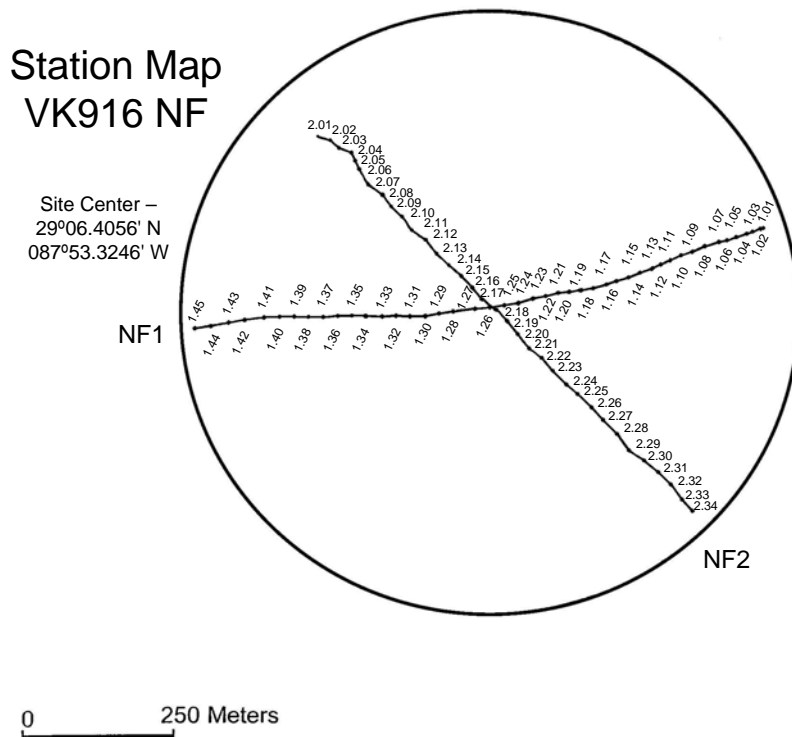


**Figure 6.24.** Viosca Knoll Block 916 near-field (NF) station map, showing positions of sediment profile imaging transects and stations. The NF site radius is 500 m.

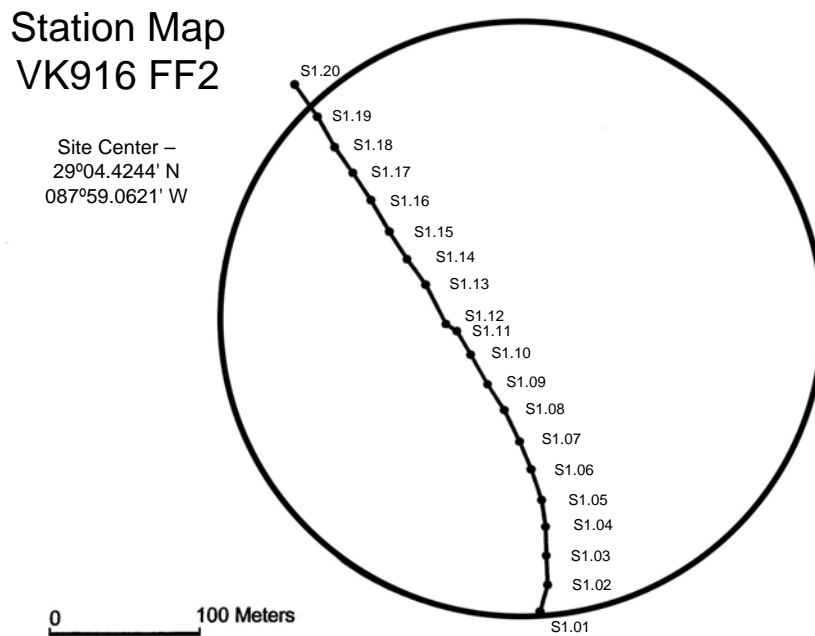


**Figure 6.25.** Viosca Knoll Block 916 Far-field 2 (FF2) station map, showing positions of sediment profile imaging transects and stations. The FF site radius is 204 m.

### Station Map VK916 FF4

Site Center –  
29°09.8071' N  
087°46.5882' W

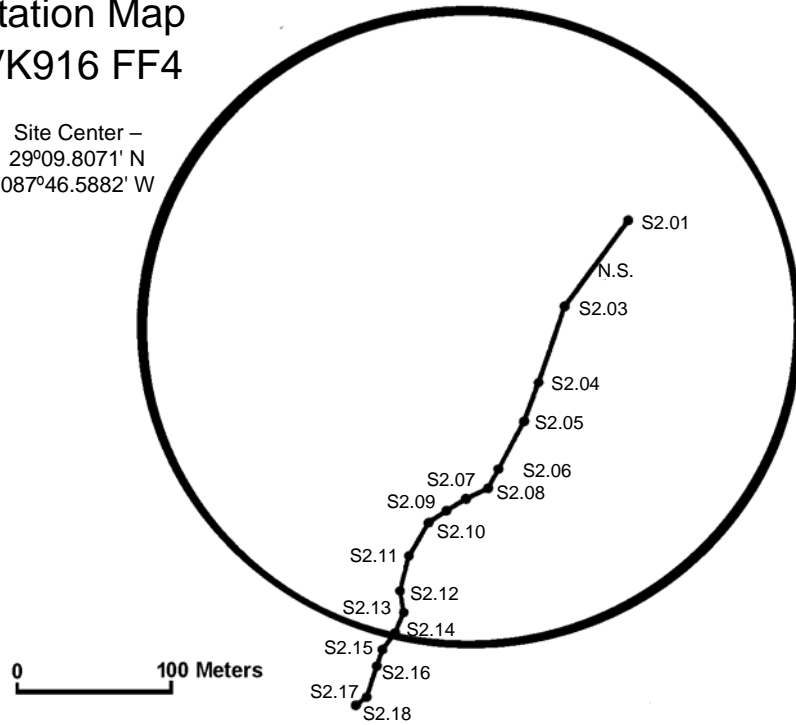


**Figure 6.26.** Viosca Knoll Block 916 Far-field 4 (FF4) station map, showing positions of sediment profile imaging transect and stations. The FF site radius is 204 m.

### Station Map VK916 FF6

Site Center –  
29°11.1643' N  
087°43.9900' W

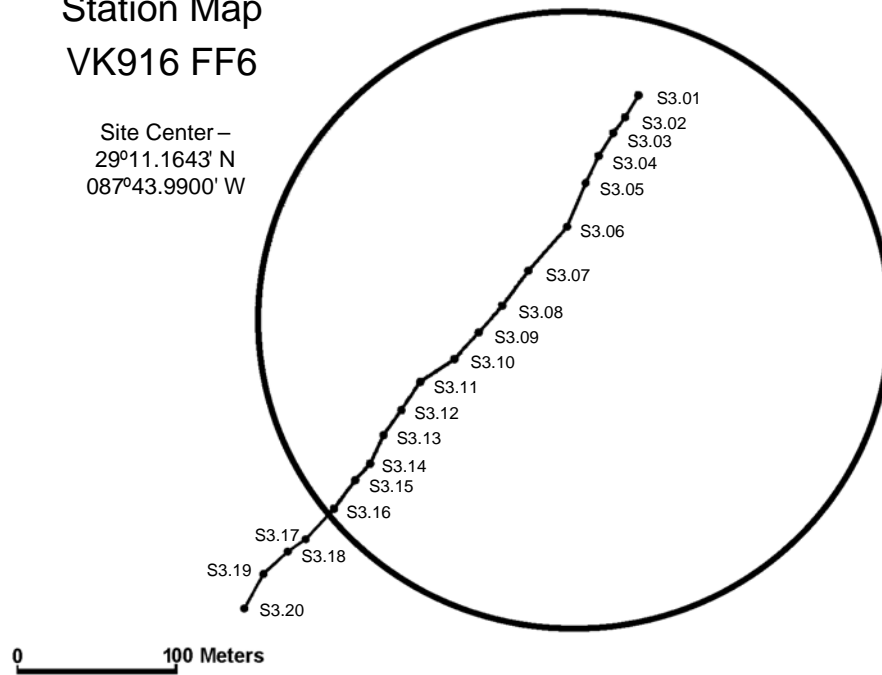


**Figure 6.27.** Viosca Knoll Block 916 Far-field 6 (FF6) station map, showing positions of sediment profile imaging transect and stations. The FF site radius is 204 m.

## 6.4.2 Sediment Fabric, Texture, Color, and Small-Scale Stratigraphy

As described in *Section 6.3.2*, a variety of sedimentary features that can be observed in sediment profile images such as changes in sediment texture, color, fabric, boundary roughness, and microstratigraphy can help elucidate sedimentary processes in the region undergoing examination.

### 6.4.2.1 Near-Field Stations

All near-field stations show sediments in the seabed that consist of a near-surface interval of reddish-brown sediment overlying a light to medium gray clay at depth. The mean thickness of the reddish brown layer at NF-1 stations is 5.53 cm (range = 2.75 to 9.11 cm), and NF-2 stations have a mean red layer thickness of 4.75 cm (range = 2.01 to 8.61 cm). The reddish color of these surficial sediments is due to ferric hydroxide coatings (“rust”) on the surfaces of sediment particles. The oxidation state of these particles indicates that they have been exposed to dissolved oxygen before and/or during sedimentation.

The origin of small-scale boundary roughness could not be determined for all stations, but at those stations where roughness elements were apparent, the generic source was estimated as being dominated either by biological activities or physical processes. Sediment-water interface boundary roughness along Transect NF-1 apparently is predominately (97%) due to biogenic features such as tube aggregations, feeding pits, etc. Transect NF-2, on the other hand, has boundary roughness that appears to be mainly (70%) due to surface erosion or bottom scour.

The texture of the upper few centimeters of the reddish-brown layer consists of sand, mainly 2-1 phi (fine sand), but may range from very fine sand (4-3 phi) to medium sand (3-2 phi). As reported in *Chapter 5*, samples of the top 2 cm indicate a mean grain size in the range of 9 to 8 phi. The sediment fabric is burrow mottled. This sand is composed of aggregates of silt and clay bound into sand-sized particles. The process of aggregation is interpreted to represent the biological “packaging” of silt and clay into sand-sized pellets, pseudofeces, small tubes, or parcels of sediment that were broken up in the process of sediment bioturbation (foraging and/or burrowing). At depth, these aggregates tend to lose their sand-sized outlines due to compaction, and the texture appears to be predominantly very coarse silt and clay (>4 phi). The underlying gray clay appears homogeneous and is entirely composed of cohesive clay-sized particles. The contact between the overlying rust-colored sediment and the underlying gray clay appears to be very sharp but irregular. The thickness of the gray clay cannot be determined as it extends below the camera’s field of view. All near-field stations have similar gradients in fabric, texture, structure, and microstratigraphy. Examples of typical sediment profile images from Transects NF-1 and NF-2 are shown in *Plate 9*.

The geotechnical consistency of the underlying gray clay is stiff and cohesive, and the clay tends to adhere to the camera’s optical window. Many images show ribbon-like pieces of gray clay at, or near, the surface that were wiped off the prism window by its wiper as the optical prism entered the bottom. The cohesive nature of this clay suggests that it has a water content of 50% or less (Boswell 1961) and is therefore geotechnically considered to be “over consolidated.” It is likely that the contact between the overlying oxidized, bioturbated sediment and the underlying gray clay may represent a significant temporal interruption. Therefore, the underlying clay is

hypothesized to be much older (e.g., Pleistocene) than the rust-colored sediment accumulating above this cohesive unit.

#### 6.4.2.2 Far-Field Stations

All of the far-field stations were similar to the near-field stations in texture, gradients in color, fabric, and microstratigraphy. The detailed description that appears above for near-field stations also applies to the far-field stations. The mean thickness (with ranges) of the reddish-brown oxidized surface sediment for the three far-field transects are FF2 = 5.06 cm (2.84 to 9.96 cm), FF4 = 5.12 cm (4.43 to 8.80 cm), and FF6 = 4.50 (2.90 to 6.48 cm). Small-scale boundary roughness is dominated (54% to 75%) by biological features. Typical far-field sediment profile images are shown in *Plates 10* (FF2 and FF4) and *11* (FF6).

#### 6.4.3 Depth of the Apparent Redox Potential Discontinuity

The near-surface zone of intensive particle mixing and interstitial water exchange is recognized in SPI images as a difference in color between the mixed zone (light tan/pink) and underlying sediment (darker red, gray, or black). The color difference is imparted by the oxidation state of particulate iron (or manganese) coatings on sediment particles (ferric hydroxide or manganese carbonate) and the relative absence of reduced compounds such as hydrogen sulfide and/or iron or manganese sulfides. Because we are inferring the oxidation state from sediment color, this parameter is called the “apparent” RPD. The true RPD (depth at which the Eh = 0 potential) can only be measured with a polarographic electrode, and experience has shown that the Eh = 0 depth is usually shallower than the apparent RPD as estimated by sediment color changes (Pearson and Stanley 1979; Revsbech et al. 1979). In addition, once ferric hydroxide coatings have developed on sediment particles, they can remain oxidized even though they subsequently may have been buried below the true redox (i.e., in a reducing environment). This is the primary reason that the apparent RPD overestimates the true RPD. Nevertheless, spatial gradients in the depth of the apparent RPD can prove useful in mapping organic enrichment, bioturbation depths, and the presence of low bottom-water dissolved oxygen tensions (Pearson and Stanley 1979; Rhoads and Germano 1982).

In general, the apparent RPD depth was difficult to measure at the VK 916 near-field and far-field sites for two reasons. First, the biological mixing depth appears to be very shallow, and second, the color difference between the mixing zone and underlying oxidized sediment is difficult to resolve.

##### 6.4.3.1 Near-Field Stations

**Figure 6.28** shows the mapped distribution of mean apparent RPD depths at the near-field stations. The hatched area delimits those stations with mean apparent RPD depths greater than 0.5 cm. All stations on Transect NF-2 have mean apparent RPD depths greater than 0.5 cm. However, 25% of the stations on Transect NF-1 have RPD depths that are less than 0.5 cm. These stations are distributed along Transect NF-1 in a patchy manner, although the majority occur in the western half of the transect. For all near-field stations where RPD depth could be determined ( $n = 74$ ), the mean apparent RPD depth was 0.93 cm. The histograms (**Figure 6.29**) of mean apparent RPD depth classes for both near-field transects show that the mean apparent RPD depth for Transect NF-1 (0.78 cm) is shallower than that for Transect NF-2 (1.14 cm).

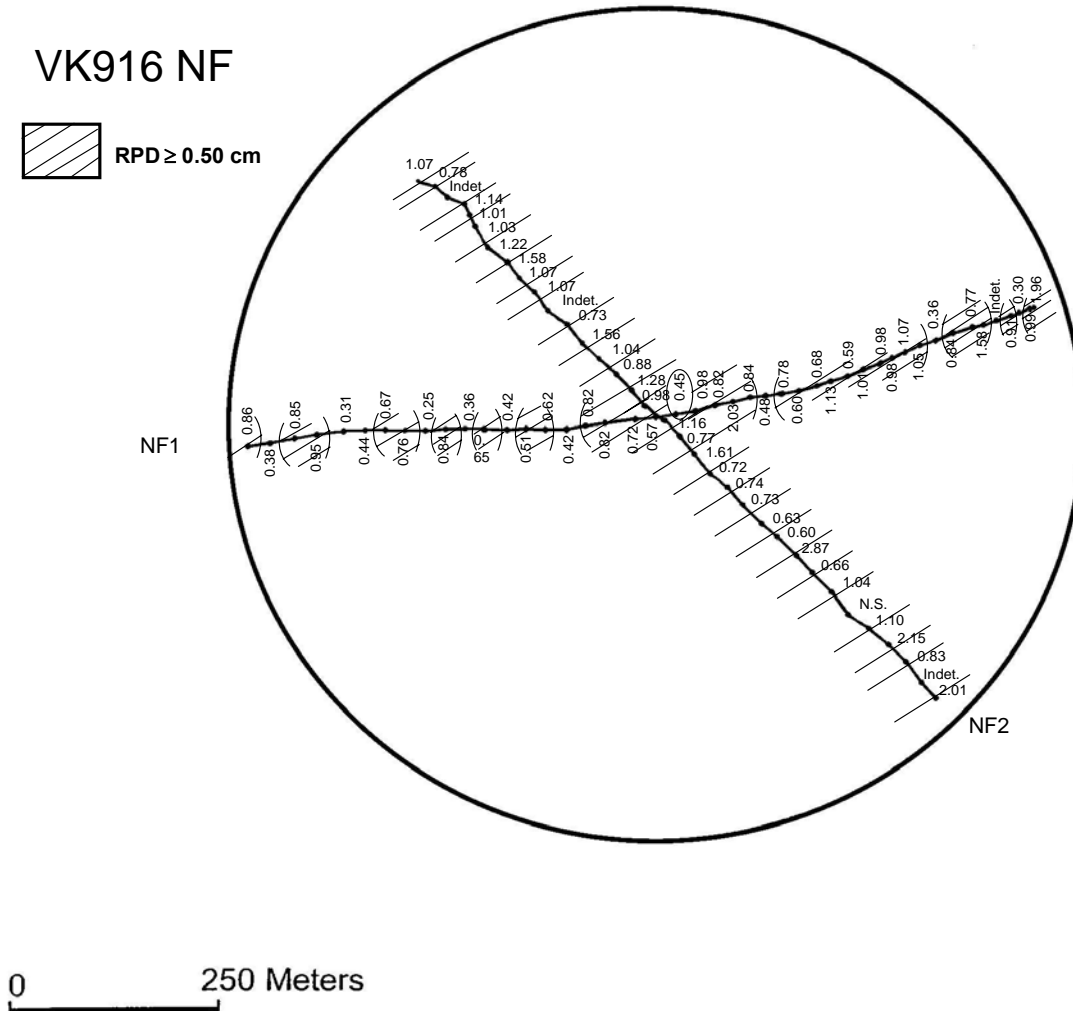


**Figure 6.28.** Mapped distribution of apparent redox potential discontinuity (RPD) depth, in centimeters, along the two near-field transects in Viosca Knoll Block 916 during pre-drilling Cruise 1B (October-November 2000). The NF site radius is 500 m.

#### 6.4.3.2 Far-Field Stations

The deepest mean apparent RPD depths were mapped along Transect FF2 (**Figure 6.30**). Most values are greater than 1.00 cm, with a transect mean of 1.36 cm (**Figure 6.31**). In comparison, all stations along Transect FF4 (**Figure 6.32**) and most stations along Transect FF6 (**Figure 6.33**) have mean apparent RPD depth values less than 1.00 cm. For all far-field stations where RPD depth could be determined ( $n = 51$ ), the mean apparent RPD depth was 0.91 cm. RPD frequency histograms show that the mean apparent RPD values for both Transects FF4 and FF6 are less than 1.00 cm (**Figure 6.31**).

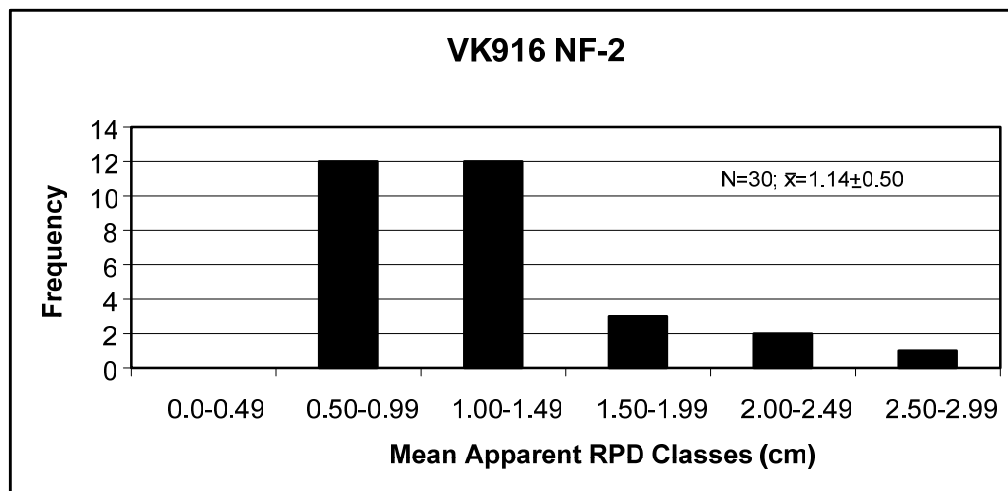
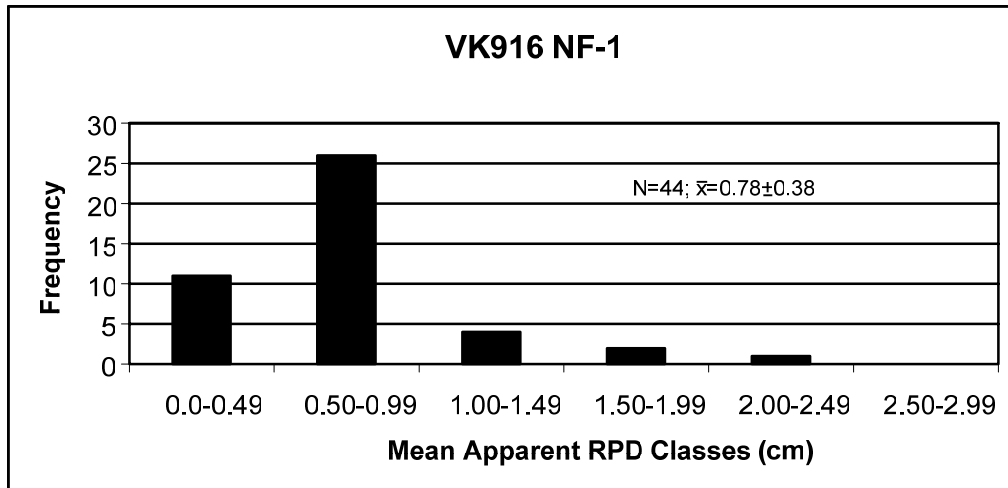


**Figure 6.29.** Redox potential discontinuity (RPD) depth-frequency distributions at two near-field transects in Viosca Knoll Block 916 during pre-drilling Cruise 1B.

#### 6.4.4 Infaunal Successional Stages

Infaunal successional stages are defined in *Sections 6.2 and 6.3.4*. As for the GB 516 site, knowledge about possible Stage II seres is lacking for the VK 916 area, and thus, Stage II seres cannot be identified. At both the near-field and far-field transects, all stations were occupied by infauna. No azoic stations were observed. In the VK 916 survey, we identified two successional bottom types:

1. Bottom sediments that exhibit only Stage I pioneers (Stage I seres); and
2. Bottom sediments that show evidence of subsurface feeding voids (with or without Stage I species at the surface) and that are mapped as Stage I-III or Stage III seres.

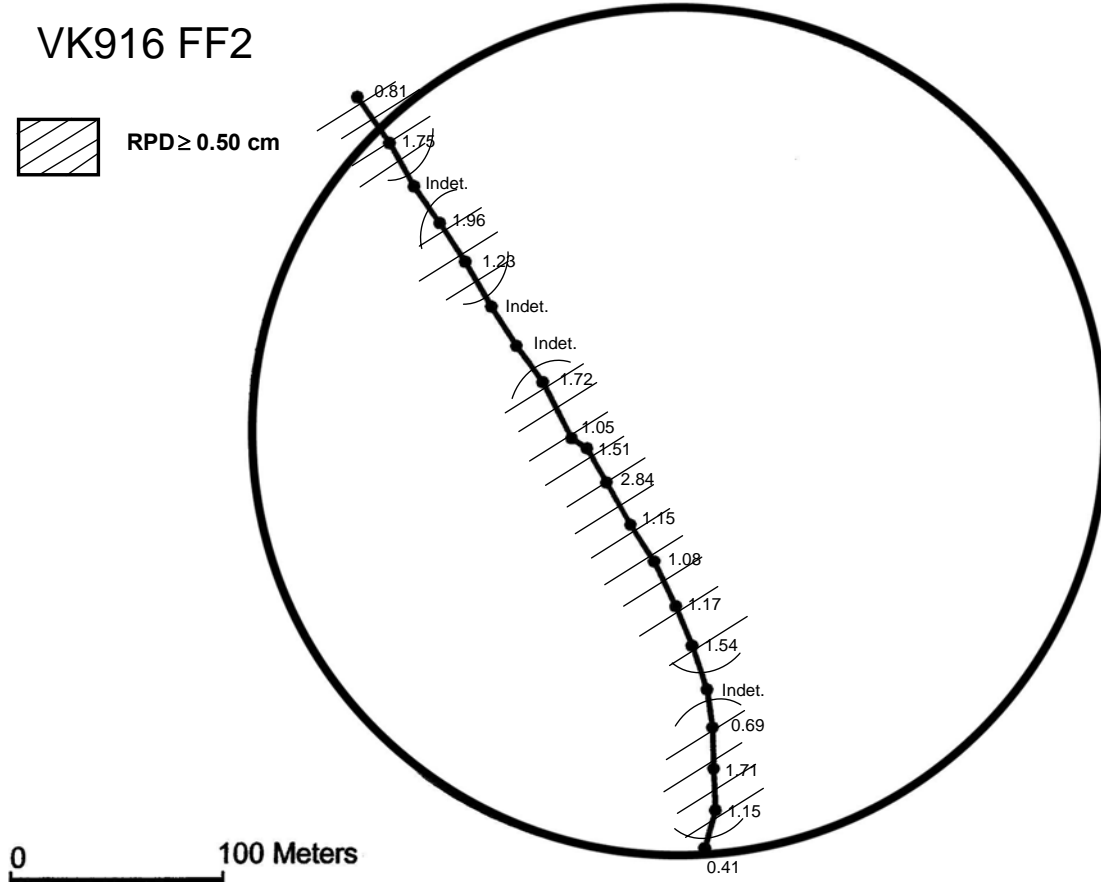


**Figure 6.30.** Redox potential discontinuity (RPD) depth-frequency distributions along Transect FF2 at Viosca Knoll Block 916 during pre-drilling Cruise 1B (October-November 2000). The FF site radius is 204 m.

We note that both Stage I and Stage III infauna observed in profile images were small in size and low in density. This observation is similar to observations made during a previous benthic sampling program, which indicated that the deeper water soft bottoms of the Gulf of Mexico appear to represent oligotrophic benthic systems dominated by sparse populations of very small infaunal organisms dominated by polychaetes (Yingst and Rhoads 1985).

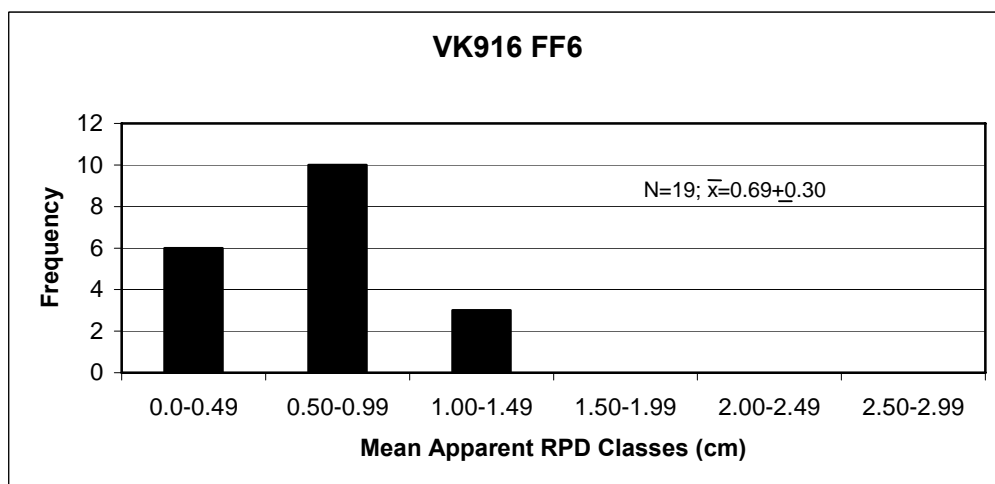
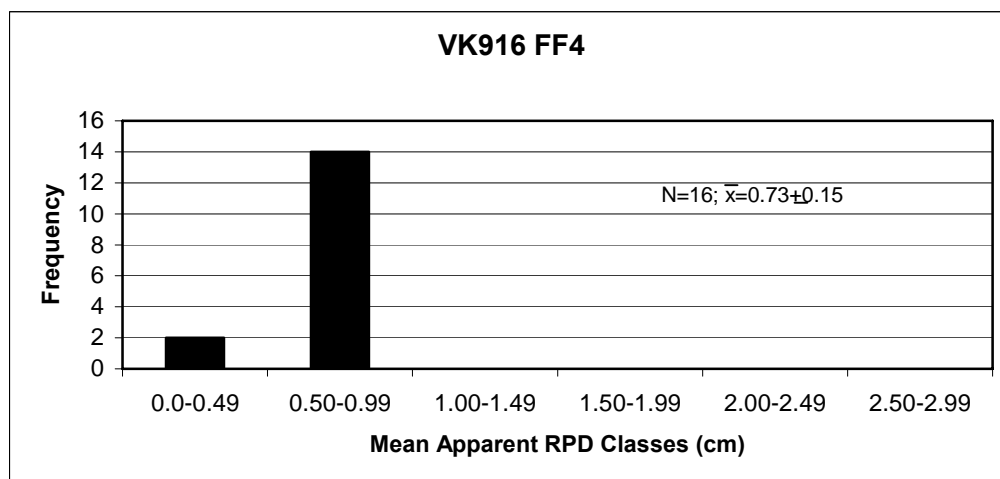
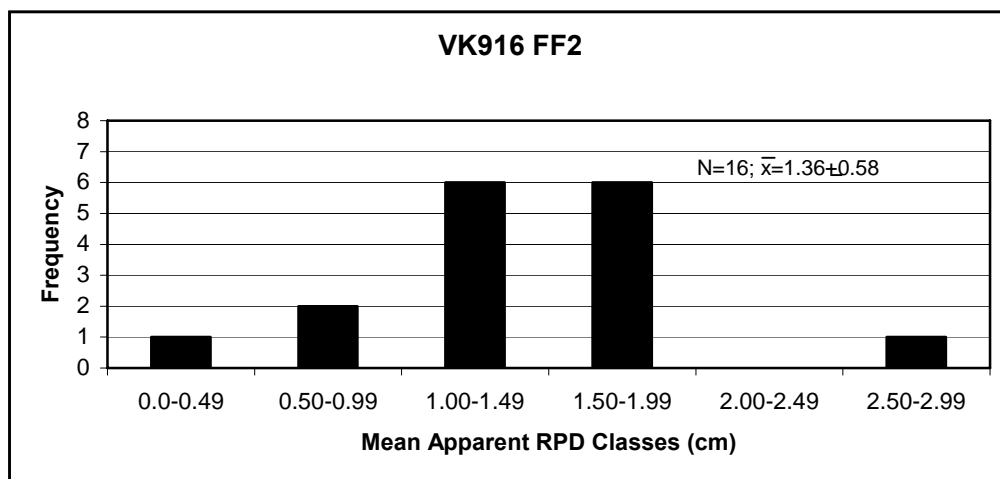


**Figure 6.31.** Redox potential discontinuity (RPD) depth-frequency distributions at three far-field transects sampled at Viosca Knoll Block 916 during pre-drilling Cruise 1B (October-November 2000).



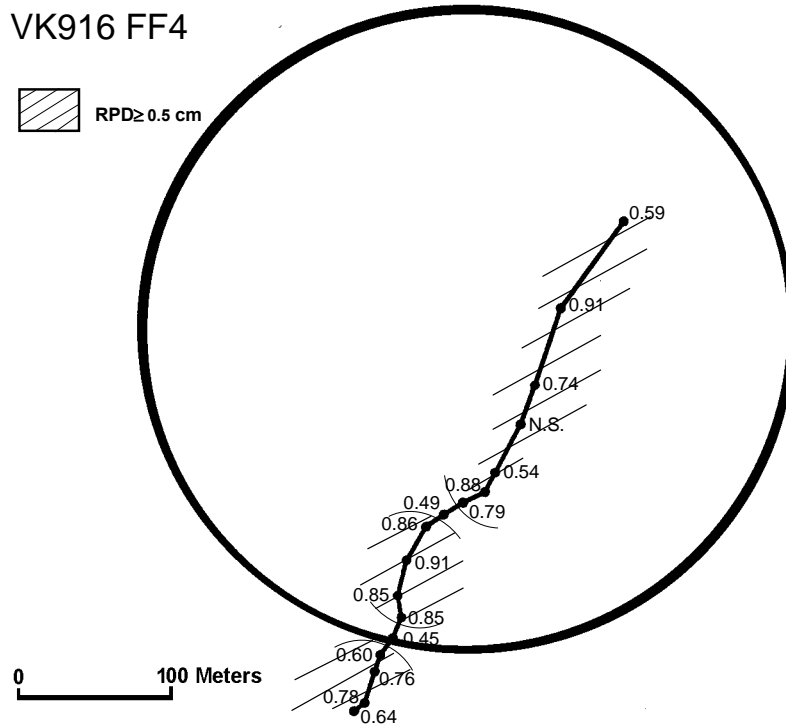


**Figure 6.32.** Redox potential discontinuity (RPD) depth-frequency distributions along Transect FF4 at Viosca Knoll Block 916 during pre-drilling Cruise 1B (October-November 2000). The FF site radius is 204 m.

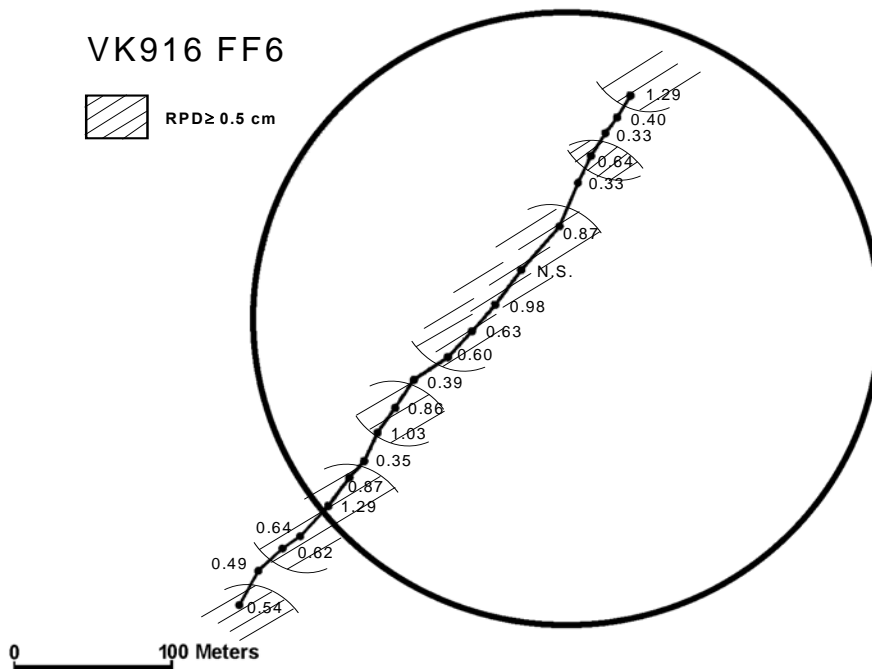


**Figure 6.33.** Redox potential discontinuity (RPD) depth-frequency distributions along Transect FF6 at Viosca Knoll Block 916 during pre-drilling Cruise 1B (October-November 2000). The FF site radius is 204 m.

#### 6.4.4.1 Near-Field Stations

The distribution of successional seres in the near-field shows that Stage I-III seres predominate, with five local patches consisting of 3 to 6 adjacent stations dominated by Stage I seres (**Figure 6.34**). The mosaic pattern of Stage I and Stage I-III seres found at the near-field site shows the scale of local seafloor disturbances.

#### 6.4.4.2 Far-Field Stations

Far-field Transect FF2 consists of a patchy mixture of Stage I and Stage I-III seres. These successional stage sere clusters are equally represented in number along this transect, and Stage I seres appear to be concentrated in one large and two smaller areas (**Figure 6.35**). Likewise, Transects FF4 and FF6 both show three clusters of stations dominated by pioneering seres (Stage I) (**Figures 6.36** and **6.37**). The patch size of successional seres at all the mapped sites suggests that the benthic community represents a mosaic of past disturbances, and the scale of these disturbances are on the order of tens to a hundred meters across. The actual patch size is difficult to estimate from a single transect. In order to estimate patch dimensions more effectively, successional stages would need to be mapped on a two-dimensional station matrix.

### 6.4.5 Organism-Sediment Index

The OSI, a parameter that depicts overall benthic habitat quality, is described in *Sections 6.2* and *6.3.5*. The value of the index can range from +11 (highest habitat value) to -10 (negative habitat value). Values of the OSI below +6 tend to be associated with disturbed benthic habitats. VK 916 and associated far-field transects have OSI values ranging from +2 to +9. No negative OSI values were present (see below).

#### 6.4.5.1 Near-Field Stations

Near-field Transects NF-1 and NF-2 show a patchy distribution of OSI values ranging from +2 to +8 (**Figure 6.38**). The OSI frequency histograms for Transects NF-1 and NF-2 both show distinctive bimodal distributions (**Figure 6.39**). The +7 to +8 class contains the greatest number of stations, indicating that most of the site is representative of high-quality habitat. The bimodality shown in the histogram is caused by the successional stage assignment at each station and by the fact that physical and chemical disturbances are at a minimum. Stations with only Stage I seres present and with thin mean apparent RPD depths tend to yield the OSI value of +2. Stations with Stage I-III seres and deeper mean apparent RPD depths produce the major mode of +7, thereby causing the demonstrated bimodal distribution.

# VK916 NF

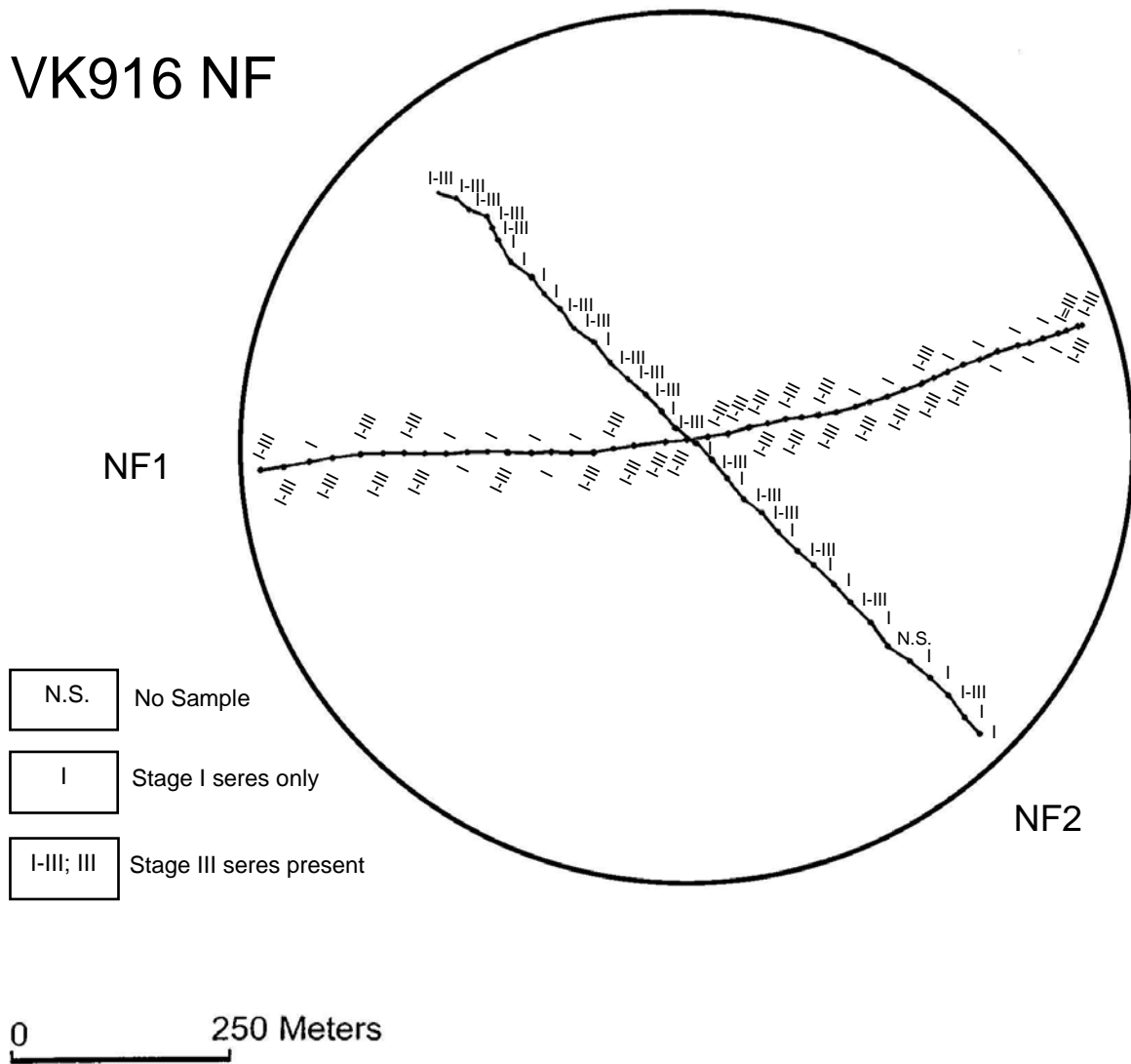


**Figure 6.34.** Mapped distribution of infaunal successional stages along Transects NF-1 and NF-2 at Viosca Knoll Block 916 during pre-drilling Cruise 1B (October-November 2000). The NF site radius is 500 m.

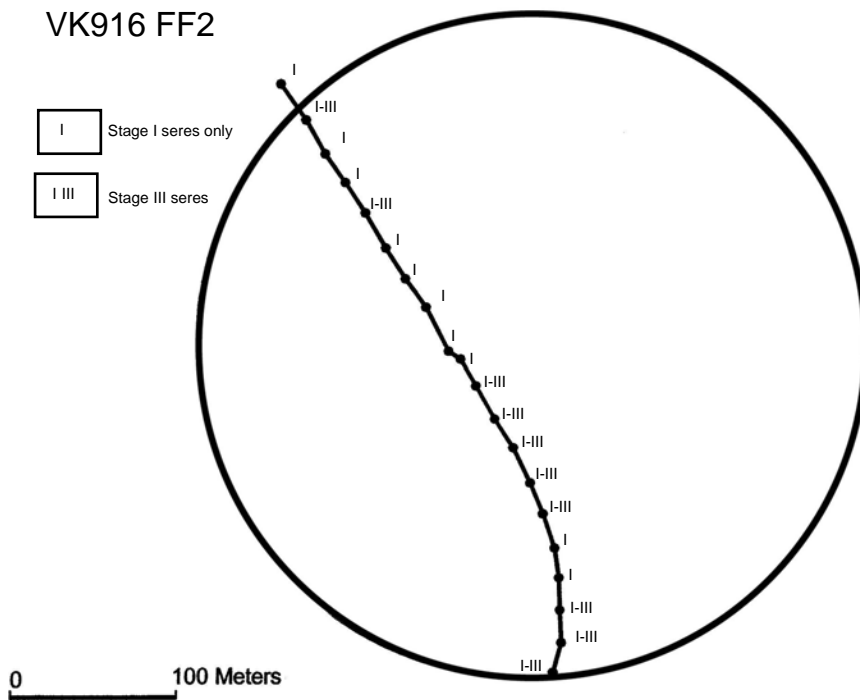


**Figure 6.35.** Mapped distribution of successional stages along Transect FF2 at Viosca Knoll Block 916 during pre-drilling Cruise 1B (October-November 2000). The FF site radius is 204 m.

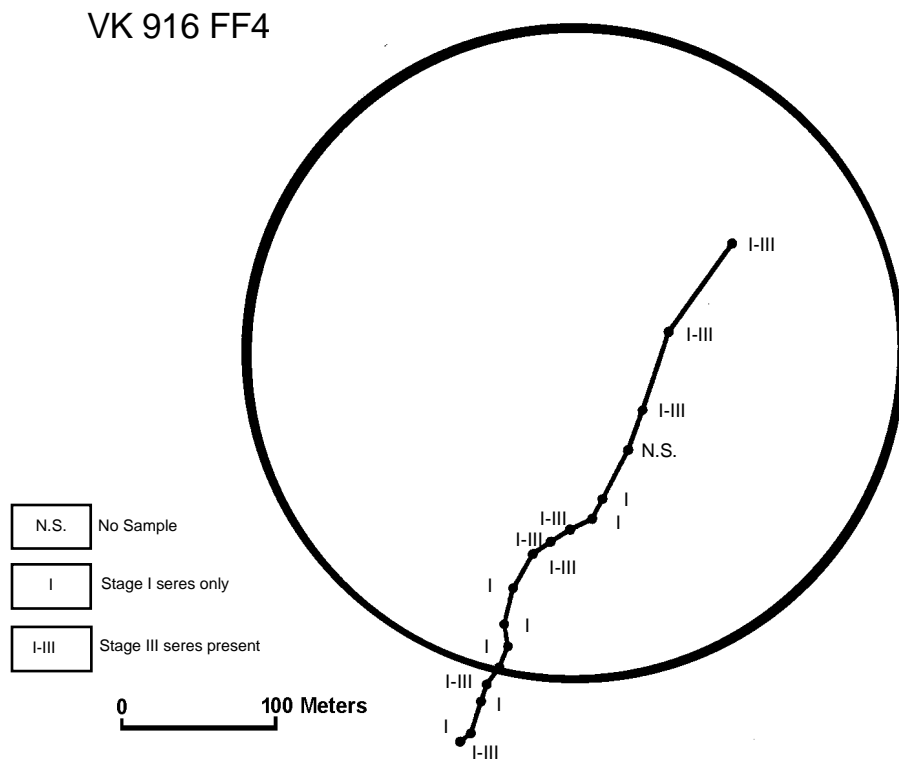


**Figure 6.36.** Mapped distribution of successional stages along Transect FF4 at Viosca Knoll Block 916 during pre-drilling Cruise 1B (October-November 2000). The FF site radius is 204 m.

## VK916 FF6

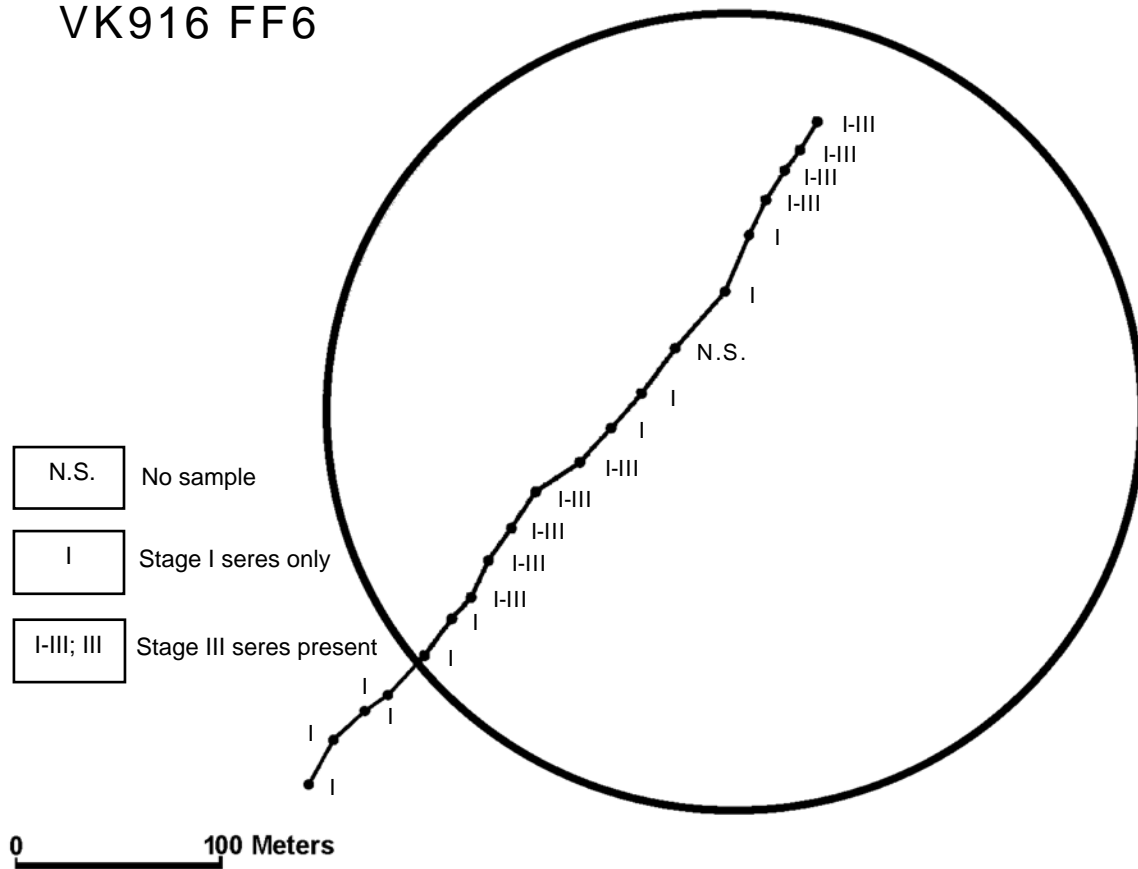


**Figure 6.37.** Mapped distribution of successional stages along Transect FF6 at Viosca Knoll Block 916 during pre-drilling Cruise 1B (October-November 2000). The FF site radius is 204 m.

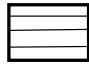
### 6.4.5.2 Far-Field Stations

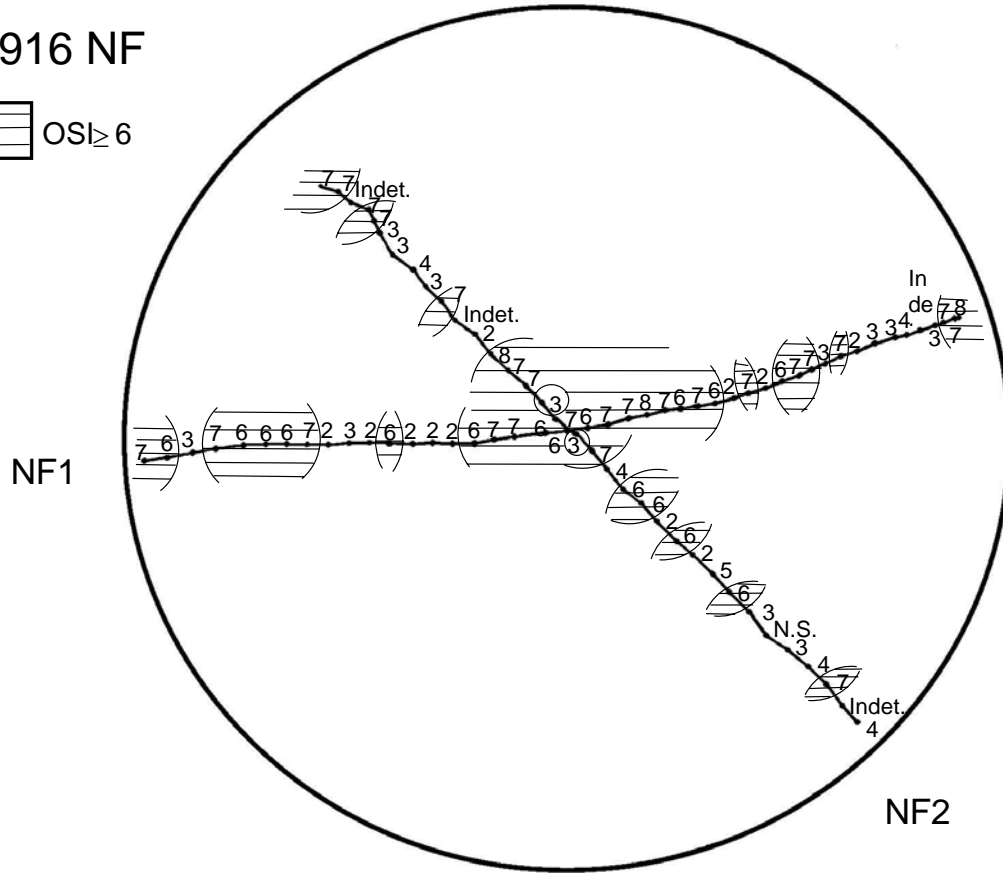
Far-field Transect FF2 also shows a patchy bimodal distribution of OSI values (**Figures 6.40** and **6.41**). The OSI frequency distribution for FF2 is comparable to that described for both near-field transects (**Figure 6.39**), with the major mode falling within the +7 to +8 class.

Organism-sediment indices at Transects FF4 and FF6 also have patchy (**Figures 6.42** and **6.43**) as well as bimodal distributions (**Figure 6.41**) but have most OSI values falling below +7.

Frequency histograms for the combined far-field OSI values compared to the combined near-field values (**Figure 6.44**) show that the near-field and far-field populations are similar, indicating that, before drilling commenced, the VK 916 site is comparable to the far-field reference transects in habitat quality as measured with the OSI parameter.

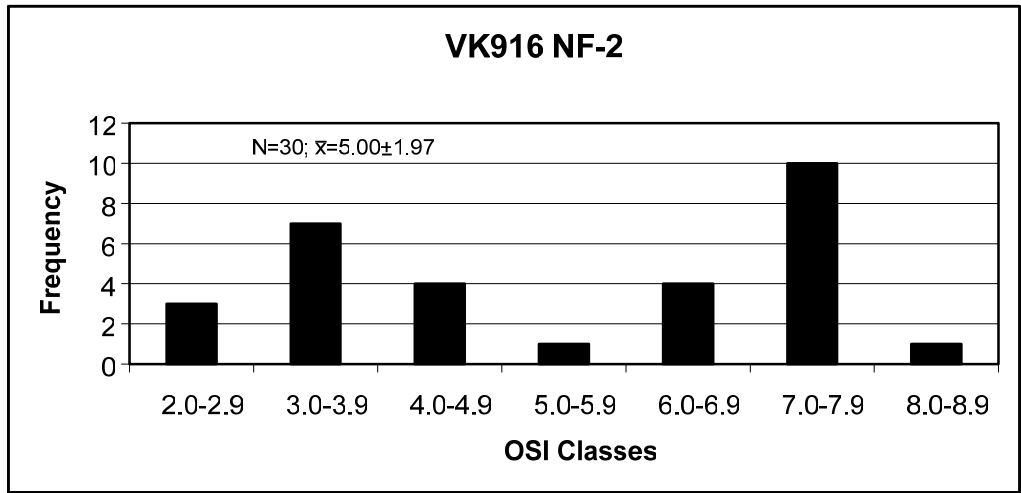
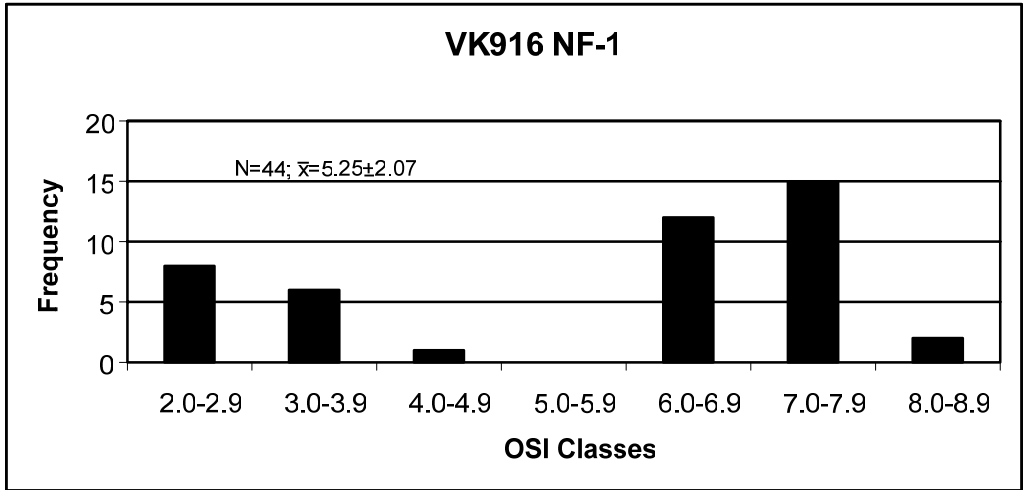
VK916 NF

 OSI ≥ 6



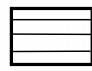
0 250 Meters

**Figure 6.38.** Mapped distribution of the Organism-Sediment Index (OSI) along the two near-field transects taken at Viosca Knoll Block 916 during pre-drilling Cruise 1B (October-November 2000). The NF site radius is 500 m.



**Figure 6.39.** Organism-Sediment Index (OSI) class-frequency distributions at two near-field transects in Viosca Knoll Block 916 during pre-drilling Cruise 1B (October-November 2000).

# VK916 FF2

 OSI ≥ 6

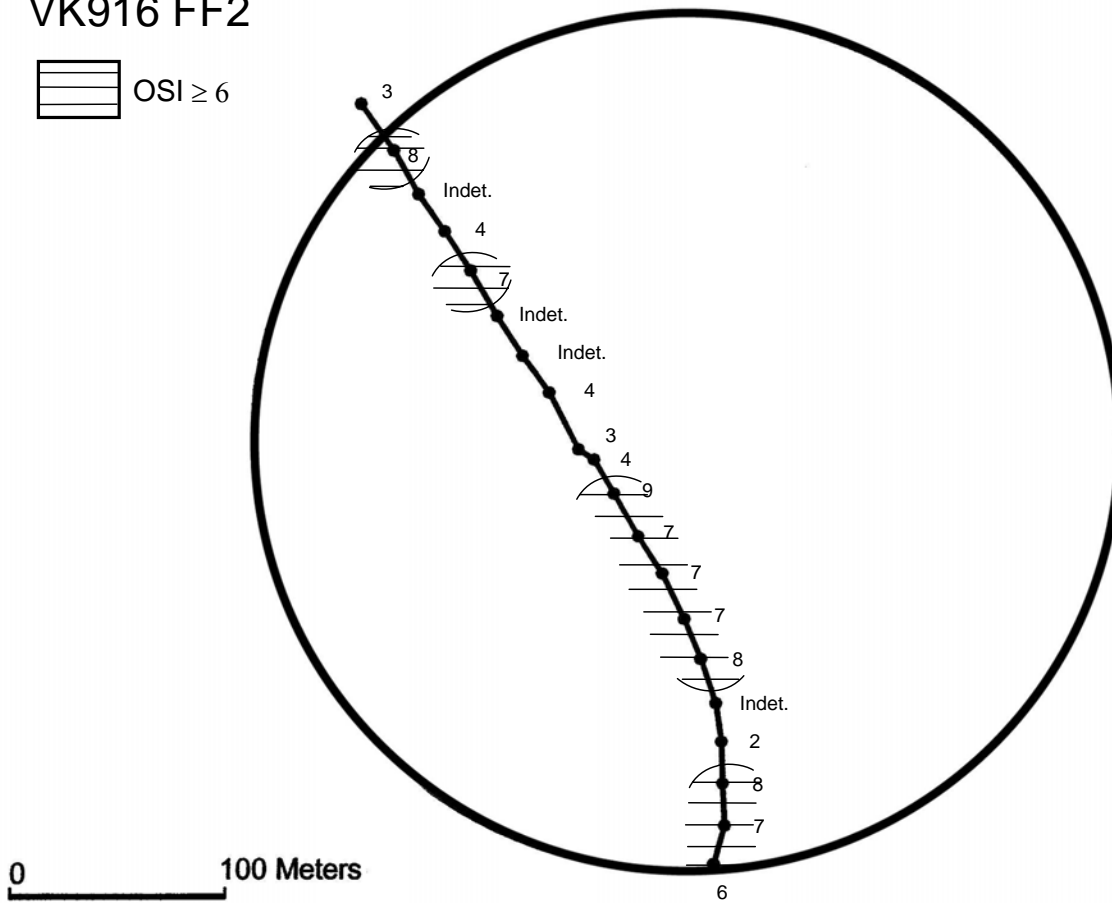


**Figure 6.40.** Mapped distribution of the Organism-Sediment Index (OSI) along Transect FF2 at Viosca Knoll Block 916 during pre-drilling Cruise 1B (October-November 2000). The FF site radius is 204 m.



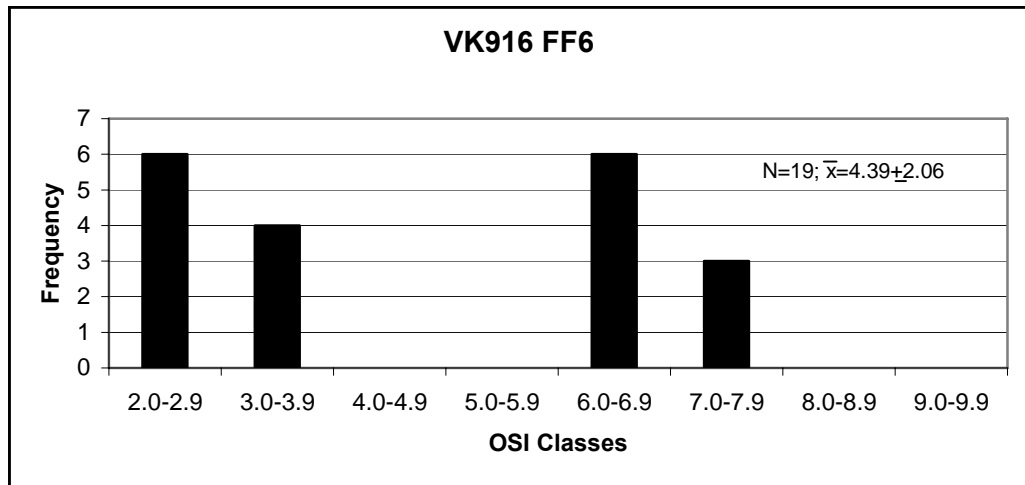
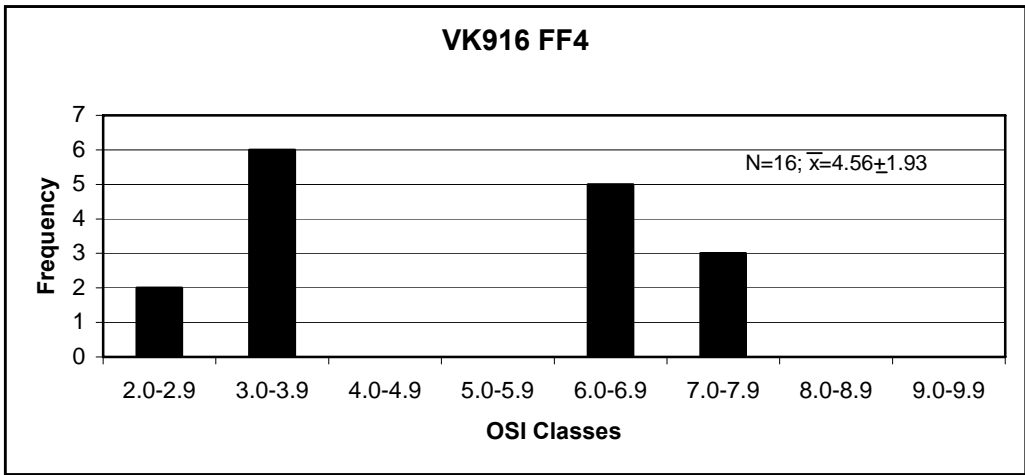
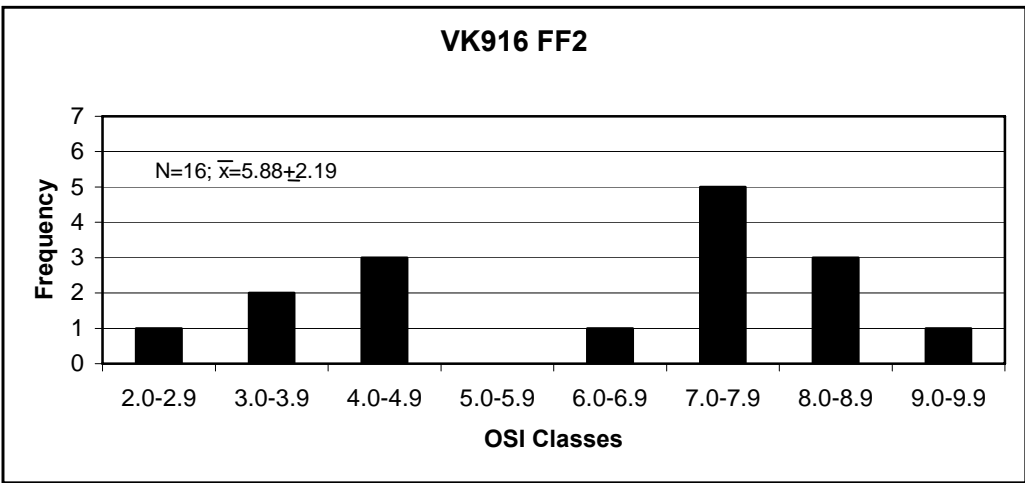


**Figure 6.41.** Organism-Sediment Index (OSI) class-frequency distributions at three far-field transects in Viosca Knoll Block 916 during pre-drilling Cruise 1B (October-November 2000).

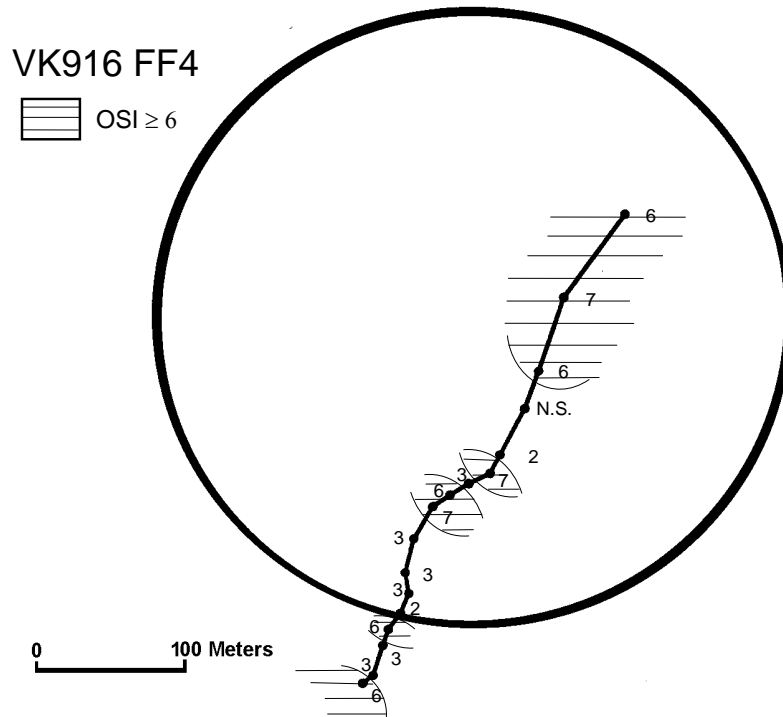


**Figure 6.42.** Mapped distribution of the Organism-Sediment Index (OSI) along Transect FF4 at Viosca Knoll Block 916 during pre-drilling Cruise 1B (October-November 2000). The FF site radius is 204 m.

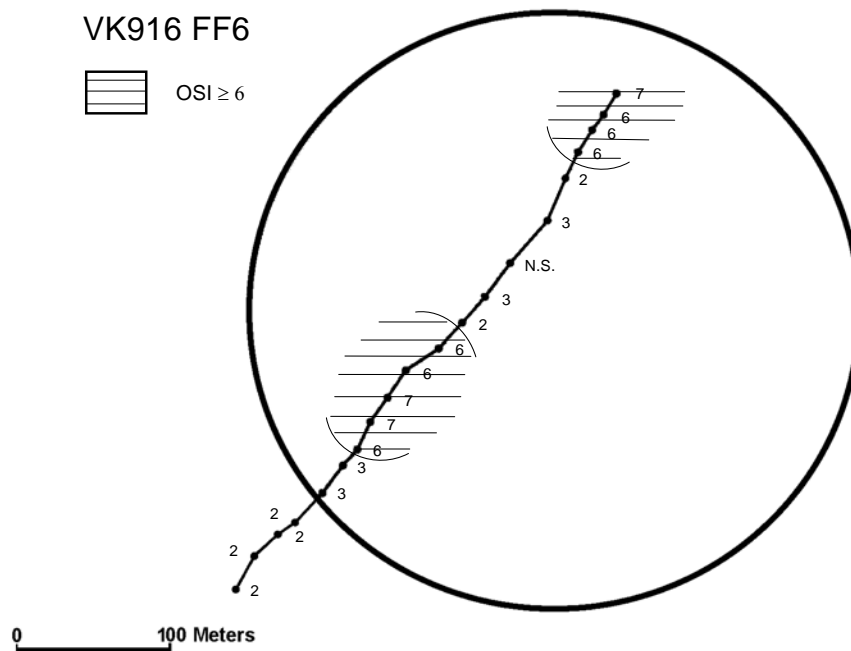


**Figure 6.43.** Mapped distribution of the Organism-Sediment Index (OSI) along Transect FF6 at Viosca Knoll Block 916 during pre-drilling Cruise 1B (October-November 2000). The FF site radius is 204 m.

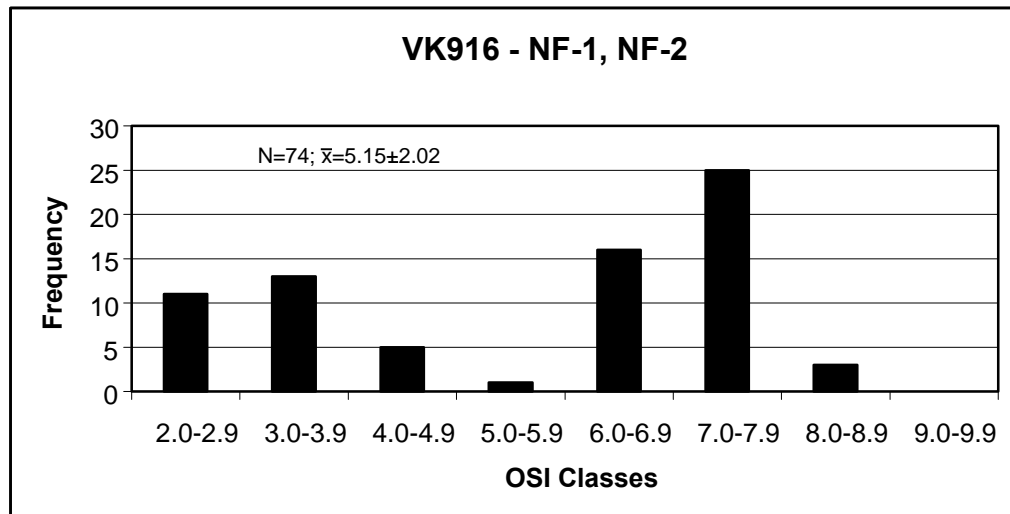
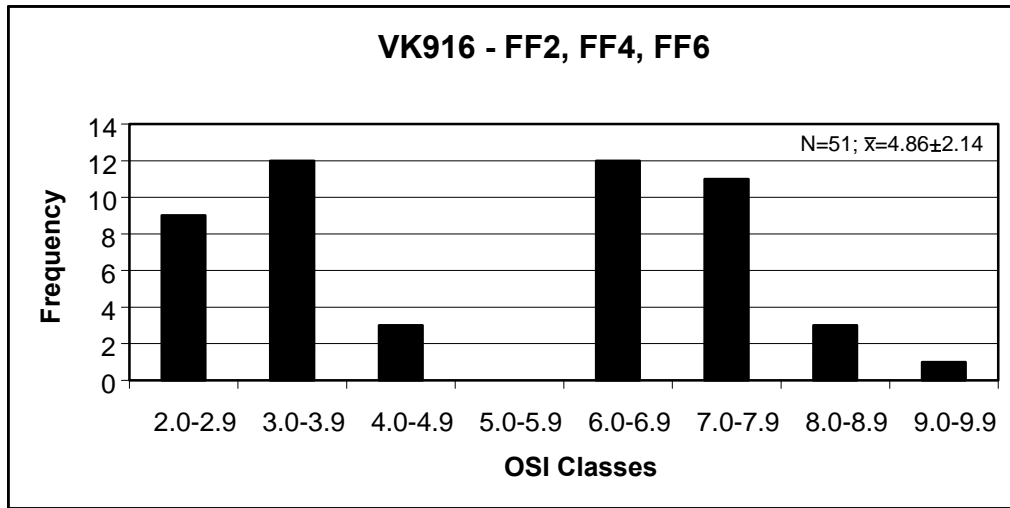


**Figure 6.44.** Organism-Sediment Index (OSI) class-frequency distributions at all near-field and far-field transects sampled at Viosca Knoll Block 916 during pre-drilling Cruise 1B (October-November 2000).

## 6.5 GARDEN BANKS BLOCK 516 – CRUISE 2B

### 6.5.1 Survey Design and Location

A second sediment profile image survey of GB 516 was conducted in mid-July 2001 (Cruise 2B) after the completion of additional drilling there (see *Chapter 3*). Three transects were sampled at the near-field site. In addition, images were collected along three control transects in the far-field. The relative locations of the near-field and far-field sites have been shown previously in **Figure 6.1**. Two images per station were acquired in this mapping survey designed to rapidly delineate spatial gradients in benthic habitat quality. The image showing deeper penetration of the camera, as long as the sediment-water interface was visible, was chosen for analysis.

### 6.5.1.1 Near-Field Stations

Three sampling transects (NF-1, NF-2, and NF-3) were located within the 1,000-m diameter circle defining the area of interest within Block 516 (**Figure 6.45**). Each transect consisted of 36 stations, and image data were successfully obtained at all stations except for one station on Transect NF-3. As spacing between stations is shortest at Transect NF-3, intermediate at Transect NF-1, and longest at Transect NF-2, there are differing scales of spatial resolution.

### 6.5.1.2 Far-Field Stations

Far-field stations, presumably representing ambient conditions, were imaged at three localities (Transects FF3, FF4, and FF5). The diameter for each circle of interest in the far-field was 408 m. Stations at Transect FF3 were located along two adjacent sub-parallel transects comprising 40 stations (**Figure 6.46**). Transect FF4 was a single transect consisting of 36 stations (**Figure 6.47**). No successful pictures were obtained from Station FF4.28 and so the sample size was reduced to  $n = 35$ . Transect FF5 was a single transect consisting of 36 stations, and images were obtained at all stations (**Figure 6.48**).

## 6.5.2 Sediment Fabric, Texture, Color, and Small-Scale Stratigraphy

As described in *Section 6.3.2*, sediment profile images may provide information about small-scale vertical gradients in the sediment structure that can be used, in conjunction with other SPI parameters, to infer sedimentation, geochemical, and biological processes.

### 6.5.2.1 Near-Field Stations

The bulk sediment texture at all stations on the three near-field transects is very fine-grained with silt and clay particles ( $>4 \phi$ ) comprising the majority of the sediment. However, the upper few millimeters of the sediment surface generally have a sandy texture, owing to the presence of sand-sized grain aggregates, as shown, for example, at Station NF-1.6B (*Plate 12*). These aggregates commonly are produced by meiofaunal burrowing as well as by pelletization of the sediment by the macrofauna. All of these sediments show a remarkable diversity of thinly bedded or laminated intervals within the images. Profile images show from 2 to 11 layers within the field of view (FOV), with most images showing between 4 and 7 layers. The layering is recognizable by differences in sediment color rather than from textural gradients. Red to brown oxidized intervals are layered within thin black to gray reduced sediments (*Plate 12*: NF-1.6B, 4 layers; *Plate 13A*: NF-3.27B, 6 layers; and *Plate 13B*: NF-2.35B, 7 layers).

Near-field Transects NF-1 and NF-2 show significant accumulations of black, presumably sulfidic sediment. Eleven contiguous stations along Transect NF-2 show this phenomenon as do 10 stations at the northern end of NF-1. At some stations, these black layers are present right up to the sediment-water interface. These black units are bounded above and/or below by light gray sediment (*Plates 14A and 14B*: NF-1.25B, 1.28B; *Plates 15A and 15B*: NF-2.17A, 2.18A; *Plates 16A and 16B*: NF-2.19A, 2.20A; and *Plate 17*: NF-2.25A). At other stations, the black stratigraphic unit, bounded by the light gray sediment, is located under (ambient?) reddish brown sediment (*Appendix E4, Plates 18A and 18B*: NF-1.19B, 1.12B). The genesis of the black and light gray layers is unknown but may be stratigraphy that is related to drilling muds. Chemical analysis of samples would be required to determine origins.

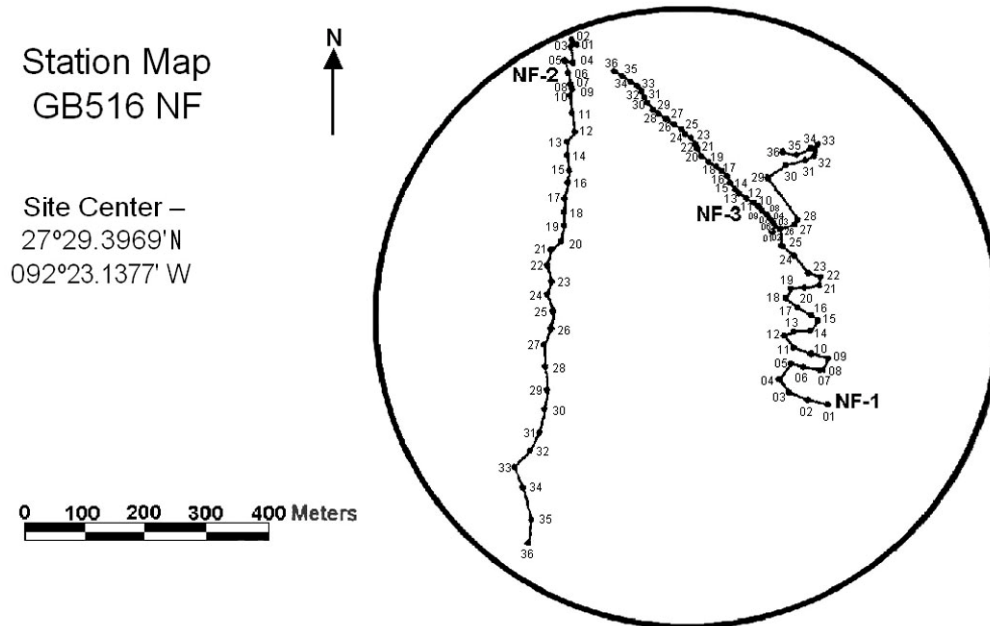


**Figure 6.45.** Garden Banks Block 516 near-field (NF) map showing transects and stations sampled during Cruise 2B (July 2001). The NF site radius is 500 m.

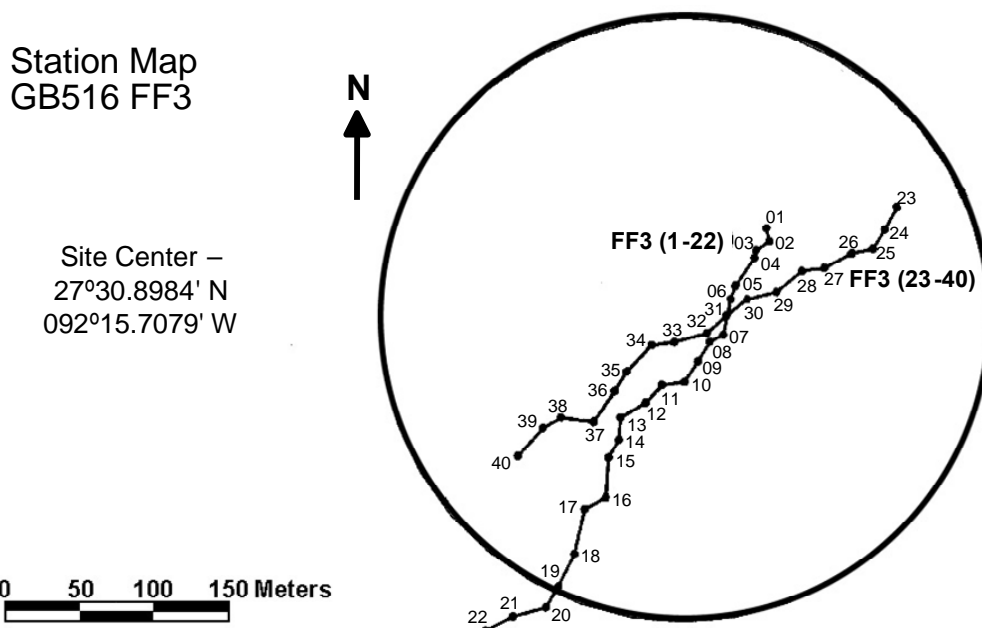


**Figure 6.46.** Garden Banks Block 516 Far-field 3 (FF3) station map, showing transects and stations sampled during Cruise 2B (July 2001). The FF site radius is 204 m.

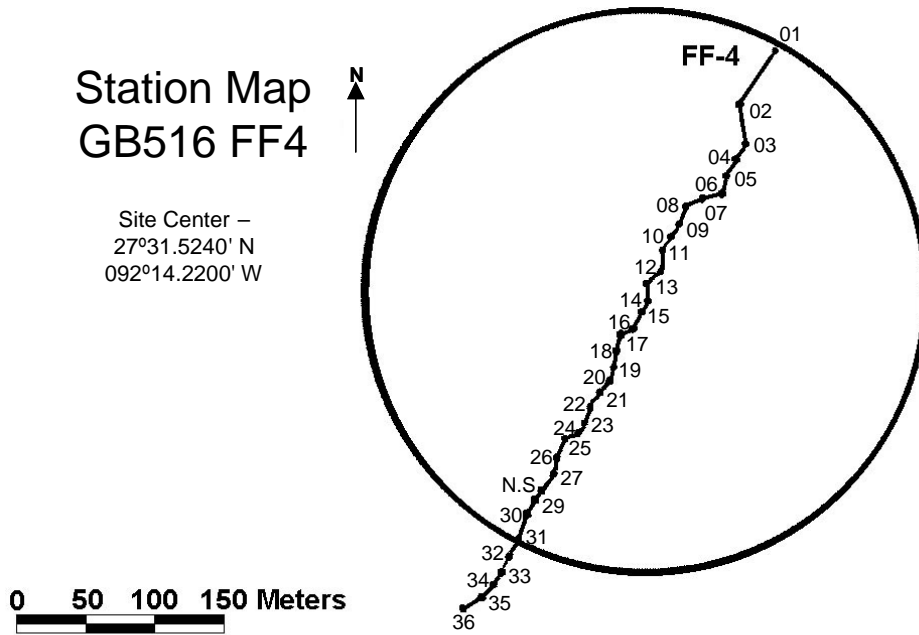


**Figure 6.47.** Garden Banks Block 516 Far-field 4 (FF4) station map, showing transects and stations sampled during Cruise 2B (July 2001). The FF site radius is 204 m.

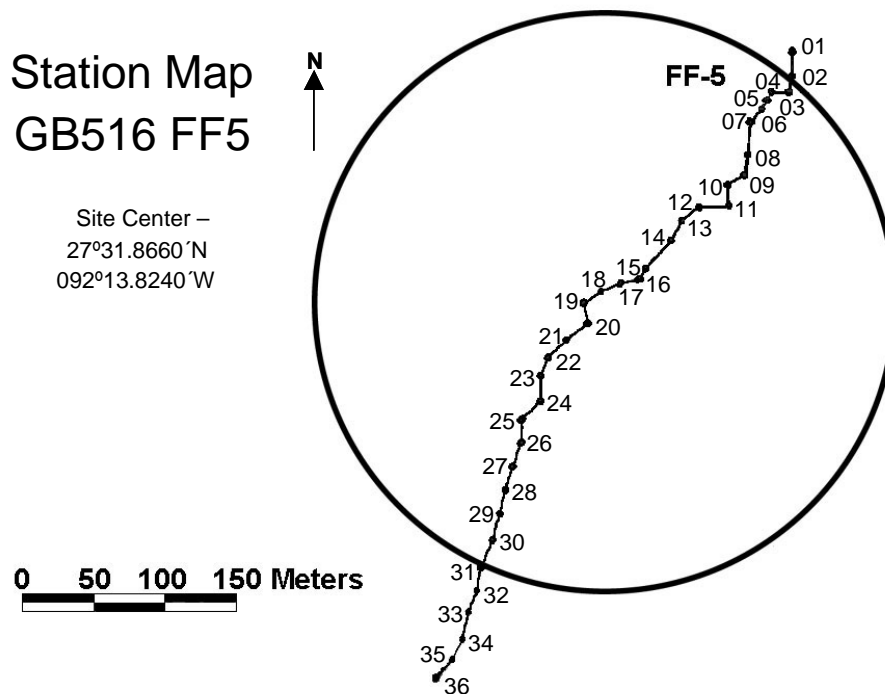


**Figure 6.48.** Garden Banks Block 516 Far-field 5 (FF5) station map, showing transects and stations sampled during Cruise 2B (July 2001). The FF site radius is 204 m.

### 6.5.2.2 Far-Field Stations

The bulk sediment texture of far-field stations consists of silt-clay sized particles (>4 phi) overlain by surficial pelletal sands. These sediments also show subsurface color layering but lack the dominance of gray to black reduced zones that are so common in the near-field stations (*Plates 14-18*). *Plate 19* (FF3-13B) shows a typical profile image of the ambient far-field seafloor. Tan to reddish brown sediments show many infaunal organisms, subsurface feeding voids, and homogeneously burrowed intervals. If layers are present at depth, they tend to be indistinct due to mixing by bioturbation.

### 6.5.3 Depth of the Apparent Redox Potential Discontinuity

The near-surface zone of intensive particle mixing and interstitial water exchange is recognized in SPI images by a difference in color between the mixed zone (light tan) and underlying sediment (dark red, gray, or black). The light tan to reddish brown color in the mixed zone is imparted by the oxidation of particulate iron coatings on sediment particle surfaces (ferric hydroxide) and the relative absence of reduced compounds such as hydrogen sulfide and/or metal sulfides. The zone of intensive mixing can be related to physical processes such as sediment resuspension or bed-load transport, but in most cases, mixing is related to bioturbation by resident infauna.

Vertical gradients in sediment color, as described above, are related to the oxidation state of the sediments. However, as we are inferring the oxidation state from sediment color, this parameter is called the “apparent” RPD. The true RPD (as measured with polarigraphic electrodes) is usually shallower than the apparent RPD. Once surface sediment is oxidized, the grain coatings may remain in an oxidized state even through the particles may be advected downward into deeper anoxic sediment. Oxidized particle coatings may be metastable for long periods of time. The long time constant of oxidized sediment contributes to the disparity between the apparent RPD and the true chemical RPD.

Deeply oxidized sediment (i.e., a deep apparent RPD) is usually indicative of a well developed and active bioturbating infauna in a benthic habitat overlain by oxygen-rich water (see *Plate 19* for an imaged example). Surface mixed zones that are shallow or absent usually are associated with ecologically stressed benthic systems, such as recently disturbed seabeds devoid of infauna or early successional stages, or bottom areas overlain by hypoxic or anoxic bottom water. Koenig et al. (2001) give further information about the imaging of oxygen distributions at benthic interfaces.

#### 6.5.3.1 Near-Field Stations

**Figure 6.49** shows the mapped distribution of mean apparent RPD depths for the three near-field transects. All transect stations have mean apparent RPD depths less than 0.5 cm thick, with the exception of Transect NF-3, Station NF-3.6. A cluster of contiguous stations (n = 10) on Transect NF-1 either lack an apparent RPD (zero thickness) or possess an apparent RPD that is anomalously thin relative to other stations on the transect. Black reducing sediments dominate the surface stratigraphy at these stations. Similarly, Transect NF-2 has a cluster of 11 stations in the middle of the transect that are devoid of an apparent RPD or have anomalously thin oxidized surface layers and are dominated by black surface sediment (*Plates 14-18*). For all near-field stations where RPD could be determined (n = 106), the mean apparent RPD was 0.18 cm.

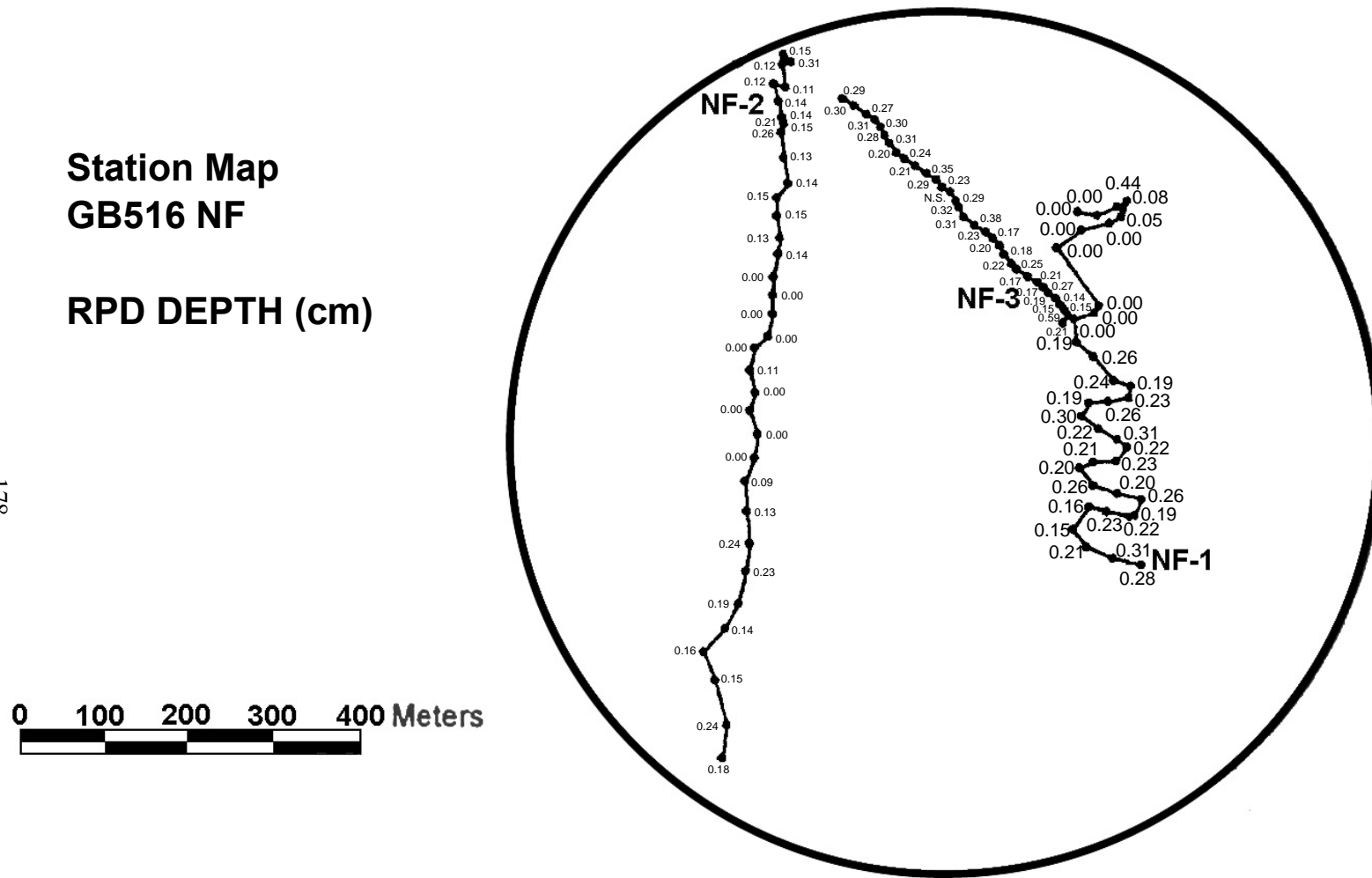


**Figure 6.49.** Mapped distribution of apparent redox potential discontinuity (RPD) depth, in centimeters, along the three near-field transects taken at Garden Banks Block 516 during Cruise 2B (July 2001). The NF site radius is 500 m.



The mapped patterns are reflected in the bimodal RPD-frequency distributions for Transects NF-1 and NF-2 (**Figure 6.50**) reflecting oxygen stressed stations versus normally aerated sediments. Near-field Transect NF-3 has a more normally distributed frequency distribution, as all stations had measurable apparent RPD depths (**Figure 6.50**).

#### 6.5.3.2 Far-Field Stations

**Figures 6.51, 6.52, and 6.53** show the mapped distributions of mean apparent RPD values for Transects FF3, FF4, and FF5, respectively. The two sub-parallel transects at FF3 show values similar to those mapped at near-field Transect NF-3, and both have the same population mean (0.25 cm). No values of 0.50 cm or greater were measured along Transect FF3, and the frequency distribution approximates a normal distribution (**Figure 6.54**).

Far-field Transect FF4 has two stations with mean apparent RPD depths >0.50 cm (Stations FF4.33 and FF4.35). Both stations are located at the extreme southwest end of the transect (**Figure 6.52**). The resulting RPD-frequency distribution is shifted toward deeper RPD depths relative to Transect FF3, with a mean of 0.29 cm (**Figure 6.54**). Transect FF5 has 6 stations with mean RPD depths equal to or greater than 0.50 cm, and these stations are distributed along the length of the entire transect (**Figure 6.53**). Transect FF5 had the highest mean apparent RPD depth (0.38 cm) (**Figure 6.54**). For all far-field stations where RPD depths could be determined (n = 110), the mean apparent RPD depth was 0.30 cm.

#### 6.5.4 Infaunal Successional Stage

Infaunal successional stage designations are described in *Sections 6.2 and 6.3.4*.

We identified three kinds of successional bottom types in images collected during Cruise 2B at GB 516:

1. Bottom sediments that are retrograde areas where there are apparently no macrofauna present (no Stage I tubes visible at the sediment surface and no subsurface Stage III feeding voids observed). These heavily impacted stations are called “azoic” (see *Plates 14-18*).
2. Bottom sediments that exhibit only Stage I pioneers (Stage I seres).
3. Bottom sediments that show evidence of subsurface feeding voids (with, or without Stage I species at the surface). These are mapped as Stage I-III or Stage III seres.

The three-stage sequence outlined above, when mapped along a spatial (or temporal) gradient, is used to identify zones of impact and benthic habitat quality. The interplay between degrees and spatial scales of disturbance and succession is discussed further by Zajac (2001).

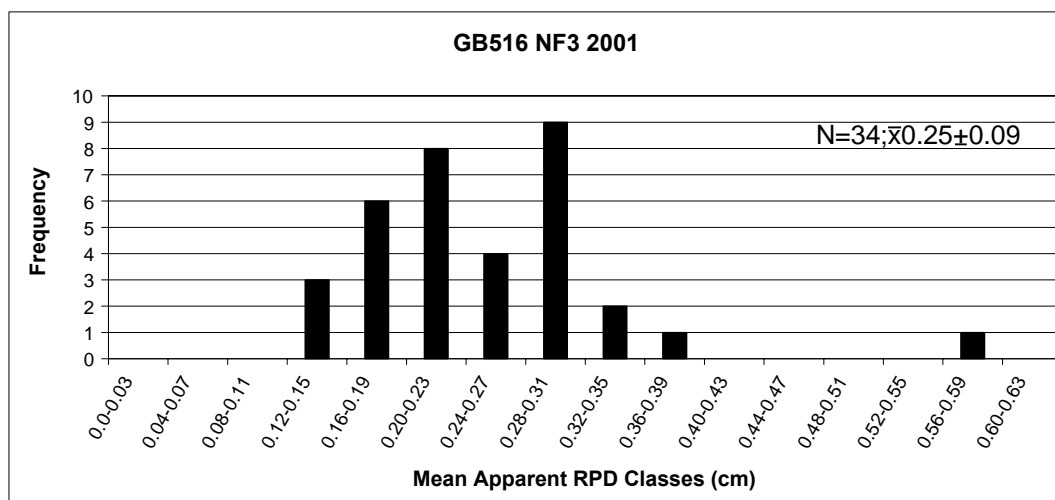
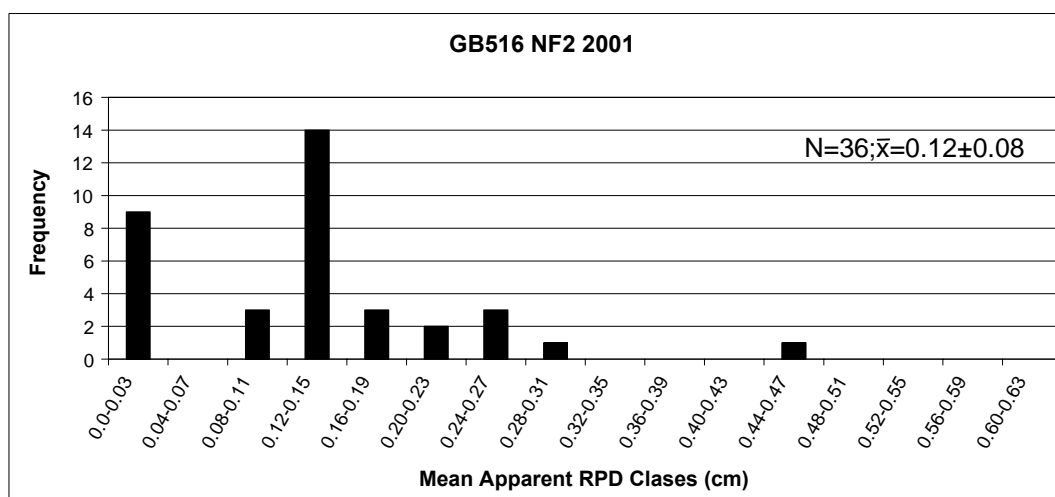
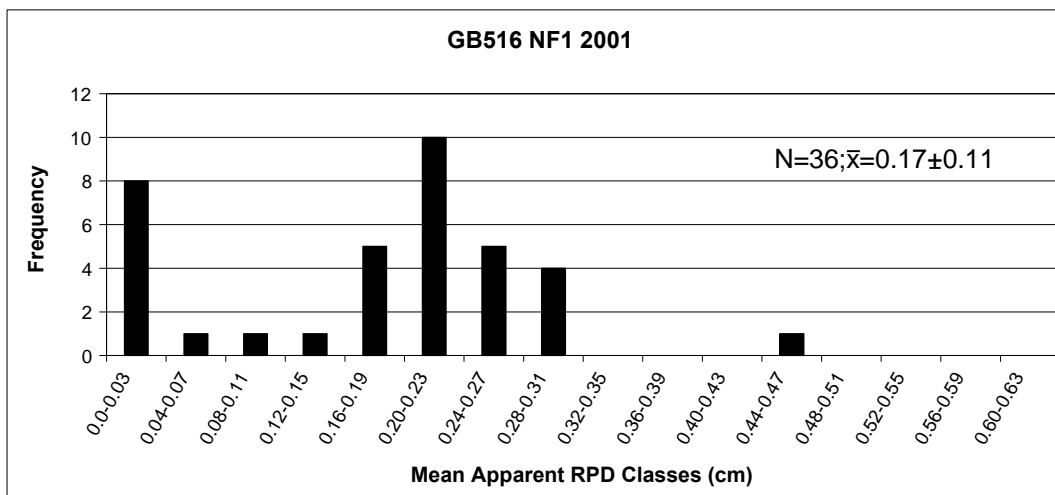


**Figure 6.50.** Redox potential discontinuity (RPD) depth-frequency distributions at three near-field transects sampled at Garden Banks Block 516 during Cruise 2B (July 2001).

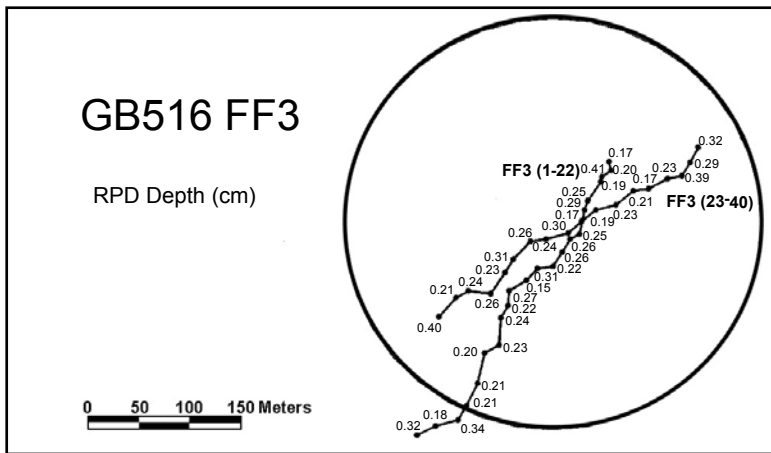


**Figure 6.51.** Mapped distribution of apparent redox potential discontinuity (RPD) depth, in centimeters, along the two transects surveyed at Far-field 3 (FF3) during Cruise 2B (July 2001). The FF site radius is 204 m.

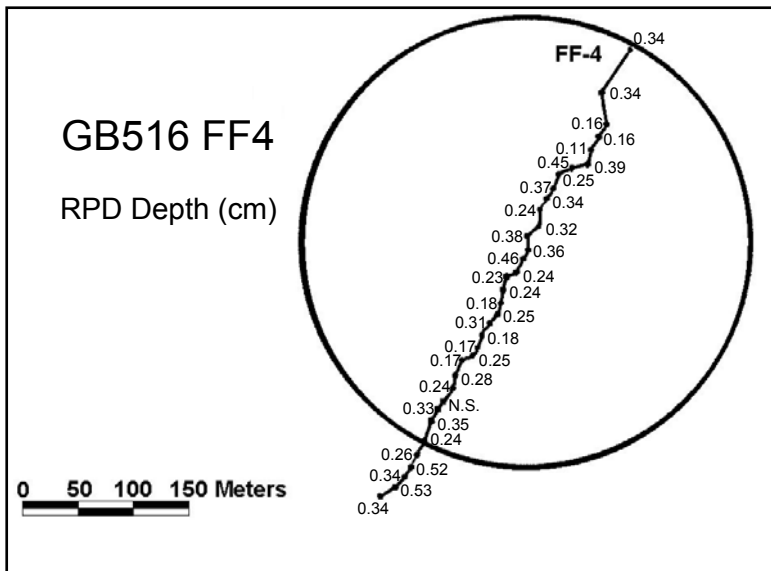


**Figure 6.52.** Mapped distribution of apparent redox potential discontinuity (RPD) depth, in centimeters, along Transect FF4 at Garden Banks Block 516 during Cruise 2B (July 2001). The FF site radius is 204 m.

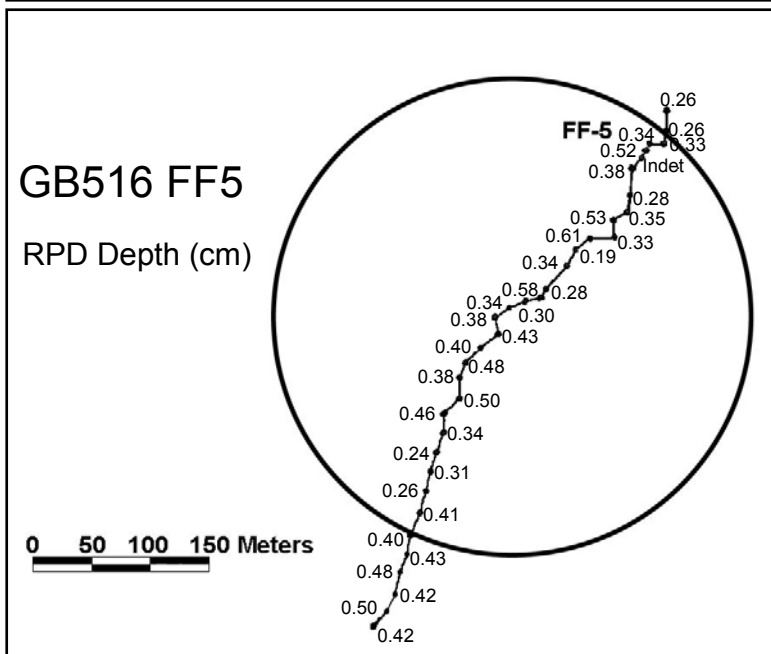


**Figure 6.53.** Mapped distribution of apparent redox potential discontinuity (RPD) depth, in centimeters, along Transect FF5 at Garden Banks Block 516 during Cruise 2B (July 2001). The FF radius is 204 m.

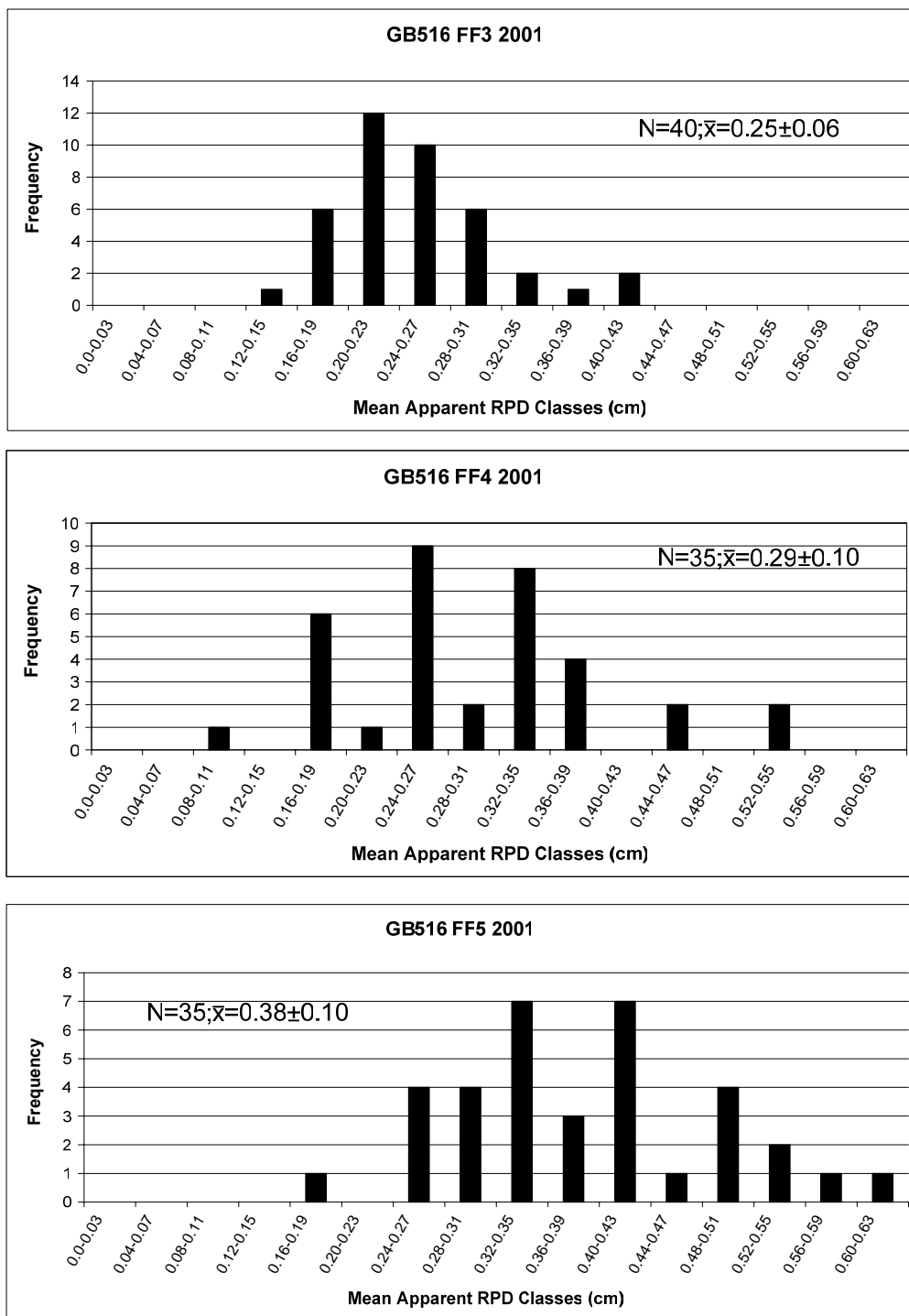


**Figure 6.54.** Redox potential discontinuity (RPD) depth-frequency distributions at three far-field transects sampled at Garden Banks Block 516 during Cruise 2B (July 2001).

#### 6.5.4.1 Near-Field Stations

Transect NF-1 shows a patchy distribution of Stage I and Stage I-III seres over the southern two thirds of the transect (**Figure 6.55**). The northern end of the transect (Stations NF-1.27 through 1.36) consists of five Stage I and four azoic stations. This is the same end of the transect that showed the accumulation of sulfidic black sediment and associated thin to zero thickness apparent RPDs. The successional status at the northern end of this transect is poor. Near-field Transect NF-1 has only 33% of the stations in a high-order successional stage (I-III).

Transect NF-2 similarly has a cluster of mid-transect stations ( $n = 8$ ) that apparently lack macrofauna and are mapped as being azoic. These stations include those with accumulations of black sulfidic sediment and thin to zero RPD depths (*Plates 15-17*). Of the seven southernmost stations on Transect NF-2, six of seven stations are dominated by Stage I seres (**Figure 6.55**). Only 34% of NF-2 stations are in a high order stage (I-III).

Transect NF-3 is a patchy mosaic of Stage I and Stage I-III seres. Interestingly, a section of Transect NF-3 that is located adjacent to the degraded portion of Transect NF-1 (Stations NF-3.01 through about 3.14), does not appear to be dominated by Stage I or azoic seres (**Figure 6.55**). This suggests that the factors that have had a negative impact on the benthic infauna at the northern end of Transect NF-1 have not adversely affected nearby stations on Transect NF-3. Half of Transect NF-3 stations are in the highest successional status (I-III).

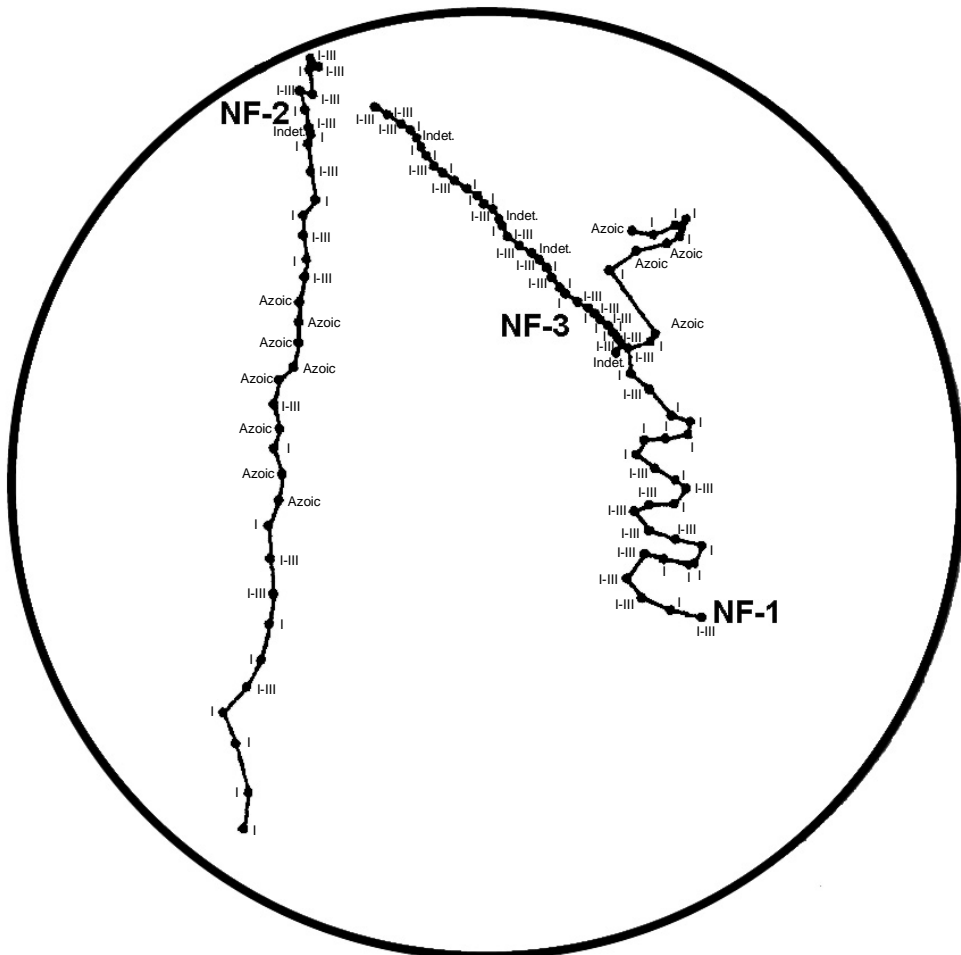
#### 6.5.4.2 Far-Field Stations

Both transects at FF3 show over 60% of the stations in a Stage I-III status. No clearly defined successional gradients are apparent from the mapped distributions (**Figure 6.56**). Transect FF4 consists of a patchy mosaic of Stage I and Stage I-III over the length of the transect, with no clear large-scale gradients in successional status (**Figure 6.57**). Only 42% of the stations are represented by the highest successional seres (I-III). Similarly, Transect FF5 consists of a patchy mosaic of seres with no clear successional gradients and with 61% of the stations populated by Stage I-III seres (**Figure 6.58**).

Overall, one can rank and compare the successional status of the near-field and far-field transects by the percentage of the stations that show the highest successional status (i.e., presence of Stage III seres). The lowest percentage of Stage III seres is found at Transects NF-1 (33%) and NF-2 (34%). Transect NF-3 had 50% of the stations showing Stage III seres. Far-field Transects FF3 and FF5 had more than 60% of the sampled stations showing Stage III seres (64% and 61%, respectively). Transect FF4 had 42% of the stations showing Stage III infauna.

# GB 516 NF

- Azoic No macrofauna present
- I Stage I seres only
- I-III; III Stage III seres present



184

**Figure 6.55.** Mapped distribution of infaunal successional stages along all three near-field transects at Garden Banks Block 516 during Cruise 2B (July 2001). The NF site radius is 500 m.

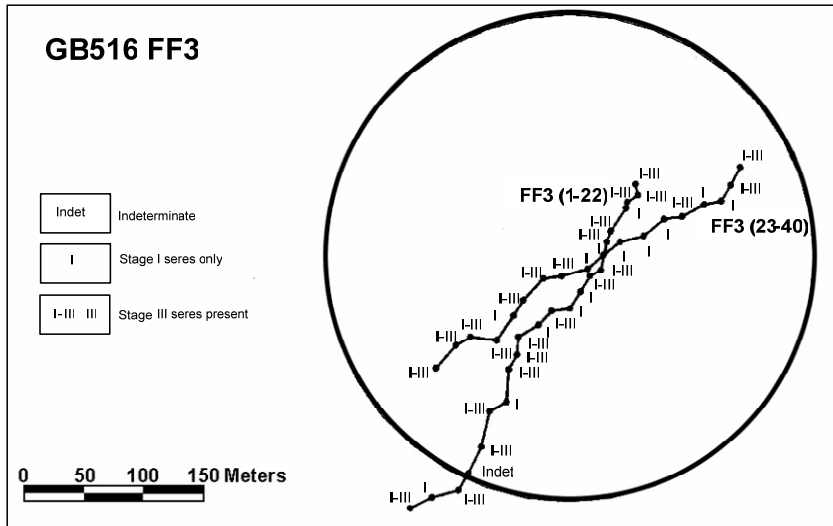


**Figure 6.56.** Mapped distribution of infaunal successional stages along the two transects at Garden Banks Block 516, Far-field 3 (FF3) during Cruise 2B (July 2001).

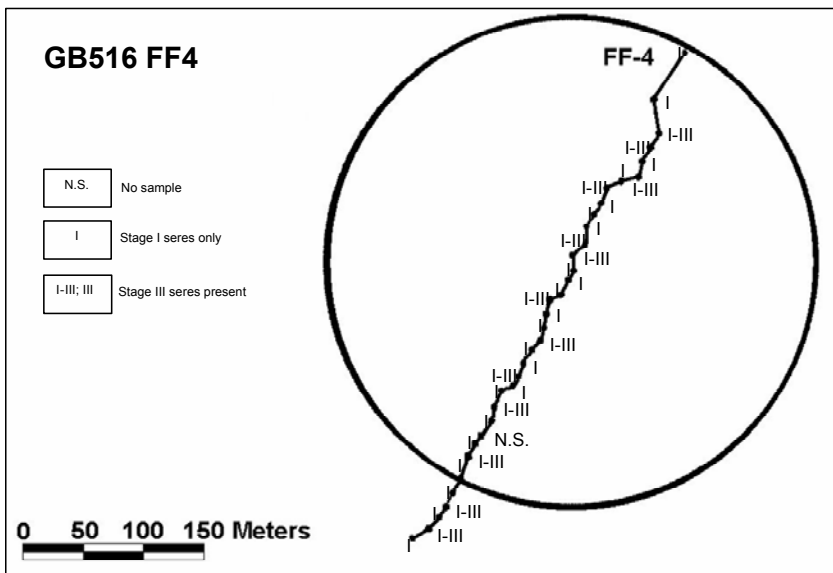


**Figure 6.57.** Mapped distribution of infaunal successional stages along Transect FF4 at Garden Banks Block 516 during Cruise 2B (July 2001). The FF site radius is 204 m.

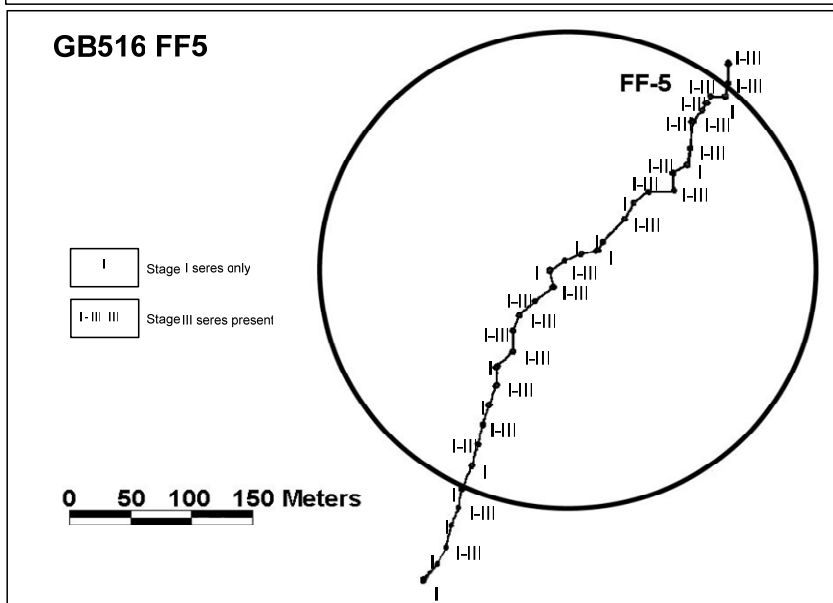


**Figure 6.58.** Mapped distribution of infaunal successional stages along Transect FF5 at Garden Banks Block 516 during Cruise 2B (July 2001). The FF site radius is 204 m.

### 6.5.5 Organism-Sediment Index

The OSI is described in *Sections 6.2 and 6.3.5*. The value of the index can range from +11 (highest habitat value) to -10 (worst habitat value). Values of the OSI below +6 tend to be associated with disturbed benthic habitats. Disturbance need not be related to anthropogenic activity. For example, disturbance may be naturally induced, such as bottom excavations by foraging by predators (especially large fish such as skates and rays), or natural hypoxia, brine, or hydrocarbon seeps.

Negative OSI values are associated with highly disturbed benthic habitats such as impacts due to dredging and disposal, chemical contamination or hypoxic/brine water. The GB 516 Cruise 2B data set includes values ranging from -8 to +6, thus encompassing stations representing a wide range of habitat quality.

#### 6.5.5.1 Near-Field Stations

The stations with degraded habitat as indicated by low OSI values at GB 516 during Cruise 2B were located at the northernmost end of Transect NF-1 (Stations NF-1.27 through 1.32 and NF-1.34 through 1.36) and the mid-region of Transect NF-2 (Stations NF-2.17 through 2.21 and NF-2.23 through 2.26) (**Figure 6.59**). The low OSIs at these stations are related to the presence of black sulfidic sediment, thin (or zero) apparent RPDs and their azoic status. No methanogenic sediments were observed in this survey (at least no methane gas bubbles were seen in the profile photos). Transect NF-3 had no negative OSI values.

The OSI frequency distribution (**Figure 6.60**) for stations on all near-field stations combined shows a polymodal distribution. The negative values form clusters around -8.0, and -4.0 to -2.0, and correspond to highly impacted stations. The highest OSI values, representing the stations with the best habitats, form a modality at +6.0 to 6.9. The major mode is located at +2.0-2.9 and represents an intermediate class of impacted stations.

#### 6.5.5.2 Far-Field Stations

**Figure 6.61** shows the spatial distribution of OSI values over the FF3 transects. No apparent spatial trends in OSI values are seen, and no negative values are present. Most values (64%) fall within the 6.0 to 6.9-frequency class (**Figure 6.62**). Stations with OSI values of +6 or more are considered to be minimally impacted relative to stations with lower OSI values.

Transect FF4 has no apparent spatial trends in OSI values, and no negative values are present (**Figure 6.63**). The dominant OSI frequency falls within the 2.0-2.9 class (**Figure 6.62**). Only 37% of the values are within the 6.0 to 6.9-frequency class.

Sixty-six percent of stations on Transect FF5 have OSI values within the 6.0 to 6.9-frequency class (**Figures 6.62 and 6.64**). These higher values are interspersed with stations having OSI values within the 2.0 to 2.9 class.



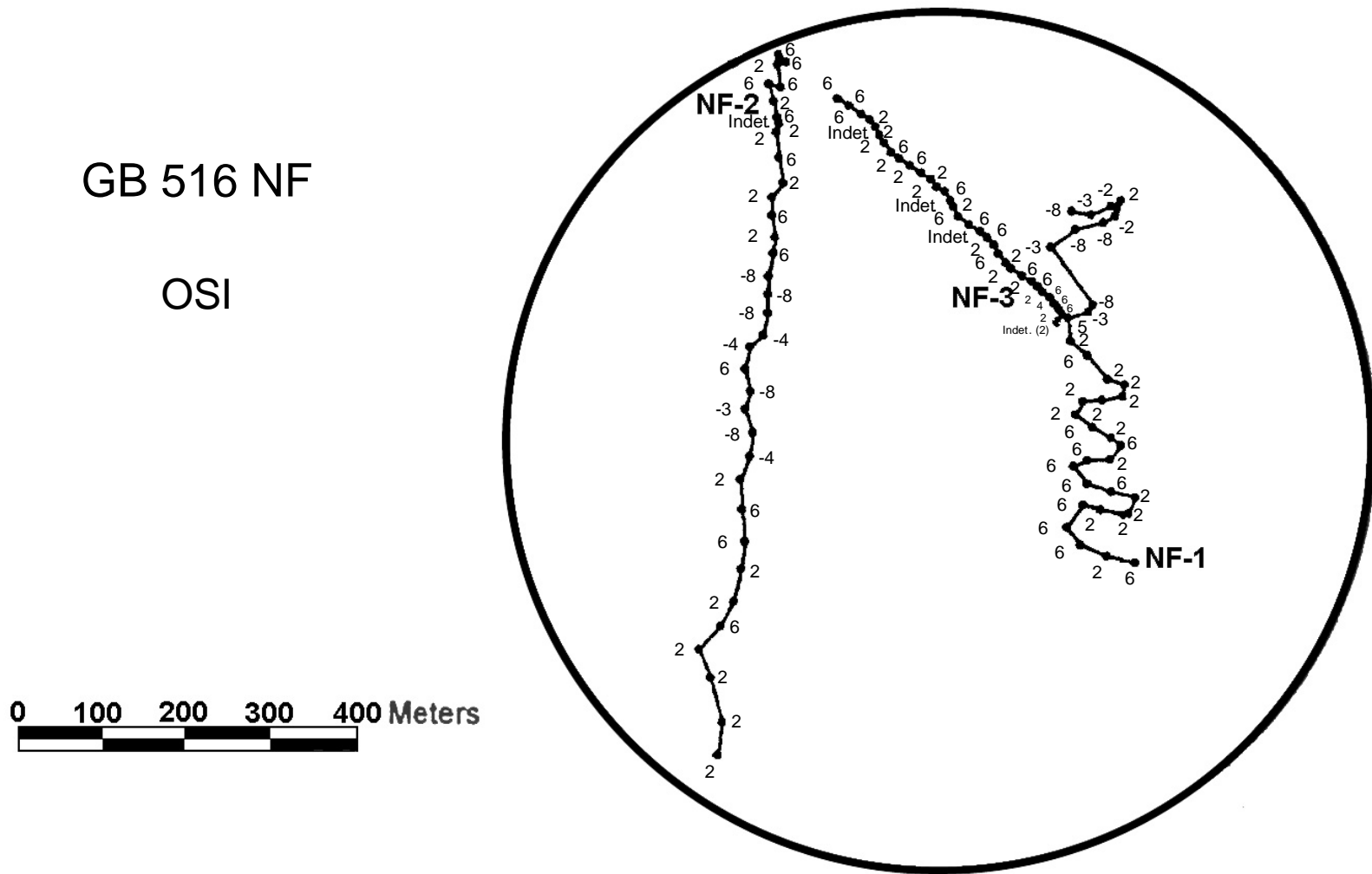


**Figure 6.59.** Mapped distribution of the Organism-Sediment Index (OSI) along all three near-field transects at Garden Banks Block 516 during Cruise 2B (July 2001). The NF site radius is 500 m.

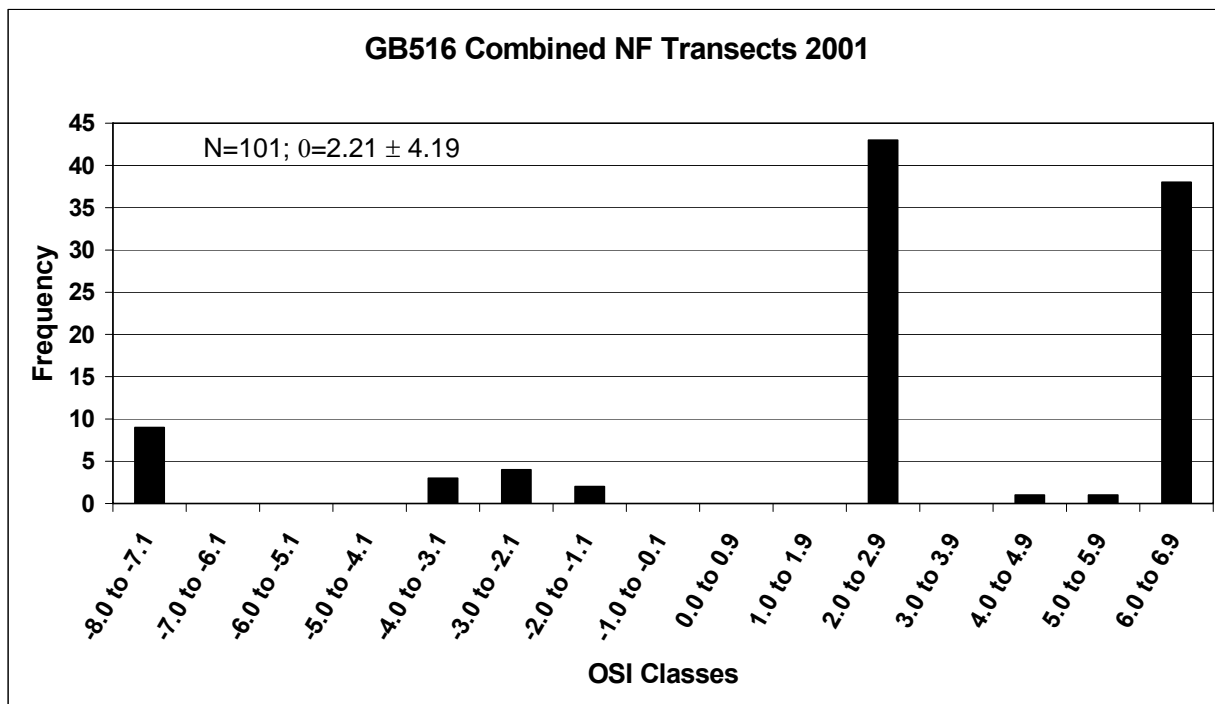


**Figure 6.60.** Organism-Sediment Index (OSI) class-frequency distribution for all stations belonging to all three near-field transects surveyed at Garden Banks Block 516 during Cruise 2B (July 2001).

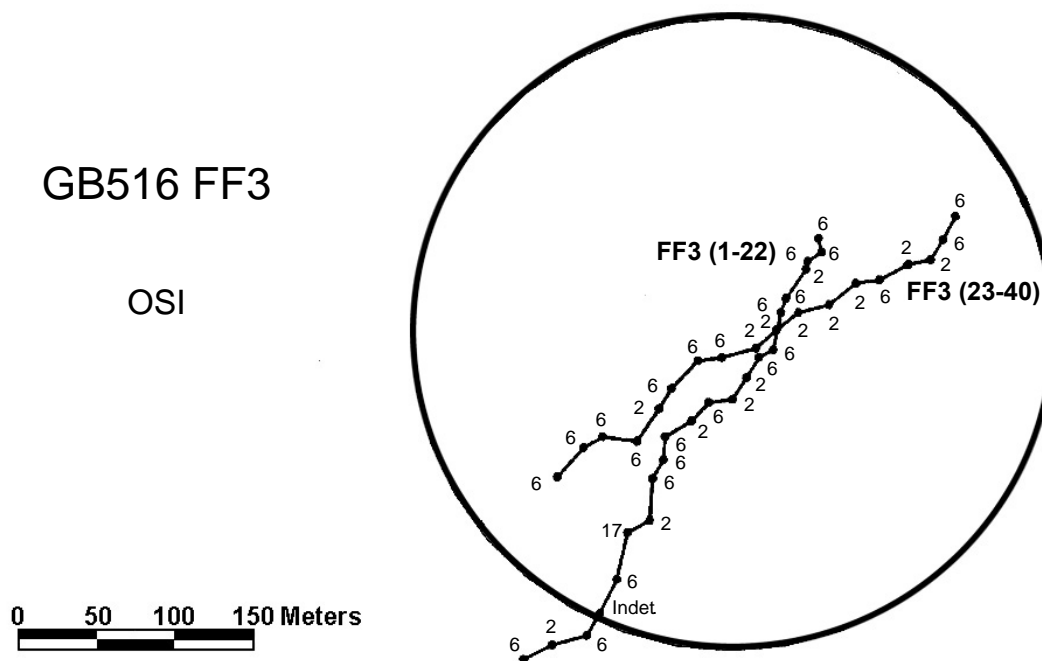


**Figure 6.61.** Mapped distribution of the Organism-Sediment Index (OSI) along far-field transects at FF3 at Garden Banks Block 516 during Cruise 2B (July 2001). The FF site radius is 204 m.

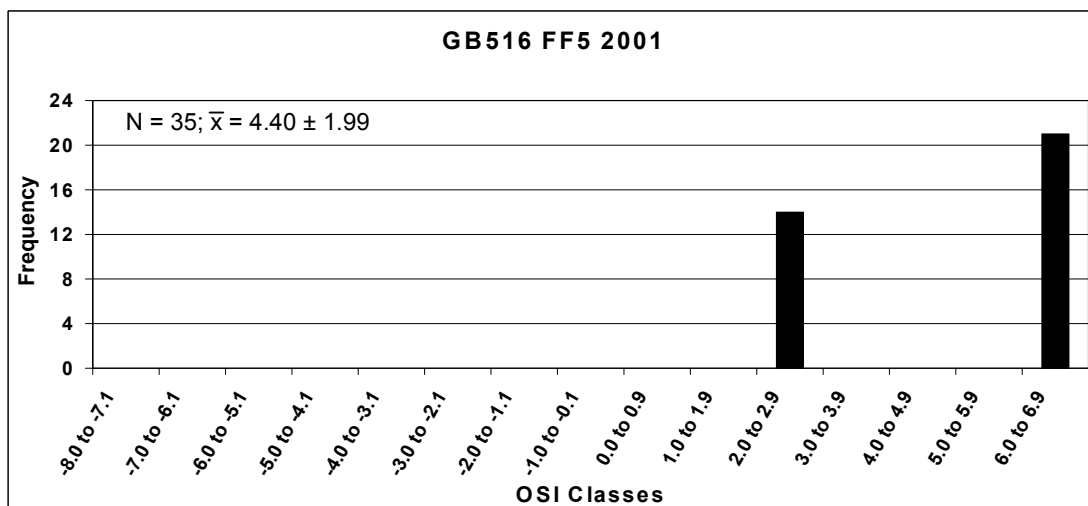
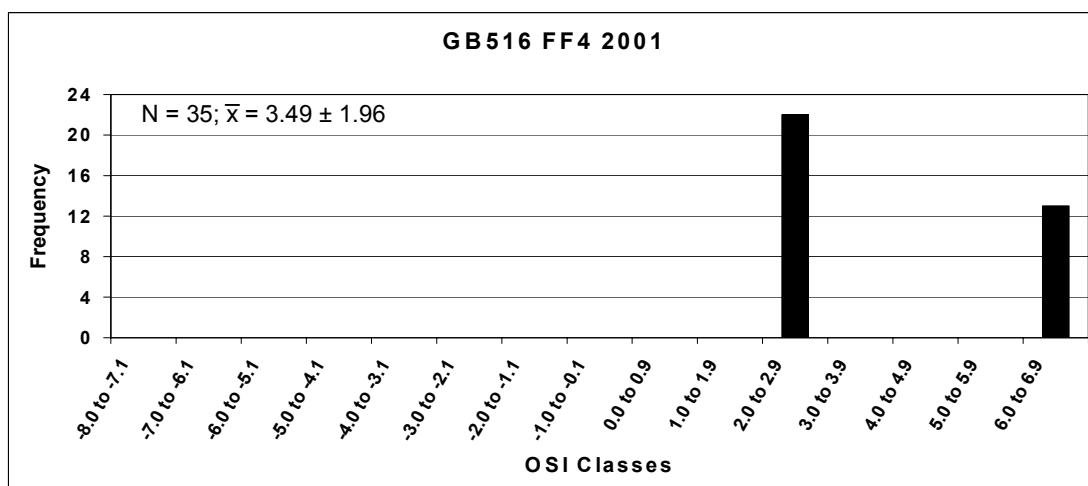
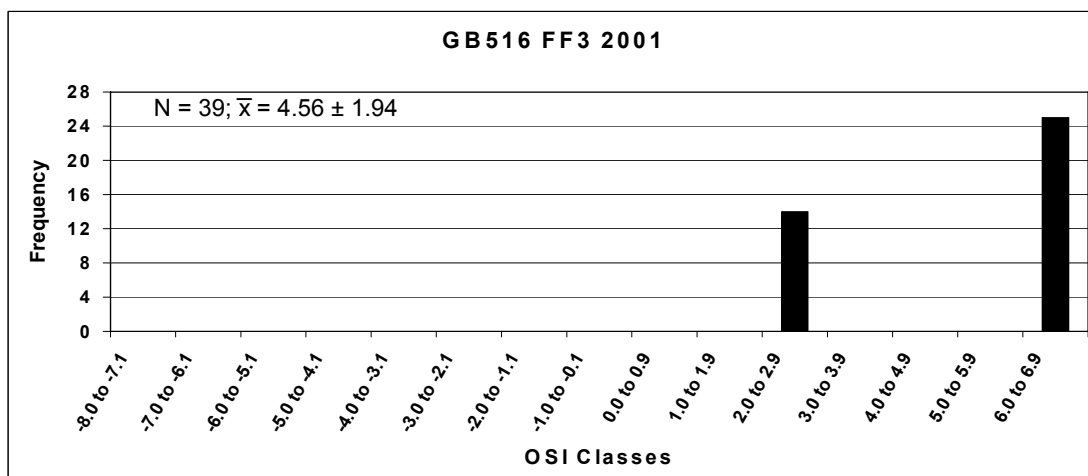


**Figure 6.62.** Organism-Sediment Index (OSI) frequency distributions at the three far-field transects at Garden Banks Block 516 (GB516) during Cruise 2B (July 2001).

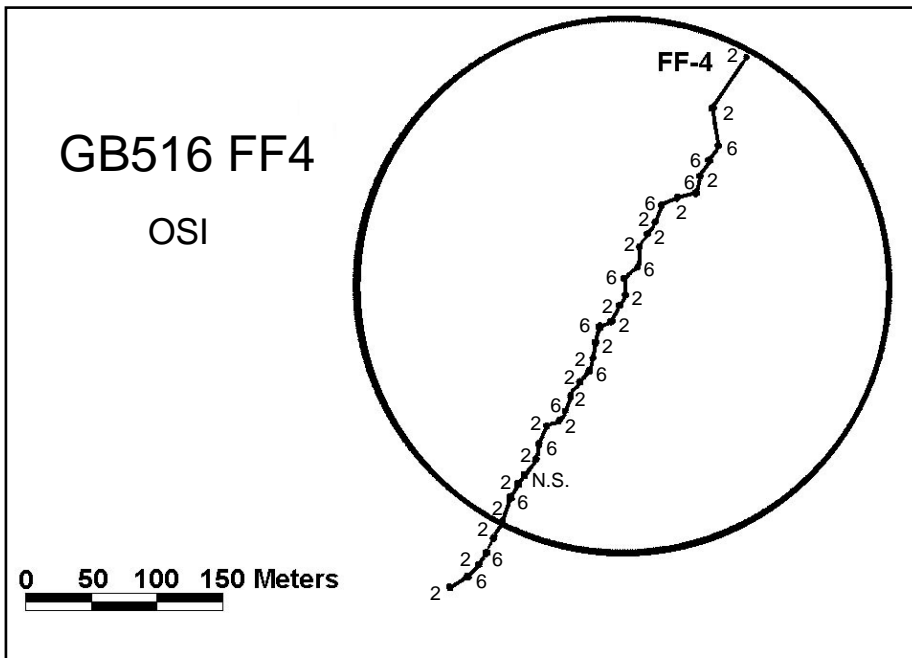


**Figure 6.63.** Mapped distribution of the Organism-Sediment Index (OSI) along Transect FF4 at Garden Banks Block 516 during Cruise 2B (July 2001). The FF site radius is 204 m.

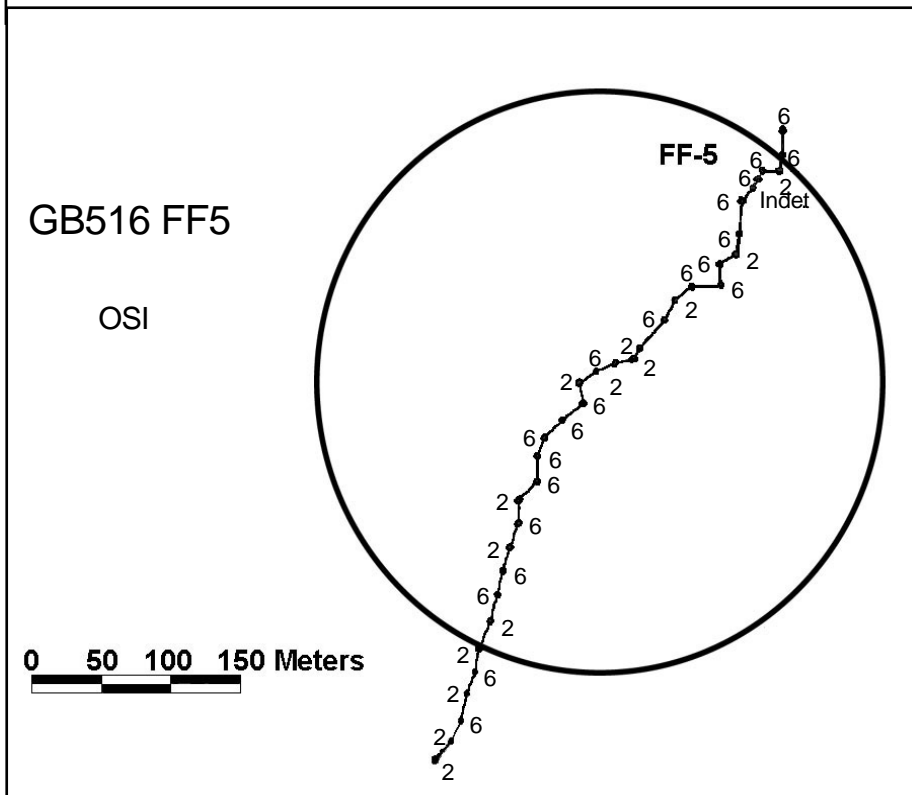


**Figure 6.64.** Mapped distribution of the Organism-Sediment Index (OSI) along Transect FF5 at Garden Banks Block 516 during Cruise 2B (July 2001). The FF site radius is 204 m.

## **6.6 VIOSCA KNOLL BLOCK 916 – CRUISE 3B (POST-DRILLING)**

### **6.6.1 Survey Design and Location**

The post-drilling sediment profile image survey of VK 916 was conducted on 7 to 8 August 2002 (Cruise 3B), immediately after drilling was completed. Three transects were sampled at the near-field site. Station locations are shown on **Figure 6.65**.

#### *6.6.1.1 Near-Field Stations*

There were 119 near-field stations located on three transects. Transects NF-1 and NF-2 each consisted of 40 stations, while Transect NF-3 had 39 stations. Usable SPI images were obtained at 112 of the 119 stations attempted (no data were collected at Stations NF-1.22, NF-2.1, NF-2.2, NF-2.8, NF-2.24, NF-3.1, and NF-3.33). Seventy-five percent of the usable images ( $n = 83$ ) were located within the 1,000-m site diameter. Thirty-three stations (29 with usable SPI images) were located outside of the circle perimeter.

#### *6.6.1.2 Far-Field Stations*

No usable far-field data were obtained at VK 916 during Cruise 3B. Far-field transects were attempted at two sites; however, due to camera problems, no usable data were collected. Therefore, results presented in the following sections are limited to near-field conditions as defined by the three near-field transects.

### **6.6.2 Sediment Fabric, Texture, Color, and Small-Scale Stratigraphy**

Images from all stations on the three near-field transects show at least three microstratigraphic units. First, the uppermost surface layer tends to consist of a pink to red high-water content layer (*Plates 20-24 and 27-29*). The mean thickness of the surface pink to red layer is comparable in all three transects (NF-1 = 3.30 cm, NF-2 = 3.44 cm, and NF-3 = 3.26 cm). The assumption of high-water content is based on the floccular appearance of this layer and the presence of dewatering pipes observed in some images (see arrows just below sediment-water interface in *Plate 20*). Dewatering structures typically are observed in rapidly deposited (or redeposited) fine sediments. A few stations lack this red to pink layer, especially where the surface is experiencing apparent anaerobic conditions (*Plates 30-35*). Chemical reduction imparts a gray to black color to the sediment due to the presence of sulfides.

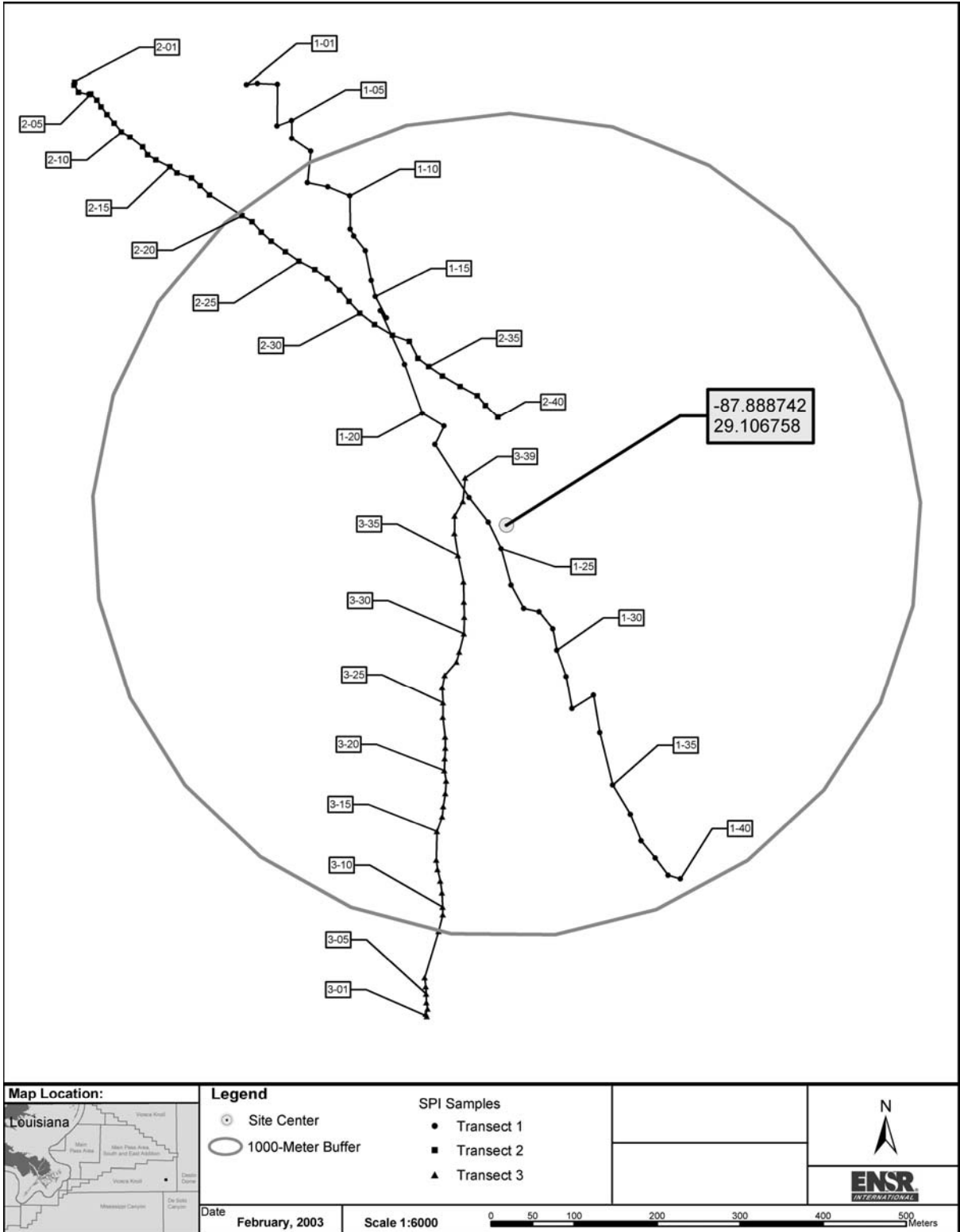


**Figure 6.65.** Viosca Knoll Block 916 near-field station map showing positions of sediment profile imaging transects and stations surveyed during post-drilling Cruise 3B (August 2002). The NF site radius is 500 m.

The dominant major-modal grain size of the surface layer sediments is sand ranging from 3-2 phi (fine sand) to 2-1 phi (medium sand). These sand-sized particles are formed from organic-mineral aggregates that result in small mud clasts and/or pellets. The sediment surface layer has a chaotic fabric, that is, an apparently random fabric consisting of subrounded to angular gray mud clasts intermixed with oxidized red to pink sand or reduced gray to black fluid mud. The sand-sized floccular surface sediment occupies interstitial spaces between these larger clasts. The cohesive gray clasts appear to have their origin in the underlying cohesive gray homogeneous clay (>4 phi major mode). The boundary between the surface unit (red-pink or black-black sand) and underlying cohesive clay is dominated by these mud clasts, which form an uneven and irregular contact (*Plates 20-35*). Cohesive sediment (plucking) erosion appears to have taken place near the surface of the cohesive gray clay layer either before or during deposition of the surface layer, resulting in clay clasts being mixed into the overlying surface layer (see *Plates 20-35*). These clay clasts also were observed in the pre-drilling survey. Small scale surface roughness is dominated by physical processes (e.g., erosional relief or dewatering mounds) at all stations – i.e., no biological structures, such as feeding mounds or pits, were observed that could explain surface topography.

### 6.6.3 Depth of the Apparent Redox Potential Discontinuity

**Figure 6.66** shows the mapped distribution of the apparent RPD as recognized by the surface mixed zone (light tan to pink or red) and underlying darker red, gray, or black sediment. This color transition was very difficult to detect and apparently was absent in most profile images. No apparent RPD was observed in sediments at any stations sampled along Transects NF-1 and NF-2. Transect NF-3 also was dominated by sediments showing zero RPD thickness, but 21 stations did show the presence of a very thin mean apparent RPD layer, less than 1.5 cm thick. The frequency distributions of the apparent RPD classes for stations sampled within the 1,000-m target circle are shown in **Figure 6.67**. The thin or absent RPD in these sediments strongly suggests that surface sediments have been deposited recently and have not yet been exposed to surficial oxidation.

### 6.6.4 Infaunal Successional Stages

Infaunal successional stages are defined in *Section 6.3.4*. Because the structure of Stage II assemblages in the VK 916 area is unknown, our mapping effort is confined to the following three successional bottom types:

1. Azoic bottom sediments that show no apparent signs of macrofaunal life at the surface of the bottom or at depth. However, this does not preclude the presence of microbial mats. In fact, most stations designated as azoic have visible evidence of bacterial aggregations or mats. (Examples are shown in *Plates 25-26* and *30-35*).
2. Bottom sediments that show evidence of only Stage I pioneering organisms near the sediment surface (Stage I seres).
3. Bottom sediments that show evidence of subsurface feeding voids (with or without Stage I species at the surface). These seres are mapped as Stage I-III or III. Examples are shown in *Plates 22-25* and *28-35*).

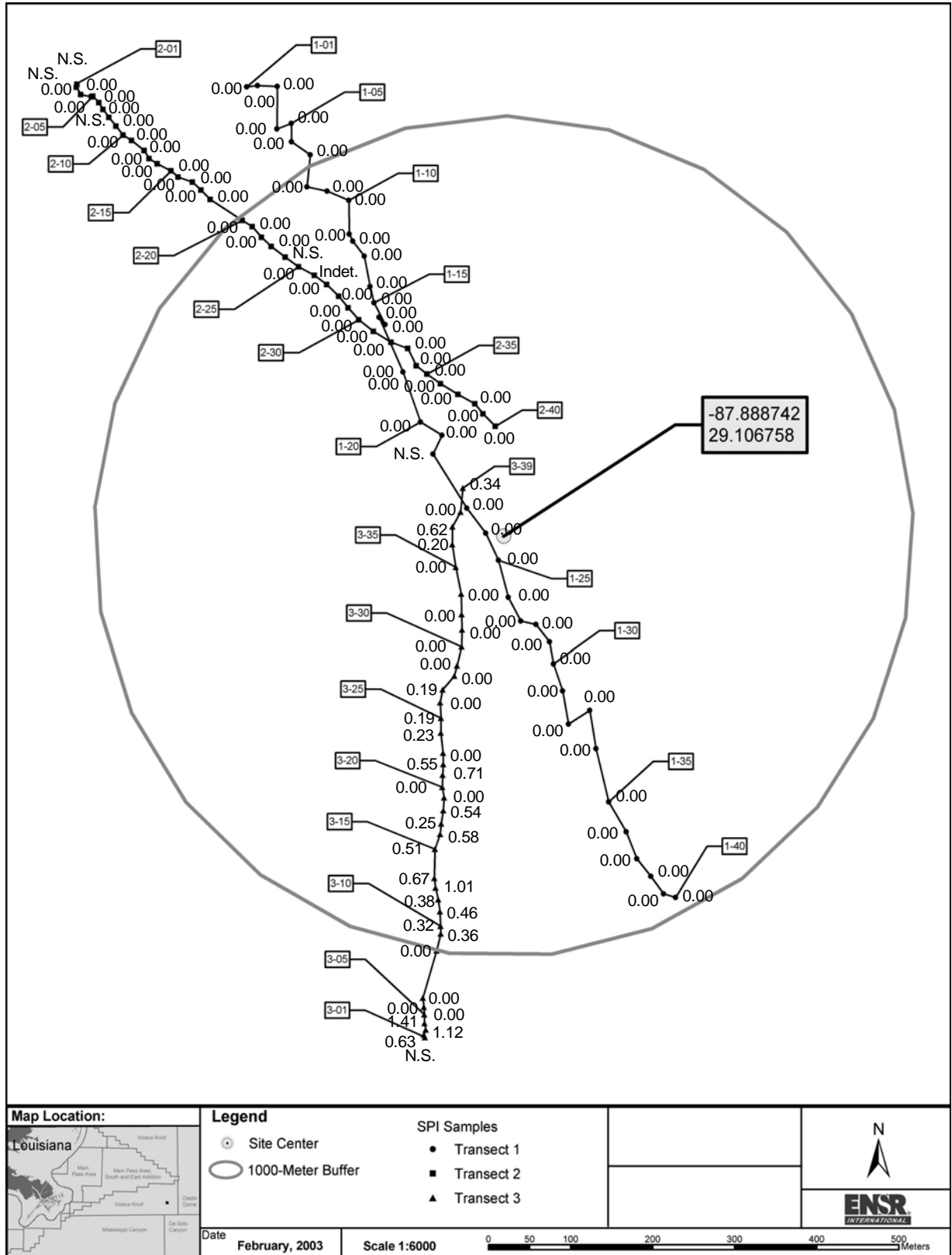


**Figure 6.66.** Mapped distribution of apparent redox potential discontinuity depth in centimeters, along the three near-field transects at Viosca Knoll Block 916 during post-drilling Cruise 3B (August 2002). The NF site radius is 500 m.



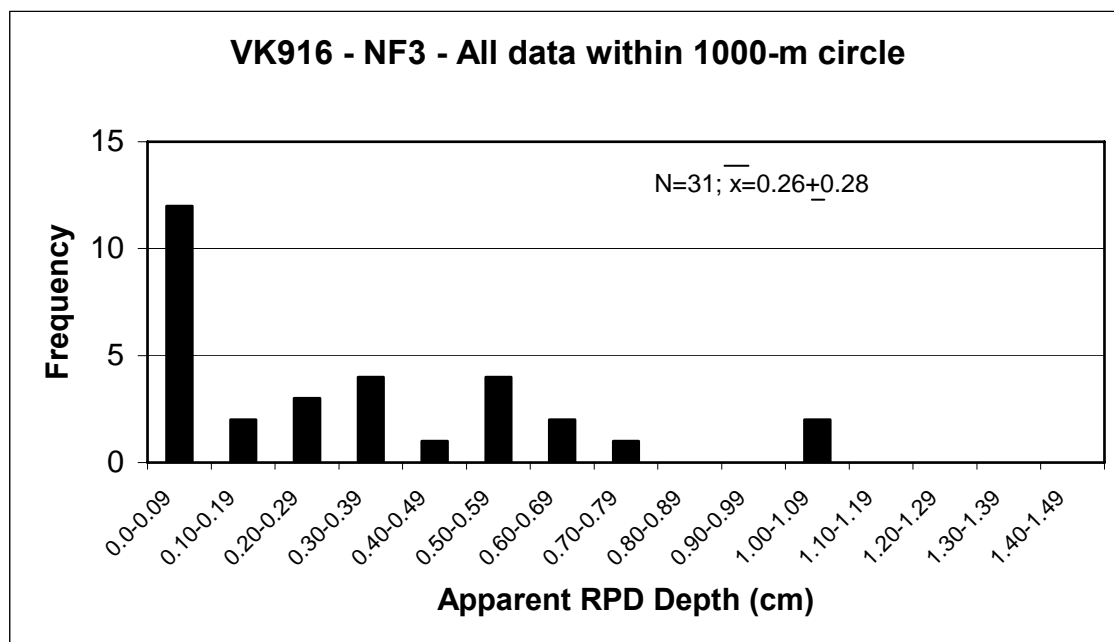
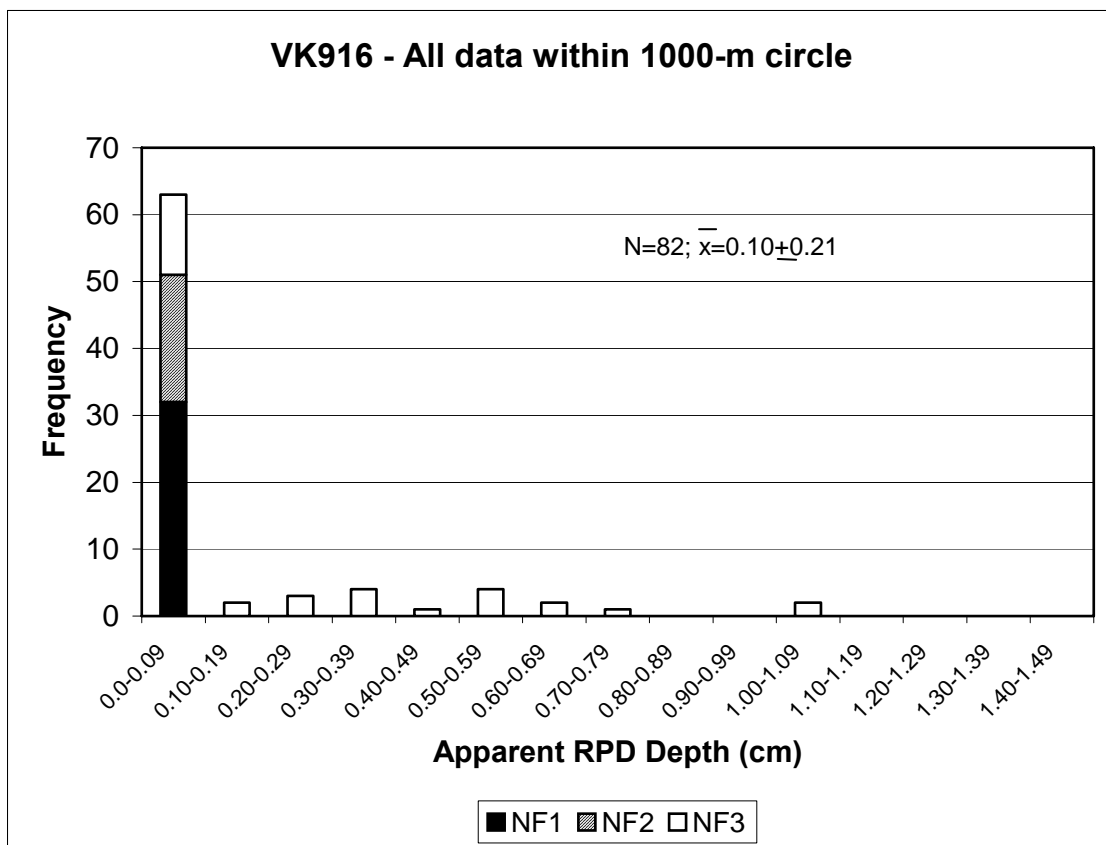


**Figure 6.67.** Apparent redox potential discontinuity (RPD) depth-frequency distributions at the three near-field transects at Viosca Knoll Block 916 during post-drilling Cruise 3B (August 2002). The lower box presents an expansion of the data for NF-3.

**Figure 6.68** shows the mapped distribution of successional stages along the three near-field transects. Transect NF-1 has 7 stations that are apparently azoic, Transect NF-2 has 13 azoic stations, and Transect NF-3 has 8 azoic stations. Therefore, about 25% of the near-field stations with usable SPI images ( $n = 112$ ) show no visual evidence of macrofaunal life on those images.

This is a significant change from the pre-drilling survey, where no stations were classified as azoic. These apparently azoic stations are patchily distributed over the three transects and are separated by stations showing evidence of Stages I-III or III.

Stage I seres are seen only occasionally in the SPI images from this survey. For example, no Stage I seres are observed in Transect NF-1 and are visible in only 22% and 14% of the stations with usable SPI images in Transects NF-2 and NF-3, respectively. The VK 916 post-drilling survey shows that the deeper Stage III seres dominate those stations where evidence of infauna is present in the surveyed area. The paucity of Stage I seres at the sediment surface suggests that recent surface disturbance (deposition, resuspension, and/or erosion) may have selectively compromised near surface-dwelling species relative to deeper-living infauna. A similar phenomenon has been noted in studies of the ecological effects of bottom trawling (Rosenberg et al. 2003). In contrast, Stage I seres dominated all near-field stations in the pre-drilling survey.

#### **6.6.5 Organism-Sediment Index**

The OSI, a parameter that provides a scale of overall benthic habitat quality, is described in *Section 6.3.5*. The value of the index can range from +11 (best habitat quality) to -10 (worst habitat quality). Values of OSI below +6 tend to be associated with disturbed habitats.

Because the apparent RPD depths were very shallow (even nonexistent at many stations) and several stations were azoic, the overall distribution of OSI values ranges from -7 to +6 (**Figure 6.69**). Those stations with zero RPD depths and an azoic status tend to map as OSI = -4. Stations with relatively deep RPD depths and associated Stage III seres map in the +6 to +7 range. The OSI frequency distributions for each of the three near-field transects are shown in **Figure 6.70**. The major modal OSI class for Transects NF-1 and NF-2 falls just below +6 (class +5.0 to +5.9), while the major mode on Transect NF-3 is within the class +6.0 to +6.9. However, Transect NF-3 also shows the greatest range (-7 to +7) of values, with 8 stations having negative OSI values.

Overall, the post-drilling survey indicates that the near-field benthic system is near, or just below, the OSI threshold of +6 (disturbed habitat criterion) and that 22% of the stations show very poor habitat quality as manifested by negative OSI values. In the pre-drilling survey, near-field stations ranged from +2 to +9, and no negative values were present. The major mode fell within the +7 to +8 classes (**Figure 6.39**), an overall indication of very good habitat quality. Using the OSI as a general measure of benthic habitat quality, a significant negative change in habitat conditions has been documented in the post-drilling survey at VK 916.

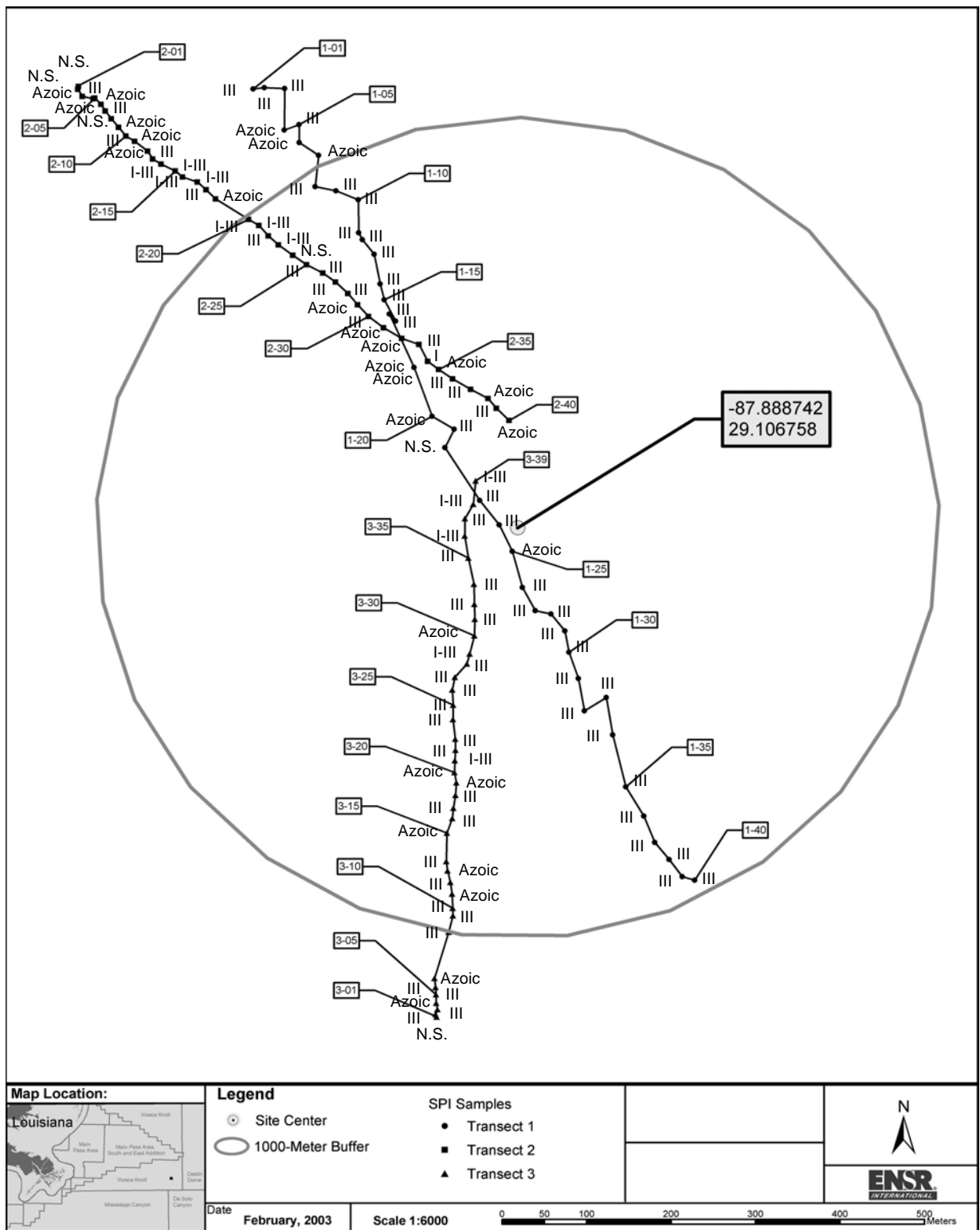


**Figure 6.68.** Mapped distribution of infaunal successional stages along all three near-field transects surveyed at Viosca Knoll Block 916 during post-drilling Cruise 3B (August 2002). The NF site radius is 500 m.

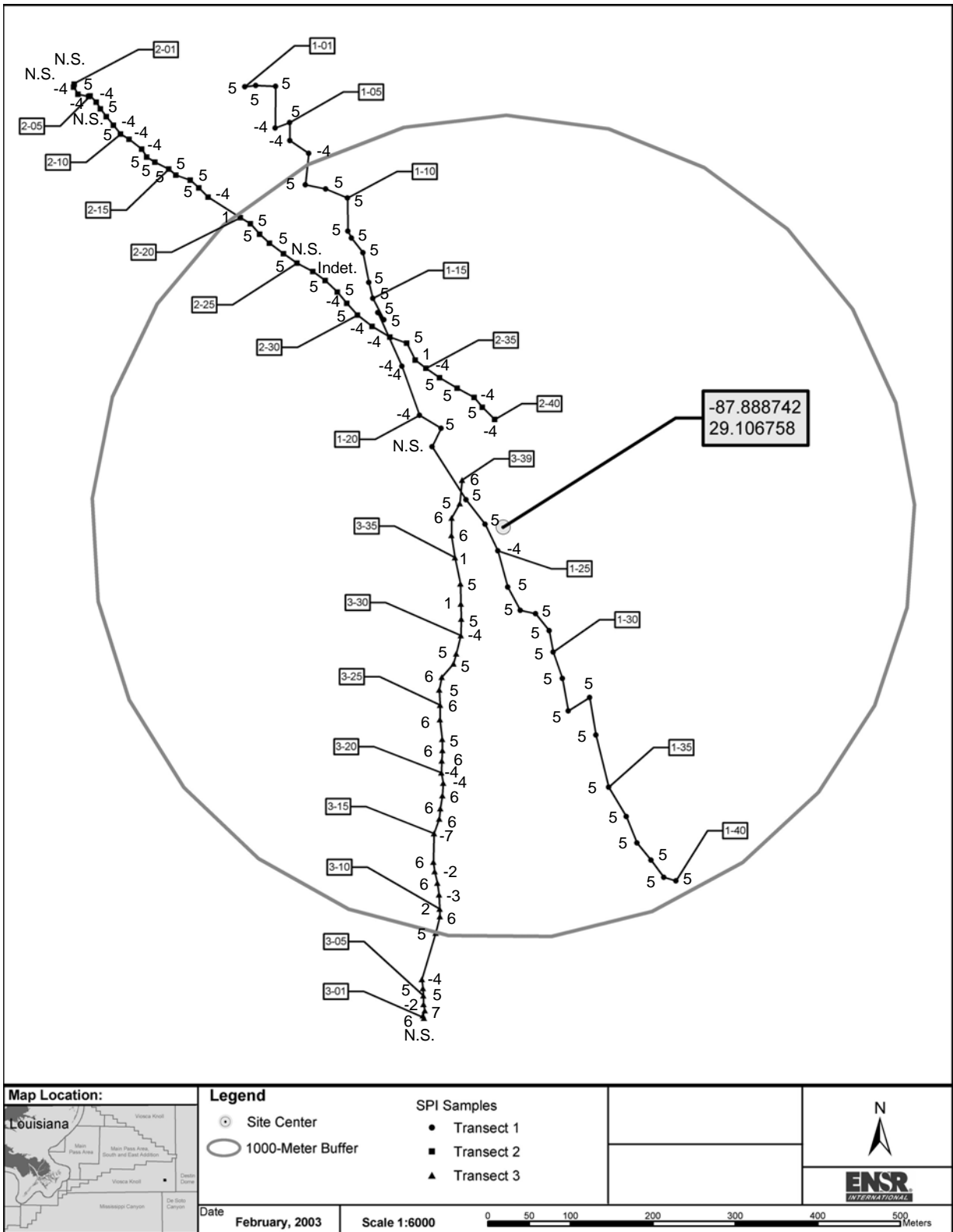


**Figure 6.69.** Mapped distribution of the Organism-Sediment Index (OSI) along the three near-field transects at Viosca Knoll Block 916 during post-drilling Cruise 3B (August 2002). The NF site radius is 500 m.

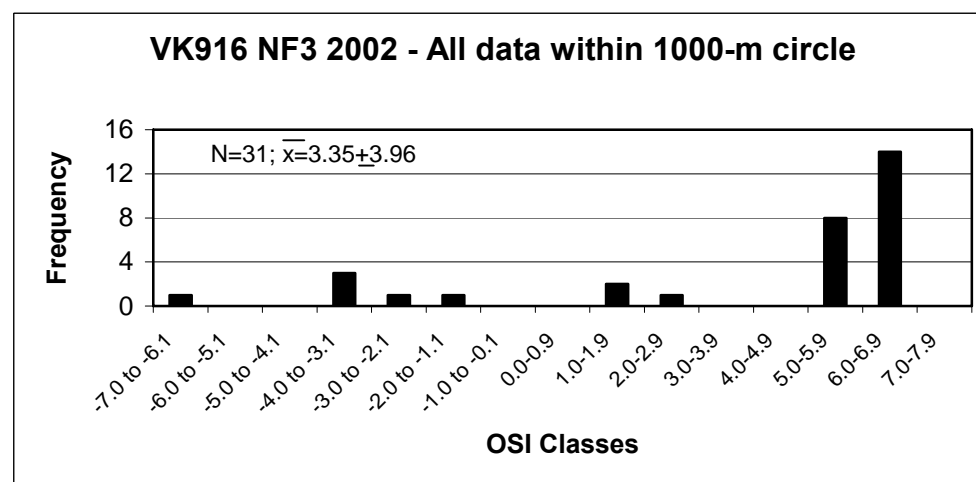
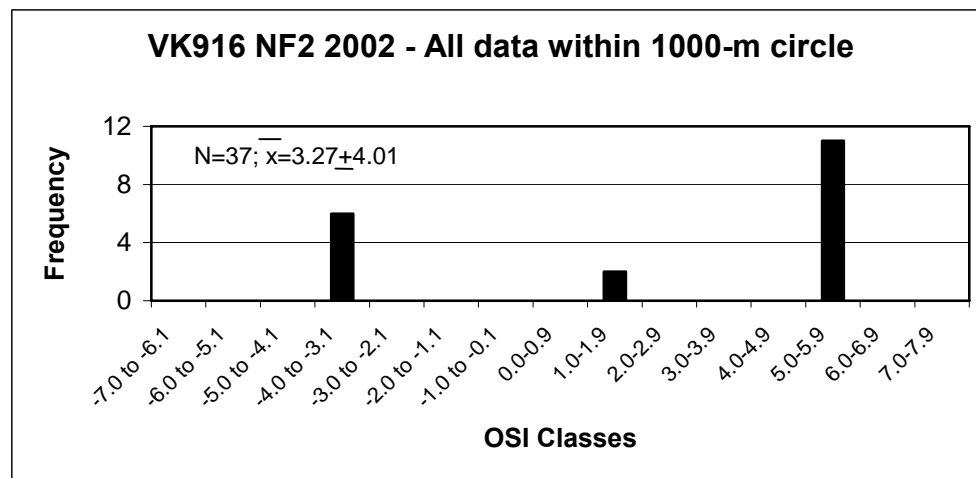
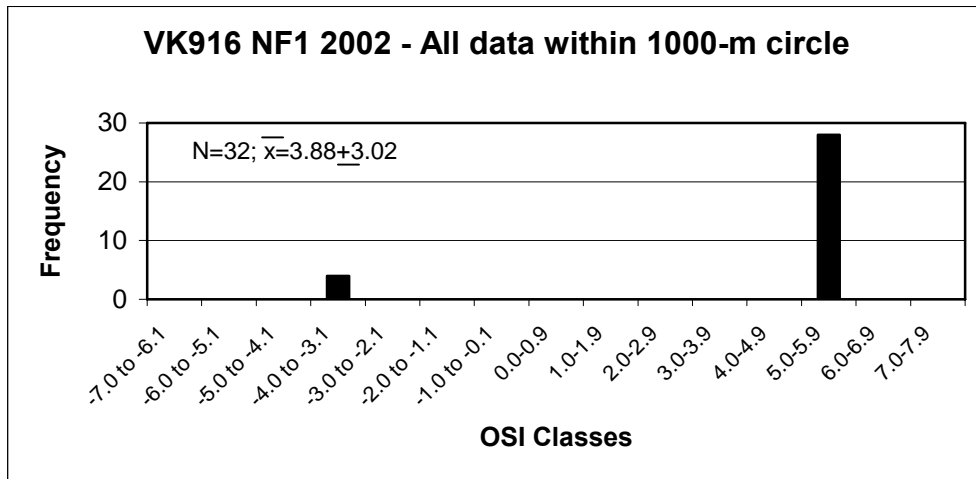


**Figure 6.70.** Organism-Sediment Index (OSI) class-frequency distributions at the three near-field transects at Viosca Knoll Block 916 during post-drilling Cruise 3B (August 2002).

## 6.7 SUMMARY AND CONCLUSIONS

In order to systematically compare benthic conditions between the two surveys at each site, tables of SPI observations and parameters have been prepared for both GB 516 (**Table 6.1**) and VK 916 (**Table 6.2**).

### 6.7.1 Garden Banks Block 516

#### 6.7.1.1 *Depth of the Mean Apparent Redox Potential Discontinuity*

The Cruise 1B (post-exploration) survey of near-field transect stations showed that mean apparent RPD depths were skewed toward low (less than 1 cm deep) values (**Table 6.1**). Stations with mean apparent RPD depths equal to or greater than 1.0 cm ranged from only 7% at Transect NF-2 to 35% at Transect NF-3. Seven stations on Transect NF-1 and 14 stations on Transect NF-2 had mean apparent RPD depths of zero, that is, there was no measurable apparent RPD. In contrast, during the same cruise, all stations on Transect NF-3 and on all three far-field transects had mean apparent RPD depths greater than zero. Stations with mean apparent RPD depths greater than 1.0 cm ranged from 20% along Transect FF6 to 36% at Transect FF2.

During Cruise 2B (post-development), the survey transects were located in slightly different positions from those mapped on Cruise 1B and so a transect-by-transect or station-by-station comparison is not possible. Nevertheless, the overall frequency distribution of mean apparent RPD depths showed most values skewed to low values. No near-field or far-field stations had mean apparent RPD depths greater than 1.0 cm deep. In the Cruise 2B survey, 8 stations on Transect NF-1 and 9 stations on Transect NF-2 had RPD depths of zero. All far-field stations had shallow yet measurable mean apparent RPD depths, although, as described above, all were found to be less than 1.0 cm deep.

In summary, a comparison of mean apparent RPD depths between Cruises 1B and 2B shows that the shallowest (i.e., zero) RPD depths exist at near-field stations in both surveys. However, a comparison of frequency distributions of RPD depths at all near-field stations combined between surveys shows that mean apparent RPD depths at near-field stations during Cruise 1B were nearly five times deeper than those measured during Cruise 2B. Similarly, far-field stations had mean apparent RPD depths more than three times greater on Cruise 1B than on Cruise 2B.

Experience in mapping apparent RPD depths in a wide range of marine environments and depths indicates that the range of values measured at the near-field and far-field stations at GB 516 is extremely narrow compared to measurements made in shallow water environments (typically from 0 to 10 cm). This suggests that surficial biogenic mixing at GB 516 is shallow compared to that normally seen in shallow water locations. While the range in apparent RPD depths is small in both surveys, the most significant and objective findings are that zero apparent RPD depths are present at some near-field stations in both surveys. The positive, albeit qualitative, correlation of those stations with RPD depth of 0.00 cm, with the presence of sulphidic surface sediments and a negative correlation with abundant infaunal macroinfaunal life, as discussed further below, supports the interpretation that such bottom areas are ecologically stressed.

**Table 6.1.** Comparison between Cruise 1B (post-exploration) and Cruise 2B (post-development) sediment profile imaging (SPI) survey results for Garden Banks Block 516 near-field stations.

SPI Parameter	Cruise 1B (Oct-Nov 2000)	Cruise 2B (July 2001)	Conclusions
Sediment conditions	Surface sediments consist of organic-mineral aggregate sand (3-2 to 2-1 phi) overlying >4 phi tan to gray clay. Evidence of reduced layers at depth. Reducing conditions at the sediment surface were seen at 28% of the sampled stations.	Surface consists of sand-sized aggregates. Sediment is >4 phi at depth and consists of black to gray layers intercalated with red to brown layers. There is some black sediment at the sediment surface.	Comparable results.
Mean thickness of apparent redox potential discontinuity (RPD)	The major modal mean RPD thickness is 0.00 to 0.99 cm. RPD depth is 0.00 cm at 21 stations.	The major modal RPD thickness lies within 0 to 0.31 cm. RPD depth is 0.00 cm at 17 stations.	Comparable results.
Successional status	74% to 87% of NF-1 and NF-2 stations, respectively, are either azoic or Stage I. Half of the NF-3 stations contain Stage I-III infauna. Microbial mats are present near the sediment surface at 22 stations (29%).	43% (NF-3) to 67% (NF-1 and NF-2) of stations are either azoic or Stage I. No stations had surficial microbial mats; however, 16 stations (15%) had thick layers of black sulfidic sediments extending to the sediment surface.	Cruise 2B shows slight improvement. Microbial mats reduced in frequency.
Organism-Sediment Index (OSI)	Transects NF-1 and NF-2 are dominated by OSI classes <+6 with negative indices at many stations (33%). At Transect NF-3, many stations (61%) have OSI values $\geq$ +6, and no station has a negative OSI value.	For all combined near-field transects, the OSI major mode was +2 to +2.9, and a minor mode of +6 to +6.9 was present. OSI values were negative at 18 near-field stations (18%).	Benthic habitat quality marginally improved between surveys. Bimodal patches of poor habitat quality interspersed with relatively good habitat quality.

**Table 6.2.** Comparison between Cruise 1B (pre-drilling) and Cruise 3B (post-drilling) sediment profile imaging (SPI) survey results for Viosca Knoll Block 916 near-field stations.

SPI Parameter	Cruise 1B (Oct-Nov 2000)	Cruise 3B (Aug 2002)	Conclusions
Sediment conditions	<ul style="list-style-type: none"> <li>• Thickness of surface red to pink layer is 4.89 to 5.59 cm.</li> <li>• Surface sediment grain size is 4-3 to 2-1 phi (organic mineral aggregates). Subsurface grain size is &gt;4 phi gray clay.</li> <li>• Boundary roughness, where determinable, is 30% (NF-2) to 97% (NF-1) biogenic.</li> </ul>	<ul style="list-style-type: none"> <li>• Thickness of surface red to pink layer is 3.26 to 3.44 cm.</li> <li>• Grain size is the same as baseline</li> <li>• Boundary roughness is 100% physical.</li> </ul>	<ul style="list-style-type: none"> <li>• Loss of about 2.0 cm of red-pink layer.</li> <li>• No change in sediment grain-size.</li> <li>• Loss of biogenic roughness.</li> </ul>
Mean thickness of apparent redox potential discontinuity (RPD)	<ul style="list-style-type: none"> <li>• The major modal mean RPD thickness is 0.78 to 1.14 cm.</li> <li>• There are no zero values.</li> </ul>	<ul style="list-style-type: none"> <li>• The 0.00 cm thickness class dominates with sulfides at the surface at several sites.</li> </ul>	<ul style="list-style-type: none"> <li>• Loss of RPD at most stations.</li> </ul>
Successional status	<ul style="list-style-type: none"> <li>• Stage I-III dominates most stations.</li> <li>• There are no azoic stations.</li> </ul>	<ul style="list-style-type: none"> <li>• 25% of stations are azoic.</li> <li>• Stage I organisms are rare and were seen at 0% (NF-1) to 22% (NF-2) of stations; this included stations classified as Stage I-III.</li> <li>• Stage III dominates.</li> <li>• Microbial mats are present at several stations.</li> </ul>	<ul style="list-style-type: none"> <li>• Retrograde successional conditions.</li> </ul>
Organism-Sediment Index (OSI)	<ul style="list-style-type: none"> <li>• Most OSI values are &gt;+6 with a major mode of +7.0 to +7.9.</li> <li>• Range is +2 to +9.</li> <li>• No negative values were recorded.</li> </ul>	<ul style="list-style-type: none"> <li>• The OSI has a major mode of +5.0 to +5.9.</li> <li>• 25% of the stations had negative OSI values.</li> </ul>	<ul style="list-style-type: none"> <li>• Change from good benthic habitat quality in baseline to marginal to poor habitat quality in the post-drilling survey.</li> </ul>



### 6.7.1.2 Successional Status

The Cruise 1B survey showed that segments of near-field Transects NF-1 and NF-2 were apparently devoid of any evidence of infaunal macroinfaunal life, either as imaged organisms or biogenic structures such as active feeding voids, tubes, or burrows. Transect NF-1 displayed azoic conditions at 16% of the stations on the northwest end. Forty-three percent of those stations located at the northwest end of Transect NF-2 also were interpreted to be azoic with respect to macrofauna. Microbial mats (*Plates 2-5*) were also widespread at the northwest ends of Transects NF-1 and NF-2. Those stations with no apparent macrofauna, but with microbial mats, are the same stations with zero mean apparent RPD depths as described above. This makes ecological sense, as biogenic mixing of surface sediment is nil under anoxic/sulfidic conditions. Some patchy microbial mats also were observed at stations located along the southeastern portion of Transect NF-1 and at Stations NF-2.11 and NF-2.12, but these clusters of stations showed evidence of Stage I worms at the sediment surface. In addition, those stations with patchy microbial mats and Stage I infauna at the southeastern portion of Transect NF-1 all had measurable apparent RPD depths.

The Cruise 2B survey also found stations apparently devoid of macrofauna on near-field Transects NF-1 and NF-3 (Note: these transect numbers are not equivalent in position to Transects NF-1 and NF-3 in the Cruise 1B survey). Four stations (11%) at the northern end of Transect NF-1 were azoic, and nearby stations were in a Stage I sere. The mid-region of Transect NF-2 had 8 stations (23%) devoid of macrofauna. As described above, these retrograde successional stations are the same stations where thin or zero apparent RPD depths were mapped. Black to gray sulfidic sediment, at or near the sediment-water interface, also was mapped at near-field stations during Cruise 2B (*Plates 14-18*), but no well-developed microbial mats were observed in the sediment profile images taken during this survey. Well-developed microbial mats were observed only during Cruise 1B. The reason for this difference is unknown.

The successional status at far-field stations was similar on both surveys. Macrofauna were found at all stations where the successional status could be determined. Stage I seres appear to be ubiquitous, and Stage III seres, as inferred from the presence of subsurface feeding voids, were also present at some of these stations. No sulfidic sediment or microbial mats were imaged at any far-field stations on either survey.

### 6.7.1.3 Organism-Sediment Index and Overall Benthic Habitat Quality

The OSI is a summary index that combines the mean depth of the RPD and successional status into a single number, useful for mapping benthic disturbance gradients in space and time (see methods section). Experience in mapping this parameter in a wide variety of environments has shown that OSI values of +6 or more represent relatively undisturbed benthic habitats, in relation to physical disturbance and/or chemical stress factors. At the other end of the spectrum, OSI values that are negative represent highly impacted and stressed benthic habitats. OSIs in the intermediate range, less than +6 but still positive, represent intermediate mosaics of disturbance or recovery.

On Cruise 1B, along GB 516 near-field transects, OSI values at 71% of the stations fell below +6 and were negative at 36% of the stations. In contrast, considering all three far-field stations together, half (50%) had OSI values below +6, and no negative OSI indices were recorded.

During Cruise 2B, the GB 516 near-field stations had slightly fewer OSI values below +6 (62%) than found during the earlier survey, and only 18% of stations had negative OSI values. Of far-field stations sampled during Cruise 2B, 46% of stations had OSI values below +6, and no negative values were seen.

Based on the OSI statistics outlined above, no difference is detected in the far-field stations between the two surveys. The OSI values at near-field stations appear to be somewhat higher during Cruise 2B. The proportion of negative OSIs during Cruise 2B is less than half that of Cruise 1B. However, this comparison is compromised by the fact that the spatial location of the near-field transects was not the same in the two surveys. This brings into question whether spatial variation in the OSI can equal or exceed temporal differences and points out the importance of reoccupying the same stations and transects over time to detect habitat change.

Overall, the most important findings of the two surveys were that black sulphidic muds with azoic or retrograde benthic communities are present in the near-field area. These degraded benthic habitats stand in marked contrast to habitats seen at far-field stations that exhibit aerobic boundary layer conditions with well-developed Stage I and I-III communities.

Drilling discharges are assumed to be the main cause for the degraded benthic habitats at some near-field stations. Two exploration wells had been drilled at the GB 516 site about 14 months prior to Cruise 1B, and five development wells were drilled between Cruise 1B and Cruise 2B (see *Chapter 3*). Sediment profile images showed the presence of buried sulfidic layers between oxidized sediment layers at depth within the bottom (*Plates 12, 13A, 13B, 16B, 18A, and 18B*). While these may be due to drilling discharges, natural processes may also be a contributing factor, as buried dark layers also can be seen at some far-field stations (*Plate 7*). These buried layers may represent past benthic anoxic and/or eutrophication events having spatial scales less than 1,000 m (as judged by the mapped distribution of impacted stations in our surveys). These events may be associated with local eutrophication, deposition of reactive organic matter, and enhanced anaerobic microbial production. These phenomena would explain the storage of sulfidic sediment in the sediment column in the form of black to gray layers. As these transient anoxic events pass, normal pelagic sedimentation would resume and the gray/black layers would be covered with tan oxidized sediment containing normal benthic communities.

#### 6.7.1.4 Summary of Results

**Table 6.1** summarizes SPI observations and measurements for the GB 516 site for Cruise 1B (October-November 2000) and Cruise 2B (July 2001). Given the observed change (or no apparent change) in SPI parameters over the period of observation, conclusions are drawn as to changes in benthic habitat conditions at the site. It can be seen from **Table 6.1** that SPI parameters range from comparable to an apparent improvement in benthic habitat conditions in the Cruise 2B survey compared to the Cruise 1B survey. This comparison is somewhat compromised by the fact that the transects and station locations between the surveys are not exactly the same. Nevertheless, the GB 516 site consists of a mosaic of very poor benthic

conditions alternating with areas of the bottom that represent moderately high benthic habitat quality. This finding is consistent for both surveys.

### **6.7.2 Viosca Knoll Block 916**

The summary below includes the baseline (Cruise 1B) results from the far-field stations, but the pre-drilling and post-drilling comparison is limited to the near-field area as no far-field stations were sampled on the post-drilling survey (Cruise 3B). Due to camera problems, no usable data were collected in the far-field on Cruise 3B.

#### *6.7.2.1 Depth of the Mean Apparent Redox Potential Discontinuity*

The baseline survey (Cruise 1B) showed that the surface sediment mixing depths (apparent RPD) at the VK 916 near-field stations are thin, with 66% of the values falling below 1.0 cm in depth. Far-field stations also are shallowly mixed, with 69% of the values falling below 1.0 cm in depth. No zero depths were recorded.

The post-drilling survey (Cruise 3B) was limited to the near-field site. Stations were located in slightly different positions from those occupied in the pre-drilling survey so that a station-by-station comparison is not possible. However, post-drilling images showed that the depth of the apparent RPD is zero (0.00 cm) at more than 80% of the stations (n = 91).

A comparison of mean apparent RPD depths between the baseline and post-drilling survey in the near-field shows that the apparent RPD depth is much shallower in the post-drilling survey as evidenced by an increase in the percentage of stations showing no RPD (i.e., no oxidized sediment at the sediment surface) from 0% to 80%.

#### *6.7.2.2 Successional Status*

The pre-drilling survey showed that Stage I-III seres dominate all near-field and far-field transect stations. No azoic stations were encountered. On Cruise 1B, the VK 916 benthic environment was in a higher successional status than the GB 516 site (due to the impacts of previous drilling at GB 516).

The post-drilling survey in the VK 916 near-field area found that 25% of the stations were azoic. Stage I seres alone were seen at only one station. Only 14% of stations where Stage III organisms were present also had Stage I organisms and could be classified as Stage I-III. The dominant seres found during the post-drilling survey were Stage III. Microbial mats were seen at several stations.

Stage I organisms were much reduced in numbers in the post-drilling survey, indicating a retrograde successional condition. This reduction is interpreted to be caused by a recent disturbance of the sediment surface.

#### *6.7.2.3 Organism-Sediment Indices and Overall Benthic Habitat Quality*

The baseline VK 916 survey found that in the near-field site, only 40% of the stations have OSI values less than +6. This means that 60% of the stations have a high habitat quality. No negative

values were present. Far-field transects had 47% of stations with OSI values less than +6. No negative OSI values were present. More than half of the near-field and far-field stations are characterized as having high benthic habitat quality based on this index. As a comparison, the near-field and far-field OSIs at VK 916 are comparable to the OSI distributions for GB 516 far-field areas as mapped in both surveys.

The VK 916 post-drilling survey showed that 25% of the near-field stations surveyed had negative OSI values and that the OSI major mode was +5 to +5.9. This indicates marginal to poor habitat quality. There was a distinct degradation of habitat quality from good in the pre-drilling survey to marginal or poor seen in the post-drilling study.

The shallow stratigraphy of the VK 916 area, as imaged in sediment profile photographs, is different from that mapped at GB 516. On Cruise 1B, no buried black or gray layers were observed at or under the surface of the seafloor in the VK 916 area. There is, instead, a thin layer of oxidized tan bioturbated sediment overlying a homogeneous light gray clay (*Plates 9A, 9B, 10A, 10B, and 11*). The gray clay appears to be an older over-consolidated deposit, as it prevented deep camera prism penetration and the clay adhered to the prism window, suggesting that it had low water content.

Some of the post-drilling stations sampled in the near-field showed a similar stratigraphy (*Plates 20-24 and 27-29*). Degraded areas, absent in the baseline survey, showed black sulfidic sediments at or near the sediment surface (*Plates 25-26 and 30-35*).

#### 6.7.2.4 Summary of Results

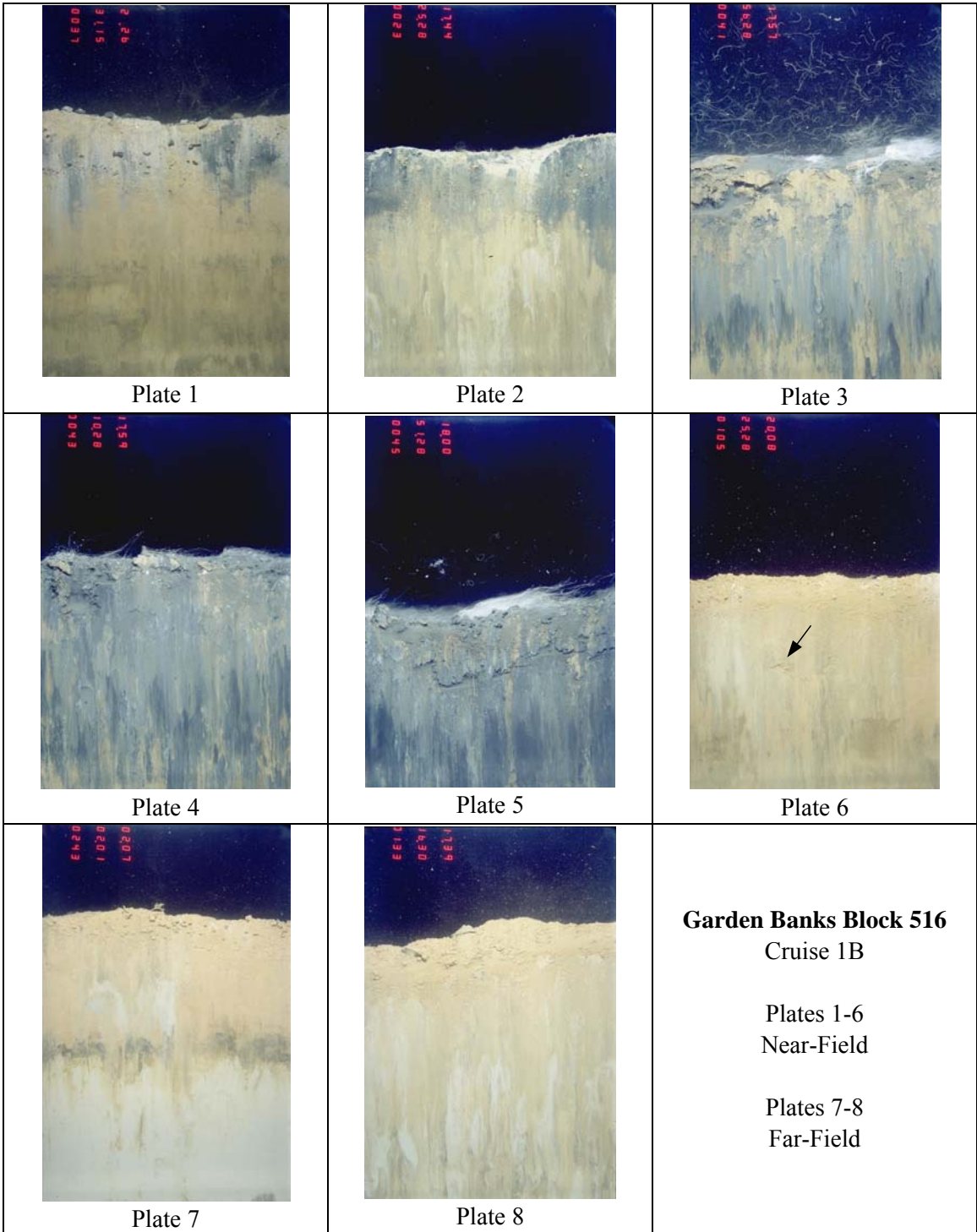
**Table 6.2** summarizes baseline (Cruise 1B, October-November 2000) and post-drilling (Cruise 3B, August 2002) SPI results at the VK 916 site with conclusions regarding change in habitat quality. Unlike the GB 516 results, major changes were detected in all SPI parameters at VK 916. Firstly, about 2 cm of red to pink surface layer apparently were lost to erosion. Also, as a consequence of erosion, the thin layer of oxidized surface sediment observed in the baseline survey was missing at most stations. All of the boundary roughness is interpreted to be due to physical (rather than biological) processes. Secondly, one of the most significant observations is the presence of reduced sulfidic surface sediments associated with anaerobic bacterial mats seen in the post-drilling survey. Sulfidic sediments and bacterial mats were not observed in the VK 916 pre-drilling survey. Thirdly, the post-drilling survey shows retrograde successional conditions at VK 916 relative to the baseline. Twenty-five percent of the post-drilling stations apparently are azoic, and Stage I seres are rarely encountered. This observation is consistent with intensive surface erosion/disturbance and is a phenomenon commonly encountered in SPI surveys of areas that have been trawled (Rosenberg et al. 2003). In the VK 916 case, trawling is less probable than anchor chain disturbance. However, the data are not conclusive about whether the erosion is related to anchoring since some evidence of erosion was observed on the pre-drilling survey and no far-field, post-drilling data were available for comparison. Lastly, the habitat summary parameter (OSI) shows a significant decline in benthic habitat quality in the post-drilling survey. The baseline major modal OSI determined in the pre-drilling survey was in the +7.0 to +7.9 class, and no negative OSI values were seen. In the post-drilling survey, the major modal OSI had dropped two OSI units to +5.0 to +5.9, and 22% of the stations had negative OSI values.






## 6.8 PLATES

Reduced versions of the photographs (plates) cited in the text are shown on the following pages. Larger versions of the images are shown in *Appendix E4*. Original image width is 15 cm.







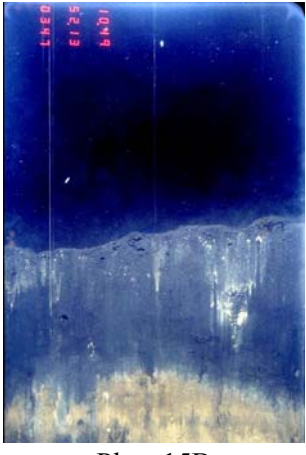
Plate	Station	Description/Notes
<b>Garden Banks Block 516, Cruise 1B</b>		
1	NF-1.19	Granular surface layer of pink to reddish-tan sediment underlain by a dark gray to black sulfidic layer.
2	NF-2.12	White microbial mat at the sediment surface overlies a sulfidic gray layer, which in turn overlies a mottled light gray to tan sediment.
3	NF-2.21	A white surface microbial mat is present on the right.
4	NF-2.22	Shows a microbial mat and a gray mottled sediment column at sediment profile imaging camera penetration depth.
5	NF-2.23	A microbial mat and the sediment column below completely gray to black; very little ferric hydroxide (yellow to tan color) is observed.
6	NF-3.17	Burrow-mottled oxidized sediment with only a hint of gray layering at the camera penetration depth. A feeding void is present (arrow).
7	FF6-3.13	Pink to tan mottled surface sediments underlain by a thin layer of sulfidic gray to black sediment, which in turn, overlies a homogeneous light gray layer.
8	FF2-1.4	Near-surface layer of mottled pink to tan sediment overlying faint gray layers at depth.
<b>Viosca Knoll Block 916, Cruise 1B</b>		
9A,B	A: NF-1.22 B: NF-2.27	Layer of reddish-brown sediment overlying a homogeneous gray clay. Feeding voids (arrows) are present in both pictures, and a worm is seen at depth in 9A.
10A,B	A: FF2-1.11 B: FF4-2.7	Images typical of VK 916 far-field sites during the pre-drilling cruise.
11	FF6-3.18	Image typical of VK 916 far-field sites during the pre-drilling cruise.
<b>Garden Banks Block 516, Cruise 2B</b>		
12	NF-1.6B	The upper few millimeters of the sediment consist of sand-sized grain aggregates; four layers of oxidized and reduced sediments are visible.
13A,B	A: NF-3.27B B: NF-2.35B	13A shows six layers of oxidized and reduced sediments, and 13B has seven layers of oxidized and reduced sediments.
14A,B	A: NF-1.25B B: NF-1.28B	Black reduced sediments extending to the sediment-water interface and bounded above and below (A) or only below (B) by light gray sediment.
15A,B	A: NF-2.17A B: NF-2.18A	Black reduced sediments extending to the sediment-water interface and bounded below by light gray sediment.
16A,B	A: NF-2.19A B: NF-2.20A	Black reduced sediments extending to the sediment-water interface and bounded below (A) or above and below (B) by light gray sediment.
17	NF2-25A	Black reduced sediments extending to the sediment-water interface and bounded below by light gray sediment.
18A,B	A: NF-1.19B B: NF-3.12B	Black reduced sediments bounded by light gray sediment, and under ambient? reddish-brown sediment.
19	FF3-13B	Image typical of far-field sites during Cruise 2B, showing absence of dark black reduced sediments. Feeding voids (arrows) are present.
<b>Viosca Knoll Block 916, Cruise 3B</b>		
20	NF-1.01 (1808)	Shows a layer of red to reddish-gray sediment over a region of chaotic fabric, which in turn, overlays a homogeneous gray clay. The surface is erosional, and no Stage I tubes are visible. Dewatering channels are present (3 arrows near surface) in the uncompacted surface region. A tiny feeding void (arrow) is present at 18-cm depth.
21	NF-1.37 (1919)	Numerous infaunal feeding voids (arrows).
22	NF-1.40 (1924)	Shows chaotic fabric, feeding voids (arrows), and small reddish patches of lignosulfate.







Plate	Station	Description/Notes
23	NF-2.14 (0155)	Shows Stage I infauna on the sediment surface (white arrows) and feeding voids (black arrows).
24	NF-2.21 (0207)	A layer of red to reddish-gray sediment over a region of chaotic fabric, which in turn, overlays a homogeneous gray clay. Stage I tubes (white arrows) are visible on the sediment surface. A tiny feeding void (black arrow) is present at 18-cm depth.
25	NF-2.39 (0235)	Shows sulfidic areas within the layer of red to reddish-gray sediment. Thin strands of a small disturbed bacterial mat are visible in the upper layer (white arrows). A region of chaotic fabric is still present between the red layer and the homogeneous gray clay. The surface is erosional, and no Stage I tubes are visible. A tiny feeding void (black arrow) is present at 18-cm depth.
26	NF-2.40 (0236)	Shows sulfidic areas within the layer of red to reddish-gray sediment. Thin strands of a small disturbed bacterial mat are visible in the upper layer (white arrows). A region of chaotic fabric is still present between the red layer and the homogeneous gray clay. A few recumbent tubes are present near the surface. No voids are present.
27	NF-3.14 (0449)	Shows a redox potential discontinuity (light pinkish-red sediment at surface).
28	NF-3.21 (0502)	Shows a redox potential discontinuity (light-brown sediment at surface). Stage I tubes are present on the sediment surface (white arrows). A feeding void is present at 16-cm depth (black arrow). An example of successional Stage I-III.
29	NF3-29 (0514)	Shows a thin redox potential discontinuity (patches of light-brown sediment at surface). Stage I tubes are present on the sediment surface (white arrows). A feeding void is present at 16-cm depth (black arrow).
30	NF-3.34 (0522)	Shows sulfidic areas within the layer of red to reddish-gray sediment. Thin strands of a small disturbed bacterial mat are visible in the upper layer (white arrows). A region of chaotic fabric is still present between the upper layer and the homogeneous gray clay. A recumbent tube is present on the surface (white dashed arrow). Feeding voids are visible at depth (black arrows).
31	NF-3.35 (0523)	Shows sulfidic areas within the layer of red to reddish-gray sediment. Thin strands of a small disturbed bacterial mat are visible in the upper layer (white arrows). A region of chaotic fabric is still present between the upper layer and the homogeneous gray clay. Recumbent/buried tubes are present on the surface (white dashed arrows). Feeding voids are visible at depth (black arrows).
32	NF-3.36 (0525)	Shows a thick sulfidic area underlying a thin redox potential discontinuity (<1 cm). A patchy white bacterial mat is visible in the upper layer (white arrows). Stage I tubes (dashed white arrows) are present on the surface. Small feeding voids are visible at depth (black arrows). The successional stage is I-III; Organism-Sediment Index is 6.
33	NF-3.37 (0527)	Shows a sulfidic area underlying a thin redox potential discontinuity (<1 cm). Patches of a buried white bacterial mat are visible in the upper layer (white arrows). Recumbent/buried tubes (dashed white arrows) are present near the surface. A small feeding void is visible at depth (black arrow).
34	NF-3.38 (0529)	Shows a patchy sulfidic layer and bacterial mat. The red layer is absent. Patches of a buried white bacterial mat are visible in the upper layer (dashed black arrows). Stage I tubes (white arrows) are present on the surface. A feeding void is visible at depth (black arrow). The successional stage is I-III; Organism-Sediment Index is 5.
35	NF-3.39 (0531)	Shows a sulfidic layer underlying a thin redox potential discontinuity. The red layer is absent. Patches of a buried white bacterial mat are visible in the upper layer (dashed black arrows). A few Stage I tubes (white arrows) are present on the surface. Feeding voids are visible at depth (black arrows). The successional stage is I-III; Organism-Sediment Index is 6.



	
	
	<p><b>Viosca Knoll Block 916</b>  Cruise 1B  (pre-drilling)</p> <p>Plates 9A, 9B  Near-Field</p> <p>Plates 10A, 10B, 11  Far-Field</p>



		
		
		<p><b>Garden Banks Block 516</b> Cruise 2B</p> <p>Plates 12, 13A, 13B 14A, 14B, 15A, 15B Near-Field</p>

		
<p>Plate 16A</p> 	<p>Plate 16B</p> 	<p>Plate 17</p> 
		<p><b>Garden Banks Block 516</b> Cruise 2B</p> <p>Plates 16A, 16B, 17, 18A, 18B Near-Field</p> <p>Plate 19 Far-Field</p>

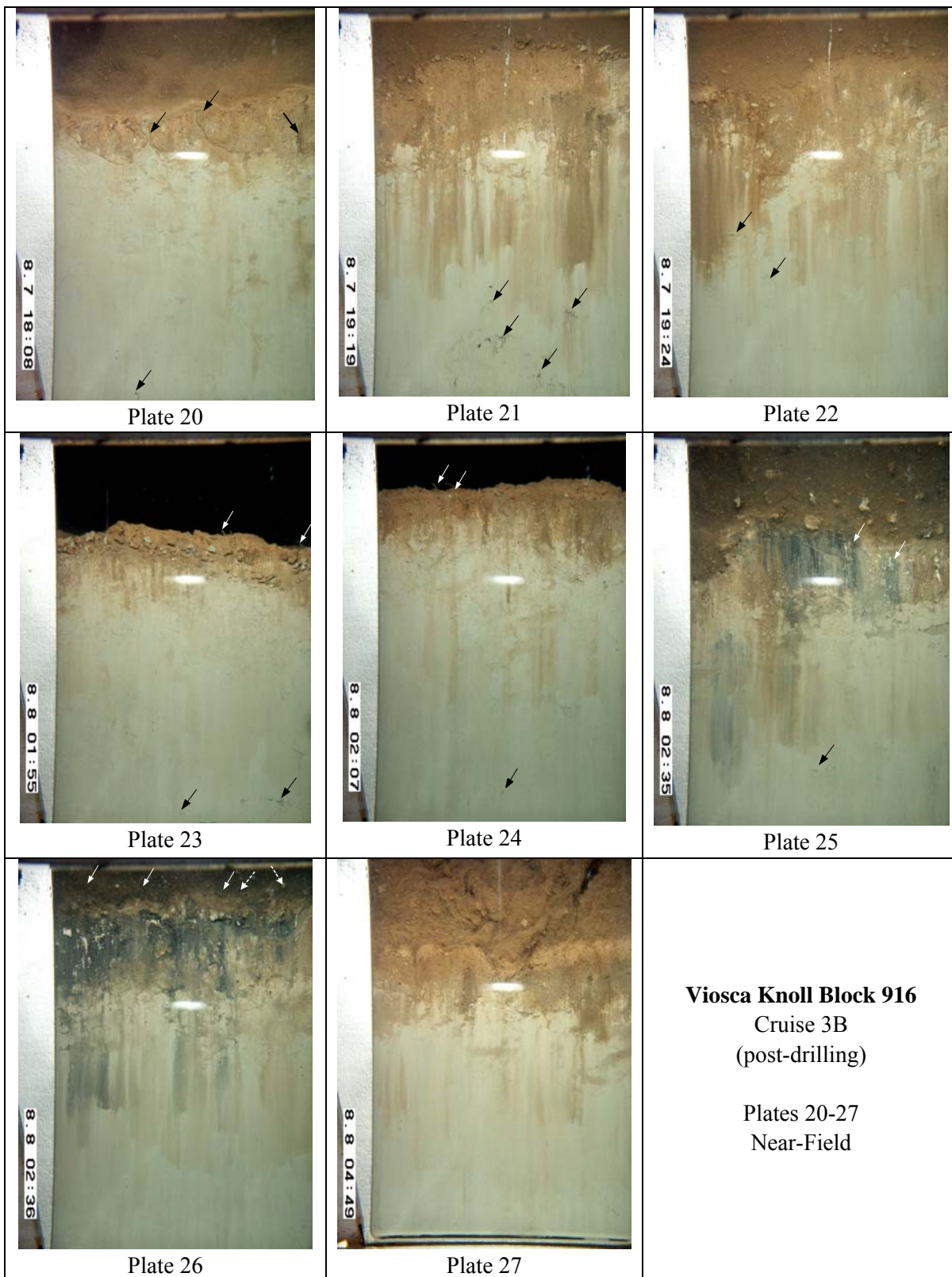




Plate 28



Plate 29



Plate 30



Plate 31



Plate 32



Plate 33



Plate 34

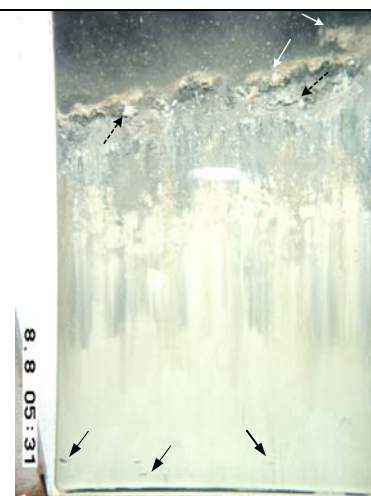


Plate 35

**Viosca Knoll Block 916**  
Cruise 3B  
(post-drilling)  
  
Plates 28-35  
Near-Field

## Chapter 7 Sediment Profile Imaging at Post-Development Sites

Robert J. Diaz  
Virginia Institute of Marine Science

---

### 7.1 INTRODUCTION

Rhoads and Cande (1971) developed sediment profiling as a means of obtaining *in situ* data to investigate processes structuring the sediment-water interface. The technology of remote ecological monitoring of the seafloor (REMOTS – Rhoads and Germano 1982) or sediment profile imaging (SPI) has allowed for the development of a better understanding of the complexity of sediment dynamics, from both a biological and physical point of view (for examples, see Rhoads and Germano [1986], Valente et al. [1992], Diaz et al. [1994], Bonsdorff et al. [1996], Nilsson and Rosenberg [2000], and Rosenberg et al. [2001]). This approach to evaluating the environment, and potential impacts, can be easily combined with classical approaches to habitat and impact assessment, providing scientists and managers with a more holistic ecosystem view. In addition, SPI serves to provide ground-truth data for acoustic methods such as side-scan and multibeam sonar.

This chapter deals only with sediment profile camera surveys at post-development sites GB 602 and MC 292. For SPI data from the other two sites, see *Chapter 6*.

### 7.2 METHODS

#### 7.2.1 Survey Design and Transect Location

An SPI survey was conducted in July 2001 (Cruise 2B) at GB 602 and MC 292. The general rationale for the field sampling design can be found in *Chapter 2*. For the SPI component, a basic transect design was adopted. Along each transect, a Benthos sediment profile camera was deployed, generally 36 times (actual numbers of usable photographs for each transect are given in the Results section)

Transects were surveyed at a near-field area, located near previous oil and gas drilling site(s), and three far-field areas, located at least 10 km from the near-field and presumably outside the influence of oil development activities (**Figures 7.1** and **7.2**). At GB 602, three near-field transects and three far-field transects were completed. At MC 292, two near-field transects and three far-field transects were surveyed.

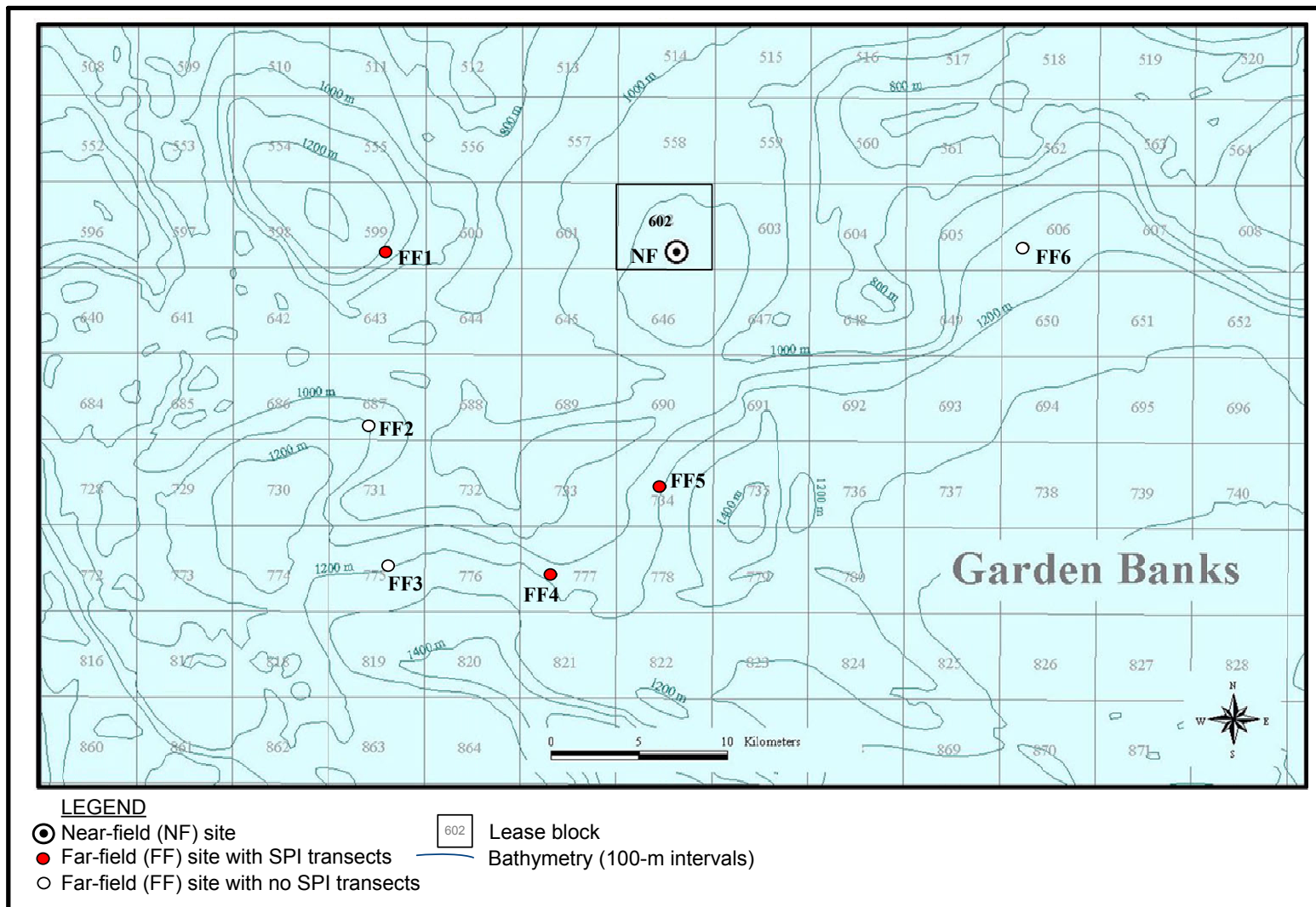


**Figure 7.1.** Location of Garden Banks Block 602 post-development site and associated reference areas where sediment profile imaging (SPI) transects were surveyed.

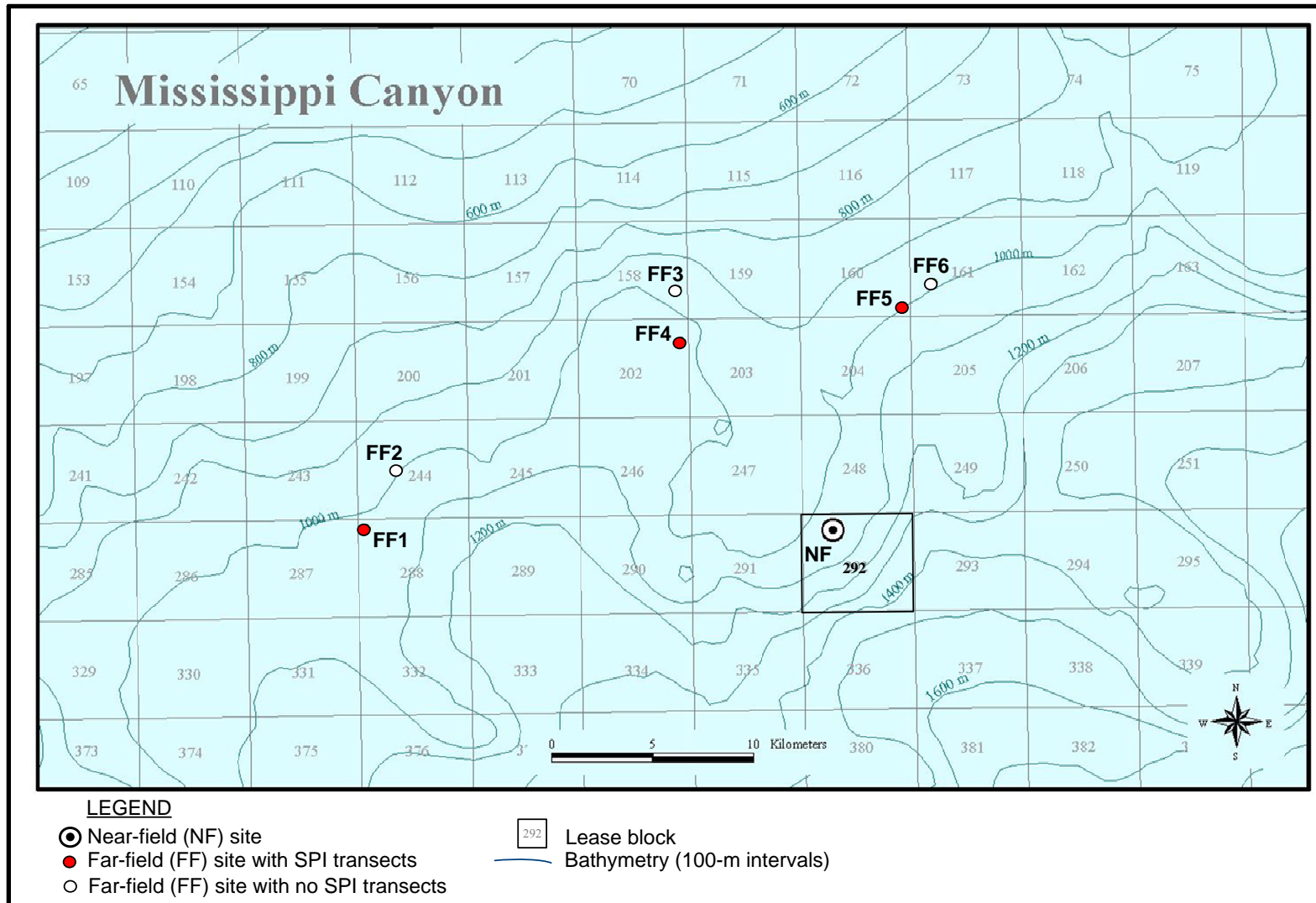


**Figure 7.2.** Location of Mississippi Canyon Block 292 post-development site and associated reference areas where sediment profile imaging (SPI) transects were surveyed.

All near-field SPI images were taken along transects located near or within a 500-m radius circle centered on previous wellsites (**Figures 7.3 and 7.4**). At GB 602, three near-field transects were sampled – two in an east-to-west direction (NF-1 and NF-2) and one north-to-south (NF-3) (**Figure 7.3**). Transect NF-1 was located north of the wellsites, the first half passing through an area with several fingers of possible cuttings as mapped by the side-scan sonar data. Transect NF-2 went within 100 m of the wellsites, with over half of the transect over bottom classified as possible cuttings based on side-scan sonar data. Transect NF-3, to the east of the wellsites by about 250 m, crossed several fingers of possible cuttings as mapped by the side-scan sonar (**Figure 7.3**). Samples were collected along three transects at far-field areas (Transects FF1, FF4, and FF5) intended to represent ambient or reference bottom conditions (**Figure 7.5**).

At MC 292, two near-field transects were sampled, one in a southwest-to-northeast direction (NF-1) and the other in a northwest-to-southeast direction (NF-2) (**Figure 7.4**). Transect NF-1 passed about 200 m northwest of the wellsites in an area with thin fingers of possible cuttings as defined by the side-scan sonar data. Transect NF-2 passed about 200 m to the southwest from wellsites with a little less than half of the transect over bottom classified as possible cuttings based on the side-scan sonar (**Figure 7.4**). Additional samples were collected along three far-field transects (FF1, FF4, and FF5) located at least 10 km from the near-field (**Figure 7.6**).

## 7.2.2 Camera Operation and Field Sampling

A Benthos Model 3731 sediment profile camera was used to collect images (see *Chapter 2*, Figure 2.9). The profile camera works like an inverted periscope with a deep-sea 35-mm camera mechanism mounted horizontally inside a water-tight housing on top of a wedge-shaped prism. The prism has a Plexiglas® faceplate at the front with a mirror placed at a 45° angle at the back. The camera lens looks down at the mirror, which is reflecting the image from the faceplate. The prism has an internal strobe mounted inside at the back of the wedge to provide illumination for the image; this chamber is filled with distilled water, so the camera always has an optically clear path to shoot through. This wedge assembly is mounted on a moveable carriage within a stainless steel frame. The frame is lowered to the seafloor on a winch wire, and the tension on the wire keeps the prism in its “up” position. When the frame comes to rest on the seafloor, the winch wire goes slack, and the camera prism descends into the sediment at a slow, controlled rate by the dampening action of a hydraulic piston so as not to disturb the sediment-water interface. On the way down, it trips a trigger that activates a time-delay circuit to allow the prism to penetrate the seafloor before any image is taken. The knife-sharp edge of the prism transects the sediment, and the prism penetrates the bottom. The strobe is discharged twice with each lowering to obtain two cross-sectional images of the upper 20 cm of the sediment column. After the two replicate images are obtained at the first location, the camera is then raised up about 2 to 3 m off the bottom to allow the strobe to recharge. The strobe recharges within 5 seconds, and the camera is ready to be lowered again for another two images. When the camera is raised between photographs, a wiper blade cleans the faceplate. Surveys can be accomplished rapidly by “pogo-sticking” the camera across an area of seafloor while recording positional fixes on the surface vessel. The resulting images give the viewer the same perspective as looking through the side of an aquarium half-filled with sediment.



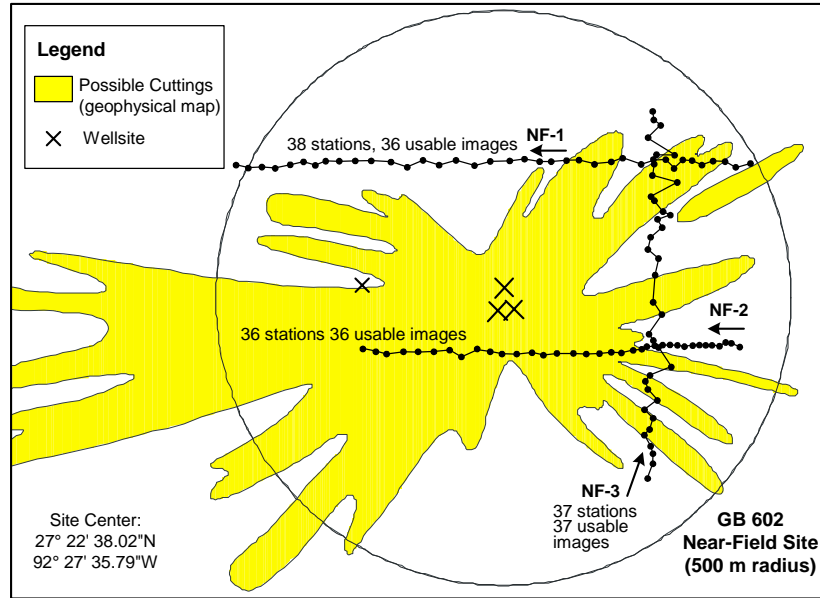


**Figure 7.3.** Locations of sediment profile imaging (SPI) transects at Garden Banks Block 602 near-field site on Cruise 2B (July 2001). Arrows indicate transect direction, and dots are sequentially numbered SPI stations. Geophysically mapped areas of possible cuttings (see *Chapter 4*) are also shown.

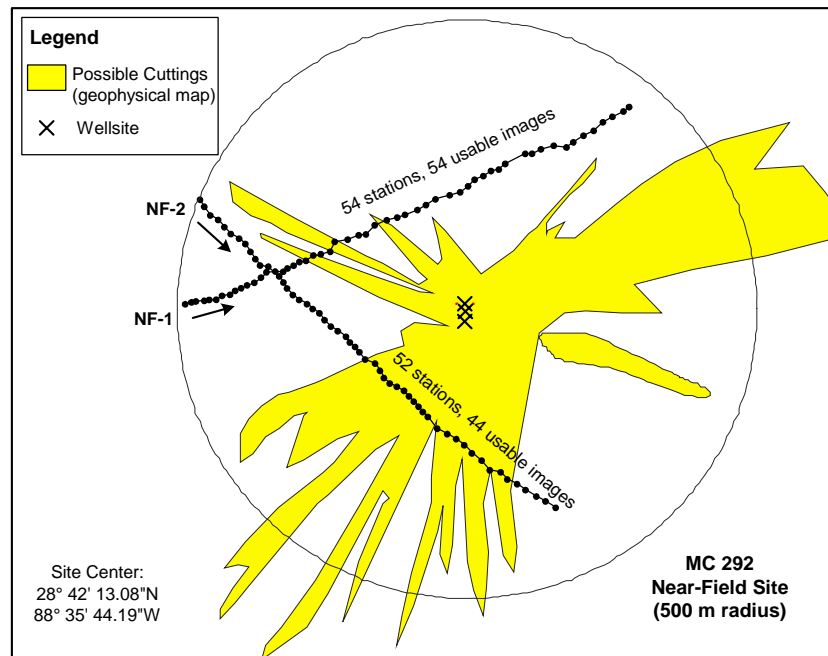


**Figure 7.4.** Locations of sediment profile imaging (SPI) transects at Mississippi Canyon Block 292 near-field site on Cruise 2B (July 2001). Arrows indicate transect direction, and dots are sequentially numbered SPI stations. Geophysically mapped areas of possible cuttings (see *Chapter 4*) are also shown.

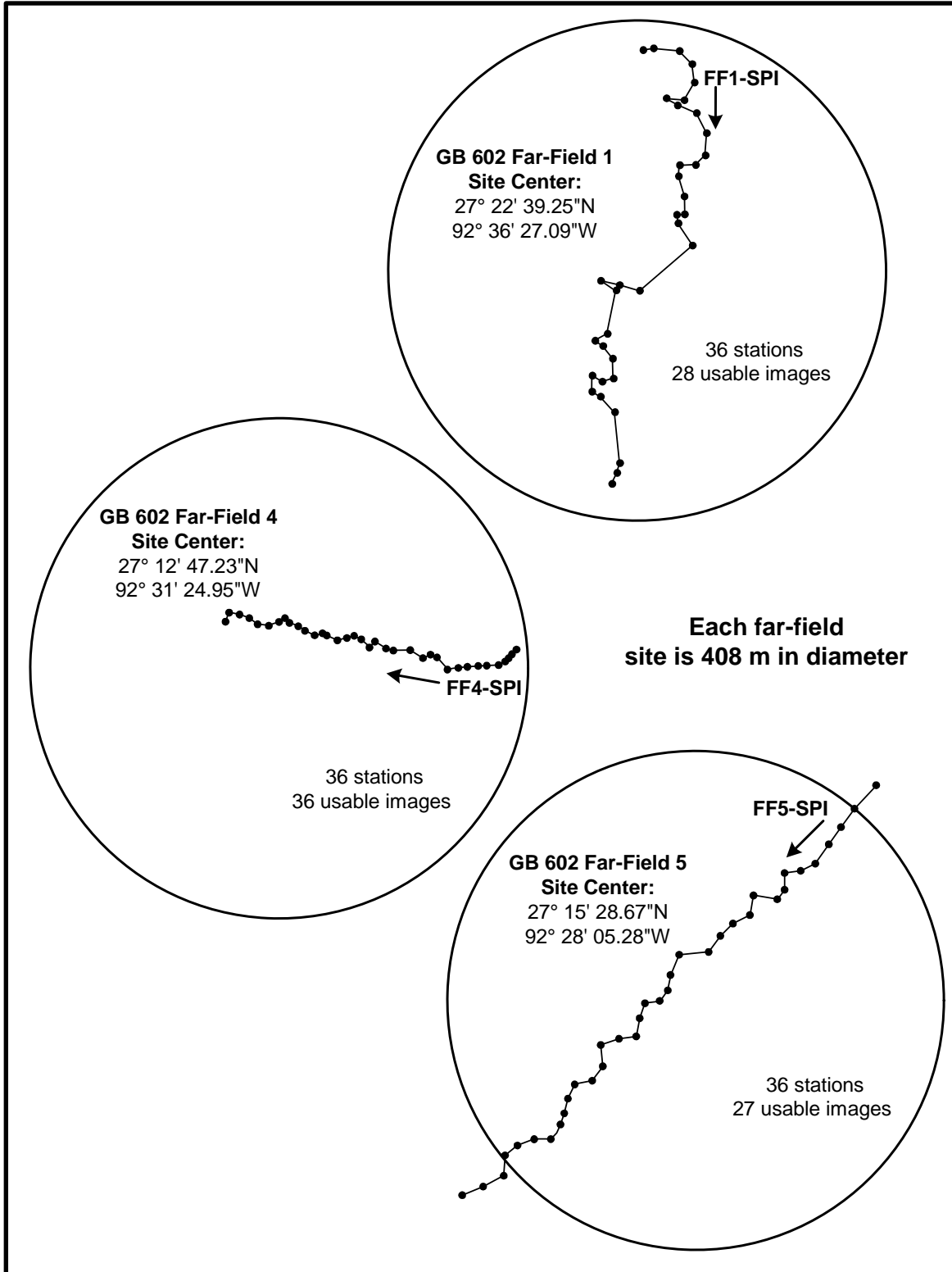


**Figure 7.5.** Locations of sediment profile imaging (SPI) transects at Garden Banks Block 602 far-field sites on Cruise 2B (July 2001). Arrows indicate transect direction, and dots are sequentially numbered SPI stations.

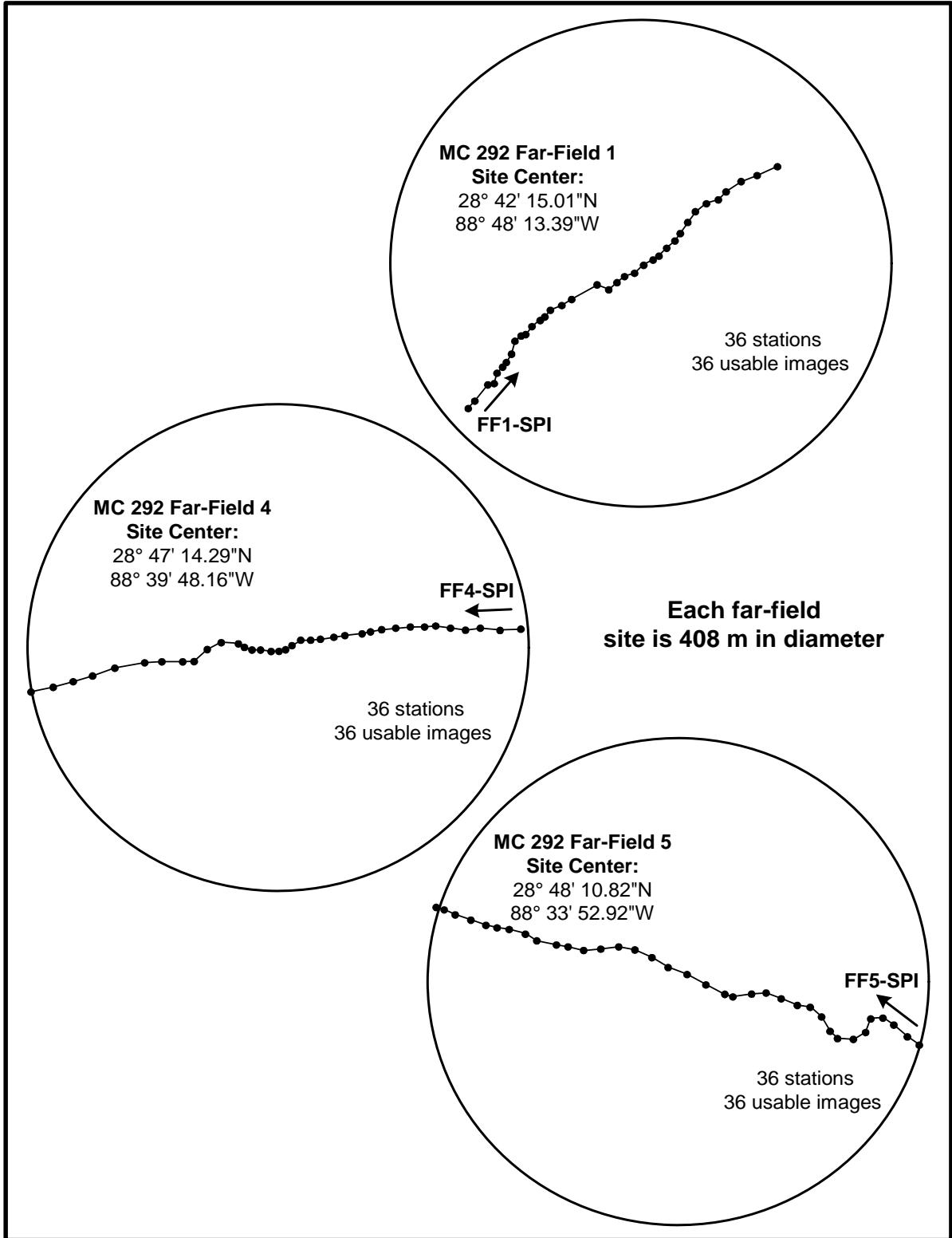


**Figure 7.6.** Locations of sediment profile imaging (SPI) transects at Mississippi Canyon Block 292 far-field sites on Cruise 2B (July 2001). Arrows indicate transect direction, and dots are sequentially numbered SPI stations.

Kodak Ektachrome® color slide film (ISO 200) was used throughout the survey. At the beginning of each survey day, the time on the camera's internal data logger was synchronized with the internal clock on the computerized navigation system being used to conduct the survey. A Benthos Model 2216 Deep Sea Pinger was attached to the camera frame and wired to the camera housing; when the strobe discharged, the ping rate doubled for 10 seconds. By monitoring the pinger signals through the use of a hydrophone on the research vessel, the scientist operating the camera was able to verify that a picture had been taken at each station. After the ship got into position at the start of a camera transect sampling line, the camera was lowered to the bottom and remained near the bottom until all the stations along the transect had been sampled. Each SPI replicate is identified by the time recorded on the film and on disk along with vessel position. Even though multiple images were taken at each location, each image was assigned a unique frame number by the data logger and cross-checked with the time stamp in the navigational system's computer data file. Redundant sample logs were kept by the field crew.

Test exposures of the Kodak® Color Separation Guide (Publication No. Q-13) were fired on deck at the beginning and end of each roll of film to verify that all internal electronic systems were working to design specifications and to provide a color standard against which final film emulsion can be checked for proper color balance. Charged spare batteries were carried in the field at all times to ensure uninterrupted sample acquisition. After deployment of the camera at each station, the frame counter also was checked to ensure that the requisite number of replicates had been taken at each location. In addition, a prism penetration depth indicator on the camera frame was checked to verify that the optical prism had actually penetrated the bottom to a sufficient depth to acquire a profile image. If images were missed (frame counter indicator), additional replicates were taken.

### **7.2.3 Image Analysis**

Sediment profile images were analyzed visually by projecting the images and recording all features seen into a preformatted standardized spreadsheet file. The images were then digitized using a Nikon LS-2000 scanner and analyzed using Adobe® PhotoShop®, Image Pro®, and the public domain Image program (available through the National Technical Information Service). Steps in the computer analysis of each image were standardized and followed the basic procedures in Viles and Diaz (1991). Data from each image were sequentially saved to a spreadsheet file for later analysis. Details of how these data were obtained can be found in Diaz and Schaffner (1988) and Rhoads and Germano (1986). Two derived image parameters, estimated infaunal successional stage and the organism-sediment index (OSI) (see Rhoads and Germano 1986), were not calculated because of the uniformity of images and general lack of biogenic activity. A summary of major parameters measured follows.

#### *7.2.3.1 Prism Penetration*

This parameter provided a geotechnical estimate of sediment compaction with the profile camera prism acting as a dead weight penetrometer. The further the prism entered into the sediment, the softer the sediments, and presumably the higher the water content. Penetration was measured as the distance the sediment moved up the 23-cm length of the faceplate. The weight on the camera frame was kept at 90 kg, so prism penetration provided a means for assessing the relative compaction between stations.

### *7.2.3.2 Surface Relief*

Surface relief or boundary roughness was measured as the difference between the maximum and minimum distance the prism penetrated. This parameter also estimated small-scale bed roughness, on the order of the prism faceplate width (16.5 cm). The origin of bed roughness can be determined from visual analysis of the images. In physically dominated habitats, features such as bedforms and sediment granularity cause bed roughness. In biologically dominated habitats, bed roughness is a result of biogenic activity such as tube structures, defecation mounds, feeding pits, or epifaunal organisms such as hydroids.

### *7.2.3.3 Apparent Color Redox Potential Discontinuity Layer*

This parameter is an important estimator of benthic habitat quality (Rhoads and Germano 1986; Diaz and Schaffner 1988; Nilsson and Rosenberg 2000), providing an estimate of the depth to which sediments appear to be oxidized. The term apparent is used in describing this parameter because no actual measurement was made of the redox potential in these samples. It is assumed that given the complexities of iron and sulfate reduction-oxidation chemistry, the reddish-brown sediment color tones (Diaz and Schaffner 1988; Rosenberg et al. 2001) indicate sediments are in an oxidative geochemical state, or at least are not intensely reducing. This is in accordance with the classical concept of RPD layer depth, which associates it with sediment color (Fenchel 1969; Vismann 1991). The apparent color RPD has been very useful in assessing the quality of a habitat for epifauna and infauna from both physical and biological points of view. Rhoads and Germano (1986), Bonsdorff et al. (1996), Nilsson and Rosenberg (2000), and Rosenberg et al. (2001) all found the depth of the RPD layer from sediment profile images to be directly correlated to the quality of the benthic habitat. These authors all found that deeper RPD layers were always associated with higher benthic habitat quality.

### *7.2.3.4 Sediment Grain Size*

Grain size is an important parameter for determining the nature of the physical forces acting on a habitat and is a major factor in determining benthic community structure (Rhoads 1974). The sediment type descriptors used for image analysis follow the Wentworth classification as described in Folk (1974) and represent the major modal class for each image. Maximum grain size also was estimated. Grain size was determined by comparison of collected images with a set of standard images for which mean grain size had been determined in the laboratory. **Table 7.1** provides phi scale sizes corresponding to sediment descriptors used in the current analysis.

**Table 7.1.** Phi scale sizes and sediment descriptors.

Phi Scale	Upper Limit Size (mm)	Grains per cm of image	SPI Descriptor	Sediment Size Class and Subclass
-6 to -8	256.0	<1	CB	Cobble
-2 to -6	64.0	<1	PB	Pebble
-1 to -2	4.0	2.5	GR	Gravel
1 to -1	2.0	5	CD	Coarse sand
2 to 1	0.5	20	MS	Medium sand
4 to 2	0.25	40	FS	Fine sand
4 to 3	0.12	80	VFS	Very fine sand
5 to 4	0.06	160	FSSI	Fine sandy silt
8 to 5	0.0039	>320	SI	Silt
6 to 5	0.0039	>320	SIFS	Silty fine sand
8 to 6	<0.0039	>320	CLSI	Clayey silt
>8 to 7	<0.0039	>320	SICL	Silty clay
>8	<0.0005	>2,560	CL	Clay

#### 7.2.3.5 Surface Features

These parameters included a wide variety of features (beds, biogenic mounds, shell, amphipod tubes, worm tubes). Each contributes information on the type of habitat and its quality for supporting benthic species. The presence of certain surface features is indicative of the overall nature of a habitat. For example, bedforms are always associated with physically dominated habitats, whereas the presence of worm tubes or feeding pits would be indicative of a more biologically accommodated habitat (Rhoads and Germano 1986; Diaz and Schaffner 1988). Surface features were visually evaluated from each image and compiled by type and frequency of occurrence.

#### 7.2.3.6 Subsurface Features

Like surface features, these parameters included a wide variety of features and revealed a great deal about physical and biological processes influencing the bottom (infauna, burrows, water-filled voids, gas voids, sediment layering). For example, habitats with grain-size layers or homogeneous color layers are generally dominated by physical processes, while habitats with burrows, infaunal feeding voids, and/or visible infauna are generally dominated by biological processes (Rhoads and Germano 1986; Diaz and Schaffner 1988; Valente et al. 1992; Nilsson and Rosenberg 2000). Subsurface features were visually evaluated from each image and compiled by type and frequency of occurrence.

#### 7.2.3.7 Statistics

For statistical analysis, each station on a transect was considered a replicate representing a sequential sampling of the given area. Analysis of variance or t-tests were used to test for differences between and within transects and areas. Normality was checked with the Shapiro-Wilk test and homogeneity of variance with Bartlett's test. Data were square-root or log

( $x + 1$ ) transformed when necessary. Data that were not normally distributed were analyzed with Kruskal-Wallis test (Zar 1999).

## 7.3 RESULTS

### 7.3.1 Garden Banks Block 602

All SPI data from GB 602 are contained in *Appendix F1*.

#### 7.3.1.1 GB 602 Near-field Transects

The three near-field transects are shown in **Figure 7.3**. Transect NF-1 contained 36 usable (i.e., image quality that allowed analysis) SPI images obtained from the 38 stations sampled. All 36 stations on Transect NF-2 had usable SPI images, and all 37 stations on Transect NF-3 had usable images. Stations along transects were spaced approximately at intervals of 30 to 50 m.

#### 7.3.1.2 GB 602 Far-field Transects

The three far-field transects are shown in **Figure 7.5**. Transect FF1 had 36 stations with 28 usable images, and all 36 stations from Transect FF4 had usable images, as did 27 of the 36 stations from Transect FF5.

#### 7.3.1.3 GB 602 Near-field Sediment Conditions

Sediment grain size at SPI stations along the GB 602 near-field transects was very uniform, with all stations being silty-clay ( $>8$  to 7 phi). While there was little variation in sediment grain size, sediment texture did vary with depth below the sediment-water interface. Deeper sediment appeared to be more compacted than surface sediments, while the upper few centimeters of the sediment appeared to have higher porosity. Sediment fabric tended to be homogeneous within a layer, which was an indication that the layers have not been significantly reworked by biogenic processes.

The most striking feature of the GB 602 near-field transects was the color layering that occurred along all three transects (**Figure 7.7**). Of the 109 near-field stations, only NF-1.13 and NF-2.04 did not have color layering. At both of these stations, the prism penetration was shallow, 5.6 cm at NF-1.13 and 2.7 cm at NF-2.04, and no layers were detected. The sediment-water interface at both stations also appeared to be disturbed, which would have destroyed surface sedimentary layering. The average number of layers per image was significantly different between transects, (Kruskal-Wallis,  $df = 2$ ,  $p = 0.013$ ) with Transect NF-1 (mean of 3.5 layers/image, 0.25 SE) having more layers per image than Transects NF-2 and NF-3 ( $2.7 \pm 0.28$  and  $2.8 \pm 0.16$ , respectively). However, there did not appear to be any broad spatial pattern to the layering (**Figure 7.7**). Along Transect NF-2, the number of layers per image was lower in the area mapped as being possible cuttings (mean of 3.3 layers/image, 0.39 SE) relative to the rest of the transect ( $2.1 \pm 0.38$ ), (t-test,  $df = 33$ ,  $p = 0.039$ ).

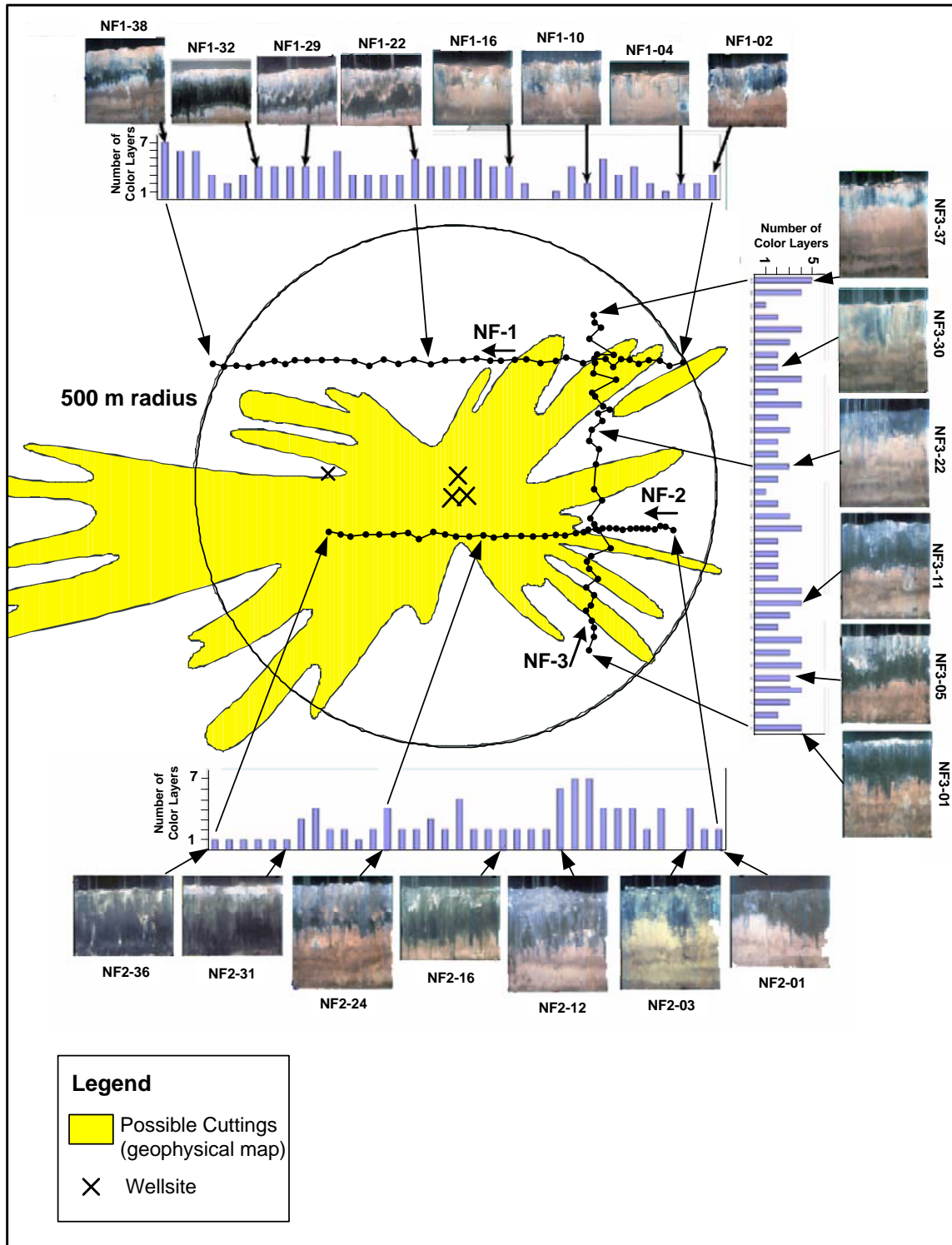


**Figure 7.7.** Number and appearance of color sediment layers at stations along GB 602 near-field transects. Dark sediment layers are likely due to deposition of cuttings and drilling mud. Arrows point to location of stations along transects. All example images are 15 cm wide.



Sediments composing the layers were light to very dark in color. The darker gray to black colors could have been an indication of the presence of cuttings and drilling mud (also see *Chapter 12*). Even though the color of the layers at the near-field varied, there did not appear to be any variation in the sediment grain size between color layers. The coarsest sediment grains appeared to be silt (4 to 8 phi) and the finest clay (>8 phi).

Many of the stations along the near-field transects had obvious signs of sediment oxygen depletion at the time of sampling. At the six stations from NF-2.31 to NF-2.36, there were indications of severe oxygen depletion, with the possible presence of bacterial mats on the sediment surface. In all cases, the whitish microbial mat on the sediment surface overlaid dark gray sediment. Under normal conditions and with an unimpacted benthic community, the depth of the RPD layer in these types of muddy sediments should have been >0.5 cm. However, 83% of the near-field stations had RPD depths of 0.5 cm or less (**Figure 7.8**). By comparison, on far-field transects, only 9% of the stations had RPD depths of 0.5 cm or less and there was no evidence of severe oxygen depletion.

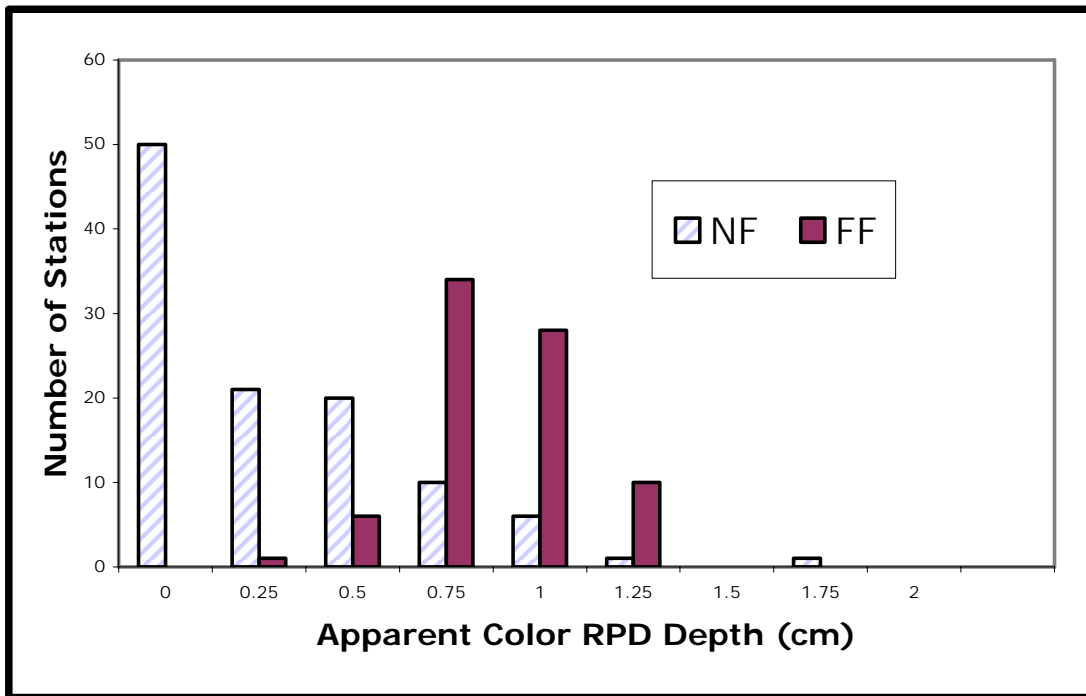


**Figure 7.8.** Histogram showing the distribution of apparent color redox potential discontinuity (RPD) layer depth for Garden Banks Block 602 near-field (NF) and far-field (FF) transects. Values for RPD are midpoint of intervals in centimeters.

There were no signs of a well developed, deep dwelling, bioturbating infauna at any of the near-field stations. There was also no indication of the presence of epifaunal organisms. Small tubes, <1 mm diameter, at the sediment-water interface were the most common biogenic structure and were present at 51% (56 of 109) of the stations along the near-field transects. No burrow structures or active feeding voids were observed at any station in the near-field or far-field, but small infaunal worms occurred at a total of six stations (NF-2.11, NF-2.23, NF-2.29, NF-3.08, NF-3.11, and NF-3.15).

Overall, sediment color, fabric, and microstratigraphy at stations taken along all three near-field transects (NF-1, NF-2, and NF-3) were similar, suggesting that drilling muds and cuttings were widespread and present at all sampled stations.

#### 7.3.1.4 GB 602 Far-field Sediment Conditions

Sediment grain size at SPI stations along the GB 602 far-field transects also was very uniform, with all stations being silty-clay (>8 to 7 phi). Overall, the stations along the far-field transects appeared to have a higher clay content relative to the near-field transects. Based on the sediment grain-size analysis from box core samples, the average grain-size for GB 602 far-field stations was 9.8 phi and 8.3 phi for near-field stations (see *Chapter 5*). Sediment fabric of the far-field station was also homogeneous, with little evidence of the presence of a bioturbating infauna. Even though layered, surface sediments appeared to be just as compact as deeper sediments.

Relative to the near-field, the most striking feature of the GB 602 far-field transects was the lack of dark color layering. Unlike the near-field transects, which had prominent dark color layering, sediments on the far-field transects were more uniform in color. Layers that did occur were various tones of reddish-brown along all three transects and not the dark gray layer that was interpreted as indicative of cuttings or drilling muds on the near-field transects (**Figure 7.9**).

Of the 91 far-field stations, 79% (71 stations) had some evidence of color layering. For comparison, 98% of the near-field stations had color layering. Transect FF1, located about 15 km west of the near-field site, had the least number of layers, with only one layer at 19 stations. At the other nine stations on Transect FF1, no layers were detected. The average number of layers per image was significantly different between transects (Kruskal-Wallis,  $df = 2$ ,  $p = <0.0001$ ), with Transect FF1 (mean of 0.7 layers/image, 0.09 SE) having fewer layers per image than Transect FF5 ( $2.4 \pm 0.16$ ), which in turn had fewer layers than Transect FF4 ( $1.3 \pm 0.21$ ). Transect FF5 was about 13 km south, and Transect FF4 was about 19 km south of the near-field site. Within a far-field transect, there did not appear to be any spatial pattern to the layering.

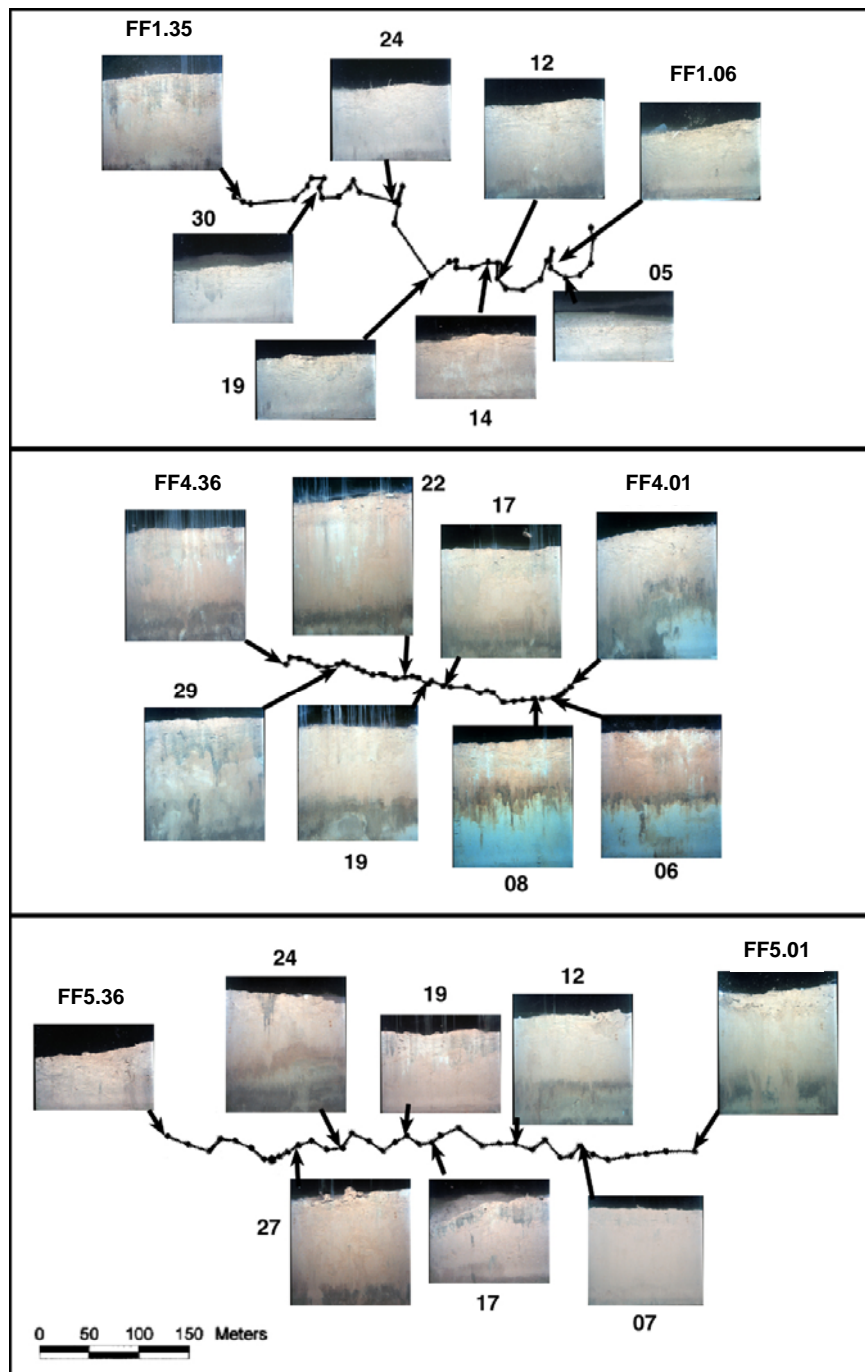


**Figure 7.9.** Appearance of color sediment layers at stations along Garden Banks Block 602 far-field transects. Transects are not in original orientation; see **Figure 7.5**. Arrows point to location of stations along transects. All example images are 15 cm wide.

At the first four stations (FF4.1, FF4.6, FF4.7, and FF4.8) along the eastern end of Transect FF4, there appeared to be some variation in the sediment grain size between color layers. Surface sediment layers appeared to be siltier than deeper sediment layers, with the deeper layers having higher clay content. The deeper sediments also were bluer-gray in color at these four stations (**Figure 7.9**). Sediments along Transect FF1 were similar between stations, being uniformly light reddish-brown. Surface sediments along Transect FF5 were similar in color to the other two transects, but deeper sediments tended to be darker brown. There was no dark gray sediment at the far-field sites.

The color layers at the far-field transects tended to be thicker than the near-field transects. Layers at Transects FF1 and FF5 were thicker than all other transects (Kruskal-Wallis,  $df = 5$ ,  $p = <0.0001$ ), and Transect NF-1 had significantly thinner layers than all other transects (**Figure 7.10**). The larger number of thinner layers in the near-field may be an indication of multiple disturbance events associated with oil and gas development activities. Thicker and less color differences between layers in the far-field may be more representative of natural sedimentary conditions.

There were few indications of the presence of infaunal organisms and no epifauna observed at far-field stations. Infaunal organisms were observed at only four far-field stations (FF1.19, FF1.21, FF4.07, and FF4.10). Tubes at the sediment-water interface were the most common biogenic structure and were present at 48% (44 of 91) of the stations along the far-field transects. The highest number of tubes per image was 10 at FF1.19. The tubes were all small, with diameters of about 1 mm. There did not appear to be a well developed infaunal community along any of the far-field transects.

In contrast to the near-field transects, all far-field stations appeared to have oxidized sediments at the sediment-water interface. Overall, near-field RPD layers were shallower than far-field (**Figure 7.11**). The shallowness of the RPD layer ( $<0.5$  cm) at many stations indicated that bioturbation was not an important factor in mixing surface sediment. The RPD along Transect FF5 averaged 0.6 cm (0.03 SE) and averaged 0.8 cm (0.03) along both Transects FF4 and FF5. Even though the difference between the transects was small, Transect FF5 had thinner RPD layers (analysis of variance [ANOVA],  $df = 2$ ,  $p = <0.0001$ ) compared to Transects FF1 and FF4 (**Figure 7.11**).

Overall, sediment color, fabric, and microstratigraphy at stations taken along all three far-field transects (FF1, FF4, and FF5) were similar, with slightly more variation in grain size and less variation in layer color than near-field transects.

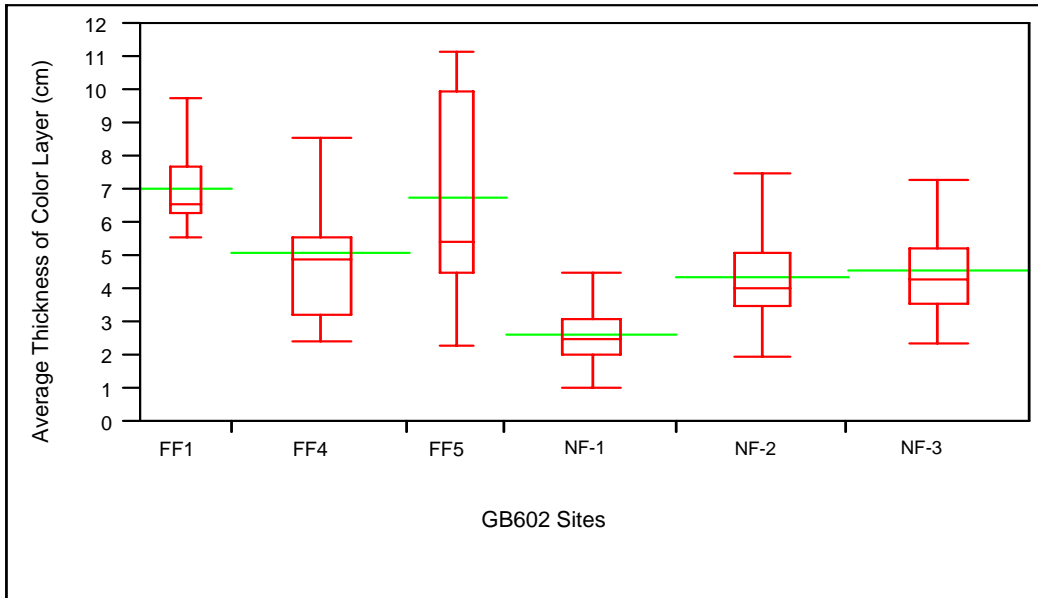


**Figure 7.10.** Average thickness of color layers (cm) at Garden Banks Block 602 sites. Box is interquartile range, tails are range, line in box is median, and line extended from box is mean, and width of box is proportional to sample size.

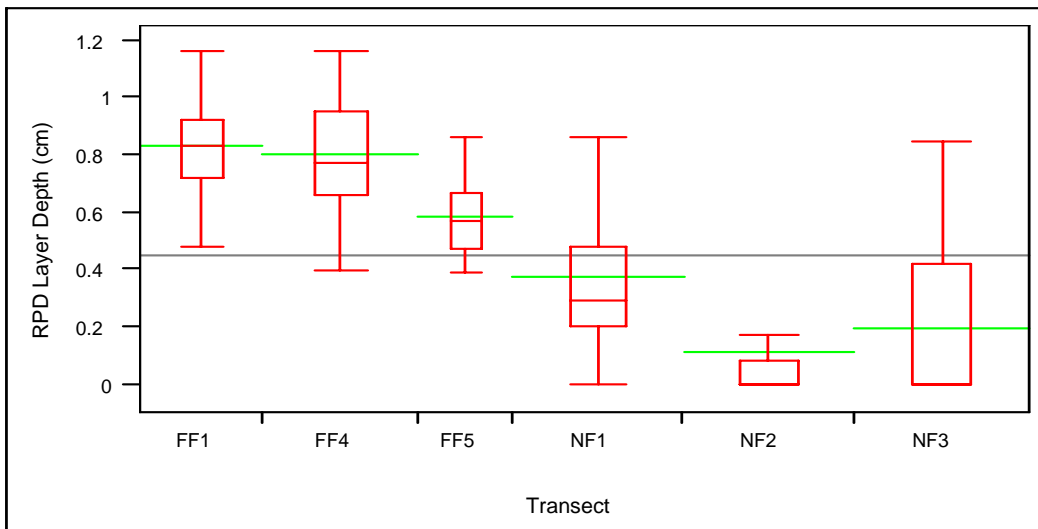


**Figure 7.11.** Average depth of apparent color redox potential discontinuity (RPD) layer (cm) at Garden Banks Block 602 far-field (FF) and near-field (NF) transects. Box is interquartile range, tails are range, line in box is median, line extended from box is mean, horizontal line is grand mean, and width of box is proportional to sample size.

### 7.3.2 Mississippi Canyon Block 292

All SPI data from MC 292 are contained in *Appendix F2*.

#### 7.3.2.1 MC 292 Near-field Transects

The two near-field transects are shown in **Figure 7.4**. Usable images were obtained from all 54 stations on Transect NF-1 and 44 of 52 stations on Transect NF-2. Toward the end of Transect NF-2, the SPI camera ran out of film, so images were not obtained from the last eight stations. Stations along transects were spaced at intervals of approximately 30 to 50 m.

#### 7.3.2.2 MC 292 Far-field Transects

The three far-field transects are shown in **Figure 7.6**. All three transects had 36 stations with 36 usable images.

#### 7.3.2.3 MC 292 Near-field Sediment Conditions

Sediment grain size at SPI stations along the MC 292 near-field transects was rather uniform, with 16 stations being silty-clay (>8 to 7 phi) and 82 being clay (>8 phi). The slightly siltier sediments tended to occur in patches along the transects. On Transect NF-1, the 10 stations from NF-1.33 to NF-1.42 were silty-clay as were the 2 stations at the eastern end of Transect NF-1. Along Transect NF-2, silty-clay occurred in two small patches, Stations NF-2.25 and NF-2.26, and NF-2.32 and NF-2.33. The texture of the silty-clay sediments was more variable with depth below the sediment-water interface. Deeper sediment appeared to be more compacted than surface sediments, while the upper few centimeters of the sediment appeared to have higher porosity. The texture of clay sediments was more uniform. Sediment fabric tended to be homogeneous for both sediment types, which was an indication that biogenic processes were not a major factor in reworking the sediments.

The most striking feature of the MC 292 near-field transects was the uniformity of the color layering that occurred along both transects (**Figure 7.12**). The only variation in the color of the layers was associated with the stations that had silty-clay sediments. At the 16 stations that were silty-clay, layering tended to be darker gray. All of the other 82 near-field stations had reddish brown color layering. (At Station NF-2.25, the sediment-water interface was disturbed and no layer could be measured).

There was little variation in the number of layers per image, with most of the near-field stations having one. All stations on Transect NF-2 and all but 12 stations on Transect NF-1 had one layer. The 12 stations with 2 layers were also those with silty-clay sediments and concentrated from the midpoint to the eastern end of Transect NF-1 (**Figure 7.12**).

Sediments composing the layers were reddish brown and darker in hue than underlying sediments, which were light grayish. The darker gray to black colored sediments along Transect NF-1 could be an indication of the presence of cuttings and drilling mud (also see *Chapter 12*). While the clay content of sediments appeared to be very high at all stations, those stations with darker gray layers appeared to be slightly coarser (siltier).

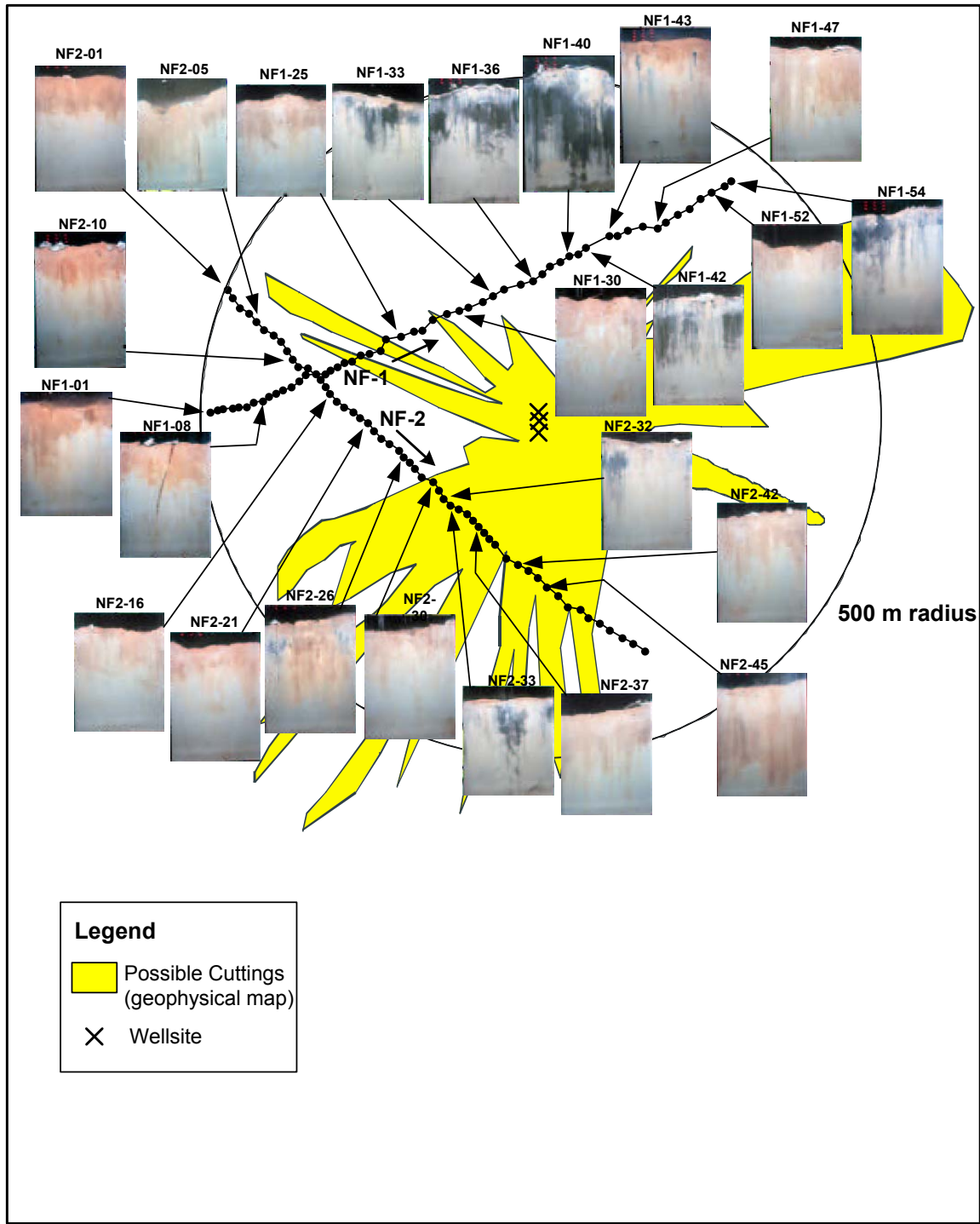


**Figure 7.12.** Appearance of color sediment layers at stations along Mississippi Canyon Block 292 near-field transects. Dark sediment layers are likely due to deposition of cuttings and drilling mud. Arrows point to location of stations along transects. All example images are 15 cm wide.

The distribution of the apparent color RPD layer depth suggests that sediment oxygen levels may have been low at some of the silty-clay stations along Transect NF-1 (Stations NF-1.34, NF-1.35, NF-1.36, NF-1.38, NF-1.39, and NF-1.40). None of the stations along near-field Transect NF-2 or any of the far-field transects had obvious signs of oxygen depletion at the time of sampling. Under normal conditions and with an unimpacted benthic community, the depth of the RPD layer in these types of muddy sediments should have been  $>0.5$  cm (**Figure 7.13**). The distribution of RPD layer depths between near-field and far-field transects was similar, except for the shallowest values occurring along Transect NF-1 (**Figures 7.12 and 7.13**). While some evidence of infaunal activity (infauna, burrows, tubes, and feeding voids) was observed at 82% (80 of 98) of the near-field stations, there did not appear to be a well developed bioturbating benthic community. The clayey sediments did not appear to be biogenically mixed. There were signs of deep dwelling infauna at 21% (21 of 98) of the near-field stations, with infauna occurring from 0.3 to 13.2 cm below the sediment-water interface. There was no indication of the presence of epifaunal organisms on the sediment surface at any near-field station. Small tubes,  $<1$  mm diameter, at the sediment-water interface were the most common biogenic structure and were present at 70% of the stations along the near-field transects. Burrow structures were observed at 22% of near-field stations. The largest burrow at the MC 292 site was observed at Station NF-1.08 (**Figure 7.14**). Only Station NF-2.07 appeared to have an active feeding void.

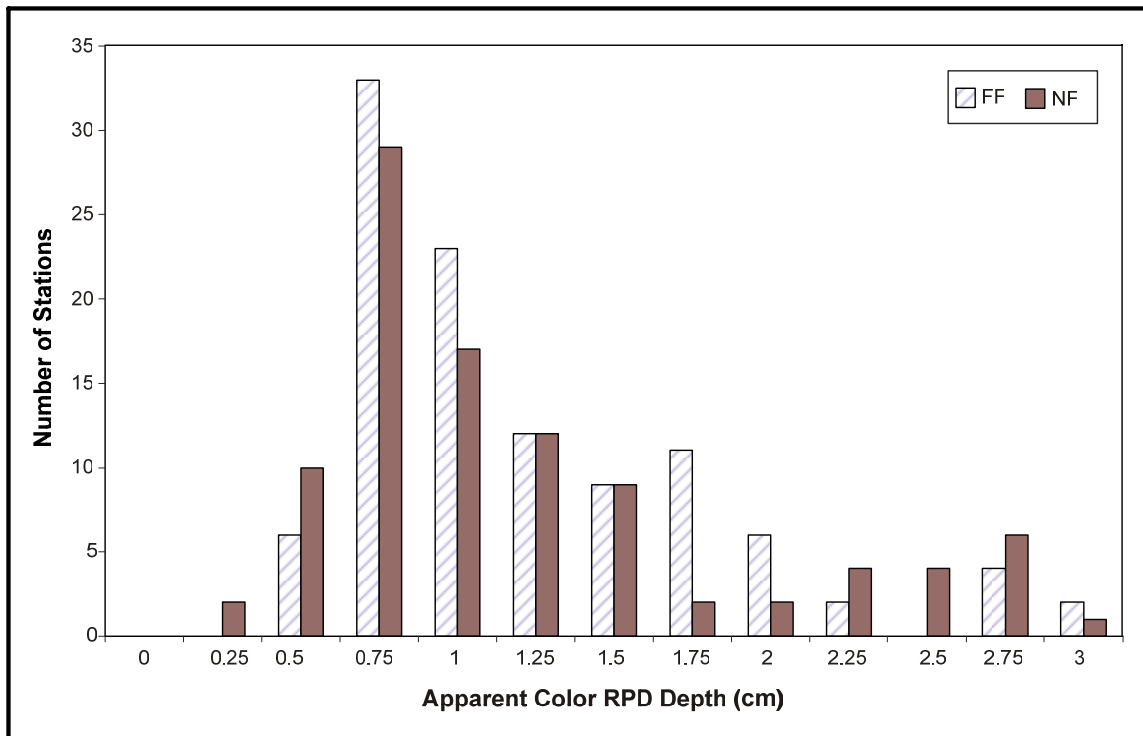


**Figure 7.13.** Histogram showing the distribution of apparent color redox potential discontinuity (RPD) layer depth for Mississippi Canyon Block 292 near-field (NF) and far-field (FF) transects. Values for RPD are mid-point of intervals in centimeters.





**Figure 7.14.** Sediment profile imaging image from Mississippi Canyon Block 292, Station NF-1.08, showing a large burrow structure near the center and extending down from sediment-water interface to bottom of image. Image is 15 cm wide.

Overall, sediment color, fabric, and microstratigraphy at stations taken along all two near-field transects (NF-1 and NF-2) could be divided into two classes that may be related to the presence/absence of drilling muds and cuttings. The largest class of stations (80 of 98) had reddish-brown surficial sediments overlaying light grayish clayey sediments. The smaller class of stations (18 of 98) had darker gray sediments, either at or near the sediment surface, which may have been due to the presence of drilling muds and cuttings. The difference in these two classes can be seen in **Figure 7.12**.

#### 7.3.2.4 MC 292 Far-field Sediment Conditions

Sediment grain size and texture at SPI stations along the MC 292 far-field transects was very uniform, with all stations being clay (>8 phi) and having a consistent texture with depth from the

sediment surface. Sediment fabric was also homogeneous with depth from the sediment surface, indicating that the level of biogenic activity was not sufficient to significantly rework and mix the sediments.

Overall, the stations along the far-field transects appeared to have a slightly higher clay content relative to some of the stations on near-field transects. Based on the sediment grain size analysis from box core samples, the average grain size for MC 292 was 9.9 phi for far-field stations and 9.6 phi for near-field stations (see *Chapter 5*). Sediment fabric of the far-field stations was also homogeneous, with little evidence of the presence of bioturbating infauna.

Relative to the near-field, the most striking feature of the MC 292 far-field transects was the lack of dark color layering. Unlike the near-field transects, which did have stations with prominent dark color layering, sediments on the far-field transects were uniform in color. Layering that did occur was various tones of reddish-brown along all three transects and not the darker gray layering that was interpreted as indicative of cuttings or drilling muds along the near-field transects (**Figure 7.15**). While all of the 108 far-field stations had evidence of color layering with all but 1 station having one layer (the exception was FF1.10, which had 2 layers), there was little variation in sediments between transects (**Figure 7.15**).

The clayey sediment station in the near-field and far-field appeared to be similar in color, texture, and fabric (**Figures 7.12 and 7.15**). Within and between far-field transects, there did not appear to be any spatial pattern relative to sediment properties. Thus, sediments over the entire MC 292 study area may be similar, with the exception of the silty-clay near-field stations, which may have drilling muds and cuttings present. Far-field Transect FF1 was located about 20 km west of the MC 292 near-field site, Transect FF4 about 11 km northwest, and Transect FF5 about 11 km to the north.

The thickness of color layers at near-field and far-field transects was different for only Transect NF-2, which had thicker color layers than all other transects (Kruskal-Wallis,  $df = 4$ ,  $p = <0.0001$ ). Layers at far-field transects tended to have a narrower range than near-field transects (**Figure 7.16**). This difference between near- and far-field for MC 292 is reversed from GB 602, where far-field layers were thicker. This may be a reflection of the fact that most of the MC 292 near-field stations did not appear to be impacted by drilling mud and cuttings.

There was evidence of infaunal activity (infauna, burrows, tubes, and feeding voids) observed at 76% (82 of 108) of the far-field stations, but there did not appear to be a well developed bioturbating benthic community. The clayey sediments did not appear to be biogenically mixed. There were signs of deep dwelling infauna at 31% (33 of 108) of the far-field stations, with infauna occurring from 1.1 to 14.2 cm below the sediment-water interface. There was only one visible epifaunal organism on the sediment surface at Station FF1.16. This organism appeared to be a small hexacoral (**Figure 7.17a**). Small tubes, <1 mm diameter, at the sediment-water interface were the most common biogenic structure and were present at 61% of the stations along the far-field transects (**Figure 7.17b**). Burrow structures were observed at 15% of far-field stations. Only three stations (FF1.21, FF1.25, and FF5.25) appeared to have an active feeding void. The largest void was observed at Station FF5.25 (**Figure 7.17b**).

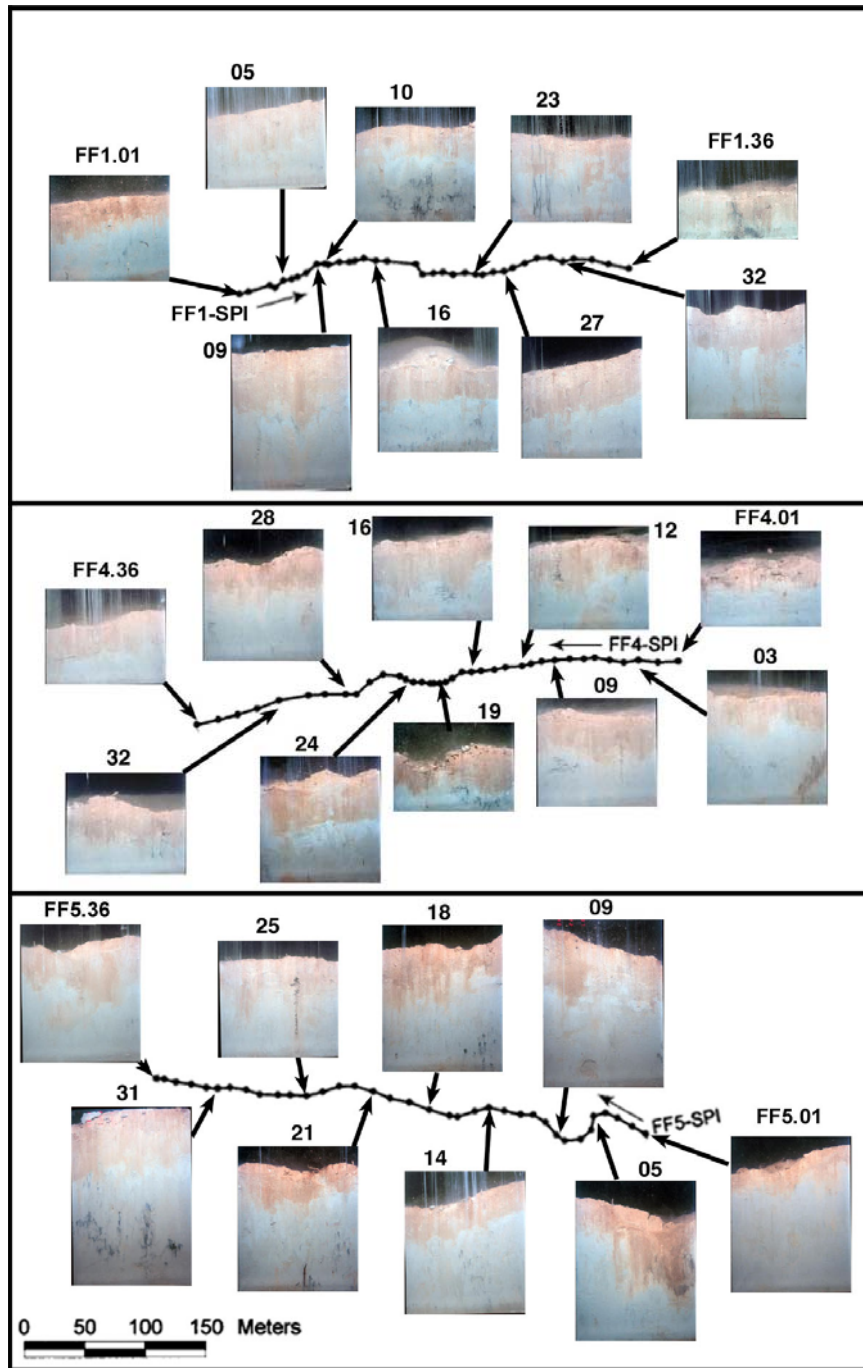


**Figure 7.15.** Appearance of color sediment layers at stations along Mississippi Canyon Block 292 far-field transects. Transects are not in original orientation (see **Figure 7.6**). Arrows point to location of stations along transects. All example images are 15 cm wide.

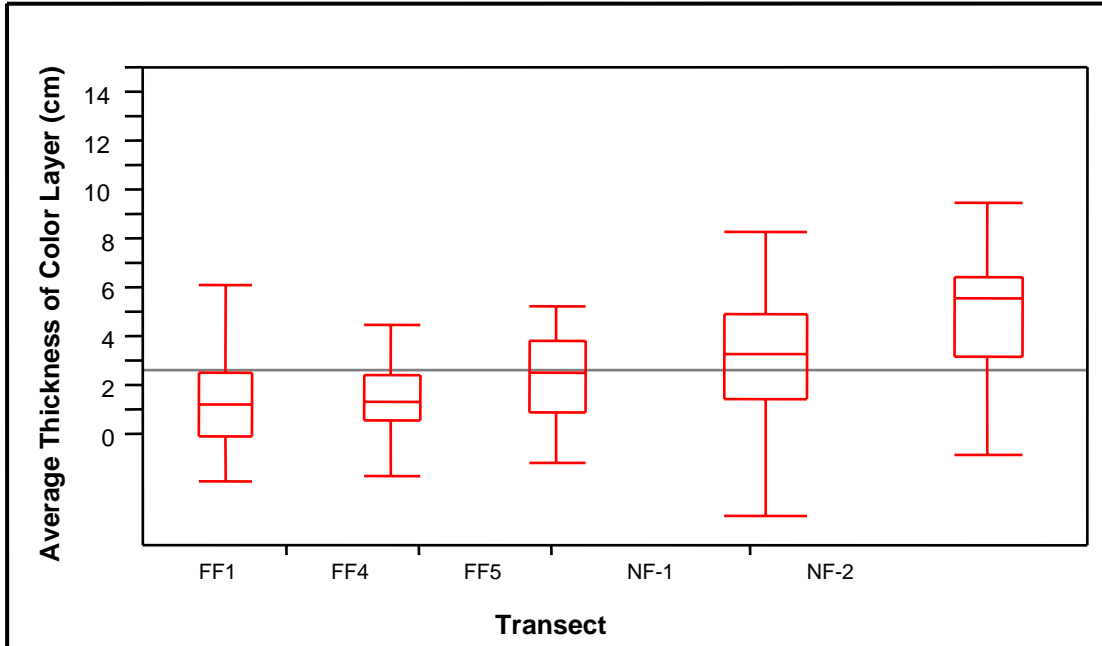


**Figure 7.16.** Average thickness of color layers (cm) at Mississippi Canyon Block 292 sites. Box is interquartile range, tails are range, line in box is median, line extended from box is mean, and width of box is proportional to sample size.

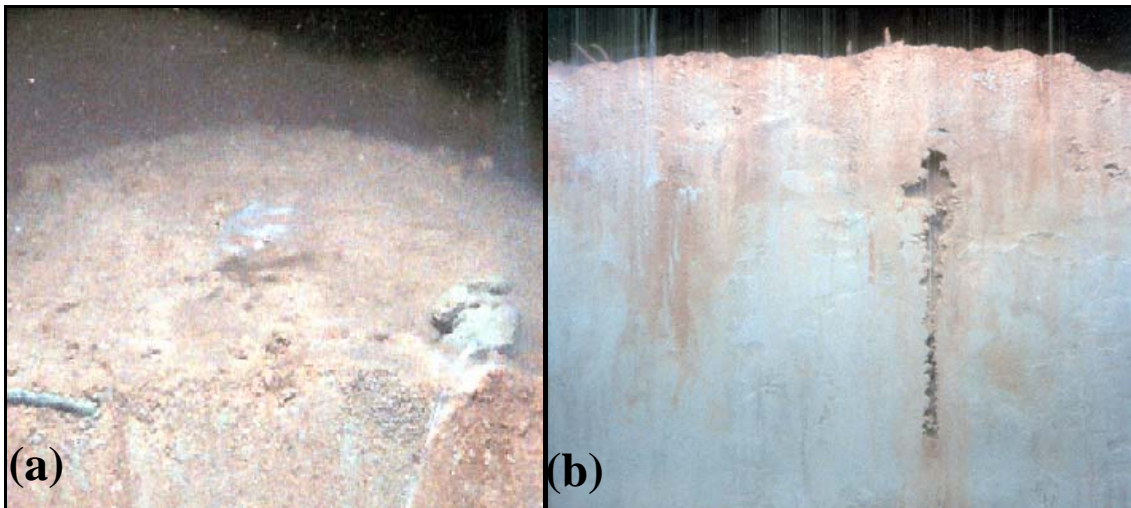


**Figure 7.17.** Fauna from Mississippi Canyon Block 292. a: Hexacoral (center of image) at Station FF1.16. Image is 5 cm wide. b: Small tubes at sediment-water interface and large oxic feeding void at Station FF5.25. Image is 15 cm wide.

In contrast to the near-field transects, all far-field stations appeared to have oxidized sediments at the sediment-water interface. The thickness of the RPD layers at far-field stations indicated that bioturbation was an important factor in mixing surface sediment (**Figure 7.13**). The RPD layers along Transect FF5 were deeper than at Transects FF1 and FF4 and averaged 1.6 cm (0.09 SE), (ANOVA,  $df = 2$ ,  $p = <0.0001$ ). Along Transect FF4, the RPD layer depth averaged 1.0 cm (0.10) and 0.7 cm (0.10) along Transect FF1 (**Figure 7.18**). RPD layer depths at the near-field were not significantly different than far-field transects (**Figure 7.18**).

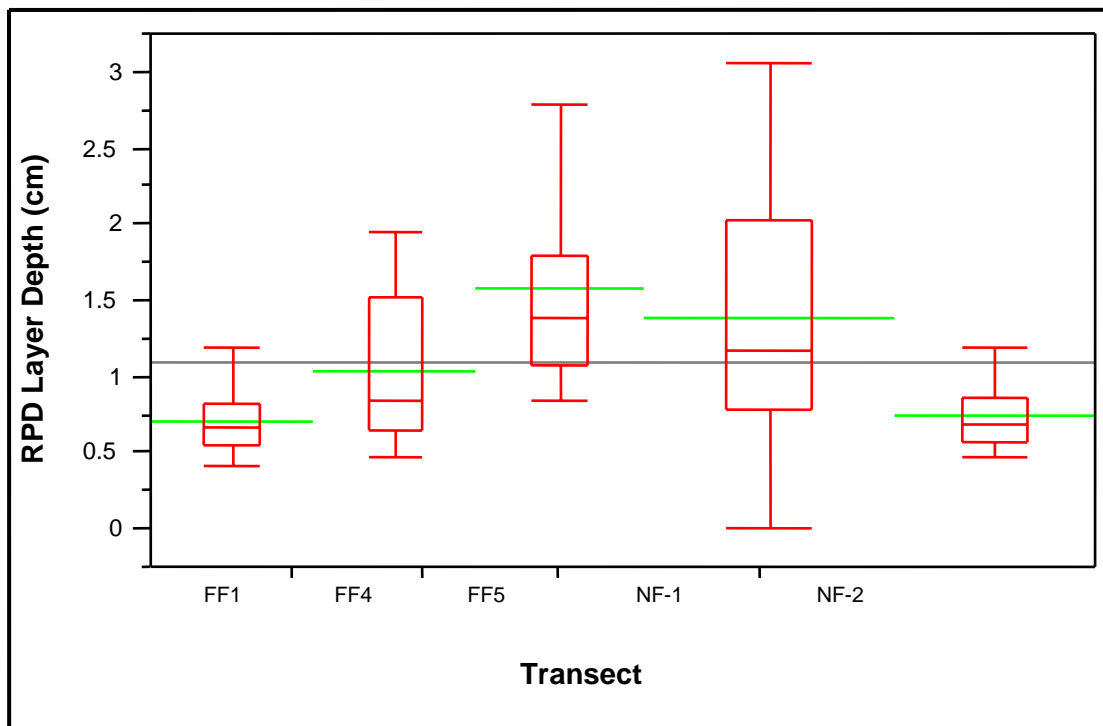


**Figure 7.18.** Average depth of apparent color redox potential discontinuity (RPD) layer (cm) at Mississippi Canyon Block 292 far-field (FF) and near-field (NF) transects. Box is interquartile range, tails are range, line in box is median, line extended from box is mean, horizontal line is grand mean, and width of box is proportional to sample size.

Overall, sediment color, fabric, and microstratigraphy at stations taken along all three far-field transects (FF1, FF4, and FF5) were similar, with no apparent variation in grain size or in layer color.

## 7.4 DISCUSSION

### 7.4.1 Garden Banks Block 602

The sediment type at GB 602 stations was uniform, with all near-field and far-field stations being silty-clay (>8 to 7 phi), but the appearance of near-field and far-field stations was different in terms of the color and number of sedimentary layers (**Figures 7.7 and 7.8**). Near-field layers were dark gray in color, which was consistent with the presence of drilling muds and cuttings (see

*Chapters 4 and 8*). Layers at the far-field stations were reddish-brown and appeared to be similar to surficial sedimentary layers in other silty-clay deep-sea habitats (Diaz et al. 1994).

Sediment oxygen levels may have been low at 83% of the near-field stations at the time of sampling. The six stations from NF-2.31 to NF-2.36 appeared to be affected by severe oxygen depletion, with the possible presence of bacterial mats on the sediment surface. At the far-field transects, only 9% of the stations appeared to be hypoxic, with no evidence of severe oxygen depletion.

There were no signs of a well developed, deep dwelling, bioturbating infauna at any of the near-field stations. Infauna and biogenic structures were more common at far-field stations but were still not sufficient to bioturbate sediments. Sediment fabric tended to be homogeneous within the color layers, which also was an indication that the layers have not been significantly reworked by biogenic processes.

#### **7.4.2 Mississippi Canyon Block 292**

The sediment type at MC 292 near-field stations varied over a narrow range of silty-clay (>8 to 7 phi) to clay (>8 phi), with most stations being clay. All far-field stations were clay. The appearance of all near-field and far-field stations was similar, with the exception of 16 near-field silty-clay stations, which had darker gray colored layers (**Figures 7.12 and 7.15**). Layers at all other MC 292 stations were reddish-brown and appeared to be similar to surficial sedimentary layers in other silty-clay deep-sea habitats (Diaz et al. 1994).

The darker gray to black colored sediments at some of the near-field stations could indicate the presence of cuttings and drilling mud. There was little variation in the number of layers per image, with most of the near-field and all of the far-field stations having one. Stations with two layers were also those with silty-clay sediments. Based on the apparent color RPD layer depth, bottom water may have been hypoxic at some of the silty-clay near-field stations. None of the other near-field or far-field stations had obvious signs of oxygen depletion at the time of sampling.

While evidence of infaunal activity (infauna, burrows, tubes, feeding voids) was observed at 82% of near-field and 76% of far-field stations, there did not appear to be a well developed bioturbating benthic community. The clayey sediments did not appear to be biogenically mixed as the sediment fabric was homogeneous with depth from the sediment surface, indicating that the level of biogenic activity was not sufficient to significantly rework and mix the sediments.

### **7.5 CONCLUSIONS**

#### **7.5.1 Garden Banks Block 602**

All the near-field stations at GB 602 appeared to be impacted from oil and gas development activities. Sediment color, fabric, and microstratigraphy at near-field stations were all similar and consistent with the presence of drilling muds and cuttings. At far-field stations, sediment color, fabric, and microstratigraphy were similar, with slightly more variation in grain size and reddish-brown layers consistent with background sedimentary conditions. While it appeared that

oil and gas development impacts did extend outside the boundary of the GB 602 near-field site, impacts did not extend out to the far-field sites.

### **7.5.2 Mississippi Canyon Block 292**

At MC 292, sediment color, fabric, and microstratigraphy at near-field stations could be divided into two classes that may be related to the presence/absence of drilling muds and cuttings. The largest class, 82% of stations, had reddish-brown surficial sediments overlaying light grayish clayey sediments. The smaller class, 18% of stations, had darker gray sediments, either at or near the sediment surface, which are interpreted as indicating the presence of drilling muds and cuttings. The difference in these two classes can be seen in **Figure 7.12**. At all far-field stations, sediment color, fabric, and microstratigraphy were similar, with no apparent variation in grain size or in layer color consistent with background sedimentary conditions. It appeared that oil and gas development impacts did not extend to the far-field sites.

## Chapter 8 Metals, Total Organic Carbon, and Redox Conditions in Sediments

*John H. Trefry, Robert P. Trocine,  
Robert D. Rember and Michelle L. McElvaine  
Florida Institute of Technology*

---

### 8.1 INTRODUCTION

The chemistry study described in this chapter was designed to help identify spatial and temporal trends in (1) the presence of drilling discharges and (2) redox conditions in sediments at each site. The supporting data set is quite diverse and includes the following: (1) data for 13 metals: aluminum (Al), arsenic (As), barium (Ba), cadmium (Cd), chromium (Cr), copper (Cu), iron (Fe), mercury (Hg), manganese (Mn), nickel (Ni), lead (Pb), vanadium (V), and zinc (Zn), and total organic carbon (TOC) in sediments, (2) data for 11 metals in biota (As, Ba, Cd, Cr, Cu, Fe, Hg, Ni, Pb, V, and Zn), (3) sedimentation rates, (4) vertical profiles for dissolved oxygen and redox potential (Eh) in sediment, and (5) data for selected redox-active chemicals in interstitial water. The data set is summarized by site and cruise for each sample type in **Table 8.1**. The complete data set is tabulated by cruise in *Appendix G*.

Concentrations of metals and TOC in sediments provide information about sediment composition, redox state, and the presence of drilling discharges or other anthropogenic inputs. Aluminum is a good indicator of the relative abundance of clay minerals and other aluminosilicates. The Al content of suspended sediment introduced to the Gulf of Mexico by the Mississippi River averages ~8.6% (Trefry and Presley 1982). Concentrations of Ba help identify the presence of drilling discharges because barite ( $\text{BaSO}_4$ ) is a common component of drilling fluids. Elevated levels of Ba in sediments, in the absence of SBFs, help support the presence of water-based drilling mud. Concentrations of Fe generally correlate well with concentrations of Al and support identification of the terrigenous fraction of sediment. Manganese is a redox-sensitive metal that can be depleted in nearshore, reducing sediments relative to Mississippi River suspended sediment, and greatly enriched in slowly accumulating and oxidizing slope sediments relative to river suspended sediments (Trefry and Presley 1982). Concentrations of TOC vary with sediment accumulation rate and biological productivity in the overlying water column. The rate of accumulation of organic carbon plays a role in controlling the redox state of the sediment. The other nine metals (As, Cd, Cr, Cu, Hg, Ni, Pb, V, and Zn) are naturally occurring in sediments from the Gulf of Mexico, with any enrichment due to a variety of possible sources. For example, concentrations of Hg may be elevated in sediments around drilling sites due to inputs of  $\text{BaSO}_4$ , in which Hg is a natural impurity (Trefry et al. 2003). Concentrations of Pb and Zn can be elevated from a variety of sources including pipe dope used during drilling operations.

Both surface samples (0 to 2 cm) and sediment cores (0 to 10 cm) were collected for this study. The cores provide information on the thickness of layers containing Ba or SBF. A few representative cores were age-dated using  $^{137}\text{Cs}$  and excess  $^{210}\text{Pb}$  techniques.



**Table 8.1.** Number of samples collected and analyzed for various parameters at each site.

Site	Cruise	Surface Sediment Metals, TOC	Sediment Cores Metals, TOC	Probe O <sub>2</sub> and Eh Profiles	Metals in Biota	(S) or (IW)
VK 916	1B	NF 12	---	NF 12	---	2 S (NF, FF)
	Pre-exploration	FF 10		FF 10		2 IW (NF, FF)
	3B	NF 12	3 NF cores	NF 13	---	2 IW (NF, FF)
	Post-exploration	FF 12	(n = 15)	FF 8		
GB 516	1B	NF 12	---	NF 12	---	1 S (FF)
	Post-exploration	FF 12		FF 11		2 IW (NF, FF)
	2B	NF 12	3 NF cores	NF 13	---	1 IW (FF)
	Post-development	FF 12	(n = 15)	FF 12		
GB 602	2B	NF 12	3 NF cores	NF 15	NF 12	1 S (FF)
	Post-development	FF 12	(n = 15)	FF 12	FF 6	2 IW (NF, FF)
MC 292	2B	NF 12	3 NF cores	NF 15	NF 12	1 S (FF)
	Post-development	FF 12	(n = 15)	FF 12	FF 12	2 IW (NF, FF)

FF = far-field; GB = Garden Banks; IW = interstitial water; MC = Mississippi Canyon; NF = near-field; S = sedimentation rate; TOC = total organic carbon; VK = Viosca Knoll.

Vertical profiles for concentrations of dissolved oxygen in sediment and the overall redox state (Eh) of the sediment column were obtained at most sites (**Table 8.1**). Concentrations of dissolved oxygen and Eh are primarily controlled by the input rate of organic matter as influenced by the following factors: (1) biological productivity in the surface water and benthic environment, (2) the rate at which terrestrial organic matter is added via rivers, and/or (3) introduction of organic matter from discharges of various municipal and industrial waste materials. Changes in redox environment at the sediment-water interface and in the upper layers of the sediment column can play a role in controlling the spatial distribution of benthic fauna. Synthetic-based drilling fluids contain hydrocarbons (olefins) that can be metabolized by sediment bacteria. The presence of this additional source of sediment organic matter may alter the background redox environment. In addition to probe measurements, more complete redox information was obtained at a few representative sites where interstitial water was collected and analyzed for dissolved Mn<sup>2+</sup>, Fe<sup>2+</sup>, ammonium (NH<sub>4</sub><sup>+</sup>), nitrate (NO<sub>3</sub><sup>-</sup>), sulfate (SO<sub>4</sub><sup>2-</sup>), phosphate (PO<sub>4</sub><sup>3-</sup>), and alkalinity. Each of these parameters provides additional information about the redox environment in the sediments.

In this chapter, the results are presented by drilling site in the following order: (1) VK 916 for pre- and post-exploratory drilling, (2) GB 516 for exploratory/development drilling, and (3) GB 602 and MC 292 for the post-development phase. In each case, results for metals and TOC are presented first. This information helps to define the sediment composition at random near-field (near-field at <1,000 m from the drilling site) and random far-field (far-field at >3 km from drilling site) locations. In some instances, sediment cores were collected at additional, fixed near-field stations, which are denoted as discretionary (DS) stations. Then, results for vertical profiles for dissolved oxygen and Eh (redox potential) in sediment cores (and pH in some cores) are introduced along with the smaller data set for sediment interstitial water. The collective data will be used to test for significant differences in sediment composition and properties (1) between near-field and far-field stations, and/or (2) between pre- and post-development as appropriate.

Samples of biota were collected only from the post-development sites (GB 602 and MC 292) and will be discussed along with other parameters for those sites. Finally, an overview section on trace metals is presented at the end of the chapter to augment information introduced in each separate section and to provide a study-wide perspective on possible metal contamination at drilling sites.

## 8.2 METHODS

### 8.2.1 Sampling and Field Measurements

Sediments were collected using a stainless steel box corer (50 cm x 50 cm x 50 cm) as described in *Chapter 2*. For metals, the surface 2 cm of sediment were removed using a Teflon<sup>®</sup> spatula and placed in a plastic vial. The vial was sealed with a layer of Parafilm<sup>®</sup> and stored frozen. At three discretionary stations from each site, the box core was carefully subsampled by pushing a 10-cm diameter Teflon<sup>®</sup> tube into the sediment. The sediment was extruded from the top, and 2-cm sections were sliced off, placed in plastic vials, and stored frozen.

One subsample from each box core was collected for probe measurements of dissolved oxygen and Eh. Values for pH were determined for selected cores as time permitted. Each core was immediately analyzed for oxygen using a 5-cm long microprobe (Microelectrodes, Inc. MI-730 O<sub>2</sub> probe) lowered from the top of the core (**Figure 8.1**). The probe was mounted on a microscope stage that was fixed vertically above the core. By lowering the microscope stage in millimeter increments, according to the attached scale, oxygen measurements were taken to the depth of oxygen depletion. Next, Eh and pH were measured through holes pre-drilled at 2-cm intervals in the wall of the core tube (**Figure 8.1**). The holes were covered with tape during sampling, and the tape was removed immediately before inserting a probe. The Eh was measured first (Orion Model 96-78-00 Platinum Redox Electrode), and pH and temperature measurements followed (Sentron Red Line pH probe).

All probes were calibrated prior to use for each core. The oxygen probe was calibrated using two beakers of deionized water: one that was equilibrated with the atmosphere using an air stone and one that was deoxygenated by purging with nitrogen. The oxygen meter was adjusted to 20.9% while the probe was immersed in the first solution and was zeroed with the probe submerged in deoxygenated water. A one point calibration with an Orion redox standard was performed for the Eh probe. The pH probe was calibrated with pH 7 and pH 10 buffers.

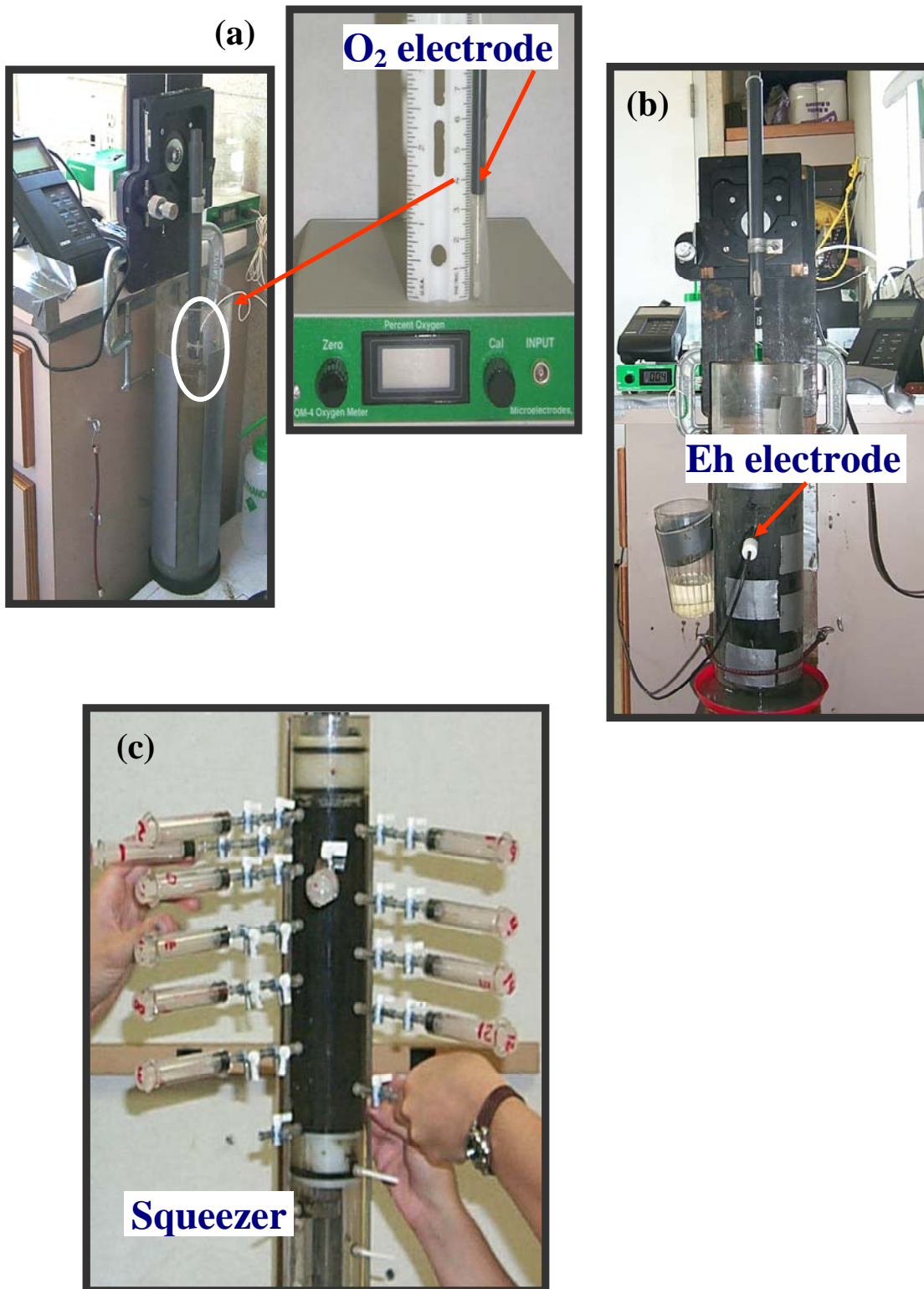


**Figure 8.1.** Photographs showing (a) oxygen probe inserted in top of sediment core and close-up of electrode and electronic control box, (b) redox potential (Eh) electrode inserted in sediment core, and (c) whole-core squeezer.

## 8.2.2 Interstitial Water Collection and Analysis

To obtain interstitial water, one 7-cm diameter subcore was transferred to a whole core squeezer, similar to that described by Bender et al. (1987) for interstitial water extraction (**Figure 8.1**). By raising the lower piston to apply pressure to the core, 16 interstitial water samples were simultaneously collected from depths of 0 to 34 cm. Samples were collected directly into acid-washed glass syringes at 1-cm intervals in the uppermost 5 cm, 2-cm intervals from 5 to 13 cm, and 3-cm intervals below 13 cm. At the completion of interstitial water collection, samples were filtered through Type A/E glass fiber filters and divided for analysis. A 1-ml sample was diluted five-fold and analyzed for phosphate using the ascorbic acid method (Clesceri et al. 1989). A 0.5-ml sample was diluted four-fold and analyzed for ammonia using the oxidation method (Matsunaga and Nishimura 1974). All colorimetric analyses performed aboard ship were carried out within 24 hours of sample collection using a Spectronic Instruments Spec 20 Genysis spectrometer. The remaining interstitial water was divided into three portions (frozen, acidified, and unaltered) for further analysis at Florida Institute of Technology (FIT).

The frozen portion ( $\geq 3$  ml) was used to determine concentrations of nitrate and sulfate using a Dionex DX-600 ion chromatograph (IC). Before injection into the system, samples and standards were passed through Dionex OnGuard II<sup>®</sup> Ag cartridges to remove chloride. Standards were prepared from mixtures of standard seawater (from the International Association for the Physical Sciences of the Ocean, IAPSO) and Dionex Five Anion Standard. The IC was operated under the following conditions: 9 mM Na<sub>2</sub>CO<sub>3</sub> eluent, 1.00 ml/min flow rate, Dionex IonPac<sup>®</sup> AS9-HC 4-mm column, 100-mA suppressor current, and 35°C oven temperature.

The acidified portion (1.5 to 2 ml) was acidified immediately upon collection with 20  $\mu$ L of 6 N hydrochloric acid (HCl). It was later analyzed for Fe and Mn by atomic absorption spectrometry (AAS) using a Perkin-Elmer Model 4000 instrument. To eliminate the effects of dissolved salts, samples were diluted by a factor of four before analysis. Standards and blanks were prepared in 1:4 seawater: deionized water (DIW). The concentrations of Fe and Mn measured in the interstitial water represent the dissolved fraction and will be referred to as Fe<sup>2+</sup> and Mn<sup>2+</sup> concentrations.

The unaltered interstitial water sample was used for chlorinity and alkalinity analysis. Chlorinity was determined by Mohr titration whereby a 0.5-ml sample was added to 20 ml DIW and titrated with  $\sim 0.04$  N AgNO<sub>3</sub>. Standard seawater (IAPSO) was titrated and used to standardize the analysis. Alkalinity was determined by titrating a 2-ml sample with 0.01 N HCl until the pH reached 4.00 or lower. The pH probe used to monitor the titration was first calibrated with pH 4 and pH 7 buffers. The volume of acid and final pH were used to calculate the alkalinity using an equation modified from Strickland and Parsons (1972).

## 8.2.3 Laboratory Analysis

### 8.2.3.1 Metals in Sediments

After being transported to FIT, sediment samples were initially brought to room temperature, and then each wet sediment sample was homogenized in the original 75-ml plastic vial using a Teflon<sup>®</sup> mixing rod. A portion ( $\sim 2$  g) of each sample was then transferred into a preweighed

plastic vial to determine water content. Once transferred, the wet sediment and the vial were reweighed. In addition, 2 to 4 g of sediment were transferred into polypropylene-copolymer centrifuge tubes to be used for the determination of sediment Hg content. Samples intended for determination of water content were frozen, freeze dried, and reweighed to determine the water content. The dried sediment samples were again homogenized using a Teflon<sup>®</sup> mixing rod.

For analysis of total Al, As, Ba, Cd, Cr, Fe, Mn, Ni, Pb, V, and Zn, about 0.4 g of sediment were digested in Teflon<sup>®</sup> beakers with HClO<sub>4</sub>-HNO<sub>3</sub>-HF and diluted to 20 ml (Trefry and Metz 1984). Total digestion of the sediments is preferred as a starting point in environmental evaluations because then no doubt remains about the absolute amount of metal associated with a sample. In the digestion process, 1 ml HClO<sub>4</sub>, 1 ml HNO<sub>3</sub>, and 3 ml HF were added to the sediment in the Teflon<sup>®</sup> beaker and heated at 50°C with a Teflon<sup>®</sup> watch cover in place until a moist paste formed. The mixture was heated for another 3 hours at 80°C with an additional 2 ml HNO<sub>3</sub> and 3 ml HF before bringing the sample to dryness. Finally, 1 ml HNO<sub>3</sub> and about 30 ml of DIW were added to the sample and heated strongly to dissolve perchlorate salts and reduce the volume. The completely dissolved and clear samples were diluted to 20 ml with DIW. This technique is 100% efficient with no loss of the elements studied and has been used successfully in the laboratory at FIT for many years with a variety of sediment types. For samples determined to have very high concentrations of Ba, based on residual white solids after digestion, a smaller mass of sample (10 to 20 mg of sediment) was digested and reanalyzed for Ba. A certified reference material (CRM), MESS-2, a marine sediment from the National Research Council (NRC) of Canada, also was digested (in 0.4-g and 20-mg amounts) and analyzed to check the accuracy of the method.

Sediment subsamples to be analyzed for Hg were digested by heating 2 to 4 g of wet sediment in acid-washed, polypropylene-copolymer centrifuge tubes with 4 ml HNO<sub>3</sub> and 2 ml H<sub>2</sub>SO<sub>4</sub>. Sample tubes were heated for 1 hour in a 90°C water bath and allowed to cool. Each tube was centrifuged at 2,000 rpm, and the supernatant was decanted into a 25-ml graduated cylinder. The sediment pellet was rinsed twice with 5 ml DIW, centrifuged, and decanted into the graduated cylinder before diluting to a final volume of 20 ml with DIW. The CRM MESS-2 was again digested and analyzed to check the accuracy of the method.

Sediment samples, CRMs, and procedural and reagent blanks were analyzed by flame atomic absorption spectrometry (FAAS), graphite furnace atomic absorption spectrometry (GFAAS), cold vapor atomic absorption spectrometry (CVAAS) or inductively coupled plasma – mass spectrometry (ICP-MS). Mercury concentrations were measured by CVAAS using a Laboratory Data Control Model 1235 Mercury Monitor. Concentrations of Al, Cr, Cu, Fe, Mn, V, and Zn were determined by FAAS. Concentrations of As were determined by GFAAS using a Perkin-Elmer Model 5100 instrument. Concentrations of Ba, Cd, Ni, and Pb were determined by ICP-MS using a Perkin-Elmer ELAN<sup>®</sup> 5000 instrument. All analytical techniques followed manufacturers' specifications and standard operating procedures (SOPs) on file at FIT. These methods are closely akin to the U.S. Environmental Protection Agency (USEPA) methods described for Series 7000 FAAS, and GFAAS, Series 7470 CVAAS, and Series 6010A ICP-MS (USEPA 1991). Method detection limits (MDLs) and data quality information are listed in **Tables 8.2 and 8.3** and *Appendix G*.

**Table 8.2.** Summary of instrumental methods and method detection limits (MDLs) for metal analysis of sediment and organisms.

Parameter	Sediments		Organisms	
	Method	MDLs ( $\mu\text{g}$ metal/g dry sediment)	Method	MDLs ( $\mu\text{g}$ metal/g tissue dry weight)
<b>Metals</b>				
Al – aluminum	FAAS	10	--	--
As – arsenic	GFAAS	0.2	GFAAS	0.03
Ba – barium	ICP-MS	2	ICP-MS	0.01
Cd – cadmium	ICP-MS	0.01	GFAAS	0.001
Cr – chromium	FAAS	3	GFAAS	0.003
Cu – copper	FAAS	3	FAAS	0.7
Fe – iron	FAAS	10	FAAS	2.5
Hg – mercury	CVAAS	0.001	CVAAS	0.001
Mn – manganese	FAAS	2.5	--	--
Ni – nickel	ICP-MS	0.5	GFAAS	0.01
Pb – lead	ICP-MS	0.2	ICP-MS	0.001
V – vanadium	FAAS	4.5	GFAAS	0.007
Zn – zinc	FAAS	0.4	FAAS	0.4
<b>Other Parameters</b>				
TOC – total organic carbon	Shimadzu Carbon System	0.06%	--	--

CVAAS = cold vapor atomic absorption spectrometry; FAAS = flame atomic absorption spectrometry; GFAAS = graphite furnace atomic absorption spectrometry; ICP-MS = inductively coupled plasma-mass spectrometry; MDL = method detection limit.

**Table 8.3.** Data quality objectives and criteria.

Element or Sample Type	Minimum Frequency	Data Quality Objective/ Acceptance Criteria
Initial calibration	Prior to every batch of samples	3 to 5 point curve depending on the element and a blank. Standard curve correlation coefficient $r \geq 0.999$ for all analytes
Continuing calibration	Must end every analytical sequence; for flame, repeat all standards every 5 samples; for graphite furnace and ICP-MS, recheck standard after every 8 to 10 samples	% RSD <15% for all analytes
Certified and standard reference materials	One per batch of 20 samples	Values must be within 20% of accepted values for >85% of the certified analytes and within 25% for Hg
Method blank	One per batch of 20 samples	No more than 2 analytes to exceed 5x MDL
Matrix spike and spike method blank	One per batch of 20 samples	% RSD 80% to 120%
Lab duplicate	One per batch of 20 samples	RSD <25% for 65% analytes

ICP-MS = inductively coupled plasma-mass spectrometry; MDL = method detection limit; RSD = relative standard deviation.

Labware used in the digestion process was acid washed with hot, 8N HNO<sub>3</sub> and rinsed three times with DIW. Two procedural blanks, two duplicate samples, and two CRMs were prepared with each set of 40 samples.

#### 8.2.3.2 *Metals in Biota*

Concentrations of 11 metals (As, Ba, Cd, Cr, Cu, Fe, Hg, Ni, Pb, V, and Zn) were determined in samples of the giant isopod *Bathynomus giganteus* and the red crab *Chaceon quinquegens* from near-field and far-field stations at sites GB 602 and MC 292. In the field, the internal organs were removed, combined, homogenized, and freeze-dried. In the laboratory, prior to acid digestion, the homogenized tissue samples were thawed and remixed with a Teflon® stirring rod. The samples were then split into two portions, one subsample to be digested wet for Hg and the other to be freeze-dried and digested for determination of the remaining trace metals. The freeze-dried subsamples also were used to calculate the percent water content so that Hg concentrations could be presented on a wet-weight and dry-weight basis.

The concentrations of all metals (except Hg) were determined using 4 to 6 g of wet weight tissue weighed into 100-ml glass digestion flasks. These subsamples were freeze-dried, reweighed for percent water content, and then digested by the sequential addition of concentrated, high-purity HNO<sub>3</sub>, hydrogen peroxide (H<sub>2</sub>O<sub>2</sub>), and HCl, with gentle refluxing. Tissue CRMs were digested at the same time as the experimental samples. Once the tissue samples and CRMs were completely dissolved, the clear solutions were transferred to graduated cylinders, diluted to 20 ml with DIW rinses of the digestion flasks, and then stored in labeled 30-ml polyethylene screw-cap bottles for trace metal analysis.

Mercury determinations were carried out using 0.4 to 0.7 g of wet tissue, and dry SRMs were weighed into 50-ml glass digestion tubes. These subsamples were digested by the addition of concentrated, high-purity HNO<sub>3</sub> and H<sub>2</sub>SO<sub>4</sub> and refluxing at 90°C for 1 hour in the sealed tubes. The dissolved samples were transferred to graduated cylinders, diluted to 20 ml with DIW rinses of the digestion tubes, and then stored in labeled 30-ml polyethylene screw-cap bottles.

Metal concentrations in the digested tissue samples, CRMs, and blanks were determined by FAAS, GFAAS, CVAAS, or ICP-MS. The method used for each element and the corresponding MDLs are given in **Table 8.2**. All analytical techniques followed manufacturers' specifications and SOPs on file at FIT. These methods are based on USEPA methods described for Series 7000 (FAAS and GFAAS), Series 7470 (CVAAS), and Series 6010A (ICP-MS) (USEPA 1991).

#### 8.2.3.3 *Total Organic Carbon*

A 0.5 to 1 g portion of the freeze-dried sediment was placed in a 10-ml Pyrex® beaker and wetted with 10% H<sub>3</sub>PO<sub>4</sub> to remove any inorganic carbon that was present. The sediment was dried at 60°C and reweighed to determine the increase in weight due to the formation of CaHPO<sub>4</sub> as a result of adding phosphoric acid. Then, approximately 200 to 400 mg of pre-treated sediment were weighed into ceramic boats and combusted at 900°C in a Shimadzu TOC-5050A carbon system with SSM-5000A solid sampling module following the manufacturer's instructions. The TOC content of the sediment samples was determined using a four-point calibration curve with pure sucrose as the standard and MESS-2 as the CRM. The TOC concentrations were corrected

to account for increases in sediment mass following addition of H<sub>3</sub>PO<sub>4</sub>. The calibration curve was checked every 10 samples by analyzing pure sucrose.

#### 8.2.3.4 Sediment Geochronology

Sediment geochronology was determined using <sup>137</sup>Cs and excess <sup>210</sup>Pb following methods described by Kang et al. (2000). Vials containing about 10 g of freeze-dried sediment were counted for 2 to 3 days until peak areas were sufficient to provide <10% counting error for total <sup>210</sup>Pb. The activities of <sup>210</sup>Pb, <sup>214</sup>Pb, <sup>214</sup>Bi, and <sup>137</sup>Cs were determined using a well-type, intrinsic germanium detector (WiGe, Princeton Gamma Tech). Detector efficiency was determined using the following: NBS 4350B, river sediment and NBS 4354, freshwater lake sediment from National Institute of Standards and Technology (NIST), and RGU-1 and RGTh-1 from the International Atomic Energy Agency. The specific activity (dpm/g) of each sediment sample was calculated from the detector efficiency, gamma intensity, geometry factor, and sample weight (Kang et al. 2000). All values were decay corrected to the date of coring. Errors are shown on the basis of 1-sigma counting statistics.

### 8.2.4 Quality Control and Quality Assurance

#### 8.2.4.1 Sample Tracking Procedure

All sediment samples were collected by, transported by, and stored by personnel from FIT. Biota samples were in the custody of Continental Shelf Associates, Inc. until transferred to FIT. Standard chain-of-custody procedures were followed for all samples. Upon return to or arrival at the laboratory, each sample was inspected to ensure that it was intact and that the identification number was clearly readable. All sediment and organism samples were kept frozen (-20°C) until processed for analysis.

#### 8.2.4.2 Quality Control Measurements for Analysis

Quality control measures included balance calibration, instrument calibration (FAAS, GFAAS, CVAAS, ICP-MS, TOC analyzer, and *in-situ* instrument sensors), matrix spike analysis for each metal, duplicate sample analysis, analysis of CRMs and standard reference materials (SRMs), procedural blank analysis, and standard checks. With each batch of up to 40 samples, two procedural blanks, two CRMs, two duplicate samples, and two matrix-spiked samples were analyzed. Data quality objectives (DQOs) for these quality control measurements are provided in **Table 8.3**.

#### 8.2.4.3 Instrument Calibration

Electronic balances used for weighing samples and reagents were calibrated prior to each use with certified NIST traceable standard weights. All pipets (electronic or manual) were calibrated prior to use. Each of the spectrometers used for metal analysis was initially standardized with a three- to five-point calibration with a linear correlation coefficient of  $r \geq 0.999$  required before experimental samples could be analyzed. Analysis of complete three- to five-point calibrations and/or single standard checks alternated every 5 to 10 samples until all the analyses were complete. The relative standard deviation (RSD) between complete calibration and standard



check was required to be <15%, or recalibration and reanalysis of the affected samples were performed.

#### *8.2.4.4 Matrix Spike Analysis*

Matrix spikes were prepared for a minimum of 5% of the total number of samples analyzed and included each metal to be determined. Results from matrix spike analysis using the method of standard additions provide information on the extent of any signal suppression or enhancement due to the sample matrix. If necessary (i.e., spike results outside 80% to 120% limit), spiking frequency was increased to 20%, and a correction was applied to the metal concentrations of the experimental samples.

#### *8.2.4.5 Duplicate Sample Analysis*

Duplicate samples from homogenized field samples (as distinct from field replicates) were prepared in the laboratory for a minimum of 5% of the total samples. These laboratory duplicates were included as part of each set of sample digestions and analyses and provide a measure of analytical precision.

#### *8.2.4.6 Procedural Blank Analysis*

Two procedural blanks were prepared with each set of 40 samples to monitor potential contamination resulting from laboratory reagents, glassware, and processing procedures. These blanks were processed using the same analytical scheme, reagents, and handling techniques as used for the experimental samples.

#### *8.2.4.7 Certified Reference Material and Standard Reference Material Analysis*

A common method used to evaluate the accuracy of environmental data is to analyze reference materials, samples for which consensus or "accepted" analyte concentrations exist. The following CRMs and SRMs were used: Marine Sediment CRM MESS-2 (NRC), Lobster Hepatopancreas CRM TORT-2 (NRC), Dogfish Muscle CRM DORM-2 (NRC), and Trace Elements in Water SRM #1643d (NIST). Metal concentrations obtained for the reference materials were required to be within 20% of accepted values for >85% of other certified analytes.

Data for quality assurance/quality control measurements for each cruise are given with the complete data sets in *Appendix G*.

### **8.3 VIOSCA KNOLL BLOCK 916 – EXPLORATION SITE**

#### **8.3.1 Metals and Total Organic Carbon**

Means, standard deviations, maximums and minimums for concentrations of metals, and TOC for surface (0 to 2 cm) sediments from site VK 916 are summarized in **Table 8.4**. The data in **Table 8.4** are for random stations in near-field and far-field zones and do not include results from the discretionary stations that were sampled during Cruise 3B. The complete data set is presented in *Appendix G*. Comparisons discussed here are between cruises and zones.

**Table 8.4.** Means  $\pm$  standard deviations with ranges in parentheses for metals, and total organic carbon (TOC) for Viosca Knoll 916 for pre- and post-exploration cruises.

Element	Far-Field		Near-Field	
	Pre-Exploration Cruise 1B	Post-Exploration Cruise 3B	Pre-Exploration Cruise 1B	Post-Exploration Cruise 3B
Al (%)	7.04 $\pm$ 0.58 (5.78-7.79)	7.11 $\pm$ 0.57 (5.93-7.72)	7.29 $\pm$ 0.20 (6.92-7.57)	6.82 $\pm$ 0.82 (4.75-7.69)
As ( $\mu\text{g/g}$ )	12.3 $\pm$ 1.7 (9.6-14.4)	12.4 $\pm$ 1.8 (8.9-14.8)	12.6 $\pm$ 0.8 (11.1-13.7)	13.8 $\pm$ 2.5 (10.1-19.9)
Ba (%)	0.087 $\pm$ 0.017 (0.070-0.118)	0.094 $\pm$ 0.022 (0.067-0.139)	0.109 $\pm$ 0.016 (0.080-0.129)	3.59 $\pm$ 5.26 (0.105-17.1)
Cd ( $\mu\text{g/g}$ )	0.22 $\pm$ 0.02 (0.17-0.24)	0.17 $\pm$ 0.02 (0.14-0.21)	0.28 $\pm$ 0.04 (0.18-0.33)	0.23 $\pm$ 0.06 (0.14-0.32)
Cr ( $\mu\text{g/g}$ )	73.2 $\pm$ 4.4 (65.8-78.4)	76.3 $\pm$ 3.2 (70.3-83.2)	52.7 $\pm$ 14.2 (31.2-68.0)	73.6 $\pm$ 6.3 (62.7-80.2)
Cu ( $\mu\text{g/g}$ )	25.2 $\pm$ 1.1 (23.1-27.0)	26.6 $\pm$ 1.1 (24.4-28.7)	26.8 $\pm$ 1.1 (25.1-28.5)	31.0 $\pm$ 6.7 (25.8-48.0)
Fe (%)	3.34 $\pm$ 0.10 (3.18-3.53)	3.41 $\pm$ 0.10 (3.27-3.60)	3.47 $\pm$ 0.13 (3.31-3.75)	3.15 $\pm$ 0.38 (2.42-3.68)
Hg (ng/g)	71 $\pm$ 4 (62-78)	77 $\pm$ 8 (64-87)	71 $\pm$ 3 (65-75)	90 $\pm$ 28 (71-153)
Mn ( $\mu\text{g/g}$ )	6,250 $\pm$ 2,110 (2,810-10,000)	6,760 $\pm$ 2,500 (2,070-12,000)	8,790 $\pm$ 1,550 (5,780-10,900)	6,360 $\pm$ 3,500 (1,040-10,400)
Ni ( $\mu\text{g/g}$ )	40.3 $\pm$ 1.4 (38.6-42.5)	39.7 $\pm$ 2.2 (36.1-42.7)	40.7 $\pm$ 2.0 (37.3-44.0)	36.6 $\pm$ 7.2 (23.2-43.6)
Pb ( $\mu\text{g/g}$ )	28.3 $\pm$ 1.8 (25.3-30.9)	25.4 $\pm$ 1.4 (22.4-27.4)	30.3 $\pm$ 3.3 (25.0-34.8)	29.9 $\pm$ 3.5 (26.3-36.9)
V ( $\mu\text{g/g}$ )	133 $\pm$ 7 (123-144)	124 $\pm$ 7 (115-137)	137 $\pm$ 4 (130-144)	115 $\pm$ 18 (88-130)
Zn ( $\mu\text{g/g}$ )	104 $\pm$ 3 (99-106)	107 $\pm$ 4 (101-116)	108 $\pm$ 2 (106-110)	106 $\pm$ 13 (88-142)
TOC (%)	1.44 $\pm$ 0.11 (1.32-1.58)	1.53 $\pm$ 0.13 (1.35-1.73)	1.54 $\pm$ 0.21 (1.30-1.90)	2.02 $\pm$ 0.77 (1.39-3.45)

Mean concentrations of Al and Fe in surface sediments collected during pre- and post-exploration cruises for near-field and far-field stations varied by  $<10\%$  (**Table 8.4**). The mean Fe/Al ratio of 0.47 for all far-field and near-field surface sediments from site VK 916 was about 10% lower than the value of 0.53 for suspended sediment (4.61% Fe/8.65% Al) from the Mississippi River (Trefry and Presley 1982). The uniformity in the Fe/Al ratios for sediments from site VK 916 support a similar terrigenous source for these sediments. The 13% discrepancy in Fe/Al ratios for sediments at site VK 916 versus suspended sediment from the Mississippi River is small enough to assume that the Mississippi River is the primary source of the aluminosilicates at this site with possible, minor alteration of Fe levels over time due to scavenging or sediment diagenesis.

Concentrations of Mn in surface sediments for far-field stations at site VK 916 varied by as much as a factor of six (**Table 8.4**) and show some spatial variability in the redox environment across the study area. Concentrations of Mn in suspended sediment from the Mississippi River are reported at  $\sim 1,300 \pm 200 \mu\text{g/g}$  (Trefry and Presley 1982); therefore, sediments from far-field stations at site VK 916 contained 2 to 10 times more Mn than incoming river particles. These higher Mn values in slope sediments are consistent with an upward flux of reduced  $\text{Mn}^{2+}$  from deeper in the sediment column to the more oxygenated surface layer of sediment where the  $\text{Mn}^{2+}$  oxidizes and precipitates as  $\text{MnO}_2$  (Trefry and Presley 1982). The variability in Mn concentrations for surface sediments from far-field stations partly results from sampling a fixed layer of sediment (0 to 2 cm) where the thickness of the Mn-rich layer is variable and most often  $< 2$  cm.

Concentrations of Mn in surface sediments at near-field stations show a similar degree of variability to those at far-field stations. The only three values for Mn that were  $< 2,000 \mu\text{g/g}$ , considering all stations from VK 916, were found for near-field stations during the post-exploration cruise. Sediment from these three stations contained 2.2% to 3.4% TOC relative to 1.5% TOC in far-field samples. These observations support reductive dissolution of Mn and diffusion of  $\text{Mn}^{2+}$  from the sediment to the overlying water column at some near-field stations when reducing conditions develop where drilling discharges are found. This information and the results for Mn in sediment cores will be further considered in discussions regarding the redox state of the sediment.

Mean concentrations of Ba were not statistically different for far-field versus near-field sediments during the pre-exploration cruise (**Tables 8.4 and 8.5** and **Figure 8.2**). However, mean concentrations of Ba increased by  $\sim 30$ -fold at near-field stations following exploratory drilling (**Figure 8.2**). The maximum concentration of Ba during the post-exploration survey was 17.1% at Station B01 (**Figure 8.3**). The maximum Ba level represents a sediment content of  $\sim 32\%$  barite (using a Ba level of 53% for industrial barite; Trefry et al. 2003). Sediments at nine stations from the center portion of the near-field zone contained Ba at levels of  $\sim 1\%$  or greater. In the peripheral areas of the near-field zone, concentrations of Ba in sediments approached background levels. The highest Ba concentration in the near-field zone during the pre-exploration cruise was 0.13%.

**Table 8.5.** Results of statistical comparisons (t-tests) for concentrations of metals among cruises (1B for pre-exploration and 3B for post-exploration) and zones for Viosca Knoll 916. Results for discretionary stations were not included in the statistical tests.

Dependent Variable	Independent Variable	Probability > F	Interpretation
Log Ba	zone	$< 0.0001$	NF post-expl. > NF pre-expl.
Cd	cruise	0.0026	FF pre-expl. > FF post-expl.
Cr	cruise	0.0005	NF post-expl. > NF pre-expl.
Hg	cruise	0.039	NF post-expl. > NF pre-expl.
Mn	cruise	0.018	NF post-expl. < NF pre-expl.
TOC	cruise/zone	$< 0.0001$	NF post-expl. > NF pre-expl.

FF = far-field; NF = near-field; TOC = total organic carbon.

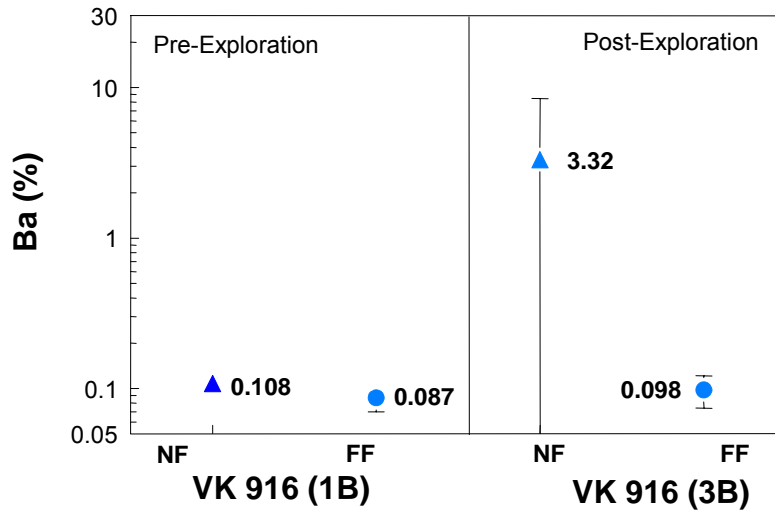


**Figure 8.2.** Concentrations of barium (Ba) with markers and numbers showing means and lines showing standard deviations in sediment from near-field (NF) and far-field (FF) stations at Viosca Knoll (VK) 916 during pre-exploration drilling Cruise 1B and post-exploration drilling Cruise 3B. In some cases, the line for the standard deviation is obscured by a marker or appears skewed due to the logarithmic scale.

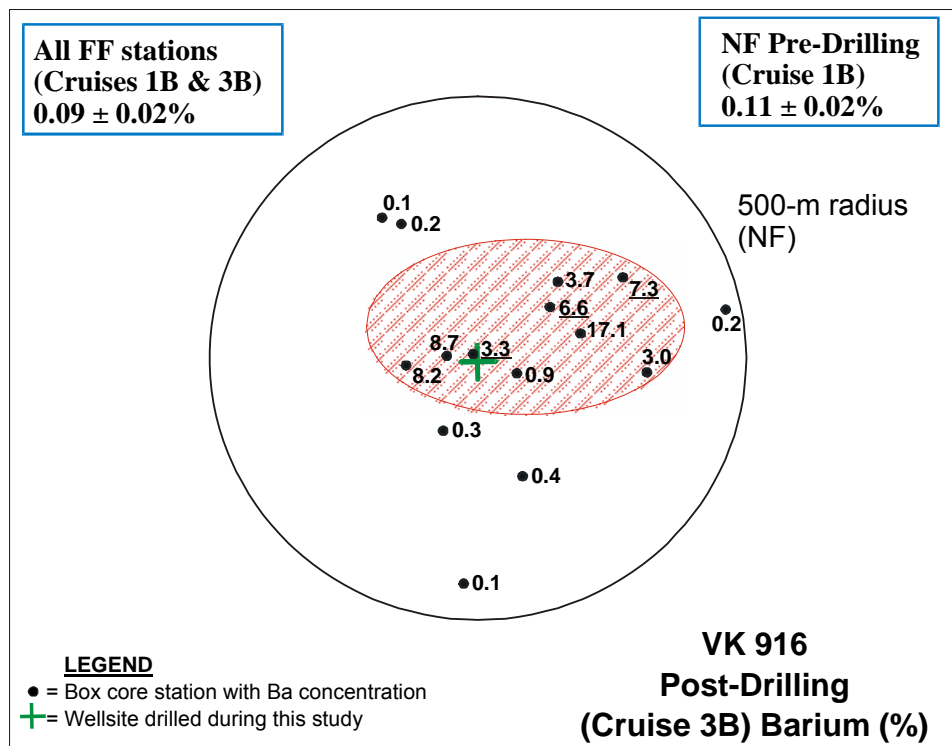


**Figure 8.3.** Concentrations of barium (Ba) at Viosca Knoll (VK) 916 near-field (NF) stations during post-drilling Cruise 3B. Inset boxes show mean barium concentrations at all far-field (FF) stations and at NF stations during pre-drilling Cruise 1B. Data for the discretionary stations are underlined. The bold NF circle represents a radius of 500 m. Shaded oval highlights area where Ba concentrations are ~1% or greater.

Vertical profiles for Ba in sediments were obtained for the three discretionary stations during the post-exploration cruise. The cores were subsectioned in five, 2-cm thick intervals over the top 10 cm. Concentrations of Ba were at background levels ( $\sim 0.1\%$ ) at less than 2 to 4 or less than 4 to 6 cm in each instance (**Figure 8.4**). The three discretionary stations were located in the shaded area on **Figure 8.3**. Based on the sediment Ba data, the sphere of influence for drilling discharges is well contained within the 500-m near-field zone and extends to depths  $\leq 4$  cm.

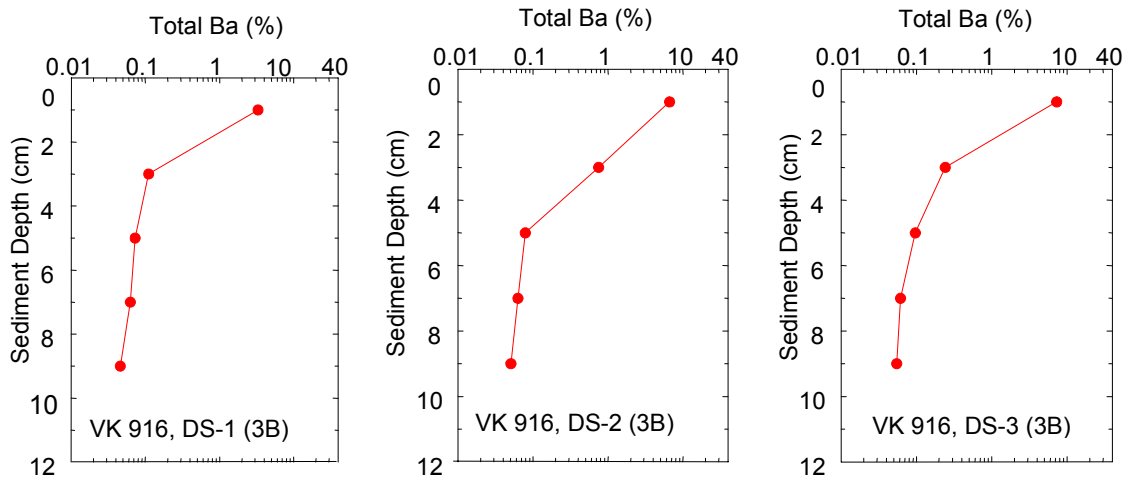


**Figure 8.4.** Vertical profiles for concentrations of barium (Ba) in sediment from discretionary (DS) stations during post-exploration Cruise 3B to Viosca Knoll (VK) 916.

Mean concentrations of Al, As, Cu, Fe, Ni, Pb, V, and Zn were not significantly different among far-field and near-field stations for both the pre-exploration and post-exploration cruises (**Tables 8.4** and **8.5**). However, concentrations of Mn, Cr, and Hg, like Ba, showed a near-field zone-wide shift in concentrations that can be related to exploratory drilling. Some isolated shifts in metal concentrations were identified by examining metal data for sediment from Station B01 (post-exploration), where Ba levels were 17.1%. Concentrations of Al, Fe, Ni, and V were  $\sim 30\%$  lower at this station due to dilution of the natural aluminosilicate material, with  $\sim 30\%$  barite in the sediments that was associated with drilling discharges. However, concentrations of As, Cu, and Zn were greater in sediment from Station B01 (post-exploration) than levels in background sediment by about 40%, 80%, and 30%, respectively. These increases are directly related to increases in concentrations of Ba; however, such increases were not clearly observed in other samples with as much as 8% Ba, except for Cu at Station B07 (Cu = 39.1  $\mu\text{g/g}$ ; Ba = 8.2%). Four near-field samples from Cruise 3B that contained  $>3\%$  Ba also contained 20% to 50% higher levels of Hg (**Figure 8.5**). Vertical profiles for Hg in sediments from discretionary stations from Cruise 3B show the same minor enhancement in Hg levels at the tops of the cores at Stations DS-2 and DS-3 (**Figure 8.6**). A more detailed, separate section on trace metals in sediments that provides an overview of all drilling sites is presented at the end of the chapter.

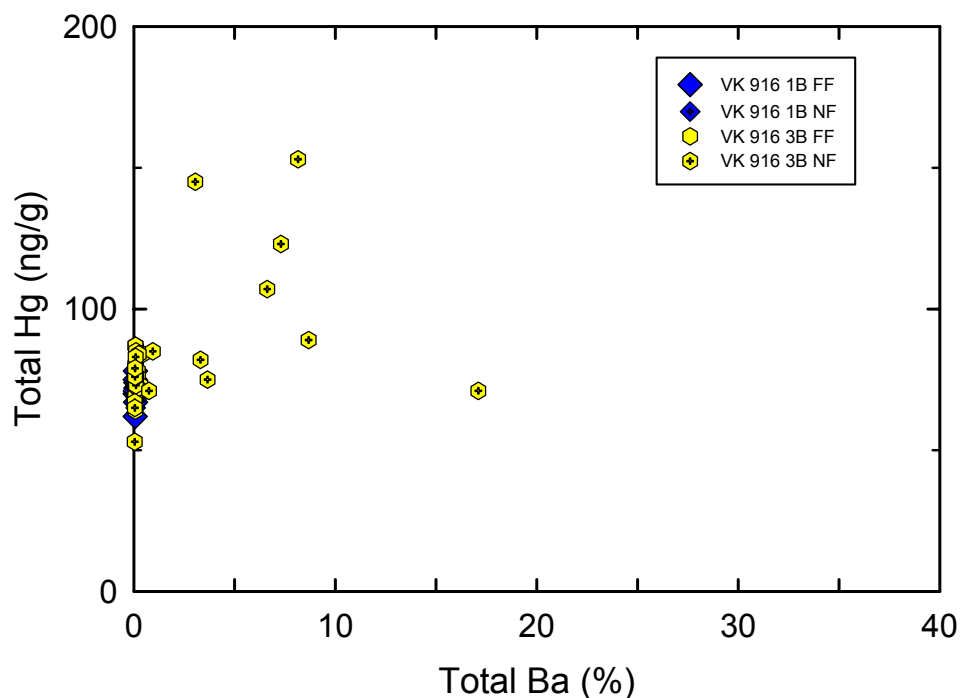


**Figure 8.5.** Concentrations of barium (Ba) versus mercury (Hg) for sediments from far-field (FF) and near-field (NF) stations from Viosca Knoll (VK) 916 collected during pre-exploration Cruise 1B and post-exploration Cruise 3B. Most points from FF samples and NF samples from Cruise 1B are hidden beneath the NF data points from Cruise 3B at low concentrations of Ba.

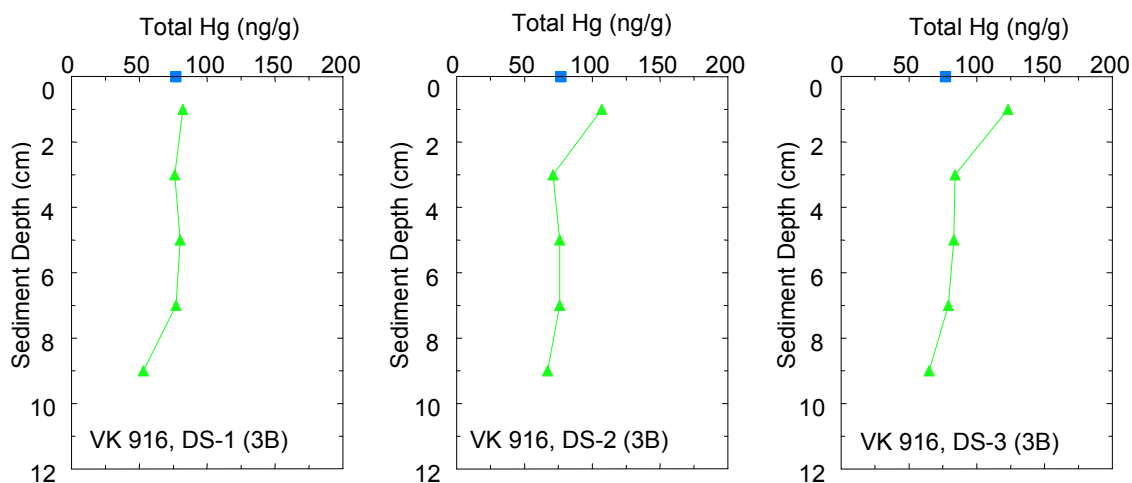


**Figure 8.6.** Vertical profiles for concentrations of mercury (Hg) in sediment from discretionary (DS) stations during post-exploration Cruise 3B to Viosca Knoll (VK) 916. Squares at 0 cm on each graph represent mean Hg values at far-field stations.

Concentrations of TOC in near-field surface sediments during the post-exploration cruise (3B) averaged about one-third greater than found in far-field samples or near-field samples from the pre-exploration cruise (**Table 8.4** and **Figure 8.7**). The maximum value for TOC in far-field or near-field samples from Cruise 1B was 1.9%. Four near-field samples and the three discretionary samples from Cruise 3B contained >2% TOC, with a maximum level of 3.45%. Each of the seven samples with >2% TOC contained >3% Ba (**Figure 8.8**). Vertical profiles for TOC (**Figure 8.9**) show similar trends to those observed for Ba (**Figure 8.4**), with elevated levels of TOC restricted to the top 2 to 4 cm of the sediment column.

### 8.3.2 Sediment Geochronology

Vertical profiles for excess  $^{210}\text{Pb}$  at Stations FF3 and NF-3 for site VK 916 from Cruise 1B are remarkably similar and provide a good test of how representative a single core can be from one of these deepwater sites (**Figure 8.10**). In both cores, two different slopes for excess  $^{210}\text{Pb}$  versus depth are observed (**Figure 8.10**). Possible explanations for the two slopes are sediment mixing (biological and/or physical) in the top 5 to 7 cm or a shift in sedimentation rate. The  $^{137}\text{Cs}$  profile was not preserved in either core, and thus confirmation of mixing was not independently determined. Based on results to be presented for the other deepwater sites, the sedimentation rate of 0.06 cm/y, based on the lower portion of the excess  $^{210}\text{Pb}$  profile, is most likely a better estimate for this site. Geochronology at near-field stations is distorted in the presence of drilling discharges. This distortion shows the presence of drilling mud or cuttings but does not differentiate between the two fractions. More detail on near-field samples is given in the results for GB 516 where a far-field core and a near-field core were studied.

### 8.3.3 Sediment Oxygen Levels and Redox Conditions

Vertical profiles for dissolved  $\text{O}_2$  and Eh were obtained using probes at near-field, far-field, and discretionary stations during both the pre- and post-exploration cruises. Measurement of pH was carried out at as many stations as time permitted. However, similar results were obtained for most stations, and thus the pH measurements were not carried out if they delayed processing of the subsequent core. The complete data set for oxygen, Eh, and pH is presented in tabular and graphical forms in *Appendix G*.

Values for Eh represent the sum of all oxidation/reduction reactions that are occurring in the sediment. An approximate Eh value can be given for the occurrence of various redox reactions (**Figure 8.11**). For example, the onset of bacterial reduction of nitrate (a replacement bacterial oxidizing agent for oxygen) to ammonia occurs at an Eh somewhat <200 mV. The onset of sulfate reduction to  $\text{H}_2\text{S}$  occurs as Eh values fall below -100 mV (**Figure 8.11**).

At VK 916, concentrations of dissolved oxygen in the sediment range from ~200  $\mu\text{M}$  (or 6.4 mg/L where 1 mg/L = 31.2  $\mu\text{M}$ ) in the bottom water collected in the box core (bottom water value is plotted at a depth of 0.0 cm on each graph) to <2  $\mu\text{M}$  (MDL) at varying depths in the cores. Concentrations of dissolved oxygen in the overlying water from the box core probably do not provide an exact measure of  $\text{O}_2$  levels in near-bottom water; however, they provide a comparable and useful point of reference for each sediment core. Dissolved oxygen levels in the overlying water, at 1 to 2 m above bottom, are typically in the range of 200 to 250  $\mu\text{M}$ .

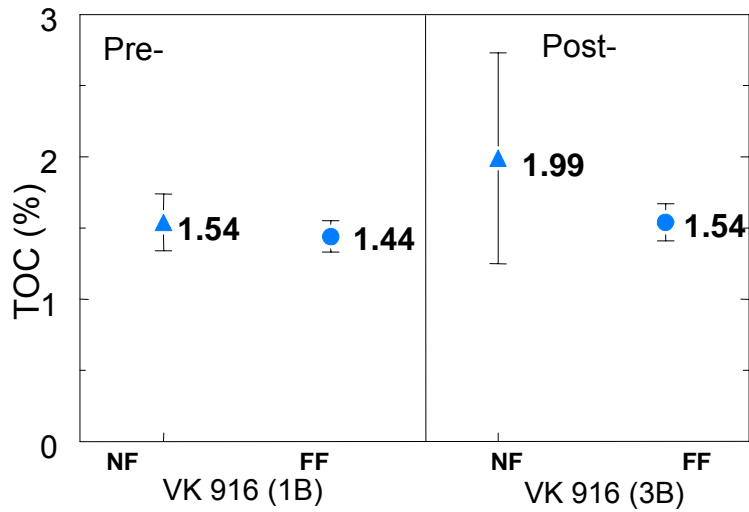


**Figure 8.7.** Concentrations of total organic carbon (TOC) with circles and numbers showing means and lines showing standard deviations in sediment from near-field (NF) and far-field (FF) stations from Viosca Knoll (VK) 916 during pre-exploration drilling Cruise 1B and post-exploration drilling Cruise 3B.

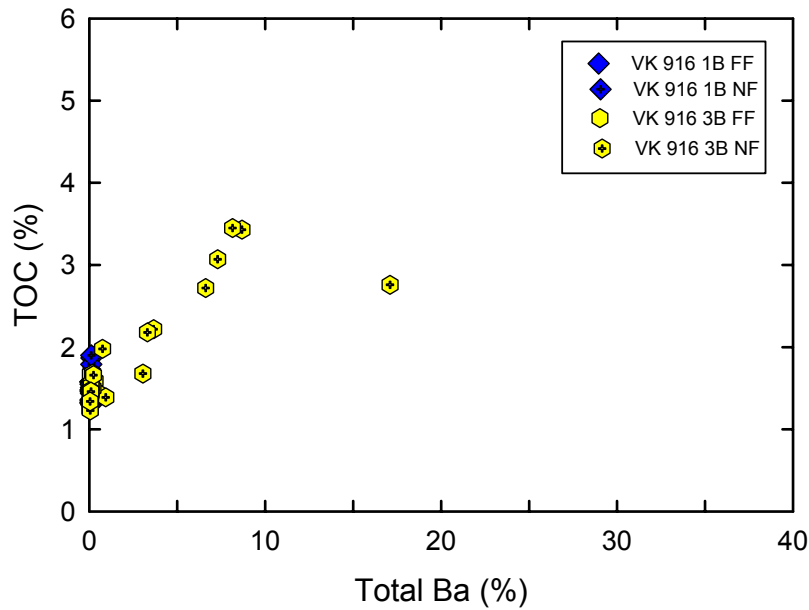


**Figure 8.8.** Concentrations of barium (Ba) versus total organic carbon (TOC) for sediments from far-field (FF) and near-field (NF) stations from Viosca Knoll (VK) 916 collected during pre-exploration Cruise 1B and post-exploration Cruise 3B. Some points from FF samples and NF samples from Cruise 1B are hidden beneath the NF data points for Cruise 3B at low concentrations of Ba.



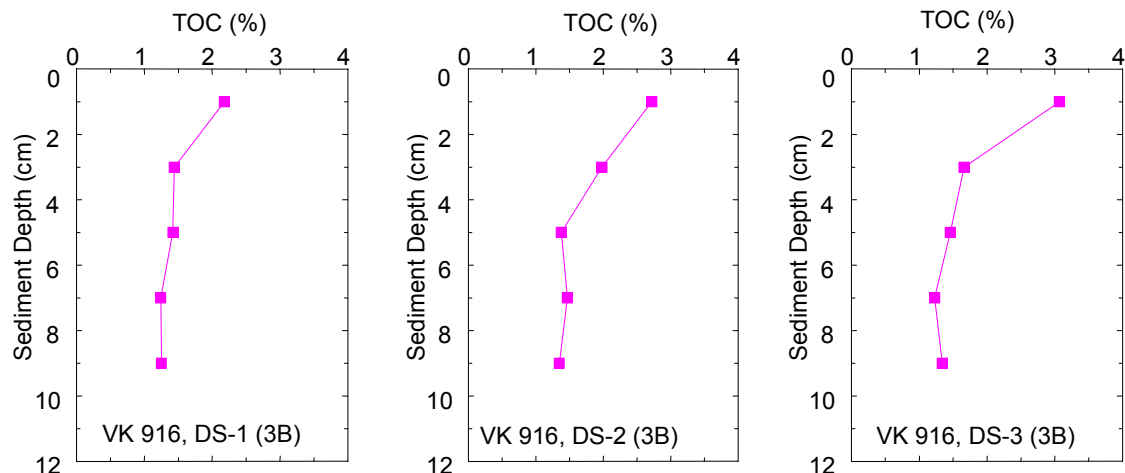


**Figure 8.9.** Vertical profiles for concentrations of total organic carbon (TOC) in sediment from discretionary (DS) stations for post-exploration Cruise 3B to Viosca Knoll (VK) 916.

Concentrations of dissolved  $O_2$  in sediment from both far-field and near-field sites during the pre-exploration cruise decreased to non-detectable levels ( $<2 \mu\text{M}$ ) at sediment depths of 1.6 to 3.5 cm (**Table 8.6** and **Figure 8.12**). Ranges in Eh and pH values also were similar for far-field and near-field sediments from Cruise 1B (**Table 8.6**). A typical vertical profile for dissolved oxygen at Station FF3 shows an exponential decrease in dissolved  $O_2$  in the sediment (**Figure 8.12**). At the same depth of  $\sim 3$  cm, where oxygen concentrations approached zero at Station FF3, the Eh decreased sharply from +400 to +100 mV (**Figure 8.12**, note different depth scales for oxygen and Eh). This shift signals a change from oxic to suboxic conditions where nitrate and manganese and iron oxides, instead of oxygen, serve as electron acceptors during the oxidation of organic matter (**Figure 8.11**). The conditions summarized in **Table 8.6** and shown in **Figure 8.12** also identify background conditions in sediments at this study site.

**Table 8.6.** Summary data for dissolved oxygen, redox potential (Eh), and pH for sediment from Viosca Knoll (VK) 916 at near-field (NF), far-field (FF), and discretionary (DS) stations during pre-exploration Cruise 1B and post-exploration Cruise 3B.

Site	Zone	Zero $O_2$ depth (cm)	Eh <sub>1 cm</sub> range (mV)		Eh <sub>10 cm</sub> range (mV)		pH
VK 916							
Pre-Exploration (Cruise 1B)	NF	1.6 – 3.5	+675	+328	+331	+69	7.3 – 7.9
	FF	2.4 – 3.1	+614	+135	+175	+56	7.4 – 8.0
VK 916							
Post-Exploration (Cruise 3B)	NF	0.2 – 3.0	+529	-79	+428	+66	--
	DS	0.1 – 0.5	+31	-65	+107	-16	--
	FF	0 – 3.2	+514	+218	+195	+91	--

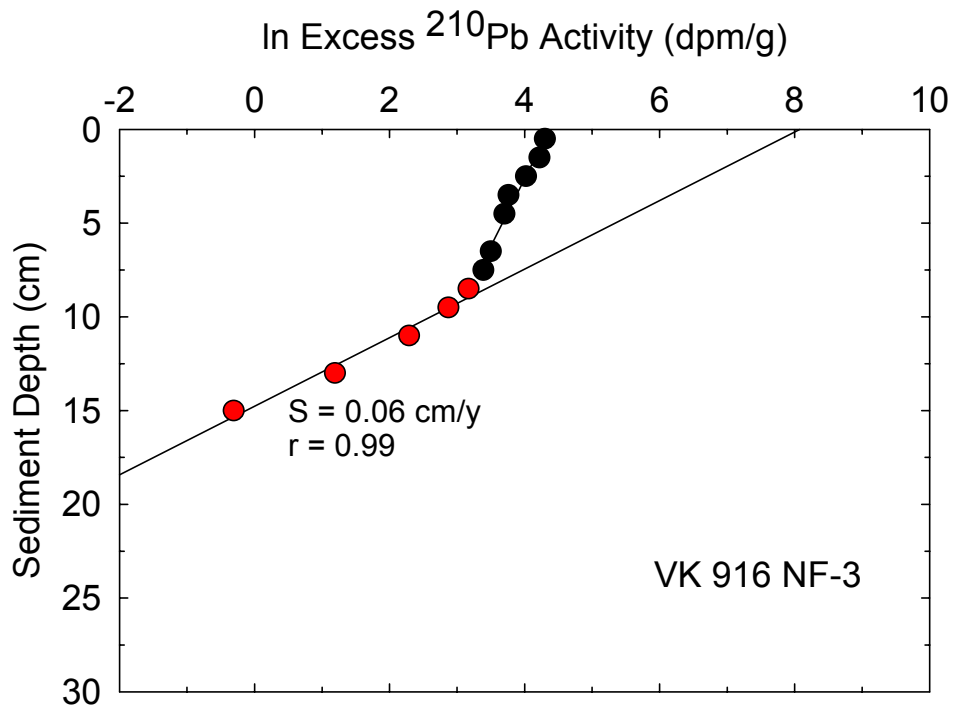
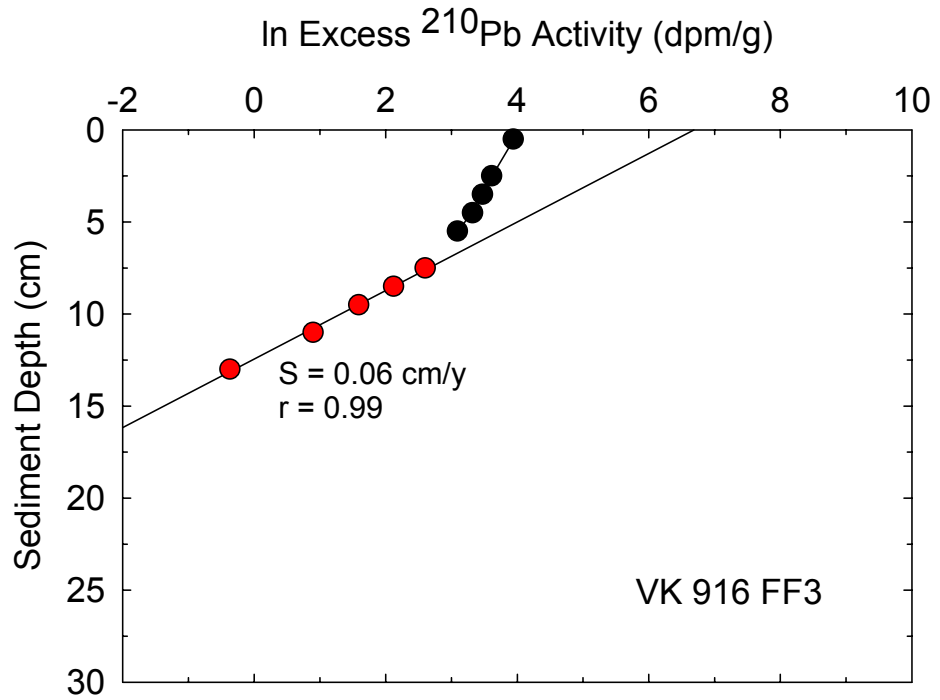


**Figure 8.10.** Vertical profiles for activities of excess  $^{210}\text{Pb}$  in sediment from far-field (FF) and near-field (NF) stations at Viosca Knoll (VK) 916 for Cruise 1B ( $S$  = sedimentation rate,  $r$  = correlation coefficient, calculated using only the red points).

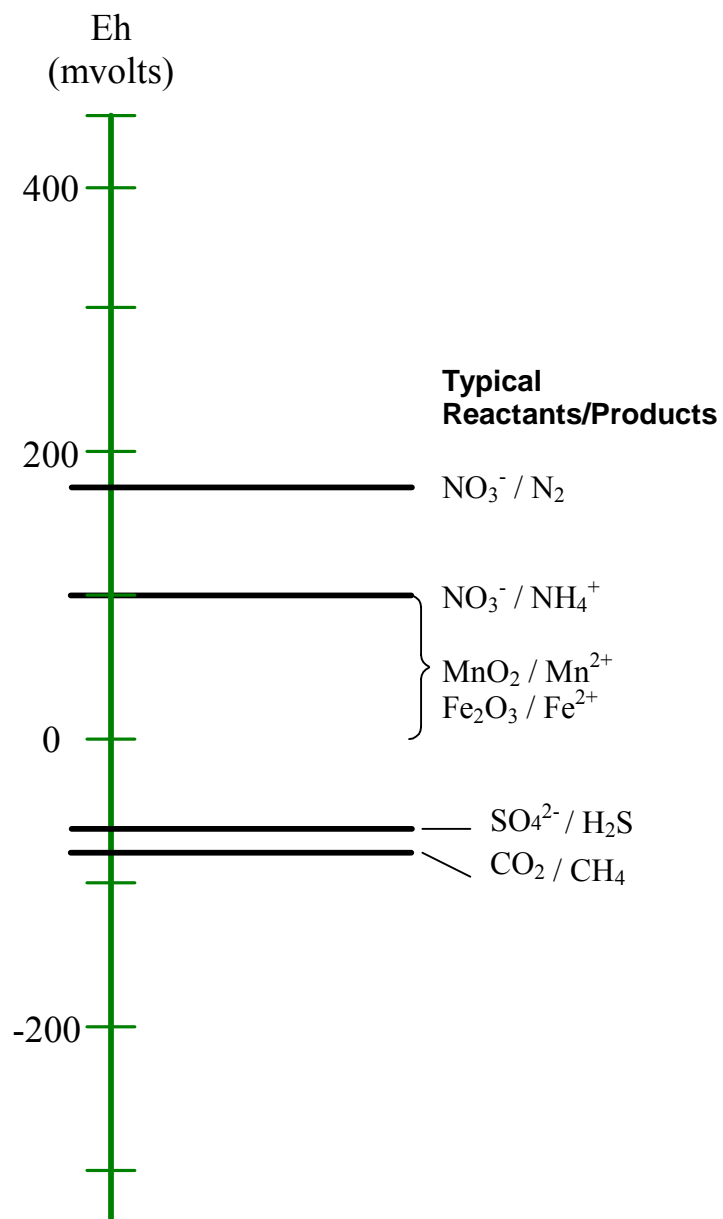
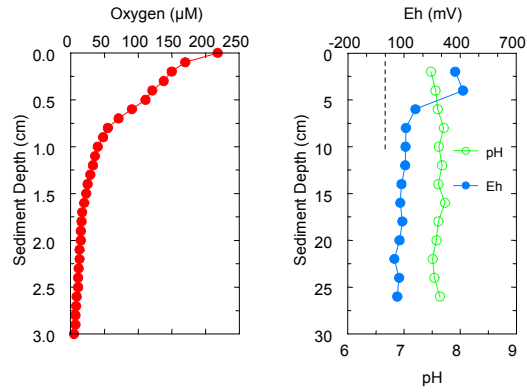
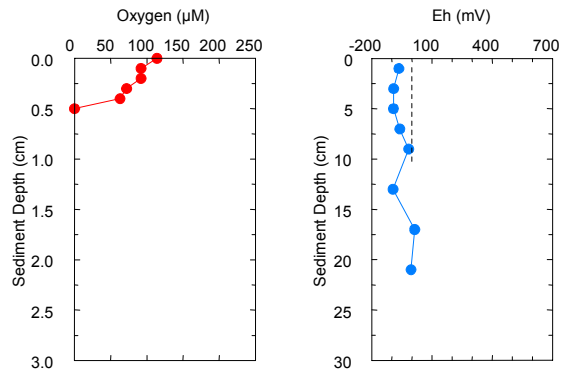


**Figure 8.11.** Approximate redox potential (Eh) values at which various redox reactions occur in water (after Drever 1997).

MMS Deep Gulf of Mexico Cruise 1B: VK 916 FF3-B01



MMS Deep Gulf of Mexico Cruise 3B: VK 916 DS-B01



MMS Deep Gulf of Mexico Cruise 3B: VK 916 NF-B02

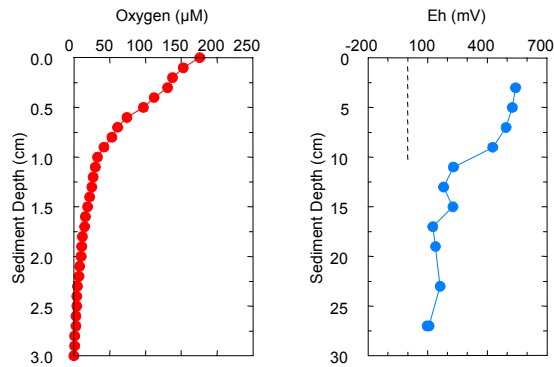


**Figure 8.12.** Vertical profiles for dissolved oxygen, redox potential (Eh), and pH in sediment from representative near-field (NF), far-field (FF), and discretionary (DS) stations from Viosca Knoll (VK) 916 (note different depth scales for oxygen versus Eh).

During the post-exploration cruise, values for dissolved oxygen and Eh at many near-field and discretionary stations were considerably lower than at far-field stations. For example, the lowest Eh levels in the top 1 cm of the sediment at near-field and discretionary stations were -79 and -65 mV, respectively, relative to +218 mV in far-field sediments (**Table 8.6** and **Figure 8.12**). Likewise, the sediment depth to zero oxygen was generally closer to the sediment-water interface at near-field and discretionary stations from the post-exploration cruise relative to far-field stations (**Table 8.6**). At some near-field stations where no drilling discharges were identified (**Figure 8.3**), vertical profiles for oxygen and Eh were similar to those observed at far-field stations (**Figure 8.12**).

To help summarize and simplify the O<sub>2</sub> data, the results for dissolved oxygen also are presented as the integrated (total) amount of oxygen in the sediment column (as nmoles/cm<sup>2</sup>). These oxygen inventories are presented as the average and standard deviation for near-field, far-field, and discretionary stations from the pre- and post-exploration cruises. The mean integrated amounts of oxygen ( $\Sigma\text{O}_2$ ) in the sediments at far-field stations from Cruises 1 and 2 and near-field stations from Cruise 1B are not statistically different at 84 to 90 nmol/cm<sup>2</sup> (**Figure 8.13**). In contrast, values for  $\Sigma\text{O}_2$  in sediments collected at near-field and discretionary stations during the post-exploration cruise averaged about one-half and one-eighth of pre-exploration values, respectively (**Figure 8.13**). This shift is directly related to the presence of drilling discharges. The rapid deposition of several centimeters of more organic-rich sediment at many stations in the near-field zone leads to an increasing rate of bacterial activity with resulting depletion of dissolved oxygen.

### 8.3.4 Interstitial Water Composition

Interstitial water was collected at one far-field and one near-field station from both the pre- and post-exploration cruises. The interstitial water data will be used here to determine how well the dissolved oxygen and Eh data predict the reactants and products of bacterial decomposition of organic matter in sediments. The interstitial water data, along with the oxygen and Eh data, also will be used to further identify changes in the redox state of the sediments in the presence of drilling discharges. The interstitial water data are tabulated in *Appendix G*, and vertical profiles for selected chemical species in several cores are presented below.

As background information, **Table 8.7** shows some of the reactions that may occur as oxygen and subsequent oxidizing agents are used by bacteria to facilitate energy production from the oxidation of organic matter. As oxygen is depleted during oxidation of organic matter, nitrate (and nitrite) are produced as shown in Eq. 1 (**Table 8.7**). The shift from oxic decomposition of detrital organic matter by bacteria can occur abruptly at rather shallow depths in the sediment to sub-oxic (nitrate reduction) decomposition (Eq. 2, **Table 8.7**). Upon depletion of oxygen and nitrate, other less efficient oxidizing agents, such as Mn and Fe oxides and sulfate are used by resident bacteria (Eqs. 3, 4, and 5, **Table 8.7**). Levels of Mn<sup>2+</sup> and Fe<sup>2+</sup> in interstitial water increase as metal oxides are chemically reduced and solubilized. Throughout the process of organic matter decomposition, concentrations of various by-products, such as dissolved ammonia, H<sub>2</sub>S, CO<sub>2</sub>, and phosphate, increase (**Table 8.7**).

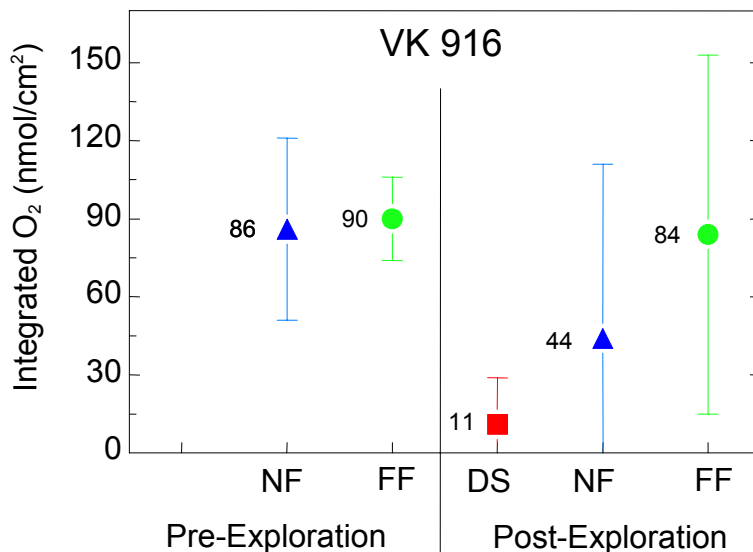


**Figure 8.13.** Integrated amounts of oxygen in the sediment column at near-field (NF), far-field (FF), and discretionary (DS) stations at Viosca Knoll (VK) 916 for pre-exploration Cruise 1B and post-exploration Cruise 3B. Markers and numbers show means, and lines show standard deviations.

**Table 8.7.** Selected reactions showing the decomposition of organic matter by various oxidation agents (after Froelich et al. 1979).

$(\text{CH}_2\text{O})_{106}(\text{NH}_3)_{16}\text{H}_3\text{PO}_4 + 138 \text{O}_2 = 106 \text{CO}_2 + 16 \text{HNO}_3 + \text{H}_3\text{PO}_4 + 122 \text{H}_2\text{O}$	Eq. 1
$(\text{CH}_2\text{O})_{106}(\text{NH}_3)_{16}\text{H}_3\text{PO}_4 + 94.4 \text{HNO}_3 = 106 \text{CO}_2 + 55.2 \text{N}_2 + \text{H}_3\text{PO}_4 + 177.2 \text{H}_2\text{O}$	Eq. 2
$(\text{CH}_2\text{O})_{106}(\text{NH}_3)_{16}\text{H}_3\text{PO}_4 + 212 \text{MnO}_2 + 424 \text{H}^+ = 106 \text{CO}_2 + 16 \text{NH}_3 + \text{H}_3\text{PO}_4 + 212 \text{Mn}^{2+} + 318 \text{H}_2\text{O}$	Eq. 3
$(\text{CH}_2\text{O})_{106}(\text{NH}_3)_{16}\text{H}_3\text{PO}_4 + 212 \text{Fe}_2\text{O}_3 \text{ (or } 424 \text{FeOOH)} + 848 \text{H}^+ = 106 \text{CO}_2 + 16 \text{NH}_3 + \text{H}_3\text{PO}_4 + 424 \text{Fe}^{2+} + 530 \text{H}_2\text{O}$	Eq. 4
$(\text{CH}_2\text{O})_{106}(\text{NH}_3)_{16}\text{H}_3\text{PO}_4 + 53 \text{SO}_4^{2-} + 424 \text{H}^+ = 106 \text{CO}_2 + 16 \text{NH}_3 + \text{H}_3\text{PO}_4 + 53 \text{S}^{2-} + 318 \text{H}_2\text{O}$	Eq. 5

Results for interstitial water from one far-field and one near-field station from the pre-exploration cruise (1B) for site VK 916 are very similar (**Figures 8.14** and **8.15**). The Eh of  $>+600$  mV in the top layer of the core decreased to  $+200$  to  $+100$  mV by depths of 5 to 10 cm and did not decrease below about  $+100$  mV deeper in both cores. These Eh values for both the far-field and near-field cores from site VK 916 are consistent with a transition from oxic to sub-oxic conditions over the top few centimeters of the core. Nitrate was detected in the top 5 cm of each core, and  $\text{Mn}^{2+}$  and  $\text{Fe}^{2+}$  were not detected in the top few cm of each core (**Figures 8.14** and **8.15**). As Eh decreased

### Pore Water Results for VK 916 FF-B02 (Cruise 1B)

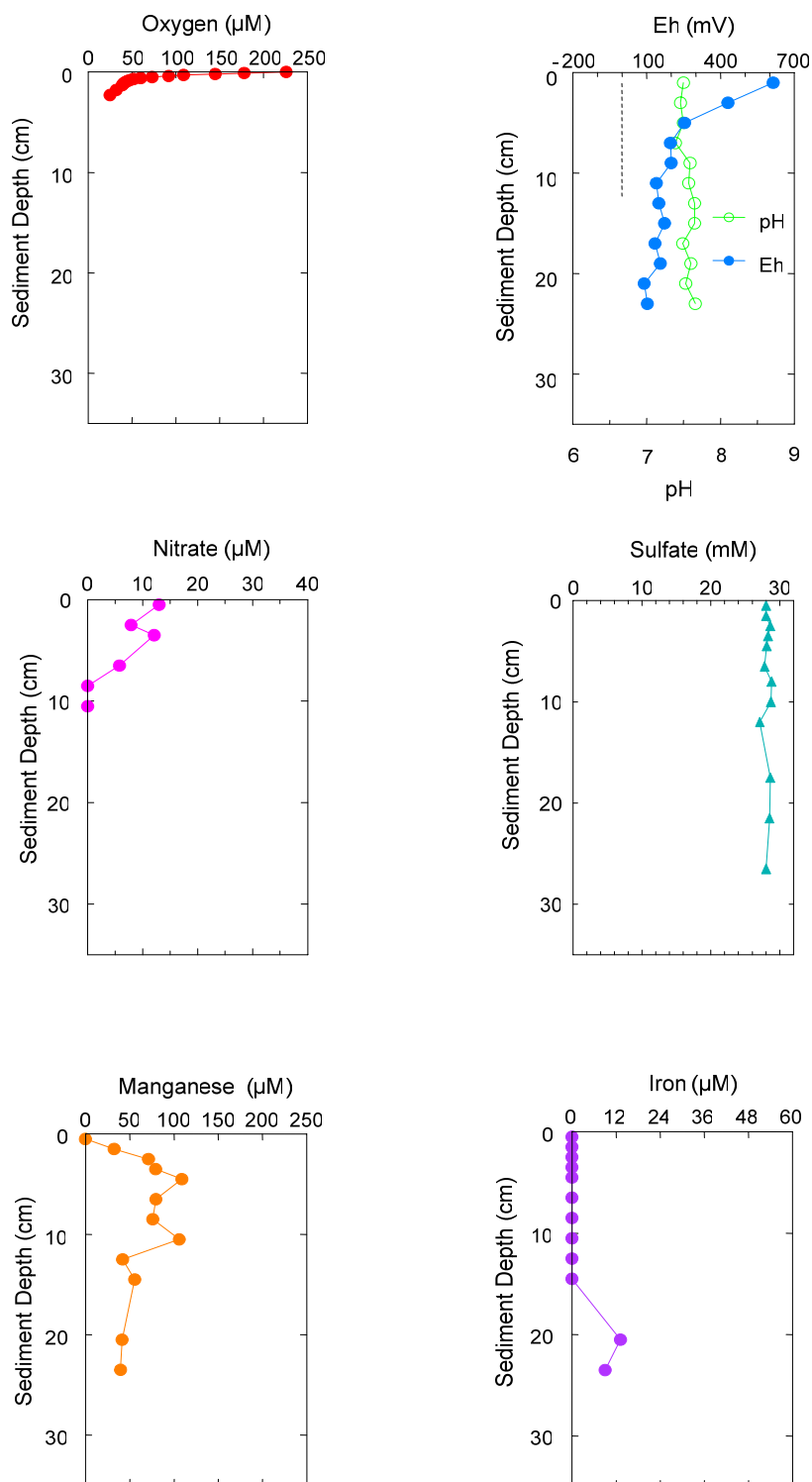


**Figure 8.14.** Vertical profiles for dissolved oxygen, Eh, nitrate, sulfate, manganese, and iron from interstitial water from Station FF-B02, Viosca Knoll (VK) 916, for pre-exploration Cruise 1B.

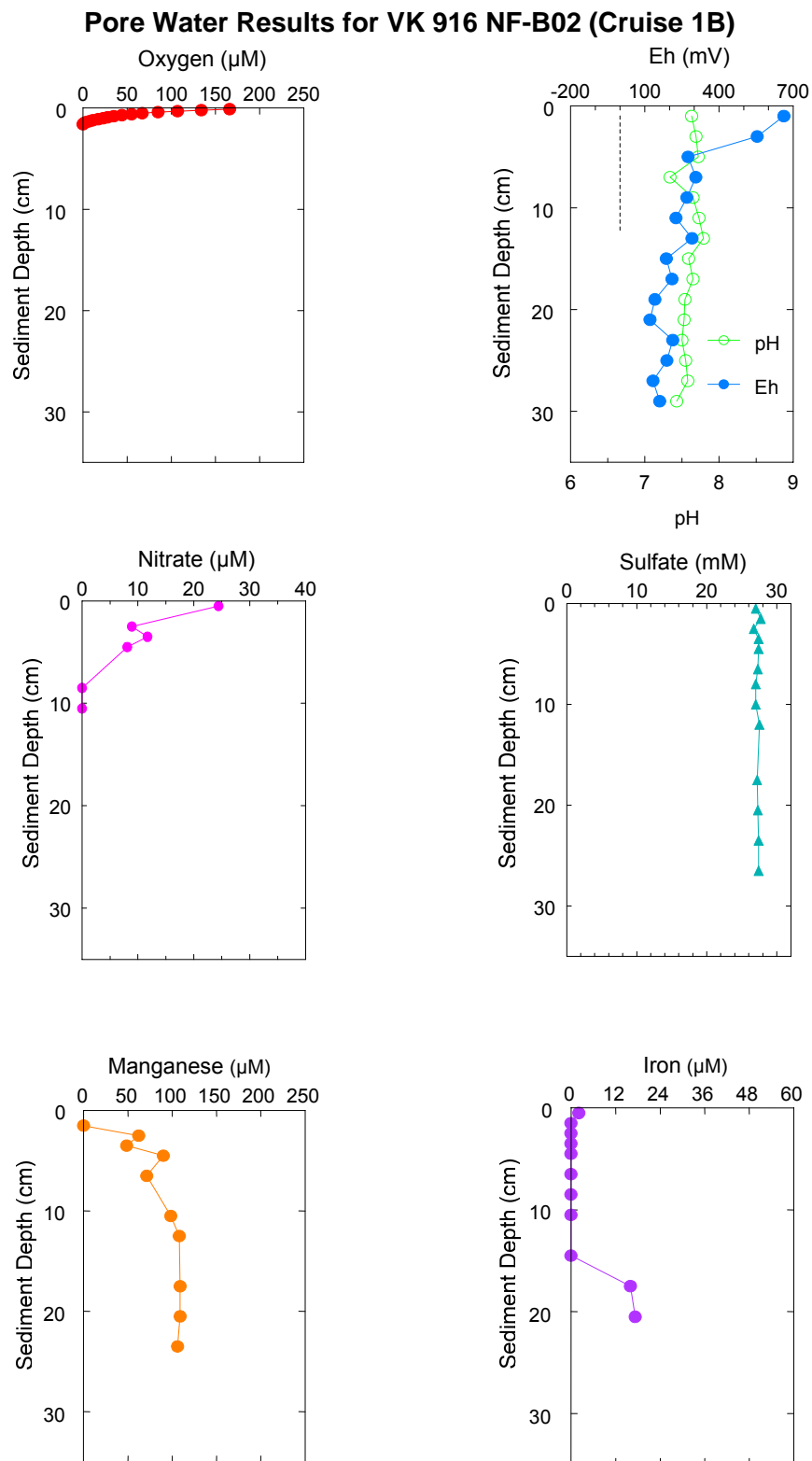


**Figure 8.15.** Vertical profiles for dissolved oxygen, Eh, nitrate, sulfate, manganese, and iron from interstitial water from Station NF-B02, Viosca Knoll (VK) 916, for pre-exploration Cruise 1B.



in the upper few centimeters, concentrations of  $\text{Mn}^{2+}$  in the interstitial water increased (**Figures 8.14 and 8.15**). Concentrations of  $\text{Fe}^{2+}$  did not increase until depths  $>15$  cm, and no discernible sulfate reduction or detectable sulfide (i.e.,  $<2$   $\mu\text{M}$  total  $\text{H}_2\text{S}$ ) were observed in either core (**Figures 8.14 and 8.15**). Thus, the dominant reactions in the far-field core were those described for Eqs. 2, 3, and 4 (**Table 8.7 and Figure 8.11**). The good relationship of the probe results for oxygen and Eh with the interstitial water data for both far-field and near-field stations during Cruise 1B support use of the probe data to assess the redox state of the sediments at the other stations. The similar data for depth to zero oxygen, Eh (**Table 8.6**), and integrated oxygen (**Figure 8.13**) for both far-field and near-field stations from site VK 916, coupled with agreement for the limited interstitial water data, show that the redox state in sediments from the far-field and near-field zones was similar during the pre-exploration phase of this study.

Interstitial water was collected from Stations FF3 and DS-2 during the post-exploration cruise. At Station DS-2, the top two sections of the sediment core at 0 to 2 cm and 2 to 4 cm contained 6.6% and 0.8% Ba and 2.7% and 2.0% TOC, respectively, relative to background levels of about 0.1% Ba and 1.5% TOC at far-field stations. Oxygen levels were below detection limits ( $<2$   $\mu\text{M}$ ) in the top millimeter of sediment at Station DS-2 to yield an integrated oxygen level of 0  $\text{nmol}/\text{cm}^2$ , relative to an oxygen penetration depth of 3.1 cm and an integrated oxygen level of 88  $\text{nmol}/\text{cm}^2$  at Station FF3 (**Figures 8.16 and 8.17**). The Eh at Station FF3 decreased from  $\sim+500$  mV in the top 2 cm to +100 mV from 8 cm to the base of the core (**Figure 8.16**). At Station DS-2, the Eh was about 0 mV in the top 2 cm and then about +100 mV through the remainder of the core (**Figure 8.17**). Concentrations of dissolved ammonia were below detection limits ( $<1$   $\mu\text{M}$ ) in the top of the core from Station FF3, increasing to  $\sim 50$   $\mu\text{M}$  at 25 cm (**Figure 8.16**). Dissolved ammonia levels of 16 to 40  $\mu\text{M}$  were found in the top 4 cm of the core from Station DS-2, with maximum levels downcore of 70  $\mu\text{M}$  (**Figure 8.17**). A somewhat similar comparison is observed for  $\text{Mn}^{2+}$ , with low  $\text{Mn}^{2+}$  levels of 10  $\mu\text{M}$  at the top of the core from Station FF3 relative to 200 to 500  $\mu\text{M}$  at Station DS-2 (**Figures 8.16 and 8.17**). No sulfate reduction was discernible in either core; and, the vertical profiles for  $\text{Fe}^{2+}$  were similar in both cores (**Figures 8.16 and 8.17**).

The thickness of layers containing drilling discharges observed during the post-exploration cruise, based on concentrations of Ba and TOC, was  $\sim 4$  cm in each of the three discretionary cores collected. The thin layer of material leads to depletion of dissolved oxygen in the sediments and a distinct decrease in redox potential as previously described (**Figure 8.13 and Table 8.6**). The apparent impact on the chemical composition of the interstitial water seems limited to the top of the core and is most obvious for concentrations of dissolved ammonia and  $\text{Mn}^{2+}$ . Concentrations of sediment Mn in the top 2 cm of the cores from the three discretionary stations (Cruise 3B) range from 1,600  $\mu\text{g}/\text{g}$  at Station DS-2 to 5,300  $\mu\text{g}/\text{g}$  at Station DS-1, relative to average levels of  $\sim 7,000$   $\mu\text{g}/\text{g}$  in far-field sediments (**Figure 8.18**). However, sediment Mn levels increased to  $>6,000$   $\mu\text{g}/\text{g}$  in the 2 to 4 cm section from all three discretionary cores (**Figure 8.18**). Significantly lower levels of sediment Mn in the top layers of sediment from discretionary and near-field stations during the post-exploration cruise result from lower Mn levels in the drilling discharges and a diffusive flux of  $\text{Mn}^{2+}$  from the sediment column at these stations. Overall, the shift in redox state is readily discernible, yet limited to the top 4 cm of the sediment column.

### Pore Water Results for VK 916 FF-B03 (Cruise 3B)

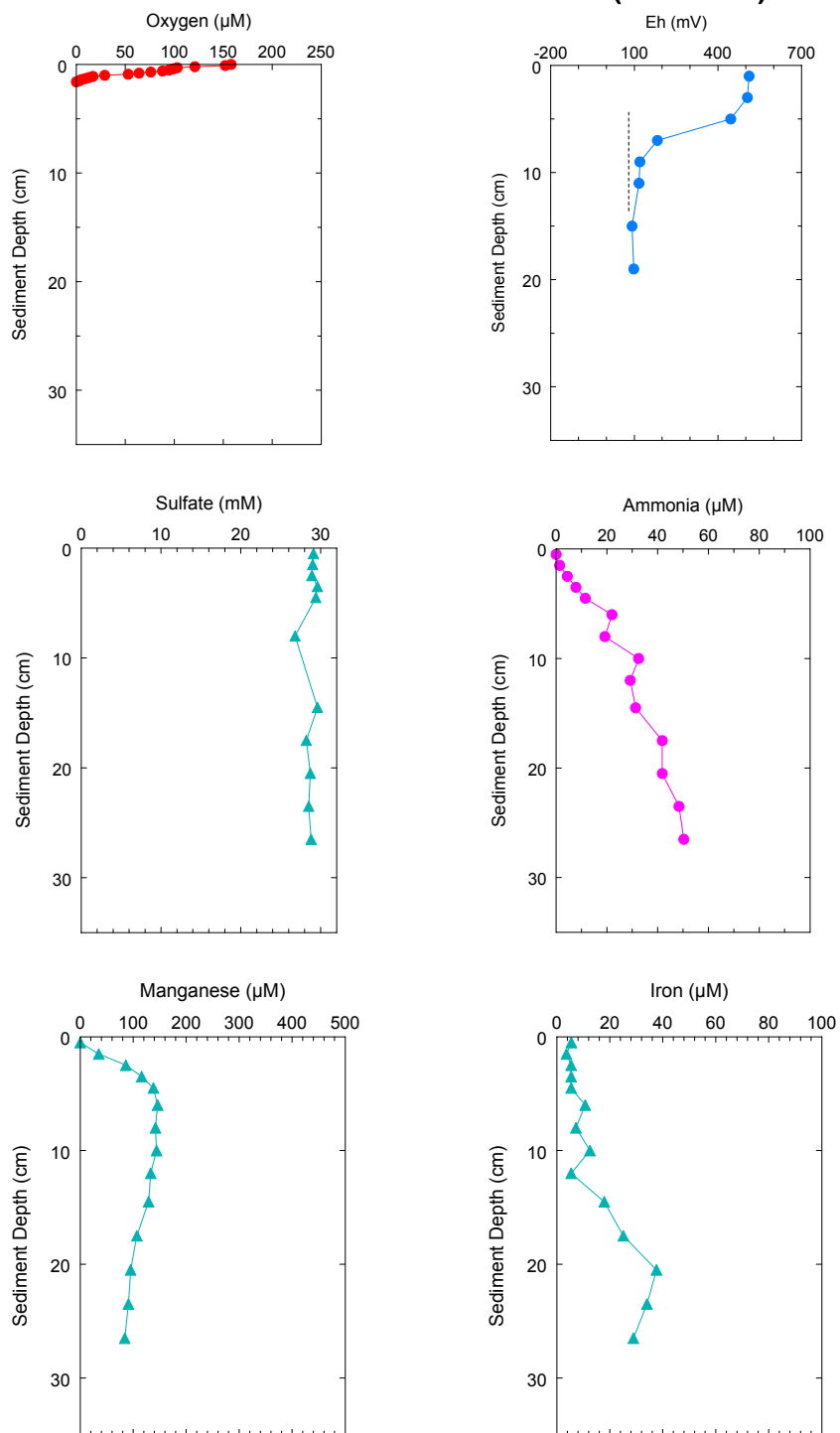


**Figure 8.16.** Vertical profiles for dissolved oxygen, Eh, sulfate, ammonia, manganese, and iron from interstitial water at Station FF-B03, Viosca Knoll (VK) 916, for post-exploration Cruise 3B.

### Pore Water Results for VK 916 DS-2 (Cruise 3B)

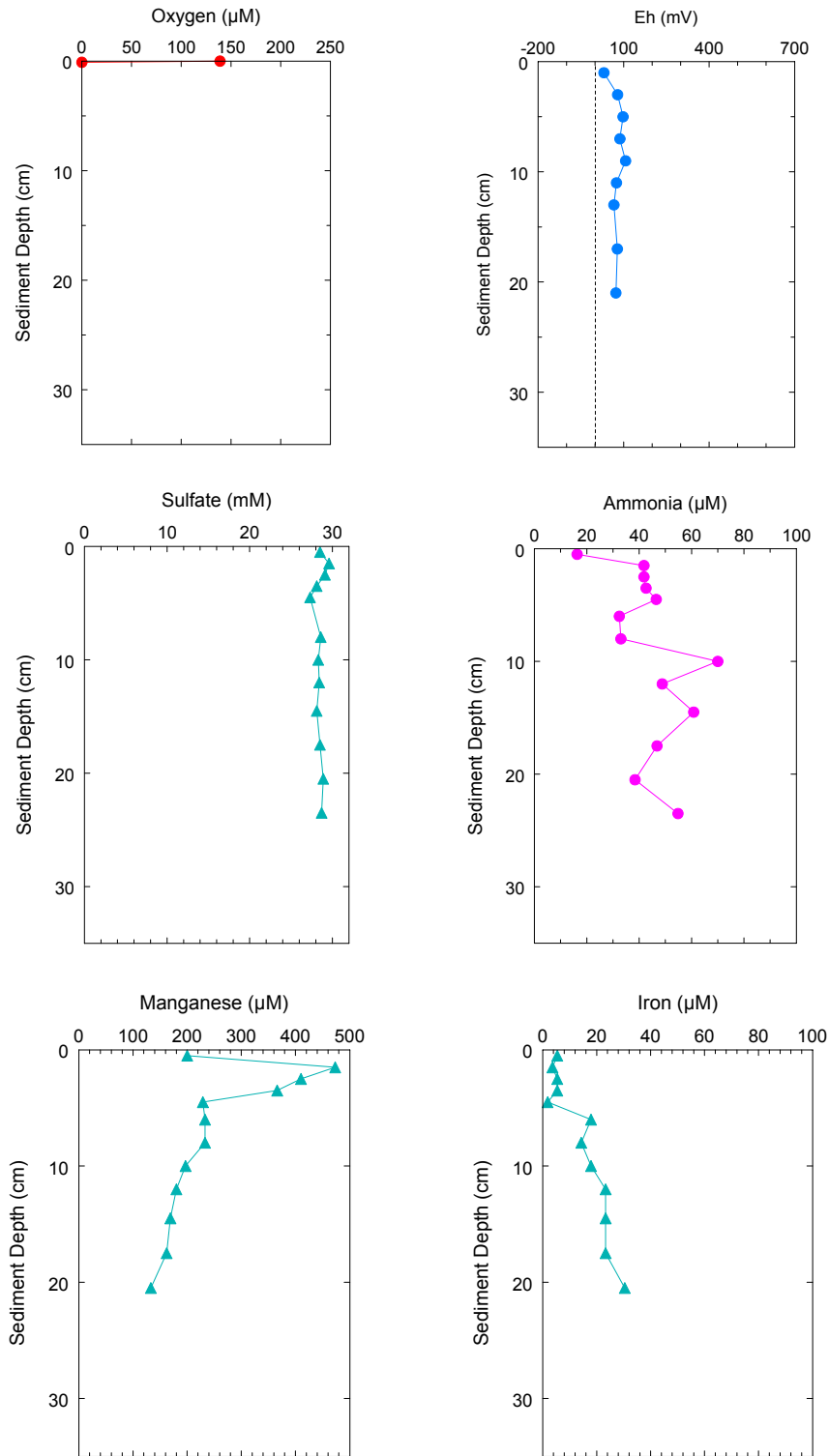


**Figure 8.17.** Vertical profiles for dissolved oxygen, Eh, sulfate, ammonia, manganese, and iron from interstitial water at Station DS-2, Viosca Knoll (VK) 916, for post-exploration Cruise 3B.

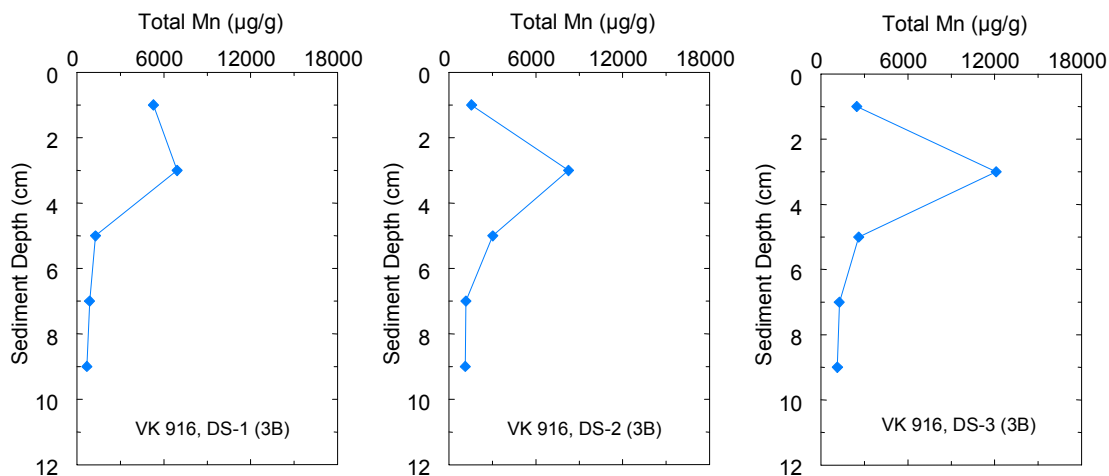


**Figure 8.18.** Vertical profiles for concentrations of manganese (Mn) in sediment from discretionary (DS) stations for post-exploration Cruise 3B to Viosca Knoll (VK) 916.

## 8.4 GARDEN BANKS BLOCK 516 – EXPLORATION/DEVELOPMENT SITE

### 8.4.1 Metals and Total Organic Carbon

Means, standard deviations, maximums and minimums for concentrations of metals, and TOC for surface (0 to 2 cm) sediments from site GB 516 are summarized in **Table 8.8**. The data in **Table 8.8** are for random stations in near-field and far-field zones and do not include results from the fixed, discretionary stations. The complete data set is presented in *Appendix G*. Once again, comparisons discussed here are between cruises and zones. However, as discussed in *Chapter 3*, some exploratory drilling and drilling discharges occurred prior to Cruise 1B at site GB 516, and additional wells were drilled prior to Cruise 2B. Thus, the data from GB 516 evaluate part of a continuum in the exploration/development process rather than the clearer pre- and post-exploration sampling at VK 916.

Mean concentrations of Al and Fe in surface sediments collected during Cruises 1B and 2B for near-field and far-field stations varied by <10% (**Table 8.8**), and the mean Fe/Al ratio of 0.47 for all surface sediments from GB 516 is the same as observed at VK 916. Data for Al versus Fe from all 213 data points in the complete study are shown in **Figure 8.19a**. The good linear fit of the data ( $r = 0.95$ ) supports a uniform source (the Mississippi River) for aluminosilicates throughout the study area. Points with low levels of both Fe and Al are observed when the normal aluminosilicates are mixed with and diluted by drilling discharges. Lower levels of Fe and Al were observed in near-field sediments from GB 516 (**Table 8.8**) relative to far-field stations due to the influence of drilling discharges. The effect is greatest for samples from Station DS-2 for Cruise 2B, where all Fe and Al levels were <1% and <2%, respectively (**Figure 8.19a**). Overall, sediments with concentrations of Al <6% also contain Ba levels >1% (**Figure 8.19b**). All data points at lower levels of Al and elevated concentrations of Ba are from near-field or discretionary stations. As the fraction of drilling discharges increases (as represented by Ba concentrations), the proportion of terrigenous clay (as represented by Al

concentrations) decreases (**Figure 8.19b**). Data for samples from far-field stations have low levels of Ba (<0.2%) relative to those where drilling discharges are present and thus plot along the baseline at about 6% to 7% Al on **Figure 8.19b**.

**Table 8.8.** Means  $\pm$  standard deviations with ranges in parentheses for metals, and total organic carbon (TOC) for Garden Banks 516 for Cruises 1B and 2B.

Element	Far-Field		Near-Field	
	Post-Exploration Cruise 1B	Post-Development Cruise 2B	Post-Exploration Cruise 1B	Post-Development Cruise 2B
Al (%)	6.40 $\pm$ 0.18 (6.00-6.62)	6.03 $\pm$ 0.21 (5.76-6.37)	6.25 $\pm$ 0.92 (4.59-8.17)	5.78 $\pm$ 1.00 (3.29-6.84)
As ( $\mu\text{g/g}$ )	11.0 $\pm$ 0.7 (9.7-12.2)	11.1 $\pm$ 0.8 (9.8-12.6)	10.3 $\pm$ 2.0 (5.2-12.3)	11.1 $\pm$ 1.2 (8.5-13.0)
Ba (%)	0.128 $\pm$ 0.034 (0.076-0.197)	0.148 $\pm$ 0.056 (0.079-0.277)	2.45 $\pm$ 3.83 (0.31-13.5)	5.90 $\pm$ 9.57 (0.86-35.1)
Cd ( $\mu\text{g/g}$ )	0.32 $\pm$ 0.03 (0.28-0.36)	0.27 $\pm$ 0.02 (0.24-0.30)	0.31 $\pm$ 0.03 (0.26-0.38)	0.28 $\pm$ 0.05 (0.23-0.41)
Cr ( $\mu\text{g/g}$ )	66.2 $\pm$ 3.0 (60.6-69.6)	59.5 $\pm$ 7.3 (39.5-68.0)	51.0 $\pm$ 9.2 (31.1-63.7)	62.6 $\pm$ 9.9 (41.4-74.7)
Cu ( $\mu\text{g/g}$ )	27.1 $\pm$ 0.6 (26.2-28.1)	28.2 $\pm$ 1.0 (26.1-29.7)	27.0 $\pm$ 1.7 (23.5-30.3)	32.7 $\pm$ 5.1 (27.0-45.8)
Fe (%)	2.93 $\pm$ 0.11 (2.75-3.11)	2.90 $\pm$ 0.17 (2.52-3.15)	2.82 $\pm$ 0.41 (2.20-3.64)	2.83 $\pm$ 0.43 (1.76-3.23)
Hg (ng/g)	108 $\pm$ 9 (92-118)	116 $\pm$ 20 (95-154)	101 $\pm$ 15 (79-128)	123 $\pm$ 39 (88-237)
Mn ( $\mu\text{g/g}$ )	4,180 $\pm$ 1,240 (3,080-7,570)	3,650 $\pm$ 585 (2,740-4,840)	3,470 $\pm$ 1,870 (658-6,970)	2,070 $\pm$ 1,140 (285-3,490)
Ni ( $\mu\text{g/g}$ )	44.2 $\pm$ 4.2 (36.2-49.1)	43.2 $\pm$ 2.6 (37.7-46.8)	39.8 $\pm$ 6.5 (24.9-47.9)	34.5 $\pm$ 7.7 (14.1-42.3)
Pb ( $\mu\text{g/g}$ )	24.5 $\pm$ 1.6 (20.9-27.3)	24.0 $\pm$ 2.0 (20.9-26.8)	24.1 $\pm$ 2.5 (18.3-28.7)	33.6 $\pm$ 10.3 (21.0-60.3)
V ( $\mu\text{g/g}$ )	124 $\pm$ 6 (116-137)	129 $\pm$ 5 (122-137)	119 $\pm$ 10 (89-128)	118 $\pm$ 22 (57-140)
Zn ( $\mu\text{g/g}$ )	90.2 $\pm$ 3.3 (83.4-95.4)	86.8 $\pm$ 3.5 (81.5-92.6)	94.4 $\pm$ 14.9 (84.1-133)	96.2 $\pm$ 38.3 (63.1-213)
TOC (%)	0.82 $\pm$ 0.08 (0.70-0.95)	1.08 $\pm$ 0.07 (0.97-1.27)	1.25 $\pm$ 0.69 (0.84-3.31)	1.32 $\pm$ 0.51 (0.82-2.87)

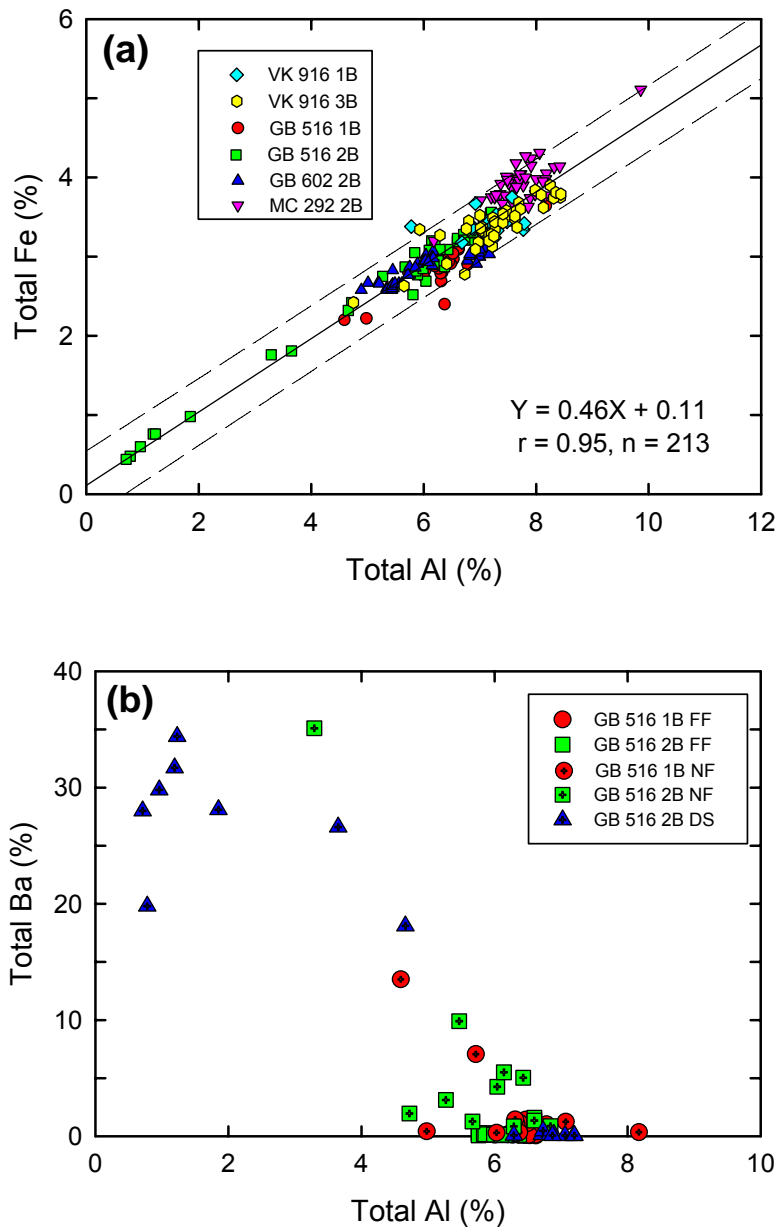


**Figure 8.19.** Concentrations of aluminum (Al) versus (a) iron (Fe) and (b) barium (Ba) for sediments from far-field (FF), near-field (NF), and discretionary (DS) stations from Garden Banks (GB) 516 collected during Cruises 1B and 2B.

At GB 516, concentrations of Ba are statistically lower for far-field versus near-field sediments during both cruises (**Tables 8.8 and 8.9** and **Figure 8.20**). Mean Ba concentrations were ~20-fold greater at near-field than far-field stations during Cruise 1B (**Table 8.8** and **Figure 8.20**). Barium levels in near-field sediments from Cruise 2B were about 40 times greater than at far-field stations (**Table 8.8** and **Figure 8.20**) but not significantly greater than at near-field stations sampled during Cruise 1B.

**Table 8.9.** Results of statistical comparisons (t-tests) for concentrations of metals among cruises (1B and 2B) and zones (NF and FF) for Garden Banks 516. Results for discretionary stations were not included in the statistical tests.

Dependent Variable	Independent Variable	Probability > F	Interpretation
Log Ba	cruise	<0.0001	NF Cruise 2B>NF Cruise 1B
Hg	cruise	0.039	NF Cruise 2B>NF Cruise 1B
Mn	cruise	0.018	NF Cruise 2B<NF Cruise 1B
TOC	zone	<0.0001	NF>FF (both cruises)

FF = far-field; NF = near-field; TOC = total organic carbon.

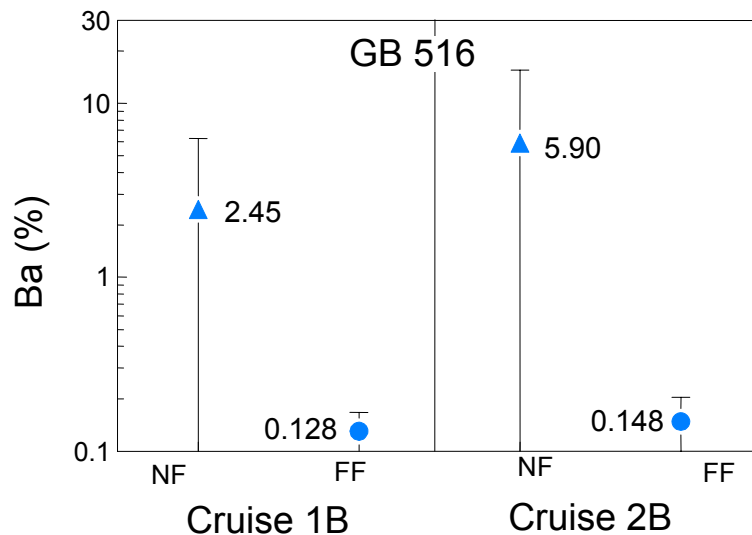


**Figure 8.20.** Concentrations of barium (Ba) with markers and numbers showing means and lines showing standard deviations in sediment from near-field (NF) and far-field (FF) stations at Garden Banks (GB) 516 during Cruises 1B and 2B. In some cases, the line for the standard deviation appears skewed due to the logarithmic scale.

The spatial distribution of Ba in sediments for both cruises is shown in **Figure 8.21**. The inner portion of the near-field zone with sediments containing >5% Ba is similar in size for both sampling periods; however, the number of data points and the magnitude of the Ba concentrations are greater for the second cruise (**Figure 8.21**). The area of the near-field zone with sediment samples containing >1% Ba approximately doubled between the two cruises (**Figure 8.21**).

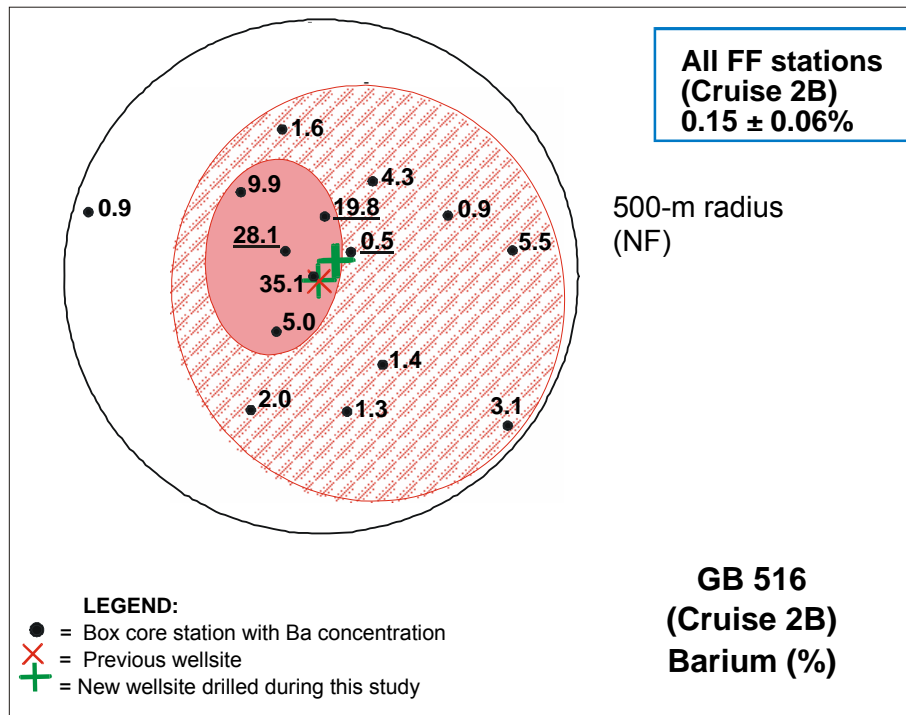
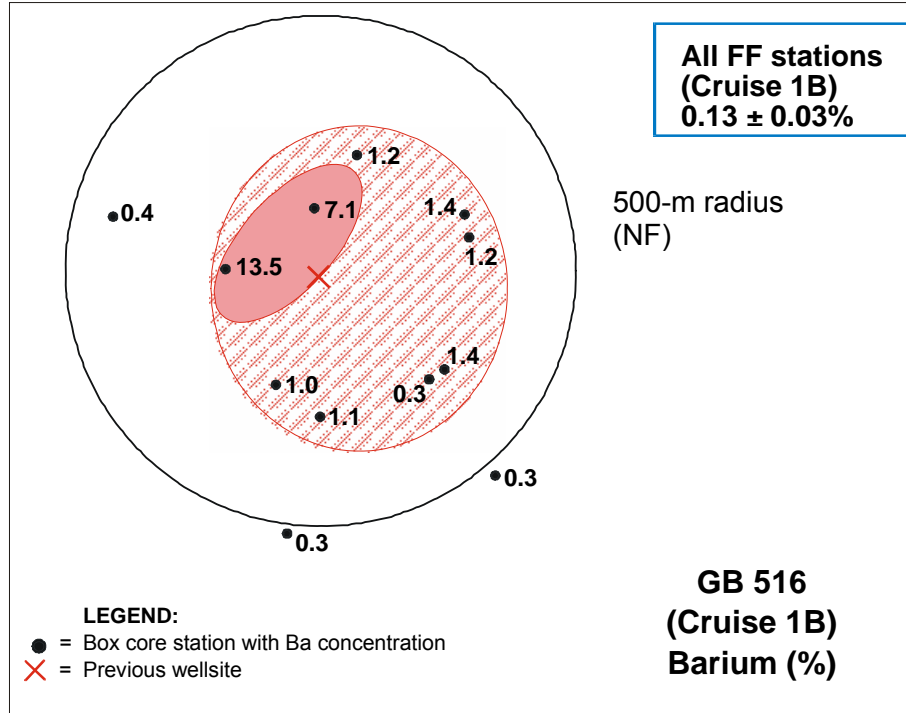


**Figure 8.21.** Concentrations of barium (Ba) at Garden Banks (GB) 516 near-field (NF) stations during Cruises 1B and 2B. Inset boxes show mean Ba concentrations at all far-field (FF) stations. Data for the discretionary stations from Cruise 2B are underlined. The bold NF circle represents a radius of 500 m. The darker shaded oval highlights area where Ba concentrations are  $\geq 5\%$ , and the lighter shaded, larger oval highlights area where Ba concentrations are  $\geq 1\%$ .



Vertical profiles for Ba in sediments were obtained for the three discretionary stations during Cruise 2B. Concentrations of Ba were above background levels (~0.1%) in surficial sediments from each discretionary station (**Figure 8.22**). The elevated Ba concentrations decreased to background levels at 4 to 6 cm and 6 to 8 cm for Stations DS-3 and DS-1, respectively (**Figure 8.22**). At Station DS-2, Ba concentrations were >30% at 8 to 10 cm, the deepest layer analyzed. Vertical profiles for Al in the sediment column mirror the profiles for Ba, with lower levels of Al in the presence of greater amounts of Ba (**Figure 8.22**). Based on the sediment Ba data, the sphere of influence for drilling discharges was directed toward the southwest and may have extended beyond the near-field zone (**Figure 8.21**). Drilling discharges were found at sediment depths  $\geq 10$  cm at one station.

Concentrations of Mn in surface sediments at near-field stations show a larger range in concentrations relative to far-field stations (**Table 8.8**). All nine surface sediment samples with Mn levels <2,000  $\mu\text{g/g}$  were collected at near-field stations, two during Cruise 1B and seven during Cruise 2B (**Figure 8.23**). These observations support reductive dissolution of Mn at some near-field stations when reducing conditions develop where drilling discharges are found. This information and the results for Mn in sediment cores will be further considered in discussions regarding the redox state of the sediment.

Mean concentrations of Al, As, Cd, Fe, Ni, Pb, V, and Zn were not significantly different among far-field and near-field stations for both the two cruises (**Tables 8.8** and **8.9**). The metal that showed the greatest zone-wide shift in concentrations that can be related to drilling was Ba, with a significant change also observed for Hg (**Table 8.9**). Some isolated shifts in metal concentrations can be identified by examining metals data on a station-by-station basis. For example, at Station NF-B03A (Cruise 2B), Ba levels were 35.1%, and concentrations of Al, Fe, Ni, and V were 40% to 70% lower at this station due to dilution of the natural aluminosilicate material, with ~65% barite in the sediments, which was associated with drilling discharges. However, concentrations of Cu, Hg, and Pb were greater in sediment from Station NF-B03A (Cruise 2B) than levels in background sediment by about 60%, 100%, and 250%, respectively. These increases are directly related to increases in concentrations of Ba as shown for Hg and Pb in **Figure 8.24**

Vertical profiles for Hg in sediments from discretionary stations from Cruise 2B show minor enhancement in Hg levels at the top of the core at Station DS-1, high Hg levels throughout the core at Station DS-2, and no enrichment at Station DS-3 (**Figure 8.25**). A more detailed, separate section on trace metals in sediments, which provides an overview of all drilling sites, is presented at the end of the chapter.

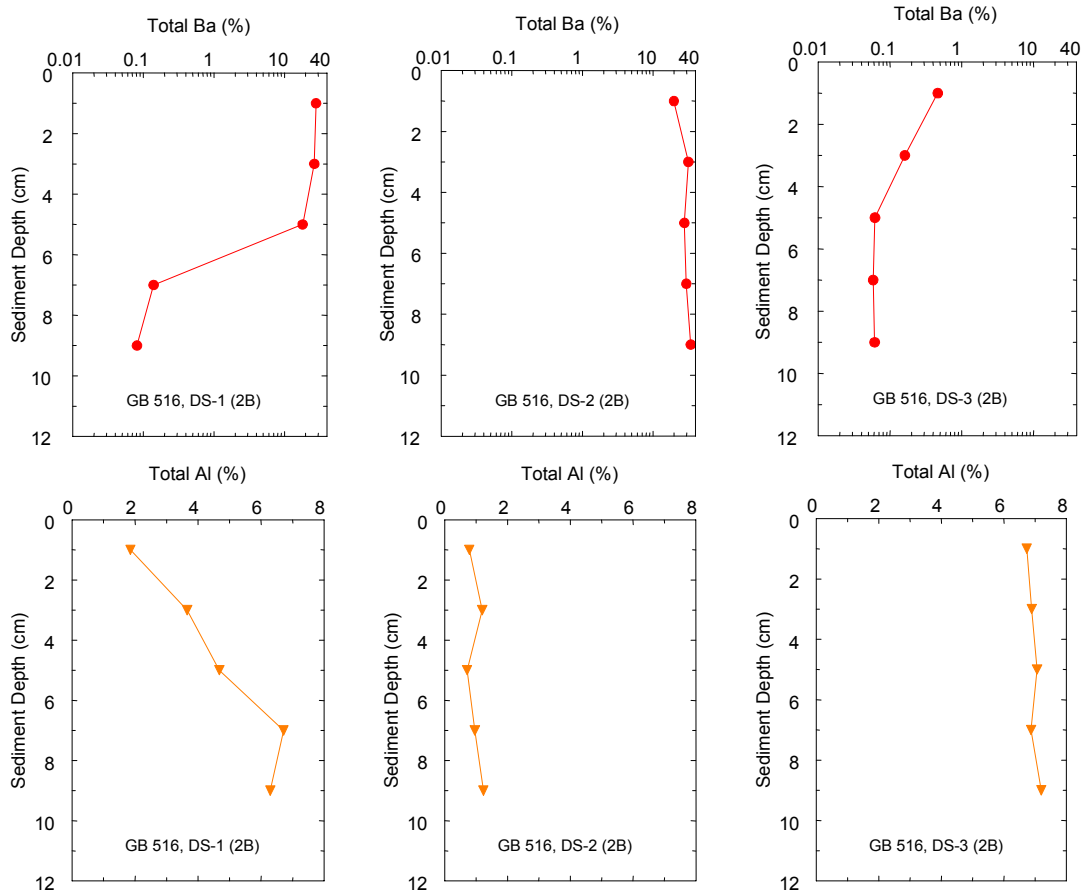


**Figure 8.22.** Vertical profiles for concentrations of barium (Ba) and aluminum (Al) in sediment from discretionary (DS) stations at Garden Banks (GB) 516 for Cruise 2B.

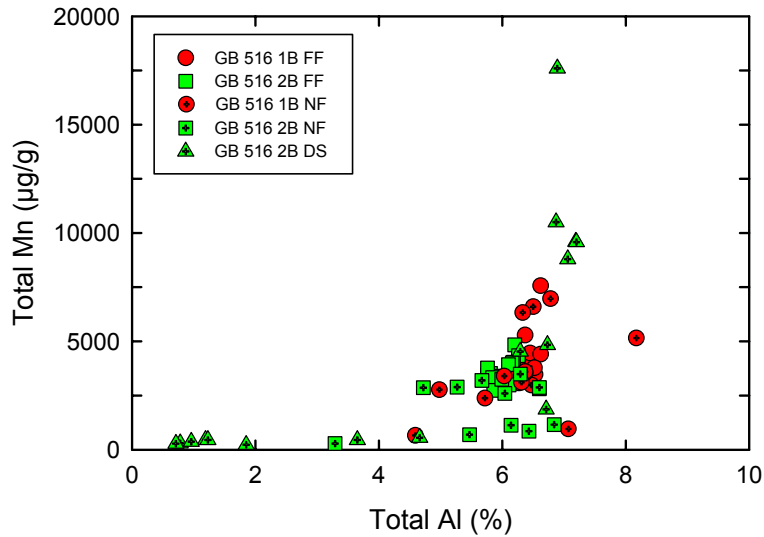


**Figure 8.23.** Concentrations of aluminum (Al) versus manganese (Mn) for sediments from far-field (FF), near-field (NF), and discretionary (DS) stations from Garden Banks (GB) 516 collected during Cruises 1B and 2B.

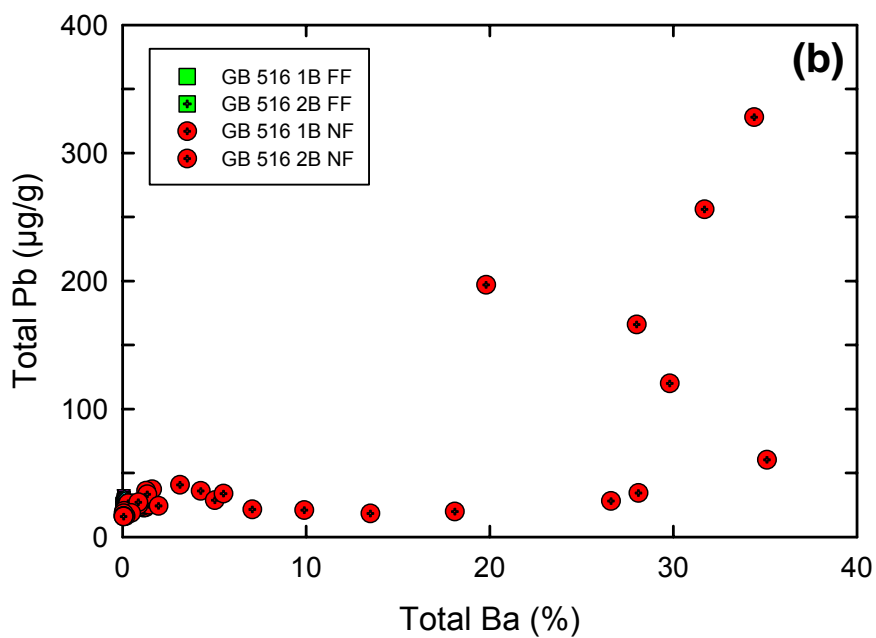
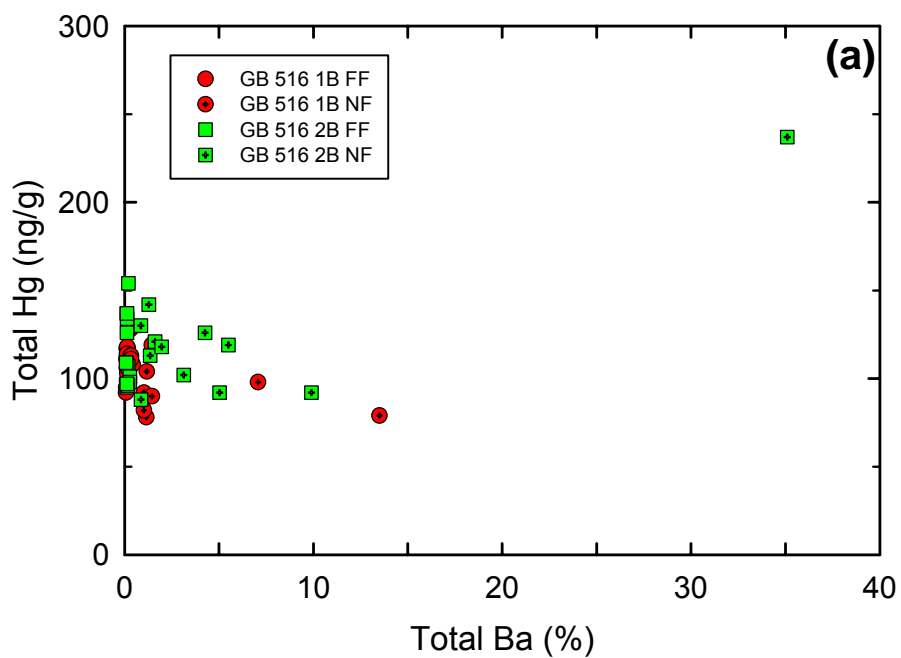


**Figure 8.24.** Concentrations of barium (Ba) versus (a) mercury (Hg) and (b) lead (Pb) for sediments from far-field (FF) and near-field (NF) stations from Garden Banks (GB) 516 collected during Cruises 1B and 2B. Points from FF samples are hidden beneath points for NF samples at Ba levels <0.2%.

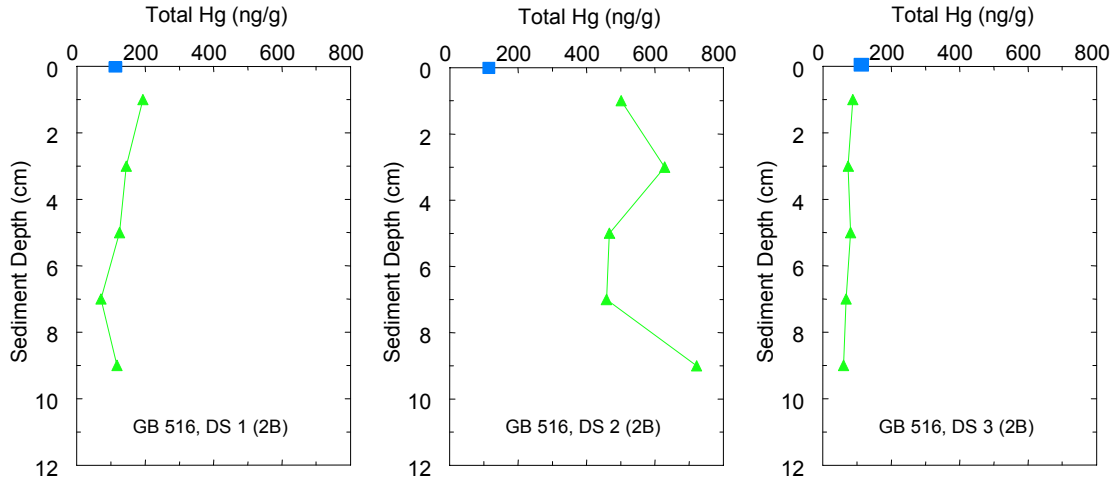


**Figure 8.25.** Vertical profiles for concentrations of mercury (Hg) in sediment from discretionary (DS) stations for Cruise 2B at Garden Banks (GB) 516. Square at 0 cm on each graph represents mean Hg values at far-field stations.

Concentrations of TOC in near-field surface sediments are statistically higher than at far-field stations during both cruises (**Table 8.9** and **Figure 8.26**). The maximum values for TOC in near-field samples from both cruises are about three times greater than levels at far-field stations. Surface sediments from two near-field stations and two discretionary stations contain >2% TOC, with a maximum level of 7.16%. Each of the samples with >2% TOC contains  $\geq 10\%$  Ba (**Figure 8.27**). Vertical profiles for TOC (**Figure 8.28**) show similar trends to those observed for Ba (**Figure 8.22**), with elevated levels of TOC at Station DS-1 restricted to the top 2 to 4 cm, very high levels of TOC throughout the 10-cm length of the core at Station DS-2, and no enrichment at Station DS-3.

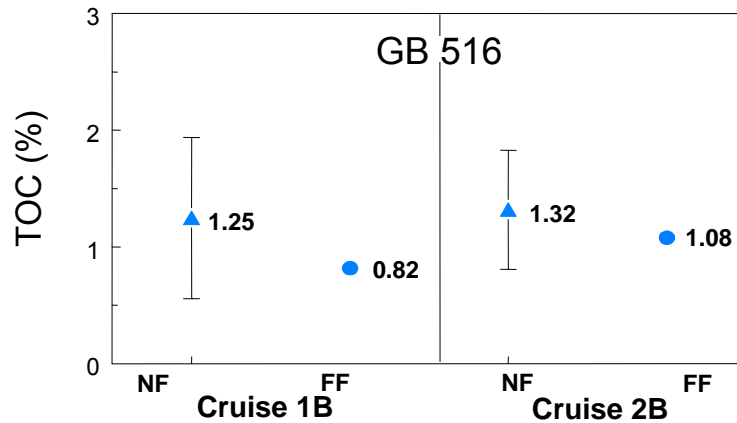


**Figure 8.26.** Concentrations of total organic carbon (TOC) with markers and numbers showing means and lines showing standard deviations in sediment from near-field (NF) and far-field (FF) stations from Garden Banks (GB) 516 during Cruises 1B and 2B. The lines for the standard deviations for the FF data are obscured by the markers.

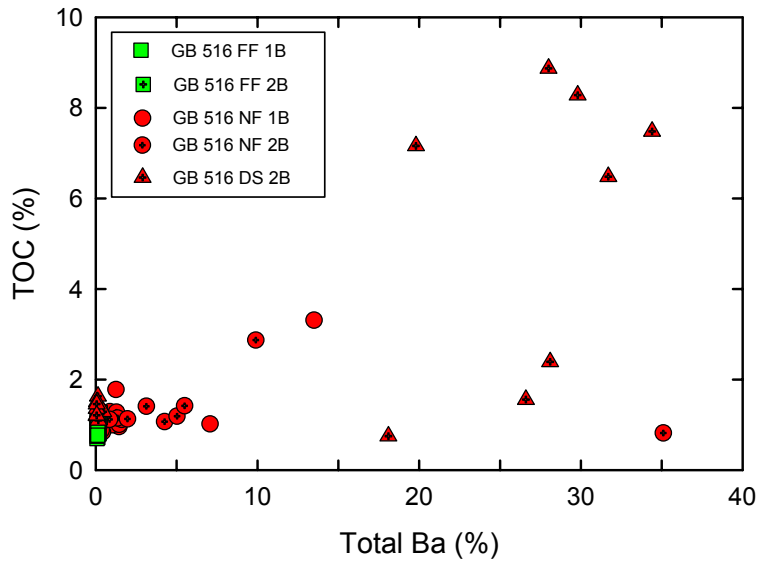


**Figure 8.27.** Concentrations of barium (Ba) versus total organic carbon (TOC) for sediments from far-field (FF), near-field (NF), and discretionary (DS) stations from Garden Banks (GB) 516 collected during Cruises 1B and 2B. Some points from FF and NF samples are hidden beneath the NF and DS data points for Cruise 2B at low concentrations of Ba.

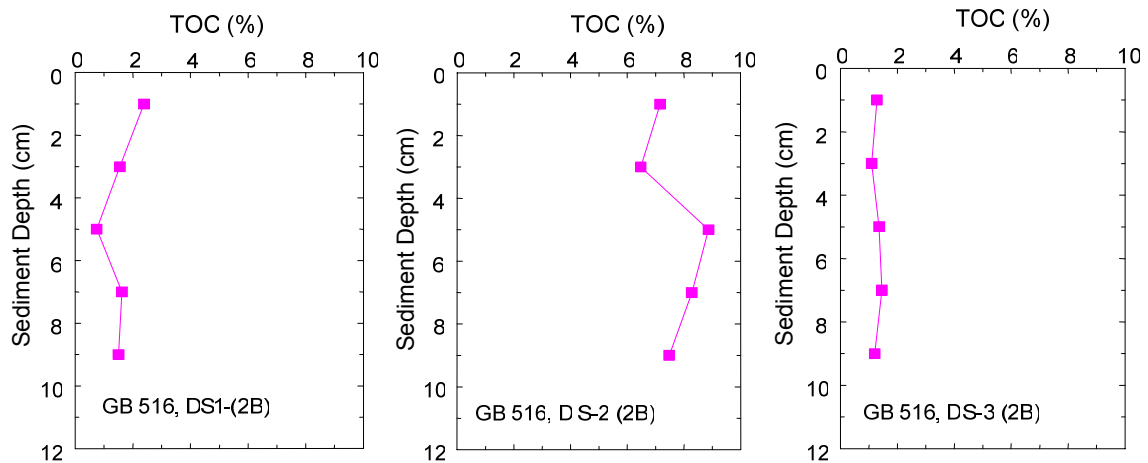


**Figure 8.28.** Vertical profiles for concentrations of total organic carbon (TOC) in sediment from discretionary (DS) stations for Cruise 2B at Garden Banks (GB) 516.

#### 8.4.2 Sediment Geochronology

The vertical profile for excess  $^{210}\text{Pb}$  at Station FF6 from Cruise 2B was used to calculate a sedimentation rate of 0.07 cm/y (**Figure 8.29**). This rate is similar to the value of 0.06 cm/y determined for VK 916 and is consistent with expected rates on the slope.

At Station NF-B02 from Cruise 2B, the top 2 cm of sediment have ~2 times lower activities of excess  $^{210}\text{Pb}$  than found in the next three, deeper layers (**Figure 8.29**). Barium concentrations in the 0 to 2 cm section of sediment from Station NF-B02 were 1.6% relative to background levels of ~0.1%. Thus, some drilling mud and cuttings are most likely distorting the expected activity of excess  $^{210}\text{Pb}$ . Below the surface anomaly, a continuous decrease in the activities of excess  $^{210}\text{Pb}$  was used to calculate a sedimentation rate of 0.06 cm/y, the same as found for the undistorted core from Station FF6. The excess  $^{210}\text{Pb}$  data for Station NF-B02 identify the presence of drilling discharges in the top 2 cm, but do not help distinguish between drilling mud versus cuttings.

#### 8.4.3 Sediment Oxygen Levels and Redox Conditions

Concentrations of dissolved  $\text{O}_2$  in sediment from far-field stations at GB 516 are similar for both sampling periods and decrease to non-detectable levels ( $<2 \mu\text{M}$ ) at sediment depths of 2.7 to 5.8 cm (**Figures 8.30** and **8.31** and **Table 8.10**). Ranges in Eh and pH values also are generally similar for far-field sediments from both cruises (**Table 8.10**). Typical vertical profiles for dissolved oxygen for far-field stations at GB 516 during the two cruises show exponential decreases in dissolved  $\text{O}_2$  in the sediment (**Figures 8.30** and **8.31**). At the same depth of ~5 cm, where that oxygen concentrations approached zero at Station FF3 (Cruise 1B), the Eh decreases sharply from +600 to +300 mV (**Figure 8.30**, note different depth scales for oxygen and Eh). This shift signals a change from oxic to suboxic conditions, where nitrate and manganese and iron oxides serve as electron acceptors during the oxidation of organic matter (**Figure 8.11**). At Station FF6 during Cruise 2B, the oxygen and Eh profiles were slightly different, with a sharper decrease in oxygen levels with increasing depth and lower levels of Eh (**Figure 8.31**). These two profiles highlight observed differences at far-field stations as summarized in **Table 8.10**. For example, the Eh in the top 1 cm ranged from +692 mV to +104 mV for all far-field stations (**Table 8.10**). Data for near-field stations during Cruise 1B were highly variable, with Eh levels as low as -163 mV in the top 1 cm of sediment and oxygen penetration depths as low as 0.3 cm (**Table 8.10** and **Figure 8.30**). However, results for other near-field stations were similar to those observed for far-field stations (e.g., NF-B10, **Figure 8.30**). As discussed previously, evidence for the presence of drilling discharges was found during Cruise 1B.

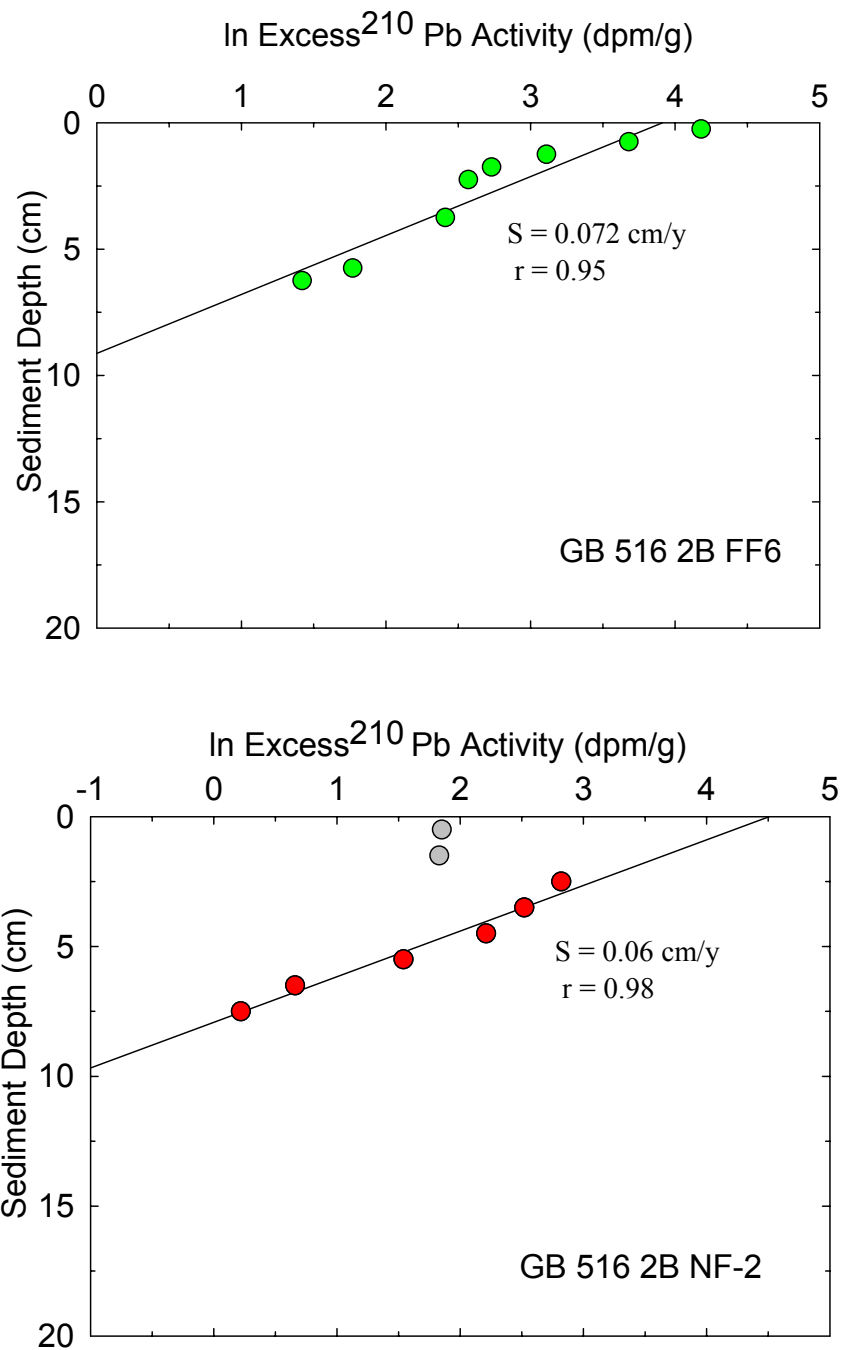


**Figure 8.29.** Vertical profiles for activities of excess <sup>210</sup>Pb in sediment from Garden Banks (GB) 516 for Station FF6 during Cruise 2B and Station NF-B02 for Cruise 2B ( $S$  = sedimentation rate,  $r$  = correlation coefficient, calculated using all points for FF6 and only the red points for NF-B02).

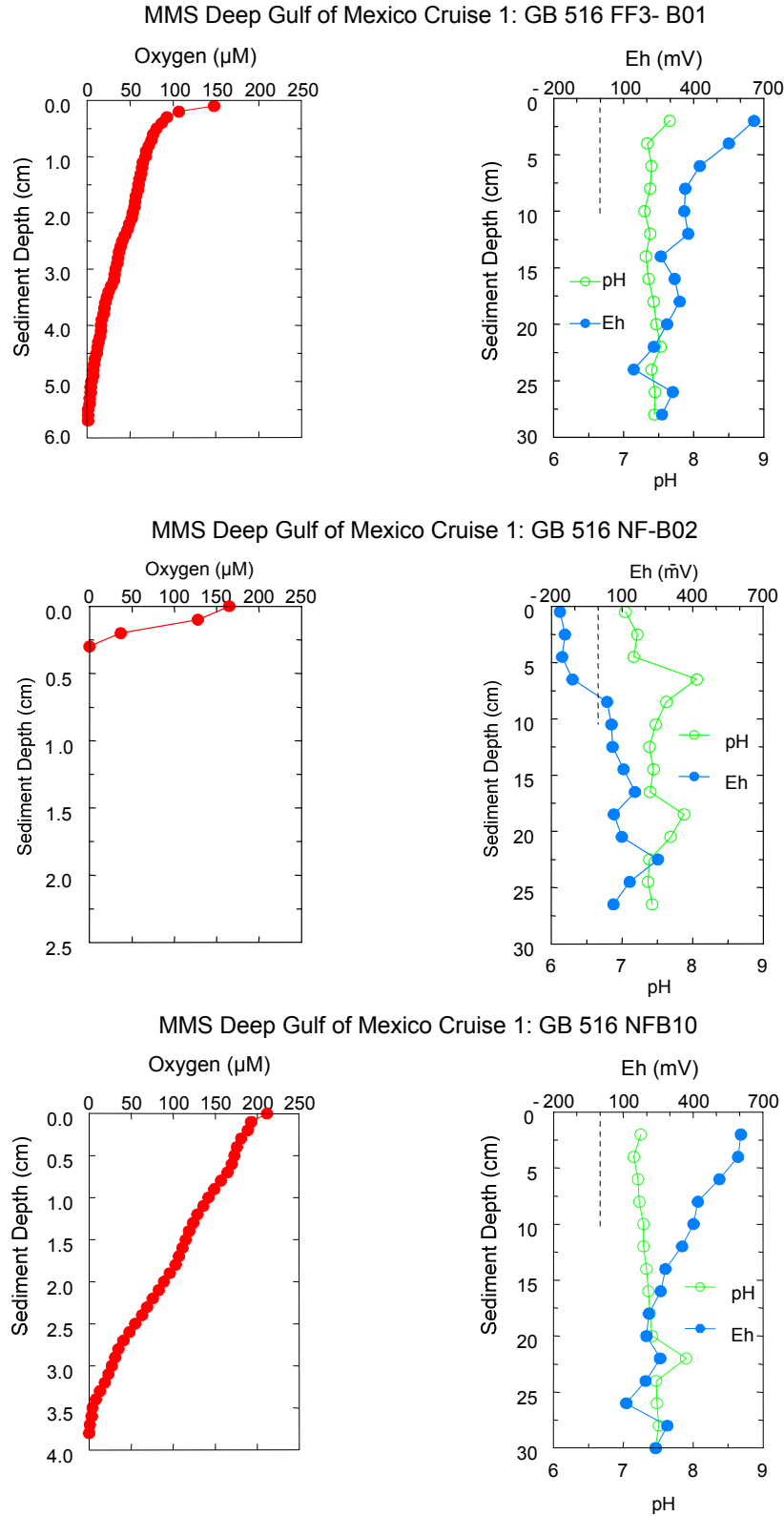


**Figure 8.30.** Vertical profiles for dissolved oxygen, redox potential (Eh), and pH in sediment from representative near-field (NF) and far-field (FF) stations at Garden Banks (GB) 516 from Cruise 1B (note different depth scales for oxygen versus Eh).



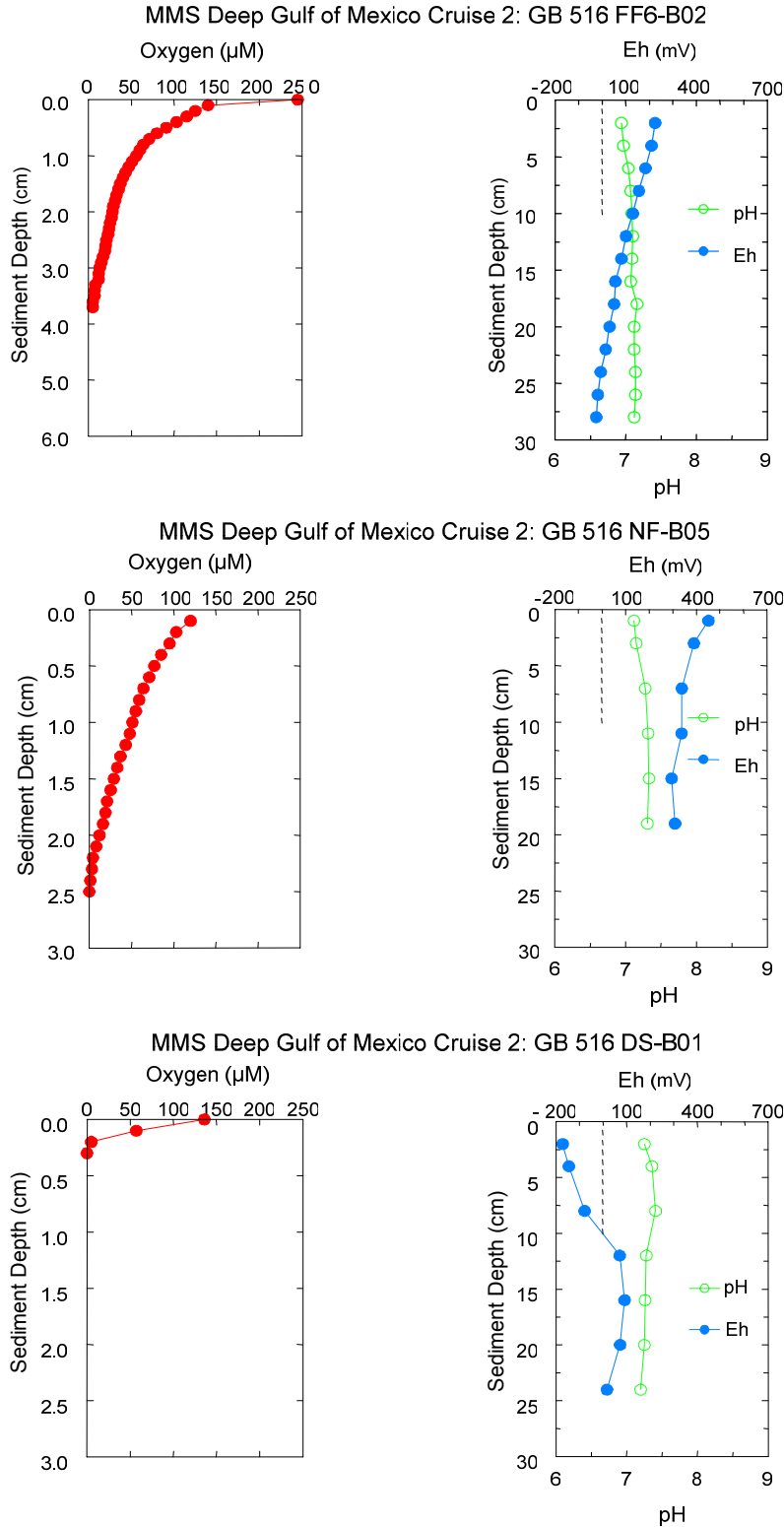


**Figure 8.31.** Vertical profiles for dissolved oxygen, redox potential (Eh), and pH in sediment from representative near-field (NF), and far-field (FF), and discretionary (DS) stations from Garden Banks (GB) 516 from Cruise 2B (note different depth scales for oxygen versus Eh).

**Table 8.10.** Summary data for dissolved oxygen, redox potential (Eh), and pH for sediment from Garden Banks (GB) 516 at near-field (NF), far-field (FF), and discretionary (DS) stations during Cruises 1B and 2B.

Site	Zone	Zero O <sub>2</sub> depth (cm)	Eh <sub>1 cm</sub> range (mV)		Eh <sub>10 cm</sub> range (mV)		pH
GB 516 (Cruise 1B)	NF	0.3 – 5.7	+664	-163	+528	+56	6.8 – 8.1
	FF	3.4 – 5.8	+692	+406	+598	+303	7.3 – 8.3
GB 516 (Cruise 2B)	NF	0.2 – 2.5	+506	-107	+259	+29	6.9 – 7.8
	DS	0.1 – 0.3	+196	-171	+39	-78	6.6 – 10.5
	FF	2.7 – 5.7	+492	+104	+390	+101	6.9 – 7.9

During Cruise 2B, values for dissolved oxygen and Eh at many near-field and all three discretionary stations were considerably lower (**Table 8.10**). For example, the lowest Eh level in the top 1 cm of the sediment at near-field and discretionary stations was -107 and -171 mV, respectively, relative to +104 mV in far-field sediments (**Table 8.10** and **Figure 8.31**). Likewise, the sediment depth to zero oxygen was closer to the sediment-water interface at near-field and discretionary stations from Cruise 2B relative to far-field stations (**Table 8.10**). Some near-field stations (e.g., NF-B05, **Figure 8.31**), had similar oxygen and Eh profiles as observed at far-field stations. Overall, the sediment depth to zero oxygen and the Eh values were lower at near-field stations from Cruise 2B than during Cruise 1B (**Table 8.10**), yet results for the near-field stations from Cruise 1B showed lower levels of oxygen and Eh.

The mean integrated amounts of oxygen ( $\Sigma\text{O}_2$ ) in the sediments at far-field stations from Cruises 1B and 2B and near-field stations from Cruise 1B were not statistically different, even though the mean value for the near-field stations from Cruise 1B was about 20% lower than at far-field stations (**Figure 8.32**). Absolute mean values for  $\Sigma\text{O}_2$  at the far-field stations for GB 516 (153 and 165 nmol/cm<sup>2</sup>) are significantly greater than at VK 916 (90 and 84 nmol/cm<sup>2</sup>), most likely a function of higher levels of TOC at VK 916 (~1.5% TOC) relative to GB 516 (~1.0% TOC) because sedimentation rates are similar.

In contrast, values for  $\Sigma\text{O}_2$  in sediments collected at near-field and discretionary stations during Cruise 2B averaged about 15% and 10% of far-field values, respectively (**Figure 8.32**). This shift is directly related to the presence of drilling discharges. The rapid deposition of several centimeters of more organic-rich sediment at many stations in the near-field zone leads to an increasing rate of bacterial activity with resulting depletion of dissolved oxygen. The mean value for  $\Sigma\text{O}_2$  for near-field stations from Cruise 2B was about 20% of the value from Cruise 1B. Therefore, most of the change in the redox environment of the sediments that resulted from drilling discharges occurred between the two cruises.

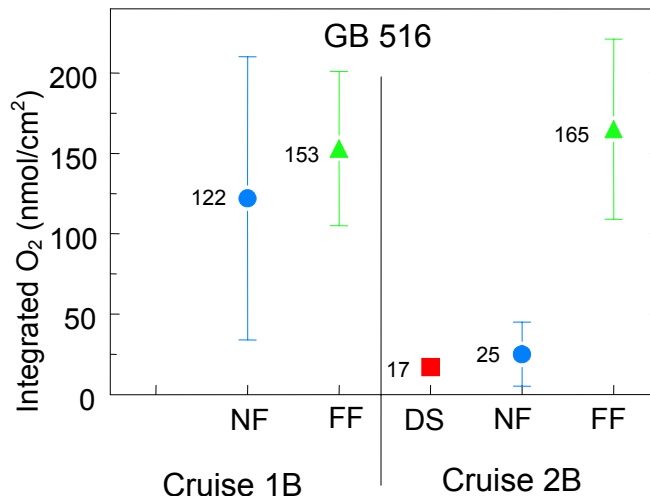


**Figure 8.32.** Integrated amounts of oxygen in the sediment column at near-field (NF), far-field (FF), and discretionary (DS) stations at Garden Banks (GB) 516 for Cruises 1B and 2B. Markers and numbers show means, and lines show standard deviations. The line for the standard deviation for the DS data is obscured by the marker.

#### 8.4.4 Interstitial Water Composition

Results for interstitial water from one far-field and one near-field station from Cruise 1B for GB 516 show some similarities and some distinct differences (**Figures 8.33** and **8.34**). Levels of  $\Sigma\text{O}_2$  were 251 nmol/cm<sup>2</sup> in the far-field core relative to 74 nmol/cm<sup>2</sup> in the near-field core. The Eh of >+600 mV in the top layer of the far-field core decreased gradually to +200 to +100 mV by depths of 15 to 20 cm. In the near-field core, the Eh at the top of the core was about +200 mV and increased to +400 mV from 5 to 15 cm and then decreased to +200 to +100 mV at 20 cm. No discernible sulfate reduction or detectable sulfide (i.e., <2  $\mu\text{M}$  total H<sub>2</sub>S) were observed in either core (**Figures 8.33** and **8.34**). Nitrate was detected in the top layers of both cores (**Figure 8.33**). Concentrations of Fe<sup>2+</sup> increased at depths below 20 cm in both cores; however, Fe<sup>2+</sup> also was detected in the top few centimeters of the near-field core. Levels of Mn<sup>2+</sup> were below detection limits in the top centimeters of the far-field core, with a gradual increase to ~100  $\mu\text{M}$  at a depth of ~20 cm. In contrast, the Mn profile in the near-field core was marked by a sharp increase in the top few centimeters and a decrease to ~100  $\mu\text{M}$  by 5 cm.

The sediments from Station FF2 (Cruise 1B) show no evidence of drilling discharges (0.13% Ba), and levels of TOC were 0.9%. In contrast, the top layer of sediment at Station NF-B01 (Cruise 1B) contained 1.2% Ba and 1.8% TOC. Collectively, the interstitial water results for far-field and near-field stations during Cruise 1B show that the upper few centimeters of sediment grade from oxic to sub-oxic in both cores, with the inventory of oxygen being more depleted in the near-field core. Once again, the surface 10 cm of the Mn<sup>2+</sup> profiles are very different between the far-field and near-field stations during Cruise 1B, with much greater amounts of Mn<sup>2+</sup> being produced in the near-field core, where oxygen levels are depleted within the top 2 cm of the sediment column. These shifts are directly related to the loading of TOC and sediment from drilling discharges.

### Pore Water Results for GB 516 FF-B02 (Cruise 1B)

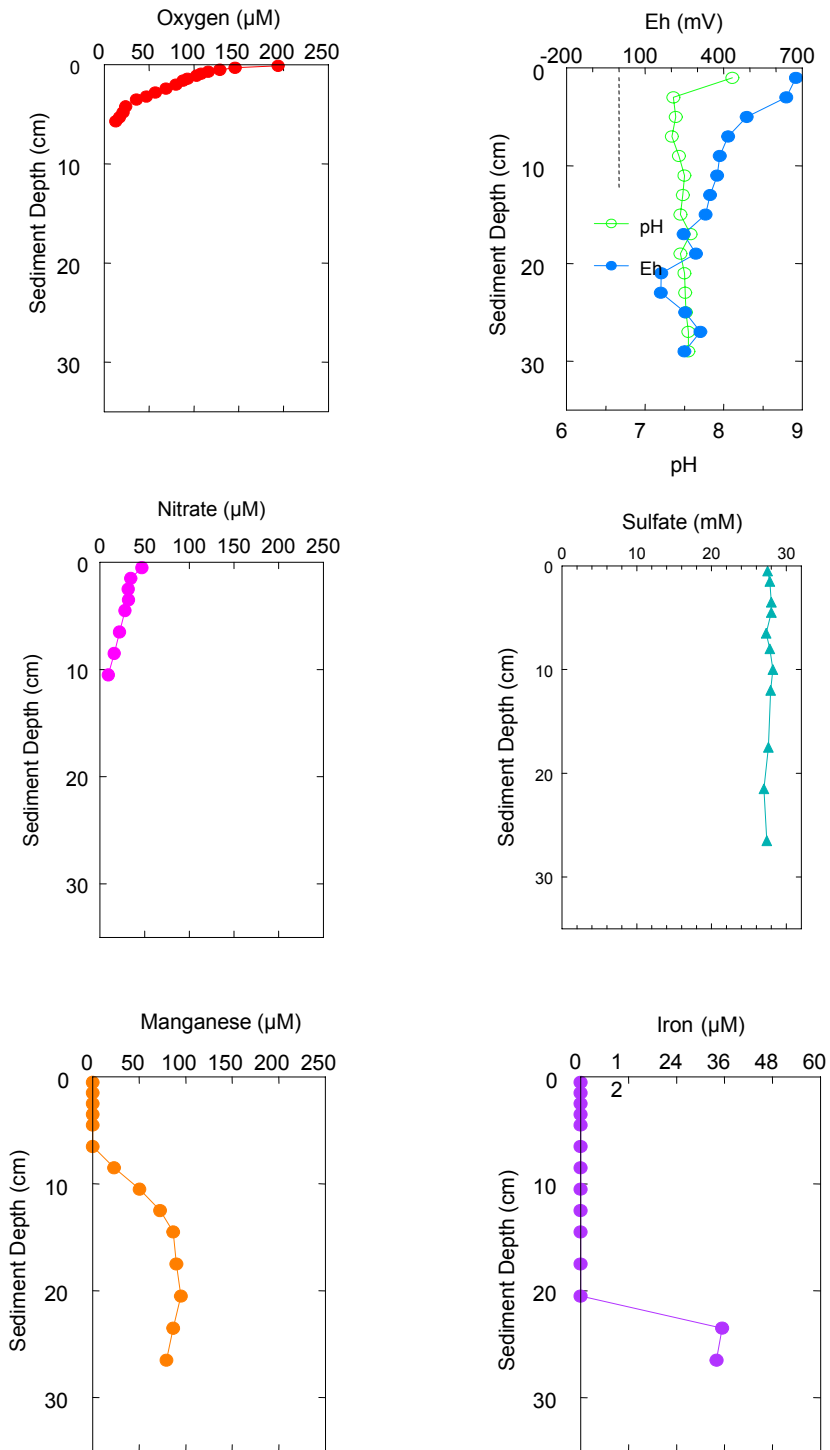


**Figure 8.33.** Vertical profiles for dissolved oxygen, Eh, nitrate, sulfate, manganese, and iron from interstitial water from Station FF-B02 at Garden Banks (GB) 516 during Cruise 1B.

### Pore Water Results for GB 516 NF-B01 (Cruise 1B)

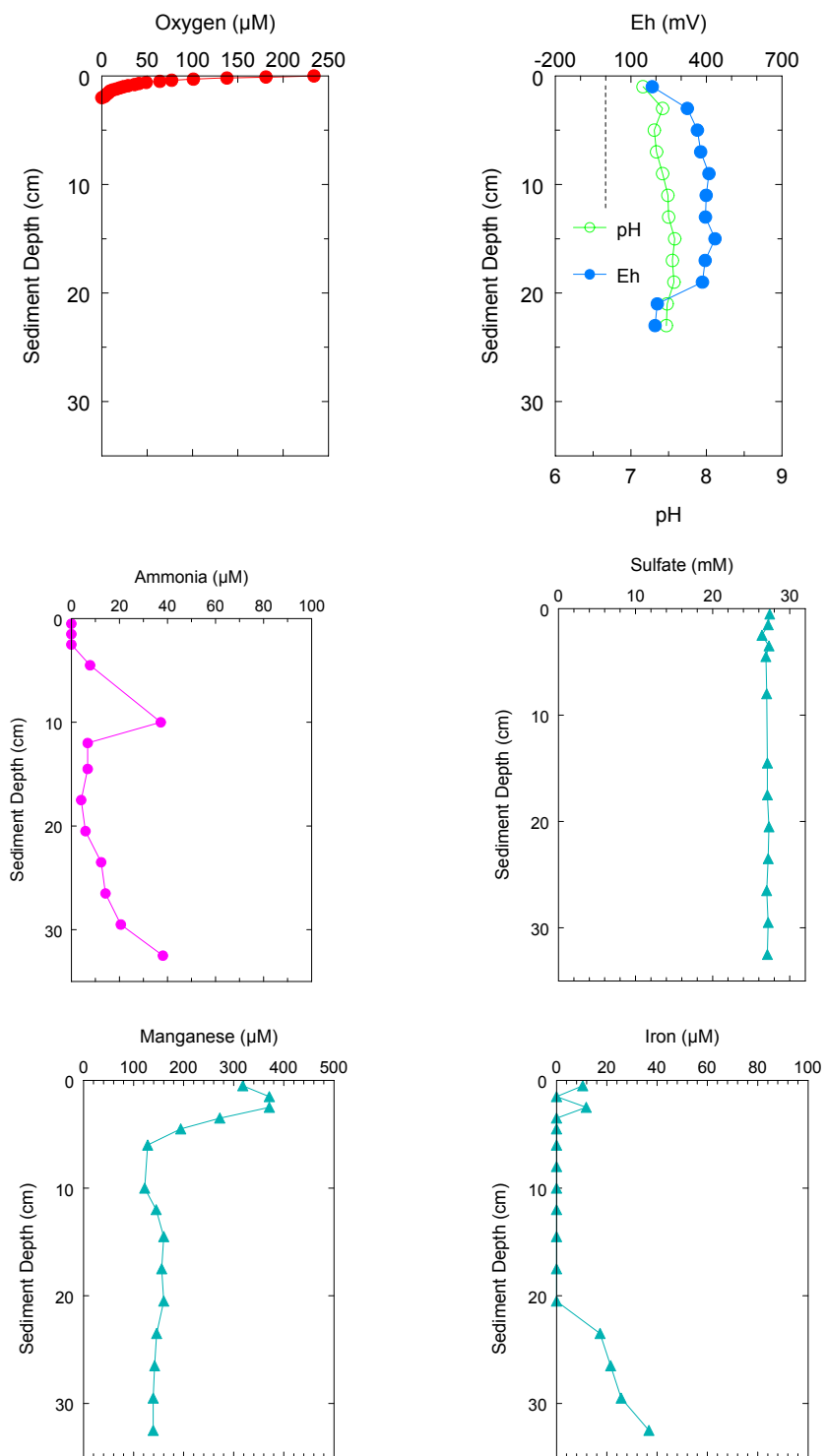


**Figure 8.34.** Vertical profiles for dissolved oxygen, Eh, ammonia, sulfate, manganese, and iron from interstitial water from Station NF-B01 at Garden Banks (GB) 516 during Cruise 1B.

During Cruise 2B, interstitial water was collected at Station FF6. The profiles for various chemical constituents in the interstitial water from Station FF6 during Cruise 2B are similar to those for the Cruise 1B samples in that no sulfate reduction and no sulfide are detected and the  $Mn^{2+}$  and  $Fe^{2+}$  profiles are similar to those at Station FF2 from Cruise 1B (**Figure 8.35**). However, the sediments from Station FF6 (Cruise 2B) are more reducing than was observed in the two cores previously described for GB 516. This manifests in lower levels of Eh (+100 to -100 mV) and higher levels of dissolved ammonia at the top of the core (**Figure 8.35**). However, this difference is most likely part of the continuum of background stations, as Ba levels (0.12%) and concentrations of TOC (1%) are compatible with natural levels and show no indication of the presence of drilling discharges.

Sediment cores were collected during Cruise 2B at each of the discretionary stations for chemical analysis of sediment solids. Sediments from Stations DS-1 and DS-2 contained elevated levels of Ba and TOC relative to Station DS-3 (**Figure 8.36**). As a result of the presence of drilling discharges, remobilization and loss of Mn from the sediments via the interstitial water is clearly observed at Stations DS-1 and 2, but not Station DS-3.

## **8.5 GARDEN BANKS BLOCK 602 AND MISSISSIPPI CANYON BLOCK 292 – POST-DEVELOPMENT SITES**

### **8.5.1 Metals and Total Organic Carbon**

Means, standard deviations, maximums, and minimums for concentrations of metals, and TOC for surface (0 to 2 cm) sediments from development sites GB 602 and MC 292 are summarized in **Table 8.11**. The data in **Table 8.11** are for random stations in near-field and far-field zones and do not include results from fixed discretionary stations. The complete data set is presented in *Appendix G*. Comparisons discussed here are between zones at each site because each site was sampled only once after undergoing some degree of development.

Mean concentrations of Al and Fe in surface sediments from near-field versus far-field stations at each site varied by <10% (**Table 8.11**). The mean Fe/Al ratios of 0.52 at MC 292 and 0.49 at site GB 602 are close to a value of 0.53 for suspended sediment (4.61% Fe/8.65% Al) from the Mississippi River (Trefry and Presley 1982). The uniformity in the Fe/Al ratios for sediments from these two sites supports a similar terrigenous source via the Mississippi River for these sediments, as previously discussed.

Mean concentrations of Ba concentrations were ~60-fold and ~12-fold greater at near-field than far-field stations for GB 602 and MC 292, respectively (**Table 8.11** and **Figure 8.37**). At each site, Ba levels are statistically higher in the near-field zone than in the far-field zone (**Table 8.12**), with a much greater degree of enrichment in sediment Ba levels at GB 602. The spatial distribution of Ba in sediments for GB 602 shows two zones where concentrations were >5% (**Figure 8.38**). No Ba concentrations >5% were found in sediments from MC 292 (**Figure 8.38**). Concentrations of Ba >1%, relative to background levels of ~0.1%, are found throughout the ~500 m radius from the center of drilling site GB 602, but only for a small portion of MC 292 (**Figure 8.38**).

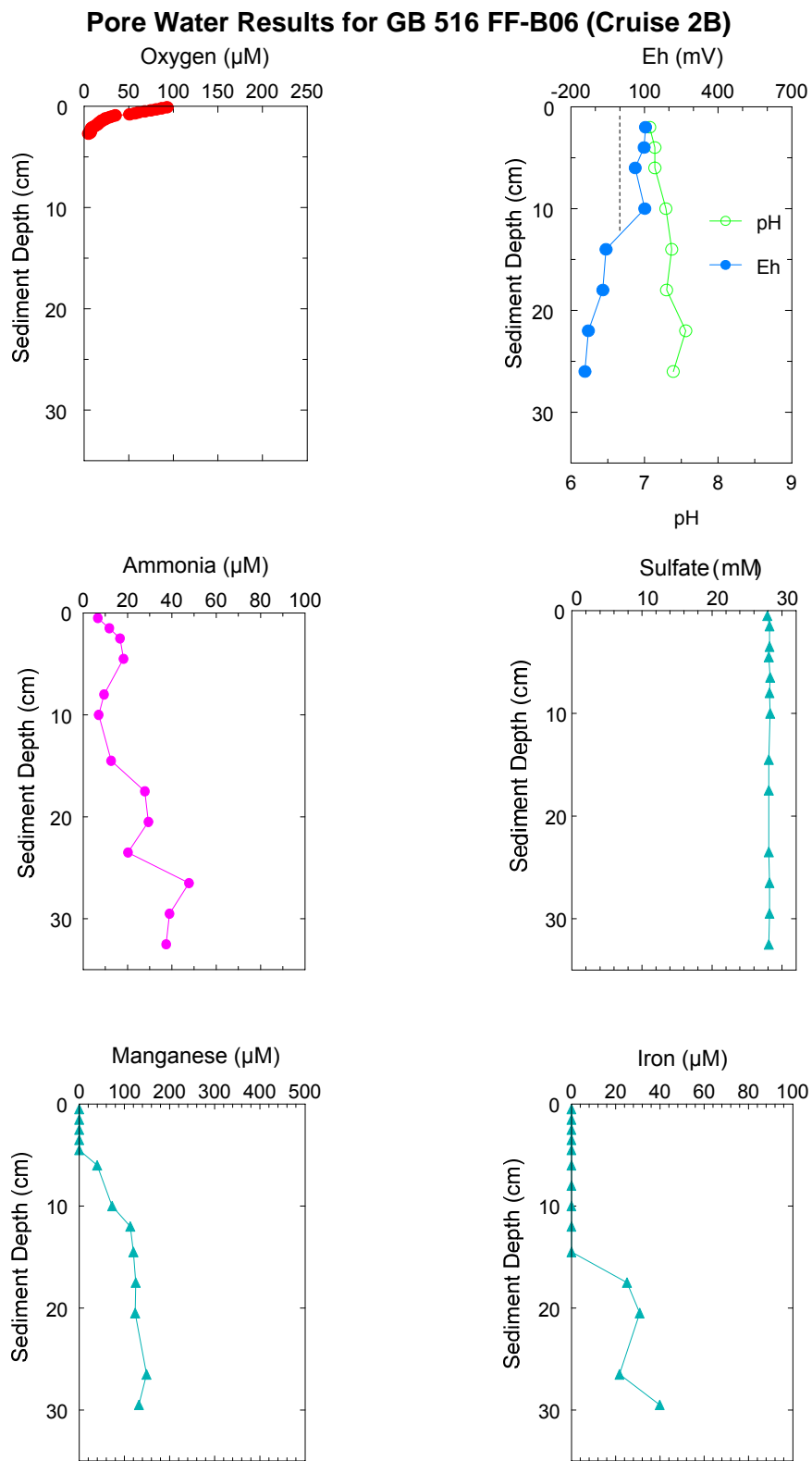


**Figure 8.35.** Vertical profiles for dissolved oxygen, Eh, ammonia, sulfate, manganese, and iron from interstitial water from Station FF-B06 at Garden Banks (GB) 516 during Cruise 2B.

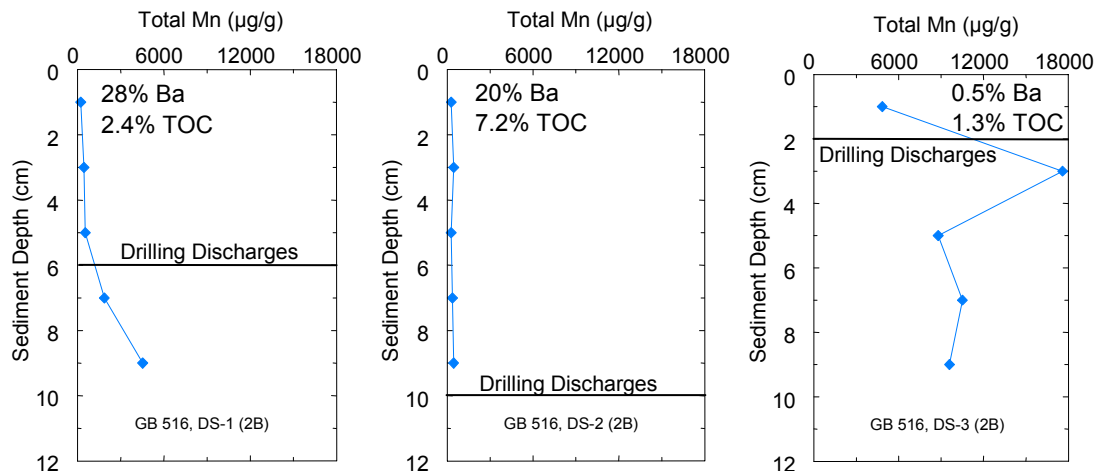


**Figure 8.36.** Vertical profiles for concentrations of manganese (Mn) in sediment from discretionary (DS) stations at Garden Banks (GB) 516 for Cruise 2B. Line shows demarcation of the presence of drilling discharges (above the line). Data are for concentrations of barium (Ba) and total organic carbon (TOC) in the 0 to 2 cm section of the core.

Vertical profiles for Ba in sediments were obtained for three near-field discretionary stations at each site during Cruise 2B (**Figure 8.39**). Concentrations of Ba are above background levels of ~0.1% in the top 2 cm in all six cores (**Figure 8.39**). However, elevated Ba levels are found no deeper than 6 cm in any of the cores (**Figure 8.39**). As observed for the surface samples, concentrations of Ba in the cores from GB 602 are as much as 10 times greater than at MC 292.

Concentrations of Mn in surface sediments at near-field stations show a larger range in concentrations relative to far-field stations (**Table 8.11**). All nine samples with values for Mn <2,000 µg/g at GB 602 and four of five samples with Mn levels <2,000 µg/g at MC 292 were collected from the near-field zone. These observations support reductive dissolution of Mn and diffusion of Mn<sup>2+</sup> from the sediments to the overlying water column at some near-field stations when reducing conditions develop where drilling discharges are found. This information and the results for Mn in sediment cores will be further considered in discussions regarding the redox state of the sediment.

Mean concentrations of Al, As, Cd, Fe, and V are not significantly different between far-field and near-field stations for surface sediments from both sites GB 602 and MC 292 (**Tables 8.11** and **8.12**). At GB 602, concentrations of Ba, Cr, Cu, Pb, and Zn are significantly greater at near-field stations than at far-field stations, whereas levels of Ni are significantly lower at near-field stations than far-field stations (**Tables 8.11** and **8.12**). The only metal that shows a zone-wide shift in concentrations that can be related to drilling at site MC 292 is Ba.



**Table 8.11.** Means, standard deviations, and ranges for metals and total organic carbon (TOC) for Garden Banks (GB) 602 and Mississippi Canyon (MC) 292 during post-development Cruise 2B.

Element	GB 602 Far-field	GB 602 Near-field	MC 292 Far-field	MC 292 Near-field
Al (%)	5.61 ± 0.26 (5.34-6.08)	5.74 ± 0.48 (4.89-6.17)	7.85 ± 0.84 (6.18-9.86)	7.44 ± 0.25 (7.01-7.91)
As (µg/g)	10.6 ± 0.3 (10.0-11.0)	11.5 ± 1.3 (9.1-13.2)	14.5 ± 1.9 (11.8-17.1)	14.0 ± 2.0 (10.1-16.5)
Ba (%)	0.085 ± 0.030 (0.057-0.155)	5.08 ± 3.19 (1.66-11.6)	0.076 ± 0.011 (0.063-0.092)	0.90 ± 1.10 (0.126-3.97)
Cd (µg/g)	0.27 ± 0.07 (0.22-0.46)	0.33 ± 0.10 (0.19-0.54)	0.20 ± 0.03 (0.17-0.25)	0.21 ± 0.04 (0.17-0.32)
Cr (µg/g)	50.9 ± 5.6 (39.6-57.8)	62.2 ± 4.8 (55.3-68.0)	77.0 ± 9.7 (63.2-103)	74.5 ± 13.6 (43.7-91.0)
Cu (µg/g)	28.7 ± 0.6 (27.7-29.8)	36.0 ± 6.0 (30.9-49.6)	27.7 ± 3.8 (20.5-36.0)	28.2 ± 1.3 (26.8-31.3)
Fe (%)	2.71 ± 0.14 (2.58-2.95)	2.87 ± 0.15 (2.58-3.07)	4.04 ± 0.42 (3.20-5.11)	3.88 ± 0.17 (3.71-4.24)
Hg (ng/g)	98 ± 7 (84-108)	104 ± 27 (70-167)	70 ± 6 (61-82)	82 ± 12 (61-109)
Mn (µg/g)	3,170 ± 283 (2,850-3,700)	2,320 ± 1,990 (417-5,990)	3,570 ± 1,420 (921-5,610)	3,890 ± 2,050 (722-6,730)
Ni (µg/g)	41.0 ± 2.3 (37.7-44.8)	32.2 ± 6.1 (23.6-43.8)	39.1 ± 4.1 (28.9-46.3)	38.1 ± 2.9 (31.7-41.7)
Pb (µg/g)	21.6 ± 1.5 (19.5-24.1)	41.8 ± 10.0 (22.1-57.0)	31.4 ± 1.1 (30.2-34.0)	30.1 ± 5.0 (24.6-44.4)
V (µg/g)	116 ± 5 (109-125)	118 ± 9 (100-130)	157 ± 18 (119-199)	157 ± 8 (147-177)
Zn (µg/g)	77.4 ± 5.2 (71.8-89.3)	90.3 ± 8.9 (76.2-101)	113 ± 12 (90-141)	120 ± 58 (50-294)
TOC (%)	1.12 ± 0.13 (0.91-1.32)	1.44 ± 0.28 (1.13-1.99)	1.41 ± 0.08 (1.26-1.51)	1.35 ± 0.12 (1.20-1.63)

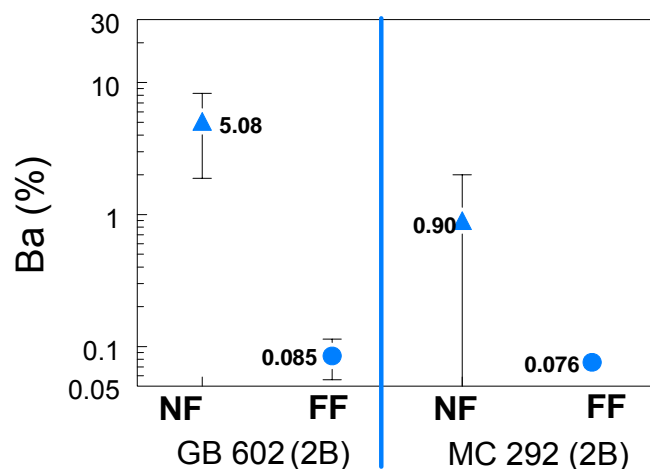


**Figure 8.37.** Concentrations of barium (Ba) with markers and numbers showing means and lines showing standard deviations in sediment from near-field (NF) and far-field (FF) stations at Garden Banks (GB) 602 and Mississippi Canyon (MC) 292 during post-development Cruise 2B. In some cases, the line for the standard deviation appears skewed due to the logarithmic scale. The line for standard deviation for the FF data at MC 292 is obscured by the marker.

**Table 8.12.** Results of statistical comparisons (t-tests) for post-development Garden Banks (GB) 602 and Mississippi Canyon (MC) 292 during Cruise 2B. Comparisons are between near-field (NF) and far-field (FF) stations at each site during one sampling trip. Results for discretionary stations were not included in the statistical tests.

Dependent Variable	Independent Variable	Probability > F	Interpretation
<b>GB 602</b>			
log Ba	zone	<0.0001	NF > FF
Cr	zone	<0.0001	NF > FF
Cu	zone	0.003	NF > FF
Ni	zone	<0.0011	FF > NF
Pb	zone	<0.0001	NF > FF
Zn	zone	0.0007	NF > FF
TOC	zone	0.0033	NF > FF
<b>MC 292</b>			
log Ba	zone	<0.0001	NF > FF
Hg	zone	0.011	NF > FF

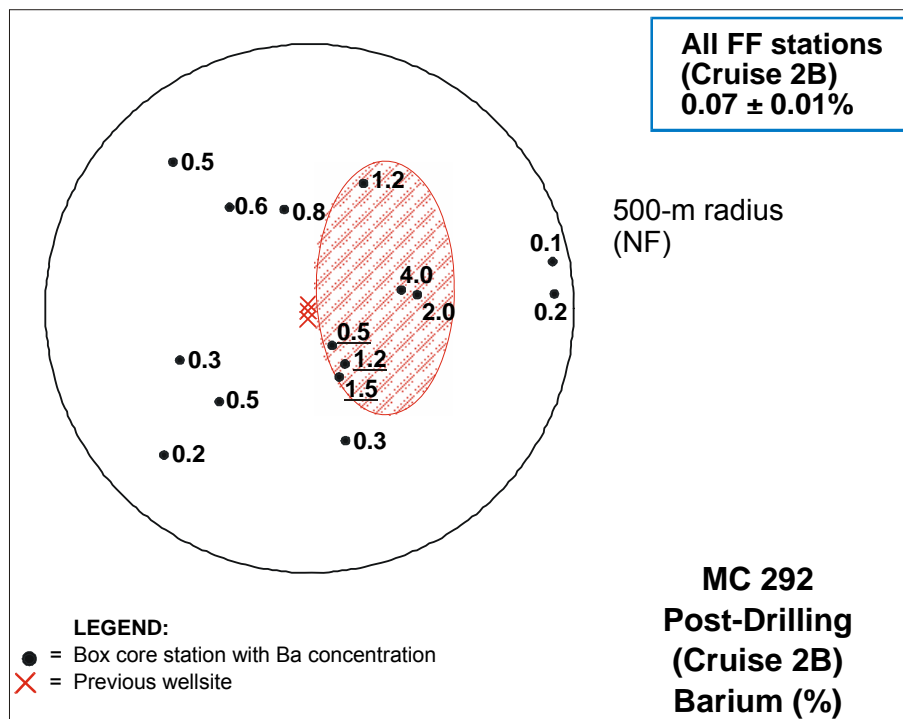
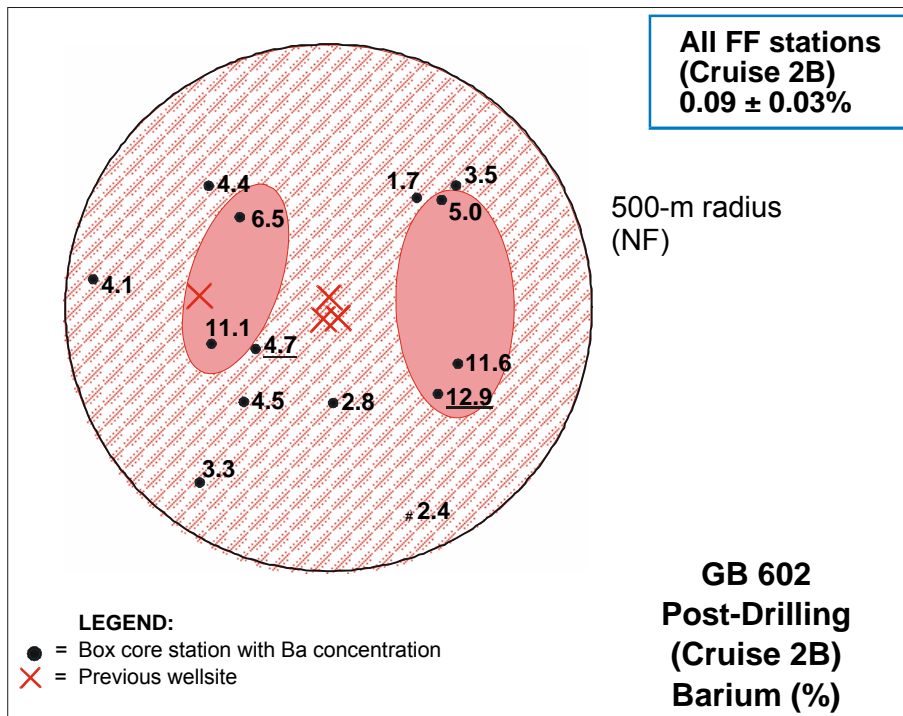


**Figure 8.38.** Concentrations of barium (Ba) at Garden Banks (GB) 602 and Mississippi Canyon (MC) 292 near-field (NF) stations during post-development Cruise 2B. Inset boxes show mean Ba concentrations at all far-field (FF) stations. Data for the discretionary stations are underlined. The circle represents a radius of 500 m. The darker shaded ovals highlight areas where Ba concentrations are  $\geq 5\%$ , and the lighter shaded, larger oval highlights area where Ba concentrations are  $\geq 1\%$ .

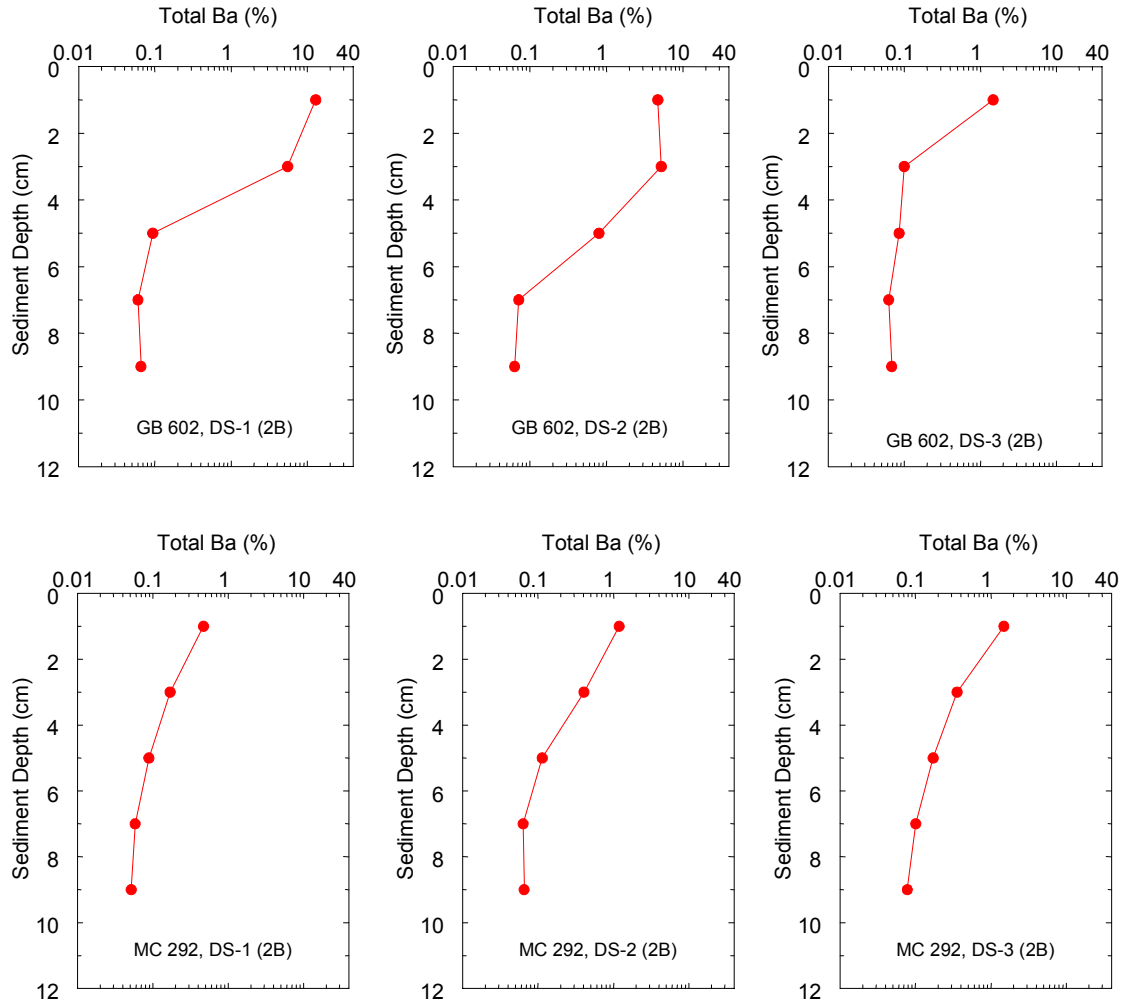


**Figure 8.39.** Vertical profiles for concentrations of barium (Ba) in sediment from discretionary (DS) stations at Garden Banks (GB) 602 and Mississippi Canyon (MC) 292.

Some elevated levels of selected metals were observed at each site. Concentrations of Pb at  $>50 \mu\text{g/g}$  were found at five (near-field + discretionary) stations from site GB 602 and none from site MC 292 relative to background levels of 20 to 35  $\mu\text{g/g}$  (**Figure 8.40a**). The elevated Pb levels were found for stations where sediment Ba concentrations also were elevated. Mercury concentrations greater than about 0.15  $\mu\text{g/g}$  were found at three (near-field + discretionary) stations from GB 602 and none from MC 292 relative to background levels of 70 to 100  $\text{ng/g}$  (**Figure 8.40b**). No significant difference was found for Hg concentrations in sediments from near-field versus far-field stations for both sites (**Figure 8.41**). Vertical profiles for Hg in sediments from discretionary stations show significantly elevated Hg levels only in one core from GB 602 to a depth of 2 cm (**Figure 8.42**). The lack of any high levels of Hg is most likely due to the lack of sediment samples with greatly elevated levels of Ba ( $>20\%$ ). The highest Zn concentration, of 294  $\mu\text{g/g}$ , was found at one near-field station from MC 292. A more detailed discussion of the complete data set for metals in sediments from all sites is presented in a later section of this chapter.

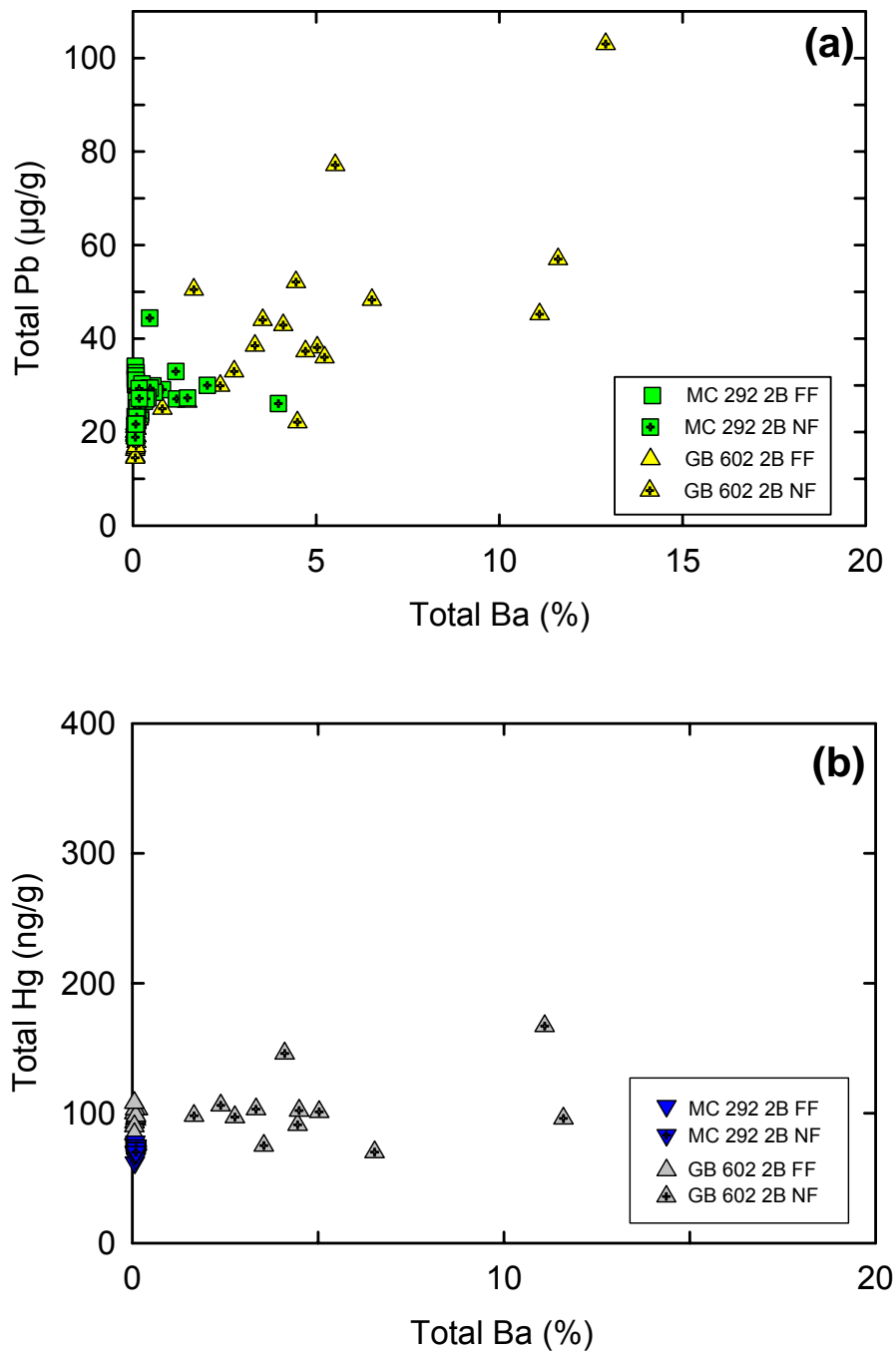


**Figure 8.40.** Concentrations of barium (Ba) versus (a) lead (Pb) and (b) mercury (Hg) for sediments from far-field (FF) and near-field (NF) stations from Garden Banks (GB) 602 and Mississippi Canyon (MC) 292 collected during Cruise 2B. Points from FF samples are hidden beneath points for NF samples at Ba levels <0.2%.

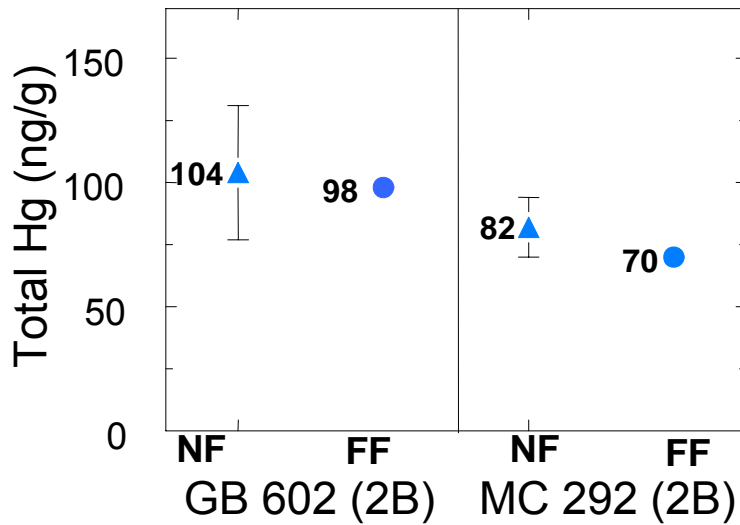


**Figure 8.41.** Concentrations of mercury (Hg) with markers and numbers showing means and lines showing standard deviations in sediment from near-field (NF) and far-field (FF) stations at Garden Banks (GB) 602 and Mississippi Canyon (MC) 292 during Cruise 2B. The lines for standard deviation for the FF data are obscured by the markers.

Concentrations of TOC in surface sediments from near-field stations are statistically higher than at far-field stations for GB 602 but not for MC 292 (**Figure 8.43**). The maximum values for TOC in near-field or discretionary samples from GB 602 and MC 292 were 2.07% and 1.63%, respectively. These maximum levels are not greatly enriched above background levels of 1.1% to 1.4% and are considerably below maximum values of 7.2% at GB 516 and 3.4% at VK 916, even though average Ba concentrations for GB 602 of 5.1% are similar to mean levels of 3.6% at VK 916 (post-development) and 5.9% at GB 516 (post-development). Vertical profiles for TOC (**Figure 8.44**) show relatively uniform trends at close to background values with the exception of Station DS-1 from GB 602, where values for the top 4 cm are 70% to 140% greater than background values.

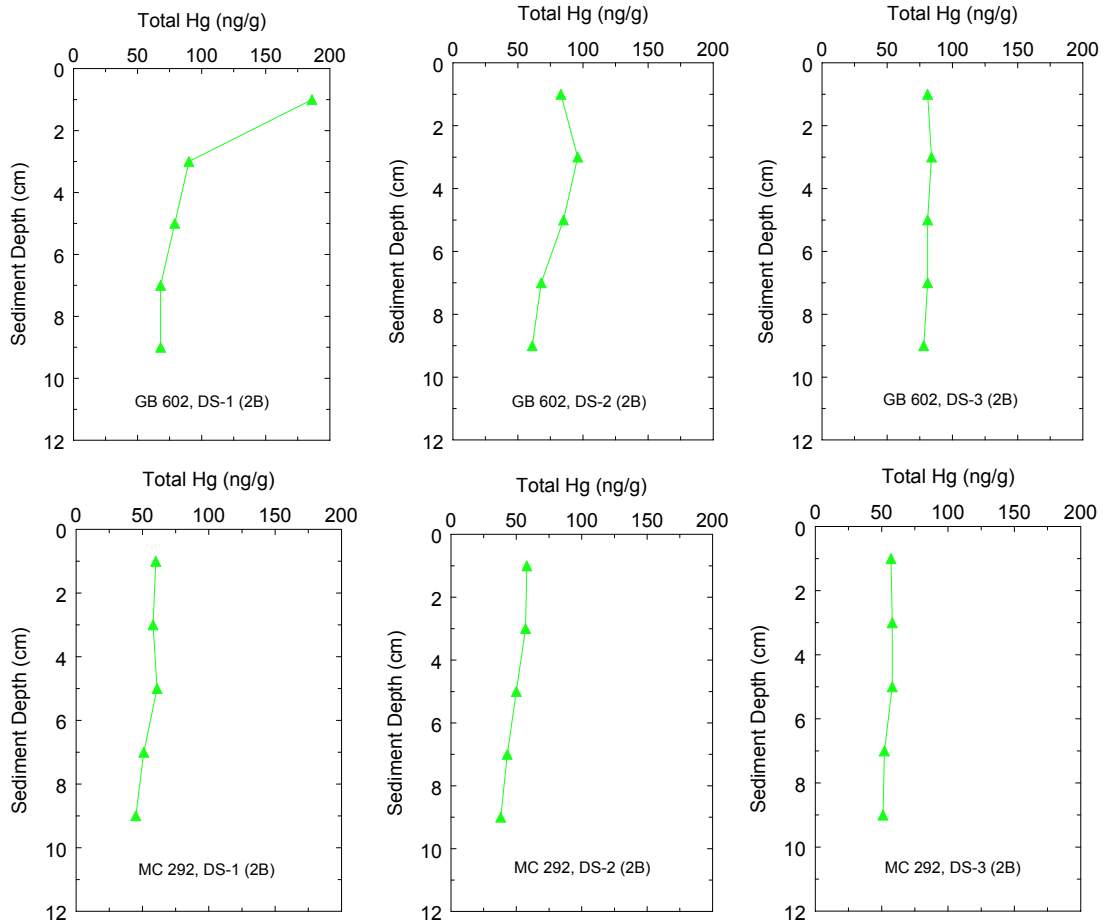


**Figure 8.42.** Vertical profiles for concentrations of mercury (Hg) in sediment from discretionary (DS) stations at Garden Banks (GB) 602 and Mississippi Canyon (MC) 292.

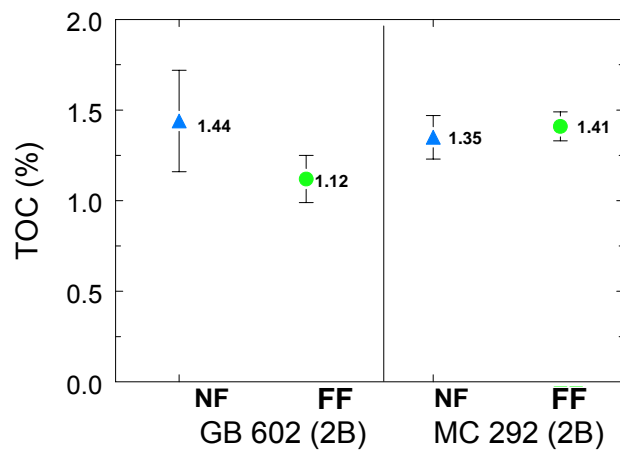


**Figure 8.43.** Concentrations of total organic carbon (TOC) with markers and numbers showing means and lines showing standard deviations in sediment from near-field (NF) and far-field (FF) stations at Garden Banks (GB) 602 and Mississippi Canyon (MC) 292 during post-development Cruise 2B.

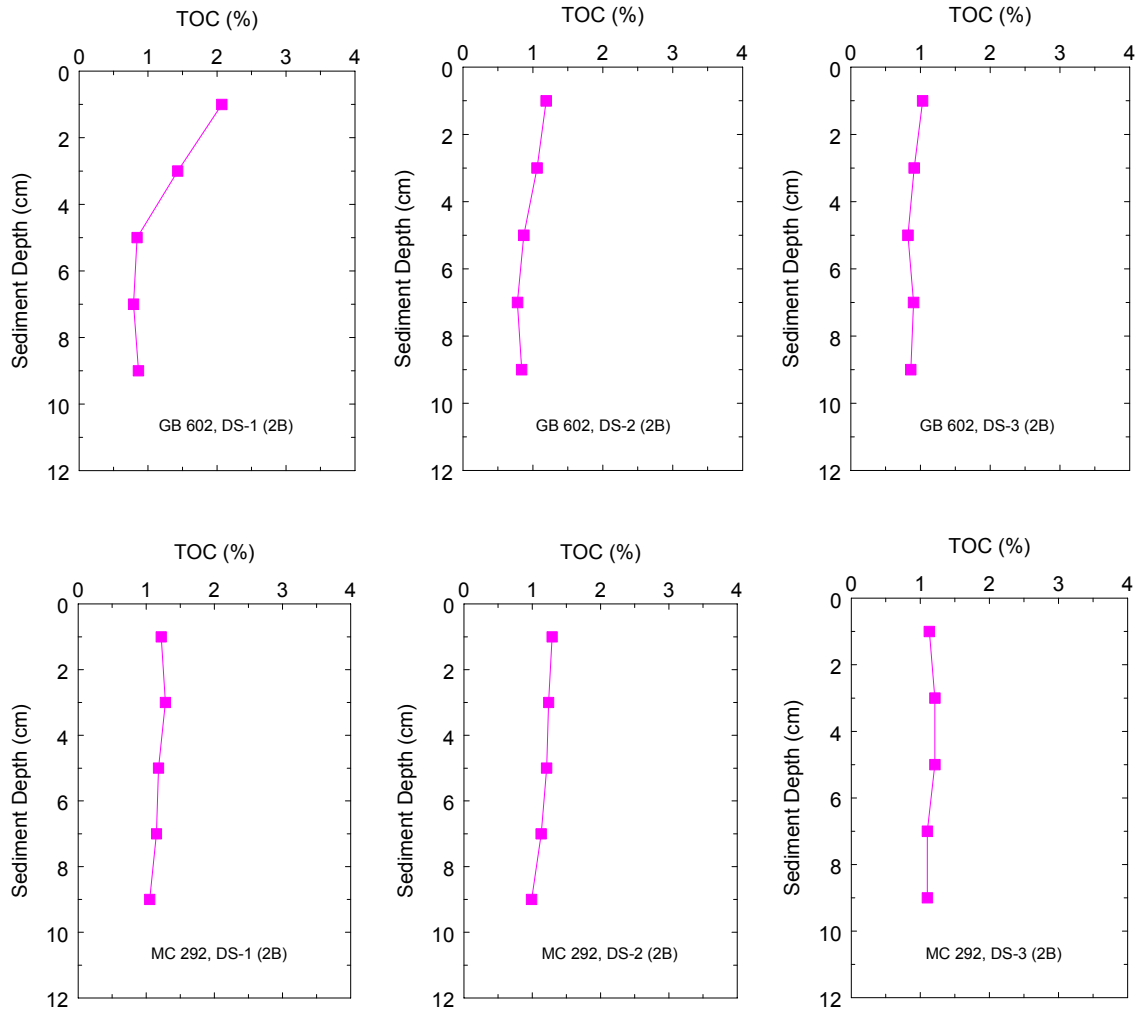


**Figure 8.44.** Vertical profiles for concentrations of total organic carbon (TOC) in sediment from discretionary (DS) stations at Garden Banks (GB) 602 and Mississippi Canyon (MC) 292.

### 8.5.2 Sediment Geochronology

The vertical profile for excess  $^{210}\text{Pb}$  at Station FF5 for GB 602 from Cruise 2B shows an exponential decrease with depth on the natural logarithm plot (**Figure 8.45**). The resulting sedimentation rate of 0.04 cm/y is similar to results obtained for VK 916 and GB 516. In contrast, the sedimentation rate at MC 292 is more than three times greater at 0.14 cm/y. The  $^{137}\text{Cs}$  profile is well defined for MC 292 and supports a sedimentation rate of  $\sim 0.1$  cm/y (5 cm/50 y). The higher sedimentation rate at MC 292 relative to the other three slope locations (VK 916, GB 516, and GB 602) is consistent with the location of MC 292 closer to the pathway of sediment transport from the Mississippi River.



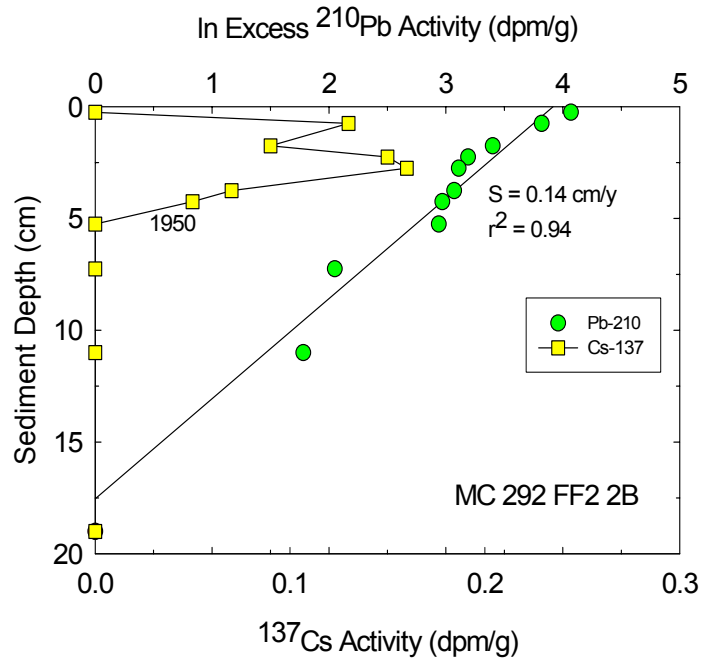
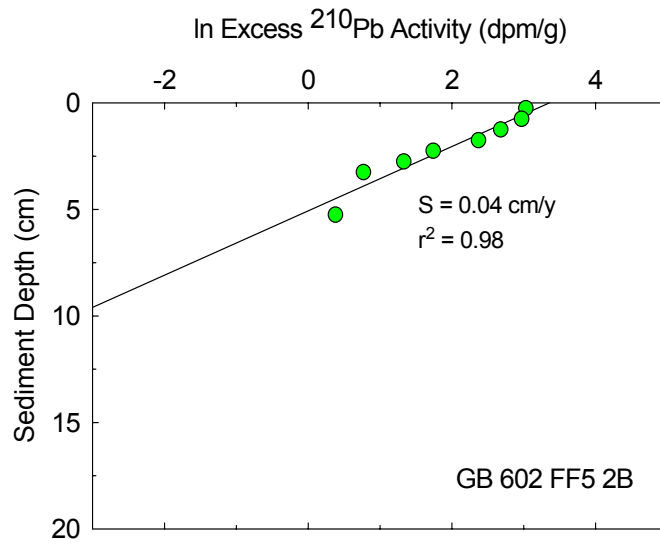


**Figure 8.45.** Vertical profiles for activities of excess  $^{210}\text{Pb}$  in sediment from Garden Banks (GB) 602 Station FF-B05 and excess  $^{210}\text{Pb}$  and  $^{137}\text{Cs}$  from Mississippi Canyon (MC) 292 Station FF-B02 ( $S$  = sedimentation rate,  $r$  = correlation coefficient).

### 8.5.3 Sediment Oxygen Levels and Redox Conditions

At GB 602, concentrations of dissolved O<sub>2</sub> in sediment from far-field sites decreased to non-detectable levels (<2 μM) at sediment depths of 2.8 to more than 6.7 cm; all of which were greater than maximum levels at the near-field and discretionary stations (**Table 8.13** and **Figure 8.46**). Similarly, the minimum value for Eh in the top centimeter from far-field stations of +225 mV was much greater than the lowest values of -167 and -296 mV when considering all near-field and all discretionary stations, respectively (**Table 8.13**). The contrast is quite striking in **Figure 8.46** for the far-field versus near-field and discretionary examples shown. Consistent with these trends, the mean value for ΣO<sub>2</sub> for the far-field sites is ~10 times greater than at near-field or discretionary stations (**Figure 8.47**).

**Table 8.13.** Summary data for dissolved oxygen, redox potential (Eh), and pH for sediment from Garden Banks (GB) 602 and Mississippi Canyon (MC) 292 at near-field (NF), far-field (FF), and discretionary (DS) stations during post-development Cruise 2B.

Site	Zone	Zero O <sub>2</sub> depth (cm)	Eh <sub>1 cm</sub> range (mV)		Eh <sub>10 cm</sub> range (mV)		pH
GB 602 (Cruise 2B)	NF	0.1-2.8	+402	-167	+358	-85	6.8-8.0
	DS	0.2-1.7	+424	-296	+273	-165	7.2-8.0
	FF	2.8->6.1	+462	+225	+368	+93	7.0-7.5
MC 292 (Cruise 2B)	NF	0.2-3.0	+350	-163	+155	-387	6.5-7.6
	DS	0.8-1.7	+321	+29	+102	+85	7.1-7.4
	FF	0.2->3.3	+449	+158	+164	-49	7.0-8.0

At MC 292, differences between far-field and near-field stations are less striking. For example, the sediment depth to zero oxygen ranged from 0.2 to about 3.3 at both far-field and near-field stations. Thus, the profiles for dissolved oxygen (**Figure 8.48**) and the values for ΣO<sub>2</sub> are more similar among far-field, near-field, and discretionary stations (**Figure 8.47**). This degree of similarity is partly due to lower levels of ΣO<sub>2</sub> at far-field stations from site MC 292 (65 nmol/cm<sup>2</sup>) than for far-field stations from GB 602 (227 nmol/cm<sup>2</sup>). This difference in background conditions between the two sites is most likely related to the proximity of MC 292 to the Mississippi River delta and the higher sedimentation rate.

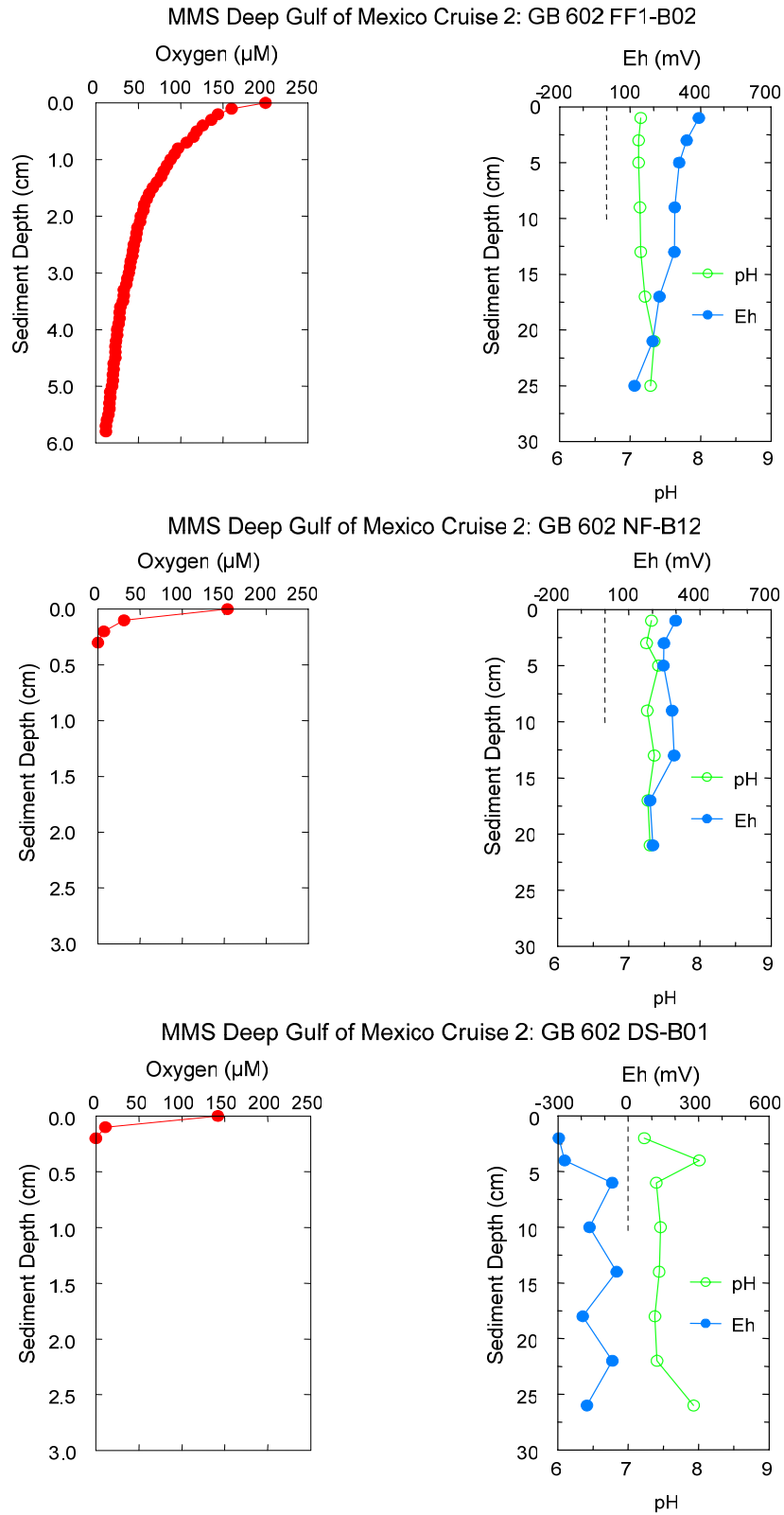


**Figure 8.46.** Vertical profiles for dissolved oxygen, redox potential (Eh), and pH in sediment from representative near-field (NF), far-field (FF), and discretionary (DS) stations at Garden Banks (GB) 602 (note different depth scales for oxygen versus Eh).

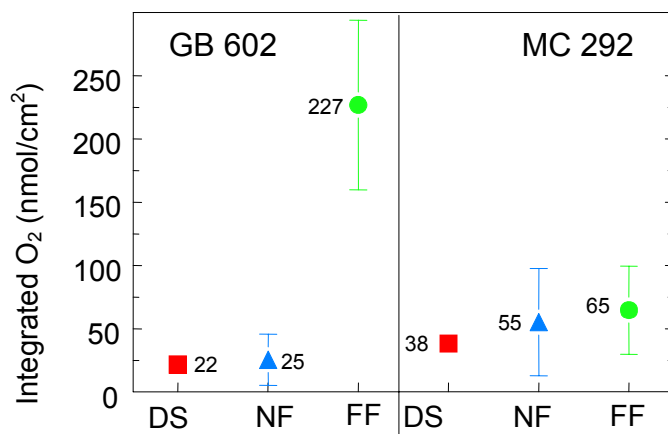


**Figure 8.47.** Integrated amounts of oxygen in the sediment column at near-field (NF), far-field (FF), and discretionary (DS) stations at Garden Banks (GB) 602 and Mississippi Canyon (MC) 292. Markers and numbers show means and lines show standard deviation.

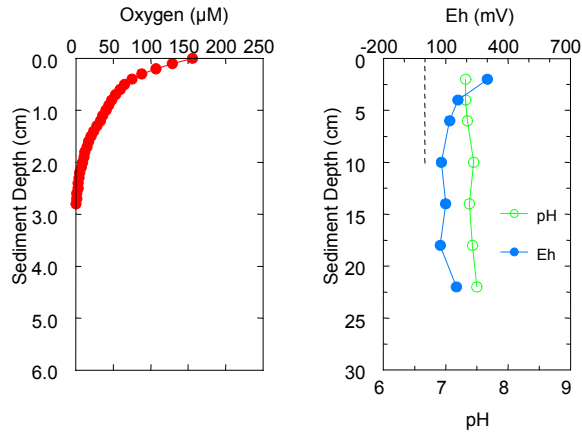
#### 8.5.4 Interstitial Water Composition

At GB 602, the Eh was between +300 to +400 mV throughout the core from Station FF5 relative to 0 to -250 mV at Station DS-2 (**Figures 8.49 and 8.50**). A 6-cm thick layer of sediment containing drilling discharges was observed at Station DS-2 (>3% Ba, but only ~1.1% TOC). The lower Eh in the DS-2 core is consistent with the differences in the depth of oxygen penetration of ~6 cm at Station FF5 relative to ~0.5 cm at Station DS-2 (**Figures 8.49 and 8.50**). Strongly reducing conditions in the top 6 cm of the core from Station DS-2 lead to large concentrations of dissolved Mn<sup>2+</sup> and NH<sub>4</sub><sup>+</sup> relative to the far-field core, where concentrations of both chemical species were near detection limits (**Figures 8.49 and 8.50**). Once again, the difference in redox conditions between far-field and near-field stations is very clear, and the Eh and dissolved oxygen data provide a reasonably good picture of chemical conditions in the interstitial water.

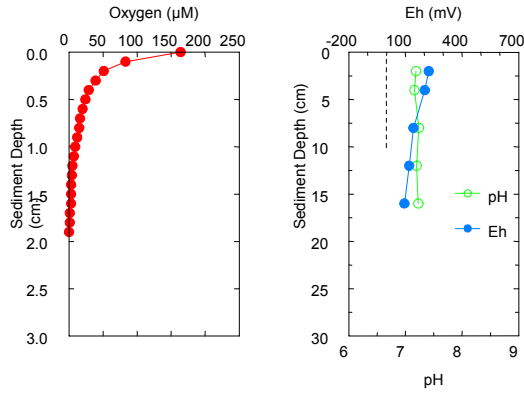
At MC 292, differences in redox state between the far-field and discretionary cores, as demonstrated by dissolved oxygen, Eh, dissolved Mn<sup>2+</sup>, and ammonia, are minor (**Figures 8.51 and 8.52**). This lack of difference is partly related to the low levels of material from drilling discharges (<1% Ba and no difference in levels of TOC), as well as the naturally more reducing environment in the more rapidly accumulating sediments at MC 292.

The distinction between the discretionary stations at GB 602 versus MC 292 is further demonstrated by the vertical profiles for sediment Mn (**Figure 8.53**). At GB 602, the surface layer of sediment contains very low levels of Mn (~600 µg/g), most likely the result of reduction of Mn oxides in the surface layer of sediment, with subsequent diffusion of Mn<sup>2+</sup> from the sediments to the overlying water. In contrast, at MC 292, the surface layer of sediment contains ~4,000 µg/g of Mn, showing much less, if any, reduction loss of Mn from the sediments. These observations are consistent with a lesser impact from drilling discharges at MC 292 than at GB 602.

MMS Deep Gulf of Mexico Cruise 2: MC 292 FF5-B01



MMS Deep Gulf of Mexico Cruise 2: MC 292 NF-B09



MMS Deep Gulf of Mexico Cruise 2: MC 292 DS-B01

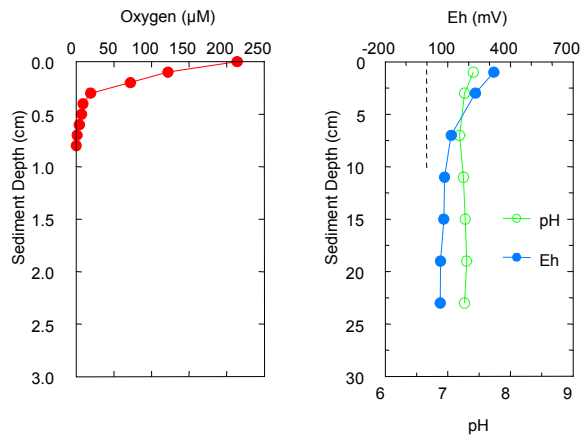


**Figure 8.48.** Vertical profiles for dissolved oxygen, redox potential (Eh), and pH in sediment from representative near-field (NF), far-field (FF), and discretionary (DS) stations at Mississippi Canyon (MC) 292 (note different depth scales for oxygen versus Eh).

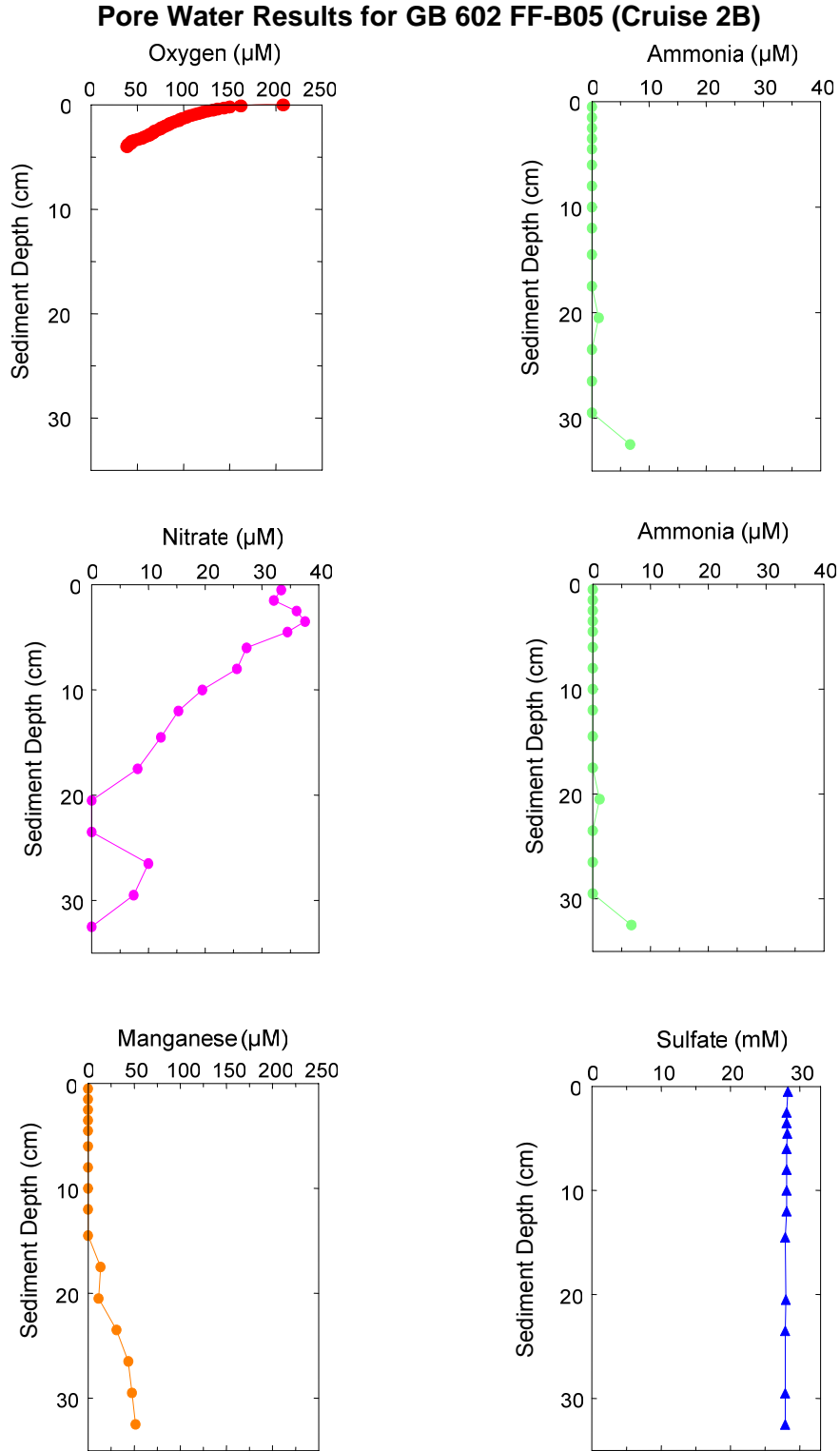


**Figure 8.49.** Vertical profiles for dissolved oxygen, Eh, nitrate, ammonia, manganese, and sulfate from interstitial water from Station FF-B05 at site Garden Banks (GB) 602 during post-development Cruise 2B.

### Pore Water Results for GB 602 DS-2 (Cruise 2B)

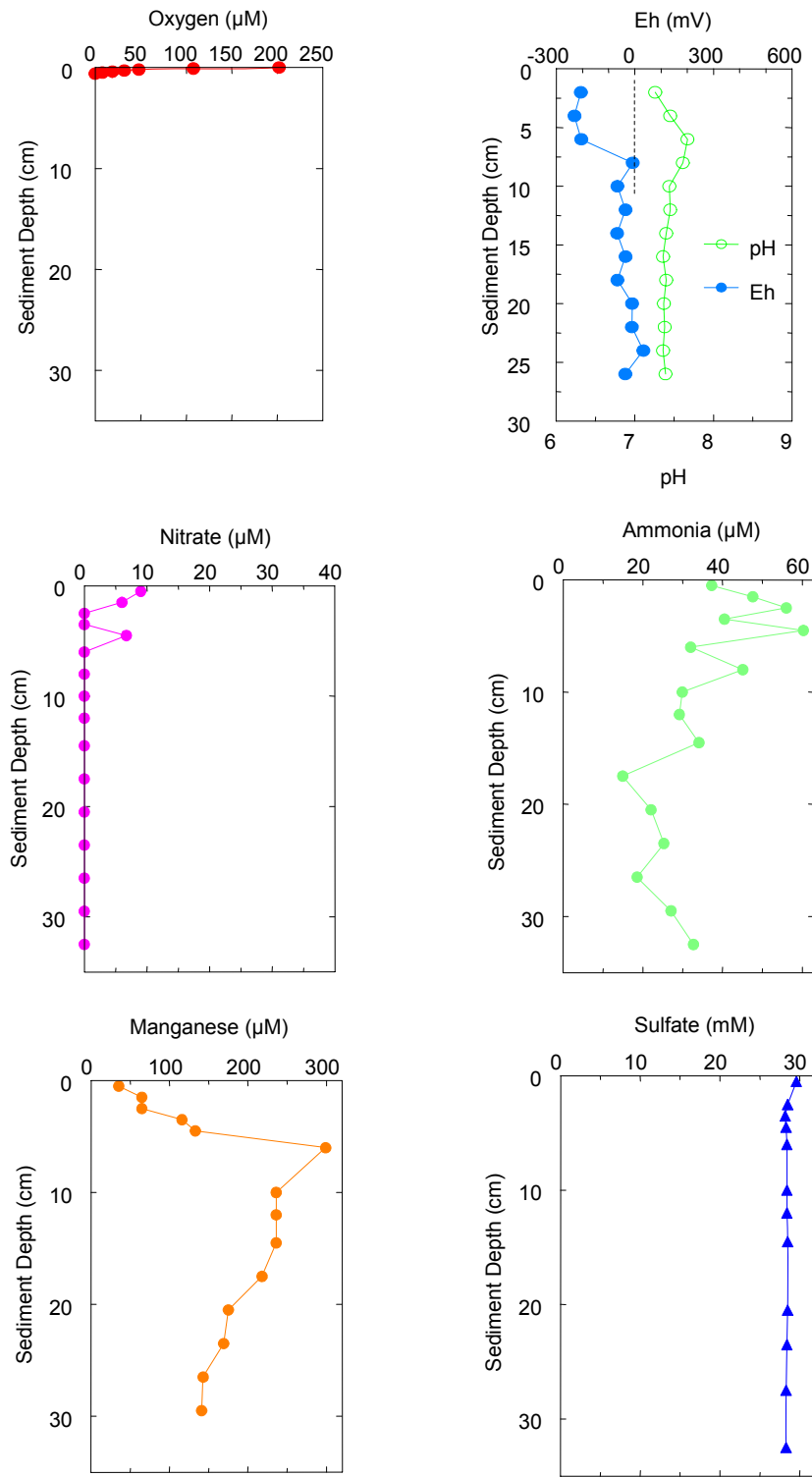


**Figure 8.50.** Vertical profiles for dissolved oxygen, Eh, nitrate, ammonia, manganese, and sulfate from interstitial water from discretionary station DS-2 at Garden Banks (GB) 602 during post-development Cruise 2B.

### Pore Water Results for MC 292 FF-B02 (Cruise 2B)

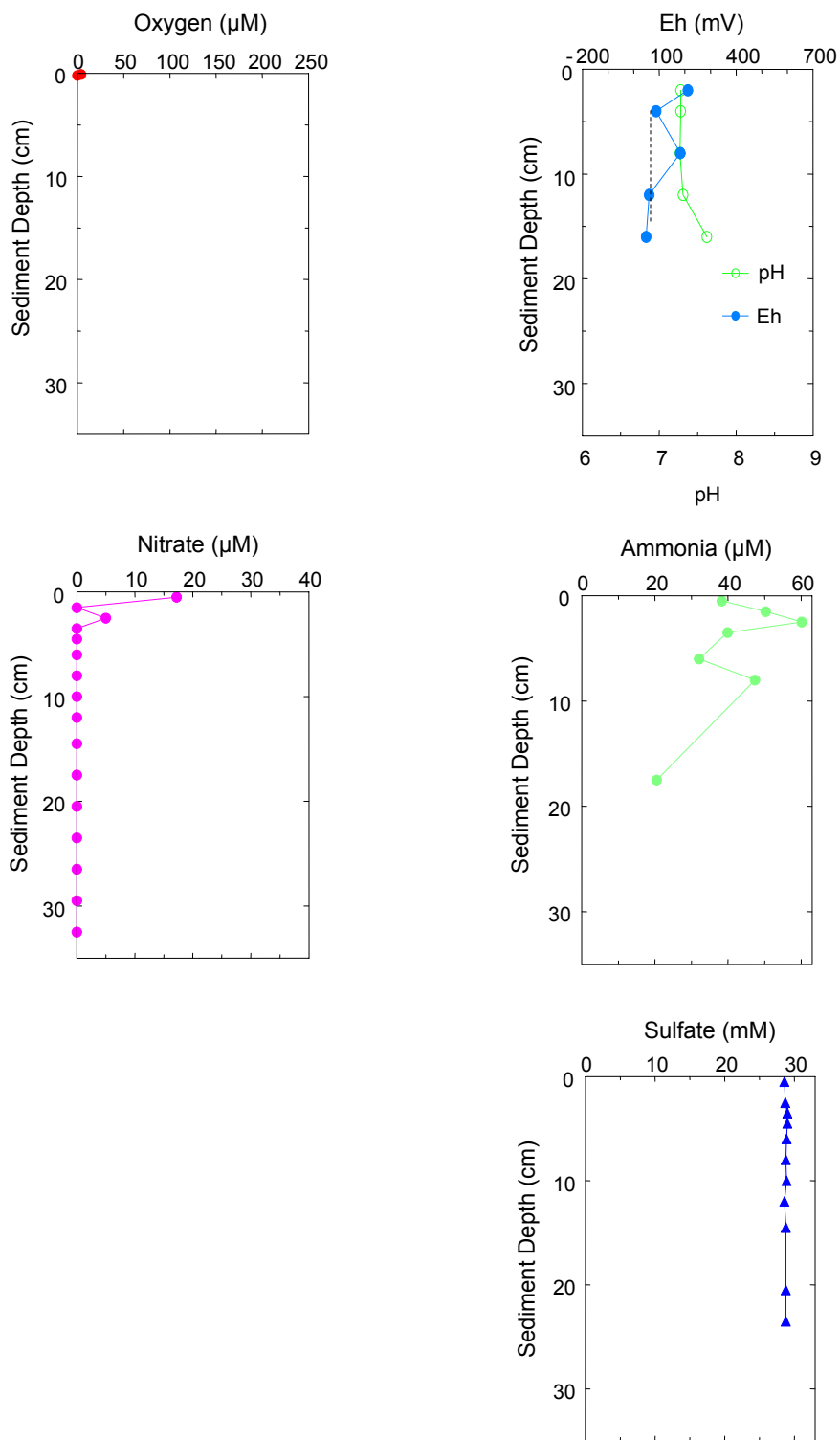


**Figure 8.51.** Vertical profiles for dissolved oxygen, Eh, nitrate, ammonia, and sulfate from interstitial water from Station FF-B02 at Mississippi Canyon (MC) 292 during post-development Cruise 2B.



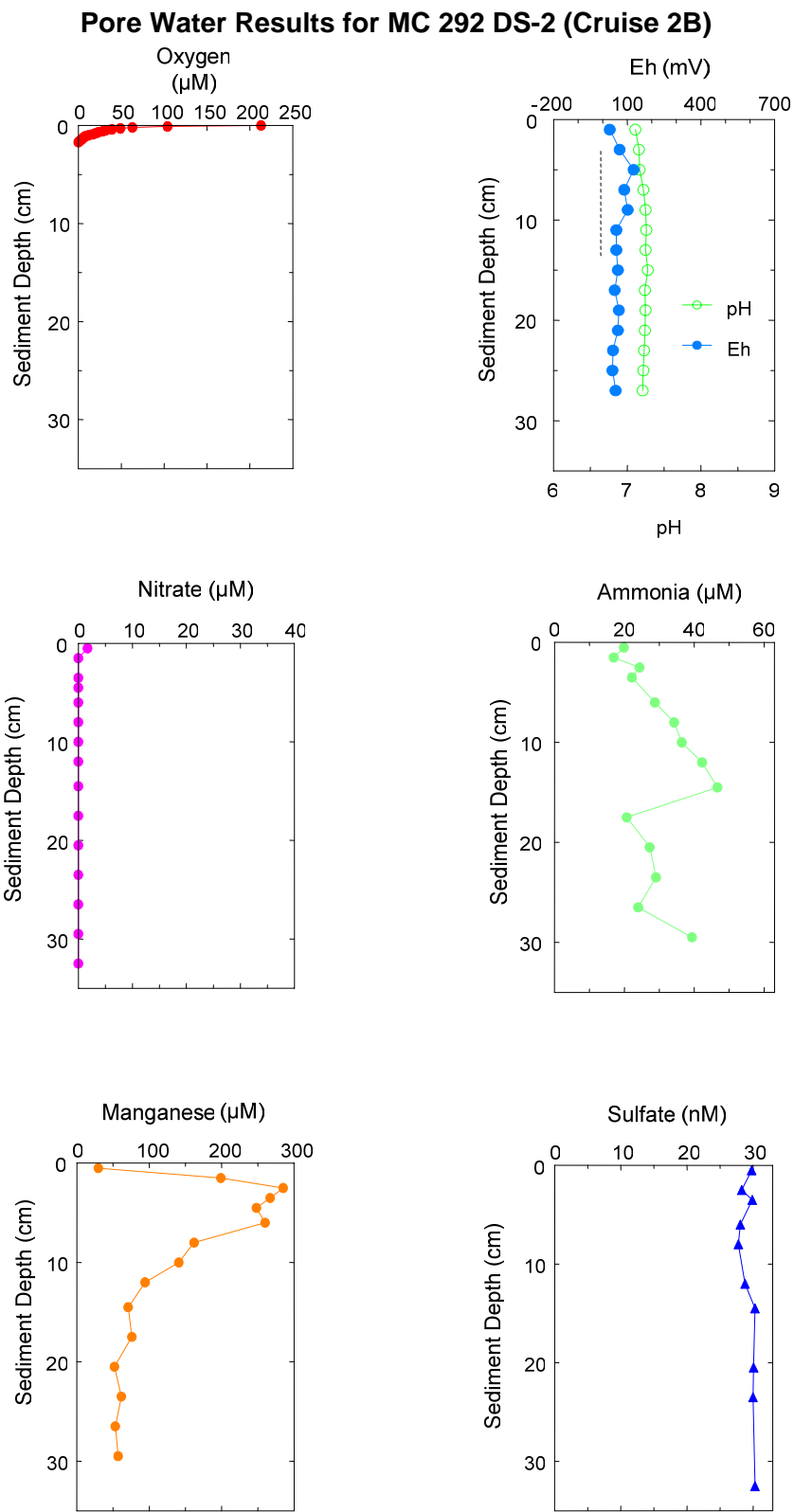


**Figure 8.52.** Vertical profiles for dissolved oxygen, Eh, nitrate, ammonia, manganese, and sulfate from interstitial water from discretionary station DS-2 at Mississippi Canyon (MC) 292 during post-development Cruise 2B.

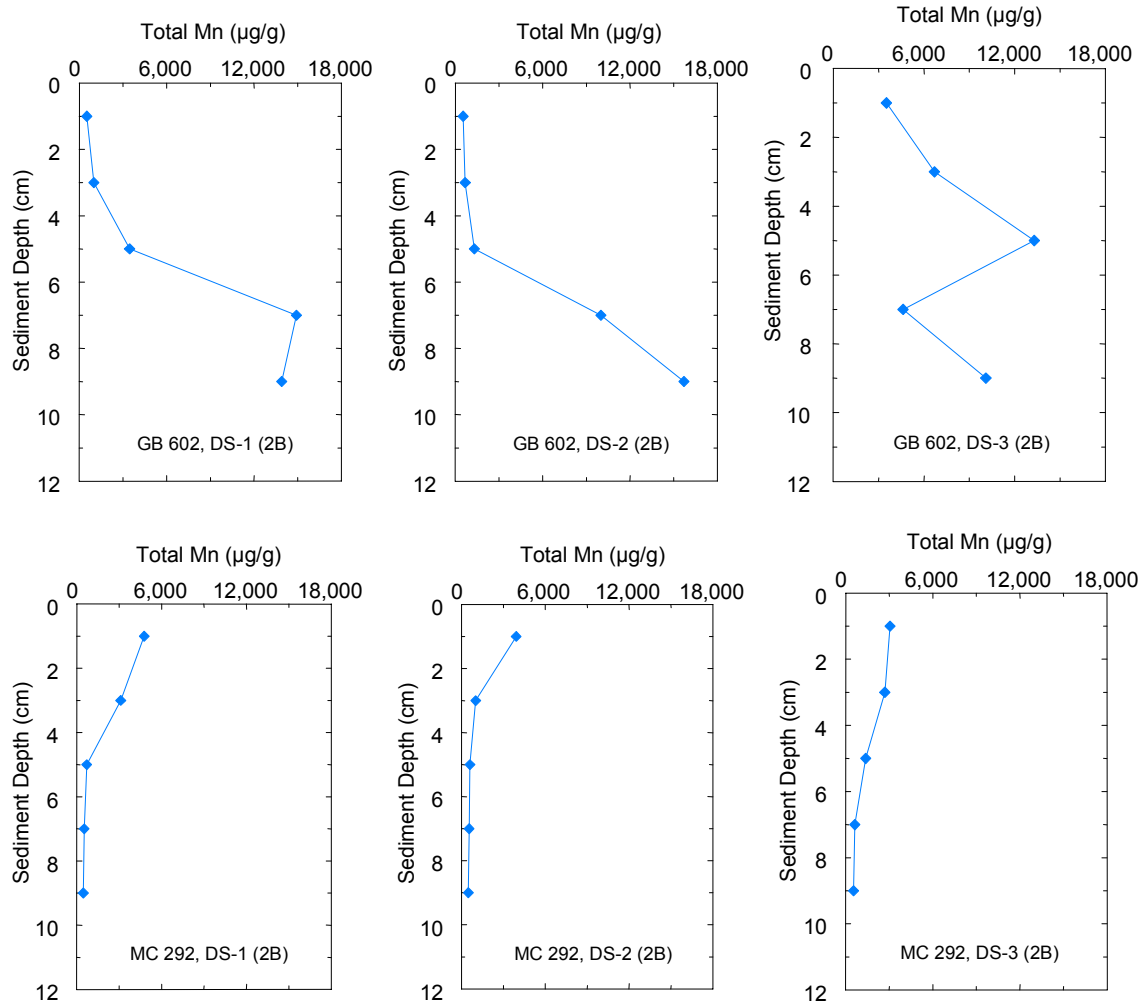


**Figure 8.53.** Vertical profiles for concentrations of manganese (Mn) in sediment from discretionary (DS) stations at Garden Banks (GB) 602 and Mississippi Canyon (MC) 292 for post-development Cruise 2B.

### 8.5.5 Metals in Isopods and Crabs

Concentrations of 11 metals (As, Ba, Cd, Cr, Cu, Fe, Hg, Ni, Pb, V, and Zn) were determined in samples of the giant isopod *Bathynomus giganteus* (**Figure 8.54**) and the red crab *Chaceon quinque-dens* (**Figure 8.55**) from near-field and far-field stations at GB 602 and MC 292. The concentrations are presented here on a dry weight basis; however, water content is available for each sample in *Appendix G*. In general, the water content in each species is 70% to 80% by weight. In many cases, the standard deviation for each metal is large, with a coefficient of variance of 50% or more (**Tables 8.14** and **8.15**).



**Figure 8.54.** Photograph of giant amphipod *Bathynomus giganteus* from the Gulf of Mexico.



**Figure 8.55.** Photograph of red crab *Chaceon quinqueedens* from the Gulf of Mexico.

Due to the large standard deviations and small number of samples from each station, most differences among the various metals for near-field versus far-field were not statistically significant as tested by ANOVA. However, for *Bathynomus giganteus*, levels of Ba, Cr, and Pb at GB 602 were greater at near-field stations than far-field stations, and concentrations of Cd and Hg were greater at far-field stations than near-field stations (Table 8.14 and Figures 8.56 and 8.57). In contrast, no significant differences were observed for metal concentrations for near-field versus far-field specimens of *Bathynomus giganteus* from MC 292 (Table 8.14 and Figures 8.56 and 8.57). Some isopods from GB 602 may have contained sediment that led to the higher levels of Ba observed.

**Table 8.14.** Means  $\pm$  standard deviations for samples of the giant amphipod *Bathynomus giganteus* from far-field (FF) and near-field (NF) stations from post-development sites Garden Banks (GB) 602 and Mississippi Canyon (MC) 292.

	As ( $\mu\text{g/g}$ )	Ba ( $\mu\text{g/g}$ )	Cd ( $\mu\text{g/g}$ )	Cr ( $\mu\text{g/g}$ )	Cu ( $\mu\text{g/g}$ )	Fe ( $\mu\text{g/g}$ )	Hg ( $\mu\text{g/g}$ )	Ni ( $\mu\text{g/g}$ )	Pb ( $\mu\text{g/g}$ )	V ( $\mu\text{g/g}$ )	Zn ( $\mu\text{g/g}$ )
<b>GB 602</b>											
FF (n = 3)	61 $\pm 33$	15 $\pm 9$	14 $\pm 6$	0.43 $\pm 0.04$	95 $\pm 86$	1,450 $\pm 540$	8.1 $\pm 6.8$	0.55 $\pm 0.45$	0.26 $\pm 0.06$	1.7 $\pm 1.5$	327 $\pm 94$
NF (n = 6)	39 $\pm 28$	164 $\pm 136$	7 $\pm 4$	1.2 $\pm 1.2$	51 $\pm 50$	979 $\pm 549$	3.1 $\pm 1.3$	1.3 $\pm 0.8$	0.61 $\pm 0.39$	2.8 $\pm 1.5$	344 $\pm 272$
<b>MC 292</b>											
FF (n = 3)	28 $\pm 23$	16 $\pm 15$	16 $\pm 17$	1.5 $\pm 1.3$	73 $\pm 59$	2,250 $\pm 2,530$	4.3 $\pm 4.4$	0.9 $\pm 0.6$	0.46 $\pm 0.38$	3.0 $\pm 1.7$	360 $\pm 339$
NF (n = 6)	39 $\pm 21$	17 $\pm 8$	14 $\pm 10$	1.1 $\pm 0.8$	75 $\pm 86$	1,310 $\pm 1,220$	3.3 $\pm 2.8$	0.9 $\pm 0.5$	0.38 $\pm 0.27$	2.8 $\pm 1.1$	264 $\pm 183$

**Table 8.15.** Means  $\pm$  standard deviations for samples of the red crab *Chaceon quinqueedens* from far-field (FF) and near-field (NF) stations from post-development sites Garden Banks (GB) 602 and Mississippi Canyon (MC) 292.

	As ( $\mu\text{g/g}$ )	Ba ( $\mu\text{g/g}$ )	Cd ( $\mu\text{g/g}$ )	Cr ( $\mu\text{g/g}$ )	Cu ( $\mu\text{g/g}$ )	Fe ( $\mu\text{g/g}$ )	Hg ( $\mu\text{g/g}$ )	Ni ( $\mu\text{g/g}$ )	Pb ( $\mu\text{g/g}$ )	V ( $\mu\text{g/g}$ )	Zn ( $\mu\text{g/g}$ )
<b>GB 602</b>											
FF (n = 3)	170 $\pm 29$	11 $\pm 7$	12 $\pm 5$	0.7 $\pm 0.2$	151 $\pm 65$	254 $\pm 81$	1.5 $\pm 0.4$	9.2 $\pm 2.4$	0.32 $\pm 0.14$	3.3 $\pm 1.0$	261 $\pm 31$
NF (n = 6)	65 $\pm 25$	54 $\pm 46$	2.1 $\pm 1.1$	1.0 $\pm 0.6$	59 $\pm 45$	216 $\pm 111$	0.54 $\pm 0.14$	3.4 $\pm 1.6$	0.26 $\pm 0.10$	1.3 $\pm 0.7$	148 $\pm 61$
<b>MC 292</b>											
FF (n = 3)	131 $\pm 46$	3.9 $\pm 1.8$	2.9 $\pm 2.3$	0.6 $\pm 0.4$	199 $\pm 70$	612 $\pm 215$	0.8 $\pm 0.4$	10 $\pm 3.2$	0.25 $\pm 0.12$	2.8 $\pm 1.3$	226 $\pm 27$
NF (n = 6)	133 $\pm 37$	43 $\pm 38$	101 $\pm 13$	2.5 $\pm 2.0$	248 $\pm 73$	1,340 $\pm 1,100$	1.0 $\pm 0.4$	14 $\pm 4.6$	0.89 $\pm 0.70$	6.0 $\pm 4.0$	230 $\pm 107$

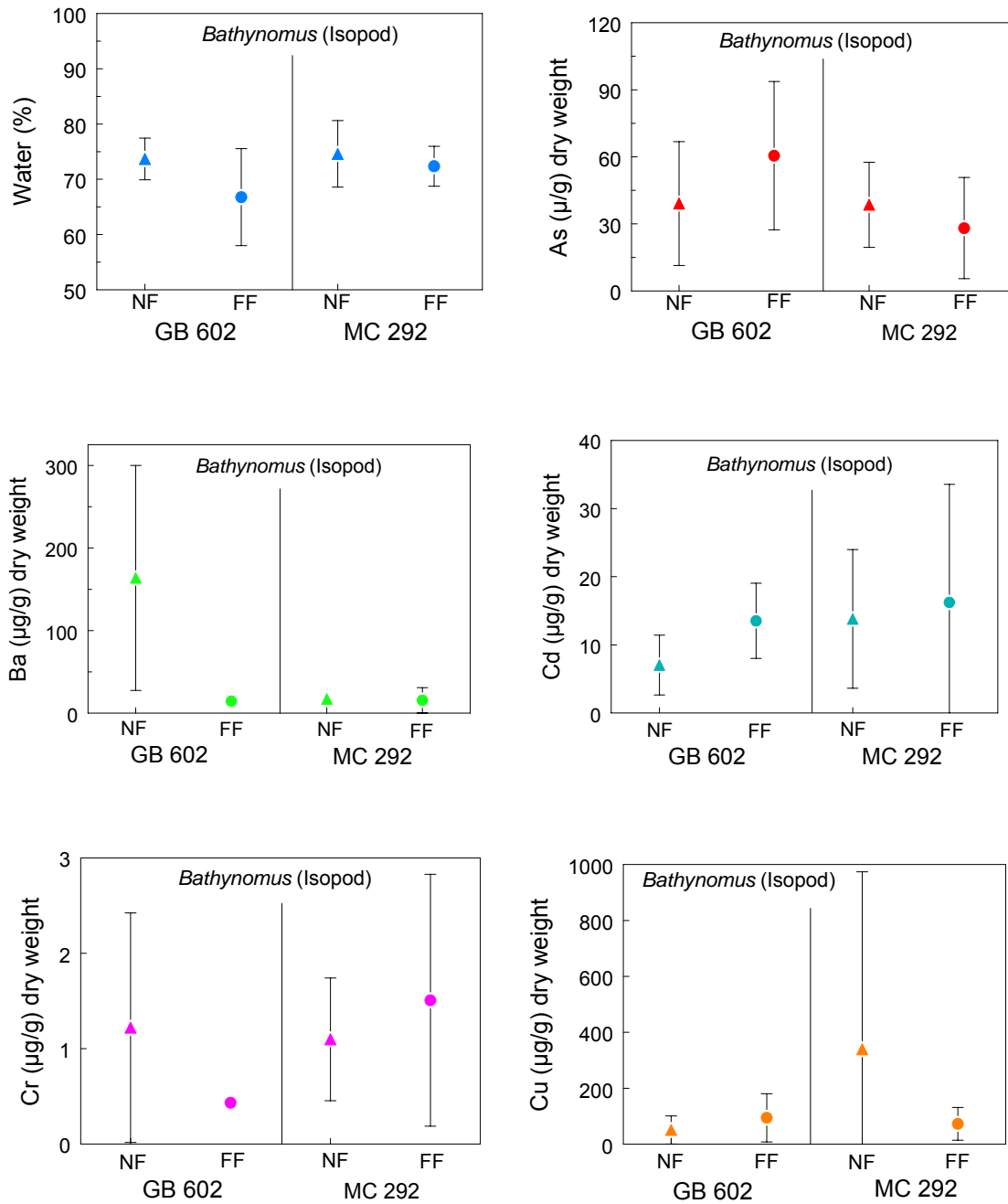


**Figure 8.56.** Water content and concentrations of arsenic (As), barium (Ba), cadmium (Cd), chromium (Cr), and copper (Cu) in soft tissue from the isopod *Bathynomus giganteus* from near-field (NF) and far-field (FF) stations from post-development sites Garden Banks (GB) 602 and Mississippi Canyon (MC) 292.

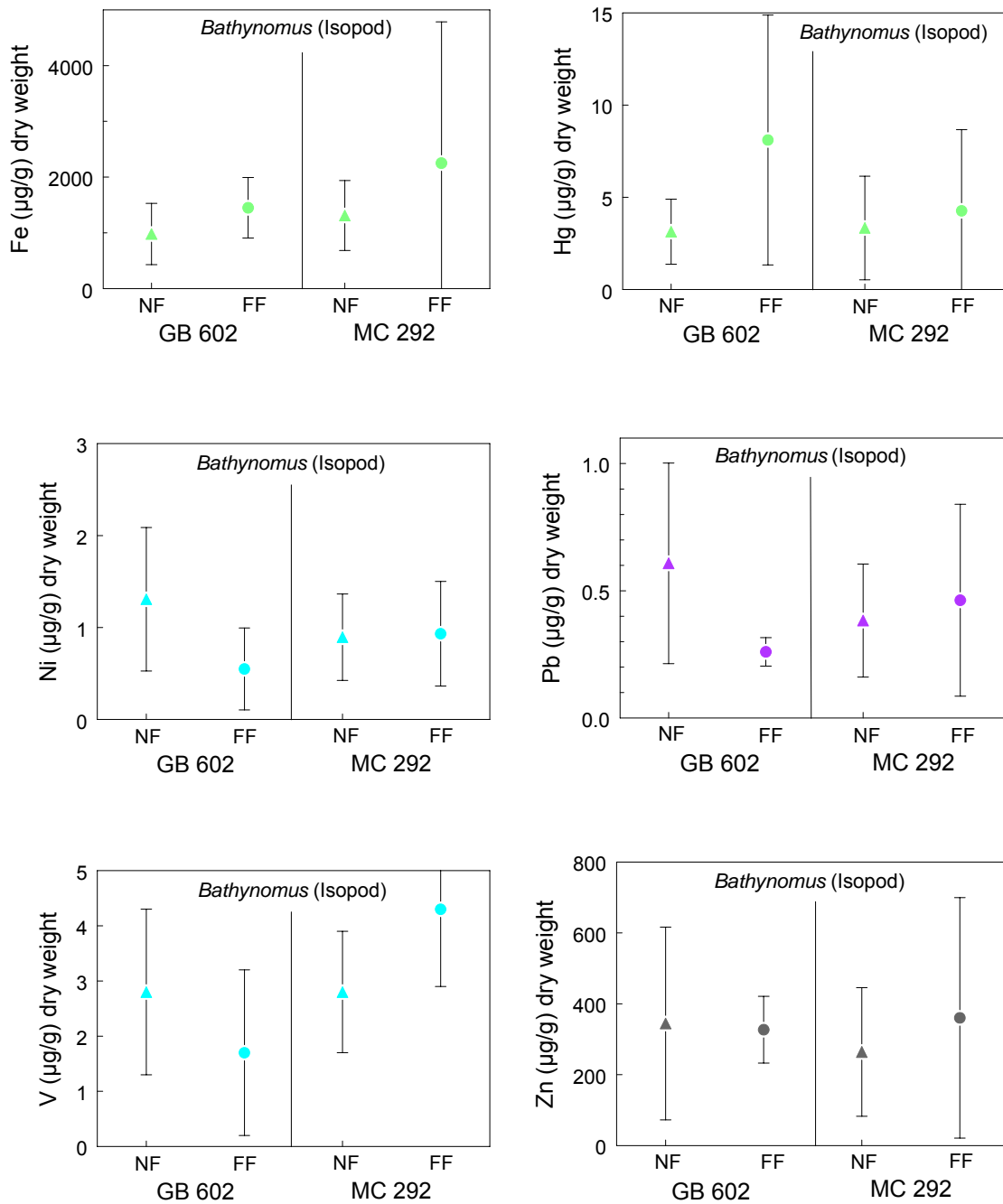


**Figure 8.57.** Concentrations of iron (Fe), mercury (Hg), nickel (Ni), lead (Pb), vanadium (V), and zinc (Zn) in soft tissue from the isopod *Bathynomus giganteus* from near-field (NF) and far-field (FF) stations from post-development sites Garden Banks (GB) 602 and Mississippi Canyon (MC) 292.

For the red crab *Chaceon quinquegens*, concentrations of Ba are greater in specimens from near-field versus far-field stations at GB 602, whereas concentrations of As, Cd, Cu, Hg, Ni, V, and Zn are greater in specimens from far-field stations than near-field stations (**Table 8.15** and **Figures 8.58** and **8.59**). For MC 292, concentrations of Ba, Cd, Cr, and V were greater in samples collected at near-field stations than at far-field stations (**Table 8.15** and **Figures 8.58** and **8.59**).

## 8.6 DISCUSSION OF SEDIMENT TRACE METALS

Concentrations of 13 metals (Al, As, Ba, Cd, Cr, Cu, Fe, Hg, Mn, Ni, Pb, V, and Zn) were determined in 163 surface sediments (0 to 2 cm) and 50 subsurface sediments (from 12 cores) at all four sites (VK 916, GB 516, GB 602, and MC 292) during this study. The data set is used here to evaluate possible sediment contamination from trace metals at near-field versus far-field sites and pre- versus post-exploration/development.

Concentrations of Fe in sediments from far-field, near-field, and discretionary stations from all sites follow a strong, positive linear trend versus Al ( $r = 0.95$ , **Figure 8.60**) as described previously. Concentrations of trace metals in sediments generally correlate well with concentrations of Al and Fe because concentrations of most metals are very low in quartz sand or carbonate shell material and much higher in fine-grained aluminosilicates. Aluminum and Fe are rarely introduced by anthropogenic processes and are present at percent levels in most sediment relative to parts per million ( $\mu\text{g/g}$ ) levels for trace metals. Concentrations of Al and Fe often can be used to normalize concentrations of trace metals and thereby incorporate the metal-controlling variables of grain size, organic carbon content, and mineralogy. In the ideal case, under natural conditions, a good linear correlation is observed between concentrations of a trace metal and Al and/or Fe. Plots of trace metal concentrations versus Fe or Al have been used in various forms for many years to identify sediment metal contamination (Trefry and Presley 1976; Schropp et al. 1990).

Under background conditions, concentrations of trace metals in sediments generally follow a strong linear trend versus Al and/or Fe in a given depositional environment. For example, concentrations of V in sediments from all far-field, near-field, and discretionary stations from this study correlate well with Al ( $r = 0.91$ , **Figure 8.61**) and Fe ( $r = 0.96$ ) for all surface and subsurface sediments collected. The broad range in V concentrations, yet good linear fit for Al (and Fe) versus V, is consistent with mixing of relatively uniform composition, metal-rich aluminosilicate phases with metal-poor quartz sand and carbonates. Aluminum was chosen for normalization in the present study because it is least affected by chemical weathering and diagenesis. Vanadium levels in background sediment from the Gulf of Mexico are predicted to follow the trend presented in **Figure 8.61**. Thus, the strong relationship for Al versus V in **Figure 8.61** also supports a lack of anthropogenic inputs of V and no impact on V levels due to sediment diagenesis. The three points that plot slightly above the upper prediction interval on **Figure 8.61** exceed that limit by <10% and are consistent with the statistical boundaries of a 95% prediction interval. Eight samples with concentrations of Al and V at <4% and <60  $\mu\text{g/g}$ , respectively, contain 30% to 60% industrial barite (18% to 34% Ba), which contains no significant amounts of Al or V and thus results in a dilution of these two metals.

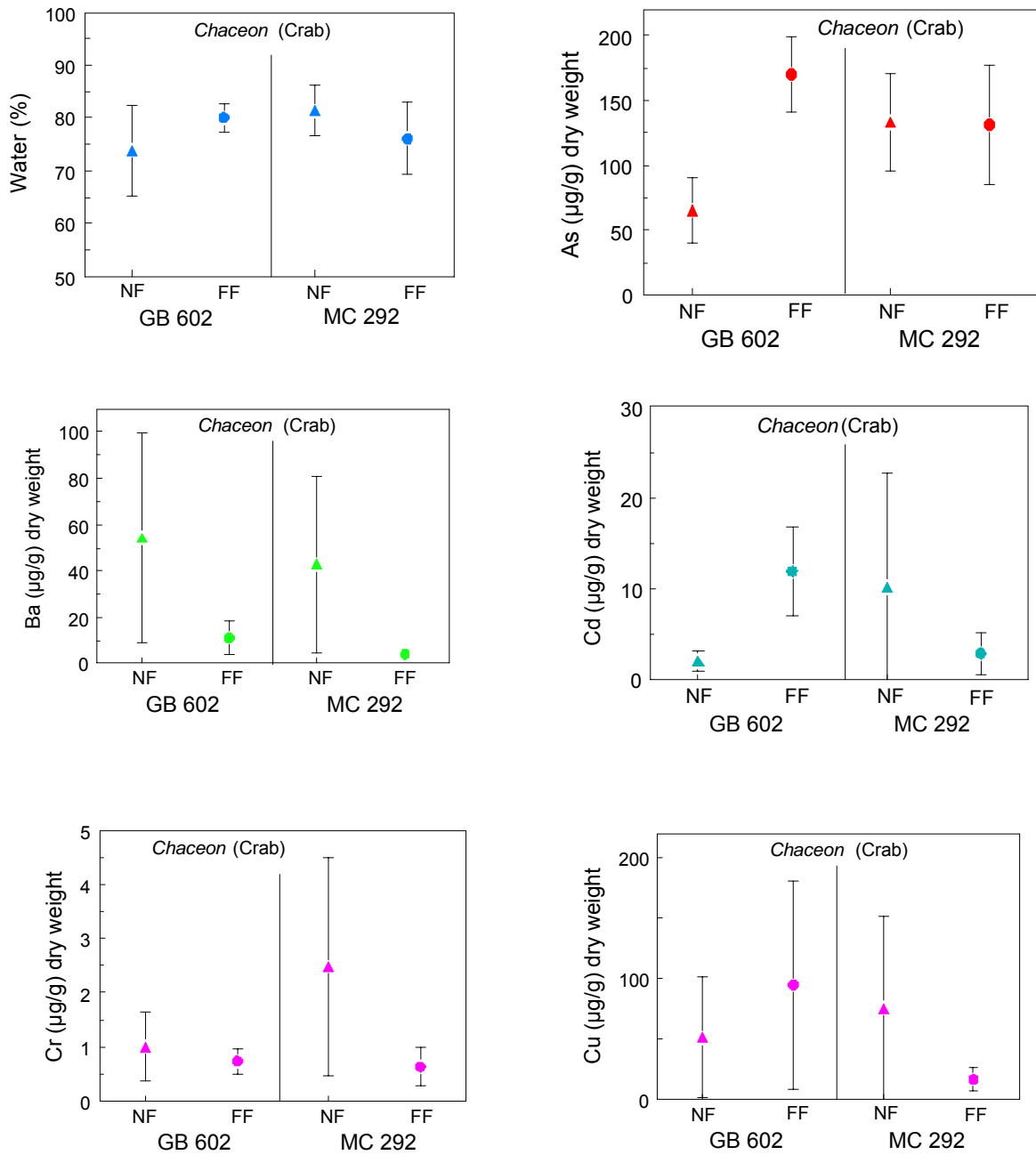


**Figure 8.58.** Water content and concentrations of arsenic (As), barium (Ba), cadmium (Cd), chromium (Cr), and copper (Cu) in soft tissue from the crab *Chaceon* from near-field (NF) and far-field (FF) stations from post-development sites Garden Banks (GB) 602 and Mississippi Canyon (MC) 292.



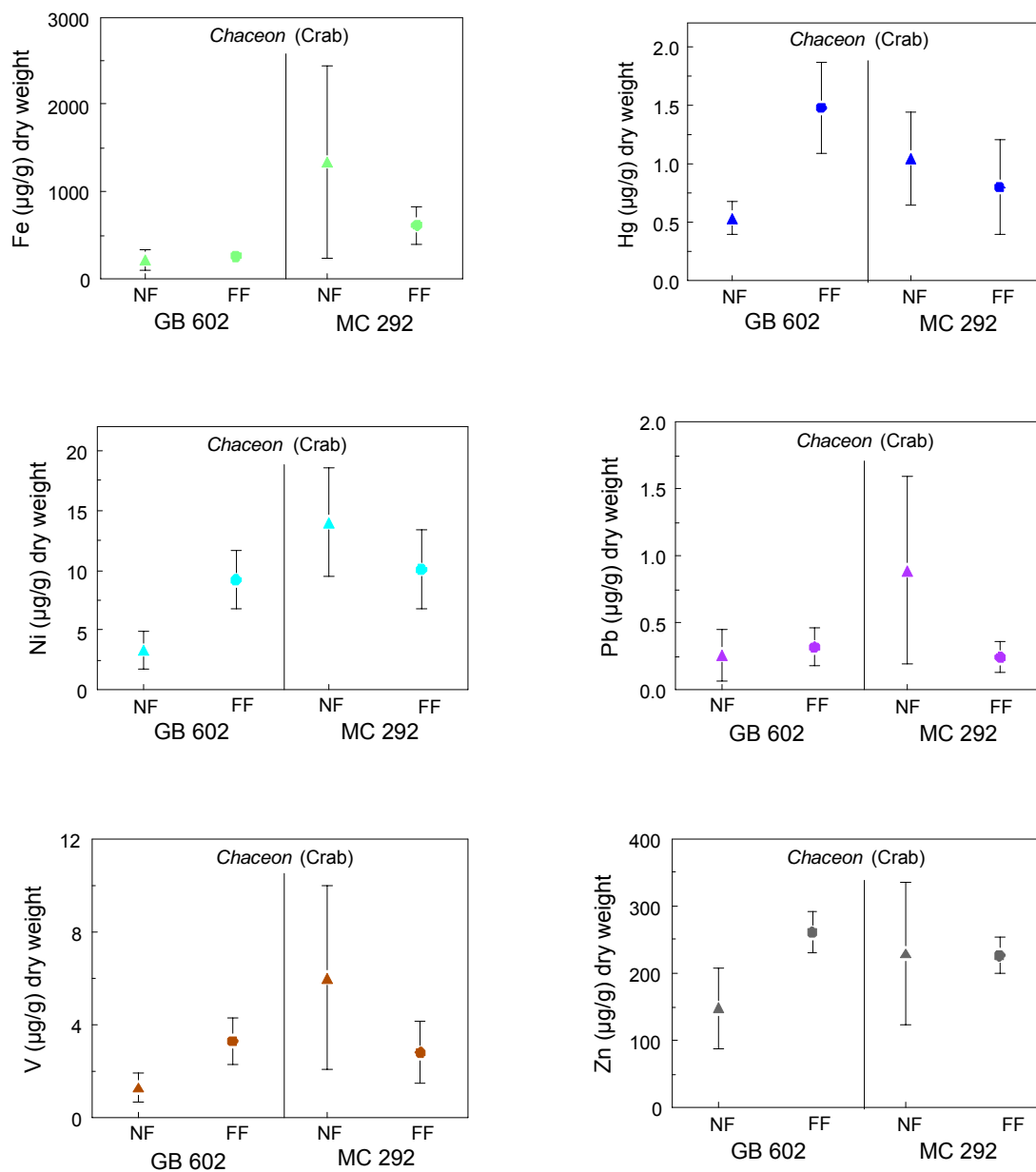


**Figure 8.59.** Concentrations of iron (Fe), mercury (Hg), nickel (Ni), lead (Pb), vanadium (V), and zinc (Zn) in soft tissue from the crab *Chaceon* from near-field (NF) and far-field (FF) stations from post-development sites Garden Banks (GB) 602 and Mississippi Canyon (MC) 292.

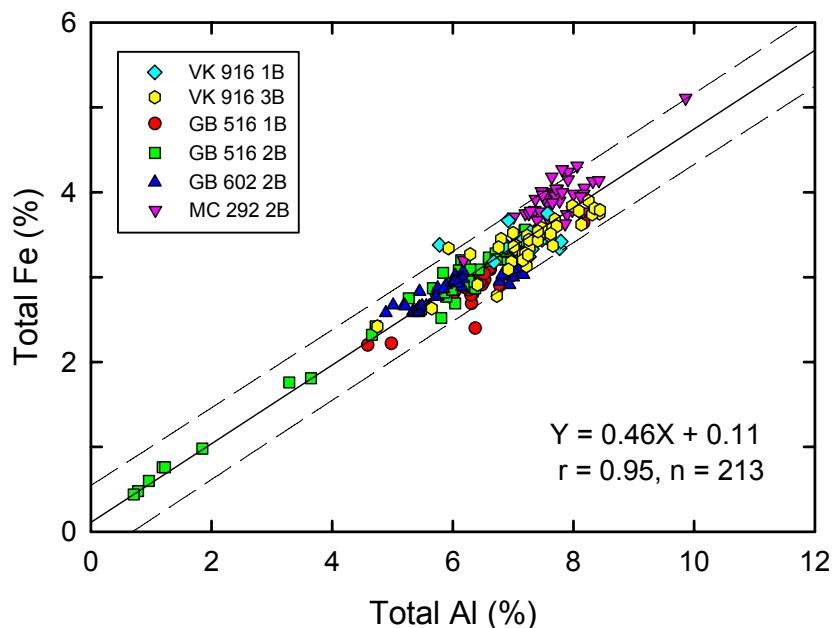


**Figure 8.60.** Concentrations of aluminum (Al) versus iron (Fe) for sediments from all stations. Solid line is from linear regression with equation, correlation coefficient (r), and number of data points (n). Dashed lines show 95% prediction interval.

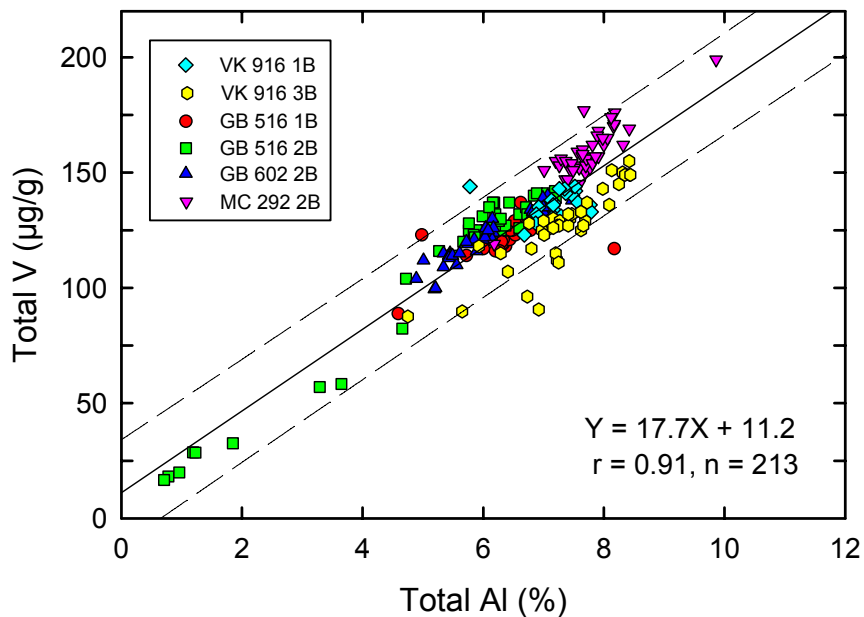


**Figure 8.61.** Concentrations of aluminum (Al) versus vanadium (V) for all sediments collected during the project. Solid line is from linear regression for all samples with equation, correlation coefficient (r), and number of samples (n). Dashed lines show 95% prediction interval.

When a graph for Al versus Zn was constructed using all the data, at least 10 values did not fit a simple linear trend (**Figure 8.62**). Thus, a line and prediction interval were constructed for Al versus Zn using only the far-field data (**Figure 8.62a**). The resulting good correlation coefficient for the far-field data supports a linear relationship for Al versus Zn in background sediments (**Figure 8.62a**). When data from the near-field and discretionary stations are added to the Al versus Zn plot, 11 or more points plot at values of Zn that are  $\geq 25\%$  above the upper prediction interval (**Figure 8.62b**). Six of the anomalous points are for discretionary stations from GB 516 (Cruise 2B). The other anomalous points are from selected near-field stations, all of which are post-exploration or post-development samples (**Figure 8.62b**).

Results for Pb follow a similar trend as described for Zn with ~20 data points that plot as positive anomalies with respect to the x axis (**Figure 8.63**). Once again, the data for the far-field samples were used to define background conditions (**Figure 8.63**). Six Pb values, five from discretionary stations at GB 516 and one from a discretionary station at GB 602, exceed 100  $\mu\text{g/g}$ . An additional 10 samples have Pb levels that are greater than 40  $\mu\text{g/g}$  (**Figure 8.63**). All of the anomalous points are from GB 516 or GB 602. In addition to the anomalous data described above, 12 other samples contain Pb at concentrations that are  $>25\%$  above the upper prediction interval on the Al versus Pb graph (**Figure 8.63**). In contrast with the positive anomalies, about 15 data points for post-exploration or post-development samples show lower Pb levels than predicted based on Al concentrations in the sediments. These lower Pb levels may be due to the presence of clays in drilling mud or cuttings (source of Al), which are low in Pb.

Nine sediment samples contain As at levels that plot above the upper prediction interval in **Figure 8.64**. Seven of the samples with elevated As concentrations are from GB 516. Most of the samples with Pb concentrations that plot below the lower prediction interval follow the same trend as for As.

Considerable interest has been generated regarding concentrations of Hg in sediments adjacent to drilling sites because concentrations of total Hg near drilling sites are often 2 to 10 times higher than in nearby background sediments (Neff 2002a). This Hg is known to be a natural impurity in barite (Kramer et al. 1980; Trefry and Smith 2003).

When concentrations of Hg from this study are normalized to concentrations of Al, about 15 samples have Hg levels that are elevated above the trend observed in the Hg/Al ratio for far-field sediments (**Figure 8.65a**). Two separate background lines are developed in the Al versus Hg plot using far-field samples from (1) GB 516 and GB 602 and (2) MC 292 and VK 916 because Hg levels are naturally higher at the GB sites, where sediments accumulate more slowly and increase the scavenging time for particles to adsorb Hg from the water column. With respect to Hg concentrations determined during this study, five samples from GB 516 contain Hg at levels  $>400$  ng/g (**Figure 8.65a**). At eight additional stations, concentrations of Hg are  $>150$  ng/g.

Most of the sediments with elevated concentrations of Hg also contain elevated levels of Ba (**Figure 8.65b**). Previous work, as summarized by Trefry and Smith (2003), shows that the barite-bound Hg has a very low degree of bioavailability.

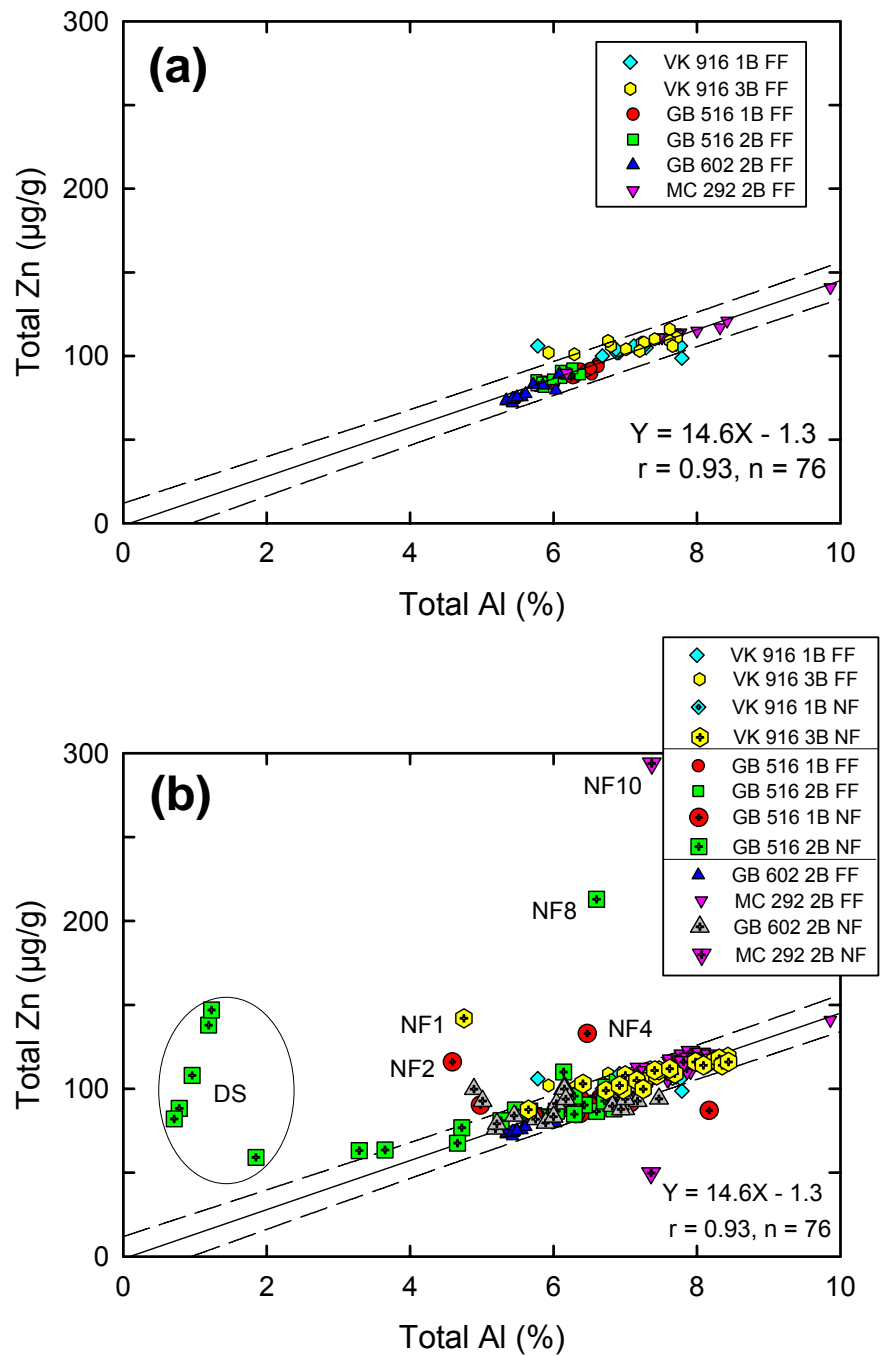


**Figure 8.62.** Concentrations of aluminum (Al) versus zinc (Zn) for sediments from (a) far-field (FF) stations and (b) all stations (FF and near-field [NF], including discretionary [DS] stations). Solid lines on both graphs are from linear regression for FF samples with equations, correlation coefficient ( $r$ ), and number of samples ( $n$ ). Dashed lines above and below solid line show 95% prediction interval.

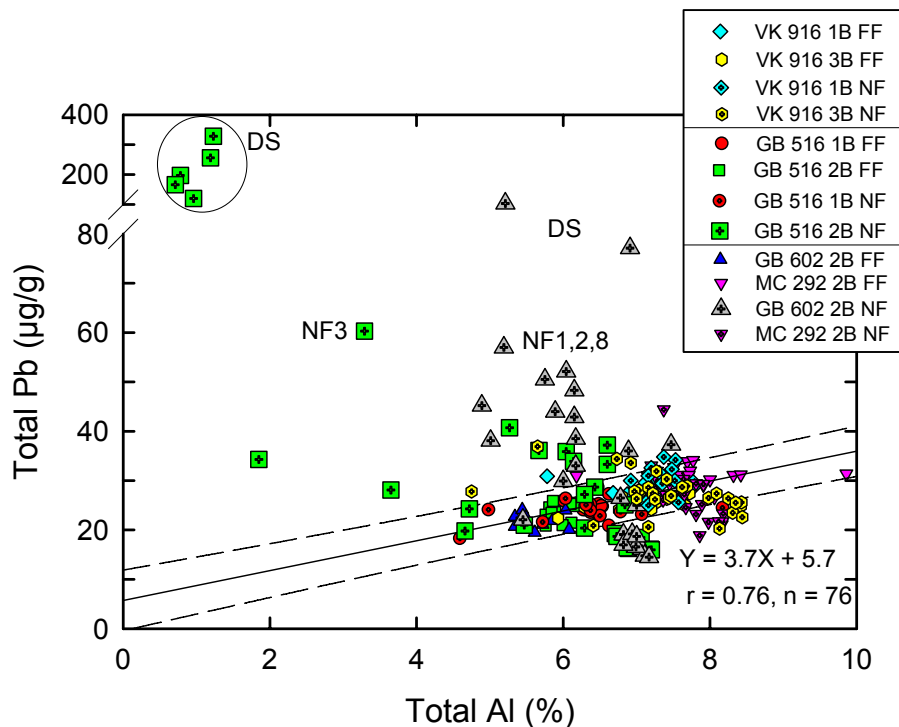


**Figure 8.63.** Concentrations of aluminum (Al) versus lead (Pb) for sediments from far-field (FF) and near-field (NF) stations (data for discretionary [DS] stations are plotted as NF samples). Solid line is from linear regression for FF samples with equations, correlation coefficient ( $r$ ), and number of samples ( $n$ ). Dashed lines above and below solid line show 95% prediction interval.

Correlations between concentrations of Ba and total Hg can sometimes be used to help confirm that excess total Hg in sediment is associated with barite. Trefry et al. (2003) obtained values of  $r > 0.92$  for Ba versus Hg in sediments adjacent to drilling sites when sufficient data were available to create separate plots for each site. The Ba versus Hg relationship also can be used to calculate the concentration of total Hg in the barite used at a particular site. Barite has been specifically identified by x-ray diffraction in many near-field samples from the study area. In this study, the following two data sets contained high enough Ba levels to estimate the Hg content of the industrial barite: (1) five samples from DS-2 stations at GB 516 and (2) the remaining near-field samples ( $n = 35$ ) at GB 516 (**Figure 8.65b**). If the two regression lines in **Figure 8.65b** are extrapolated to pure barite at 58.8% Ba, the concentrations of total Hg are 944 and 260 ng/g (obtained by substituting 58.8% Ba for  $x$  in the equations in **Figure 8.65b**). Typical “industrial barite” contains 85% to 95% barite (i.e., 50% to 56% Ba). Based on the range of Ba levels in industrial barite (50% to 56% Ba), the average values for total Hg in the (apparently) two different barites used at GB 516 are ~870 and 240 µg/g (at 53% Ba). These calculated values are in line with USEPA regulations, which allow a maximum Hg level of 1,000 ng/g (1 µg/g) in barite (USEPA 1993).

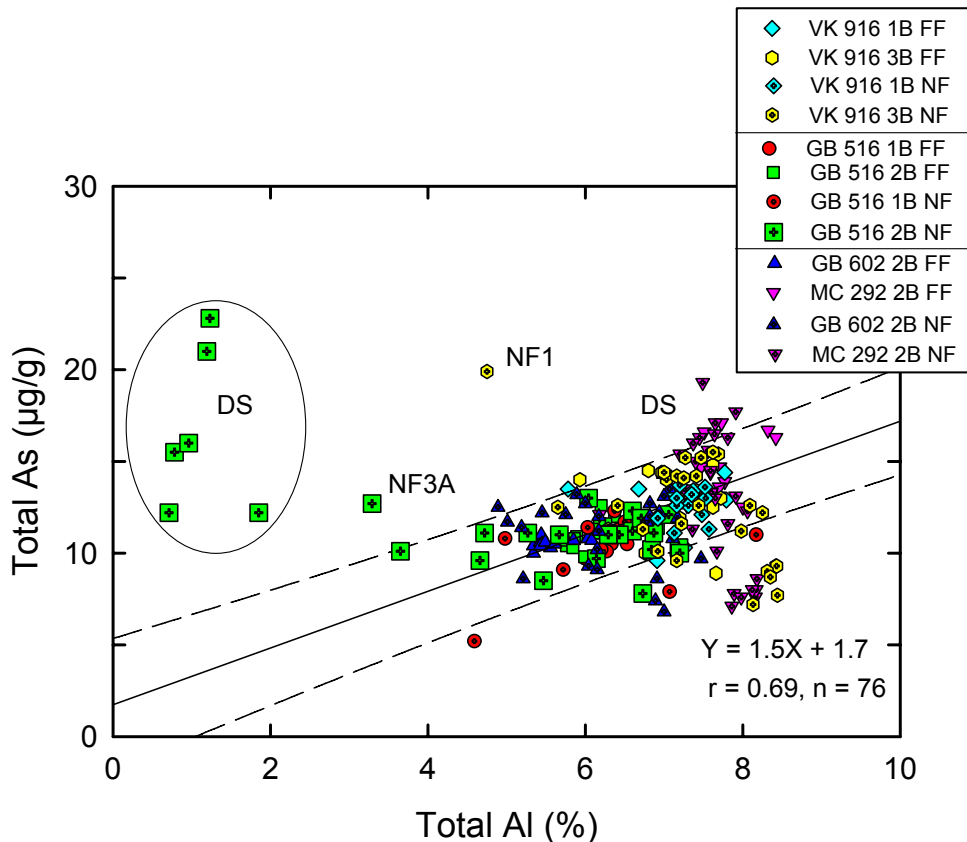


**Figure 8.64.** Concentrations of aluminum (Al) versus arsenic (As) for sediments from far-field (FF) and near-field (NF) stations (data for discretionary [DS] stations are plotted as NF samples). Solid line is from linear regression for FF samples with equations, correlation coefficient ( $r$ ), and number of samples ( $n$ ). Dashed lines above and below solid line show 95% prediction interval.

The graph for Al versus Cd (**Figure 8.66**) does not show the same goodness of fit as observed for V and Zn, partly because of the greater variability in Cd concentrations. All Cd concentrations are  $<0.6 \mu\text{g/g}$ ; however, samples from discretionary stations at GB 516 and GB 602 plot above the other data in a manner similar to that observed for Pb. These samples may have a minor anthropogenic contribution of Cd. Concentrations of Cu (**Figure 8.66**) from sediments with Al levels of 5%-8% are similar and do not yield a clear trend. However, samples from the discretionary stations at site GB 516 show distinct positive anomalies relative to the other samples. Plots for both Ni and Cr (**Figure 8.67**) show no anomalously high values, yet some low concentrations are observed in a manner similar to that described for Pb.

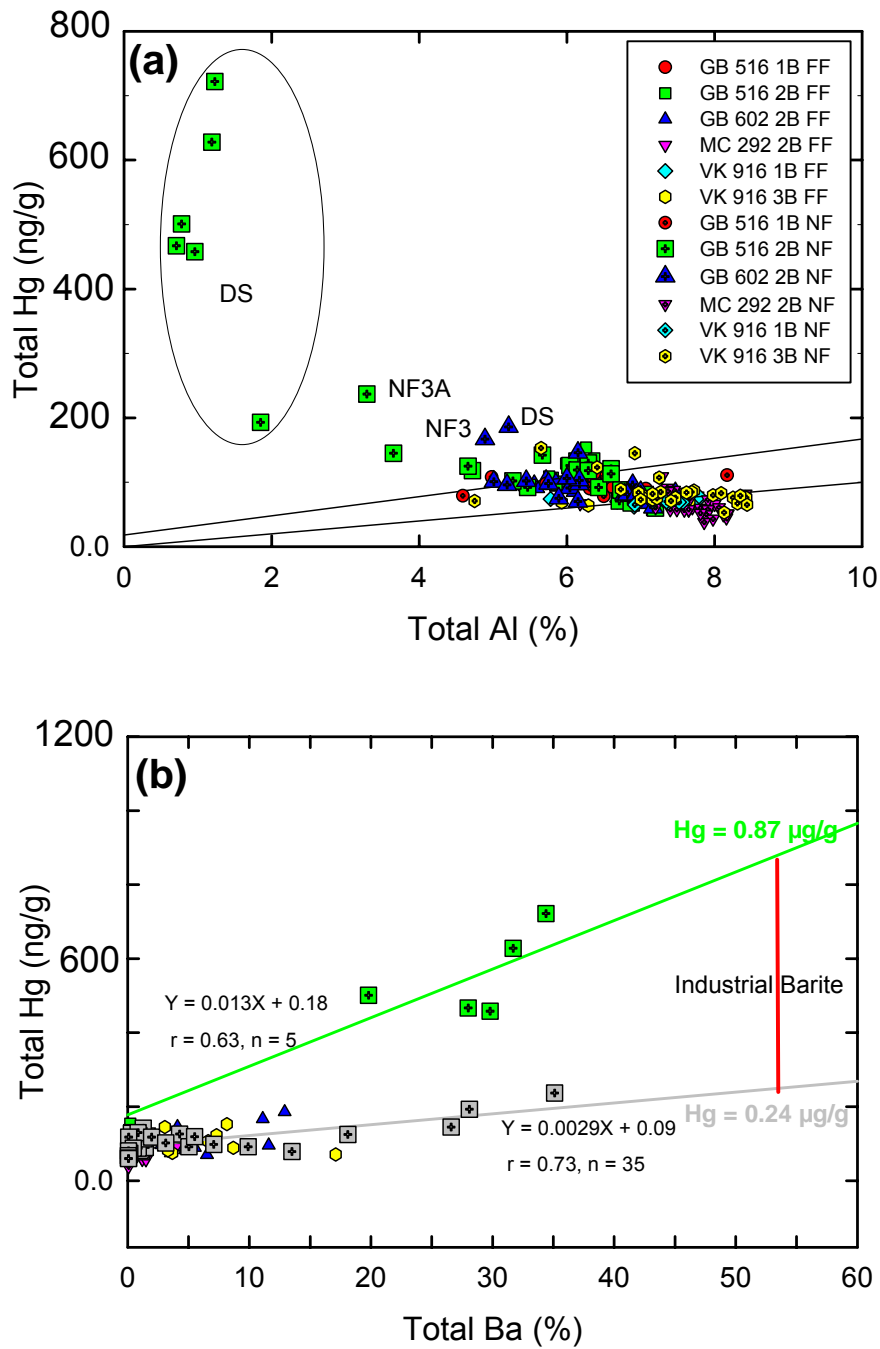


**Figure 8.65.** Concentrations of (a) aluminum (Al) versus mercury (Hg) and (b) barium (Ba) versus Hg for sediments from far-field (FF) and near-field (NF) stations (data for discretionary [DS] stations are plotted as NF samples). Solid lines on (a) are from linear regression for FF samples as described in the text. Solid lines on (b) are for NF samples from Garden Banks (GB) 516 with equations, correlation coefficient (r), and number of samples (n). Extrapolated concentrations of Hg, based on 53% Ba in industrial barite, are shown in (b) along vertical line.

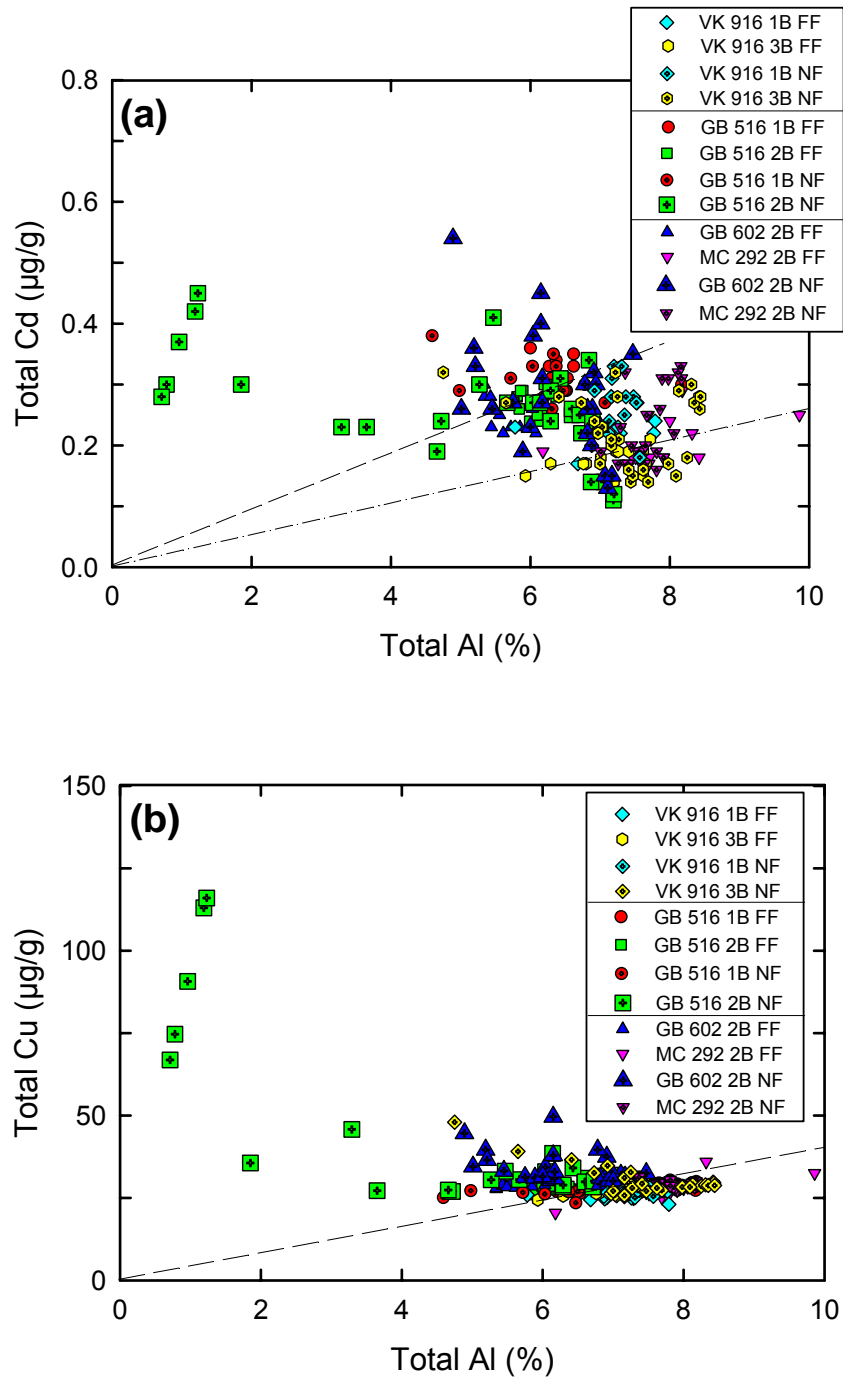


**Figure 8.66.** Concentrations of aluminum (Al) versus (a) cadmium (Cd) and (b) copper (Cu) for sediments from far-field (FF) and near-field (NF) stations (data for discretionary stations are plotted as NF samples). Solid lines are from linear regression (set through the origin) for FF samples.



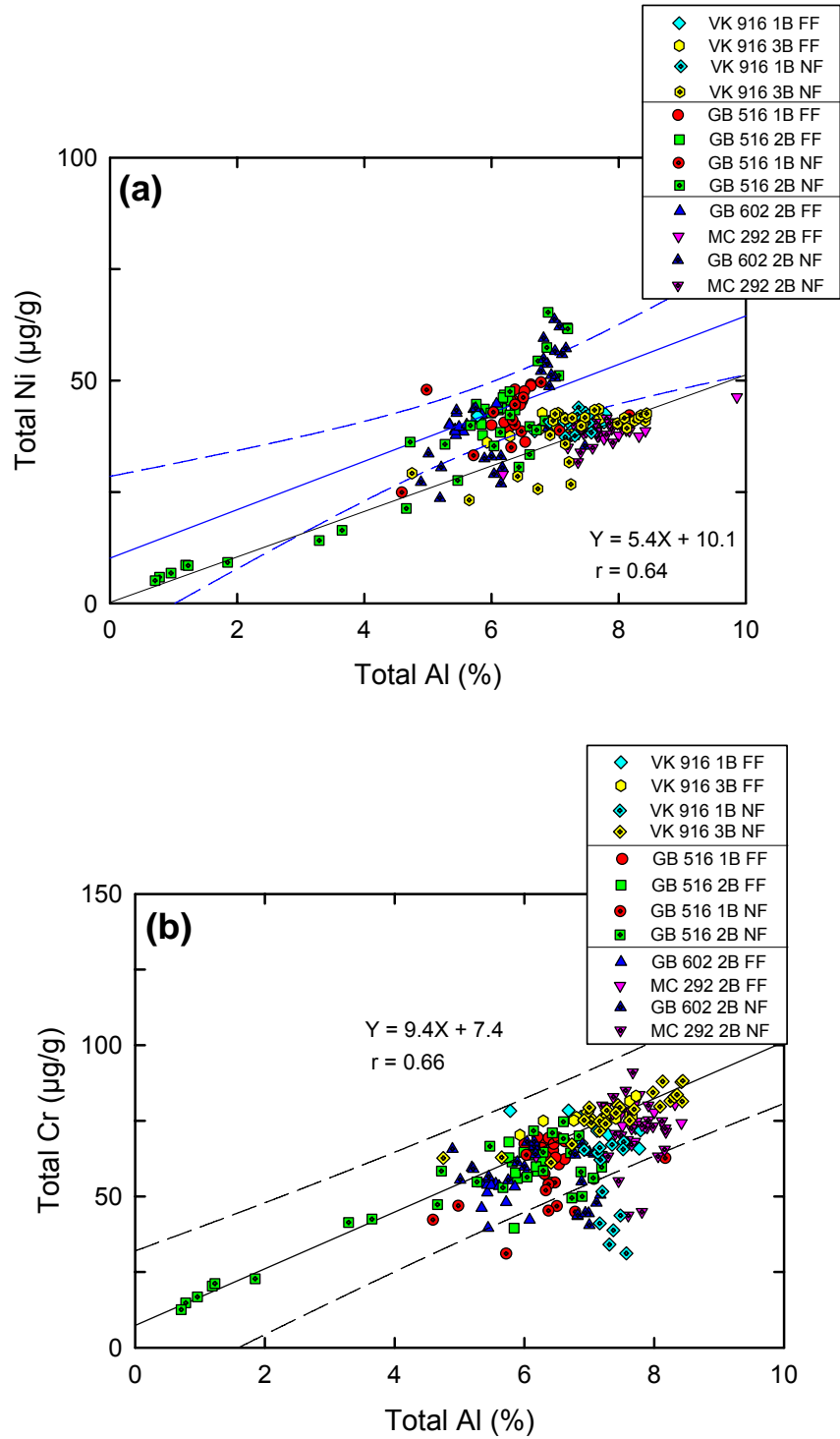


**Figure 8.67.** Concentrations of aluminum (Al) versus (a) nickel (Ni) and (b) chromium (Cr) for sediments from far-field (FF) and near-field (NF) stations (data for discretionary stations are plotted as NF samples). Solid lines are from linear regression for FF samples with equations, correlation coefficient ( $r$ ), and number of samples ( $n$ ). Dashed lines show 95% prediction intervals.

## 8.7 CONCLUSIONS

The data for metals, TOC, and redox parameters include one set of pre-drilling samples (VK 916 on Cruise 1B) and four sets of post-drilling samples (GB 516 on Cruise 1B and Cruise 2B; GB 602 and MC 292 on Cruise 2B). Overall, the following general trends were observed at sites where drilling discharges had occurred:

- Concentrations of Ba were typically enriched by >10 fold at NF versus FF stations. The degree of enrichment was typically on the order of 20- to 40-fold.
- Concentrations of Hg, Zn, As, and Pb were elevated in 6% to 15% of the NF samples relative to FF samples. These increases were directly related to increases in concentrations of Ba. Calculations indicate that Hg concentrations in barite deposited at these sites were in line with USEPA regulations.
- Concentrations of TOC were typically about one-third greater in NF sediments relative to FF sediments.
- The amount of integrated O<sub>2</sub> was commonly 2 to 10 times lower in NF sediments relative to FF sediments.

Most NF versus FF differences in tissue metals in the giant isopod *Bathynomus giganteus* and the red crab *Chaceon quinquegens* were not significant. This was due to the large standard deviations and small number of samples from the two sites (GB 602 and MC 292) where these animals were collected. However, for isopods at GB 602, concentrations of Ba, Cr, and Pb were greater at NF stations than FF stations and concentrations of Cd and Hg were greater at FF stations than NF stations. No significant differences were observed for isopods from MC 292. For red crabs at GB 602, concentrations of Ba were greater in specimens from NF versus FF stations whereas concentrations of As, Cd, Cu, Hg, Ni, V, and Zn were greater in specimens from FF stations than NF stations. For MC 292, concentrations of Ba, Cd, Cr, and V were greater in samples collected at NF stations than at FF stations. The most consistent finding was elevated Ba, which may be due to sediment particles retained in the gut.

## Chapter 9 Sediment and Tissue Hydrocarbons

Thomas J. McDonald and James M. Brooks  
TDI-Brooks International, Inc.

---

### 9.1 INTRODUCTION

During three cruises, sediments were collected for hydrocarbon analysis from four deepwater sites in the northern Gulf of Mexico:

- VK 916 – exploration site
- GB 516 – exploration/development site
- GB 602 – post-development site
- MC 292 – post-development site

Cruise 1B (October/November 2000) was the pre-drilling survey for GB 516 and VK 916. Cruise 2B (July 2001) was the post-drilling survey for GB 516 and the two post-development sites (GB 602 and MC 292). Cruise 3B (August 2002) was the post-drilling survey at VK 916. Further details of surveys and general sampling methods are provided in *Chapter 2*.

Sediment samples were collected at 12 near-field stations and 12 far-field stations at each site. In addition to these routinely collected sediments, three discretionary box-core samples were located in suspected cuttings depositional areas mapped during geophysical surveys. All of the sediment samples were analyzed for the presence of polycyclic aromatic hydrocarbons (PAH) by gas chromatography-mass spectrometry (GC/MS) and synthetic based fluid (SBF) by gas chromatography-flame ionization detection (GC-FID). Detailed results for each sample are provided in *Appendix H*.

PAHs are widely used as an indicator of petroleum input in environmental samples. PAHs containing condensed rings and simple alkylations (naphthalenes, fluorenes, phenanthrenes, dibenzothiophenes, fluoranthenes, and chrysenes, etc.) are generally the analytes of interest. PAHs are ubiquitous in the marine environments and can have multiple sources such as petroleum, early diagenesis, coals, combustion, immature/mature sediments, and anthropogenic inputs.

Synthetic hydrocarbons used in SBMs include linear- $\alpha$ -olefins, poly- $\alpha$ -olefins, internal olefins, and esters. A GC-FID chromatogram displaying a typical background deep-sea sediment hydrocarbon distribution is shown in **Figure 9.1**. **Figure 9.2** displays a deep-sea sediment hydrocarbon distribution pattern that is dominated by SBF. The types of SBMs used at the study sites included internal olefins, linear- $\alpha$ -olefins, and esters as discussed in *Chapter 3*.

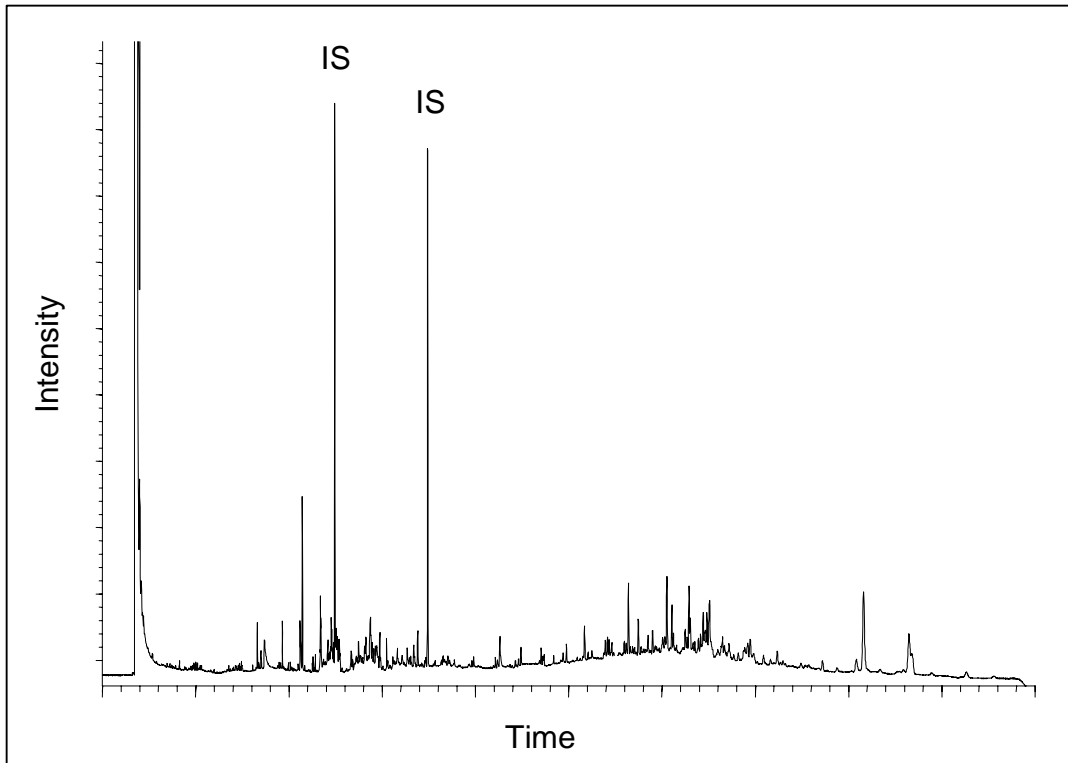


**Figure 9.1.** Typical background hydrocarbon distribution in deep sea sediment. The two large peaks are internal standards (IS). The first peak is the solvent peak.

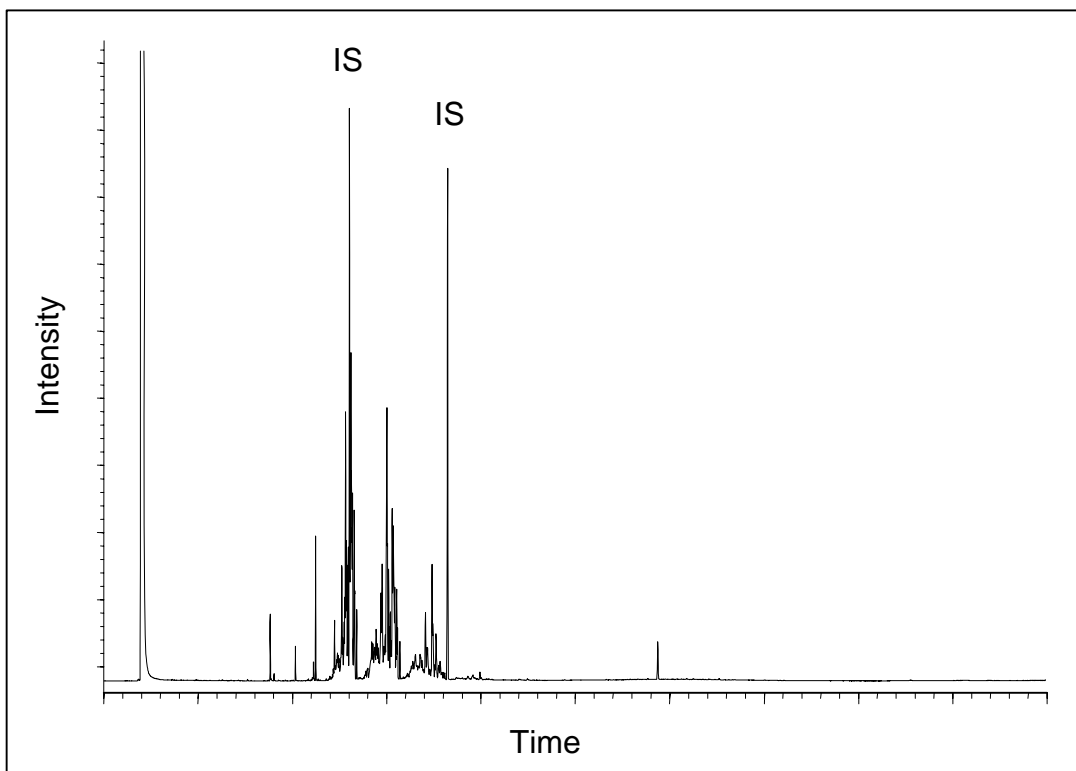


**Figure 9.2.** A sediment hydrocarbon sample that displays a synthetic based fluid pattern.

## **9.2 ANALYTICAL METHODS**

### **9.2.1 Extraction of Sediments for Aromatic and Saturated Hydrocarbons**

An automated extraction apparatus (Dionex ASE200 Accelerated Solvent Extractor - USEPA Method SW-846 3545) was used to extract various organics from 2 to 20 g of pre-dried samples. The extractions were performed using methylene chloride solvent inside stainless steel extraction cells held at elevated temperature and solvent pressure. The extracts dissolved in the solvent were then transferred from the heated extraction cells to glass collection vials containing activated Cu granules to minimize matrix interference during quantitative determinations. The extracts were subjected to silica gel/alumina columns to remove biogenic organic material that can cause positive interference with this method. The extracts were then concentrated to a final volume of 1 mL using an evaporative solvent reduction apparatus. Final extracts were submitted for determination of aromatic and aliphatic hydrocarbon analytes including SBF.

### **9.2.2 Extraction of Tissues for Aromatic Hydrocarbons**

An automated extraction apparatus (Dionex ASE200 Accelerated Solvent Extractor - USEPA Method SW-846 3545) was used to extract various organics from 2 to 15 g of pre-dried samples (chemically dried or freeze-dried). The extractions were performed using methylene chloride solvent inside stainless steel extraction cells held at elevated temperature and solvent pressure. The extracts dissolved in the solvent were then transferred from the heated extraction cells to glass collection vials. Extracts were then concentrated to a final volume of 4 mL using an evaporative solvent reduction apparatus. These extracts were then subjected to high performance liquid chromatography (HPLC) cleanup for lipid removal. After HPLC, the extracts were then concentrated to 0.5 mL using an evaporative solvent reduction apparatus and submitted for determination of aromatic hydrocarbon analytes.

### **9.2.3 Determination of Aromatic Hydrocarbons**

PAHs and their alkylated homologues in extracts of sediment and biological tissue (Modified SW-846 8270b) were quantified by GC/MS in selected ion monitoring mode. The gas chromatograph was temperature-programmed and operated in splitless mode. The capillary column was a J&W Scientific DB-5MS<sup>®</sup> (60 m long by 0.25 mm internal diameter [ID] and 0.25  $\mu$ m film thickness) or equivalent. The data acquisition system allowed continuous acquisition and storage of all data during analysis and displayed ion abundance versus time or scan number.

Calibration solutions were prepared at five concentrations ranging from 0.02 to 1  $\mu$ g/mL by diluting a commercially available solution containing the analytes of interest (typically NIST SRM 1491). For each analyte of interest, a relative response factor (RRF) was determined for each calibration level. All five response factors were then averaged to produce a mean relative response factor for each analyte.

An analytical set consisted of standards, samples, and quality control samples. Each extraction batch was analyzed as an analytical set including samples and the following quality control samples: method blank, matrix spike, matrix spike duplicate, and SRMs.

#### 9.2.4 Determination of Aliphatic Hydrocarbons

Saturated hydrocarbons in extracts of sediment (Modified USEPA Method SW-846 8100 and USEPA Method 1663) were quantified by high resolution, capillary gas chromatography with GC-FID. Normal alkanes with 10 to 34 carbons ( $C_{10}$  to  $C_{34}$ ), the isoprenoids pristane and phytane, the unresolved complex mixture (UCM), and the total resolved peaks were determined with this procedure. The gas chromatograph was temperature-programmed and operated in split mode. The capillary column is a Restek Scientific RTX-1 (30 m long by 0.25 mm ID and 0.25  $\mu$ m film thickness). Carrier flow is by electronic pressure control. The autosampler is capable of making 1 to 5 mL injections. Dual columns and dual FIDs were used. The data acquisition system is by HP ChemStation software, capable of acquiring and processing GC data.

A calibration curve was established by analyzing each of five calibration standards (1.25, 10, 25, 40, and 50  $\mu$ g/mL) and fitting the data to a straight line using the least square technique. For each analyte of interest, a response factor (RF) was determined for each calibration level. All five response factors were then averaged to produce a mean relative response factor for each analyte. If an individual aliphatic hydrocarbon is not in the calibration solutions, an RF was estimated from the average RF of the hydrocarbon eluting immediately before the compound. The RF used to calculate UCM was an average of all response factors for n-alkanes contained in the calibration solutions.

An analytical set consists of standards, samples, and quality control samples. Each extraction batch was analyzed as an analytical set, including samples and some or all of the following quality control samples: method blank, matrix spike, duplicate, matrix spike duplicate, and SRM.

#### 9.2.5 Quality Assurance/Quality Control

The quality assurance/quality control procedure for this program included the analyses of a method blank, duplicate, blank spike, and blank spike duplicate per analytical batch of no more than 20 samples. Standard reference oil (NIST 1582) was analyzed with each extraction set. Standard reference sediment (NIST 1941a) was analyzed with each sediment batch, and standard reference tissue (NIST 1947a) was analyzed with each tissue batch. Method blanks were used to determine that sample preparation and analyses were free of contaminants. The duplicate sample was used to determine the precision of the analysis. The blank spike and blank spike duplicate were used to measure accuracy and precision of the analysis. Standard reference materials were used to evaluate accuracy. All quality assurance samples were subject to the identical preparation and analysis steps as samples. The quality assurance criterion for blanks specifies that target analytes must be less than three times the method detection limits (MDLs). The quality assurance criteria for spike recoveries were between 40% and 120%. The quality assurance criterion for valid spiked duplicates was  $\pm 25\%$ . The quality assurance criterion for valid duplicates was  $\pm 25\%$ .

Surrogate solutions equivalent to 5 to 10 times the MDL were prepared for various hydrocarbon analyses. The appropriate surrogate solution was added to every sample, including quality control samples. The data were corrected based on surrogate recovery. The quality assurance criteria for surrogate recoveries were between 40% and 120%, except d12-perylene, which ranged from 10% to 120%.

### 9.3 RESULTS – SEDIMENTS

This section summarizes data for sediment SBF and PAH concentrations. Concentrations of all analytes are presented in *Appendix H*. SBF concentrations reported here are total petroleum hydrocarbons in the SBF range. Non-zero values for far-field sites do not indicate that SBFs are present there; rather, these represent background concentrations of hydrocarbons that coelute with SBFs in the analytical procedure.

#### 9.3.1 Viosca Knoll Block 916 – Exploration Site

Sediments from the near-field and far-field stations at the VK 916 location were sampled during Cruise 1B (October/November 2000) and Cruise 3B (August 2002). In addition to the box cores collected at the near-field and far-field locations, three discretionary box cores were located in suspected cuttings depositional areas during Cruise 3B. These box cores were sampled in 2-cm intervals from 0 cm to 10 cm. The sediment SBF and total PAH concentrations are listed in **Tables 9.1** and **9.2**.

**Table 9.1.** Sediment synthetic based fluid (SBF) and total polycyclic aromatic hydrocarbon (PAH) concentrations at Viosca Knoll Block 916.

Sample	SBF ( $\mu\text{g/g}$ ) <sup>a</sup>		Total PAH (ng/g)	
	Cruise 1B Nov 2000	Cruise 3B Aug 2002	Cruise 1B Nov 2000	Cruise 3B Aug 2002
NF-B01	6.1	10,283	241	NA
NF-B02	5.1	228	249	437
NF-B03	5.5	753	225	275
NF-B04	4.8	7.5	241	244
NF-B05	6.6	6,560	254	NA
NF-B06	6.1	20,364	294	NA
NF-B07	5.1	47,920	235	NA
NF-B08	5.4	36.4	227	252
NF-B09	3.5	17.9	194	268
NF-B10	2.4	8.5	159	254
NF-B11	5.0	7.8	235	254
NF-B12	4.6	98.0	233	250
FF2-B01	4.5	12.8	175	247
FF2-B02	4.3	111 <sup>b</sup>	222	399
FF3-B01	5.7	11.7	270	315
FF3-B02	6.1	13.1	299	316
FF4-B01	4.4	2.2	236	181
FF4-B02	4.7	10.0	246	278
FF5-B01	7.2	10.9	246	297
FF5-B02	4.4	5.5	209	248
FF6-B01	4.4	11.7	237	335
FF6-B02	5.9	13.7	388	305

FF = far-field ; NF = near-field; NA = not available.

<sup>a</sup> Far-field values represent background concentrations of hydrocarbons that coelute with SBFs.

<sup>b</sup> This FF site may have been exposed to previous drilling discharges. Four wells were drilled between March and May 2002 at a wellsite 2.6 km away (see *Chapter 3*).

**Table 9.2.** Synthetic based fluid (SBF) and total polycyclic aromatic hydrocarbon (PAH) sediment concentrations in the Viosca Knoll Block 916 discretionary box core samples from Cruise 3B (August 2002).

Sample	SBF ( $\mu\text{g/g}$ )	Total PAH ( $\text{ng/g}$ )
DS-B1 (0-2)	10,431	NA
DS-B1 (2-4)	3,903	410
DS-B1 (4-6)	940	2163
DS-B1 (6-8)	283	212
DS-B1 (8-10)	178	182
DS-B2 (0-2)	28,138	NA
DS-B2 (2-4)	1,673	30.2
DS-B2 (4-6)	459	190
DS-B2 (6-8)	159	225
DS-B2 (8-10)	278	208
DS-B3 (0-2)	27,319	NA
DS-B3 (2-4)	1,425	NA
DS-B3 (4-6)	788	34.2
DS-B3 (6-8)	771	33.4
DS-B3 (8-10)	585	11.8

DS = discretionary sample; NA = not available.

SBF concentrations in the Cruise 1B near-field sediments ranged from 2.4 to 6.6  $\mu\text{g/g}$  and from 4.3 to 7.2  $\mu\text{g/g}$  in far-field sediments. SBF concentrations in Cruise 3B near-field sediments ranged from 7.5 to 47,920  $\mu\text{g/g}$  and in far-field sediments ranged from 2.2 to 111  $\mu\text{g/g}$ . Surface sediment SBF concentrations in the near-field and discretionary box core samples are displayed in **Figure 9.3**. Total PAH concentrations in Cruise 1B near-field sediments ranged from 159 to 294  $\text{ng/g}$  and in far-field sediments ranged from 175 to 388  $\text{ng/g}$ . Total PAH concentrations in Cruise 3B near-field sediments ranged from 244 to 437  $\text{ng/g}$  and in far-field sediments ranged from 181 to 399  $\text{ng/g}$ . Four of the Cruise 3B near-field locations could not be analyzed for PAH due to the high concentrations of SBF in the sediments.

Using the Tukey's Honest Significant Difference (HSD) test, there was no significant difference among the sediment SBF concentrations at Cruise 1B near-field stations, Cruise 1B far-field stations, and Cruise 3B far-field stations. However, a significant difference was detected between sediment SBF concentrations in Cruises 1B and 3B near-field stations (the post-drilling concentrations were higher). There was no significant difference among sediment PAH concentrations at near-field stations and far-field stations during both cruises.



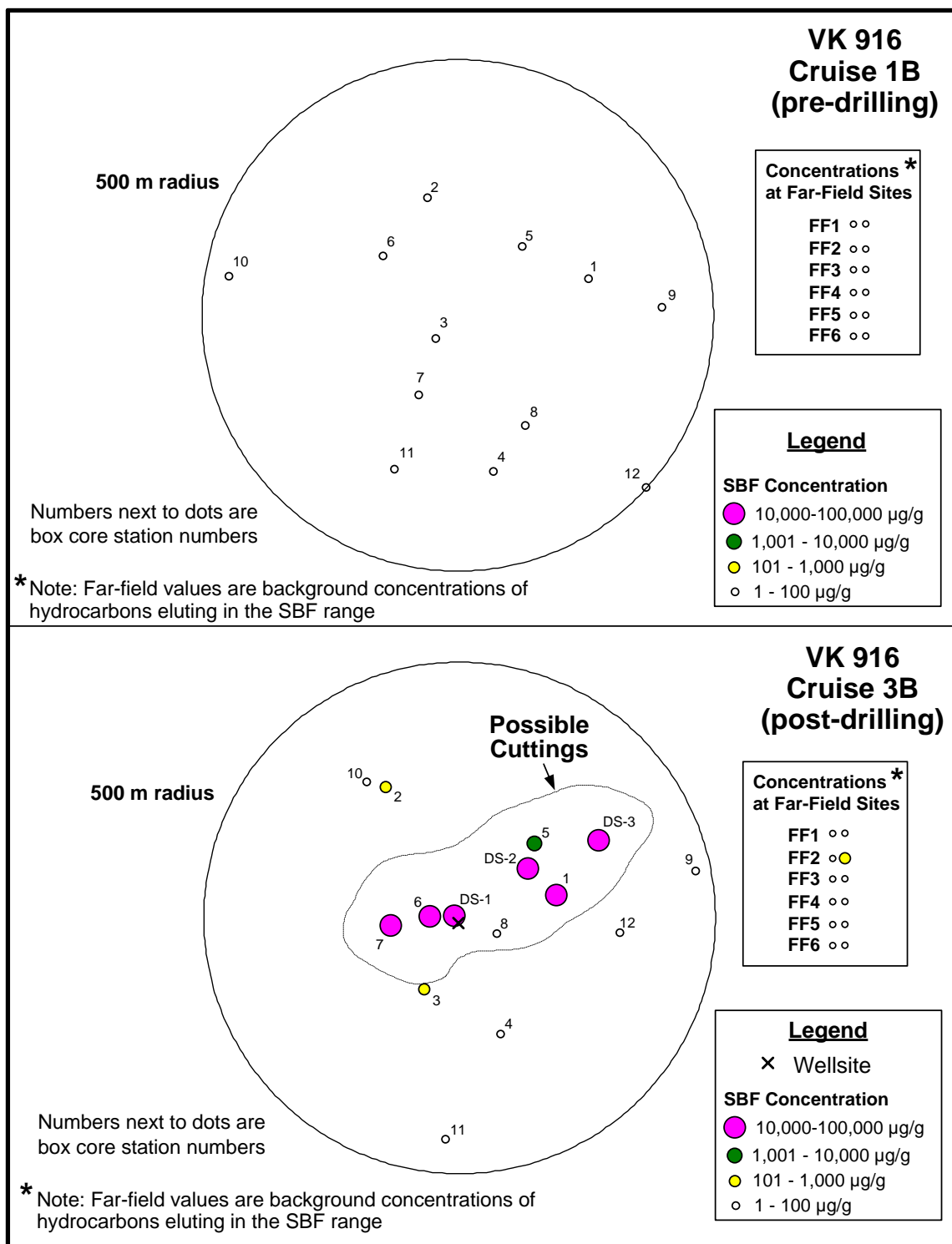


**Figure 9.3.** Spatial distribution of synthetic-based fluid (SBF) concentrations at Viosca Knoll (VK) Block 916 on Cruise 1B (pre-drilling) and Cruise 3B (post-drilling). The area of geophysically mapped cuttings is shown for the post-drilling cruise.

Sediment SBF concentrations in the three discretionary box core samples all displayed high concentrations (>10,000  $\mu\text{g/g}$ ) in the 0 to 2 cm section. SBF concentration decreased with depth in all three box cores. Sediment PAH concentrations in discretionary box cores generally decreased with depth, but all of the 0 to 2 cm sections could not be analyzed due to the high SBF concentrations.

### 9.3.2 Garden Banks Block 516 – Exploration/Development Site

Sediments from the near-field and far-field stations at the GB 516 location were sampled during Cruise 1B (October/November 2000) and Cruise 2B (July 2001). In addition to the box cores collected at both the near-field and far-field locations, three discretionary box cores were located in suspected cuttings depositional areas during Cruise 2B. These box cores were sampled in 2-cm intervals from 0 cm to 10 cm. The sediment SBF and total PAH concentrations are listed in **Tables 9.3** and **9.4**.

**Table 9.3.** Sediment synthetic based fluid (SBF) and total polycyclic aromatic hydrocarbon (PAH) concentrations at Garden Banks Block 516.

Sample	SBF ( $\mu\text{g/g}$ ) <sup>a</sup>		Total PAH (ng/g)	
	Cruise 1B Nov. 2000	Cruise 2B July 2001	Cruise 1B Nov. 2000	Cruise 2B July 2001
NF-B01	775	1,283	561	171
NF-B02	25,131	1,093	3,470	215
NF-B03	557	4,520	344	405
NF-B04	93.3	162	473	191
NF-B05	195	420	359	335
NF-B06	1,091	29,167	402	431
NF-B07	1,926	4,666	502	351
NF-B08	12.0	418	241	351
NF-B09	526	6,170	246	306
NF-B10	24.0	7.0	218	165
NF-B11	11.4	152	194	151
NF-B12	5.4	56.0	230	142
FF1-B01	9.4	3.0	224	193
FF1-B02	5.7	3.0	182	205
FF2-B01	3.6	4.0	227	162
FF2-B02	3.3	7.0	138	203
FF3-B01	6.1	4.0	242	199
FF3-B02	4.2	3.0	177	152
FF4-B01	3.6	3.0	444	203
FF4-B02	3.3	3.0	120	192
FF5-B01	2.0	5.0	115	175
FF5-B02	3.6	4.0	230	249
FF6-B01	3.4	4.0	174	217
FF6-B02	3.0	4.0	149	250

FF = far-field; NF = near-field.

<sup>a</sup> Far-field values represent background concentrations of hydrocarbons that coelute with SBFs.

**Table 9.4.** Synthetic based fluid (SBF) and total polycyclic aromatic hydrocarbon (PAH) sediment concentrations in the Garden Banks Block 516 discretionary box core samples from Cruise 2B (July 2001).

Sample	SBF ( $\mu\text{g/g}$ )	Total PAH ( $\text{ng/g}$ )
DS-B1 (0-2)	5,148	87.4
DS-B1 (2-4)	21,908	146
DS-B1 (4-6)	3,984	123
DS-B1 (6-8)	1,073	701
DS-B1 (8-10)	1,173	331
DS-B2 (0-2)	117,280	23,840
DS-B2 (2-4)	136,297	19,214
DS-B2 (4-6)	119,992	18,041
DS-B2 (6-8)	98,940	16,878
DS-B2 (8-10)	13,271	1,667
DS-B3 (0-2)	3,353	43.0
DS-B3 (2-4)	162	215
DS-B3 (4-6)	37	194
DS-B3 (6-8)	21	98.3
DS-B3 (8-10)	25	89.0

DS = discretionary sample.

SBF concentrations in Cruise 1B near-field sediments ranged from 5.4 to 25,131  $\mu\text{g/g}$  and in far-field sediments ranged from 2.0 to 9.4  $\mu\text{g/g}$ . SBF concentrations in Cruise 2B near-field sediments ranged from 7.0 to 29,167  $\mu\text{g/g}$  and in far-field sediments ranged from 3.0 to 7.0  $\mu\text{g/g}$ . Surface sediment SBF concentrations in the near-field and discretionary box core samples are displayed in **Figure 9.4**. Total PAH concentrations in the Cruise 1B near-field sediments ranged from 194 to 3,470  $\text{ng/g}$  and in far-field sediments ranged from 115 to 444  $\text{ng/g}$ . Total PAH concentrations in Cruise 2B near-field sediments ranged from 142 to 431  $\text{ng/g}$  and in far-field sediments ranged from 152 to 250  $\text{ng/g}$ .

Using the Tukey's HSD test, a significant difference was detected between the sediment SBF concentrations at near-field and far-field stations during both cruises. Near-field SBF concentrations were higher than far-field concentrations on both cruises. There was no significant difference between the sediment PAH concentrations at the near-field and far-field stations during both cruises.

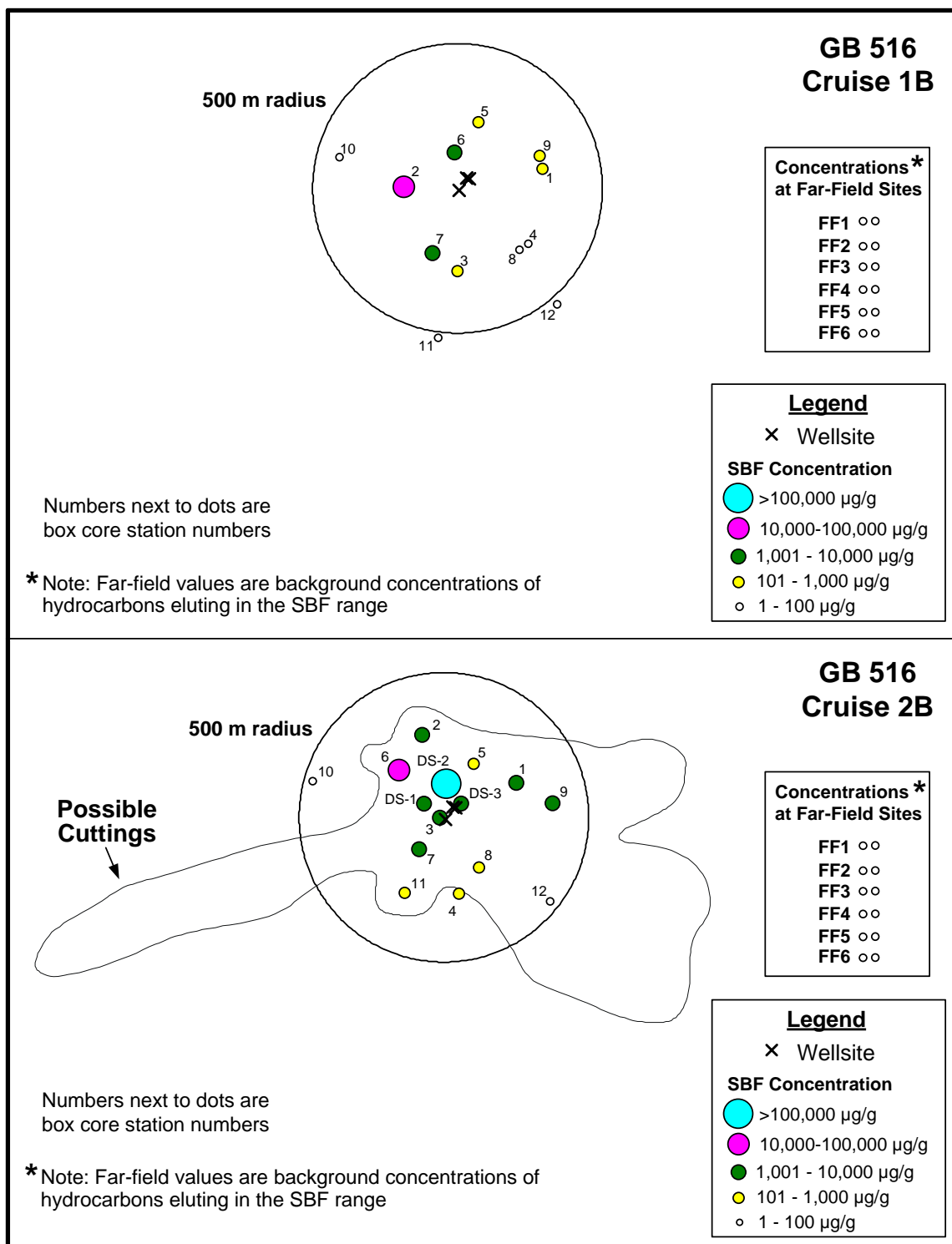


**Figure 9.4.** Spatial distribution of synthetic-based fluid (SBF) concentrations at Garden Banks (GB) Block 516 on Cruise 1B and Cruise 2B. Areas of geophysically mapped cuttings are shown for Cruise 2B (not available for Cruise 1B).

Sediment SBF concentrations in the three discretionary box core samples all displayed high concentrations (>3,000 µg/g) in the 0 to 2 cm section. SBF concentration generally decreased with depth in all three box cores, although two of the discretionary box cores had significant (>1,000 µg/g) SBF concentrations, even 10 cm. Sediment PAH concentrations in discretionary box cores generally decreased with increasing depth. Sediment PAH concentrations in DS-B2 had elevated levels ranging from 23,840 ng/g at 0 to 2 cm to 1,667 ng/g at 8 to 10 cm. The naphthalenes, biphenyl, and acenaphthene dominated the total PAH in these samples. The source of these PAHs is suggested to be from some other contaminant from the drilling activity, as SBF does not contain PAHs.

### 9.3.3 Garden Banks Block 602 – Post-Development Site

Sediments from the near-field and far-field sampling stations at the GB 602 location were sampled during Cruise 2B (July 2001). In addition to the box cores collected at both the near-field and far-field locations, three discretionary box cores were located in suspected cuttings depositional areas. These box cores were sampled in 2-cm intervals from 0 cm to 10 cm. The sediment SBF and total PAH concentrations are listed in **Tables 9.5** and **9.6**.

**Table 9.5.** Sediment synthetic based fluid (SBF) and total polycyclic aromatic hydrocarbon (PAH) concentrations at Garden Banks Block 602 on Cruise 2B (July 2001).

Sample	SBF (µg/g) <sup>a</sup>	Total PAH (ng/g)
NF-B01	462	132
NF-B02	585	495
NF-B03	8,446	552
NF-B04	1,978	256
NF-B05	4,339	208
NF-B06	3,263	499
NF-B07	1,954	245
NF-B08	13,792	539
NF-B09	1,430	170
NF-B10	1,351	405
NF-B11	2,027	219
NF-B12	985	189
FF1-B01	6.0	118
FF1-B02	5.0	127
FF2-B01	5.0	115
FF2-B02	4.0	152
FF3-B01	3.0	119
FF3-B02	4.0	93.8
FF4-B01	5.0	98.2
FF4-B02	8.0	119
FF5-B01	10.0	110
FF5-B02	6.0	143
FF6-B01	8.0	136
FF6-B02	5.0	128

FF = far-field; NF = near-field.

<sup>a</sup> Far-field values represent background concentrations of hydrocarbons that coelute with SBFs.

**Table 9.6.** Synthetic based fluid (SBF) and total polycyclic aromatic hydrocarbon (PAH) sediment concentrations in the Garden Banks Block 602 discretionary box core samples from Cruise 2B (July 2001).

Sample	SBF ( $\mu\text{g/g}$ )	Total PAH ( $\text{ng/g}$ )
DS-B1 (0-2)	10,572	582
DS-B1 (2-4)	8,798	653
DS-B1 (4-6)	3,742	436
DS-B1 (6-8)	1,293	150
DS-B1 (8-10)	291	136
DS-B2 (0-2)	3,749	436
DS-B2 (2-4)	2,706	357
DS-B2 (4-6)	764	220
DS-B2 (6-8)	62.0	123
DS-B2 (8-10)	24.0	134
DS-B3 (0-2)	930	358
DS-B3 (2-4)	532	221
DS-B3 (4-6)	37.0	123
DS-B3 (6-8)	11.0	136
DS-B3 (8-10)	12.0	135

DS = discretionary sample.

SBF concentrations in Cruise 2B near-field sediments ranged from 462 to 13,792  $\mu\text{g/g}$  and in far-field sediments ranged from 3.0 to 10.0  $\mu\text{g/g}$ . Surface sediment SBF concentrations in near-field and discretionary box core samples are displayed in **Figure 9.5**. Total PAH concentrations in Cruise 2B near-field sediments ranged from 132 to 552  $\text{ng/g}$  and in far-field sediments ranged from 93.8 to 152  $\text{ng/g}$ .

Using the Tukey's HSD test, a significant difference was detected between the sediment SBF concentrations in the Cruise 2B near-field and far-field stations (near-field concentrations were higher). There was no significant difference between the sediment PAH concentrations in Cruise 2B near-field and far-field stations.

Sediment SBF concentrations in the three discretionary box core samples all displayed high concentrations ( $>900 \mu\text{g/dry g}$ ) in the 0 to 2 cm section. SBF and PAH concentrations in discretionary box cores generally decreased with increasing depth.

**GB 602  
Cruise 2B**

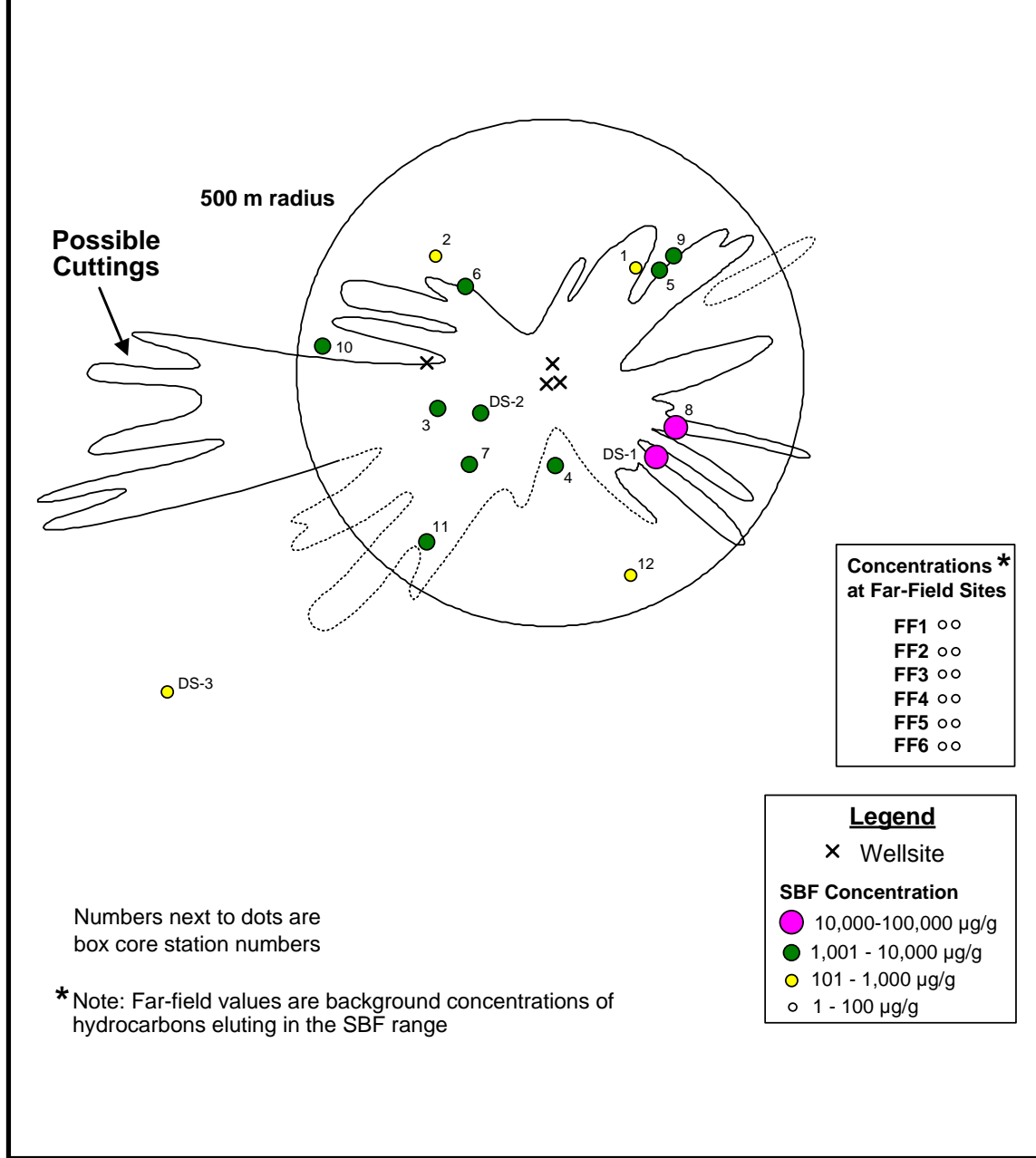


**Figure 9.5.** Spatial distribution of synthetic-based fluid (SBF) concentrations at Garden Banks (GB) Block 602 on Cruise 2B. Areas of geophysically mapped cuttings are shown.

### 9.3.4 Mississippi Canyon Block 292 – Post-Development Site

Sediments from the near-field and far-field sampling stations at the MC 292 location were sampled during Cruise 2B (July 2001). In addition to the box cores collected at both the near-field and far-field locations, three discretionary box cores were located in suspected cuttings depositional areas during Cruise 2B. These box cores were sampled in 2-cm intervals from 0 cm to 10 cm. The sediment SBF and total PAH concentrations are listed in **Tables 9.7** and **9.8**.

**Table 9.7.** Sediment synthetic based fluid (SBF) and total polycyclic aromatic hydrocarbon (PAH) concentrations at Mississippi Canyon Block 292 on Cruise 2B (July 2001).

Sample	SBF ( $\mu\text{g/g}$ ) <sup>a</sup>	Total PAH (ng/g)
NF-B01	2,408	563
NF-B02	782	200
NF-B03	86.1	297
NF-B04	<1.4	256
NF-B05	584	743
NF-B06	7.8	174
NF-B07	12.8	247
NF-B08	920	452
NF-B09	12.4	222
NF-B10	101	310
NF-B11	8.9	272
NF-B12	10.0	269
FF1-B01	6.0	395
FF1-B02	<1.4	748
FF2-B01	19.0	545
FF2-B02	<1.4	453
FF3-B01	8.0	305
FF3-B02	<1.4	279
FF4-B01	8.0	339
FF4-B02	<1.4	329
FF5-B01	6.0	249
FF5-B02	28.0	333
FF6-B01	<1.4	210
FF6-B02	<1.4	218

FF = far-field; NF = near-field.

<sup>a</sup> Far-field values represent background concentrations of hydrocarbons that coelute with SBFs.



**Table 9.8.** Synthetic based fluid (SBF) and total polycyclic aromatic hydrocarbon (PAH) sediment concentrations in the Mississippi Canyon Block 292 discretionary box core samples from Cruise 2B (July 2001).

Sample	SBF ( $\mu\text{g/g}$ )	Total PAH ( $\text{ng/g}$ )
DS-B1 (0-2)	59.1	302
DS-B1 (2-4)	76.0	521
DS-B1 (4-6)	18.0	280
DS-B1 (6-8)	10.0	233
DS-B1 (8-10)	9.0	210
DS-B2 (0-2)	714	552
DS-B2 (2-4)	60.0	329
DS-B2 (4-6)	16.0	203
DS-B2 (6-8)	14.0	155
DS-B2 (8-10)	9.0	94.0
DS-B3 (0-2)	618	524
DS-B3 (2-4)	103	398
DS-B3 (4-6)	33.0	285
DS-B3 (6-8)	15.0	140
DS-B3 (8-10)	12.0	130

DS = discretionary sample.

SBF concentrations in Cruise 2B near-field sediments ranged from  $<1.4$  to  $2,408 \mu\text{g/g}$  and in far-field sediments ranged from  $<1.4$  to  $19.0 \mu\text{g/g}$ . Surface sediment SBF concentrations in the near-field and discretionary box core samples are displayed in **Figure 9.6**. Total PAH concentrations in the Cruise 2B near-field sediments ranged from  $174$  to  $743 \text{ng/g}$  and in far-field sediments ranged from  $210$  to  $748 \text{ng/g}$ .

Using the Tukey's HSD test, a significant difference was detected between the sediment SBF concentrations in Cruise 2B near-field and far-field stations. No significant difference was detected between the sediment PAH concentrations in Cruise 2B near-field and far-field locations.

Sediment SBF concentrations in the two of three discretionary box core samples displayed elevated concentrations ( $>600 \mu\text{g/g}$ ) in the 0 to 2 cm section. The first discretionary box core samples displayed concentrations slightly above background ( $>50 \mu\text{g/g}$ ) in the 0 to 2 cm section. SBF and PAH concentrations in discretionary box cores generally decreased with increasing depth.

**MC 292  
Cruise 2B**

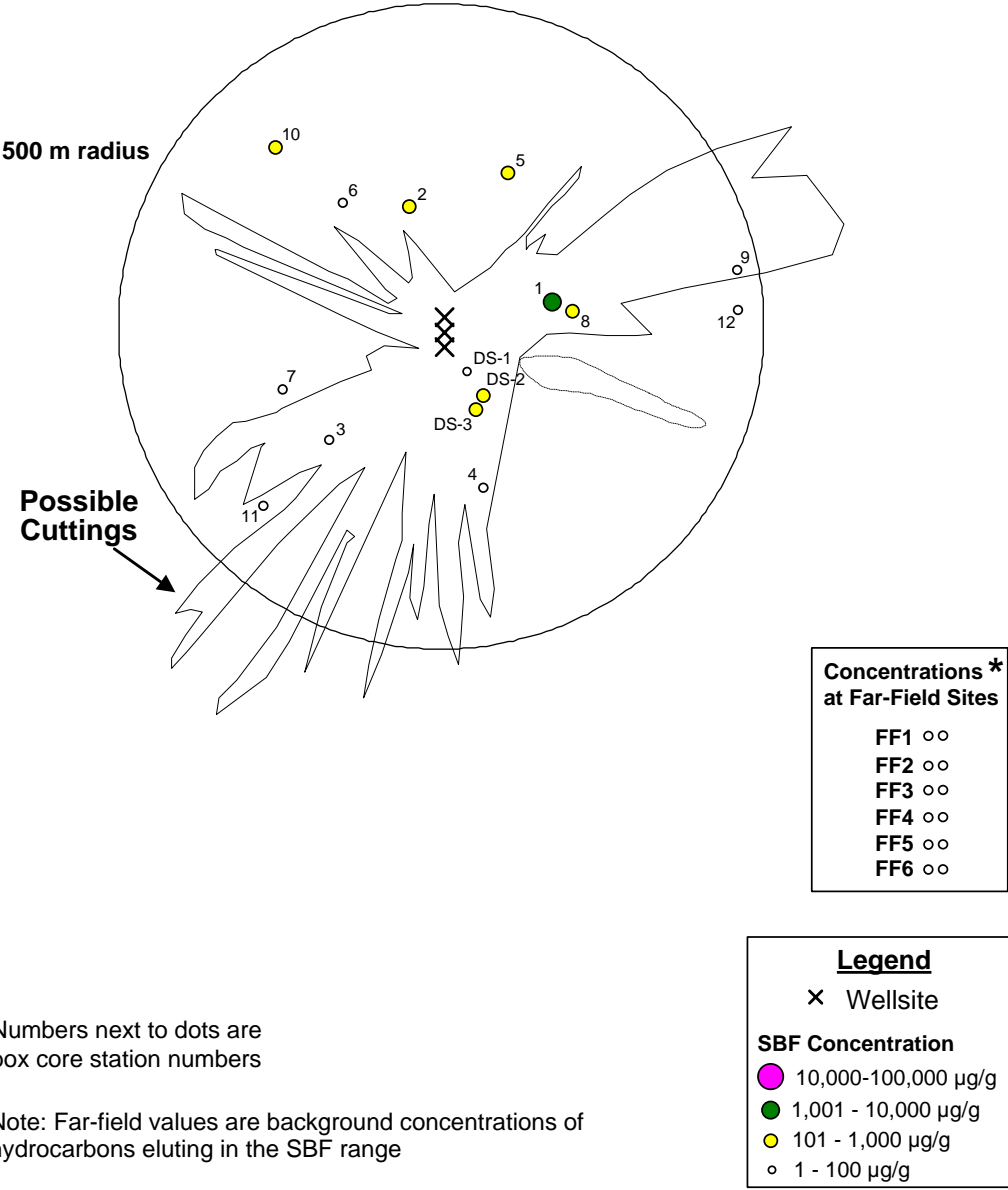


**Figure 9.6.** Spatial distribution of synthetic-based fluid (SBF) concentrations at Mississippi Canyon (MC) Block 292 on Cruise 2B. Areas of geophysically mapped cuttings are shown.

## 9.4 RESULTS – TISSUE SAMPLES

Two species of deepwater organisms, the isopod *Bathynomus giganteus* and the crab *Chaceon quinquedens*, were collected during the July 2001 (Cruise 2B) using traps located at both the near-field and far-field stations at two of the well locations (GB 602 and MC 292). Three organisms from each of the sampling locations were selected at random. The internal organs were removed, combined, and homogenized into one sample. Both species were analyzed for the presence of PAHs (Table 9.9).

**Table 9.9.** Summary of polycyclic aromatic hydrocarbons (PAH) in tissue samples from Garden Banks Block 602 (GB 602) and Mississippi Canyon Block 292 (MC 292).

Sample Location	Species	Total PAH (ng/g dry wt)
MC 292 NF Trap 1 (HC)	<i>Bathynomus giganteus</i>	86.8
MC 292 NF Trap 2 (HC)	<i>B. giganteus</i>	91.9
MC 292 FF3 (HC 1 of 2)	<i>B. giganteus</i>	416
MC 292 FF4 (HC 1 of 2)	<i>B. giganteus</i>	109
GB 602 NF Trap 1 (HC)	<i>B. giganteus</i>	132
GB 602 NF Trap 2 (HC)	<i>B. giganteus</i>	157
GB 602 FF5 (HC 1 of 2)	<i>B. giganteus</i>	131
GB 602 FF5 (HC 2 of 2)	<i>B. giganteus</i>	97.7
MC 292 NF Trap 1 (HC)	<i>Chaceon quinquedens</i>	136
MC 292 NF Trap 2 (HC 1 of 2)	<i>C. quinquedens</i>	38.6
MC 292 FF3 (HC 1 of 2)	<i>C. quinquedens</i>	108
MC 292 FF4 (HC 1 of 2)	<i>C. quinquedens</i>	107
GB 602 NF Trap 1 (HC)	<i>C. quinquedens</i>	176
GB 602 NF Trap 2 (HC)	<i>C. quinquedens</i>	94.9

FF = far-field; NF = near-field.

PAH body burden concentrations ranged from 38.6 to 416 ng/dry g. Using the student *t*-test, no significant difference was found between the total PAH body burden concentrations in the two deepwater organisms ( $\alpha= 0.05$ ). Additionally, no significant difference was found between the total PAH body burden concentrations at near-field and far-field stations ( $\alpha= 0.05$ ).

## 9.5 DISCUSSION

The lateral distribution and concentrations of SBFs in the deep-sea sediments during this study were the direct result of drilling activities. Drilling activities at each of the four locations have been summarized in *Chapter 3*. The lateral distribution and concentration of SBFs in the sediments were extremely heterogeneous. This patchy distribution of SBFs in marine sediments has been reported in other studies (Gallaway et al. 1997; McIlroy 1998; Terrens et al. 1998; Fechhelm et al. 1999). It has been suggested that the cuttings discharge depth, rate, and total mass of discharge, currents, and storm currents are the main determinants of the dimension of the cuttings accumulations near offshore platforms (Neff et al. 2000).

One way to assess the significance of the PAH contaminant load in sediments is to compare the concentrations measured in the near-field and far-field locations with previous MMS studies and the National Oceanic and Atmospheric Administration (NOAA) Status and Trends Mussel Watch Program (Brooks et al. 1989). Sediment PAH values detected at the four deepwater sites are similar to the concentrations that were detected in sediments collected during the Gulf of Mexico Offshore Operations Monitoring Experiment (GOOMEX) Study (Kennicutt et al. 1996a) and an American Petroleum Institute study (Brooks et al. 1989). The concentration ranges of the detected PAHs in the near-field and far-field locations were similar, suggesting that concentrations of PAHs in the sediments were not significantly increased due to drilling. However, there was a significant increase in the concentration of PAHs in the second discretionary box core from GB 516 during Cruise 2B. Also, some samples from VK 916 near-field locations on Cruise 3B could not be analyzed for PAHs due to the high concentrations of SBF in the sediments.

The total PAH body burden concentrations in the two test species of deepwater organisms, the isopod *Bathynomus giganteus* (152 ng/dry g  $\pm$  109 ng/dry g) and the crab *Chaceon quinquedens* (110 ng/dry g  $\pm$  45.5 ng/dry g) collected during Cruise 2B from the near-field and far-field sites in GB 602 and MC 292, were similar in concentration to other benthic samples collected during the GOOMEX Study (Kennicutt et al. 1996a). Even though the concentrations of the majority of the individual PAH analytes were at or below the MDL (see *Appendix H*), the presence of contaminants in the internal organs does represent exposure to mature hydrocarbons. The PAH contaminants detected in the internal organs of these two species are probably due to their intimate relationship with the sediments (e.g., sediment particles retained in the gut). No statistically significant differences between near-field and far-field tissue PAH concentrations were detected. Thus, there was no clear evidence of PAH bioaccumulation from drilling discharges. This issue is discussed further in *Chapter 16*.

## Chapter 10 Sediment Microbes

Paul A. LaRock  
School of the Coast and Environment  
Dept. of Oceanography and Coastal Sciences  
Louisiana State University

---

### 10.1 INTRODUCTION

The thrust of the current effort in this chapter was to determine the effects of oil drilling activities on sedimentary microbes using adenosine triphosphate (ATP) determinations as the primary analytical tool. ATP serves as a useful measure of bacterial colonization and survival in extreme or altered environments as it is directly tied to the physiological functioning of the community.

The nature and magnitude of the sedimentary bacterial community has been the subject of a number of studies. The initial approach to quantify sedimentary bacteria was to separate them from the sediment matrix and count the resultant cells using epifluorescent microscopy. A consensus developed that the size of the bacterial community was inversely proportional to sediment grain size (Dale 1974; DeFlaun and Mayer 1983; Yamamoto and Lopez 1985), and that it also varied directly with organic carbon. The reasoning for the increase in bacterial numbers with decreasing grain size was the greater availability of sediment surface area for colonization. Early experiments at sediment oxygen uptake indicated that more oxygen was consumed by small grain-size sediments than by coarser materials. However, the experiment was carried out by suspending less than a gram of material into 28-mL biochemical oxygen demand bottles and following oxygen loss (Hargrave 1972). This approach ignores *in situ* conditions and the fact that very fine materials may have more interstitial (pore) space, but the pores are so small that flow into the sediments is greatly inhibited, thus limiting the introduction of nutrients and oxygen into the sediment matrix (Maier et al. 2000). The work of Yamamoto and Lopez (1985) revealed that increased surface was only one aspect of microbial colonization and recognized that the size and shape of sediment particles affect sediment packing. Larger more sorted particles, as found in sand, would actually make nutrients more available to the sedimentary bacterial community. Both DeFlaun and Mayer (1983) and Yamamoto and Lopez (1985) noted that clays were a poor substrate for bacterial attachment.

Biochemical approaches were subsequently employed to probe the microbial activities in sediments. One such example was the fine work of Koster and Meyer-Reil (2001), who experimented with shallow coastal sediments whose compositions varied from sand to sand-mud mixtures. Measurements of phospholipid, chlorophyll a, and ATP were made to assess structural components, photosynthetic producers, and physiologically active biomass, respectively. Parallel determinations of total carbon (C) and nitrogen (N) were carried out to assess the relative availability of nutrient resources based on the notion that sediments with low C:N ratios indicated the presence of easily available dissolved organic carbon (DOC), or new material, whereas high C:N ratios indicated the presence of resilient compounds. Their results indicated that in sandy sediments, both the phospholipid and ATP were high, but as the sediments became progressively more muddy (finer grain size), the phospholipid became the dominant biomarker (accumulated),

but ATP decreased significantly. Similarly, the carbon analysis revealed that available DOC was a large fraction (about 25%) of the total organic pool in the sandy sediments, but as the sediment mud content increased, the available DOC fraction became an absolute minor component of the carbon pool. In sum, Koster and Meyer-Reil (2001) found that as sediment grain size decreased, available carbon resources were diminished, and that compounds that are microbial structural components accumulated, but the community itself was less physiologically active.

The ATP assay offers considerable advantage over conventional microbiological methods when assessing the effect of the environment on microbial communities because it is non-cultural, avoids the issue of nutrient limitations, and reflects the *in situ* properties of the community. ATP is present in physiologically active cells and thus offers a means of assessing the relationship between the microbial community and the suitability of the prevailing habitat. Environmental ATP determinations can, therefore, provide quantification of the effects of toxicants, nutrient enrichment, or other alteration of the environment. A few of the more recent applications of ATP technology have been to examine issues in marine ecology (Karl 1986; Karl 1993; Bjorkman and Karl 2001), study the effects of nutrient loading in coastal waters (Malin et al. 2001), quantify hydrothermal communities (Atkinson et al. 2000), assess river water and sediment quality (Dutka et al. 1991), follow the toxic effects of zinc released from trout farms (Martinez-Tabche et al. 2000), determine the toxicity of pollutants on wastewater treatment (Dalzell and Christofi 2002; Dalzell et al. 2002), and assess the effects of wastewater-borne heavy metals in mangroves (Yim and Tam 1999).

As the ATP assay became more widespread, it became evident that there were substances that resulted in a loss of ATP during extraction and that we needed to compensate for the loss. It was shown that suspended material in water samples, for example, was capable of reducing ATP quantification by either affecting the extraction efficiency or by inhibiting the luciferin-luciferase reaction (Lee et al. 1971; Sutcliffe and Orr 1976). Sutcliffe and Orr (1976) found that high levels of suspended particles reduced the yield of ATP by as much as 50% to 66% of that known to be in the sample.

The nature of the ATP extractant also plays a role in the overall efficacy of the determination. Bancroft et al. (1976) suggested that extractant interactions with the individual sample must be considered, especially when using an acid as this promotes the mobilization of otherwise insoluble ions. This brings up the second type of difficulty encountered with the ATP assay, that of ionic interference. To address this issue, ethylenediaminetetraacetic acid (EDTA) was initially used to complex cations (Karl and LaRock 1976), but Bancroft et al. (1976) indicated that EDTA addition was a time-consuming step that lost an additional 25% of the sample ATP, and consequently it is no longer used. Along these lines, Cunningham and Wetzel (1978) found that samples that were acid-extracted had a problem with fulvic acids, which accounted for a loss of 70% to 80% of the sample ATP. These acid-soluble organic compounds sequester and bound charged species including ATP, and in the case of fulvic acids, the inhibitory effect was not reversible. The preceding discussion serves to illustrate the importance of establishing a protocol that incorporates ATP standards that allow correction for all the potential losses encountered along the way. An obvious mechanism is to prepare replicate samples that contain a known ATP standard and note the efficiency of recovery. This necessitates multiple samples and perhaps a range of ATP standards in order to cover all possibilities (Koster and Meyer-Reil 2001). The use

of a radioactive ATP standard circumvents the need for duplicates, as will be demonstrated later in this chapter.

The work we now report used ATP determinations as the primary analytical tool. Given the work schedule, the number of samples to be processed, the chemical nature of the material, and the very fine muds encountered, it became necessary to refine the ATP assay protocol and assess the effects of sediment grain size on ATP recovery. Efforts were made to assess the turnover of <sup>14</sup>C-labeled substrates, but the anoxic nature of the sediments prevented us from doing so given the current methodology. Efforts also were made to extract and polymerase chain reaction (PCR) amplify sediment deoxyribonucleic acid (DNA) to determine whether there were differences between the pre-drilling and post-drilling materials, but unidentified inhibitory compounds in all of the post-drilling samples apparently blocked amplification, although the pre-drilling sediments were successfully extracted and amplified.

## 10.2 MATERIALS AND METHODS

As discussed in *Chapter 2*, sites were established at a depth of approximately 1,000 to 1,150 m in VK 916, GB 516, GB 602, and MC 292, off the Louisiana coast. VK 916 was an exploration site that was sampled before and after drilling of a single exploration well. GB 516 was an exploration/development site that was sampled once after exploration drilling and again after several development wells were drilled. The other two locations (GB 602 and MC 292) were post-development sites that were sampled only once, after several exploration and development wells had been drilled. The sampling strategy was to take 12 box cores in the immediate vicinity of where drilling had been or would be taking place, termed the near-field sites, and 2 box cores each at six far-field sites at least 10 km distant from the near-field site. Near-field samples are identified by the location and station number – for example, VK 916 NF-B01 through NF-B 12. Far-field stations are identified by the far-field site number (1 through 6), and box core number (01 or 02) – for example, VK 916 FF1-B01 and FF1-B02. Maps of the near-field and far-field sample locations are presented in *Chapter 2*. Numbers of microbial samples analyzed are summarized in **Table 10.1**.

**Table 10.1.** Numbers of microbial subsamples collected from box cores.

Cruise and Site	Near-Field		Far-Field				
	NF	FF1	FF2	FF3	FF4	FF5	FF6
Cruise 1B							
GB 516	11	2	2	2	2	2	2
VK 916	12	-- <sup>a</sup>	2	2	2	1	2
Cruise 2B							
GB 516	12	2	2	2	2	2	2
GB 602	10	2	2	2	2	2	2
MC 292	12	1	2	2	2	2	2
Cruise 3B							
VK 916	12	2	2	2	2	2	2

FF = far-field; NF = near-field; GB = Garden Banks; MC = Mississippi Canyon; VK = Viosca Knoll.

<sup>a</sup> No box cores collected.

### 10.2.1 ATP Assay

Conceptually, the ATP assay can be divided into two components, the initial extraction and the subsequent laboratory assay of the ATP using the luciferin-luciferase reaction. ATP was extracted using 0.6 or 1.25N sulfuric acid as previously described (Karl and LaRock 1976) since phosphoric acid resulted in a copious precipitate. The major alteration in the technique was separate corrections for adsorptive loss encountered during sediment extraction and subsequent interference during the assay procedure.

As described in *Chapter 2*, a 0.25-m<sup>2</sup> box core was used to obtain sediment from the seafloor. A sample for microbial analyses was obtained from a subcore in each box core. The top 2 cm of sediment were collected, for a total volume of 60 cc, which was then quickly stirred and subsampled using syringe corers. Two cc of sediment were added to each of four centrifuge tubes (15 x 100 mm) and 5 mL of 0.6N sulfuric acid and 0.1 mL of <sup>14</sup>C-ATP (total activity 10,000 dpm, NEC-417 or equivalent, New England Nuclear/Perkin-Elmer, Boston, MA). The mixtures were vortexed for 5 min, centrifuged in a clinical centrifuge until settled (generally 15 min), and 4 mL withdrawn to be adjusted to pH 7.8 with a graded series of sodium hydroxide solutions. The volume was then brought up to 7.0 mL with TRIZMA 7.8 (Sigma-Aldrich Chemical Co., St. Louis, MO), and the extract was frozen for subsequent laboratory analysis. The addition of a radioactive ATP internal standard allowed every sample to be corrected for adsorptive losses, which was a critical concern when working with very fine-grained sediments.

The ATP was measured by adding 1 mL of the extract to a 22-mL scintillation vial along with 0.5 mL TRIZMA 7.8 buffer to which 200 µl of luciferin-luciferase mixture (FL-AAM ATP kit, Sigma-Aldrich Chemical Co., St. Louis, MO) was injected. After a 30-second delay, the emitted light was detected using a Turner 20e Luminometer (Turner Industries Inc., Sunnyvale, CA) and the ATP determined relative to standards run with each enzyme preparation. Substances interfering with the assay were corrected for by recounting each sample and substituting a 10 to 50 ng ATP standard in 0.5 mL of TRIZMA for the plain TRIZMA used in the initial count. Adsorptive loss was corrected by determining the <sup>14</sup>C-ATP recovered in the extract relative to that which was added. In all calculations, careful attention was paid to all the dilution factors used in the various steps of the process.

The use of ATP is a powerful means of determining factors affecting microbial biomass. There are, however, corrections that must be applied to overcome inaccuracies that are associated with both the extraction of the ATP from the sediments and its subsequent assay by the luciferin-luciferase method. One approach to correct for these interferences is to add an internal standard to a second set of replicates and determine the recovery after subtracting the actual sample ATP from the sample plus standard mixture. This approach essentially doubles the workload, and the ultimate accuracy of the correction depends upon the number of replicates used. For this reason, we decided it would be better to differentiate between the adsorptive loss in the extraction process and the interference encountered during the actual ATP assay itself.

The approach we used to determine adsorptive loss was to add radioactive ATP, either <sup>14</sup>C or <sup>3</sup>H labeled, to every sample and calculate an extraction efficiency as the difference between the added and recovered radiolabeled standard. The use of a radiolabeled material allows every



sample to be treated, is the more sensitive approach, and does not add measurable ATP to the sample. To demonstrate the efficacy of this approach, we conducted a series of experiments in which a stable internal ATP standard was added to one set of samples (done in triplicate) and  $^{14}\text{C}$ -ATP to a second set of samples (also done in triplicate), and the recovery of each standard was determined. The results of this experiment are shown in **Figure 10.1** and reveal close agreement between the two approaches ( $r^2 = 0.82$ ). However, the stable ATP standard has a recovery that is only about 80% of that determined by the use of the radioisotope. We attribute the difference to the increased sensitivity of the radioassay and the fact that isotope detection is not affected by potential ionic interference as might be encountered when assaying the stable internal ATP standard.

As may be noticed in **Figure 10.1**, the recovery of the extracted ATP varied from 10% to 100%. The principal factor affecting ATP loss in the extraction process is sediment grain size, with the finer materials being more adsorptive relative to the coarser sands. To illustrate the point, we compared the ATP extraction efficiency (determined with a radioactive standard) to sediment grain-size ratio. The results are seen in **Figure 10.2** and demonstrate that as the proportion of fines increases (i.e., the grain size decreases), the ATP extraction efficiency decreases.

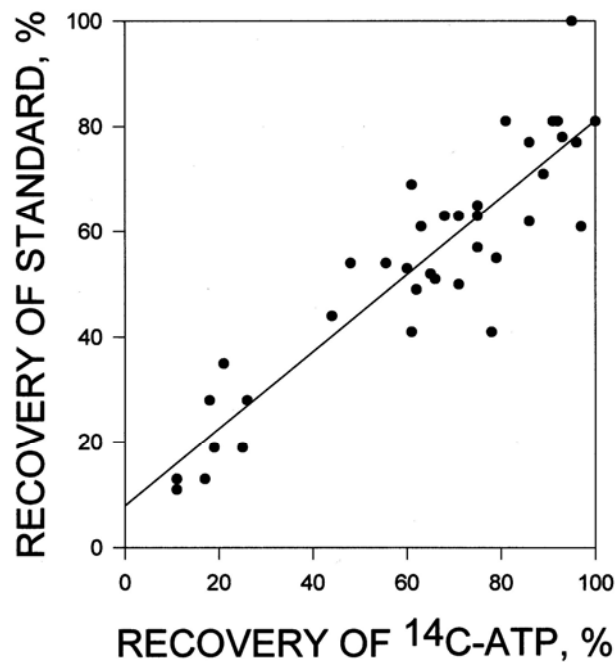


**Figure 10.1.** A comparison between the recovery of a stable internal adenosine triphosphate (ATP) standard to the recovery of the  $^{14}\text{C}$  ATP adsorption standard.

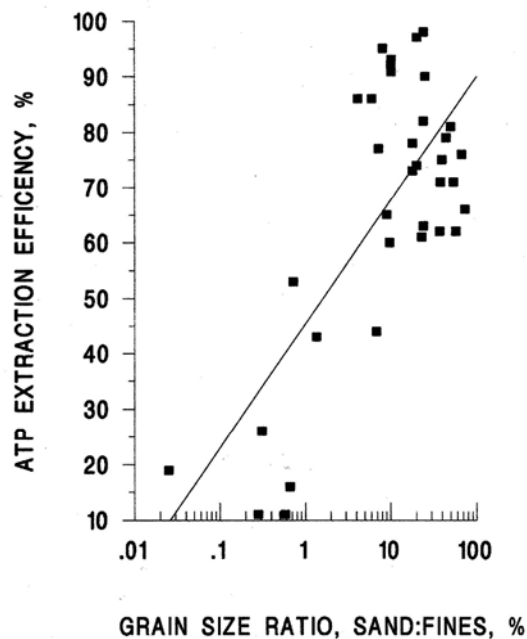


**Figure 10.2.** The effect of sediment grain size on the recovery of the  $^{14}\text{C}$  ATP extraction standard. Note that as the sediment grain size decreases, adsorption of the extracted ATP becomes significant, reducing the efficiency of extraction to as little as 10%.

As discussed in *Chapter 5*, sediments from the study sites were predominantly clay with a mean sedimentary particle diameter ranging from about 1 to 3  $\mu\text{m}$ . Over 80% of the sediment consisted of components smaller than 10  $\mu\text{m}$ ; thus, we were dealing with materials that are very fine-grained and impermeable (Maier et al. 2000).

### 10.2.2 Microbial Respiration

The method used for microbial respiration was essentially that of Deming (1993), except that pressurization was not required and that aspect of the protocol was omitted and the experiments were carried out as time series. For each box core retrieved, approximately 60 cc of sediment were collected, homogenized, and 2 cc added via a syringe corer to 10, 50-mL serum bottles, followed by 10 mL of filtered seawater to form a slurry. Formaldehyde at a final concentration of 2% was added to two of the bottles to serve as a poisoned control. The remaining eight bottles were incubated at *in situ* temperature (6°C), with duplicates being sacrificed after 30, 60, 90, and 120 minutes of incubation, and the respired  $^{14}\text{CO}_2$  collected and counted by liquid scintillation counting. Three different  $^{14}\text{C}$ -labeled compounds were used, glutamic acid (NEC 290), acetic acid (NEC 553), and glucose (NEC 042). Acetic acid was used for all samples, while the glutamic acid was used on Cruises 1B and 2B and glucose on Cruise 3B to provide assurance that the results obtained were not substrate-specific.

### 10.2.3 Sediment DNA Extraction, Quantification, and Amplification

A variety of methods were used to extract DNA from the sediments that was suitable for PCR amplification (Atlas 1993; Steffan et al. 1988; Tsai and Rochelle 2001). Extracted DNA was quantified fluorometrically using ethidium bromide as described by van Lancker and Gheysens (1986). The presence of interfering organic substances was assessed by changes in the spectrophotometric absorption of DNA over a range of 250 to 700 nm (Chen et al. 1977; Edzwald et al. 1985).

### 10.2.4 Toxicity Bioassay

A bioluminescent assay (Lumitox<sup>®</sup>) using the dinoflagellate *Pyrocystis lunula* was used to test the relative inhibitory effects of sediment extracts. A detailed methodology for the luminescent assay may be found in American Society for Testing and Materials (ASTM) Protocol E 1924, and the procedure as reported here was performed by the Lumitox Co., Slidell, LA, which developed the technique. In this particular instance, a 10-g aliquot of the desired sediment sample was weighed and diluted to a final volume of 50 mL with artificial seawater, continuously shaken for 75 minutes, and then allowed to settle. Five mL of the cleared suspension was put in a 20-mL scintillation vial, and 50 µl of this suspension was used to challenge 300 *P. lunula* suspended in 3 mL of artificial seawater contained in a 20-mL LSC vial. Pentuplicates were prepared for each sediment and control sample assayed. Each set of vials was incubated in darkness for 4 hours and then monitored for light output in a luminometer especially designed for the purpose. Negative controls consisted of a *P. lunula* suspension without any added substances (i.e., an uninhibited cell suspension). Positive controls consisted of *P. lunula* suspensions to which two different concentrations of sodium dodecyl sulfate (SDS) were added. The relative inhibitory effect of the SDS and the sediment extracts was assessed by a reduction in the light output of *P. lunula*. A total of 24 separate sediment samples was tested and was chosen such that there were two near-field and two far-field samples for both the pre-drilling and post-drilling samplings at GB 516 and VK 916. For GB 602 and MC 292, only post-drilling materials were available, and two near-field and two far-field samples were used.

## 10.3 RESULTS<sup>1</sup>

### 10.3.1 ATP Analysis

The ATP results for all stations and cruises are summarized in **Table 10.2**, and although there are some hot spots, they show that for all the post-drilling conditions, the ATP ranges between 2 to 5 ng g<sup>-1</sup>.

A comparison of the pre- and post-drilling ATP values at GB 516 and VK 916, on the average, show a marked decrease of about 5- to 15-fold after drilling. At GB 516, the average ATP concentration on Cruise 1B was 44.2 ng g<sup>-1</sup> for the near-field site and 43 ng g<sup>-1</sup> for the far-field sites. The Cruise 2B averages were 4.3 ng g<sup>-1</sup> for the near-field site and 2.5 ng g<sup>-1</sup> for the far-field sites. At VK 916, the average pre-drilling ATP concentration was 32 ng g<sup>-1</sup> for the near-field site

---

<sup>1</sup> Editor's note: In this chapter, the author classifies Cruise 1B data from GB 516 as "pre-drilling" because of subsequent development drilling there. Elsewhere in this report these samples are classified as post-drilling due to two previous exploratory wells (see *Chapter 3*). See *Chapter 15* for an alternate interpretation of these data.

and 36 ng g<sup>-1</sup> for the far-field sites. The post-drilling averages for VK-916 near-field (7.7 ng g<sup>-1</sup>) and far-field (7.1 ng g<sup>-1</sup>) indicate a five-fold reduction in the microbial ATP biomass, although it should be noted that again there is spatial heterogeneity in the data. The difference between the pre-drilling and post-drilling ATP concentrations is statistically significant (p<0.0001 for GB 516 and p<0.0002 for VK 916). Statistically, there was no significant difference between the near-field and far-field ATP levels for either GB 516 or VK 916 (p<0.137 for GB 516 and p<0.157 for VK 916) or for GB 602 and MC 292 (p<0.083). Simply stated, the far-field stations did not serve as true, unaffected controls of the drilling operation and thus the similar effect on ATP levels in both near-field and far-field locations cannot be attributed solely to drilling.

**Table 10.2.** Sediment adenosine triphosphate (ATP) concentrations (ng g<sup>-1</sup> dry wt) for all near-field and far-field sites.

Site	Sample <sup>a</sup>	GB 516		VK 916		GB 602	MC 292
		Cruise 1B	Cruise 2B	Cruise 1B	Cruise 3B	Cruise 2B	Cruise 2B
NF	B01	288.3	2.1	47.5	<1.7 <sup>b</sup>	--	4.5
	B02	418.2	0.6	42.1	<1.3 <sup>b</sup>	3.4	1.2
	B03	13.1	7.9	30.2	<1.8 <sup>b</sup>	3.3	1.4
	B04	27.9	0.5	34.5	<1.8 <sup>b</sup>	2.3	0.9
	B05	26.4	1.1	29.3	15.3	14.1	4.4
	B06	--	11.9	48.3	25.6	4.7	4.4
	B07	33.5	4.4	30.1	41.5	2.3	1.1
	B08	104.1	1.5	21.9	<0.3 <sup>b</sup>	17.6	5.4
	B09	39.2	9.6	25.1	1.1	2.7	1
	B10	29.2	0.7	23.3	1.3	15.2	1.6
	B11	56.3	5.1	23.4	<1.5 <sup>b</sup>	16.2	5.5
	B12	68.7	6.8	29.1	1.1	--	1.7
FF1	B01	28.7	5.5	--	61.1	2.1	2.9
	B02	43.4	5.8	--	1.1	1.1	--
FF2	B01	102.4	2.3	57.9	1.3	1.7	2.5
	B02	25.3	2.8	61.4	1.1	1.9	66.6
FF3	B01	92.3	0.5	34.2	2.7	3.6	1.7
	B02	35.3	3.1	29.6	<1.5 <sup>b</sup>	2.4	2.8
FF4	B01	29.1	5.4	19.7	2.7	1.1	2.1
	B02	38.1	1.1	28.4	2.3	2.2	0.7
FF5	B01	64.4	0.5	24.5	2.3	3.2	1.1
	B02	14.2	0.6	--	2.7	216.3	2.2
FF6	B01	29.3	1.4	36.4	0.9	2.6	1.5
	B02	16.7	0.8	32.1	5.6	2.7	1

<sup>a</sup> Sample locations were randomly selected on each cruise; therefore, the samples collected on two cruises at GB 516 and VK 916 are not paired samples from the same location.

<sup>b</sup> A < symbol indicates that interference reduced the sensitivity of the assay to the value indicated; thus, ATP may be present at a lower concentration but be undetectable.

GB = Garden Banks; MC = Mississippi Canyon; VK = Viosca Knoll.

These findings are shown more clearly in **Figure 10.3**, noting that the graphs are plotted logarithmically. Based on previous data from the eastern Gulf of Mexico, we might expect reasonable sedimentary ATP values at GB 516 and VK 916 (pre-drilling) of 30 to 40 ng g<sup>-1</sup> at a mean grain size of 2 to 3 μm, provided that sediment grain size was the controlling factor. Our measured ATP results are in good agreement with the projected values based on grain-size criteria for GB 516 and VK 916 pre-drilling conditions, but the post-drilling results are significantly lower.

There are three possibilities that may explain the reduction in ATP levels as a result of drilling: 1) the addition of drill cuttings simply overlays the existing sediments, creating a new and uncolonized environment; 2) the new material may contain some inhibitory compound; and 3) a combination of the above two events. One approach to sort out the possibilities is to compare the DNA content of the pre- and post-drilling samples using ethidium bromide (van Lancker and Gheysens 1986). The DNA in the post-drilling materials is about one-fifth that found in the pre-drilling materials, but that only partially accounts for the 10- to 15-fold reduction in ATP.

### 10.3.2 Toxicity Bioassay

A toxicity bioassay was performed that measured the relative changes in light output of the dinoflagellate *P. lunula* as it was exposed to extracts made from the various pre- and post-drilling sediments. The addition of SDS, either 10 or 20 μl (labeled X2 in the figures), was used as a positive control to elicit a measurable response that can be compared to the negative control (*P. lunula* with no additives). The results obtained for VK 916 are shown in **Figure 10.4** and indicate that all of the pre-drilling materials yielded the same response as the unamended *P. lunula* control, but the post-drilling samples exhibited some inhibition, with the near-field sediments being more inhibitory than the far-field sediments. Bear in mind that the design of these tests was only to indicate the relative effects of the various sediments, and that only a small aliquot of the extract was used, which may not indicate the full inhibitory potential of the materials.

The results for GB 516 (**Figure 10.5**) essentially paralleled those obtained for VK 916; namely, the post-drilling samples were inhibitory with the near-field materials exerting a stronger effect than the far-field samples did. Tests on GB 602 (**Figure 10.6a**) post-drilling sediments showed some inhibition in the bioassay, but the results for MC 292 (**Figure 10.6b**) indicated no inhibition whatsoever, which may reflect different drilling parameters or perhaps different environmental conditions affected by the proximity of the Mississippi River.

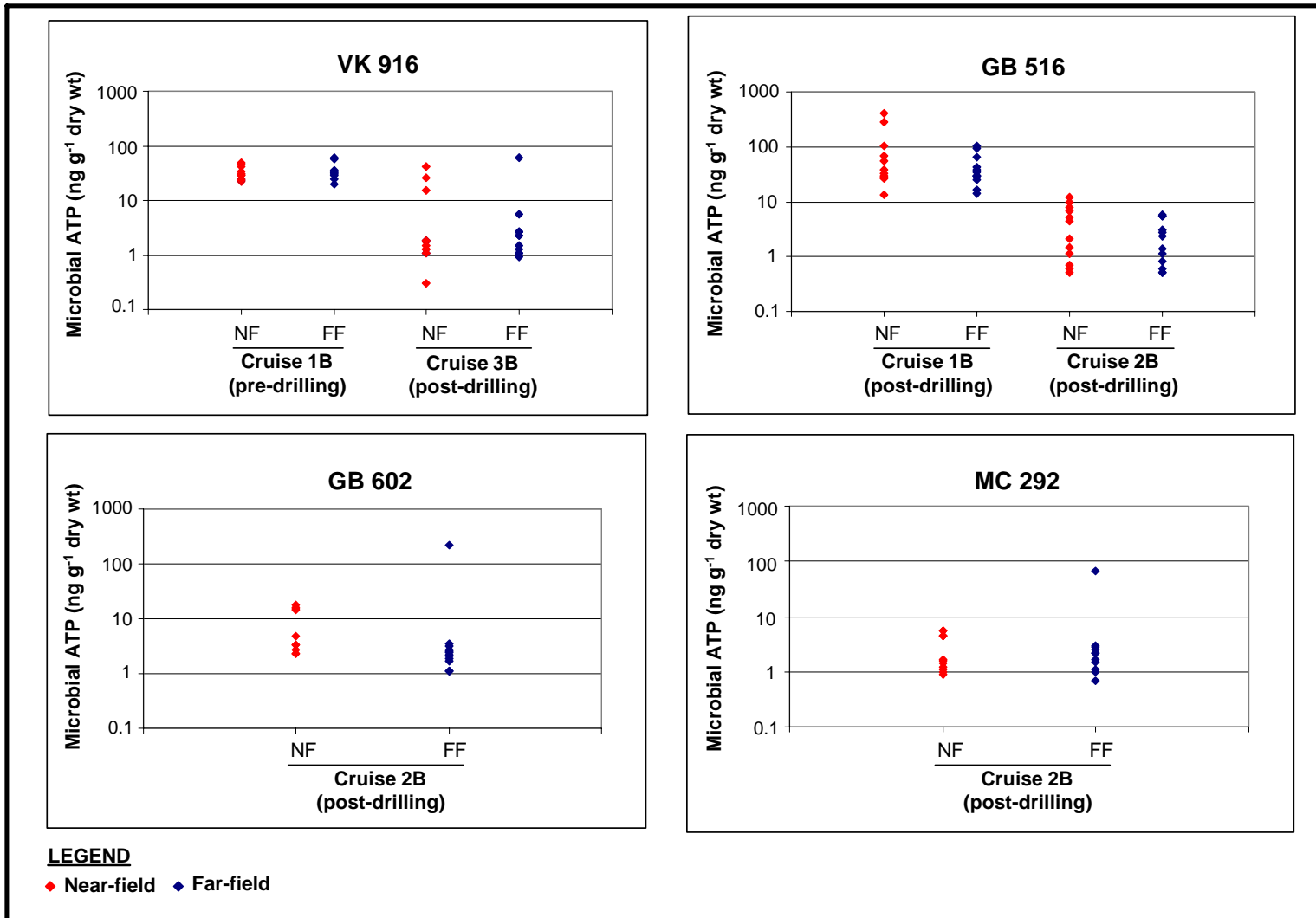


**Figure 10.3.** Microbial adenosine triphosphate (ATP) concentrations at the four study sites. Note the log scale.

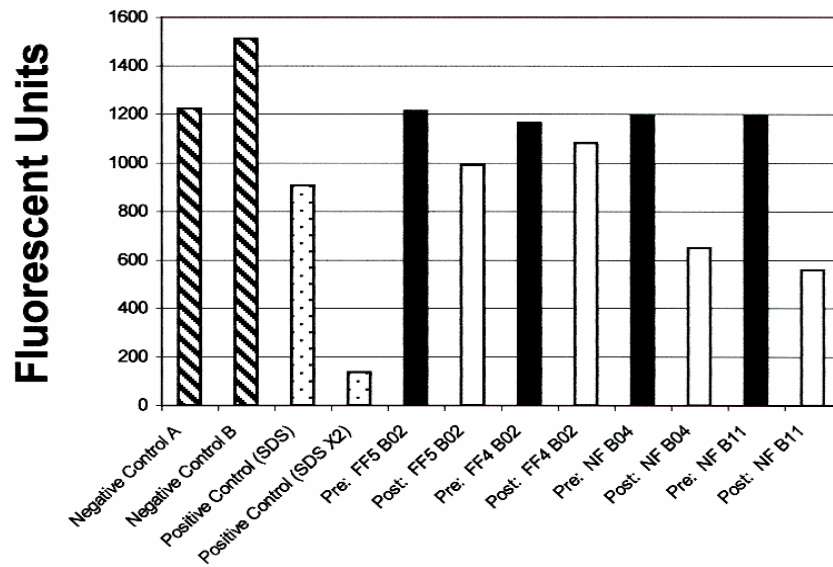


**Figure 10.4.** The relative toxicity of sediment extracts for selected sampling sites at VK 916 before and after drilling. The cross-hatched bars indicate the light output of *P. lunula* alone, the stipled bars are *P. lunula* with two different concentrations of SDS added, the black bars are *P. lunula* plus the pre-drilling sediment extract, and the white bars are *P. lunula* plus the post-drilling extract.

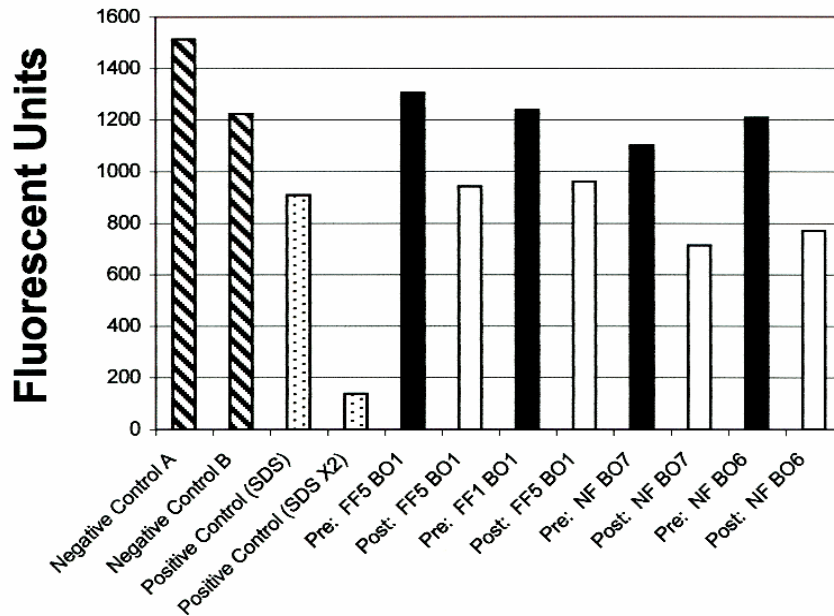


**Figure 10.5.** The relative toxicity of sediment extracts for selected sampling sites at GB 516 before and after drilling. Symbols are the same as in **Figure 10.4**.

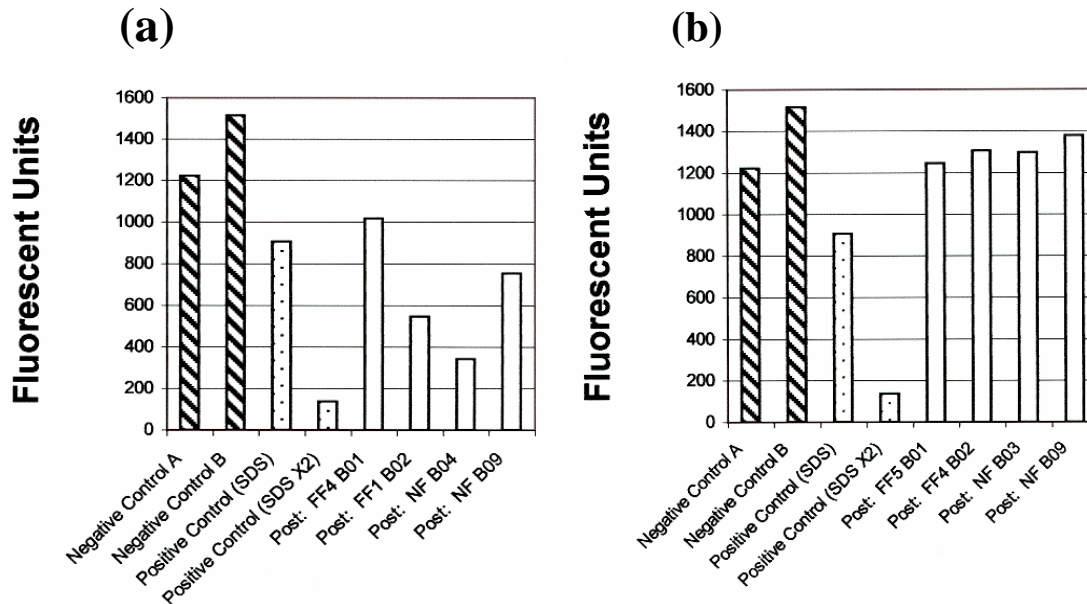


**Figure 10.6.** The relative toxicity of sediment extracts for selected sampling sites at a) GB 602 and b) MC 292. Symbols are the same as in **Figure 10.4**, except that there were no pre-drilling samples.

### 10.3.3 DNA Assay

Efforts were made to PCR amplify the extracted sedimentary DNA to look at changes in bacterial community structure that might have resulted from drilling. A variety of methods were used, beginning with the established protocols to secure DNA that could be used for PCR, which worked on the pre-drilling samples but failed on all the post-drilling samples. Attempts were made by three different laboratories to obtain clean DNA on the post-drilling materials, but all were without success. The extracts did contain DNA as determined by ethidium bromide, but some inhibiting compounds were collected as well as DNA. Drilling fluids are known to contain organic compounds, and high levels of some metals (see *Chapter 8*), both of which are known to interfere with PCR. Efforts to eliminate these potential sources of interference used Sepharose 4B for organics (Jackson et al. 1997) and Chelex 100 (Walsh et al. 1991) for the removal of metals, as well as specialized clean-up kits, and none had a positive effect.

### 10.3.4 Respiration

Efforts also were made to assess the heterotrophic activity of the sedimentary microflora by measuring the respiration of  $^{14}\text{C}$ -labeled compounds by capturing the resultant  $^{14}\text{CO}_2$  produced. The method entails making a sediment-water slurry, incubating at *in situ* temperatures, and sacrificing samples over a given time period. A total of 72 separate samples was challenged in the heterotrophic activity assay, and all yielded negative respiratory curves as seen in **Figure 10.7**, regardless of whether the labeled substrate was acetate, glutamate, or glucose. The process is carried out in a normal laboratory setting (i.e., in air), which would shut down anaerobic bacteria or those facultative organisms functioning as anaerobes, and consequently, the utilization of substrate would diminish as the redox conditions of the experiment became more



positive with time. An interesting implication of these observations is that the sediments in the areas tested are essentially anoxic with respect to the microflora.

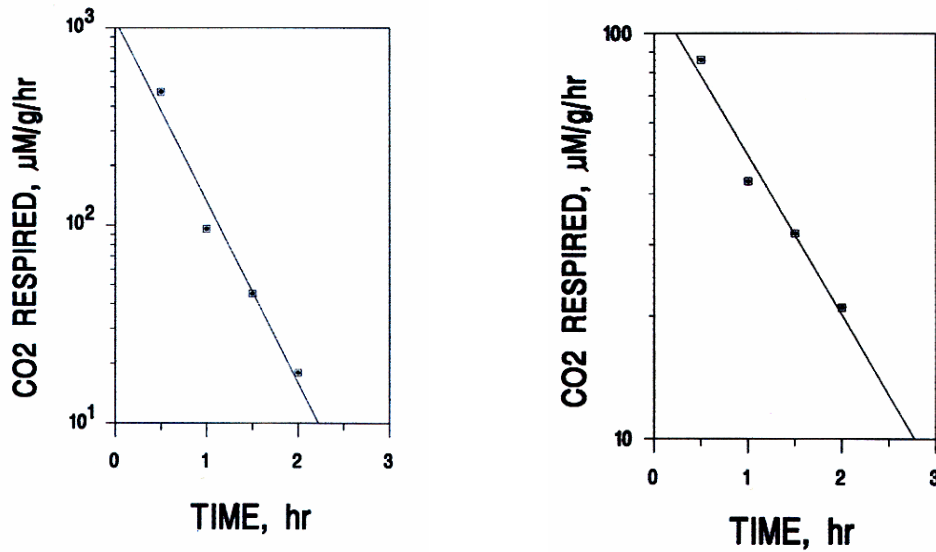


**Figure 10.7.** Respired carbon dioxide from acetate in sediments from GB 516, Cruise 1B. These curves were representative of all the heterotrophic respiration experiments and suggest that the sediments had trace amounts of oxygen or were in fact anoxic.

#### 10.4 DISCUSSION

The major issues covered in this effort were 1) the relationship between sediment grain size and living microbial ATP biomass levels; 2) the effects of drilling on microbial ATP biomass; and 3) the inhibitory effects of oil production on sediment microflora. Given the nature of the sedimentary matrix we had to deal with, we had to devise a new method of measuring ATP and compensating for interferences on a very rigorous sampling program. There are a variety of means of extracting sedimentary ATP, but a major problem for all of them is a means of correcting loss of ATP during sediment extraction by adsorption to the sediments, followed by a secondary interference encountered during the luciferin-luciferase assay. The simplest means to tackle the problem would be to add an internal standard to a duplicate set of samples and to determine the overall loss in the final counting. This approach essentially doubles the work effort and limits the number of replicates that can reasonably be processed, and for very fine-grained materials, the initial loss from adsorption to the sediments may be so great that too much of the standard is lost to be of value.

Our solution was to use radioactive ATP to follow the adsorptive loss followed by an internal ATP standard added at the time of assay to determine counting efficiency. By separating the interference into two components, every sample can be used to determine adsorptive loss (the radioactive ATP is essentially at a concentration that is below detection limits), thus expediting the field aspect. When counting the extracted ATP, the internal standard can be adjusted in the laboratory if, as was the case with our work, there is severe interference in the counting process. As seen in **Figure 10.1**, there is agreement between both approaches, although the radioisotope

approach gave a better estimate of recovery. Our findings also show that as the sediments became finer in composition, the extraction efficiency fell off appreciably (**Figure 10.2**). Samples taken from our sites typically had an extraction efficiency of 8%.

There are a considerable number of reports describing the bacterial numbers found in a variety of sediments. One general conclusion based on direct microscopic evaluation is that bacterial numbers increase as sediment grain size decreases. The question that arises is whether these bacteria are active, or whether an alternative metabolic assay, such as ATP, would be a better indicator of sediment suitability for microbial colonization? In a separate analysis of microbial data from the Mississippi-Alabama-Florida (MAFLA) program in the eastern Gulf of Mexico (LaRock, unpublished data), ATP levels declined with reduced sediment particle size, which is contrary to the microscopic observation but in good agreement with the findings of Koster and Meyer-Reil (2001). Furthermore, by extrapolating the ATP-grain size regression lines to a zero ATP concentration, we arrived at a theoretical minimum grain size of about 2  $\mu\text{m}$ , which would support bacterial development.

Information on deep-sea sedimentary microbial biomass is limited, and information that is integrated to sediment grain size is even more scarce. One of the first measurements of deep-sea ATP biomass was reported by Karl et al. (1976), who found that the upper 2 cm of sediment collected from the abyssal plain in the Atlantic Ocean had a value of 2.4  $\text{ng g}^{-1}$ . More recent work by Egeberg (2000), done in conjunction with the Ocean Drilling Program, suggested that particle size may be a determining factor in regulating sediment microbes. Egeberg made down-core measurements from 1.38 to as deep as 57.8 m below the seafloor and reported ATP values as high as 6 to as low as 0.23  $\text{ng g}^{-1}$ , with an average value of 0.75  $\text{ng g}^{-1}$ . No determinations were made on surface sediments, however.

Koster and Meyer-Reil made a suite of measurements in shallow coastal waters of the Baltic Sea, which included ATP, chlorophyll a, phospholipid, and carbon species. The sediments they worked with were characterized as sandy, slightly muddy sand, and muddy sand. The TOC increased as the sediments became finer, although the available DOC (the more labile component) decreased, leading to the conclusion that the higher organic content is composed of more refractory, or aged material, which is less capable of supporting microbial metabolism. With increasing mud content, the microbial biomass, based on phospholipid determinations, increased, whereas the active biomass, based on ATP determinations, decreased. This result neatly illustrates the disparity that we observe between measurements that seek to quantify the total quantity or number of microbes without regard to whether they are functional or not. In this case, as well as with direct acridine orange direct counts (AODCs), the measured parameter (phospholipid or cell number) reflects only whether bacteria are present, and not whether they are growing or in a metabolically active state. In other words, the finer sediments may harbor more microbes, but based on ATP measurements, their geochemical potential is diminished.

The ATP values obtained by Koster and Meyer-Reil are not directly comparable to our measurements because they reported their results as a function of sediment volume (i.e.,  $\text{ng cm}^{-3}$  as opposed to  $\text{ng g}^{-1}$ ). Since our sediments were about 60% to 70% water, 1 g of sediment is a close approximation to 1  $\text{cm}^3$  of sediment slurry. With this difference in mind, the ATP values reported ranged from 673 to 2,843  $\text{ng cm}^{-3}$ , which agree well with the values we reported for the

Florida shelf off the Gulf coast. The question now is what ATP levels might one reasonably expect at 1,000 m in the sediments of the Gulf of Mexico if there were no anthropogenic impacts? A reasonable expectation might range from 1,000 ng g<sup>-1</sup> in the shallow coastal zone to 2 ng g<sup>-1</sup> in the most distant and deepest regions of the open ocean. Under the present circumstances, an approximate value might be between 50 and 100 ng g<sup>-1</sup>.

The Cruise 1B ATP values for GB 516 (**Table 10.2**) show considerable spatial variability that may, in part, be the result of gas and oil seeping from the seafloor (see the dedicated issue of *Geo Marine Letters* 14:2/3, 1994 for an extensive overview of the Louisiana seep zone). In calculating an average ATP concentration for the area, we did not include the exceptionally high values of NF-B01 and NF-B02, as these samples may be affected by gas or oil seepage.

One effect of drilling was the addition of drilling muds and cuttings to the seafloor. This is seen in the chemical analyses in *Chapter 8*, where it is apparent that the primary change is with the addition of barium to the sedimentary matrix. Barite is a major constituent of the drilling muds that are used to aid in the drilling process. Based on the change in barium concentrations alone, more of the coarser drilling discharges were deposited in the near-field sites than were found in the far-field locations, as were also seen in the GOOMEX project (Kennicutt 1995; Kennicutt et al. 1996a). In other words, heavier materials are quickly deposited, whereas the finer materials are more dispersed. Interestingly, the mean grain size for these sediments borders on the hypothetical 2- $\mu$ m threshold that we postulate to be the lower limit that will support bacterial growth. Clay sediments, because of the extremely small particle size, are highly impervious. This has the effect of inhibiting bacterial movement either into or out of the clay sediments, as well as limiting the passage of oxygen or nutrients (Maier et al. 2000).

How might drilling discharges affect the sedimentary microbial community? There are three possibilities: 1) the solid phase of the SBM simply buries the existing community; 2) there is an inhibitory component in the SBM that affects bacterial metabolism or the environment; or 3) the outcome is a combination of 1 and 2. From the oxygen data (see *Chapter 8*), it is obvious that the sediments quickly became anoxic as a result of drilling. The base chemical of SBMs (representing up to 75% of the total volume) is selected to be biodegradable as mandated by USEPA regulations; however, this organic enrichment has the effect of creating anoxia. The synthetic chemicals, usually internal and linear alpha olefins, have low solubility and bioavailability, but emulsifiers that include detergents and other additives may contribute some level of toxicity (Jerry Neff, pers. comm.; Neff et al. 2000).

Toxicity bioassays were performed in the GOOMEX project using the sea urchin *Arbacia punctulata* and following either its fertilization or embryological development (Carr and Chapman 1992; Carr 1993). Of the two approaches, the embryological development test proved to be the more sensitive in assessing pore water effects in production areas relative to an uncontaminated control site. Inhibitory effects were found only within a 150-m radius of a platform, and no inhibitory effects were found at any of the far-field sites. Based on the ATP data, it appears that bacteria are severely impacted, even at the far-field locations. Whether this was due to toxicity remained an open question. In order to add some degree of quantification to the problem, a bioassay was done by the Lumitox Co., Inc., based on the relative reduction in light emission from the dinoflagellate *P. lunula* when exposed to water extracts made from the

pre- and post-drilling sediments. The results (**Figures 10.4 and 10.5**) showed that prior to drilling, the sediments at GB 516 and VK 916 had no negative effect on the test organism, and light output from *P. lunula* was essentially equal to that of the negative controls. The post-drilling samples, however, caused a reduction in light emission, with the near-field materials exerting a more deleterious effect than the far-field materials. In a similar fashion, the post-drilling samples from GB 602 had a negative effect, but surprisingly, the samples from MC 292 had no effect at all. At the time the MC 292 samples were taken, the sea surface was noticeably green, even though we were in 1,000 m of water, suggesting terrestrial influences that might in some fashion mitigate the effects of production activities. How do these results translate into an effect that the bacterial community might experience? We cannot say precisely, but these findings together with the ATP results indicate that a stress condition had been established.

What is the nature of the inhibitory substance(s)? In the GOOMEX program it was considered to be metals, specifically barium, but in our study, the barium concentration at the far-field stations did not increase significantly after drilling, compared to a one to two orders of magnitude increase at the near-field locations. This suggested that some other factor was responsible for the ATP and toxicity test results, which we believe is organic in nature. Attempts were made by three different laboratories to extract and amplify DNA for characterization using a variety of techniques and clean-up kits, which worked with the pre-drilling sediments but all failed when applied to the post-drilling sediments. DNA was extracted from the sediments as determined by the ethidium bromide technique, but the problem arose in the polymerase amplification. In a similar vein, the sensitivity of the ATP assay was greatly reduced when we counted the post-drilling samples. The analytical system we use is routinely able to detect  $0.1 \text{ ng g}^{-1}$ , but the limit of detection for the post-drilling samples was raised to 1.5 to  $1.8 \text{ ng g}^{-1}$ , which accounts for the less than symbols in **Table 10.2**. Note also that the interfering effect was most pronounced for the near-field stations. In other words, something is interfering with enzyme function.

How long do these deleterious effects last? That is difficult to say, but they do not appear to be permanent. GB 516 had been developed and then abandoned a number of years ago and then redeveloped in 2000-2001. Based on ATP and toxicity measurements prior to the secondary development, it is apparent that the sediments had fully recovered from the earlier drilling.

## Chapter 11 Meiofauna and Macrofauna

*Barry A. Vittor & Associates, Inc.*

*Continental Shelf Associates, Inc.*

---

### 11.1 INTRODUCTION

Responses of benthic organisms to offshore Gulf of Mexico petroleum exploration and production have been studied extensively on the continental shelf. Investigations of acute effects of drilling muds and cuttings on macroinfaunal communities have been sponsored by the MMS and American Petroleum Institute in particular, and include studies such as the Central Gulf of Mexico platform project (Baker et al. 1981), drilling discharges fate and effects in shallow nearshore waters in south Texas (Continental Shelf Associates, Inc. 1989), and the Buccaneer gas and oil field benthic community study (Harper et al. 1981). Some studies have addressed meiofaunal and macroinfaunal community structure and detected effects on these organisms by surveying around drilling/production sites of varied duration. The Gulf of Mexico Offshore Operations Monitoring Experiment (GOOMEX) investigated potential chronic, sublethal, and long-term oil and gas production effects on meiofauna and macrofauna, as well as other ecosystem components on the continental shelf (Montagna and Harper 1996). That program detected changes in benthic assemblages due to both organic enrichment and toxicity of drilling muds and cuttings discharged to the bottom. The present investigation used some of the same methods but focused on meiofaunal and macroinfaunal community responses to drilling discharges in the deepwater Gulf of Mexico. Previous studies that provide some information about benthic effects of SBMs on the Gulf of Mexico continental slope include an opportunistic survey of a wellsite in the Mississippi Canyon area (Gallaway et al. 1997; Fechhelm et al. 1999) and a study of several continental slope and shelf sites by Continental Shelf Associates, Inc. (2004).

Background information on deepwater benthic communities is available from the MMS northern Gulf of Mexico continental slope study (Gallaway 1988; Pequegnat et al. 1990). More recently, the MMS deep Gulf of Mexico benthos study has expanded the depth range and geographic coverage of the previous continental slope study (Rowe and Kennicutt 2002). The study included stations at depths from 300 m to greater than 3,000 m.

### 11.2 MATERIALS AND METHODS

Study design has been described in *Chapter 2*. Briefly, benthos were sampled at four sites on the northern Gulf of Mexico continental slope. VK 916 was an exploration site sampled before and after drilling of a single exploration well. GB 516 was an exploration/development site that was sampled once after exploration drilling and again after several development wells were drilled. GB 602 and MC 292 were post-development sites sampled once after several exploration and development wells had been drilled.

Benthic samples were collected on three cruises. Cruise 1B (October-November 2000) was a pre-drilling survey of VK 916 and a snapshot of GB 516 after exploration drilling and prior to

development drilling. Cruise 2B (July 2001) was a post-drilling survey following development drilling at GB 516, GB 602, and MC 292. Cruise 3B (August 2002) was the post-drilling survey at VK 916. On each cruise, box core samples were collected at 12 randomly selected locations within the 500-m near-field radius at each study site visited. Samples also were collected at 12 far-field locations (two locations selected randomly within each of six far-field sites).

Macroinfauna (animals retained on a 300- $\mu$ m screen) and meiofauna (those passing through a 300- $\mu$ m screen but retained on a 63- $\mu$ m screen) were counted and identified to major group (order or higher taxonomic level in most cases). In most cases, annelids were identifiable to class (Polychaeta or Oligochaeta), and the overwhelming majority of these were polychaetes. However, in some data sets (e.g., all Cruise 3B samples), they were identified only as annelids. For consistency in making comparisons among sites and cruises, all of these observations are reported here as Annelida. Meiofaunal nematodes from GB 602 and MC 292 during Cruise 2B were identified to family to determine changes in feeding types among these taxa; feeding types of nematode families were adopted from Jensen (1986). Harpacticoid copepod reproductive condition also was noted at these two sites to detect potential sublethal effects of synthetic drilling muds. Benthic data reduction included individual and taxon abundance, taxon diversity, evenness, and richness. Statistical treatment of the data involved ANOVA for differences in meiofaunal or macroinfaunal individual abundances between survey sites and cruises.

Twenty-four stations were selected for more in-depth taxonomic identification of macroinfauna to the Lowest Practical Identification Level (LPIL). These analyses included near-field and far-field samples from each site and each cruise. For the 24-station analysis of macroinfaunal data, spatial and temporal patterns were examined using multivariate techniques, including cluster analysis, non-metric multidimensional scaling (MDS), and similarity percentage breakdown (SIMPER). These analyses were performed on a similarity matrix constructed from a raw data matrix consisting of taxa and samples (station-cruise). To weight the contributions of common and rare taxa, raw counts of each taxon in a sample ( $n$ ) were transformed to logarithms [ $\log_{10}(n+1)$ ] prior to similarity analysis. Cluster analysis was followed by MDS ordination of the similarity matrix to corroborate cluster results. Species accounting for observed assemblage differences among groups and within groups of stations were identified using the SIMPER procedure, which determines the average contribution of each species characterizing a station group or discriminating between pairs of station groups (Clarke 1993). These analyses (MDS and SIMPER) were performed with the PRIMER v5 package (Clarke and Gorely 2001).

### **11.3 MEIOFAUNAL RESULTS AND DISCUSSION**

A complete list of meiofaunal taxa collected is presented in *Appendix II*.

#### **11.3.1 Viosca Knoll Block 916**

VK 916 was sampled on Cruise 1B (November 2000) and Cruise 3B (August 2002). The two cruises served as pre- and post-drilling surveys for this site.

**Table 11.1** summarizes meiofaunal community statistics for VK 916 including density, diversity, evenness, and richness. There was considerable spatial and temporal variation in all of the community statistics. As shown in the table and illustrated in **Figure 11.1**, total densities decreased by about an order of magnitude between the two cruises at both near-field and far-field sites. Mean densities on Cruise 1B were 608 and 544 individuals/10 cm<sup>2</sup> for near-field and far-field, respectively, as compared with 96 and 19 individuals/10 cm<sup>2</sup> for Cruise 3B. On both surveys, there was considerable overlap in the range of densities between near-field and far-field sites (i.e., densities at some near-field stations were similar to those at far-field stations). On the pre-drilling cruise (1B), the near-field site showed a greater range of densities, including both higher and lower values than the far-field sites. On the post-drilling cruise (3B), near-field densities tended to be higher than far-field densities, with some overlap.

**Figure 11.2** illustrates the taxonomic composition of the meiofaunal samples at VK 916. On Cruise 1B, both the near-field and far-field sites were numerically dominated by nematodes and harpacticoid copepods, which together accounted for over 90% of the total numbers. On Cruise 3B, the composition of the near-field samples was markedly different, with annelids and aplacophoran molluscs contributing over 50% of the individuals. At the far-field site, nematodes accounted for about the same proportion as on the pre-drilling survey, but annelids were relatively more abundant and harpacticoids relatively less abundant than on the pre-drilling cruise.

It also is instructive to look at the two near-field stations having the highest density on each survey. On Cruise 1B, these were Stations NF-B02 and NF-B08. Nematodes accounted for 90% of the individuals at NF-B02 and 83% of the individuals at NF-B08. On Cruise 3B, the two highest densities were observed at NF-B05 and NF-B08. Annelids were the most abundant group at NF-B05, accounting for 61% of the total. At NF-B08, nematodes were the most abundant group (48%), but aplacophorans (31%) and annelids (19%) were significant components.

ANOVA was conducted for the most abundant groups in the VK 916 samples to test for spatial and temporal differences (**Table 11.2**). Significant ( $p < 0.05$ ) differences were as follows:

- Harpacticoid copepods and nematodes were significantly less abundant during Cruise 3B than during Cruise 1B. The same was true for aplacophorans, but only at the far-field sites.
- On Cruise 3B, annelids and aplacophorans were more abundant at the near-field than at the far-field sites. There were no significant near-field vs. far-field differences in mean density for nematodes or harpacticoids.

### 11.3.2 Garden Banks Block 516

GB 516 was sampled on Cruise 1B (October-November 2000) and Cruise 2B (July 2001). Both cruises were post-drilling, with exploration wells drilled prior to the first cruise and several development wells drilled between cruises (see *Chapter 3*).

**Table 11.1.** Meiofaunal community statistics for Viosca Knoll Block 916.

Station	No. Taxa	Density No./10 cm <sup>2</sup>	H' Diversity	J' Evenness	D Richness
<b>Cruise 1B (October-November 2000)</b>					
<b>Near-Field</b>					
NF-B01	10	122	1.77	0.77	1.87
NF-B02	7	1,452	0.41	0.21	0.82
NF-B03	9	387	0.89	0.40	1.34
NF-B04	9	468	1.15	0.52	1.30
NF-B05	9	700	0.60	0.27	1.22
NF-B06	6	398	0.96	0.53	0.84
NF-B07	11	898	0.80	0.33	1.47
NF-B08	14	1,872	0.69	0.26	1.73
NF-B09	7	230	0.54	0.28	1.10
NF-B10	2	18	0.21	0.31	0.35
NF-B11	6	141	0.77	0.43	1.01
<b>Far-Field</b>					
FF2-B1	10	896	0.57	0.25	1.32
FF2-B2	8	574	1.16	0.56	1.10
FF3-B1	8	596	0.80	0.39	1.10
FF3-B2	9	514	1.03	0.47	1.28
FF4-B1	8	744	0.75	0.36	1.06
FF4-B2	7	414	0.89	0.46	1.00
FF5-B1	6	217	0.40	0.22	0.93
FF5-B2	4	74	0.56	0.40	0.70
FF6-B1	8	783	0.61	0.29	1.05
FF6-B2	7	626	0.45	0.23	0.93
<b>Cruise 3B (August 2002)</b>					
<b>Near-Field</b>					
NF-B01	4	40	1.10	0.80	0.81
NF-B02	10	136	1.50	0.65	1.83
NF-B03	7	92	1.45	0.75	1.33
NF-B04	8	92	1.69	0.81	1.55
NF-B05	6	187	1.03	0.58	0.96
NF-B06	4	107	0.95	0.69	0.64
NF-B07	4	21	1.00	0.72	0.99
NF-B08	7	245	1.14	0.59	1.09
NF-B09	3	29	0.76	0.69	0.59
NF-B10	3	19	0.86	0.79	0.68
NF-B11	6	119	1.35	0.75	1.05
NF-B12	6	67	1.17	0.65	1.19
<b>Far-Field</b>					
FF1-B01	5	32	1.16	0.72	1.15
FF1-B02	1	11	0.00	N/A	0.00
FF2-B01	4	30	0.73	0.53	0.88
FF2-B02	4	17	0.89	0.64	1.06
FF3-B01	1	4	0.00	N/A	0.00
FF3-B02	2	3	0.64	0.92	0.91
FF4-B01	4	40	0.80	0.57	0.81
FF4-B02	4	38	0.53	0.38	0.82
FF5-B01	2	24	0.56	0.81	0.31
FF5-B02	3	23	0.80	0.73	0.64
FF6-B01	1	1	0.00	N/A	N/A
FF6-B02	2	6	0.45	0.65	0.56

N/A = not applicable.



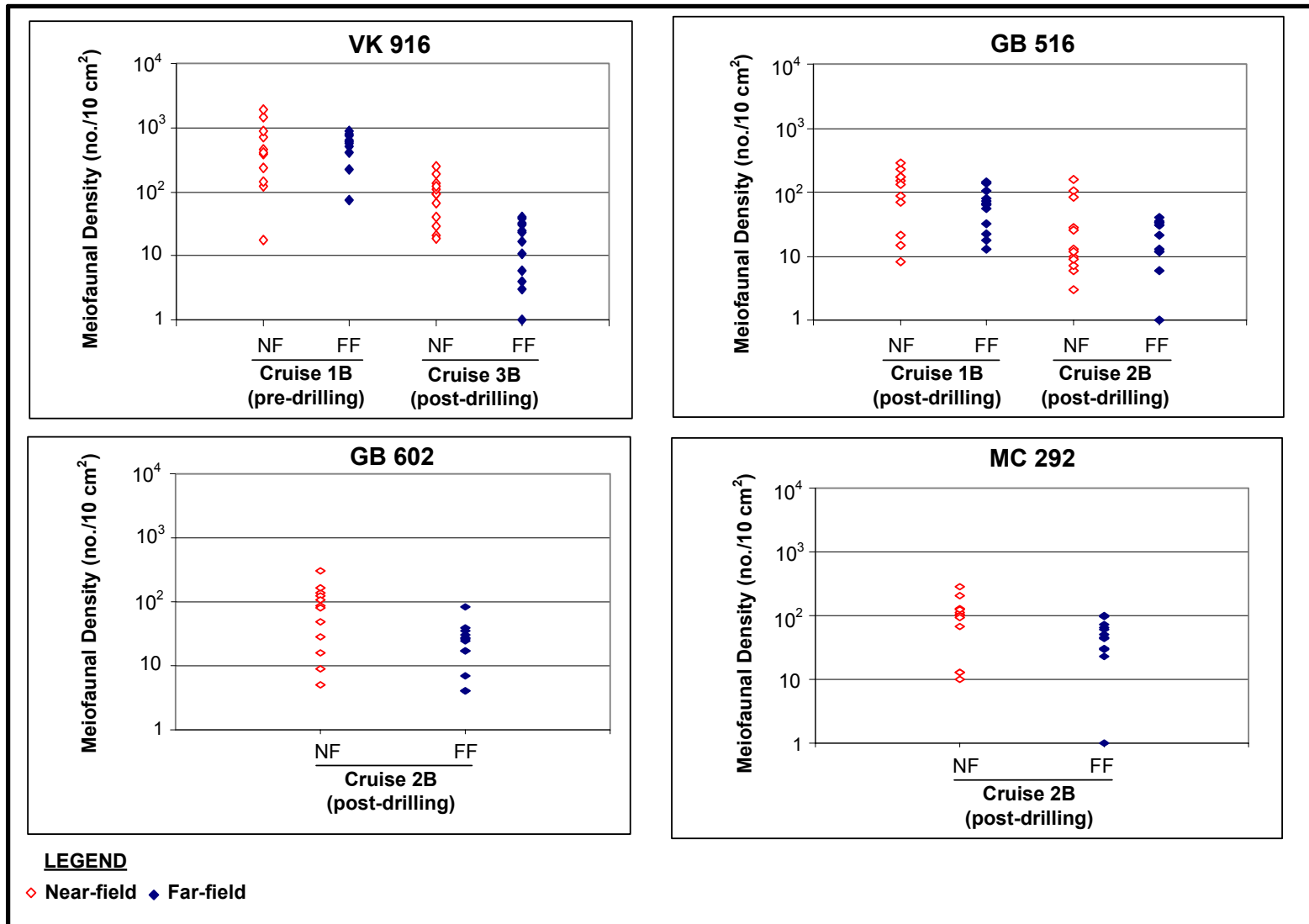
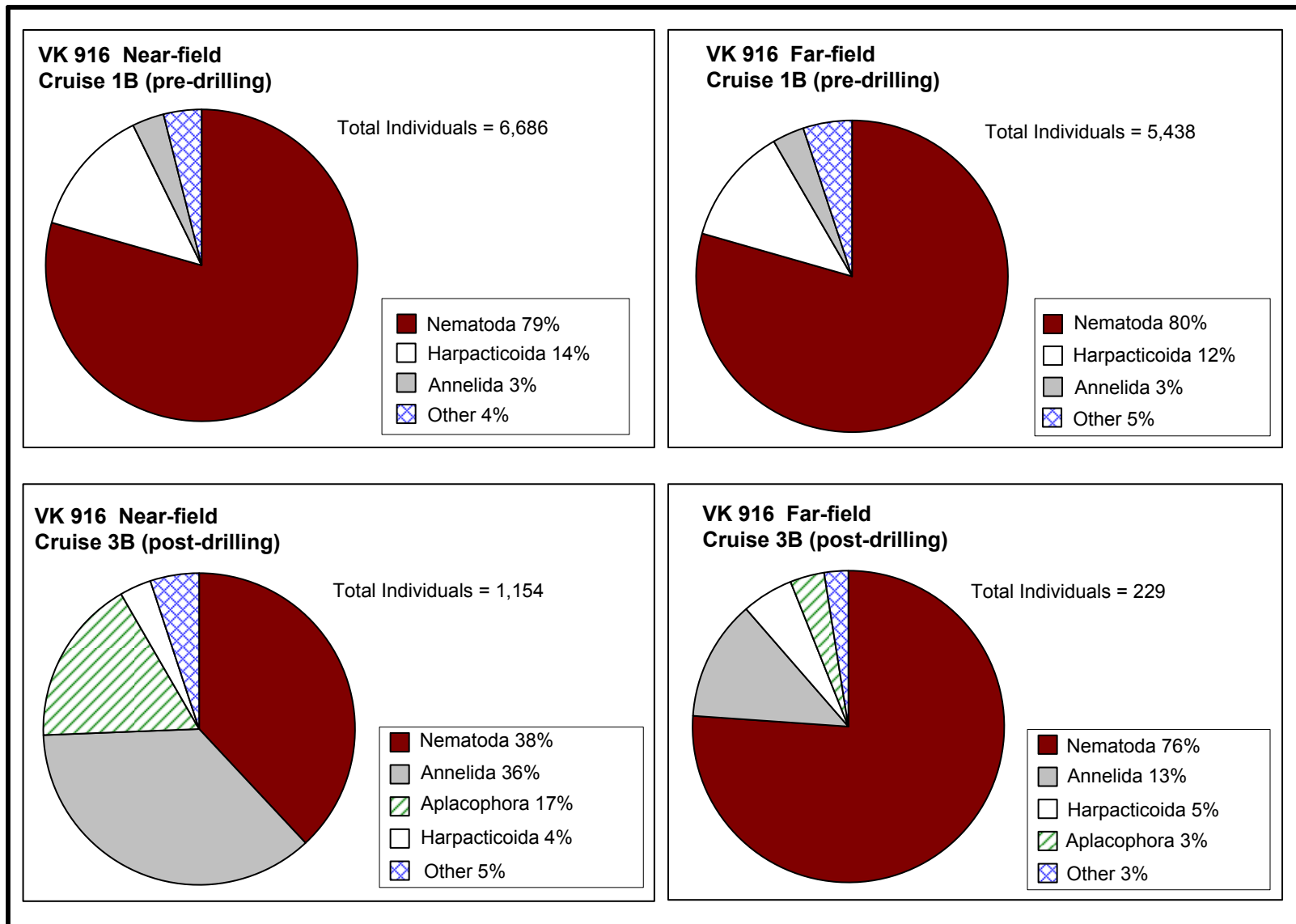


Figure 11.1. Total meiofaunal densities at the four study sites. Note the log scale.



**Figure 11.2.** Taxonomic composition of meiofauna at Viosca Knoll Block 916.

**Table 11.2.** ANOVA results for meiofaunal groups. Significance level  $\alpha = 0.05$ . In the interaction column, cruise/site combinations are listed in order of decreasing abundance, and vertical lines group cruises/sites that are not significantly different.

Site	Group	ANOVA Result		
		Cruise	Site	Interaction
Viosca Knoll 916	Annelida	Interaction significant; see last column	Interaction significant; see last column	Cr 3B NF Cr 1B FF Cr 1B NF Cr 3B FF
	Aplacophora	Interaction significant; see last column	Interaction significant; see last column	Cr 3B NF Cr 1B FF Cr 1B NF Cr 3B FF
	Harpacticoida	Cr 1B > Cr 3B	n.s.	n.s.
	Nematoda	Cr 1B > Cr 3B	n.s.	n.s.
Garden Banks 516	Annelida	n.s.	NF > FF	n.s.
	Harpacticoida	n.s.	n.s.	n.s.
	Nematoda	Cr 1B > Cr 2B	n.s.	n.s.
Garden Banks 602	Annelida	N/A	n.s.	n.s.
	Harpacticoida	N/A	n.s.	n.s.
	Nematoda	N/A	n.s.	n.s.
Mississippi Canyon 292	Annelida	N/A	NF > FF	n.s.
	Harpacticoida	N/A	n.s.	n.s.
	Nematoda	N/A	n.s.	n.s.

FF = far-field; NF = near-field; N/A = not applicable (only one cruise at GB 602 and MC 292); n.s. = not significant.

**Table 11.3** summarizes meiofaunal community statistics for GB 516 including density, diversity, evenness, and richness. There was considerable spatial and temporal variation in all of the community statistics. As shown in the table and illustrated in **Figure 11.1**, densities apparently decreased between the two cruises at both near-field and far-field sites. Mean densities on Cruise 1B were 122 and 68 individuals/10 cm<sup>2</sup> for near-field and far-field, respectively, as compared with 38 and 22 individuals/10 cm<sup>2</sup> for Cruise 2B. On both surveys, there was considerable overlap in the range of densities between near-field and far-field sites. On Cruise 1B, the near-field site included both the highest and lowest values. On Cruise 2B, the near-field site had the highest densities, and the far-field site had the lowest density.

**Figure 11.3** illustrates the taxonomic composition of the meiofaunal samples at GB 516. At the far-field sites on both cruises, nematodes and harpacticoid copepods together contributed 88% to 89% of the total population. At the near-field site, these groups were less numerically dominant (66% to 79% combined percentage), and the proportion of annelids was higher.

**Table 11.3.** Meiofaunal community statistics for Garden Banks Block 516.

Station	No. Taxa	Density No./10 cm <sup>2</sup>	H' Diversity	J' Evenness	D Richness
<b>Cruise 1B (October-November 2000)</b>					
<b>Near-Field</b>					
NF-B01	2	8	0.66	0.95	0.48
NF-B02	3	21	0.98	0.89	0.66
NF-B03	3	170	1.07	0.97	0.39
NF-B04	7	226	1.13	0.58	1.11
NF-B05	5	86	0.91	0.56	0.90
NF-B06	4	152	0.89	0.64	0.60
NF-B07	4	15	1.17	0.84	1.11
NF-B08	4	171	0.93	0.67	0.58
NF-B09	4	71	0.87	0.63	0.70
NF-B10	6	288	0.90	0.50	0.88
NF-B11	4	131	0.79	0.57	0.62
<b>Far-Field</b>					
FF1-B1	6	137	1.02	0.57	1.02
FF1-B2	6	66	1.02	0.57	1.19
FF2-B1	5	80	1.34	0.83	0.91
FF2-B2	4	106	0.81	0.59	0.64
FF3-B1	4	32	0.95	0.69	0.87
FF3-B2	5	56	1.37	0.85	0.99
FF4-B1	4	18	1.04	0.75	1.04
FF4-B2	6	62	0.73	0.41	1.21
FF5-B1	9	146	1.04	0.47	1.61
FF5-B2	8	72	1.52	0.73	1.64
FF6-B1	2	13	0.43	0.62	0.39
FF6-B2	4	22	0.98	0.71	0.97
<b>Cruise 2B (July 2001)</b>					
<b>Near-Field</b>					
NF-B01	1	3	0.00	N/A	0.00
NF-B02	4	6	1.24	0.90	1.67
NF-B03A	5	107	1.11	0.69	0.86
NF-B04	5	156	0.69	0.43	0.79
NF-B05	3	7	0.96	0.87	1.03
NF-B06	3	13	0.54	0.49	0.78
NF-B07	3	10	1.05	0.96	0.87
NF-B08	3	9	0.85	0.77	0.91
NF-B09	4	84	0.79	0.57	0.68
NF-B10	3	28	0.74	0.67	0.60
NF-B11	4	26	1.08	0.78	0.92
NF-B12	3	12	1.10	1.00	0.80
<b>Far-Field</b>					
FF1-B1	3	13	0.54	0.49	0.78
FF1-B2	1	1	0.00	N/A	N/A
FF2-B1	2	6	0.64	0.92	0.56
FF2-B2	3	12	0.92	0.84	0.80
FF3-B1	2	30	0.68	0.99	0.29
FF3-B2	4	12	1.08	0.78	1.21
FF4-B1	6	35	1.43	0.80	1.41
FF4-B2	3	30	0.80	0.73	0.59
FF5-B1	4	21	0.90	0.65	0.99
FF5-B2	4	33	0.88	0.64	0.86
FF6-B1	5	41	0.89	0.55	1.08
FF6-B2	3	34	0.71	0.65	0.57

N/A = not applicable.

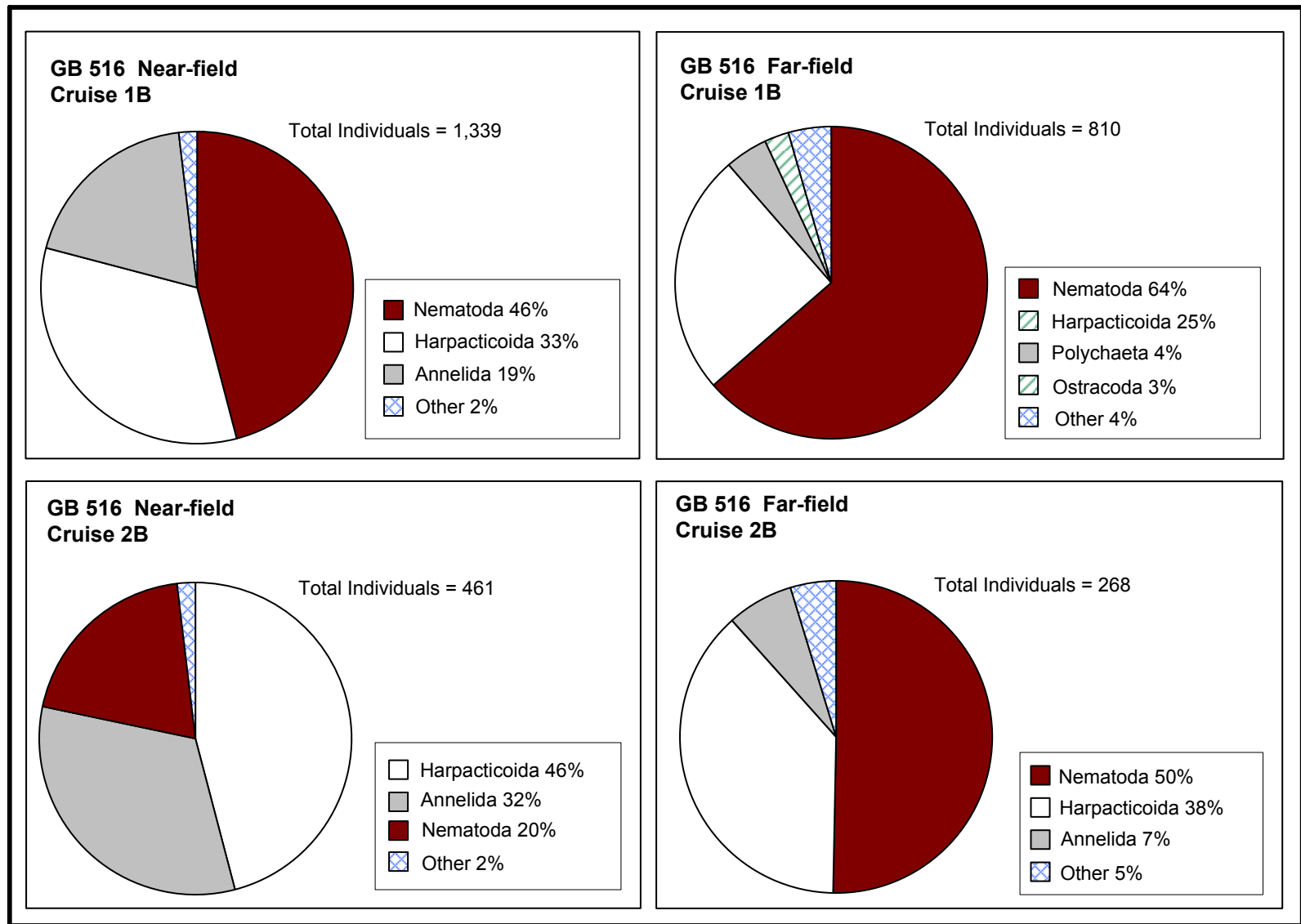


**Figure 11.3.** Taxonomic composition of meiofauna at Garden Banks Block 516.

On Cruise 1B, the two highest densities at the near-field site were observed at NF-B10 and NF-B04. Harpacticoids and nematodes together accounted for 85% of total individuals at NF-B04 and 95% at NF-B10. On Cruise 2B, harpacticoids and nematodes also dominated at the station with the highest abundance (combined 95% of individuals at NF-B04). However, at the station with the second highest abundance (NF-B03A), annelids accounted for 50% of the total individuals.

ANOVA was conducted for the most abundant groups at GB 516 to test for spatial and temporal differences (**Table 11.2**). Results were as follows:

- Nematodes were significantly more abundant on Cruise 1B than on Cruise 2B, whereas the abundance of annelids and harpacticoids did not differ between cruises.
- Annelids were significantly more abundant in the near-field than the far-field.
- There were no significant differences in nematode or harpacticoid copepod abundance between the near-field and far-field.

### 11.3.3 Garden Banks Block 602

GB 602 was sampled only on Cruise 2B (July 2001). **Table 11.4** summarizes meiofaunal community statistics for GB 602 including density, diversity, evenness, and richness. There was considerable spatial variation in all of the community statistics. As shown in **Table 11.4** and **Figure 11.1**, there was considerable overlap in the range of densities between near-field and far-field sites. However, several near-field stations had higher densities than any of the far-field stations. Mean densities were 93 individuals/10 cm<sup>2</sup> for the near-field and 26 individuals/10 cm<sup>2</sup> for the far-field.

**Figure 11.4** illustrates the taxonomic composition of the meiofaunal samples at GB 602. At the far-field sites, nematodes and harpacticoid copepods together contributed 87% of the total population. However, at the near-field site, annelids were the second most abundant group (31%, compared with 49% for nematodes), and nematodes and harpacticoids together contributed only 66% of the total population.

The two near-field stations having the highest density were NF-B03 and NF-B12. At NF-B03, annelids were dominant (54%), followed by nematodes (40%). At NF-B12, nematodes were the most abundant group (46%), followed by annelids (38%).

ANOVA did not detect any significant differences between near-field vs. far-field sites with respect to abundance of the most abundant meiofaunal groups at GB 602 (**Table 11.2**). No temporal comparisons are possible because the site was sampled only on Cruise 2B.

**Table 11.4.** Meiofaunal community statistics for Garden Banks Block 602, Cruise 2B (July 2001).

Station	No. Taxa	Density No./10 cm <sup>2</sup>	H' Diversity	J' Evenness	D Richness
<b>Near-Field</b>					
NF-B01	4	16	0.69	0.50	1.08
NF-B02	10	140	0.57	0.26	1.62
NF-B03	7	163	0.91	0.57	0.79
NF-B04	8	86	1.31	0.67	1.35
NF-B05	6	48	1.31	0.81	1.03
NF-B06	6	126	0.82	0.51	0.83
NF-B07	5	81	1.16	0.72	0.91
NF-B08	4	5	1.33	0.96	1.86
NF-B09	4	28	1.09	0.79	0.90
NF-B10	5	9	1.43	0.89	1.82
NF-B11	9	107	1.42	0.68	1.50
NF-B12	11	305	1.18	0.54	1.40
<b>Far-Field</b>					
FF1-B1	12	35	1.78	0.81	2.25
FF1-B2	7	26	1.30	0.73	1.53
FF2-B1	14	39	1.57	0.63	3.00
FF2-B2	10	25	1.77	0.85	2.17
FF3-B1	3	4	1.04	0.95	1.44
FF3-B2	8	30	1.39	0.67	2.06
FF4-B1	2	4	0.56	0.81	0.72
FF4-B2	9	84	1.59	0.76	1.58
FF5-B1	5	17	1.30	0.81	1.41
FF5-B2	3	7	0.96	0.87	1.03
FF6-B1	6	17	1.22	0.76	1.41
FF6-B2	11	27	1.84	0.80	2.73

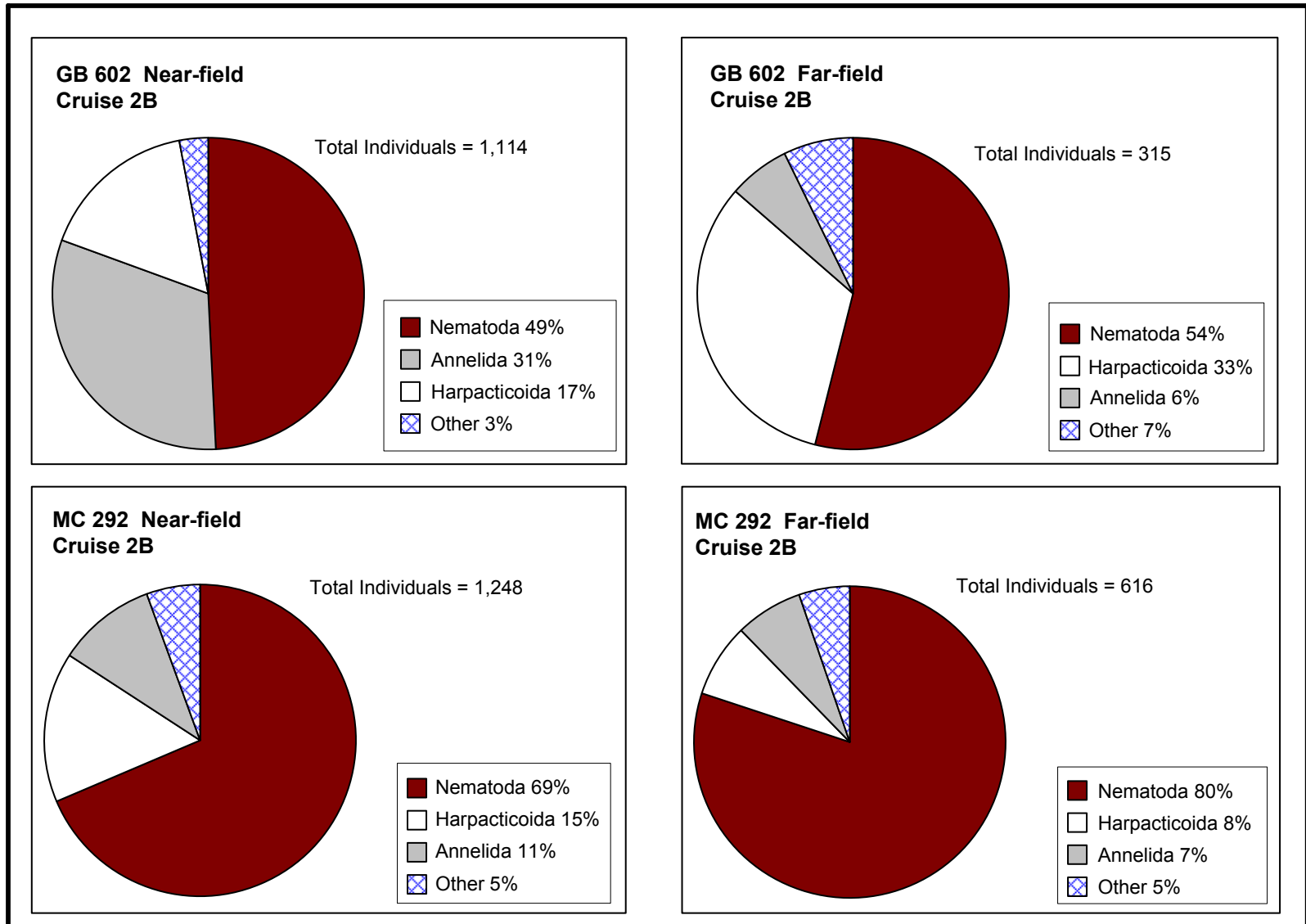


**Figure 11.4.** Taxonomic composition of meiofauna at Garden Banks Block 602 and Mississippi Canyon Block 292.



#### 11.3.4 Mississippi Canyon Block 292

MC 292 was sampled only on Cruise 2B (July 2001). **Table 11.5** summarizes meiofaunal community statistics for MC 292 including density, diversity, evenness, and richness. There was considerable spatial variation in all of the community statistics. As shown in **Table 11.5** and **Figure 11.1**, there was considerable overlap in the range of densities between near-field and far-field sites. However, the highest densities were seen in the near-field. Mean densities were 104 individuals/10 cm<sup>2</sup> for the near-field and 51 individuals/10 cm<sup>2</sup> for the far-field (including one zero value).

**Figure 11.4** illustrates the taxonomic composition of the meiofaunal samples at MC 292. At the far-field sites, nematodes were by far the dominant group, contributing 80% of the total population. At the near-field site, nematodes were slightly less dominant (69%), and harpacticoid copepods and annelids were relatively more abundant than at the far-field sites.

The two near-field stations having the highest density were NF-B01 and NF-B05. At NF-B01, nematodes were dominant (78%). At NF-B05, nematodes were the most abundant group (50%), followed by annelids (20%).

ANOVA indicated that annelids were more abundant in the near-field than in the far-field, but there were no significant differences for nematodes or harpacticoids (**Table 11.2**). No temporal comparisons are possible because the site was sampled only on Cruise 2B.

#### 11.3.5 Individual Groups and Environmental Correlations

The three most abundant groups from the meiofaunal data (annelids, harpacticoid copepods, and nematodes) were selected for further plotting and analysis. **Figure 11.5** shows densities of these individual groups in all post-drilling samples, with each point representing an individual sample. The figure shows that for all three groups, there is a tendency for at least some near-field stations to have higher densities than their far-field counterparts. This pattern is most pronounced for annelids, which clearly tended to be more abundant in the near-field (as confirmed by significant ANOVAs, see **Table 11.2**). Although the ANOVA did not detect a significant difference between near-field and far-field means for nematodes or harpacticoids, **Figure 11.5** shows there were higher densities at some near-field stations.

**Table 11.5.** Meiofaunal community statistics for Mississippi Canyon Block 292, Cruise 2B (July 2001).

Station	No. Taxa	Density No./10 cm <sup>2</sup>	H' Diversity	J' Evenness	D Richness
<b>Near-Field</b>					
NF-B01	9	279	0.85	0.41	1.24
NF-B02	6	104	1.10	0.61	1.08
NF-B03	16	112	1.93	0.73	2.76
NF-B04	12	130	1.25	0.54	1.85
NF-B05	12	202	1.41	0.61	1.70
NF-B06	5	13	1.44	0.89	1.56
NF-B07	9	67	1.71	0.78	1.90
NF-B08	9	100	1.56	0.75	1.52
NF-B09	9	124	1.17	0.56	1.45
NF-B10	8	94	1.43	0.69	1.54
NF-B11	4	10	0.94	0.86	0.87
NF-B12	4	13	1.31	0.94	1.17
<b>Far-Field</b>					
FF1-B1	11	65	1.42	0.62	2.16
FF1-B2	7	97	1.03	0.53	1.31
FF2-B1	0	0	N/A	N/A	N/A
FF2-B2	8	100	1.38	0.66	1.52
FF3-B1	3	43	0.99	0.90	0.53
FF3-B2	7	60	0.97	0.54	1.22
FF4-B1	7	51	1.46	0.75	1.53
FF4-B2	10	72	1.46	0.66	1.87
FF5-B1	5	23	1.35	0.84	1.28
FF5-B2	5	31	1.29	0.80	1.16
FF6-B1	7	45	1.25	0.70	1.31
FF6-B2	4	29	0.88	0.64	0.89

N/A = not applicable.

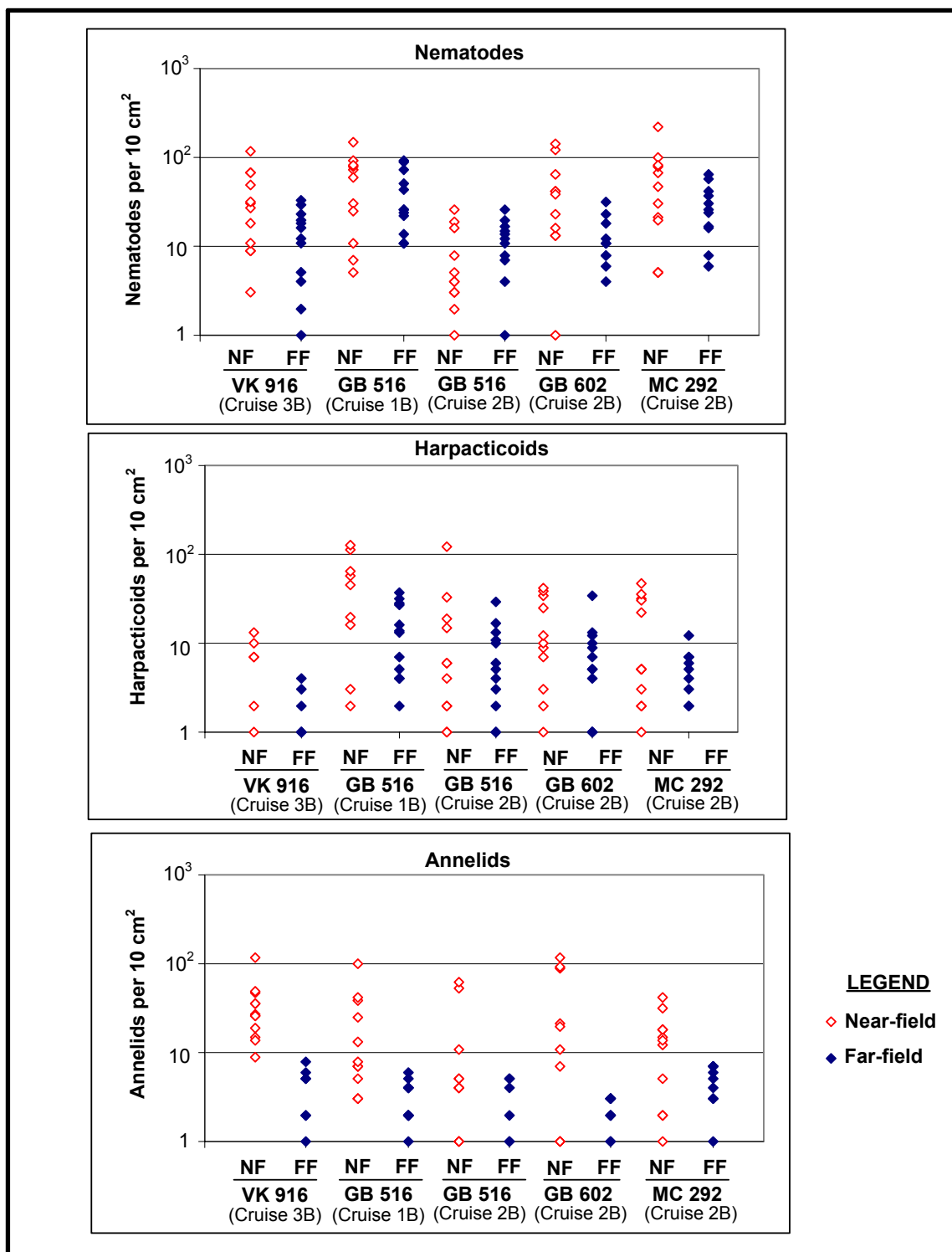


Figure 11.5. Comparison of near-field and far-field abundances of meiofaunal nematodes, harpacticoids, and annelids in post-drilling samples.

Correlations were calculated between densities of these meiofaunal groups and environmental variables (barium, SBF, and TOC concentrations; sediment sand, silt, and clay percentages). Only stations exposed to drilling discharges were included in this analysis (i.e., near-field, post-drilling). Results are summarized in **Table 11.6**. Most of the correlation coefficients were not significant. There was no consistent relationship between any of the selected environmental variables and the abundance of annelids, harpacticoid copepods, or nematodes. At MC 292, annelid densities were positively correlated with barium and SBF. Annelid densities also were positively correlated with barium at GB 516 (Cruise 2B), but there was little or no relationship with barium or SBF at VK 916 or GB 602. Harpacticoid densities were correlated negatively with SBF at GB 516 (Cruise 1B), and at GB 602, were correlated positively with sand and negatively with silt. Nematode densities were negatively correlated with barium and SBF at GB 516 (Cruise 1B) and negatively correlated with silt at GB 602.

### 11.3.6 Nematode Feeding Groups and Harpacticoid Reproductive Status

During Cruise 2B, samples from GB 602 and MC 292 were selected for further analysis. Where possible, nematodes were identified to family, and the families were assigned to feeding types (deposit feeder or predator) based on Jensen (1986). Harpacticoid reproductive condition was also noted (ovigerous vs. non-ovigerous females).

**Table 11.7** summarizes the results of these analyses. The proportion of the nematode population that could be identified to family level ranged from 6% to 36% among the sites. The following results were noted:

- Densities of deposit feeders were about six times higher at MC 292 than at GB 602.
- Densities of predators also were apparently higher at MC 292 than at GB 602.
- Near-field vs. far-field sites had similar densities of deposit feeders at both GB 602 and MC 292.
- Near-field sites had higher densities of predators at both locations.
- The ratio of deposit feeders to predators was 3.5 and 4.2 at the two near-field sites and 13.9 and 14 at the two far-field sites. That is, predators were more abundant (relative to deposit feeders) at the near-field sites.

The ratio of non-ovigerous females to ovigerous females was higher at GB 602 (7.0 and 6.5 for near-field and far-field sites, respectively) than at MC 292 (2.3 and 4.0 for near-field and far-field sites, respectively). There was no indication that near-field sites were consistently higher or lower than far-field sites with respect to this ratio, or with respect to densities of ovigerous or non-ovigerous females. Due to the small number of ovigerous females noted at any site, this analysis was not considered very useful.

### 11.3.7 Discussion

Deep-sea meiofaunal organisms typically occupy the top 2 cm of sediment. Data compiled from a variety of studies by Bett et al. (1994) indicated that about two-thirds of meiofauna occur in this layer of surficial sediment, on average. These organisms are therefore readily exposed to surface sediment disturbance, such as deposition of drilling muds and cuttings from gas and oil exploratory and development activities.

**Table 11.6.** Rank correlation coefficients (Spearman's rho) between meiofaunal densities and environmental variables within areas exposed to drilling discharges (near-field sites on post-drilling cruises). Statistically significant correlation coefficients ( $p < 0.05$ ), i.e., those large enough that they are probably not due to chance, are bold and double-underlined.

Group	Site	Cruise	Correlation Coefficient vs. Environmental Variable					
			Barium	SBF	TOC	Sand	Silt	Clay
Annelida	VK 916	3B	-0.052	-0.147	-0.242	0.105	0.115	-0.150
	GB 516	1B	0.365	0.050	0.041	0.153	-0.265	0.265
	GB 516	2B	<b><u>0.764</u></b>	0.416	0.203	0.316	0.082	-0.195
	GB 602	2B	0.049	0.219	0.117	<b><u>0.638</u></b>	-0.198	-0.109
	MC 292	2B	<b><u>0.653</u></b>	<b><u>0.832</u></b>	0.533	0.179	0.502	<b><u>-0.582</u></b>
Harpacticoida	VK 916	3B	-0.340	-0.201	-0.294	0.044	-0.007	0.026
	GB 516	1B	-0.501	<b><u>-0.733</u></b>	0.000	-0.224	0.068	-0.068
	GB 516	2B	-0.067	-0.446	-0.312	0.049	0.004	-0.186
	GB 602	2B	0.189	0.133	-0.308	<b><u>0.594</u></b>	<b><u>-0.622</u></b>	0.427
	MC 292	2B	0.473	0.374	0.171	0.444	0.155	-0.388
Nematoda	VK 916	3B	0.017	0.018	-0.165	0.164	-0.115	-0.049
	GB 516	1B	<b><u>-0.600</u></b>	<b><u>-0.845</u></b>	-0.191	-0.068	0.145	-0.145
	GB 516	2B	-0.032	-0.172	-0.054	-0.116	-0.025	-0.056
	GB 602	2B	-0.252	-0.228	-0.249	0.501	<b><u>-0.595</u></b>	0.368
	MC 292	2B	0.352	0.493	0.272	-0.021	0.049	-0.084

GB = Garden Banks; MC = Mississippi Canyon; VK = Viosca Knoll; SBF = synthetic-based fluid; TOC = total organic carbon.

**Table 11.7.** Additional meiofaunal analyses from Cruise 2B: nematode trophic groups and harpacticoid copepod reproductive condition. Densities are number of individuals per 10 cm<sup>2</sup>.

Statistic	Garden Banks Block 602		Mississippi Canyon Block 292	
	Near-Field	Far-Field	Near-Field	Far-Field
Nematode density (total)	45.8	14.2	71.5	41.0
Deposit feeders <sup>a</sup>	2.1	2.8	11.7	13.9
Predators <sup>a</sup>	0.6	0.2	2.8	1.0
Not determined	43.1	11.2	57.0	26.1
Ratio deposit/predators	3.5	14.0	4.2	13.9
Harpacticoid density (total)	15.3	8.5	15.9	4.0
Non-ovigerous females	1.4	1.3	1.4	0.4
Ovigerous females	0.2	0.2	0.6	0.1
Ratio non-ovig./ovigerous	7.0	6.5	2.3	4.0

<sup>a</sup> Nematode trophic groups are based on identification to family, with feeding types of families assigned based on Jensen (1986).

In the present study, we observed a wide range in meiofaunal abundance among the four study sites and between surveys. Average meiofaunal densities ranged from 19 to 608 per 10 cm<sup>2</sup>. For comparison, a regression equation developed during the MMS northern Gulf of Mexico continental slope study (Gallaway et al. 1988) predicts a meiofaunal density of about 490 per 10 cm<sup>2</sup> for a water depth of 1,000 m. Preliminary data from the new MMS deep Gulf of Mexico benthos study indicate typical meiofaunal densities at a water depth of 1,000 m are in the range of 100 to 200 per 10 cm<sup>2</sup> (Rowe and Kennicutt 2002). An inverse relationship between water depth and meiofaunal abundance has been widely reported (Jumars and Gallagher 1982; Montagna and Harper 1996; Rowe and Kennicutt 2002). Bett et al. (1994) reported higher densities at similar water depths in the northeast Atlantic (over 1,000 per 10 cm<sup>2</sup>) due to higher nematode densities than in the present study.

Two general patterns are evident in the meiofaunal data and are discussed further below:

- Densities declined between Cruise 1B and the subsequent cruises.
- Densities tended to be higher in the near-field than the far-field.

The meiofaunal data indicate a decrease in density over time at both near-field and far-field sites. At GB 516, average densities decreased by a factor of three at both the near-field and far-field sites between Cruise 1B (October-November 2000) and Cruise 2B (July 2001). At VK 916, average densities decreased by a factor of six at the near-field site and by a factor of 28 at the far-field sites between Cruise 1B and Cruise 3B (August 2002). No cruise-to-cruise comparisons are possible for GB 602 or MC 292; however, the Cruise 2B densities for GB 602 far-field sites are similar to densities at nearby GB 516 during this time.

The reason for this decline over time is unknown. It is similar to the decline in microbial biomass noted in *Chapter 10* between cruises. There was no area-wide change in sediment grain size (see *Chapter 5*) or TOC (see *Chapter 8*) between cruises. At VK 916, TOC increased by about one-third at the near-field site, but not at the far-field site. At GB 516, there was no significant difference between TOC between cruises for either far-field or near-field sites. The decline is not attributable to drilling discharges because little or no exposure of far-field sites to drilling effluents was detected (e.g., elevated barium or SBF concentrations; see *Chapters 8 and 9*); this issue is discussed further in *Chapter 15*.

The broad decline in meiofaunal abundance between cruises complicates interpretation. Because of the magnitude of this change, it would be difficult to determine whether differences between cruises are due to drilling impacts. Therefore spatial comparisons (near-field vs. far-field) are more useful in detecting impacts. In particular, although there was considerable overlap between near-field and far-field densities, the highest densities were always seen in the near-field.

The high total densities in the near-field reflected the increased abundance of several groups. As shown in **Figure 11.5**, in post-drilling samples, the highest densities of annelids, harpacticoid copepods, and nematodes were always seen in the near-field.

VK 916 offers the only straightforward pre- vs. post-drilling comparison. On average, the magnitude of population decline between cruises was much greater at the far-field sites than at the near-field site, suggesting a possible enrichment effect in the near-field. Groups that showed

higher densities in the near-field on the post-drilling cruise were annelids and aplacophoran molluscs. These two groups contributed over 50% of the individuals in the near-field on Cruise 3B. In contrast, the far-field sites (and the pre-drilling near-field site) were numerically dominated by nematodes and harpacticoid copepods, which together accounted for over 90% of total numbers.

GB 516 provides evidence of an apparent numerical response of annelids to drilling discharges (higher densities near drilling). At the far-field sites, nematodes and harpacticoid copepods together contributed 88% to 89% of the total population. At the near-field site, nematodes and harpacticoids were less numerically dominant (67% to 79% combined percentage), and there was a noticeable population of annelids on both cruises.

At MC 292, annelid densities were significantly higher in the near-field than the far-field. But at GB 602, there were no significant differences between near-field and far-field sites with respect to densities of individual meiofaunal groups. However, there is some indication of differences in community composition at GB 602 that could reflect drilling impacts. At the GB 602 near-field site, annelids were the second most abundant group (31%, compared with 49% for nematodes), much different from the far-field sites, where nematodes and harpacticoid copepods together contributed 87% of the total population.

Our results contrast with those found previously in the GOOMEX study. Montagna and Harper (1996) found that nematodes were more abundant near platforms and harpacticoids were less abundant. They attributed the nematode increase to organic enrichment and the harpacticoid decrease to toxicity of metals in drilling discharges. In our study, harpacticoid densities were not reduced in the near-field. A similar result (higher densities in the near-field) is reported in *Chapter 13* for one particular harpacticoid, *Bathycletopsyllus* sp. The only group that had lower densities in the near-field was ostracods at GB 516, but this group was not common enough in the meiofauna to establish a general pattern (see further information on this group in the Macroinfauna section).

Although meiofaunal annelid, nematode, and harpacticoid copepod densities tended to be highest in the near-field, there were no consistent correlations between abundances of these groups and drilling discharge indicators (e.g., barium and SBF concentrations) within near-field sites.

The detailed analyses of nematode feeding types and harpacticoid copepod reproductive status were not very useful because of the small number of organisms identified. The nematode analysis indicated that nematode families classified as predators were more abundant (relative to deposit feeders) in the near-field than the far-field. This seems to be the opposite of what one might expect in the presence of near-field organic enrichment (Montagna and Harper 1996). The ratio of harpacticoid non-ovigerous females to ovigerous females was higher at GB 602 than at MC 292, but there was no indication that near-field sites were consistently higher or lower than far-field sites with respect to this ratio.

## 11.4 MACROINFAUNAL RESULTS AND DISCUSSION

A complete list of macroinfaunal taxa is presented in *Appendix I2*.

### 11.4.1 Viosca Knoll Block 916

VK 916 was sampled on Cruise 1B (October-November 2000) and Cruise 3B (August 2002). The two cruises served as pre- and post-drilling surveys for this site.

**Table 11.8** summarizes macroinfaunal community statistics for VK 916 including density, diversity, evenness, and richness. There was considerable spatial and temporal variation in all of the community statistics. As shown in **Table 11.8** and illustrated in **Figure 11.6**, generally, densities decreased by a factor of six between the two cruises at both near-field and far-field sites. Similar declines were observed in microbial biomass (see *Chapter 10*) and meiofaunal densities (see *Section 11.3.7*).

Mean densities on Cruise 1B were 8,517 and 8,751 individuals/m<sup>2</sup> for near-field and far-field, respectively, as compared with 1,633 and 1,256 individuals/m<sup>2</sup>, respectively, for Cruise 3B. There was considerable overlap between near-field and far-field densities on both cruises. On the pre-drilling cruise (1B), the highest densities were seen at the far-field sites. On the post-drilling cruise (3B), the highest densities were seen in the near-field.

**Figure 11.7** illustrates the taxonomic composition of the macroinfaunal samples at VK 916. On Cruise 1B, the community was similar at near-field and far-field sites, with annelids the most abundant group, followed by ostracods and aplacophoran molluscs. On the post-drilling cruise (3B), the near-field and far-field sites differed noticeably, with the near-field site having higher proportions of annelids and gastropods and lower proportions of ostracods and amphipods than the far-field.

On the post-drilling cruise, the two near-field stations with the highest densities were dominated by annelids (98% at NF-B06) or a combination of annelids and gastropods (68% and 30% respectively, at NF-B07).

ANOVA was conducted for individual macroinfaunal groups to test for spatial and temporal differences (**Table 11.9**). The significant ( $p < 0.05$ ) differences were as follows:

- For annelids, amphipods, aplacophorans, bivalves, gastropods, harpacticoids, ostracods, rhyncocoels, and tanaids, Cruise 1B densities were higher than Cruise 3B densities.
- For ostracods, far-field densities were higher than near-field densities.



**Table 11.8.** Macroinfaunal community statistics for Viosca Knoll Block 916.

Station	No. Taxa	No. Individuals	Density (no./m <sup>2</sup> )	H' Diversity	J' Evenness	D Richness
<b>Cruise 1B (October-November 2000)</b>						
<b>Near-Field</b>						
NF-B01	14	933	9,330	1.56	0.59	1.90
NF-B02	15	435	4,350	1.68	0.62	2.30
NF-B03	16	1,034	10,340	1.69	0.61	2.16
NF-B04	17	1,254	12,540	1.67	0.59	2.24
NF-B05	18	1,240	12,400	1.70	0.59	2.39
NF-B06	15	1,186	11,860	1.49	0.55	1.98
NF-B07	16	759	7,590	1.34	0.48	2.26
NF-B08	14	1,252	12,520	1.58	0.60	1.82
NF-B09	15	726	7,260	1.59	0.59	2.13
NF-B10	14	399	3,990	1.43	0.54	2.17
NF-B11	14	825	8,250	1.62	0.61	1.94
NF-B12	1	177	1,770	0.00	N/A	0.00
<b>Far-Field</b>						
FF2-B1	15	1,356	13,560	1.64	0.61	1.94
FF2-B2	17	1,144	11,440	1.59	0.56	2.27
FF3-B1	17	1,738	17,380	1.62	0.57	2.14
FF3-B2	14	344	3,440	1.30	0.49	2.23
FF4-B1	16	1,110	11,100	1.75	0.63	2.14
FF4-B2	16	838	8,380	1.67	0.60	2.23
FF5-B1	14	220	2,200	1.42	0.54	2.41
FF5-B2	13	586	5,860	1.61	0.63	1.88
FF6-B1	14	1,251	12,510	1.76	0.67	1.82
FF6-B2	11	164	1,640	1.57	0.65	1.96
<b>Cruise 3B (August 2002)</b>						
<b>Near-Field</b>						
NF-B01	6	61	610	1.13	0.63	1.22
NF-B02	8	140	1,400	1.66	0.80	1.42
NF-B03	12	193	1,930	1.80	0.72	2.09
NF-B04	12	158	1,580	1.72	0.69	2.17
NF-B05	4	217	2,170	0.29	0.21	0.56
NF-B06	4	391	3,910	0.09	0.07	0.50
NF-B07	4	447	4,470	0.68	0.49	0.49
NF-B08	12	130	1,300	2.01	0.81	2.26
NF-B09	2	49	490	0.10	0.14	0.26
NF-B10	8	67	670	0.85	0.41	1.66
NF-B11	7	71	710	1.50	0.77	1.41
NF-B12	7	36	360	1.32	0.68	1.67
<b>Far-Field</b>						
FF1-B1	8	87	870	1.45	0.70	1.57
FF1-B2	13	186	1,860	1.68	0.65	2.30
FF2-B1	13	162	1,620	1.80	0.70	2.36
FF2-B2	12	142	1,420	1.86	0.75	2.22
FF3-B1	8	84	840	0.99	0.48	1.58
FF3-B2	12	147	1,470	1.81	0.73	2.20
FF4-B1	11	123	1,230	1.74	0.73	2.08
FF4-B2	11	153	1,530	1.69	0.70	1.99
FF5-B1	9	145	1,450	1.75	0.80	1.61
FF5-B2	9	119	1,190	1.51	0.69	1.67
FF6-B1	5	29	290	0.92	0.57	1.19
FF6-B2	10	130	1,300	1.74	0.76	1.85

N/A = not applicable.

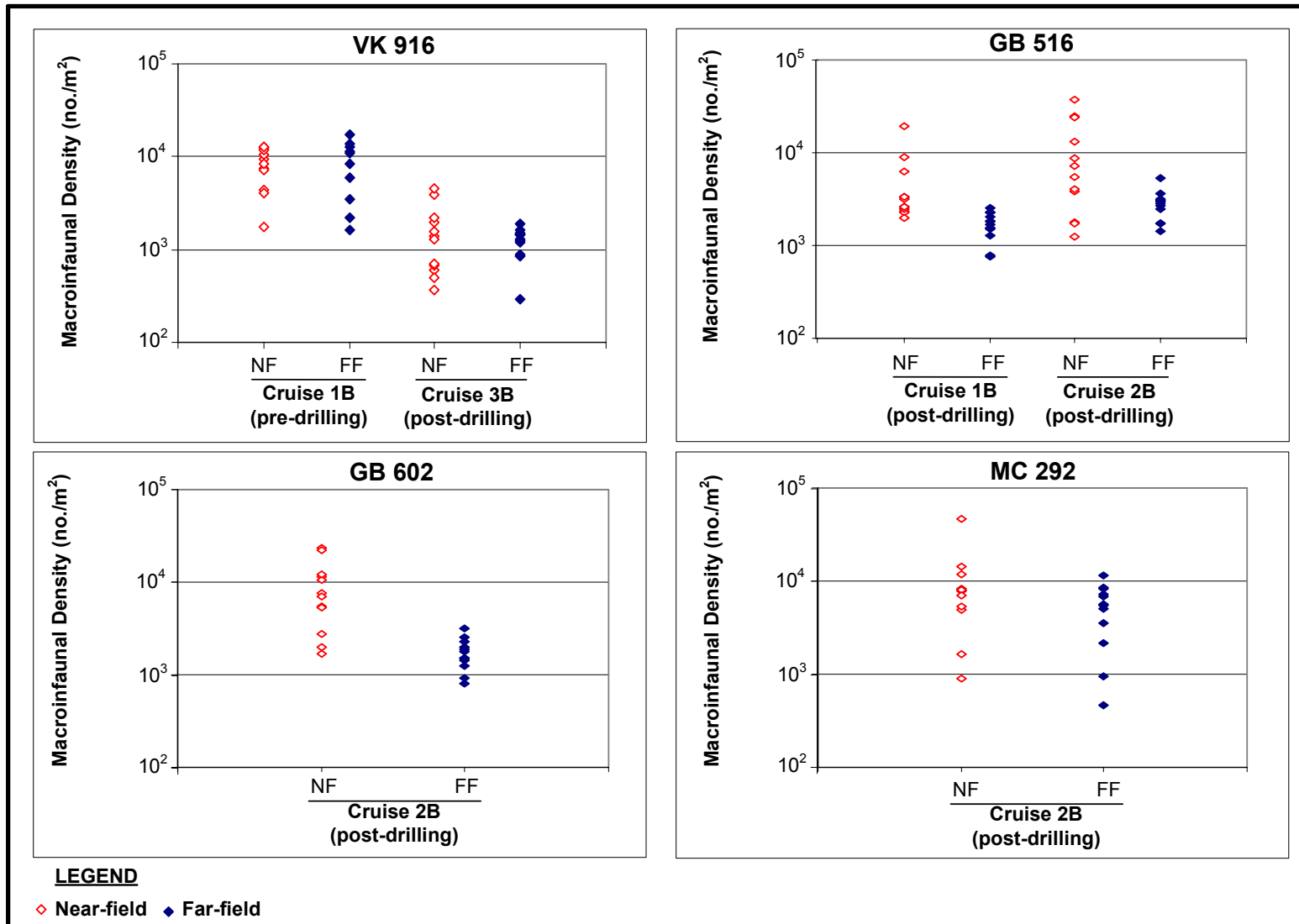
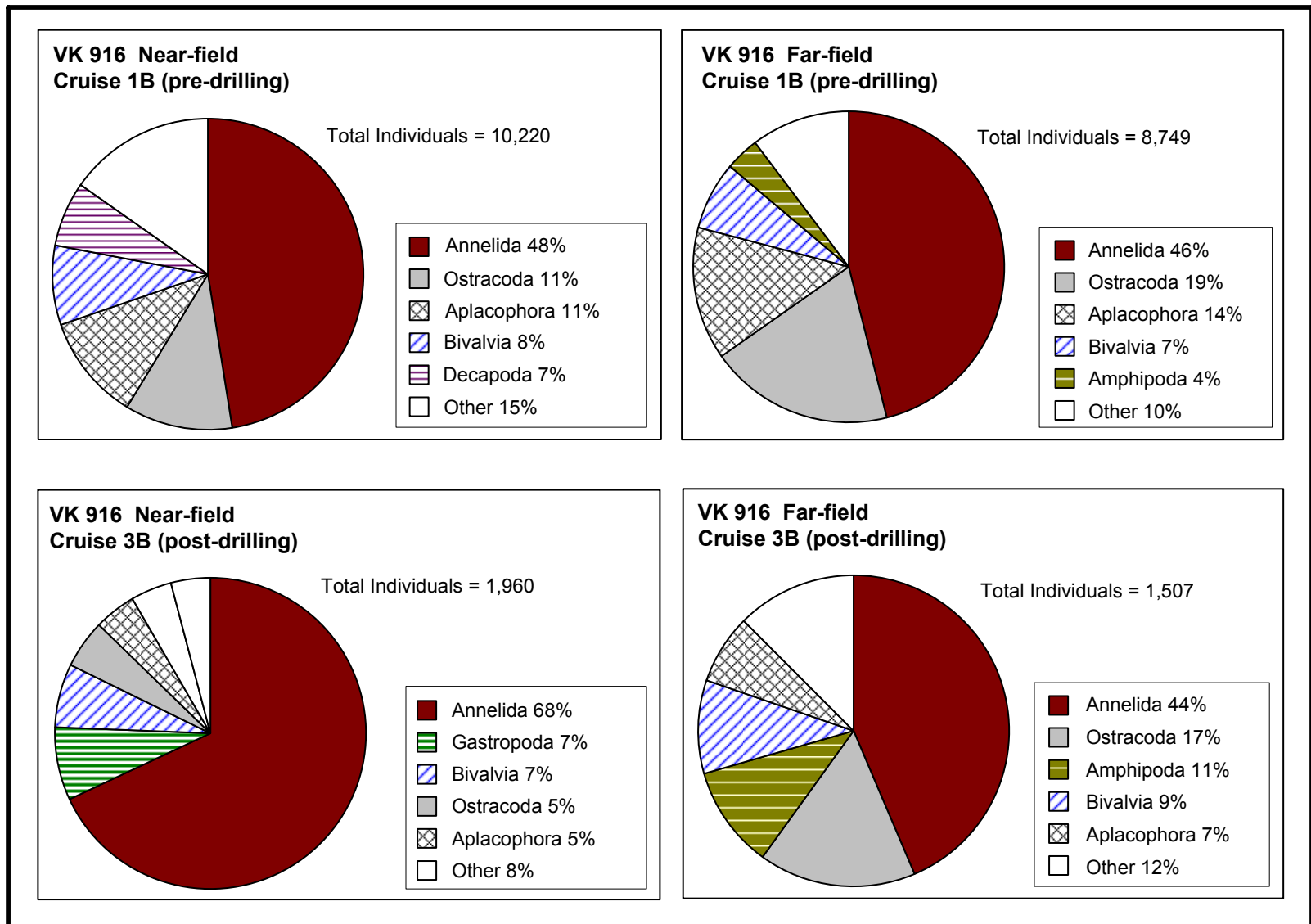


Figure 11.6. Total macroinfaunal densities at the four study sites. Note the log scale.



**Figure 11.7.** Taxonomic composition of macroinfauna at Viosca Knoll Block 916.

**Table 11.9.** ANOVA results for macroinfaunal groups. Significance level  $\alpha = 0.05$ . In the interaction column, cruise/site combinations are listed in order of decreasing abundance, and vertical lines group cruises/sites that are not significantly different.

Site	Group	ANOVA Result		
		Cruise	Site	Interaction
VK 916	Annelida	1B > 3B	n.s.	n.s.
	Amphipoda	1B > 3B	n.s.	n.s.
	Aplacophora	1B > 3B	n.s.	n.s.
	Bivalvia	1B > 3B	n.s.	n.s.
	Decapoda	n.s.	n.s.	n.s.
	Gastropoda	1B > 3B	n.s.	n.s.
	Harpacticoida	1B > 3B	n.s.	n.s.
	Ostracoda	1B > 3B	FF > NF	n.s.
	Rhyncocoela	Interaction significant; see last column	Interaction significant; see last column	1B NF 1B FF 3B FF 3B NF
	Tanaidacea	1B > 3B	n.s.	n.s.
GB 516	Annelida	n.s.	NF > FF	n.s.
	Amphipoda	Interaction significant; see last column	Interaction significant; see last column	2B FF 1B FF 1B NF 2B NF
	Aplacophora	n.s.	n.s.	n.s.
	Bivalvia	n.s.	NF > FF	n.s.
	Gastropoda	n.s.	NF > FF	n.s.
	Harpacticoida	2B > 1B	n.s.	n.s.
	Nematoda	2B > 1B	n.s.	n.s.
	Ostracoda	n.s.	FF > NF	n.s.
	Rhyncocoela	n.s.	n.s.	n.s.
	Tanaidacea	n.s.	FF > NF	n.s.
GB 602	Annelida	N/A	NF > FF	--
	Aplacophora	N/A	NF > FF	--
	Bivalvia	N/A	NF > FF	--
	Gastropoda	N/A	NF > FF	--
	Harpacticoida	N/A	NF > FF	--
	Nematoda	N/A	FF > NF	--
	Rhyncocoela	N/A	NF > FF	--
	Tanaidacea	N/A	FF > NF	--
MC 292	Annelida	N/A	NF > FF	--
	Amphipoda	N/A	n.s.	--
	Aplacophora	N/A	n.s.	--
	Bivalvia	N/A	NF > FF	--
	Harpacticoida	N/A	NF > FF	--
	Nematoda	N/A	n.s.	--
	Ostracoda	N/A	n.s.	--
	Tanaidacea	N/A	n.s.	--

FF = far-field; NF = near-field; N/A = not applicable (only one cruise at GB 602 and MC 292);  
n.s. = not significant.

#### 11.4.2 Garden Banks Block 516

GB 516 was sampled on Cruise 1B (October-November 2000) and Cruise 2B (July 2001). Exploration wells were drilled at this site prior to the first cruise, and therefore both cruises were post-drilling. Several development wells were drilled between the two cruises (see *Chapter 3*).

**Table 11.10** summarizes macroinfaunal community statistics for GB 516 including density, diversity, evenness, and richness. There was considerable spatial and temporal variation in all of the community statistics. As shown in **Table 11.10** and illustrated in **Figure 11.6**, both near-field and far-field densities generally increased between the two cruises. Mean density at the near-field site was 4,901 individuals/m<sup>2</sup> on Cruise 1B and 11,087 individuals/m<sup>2</sup> on Cruise 2B. At the far-field sites, mean density was 1,692 individuals/m<sup>2</sup> on Cruise 1B and 2,838 individuals/m<sup>2</sup> on Cruise 2B. There was considerable overlap between near-field and far-field densities on both cruises. However, the range of densities was much greater in the near-field than in the far-field. Most notably, on both cruises, the near-field site included several stations that had much higher densities than any far-field sample.

**Figure 11.8** illustrates the taxonomic composition of the macroinfaunal samples at GB 516. At both near-field and far-field sites, annelids were the most abundant group on both cruises (37% to 50%). However, gastropods were the second most abundant group in the near-field (25% to 30%), compared with only 1% at the far-field sites.

Gastropod and/or annelid dominance also was evident when looking at some individual samples in the near-field. On Cruise 1B, the two near-field stations with the highest densities were NF-B02 and NF-B06. At NF-B02, gastropods accounted for 89% of the total population. At NF-B06, annelids were 78% of the total. On Cruise 2B, the two near-field stations with the highest densities were NF-B03 (48% annelids and 26% gastropods) and NF-B06 (66% gastropods).

ANOVA was conducted for individual macroinfaunal groups to test for spatial and temporal differences (**Table 11.9**). The significant ( $p < 0.05$ ) differences were as follows:

- For harpacticoids and nematodes, densities were significantly higher on Cruise 2B than on Cruise 1B.
- For annelids, bivalves, and gastropods, near-field densities were significantly higher than far-field densities.
- For ostracods and tanaids, far-field densities were significantly greater than near-field densities.

For amphipods, densities at far-field sites (both cruises) and the near-field on Cruise 1B were higher than for the near-field on Cruise 2B.

**Table 11.10.** Macroinfaunal community statistics for Garden Banks Block 516.

Station	No. Taxa	No. Individuals	Density (no./m <sup>2</sup> )	H' Diversity	J' Evenness	D Richness
<b>Cruise 1B (October-November 2000)</b>						
<b>Near-Field</b>						
NF-B01	10	636	6,360	0.90	0.39	1.39
NF-B02	8	1922	19,220	0.43	0.21	0.93
NF-B03	13	237	2,370	0.87	0.34	2.19
NF-B04	13	225	2,250	1.11	0.43	2.22
NF-B05	12	244	2,440	1.15	0.46	2.00
NF-B06	12	907	9,070	0.84	0.34	1.62
NF-B07	14	196	1,960	1.43	0.54	2.46
NF-B08	16	336	3,360	1.68	0.61	2.58
NF-B09	13	317	3,170	1.29	0.50	2.08
NF-B10	13	263	2,630	1.53	0.59	2.15
NF-B11	16	335	3,350	1.71	0.62	2.58
NF-B12	15	263	2,630	1.70	0.63	2.51
<b>Far-Field</b>						
FF1-B1	14	153	1,530	1.62	0.61	2.58
FF1-B2	13	226	2,260	1.57	0.61	2.21
FF2-B1	17	251	2,510	2.10	0.74	2.90
FF2-B2	12	75	750	1.89	0.76	2.55
FF3-B1	14	202	2,020	1.78	0.67	2.45
FF3-B2	12	78	780	1.80	0.72	2.52
FF4-B1	15	170	1,700	1.89	0.70	2.73
FF4-B2	16	152	1,520	1.63	0.59	2.99
FF5-B1	14	129	1,290	1.76	0.67	2.68
FF5-B2	15	181	1,810	1.85	0.68	2.69
FF6-B1	14	185	1,850	1.64	0.62	2.49
FF6-B2	13	228	2,280	1.72	0.67	2.21
<b>Cruise 2B (July 2001)</b>						
<b>Near-Field</b>						
NF-B01	7	177	1,770	1.42	0.73	1.16
NF-B02	12	716	7,160	1.59	0.64	1.67
NF-B03	11	3,738	37,380	1.42	0.59	1.22
NF-B04	14	380	3,800	1.16	0.44	2.19
NF-B05	12	542	5,420	1.93	0.78	1.75
NF-B06	5	2,446	24,460	0.71	0.44	0.51
NF-B07	16	1,302	13,020	1.34	0.48	2.09
NF-B08	15	862	8,620	1.37	0.51	2.07
NF-B09	8	2,434	24,340	0.85	0.41	0.90
NF-B10	12	173	1,730	1.68	0.67	2.13
NF-B11	12	126	1,260	1.75	0.70	2.27
NF-B12	16	408	4,080	1.82	0.66	2.50
<b>Far-Field</b>						
FF1-B1	17	174	1,740	2.29	0.81	3.10
FF1-B2	21	359	3,590	2.15	0.71	3.40
FF2-B1	12	142	1,420	1.92	0.77	2.22
FF2-B2	15	268	2,680	1.83	0.67	2.50
FF3-B1	15	284	2,840	1.86	0.69	2.48
FF3-B2	12	296	2,960	1.75	0.70	1.93
FF4-B1	17	174	1,740	2.20	0.78	3.10
FF4-B2	15	308	3,080	2.04	0.75	2.44
FF5-B1	16	248	2,480	2.12	0.76	2.72
FF5-B2	15	538	5,380	2.00	0.74	2.23
FF6-B1	17	296	2,960	1.94	0.68	2.81
FF6-B02	16	318	3,180	1.87	0.67	2.60

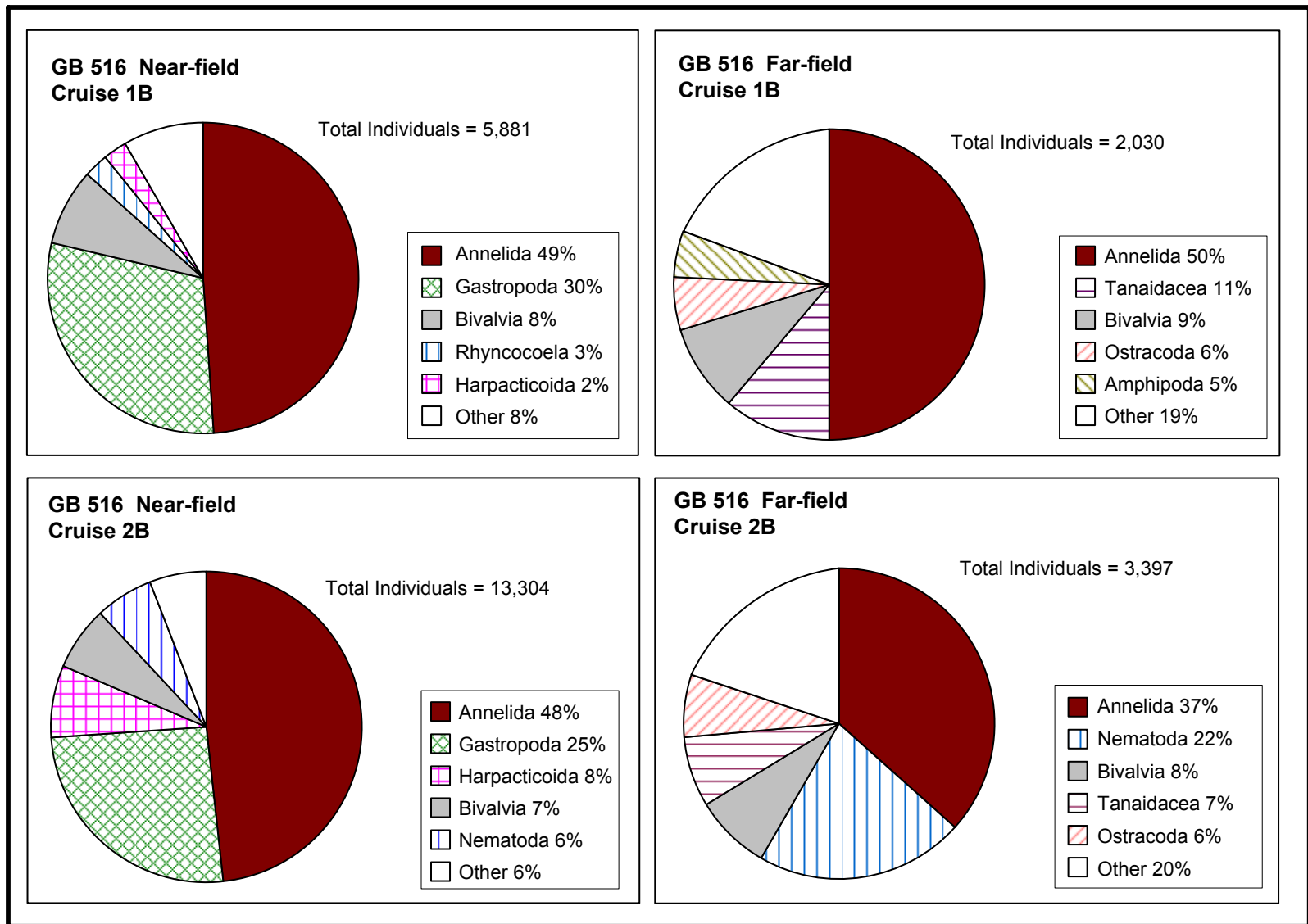


**Figure 11.8.** Taxonomic composition of macroinfauna at Garden Banks Block 516.

#### 11.4.3 Garden Banks Block 602

GB 602 was sampled only on Cruise 2B. **Table 11.11** summarizes macroinfaunal community statistics for GB 602 including density, diversity, evenness, and richness. There was considerable spatial and temporal variation in all of the community statistics. As shown in **Table 11.11** and in **Figure 11.5**, there was considerable overlap between near-field and far-field densities. However, the range of densities was much greater in the near-field than in the far-field. The near-field site included several stations that had much higher densities than any far-field sample. The lowest densities were seen at the far-field sites. Mean densities were 9,251 individuals/m<sup>2</sup> in the near-field and 1,743 individuals/m<sup>2</sup> in the far-field.

**Figure 11.9** illustrates the taxonomic composition of the macroinfaunal samples at GB 602. Annelids were the most abundant group in the near-field (47%) followed by harpacticoid copepods (20%) and gastropods (11%). The far-field was different in that nematodes were the most abundant group (34% vs. 26% for annelids), and gastropods accounted for less than 1% of the total.

Annelid and/or harpacticoid dominance was evident at near-field stations with high densities. The two near-field stations with the highest densities were NF-B03 and NF-B05. At NF-B03, annelids accounted for 88% of the total population. At NF-B05, harpacticoid copepods were 60% of the total.

ANOVA was conducted for individual macroinfaunal groups to test for spatial and temporal differences (**Table 11.9**). The significant ( $p < 0.05$ ) differences were as follows:

- Annelids, aplousobranchs, bivalves, gastropods, harpacticoids, and rhynchocoelans were more abundant at the near-field site than at the far-field sites.
- Nematodes and tanaids were more abundant at the far-field sites than at the near-field site.

#### 11.4.4 Mississippi Canyon Block 292

MC 292 was sampled only on Cruise 2B. **Table 11.12** summarizes macroinfaunal community statistics for GB 602 including density, diversity, evenness, and richness. There was considerable spatial and temporal variation in all of the community statistics. As shown in **Table 11.12** and in **Figure 11.5**, there was considerable overlap between near-field and far-field densities. The near-field site included several stations that had much higher densities than any far-field sample. The lowest density was observed at one far-field site. Mean densities were 10,327 individuals/m<sup>2</sup> in the near-field and 5,448 individuals/m<sup>2</sup> in the far-field.

**Figure 11.9** illustrates the taxonomic composition of the macroinfaunal samples at MC 292. Annelids were the most abundant group in the near-field (39%) followed by harpacticoid copepods (20%) and nematodes (18%). The far-field was different in that nematodes were the most abundant group (30% vs 24% for annelids), and harpacticoid copepods were less than 1% of the population.

The two near-field stations with the highest densities were NF-B01 and NF-B03. At NF-B01, harpacticoids were 48%, and annelids accounted for 41% of the total population. At NF-B03, nematodes and annelids each accounted for 34% of the total.



**Table 11.11.** Macroinfaunal community statistics for Garden Banks Block 602, Cruise 2B (July 2001).

Station	No. Taxa	No. Individuals	Density (no./m <sup>2</sup> )	H' Diversity	J' Evenness	D Richness
<b>Near-Field</b>						
NF-B01	14	278	2,780	1.80	0.68	2.31
NF-B02	7	1,144	11,440	1.31	0.67	0.85
NF-B03	6	2,310	23,100	0.47	0.26	0.65
NF-B04	8	196	1,960	1.77	0.85	1.33
NF-B05	13	2,192	21,920	1.10	0.43	1.56
NF-B06	7	761	7,610	1.08	0.55	0.90
NF-B07	5	170	1,700	1.45	0.90	0.78
NF-B08	9	1,045	10,450	0.62	0.28	1.15
NF-B09	10	1,218	12,180	1.25	0.54	1.27
NF-B10	9	554	5,540	1.52	0.69	1.27
NF-B11	7	538	5,380	1.65	0.85	0.95
NF-B12	13	695	6,950	1.73	0.67	1.83
<b>Far-Field</b>						
FF1-B1	11	143	1,430	1.92	0.80	2.01
FF1-B2	16	315	3,150	1.73	0.62	2.61
FF2-B1	11	151	1,510	1.81	0.76	1.99
FF2-B2	20	176	1,760	2.01	0.67	3.67
FF3-B1	13	196	1,960	1.91	0.74	2.27
FF3-B2	14	125	1,250	1.72	0.65	2.69
FF4-B1	16	252	2,520	2.02	0.73	2.71
FF4-B2	12	186	1,860	1.69	0.68	2.10
FF5-B1	14	80	800	2.13	0.81	2.97
FF5-B2	14	150	1,500	2.18	0.83	2.59
FF6-B1	16	227	2,270	2.08	0.75	2.77
FF6-B2	10	91	910	1.87	0.81	2.00

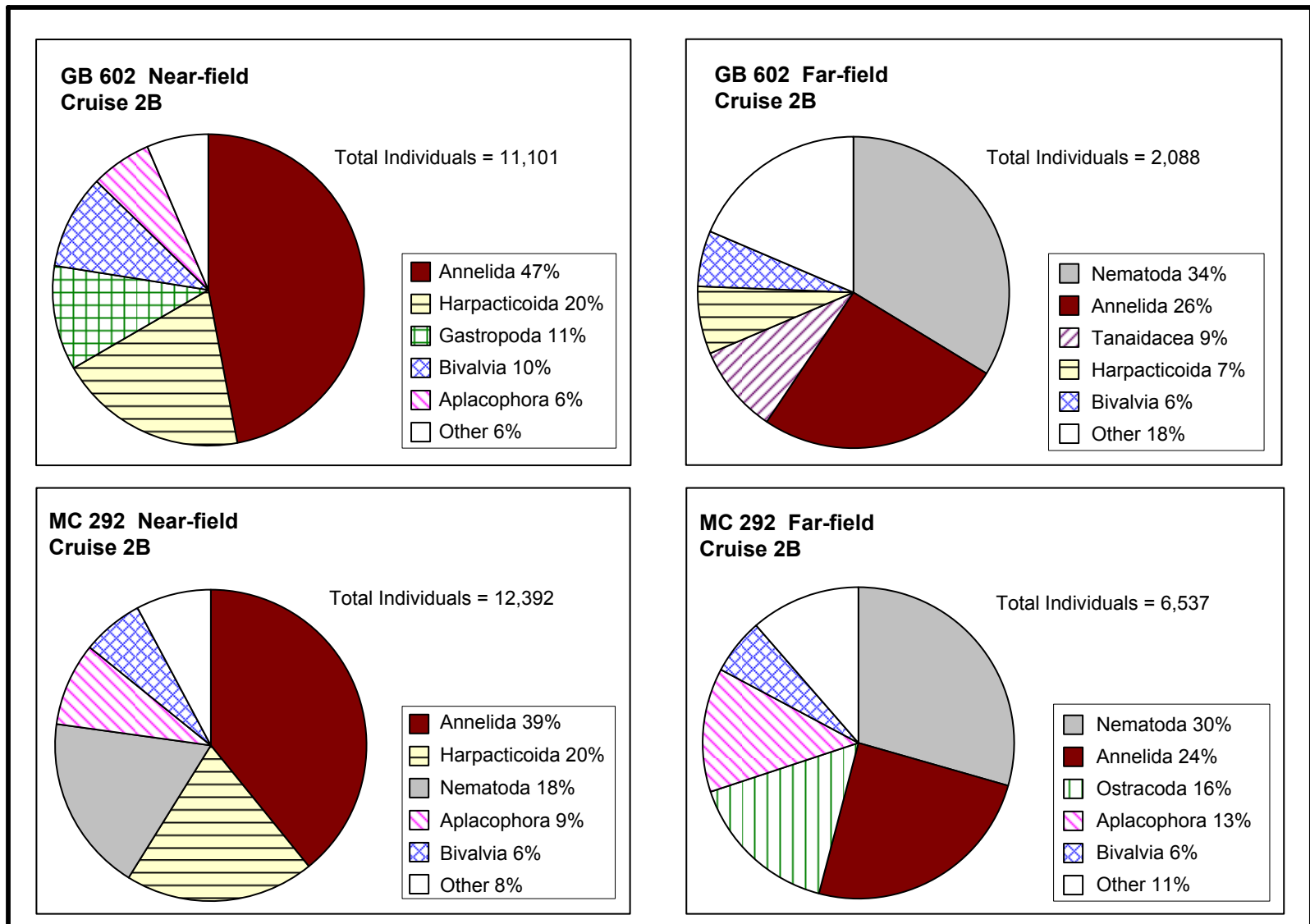


**Figure 11.9.** Taxonomic composition of macroinfauna at Garden Banks Block 602 and Mississippi Canyon Block 292.

**Table 11.12.** Macroinfaunal community statistics for Mississippi Canyon Block 292, Cruise 2B (July 2001).

Station	No. Taxa	No. Individuals	Density (no./m <sup>2</sup> )	H' Diversity	J' Evenness	D Richness
<b>Near-Field</b>						
NF-B01	11	4,580	45,800	1.13	0.47	1.19
NF-B02	9	492	4,920	1.15	0.52	1.29
NF-B03	15	1,423	14,230	1.69	0.62	1.93
NF-B04	17	785	7,850	1.95	0.69	2.40
NF-B05	14	820	8,200	1.70	0.64	1.94
NF-B06	16	1,186	11,860	1.51	0.54	2.12
NF-B07	17	814	8,140	1.71	0.60	2.39
NF-B08	9	538	5,380	1.11	0.50	1.27
NF-B09	14	811	8,110	1.77	0.67	1.94
NF-B10	14	691	6,910	1.63	0.62	1.99
NF-B11	8	89	890	1.13	0.55	1.56
NF-B12	13	163	1,630	1.59	0.62	2.36
<b>Far-Field</b>						
FF1-B1	15	560	5,600	1.90	0.70	2.21
FF1-B2	13	846	8,460	1.46	0.57	1.78
FF2-B1	2	46	460	0.57	0.83	0.26
FF2-B2	17	683	6,830	1.62	0.58	2.30
FF3-B1	14	350	3,500	1.69	0.64	2.22
FF3-B2	14	215	2,150	1.97	0.75	2.42
FF4-B1	15	725	7,250	1.88	0.69	2.13
FF4-B2	16	831	8,310	1.86	0.67	2.23
FF5-B1	13	509	5,090	1.88	0.73	1.93
FF5-B2	12	95	950	1.85	0.74	2.42
FF6-B1	16	1,133	11,330	1.78	0.66	1.99
FF6-B2	14	545	5,450	1.83	0.69	2.06

ANOVA was conducted for individual macroinfaunal groups to test for spatial and temporal differences (**Table 11.9**). The significant ( $p < 0.05$ ) differences were as follows:

- Annelids, bivalves, and harpacticoid copepods were more abundant at the near-field site than at far-field sites.

Taxa that did not exhibit differences in abundance between near-field and far-field sites were amphipods, aplacophorans, nematodes, ostracods, and tanaids.

#### 11.4.5 Individual Groups and Environmental Correlations

The six most abundant groups from the macroinfaunal data (annelids, gastropods, bivalves, amphipods, ostracods, and aplacophorans) were selected for further plotting and analysis.

**Figures 11.10** and **11.11** show densities of these individual groups in all post-drilling samples, with each point representing an individual sample. For annelids, gastropods, and bivalves, there was a strong, consistent tendency for the highest densities to occur in the near-field.

Aplacophorans showed a similar trend at GB 516 and GB 602, though not at VK 916. The opposite was true for amphipods and ostracods, with the highest densities occurring at one or more far-field stations (except for GB 516 on Cruise 1B).

Correlations were calculated between densities of these macroinfaunal groups and environmental variables (barium, SBF, and TOC concentrations; sediment sand, silt, and clay percentages).

Only stations exposed to drilling discharges were included in this analysis (i.e., near-field, post-drilling). Results are summarized in **Table 11.13**.

Selected relationships between densities of individual groups and barium, SBF, and TOC concentrations are illustrated in **Figures 11.12** and **11.13** (annelids), **Figure 11.14** (gastropods), **Figure 11.15** (amphipods), and **Figure 11.16** (ostracods).

##### 11.4.5.1 Annelids

Annelid densities tended to be positively correlated with sediment barium, SBF, and TOC, though the correlation was significant in only a few cases (**Table 11.13**). Overall, barium was the strongest correlate. Nearly all far-field stations and some near-field stations had annelid densities less than 2,000 individuals/m<sup>2</sup>. Some near-field stations on post-drilling cruises had up to 10 times higher densities. Generally, stations with elevated annelid densities had barium concentrations of 10,000 µg/g or higher (**Figure 11.12**) and SBF concentrations of 1,000 µg/g or higher (**Figure 11.13**).

##### 11.4.5.2 Gastropods

Gastropod densities tended to be positively correlated with sediment barium, SBF, and to a lesser extent, TOC (**Table 11.13**). Densities also tended to be positively correlated with sand percentages. Only a few of the correlations were significant.

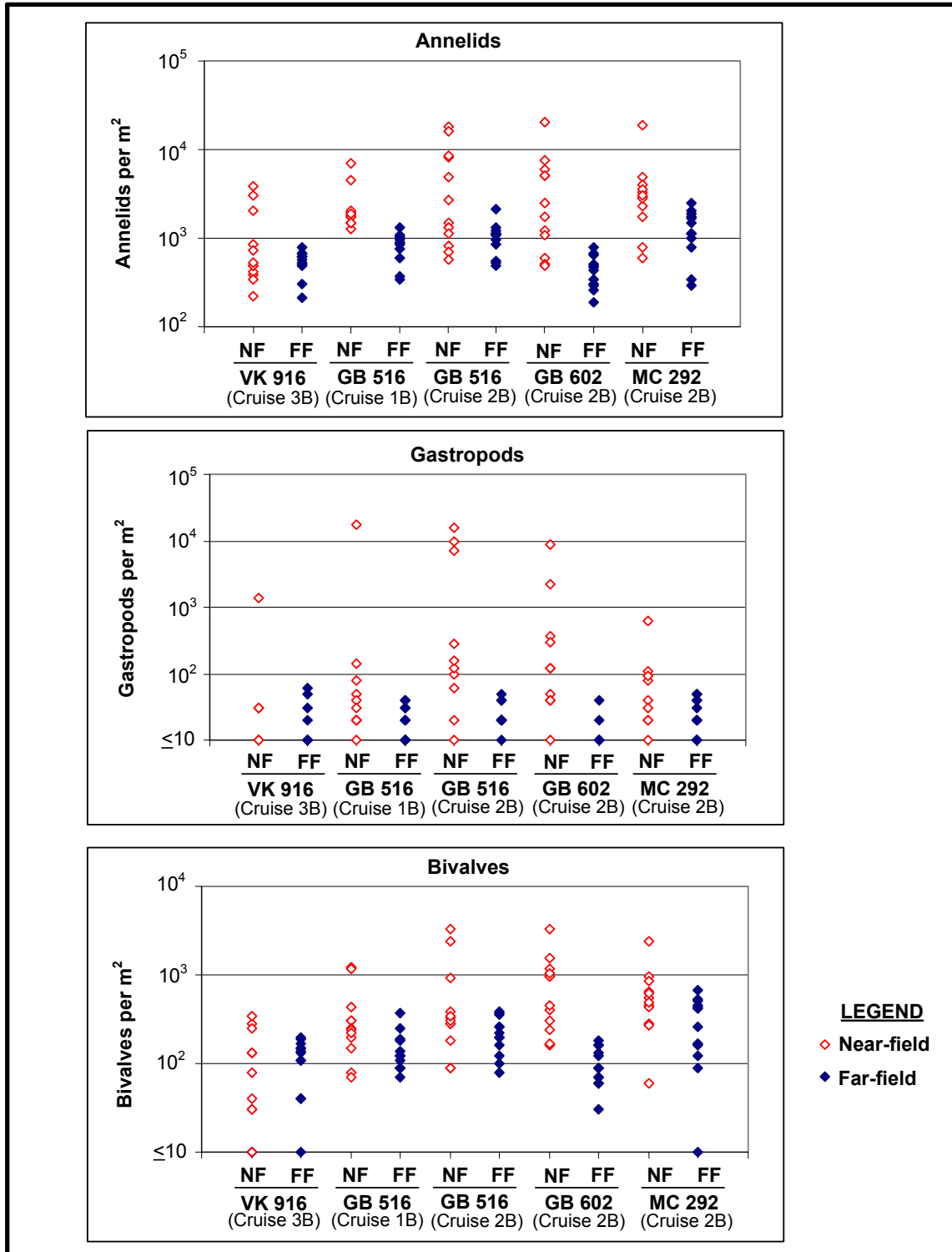


**Figure 11.10.** Comparison of near-field and far-field abundances of macroinfaunal annelids, gastropods, and bivalves in post-drilling samples. Note the log scale.

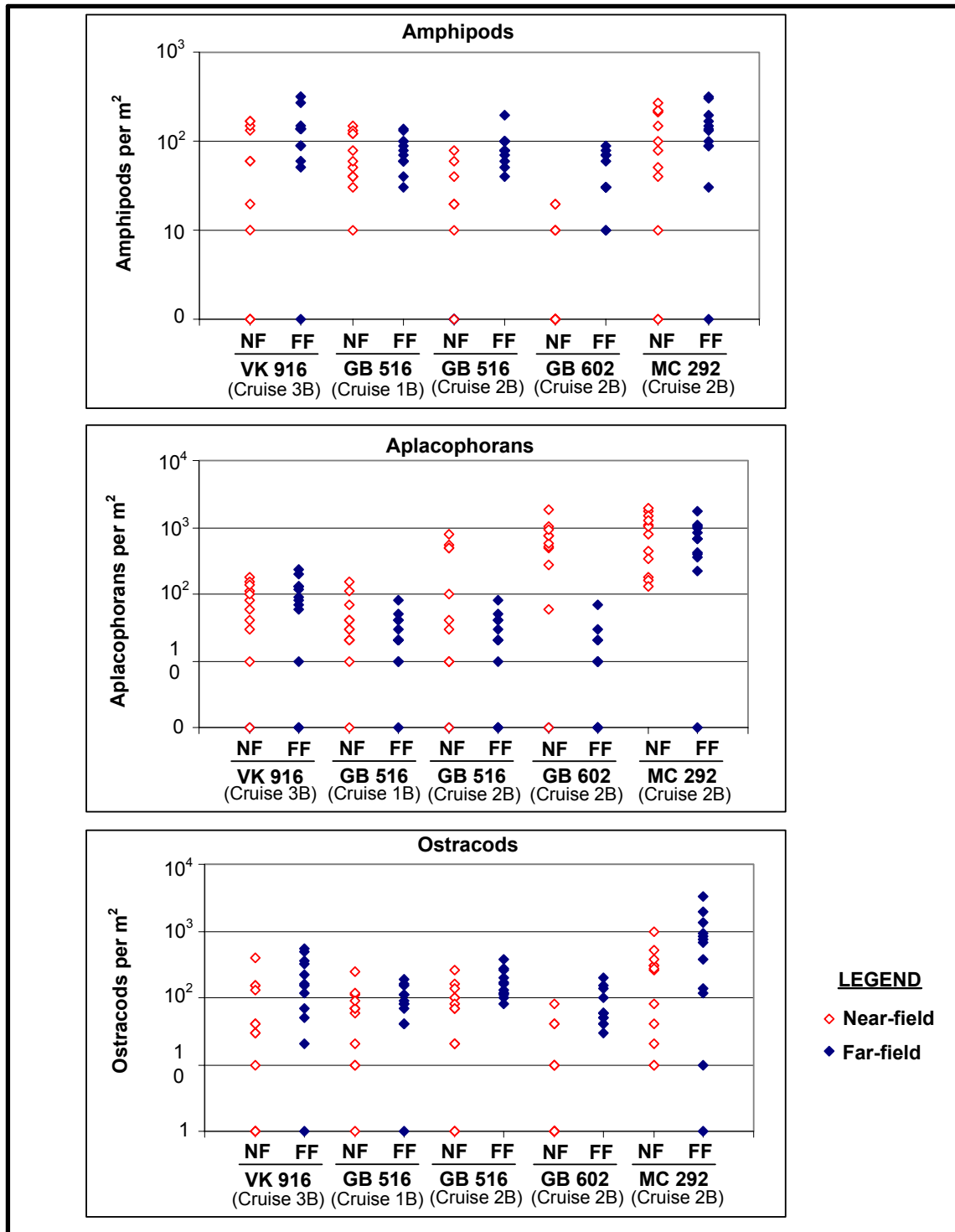
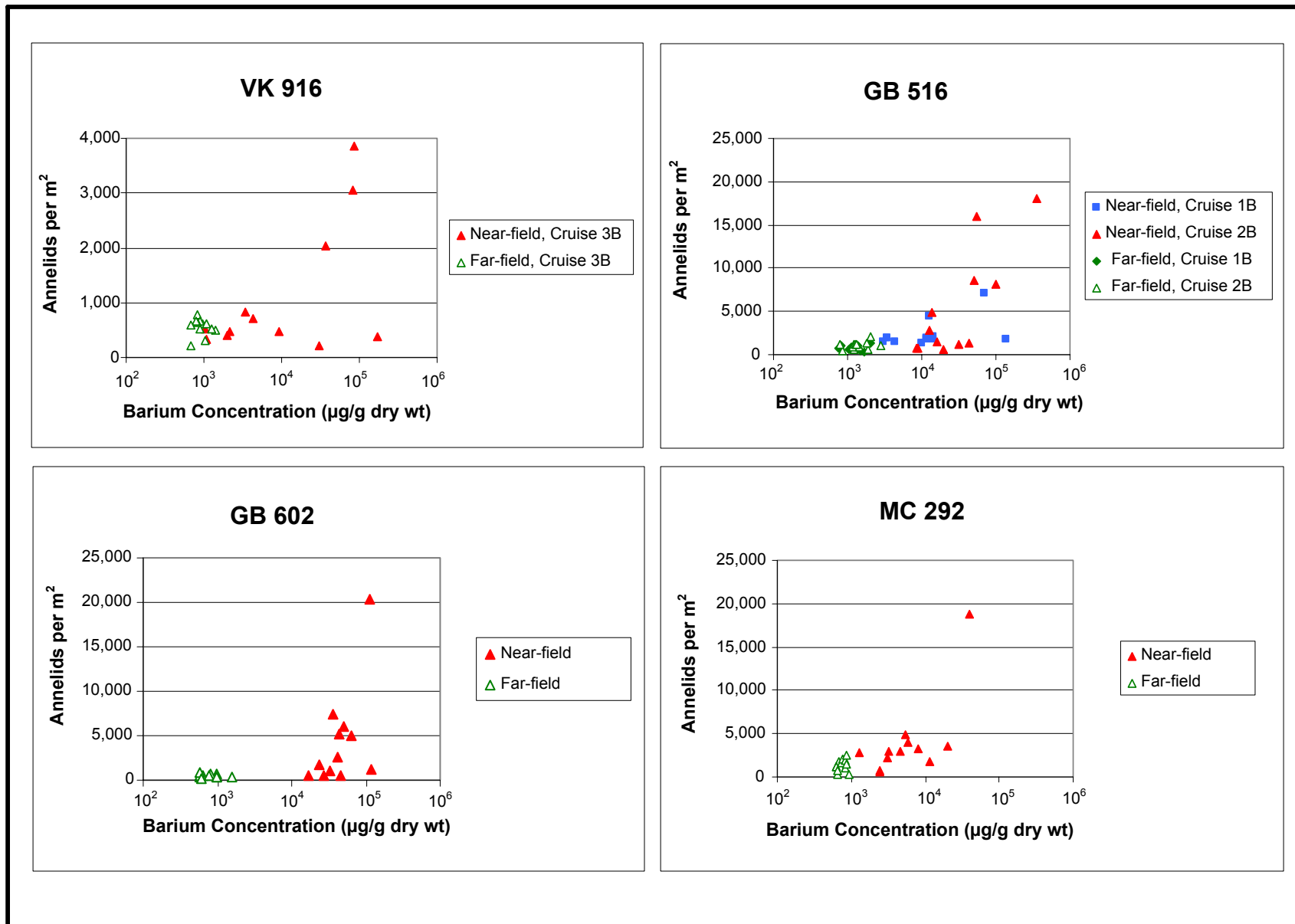


Figure 11.11. Comparison of near-field and far-field abundances of macroinfaunal amphipods, aplacophorans, and ostracods in post-drilling samples. Note the log scale.

**Table 11.13.** Rank correlation coefficients (Spearman's rho) between macroinfaunal densities and environmental variables within areas exposed to drilling discharges (near-field sites on post-drilling cruises). Statistically significant correlation coefficients ( $p < 0.05$ ), i.e., those large enough that they are probably not due to chance, are bold and double-underlined.

Group	Site	Cruise	Correlation Coefficient vs. Environmental Variable					
			Barium	SBF	TOC	Sand	Silt	Clay
Annelida	VK 916	3B	0.319	0.459	0.347	0.291	0.084	-0.277
	GB 516	1B	0.452	0.263	0.280	-0.049	-0.035	0.035
	GB 516	2B	<b><u>0.706</u></b>	<b><u>0.748</u></b>	0.126	0.210	0.566	-0.483
	GB 602	2B	0.420	0.210	<b><u>0.585</u></b>	0.090	-0.035	-0.035
	MC 292	2B	<b><u>0.671</u></b>	0.504	0.046	-0.007	-0.357	0.147
Gastropoda	VK 916	3B	0.324	0.505	0.257	0.373	0.516	-0.516
	GB 516	1B	0.399	0.135	-0.170	<b><u>0.731</u></b>	0.089	-0.089
	GB 516	2B	<b><u>0.883</u></b>	<b><u>0.669</u></b>	0.221	<b><u>0.595</u></b>	0.462	-0.493
	GB 602	2B	0.429	<b><u>0.615</u></b>	<b><u>0.866</u></b>	0.169	0.018	-0.109
	MC 292	2B	0.557	0.444	0.405	0.296	-0.138	-0.208
Bivalvia	VK 916	3B	-0.148	-0.163	-0.281	0.113	0.049	-0.039
	GB 516	1B	0.438	0.322	0.193	-0.014	0.165	-0.165
	GB 516	2B	0.442	0.411	-0.311	0.151	0.295	-0.133
	GB 602	2B	-0.287	-0.504	-0.515	0.077	-0.357	0.385
	MC 292	2B	<b><u>0.566</u></b>	0.504	0.298	0.329	0.014	-0.231
Amphipoda	VK 916	3B	-0.475	-0.507	<b><u>-0.637</u></b>	-0.354	-0.007	0.239
	GB 516	1B	<b><u>-0.850</u></b>	<b><u>-0.691</u></b>	-0.081	-0.189	-0.131	0.131
	GB 516	2B	-0.168	-0.409	-0.307	-0.219	-0.226	0.307
	GB 602	2B	-0.158	-0.138	0.039	-0.296	0.237	-0.217
	MC 292	2B	-0.488	-0.526	<b><u>-0.633</u></b>	-0.091	0.021	-0.067
Ostracoda	VK 916	3B	-0.262	-0.142	-0.250	-0.046	0.145	0.060
	GB 516	1B	<b><u>-0.620</u></b>	<b><u>-0.635</u></b>	0.004	0.208	-0.212	0.212
	GB 516	2B	-0.014	-0.134	0.032	0.003	-0.049	0.063
	GB 602	2B	-0.385	-0.196	0.315	<b><u>-0.599</u></b>	0.136	0.004
	MC 292	2B	-0.281	-0.446	<b><u>-0.640</u></b>	0.098	-0.007	-0.091
Aplacophora	VK 916	3B	-0.235	-0.326	-0.456	-0.003	0.249	-0.084
	GB 516	1B	0.269	0.276	0.322	-0.182	<b><u>-0.594</u></b>	<b><u>0.594</u></b>
	GB 516	2B	0.339	0.152	-0.527	0.244	-0.046	0.018
	GB 602	2B	-0.361	-0.491	<b><u>-0.576</u></b>	0.102	-0.425	0.470
	MC 292	2B	0.000	-0.035	-0.098	0.091	-0.091	-0.140



**Figure 11.12.** Annelid (predominantly polychaete) densities vs. barium concentrations on post-drilling cruises. Note the log scale for barium concentrations and the different density scale for VK 916.



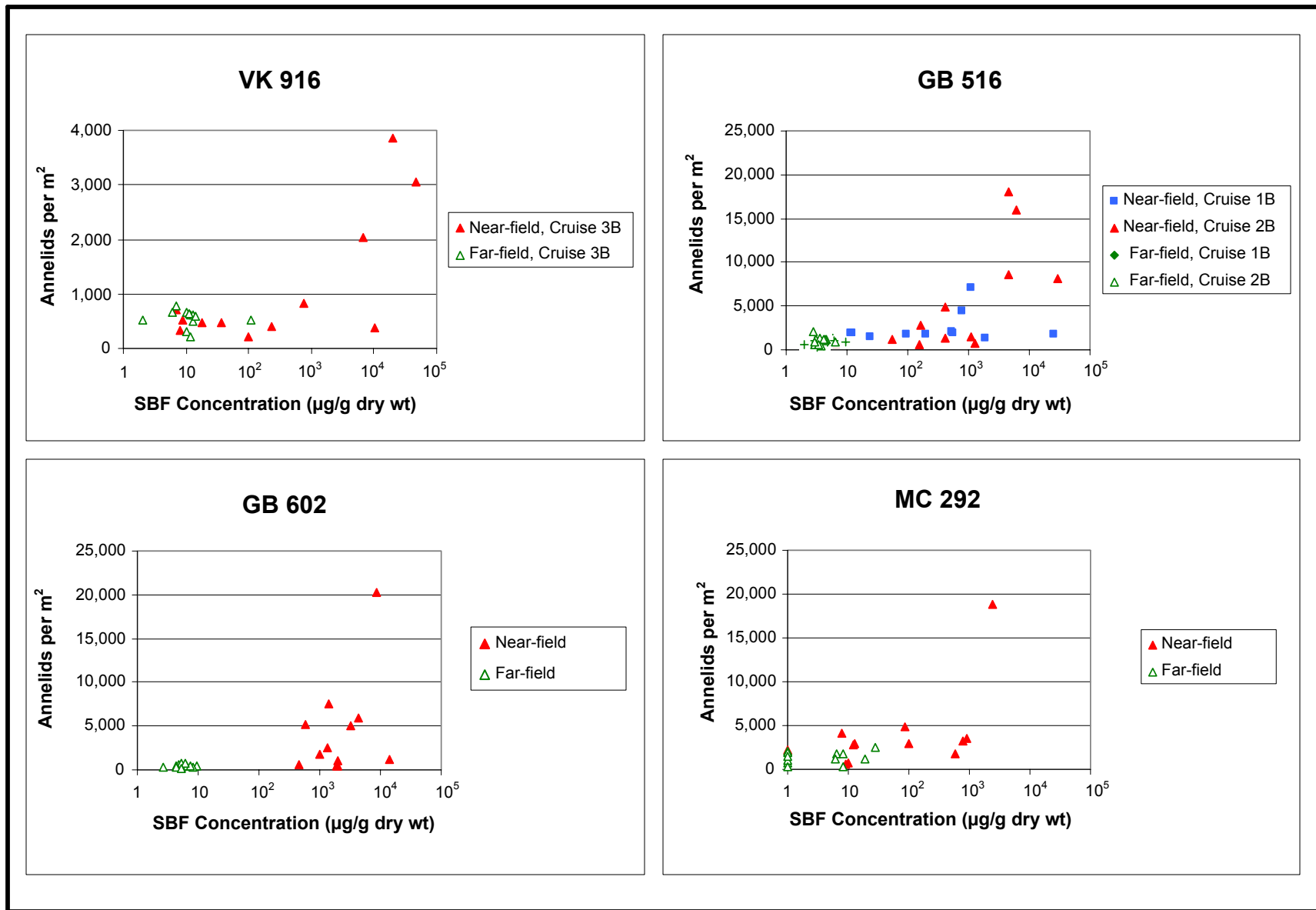


**Figure 11.13.** Annelid (predominantly polychaete) densities vs. synthetic-based fluid (SBF) concentrations on post-drilling cruises. Note the log scale for SBF concentrations and the different density scale for VK 916.

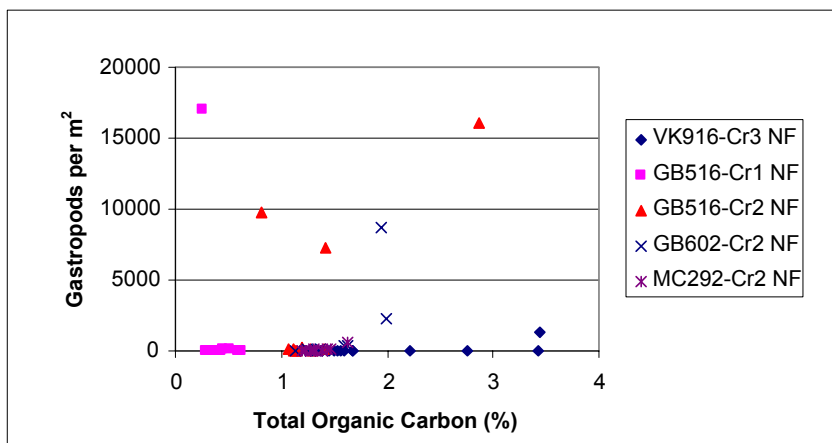
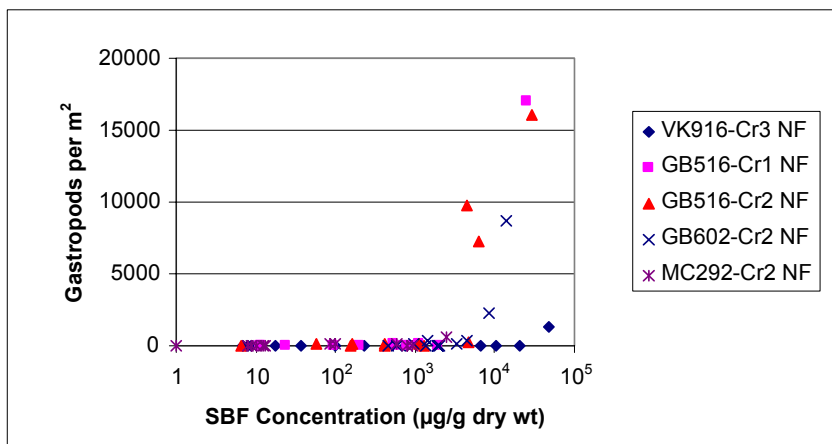
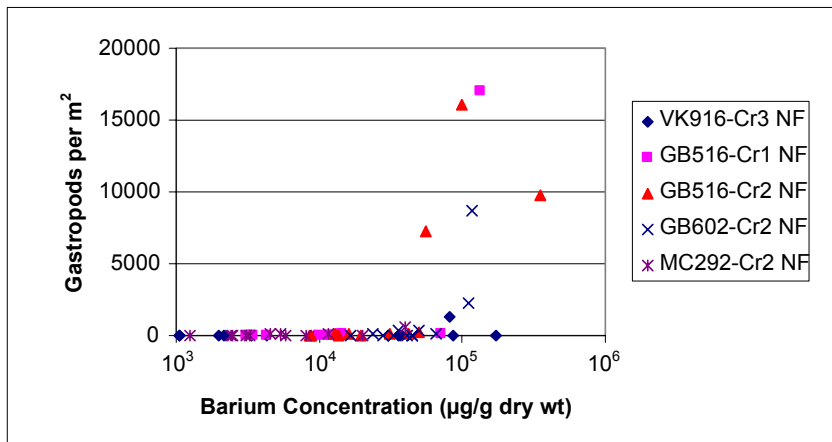


**Figure 11.14.** Gastropod densities vs. sediment barium, synthetic-based fluid (SBF), and total organic carbon concentrations at near-field (NF), post-drilling stations. Note the log scale for barium and SBF concentrations.

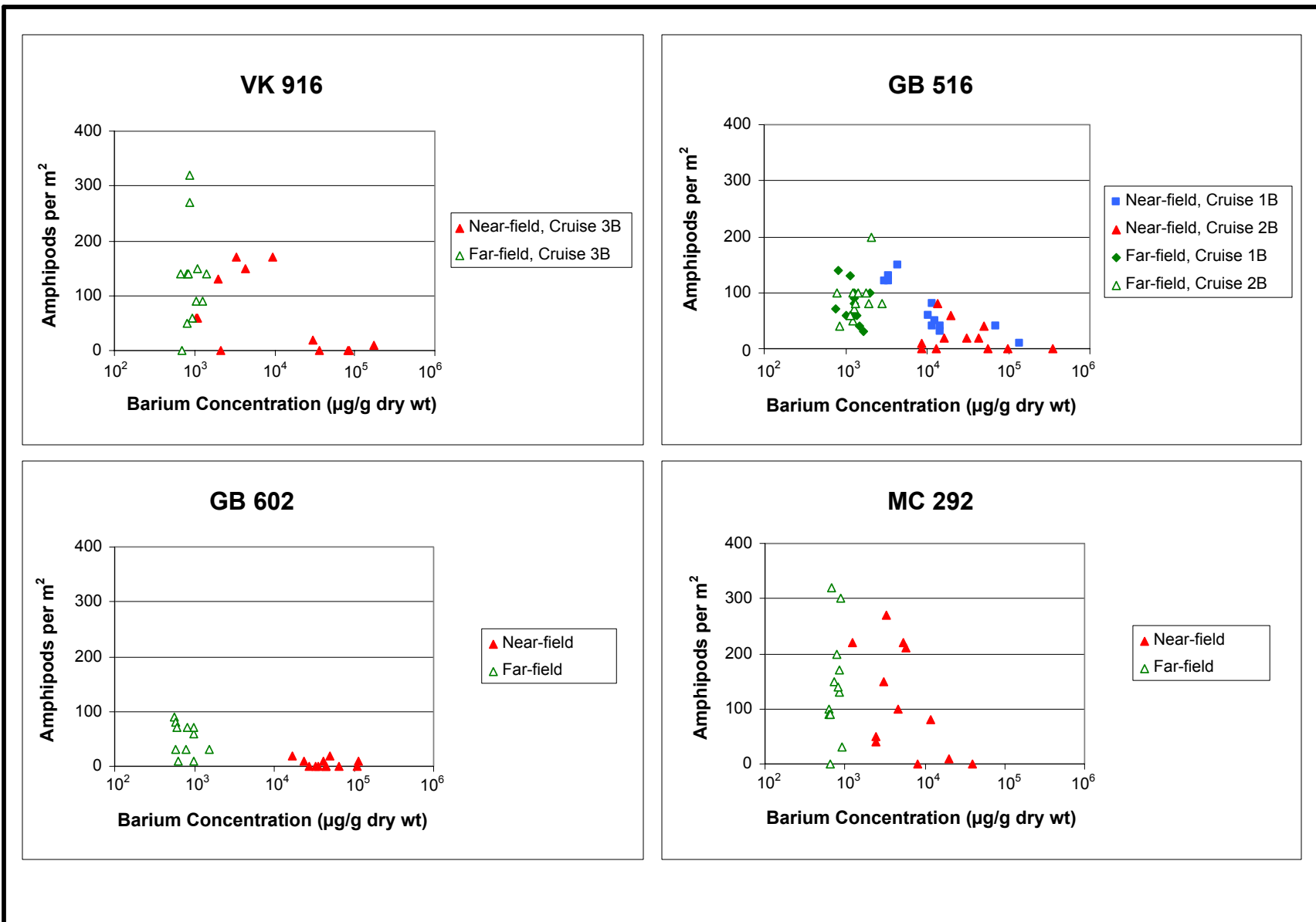


**Figure 11.15.** Amphipod densities vs. sediment barium concentrations on post-drilling cruises. Note the log scale for barium concentrations.

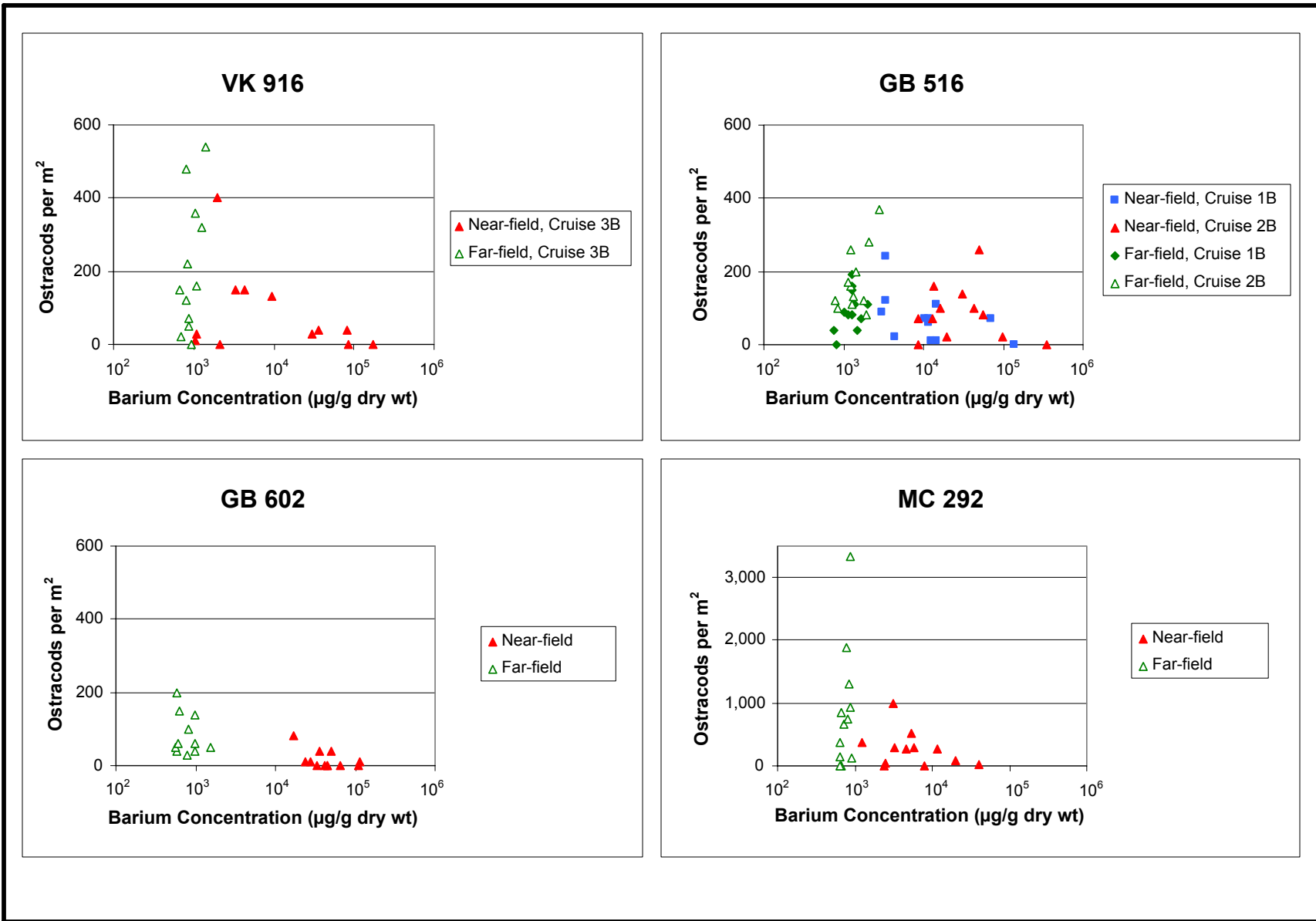


Figure 11.16. Ostracod densities vs. sediment barium concentrations on post-drilling cruises. Note the log scale for barium concentrations.

As shown in **Figure 11.14**, the relationship between gastropods and drilling fluid indicators was striking. All far-field stations and most near-field stations had low gastropod densities (generally less than 100 individuals/m<sup>2</sup>). However, a few near-field stations at GB 516 and GB 602 had much higher densities, up to 17,000 individuals/m<sup>2</sup>. The extremely high densities were associated with SBF concentrations of 4,500 µg/g or higher and barium concentrations of 55,000 µg/g and higher. Much weaker relationships were observed at VK 916 and MC 292. VK 916 had several stations with high SBF concentrations and few gastropods (or none). **Figure 11.14** also shows there is no overall consistent relationship between gastropod densities and TOC.

#### 11.4.5.3 Bivalves

There were no strong, consistent correlations between bivalve abundance and sediment barium, SBF, TOC, or grain size fractions. There was a significant positive correlation with barium at MC 292 on Cruise 2B (**Table 11.13**).

#### 11.4.5.4 Amphipods

Amphipod densities tended to be negatively correlated with barium, SBF, and TOC concentrations, though only a few of the correlations were significant (**Table 11.13**). The weakest correlations were at GB 602. As shown in **Figure 11.15**, amphipod densities at far-field stations ranged from 0 to 320 individuals/m<sup>2</sup>. Generally, near-field stations with barium concentrations higher than about 10,000 µg/g and/or SBF concentrations greater than about 1,000 µg/g had low amphipod densities.

#### 11.4.5.5 Ostracods

Ostracod densities tended to be negatively correlated with barium and SBF concentrations, though the correlations were significant only at GB 516 on Cruise 1B (**Table 11.13**). At GB 602, ostracod abundance was negatively correlated with sand. At MC 292, ostracod abundance was negatively correlated with TOC. With the exception of GB 516, near-field stations with barium concentrations higher than about 10,000 µg/g (**Figure 11.16**) and/or SBF concentrations greater than about 1,000 µg/g had low ostracod densities.

#### 11.4.5.6 Aplacophorans

There were no consistent correlations between aplacophoran abundance and sediment barium, SBF, TOC, or grain size fractions (**Table 11.13**). At GB 516 on Cruise 1B, aplacophoran abundance was correlated negatively with silt and positively with clay. At GB 602, aplacophoran abundance was negatively correlated with TOC.

### 11.4.6 Detailed Macroinfaunal Taxonomic Analysis

#### 11.4.6.1 Community Characteristics

Twenty-four stations were selected for detailed taxonomic analysis. These included near-field and far-field locations at each site on each cruise (**Table 11.14**).

**Table 11.14.** Samples included in the 24-station analysis of macroinfauna.

Site	Cruise	Samples Included
Viosca Knoll Block 916	1B	NF-B04
		NF-B11
		FF2-B01
	3B	FF6-B01
		NF-B03
		NF-B07
FF1-B02		
Garden Banks Block 516	1B	FF5-B01
		NF-B02
		NF-B06
	2B	FF1-B02
		FF6-B02
		NF-B03
Garden Banks Block 602	2B	NF-B08
		FF3-B02
		FF5-B02
	2B	NF-B01
		NF-B03
		FF1-B01
Mississippi Canyon Block 292	2B	FF4-B01
		NF-B03
		NF-B06
		FF4-B02
		FF6-B01

In the detailed taxonomic analysis, 266 macroinfaunal taxa were identified, including 119 polychaetes, 86 crustaceans, 26 bivalves, 21 gastropods, two echinoderms, two rhynchocoels, two scaphopods, one oligochaete, and seven other taxa that were identified only to phylum (nematodes, sipunculids, sponges, turbellarians), order (actinarians), or class (aplacophorans, enteropneusts) (*Appendix I2*). The most abundant macroinfauna were the polychaete *Aphelocheata* sp. B (17.2% of collected individuals), the gastropods *Solariella* sp. A (8.5%) and *Ganosa* sp. A (6.7%), Nematoda (LPIL) (5.7%), and Aplacophora (LPIL) (5.5%) (**Table 11.15**). The most widespread taxa were non-identified bivalves and spionid polychaetes, both of which were collected at 22 of the 24 stations, followed by non-identified aplacophorans, maldanid polychaetes, and rhychocoels found at 20 stations.

The basic community statistics for each of the 24 stations are summarized in **Table 11.16**. (The values differ from those presented earlier for the same stations because individuals were identified to LPIL for this analysis.) The total number of taxa per sample ranged from 13 to 123. Total number of individuals ranged from 138 to 3,818.  $H'$  ranged from 0.58 to 3.85,  $J'$  ranged from 0.22 to 0.90, and D ranged from 1.72 to 17.21.

**Table 11.15.** Ten most abundant macroinfaunal taxa for the 24-station analysis.

Taxon	Type of Organism	Count
<i>Aphelocheata</i> sp. B	Polychaete	3,426
<i>Solariella</i> sp. A	Gastropod mollusc	1,701
<i>Ganesa</i> sp. A	Gastropod mollusc	1,326
Nematoda (LPIL)	Nematode	1,143
Aplacophora (LPIL)	Aplacophoran mollusc	1,093
Harpacticoida (LPIL)	Harpacticoid copepod	845
Maldanidae (LPIL)	Polychaete	796
Bivalvia (LPIL)	Bivalve mollusc	682
<i>Actinocythereis</i> sp. E	Ostracod	620
<i>Ophryotrocha</i> sp. D	Polychaete	464

**Table 11.16.** Macroinfauna community statistics for the 24-station analysis.

Station	Cruise	No. Taxa	No. Individ.	H' Diversity	J' Evenness	D Richness
<b>Viosca Knoll Block 916</b>						
VK916-NF-B04	1B	123	1,197	3.79	0.79	17.21
VK916-NF-B11	1B	86	655	3.48	0.78	13.11
VK916-FF2-B01	1B	94	1,108	3.48	0.77	13.27
VK916-FF6-B01	1B	82	1,117	3.13	0.71	11.54
VK916-NF-B03	3B	60	191	3.63	0.89	11.23
VK916-NF-B07	3B	13	451	0.82	0.32	1.96
VK916-FF1-B02	3B	35	184	2.88	0.81	6.52
VK916-FF5-B01	3B	45	139	3.43	0.90	8.92
<b>Garden Banks Block 516</b>						
GB516-NF-B02	1B	14	1,903	0.58	0.22	1.72
GB516-NF-B06	1B	56	878	2.55	0.63	8.12
GB516-FF1-B02	1B	65	215	3.44	0.82	11.92
GB516-FF6-B02	1B	72	214	3.85	0.90	13.23
GB516-NF-B03	2B	34	3,818	2.31	0.65	4.00
GB516-NF-B08	2B	55	796	2.67	0.67	8.08
GB516-FF3-B02	2B	59	270	3.43	0.84	10.36
GB516-FF5-B02	2B	72	488	3.65	0.85	11.47
<b>Garden Banks Block 602</b>						
GB602-NF-B03	2B	19	2,316	0.75	0.25	2.32
GB602-NF-B01	2B	42	270	2.54	0.68	7.32
GB602-FF1-B01	2B	53	138	3.54	0.89	10.55
GB602-FF4-B01	2B	65	149	3.60	0.86	12.79
<b>Mississippi Canyon Block 292</b>						
MC292-NF-B03	2B	99	1,433	2.90	0.63	13.48
MC292-NF-B06	2B	84	638	3.43	0.77	12.85
MC292-FF4-B02	2B	63	612	2.86	0.69	9.66
MC292-FF6-B01	2B	72	736	3.26	0.76	10.76

**Figure 11.17** shows the same data, but with stations grouped into two subsets:

- Near-drilling = all near-field stations at GB 516, GB 602, and MC 292, plus near-field stations at VK 916 on Cruise 3B (post-drilling).
- Away from drilling = all far-field stations plus VK 916 near-field stations from Cruise 1B (pre-drilling).

As summarized in the figure, some stations “near drilling” had higher densities, lower diversity, lower evenness, and lower richness indices compared with stations “away from drilling.” Other “near-drilling” stations had community characteristics similar to those of the “away from drilling” stations.

#### 11.4.6.2 Community Structure Comparisons

**Figure 11.18** summarizes the results of MDS ordination for the 24-station dataset. MDS ordination identified four main station (sample) groups (A through D) that were similar with respect to species composition and relative abundance (**Table 11.17**). Two individual stations were dissimilar to the others and were designated as Groups E and F.

Some geographic influence is evident in the groupings. Groups A and B consist of stations from GB 516 and GB 602, which are very close geographically (within tens of kilometers). Groups C and D include stations from VK 916 (Group C) or both VK 916 and MC 292 (Group D), which are relatively close to each other, but about 400 km from the two Garden Banks sites.

Drilling impacts also are evident in the groupings. The two “outlier” stations (Groups E and F) are both near-field, post-drilling stations, and they had the highest SBF concentrations among the 24 stations (47,920  $\mu\text{g/g}$  and 25,131  $\mu\text{g/g}$ , respectively) (**Figure 11.19**). Both were dominated by taxa that were not found at other stations. Group E (Station VK916-NF-B07) was numerically dominated by the polychaete *Capitella capitata*, a classic indicator of organic enrichment, and Group F (Station GB516-NF-B02) was numerically dominated by the gastropod *Solariella* sp. A.

Group A includes only near-field, post-drilling stations at GB 516 and GB 602. These stations had barium concentrations ranging from 13,500 to 351,000  $\mu\text{g/g}$  and SBF concentrations ranging from 418 to 8,446  $\mu\text{g/g}$ . Groups B, C, and D presumably reflect little or no drilling impact. Most of the stations are far-field or near-field pre-drilling. Each group included one or two near-field post-drilling stations, but those tended to be at the low end of the range compared to the high barium and SBF concentrations seen for Groups A, E, and F.

Taxa typifying station groups, determined with SIMPER, are presented in **Table 11.18**. As indicated by lower average levels of similarity, Groups A and B had more assemblage variability between stations than Groups C and D. Group A was distinguished from other groups mostly due to high abundances of the polychaete *Aphelochoeta* sp. B. This genus has been identified as an indicator of organic enrichment in some studies (Llansó et al. 1998). Group B stations yielded relatively high abundances of non-identified spionid polychaetes and nematodes. Group C stations yielded certain taxa that were rare at other stations, such as the polychaete *Sthenolepis* sp. D and the amphipod *Harpiniopsis* sp. A. Group D stations yielded high abundances of non-identified maldanid polychaetes and aplacophorans, as well as polychaetes such as *Cossura soyeri* and *Scoletoma verrilli*, which were rare or absent at stations in Groups A through C.



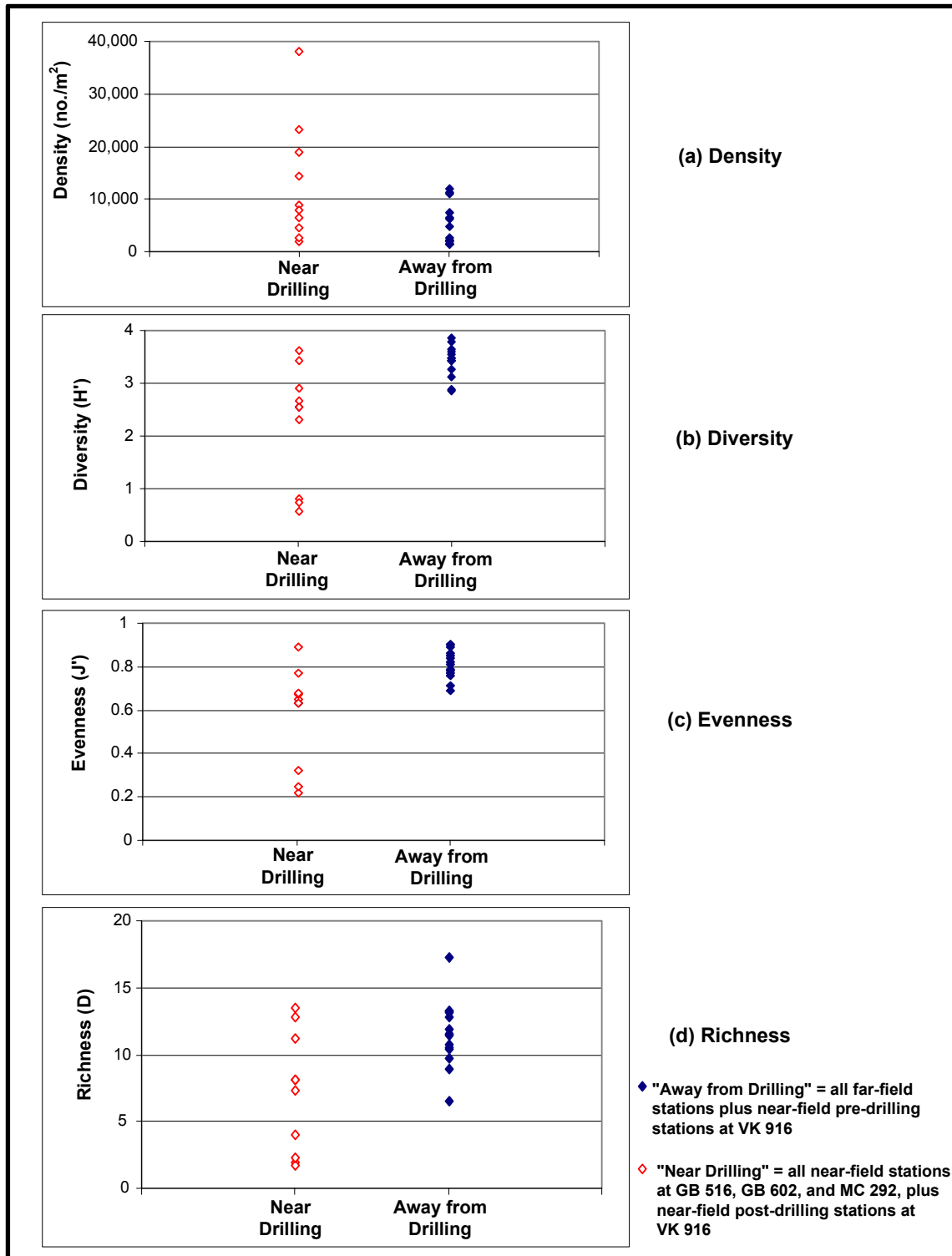
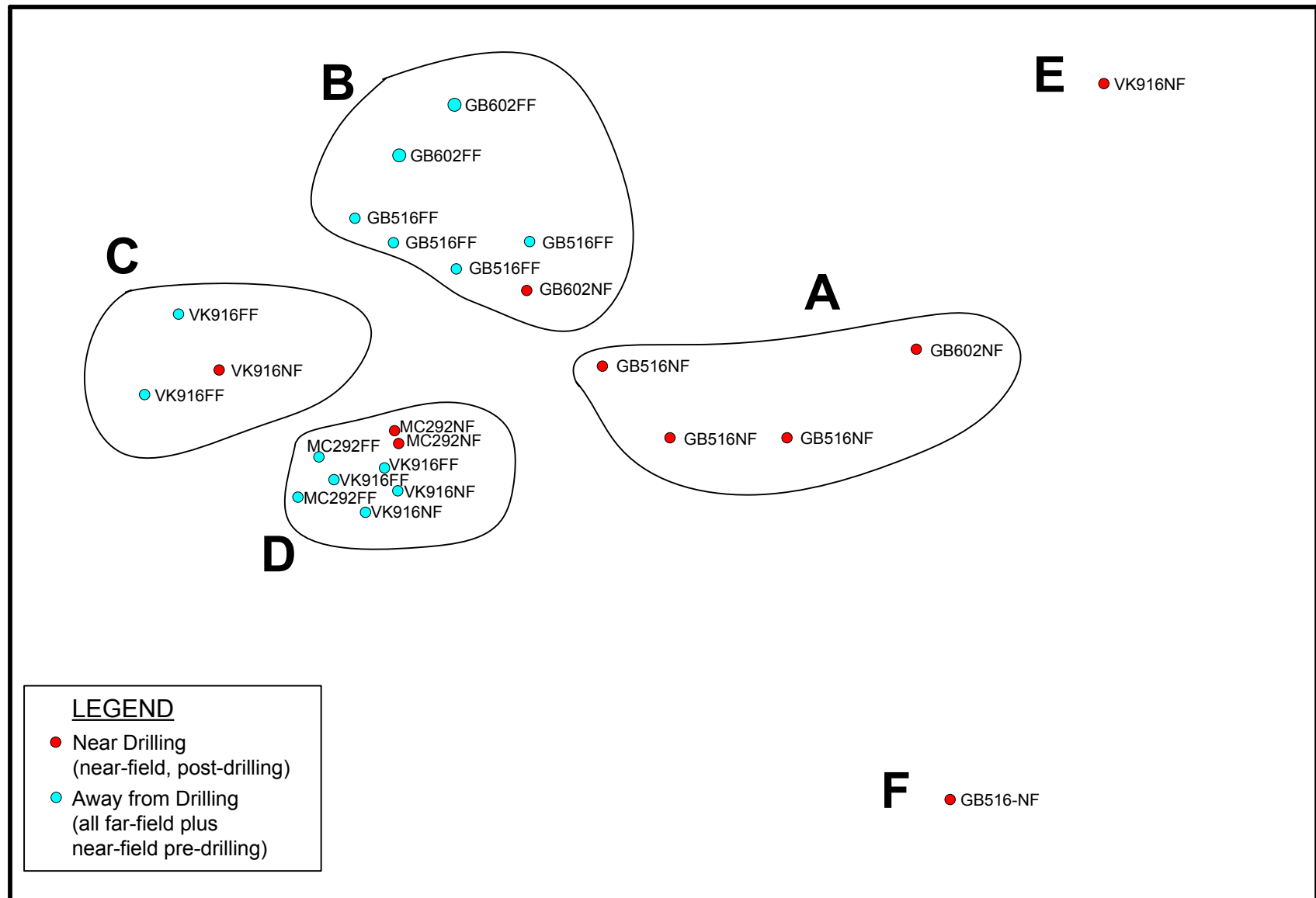


Figure 11.17. Macroinfaunal community characteristics for the detailed, 24-station analysis.



**Figure 11.18.** Station/cruise groups resolved by multidimensional scaling of macrofaunal data from the 24-station dataset.

**Table 11.17.** Station groups (A through D) resolved by multi-dimensional scaling (MDS).  
MDS plot labels refer to **Figure 11.18**.

Station Group	MDS Plot Label	Full Label	Cruise
A	GB516-NF	GB516-NF-B03	2B
	GB602-NF	GB602-NF-B03	2B
	GB516-NF	GB516-NF-B06	1B
	GB516-NF	GB516-NF-B08	2B
B	GB602-FF	GB602-FF1-B01	2B
	GB602-FF	GB602-FF4-B01	2B
	GB602-NF	GB602-NF-B01	2B
	GB516-FF	GB516-FF3-B02	2B
	GB516-FF	GB516-FF5-B02	2B
	GB516-FF	GB516-FF1-B02	1B
	GB516-FF	GB516-FF6-B02	1B
C	VK916-FF	VK916-FF5-B01	3B
	VK916-FF	VK916-FF1-B02	3B
	VK916-NF	VK916-NF-B03	3B
D	MC292-FF	MC292-FF6-B01	2B
	MC292-NF	MC292-NF-B03	2B
	VK916-NF	VK916-NF-B04	1B
	MC292-NF	MC292-NF-B06	2B
	VK916-FF	VK916-FF2-B01	1B
	VK916-NF	VK916-NF-B11	1B
	MC292-FF	MC292-FF4-B02	2B
	VK916-FF	VK916-FF6-B01	1B
E	VK916-NF	VK916-NF-B07	3B
F	GB516-NF	GB516-NF-B02	1B

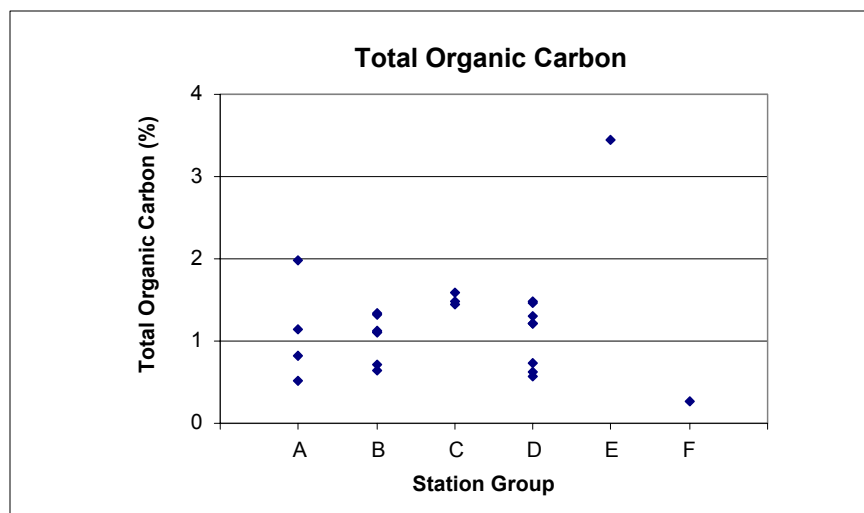
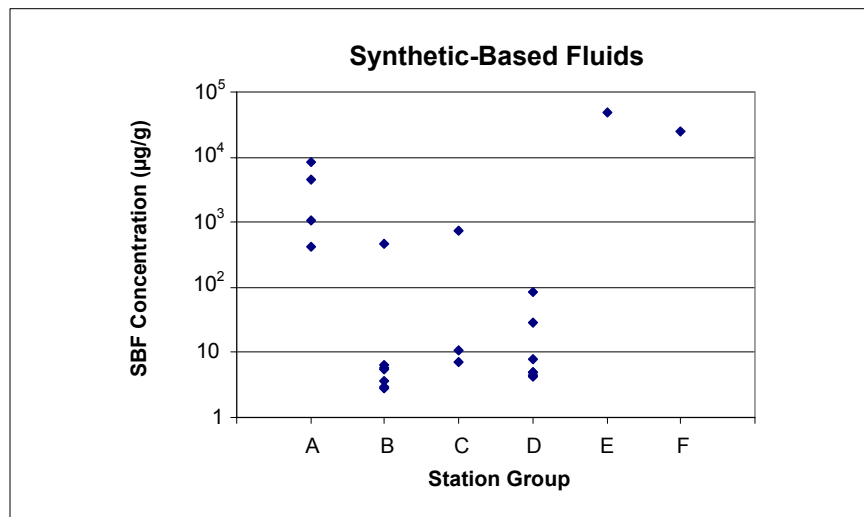
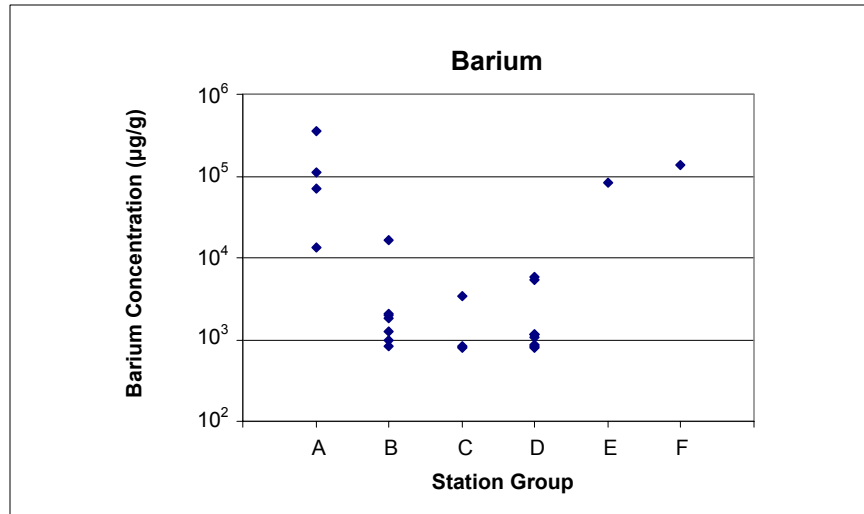


**Figure 11.19.** Comparison of sediment barium, synthetic-based fluid (SBF), and total organic carbon concentrations at station groups identified from multidimensional scaling ordination.

**Table 11.18.** Average abundance of infaunal species accounting for at least 50% of the within-group similarity in station (sample) groups A through D. Groups E and F (not shown) were dominated by the polychaete *Capitella capitata* and the gastropod *Solariella* sp. A, respectively. Numbers in bold represent the average similarity for each group as a whole.

Group	Taxa	Average Abundance	Average Similarity
A	Aphelochaeta sp. B	848.00	11.22
	Harpacticoida (LPIL)	133.75	2.95
	Phyllodocidae Genus E	36.00	2.47
	Prionospio sp. O	30.25	2.45
	Bivalvia (LPIL)	58.00	2.31
			<b>38.50</b>
B	Spionidae (LPIL)	17.86	2.94
	Harpacticoida (LPIL)	22.29	2.17
	Nematoda (LPIL)	36.86	1.74
	Bivalvia (LPIL)	4.57	1.56
	Paraonidae (LPIL)	6.00	1.45
	Aplacophora (LPIL)	4.57	1.41
	Maldanidae (LPIL)	8.14	1.19
	Pseudotanais (LPIL)	6.00	1.17
	Syllidae (LPIL)	5.14	1.13
	Monticellina dorsobranchialis	1.86	1.08
	Ostracoda (LPIL)	2.14	0.92
	Paraonidae Genus B	9.57	0.89
			<b>34.14</b>
C	Sthenolepis sp. D	16.33	4.69
	Harpiniopsis sp. A	9.67	3.57
	Aplacophora (LPIL)	11.33	3.55
	Cirratulidae (LPIL)	10.00	3.24
	Aricidea (LPIL)	9.33	3.12
	Actinocythereis sp. E	16.33	2.88
	Ophelina sp. F	3.67	2.23
			<b>46.07</b>
D	Maldanidae (LPIL)	89.50	3.44
	Aplacophora (LPIL)	119.75	2.95
	Bivalvia (LPIL)	51.63	2.59
	Ophelina sp. F	26.63	2.03
	Cirratulidae (LPIL)	26.63	1.93
	Actinocythereis sp. E	71.38	1.71
	Cossura soyeri	22.38	1.69
	Aricidea (LPIL)	24.00	1.68
	Sthenolepis sp. D	29.00	1.62
	Podocopida (LPIL)	19.13	1.22
	Harpacticoida (LPIL)	19.25	1.15
	Scoletoma verrilli	8.88	1.15
	Levensenia sp. T	7.75	1.06
			<b>47.77</b>

In conclusion, the ordination identified groups of stations that reflect both geographic location and drilling impacts. The three station/cruise groups most likely affected by drilling (Groups A, E, and F) were dominated by high abundances of one or a few deposit-feeding species.

#### 11.4.7 Discussion

In the present study, we observed a wide range in macroinfaunal abundance among the four study sites and between surveys. Mean densities ranged from 1,256 to 11,087 individuals/m<sup>2</sup>. This compares well with preliminary data from the new MMS deep Gulf of Mexico benthos study, which show macroinfaunal densities at a water depth of 1,000 m range from a few thousand to over 10,000 individuals/m<sup>2</sup>, with an average of about 6,000 individuals/m<sup>2</sup> (Rowe and Kennicutt 2002). Earlier data from the MMS northern Gulf of Mexico continental slope study indicated somewhat lower densities of about 2,500 individuals/m<sup>2</sup> for a water depth of 1,000 m (Galloway et al. 1988).

The study results correspond well with prior deepwater observations of macroinfaunal community structure. Jumars and Gallagher (1982) noted that polychaetes usually constitute 50% to 75% of the individuals in deepwater sediments, and usually include the most abundant species. In the 24-station analysis, the most speciose polychaete families were Paronidae (11 species), Cirratulidae (9 species), Lumbrineridae (8 species), Capitellidae (7 species), Lumbrineridae (7 species), Pilargidae (7 species), Syllidae (7 species), and Spionidae (6 species). The taxa census for the present study is similar to that found in other studies (Hartman 1965; Fauchald 1972). Fauchald (1972) reported that in deepwater benthic collections from western Mexico and adjacent areas of the eastern Pacific, the families Ampharetidae, Capitellidae, Lumbrineridae, Maldanidae, Onuphidae, Paronidae, and Spionidae were well represented. Hartman (1965) reported similar deepwater macroinfauna from the western Atlantic, including members of Syllidae, in a list of commonly occurring taxa.

Unlike the meiofaunal data, macroinfaunal densities did not consistently decrease between cruises. At VK 916, mean densities decreased by a factor of six between Cruises 1B and 3B at both near-field and far-field sites. However, at GB 516, mean densities increased (approximately doubled) at both near-field and far-field sites.

Nematodes are normally considered meiofaunal taxa, but due to the small screen mesh used in deep sea studies (300 µm), the larger individuals can be retained with the macroinfauna. For example, at both GB 602 and MC 292, nematodes were the most abundant group in the far-field macrofaunal samples. Nematodes were significantly more abundant in the far-field than in the near-field at GB 602. This is the opposite of the result seen in the meiofaunal data, where nematodes were more abundant in the near-field. However, at most stations, the macrofaunal nematodes accounted for <2% of the total population. If both macrofaunal and meiofaunal nematodes are combined, the pattern is the same as discussed previously under Meiofauna – i.e., the highest densities tend to occur in the near-field (see **Figure 11.5**).

Drilling impacts were evident in spatial comparisons. In post-drilling samples, there was considerable overlap in macroinfaunal densities between near-field and far-field sites, but the highest total densities were always seen in the near-field (**Figure 11.6**). The elevated total densities reflect higher numbers of annelids, gastropods, and bivalves in the near-field

**(Figure 11.10).** A similar but weaker trend was evident for aplacophorans. Two groups that tended to have higher abundances away from drilling were amphipods and ostracods. In terms of community statistics, some stations “near drilling” had lower diversity, lower evenness, and lower richness indices compared with stations “away from drilling” (**Figure 11.17**).

In previous studies, drilling discharges have been shown to affect macrofaunal communities in a variety of ways, including burial and smothering, alterations in sediment grain size and mineralogy, and toxicity of drilling fluid components (National Research Council 1983; Neff 1987; Continental Shelf Associates, Inc. 1989; Montagna and Harper 1996). Where SBM cuttings are discharged, organic enrichment and anoxia are additional factors (Neff et al. 2000).

Some of the impacts noted here are similar to those observed in the GOOMEX study, which focused on long-term production sites on the continental shelf (Montagna and Harper 1996). Although GOOMEX did not involve SBMs, an organic enrichment effect was noted, with higher macrofaunal densities near platforms – particularly, increased abundance of deposit-feeding polychaetes. In GOOMEX, the organic enrichment apparently was due to sloughing of biofouling organisms from submerged structures over a period of years, whereas in the present study, SBM cuttings are the presumed source of organic enrichment. Montagna and Harper (1996) attributed reduced abundances of amphipods and harpacticoid copepods near platforms to toxicity of metals from water-based drilling fluids, though no metal toxicity studies were conducted. In the present study, harpacticoid abundance was actually higher near drilling (see Meiofauna section), and reduced abundances of amphipods and ostracods in the near-field were not significantly correlated with metal concentrations other than barium (drilling fluid indicator). Potential toxicity is addressed further in *Chapter 14*.

There have been few previous studies of SBM cuttings impacts on the Gulf of Mexico continental slope. An opportunistic survey was conducted after development drilling at the Pompano development site in MC 28 (water depth of 565 m) (Gallaway et al. 1997; Fechhelm et al. 1999). All observations were within 90 m of the drillsite, and this area had elevated macroinfaunal densities (up to 13,724 individuals/m<sup>2</sup>) and low diversity relative to baseline conditions. Macroinfaunal populations were dominated by epibenthic scavengers including cyclopoid copepods and gastropods, and the authors suggested that true infaunal dwellers (e.g., tube-dwelling polychaetes) had been buried by cuttings discharges. There was no consistent pattern of increasing or decreasing density in relation to distance or SBF concentration. The increased macrofaunal densities are consistent with the results seen in the present study. However, the benthic effects observed here are more complex and patchy than observed in the Pompano study. Sediment profile imaging data (see *Chapters 6 and 7*) indicate a range of post-drilling conditions including areas of azoic sediment column, areas of dominance by surface-dwelling pioneering assemblages, and areas where recent disturbance has selectively compromised near-surface species relative to deeper-living infauna. Differences between the studies include the range of distances from the drillsite (within 90 m in Pompano, within 500 m in this study) and the amount of time elapsed since the most recent drilling discharges (4 months in Pompano, 5 months to 2 years in this study).

More recently, a comprehensive study of SBM impacts was conducted at several continental slope and shelf sites in the Gulf of Mexico (Continental Shelf Associates, Inc. 2004). However,

that study did not include box core sampling at continental slope sites. Benthic community impacts were documented at three shallower sites on the continental shelf. At one site with relatively high SBF concentrations, the abundance and diversity of the benthic community were reduced within 250 m of the site center. There was evidence of recovery during the year between sampling cruises at this site. Near- and mid-field sediments at two other sites (with lower SBF concentrations) had only moderately disturbed benthic community structure. Variability of diversity and evenness was greatest in the near-field zone and generally much lower in the far-field zone. In the near-field zone, this variability was probably due to variations in sediment textures and patchy distributions of cuttings.

## **11.5 CONCLUSIONS**

### **11.5.1 Meiofauna**

- Meiofaunal densities declined by about an order of magnitude between October-November 2000 (Cruise 1B) and the subsequent surveys (Cruise 2B, July 2001 and Cruise 3B, August 2002) at both near-field and far-field sites. The cause is unknown, but the decrease is not attributable to drilling activities.
- Meiofaunal densities tended to be higher near drilling. Although there was considerable overlap in near-field vs. far-field densities, the highest densities of nematodes, harpacticoid copepods, and especially annelids occurred in the near-field.
- Meiofaunal densities in the near-field were not consistently correlated with drilling indicators (barium, SBF) or other sediment variables (TOC, grain size fractions).
- The elevated meiofaunal densities seen here are similar to the nematode enrichment effect previously reported in the GOOMEX study by Montagna and Harper (1996) for platforms in shallower Gulf waters. However, we did not see lower harpacticoid densities near drilling as reported in GOOMEX.

### **11.5.2 Macroinfauna**

- Macroinfaunal densities tended to be higher near drilling. Although there was considerable overlap in near-field vs. far-field densities, the highest densities occurred in the near-field.
- For annelids (predominantly polychaetes), gastropods, and bivalves, there was a strong, consistent tendency for the highest densities to occur in the near-field. Aplacophorans showed a similar trend at GB 516 and GB 602, though not at VK 916. The opposite was true for amphipods and ostracods, with the highest densities generally occurring at one or more far-field stations.
- In terms of community statistics, some stations “near drilling” had lower diversity, lower evenness, and lower richness indices compared with stations “away from drilling.”
- Annelid (predominantly polychaete) densities in the near-field were positively correlated with drilling indicators (barium, SBF). Some near-field stations with barium concentrations higher than about 10,000  $\mu\text{g/g}$  and/or SBF concentrations greater than about 1,000  $\mu\text{g/g}$  had elevated polychaete densities.
- Gastropod densities in the near-field were positively correlated with drilling indicators (barium, SBF). A few near-field stations at GB 516 and GB 602 had very high gastropod densities, which were associated with barium concentrations of 55,000  $\mu\text{g/g}$  or higher and SBF concentrations of 4,500  $\mu\text{g/g}$  or higher. Much weaker relationships were observed at VK 916 and MC 292.



- Amphipod densities in the near-field were negatively correlated with drilling indicators (barium, SBF). Generally, near-field stations with barium concentrations higher than about 10,000  $\mu\text{g/g}$  and/or SBF concentrations greater than about 1,000  $\mu\text{g/g}$  had low amphipod densities.
- A detailed taxonomic analysis of 24 stations showed that species composition reflects both geographic location and drilling impacts. The three station/cruise groups most likely affected by drilling (as indicated by high barium and SBF concentrations) were dominated by high abundances of one or a few deposit-feeding species.

## Chapter 12 Megafauna and Image Analysis

*Robert S. Carney  
Coastal Ecology Institute  
Louisiana State University*

---

### 12.1 INTRODUCTION: IMAGE-BASED SAMPLING

Image-based sampling is extremely appealing but must be considered critically in designing studies. What is the purpose of the images to be obtained? Hecker's camera sled work is noteworthy both in terms of relating animals to structure (Hecker 1982) and sampling in deep-sea canyons where coring is inapplicable and trawling impossible (Hecker 1990). Excellent quantification and aggregation analysis for dominant megafauna have been obtained from submersibles (Grassle et al. 1975) and cameras mounted to beam trawls (Wakefield and Genin 1987). However, the literature presenting successful studies gives no hint of the vast majority of photo and video surveys, which are never analyzed. Bulk-load survey cameras can take approximately 800 frames per deployment, while video takes tens of thousands. Extracting useful final data from such massive raw data usually proves to be overwhelming. Imaging technology is appealing, but the actual benefits are not often evident. Unless specimens are required for other analysis, image-based sampling generally gives a better measure of items on the seafloor, but not those buried (Kidd and Huggett 1981).

The most extensive photographic survey of the deep Gulf of Mexico was carried out as a component of the Northern Gulf of Mexico Continental Slope Study (Gallaway 1988). Sixty surveys were conducted, producing a total of 48,000 images. An Edgerton-type pressure housed 35-mm camera and strobe were configured to drift 2 m above bottom. The length of survey was determined by drift rate, ranging from 1,500 to 5,000 m long. Analysis of the images was conducted by G. Boland, with data processing and management by J. Baker. The daunting task of analyzing so many images was made manageable by randomly subsampling 100 or 200 images. In all, 9,147 images (24,590 m<sup>2</sup> of bottom) were analyzed for fauna and lebensspuren (life marks). The primary use of the results was to provide density and patchiness estimates for dominant megafauna.

Due to the overall paucity of fauna captured in bottom photos and the comparable abundance of tracks, trails, burrows, and mounds, there has been a persistent interest in obtaining information about the bottom habitat from analyses of lebensspuren. The present study did not include a study of specific marks but did include an exploratory effort to quantify the overall extent of biological structure seen on the bottom. As such, the study sought to bridge the three ways in which lebensspuren has been examined:

1. A description of an obvious and pervasive small-scale topography (Ewin and Davis 1967; Heezen and Hollister 1971).
2. A surrogate for observations of actual animals that provide estimates of population density.
3. As a record of habitat-influenced foraging behavior (Seilacher 1967).

Tried alone, none of these three approaches has proven to be informative in either an ecological or management sense. Local patterns of specific marks have been found, but no obvious relationships to habitat difference could be identified (Gallaway 1988). There is the confusing factor of erasure of marks both by erosional events and by bioturbation (Wheatcroft et al. 1988). Predictions that habitat changes in foraging patterns might be found have been disproved in the case of depth (Kitchell 1979).

The approach taken in this study was less ambitious. It was assumed that lebensspuren could be a surrogate of overall sediment processing by organisms. If simply quantified, it would be an easily assessed parameter that might indicate impacts in the vicinity of development.

## **12.2 METHODS**

### **12.2.1 Field Sampling**

A Benthos Edgerton-type camera and single strobe were sled mounted and dragged along the bottom by cable (see *Chapter 2*). A down weight on the cable reduced the amount of wire played out. Time of exposure was recorded by an image data chamber, while ship position and time were logged by the towing vessel. The camera was oriented straight down as in the Northern Gulf of Mexico Continental Slope Study, unlike other camera sled surveys, in which the camera looks forward of the sled. There are pros and cons to all methods. Down-facing cameras tethered above bottom give excellent large area coverage, but fixed distance to bottom is hard to maintain. Sleds assure a fixed distance at the cost of area imaged. Angled cameras photograph a larger panoramic scene. However, fauna quantification becomes somewhat problematic, and inconsistent illumination limits digital analysis. In effect, the lighting pattern becomes the dominant information in the image.

The intended design was to carry out photographic surveys at four locations: VK 916, GB 516, GB 602, and MC 292. At each, three tows crossed a near-field 500-m radius circle centered around existing or planned drilling activity (**Figures 12.1, 12.2, 12.3, and 12.4**). Exact tracks across that circle were determined by sea conditions and obstacle avoidance. Three additional tows were carried out in the far-field at stations greater than 10 km from the near-field. This near-field and far-field pairing was intended to test for effects of development. The design was also to include before/after comparisons at GB 516 and VK 916, with the three near-field and three far-field samplings being carried out prior to and after drilling was initiated. Unfortunately, this part of the study was compromised by prior drilling at the GB 516 site (see *Chapter 3*).

### **12.2.2 Image Processing**

Images were scanned on a Nikon Cool-Scan 4000 at a density of 1,208 by 1,937 pixels using Nikon Scan software as an Adobe Photoshop plug-in in a Microsoft® Windows 2000 environment. The resulting raw scan was cropped as necessary and stored as a tagged image format (tif) file without compression, 7.1 megabytes. The actual pixel sizes were somewhat arbitrary. They produced high-resolution images, and images could be stored on an ordinary CD-ROM. Auto exposure was defeated during scanning so that actual image-to-image differences were maintained for later analysis. The name of each image file was derived from the information of the data chamber (roll number, day, hour, minute, and second).

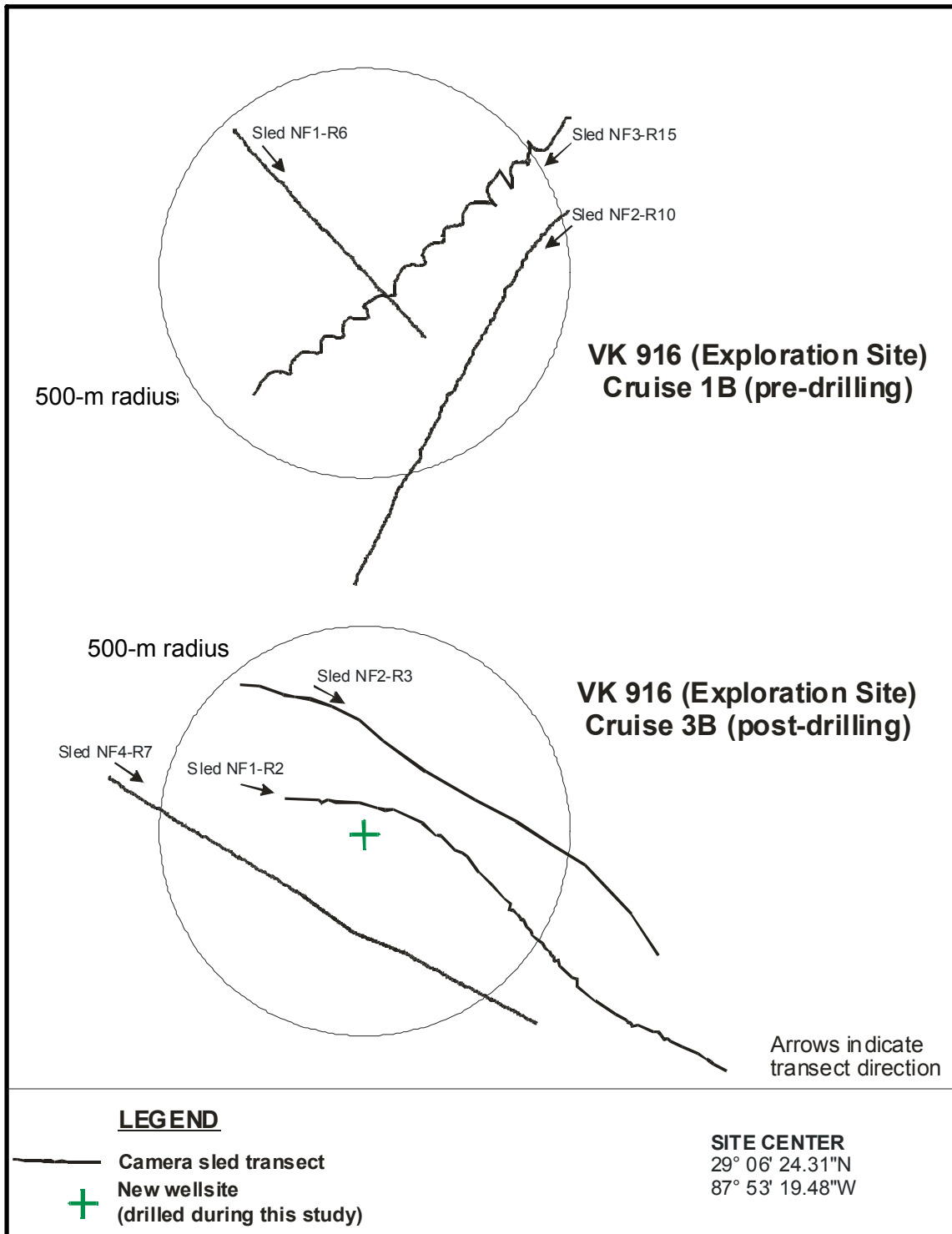


**Figure 12.1.** Locations of camera sled transects at Viosca Knoll (VK) Block 916 near-field site. Arrows indicate direction of tow.

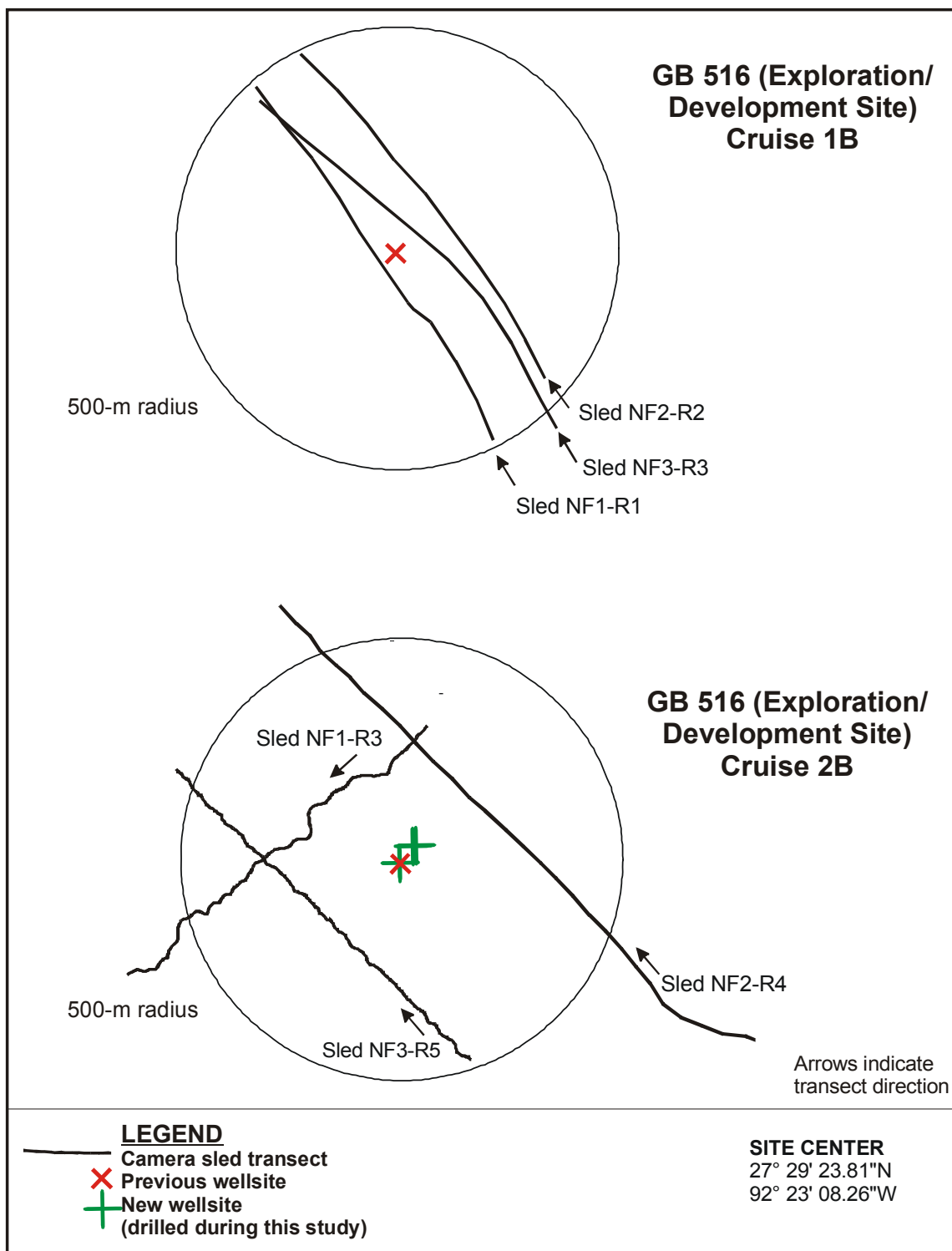


**Figure 12.2.** Locations of camera sled transects at Garden Banks Block (GB) Block 516 near-field (NF) site. Arrows indicate direction of tow.

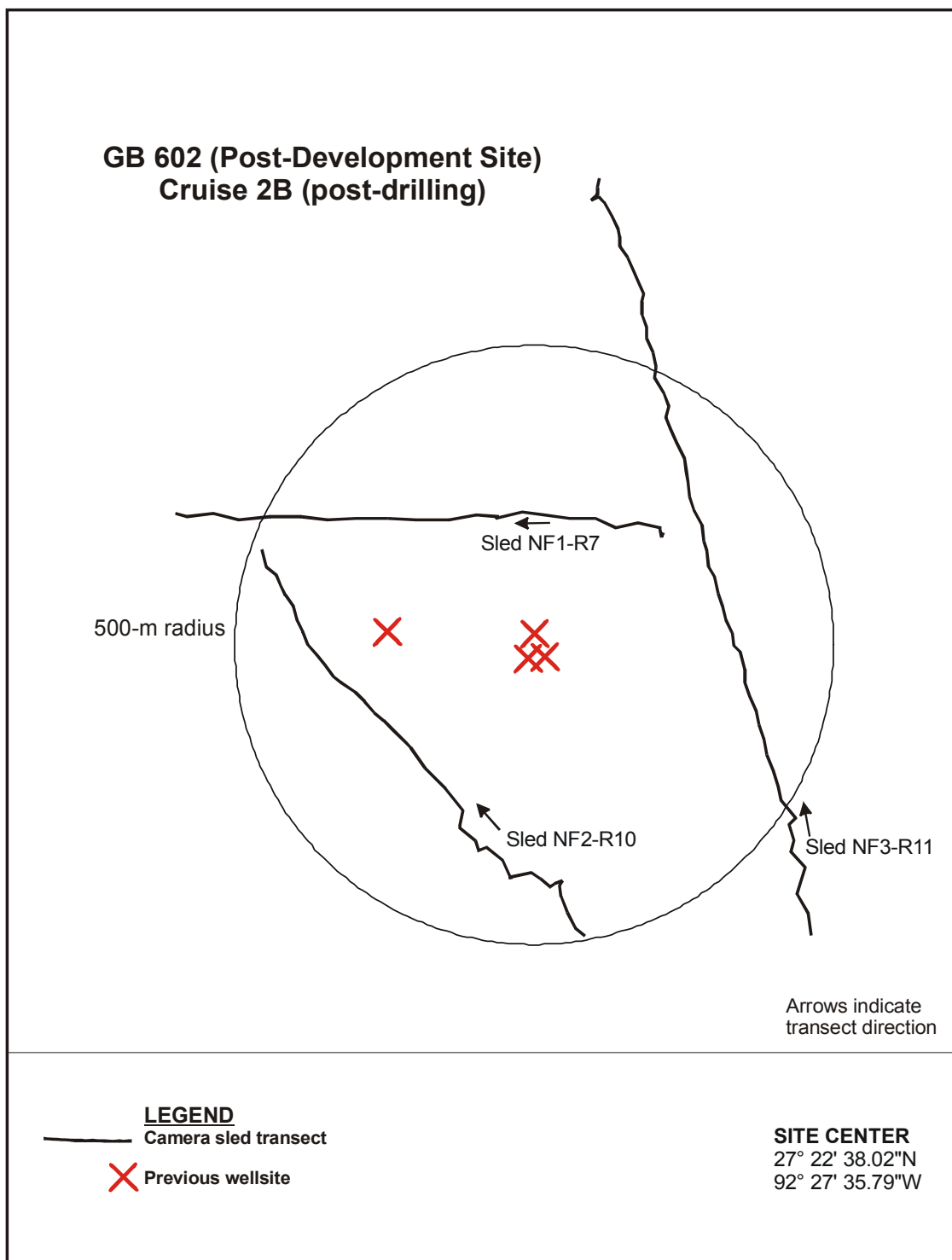


**Figure 12.3.** Locations of camera sled transects at Garden Banks Block (GB) Block 602 near-field (NF) site. Arrows indicate direction of tow.

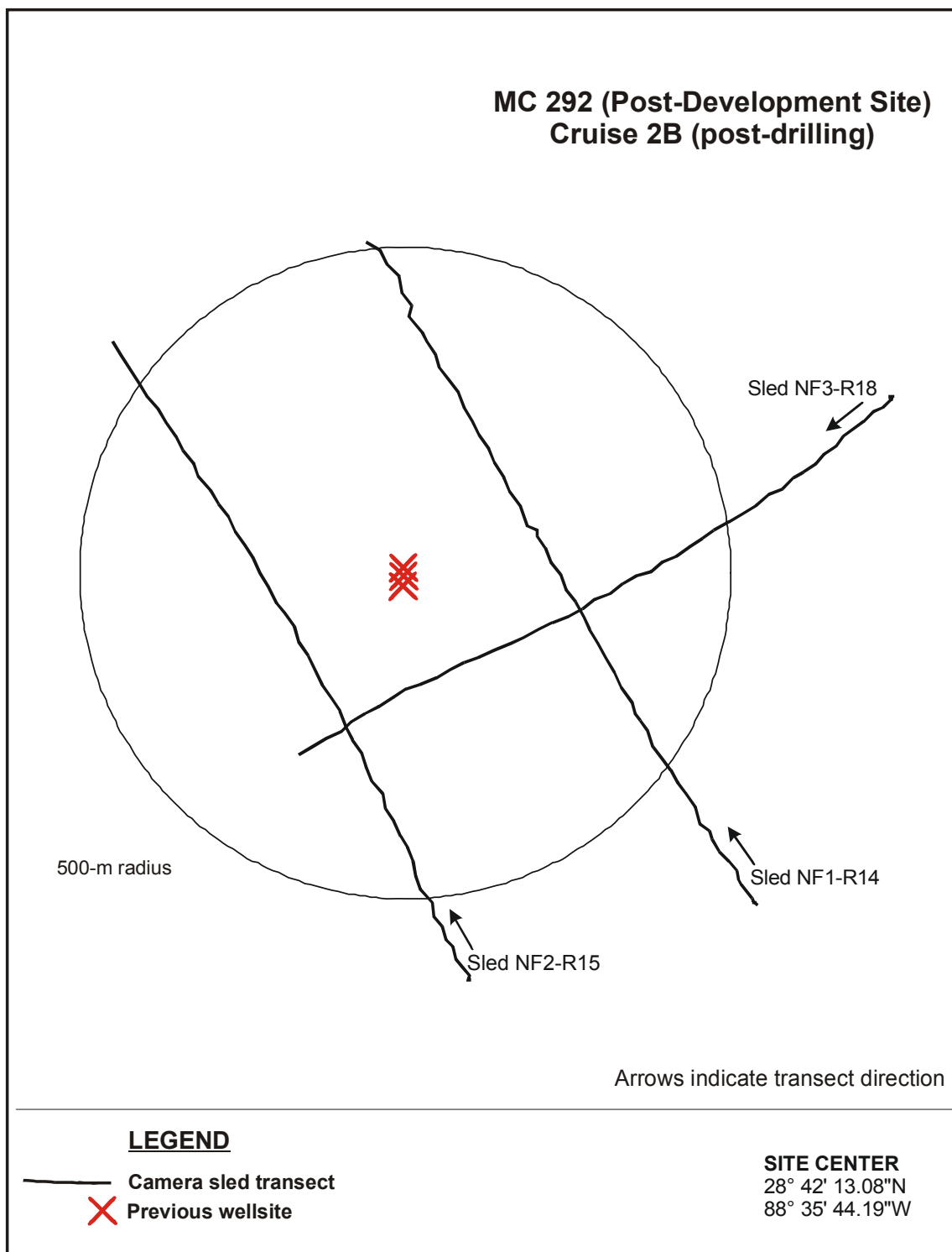


**Figure 12.4.** Locations of camera sled transects at Mississippi Canyon (MC) Block 292 near-field (NF) site. Arrows indicate direction of tow.

Visual inspection was based upon a dual examination. The film was examined under magnification, and the digital image was examined subsequently. Data logged were data chamber content, image quality, confirmation that the camera was moving (non-redundant image), and an inventory and count of all fauna and objects. Handwritten logs were then converted into Microsoft<sup>®</sup> Excel tabular files.

Analysis of image color and texture was carried out using custom written programs employing the Precision Visuals Workstation Analysis and Visualization (PV-WAVE) image processing and statistics tool kits. These were run on a 64-bit Unix workstation. Color analysis (calculation of hue) and textural analyses were run on a 1,000 x 1,000 pixel area in the center of each image. This area was unaffected by color bleeding from the red data chamber insert and was uniformly lighted by the strobe.

### **12.2.3 Color Analysis**

The color of the seafloor can be a useful indicator of ecological condition. In typical deep-sea habitats, the top 1 to 2 cm of sediment are well oxidized and appear brownish in color; underlying these are more reduced sediments that are more gray. When bioturbation is active, mounds of the excavated gray sediment are conspicuous on top of the brown surface. The more extensive the burrowing, the greater the shift from brown to gray. The deep-sea floor normally does not become sulfidic in the top few centimeters, but sulfate reduction can occur when there is an usually high input of organics, either from detritus, seeping hydrocarbons, and/or man-made sources. The resulting sulfidic sediments are typically black and may be colonized by white to orange bacterial mats.

### **12.2.4 Color Models**

There are several methods of mathematically describing the perceived colors. Computer imaging typically uses the RGB (red, green, and blue) model in which each pixel (picture element) is represented by three values. In the most common 8-bit systems, values range from 0 to 255 for each. These data are easily converted to a displayed image via the RGB primary colors of display devices. In analysis of seafloor images, RGB data are not especially useful since we are more interested in describing colors than displaying them.

Hue is a basic concept in color perception, selecting colors, and describing colors. Descriptions such as “brownish,” “bluish,” etc. all describe the hue of an image. Full description of a color requires two other terms, S (saturation) and L (lightness). Of these, L is more readily understood in terms of exposure, being a measure of where between maximum lightness (white) and minimum lightness (black) an image falls. S refers to the intensity of the hue. For example, the brightest red possible for a given film image is said to be fully saturated. A poorly saturated red would appear to be a grayish pink ranging from very light pink at high L to a dark gray at low L.

H, S, and L are readily calculated from RGB by conversion from the RGB to hue/saturation/light color models. Hue is expressed as an angle between 1 and 360 degrees, much like a color wheel. The algorithm employs scalings between the maximum and minimum values of the RGB representation. The conversion was carried out using the COLOR\_CONVERT function of PV-WAVE. The average hue was calculated for a 1,000 x 1,000 pixel area.



Texture analysis was considered highly exploratory. One hundred images were selected by examination, which ranged from a uniform, almost featureless bottom up to images with multiple mounds and burrows with associated large shadows. Texture statistics were then calculated using three texture models in the PV-WAVE Image Processing Toolkit. Each model produced a single value or suite of texture statistics. The ranking of the calculated statistic was then compared to the initial visual assessment.

## 12.3 RESULTS

### 12.3.1 Texture Analysis

The trial effort at digital texture analysis was not successful. Objectively, some sites had distinct and consistent textures. Notably, most smooth bottom images were found at GB 516, and most coarsely burrowed bottom images were found at MC 292. None of the three texture models reflected these subjective patterns. The primary difficulty is identification of the most appropriate scale at which to seek patterns. The pixel-level analyses attempted were probably at too fine of scale to reflect burrows and mounds a few hundred pixels across.

### 12.3.2 Color Analysis

Calculation of hue and plotting of values against time of image were exceptionally successful, but for unanticipated reasons. The anticipated local shifts in hue due to bioturbation were not found. Rather, all or most camera tows in near-field areas where development had taken place revealed areas where the normal brownish-gray bottom shifted progressively to areas of dark blue-black. These dark bottoms are most likely due to anoxia caused by drilling muds adhering to cuttings. No such shifts from normal to dark bottom were found in any far-field tow or in the VK 916 near-field prior to development.

#### 12.3.2.1 Viosca Knoll 916 (**Figures 12.5, 12.6, 12.7, and 12.8**)

There were no hue shifts on any Cruise 1B tows, a result consistent with the lack of drilling activity. On Cruise 3B (post-drilling), all three near-field tows crossed one or two dark bottom areas. Locations of dark bottom areas were consistent with geophysically mapped cuttings deposits (**Figure 12.8**). Bacterial mats were not observed (though they were seen in some sediment profile images from this site; see *Chapter 6*). Far-field images showed no hue shifts.

#### 12.3.2.2 Garden Banks 516 (**Figures 12.9, 12.10, and 12.11**)

The dark bottom in the near-field was crossed by all three tows on Cruise 1B. It appears to be a feature at least 250 m across and lying to the north of the center. The dark bottom is covered in some images by white to red mats consistent with the sulfide-using bacteria *Beggiatoa*. These bacterial areas may reflect site of local bottom anoxia supported by bacterial degradation of discharged drilling fluids. Cruise 2B results were similar except that no bacterial mats were seen.

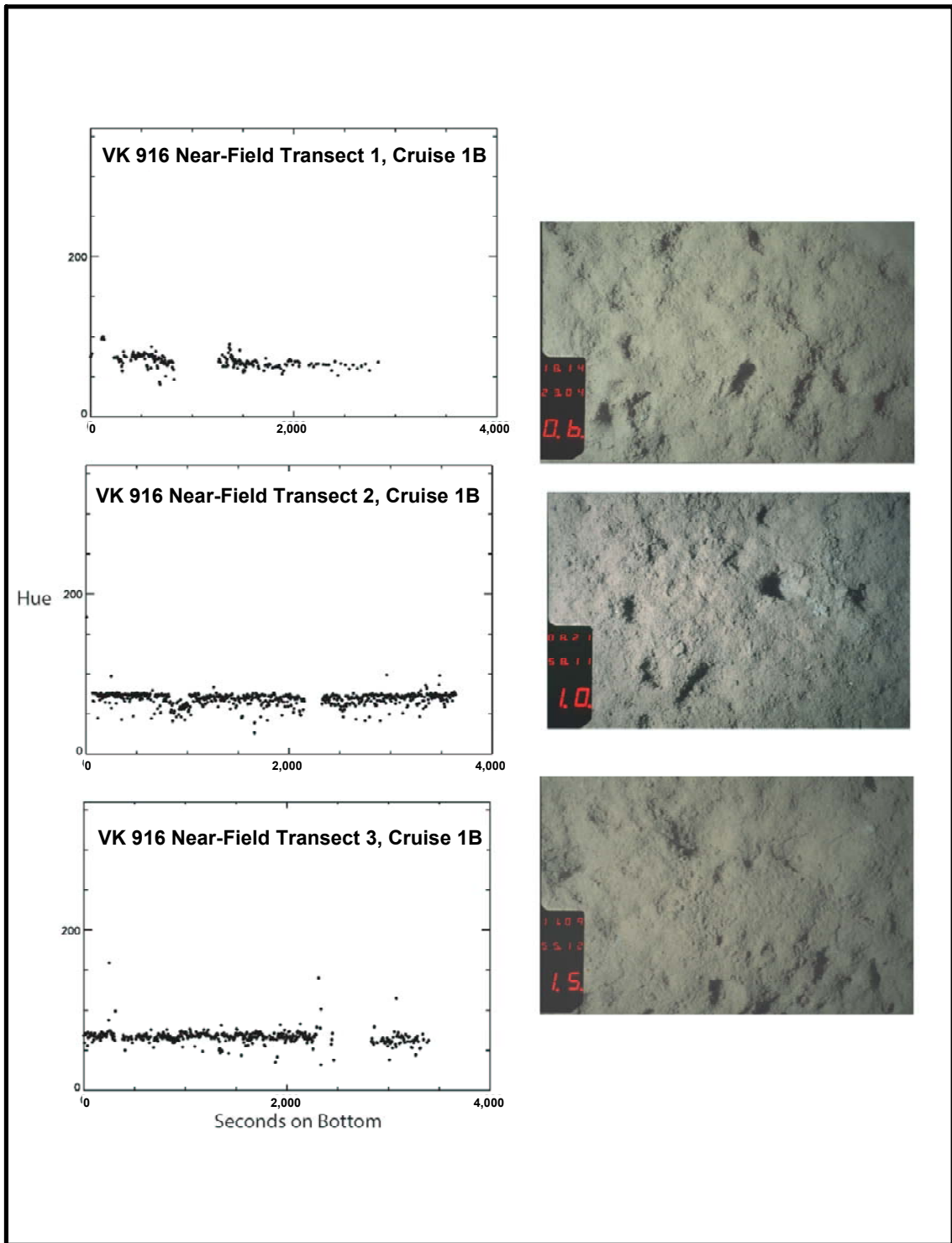
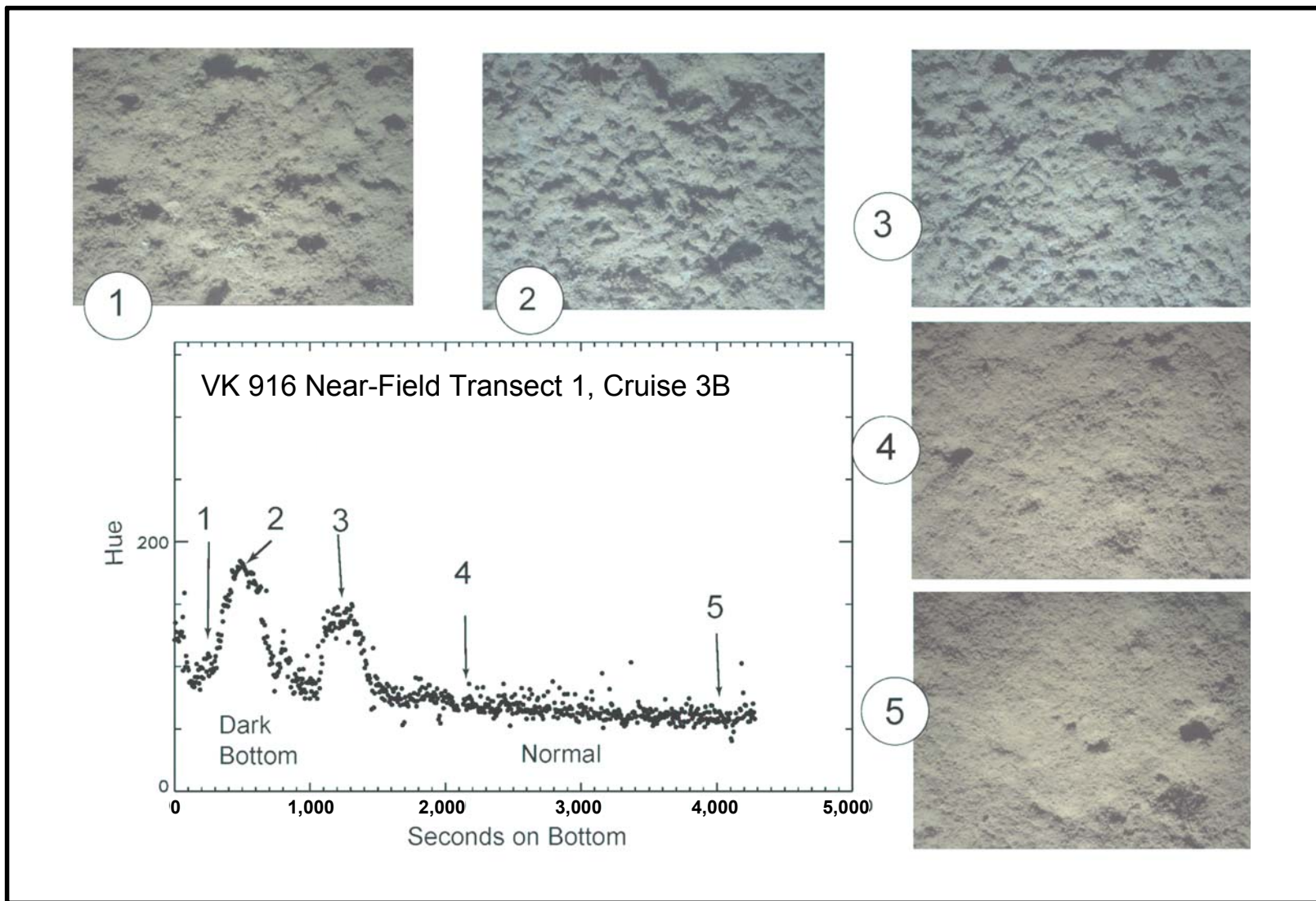
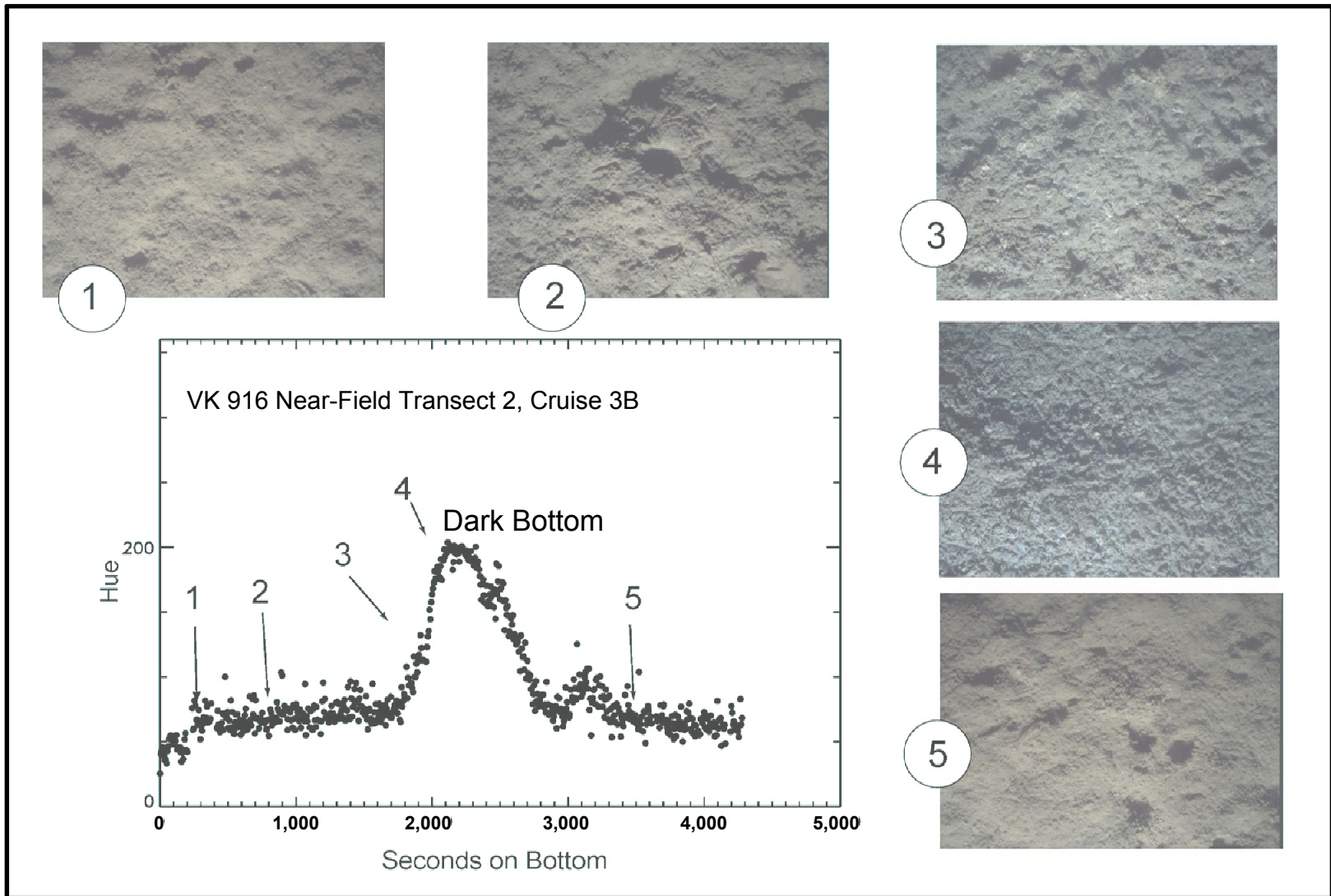


Figure 12.5. Image analysis results for Viosca Knoll (VK) Block 916, Cruise 1B, near-field transects.



**Figure 12.6.** Image analysis results for Viosca Knoll (VK) Block 916, Cruise 3B, Near-field Transect 1.



**Figure 12.7.** Image analysis results for Viosca Knoll (VK) Block 916, Cruise 3B, Near-field Transect 2.

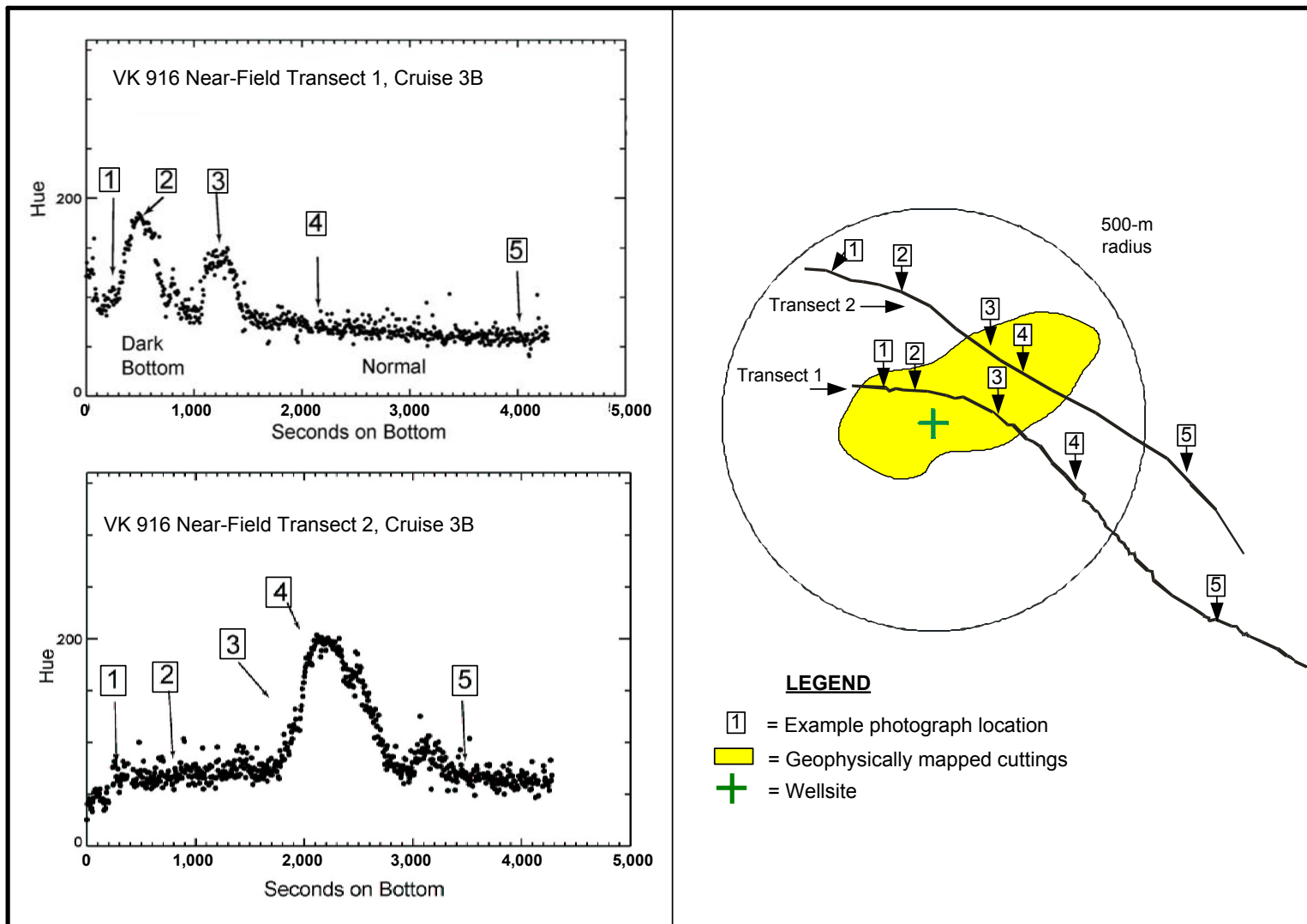


**Figure 12.8.** Locations of example photographs in relation to geophysically mapped cuttings deposits at Viosca Knoll (VK) Block 916 on Cruise 3B.

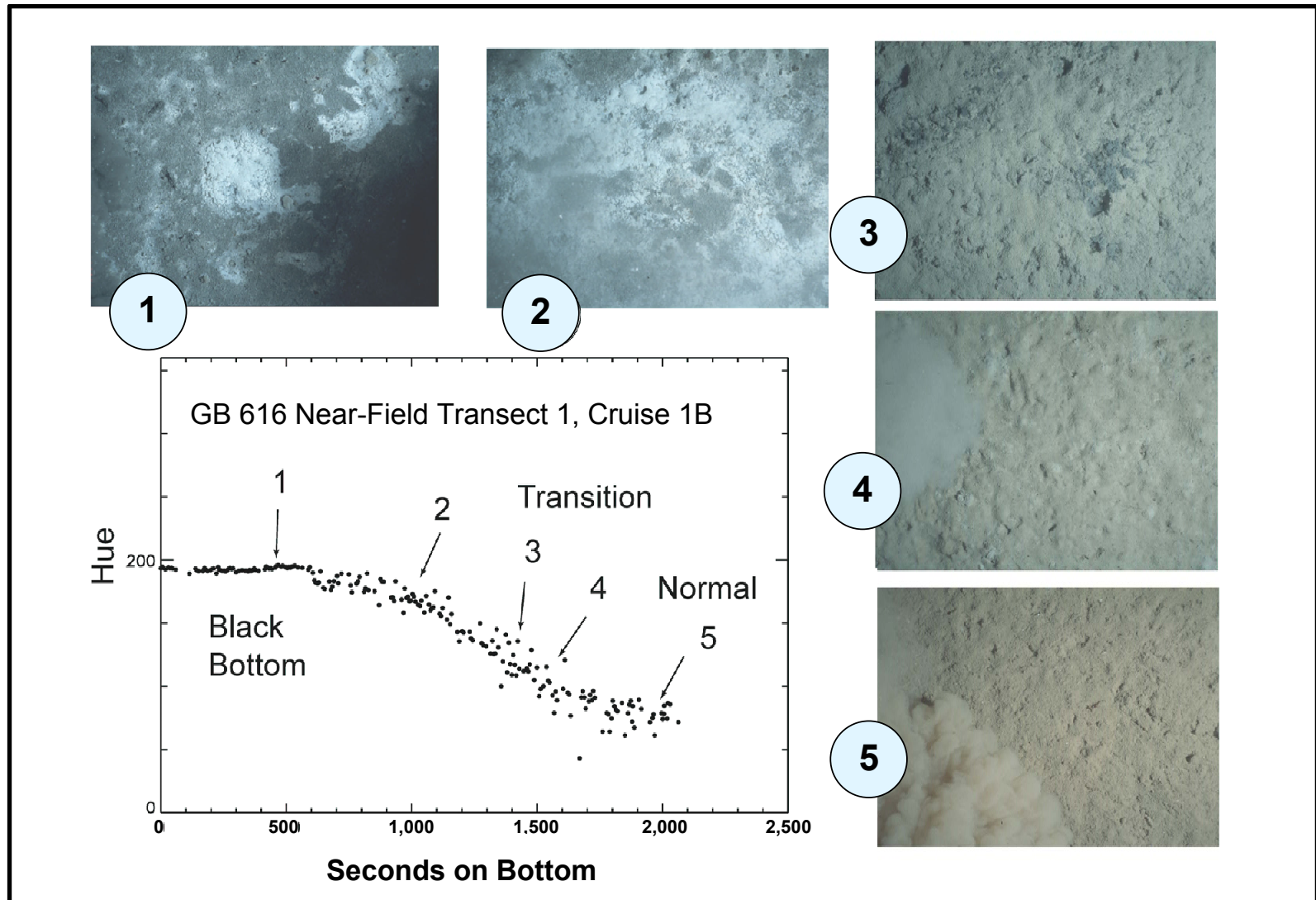
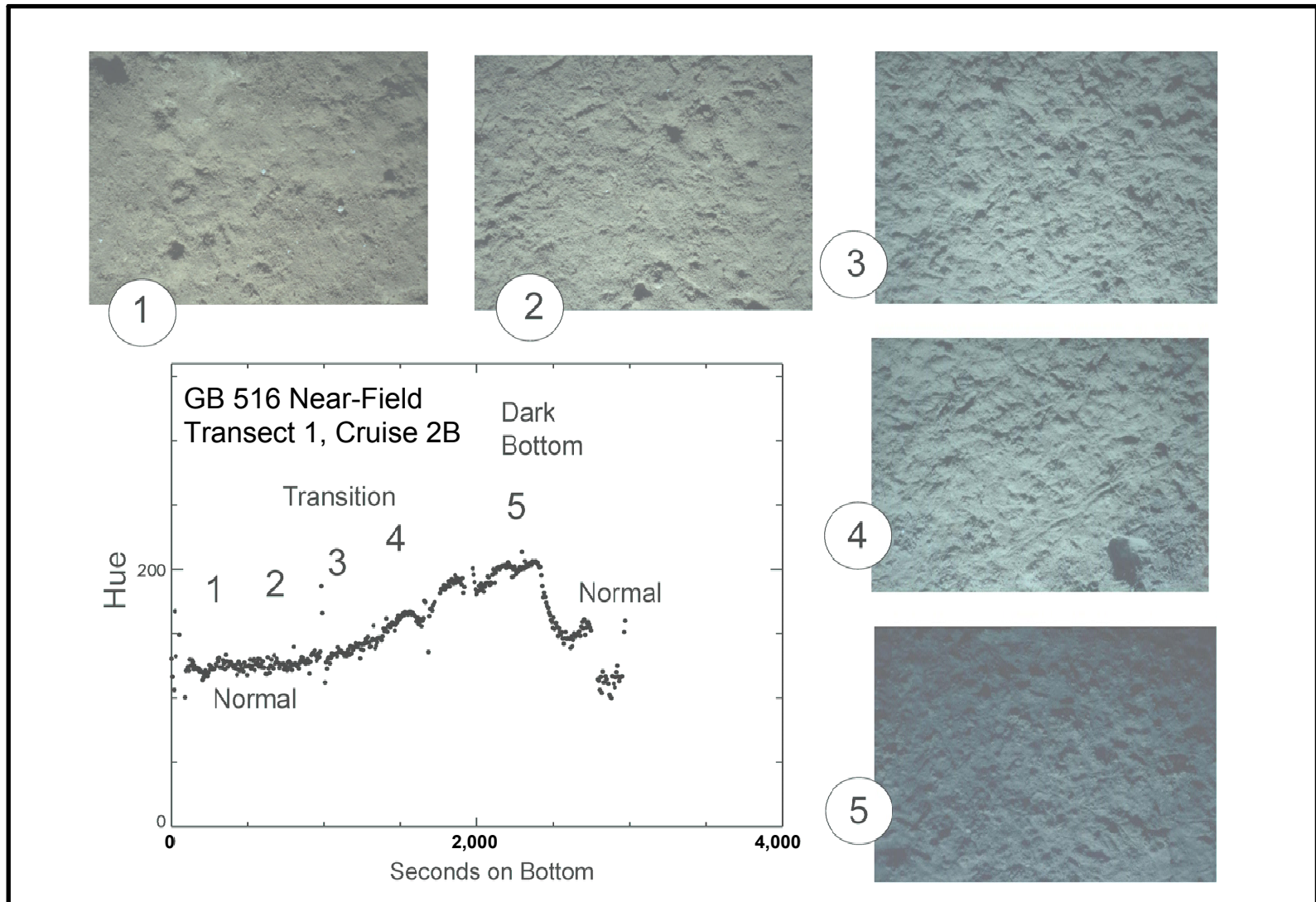
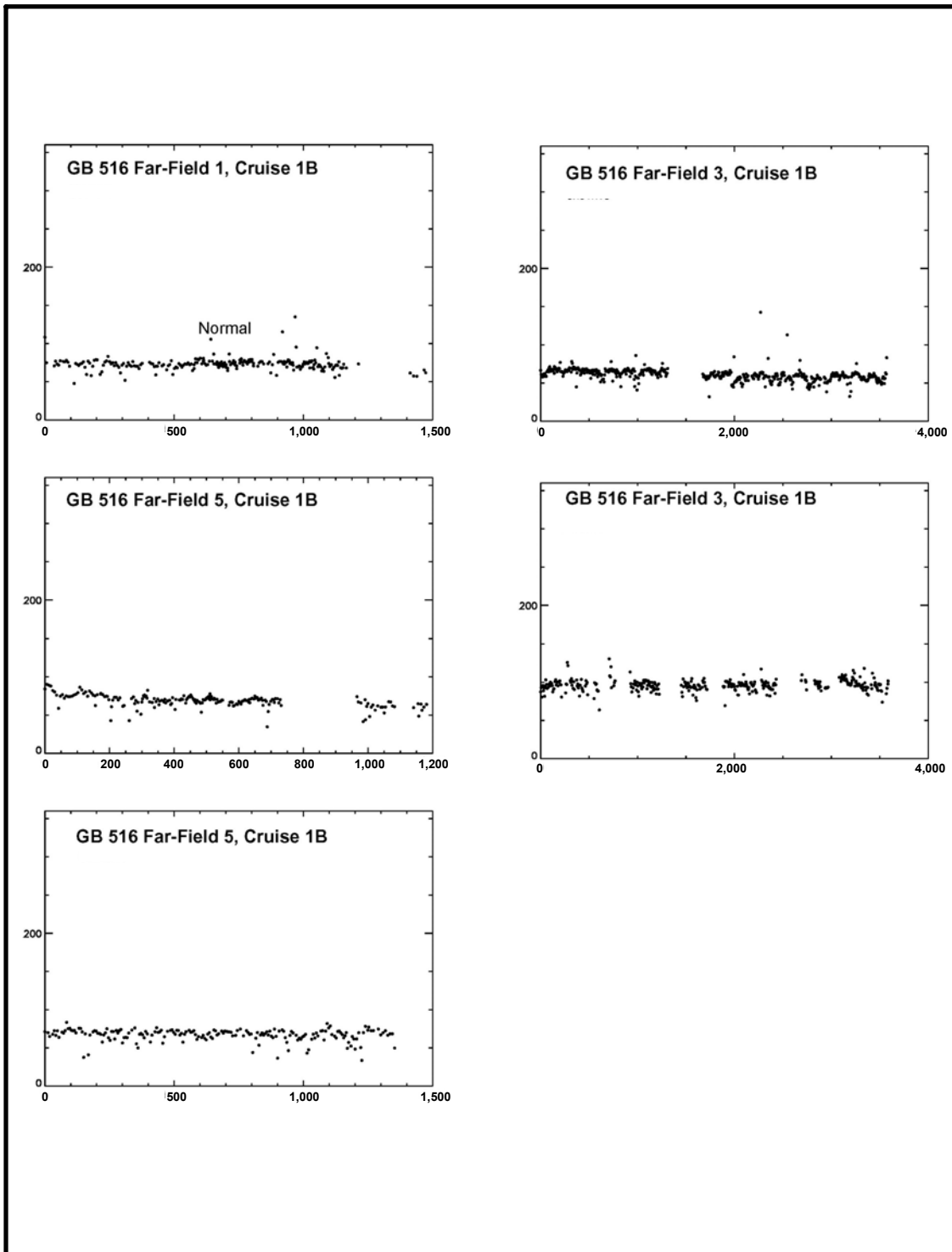


Figure 12.9. Image analysis results for Garden Banks (GB) Block 516, Cruise 1B, Near-field Transect 1.



**Figure 12.10.** Image analysis results for Garden Banks (GB) Block 516, Cruise 2B, Near-field Transect 1.



**Figure 12.11.** Image analysis results for Garden Banks (GB) Block 516, Cruise 1B, far-field transects.



### 12.3.2.3 Garden Banks 602 (Figures 12.12 and 12.13)

The normal-dark shift in near-field images was somewhat more difficult to identify since most images produced hue values indicative of dark bottoms. Only the third tow had the dramatic shift found at other sites. It appears as though GB 602 has cuttings more thinly spread over a larger area. Far-field results were typical, with no indication of dark bottom.

### 12.3.2.4 Mississippi Canyon 292 (Figures 12.14 and 12.15)

The normal-dark shift was again obvious in the near field, and far-field images showed only normal bottom. As an interesting note, the bottom at MC 292 showed a distinctive texture in all tows. There was a mosaic of overlapping circles about 10 cm across. These appear to be filled-in feeding pits. The maker of the pits was never photographed.

## 12.4 FAUNAL ANALYSIS

Results of faunal analysis are summarized in **Table 12.1**. Thirty-eight rolls of film had usable images on them. Camera difficulties required extra tows at GB 516 on Cruise 1B, and only five tows were successful at VK 916 on Cruise 2B. Otherwise, the original design was reasonably well achieved. Fauna were counted in 16,770 images. For the entire data set, approximately 7.5% of images contained identifiable fauna. At all sites except MC 292, this value ranged from a high at GB 516 of 9% to 6.6% at GB 602. Distinctively lower was the 2% at MC 292. MC 292 had a distinctive bottom texture that both indicates a unique habitat and may obscure fauna.

The small area of the images proved to be more of a problem than anticipated. Originally, it was assumed that higher resolution images of small areas would miss large animals but allow identification and enumeration of many animals at the lower limit of the megafauna size range, 1 cm. This did not prove to be the case. Large fishes, crabs, and the rare holothuroid usually appear in only part of the image frame. Some distinctive small fauna was seen, notably retracted anemones and hermit crabs as small as 1 cm, but little else. Animals in the 1 to 2 cm size range are either very rare, buried, or obscured by microtopography.

For statistical analysis, fauna were placed into six categories:

1. Benthic coelenterates were most abundant, but the category has a high degree of uncertainty. It contains a few obvious burrowing anemones and sea pens, along with a great many organisms that might be retracted anemones. All were benthic and partially buried.
2. Shrimps consisted of unidentifiable penaeids usually seen a few centimeters off bottom along with *Glyphocrangon* sp. seen on the bottom.
3. Ophiuroids could not be identified to species. Partially buried specimens were common, suggesting that a large number of fully buried specimens were not imaged.
4. Fishes were seldom imaged whole; that and the camera angle made identification uncertain. Coryphanoidids were most common, followed by synphobranchid eels and a few rays identifiable as *Bathyraja* sp.
5. Crabs were predominantly small (<2 cm) hermit crabs. *Chaceon quinquegens* was imaged in very low numbers.
6. Gastropods were small (<2 cm). Most were found on a trail, but there is no certainty that they were live or occupied by a withdrawn hermit crab.

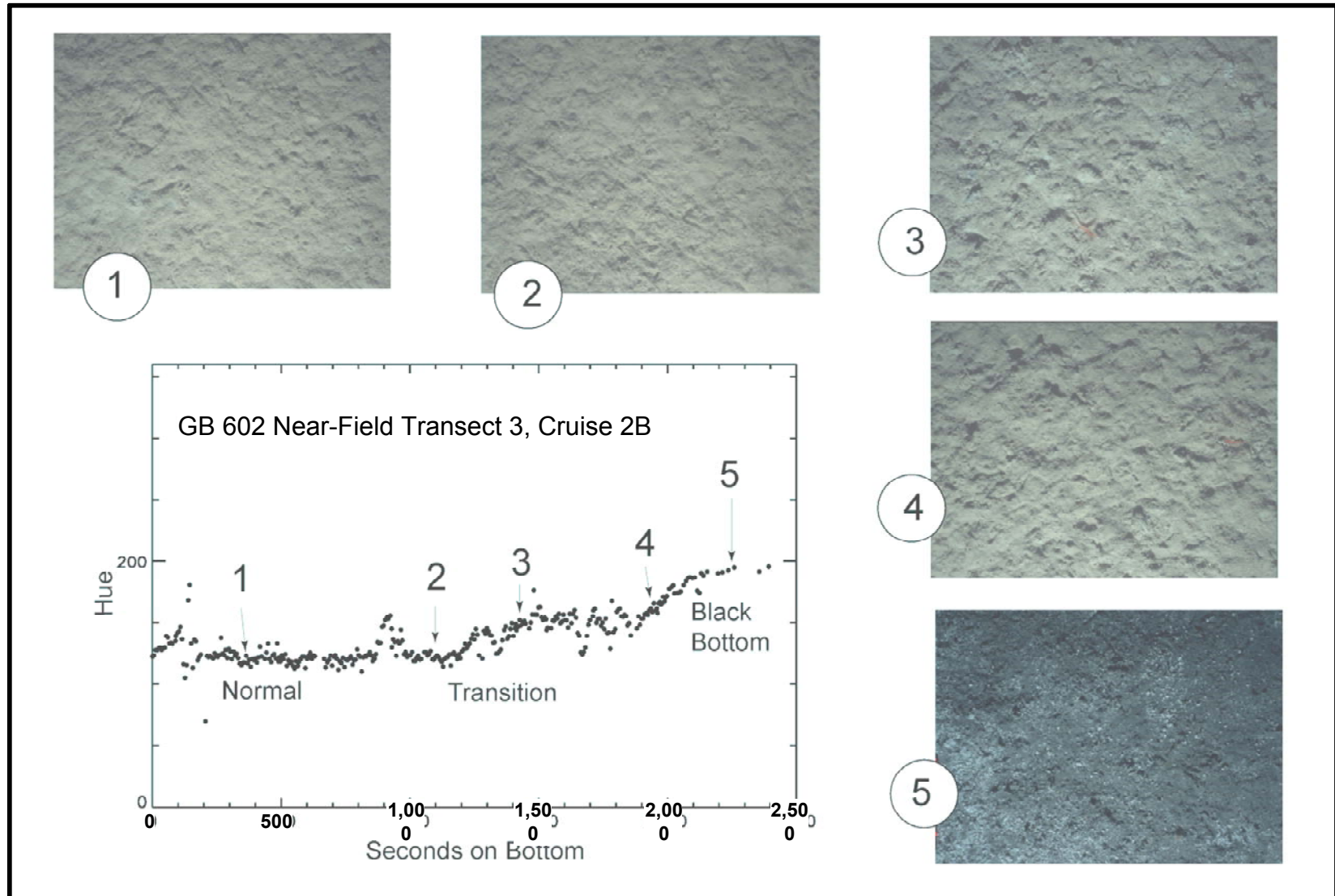


**Figure 12.12.** Image analysis results for Garden Banks (GB) Block 602, Cruise 2B, Near-field Transect 3.

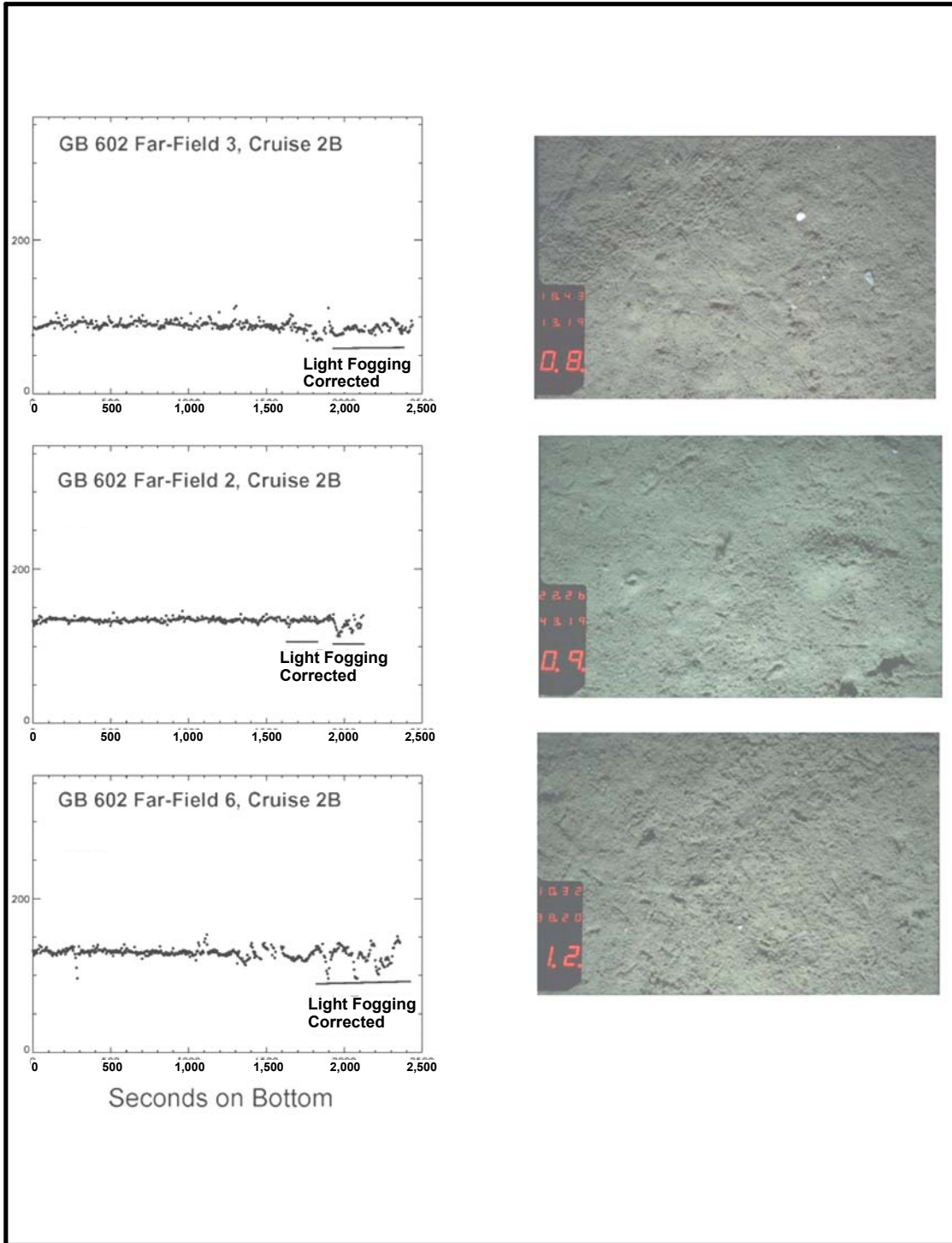


**Figure 12.13.** Image analysis results for Garden Banks (GB) Block 602, Cruise 2B, far-field transects.

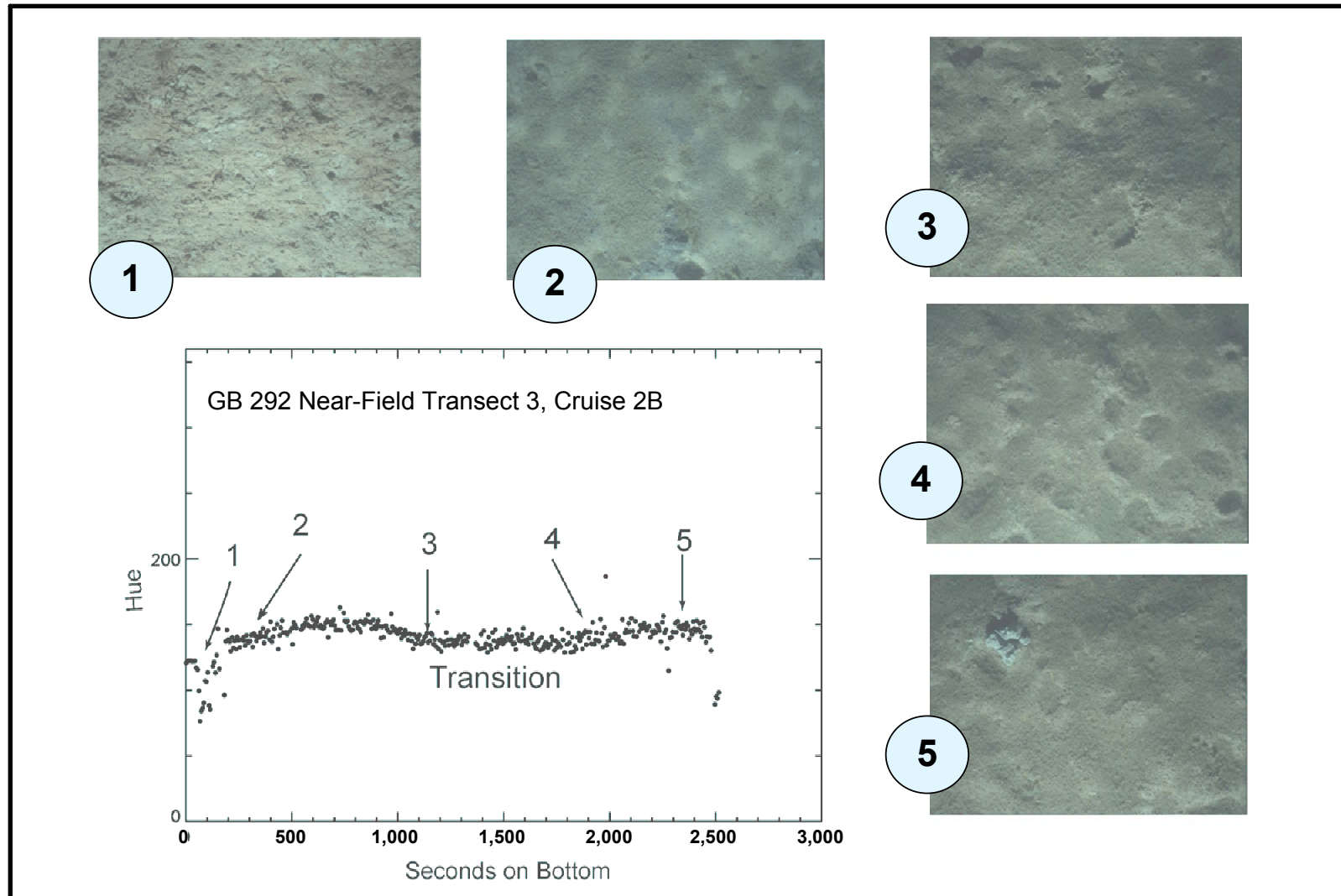


**Figure 12.14.** Image analysis results for Mississippi Canyon (MC) Block 292, Cruise 2B, Near-field Transect 3.

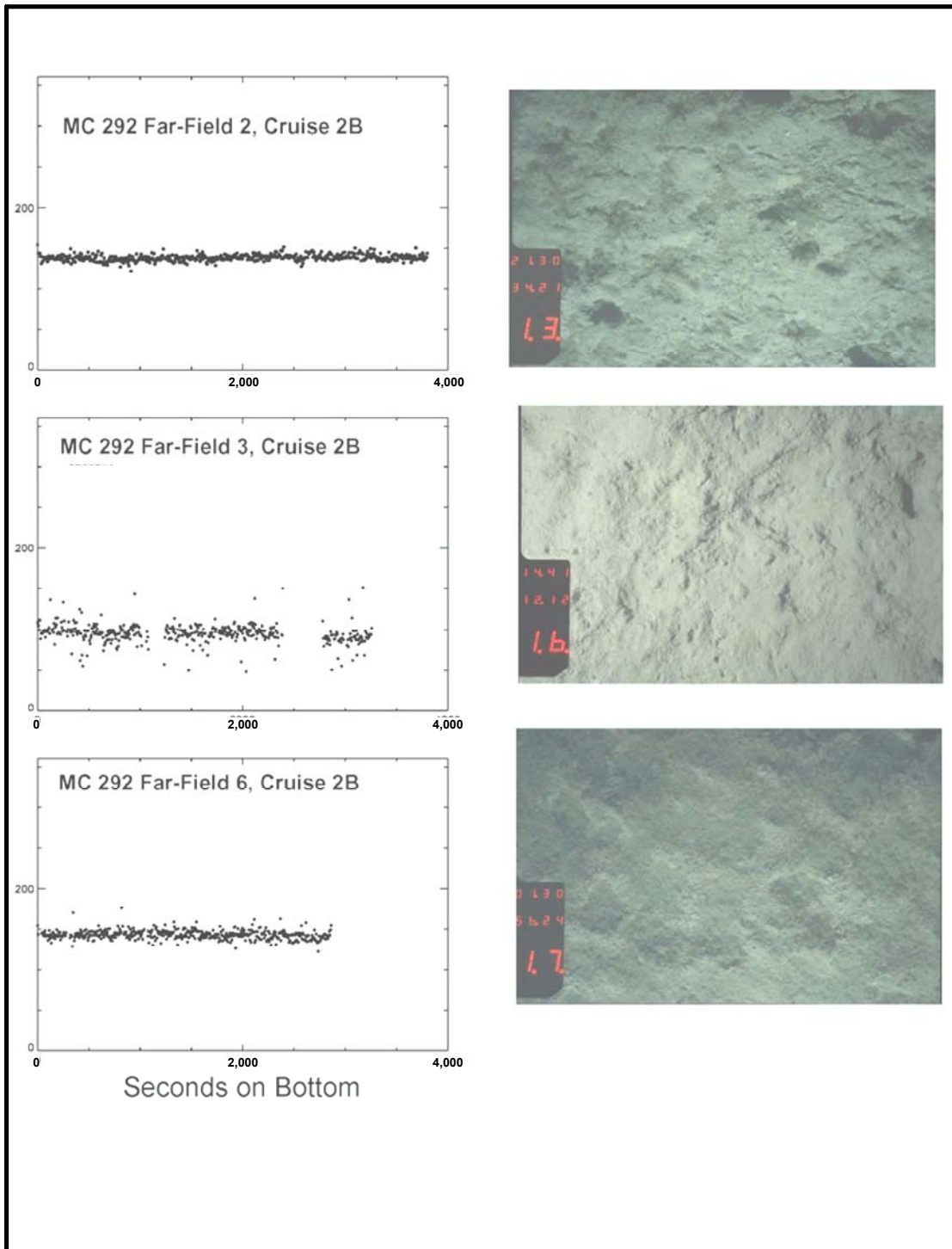


Figure 12.15. Image analysis results for Mississippi Canyon (MC) Block 292, Cruise 2B, far-field transects.

**Table 12.1.** Results of photographic faunal survey. Data are counts of each type of animal seen in photographs from each transect.

Site	Far/Near	Cruise/Film	No. of Images	No. of Animals						
				Total	Coelenterates	Shrimps	Ophiuroids	Fishes	Crabs	Gastropods
<b>Viosca Knoll Block 916</b>										
<i>Cruise 1B "pre-drilling"</i>										
VK 916	FF3	C-1-R-14	490	49	12	2	17	3	6	9
VK 916	FF4	C-1-R-13	64	2	1	0		0	1	0
VK 916	FF4	C-1-R-16	442	19	2	2	8	6		1
VK 916	FF5	C-1-R-11	433	30	2	3	13	8	1	3
VK 916	NF-1	C-1-R-6	246	15	3	3	3	2	1	3
VK 916	NF-2	C-1-R-10	406	23	6	3	7	3	3	1
VK 916	NF-3	C-1-R-15	453	26	2	2	6	4	8	4
		Average	362.00	23.43	4.00	2.14	9.00	3.71	3.33	3.00
		Image/Count <sup>a</sup>		0.0647	0.0110	0.0059	0.0249	0.0103	0.0092	0.0083
<i>Cruise 3B "post-drilling"</i>										
VK 916	FF4	C-3-R-6	698	68	16	30	7	7	1	7
VK 916	FF5	C-3-R-5	710	56	19	20	10	3	2	2
VK 916	NF-1	C-3-R-2	695	47	17	7	7	12	4	0
VK 916	NF-2	C-3-R-3	712	47	9	6	3	23	2	4
VK 916	NF-4	C-3-R-7	753	50	26	6	6	6	2	4
		Average	713.60	53.60	17.40	13.80	6.60	10.20	2.20	3.40
		Image/Count <sup>a</sup>		0.0751	0.0244	0.0193	0.0092	0.0143	0.0031	0.0048

**Table 12.1.** (Continued).

Site	Far/Near	Cruise/Film	No. of Images	No. of Animals						
				Total	Coelenterates	Shrimps	Ophiuroids	Fishes	Crabs	Gastropods
<b>Garden Banks Block 516</b>										
<i>Cruise 1B</i>										
GB 516	FF1	C-1-R-19	240	28	9	5	12	0	0	2
GB 516	FF3	C-1-R-18	560	36	9	3	15	5	3	1
GB 516	FF3	C-1-R-4	580	17	2	5	8	1	1	0
GB 516	FF5	C-1-R-17	300	25	4	5	12	3	0	1
GB 516	FF5	C-1-R-5	280	15	1	5	8	1	0	0
GB 516	NF-1	C-1-R-1	300	28	9	5	12	0	0	2
GB 516	NF-2	C-1-R-2	650	96	70	12	2	12	0	0
GB 516	NF-3	C-1-R-3	580	71	59	6	1	3	2	0
		Average	436.25	39.5	20.375	5.75	8.75	3.125	0.75	0.75
		Image/Count <sup>a</sup>		0.0905	0.0467	0.0132	0.0201	0.0072	0.0017	0.0017
<i>Cruise 2B</i>										
GB 516	FF1	C-2-R-6	340	4	0	3		0	1	
GB 516	FF2	C-2-R-1	510	58	16	19	17	5	1	0
GB 516	FF6	C-2-R-2	440	40	6	14	15	2	3	0
GB 516	NF-1	C-2-R-3	460	28	11	12	0	5	0	0
GB 516	NF-2	C-2-R-4	440	60	31	16	1	11	1	0
GB 516	NF-3	C-2-R-5	440	28	1	10	5	11	1	0
		Average	438.33	36.33	10.83	12.33	7.60	5.67	1.17	0.00
		Image/Count <sup>a</sup>		0.0829	0.0247	0.0281	0.0173	0.0129	0.0027	0.0000

Table 12.1. (Continued).

Site	Far/Near	Cruise/Film	No. of Images	No. of Animals						
				Total	Coelenterates	Shrimps	Ophiuroids	Fishes	Crabs	Gastropods
<b>Garden Banks Block 602</b>										
<i>Cruise 2B "post-drilling"</i>										
GB 602	FF2	C-2-R-9	370	10	3	4	0	1	2	0
GB 602	FF3	C-2-R-8	380	11	1	3	3	2	2	0
GB 602	FF6	C-2-R-12	435	12	1	3	3	2	1	2
GB 602	NF-1	C-2-R-7	180	18	0	15	0	3	0	0
GB 602	NF-2	C-2-R-10	175	24	1	22	0	1	0	0
GB 602	NF-3	C-2-R-11	342	50	2	39	2	7	0	0
		Average	313.67	20.83	1.33	14.33	1.33	2.67	0.83	0.33
		Image/Count <sup>a</sup>		0.0664	0.0043	0.0457	0.0043	0.0085	0.0027	0.0011
<b>Mississippi Canyon Block 292</b>										
<i>Cruise 2B "post-drilling"</i>										
MC 292	FF2	C-2-R-13	348	8	1	1	3	2	1	0
MC 292	FF3	C-2-R-16	413	11	1	2	2	5	0	1
MC 292	FF6	C-2-R-17	481	9	1	4	2	1	0	1
MC 292	NF-1	C-2-R-14	540	5	0	1	2	2	0	0
MC 292	NF-2	C-2-R-15	412	11	0	1	2	3	4	1
MC 292	NF-3	C-2-R-18	472	12	2	2	1	5	1	1
		Average	444.33	9.33	0.83	1.83	2.00	3.00	1.00	0.67
		Image/Count <sup>a</sup>		0.0210	0.0019	0.0041	0.0045	0.0068	0.0023	0.0015
<b>Total</b>			<b>16,770</b>	<b>1,147</b>	<b>356</b>	<b>301</b>	<b>215</b>	<b>170</b>	<b>55</b>	<b>50</b>
<b>Image/Count<sup>a</sup></b>				<b>0.0684</b>	<b>0.0212</b>	<b>0.0179</b>	<b>0.0128</b>	<b>0.0101</b>	<b>0.0033</b>	<b>0.0030</b>

FF = far-field; NF = near-field.

<sup>a</sup> Proportion of images that contained identifiable fauna.



Fauna imaged but omitted from analysis include the holothuroid *Mesothuria lactea* and the starfish *Dytaster* sp. Fewer than five were seen of each in the entire survey.

The primary hypothesis behind the image analysis task was that fauna in the near-field and in the far-field are equal within natural variation. A traditional approach to testing this hypothesis might have estimated faunal densities near and far, and then tested for uniformity of the densities. Due to the small area of bottom captured in each photograph, most images contained no fauna, and with very few exceptions, only one animal was seen in any picture. These facts made a goodness-of-fit analysis, based on percentages of images with fauna, a simple and informative approach.

Roll 13 of Cruise 1B at VK 916 was omitted due to the very limited number of images, leaving 37 camera tows to be divided into two categories: close to development (n=15) and far from development (n=22). The division followed the original plan of near- and far-fields, with two important exceptions. The VK 916 near-field pre-drilling sites were considered far from development. The GB 516 Cruise 1B near-field tows were categorized as being in the vicinity of development due to prior drilling activity. Results are presented in **Table 12.2**.

**Table 12.2.** Results of comparisons between near-field and far-field tows.

Images	Total	Coel.	Shrimps	Ophiuroids	Fishes	Crabs	Gastropods
Near-field w. fauna	575	238	160	44	104	17	12
Far-field w. fauna	570	117	141	171	66	37	38
Kolmogorov Z	1.0316	0.8506	0.7692	1.701	1.384	0.8959	0.9049
Prob. greater by chance	0.1639	0.3408	0.4644	<b>0.0022*</b>	<b>0.0239*</b>	0.2937	0.2776

\* Significant result (null hypothesis rejected).

A Kolmogorov two-sample test was performed using the statistical package of PV-WAVE. One sample consisted of results from each of the near-field tows, and the other consisted of results from each of the far-field tows. The differences (higher or lower) in proportion of images with and without fauna may occur by chance alone, with a probability of 0.1639. Thus the hypothesis of faunal independence is accepted using the traditional criteria of  $\alpha = 0.05$ . No clear effect of proximity for all fauna could be convincingly detected.

For fishes and ophiuroids, significant results were obtained. For fishes, the probability of the observed differences in proportions being to chance alone were 0.0239. Thus, for fishes, the hypothesis of similar fauna must be rejected by the criteria of  $\alpha = 0.05$ . Fishes are more abundant near development than far from it. For ophiuroids, a similar probability of the results by chance was 0.0022, also significant. The direction of the near-field versus far-field changes is opposite. Fishes were significantly more abundant near development activity, while ophiuroids were more abundant remote from development.

The intended before/after comparison at GB 516 and VK 916 was seriously compromised by the fact that the GB 516 site had been drilled prior to the “before” sampling (as well indicated in the

color analysis). The VK 916 site produced problematic results. Both near- and far-field sites produced generally higher numbers during the “after” cruise. By the design criteria, these changes must be attributed to an overall increase independent of drilling effects. Conceptually, it is still possible to carry out a low power before/after control comparison. The low number of images with fauna, however, causes small changes to have disproportionate effects. Thus, natural increase cannot be partitioned from any drilling effects.

## **12.5 DISCUSSION**

The results of this image analysis task are important from three perspectives:

1. The study did produce definitive indications of near-field versus far-field effects.
2. The color analysis greatly increased the data utility of images.
3. The pros and cons of small area images could be considered.

### **12.5.1 Faunal Results**

The faunal results were consistent with previous findings in shallow water. Color analysis, combined with the results of geophysical surveys (*Chapter 4*) and chemical analyses (*Chapters 8 and 9*), suggest that the near-field images were taken in or very close to deposits of drilling discharges. Thus, there is no uncertainty as to the presence of a potentially impacting process. Overall, small megafauna showed little impact; there was no gross reduction or increase in imaged fauna. Localized significant shifts were found for two component groups. Fishes were more abundant in the near-field consistent with attraction to disturbance and structure. Ophiuroids were less abundant in the near-field. An exact cause is less easily suggested. The very flat organisms might have been buried by cuttings, or there may be a behavior shift, which resulted in fewer animals being seen in the near-field.

### **12.5.2 Color Analysis**

Using hue rather than digital RGB as a descriptive parameter for color proved exceptionally successful. Subjective classification of images was quantified and made more useful for (GIS)-type display. The patterns of dark bottom coincided with acoustic mapping of cuttings reasonably well. Such a linkage between biological sampling and geological survey has the potential to greatly increase the reliability of impact studies.

### **12.5.3 Consideration of Size**

The use of small-area, straight-down imaging in this study was unique. It probably contributed to the detection of a difference in the ophiuroids, and it did not prevent detection of a difference in the larger fishes. It did not, however, make available a new suite of species for observation. Making some simplistic assumptions about density-area relationships, it can be predicted that quadrupling the area of the image (doubling the linear dimensions) would produce a four-fold increase in the number of images capturing fauna, about 28% based on the current studies. Such an increase in size would not lose too many animals below the limits of resolution.

## Chapter 13 Genetic Diversity of Harpacticoid Copepods

*Christopher S. Gregg, David W. Foltz, and John W. Fleeger  
Louisiana State University*

---

### 13.1 INTRODUCTION

The deep sea in the northern Gulf of Mexico is an increasingly active area for exploration of oil resources. The ecological (Peterson et al. 1996) and genetic (Street and Montagna 1996) impacts of offshore oil exploration and production have been studied in shallow continental shelf habitats; however, there are currently no data on the effects of oil exploration and production on genetic diversity of deep-sea infauna (Creasy and Rogers 1999).

In shallow water, reductions in genetic diversity have been observed in populations of harpacticoid copepods living near offshore oil platforms compared to reference sites (Street and Montagna 1996). Studies of natural populations of fishes (Murdoch and Hebert 1994) and aquatic insects (Beaty et al. 1998) have also noted reductions in genetic diversity in populations exposed to contaminants compared to those from uncontaminated sites. Additionally, laboratory experiments on harpacticoid copepods have shown reductions in genetic diversity when copepods were exposed to xenobiotics such as PAHs (Street et al. 1998) or pesticides (Schizas et al. 2001). Two mechanisms that may cause the observed reductions in genetic diversity in natural populations exposed to contaminants are natural selection and population bottlenecks (reviewed in Hebert and Luiker 1996; Bickham et al. 2000; Belfiore and Anderson 2001). Natural selection reduces genetic diversity by the differential survival of tolerant genotypes compared to less tolerant genotypes. Schizas et al. (2001) demonstrated that *Microarthridion littorale* that possessed one mitochondrial lineage had greater survival when exposed to pesticides compared to those possessing other lineages, thus bolstering the argument for natural selection. Genetic diversity can be decreased in a population that has undergone a rapid decrease in population size, a bottleneck, through the loss of rare alleles by the random process of genetic drift. Additionally, a small population that has undergone a rapid increase in size may show low diversity because mutation and gene flow would not have had time to introduce new alleles (reviewed in Harpending et al. 1998).

Undetected cryptic species (i.e., morphologically similar but genetically divergent species) may also be a factor in observed reduction in genetic diversity. Molecular analysis within some previously well-studied species has revealed genetic divergence suggestive of interspecific differences (Knowlton 1993, 2000). Cryptic species have been found to occur in widely-studied pollution indicator species (e.g., Grassle and Grassle 1976; Lobel et al. 1990) and in harpacticoids (Ganz and Burton 1995; Rocha-Olivares et al. 2001). The presence of cryptic species may contribute to an observed loss in genetic diversity, if they differ in their tolerance to contaminants and if they are sympatric at uncontaminated sites. This would represent a loss of species diversity as opposed to genotypic selection. Fleeger et al. (2001) demonstrated that cryptic species within the genus *Cletocamptus*, which co-occur in Louisiana salt marshes, exhibited differential

tolerances to heavy metals. The possibility of cryptic species must be accounted for when examining the effect of pollution on genetic diversity.

In the present study, we intended to determine if genetic diversity in harpacticoid copepods was reduced in populations near development drilling sites compared to populations from reference sites (*sensu* Street and Montagna 1996). Sites adjacent to (near-field) and distant from (far-field) development drilling sites were sampled at two locations off the coast of Louisiana at water depths slightly greater than 1,000 m. Analysis of samples taken near the drillsites and at reference sites indicated that two very different harpacticoid communities with few species in common were present. Near-field sites were characterized by a relatively low species diversity, high dominance community. Large numbers of a single species, *Bathyletopsyllus* sp., typified near-field sites, although other species were present in unusually high densities for the deep sea. Far-field sites were characterized by high species diversity and low dominance, more typical of undisturbed deep-sea communities. Almost no species were in common at near-field sites and far-field sites (*Bathyletopsyllus* sp. was found in only one far-field site, represented by one individual). We concluded that *Bathyletopsyllus* sp. was likely an opportunistic species, present in low numbers in undisturbed deep-sea habitats, but able to undergo a population expansion in response to disturbance associated with oil drilling and production activities.

*Bathyletopsyllus* sp. is a benthic harpacticoid copepod in the family Cleptopsyllidae (Huys and Lee 1998/99). Thus far, only one species, *Bathyletopsyllus hexarthra*, of this genus has been described from the Indian Ocean off Le Réunion at a depth of 400 m in muddy sediments (Huys and Lee 1998/99). The species examined in the present study has not been described, but it is approximately 0.9 mm in body length. The females brood their larvae in an attached egg sac (personal obs.), typical of harpacticoid copepods (Hicks and Coull 1983).

The objectives of the present study were to examine the genetic diversity and population structure of *Bathyletopsyllus* sp. at the two development drilling sites, which are approximately 407 km distant from each other in the northern Gulf of Mexico. Additionally, DNA sequence data were used to determine whether the harpacticoids examined were a single species or a complex of cryptic species. We examined DNA sequence variation of the mitochondrial cytochrome c oxidase subunit I (COX I) gene. Mitochondrial genes have been used extensively to study the population genetics of harpacticoid copepods (Burton and Lee 1994; Burton 1998; Schizas et al. 1999; Edmands 2001; Schizas et al. 2001) as well as to examine the effects of pollution on harpacticoids (Street et al. 1998; Fleeger et al. 2001; Schizas et al. 2001). The presence of cryptic species among harpacticoid copepods (Ganz and Burton 1995; Rocha-Olivares et al. 2001) has also been detected using the COX I gene. The patterns of population genetic diversity and genetic structure or the presence of cryptic species were used to determine how *Bathyletopsyllus* sp. may have responded to environmental disturbance associated with oil production activities. The present study was also the first to examine the population genetics of a deep-sea harpacticoid species using data from a mitochondrial gene.

## 13.2 METHODS

### 13.2.1 Collection and Processing of Samples

Two post-development drilling sites were sampled in July 2001. GB 602 and MC 292 are located off the coast of Louisiana at depths of 1,125 m and 1,034 m, respectively (see *Chapter 2*). Sediment samples were collected by box core from which subsamples were taken by coring. Three 7.6-cm diameter cores were taken from each box core to obtain harpacticoid copepods for genetic analysis. Twelve box cores were collected at both GB 602 and MC 292 from randomly selected locations within 500 m of each post-development site. Subsamples from box cores were combined into one collection jar and were preserved onboard ship in 95% ethanol. Details of the sampling sites and general sampling methods are given in *Chapter 2* of the present report.

Sediment samples were stained with rose bengal and stored at 4°C upon arrival at Louisiana State University. Processing consisted of sieving on a 63- $\mu$ m sieve, then sorting and removing the harpacticoid copepods under a stereo dissection microscope. All sorting was done in SED buffer (Seutin et al. 1991) to minimize DNA degradation. Identification of the harpacticoids to the lowest taxonomic level was done by one of us (John W. Fleeger), and one species in the genus *Bathycletopsyllus* was found to be abundant at near-field sites at both GB 602 and MC 292.

### 13.2.2 Genetic Methods

DNA was extracted from individual copepods using the Gene Releaser (BioVentures, Inc.) protocol described by Schizas et al. (1997). A 710-base pair portion of the mitochondrial COX I gene was amplified by the PCR using primers developed by Folmer et al. (1994) (LCOI: 5'-GGTCAACAAATCATAAAGATATTGG-3'; HCOI: 5'-TAAACTTCAGGGTGACCAAAAAATCA-3'). Reactions were done at 50- $\mu$ l final volume, and the final concentrations of the reagents were as follows: 1X Promega Reaction Buffer A; 2.5 mM MgCl<sub>2</sub>; 0.2 mM total dNTPs; 1  $\mu$ M of both forward and reverse primers; three units Promega Taq polymerase; 2- $\mu$ l DNA extract; sterile H<sub>2</sub>O to bring volume to 50  $\mu$ l. The PCR was done in a Perkin-Elmer DNA Thermal Cycler under the following conditions: 1 cycle 95°C for 3 min; 40 cycles of 95°C for 30 sec, 47°C for 45 sec, and 74°C for 1 min; 1 cycle 74°C for 7 min. Three  $\mu$ l of each PCR product was electrophoresed into a 2% agarose gel, stained with ethidium bromide, and visualized by ultraviolet transillumination.

Because of the small size of the organisms (<1 mm) and poor preservation of some samples, initial amplifications with the LCOI and HCOI primers of Folmer et al. (1994) had a low success rate, and DNA sequencing revealed contaminating coamplicons. Primers internal to LCOI – HCOI were designed, BathyLCOI (5'-ATATTGGTACCTTGAATTTGTTAGC-3') and BathyHCOI (5'-CCAAAAAATCAAAATAAATGCTGGT-3'), by examining preliminary sequence data from the LCOI – HCOI fragment. This led to a higher success rate and elimination of contaminating coamplicons. Additionally, two primers were designed from the middle of the PCR fragment, BathyCOI K (5'-GGGCHCCTGATATGGCTTTTCC-3', modified from Burton and Lee 1994) and Bathy iR (5'-ATTATTTAATCGAAGAAAAGCCATA-3') to provide greater overlapping coverage of the COX I gene for unambiguous assembly of contigs.

DNA sequences of the COX I gene were obtained from individuals chosen at random; a total of 33 individuals from GB 602 and 28 from MC 292 was analyzed. The PCR products were

purified using Exo-SAP IT (USBiochemicals) following the manufacturer's protocols, then sequenced using the ABI-Prism Big-Dye cycle sequencing chemistry (Applied Biosystems). The sequencing reactions were scaled down to 10- $\mu$ l reaction volumes, as described by Rocha-Olivares et al. (2001), and run on an ABI-377 Gene Analyzer (Applied Biosystems).

### 13.2.3 Data Analysis

A genealogy of the COX I gene in *Bathycletopsyllus* sp. was constructed to show the relationships among the different haplotypes observed in the two populations. A minimum-spanning tree was constructed using Arlequin v. 2.0 (Schneider et al. 2000), and a statistical-parsimony network was constructed using TCS v. 1.13 (Clement et al. 2000), with genealogies from both methods producing identical topologies. Network approaches were chosen over traditional phylogenetic approaches, represented by a bifurcating tree, because in intraspecific studies, ancestral haplotypes are usually extant and give rise to multiple descendent haplotypes (Smouse 1998; Posada and Crandall 2001).

Genetic subdivision of the populations was examined by analysis of molecular variance (AMOVA; Excoffier et al. 1992) using the program Arlequin v. 2.0 (Schneider et al. 2000). A hierarchical design was implemented to test the null hypotheses of no heterogeneity of haplotype frequencies between sites, among box cores within sites, and within box cores. The distance matrix used in the analysis consisted of pairwise differences among haplotypes; additionally, conventional F-statistics were determined based only on allele frequencies where distances between all pairs of non-identical haplotypes were set to one. The null distribution for significance tests was obtained by 644 random permutations of the data matrix.

Two methods were used to make inferences regarding population demographics of *Bathycletopsyllus* sp. at the two drilling sites: comparison of haplotype and nucleotide diversities and mismatch distribution analysis. Haplotype diversity (probability that two randomly chosen haplotypes are different;  $h$ ) and nucleotide diversity (probability that two homologous nucleotides are different;  $\pi_n$ ) were calculated for both populations. Low values for  $h$  and/or  $\pi_n$  are expected in recently founded populations or populations that have undergone a demographic bottleneck, and high values are expected in large populations in equilibrium (Bowen and Grant 1997; Avise 2000). Mismatch distributions, the frequency distribution of the number of nucleotide differences between pairs of individuals, were determined for both populations and compared to a sudden population expansion model (Rogers and Harpending 1992; Rogers 1995). Slatkin and Hudson (1991) and Rogers and Harpending (1992) have demonstrated that populations that have undergone a relatively recent population expansion exhibit a unimodal mismatch distribution, while populations in equilibrium exhibit a multimodal distribution. A Kolmogorov-Smirnov two-sample test was used to test the null hypothesis that the mismatch distributions for the populations at both sites did not differ (Sokal and Rohlf 1995). Also, the fit of the observed mismatch distribution for both populations to a sudden expansion model (Li 1977) was tested using the procedure of Schneider and Excoffier (1999). The sudden expansion model determines a frequency distribution of the expected number of nucleotide differences between two randomly chosen haplotypes in a population that has undergone an expansion. The molecular indices ( $h$  and  $\pi_n$ ) were calculated, and the mismatch distribution analysis was performed using Arlequin v. 2.0 (Schneider et al. 2000).

## 13.3 RESULTS

### 13.3.1 Numerical Response to Disturbance by *Bathyletopsyllus* sp.

One species of harpacticoid copepod in the genus *Bathyletopsyllus* was present in sufficient numbers at near-field samples from both GB 602 and MC 292 for genetic analysis (**Table 13.1**). At GB 602, a total of 459 *Bathyletopsyllus* sp. was found and removed from all 12 near-field samples, where 9 of 12 samples had 10 or more individuals, and 4 of 12 had greater than 50 individuals. *Bathyletopsyllus* sp. was less common at MC 292, with 183 individuals sorted from all 12 near-field samples, but was still present in sufficient numbers for genetic analysis. Two out of 12 samples had more than 10 individuals.

The density of *Bathyletopsyllus* sp. appeared to be related to the concentration of SBF hydrocarbons (see *Chapter 9*) in a complex fashion. At near-field GB 602, SBF concentrations were an order of magnitude greater than at the MC 292 site, and there was no relationship between SBF concentration and *Bathyletopsyllus* sp. density ( $r^2 = 0.04$ , **Figure 13.1a**). At the MC 292 near-field site, there was a positive relationship between SBF concentration and *Bathyletopsyllus* sp. density ( $r^2 = 0.85$ , **Figure 13.1b**). Regression of SBF concentrations with copepod numbers at GB 602 with observations from box cores with SBF concentrations less than 2,500  $\mu\text{g}/\text{dry g}$  revealed a positive linear relationship ( $r^2 = 0.52$ , **Figure 13.1c**). The SBF concentration above 2,500  $\mu\text{g}/\text{dry g}$  was chosen because it was near the maximum concentration observed at MC 292. These data suggest that *Bathyletopsyllus* sp. responds positively to increasing levels of disturbance/hydrocarbons up to a certain threshold level, but then density decreases with increasing concentration above the threshold.

### 13.3.2 Genetic Divergence

The analyzed dataset consisted of 605 base pairs of the mitochondrial COX I gene with sequence data collected from 33 *Bathyletopsyllus* sp. from GB 602 and 28 from MC 292. Among the COX I gene sequence data, 9 haplotypes and 13 polymorphic sites were observed from GB 602 individuals, while 11 haplotypes and 14 polymorphic sites were observed from MC 292 individuals. The average transition to transversion ratios for the GB 602 and MC 292 data were 8.9 and 3.6, respectively. The nucleotide composition showed that thymine (T) was the most common nucleotide, and cytosine (C) was the least common at both sites, with C = 14.9%, T = 35.9%, adenine (A) = 26.3%, and guanine (G) = 22.9% for GB 602, and C = 14.7%, T = 36.0%, A = 26.5%, and G = 22.8% for MC 292. The maximum P-distance was 1.6%, and the mean P-distance was 0.5% as calculated in MEGA 2.1 (Kumar et al. 2001). The maximum observed P-distance was within the range of values expected for within-species variation; thus the two populations likely represent a single species and not a complex of cryptic species.

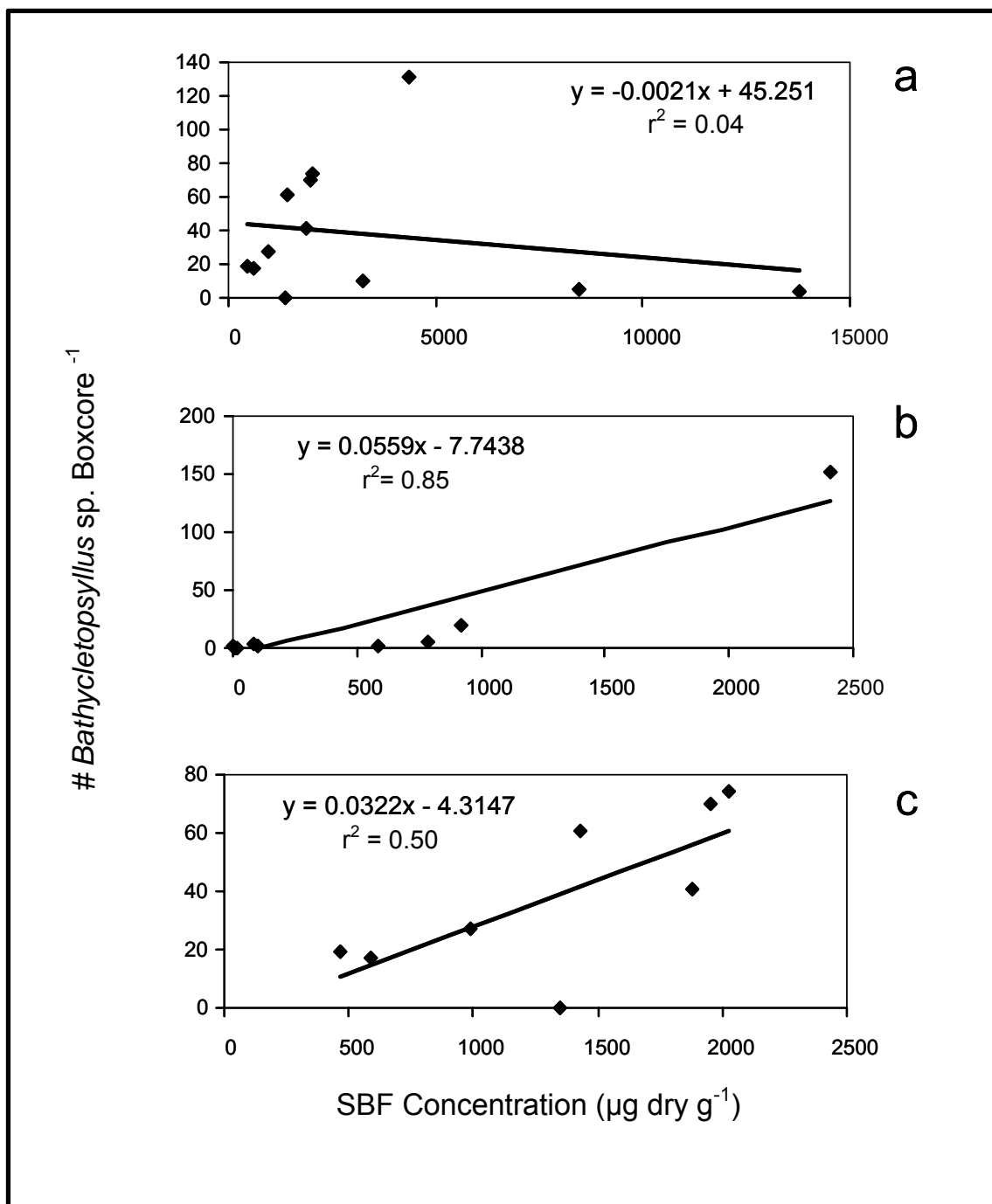


**Figure 13.1.** Relationship between synthetic based fluid (SBF) concentration and the number of *Bathycletopsyllus* sp. per box core at the near-field sites. (a) Relationship at Garden Banks Block 602 including all box cores. (b) Relationship at Mississippi Canyon Block 292 including all box cores. (c) Relationship at Garden Banks Block 602 excluding box cores with SBF concentrations greater than 2,500 μg dry g<sup>-1</sup>.



**Table 13.1.** Numbers of *Bathycletopsyllus* sp. collected from box cores at the near-field sites of Garden Banks (GB) Block 602 and Mississippi Canyon (MC) Block 292. The numbers are the total number of *Bathycletopsyllus* sp. found in three, 7.6-cm diameter cores taken from box core samples.

Box Core	Site	
	GB 602	MC 292
B01	19	151
B02	17	6
B03	5	3
B04	41	1
B05	131	1
B06	10	0
B07	70	0
B08	4	20
B09	61	0
B10	0	1
B11	74	0
B12	27	0
Total	459	183

The haplotype cladogram revealed the presence of three distinct clades, which will henceforth be referred to as Clades BI, BII, and BIII for *Bathycletopsyllus* clade (**Figure 13.2**). Clade BI was separated from both Clades BII and BIII by three mutational steps, and Clades BII and BIII were separated from each other by a minimum of six mutational steps. The distribution of haplotypes was spatially heterogeneous as there were few haplotypes shared among sampling sites. Eighty-three percent of the individuals in Clade BI was from GB 602, while 88% and 89% of the individuals from Clades BII and BIII were from MC 292, respectively (**Table 13.2**). Haplotype A was the most frequently occurring haplotype in Clade BI, from which all other Clade BI haplotypes appear to have arisen. Haplotype I was the most frequently occurring haplotype in Clade BII; however, the relationships among the other haplotypes were more complex in that they do not all radiate from this haplotype in a “star phylogeny” (Slatkin and Hudson 1991) as in Clade BI. Only three haplotypes were observed in Clade BIII, with no single haplotype numerically dominant.

### 13.3.3 Population Structure

The AMOVA indicated genetic heterogeneity between *Bathycletopsyllus* sp. populations at the GB 602 and MC 292 sites. Significant genetic structuring was noted between the two sites sampled using both pairwise distances ( $\Phi_{st} = 0.35$ ;  $P < 0.0001$ ) and haplotype frequencies ( $F_{st} = 0.21$ ;  $P < 0.0001$ ) (**Table 13.3**). There was no evidence of genetic structure among the subpopulations represented by box cores within sites in AMOVAs using both pairwise differences ( $\Phi_{sc} = 0.043$ ;  $P = 0.075$ ) and haplotype frequencies ( $F_{sc} = 0.0013$ ;  $P = 0.37$ ) (**Table 13.3**).

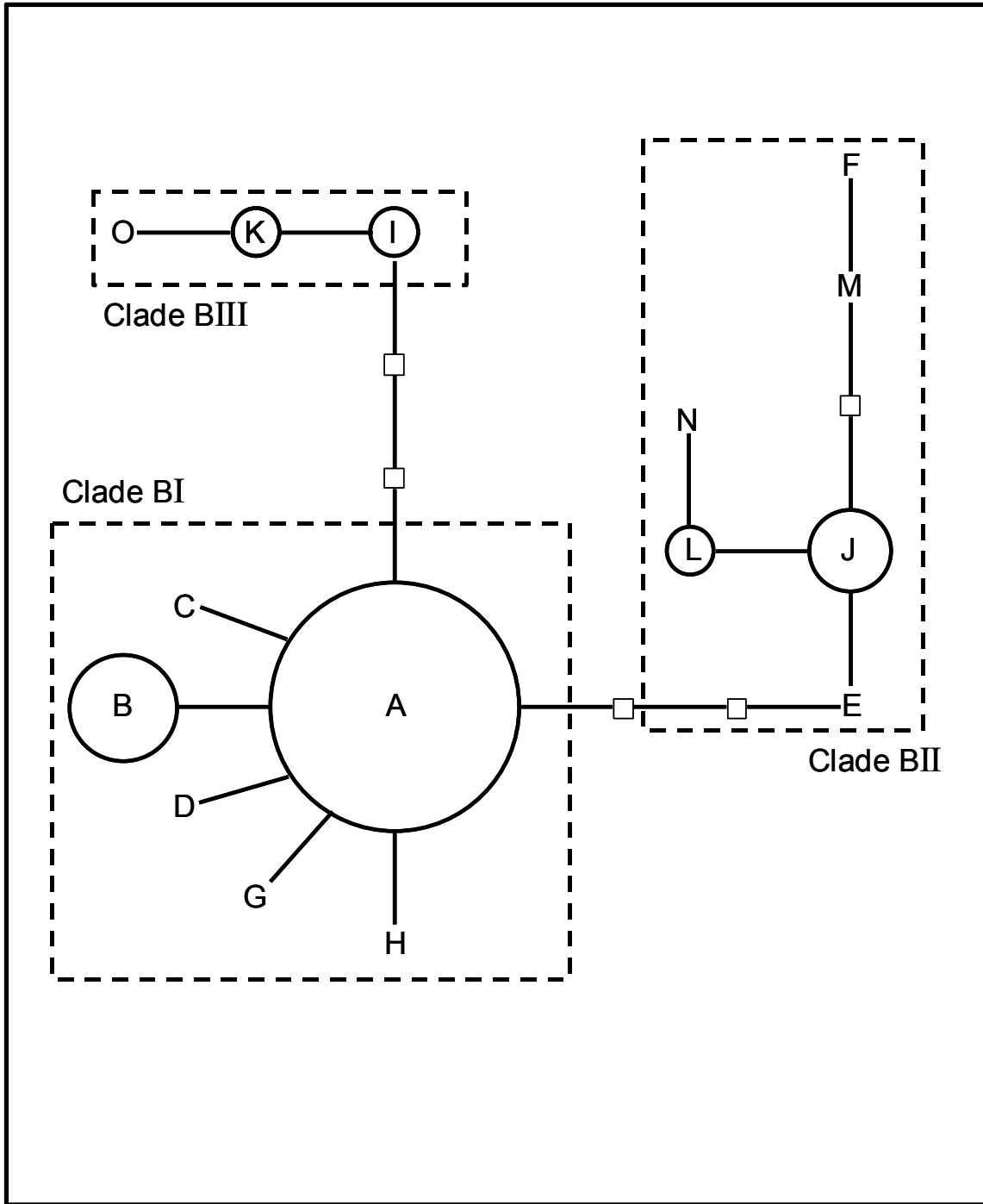


**Figure 13.2.** Haplotype network of 15 unique cytochrome c oxidase subunit I COX I sequences. Letters represent different haplotypes. Circles are drawn proportional to the number of individuals sharing a certain haplotype. Haplotypes without circles had 2 individuals. Each line represents a nucleotide substitution, and  $\square$  represent unobserved or extinct haplotypes.

**Table 13.2.** Distribution of *Bathycletopsyllus* sp. haplotypes at each sampled location in Garden Banks Block 602 and Mississippi Canyon Block 292. Clades correspond to those shown in **Figure 13.2**.

Box core	Haplotype															Total
	A	B	C	D	E	F	G	H	I	J	K	L	M	N	O	
Garden Banks 602																
B01	3	1											1			5
B02	3	1		1												5
B04	4						1									5
B05	1	1														2
B07	1	1			1	1										4
B08		1														1
B11	4	1	1													6
B12	4							1								5
Mississippi Canyon 292																
B01								2	2	1			2	3	1	11
B02								3						1		4
B03												1				1
B04									1							1
B08	1	3			1	1			2	1	1		1			11
Total	21	9	1	1	2	2	1	1	7	4	2	1	4	4	1	61
Total Clade BI = 36							Total Clade BII = 16					Total Clade BIII = 9				

**Table 13.3.** Analysis of molecular variance across the populations from the Garden Banks 602 and Mississippi Canyon 292 sites. For each analysis, the percentage of the variance explained (%) and the probability of more extreme values from 644 permutation tests (P) are presented. Values outside the parentheses are from the analysis of molecular variance (AMOVA) weighted by pairwise differences between haplotypes. Those within parentheses are from the unweighted AMOVA.

Source of Variation	%	P
Among sites	32 (21.4)	0.0015 (<0.0001)
Among box cores within sites	3 (0.10)	0.075 (0.37)
Within sites	65 (78.5)	<0.0001 (<0.0001)

$\Phi_{st} = 0.35$ ;  $\Phi_{sc} = 0.043$ ;  $\Phi_{ct} = 0.32$ .

$F_{st} = 0.21$ ;  $F_{sc} = 0.0013$ ;  $F_{ct} = 0.21$ .

### 13.3.4 Genetic Diversity

The indices measuring molecular, haplotype, and nucleotide diversity indicated different demographic histories for *Bathycletopsyllus* sp. at GB 602 and MC 292. Haplotype diversity was 0.61 (standard deviation [SD]  $\pm$  0.089) and 0.89 (SD  $\pm$  0.033), and nucleotide diversity was 0.0020 (SD  $\pm$  0.0014) and 0.0066 (SD  $\pm$  0.0038) at GB 602 and MC 292, respectively. Haplotype diversity was significantly lower at GB 602 compared to MC 292 ( $t = 15.95$ ,  $df = 59$ ,  $P < 0.001$ ). Nucleotide diversity was also significantly lower at GB 602 compared to MC 292 ( $t = 6.43$ ,  $df = 59$ ,  $P < 0.001$ ). These diversity measures reflect the distribution of and relationship among the haplotypes at the two sites. GB 602 was numerically dominated by Haplotypes A (20) and B (6) in Clade BI, whereas haplotypes were more evenly distributed among Clades BI, BII, and BIII at MC 292, with no overwhelming numerical dominance by any haplotype at this site (**Table 13.2**). The low haplotype and nucleotide diversities observed for *Bathycletopsyllus* sp. at GB 602 were comparable to other harpacticoid copepods in the genus *Cletocamptus* and some populations of the species *Microarthridion littorale* (**Figure 13.3**). *Bathycletopsyllus* sp. collected at MC 292 had high haplotype diversity and low to moderate nucleotide diversity compared to other harpacticoids. The haplotype diversity for this population was similar to that observed in some populations of *Microarthridion littorale*, while the nucleotide diversity remained low to moderate (**Figure 13.3**).

The mismatch distributions from GB 602 and MC 292 populations differed significantly from each other ( $D = 0.54 > D_{.01} = 0.11$ ), but neither distribution differed significantly from a sudden expansion model. Pairwise comparisons of the DNA sequence data from the GB 602 population resulted in a unimodal frequency distribution that did not differ significantly from the sudden expansion model ( $P = 0.071$ ; **Figure 13.4a**). The observed mean number of mismatches among randomly chosen sequences was 1.21. The mismatch distribution for MC 292 was multimodal, but it also did not differ significantly from the sudden population expansion model ( $P = 0.068$ ; **Figure 13.4b**). The distribution produced by the MC 292 sequence data had a mean number of mismatches of 3.97. These data indicate that, while both populations may have undergone a population expansion, processes affecting the mismatch distribution differed at MC 292 compared to GB 602.

## 13.4 DISCUSSION

### 13.4.1 Numerical Response to Disturbance by *Bathycletopsyllus* sp.

*Bathycletopsyllus* sp. appeared to be the most abundant harpacticoid at both the GB 602 and MC 292 near-field sites; more than 100 individuals were found in some box core samples (**Table 13.1**). In the far-field sites, only one *Bathycletopsyllus* sp. individual was observed in over 24 box cores from both GB 602 and MC 292. These data suggest that this species responds to disturbance by increasing in population size. SBF concentrations may serve as a non-biotic indicator of disturbance. SBF hydrocarbons were elevated at near-field sites compared to far-field sites (see *Chapter 9*). At GB 602, the average SBF concentration in  $\mu\text{g/dry g}$  was 3,384.3 (SD  $\pm$  3,940.7) at the near-field site and 5.75 (SD  $\pm$  2.0) at the far-field sites. At MC 292, the average SBF concentration in  $\mu\text{g/dry g}$  was 411.2 (SD  $\pm$  712.6) at the near-field site and 6.95 (SD  $\pm$  8.4) at the far-field sites.

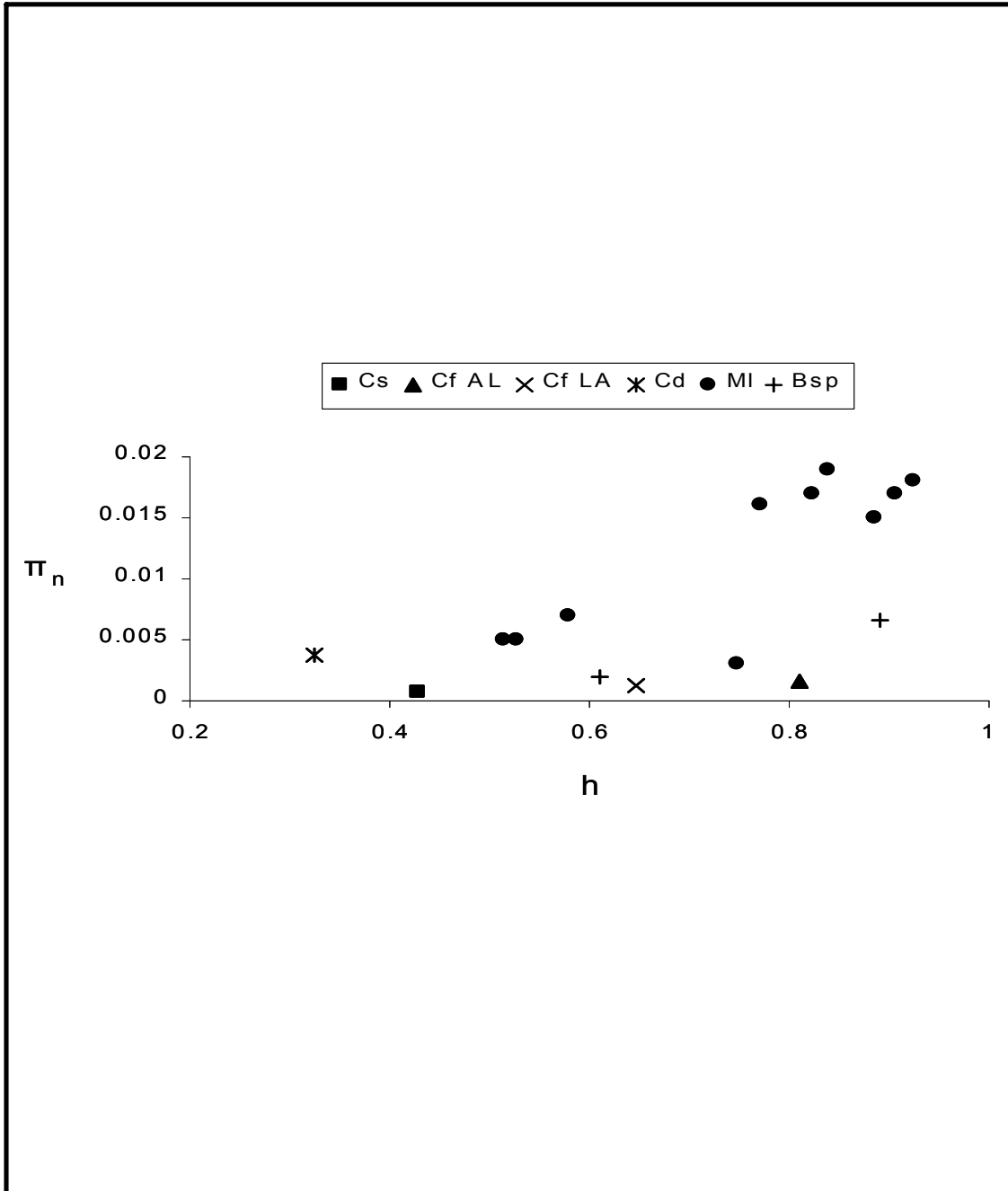


**Figure 13.3.** Relationship between haplotype diversity and nucleotide diversity of COX I sequences for five species of harpacticoid copepods including *Bathyletopsyllus* sp. The x-axis is haplotype diversity (h), and the y-axis is nucleotide diversity ( $\pi_n$ ). Cs = *Cletocamptus stimsoni*, Cf AL = *C. fourchensis* from Alabama, Cf LA = *C. fourchensis* from Louisiana, Cd = *C. deborahdexterae* (all *Cletocamptus* data were from Rocha-Olivares et al. 2001). MI = *Microarthridion littorale* (Schizas et al. 2002). Bsp = *Bathyletopsyllus* sp. All data were taken from COX I sequences except MI, which were from cytochrome b sequences.

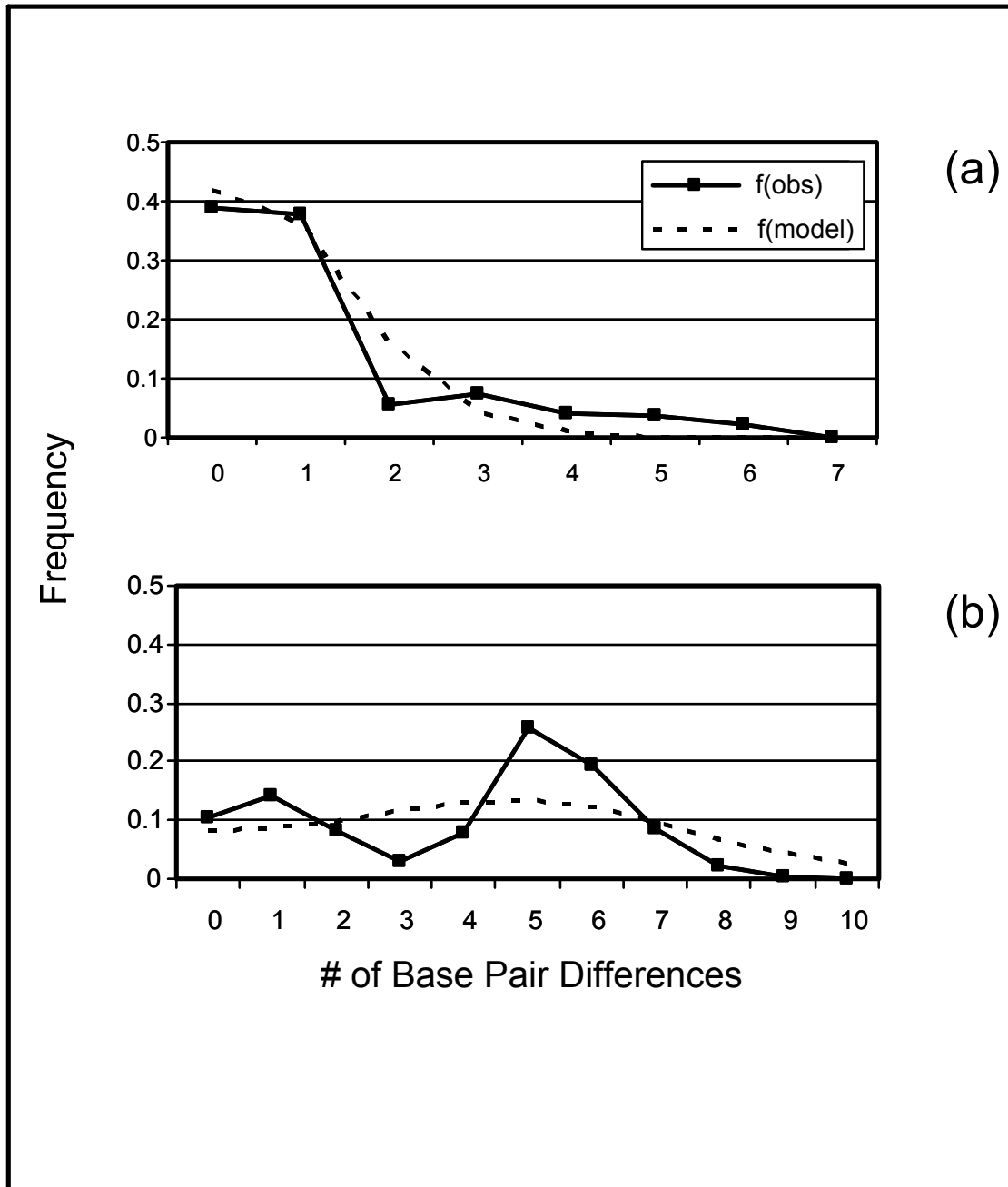


**Figure 13.4.** Mismatch distributions for pairwise haplotype distances between *Bathycletopsyllus* sp. individuals collected at Garden Banks (GB) Block 602 and Mississippi Canyon (MC) Block 292. The x-axis represents the number of base pair differences between individuals, and the y-axis represents the frequency. (a) Mismatch distribution for individuals at GB 602, (b) mismatch distribution for individuals at MC 292.  $f(\text{obs})$  = frequency of the observed number of base pair differences.  $f(\text{model})$  = frequency of the number of base pair differences expected with a sudden population expansion model.

Although the data in the present study were limited, there was a suggestion of a positive correlation between abundance of *Bathyletopsyllus* sp. and SBF hydrocarbons (see **Figure 13.1**). The relationship held only when SBF concentrations less than 2,500 µg/dry g were considered (**Figure 13.1a** and **13.1c**) at GB 602. These data suggest that *Bathyletopsyllus* sp. responds to disturbance/hydrocarbons by increasing in population size, but only up to a threshold concentration of SBF hydrocarbons, then this species decreases in number. These data must be interpreted with caution, however, because no information is available on the biology of this copepod species, let alone its tolerance to contaminants. It is possible that SBF concentrations at values below the threshold may serve as an indicator of physical disturbance to which *Bathyletopsyllus* responds. For example, a change in sediment granulometry may accompany the increased SBF concentrations associated with drilling activities. Laboratory experimentation and additional field sampling are necessary to determine cause-and-effect relationships.

#### 13.4.2 Genetic Divergence

Three discreet COX I lineages (BI, BII, and BIII) were observed in *Bathyletopsyllus* sp. populations from both GB 602 and MC 292. Clade BI was separated from Clades BII and BIII by three nucleotide differences, and Clades II and III were separated from each other by a minimum of six nucleotide differences. The maximum uncorrected difference among haplotypes was 1.6%, and the average uncorrected difference was 0.5%, which is within the range expected for intraspecific variability of the COX I gene. Therefore, the individuals sampled likely represent two populations of a single species and not a complex of cryptic species. The low level of divergence was surprising given the distance separating the two populations (407 km) and the usually low dispersal capabilities of harpacticoid copepods. High levels of divergence have been observed in other harpacticoid species over similar or even smaller spatial scales. For example, Rocha-Olivares et al. (2001) noted uncorrected genetic distances of up to 25% at the COX I gene in population comparisons of four populations of the morphologically described species *Cletocamptus deitersi*. Two of these diverged lineages are sympatric in populations from Louisiana and Alabama. Closer examination of the four genetically diverged lineages has revealed morphological differences, and they have been described as four distinct species (Gómez et al. in press). High levels of genetic differentiation at the COX I locus also have been noted in *Tigriopus californicus* populations from southern California over relatively small spatial scales (Burton and Lee 1994; Burton 1998; Edmands 2001). Burton (1998) has shown that *T. californicus* populations inhabiting the north and south sides of Santa Cruz Island exhibit as much as 22% sequence divergence at the COX I locus. In a genetic survey of *Microarthridion littorale* populations from South Carolina, Georgia, Florida, and Louisiana, Schizas et al. (1999) found high genetic divergence at another mitochondrial gene, cytochrome b (cyt b). Populations from Louisiana showed uncorrected nucleotide divergence of as much as 36%, while 10% divergences were observed among populations from South Carolina, Georgia, and Florida. In a smaller scale survey of *M. littorale* populations from South Carolina, three distinct cyt b clades that diverged by as much as 4.3% were observed (Schizas et al. 2002). The three cyt b lineages were found to co-occur at most of the sampled sites in South Carolina.

Genetic surveys of benthic invertebrates from the deep sea using mitochondrial genes have also revealed high genetic divergence over sometimes small spatial scales in morphologically similar taxa. For example, France and Kocher (1996) showed by comparing 16S rRNA sequences that

populations of the deep-sea amphipod, *Eurythenes gryllus*, diverged by 10% between depth zones. Also using the 16S rRNA gene, Chase et al. (1998) showed that populations of the bivalve, *Deminucula atacellana*, above 2,500 m, diverged from populations below 2,500 m by 4.1%. In contrast, Quattro et al. (2001), using cyt b sequences, found that populations of the deep-sea gastropod, *Frigidoalvania brychia*, at the same depth level, exhibited nucleotide divergences of up to 23%. These highly diverged populations were separated by a maximum distance of  $\approx 80$  km at the depth of 500 m. The levels of nucleotide divergence seen in these deep-sea organisms are consistent with divergence levels between species in shallow-water taxa, suggesting they may be cryptic species (Etter et al. 1999).

### 13.4.3 Population Structure

The *Bathycletopsyllus* sp. populations at GB 602 and MC 292 were genetically heterogeneous as indicated by the significant fixation indices ( $\Phi_{st} = 0.35$ ;  $F_{st} = 0.21$ ) in the AMOVA (**Table 13.3**). Examination of the distribution of haplotypes at the two sites indicates an absence of gene flow between the two populations (**Table 13.2**). Most of the individuals sampled from GB 602 were in Clade BI, while most of the individuals from MC 292 were in Clades BII and BIII. Harpacticoid copepods in general have low dispersal potential because most species brood eggs in an egg sac, which then hatch into a benthic naupliar stage (Hicks and Coull 1983). At the present time, the type of development possessed by *Bathycletopsyllus* sp. is unknown; however, females in our samples had attached egg sacs (pers. obs.), indicating that this species likely exhibits larval development typical of harpacticoid copepods. Given the likely low dispersal potential and the distance between the two sites (407 km), the observed genetic heterogeneity was not surprising.

Other species of harpacticoid copepods have shown genetic heterogeneity among populations, sometimes over small geographic distances. Surveys of allozyme variation have revealed significant genetic structure between *T. californicus* populations, separated by as little as 1.5 km, along the southern California coast (Burton et al. 1979; Burton and Lee 1994). *T. californicus* inhabits tidepools in the supralittoral zone of the rocky intertidal, and dispersal of individuals across barriers, such as sandy beaches, is thought to be rare (Burton et al. 1979). The estuarine harpacticoid copepod, *M. littorale*, has also been found to exhibit significant genetic differentiation among populations from South Carolina in surveys of the mitochondrial cyt b gene (Schizas et al. 2002). *M. littorale* can potentially be dispersed within estuarine creeks through resuspension and advection by tidal currents (Palmer and Gust 1985). However, little is known about the transport of estuarine meiofauna between adjacent estuaries, and the genetic data indicate it does not frequently occur.

Determining the underlying genetic structure of a population may be confounded if the locus examined has alleles that are selectively advantageous. An allele with a strong selective advantage is likely to become fixed in a population despite high levels of gene flow of other, less advantageous alleles (Takahata 1991). Schizas et al. (2001) demonstrated that one of three cyt b lineages of the harpacticoid copepod, *M. littorale*, survived in higher numbers when exposed to a pesticide treatment. Frequencies of this lineage are highest in *M. littorale* populations inhabiting contaminated estuaries compared to relatively pristine estuaries (Schizas et al. 2001; Schizas et al. 2002). In the present study, levels of SBF hydrocarbons were, on average, an order of magnitude higher at the GB 602 site compared to the MC 292 site (see *Chapter 9*). *Bathycletopsyllus* sp. at



GB 602 was dominated by the BI lineage of the COX I gene, whereas a more even distribution of all three lineages was observed at the MC 292 site. Therefore, it is plausible that individuals possessing a haplotype in the BI lineage had a selective advantage over the other lineages, although further study is needed to test this hypothesis.

#### 13.4.4 Genetic Diversity

Levels of haplotype diversity and nucleotide diversity observed in *Bathyletopsyllus* sp. populations differed between the two sites: GB 602 ( $h = 0.61$ ,  $SD = 0.089$ ;  $\pi_n = 0.0020$ ,  $SD = 0.0014$ ); MC 292 ( $h = 0.89$ ,  $SD = 0.033$ ;  $\pi_n = 0.0066$ ,  $SD = 0.0038$ ). These values of haplotype and nucleotide diversity fall within the range of values observed for other harpacticoid copepod species that live in muddy habitats similar to *Bathyletopsyllus* sp. (see **Figure 13.3**). For the population at GB 602, genetic diversities, both haplotype and nucleotide diversities, were moderate to low. In contrast, the population at MC 292 had high haplotype diversity and low to moderate nucleotide diversity.

Several factors may contribute to the patterns of genetic diversity observed in the *Bathyletopsyllus* sp. populations, including short- and long-term demographic processes, gene flow, and natural selection. The general demographic history of a population can be inferred by examination of haplotype and nucleotide diversities (Bowen and Grant 1997; Avise 2000). High haplotype and nucleotide diversities are usually observed in populations that have remained constant in size over a long time period, thus allowing for the accumulation of alleles through mutation. Low values of haplotype and/or nucleotide diversities signal that a population has undergone population fluctuations and alleles have been lost due to genetic drift while population sizes were small. Migration among populations may increase or decrease genetic diversity depending on the number of migrants between populations and the frequencies of alleles in the populations. Natural selection may decrease genetic diversity in a population by the differential survival of individuals possessing a favorable genotype. Each of these mechanisms may explain the observed genetic diversity in *Bathyletopsyllus* sp. at the two sites.

The haplotype diversity and nucleotide diversity for the population at the GB 602 site were low, and the values were comparable to those seen in three species of harpacticoids in the genus *Cletocamptus* (data from Rocha-Olivares et al. 2001; **Figure 13.3**). *C. deborahdexterae*, which is found in the Salton Sea, CA, had the lowest calculated haplotype diversity ( $h = 0.32$ ) and a low nucleotide diversity ( $\pi_n = 0.0038$ ). The low genetic diversities seen in this population are likely a result of the recent creation of the Salton Sea (in 1905) and its colonization by a small founder population. *C. stimpsoni*, collected from an inland brine seep in Alabama, also had low genetic diversity ( $h = 0.43$ ;  $\pi_n = 0.00067$ ). This brine seep is subject to periodic flood-drought cycles causing extreme fluctuations in salinity and water level/flooding. Species in the genus *Cletocamptus* have been shown to increase population sizes in response to increases in salinity (Dexter 1995; Simpson et al. 1998). Therefore, it is plausible that the brine seep populations undergo demographic fluctuations, which cause reductions in genetic diversity. Laboratory microcosm experiments have demonstrated that *C. fourchensis* increased in abundance compared to other harpacticoid species in sediments contaminated with diesel fuel (Carman et al. 1997). This species has subsequently been found to be tolerant of heavy metal contamination (Fleeger et al. 2001) and may increase in numbers due to a release from competition with other meiofauna

(Carman et al. 1997). Species in the genus *Cletocamptus* seem to undergo fluctuations in population size caused by environmental factors, which may explain the low genetic diversity observed in these populations. Processes similar to those affecting genetic diversity in *Cletocamptus* may have occurred in the *Bathycletopsyllus* sp. population at GB 602.

Selection for individuals from a lineage that is tolerant to contamination may also result in the low genetic diversity observed in the population at GB 602. Different intraspecific (Schizas et al. 2001) and interspecific (Fleeger et al. 2001) mitochondrial lineages of harpacticoid copepods have been shown to tolerate exposure to contaminants. This apparent selection for certain haplotypes would cause the elimination of other less tolerant types, thus reducing the genetic diversity. Since mitochondrial genes have no known detoxification functions, it is difficult to put forward a mechanistic explanation for how selection acts on the mtDNA molecule itself; however, selection acting on nuclear loci may constrain mtDNA variation (Kilpatrick and Rand 1995).

The *Bathycletopsyllus* sp. population at the MC 292 site had high haplotype diversity and low to moderate levels of nucleotide diversity compared to the other harpacticoid species. This pattern of genetic diversity suggests that the population at MC 292 also may have undergone fluctuations in numbers, but not to the same extent as at GB 602 (Bowen and Grant 1997; Avise 2000). There are three likely explanations to account for the observed genetic diversity at MC 292. First, the source populations contributing to the expansion at MC 292 may have been larger, but still unobserved in our sampling, compared to the GB 602 site. With less dramatic population fluctuations, there would be a decreased chance of losing rare haplotypes, resulting in higher haplotype diversity. Second, the population at MC 292 may be an admixture from two or more populations that diverged in the past and have recently come into contact. Individuals falling into Clades BII and BIII have the highest frequency at the MC 292 site, and **Figure 13.2** shows that these are the most divergent clades. The maximum P-distance between haplotypes in these two clades is 1.6%. Assuming a mutation rate at the COX I gene of 1.4%/Myr (Knowlton and Weigt 1998) to 2.4%/Myr (Knowlton et al. 1993), the haplotypes observed at MC 292 have diverged over 0.67 to 1.1 Myr. Given the apparent patchy distribution of this species, the most parsimonious explanation is that the population at MC 292 has resulted from secondary contact of two allopatric populations. Lastly, as mentioned above, selective pressure may be reduced at MC 292 because of the decreased level of disturbance, thus allowing more haplotypes to coexist in this habitat.

A way of visualizing genetic diversity in a population is to plot the mismatch distribution, or the frequencies of the observed number of differences between pairs of haplotypes. The shape of this distribution is affected by the demographic history of a population. A multimodal distribution indicates a population that has been at demographic equilibrium for a long period of time, and a unimodal distribution indicates a population that has undergone a sudden bottleneck or expansion (Slatkin and Hudson 1991; Rogers and Harpending 1992). **Figure 13.4** shows that the mismatch distributions at the two sites differ in shape: GB 602 is unimodal and MC 292 is multimodal, but still not significantly different from a sudden population expansion model. Again, alternative hypotheses can be used to explain the shapes of the observed mismatch distributions, such as natural selection (GB 602) and admixture of diverged populations (MC 292).

### 13.5 CONCLUSIONS

The present study suggests that the harpacticoid copepod, *Bathyletopsyllus* sp., responds to disturbance caused by oil drilling in the deep sea. Three lines of evidence support this conclusion. First, *Bathyletopsyllus* sp. was absent from far-field sites but present in large numbers at near-field sites. Second, the abundances were related to concentration of SBF in the sediments up to a concentration of about 2,500 µg/dry g. Third, the low genetic diversity observed in both *Bathyletopsyllus* sp. populations was consistent with what would be expected from a population that underwent an expansion from a small population size. Only two drilling sites were sampled in the present study, so our conclusions are tentative at this time.

Further study of *Bathyletopsyllus* sp. is warranted to help explain the high abundance of this species near the drilling sites. For example, this species may be common at natural hydrocarbon seeps in the northern Gulf of Mexico and therefore may have evolved a tolerance to hydrocarbons. Additionally, other disturbances in the deep sea, which lead to localized carbon enrichment in the sediment (e.g., whale carcasses and phytoplankton settlement events), may provide suitable environmental conditions for opportunistic colonization by this species. If further sampling at other deep-sea oil platforms and organically enriched habitats shows similar results, then *Bathyletopsyllus* sp. may prove to be a useful marine pollution indicator species in the deep sea.

## Chapter 14 Sediment Toxicity

Roy Kropp, Battelle Marine Sciences Laboratory  
and Jerry Neff, Battelle Duxbury

### 14.1 INTRODUCTION

Acute solid-phase (sediment) toxicity tests were performed with near-field and far-field sediments from two post-development sites – Garden Banks 602 (GB 602) and Mississippi Canyon Block 292 (MC 292). The tests were conducted according to standard USEPA and ASTM protocols.

### 14.2 MATERIALS AND METHODS

#### 14.2.1 Sediment Sampling Locations

Surficial sediments were collected for laboratory sediment toxicity tests from GB 602 and MC 292 during Cruise 2B (8 to 25 July 2001). Samples were collected from 12 randomly selected near-field stations and 12 far-field stations at each site (see *Chapter 2*). Site characteristics are summarized in **Table 14.1**. Near-field stations were within 500 m of the discharge site; far-field stations were 10 to 25 km from the discharges.

#### 14.2.2 Test Organism Collection

One species of test animal, the estuarine amphipod *Leptocheirus plumulosus*, was used to evaluate the toxicity of test sediments. Although not a deepwater species, this amphipod is useful as a surrogate because it is easily cultured, exhibits high survival under a variety of environmental test conditions, and displays sensitivity to reference toxicants similar to those of other amphipods. The amphipods were obtained from in-house cultures maintained at the Battelle Marine Sciences Laboratory (MSL) and from Chesapeake Cultures, Hayes, Virginia. Organisms exhibiting abnormal behavior or appearance were not used in toxicity tests.

**Table 14.1.** Characteristics of the two development drilling sites from which sediments for solid phase toxicity testing were collected.

Parameter	Development Drilling Site	
	Garden Banks 602	Mississippi Canyon 292
Water depth (m)	1,125	1,034
Distance to Mississippi River (km)	370	69
Wells within 5-km radius	7	5
Time since last well drilled (months)	6	24
Total mud and cuttings discharge (bbl)	159,302	120,003
Synthetic based fluid types	IO, LAO, ester	IO

IO = internal olefin; LAO = linear- $\alpha$ -olefin.

### 14.2.3 Sediment Sample Preparation

Sediments were received at MSL on 31 July 2001. Cooler temperatures, which were measured upon arrival, ranged from 1.2°C to 4.7°C. All of the jars were in good condition. Laboratory control sediment, which is used to validate the test, was collected from Sequim Bay, WA. Prior to its use, the laboratory control sediment was pressed through a 0.5-mm-mesh sieve to remove any live organisms that might interfere with the test results. All sediment samples were stored in a walk-in cold room at 4°C ± 2°C until used in toxicity tests.

### 14.2.4 Toxicity Test

Acute toxicity testing was performed in accordance with guidance in USEPA (1994, 2001a) and ASTM (1999). The tests used subadult *L. plumulosus* in a 10-day static exposure with mortality as the endpoint. The animals were exposed to 48 Gulf of Mexico test sediments and a laboratory control sediment. Because of the number of sediments to be tested, the toxicity test was conducted in two batches of 24 samples. Each batch included a laboratory control sample and a concurrent reference toxicant test. Batch 1 included sediments from MC 292 and test animals from MSL in-house cultures. Batch 2 included sediments from GB 602 and test animals obtained from Chesapeake Cultures on 16 August 2001.

After preliminary water-quality measurements of the conditions (temperature, pH, dissolved oxygen, and salinity) in each container were made, the test was initiated by introducing 20 organisms into each test chamber. During the test, these water quality parameters were measured in one replicate on days 2, 4, 6, and 8, and were measured in all replicates at test termination. Organisms were randomly allocated to treatments, and treatment replicates were randomly positioned on water tables (**Figure 14.1**). Random positions for test chambers were assigned using the discrete random number generator in Microsoft Excel 97<sup>®</sup> spreadsheet software. Amphipods were not fed during the test. Each batch of the bioassay included a concurrent, 96-h, water-only, reference toxicant (cadmium chloride at seven concentrations) test to assess the sensitivity of each test population. Specific conditions for the benthic toxicity test are summarized in **Table 14.2**.



**Figure 14.1.** Sediment toxicity test system.

**Table 14.2.** Toxicity test conditions.

Parameter	Test Conditions
Treatments:	48 Gulf of Mexico sediments (2 batches of 24) 1 laboratory control (Sequim Bay) sediment with each batch
Replicates:	5
Test population per replicate:	20 individuals, total per treatment, $n = 100$
Temperature:	$25^{\circ} \pm 2^{\circ}\text{C}$
Dissolved Oxygen:	$> 50\%$ saturation ( $> 3.6 \text{ mg/mL}$ at $25^{\circ}\text{C}$ , $20\text{‰}$ )
pH:	$7.8 \pm 0.5$
Salinity:	$20\text{‰} \pm 2\text{‰}$
Feeding:	None
Reference Toxicant:	Cadmium chloride at 0, 0.156, 0.312, 0.625, 1.25, 2.5, 5.0, and 7.0 mg/L
(1 concurrent with each batch)	

## 14.3 RESULTS

Results of toxicity tests are summarized here. Test endpoint data for individual replicates and reference toxicant test data, water quality data summaries, and a sediment receipt summary are in *Appendices J1* and *J2*.

### 14.3.1 Mississippi Canyon Block 292

Toxicity tests with near-field and far-field sediments from MC 292 were initiated on 7 August 2001, using amphipods purchased from MSL in-house cultures, and completed 17 August 2001. During the 10-day test, most water quality parameters remained within the required ranges. Dissolved oxygen values for most replicates exceeded the hypothetical maximum concentration value on Day 0 and Day 10 of the test (*Appendix J1*). At test completion, three test chambers contained more than the intended stocking density ( $n = 20$ ) of amphipods (**Table 14.3**). These samples and the assumed stocking densities are shown in the table.

**Table 14.3.** Stocking density for test chambers found at test completion to have more than 20 amphipods.

Sediment	Replicate	Number of Amphipods at Termination	Assumed Stocking Density	Survival Using Assumed Stocking Density
MC292-NF-B06	1	21	21	1.00
MC292-FF2-B02	2	24	25	0.96
MC292-FF4-B02	2	38	40	0.95

Fractional survival of amphipods in the laboratory control sediments tested concurrently with MC 292 sediments was 0.99, exceeding the acceptability criterion of 0.90 survival. Mean fractional survival among the test sediments ranged from 0.41 to 0.99 (**Table 14.4**; *Appendix J1*). Mean fractional survival of amphipods in replicate chambers containing sediments from the near-field stations ( $0.76 \pm 0.21$ ) was significantly lower than mean survival among replicates from far-field stations ( $0.93 \pm 0.08$ ). Mean fractional survival in all near-field and far-field samples was  $0.84 \pm 0.15$ .

**Table 14.4.** Amphipod survival in the toxicity tests with sediments from Mississippi Canyon Block 292, performed 7 to 17 August 2001.

Sediment	Proportion Surviving		
	Mean	Standard Deviation	CV
Laboratory Control	0.99	0.02	2
MC292-NF-B01	0.47	0.22	46
MC292-NF-B02	0.41	0.18	43
MC292-NF-B03	0.84	0.11	14
MC292-NF-B04	0.84	0.10	11
MC292-NF-B05	0.71	0.12	18
MC292-NF-B06	0.94	0.08	9
MC292-NF-B07	0.92	0.04	5
MC292-NF-B08	0.71	0.13	19
MC292-NF-B09	0.74	0.22	30
MC292-NF-B10	0.71	0.25	36
MC292-NF-B11	0.96	0.02	2
MC292-NF-B12	0.81	0.13	16
MC292-FF1-B01	0.92	0.10	11
MC292-FF1-B02	0.93	0.10	11
MC292-FF2-B01	0.92	0.08	8
MC292-FF2-B02	0.89	0.11	12
MC292-FF3-B01	0.94	0.04	4
MC292-FF3-B02	0.88	0.16	18
MC292-FF4-B01	0.93	0.10	10
MC292-FF4-B02	0.98	0.03	3
MC292-FF5-B01	0.99	0.02	2
MC292-FF5-B02	0.91	0.09	10
MC292-FF6-B01	0.94	0.04	4
MC292-FF6-B02	0.97	0.04	5

CV = coefficient of variation; NF = Near-Field; FF = Far-Field.

The reference toxicant (cadmium) test was conducted 7 to 11 August 2001. The LC<sub>50</sub> for cadmium was 0.64 mg/L (*Appendix J1*), which was within the control chart range (mean  $\pm$  2 standard deviations) calculated for the species during the previous 20 tests at MSL (0.05 to 1.38 mg/L) indicating that the test population was about as sensitive as previous populations tested.

#### 14.3.2 Garden Banks Block 602

Benthic toxicity tests of sediments from GB 602 were initiated on 20 August 2001 using amphipods purchased from Chesapeake Cultures, Inc., and was completed 30 August 2001. During the 10-day test, most water quality parameters remained within the required ranges. Dissolved oxygen concentrations for most replicates exceeded the hypothetical maximum concentration value on Day 0 of the test (*Appendix J2*). Some values were above this value on Days 2 and 4. The dissolved oxygen concentration in one test chamber (sediment GB602-NF-B08, replicate 2) was below the minimum target value on Day 0; aeration in this chamber was increased slightly. All dissolved oxygen concentrations were above the minimum limit for the remainder of the test.

Fractional survival of amphipods in the laboratory control sediments during tests with GB 602 sediments was 1.0, which exceeds the acceptability criterion of 0.90 control survival. Mean fractional survival among the test sediments ranged from 0 to 0.81 (**Table 14.5**; *Appendix J2*).

The reference toxicant (cadmium chloride) test was performed 20 to 24 August 2001. The calculated LC<sub>50</sub> was 0.57 mg/L (*Appendix J2*), which was within the normal range (mean  $\pm$  2 standard deviations) calculated for the species during the previous 20 tests at MSL (0.11 to 1.36 mg/L). However, fractional control survival was 0.45; therefore, the results of this reference toxicant test may not provide an accurate description of the test population's sensitivity.

Mean fractional survival among the test sediments ranged from 0 to 0.81 (**Table 14.5**; *Appendix J2*). Mean fractional survival of amphipods in replicate chambers containing sediments from the near-field stations ( $0.17 \pm 0.18$ ) was significantly lower than mean survival among replicates from far-field stations ( $0.68 \pm 0.13$ ). Mean fractional survival in all near-field and far-field sediments was  $0.42 \pm 0.28$ . Amphipod survival in both near-field and far-field sediments from GB 602 was much lower than survival in sediments from MC 292. This may have been due in part to the poorer condition of the amphipods used in the tests with GB 602 sediments than those used in tests with MC 292 sediments.



**Table 14.5.** Amphipod survival in the toxicity tests with sediments from Garden Banks Block 602, performed 20 to 30 August 2001.

Sediment	Proportion Surviving		
	Mean	Standard Deviation	CV
Laboratory Control	1.00	0.00	–
GB602-NF-B01	0.36	0.24	66
GB602-NF-B02	0.41	0.12	30
GB602-NF-B03	0.27	0.20	75
GB602-NF-B04	0.14	0.10	69
GB602-NF-B05	0.20	0.29	146
GB602-NF-B06	0.04	0.06	161
GB602-NF-B07	0	0	–
GB602-NF-B08	0	0	–
GB602-NF-B09	0.08	0.13	163
GB602-NF-B10	0.20	0.12	59
GB602-NF-B11	0.08	0.06	71
GB602-NF-B12	0.23	0.10	45
GB602-FF1-B01	0.71	0.11	16
GB602-FF1-B02	0.59	0.19	32
GB602-FF2-B01	0.64	0.13	20
GB602-FF2-B02	0.66	0.16	24
GB602-FF3-B01	0.73	0.06	8
GB602-FF3-B02	0.74	0.08	11
GB602-FF4-B01	0.67	0.07	10
GB602-FF4-B02	0.74	0.05	7
GB602-FF5-B01	0.53	0.14	27
GB602-FF5-B02	0.81	0.07	8
GB602-FF6-B01	0.74	0.12	16
GB602-FF6-B02	0.62	0.20	33

CV = coefficient of variation; NF = Near-Field; FF = Far-Field.

## 14.4 DISCUSSION

### 14.4.1 Mississippi Canyon Block 292

A total of about 120,000 bbl (19.1 million liters) of drilling muds and cuttings had been discharged from the drilling operations at MC 292 before the sampling cruise (**Table 14.1**). The total included about 10,331 bbl of water based mud and 1,409 bbl of cuttings discharged directly to the sea floor before the risers were in place and about 93,960 bbl of water based drilling mud and 12,813 bbl of associated cuttings from the platform after the riser was in place. About 1,490 bbl of SBM cuttings were discharged, with about 10% internal olefin (Novaplus) adhering to the cuttings. The last discharge was about 24 months before the sampling cruise.

Sediments from two near-field stations, NF-B01 and NF-B02, were moderately toxic to the amphipods (fraction surviving ranged from 0.15 to 0.85 among 10 replicate test containers). Four far-field sediment replicates had fractional survival between 0.60 and 0.75. Thus, sediments from just two near-field stations can be considered moderately toxic to benthic amphipods. Station NF-B01 was in an area mapped geophysically as cuttings, but Station NF-B02 was not.

There was not a clear relationship between sediment toxicity at MC 292 and concentrations of metals in sediments (*Chapter 8*). The strongest relationship ( $r^2 = 0.50$ ) was between sediment barium concentration and mean fraction survival of amphipods in near-field and far-field sediments (**Figure 14.2**). The sediment in which fractional survival was 0.47 contained 39,700 mg/kg barium; however, the sediment with a fractional survival of 0.41 contained 39,700 mg/kg barium; however, the sediment with a fractional survival of 0.41 contained 8,040 mg/kg barium. Regressions for all other metals had lower  $r^2$  values than that for barium.

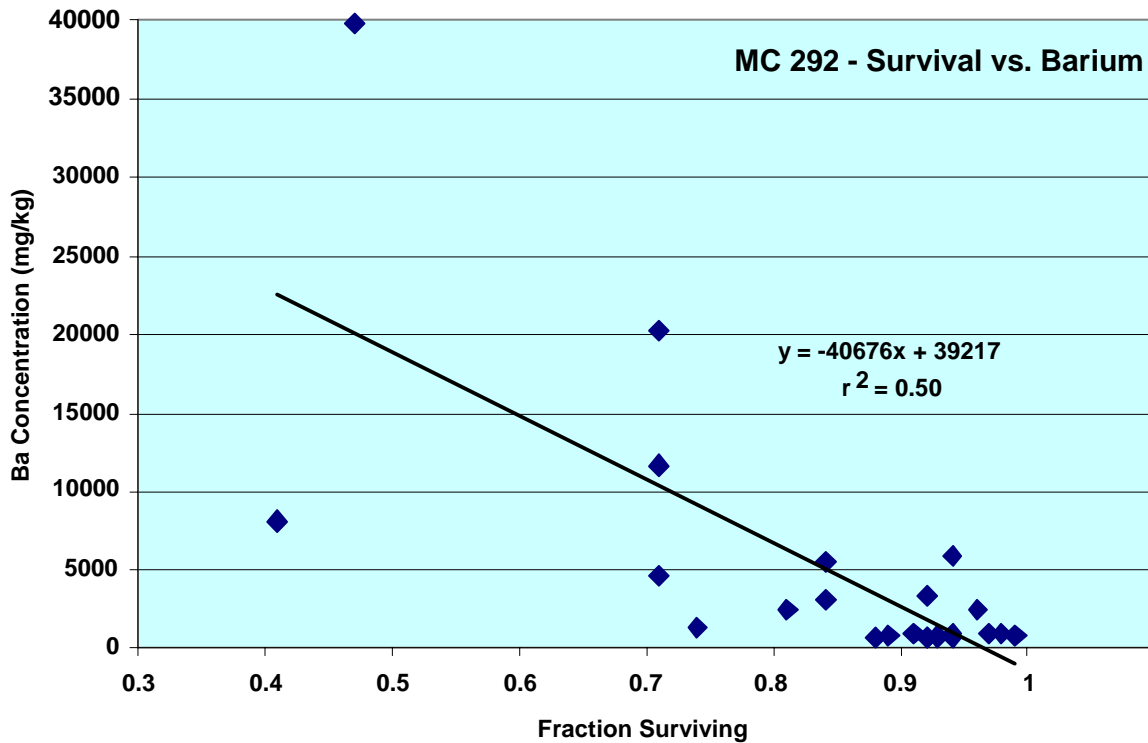


**Figure 14.2.** Regression of barium concentration against fraction of amphipods surviving in a 10-day sediment toxicity test with near-field and far-field sediments from Mississippi Canyon Block 292.  $r^2 = 0.50$ .

There was a slightly stronger relationship ( $r^2 = 0.60$ ) between the concentration of synthetic based fluids (SBF) in sediment and toxicity to benthic amphipods (**Figure 14.3**). Mean amphipod fractional survival was less than 0.74 at nearly all locations where sediment SBF concentration was higher than about 100 mg/kg. Sediments in which mean amphipod fractional survival was 0.41 and 0.47 contained 782 mg/kg and 2,408 mg/kg SBF, respectively. Two far-field sediments contained more than 15 mg/kg SBF. However, SBF was measured as total resolved and unresolved hydrocarbons in the boiling point range of the synthetic base fluid (*Chapter 9*). Thus, some of the material in these samples may be hydrocarbons or extractable organic chemicals from other sources than SBM cuttings. Water-based muds sometimes contain small amounts of petroleum hydrocarbons from lubricity additives (e.g., Mentor 26, gilsonite) added to the mud.

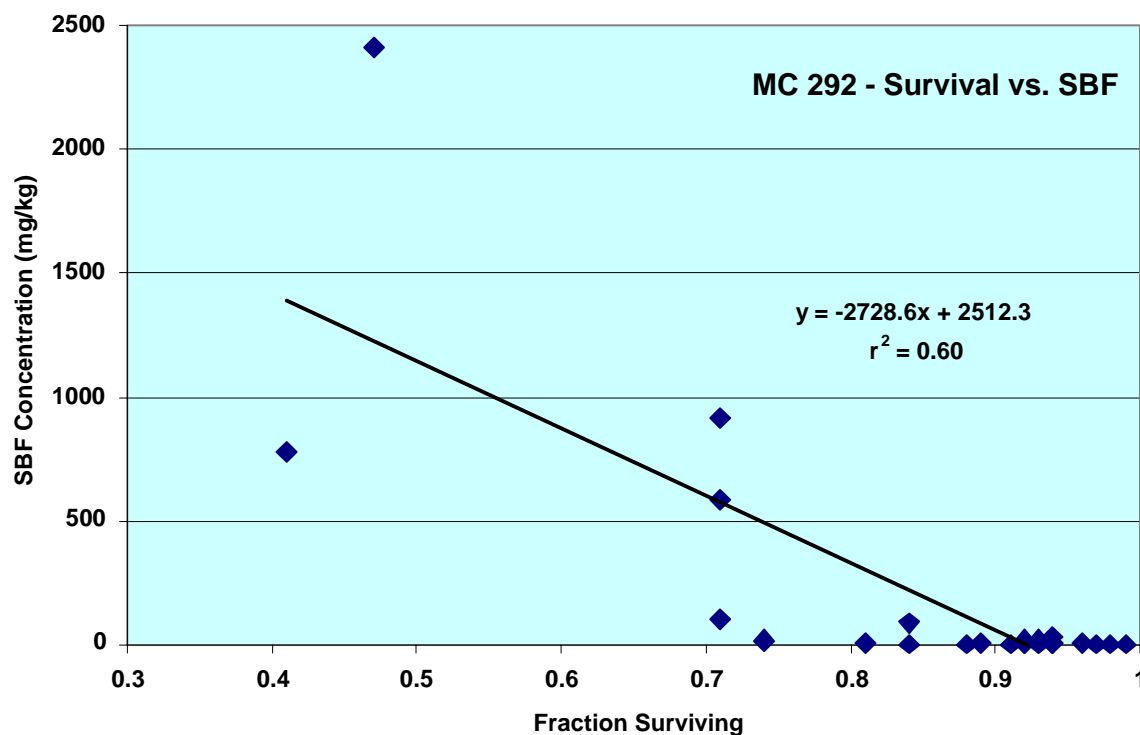


**Figure 14.3.** Regression of synthetic based fluid (SBF) concentration against fraction of amphipods surviving in a 10-day sediment toxicity test with near-field and far-field sediments from Mississippi Canyon Block 292.  $r^2 = 0.60$ .

Drilling muds and cuttings usually do not contain more than traces of polycyclic aromatic hydrocarbons (PAH), unless a diesel fuel pill was added to the mud system to free stuck pipe, or formation oil got into the mud system. Oil-contaminated drilling muds and cuttings are not permitted for ocean discharge in the Gulf of Mexico. Near-field sediments at MC 292 contained 174 to 743  $\mu\text{g}/\text{kg}$  total PAH. The highest concentration was in sediments from Station NF-B01 where mean fractional amphipod survival was 0.47. Far-field sediments actually contained higher PAH concentrations than near-field stations did (concentration range: 210 to 748  $\mu\text{g}/\text{kg}$ ). The regression of mean fractional amphipod survival against PAH concentration had an  $r^2$  of 0.03, indicating no relationship between PAH concentration in sediment and amphipod survival. Mean fractional amphipod survival in the sediment containing 748  $\mu\text{g}/\text{kg}$  PAH was 0.95, indicating that PAH probably were not causing the sediment toxicity.

#### 14.4.2 Garden Banks 602

A total of nearly 160,000 bbl (25.4 million liters) of drilling muds and cuttings had been discharged from the drilling operations at GB 602 before the sampling cruise (**Table 14.1**). The total included about 23,946 bbl of water based mud and 3,266 bbl of cuttings discharged directly to the sea floor before the risers were in place and about 91,301 bbl of water based drilling mud and 12,450 bbl of associated cuttings discharged from the platform after the riser was in place. About 28,339 bbl of SBM cuttings were discharged, with about 10% internal olefin, linear- $\alpha$ -olefin, or ester adhering to the cuttings. The last discharge was about 6 months before the sampling cruise. Because of the more recent and larger mass of mud and cuttings discharged

at GB 602 than at MC 292, it was expected that impacts on the benthic environment would be more severe.

Amphipod survival was low in nearly all replicate near-field sediment samples from GB 602. Amphipod fractional survival in sediment replicates ranged from 0 to 0.75. There were only four sediment replicates with amphipod fractional survival greater than 0.50.

The far-field sediments from GB 602 were moderately toxic to the amphipods. Amphipod fractional survival in replicate far-field sediment samples ranged from 0.30 to 0.90. This poor survival, plus the poor survival among amphipods exposed to control sediments indicates that the amphipods may have been in poor condition at the start of the bioassay. However, near-field sediments clearly were more toxic than far-field sediments at GB 602.

There was a moderate relationship ( $r^2 = 0.57$ ) between barium concentration and mean fraction surviving in sediments at near-field and far-field stations at GB 602 (**Figure 14.4**). The relationship between barium concentration and sediment toxicity was stronger for GB 602 than for MC 292.

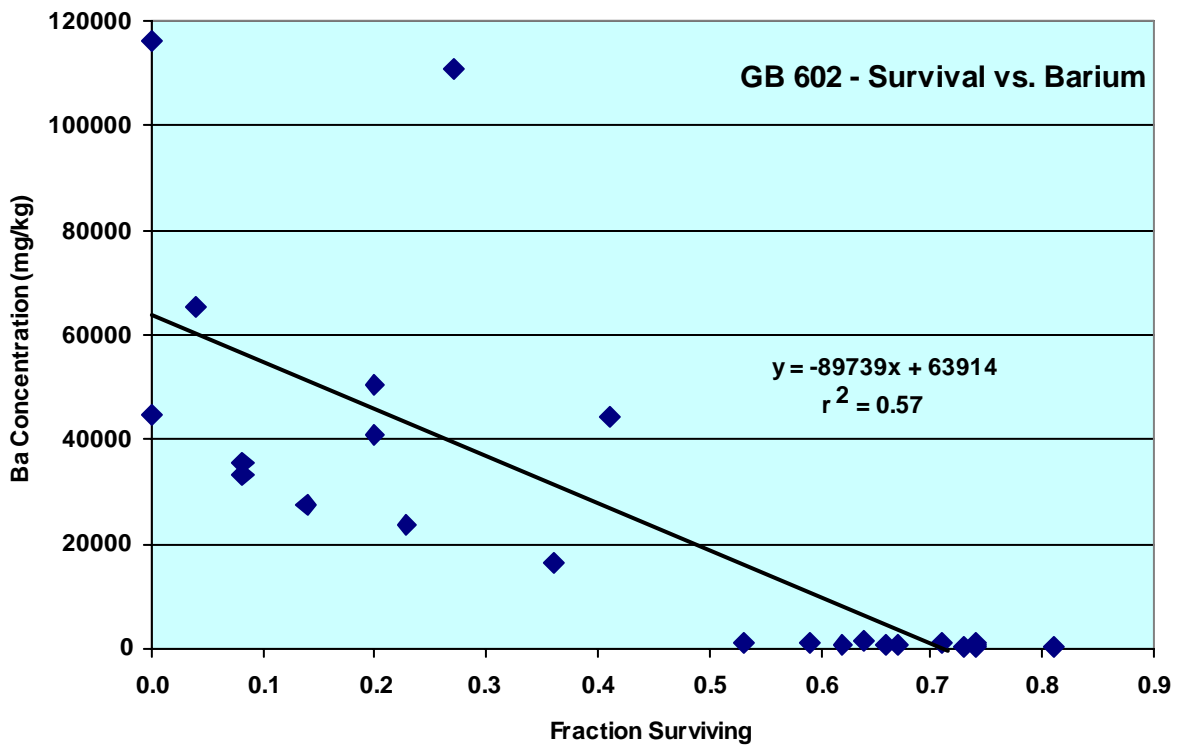


**Figure 14.4.** Regression of barium concentration against fraction of amphipods surviving in a 10-day sediment toxicity test in near-field and far-field sediments at Garden Banks Block 602.  $r^2 = 0.57$ .

The relationship between amphipod survival and SBF concentrations in near-field and far-field sediments at GB 602 is weaker than the relationship between barium concentration and survival (**Figure 14.5**). The  $r^2$  for the regression of SBF concentration versus fraction amphipod survival is 0.35.

There also was a weak relationship between PAH concentration in sediments and amphipod survival (**Figure 14.6**). The  $r^2$  for this regression is 0.40. Near-field sediments contained higher PAH concentrations ( $326 \pm 152$  ng/g) than far-field stations did ( $122 \pm 17$  ng/g). Overall, these results suggest that there is a relationship between toxicity to benthic amphipods and concentrations of drilling mud and cuttings in sediments, as indicated by elevated concentrations of barium (from drilling mud barite), SBF, and PAH.

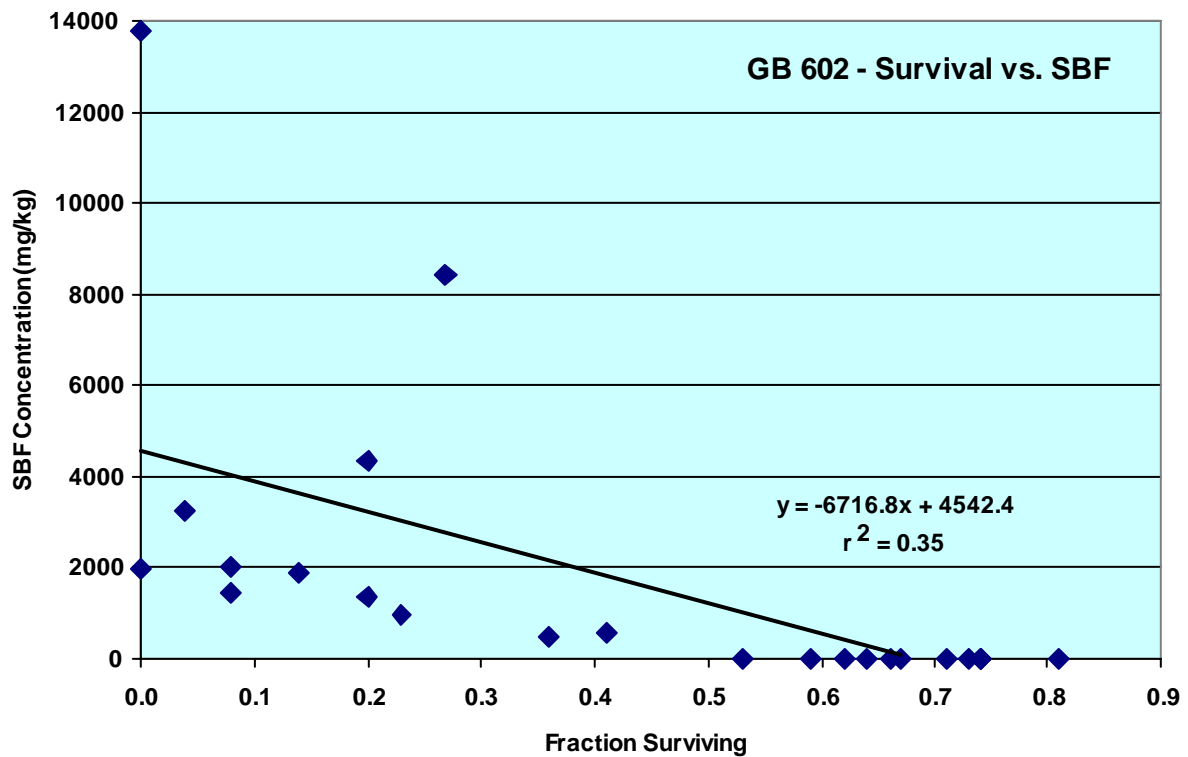


**Figure 14.5.** Regression of synthetic based fluid (SBF) concentration against fraction of amphipods surviving in a 10-day sediment toxicity test with near-field and far-field sediments from Garden Banks Block 602.  $r^2 = 0.35$ .

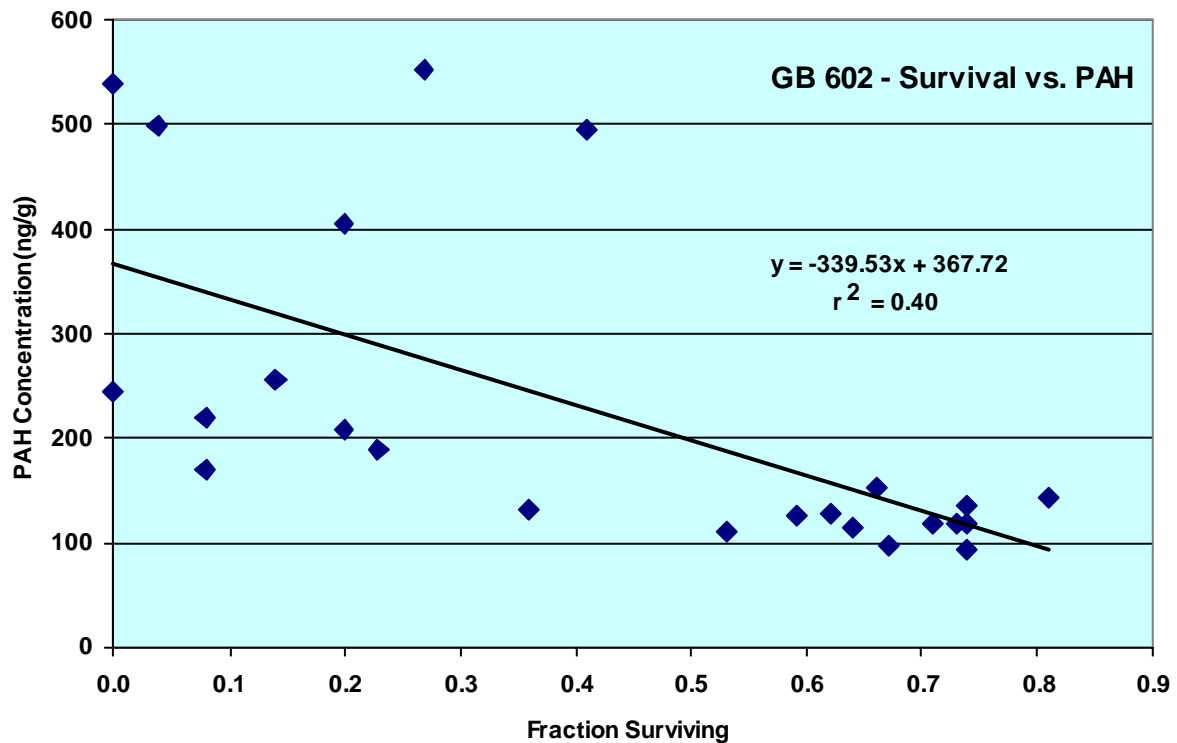


**Figure 14.6.** Regression of polycyclic aromatic hydrocarbon (PAH) concentration against fraction of amphipods surviving in a 10-day sediment toxicity test with near-field and far-field sediments from Garden Banks Block 602.  $r^2 = 0.40$ .

## 14.5 CONCLUSIONS

Acute solid-phase (sediment) toxicity tests were performed with near-field and far-field sediments from two post-development sites, MC 292 and GB 602. The tests were conducted according to standard USEPA and ASTM protocols. The principal conclusions are as follows:

- At both MC 292 and GB 602, mean amphipod survival was significantly lower in sediments from near-field stations than in sediments from far-field stations.
- Mean amphipod survival was lower at GB 602 than at MC 292 in both near-field and far-field sediments, possibly indicating that the amphipods used for the GB 602 tests were in relatively poor condition at the start.
- Mean amphipod survival was negatively correlated with drilling mud and cuttings indicators (barium and SBF) for both sites. The highest correlations were with SBF at MC 292 ( $r^2 = 0.60$ ) and barium at GB 602 ( $r^2 = 0.57$ ).
- The toxicity of near-field sediments apparently was unrelated to sediment total PAH concentrations at MC 292, but there may have been a weak negative relationship at GB 602.

Sediment toxicity is discussed further in the Ecological Risk Assessment (*Chapter 16*).

### 15.1 INTRODUCTION

This study focused on four sites on the northern Gulf of Mexico continental slope in water depths of 1,033 to 1,125 m. Two sites were in the Western Planning Area (GB 516 and GB 602), and the other two were in the eastern part of the Central Planning Area (VK 916 and MC 292).

The six cruises provide insight into impacts of both exploration and development. Two sites were sampled post-exploration (VK 916 on Cruises 3A/3B; GB 516 on Cruise 1B). Three sites were sampled post-development (GB 516, GB 602, and MC 292, all on Cruises 2A/2B). Both WBMs and SBMs were used in drilling at these sites.

The general objectives of this study were to assess the physical, chemical, and biological impacts of oil and gas development at selected exploration and development wellsites on the Gulf of Mexico continental slope. Specific objectives were to document (1) drilling mud and cuttings accumulations; (2) physical modification/disturbance of the seabed due to anchors and their mooring systems; (3) debris accumulations; (4) physical/chemical modification of sediments; and (5) effects on benthic organisms.

This chapter synthesizes findings from the preceding chapters and focuses on several topics:

- Types of impacts and their areal extent;
- Variations in impacts among sites and relationships to level of drilling activity;
- Duration/persistence of impacts; and
- Methodology evaluation.

There have been few previous environmental studies of drilling impacts on the Gulf of Mexico continental slope. A post-drilling survey of a development site (Pompano) in MC Block 28 (water depth 565 m) was reported by Gallaway et al. (1997) and Fechhelm et al. (1999). More recently, a comprehensive study of SBM impacts was conducted at several continental slope and shelf sites in the Gulf of Mexico (Continental Shelf Associates, Inc. 2004). The latter study is referred to as the SBM monitoring program. Findings from these studies are cited where appropriate in this synthesis.

#### 15.1.1 Baseline Conditions

“Baseline” characteristics of the four sites can be summarized based on far-field data. All of the sites are located on the northern Gulf of Mexico continental slope and are similar with respect to the overall environmental setting. However, water depths at GB 516 and MC 292 were about 120 m shallower than at VK 916 and GB 602 (**Table 15.1**).

**Table 15.1.** Comparison of baseline environmental characteristics based on data from far-field sites.

Site	Water Depth (m)	Approx. Dist. to Miss. R. (km)	Sedimentation Rate (cm/yr)	Sediment Characteristics			
				Mean Grain Size ( $\mu\text{m}$ )	Mean Total Organic Carbon (%)	Mean Integrated Oxygen ( $\text{nmol}/\text{cm}^2$ )	Mean Barium ( $\mu\text{g}/\text{g}$ )
VK 916	1,125	120	0.06	2.44	1.10	90	805
				1.82	1.53	84	866
GB 516	1,033	357	0.07	1.96	0.52	153	1,281
				2.40	1.08	165	1,478
GB 602	1,125	370	0.04	2.03	1.10	227	821
MC 292	1,034	69	0.14	1.64	1.44	65	754

The two Garden Banks sites are located in the Western Planning Area and are more than 350 km from the Mississippi River mouth (**Table 15.1**). The other two sites are much closer. The likely influence of the Mississippi River discharge on sedimentation rate and sediment oxygen levels has been noted in *Chapter 8*. MC 292, being the closest to the river mouth, has a sedimentation rate 2 to 3 times higher than the other sites. Baseline sediment oxygen levels were lower at both VK 916 and MC 292 than at the two Garden Banks sites.

Far-field sediment barium levels were about 50% higher at GB 516 (1,281 to 1,478  $\mu\text{g}/\text{g}$ ) than at the other three sites (754 to 866  $\mu\text{g}/\text{g}$ ). Background barium concentrations in the Gulf of Mexico typically are in the range of 200 to 800  $\mu\text{g}/\text{g}$  (Anderson et al. 1981; Trefry et al. 1981). The slight elevation at GB 516 may be due to the relatively large number of previous wells in the area compared with the nearby GB 602 site (*Chapter 3*).

**Figure 15.1** shows selected biological data for the far-field sites. Comparisons among sites are complicated by temporal differences. At the VK 916 site, there was an order of magnitude decrease in microbial biomass as well as meiofaunal and macroinfaunal densities between cruises. A similar decrease was evident at GB 516 for microbes and meiofauna but not for macroinfauna.

Excluding the high values for VK 916 and GB 516 on Cruise 1B, nearly all microbial biomass (ATP) levels at far-field sites were in the range of 1 to 5  $\mu\text{g}/\text{g}$ . Excluding the Cruise 1B samples at VK 916, most meiofaunal densities were in the range of 1 to 100 individuals/10  $\text{cm}^2$ . Typical far-field macroinfaunal densities were a few thousand individuals per square meter, except for several stations exceeding 5,000 individuals/ $\text{m}^2$  at MC 292 (Cruise 2B) and VK 916 (Cruise 1B).

Analysis of macroinfaunal data suggests there are some geographic differences in benthic community composition (*Chapter 11*). In the ordination analysis, two groups consisted of stations from GB 516 and GB 602, which are very close geographically (stations within tens of kilometers), whereas two other groups included stations from VK 916 and/or MC 292, which are relatively close to each other but about 400 km from the two Garden Banks sites.



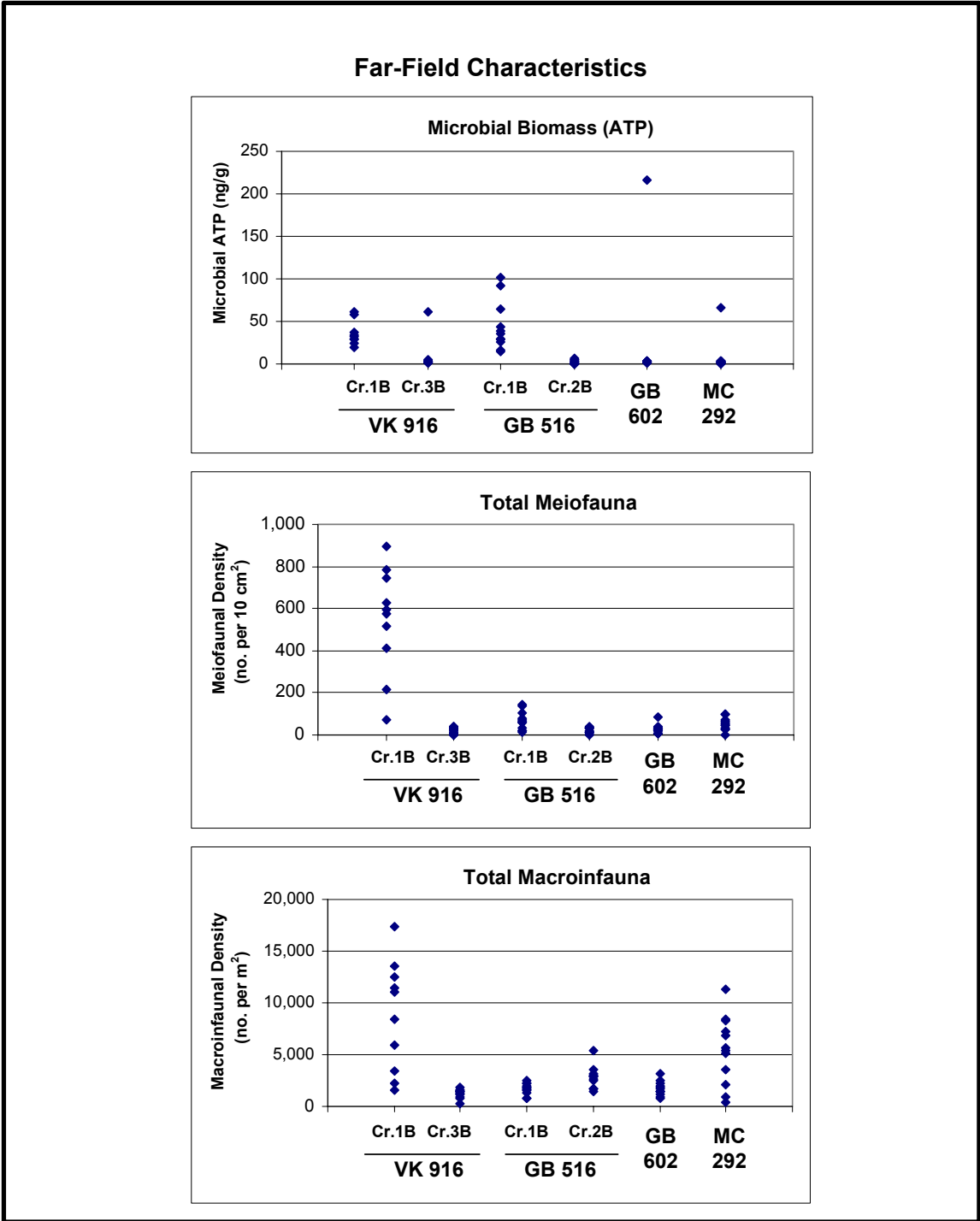


**Figure 15.1.** Microbial biomass and meiofaunal and macroinfaunal densities at far-field sites. Points are individual stations.

In conclusion, the four sites are broadly similar environmentally. Some physical/chemical and biological differences are evident between the western (GB 516 and GB 602) and central (VK 916 and MC 292) sites. Proximity to the Mississippi River mouth is an important influence on ambient conditions, as exemplified by lower sediment oxygen levels at the two central sites and the high sedimentation rate at MC 292. Significant temporal changes unrelated to drilling (e.g., in microbial biomass and meiofaunal and macroinfaunal densities) were noted at VK 916 and GB 516, and therefore, the impact analysis focuses on spatial comparisons (near-field vs. far-field).

### 15.1.2 Drilling Activities

The four sites represent a range of drilling activities (*Chapter 3*). VK 916 is the simplest case, with no previous drilling in the near-field site and a single exploration well drilled during this study. A semisubmersible drilling rig was used, and one set of anchors was deployed. Both WBMs and SBMs were used during drilling. This site was sampled before (Cruises 1A/1B) and after (Cruises 3A/3B) exploratory drilling.

GB 602 and MC 292 are development sites with several previous exploration and development wells and no new drilling during this study. Drilling occurred at various times over several years, so there were multiple drilling rigs, anchor deployments, and sets of drilling discharges. An important difference is that most of the drilling at MC 292 was done with WBM, with SBM used only for two sidetracks. Therefore, the total quantity of SBM cuttings discharged at MC 292 was the smallest among the four sites. These sites were sampled once during Cruises 2A/2B to provide a snapshot of post-development status.

GB 516 is the most complex case, with two previous exploration wells and five new development wells drilled during this study. Overall, activities were similar to those at the other development sites (GB 602 and MC 292) in that multiple wells were drilled over time, with multiple anchor deployments and drilling discharges; and subsea wellheads, manifolds, and flowlines were installed connecting to a remote platform. The difference is that two “snapshots” were obtained – once during Cruise 1B after exploration and again on Cruises 2A/2B after development.

The general sequence of events was similar for most wells (*Chapter 3*). The initial well interval was drilled (jetted) using a water-based spud mud. During this time before the marine riser was set, there were no returns to the drilling rig, and all mud and cuttings were released at the seafloor. Spud muds consisting primarily of water and bentonite clay were used for this jetting process. The wellhead was then connected to a marine riser system that returned muds and cuttings to the drilling rig during the remainder of the drilling process. Subsequently, one or more well intervals were drilled using WBM, with muds and WBM cuttings discharged from the rig. Finally, in most cases, the mud system was switched to SBM for drilling of remaining well intervals. In some cases, there were bulk discharges of remaining WBM prior to switching to SBM. During SBM intervals, SBM cuttings were discharged, but muds were retained (except for those adhering to cuttings). In addition, some quantities of SBMs were lost to the formation, lost during casing/cementing operations, or left in the wellbore for future sidetracks. Sidetracks at these sites were drilled primarily using SBMs. As noted previously, at MC 292, SBMs were used *only* during drilling of sidetracks.

**Table 15.2** summarizes the number of wells and estimated drilling fluid and cuttings discharges for each site. The GB 516 wells and discharges are divided into Exploration and Development.

**Table 15.2.** Drilling summary for wells within each near-field site.

Site	Total No. Wells Within 500-m Radius	Estimated Seafloor Discharges (bbl)		Estimated Drilling Rig Discharges (bbl)			SBM Type
		WBM	WBM Cuttings	WBM	WBM Cuttings	SBM Cuttings	
<b>Exploration</b>							
VK 916	1	3,074	419	12,807	1,746	2,510	Syn-Teq (IO)
GB 516	2	6,501	887	14,731	2,009	1,904	Novaplus (IO) or Petrofree LE (LAO)
<b>Development</b>							
GB 516	7 <sup>a</sup>	13,002	1,774	29,462	4,018	7,313	Novaplus (IO) and possibly Petrofree LE (LAO)
GB 602	7	23,946	3,266	91,301	12,450	28,339	Novadril (IO) or Petrofree ester (1 well); Novaplus (IO) or Petrofree LE (LAO) (all others)
MC 292	5	10,331	1,409	93,960	12,813	1,490	Novaplus (IO)

GB = Garden Banks; MC = Mississippi Canyon; VK = Viosca Knoll; IO = internal olefin; LAO = linear- $\alpha$ -olefin; SBM = synthetic-based mud; WBM = water-based mud.

<sup>a</sup> Totals for GB 516 post-development include the two exploration wells listed above.

The most important quantities in the table include the volume of SBM cuttings, the volume of WBM cuttings (including both seafloor and rig discharges), and the volume of WBM discharged at the seafloor. These are the discharges most likely to accumulate in detectable deposits within the near-field sites. WBM discharges from the rig are assumed to be less important because these fine particles would be widely dispersed in the water column while settling to the seafloor (Brandsma 1990).

In comparing discharges at the four sites:

- Quantities of most discharges were less at the two exploration sites than at the post-development sites, due to the smaller number of exploration wells.
- The GB 602 post-development site had by far the largest quantities of SBM cuttings discharged (about four times as much as GB 516).
- The MC 292 and GB 602 post-development sites had comparable quantities of WBM cuttings and mud discharges. The main difference is the much smaller quantity of SBM cuttings discharged at MC 292. Most of the drilling at MC 292 was done with WBM, with SBM used only for two sidetracks.

The timing of drilling activities vs. sampling cruises differed among sites. The interval between cessation of drilling and the date when the surveys began ranged from 5 months to about 2 years depending on the site (see *Section 15.3.3*).

In addition to the drilling activity, the three development sites (GB 516, GB 602, and MC 292) had structures placed on the seafloor, including subsea wellheads, flowlines and umbilicals, and associated equipment. At GB 516, these structures were emplaced during this study, between Cruises 1A/1B and 2A/2B. At the other two sites, the structures were installed prior to this study.

## 15.2 NATURE AND EXTENT OF IMPACTS

**Table 15.3** summarizes the physical, chemical, and biological impacts noted during this study. These are discussed subsequently in individual subsections.

Two types of information are available concerning the extent of impacts. Geophysical surveys (Cruises 1A, 2A, and 3A) were used to map the extent of anchor scars, debris, and drilling deposits within a radius of about 3 km around each near-field site. Biological/chemical sampling (Cruises 1B, 2B, and 3B) focused on detecting physical, chemical, and biological changes within the zone of most likely impact. Within each near-field site, eight stations were within 300 m, and the other four were between 300 m and 500 m from the site center. This stratification can be used to evaluate the extent of impacts within the near-field.

### 15.2.1 Physical

#### 15.2.1.1 Anchor Scars

Based on the geophysical surveys, anchor scars extended to the limit of the surveyed area (about 3-km radius) around the wellsites (*Chapter 4*). The anchor radius for a drilling rig is a function of water depth (typically about three times water depth in this depth range). Individual anchor scars, all in soft bottom areas, ranged from less than 100 m to over 3 km in length.

VK 916 had only one set of anchor scars associated with the exploratory drilling at this site. However, other scars remained from previous drilling in adjacent blocks (VK 872 and VK 873). The other three sites, surveyed post-development, had several sets of anchor scars, reflecting the use of different drilling rigs to drill various wells over time.

The extent of anchor scars was greater than initially expected. Exploration and development plans submitted to the MMS typically show the planned anchor locations and the catenary (“touch-down”) point where anchor chains may contact the seafloor once the anchors are tensioned from the rig. Based on these diagrams, anchor scars would be expected mainly along the outer portion of each anchor line, i.e., between the catenary point and the anchor location (a distance of a few hundred meters at this water depth). However, when anchors are being carried out to their pre-plotted locations by the anchor-handling vessel, longer portions of the anchor cable or chain may temporarily rest on the seafloor. This evidently is the cause of some of the longer scars detected by the side-scan sonar. Most of these wells were drilled at least 5 years ago and probably did not use taut-line anchoring systems. Such systems, which are now used for most deepwater anchoring, consist of polypropylene line and wire, with little or no chain that could drag on the seafloor during deployment (J. Hood, Transocean Inc., personal communication 2006).

**Table 15.3.** Impact summary.

Parameter and Chapter Reference	Impact	Extent	Notes
<b>PHYSICAL</b>			
Anchor scars (Chapter 4)	Presence of anchor scars	Within about 3-km radius from wellsites, 8 radial directions	Individual scars <100 m to >3 km in length
Seafloor equipment and debris (Chapter 4)	Presence of structures and debris on bottom	Subsea wellheads etc. within few hundred meters; flowlines and umbilicals extend many kilometers to nearby blocks; occasional debris within 3-km radius	VK 916 had the smallest number of side-scan “debris” contacts
Mappable mud and cuttings deposits (Chapter 4)	Presence of geophysically detectable mud and cuttings zones around wellsites	Well jetting deposits mostly within 100 m of wellsites. Rig discharge deposits extending from several hundred meters to about 1 km	Areal extent greatest at GB 516 and GB 602, smallest at VK 916
Sediment grain size (Chapter 5)	Increased percentage of (mainly coarse) sand at some stations	Primarily within 300-m radius	Cuttings similar in grain size to surficial sediments
Sediment color/appearance (Chapter 12)	Areas of black bottom within near-field	Extent not determined. Most consistent at GB 602; patchy at other sites	Black bottom is presumed due to the presence of cuttings and/or mud
Thickness of drilling deposits (Chapter 4, Chapter 8)	Isopach maps from subbottom profiling at VK 916 indicate thickness ranging from 0 to 45 cm	Extent not determined	Sectioning of a few discretionary cores at VK 916, GB 516, and GB 602 indicates layer of mud/cuttings several centimeters thick. Full range of thicknesses was not sampled by these cores
<b>CHEMICAL</b>			
Sediment barium (Chapter 8)	Elevated by orders of magnitude at nearly all near-field stations	Nearly all stations within 500-m radius; highest values within 300-m radius	One discretionary station 1,000 m from GB 602 site center had elevated barium; far-field data suggest slight effects at 2 to 3 km
Sediment SBF (Chapter 9)	Elevated by orders of magnitude at most near-field stations	Most stations within 500-m radius; nearly all stations within 300-m radius	One discretionary station 1,000 m from GB 602 site center had elevated SBF; far-field data suggest slight effects at 2 to 3 km
Sediment PAH (Chapter 9)	Elevated at two GB 516 stations	Within 300-m radius	Not attributable to SBM since these discharges do not contain PAH

**Table 15.3.** (continued).

Parameter and Chapter Reference	Impact	Extent	Notes
Metals other than Barium ( <i>Chapter 8</i> )	Elevated concentrations of As, Cd, Cr, Cu, Hg, Pb, and Zn at some stations; lower concentrations of Al, Fe, Mn, Ni, and V	Few stations	Differences are related to concentrations of these metals in barite, or reductive dissolution in the case of Mn
Sediment TOC ( <i>Chapter 8</i> )	Elevated at some near-field stations	Primarily within 300-m radius	High TOC is associated with high SBF concentrations
Sediment oxygen/Eh ( <i>Chapter 8</i> )	Low oxygen and negative Eh at some near-field sites	Primarily within 300-m radius	Poor redox conditions are associated with high SBF levels; least severe MC 292
Redox potential discontinuity ( <i>Chapters 6 and 7</i> )	Decreased depth of the oxidized layer in the near-field	Patchy within near-field	Poor redox conditions are associated with high SBF levels; least severe MC 292
Metals in isopods <i>Bathynomus giganteus</i> ( <i>Chapter 8</i> )	Elevated Ba, Cr, and Pb in isopods at GB 602 but not at MC 292; lower Cd and Hg in isopods at GB 602, but not at MC 292	Extent not determined	Most consistent finding is elevated barium (in isopods from GB 602 and in crabs from both GB 602 and MC 292). Possibly due to sediment particles in gut
Metals in red crabs <i>Chaceon quinquegens</i> ( <i>Chapter 8</i> )	Elevated Ba and reduced As, Cd, Cu, Hg, Ni, V, and Zn in crabs at GB 602; elevated Ba, Cd, Cr, and V in crabs at MC 292	Extent not determined	
Hydrocarbons in isopods and red crabs ( <i>Chapter 9</i> )	--	--	No impact on tissue PAH concentrations detected
<b>BIOLOGICAL</b>			
Benthic communities (general conditions) ( <i>Chapters 6 and 7</i> )	Azoic areas; areas of pioneering communities; poor organism-sediment index	Patchy within near-field	MC 292 appears least affected
Microbiota ( <i>Chapter 10</i> )	Elevated microbial biomass (ATP) at some stations	Patchy within near-field	Generally, stations with high ATP had high SBF levels; order of magnitude decrease in ATP between cruises at VK 916 and GB 516 (both near- and far-field)
Microbial mats ( <i>Chapters 6 and 7</i> )	Microbial mats seen in SPI images from several near-field stations	Patchy within near-field	Mats not seen at MC 292 or at GB 516 on Cruise 2B
Meiofauna ( <i>Chapter 11</i> )	Increased meiofaunal densities in near-field including annelids, harpacticoids, and nematodes	Primarily within 300-m radius	Order of magnitude decrease in meiofauna between cruises at VK 916 and GB 516

**Table 15.3.** (continued).

Parameter and Chapter Reference	Impact	Extent	Notes
Meiofauna - harpacticoid genetics ( <i>Chapter 13</i> )	Low genetic diversity in near-field populations of <i>Bathycyctopsyllus</i> sp.	Extent not determined	<i>Bathycyctopsyllus</i> sp. absent from far-field sites, but abundant at near-field sites; low genetic diversity is consistent with expansion from a small population
Macroinfauna ( <i>Chapter 11</i> )	Increased polychaete, gastropod, and bivalve densities in near-field; reduced amphipod and ostracod densities	Primarily within 300-m radius	--
Megafauna ( <i>Chapter 12</i> )	Higher fish densities and lower ophiuroid densities within near-field	Extent not determined	Effects evident at VK 916 and GB 516 but not at GB 602 or MC 292

GB = Garden Banks; MC = Mississippi Canyon; VK = Viosca Knoll; Al = aluminum; ATP = adenosine triphosphate; Ba = barium; Cd = cadmium; Cr = chromium; Cu = copper; Eh = redox potential; Fe = iron; Hg = mercury; Mn = manganese; Ni = nickel; PAH = polycyclic aromatic hydrocarbon; Pb = lead; SBF = synthetic-based fluid; ; SBM = synthetic-based mud; TOC = total organic carbon; V = vanadium.

#### 15.2.1.2 Seafloor Equipment and Debris

At the three sites where development drilling has occurred and production is ongoing (GB 516, GB 602, and MC 292), the geophysical survey identified known structures on the seafloor, including pipelines and flowlines, subsea wellheads, umbilical termination modules, etc. The wellheads and associated equipment were mostly within 200 m of the site centers. Pipelines and flowlines extended many kilometers to platforms or other structures in nearby lease blocks.

At all four sites, there were side-scan sonar contacts identified as debris. These could include pieces of pipe, etc. that presumably fell from the drilling rig or other vessels. VK 916 had the smallest number of contacts (4), whereas there were numerous contacts at the other sites. Debris locations were not investigated further in this study. Visual observations of debris around former drillsites in the Gulf of Mexico have been reported by Shinn et al. (1993).

#### 15.2.1.3 Mappable Cuttings and Mud Deposits

As noted in *Chapter 4*, side-scan sonar and chirp sonar subbottom records were used to map deposits of drilling mud and cuttings around the wellsites. However, there are no unique geophysical signatures for these deposits. The mapped distribution of mud and cuttings was inferred from a combination of geophysical data and information about discharges.

Two zones were recognized. Although these were identified as “drilling muds” and “drill cuttings” in the geophysical cruise reports, both zones probably consist of both muds and cuttings, and primarily the latter. First, in the area immediately around wellsites, there typically was a zone recognized by a combination of a smooth seafloor (little backscatter on side-scan sonar records) and a high amplitude response at the seafloor on high resolution subbottom profiles. This zone, identified as “drilling muds” in the geophysical cruise reports, probably

represents an area of cuttings and spud mud deposition from initial jetting of wells. Cuttings probably account for most of the materials deposited during this stage, because spud muds are primarily seawater with low solids concentrations. Typically, these initial deposits, along with excess cement from setting of the well casing, create a shallow, compact mound. Other activities including installation of subsea wellheads, flowlines, and umbilical modules at the three post-development sites (GB 516, GB 602, and MC 292) (see *Chapter 3*) may also have contributed to the observed reflectance pattern around the wellsites.

More extensive areas where side-scan sonar showed high reflectivity extending in a radial pattern around the wellsites were interpreted as primarily cuttings (with adhering muds) from rig discharges. Cuttings are derived from subsurface sediments that are much more compacted and therefore denser than surface hemipelagic sediments that drape most of the northern Gulf continental slope. When clumps of these dense, coarse sediments are scattered across the seafloor by surface discharges, they create an acoustic impedance difference that translates into a higher amplitude reflection on side-scan sonar records. Although water-based drilling muds were also discharged from the rig at all wellsites, they probably were widely dispersed before reaching the seafloor (Brandsma 1990) and would not likely be detected geophysically. Cuttings discharged during both WBM and SBM well intervals presumably included adhering muds that sank with the cuttings.

**Figure 15.2** shows the mapped distribution of these zones on post-drilling cruises at each of the four sites. For simplicity, these zones are referred to as well jetting deposits and rig discharge deposits. The only post-exploration map is for VK 916 on Cruise 3A; there was no post-exploration geophysical survey at GB 516. Post-development maps are available for GB 516, GB 602, and MC 292 from Cruise 2A.

Generally, areas mapped as well jetting deposits were identified within about 100 m of wellsites. Areas mapped as rig discharge deposits typically extended several hundred meters from wellsites, with the greatest extent (about 1 km) observed at GB 602 and GB 516. The estimated area of mud and cuttings accumulation was greatest at GB 516 (Cruise 2B) and smallest at VK 916 (**Table 15.4**).

**Table 15.4.** Geophysically estimated areal extent of drilling mud and cuttings deposits at each near-field site. Both well jetting deposits and rig discharge deposits are assumed to consist of both drilling muds and cuttings (primarily the latter). See text for caveats concerning the identification of these zones.

Site	Cruise	Stage	Well Jetting Deposits (ha)	Rig Discharge Deposits (ha)
VK 916	3A	Post-exploration	None mapped	13.37
GB 516	2A	Post-development	2.48	108.53
GB 602	2A	Post-development	1.08	43.18
MC 292	2A	Post-development	0.78	25.61

GB = Garden Banks; MC = Mississippi Canyon; VK = Viosca Knoll.



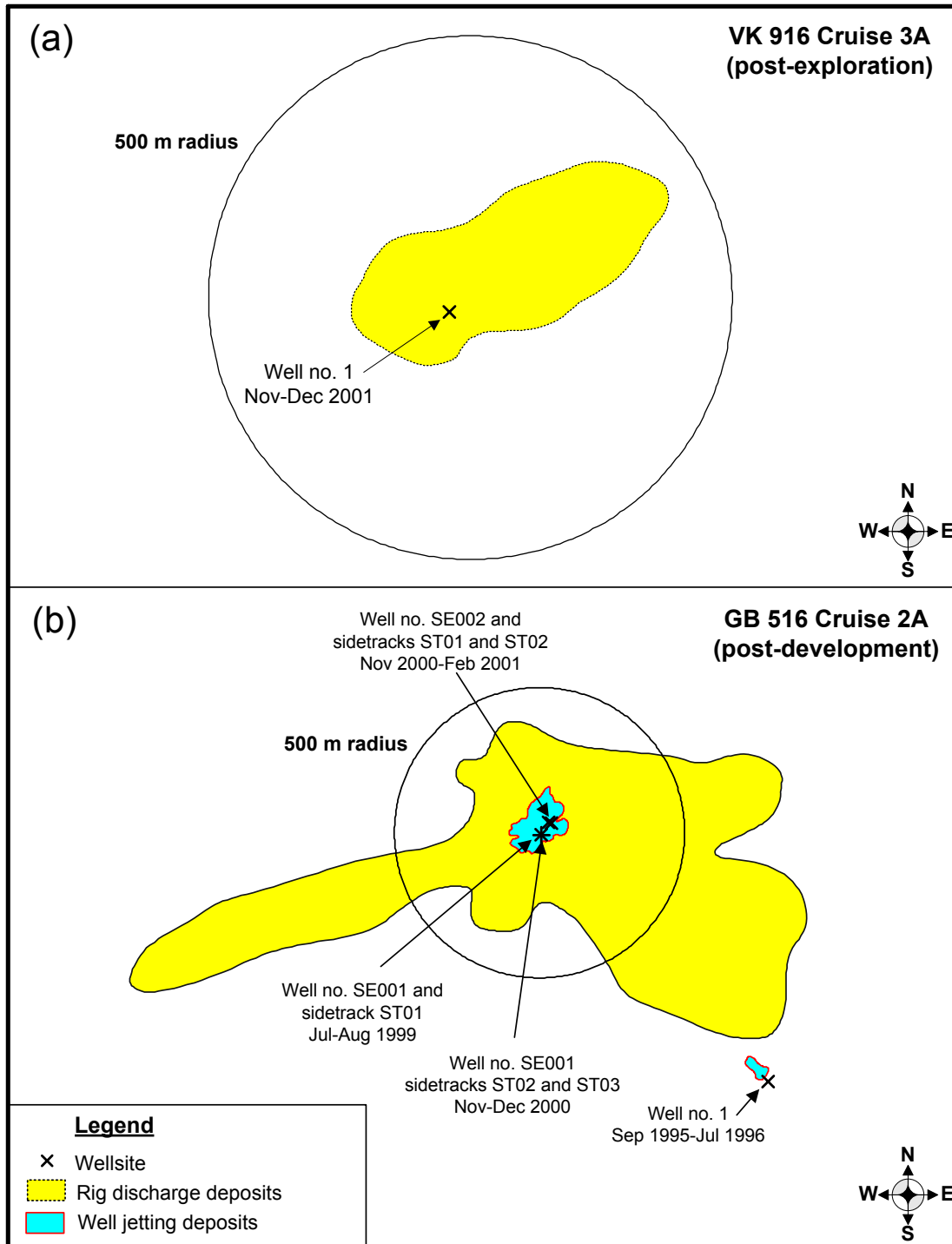


**Figure 15.2.** Extent of geophysically mapped drilling mud and cuttings deposits around (a) Viosca Knoll 916 on Cruise 3A; (b) Garden Banks 516 on Cruise 2A; (c) Garden Banks 602 on Cruise 2A; and (d) Mississippi Canyon 292 on Cruise 2A. See text for assumptions and caveats concerning mapping of these zones.

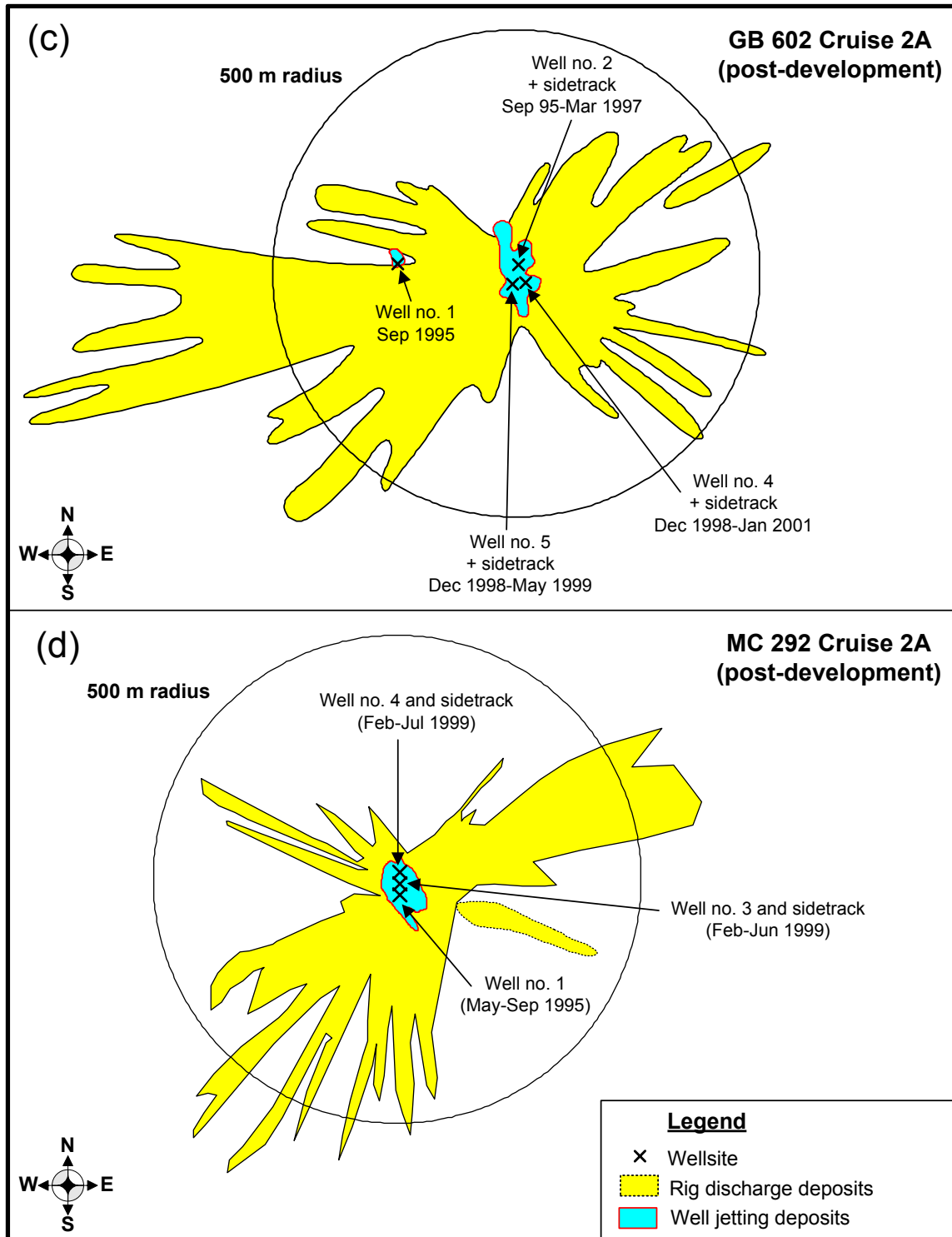


Figure 15.2. (continued).

Identification of these mapped zones is not definitive. No “ground truth” sampling or analysis was conducted to verify that cuttings or drilling mud particles were present in these zones, or to determine the minimum thickness that could be detected. In *Chapter 4*, it was noted that other processes could produce the reflectance patterns mapped as cuttings, including seafloor disturbances (grooves, furrows, etc.) caused by the process of setting anchors and the dropping of sediment clumps to the seafloor from the anchor cables as they are pulled into place. However, several lines of evidence (discussed below) suggest that the geophysically mapped areas are due to drilling discharges rather than clumps from anchor cables or other seafloor disturbances.

Typically, eight anchors are deployed radially around the drilling rig. If the high reflectivity areas were related to anchoring (scars, grooves, and clumps), they should be distributed radially. However, the high-reflectivity areas are predominantly along a SW to NE or WSW to NNE axis and are not lined up with plotted anchor locations (see **Figures 15.3** and **15.4** for VK 916 and GB 516; the other two side-scan sonar mosaics are presented in *Appendix K*). The distribution tends to be along isobaths, consistent with the expected current patterns along the continental slope (Nowlin et al. 2001; Sturges et al. 2004). Also, drilling rigs generally were present at each site for only a few months during drilling of each well. Based on what is known about colonization of submerged structures, this probably is not long enough to develop a substantial fouling biota on the anchor cables, making it unlikely that the observed patterns were created by substantial clumps of organic matter falling to the seafloor. In addition, if the deposition were caused by clumps from anchor cables, one would expect to see the patterns extending all the way out to the anchor locations, whereas the high-reflectivity areas are primarily within the 500-m near-field radius.

The association of the mapped deposits with the drilling rig (rather than anchor cables) is also evident in the isopach map (**Figure 15.5**) produced for VK 916. The plot shows thicknesses ranging from 0 to 45 cm within the mapped cuttings zone. The thickness of the deposits and the proximity to the wellsite strongly suggest that the geophysically mapped zone consists of drilling discharges.

Further confirmation is available from chemical analysis of sediments. Concentrations of barium and SBF tended to be higher in areas mapped as drilling deposits (see plots in *Section 15.2.2*). VK 916 shows the clearest pattern, with stations within the zone of rig discharge deposits having higher barium and SBF concentrations than those outside the zone. At GB 516, only one station was not in the zone of rig discharge deposits, and this station had relatively low barium and SBF concentrations. Stations in the zone of well jetting deposits at GB 516 had very high barium concentrations, and one station had very high SBF concentrations. Patterns at GB 602 and MC 292 were less clear-cut. Overall, the results suggest that the geophysically mapped zones are due to drilling discharges, though the exact boundaries do not necessarily correspond to barium and SBF contours.

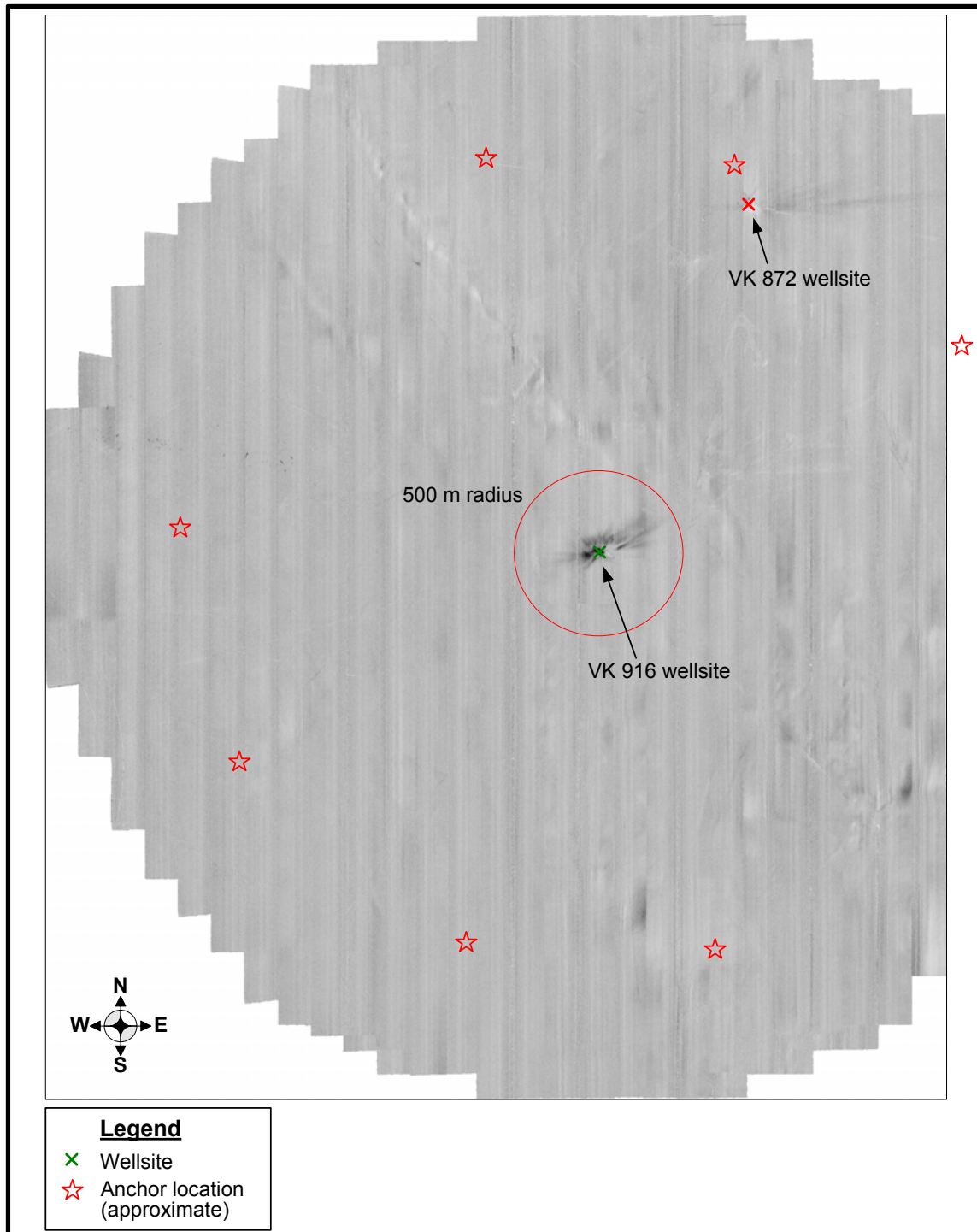


**Figure 15.3.** Side-scan sonar mosaic showing highly reflective seafloor (dark areas, presumed rig discharge deposits) at Viosca Knoll 916 on Cruise 3A (post-exploration). Dark areas are oriented predominantly WSW to ENE whereas anchors are distributed radially. A similar but fainter pattern is evident around a wellsite in VK 872 (drilled about 3.5 years earlier).

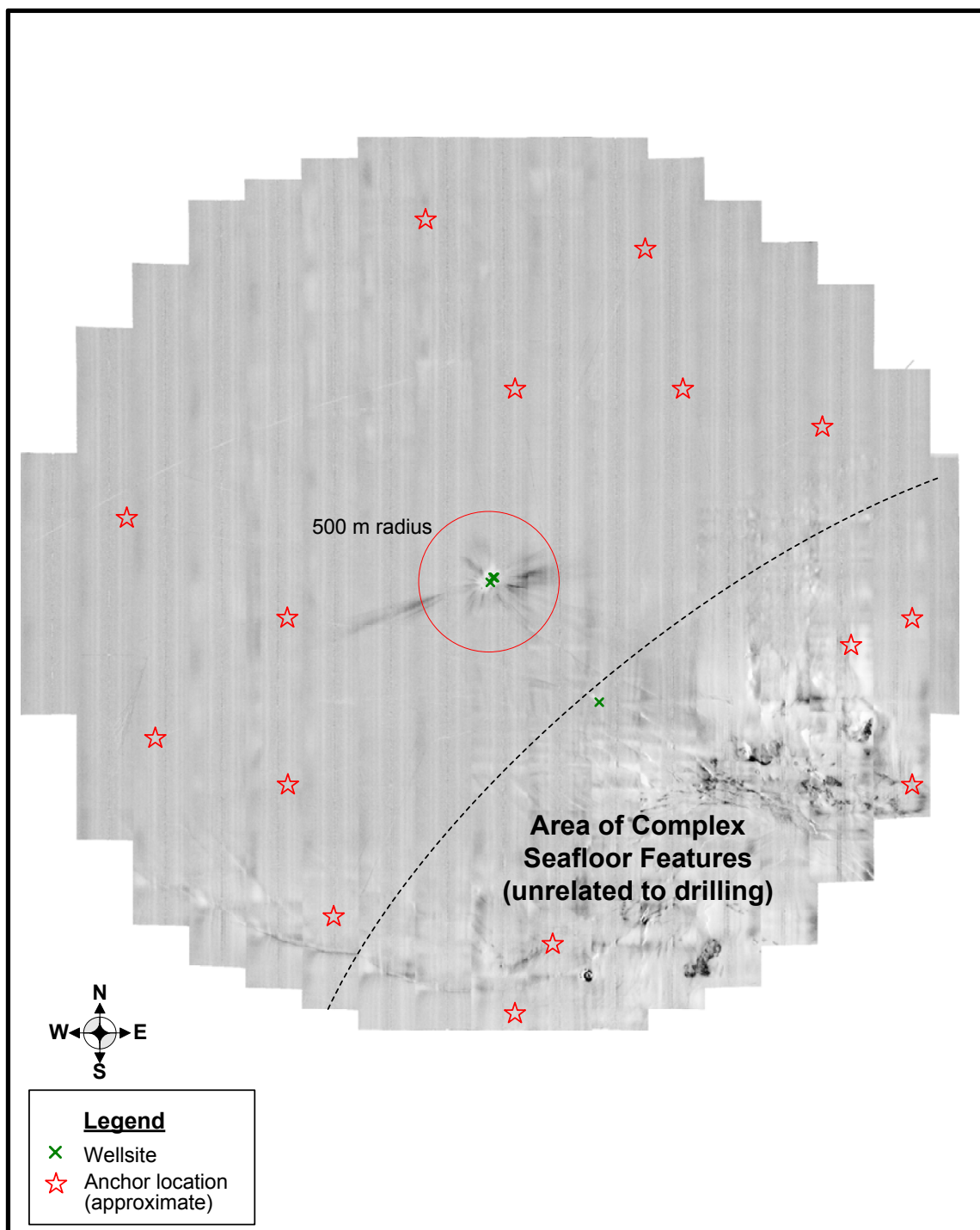


**Figure 15.4.** Distribution of highly reflective seafloor (dark areas, presumed rig discharge deposits) at Garden Banks 516 on Cruise 2A (post-development). Note that dark areas are predominantly oriented WSW to ENE around the wellsite and do not appear to be associated with anchor locations.

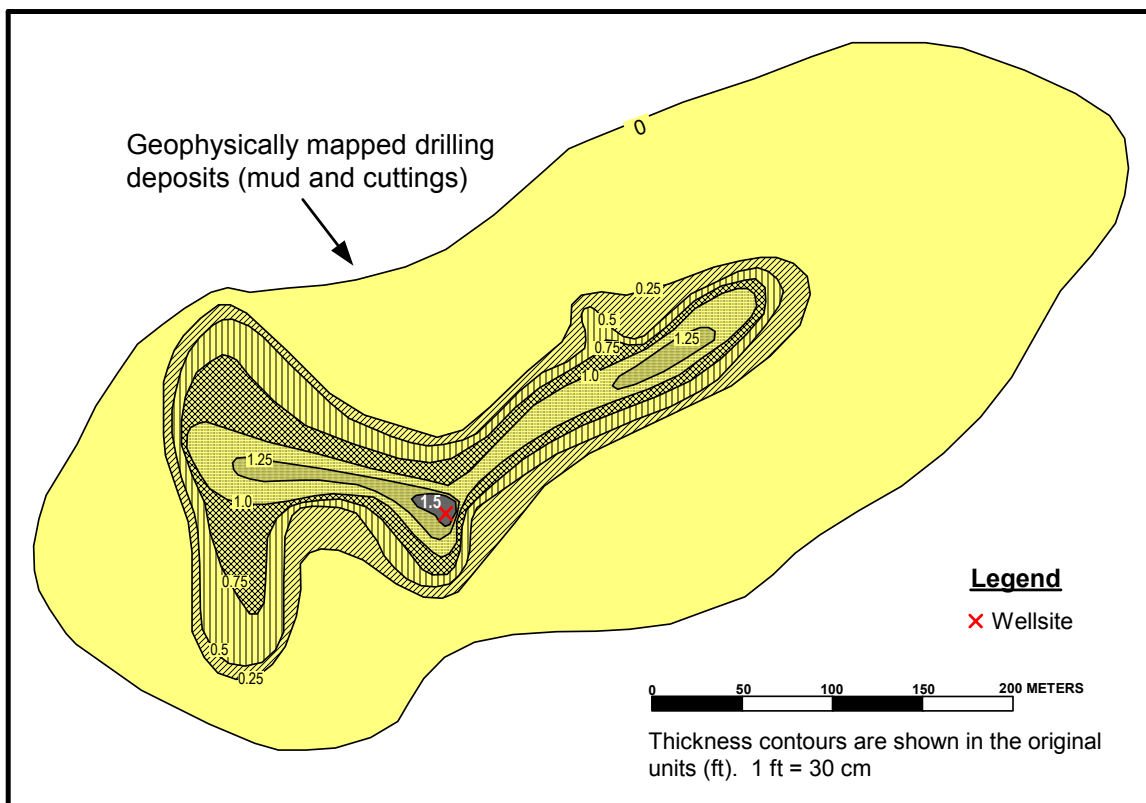


**Figure 15.5.** Isopach (thickness) plot of geophysically mapped drilling deposits at Viosca Knoll 916. Adapted from the isopach map in *Appendix C2*.

#### 15.2.1.4 Sediment Grain Size

Sediments at all four sites were predominantly clay and silt. There were no major, gross changes in sediment grain size distribution around the wellsites (*Chapter 5*). There were no gravel-sized particles ( $>2$  mm) at most stations. On Cruise 3B at VK 916, one station (NF-B01) had 0.74% gravel associated with high concentrations of barium (171,000  $\mu\text{g/g}$ ) and SBF (10,283  $\mu\text{g/g}$ ).

A few near-field samples had slightly elevated percentages of sand-sized particles. Most stations had  $<10\%$  sand. Higher percentages were evident at several stations at GB 516 on Cruise 2B (up to 18%) and at one MC 292 station (14%). GB 602 had higher sand percentages both near-field and far-field, but one near-field station had the highest value (21%). Near-field, post-drilling elevations in sand percentages were detected statistically at VK 916, GB 516 (Cruise 2B), and MC 292, but not at GB 602 nor at GB 516 on Cruise 1B (*Chapter 5*).

**Figure 15.6** shows sand, silt, and clay percentages for stations grouped into three categories:

- Far-field stations ( $>10$  km) (also includes near-field pre-drilling stations at VK 916);
- Near-field stations 300 to 500 m from site center; and
- Near-field stations within 300 m of site center.

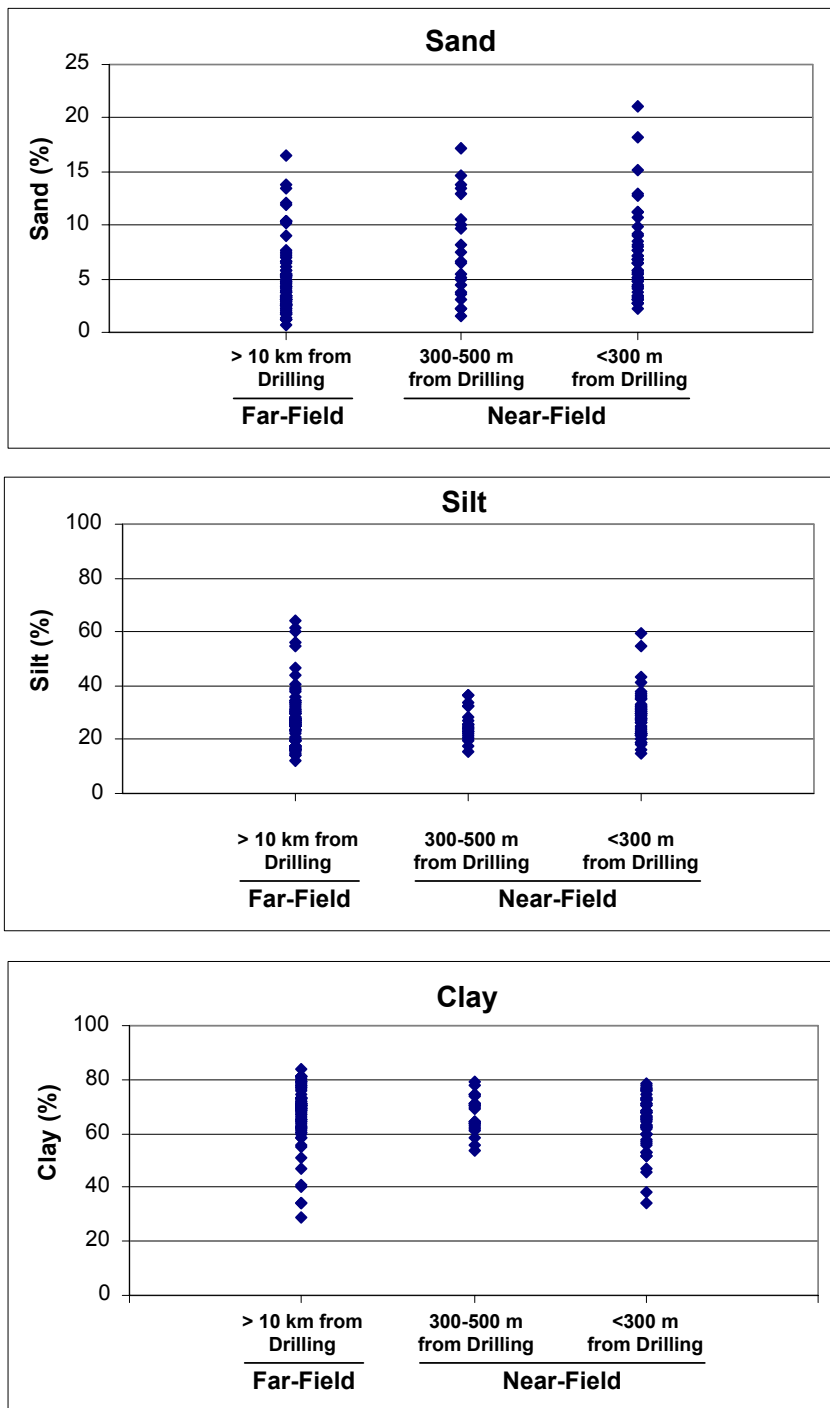


**Figure 15.6.** Sediment percentages of sand, silt, and clay in relation to proximity to drilling. Points are individual stations including non-random "discretionary" stations. "Far-field" includes near-field, pre-drilling stations at Viosca Knoll 916.

The range of sand percentages at the far-field and 300- to 500-m groups was similar. The <300-m group had two values that were slightly higher than those seen in the far-field, and overall, this group tended to have higher sand percentages than the far-field. In the near-field, both silt and clay percentages were within the range of values observed in the far-field.

Grain size variations were patchy within near-field sites and the spatial pattern did not necessarily correspond to the drilling discharge zones mapped in *Chapter 4*. Also, except for VK 916, there were no strong correlations between percentages of sand, silt, or clay and concentrations of drilling indicators such as barium and SBF. These findings suggest that grain size distribution *per se* is not a very good indicator of drilling discharge impacts. Other physical measures have been determined to be more definitive in identifying cuttings, such as visual analysis for angular or tabular particles (Continental Shelf Associates, Inc. 2004).

We assume that the materials deposited within the near-field sites consist mainly of (1) cuttings and WBMs released at the seafloor during the early stage of drilling; and (2) surface-discharged cuttings with small percentages of adhering SBMs. The latter is probably the main contributor at the near-field stations. While very coarse particles presumably attributable to seafloor discharges were noted near some drillsites in the SBM monitoring program (Continental Shelf Associates, Inc. 2004), these deposits are unlikely to have been sampled at our stations. Also, it is expected that any water-based drilling fluids discharged at the surface would be widely dispersed while settling to the bottom in a water depth of 1,000 m or more and would not appreciably affect grain size of bottom sediments.

Cuttings with adhering SBMs tend to clump together and sink rapidly when discharged (Brandsma 1996). It is this aggregation that results in detectable accumulations of SBM cuttings on the seafloor near the drillsite. Once deposited, these clumps are eventually broken up due to biological activity. Grain size determinations would not show the presence of loosely adhering clumps. However, rough seafloor texture is evident in some near-field photographs (*Chapter 12*).

#### 15.2.1.5 Sediment Color/Appearance

Color analysis of seafloor photographs (*Chapter 12*) showed that areas of “black bottom” were present on post-drilling surveys at all four near-field sites, but not at far-field sites (or VK 916 near-field on the pre-drilling survey). Black surface layers also were seen in some sediment profile images (*Chapters 6 and 7*). The black bottom was covered in some images by white-to-red mats consistent with the sulfide-using bacteria *Beggiatoa*. These bacterial areas may indicate sites of local bottom anoxia supported by bacterial degradation of SBM. Although impacts were patchy at all sites, most images at GB 602 showed dark bottom, possibly indicating that this site has cuttings more thinly spread over a larger area. The patterns of black bottom coincided with geophysical mapping of cuttings reasonably well where direct comparisons could be made.

#### 15.2.1.6 Thickness of Mud and Cuttings Deposits

The thickness of mud and cuttings deposits was estimated during the post-drilling geophysical survey at VK 916. The isopach map (**Figure 15.5**) shows thicknesses ranging from 0 to 45 cm around the wellsite. For comparison, the Pompano study estimated maximum cuttings thicknesses of 20 to 25 cm near a development well (Fechhelm et al. 1999) and the SBM



monitoring program detected layers ranging from a few centimeters to about 20-cm thick around various wellsites (Continental Shelf Associates, Inc. 2004).

In addition, discretionary samples taken in likely mud/cuttings areas during Cruises 2B and 3B provide information about the thickness of mud and cuttings at a few stations (*Chapter 8*). Cores were subsectioned in five, 2-cm thick intervals over the top 10 cm. At VK 916, the thickness of layers containing drilling discharges during Cruise 3B (post-exploration), based on concentrations of barium and TOC, was about 4 cm in each of three discretionary cores. At GB 516 on Cruise 2B (post-development), excess  $^{210}\text{Pb}$  data for one station identify the presence of drilling discharges in the top 2 cm. At GB 602, a 6-cm thick layer of sediment containing drilling discharges was observed at the NF-DS2 station on Cruise 2B (post-development). The thickness of drilling deposits at MC 292 was not estimated. As indicated by the isopach map produced for VK 916 (see above), these values do not represent the thickest deposits since the area immediately surrounding the wellsites was not sampled.

## 15.2.2 Chemical

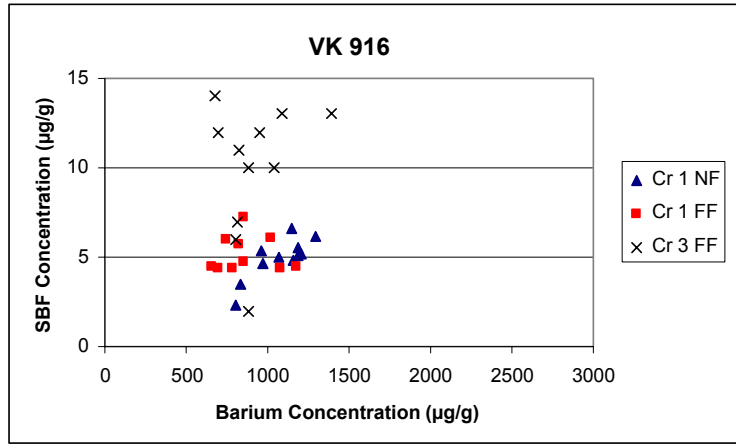
### 15.2.2.1 Drilling Fluid Tracers (Barium and SBF)

Barium and SBF are sensitive tracers of drilling fluids in this study. Barite ( $\text{BaSO}_4$ ) is a major ingredient in both WBMs and SBMs. SBF concentrations are presumed to be related to the amount of SBF adhering to discharged cuttings. Current USEPA regulations limit the SBF retention on cuttings to 6.9% internal olefins and 9.4% ester-based fluids (USEPA 2001b). However, several of the wells within the near-field sites were drilled prior to those regulations. Historical data for wells drilled in the 1990's in the Gulf of Mexico indicate an average retention on cuttings of 12.8% for poly-alpha-olefin fluids and 9.2% for internal olefin fluids (Annis 1997, as cited by Neff et al. 2000).

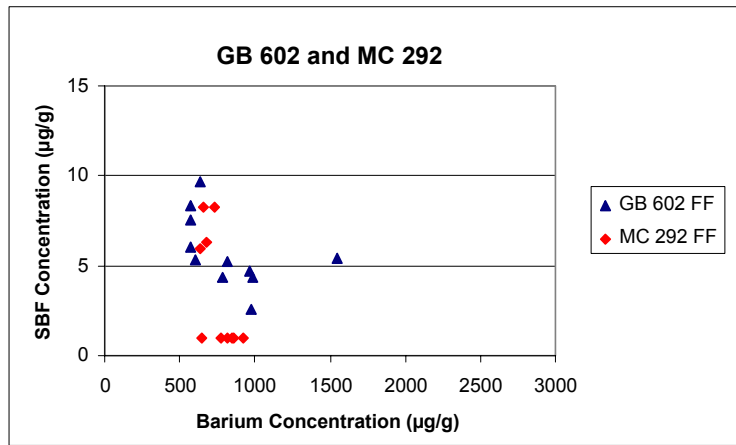
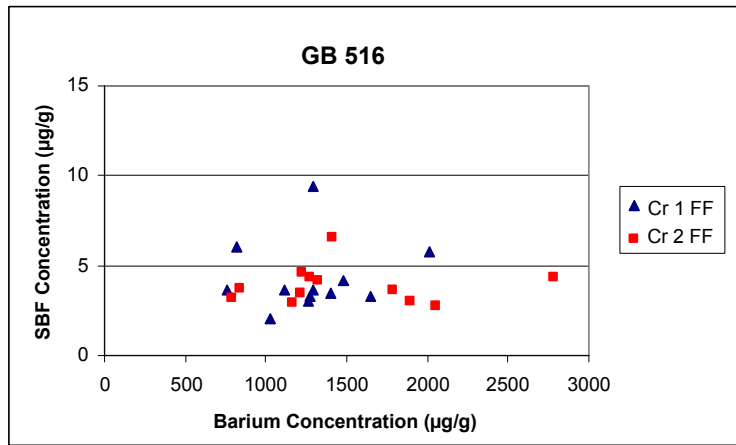
Neither barium nor SBF are ideal tracers of drilling fluids or cuttings. SBFs biodegrade over time. Although barium persists, its fate does not necessarily represent that of other drilling fluid components with different masses, shapes, solubilities, specific gravities, etc. Once drilling fluids and cuttings are released to the water column or the seafloor, the components may react, degrade, and move with different characteristics.

**Figure 15.7** shows the range of barium and SBF concentrations at far-field sites. Far-field barium values typically were between 500 and 1,500  $\mu\text{g/g}$ , except at GB 516, where values as high as 2,780  $\mu\text{g/g}$  were observed. Far-field SBF concentrations generally were less than 10  $\mu\text{g/g}$ , except for the Cruise 3B values at VK 916, which were in the 10 to 15  $\mu\text{g/g}$  range. There was one higher SBF concentration at VK 916 FF2 (111  $\mu\text{g/g}$ ), which may be due to drilling discharges from wells in an adjacent lease block (see *Chapter 3*).

All of the far-field sites had non-zero SBF concentrations (i.e., above the detection limits). However, these values do not necessarily represent the presence of SBM cuttings. These concentrations may be due to small quantities of natural hydrocarbons that eluted in the same range as SBFs in the analytical procedure. **Table 15.5** shows the confidence intervals for far-field barium and SBF concentrations.



Note: Cruise 3B plot excludes FF2-B02 (SBF=111 µg/g). This sample may have been exposed to drilling discharges from another well.



Note: MC 292 plot excludes FF6-B01 (SBF=28 µg/g) and FF1-B02 (19 µg/g). These samples may have been exposed to drilling discharges from another well.

**Figure 15.7.** Far-field concentrations of barium and synthetic-based fluids. Points are individual stations including non-random "discretionary" stations. "Far-field" includes near-field, pre-drilling stations at Viosca Knoll 916.

**Table 15.5.** Confidence intervals for far-field barium and synthetic-based fluid (SBF) concentrations.

Site	Cruise	95% Confidence Interval for an Observation	
		Barium ( $\mu\text{g/g}$ )	SBF ( $\mu\text{g/g}$ )
VK 916	1B	546 – 1,064	2.96 – 7.74
VK 916	3B	565 – 1,166	1.49 – 17.91
GB 516	1B	532 – 2,031	-0.01 – 8.55
GB 516	2B	254 – 2,702	1.38 – 6.45
GB 602	2B	169 – 1,473	1.38 – 10.12
MC 292	2B	516 – 993	-13.46 – 31.46

GB = Garden Banks; MC = Mississippi Canyon; VK = Viosca Knoll.

As discussed in *Chapters 8 and 9*, barium and SBF concentrations were significantly higher at sites near drilling (near-field, post-drilling) than at sites far from drilling (i.e., far-field sites or the near-field, pre-drilling site at VK 916). Post-drilling, near-field barium concentrations were as high as 351,000  $\mu\text{g/g}$ . The maximum barium concentration was measured at GB 516 Station NF-B03 on Cruise 2B and represents a sediment content of ~66% barite (using a barium level of 53% for industrial barite, Trefry et al. 2003). All near-field stations except two at VK 916 had barium concentrations exceeding the 95% confidence interval for far-field concentrations.

Post-drilling, near-field SBF concentrations ranged from <1.4 to 117,280  $\mu\text{g/g}$ . The highest concentration was measured in a discretionary sample at GB 516 on Cruise 2B. All near-field stations at GB 602 and 11 of 12 stations at GB 516 had SBF concentrations that exceeded the 95% confidence interval for far-field concentrations. SBF increases were not as widespread at the other two sites. At VK 916, 8 of 12 stations exceeded the far-field confidence limits, and at MC 292, only 6 of 12 stations did. (VK 916 had only a single well drilled, and MC 292 had the lowest volume of SBM discharges.)

**Figures 15.8, 15.9, 15.10, and 15.11** show barium and SBF concentrations at each of the four sites in relation to geophysically mapped zones. For VK 916 and GB 516, stations with elevated barium and SBF were mainly within these zones. For GB 602, elevated concentrations seemed to be distributed throughout the near-field site, and most stations were in or near the mapped zones in any case. MC 292 does not show the very high ranges of barium and (especially) SBF values as compared with the other sites.

**Figure 15.12** shows concentrations of barium and SBF for all sites combined, with stations grouped into the same three categories cited previously (far-field, near-field 300 to 500 m, and near-field <300 m). The figure shows that although the highest barium concentrations were seen within 300 m, most near-field stations including those between 300 m and 500 m from the center had elevated barium concentrations. Similarly, for SBF, although a 300-m station had the highest concentration, the range was fairly similar for both 300-m and 500-m radii. For both barium and SBF, some near-field stations, even within 300 m, had concentrations within the range observed for far-field stations.

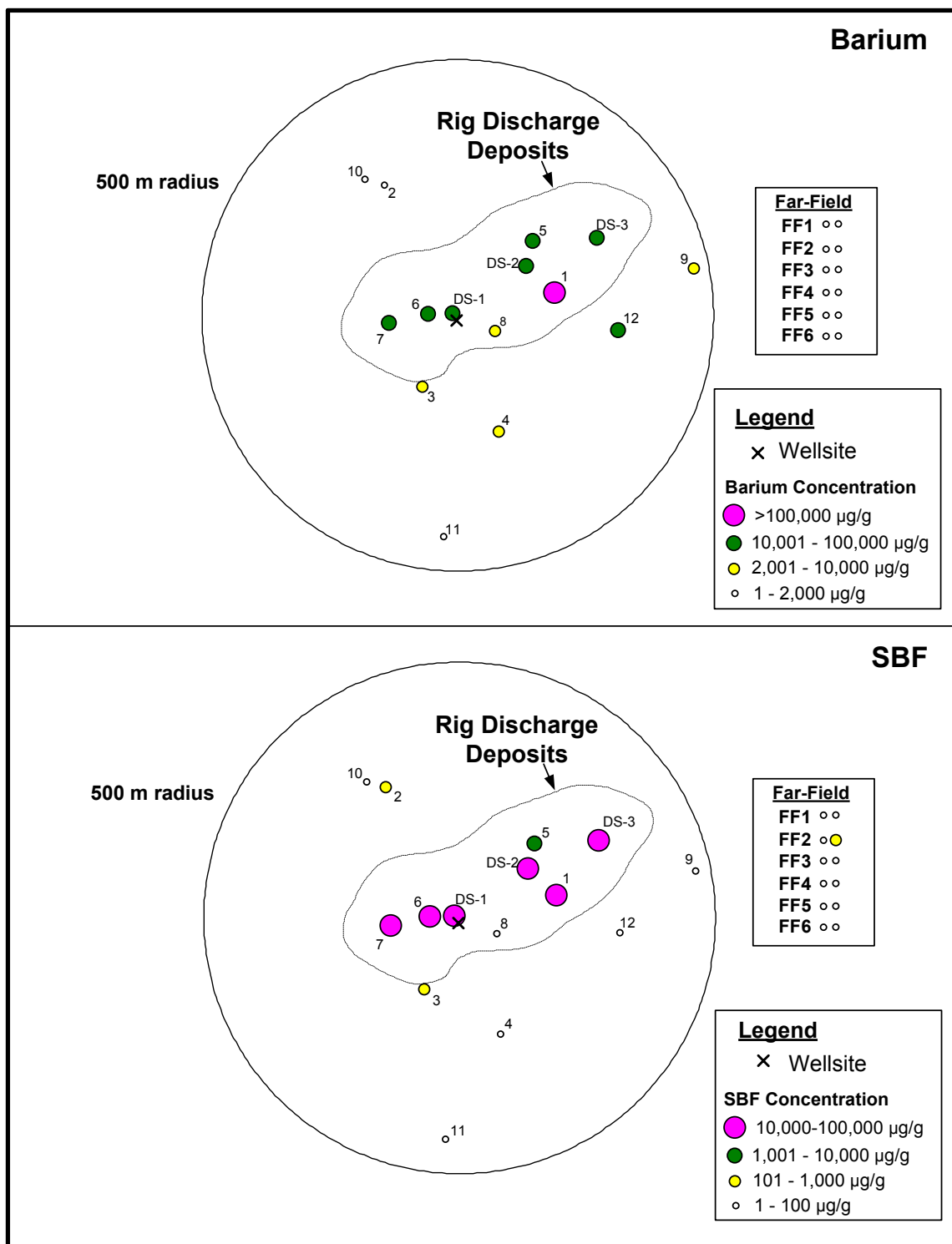


**Figure 15.8.** Barium and synthetic-based fluid (SBF) concentrations on Cruise 3B at Viosca Knoll 916 site in relation to geophysically mapped rig discharge deposits.

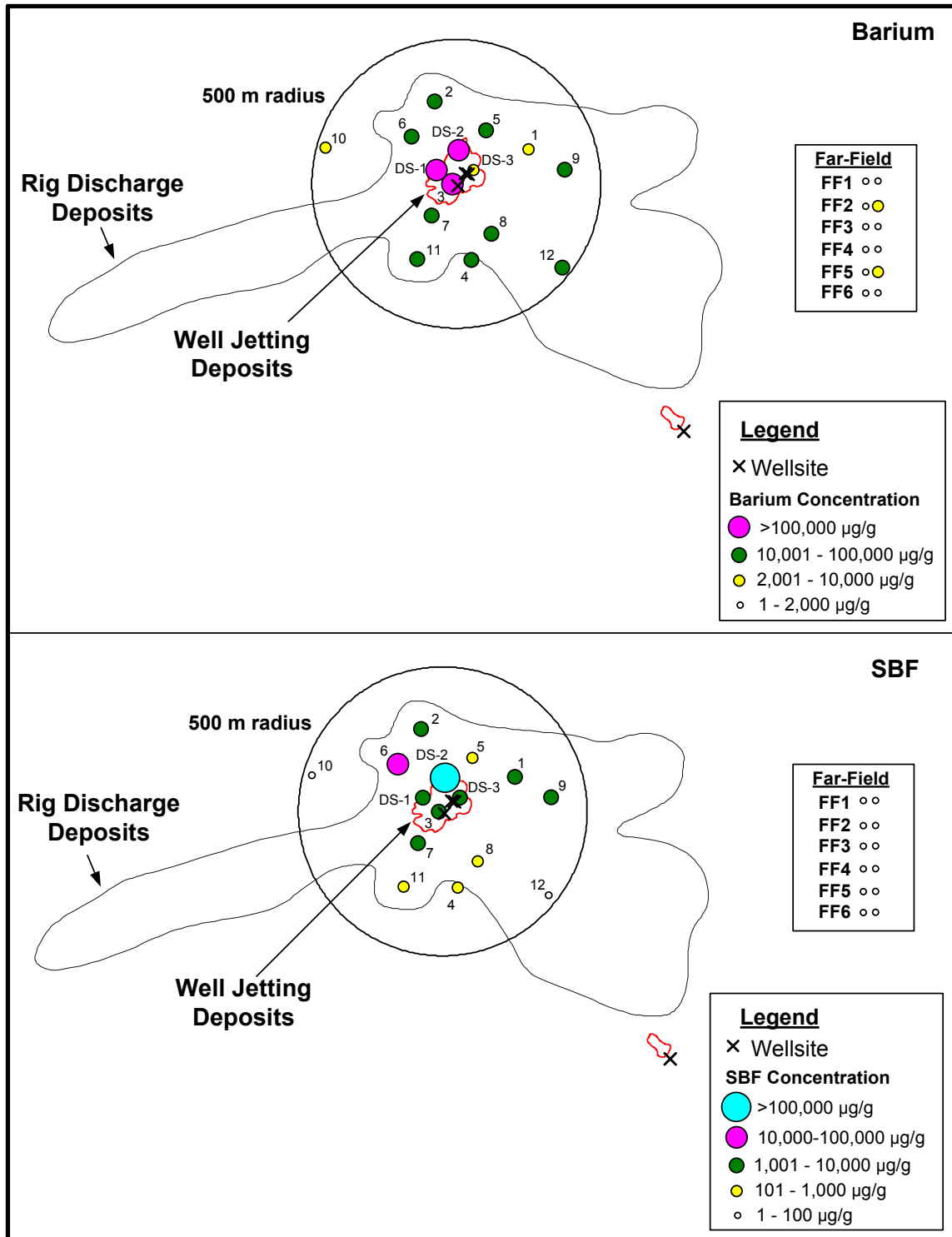


Figure 15.9. Barium and synthetic-based fluid (SBF) concentrations on Cruise 2B at Garden Banks 516 in relation to geophysically mapped mud and cuttings deposits.

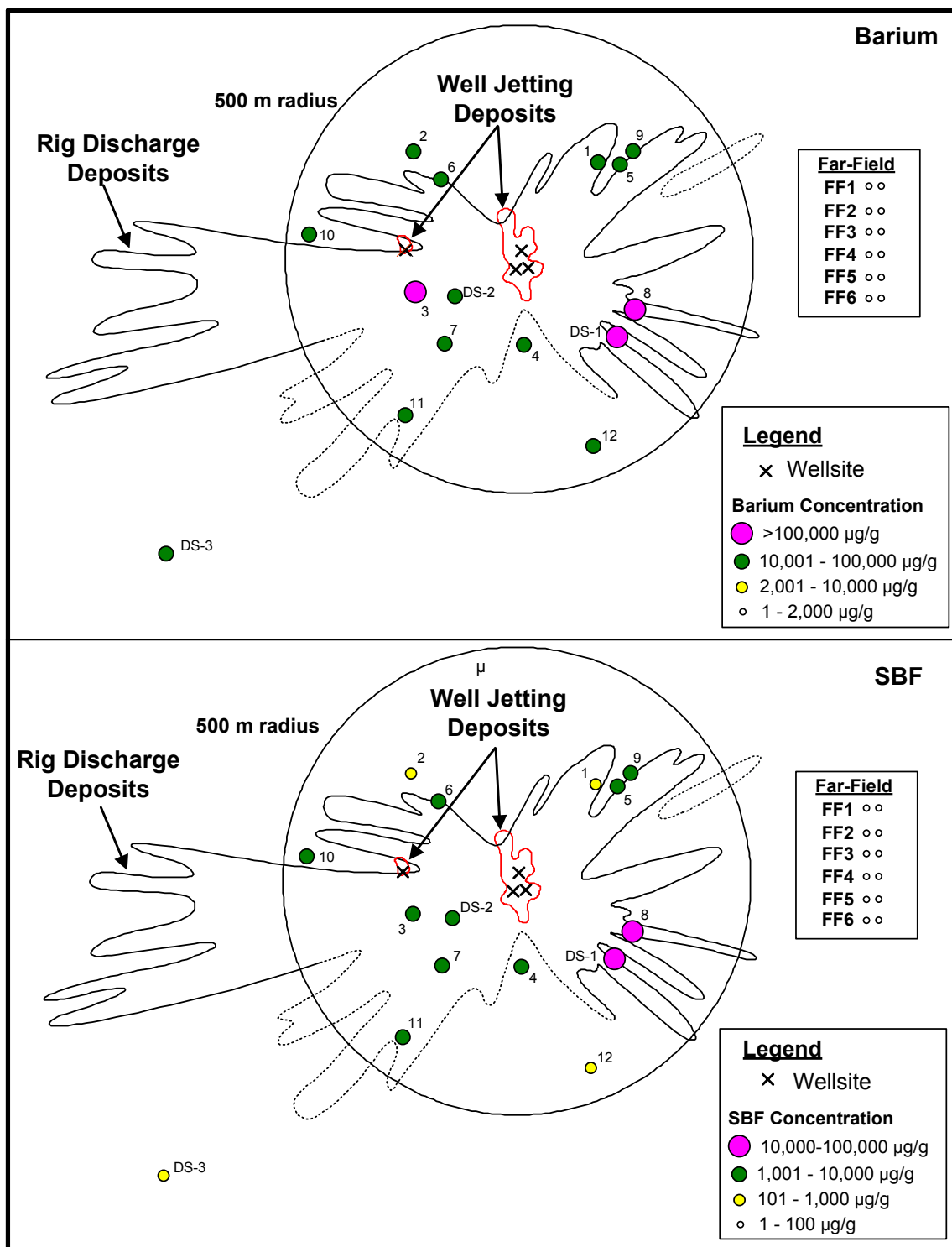


Figure 15.10. Barium and synthetic-based fluid (SBF) concentrations on Cruise 2B at Garden Banks 602 in relation to geophysically mapped mud and cuttings deposits.

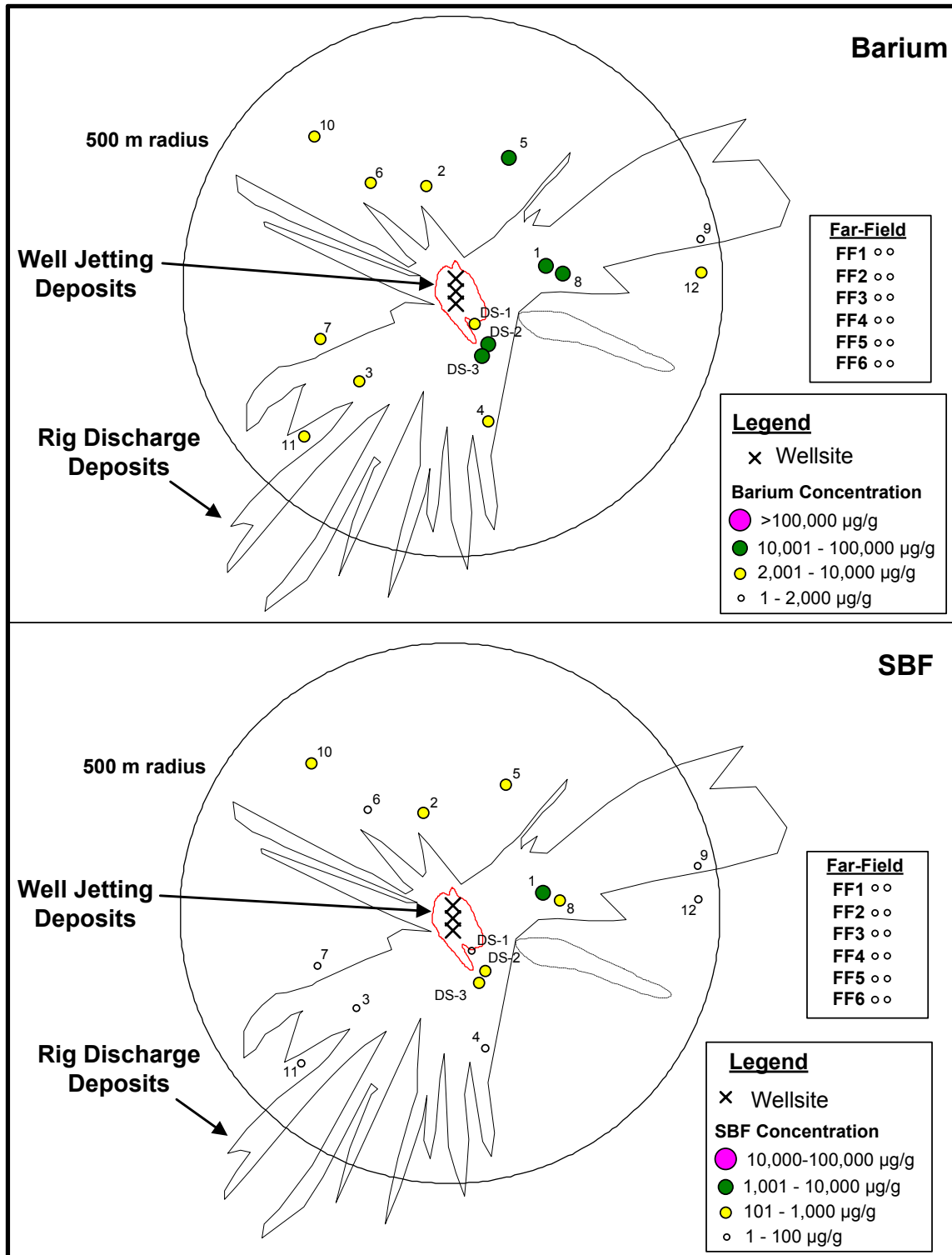
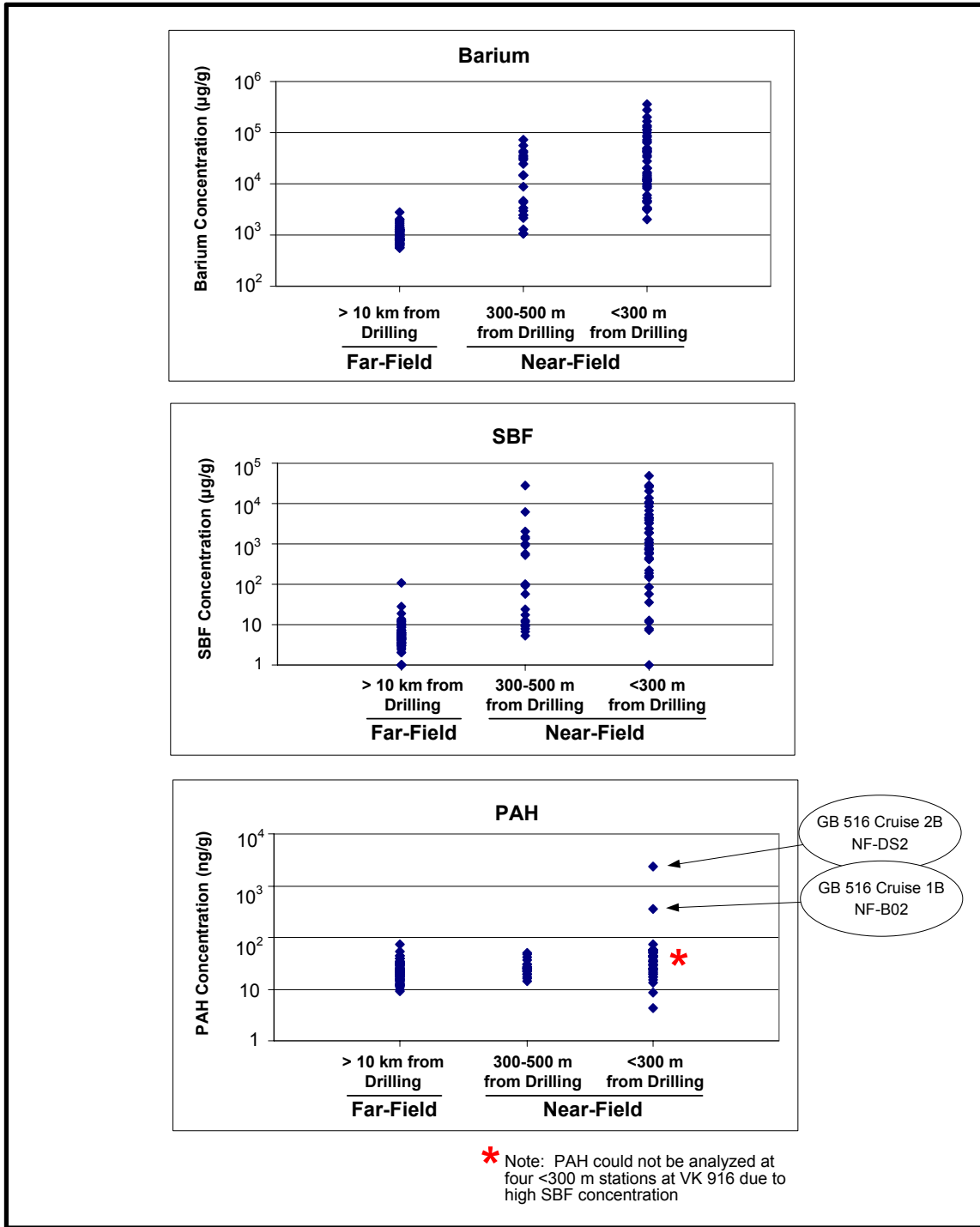


Figure 15.11. Barium and synthetic-based fluid (SBF) concentrations on Cruise 2B at Mississippi Canyon 292 site in relation to geophysically mapped mud and cuttings deposits.



**Figure 15.12.** Sediment concentrations of barium, synthetic-based fluids (SBF), and polycyclic aromatic hydrocarbons (PAH) in relation to proximity to drilling. Points are individual stations, including non-random "discretionary" stations. "Far-field" includes near-field, pre-drilling stations at Viosca Knoll 916.



The near-field data are essentially limited to the 500-m radius. However, one discretionary station at GB 602 on Cruise 2B (Station NF-DS3) was about 1,000 m southwest of the site center and had a barium concentration of 14,800  $\mu\text{g/g}$ ; in comparison, nearly all far-field values were less than 2,000  $\mu\text{g/g}$ . The SBF concentration was 930  $\mu\text{g/g}$ , compared with nearly all of the far-field values being less than 15  $\mu\text{g/g}$ . The geophysical map does not show this station within the cuttings zone, though it does show cuttings (from rig discharges) extending about this distance from the site center.

There are some indications of more distant effects. One far-field site (VK 916 FF2) had slightly elevated barium and SBF concentrations on both cruises. Four wells were drilled between April and July 1997 in VK 914, approximately 3.1 km from the FF2 site center. Subsequently, four wells were drilled in VK 915 within the 3 months preceding Cruise 3B, at a distance of 2.6 km. Drilling plans indicate that SBMs would be used in VK 915 but not in VK 914. On Cruise 3B, barium concentrations at FF2 averaged 1,315  $\mu\text{g/g}$ , compared with a mean of 865  $\mu\text{g/g}$  for the other VK 916 far-field sites. The SBF concentration at one of the VK 916 FF2 stations was 111  $\mu\text{g/g}$ , about 10 times higher than the mean of other VK 916 far-field sites on this cruise.

Based on the extent of detectable barium and SBF increases, it seems possible that prior to the first cruise, the VK 916 near-field site also may have been exposed to small quantities of drilling fluids from the two previous wells in VK 872, approximately 2.3 km to the NNE. Near-field barium concentrations averaged 1,076  $\mu\text{g/g}$ , whereas far-field concentrations (excluding FF2, as noted above) averaged 865  $\mu\text{g/g}$ . However, the barium difference is not statistically significant. There was no indication of elevated SBF concentrations (drilling plans did include SBMs).

The results are similar to those noted in the SBM monitoring program (Continental Shelf Associates, Inc. 2004). Elevated barium and SBF were detected mainly within 250 m of well sites, with small amounts detected at greater distances.

#### 15.2.2.2 Polycyclic Aromatic Hydrocarbons (PAHs)

With two exceptions, sediment PAH concentrations ranged from 43 to 748 ng/g dry wt (*Chapter 9*). Two samples at GB 516 had considerably higher concentrations. On Cruise 1B, Station NF-B02 had 3,470 ng/g, and on Cruise 2B, one of the discretionary stations (NF-DS2) had PAH levels of 23,840 ng/g in the top 2 cm. Both of these stations were within the 300-m radius (**Figure 15.12**).

The source of the PAHs is suggested to be from some other contaminant from the drilling or production activity, as SBMs do not contain PAHs. Although the geohazards report for this lease block notes that shallow gas may be seeping through the seafloor in GB 516 (Fugro-McClelland Marine Geosciences, Inc. 1997), hydrocarbon seepage probably is not the source of the elevated PAH in these two samples, for several reasons. The concentrations are much higher than the highest levels (1,040 ng/g) measured during the Deepwater Gulf of Mexico Benthos (DGoMB) program, which included stations near seep areas (Rowe and Kennicutt 2002). The naphthalenes, biphenyl, and acenaphthene dominated the total PAH in our samples, rather than perylene, which was the major PAH in many DGoMB samples (Rowe and Kennicutt 2002). Also, PAH concentrations in the discretionary core decreased vertically with depth (highest values were at the surface). This issue is discussed further in the Ecological Risk Assessment (*Chapter 16*).

### 15.2.2.3 Sediment Metals Other Than Barium

Near-field concentrations of arsenic, cadmium, chromium, copper, lead, mercury, and zinc were elevated in some near-field sediment samples as compared with far-field samples (*Chapter 8*). Generally, elevated concentrations of these metals were associated with high barium concentrations (i.e., drilling fluid). However, these elevated concentrations are within the expected range of background concentrations for uncontaminated marine sediments (Neff 1987).

Relatively low concentrations of aluminum, iron, nickel, and vanadium were measured in some near-field samples and were attributed to dilution of ambient sediments with barite, which contains no significant amounts of these metals. Also, concentrations of manganese were lower and more variable at near-field sites, a result attributed to reductive dissolution of this metal at stations where the presence of drilling discharges created reducing conditions.

Considerable interest has been generated regarding concentrations of mercury in sediments adjacent to drilling sites because concentrations of total mercury near drilling sites are often 2 to 10 times higher than in nearby background sediments (Neff 2002a). This mercury is known to be a natural impurity in barite (Kramer et al. 1980; Trefry and Smith 2003). Calculations in *Chapter 8* indicate that the mercury concentrations in barite deposited at these sites are in line with USEPA regulations, which allow a maximum level of 1 mg/kg in barite (USEPA 1993).

### 15.2.2.4 Metals and Hydrocarbons in Biota

Concentrations of 11 metals (arsenic, barium, cadmium, chromium, copper, iron, lead, mercury, nickel, vanadium, and zinc) were determined in samples of the giant isopod *Bathynomus giganteus* and the red crab *Chaceon quinque-dens* from near-field and far-field stations at sites GB 602 and MC 292 (*Chapter 8*).

In isopods from GB 602, levels of barium, chromium, and lead were greater at near-field stations, whereas concentrations of cadmium and mercury were greater at far-field stations. No significant differences were detected for isopods at MC 292.

For red crabs from GB 602, barium concentrations were higher in the near-field, whereas concentrations of arsenic, cadmium, copper, mercury, nickel, vanadium, and zinc were higher in the far-field specimens. For MC 292, concentrations of barium, cadmium, chromium, and vanadium were greater at near-field stations.

The most consistent finding in the metals data is elevated barium (in isopods from GB 602 and in crabs from both GB 602 and MC 292). The only other metal with more than one significant result is chromium (elevated in isopods from GB 602 and crabs from MC 292). All other metals either had contradictory findings between sites (cadmium and vanadium in crabs); were significant in only one organism at one site (lead in isopods at GB 602); were higher at far-field sites (arsenic, copper, nickel, and zinc in crabs at GB 602; cadmium and mercury in both isopods and crabs from GB 602); or had no significant differences (iron).

Studies have consistently shown that industrial barite (and its trace components) used in drilling muds has low bioavailability to marine organisms (Neff et al. 1989b,c). The elevated barium concentrations detected in isopods and crabs may reflect small amounts of sediment particles retained in the gut.

Both species also were analyzed for tissue PAH concentrations (*Chapter 9*). PAH body burden concentrations ranged from 38.6 to 416 ng/g dry. No significant difference was found between the total PAH body burden concentrations in the two deepwater organisms. No significant difference also was found between the total PAH body burden concentrations at near-field and far-field stations.

#### 15.2.2.5 Total Organic Carbon

Sediment TOC concentrations at far-field and pre-drilling near-field stations ranged from 0.28% to 1.73%. Near-field concentrations ranged from 0.26% to 7.16%.

Elevated TOC was patchy within near-field sites. Numbers of near-field stations exceeding the 95% confidence interval for far-field sites were as follows:

- VK 916 – 4 of 12 stations;
- GB 516 – 0 of 12 stations (Cruise 1B) and 5 of 12 stations (Cruise 2B);
- GB 602 – 4 of 12 stations; and
- MC 292 – 1 of 12 stations.

**Figure 15.13** shows TOC concentrations with stations grouped into the same three categories noted previously. With one exception, elevated TOC (greater than 2%) was observed only within 300 m of the site center. The exception was one VK 916 discretionary station at a distance of about 315 m with a TOC concentration of 3.07%.

All stations with elevated TOC had high SBF and barium concentrations. The high ratio of SBF to barium suggests that drilling deposits at those stations were primarily SBM cuttings rather than WBM cuttings or muds. TOC was strongly correlated with SBF concentration within near-field sites (**Figure 15.13**), supporting the conclusion that the organic-rich areas were due to deposition of SBM cuttings. Most of the TOC concentrations exceeding 2% occurred at either VK 916 or GB 516 (Cruise 2B). There was little or no elevated TOC at MC 292 or at GB 516 post-exploration (Cruise 1B).

#### 15.2.2.6 Sediment Redox Conditions

*Chapter 8* presents detailed discussions of sediment oxygen levels and redox conditions at each of the four sites. The sediment profile imaging studies (*Chapters 6 and 7*) also provide visual information about redox conditions.

As a useful summary measure, **Figure 15.14** compares integrated oxygen levels in the sediment column at each site. Included in these plots are both near-field and far-field stations, plus discretionary stations placed deliberately in likely cuttings deposits. With a couple of exceptions, oxygen levels were markedly reduced at near-field, post-drilling sites. This effect was most pronounced at GB 602 and at GB 516 on Cruise 2B, where all near-field and discretionary stations had much lower oxygen than the far-field.

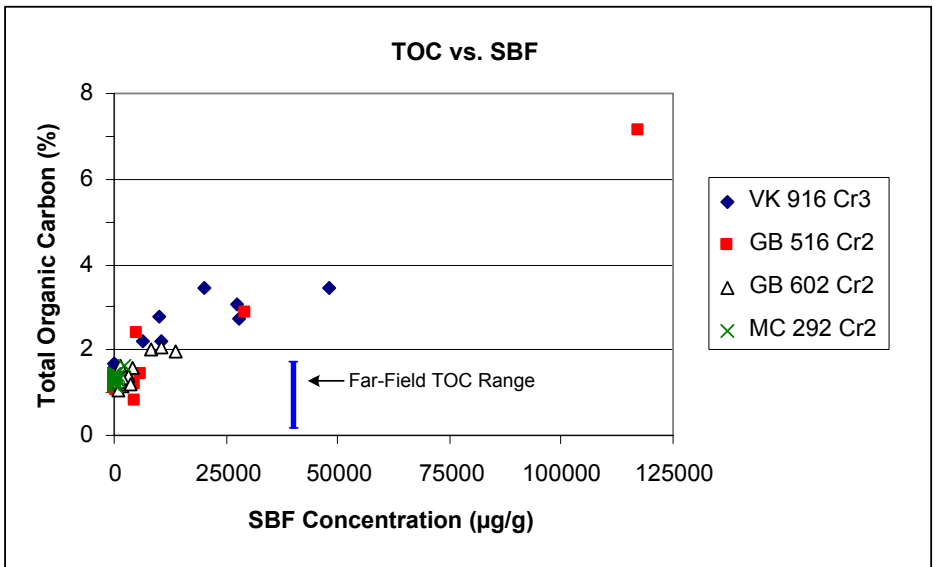
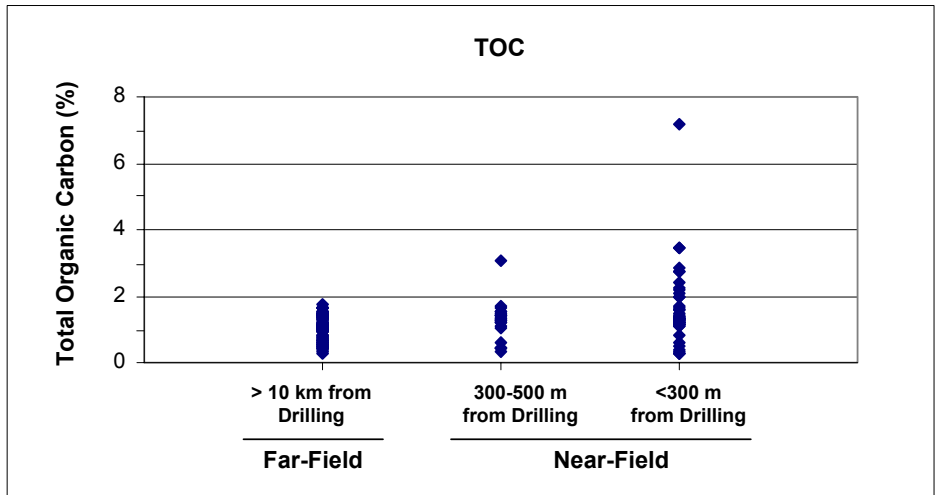
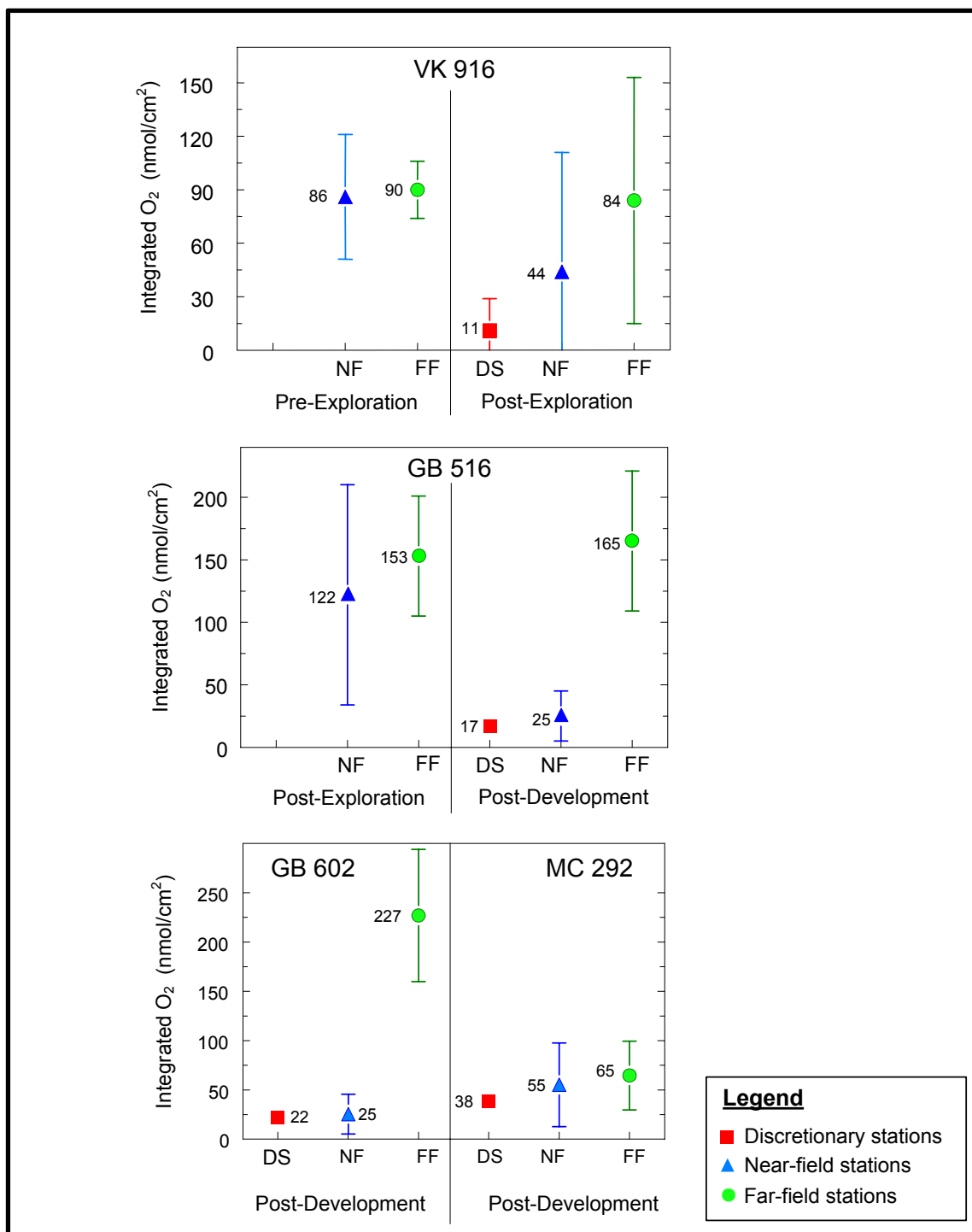


Figure 15.13. Relationship between total organic carbon (TOC) and synthetic-based fluid (SBF) concentrations in near-field sediments at the four sites.



**Figure 15.14.** Integrated amounts of oxygen in the sediment column at near-field (NF), far-field (FF), and discretionary (DS) stations at all four sites. Markers and numbers show means and lines show standard deviations. The standard deviation for some DS samples is smaller than the marker.

On Cruise 1B at VK 916, where there was no previous drilling, most near-field stations had oxygen levels similar to those seen in the far-field. Similarly, at GB 516, although there was previous drilling prior to Cruise 1B (two exploration wells), oxygen levels at many near-field stations initially were similar to those in the far-field. However, after subsequent drilling of five development wells, the near-field oxygen levels were greatly reduced on Cruise 2B (**Figure 15.14**).

At MC 292, differences between near-field and far-field stations were less striking. The degree of similarity is partly due to lower levels of oxygen at the MC 292 far-field site as compared with the other sites. The difference in background conditions may be related to the proximity of MC 292 to the Mississippi River delta and the higher sedimentation rate at this site (~0.14 cm/yr vs. 0.04 to 0.07 cm/yr for the other three sites). MC 292 and VK 916 had lower far-field oxygen levels than the two western sites (GB 516 and GB 602). In addition, MC 292 had the smallest quantities of SBM discharges and the longest time since drilling (see *Section 15.3, Site Comparisons*).

Sediment Eh profiles were obtained at most stations (*Chapter 8*). Eh represents the sum of all oxidation/reduction reactions in the sediment. Here, we use the Eh value near the sediment/water interface (1 to 3 cm depth in the sediment column, depending on the station) as an index of redox conditions. Far-field stations had Eh values ranging from 100 to 692 mV. Many near-field stations also were within this range. However, numerous near-field stations had low or negative Eh, including values as low as -296 mV. GB 602 had the most stations with negative values. **Figures 15.15** and **15.16** show that areas of low Eh were patchy/localized at the post-exploration sites (VK 916 Cruise 3B and GB 516 Cruise 1B) but more extensive at two of the post-development sites (GB 602 and GB 516 Cruise 2B). At the other post-development site (MC 292), only one near-field station had negative Eh; the others were similar to the far-field.

All stations with negative Eh at 1 to 3 cm depth had elevated barium and SBF concentrations, indicating that anoxic and reducing conditions were associated with areas of cuttings deposition.

Sediment profile imaging (*Chapters 6 and 7*) included measurements of apparent RPD depth (i.e., the depth of the oxidized layer) in each photograph. The most important findings were as follows:

- RPD depths were shallower at near-field sites on post-drilling surveys; that is, anoxic conditions were closer to the sediment surface.
- Instances of zero RPD depth were noted only on near-field, post-drilling transects.
- Among the four sites, near-field vs. far-field differences were smallest at MC 292.

In *Chapter 7*, some sediment profile images were interpreted as indicating hypoxic or anoxic conditions in near-bottom waters. However, direct measurements in *Chapter 8* show that near-bottom waters were not anoxic and oxygen levels rarely approached zero at the sediment/water interface. While the two sets of observations are not directly comparable because the SPI transects did not sample the same locations as the box cores, the difference highlights the difficulty of inferring the oxidation state from sediment color.

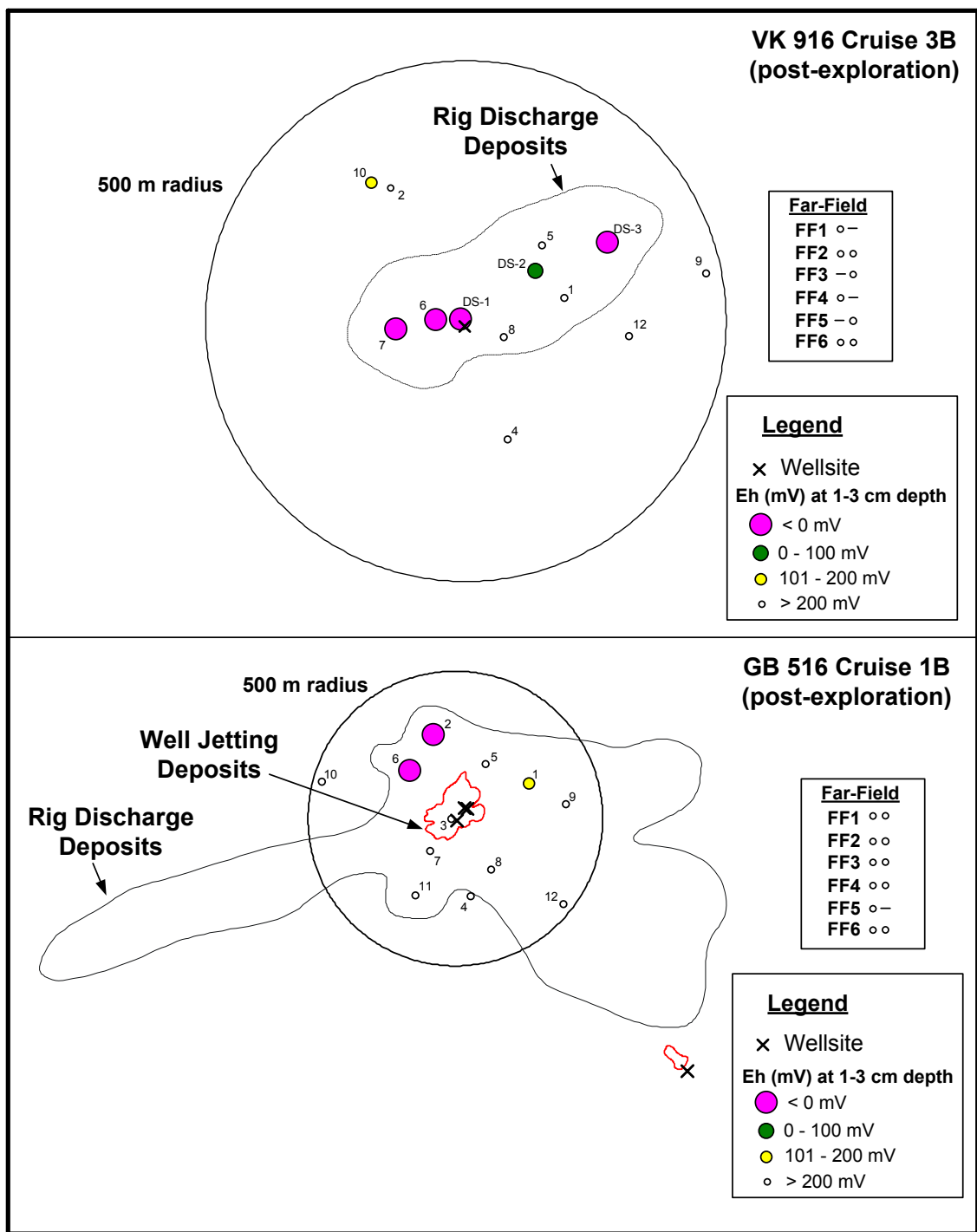


**Figure 15.15.** Redox potential (Eh) values at 1 to 3 cm depth in the sediment column at Viosca Knoll 916 and Garden Banks 516 on post-exploration cruises in relation to geophysically mapped mud and cuttings deposits.

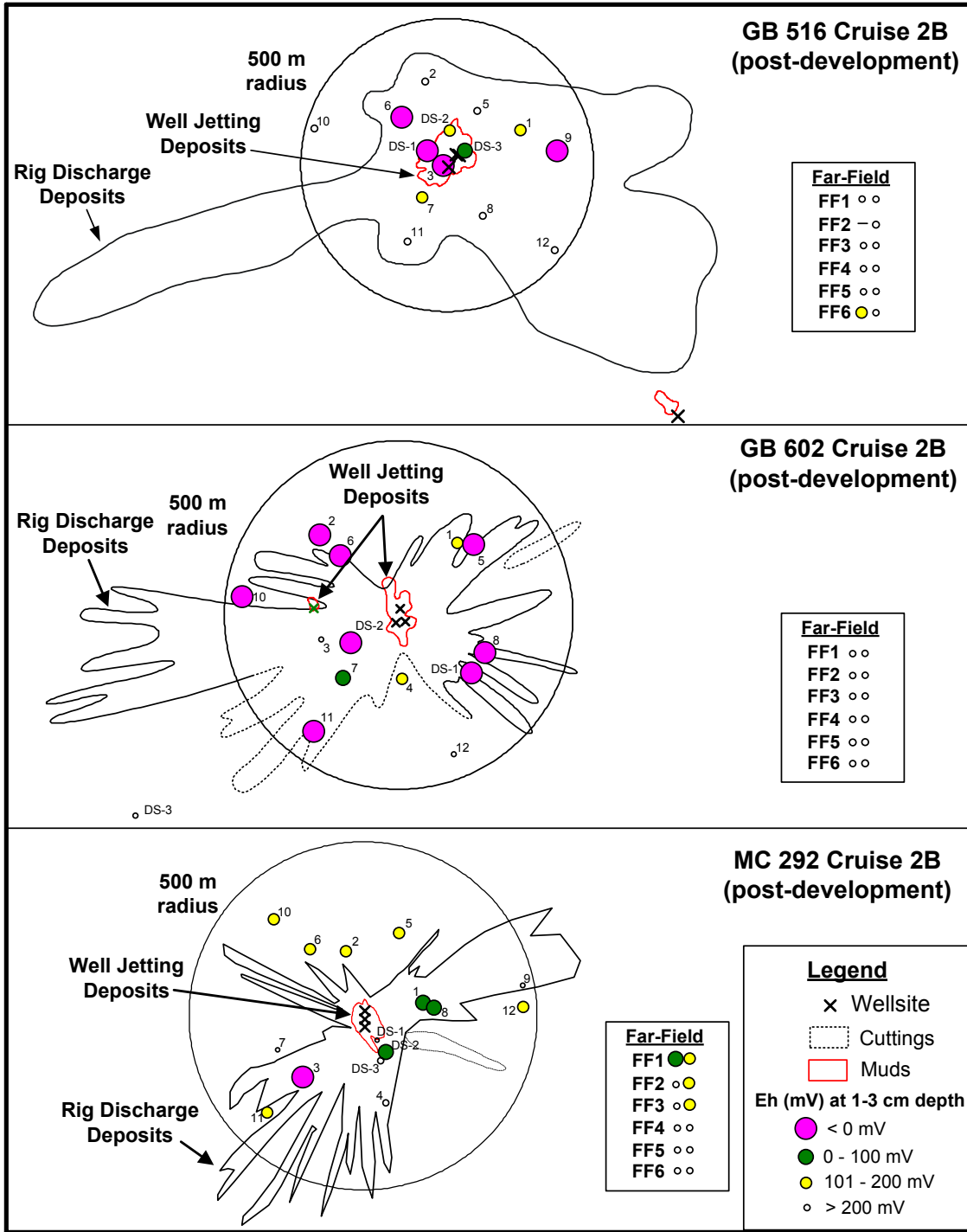


Figure 15.16. Redox potential (Eh) values at 1 to 3 cm depth in the sediment column at Garden Banks 516, Garden Banks 602, and Mississippi Canyon 292 on post-development cruises in relation to geophysically mapped mud and cuttings deposits.



### 15.2.3 Biological

This study included several biological components. Sediment profile imaging (*Chapters 6 and 7*) provides an overview of benthic community health and successional status. Box core samples were analyzed for microbial ATP (*Chapter 10*), and meiofauna and macroinfauna (*Chapter 11*). Additional studies of harpacticoid copepod genetics were conducted at GB 602 and MC 292 (*Chapter 13*). Photographs taken with the camera sled were examined for the presence of megafauna (*Chapter 12*).

#### 15.2.3.1 Benthic Community Status

Sediment profile imaging was used to characterize benthic communities at each site (*Chapters 6 and 7*). Images were analyzed to determine successional stage using a paradigm based on recolonization of disturbed shallow-water habitats (Rhoads and Germano 1982). Application of this method to our study sites is an extrapolation, as detailed knowledge about infaunal successional stages is not available for these sites. Stage I organisms live very close to the sediment-water interface, and are pioneers as they require little oxidized sediment. By their feeding and burrowing activities, these Stage I animals, often small annelids, deepen the RPD, preparing the sediment for colonization by somewhat larger animals such as amphipods (Stage II). (No Stage II assemblages were identified here because detailed knowledge of successional dynamics is not available for the study sites.) Stage III organisms are large, deep-burrowing, head-down deposit feeders, usually polychaetes and echinoderms, which aerate the sediment to several centimeters in depth. Their presence indicates an equilibrium community and a healthy environment.

In addition, an overall organism-sediment index (OSI) was calculated for each image in *Chapter 6*. The index takes into account the depth of the apparent RPD, successional stage, presence or absence of sediment methane bubbles, and presence or absence of reduced sediment near the sediment-water interface. The value of the index can range from +11 (best habitat value) to -10 (worst habitat value). Values of the OSI below +6 tend to be associated with disturbed benthic habitats. Negative OSI values reflect a highly disturbed benthos.

Post-drilling surveys indicated that the near-field zone at three of the four sites (VK 916, GB 516, and GB 602) consisted of a mosaic of poor benthic conditions (patchy areas of low or negative OSI and azoic or retrograde benthic communities) alternating with areas of moderately high benthic habitat quality. The degraded near-field habitats stand in marked contrast to those seen at far-field sites that exhibit aerobic boundary layer conditions with well-developed Stage I and I-III communities.

**Table 15.6** summarizes OSI data and successional status for VK 916 and GB 516 as an example. Negative OSI values indicative of highly disturbed benthic habitats were observed only in the near-field, post-drilling images.

**Table 15.6.** Organism-sediment index (OSI) and successional stage for Viosca Knoll 916 (VK 916) and Garden Banks 516 (GB 516).

Site and Cruise	Stage	Stations with Negative OSI (%)		Successional Stage	
		FF	NF	FF	NF
VK 916 Cruise 1B	Pre-drilling	0	0	Stage I-III (mostly)	Stage I-III (mostly)
VK 916 Cruise 3B	Post-exploration	0	25	Stage I-III (mostly)	Stage III dominates; Stage I rare
GB 516 Cruise 1B	Post-exploration	0	36	Stage I-III (mostly)	About 80% of stations are azoic or Stage I
GB 516 Cruise 2B	Post-development	0	18	Stage I-III (mostly)	About 50% of stations are azoic or Stage I

FF = far-field; NF = near-field.

Post-drilling communities at GB 516 were dominated by pioneering infauna (Stage I), which are quick to colonize disturbed habitats. Microbial mats were observed at some stations on Cruise 1B. There was some indication of slight improvement in benthic habitat conditions between Cruises 1B and 2B. This is puzzling because box core data show that redox conditions deteriorated between cruises; however, the sediment profile transects may simply have crossed less severely affected areas than those sampled by box cores on Cruise 2B.

At VK 916, the successional picture was different in that Stage I seres were rarely encountered. This observation suggests that recent surface disturbance (deposition, resuspension, and/or erosion) may have selectively compromised near surface-dwelling species relative to deeper-living infauna. A similar phenomenon has been noted in studies of the ecological effects of bottom trawling (Rosenberg et al. 2003). These observations are based on near-field sampling only; no far-field data were available for the post-drilling survey at this site.

Results for the GB 602 post-development site appear qualitatively similar to those for GB 516. However, at the other development site (MC 292), only a small number of stations appeared to have been visibly affected by drilling muds and cuttings. Only a few stations along one transect had signs of depleted oxygen conditions. There was evidence of infaunal activity at most stations, and no microbial mats were observed at this site. The relative lack of impacts is consistent with box core redox measurements and may be related to the low volume of SBM cuttings discharged at this site, as discussed further in *Section 15.3*.

#### 15.2.3.2 Microbiota

In *Chapter 10*, LaRock concluded that microbial biomass was reduced at *both* near-field and far-field sites due to drilling discharges. However, alternative explanations can be offered that are more consistent with both the microbial data and findings in other chapters. The results suggest that microbial biomass was higher, not lower, in some areas where drilling discharges were present.

**Figure 15.17** shows the microbial ATP data for the four study sites. A temporal difference in microbial biomass is evident at VK 916 and GB 516. Specifically, ATP concentrations measured on Cruise 1B were about an order of magnitude higher than those measured on Cruises 2B or 3B. The difference is statistically significant for both VK 916 and GB 516, as noted by LaRock. In *Chapter 10*, this difference is attributed to drilling discharges affecting both near-field and far-field sites. However, this interpretation has several problems:

- The decrease occurred regardless of the degree of exposure to drilling discharges. Between cruises, the near-field sites received large accumulations of drilling deposits as indicated by orders of magnitude increases in barium and SBF concentrations, whereas most far-field sites were exposed to undetectable amounts of drilling fluids, if any.
- The high ATP concentrations seen at GB 516 on Cruise 1B are not consistent with inhibition of microbial populations by drilling discharges. If drilling discharges reduce microbe populations, then this site should already have been inhibited on Cruise 1B because two wells were drilled there 14 months earlier. (The presence of drilling discharges is evidenced by barium concentrations as high as 135,000  $\mu\text{g/g}$  and SBF concentrations as high as 25,131  $\mu\text{g/g}$ .) Instead, both near-field and far-field ATP concentrations were in the same range as those at VK 916, where there was no previous drilling.
- No plausible mechanism is offered that could cause microbial inhibition at a distance of more than 10 km away. Moreover, if drilling discharges reduce microbial biomass at stations more than 10 km away, then nearly all of the Cruise 1B far-field stations, as well as the VK 916 near-field site, could already have been affected. All of the VK 916 and GB 516 far-field sites, as well as the VK 916 near-field site, had previous wells within 10 km (see *Chapter 3*).

The cause of the decrease between cruises is unknown, but we do not believe it to be attributable to drilling discharges. Temporal differences apparently unrelated to drilling are evident in some other data sets, including meiofauna and macroinfauna and megafauna. For example, meiofaunal densities declined by about an order of magnitude between Cruise 1B and the subsequent surveys at both near-field and far-field sites (*Chapter 11*). Macroinfaunal densities decreased between surveys at VK 916 (both near- and far-field) but increased at GB 516 (both near- and far-field) (*Chapter 11*).

There is ample evidence that microbial biomass, though patchy, was higher in areas where drilling discharges accumulated. For example, sediment profile camera images commonly showed microbial mats at near-field sites but not far-field sites (**Plate 15.1**; **Table 15.7**; *Chapters 6 and 7*).

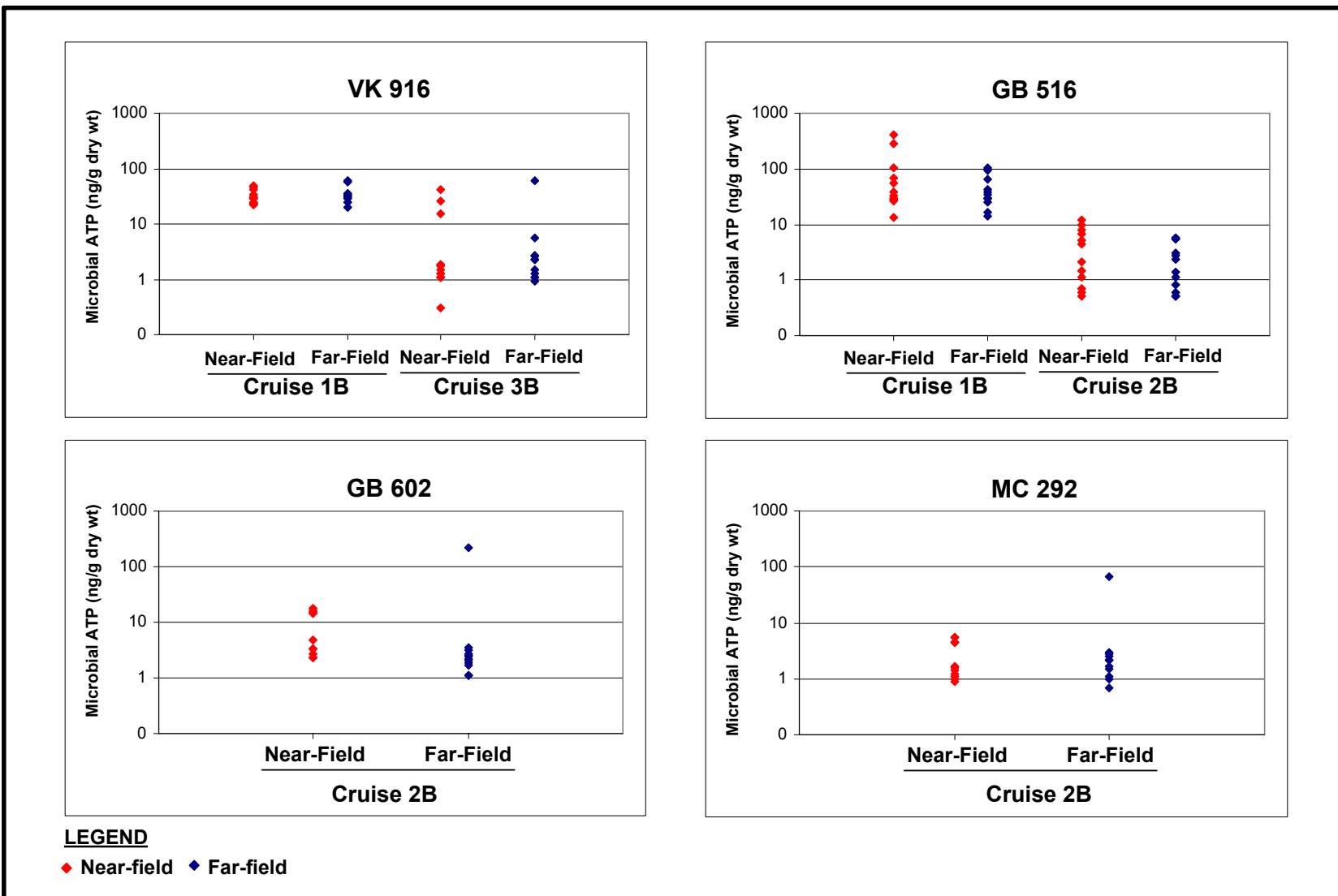
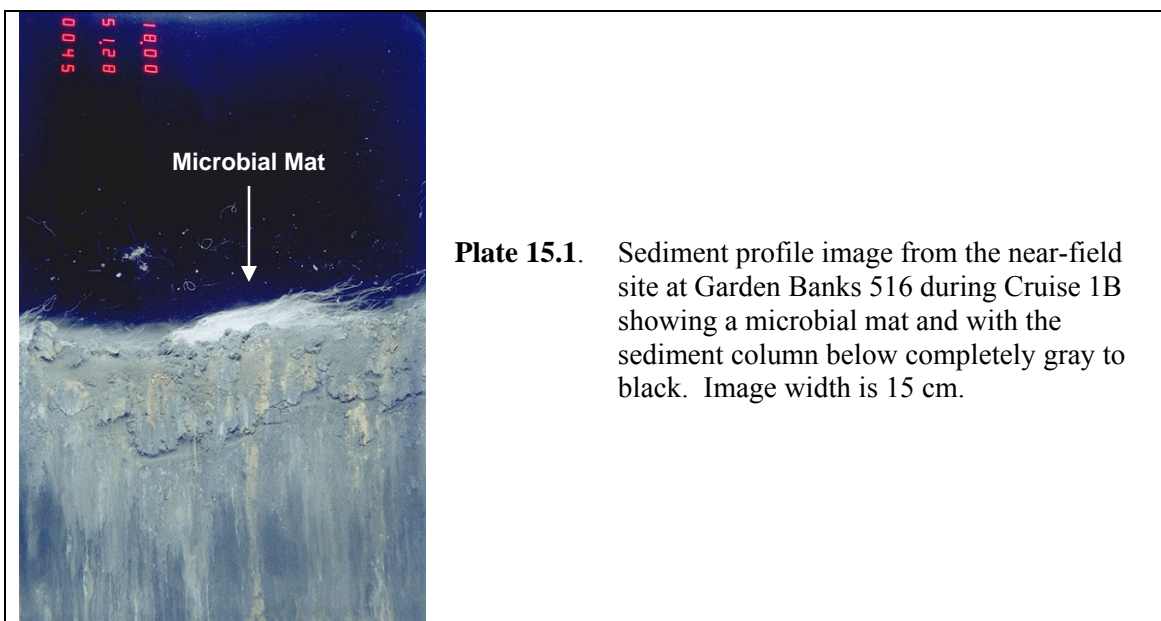


Figure 15.17. Microbial adenosine triphosphate (ATP) concentrations at the four study sites. Points are individual stations.



**Plate 15.1.** Sediment profile image from the near-field site at Garden Banks 516 during Cruise 1B showing a microbial mat and with the sediment column below completely gray to black. Image width is 15 cm.

**Table 15.7.** Presence of microbial mats as recorded in sediment profile images.

Site	Cruise	Stage	Presence of Microbial Mats	
			FF	NF
VK 916	1B	Pre-drilling	--	--
	3B	Post-exploration	--	Present at several stations
GB 516	1B	Post-exploration	--	Present at several stations (29%)
	2B	Post-development	--	--
GB 602	2B	Post-development	--	Present at several stations
MC 292	2B	Post-development	--	--

GB = Garden Banks; MC = Mississippi Canyon; VK = Viosca Knoll; FF = far-field; NF = near-field.

Within the VK 916 and GB 516 sites, the stations with the highest microbial biomass corresponded to those with the highest SBF concentrations (**Figure 15.18**). This effect was evident at SBF concentrations greater than 1,000  $\mu\text{g/g}$ . A similar effect was not evident at GB 602 or MC 292 (**Figure 15.19**); both of these sites, as well as VK 916, had one apparent “outlier” value among the far-field stations, which complicates interpretation. For example, at GB 602, Station FF5-B02 had an ATP concentration of 216.3 ng/g (compared with 1.1 to 3.6 ng/g for other GB 602 far-field samples). If this value is included, the near-field and far-field means are not significantly different ( $p=0.52$ ), but if it is omitted, the near-field mean is significantly higher ( $p=0.02$ ).

The increased microbial abundance at some near-field stations is consistent with an organic enrichment effect due to the addition of SBM cuttings. The possibility that some inhibition of microbial activity also occurs where SBM cuttings accumulate, as hypothesized in *Chapter 10* cannot be ruled out. However, if it exists, this inhibition seems to be overwhelmed by the organic enrichment effect.

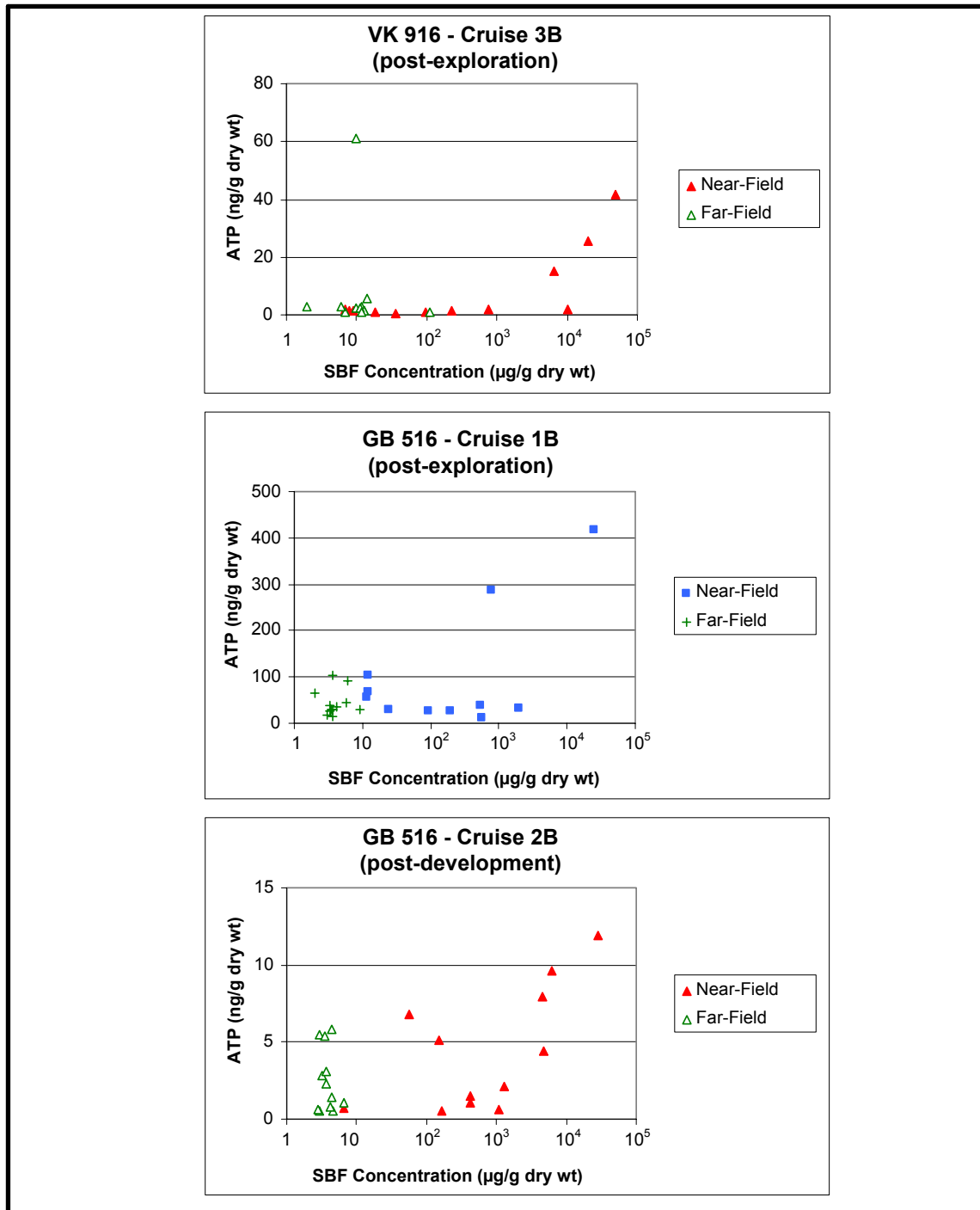


**Figure 15.18.** Microbial adenosine triphosphate (ATP) concentrations at Viosca Knoll 916 and Garden Banks 516 on post-drilling cruises in relation to sediment synthetic-based fluid (SBF) concentrations. Points are individual stations. Note the different ATP scales on each graph.

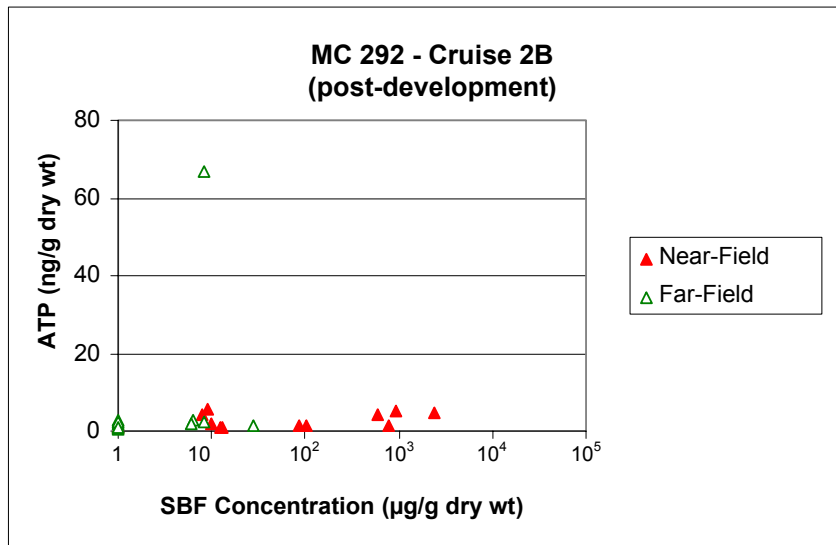
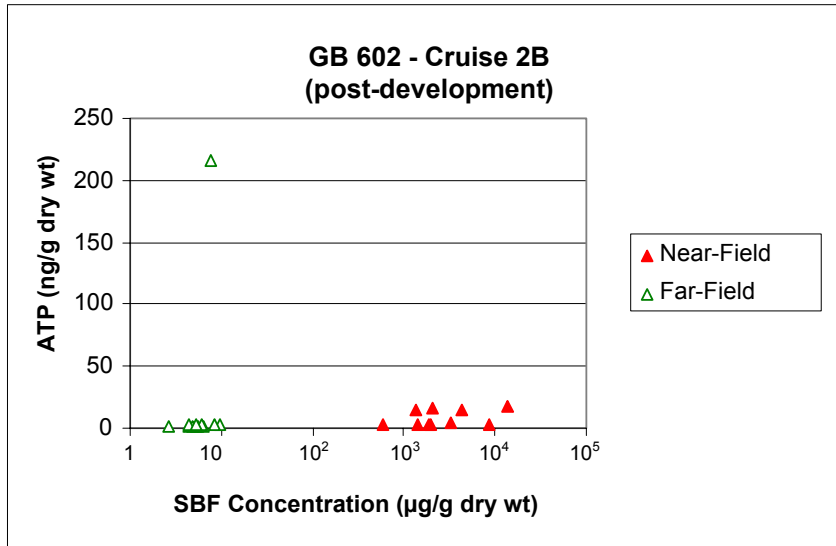


**Figure 15.19.** Microbial adenosine triphosphate (ATP) concentrations at Garden Banks 602 and Mississippi Canyon 292 on Cruise 2B (post-drilling) in relation to sediment synthetic-based fluid (SBF) concentrations. Points are individual stations. Note the different ATP scales on each graph.

### 15.2.3.3 Meiofauna

Meiofaunal densities declined by about an order of magnitude between October-November 2000 (Cruise 1B) and the subsequent surveys (Cruise 2B, July 2001 and Cruise 3B, August 2002) at both near-field and far-field sites (*Chapter 11*). The decrease is not attributable to drilling activities, for the same reasons discussed under Microbiota. However, because of the magnitude of change, impacts must be inferred from near-field vs. far-field comparisons within cruises.

Meiofaunal densities tended to be higher near drilling. Although there was considerable overlap in near-field vs. far-field densities, the highest densities of nematodes, harpacticoid copepods, and especially annelids occurred in the near-field. As shown in **Figure 15.20**, this effect was seen mainly within 300 m of the wellsite(s), although a few stations in the 300- to 500-m range also had elevated numbers. The elevated meiofaunal densities are similar to the nematode enrichment effect previously reported in the GOOMEX study by Montagna and Harper (1996) for platforms in shallower Gulf waters. In addition, unlike GOOMEX, *higher* (not lower) harpacticoid densities were found near drilling.

Meiofaunal densities in the near-field were not consistently correlated with drilling indicators (barium, SBF) or other sediment variables (TOC, grain size fractions).

A study of harpacticoid genetic diversity was conducted at GB 602 and MC 292 (*Chapter 13*). The study focused on *Bathyletopsyllus* sp., which was absent from far-field sites but abundant at near-field sites. Results showed low genetic diversity in near-field populations of *Bathyletopsyllus* sp., which is consistent with expansion from a small, pre-drilling population.

### 15.2.3.4 Macroinfauna

Macroinfaunal densities tended to be higher near drilling (*Chapter 11*). Although there was considerable overlap in near-field vs. far-field densities, the highest densities occurred in the near-field. As shown in **Figure 15.20**, this effect was seen almost entirely within 300 m of the wellsite(s).

For annelids (predominantly polychaetes), gastropods, and bivalves, there was a strong, consistent tendency for the highest densities to occur in the near-field. Aplacophorans showed a similar trend at GB 516 and GB 602, though not at VK 916. The opposite was true for amphipods and ostracods, with the highest densities generally occurring at one or more far-field stations.

Annelid (predominantly polychaete) densities in the near-field were positively correlated with drilling indicators (barium, SBF). Some near-field stations with barium concentrations higher than about 10,000  $\mu\text{g/g}$  and/or SBF concentrations greater than about 1,000  $\mu\text{g/g}$  had elevated polychaete densities (**Figure 15.21**).

Gastropod densities in the near-field were positively correlated with drilling indicators (barium, SBF). A few near-field stations at GB 516 and GB 602 had very high gastropod densities, which were associated with barium concentrations of 55,000  $\mu\text{g/g}$  or higher and SBF concentrations of 4,500  $\mu\text{g/g}$  or higher (**Figure 15.22**). Much weaker relationships were observed at VK 916 and MC 292.



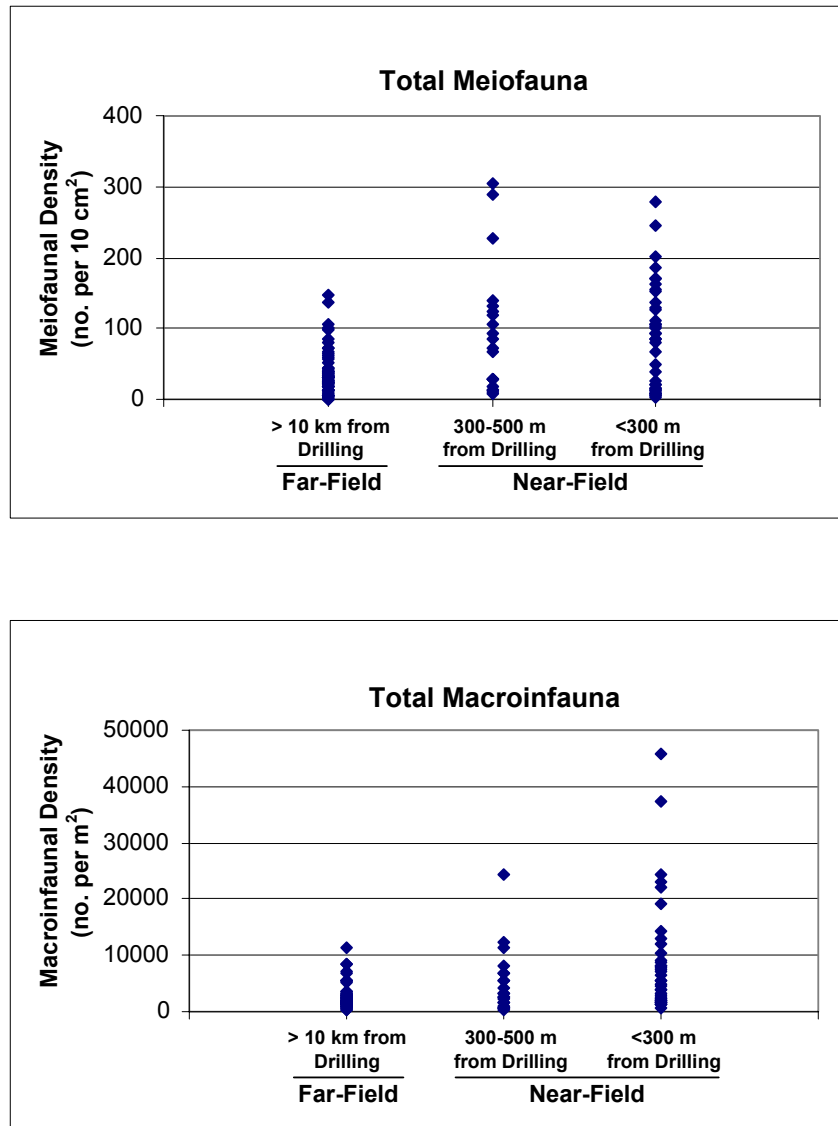


**Figure 15.20.** Meiofaunal and macroinfaunal densities in relation to proximity to drilling. Points are individual stations including non-random "discretionary" stations. The pre-drilling survey at Viosca Knoll 916 has been excluded from these plots (higher densities both near- and far-field would obscure other patterns).

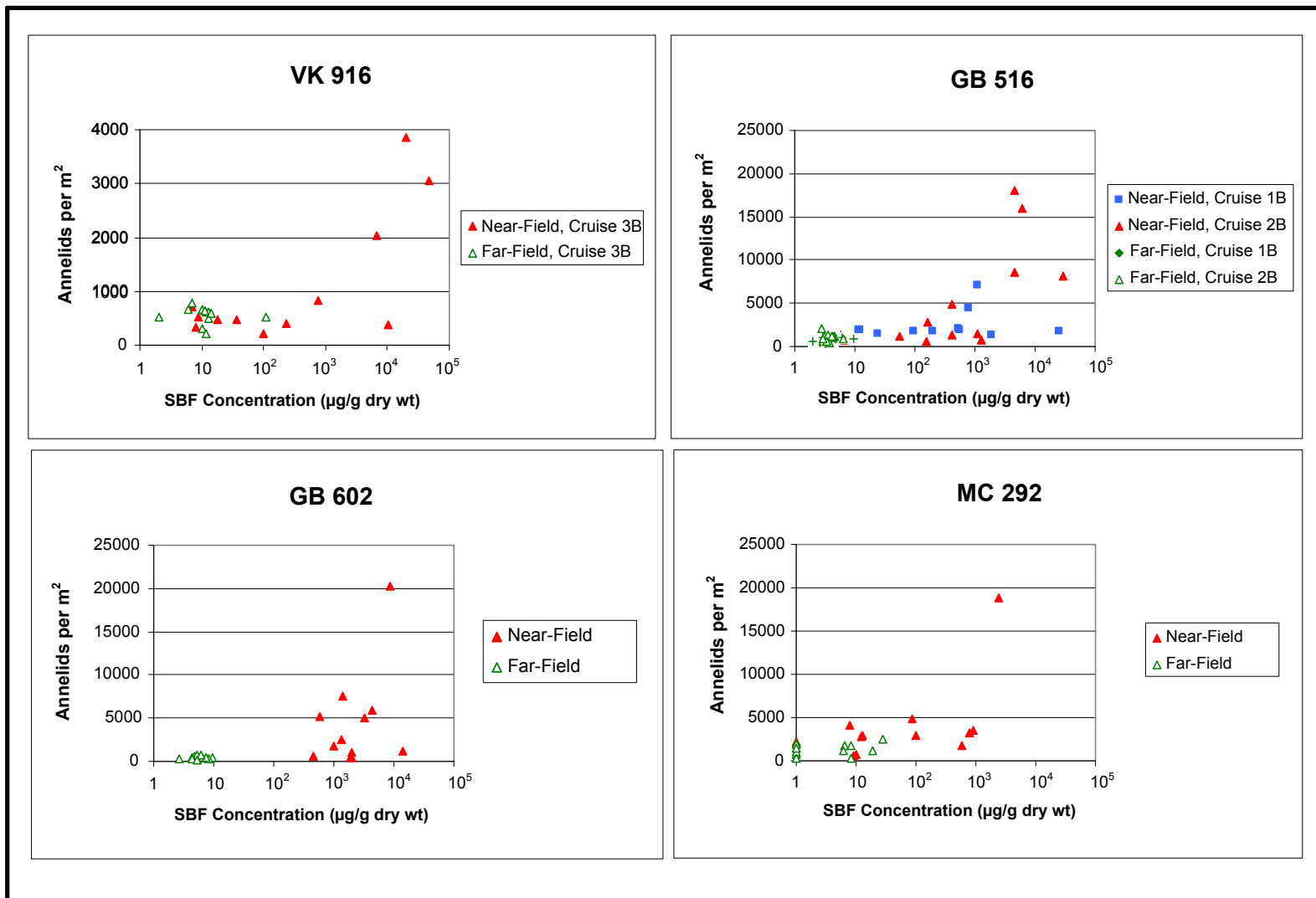


**Figure 15.21.** Annelid (predominantly polychaete) densities vs. synthetic-based fluid (SBF) concentrations on post-drilling cruises. Note the log scale for SBF concentrations and the different density scale for Viosca Knoll 916.

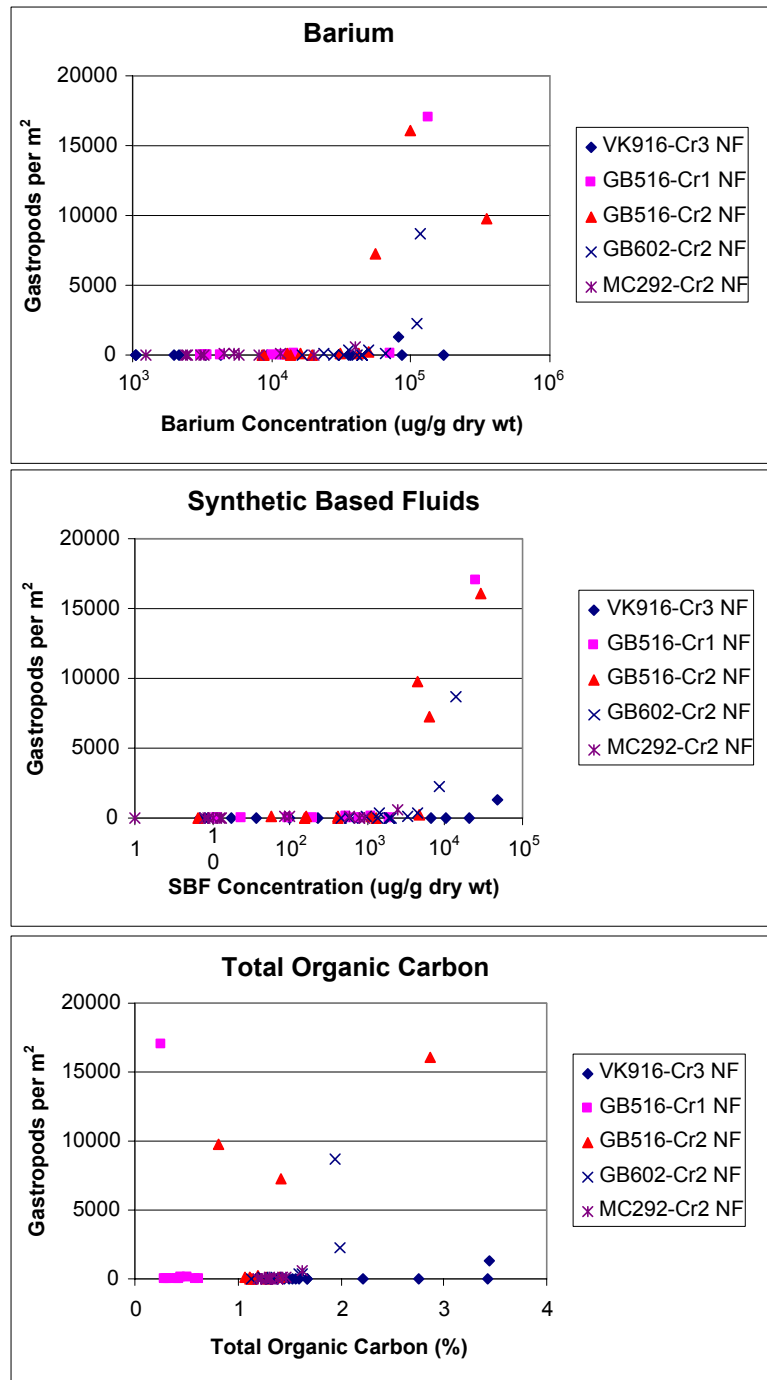


**Figure 15.22.** Gastropod densities vs. sediment barium, synthetic-based fluid (SBF), and total organic carbon concentrations at near-field (NF), post-drilling stations. Note the log scale for barium and SBF concentrations.

Amphipod densities in the near-field were negatively correlated with drilling indicators (barium, SBF). Generally, near-field stations with barium concentrations higher than about 10,000  $\mu\text{g/g}$  and/or SBF concentrations greater than about 1,000  $\mu\text{g/g}$  had low amphipod densities (**Figure 15.23**).

A detailed taxonomic analysis of 24 stations showed that species composition reflects both geographic location and drilling impacts. In terms of community statistics, some stations “near drilling” had lower diversity, lower evenness, and lower richness indices compared with stations “away from drilling” (**Figure 15.24**). Station/cruise groups most likely affected by drilling (as indicated by high barium and SBF concentrations) were dominated by high abundances of one or a few deposit-feeding species. For example, at VK 916, Station NF-B07 was numerically dominated by the polychaete *Capitella capitata*, a classic indicator of organic enrichment, and at GB 516, Station NF-B02 was numerically dominated by the gastropod *Solariella* sp. A.

#### 15.2.3.5 Megafauna

Overall, small megafauna identified in photographs showed little impact; there was no gross reduction or increase in imaged fauna (*Chapter 12*). However, localized significant shifts were found for two component groups. Fish were more abundant in the near-field, consistent with attraction to disturbance and structure (and possibly, increased food supplies in the form of elevated macroinfaunal densities). Ophiuroids were less abundant in the near-field, perhaps because these flat organisms were buried by cuttings, or perhaps there was a behavior shift, which resulted in fewer animals being seen in the near-field. **Figures 15.25** and **15.26** show that the near-field vs. far-field differences for fish and ophiuroids were seen mainly at VK 916 and GB 516. There was little or no difference between near- and far-field at GB 602 or MC 292.

#### 15.2.3.6 Discussion

The geophysical and chemical data reviewed previously indicate that a layer of cuttings and muds up to 45 cm thick was deposited within the near-field sites. Based on previous studies, one would expect impacts to include burial and smothering and changes in benthic assemblages due to altered sediment grain size and mineralogy (National Research Council 1983; Neff 1987; Continental Shelf Associates, Inc. 1989; Hinwood et al. 1994). Because SBM cuttings were discharged, toxicity, organic enrichment, and anoxia (including potentially toxic concentrations of sulfide and ammonia) are additional factors (Neff et al. 2000).

Observations consistent with burial and/or stressed conditions include

- Azoic areas observed in near-field sediment profile images from VK 916, GB 516, and GB 602;
- Absence or rarity of surface-dwelling macroinfauna in near-field sediment profile images from VK 916;
- Reduced densities of macroinfaunal amphipods and ostracods in the near-field box cores; and
- Reduced densities of ophiuroids in near-field photographs.

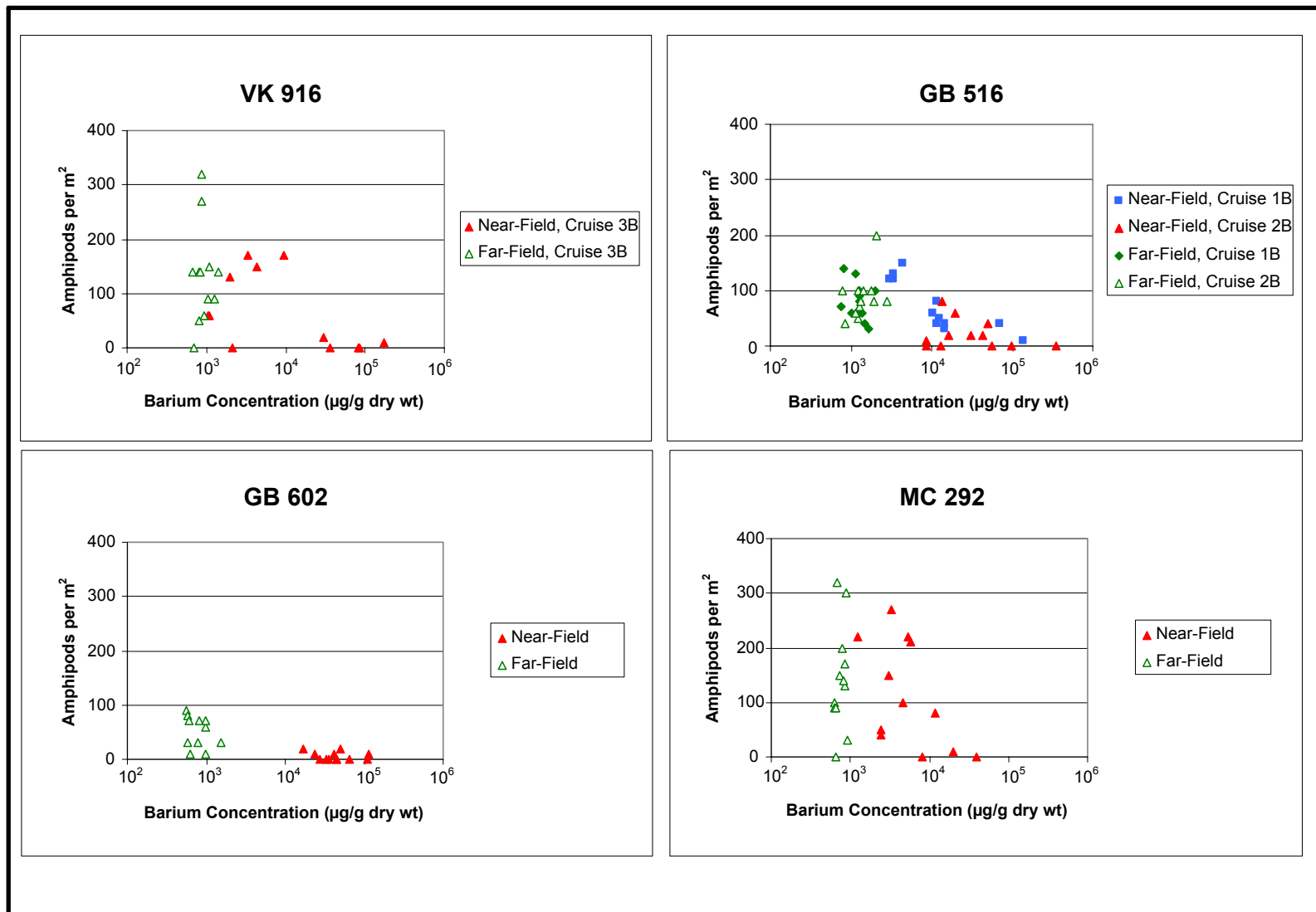


**Figure 15.23.** Amphipod densities vs. sediment barium concentrations on post-drilling cruises. Note the log scale for barium concentrations.

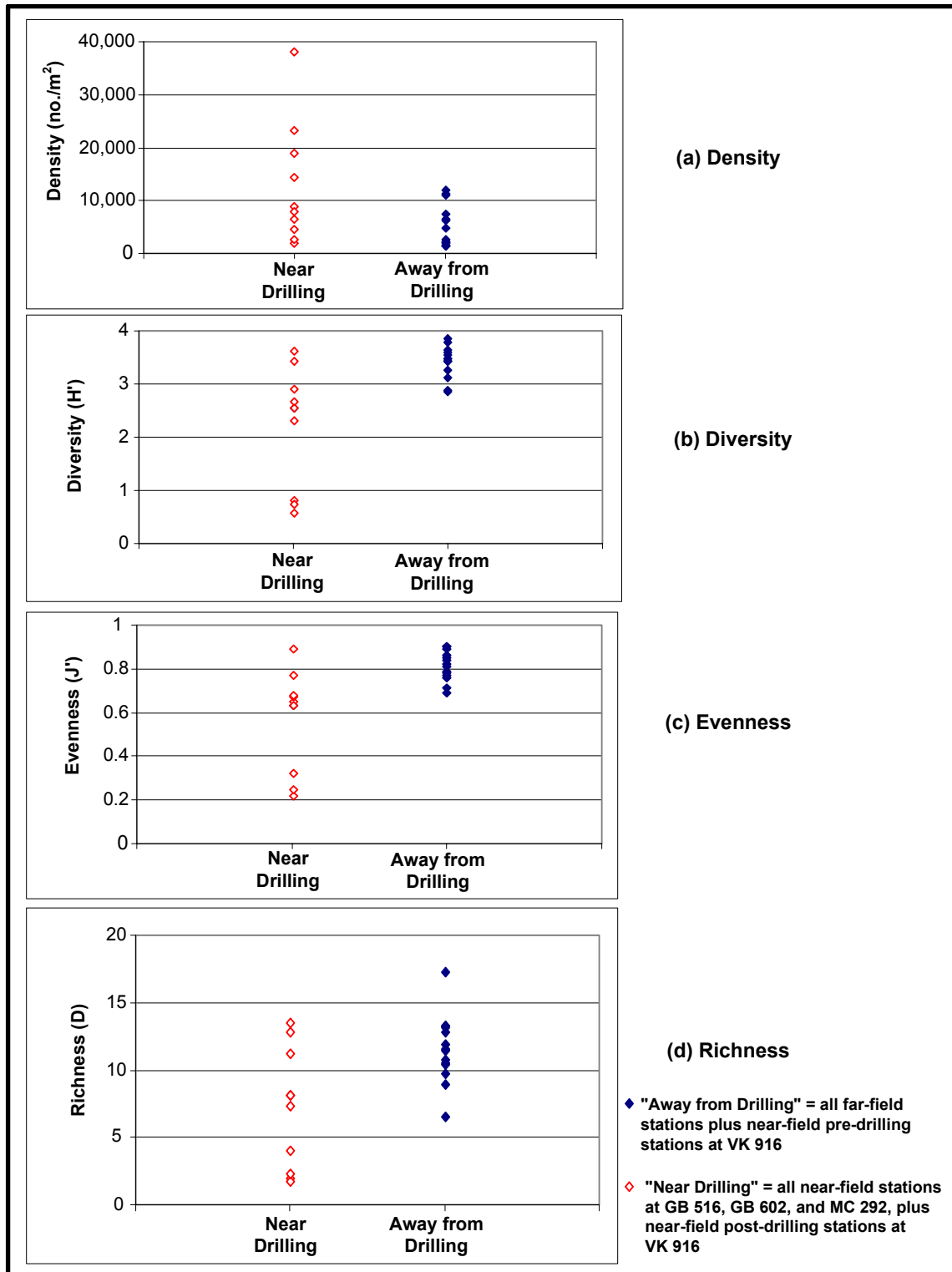


Figure 15.24. Macroinfaunal community characteristics for the detailed, 24-station analysis.

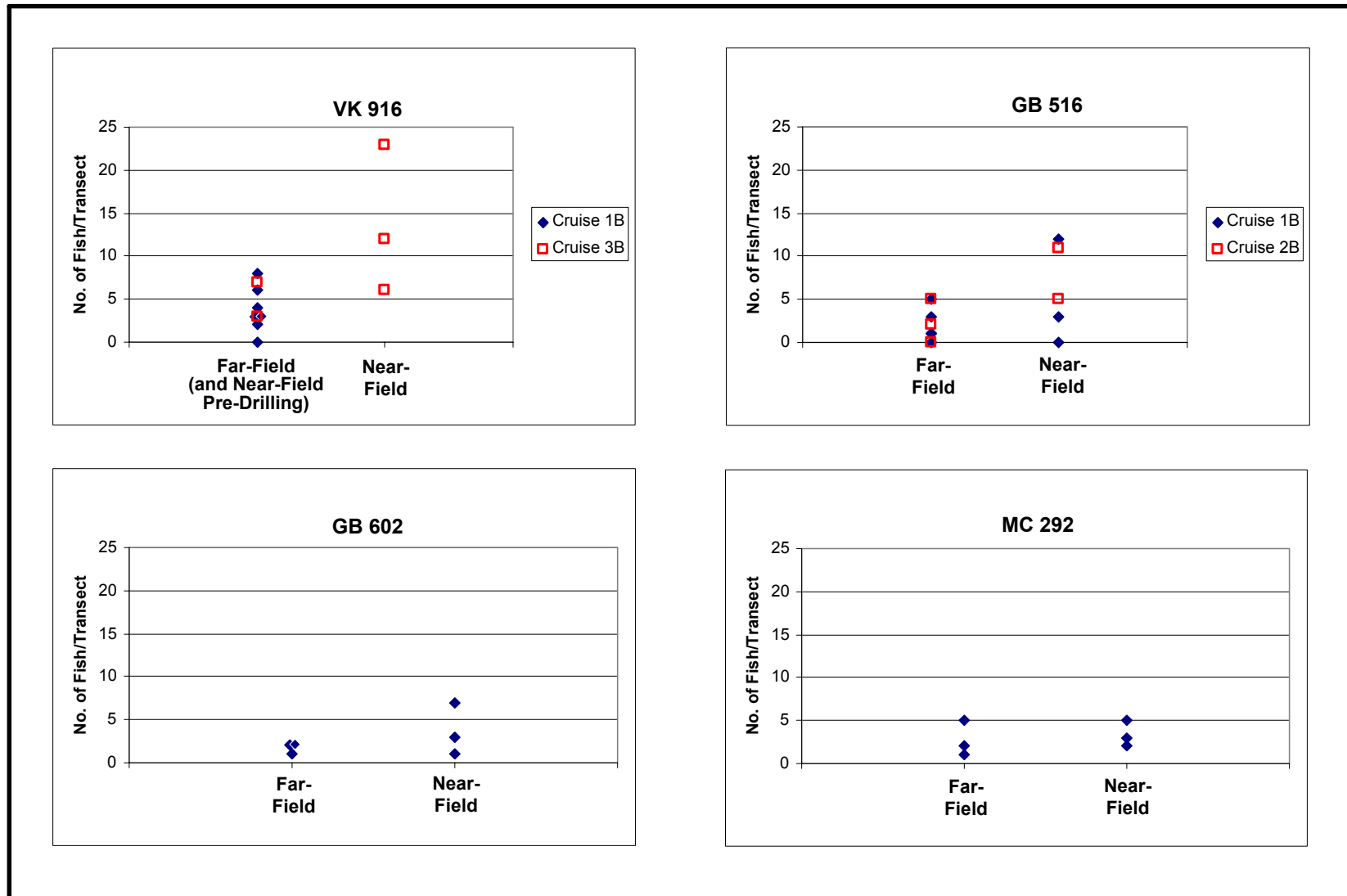


Figure 15.25. Fish abundance along camera sled transects at each site. Points are individual transects.

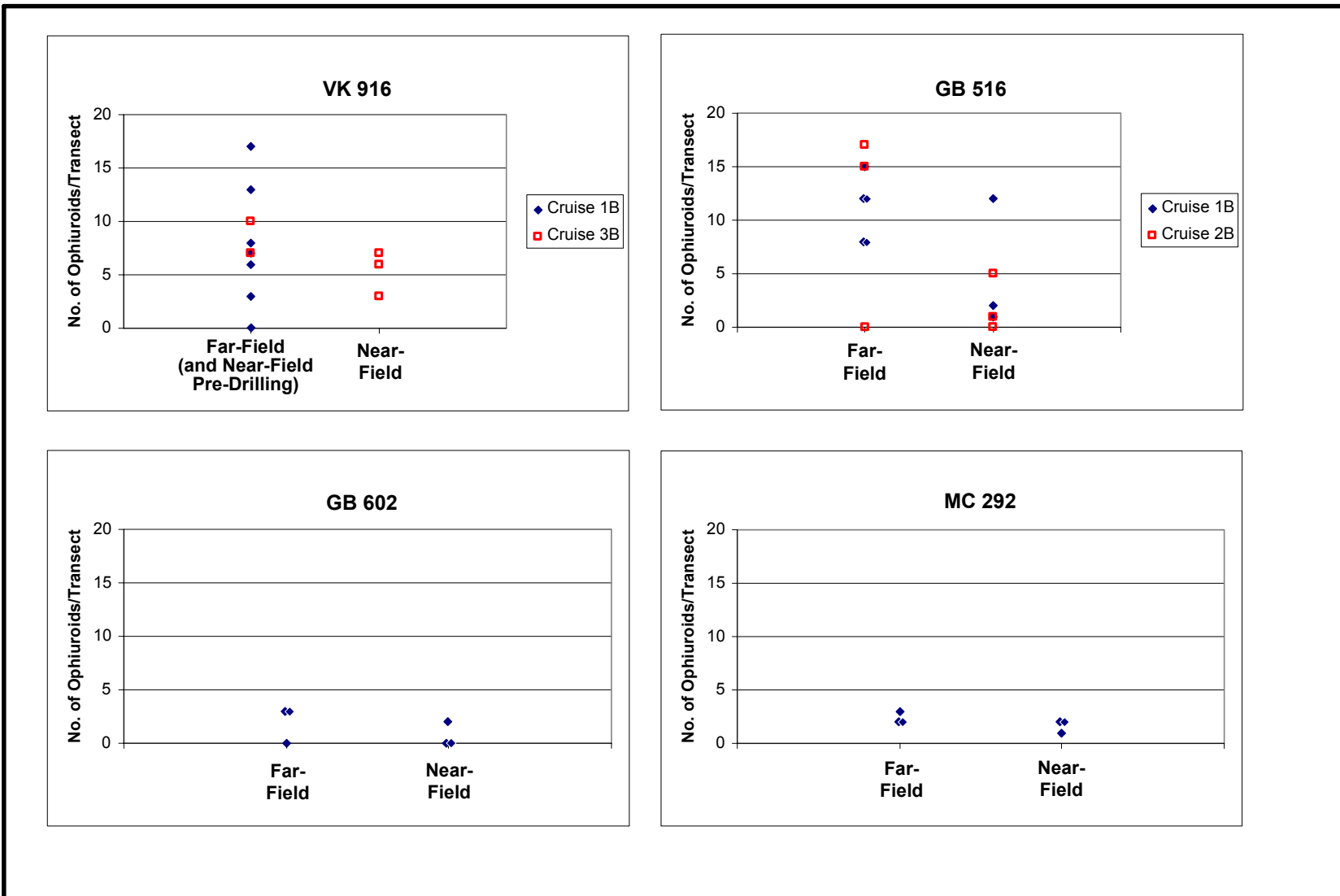


Figure 15.26. Ophiuroid abundance along camera sled transects at each site. Points are individual transects.



Sediment toxicity may be a contributing factor in the observed negative effects. Acute toxicity tests with near-field and far-field sediments from MC 292 and GB 602 showed that mean amphipod survival was significantly lower in sediments from near-field stations than in sediments from far-field stations (*Chapter 14*). Amphipod survival was negatively correlated with drilling mud and cuttings indicators (barium and SBF) for both sites. However, the bioassays were conducted with estuarine amphipods (rather than indigenous deep-sea fauna) and do not simulate actual field conditions. The potential for toxicity is addressed further in the Ecological Risk Assessment (*Chapter 16*).

On the other hand, there is evidence of elevated biological activity associated with a disturbed, organically enriched habitat. This includes

- Microbial mats observed in sediment profile images;
- Elevated microbial biomass (ATP) associated with high SBF concentrations;
- Elevated near-field densities of meiofauna, including annelids, harpacticoid copepods, and nematodes;
- Elevated near-field densities of macroinfauna, including annelids, bivalves, and gastropods;
- Predominance of pioneering stage macroinfaunal assemblages at some near-field stations; and
- Elevated near-field densities of fishes at VK 916 and GB 516.

Similar benthic impacts of SBM cuttings on the Gulf of Mexico continental slope were noted during an opportunistic survey after development drilling at the Pompano development site in MC 28 (water depth 565 m) (Gallaway et al. 1997; Fechhelm et al. 1999). All observations were within 90 m of the drillsite, and this area had elevated macroinfaunal densities (up to 13,724 individuals/m<sup>2</sup>) and low diversity relative to baseline conditions. Macroinfaunal populations were dominated by epibenthic scavengers, including cyclopoid copepods and gastropods, and the authors suggested that true infaunal dwellers (e.g., tube-dwelling polychaetes) had been buried by cuttings discharges. There was no consistent pattern of increasing or decreasing density in relation to distance or SBF concentration. The increased macrofaunal densities are consistent with the results seen in the present study. However, the benthic effects observed here are more complex and patchy than observed in the Pompano study. Sediment profile imaging data indicate a range of post-drilling conditions, including areas of azoic sediment column, areas of dominance by surface-dwelling pioneering assemblages, and areas where recent disturbance has selectively compromised near-surface species relative to deeper-living infauna. Differences between the studies include the range of distances from the drillsite (within 90 m in Pompano, within 500 m in this study) and the amount of time elapsed since the most recent drilling discharges (4 months in Pompano, 5 months to 2 years in this study).

Direct comparisons with the SBM monitoring program are not possible because that study did not include box core sampling at continental slope sites (Continental Shelf Associates, Inc. 2004). However, data were collected at three shallower sites on the continental shelf. At one site with relatively high SBF concentrations, the abundance and diversity of the benthic community were reduced within 250 m of the site center. There was evidence of recovery during 1 year between sampling cruises at this site. Near- and mid-field sediments at two other sites (with lower SBF concentrations) had only moderately disturbed benthic community structure. Variability of diversity and evenness was greatest in the near-field zone and generally much lower in the

far-field zone. In the near-field zone, this result was probably due to variations in sediment textures and patchy distributions of cuttings.

### 15.3 SITE COMPARISONS

#### 15.3.1 Areal Extent of Impacts

**Table 15.8** compares the areal extent of impacts among the four sites. Measures of areal extent include the areas of geophysically mapped mud and cuttings zones and the number of near-field stations with elevated barium and/or SBF concentrations. The latter is indicated by values exceeding the far-field 95% confidence limits. In addition, the number of stations with SBF concentrations above 1,000 µg/g and barium concentrations above 10,000 µg/g are tabulated since macroinfaunal data indicate some impacts are associated with these high levels.

**Table 15.8.** Comparison of sites with respect to areal extent of mud and cuttings deposits.

Site and Cruise	Geophysically Mapped Areal Extent (ha)		Barium		SBF	
	Well Jetting Deposits	Rig Discharge Deposits	No. NF stations >FF <sup>a</sup>	No. NF stations >10,000 µg/g	No. NF stations >FF	No. NF stations >1,000 µg/g
<b>Post-Exploration</b>						
VK 916 Cruise 3A/B	None mapped	13.37	10	5	8	4
GB 516 Cruise 1A/B	(no data)	(no data)	12	8	11	3
<b>Post-Development</b>						
GB 516 Cruise 2A/B	2.48	108.53	12	10	11	6
GB 602 Cruise 2A/B	1.08	43.18	12	12	12	9
MC 292 Cruise 2A/B	0.78	25.61	12	3	6	1

GB = Garden Banks; MC = Mississippi Canyon; VK = Viosca Knoll; FF = far-field; NF = near-field.

<sup>a</sup> Number of NF stations exceeding 95% confidence limits for FF stations (maximum = 12).

Overall, the areal extent of impacts was greatest at two post-development sites (GB 516 and GB 602). These two sites had relatively large mapped cuttings zones, and most stations had high barium and SBF concentrations. Impact extent was smallest at the VK 916 exploration site, where only a single well was drilled. Among the post-development sites, MC 292 had the smallest extent of impacts based on both the mapped extent of cuttings deposits and the relatively few stations having very high barium and SBF concentrations. The latter result may reflect the limited use of SBM at this site and the longer elapsed time since drilling ended there (see *Section 15.3.3*).

The geophysically mapped areal extent of cuttings was positively correlated ( $r = 0.70$ ) with the total number of wells; the relationship with estimated SBM cuttings volume was weaker (**Figure 15.27**). For GB 602 and MC 292, which had five and seven wells respectively, the total cuttings area was not much greater than that mapped for the single VK 916 well. Only for GB 516 (post-development) was the increase in cuttings area roughly proportional to the increase in number of wells (i.e., 7-fold). Although discharges from multiple wells presumably would fall in approximately the same pattern on the seafloor, some increase in area due to multiple wells would be expected due to variations in current patterns over time as well as redistribution of the initial deposits of muds and cuttings.

The number of stations with very high SBF concentrations ( $>1,000 \mu\text{g/g}$ ) was positively correlated with the volume of SBM cuttings discharges ( $r = 0.62$ ) (**Figure 15.28**). Similarly, the number of stations with very high barium concentrations ( $>10,000 \mu\text{g/g}$ ) was positively correlated with the estimated SBM cuttings discharges ( $r = 0.78$ ). Correlations with WBM cuttings discharges were much weaker, even for barium (0.14). This is consistent with the prediction that SBM cuttings are more likely to settle rapidly near the discharge due to clumping of hydrophobic SBM-coated cuttings particles (Brandsma 1996; Neff et al. 2000).

### 15.3.2 Severity of Impacts

**Table 15.9** compares the sites with respect to several measures of impact severity. These include maximum and mean barium and SBF concentrations in the near-field. Geometric mean is used for barium and SBF (i.e., log transformation) because of the order of magnitude differences among stations. Also included are maximum TOC concentration (as a measure of organic enrichment) and the difference in mean integrated sediment oxygen levels between near-field and far-field sites (values previously presented in **Figures 15.13** and **15.14**).

**Table 15.9.** Comparison of near-field sites with respect to impact severity.

Site and Cruise	Barium Concentrations		SBF Concentrations		TOC Max	Sediment O <sub>2</sub> Difference <sup>b</sup>
	Max	Mean <sup>a</sup>	Max	Mean <sup>a</sup>		
<b>Post-Exploration</b>						
VK 916 Cruise 3A/B	171,000	9,895	47,920	291	3.45	-40
GB 516 Cruise 1A/B	135,000	11,486	25,131	199	0.62	-31
<b>Post-Development</b>						
GB 516 Cruise 2A/B	351,000	29,960	29,167	672	2.87	-140
GB 602 Cruise 2A/B	116,000	43,385	13,792	2,073	1.99	-202
MC 292 Cruise 2A/B	39,700	5,532	2,408	56	1.63	-10

GB = Garden Banks; MC = Mississippi Canyon; VK = Viosca Knoll; SBF = synthetic-based fluid; TOC = total organic carbon.

<sup>a</sup> Geometric mean concentration.

<sup>b</sup> Difference between mean sediment integrated oxygen concentrations at near-field and far-field sites (negative values mean less oxygen in the near-field).

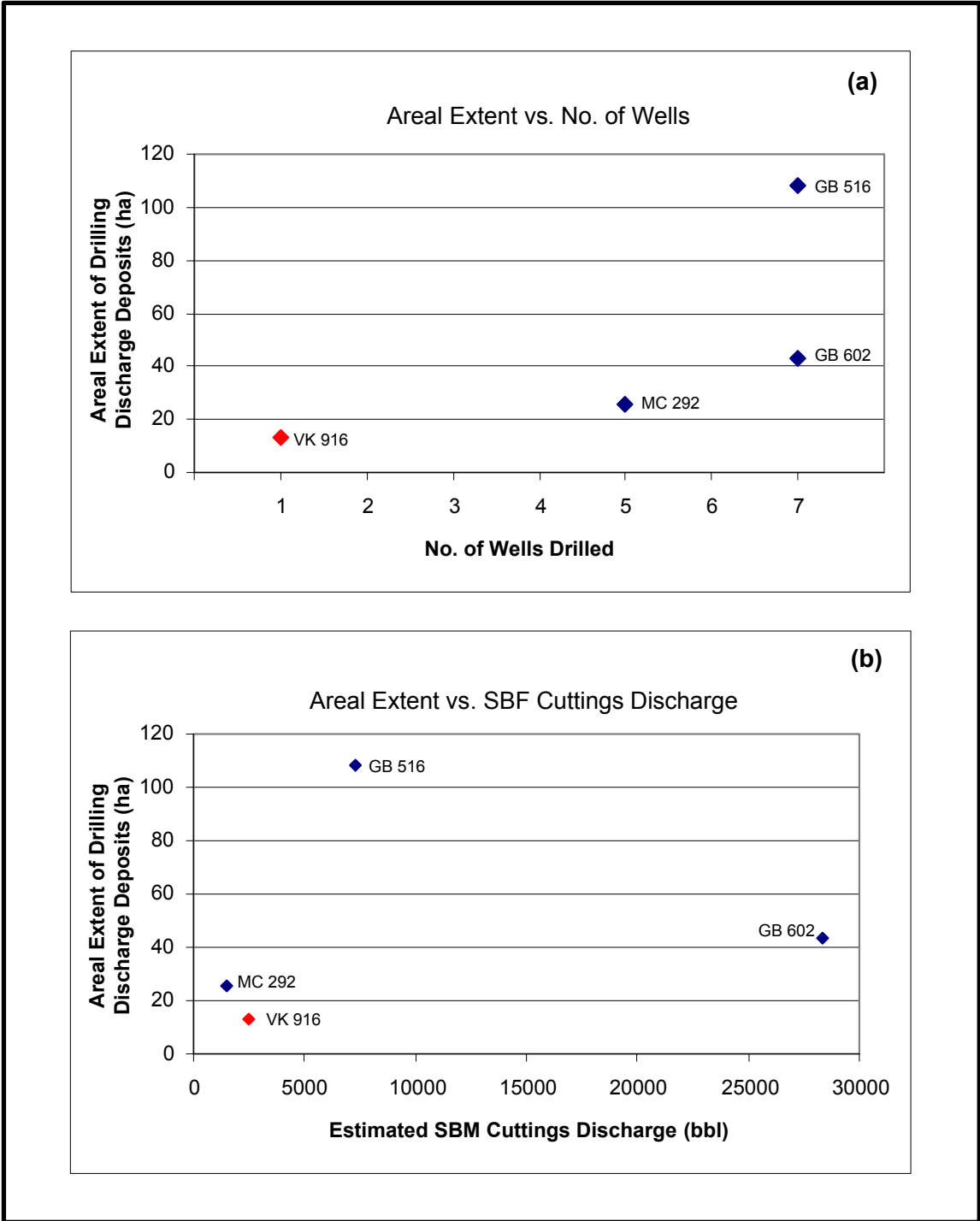


**Figure 15.27.** Geophysically mapped areal extent of drilling discharge deposits in relation to (a) number of wells drilled and (b) estimated synthetic-based mud (SBM) cuttings discharges. Viosca Knoll 916 (red dots) is the only exploration site represented (Garden Banks 516 geophysical data are for post-development only).

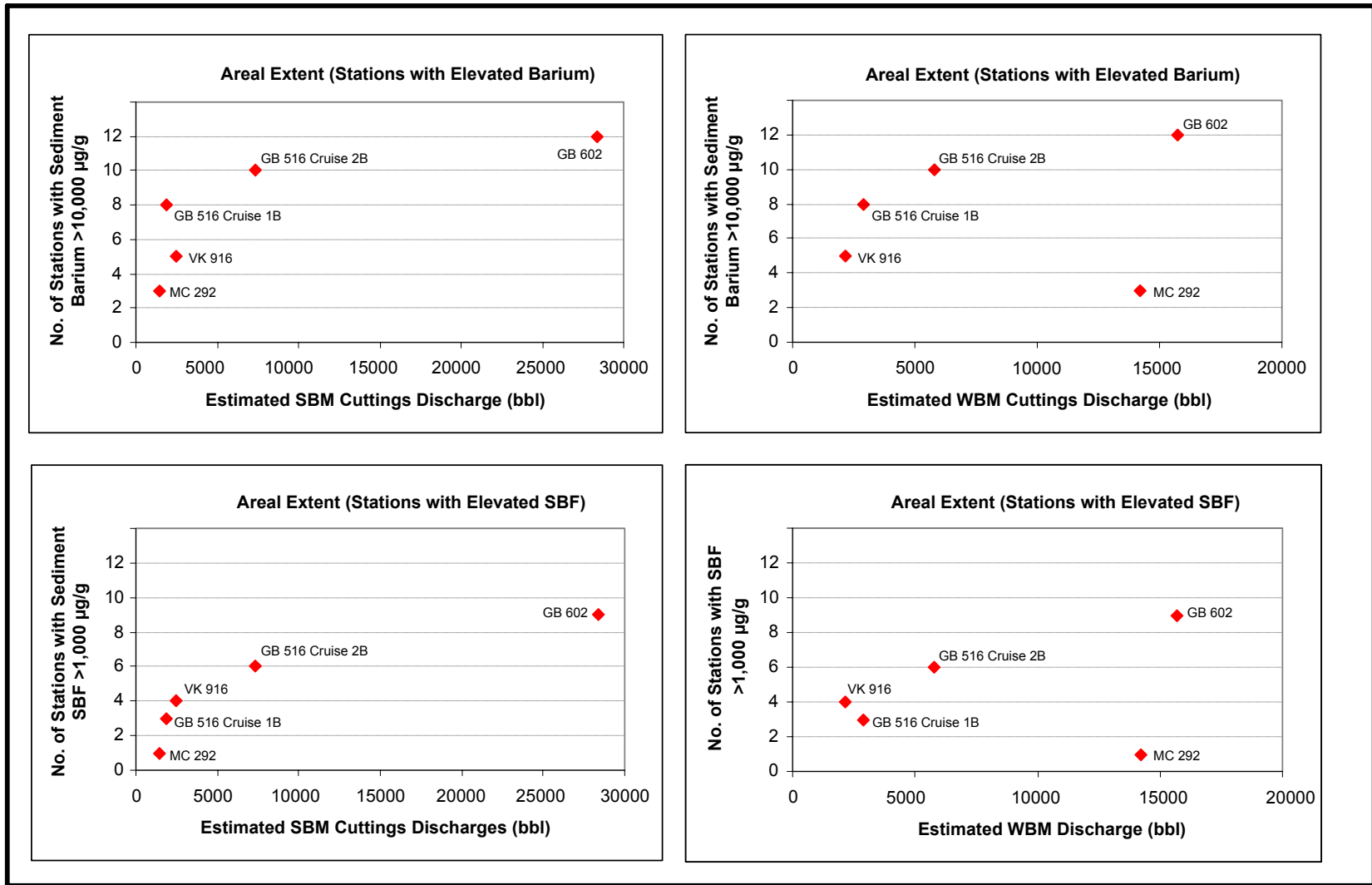


**Figure 15.28.** Areal extent of cuttings deposits (number of near-field stations with very high barium or synthetic-based fluid [SBF] concentrations) in relation to estimated synthetic-based mud (SBM) and water-based mud (WBM) cuttings discharges. The maximum number of stations is 12.

By these measures, the two Garden Banks post-development sites were the most severely affected, having high mean barium and SBF concentrations and the greatest reduction in sediment integrated oxygen levels. The VK 916 post-exploration site had the highest individual SBF and TOC values and the second highest barium value, but mean barium and SBF concentrations were not as high as at GB 516 and GB 602 because fewer stations were affected. By all measures, MC 292 was least severely affected, having low maximum and mean barium and SBF concentrations and the smallest decrease in sediment integrated oxygen levels.

**Figure 15.29** shows that two measures of impact severity, the geometric mean barium and SBF concentrations, were positively correlated with estimated SBM cuttings volume. GB 602 had the highest mean barium and SBF concentrations, corresponding to the largest SBM cuttings discharge.

The decrease in mean sediment oxygen levels was strongly negatively correlated with both mean sediment SBF concentrations and the estimated SBM cuttings discharges (**Figure 15.30**). The decrease in oxygen was greatest at the site with the highest SBF concentrations and the highest estimated SBM discharge (GB 602).

### 15.3.3 Duration of Impacts

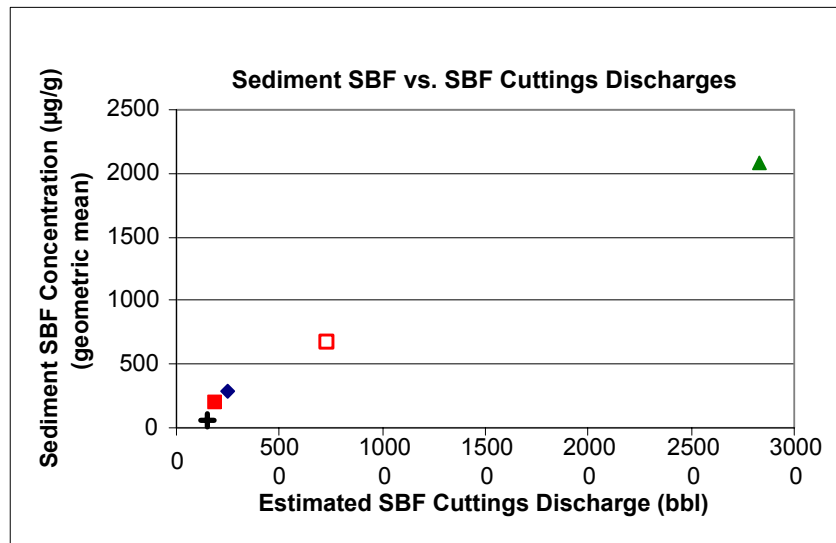
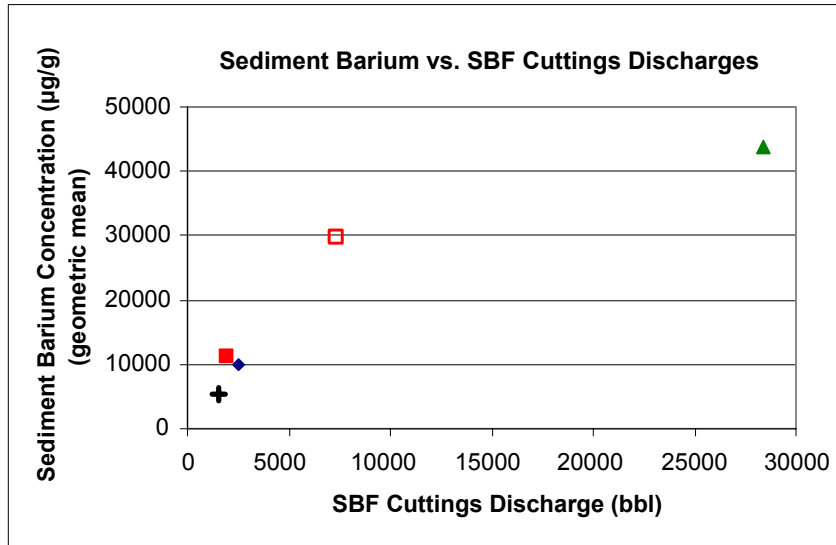
The timing of drilling activities vs. sampling cruises differed among sites. The interval between cessation of drilling and the date when the surveys began ranged from 5 months to nearly 2 years depending on the site (**Table 15.10**).

**Table 15.10.** Timing of drilling vs. cruise dates.

Site	Previous Drilling Ended	Subsequent Cruise	Cruise Dates	Time Interval (approx)
VK 916	18 Dec 2001	3A (Geophysical) 3B (Biol/chem)	7-12 Aug 2002 4-14 Aug 2002	8 months
GB 516	21 Aug 1999	1B (Biol/chem)	23 Oct-17 Nov 2000	14 months
	5 Feb 2001	2A (Geophysical) 2B (Biol/chem)	24 June-7 July 2001 8-25 July 2001	5 months
GB 602	3 Jan 2001	2A (Geophysical) 2B (Biol/chem)	24 June-7 July 2001 8-25 July 2001	6 months
MC 292	16 July 1999	2A (Geophysical) 2B (Biol/chem)	24 June-7 July 2001 8-25 July 2001	24 months

GB = Garden Banks; MC = Mississippi Canyon; VK= Viosca Knoll.

Over time, SBF residues are decomposed by microbes, resulting in significant decreases in SBF concentration (Candler et al. 1995). **Figure 15.31** shows that both time and volume of SBM cuttings discharges are factors affecting SBF concentrations in near-field sediments. On **Figure 15.31a**, the size of each circle is proportional to the geometric mean SBF concentration in the near-field. Mean SBF concentrations tend to increase with increasing SBM discharge volume, and tend to decrease with longer elapsed time since drilling.



- LEGEND**
- ◆ VK 916
  - GB 516 Cruise 1B
  - GB 516 Cruise 2B
  - ▲ GB 602
  - + MC 292

**Figure 15.29.** Relationship between post-drilling sediment barium and synthetic-based fluid (SBF) concentrations within near-field sites and estimated volumes of SBF cuttings discharges.

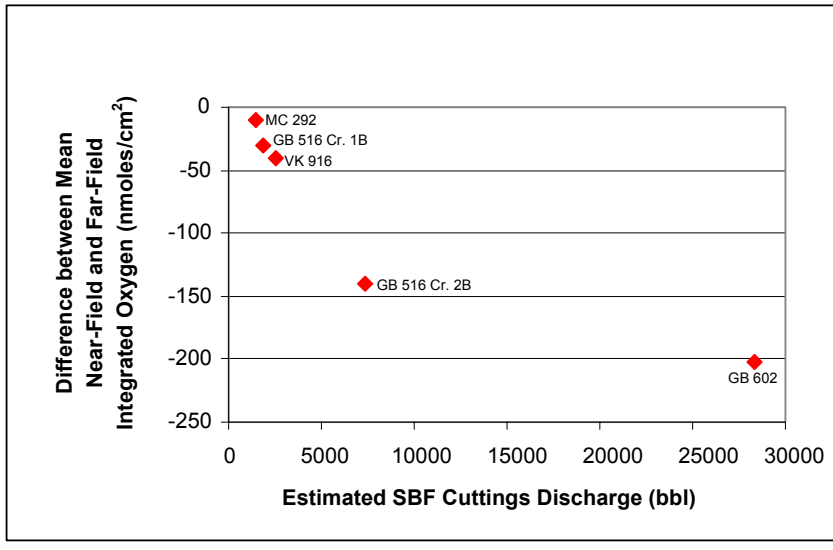
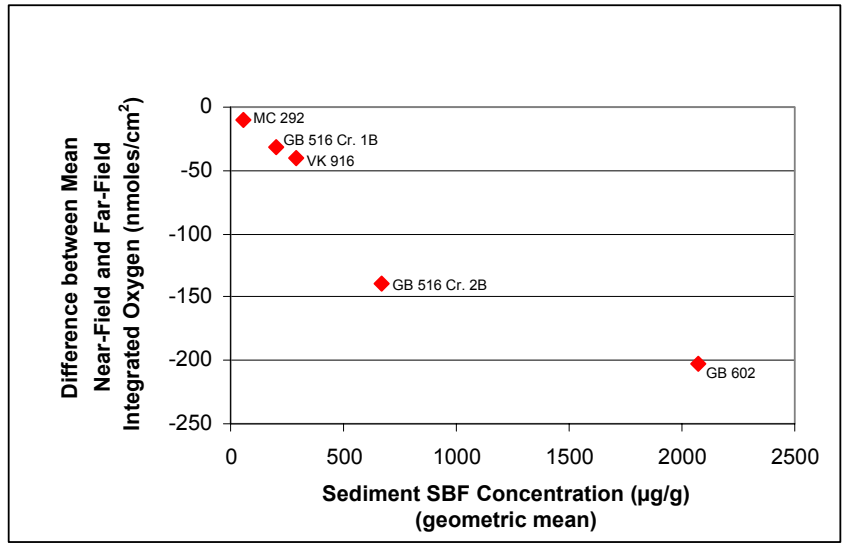


**Figure 15.30.** Difference between mean near-field (NF) and far-field (FF) sediment oxygen levels in relation to sediment synthetic-based fluid (SBF) concentrations and estimated SBF cuttings discharges.



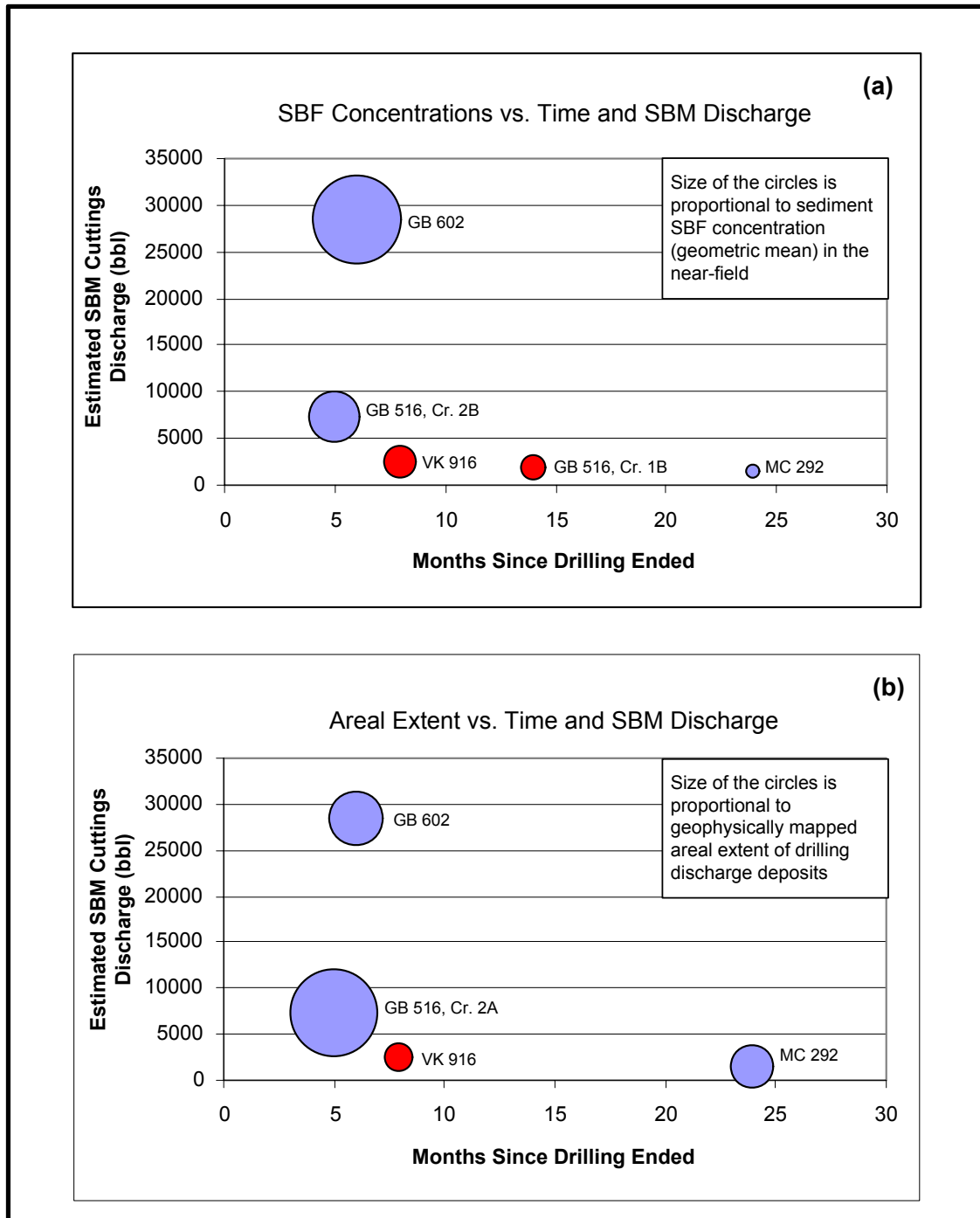


**Figure 15.31.** Plots of (a) geometric mean synthetic-based fluid (SBF) concentration and (b) geophysically mapped areal extent of drilling discharge deposits in relation to estimated synthetic-based mud (SBM) cuttings discharges. Red circles indicate post-exploration data; all others are post-development.

Similar findings were noted in the SBM monitoring program, which showed an overall trend of decreasing sediment SBF concentrations with elapsed time after drilling (Continental Shelf Associates, Inc. 2004). In addition, SBF concentrations decreased significantly when development sites were resampled 1 year after the first sampling cruise. Barium concentrations did not consistently decrease during this time. Drilling mud barite is stable and persistent in sediments near drill cuttings discharge sites. Although it can be dispersed and diluted by bed transport or burial, this apparently occurs over a longer time period than a year or two at this water depth.

In the broader view, data from the sites and adjacent blocks provide insight into the duration of drilling impacts. In addition, as discussed in *Chapter 4*, persistent cuttings and/or anchor scars from previous activities at nearby wellsites also were evident. These observations are summarized in **Table 15.11**. They suggest that geophysically detectable mud/cuttings deposits persist for 5 years or more and anchor scars may persist for 14 years or more. Because no chemical or biological sampling was done in adjacent blocks, it is not known if the mapped mud/cuttings deposits from older wells are associated with persistent elevations in barium and SBF, anoxic conditions, or altered benthic communities.

**Table 15.11.** Impacts observed at various time intervals after drilling, including wells in blocks adjacent to the study sites.

Block	Date Drilling Ended	Time Elapsed Since Drilling	Impacts Noted	
			Physical	Chemical
<b>Study Sites</b>				
GB 516 (Cruises 2A, 2B)	5 Feb 2001	5 months	Mud/cuttings deposits Anchor scars Debris	Elevated barium, SBF, TOC; low oxygen and Eh
GB 602 (Cruises 2A, 2B)	3 Jan 2001	6 months	Mud/cuttings deposits Anchor scars Debris	Elevated barium, SBF, TOC; low oxygen and Eh
VK 916 (Cruises 3A, 3B)	18 Dec 2001	8 months	Mud/cuttings deposits Anchor scars Debris	Elevated barium, SBF, TOC; low oxygen and Eh
GB 516 (Cruise 1B)	21 Aug 1999	14 months	No data	Elevated barium and SBF; low oxygen and Eh
MC 292 (Cruises 2A, 2B)	16 July 1999	24 months	Mud/cuttings deposits Anchor scars Debris	Elevated barium and SBF, but more patchy and less elevated than at other sites
<b>Adjacent Blocks</b>				
MC 248 (adjacent to MC 292)	14 Mar 2000	15 months	Mud/cuttings deposits Anchor scars	No data
VK 872 (adjacent to VK 916)	18 Dec 1998	~3.5 years	Mud/cuttings deposits Anchor scars	No data
MC 291 (adjacent to MC 292)	20 Oct 1997	~4 years	Mud/cuttings deposits Anchor scars	No data
GB 602 (Well No. 3 and two sidetracks)	7 Aug 1996	~5 years	Mud/cuttings deposits Anchor scars	No data
GB 516 (Well No. 1)	23 July 1996	~5 years	Mud/cuttings deposits Anchor scars	No data
VK 873 (adjacent to VK 916)	25 Mar 1988	~14 years	Anchor scars	No data

GB = Garden Banks; MC = Mississippi Canyon; VK = Viosca Knoll; Eh = redox potential;  
SBF = synthetic-based fluid; TOC = total organic carbon.

## 15.4 METHODOLOGY EVALUATION

This study used a combination of conventional and innovative techniques, some of which have not been used previously in environmental monitoring of deepwater drilling in the Gulf of Mexico.

### 15.4.1 Selection of Far-Field Sites

The six far-field sites for each near-field site were chosen to be at similar water depth and 10 to 25 km away. The intention also was to locate these sites away from other previous wellsites, to the extent possible. However, due to the large number of wells in the Gulf of Mexico, it was difficult to find far-field sites that were not within 10 km of previous drilling. For example, all of the VK 916 far-field sites had 25 or more previous wells within 10 km (*Chapter 3*).

As discussed in *Chapter 3*, four far-field sites had previous wells within 3 km. These were VK 916 FF1 and FF2, and MC 292 FF1 and FF2. Analysis of barium and SBF concentrations suggests that two of these (VK 916 FF2 and MC 292 FF1) may have been exposed to small amounts of drilling discharges (see *Appendix K*). At VK 916 FF2, the most likely source was four wells drilled between March and May 2002 in VK 915. This drilling occurred during the program and could not have been foreseen when the site was selected. However, the other three far-field sites had previous wells that probably could have been avoided. The initial mapping effort did not include a large enough area (15-km radius from near-field site center), and eventual mapping of previous wells for this report turned out to be a complex, iterative exercise, even working with the MMS databases. In any future study, it is recommended that more effort be devoted to initial mapping to ensure that far-field sites are not near previous drilling. This problem also highlights the importance of having multiple reference sites.

Statistically, elevated barium and SBF concentrations at some far-field sites could make it more difficult to detect near-vs.-far-field differences by increasing both the far-field mean and the variance among far-field sites. However, the far-field concentrations seen here are orders of magnitude lower than most barium and SBF concentrations in the near-field. (Keep in mind that SBF concentrations measured at most far-field sites represent background concentrations of hydrocarbons that co-elute with SBF in the analytical procedure.) For statistical comparisons of the near-field site *as a whole* vs. the far-field, the effects of slight elevations in the far-field are negligible. For example, even though VK 916 FF2 and MC 292 FF1 were included in statistical analyses in *Chapters 8* and *9*, significant near-field vs. far-field differences for both barium and SBF were detected.

The elevated barium and/or SBF levels at some far-field sites represent very small amounts of drilling fluids or fine cuttings particles. For example, a barium increase of 500  $\mu\text{g/g}$  would represent about 943  $\mu\text{g}$  of industrial barite per gram of sediment, or 0.094% (assuming industrial barite averages 53% barium; Trefry et al. 2003). Similarly, an SBF increase of 100  $\mu\text{g/g}$  would represent approximately 1,000  $\mu\text{g}$  of cuttings particles per gram of sediment, or 0.1% (assuming retention on cuttings averages about 10% on a dry weight basis).

#### 15.4.2 Geophysical Surveys

The use of an autonomous underwater vehicle (AUV) for the Cruise 2A and 3A geophysical surveys was a marked improvement over the deep-tow methods used on Cruise 1A (*Chapter 4*). The AUV saved time because it could accurately follow a pre-programmed track and did not require a large turning radius when moving from one transect to the next. In addition, this system was less vulnerable to weather delays. Geophysical data collected with the AUV proved useful in mapping the extent of drilling mud and cuttings deposits. The maps identified areas of possible cuttings, which could then be targeted for additional sampling. Other techniques, including sediment hydrocarbon and metal analyses, sediment profile imaging, and color analysis of bottom photographs generally confirmed the mapped distribution of mud and cuttings.

Although the geophysically derived maps generally corresponded with zones of suspected drilling mud and cuttings deposits, there was no “ground truthing” to determine whether deposits were accurately mapped or to estimate the minimum thickness that could be detected. Since positive identification of cuttings particles is difficult even with samples in hand, there probably is no practical way to ensure the accuracy of the mapping. Except where thickness of deposits can be estimated from subbottom profiles, the geophysical mapping is most useful as a guide to aid in station placement rather than a detailed, quantitative picture of mud and cuttings deposition.

#### 15.4.3 Seafloor Photography

In the Northern Gulf of Mexico continental slope study, bottom photographs were taken using a camera drifted approximately 2 m above the bottom (Gallaway 1988). At this altitude, the area of each photograph was about 2.3 m<sup>2</sup>. In the present study, a dragged sled was used to obtain close-up images of the seafloor looking straight down from a height of 0.6 m. The area of each photograph was much smaller, about 0.22 m<sup>2</sup>. While the closeup views of the seafloor obtained with this method made it easier to identify biota, the area was found to be too small for useful megafaunal counts, as most images showed no fauna or at most, one organism. Originally, it was assumed that higher resolution images of small areas would miss large animals but allow identification and enumeration of many animals at the lower limit of the megafaunal size range, 1 cm. This did not prove to be the case. Large fish, crabs, and the rare holothuroid usually appeared in only part of the image frame. Some distinctive small fauna was seen, notably retracted anemones and hermit crabs as small as 1 cm, but little else.

Making some simplistic assumptions about density-area relationships, it can be predicted that quadrupling the area of the image (doubling the linear dimensions) would produce a four-fold increase in the number of images capturing fauna, about 28% based on the current studies. Such an increase in size would not lose too many animals below the limits of resolution.

A digital photographic analysis of seafloor color was developed (*Chapter 12*) that identified patchy areas of dark, blue-black bottom attributed to a covering of cuttings and/or drilling fluids. However, an exploratory attempt to develop a digital texture analysis was not successful.

#### 15.4.4 Detecting Benthic Community Impacts

Sediment profile imaging (*Chapters 6 and 7*) proved a useful tool in identifying benthic communities affected by SBM cuttings. Each image included not only biological data, but also information about the physical/chemical context (e.g., redox conditions). The usefulness of this technique is based on a paradigm developed from sampling disturbed shallow-water habitats. However, it appears to be applicable to detecting SBM cuttings impacts on the continental slope.

Sediment profile imaging and box coring provide somewhat different and complementary pictures of benthic impacts. While sediment profile images showed areas dominated by pioneering assemblages, they did not provide any direct information about the very high densities of some macroinfauna and meiofauna species near drilling. Also, sediment profile imaging classified some stations as “azoic” (i.e., lacking visible benthic macroinfauna). In contrast, none of the box cores had zero macroinfauna, although some had relatively few organisms. The patchiness of macroinfaunal distribution and the different scale of observations may help to explain this discrepancy. Box core macroinfaunal samples consist of a cube of sediment 32 cm x 32 cm and 20 to 30 cm deep. The sediment profile images are 15 cm wide by 20 cm deep (maximum) and are looking at a single plane through the sediment column. In images classified as “azoic,” there may be macrofauna in the sediment column that are not in the plane of the photograph.

In the present study, most box core specimens were identified only to major group (e.g., Annelida), which is not very helpful in understanding impacts. More detailed analysis such as identification of polychaete families is necessary to understand whether the community is changing – for example, from deep, tube-dwelling species to a pioneering assemblage of surface scavengers. A subset of 24 stations was processed in greater detail by the principal investigators but was beyond the required scope of this study. For cost-effective sampling, it would appear that sediment profile imaging supplemented by box core samples processed at least to the level of family would be most useful.

### 15.5 CONCLUSIONS

The following are the main conclusions of the study:

- Geophysical and chemical measurements indicated that a layer of SBM cuttings and muds was deposited within the near-field radius. Geophysically mapped cuttings zones ranged from 13 to 109 ha in area, with larger zones observed at post-development sites. Areas mapped as cuttings typically extended several hundred meters from wellsites, with the greatest extent (about 1 km) observed at GB 602 and GB 516. The cuttings deposits were estimated to be up to 45 cm thick at one site (VK 916).
- Concentrations of drilling fluid tracers (barium and SBF) were elevated by several orders of magnitude within near-field sites. Mean sediment concentrations of barium and SBF were positively correlated with estimated discharge volumes of SBM cuttings.
- Areas of SBM cuttings deposition were associated with elevated TOC and anoxic conditions, including low dissolved oxygen, negative Eh, and shallow depth of the oxidized layer. Sites with larger volumes of SBM cuttings discharges and higher mean sediment SBF concentrations had the greatest reduction in mean sediment oxygen levels.

- Sediment profile imaging indicated that the near-field sites had patchy zones of disturbed benthic communities, including microbial mats, areas lacking visible benthic macroinfauna, zones dominated by pioneering stage assemblages, and areas where surface-dwelling species were selectively lost.
- Macroinfaunal and meiofaunal densities generally were higher near drilling, although some faunal groups were less abundant in the near-field (amphipods, ostracods). Among megafauna, increased fish densities and reduced ophiuroid densities were noted in the near-field of two sites (VK 916 and GB 516).
- Microbial biomass (ATP) was elevated in some samples near drilling and positively correlated with SBF concentrations above about 1,000  $\mu\text{g/g}$  at VK 916 and GB 516, but not at GB 602 or MC 292. The ATP data were problematic, however, with major temporal changes and apparent far-field “outliers” complicating the interpretation.
- Meiofaunal densities in the near-field were not consistently correlated with drilling indicators (barium, SBF) or other sediment variables (TOC, grain size fractions).
- Annelid (predominantly polychaete) and gastropod densities in the near-field were positively correlated with drilling indicators (barium, SBF). Some near-field stations with barium concentrations higher than about 10,000  $\mu\text{g/g}$  and/or SBF concentrations greater than about 1,000  $\mu\text{g/g}$  had elevated polychaete densities. A few near-field stations at GB 516 and GB 602 had very high gastropod densities, which were associated with barium concentrations of 55,000  $\mu\text{g/g}$  or higher and SBF concentrations of 4,500  $\mu\text{g/g}$  or higher.
- Amphipod densities in the near-field were negatively correlated with drilling indicators (barium and SBF). Generally, near-field stations with barium concentrations higher than about 10,000  $\mu\text{g/g}$  and/or SBF concentrations greater than about 1,000  $\mu\text{g/g}$  had low amphipod densities. Separately, acute toxicity tests with near-field and far-field sediments from MC 292 and GB 602 showed that mean amphipod survival was significantly lower in sediments from near-field stations than in sediments from far-field stations. Amphipod survival in the toxicity tests was negatively correlated with drilling indicators.
- Detailed taxonomic analysis of a subset of the macroinfaunal samples showed some stations near drilling had lower diversity, lower evenness, and lower richness indices compared with stations away from drilling. Species composition varied in relation to both geographic location and drilling impacts. Station/cruise groups most likely affected by drilling were dominated by high abundances of one or a few deposit-feeding species, including known pollution indicators.
- At all four near-field sites, impacts were patchy, with some stations showing conditions similar to those at the far-field sites. Impacts generally were less extensive and less severe at post-exploration sites than at post-development sites.
- Impacts attributable to SBM cuttings such as elevated TOC, poor redox conditions, and associated biological changes were least severe at MC 292, where the smallest quantities of SBM cuttings were discharged. However, the time elapsed since drilling also was longer at this site (about 2 years) than at the other three sites (5 to 14 months), and the less severe impacts may reflect recovery of this site over time.
- Observations from the study sites and adjacent lease blocks suggest that geophysically detectable mud/cuttings deposits may persist for 5 years or more and anchor scars may persist for 14 years or more. Because no chemical or biological sampling was done in adjacent blocks, it is not known if the mapped mud/cuttings from older wells are associated with persistent elevations in barium, anoxic conditions, or altered benthic communities.

## **16.1 INTRODUCTION**

An ecological risk assessment is the estimation of the likelihood of undesirable effects of human activities or natural events and the accompanying risks to non-human organisms (Suter 1997). Ecological risk assessment methods are being used with increasing frequency to predict or forecast the consequences to the environment of human activities, particularly releases of chemicals (USEPA 1992, 1998; Suter 1993, 1997). The results of ecological risk assessment should be used by risk managers and environmental regulators to make decisions about how to manage operations in such a way as to minimize or mitigate adverse environmental impacts (Maciorowski 1997).

The objective of this chapter is to estimate and evaluate the ecological risk of drilling discharges to the ocean from drilling rigs or platforms on the continental slope ( $\approx 1,000$  m) of the northern Gulf of Mexico. This risk assessment is based on the results of the study as presented in *Chapters 3 through 14* as well as the preceding Synthesis (*Chapter 15*).

An ecological risk assessment often includes four steps (USEPA 1992, 1998; Suter 1993, 1997):

- Problem formulation
- Exposure assessment
- Effects assessment
- Risk characterization

In the problem formulation, the study sites are briefly described and their physical and biological characteristics are summarized, as well as the types and amounts of drilling discharges at each site. Current understanding of the marine environmental fates and effects of drilling waste discharges (water based and synthetic based drilling muds and cuttings) is summarized. The latter summary is used as the basis for a simple conceptual model for potential impacts of drilling discharges and the four deepwater discharge sites.

The exposure assessment includes a description of the concentrations of chemicals of concern (synthetic base chemicals, hydrocarbons, metals) in near-field and far-field sediments at the four sites. The exposure assessment also contains a description of selected physical and chemical changes (sediment grain size, geochemistry, and redox state) in near-field sediments that could be caused directly or indirectly by accumulation of drilling discharge solids on the seafloor.

The effects assessment includes a brief summary of the toxicity and marine ecological impacts of the chemicals of concern (water based drilling muds and cuttings, synthetic based mud cuttings, hydrocarbons, metals), based on laboratory and field studies from the scientific literature. These published effects data are used to evaluate changes (measured mainly as difference between near-field and far-field) in benthic micro-, meio-, macro-, and mega-biota and sediment toxicity as possible direct or indirect effects of drilling discharge accumulations on the seafloor.

The risk characterization integrates and evaluates the relationships between exposure to chemicals of concern or physical/chemical alteration of the seafloor and biological changes in the benthic organisms of concern. The risk characterization produces a quantitative estimate of the risk of injury to valued ecosystem components from exposure to the chemicals of concern. “Risk” is used in this context as the probability that an organism will incur injury (harm) as a direct or indirect result of exposure to the chemicals of concern or other potential stressors evaluated.

## **16.2 PROBLEM FORMULATION**

### **16.2.1 Deepwater Drilling in the Gulf of Mexico**

Today, the outer continental shelf of the U.S. Gulf of Mexico is the most extensively developed and mature offshore petroleum province in the world (Kaiser and Mesyanzhinov 2005). In 2003, there were 7,800 active leases on the outer continental shelf and slope of the U.S. Gulf of Mexico, 54% of them in deep water (Richardson et al. 2004). Since 1947, the international oil industry has drilled more than 40,000 wells in the northern Gulf and placed more than 6,300 structures in water depths to more than 2,300 m (Kaiser and Mesyanzhinov 2005).

Technological developments have permitted oil and gas exploration in the U.S. Gulf of Mexico to move progressively farther offshore to depths exceeding 2,300 m (MMS 2000a; Richardson et al. 2004). More than 1,675 wells have been drilled in the Gulf at greater than 200 m water depth, culminating in drilling of two discovery wells in 2004 in more than 2,200 m of water in the Walker Ridge lease area, and the first well drilled in more than 3,000 m of water in 2003. There were 121 producing wells in water depths greater than 1,000 m the northern Gulf of Mexico in the first half of 2005 (MMS 2005).

Exploration for and development and production of offshore oil and gas resources is a massive, long-term undertaking that may cause physical, chemical, and biological disturbance to the local marine environment (Neff 1987, 2005). Offshore oil and gas operations can be divided into three phases: geophysical evaluation, exploration, and development/production. All three phases may occur simultaneously during development of large offshore fields. The objective of the current study was to evaluate the environmental effects of exploration and development activities at continental slope depths in the northern Gulf of Mexico.

Drilling of wells is the main activity in exploration and development. Exploration, appraisal, and development drilling are essentially the same, though the facilities from which drilling occurs sometimes are different (**Figure 16.1**). Drilling at the four sites evaluated in this risk assessment was performed from anchored semi-submersible rigs (*Chapter 3*).



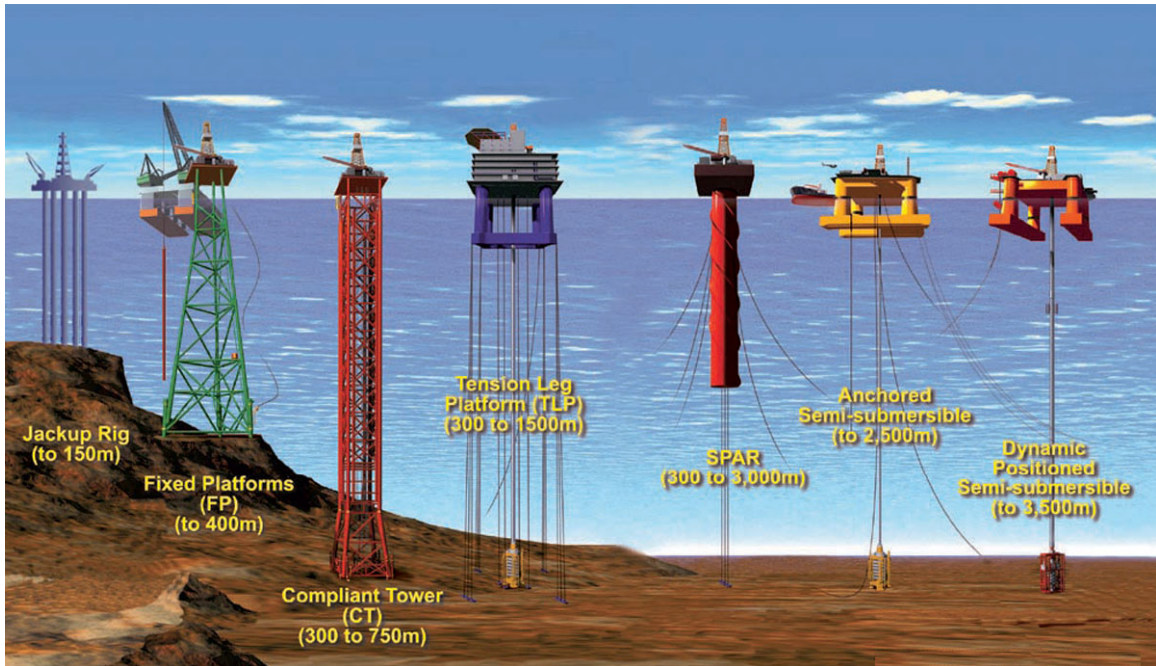


**Figure 16.1.** Facilities from which offshore wells are drilled change with water depth. As water depth increases beyond 400 m, drilling usually is performed from floating drilling units or floating production facilities. From International Association of Oil & Gas Producers (OGP 2003).

### 16.2.2 Drilling Practices and Discharge Histories

Similar practices were used for drilling exploration and development wells at the four sites evaluated in this risk assessment. Both water based drilling muds (WBM) and synthetic based drilling muds (SBM) were used to drill most wells. The surface section (to about 300 m) of exploration and most development wells (except offset or deviated wells from an existing well-bore) was drilled (spudded) or jetted with a water based spud mud, composed primarily of a slurry of bentonite clay or gel (e.g., cellulose polymers) and sometimes barite in seawater. The spud mud was pumped down the drill pipe and exited through holes in the drill bit, where it picked up cuttings (chips of crushed rock produced by the drill bit) and carried them to the seafloor surface. The spud muds and associated cuttings were discharged directly to the seafloor until the riser was put in place.

After the riser was installed, the drilling fluids and cuttings were pumped through the well annulus back to the drilling rig, where drilling fluids and cuttings were passed through the solids control equipment on the rig to separate the drilling fluid from the cuttings. The drilling fluids were returned to the mud pit to be recirculated down-hole (Neff et al. 1987). The cuttings were discharged to the ocean as allowed by the National Pollutant Discharge Elimination System (NPDES) permit.

WBM were used for the shallower segments of the wells drilled at the four sites. The treated cuttings, containing about 10% to 15% WBM solids, were discharged to the ocean during

drilling, which occurred approximately half the time during development. There also were periodic discharges of WBM to the ocean, particularly when changing the WBM system or switching over to SBM. The deeper segments of most wells, particularly if deviated, were drilled with SBM. Cuttings were removed from the SBM and cuttings returns and discharged to the ocean if they met effluent limitation guidelines in the NPDES permit. The SBM themselves were recycled down hole and eventually returned to shore for regeneration or disposal.

16.2.2.1 Viosca Knoll Block 916

VK 916 was an exploration site; only one well was drilled within the near-field site. Although 25 wells were drilled within 10 km before or during the study, most were more than 4 km away and the nearest was 2.3 km (*Chapter 3*). The near-field exploration well was drilled from an anchored semi-submersible rig. Eight anchors were deployed in a radial array with a radius of about 2,440 m around the site; each anchor had about 450 m of anchor chain on the seafloor. Scour by anchor chains at all locations contributes to physical disturbance of the seafloor at the rig site.

Both WBM and SBM were used to drill the exploratory well (**Table 16.1**). A total of about 15,880 bbl of WBM and 2,165 bbl of WBM cuttings was discharged to the ocean during spudding and drilling of the upper segments of the well. An additional 2,510 bbl of SBM cuttings (probably containing about 10% SBF chemical) also were discharged during drilling of the deepest sections of the well. The SBM was an internal olefin (IO). A total of about 20,556 bbl of drilling mud and cuttings was discharged to the ocean during drilling of this exploratory well.

**Table 16.1.** Summary of drilling activities within 500 m of the four drillsites before and during this study. bbl = barrel: 42 gallons or 159 L.

Wells and Discharges	VK 916	GB 516	GB 602	MC 292
Wells within 500 m				
Prior to study	0	2	7	5
During study	1	5	0	0
Est. Seafloor Discharges (bbl)				
WBM mud	3,074	13,002	23,946	10,331
WBM cuttings	419	1,774	3,266	1,409
Est. Drill Rig Discharges (bbl)				
WBM mud	12,807	29,462	91,301	93,960
WBM cuttings	1,746	4,018	12,450	12,813
SBM cuttings	2,510	7,313	28,339	1,490
Total Discharges	20,556	55,569	159,302	120,003
SBM Type	Syn-Teq (IO)	Novaplus (IO) Petrofree LE (LAO)	Novadril (IO) or Petrofree ester; Novaplus (IO) or Petrofree LE (LAO)	Novaplus (IO)

IO = internal olefin; LAO = linear alpha olefin; SBM = synthetic based mud; WBM = water based mud.

#### 16.2.2.2 Garden Banks Block 516

Two exploration wells (one straight well and one sidetrack) were drilled within 500 m of the site center at GB 516 before the study, and five development wells were drilled during the study (**Table 16.1**). An additional 49 wells had been drilled within 10 km of the site between 1987 and 2000. Most of these had been drilled in Blocks GB 426/471, 7.5 to 9.1 km from the site.

Both WBM and SBM were used to drill the wells at GB 516. The SBM segments drilled during exploratory drilling before the study were drilled with either an IO or a linear alpha olephin (LAO) SBM; IOs were the only SBM used to drill the five development wells drilled in 2000-2001 during the study. A total of 55,569 bbl of drilling muds and cuttings was discharged from the wells within 500 m of site center, including 42,464 bbl of WBM, 5,792 bbl of WBM cuttings, and 7,313 bbl of SBM cuttings (**Table 16.1**). A variety of gas production structures and flowlines are positioned on the seafloor at the site (*Chapter 3*).

#### 16.2.2.3 Garden Banks Block 602

GB 602 is a post-development site in 1,125 m of water. A total of seven wells were drilled within 500 m of the site and an additional 11 wells were drilled 1.3 km to 8.3 km away. Drilling at the site was from an anchored semi-submersible rig. The anchor radius was about 2,377 m, and about 914 m of anchor chain from each anchor was on the seafloor. A variety of gas production structures and flowlines are positioned on the seafloor at the site (*Chapter 3*).

Nearly 160,000 bbl of drilling muds and cuttings were discharged during drilling of the seven wells at the site center (**Table 16.1**). Discharges included 115,247 bbl of WBM, 15,716 bbl of WBM cuttings, and 28,339 bbl of SBM cuttings. This was the largest volume of SBM cuttings discharged at the four sites.

#### 16.2.2.4 Mississippi Canyon Block 292

MC 292 is a post-development site in about 1,034 m of water. A total of 16 wells had been drilled within 10 km of the site, including five wells within 500 m of site center at MC 292. The wells near site center are producing wells with a subsea manifold and flowlines carrying natural gas to VK 900, about 44 km to the north. A variety of gas production structures and flowlines are positioned on the seafloor at the site.

Three of the wells near the center of the site were drilled with WBM. Two sidetracks were drilled with an IO SBM system. A total of 120,003 bbl of drilling mud and cuttings was discharged to the ocean at this site, including 104,291 bbl of WBM, 14,222 bbl of WBM cuttings, and 1,490 bbl SBM cuttings (**Table 16.1**).

### 16.2.3 The Benthic Environment of the Study Area

The continental slope of the U.S. Gulf of Mexico ( $\approx 200$  to 2,700 m) supports unique biological communities distinct from those on the continental shelf or Sigsbee and Florida Escarpments (Rowe and Kennicutt 2002; Gallaway et al. 2003). Several investigators have identified a distinct zonation of benthic community structure with depth on the slope (Rowe and Menzies 1969). This apparent zonation is actually the result of interactions among a variety of physical and chemical

parameters that vary with distance from shore and water depth, the most important of which is the availability of organic nutrients (Rowe and Kennicutt 2002).

Slope communities are food-limited. Nutrients reach the slope benthos as a rain of dissolved and particulate organic matter and inorganic nutrients, derived primarily from production in surface waters and runoff from land. Deposition rate declines with distance from land and increasing water depth, except where water currents and bottom physiography concentrate nutrients, as in the Mississippi Trough and DeSoto Canyon (Rowe and Kennicutt 2002). Local nutrient sources, such as oil and methane seeps and brine pools, which are abundant on the upper slope of the north-central Gulf of Mexico, also increase biological production over large areas (MacDonald et al. 1996; MacDonald 1998, 2002; Gallaway et al. 2003; Sager et al. 2003). Outside these local nutrient-enriched areas, benthic biomass decreases with decreasing nutrient flux to the benthos with depth on the slope. This decrease in biomass with depth is steeper on the slope of the Gulf of Mexico than in other oceans studied (Rowe 1983), perhaps because of the lower production in surface waters of the Gulf of Mexico.

The slope communities in the Gulf of Mexico tend to be depauperate in numbers and biomass. The mean size of benthic macrofauna tends to be smaller than that of the macrofauna occurring at similar depths in the Atlantic (Rowe and Menzel 1971; Rowe et al. 1974; Gallaway et al. 2003). On the slope, the biomass of meiofauna tends to be greater than that of macrofauna, which in turn exceeds that of the megafauna (Pequegnat et al. 1990). The meiofauna are dominated by nematodes, the macrofauna by polychaetes, and the megafauna by echinoderms (particularly holothurians) or decapod crustaceans.

Rowe and Kennicutt (2002) are developing a conceptual model of the slope benthic community of the northern Gulf of Mexico. The components of the benthic/demersal food web of the slope, classed by size and trophic position, are microbiota, meiofauna, macrofauna, megafauna, and demersal fishes. Site-specific information about benthic communities of the study area have been presented in *Chapters 6 and 7* (sediment profile imaging), *Chapter 10* (sediment microbes), *Chapter 11* (meiofauna and macroinfauna), and *Chapter 12* (megafauna and image analysis).

#### 16.2.3.1 Microbiota

Benthic microbiota such as bacteria and protists, including foraminifera, are the primary consumers of the particulate organic carbon raining down from above, as well as any organic matter derived from oil/gas seeps and brine pools. Bacteria are the most abundant benthic microbiota, with densities of about  $10^9$  per mL (Rowe and Kennicutt 2002). Protists are less abundant, but most are larger than bacteria. Foraminifera are shelled protozoans that often are extremely abundant in surface layers of slope sediments, particularly where sediments are enriched with organic matter and are hypoxic. Foraminifera often are as large as or larger than most meiofauna. Foraminiferal biomass may exceed that of meiofauna, and abundance often exceeds that of meiofauna and macrofauna combined.

#### 16.2.3.2 Meiofauna

Meiofauna are metazoans between 63 and 300  $\mu\text{m}$  in size, and include nematodes, harpacticoid copepods, ostracods, kinorhynchs, small polychaetes, and several other taxa. Nematodes and

harpacticoids usually are most abundant, but polychaetes and ostracods contribute most to the meiofaunal biomass in slope sediments (Gallaway et al. 2003). Most meiofauna feed on benthic microbiota, other meiofauna, and small detritus particles. Meiofaunal production and turnover often is high, sometimes comparable to that of many microbiota. Production seems to be slower in cold, low nutrient slope sediments than in warmer, organically enriched continental shelf sediments. Nevertheless, meiofaunal biomass often is greater than that of the macrofauna in slope sediments of the Gulf of Mexico (Pequegnat et al. 1990; Rowe and Kennicutt 2002).

Because of their relatively high biomass, meiofauna may be directly or indirectly responsible for much of the organic matter metabolism in slope sediments. Meiofauna graze on particulate organic carbon directly and on the microbiota that are the primary consumers of the organic matter from surface waters and seeps. They probably are responsible for maintaining bacterial populations in log-phase growth and, therefore, are indirectly responsible for maintaining high rates of nutrient cycling (Rowe and Kennicutt 2002).

#### 16.2.3.3 Macroinfauna

Macroinfauna are invertebrates larger than about 0.3 mm (this group of benthic animals is operationally defined by the sieve size used for sampling benthic fauna). About 50% of the benthic macroinfauna of slope sediments are polychaetes (Rowe and Kennicutt 2002). Bivalve mollusks and crustaceans also are abundant. The most abundant taxa of crustaceans often are isopods, amphipods, and tanaids, though penaeid shrimp also may be abundant. Diversity of the slope macroinfaunal community in the Gulf of Mexico is relatively high (Gallaway et al. 2003).

The production-to-biomass ratio of the slope macroinfauna may be well under 1.0, indicating a low turnover rate of macrofaunal biomass. The abundance and biomass of macroinfauna decline sharply with increasing water depth on the slope, reflecting the depth-dependent decline in food availability. Abundance declines less steeply than biomass with depth, indicating that macroinfaunal size decreases with depth (Gallaway et al. 2003). Macroinfaunal abundance is much lower than that of meiofaunal abundance at the four sites evaluated in this risk assessment. For example, the maximum meiofaunal abundance at far-field sites at VK 916 at the time of Cruise 1B was almost two orders of magnitude greater than that of the macroinfauna (90 individuals/cm<sup>2</sup> vs. 1.7 individuals/cm<sup>2</sup>) (see *Chapter 11*).

The mean size of the Gulf of Mexico slope macrofauna is smaller than that of the western North Atlantic slope macroinfauna. The slope macroinfauna feed on one another, on meiofauna, and on organic detritus. Most of the slope polychaetes are selective or non-selective deposit feeders, followed by carnivores, and then scavengers (Gallaway et al. 2003). The macroinfauna in turn are consumed by megafauna and demersal fishes.

#### 16.2.3.4 Megafauna

Megafauna are benthic epifauna that can be sampled with a trawl or other net with a 2.5-cm stretch mesh and that can be seen easily in bottom photographs (about 1 cm or greater in diameter). The dominant megafauna at many slope locations are echinoderms, particularly holothurians. Decapod crustaceans and cnidarians, such as sea anemones, soft corals, and sea pens, also may be common. The giant isopod, *Bathynomus giganteus*, a benthic scavenger,

appears to be most abundant on the upper slope at water depths less than those of the four sites in this study (Barradas-Ortiz et al. 2003).

#### 16.2.3.5 Demersal Fishes

Demersal fishes live and feed on or near the seafloor. Gallaway et al. (2003) identified 153 taxa of demersal fishes in their trawl collections from the continental slope of the Gulf of Mexico. Fishes are more abundant in bottom photographs than estimated by trawls. Fish abundance is variable with depth on the slope of the Gulf of Mexico between 300 and 1,200 m, and then declines steeply to low abundances between 1,300 and 2,900 m (Gallaway et al. 2003). Photographic observations indicated a fish density of about 200 to 300 individuals/ha in the 1,000- to 1,200-m depth interval of the sites evaluated in this risk assessment (Gallaway et al. 2003).

### 16.2.4 Conceptual Model

The conceptual model for risks of drilling discharges to continental slope waters of the Gulf of Mexico describes the chemicals of potential concern (COPCs), their sources, and transport pathways. It describes valued ecosystem components (receptors of concern) at potential risk and the most likely exposure-biological response scenarios and consequences at the population or community level.

#### 16.2.4.1 Chemicals of Potential Concern

The largest volume discharges to the ocean associated with drilling of exploration and development wells for oil and gas on the continental slope of the Gulf of Mexico are drilling fluids (also called drilling muds) and drill cuttings. Three types of drilling muds are used offshore (Neff et al. 2000). They include WBM and two types of non-aqueous drilling fluids, oil based drilling fluids (OBF) and SBM. Only WBM and SBM were used to drill the wells at the sites evaluated in this risk assessment. Bulk WBM and cuttings generated with WBM or SBM are permitted for discharge to Federal waters of the Gulf of Mexico, if they meet effluent limitation guidelines.

WBM is a suspension of particulate materials, dissolved salts, and organic compounds in fresh water, seawater, or a concentrated brine. The base fluids of synthetic based muds, as the name suggests, are well-characterized chemical compounds synthesized specifically for formulation of the mud product (Neff et al. 2000). In SBM, the continuous phase is a synthetic organic ester, ether, acetyl, or olefin (ether and acetyl SBMs are not used in the U.S.). Most SBM used today in the Gulf of Mexico are LAO, internal olefins (IO), or esters (**Table 16.2**). Some SBM formulations contain a mixture of two or three synthetic organic chemicals, usually olefins and esters. LAO, IO, and ester SBM were used to drill SBM sections of the wells drilled at the sites evaluated in this risk assessment (**Table 16.1**). The synthetic chemical usually represents 30% to 90% of the volume and about 20% to 40% of the mass of the SBM (Kenny 1993). The other ingredients in SBM usually are similar to those in WBM. However, larger amounts of emulsifiers are used in SBM than in WBM.

**Table 16.2.** Names and chemical structures of synthetic chemicals used most frequently in the Gulf of Mexico for SBM (From Neff et al. 2000).

Synthetic Chemical Type	Generic Chemical Structure
Linear- $\alpha$ -Olefin (LAO)	$\text{CH}_3 - (\text{CH}_2)_n - \text{CH} = \text{CH}_2$
Internal Olefin (IO)	$\text{CH}_3 - (\text{CH}_2)_m - \text{CH} = \text{CH} - (\text{CH}_2)_n - \text{CH}_3$
Ester	$\begin{array}{c} \text{CH}_3 - (\text{CH}_2)_n - \text{C} = \text{O} \\ \quad \quad \quad \backslash \\ \quad \quad \quad \text{O} - (\text{CH}_2)_m - \text{CH}_3 \end{array}$

Drill cuttings are particles of crushed rock produced by the grinding action of the drill bit as it penetrates into the earth (Neff et al. 1987). Drill cuttings range in size from clay-sized particles ( $\sim 2 \mu\text{m}$ ) to coarse gravel ( $>30 \text{ mm}$ ) and have an angular configuration. Their chemistry and mineralogy reflect that of the sedimentary strata being penetrated by the drill and the amount of drilling mud ingredients adhering to the cuttings at the time of disposal. For example, the metals concentrations in drill cuttings discharged to offshore waters of California are similar to those of the drilling muds used to drill the wells (Phillips et al. 1998). Most of the metals associated with cuttings are in immobile forms in minerals from the geologic formations.

Most of the mass of the ingredients of drilling muds and cuttings is composed of inert solids, particularly barite and clay. Liquid or water-soluble ingredients, other than water, usually are present at low concentrations or have a very low toxicity when diluted in the ocean (most inorganic salts). The few more toxic chemicals, such as bactericides and emulsifiers, usually are used in small enough quantities that they do not pose a risk to the marine ecosystem after discharge to and initial dilution in the ocean.

The ingredients of drilling muds and cuttings of major environmental concern, because of the volumes used and discharged or their potential for toxicity, are metals and hydrocarbons, including SBF chemicals. Most of the metals in drilling muds and cuttings are associated with the drilling mud solids, barite and clay, or with cuttings particles and are in solid, immobile forms. Several metals are present in most WBM and SBM (**Table 16.3**). The metals of greatest concern, because of their potential toxicity and/or abundance in drilling fluids, include arsenic, barium, cadmium, chromium, copper, iron, lead, mercury, nickel, and zinc (Neff et al. 1987, 2000). Some of these metals are added intentionally to drilling muds as metal salts or organo-metallic compounds. Others are present as trace impurities in major mud ingredients, particularly barite and clay.

**Table 16.3.** Concentration ranges of several metals in water based muds (WBM) from different sources and in typical soils and marine sediments. Concentrations are mg/kg dry wt (ppm). Modified from Neff et al. (1987). Metals that sometimes are present in drilling muds at concentrations more than 10 times those in natural sediments are shaded and bold.

Metal	Drilling Muds <sup>1</sup>	Clay-Loam Soils <sup>2</sup>	Sediments <sup>3</sup>
<b>Barium</b>	<b>720 – 449,000</b>	<b>150 – 1,500</b>	<b>1 – 2,000</b>
<b>Chromium</b>	<b>0.1 – 5960</b>	<b>20 – 100</b>	<b>36 – 110</b>
Cadmium	0.16 – 54.4	0.01 – 7	0.1 – 0.6
Copper	0.05 – 307	7 – 70	7 – 33
Iron	0.002 – 27,000	---	20,000 – 60,000
<b>Mercury</b>	<b>0.017 – 10.4</b>	<b>&lt;0.01 – 0.90</b>	<b>0.03 – 0.14</b>
<b>Lead</b>	<b>0.4 – 4226</b>	<b>&lt;10 – 70</b>	<b>10 – 33</b>
<b>Zinc</b>	<b>0.06 – 12,270</b>	<b>20 – 220</b>	<b>27 – 88</b>
Nickel	3.8 – 19.9	5 – 50	13 – 45
Arsenic	1.8 – 2.3	1.7 – 27	6.9 – 26
Vanadium	14 – 28	---	63 – 238
Aluminum	10,800	---	10,000 – 90,000
Manganese	290 – 400	50 – 2,000	100 – 10,000

<sup>1</sup> From Neff (1982); <sup>2</sup> from Breckenridge and Crockett (1995); <sup>3</sup> from Robertson and Carpenter (1976), Siegel et al. (2000), and Neff (2002b).

The metals most frequently present in drilling muds at concentrations more than 10-fold greater than natural concentrations in soils and sediments are barium, chromium, lead, and zinc (**Table 16.3**). Mercury sometimes is present at elevated concentrations in U.S., Canadian, and North Sea drilling muds; it is derived from mercury present in drilling mud barite (Neff 2002a). The USEPA (1993) placed restrictions on the maximum concentration of mercury in drilling mud barite destined for ocean disposal. With wider use of low-trace-metal barite for drilling muds, average mercury concentrations in U.S. WBM have declined, though concentrations usually still are higher than background concentrations in clean marine sediments. Barite in drilling muds used offshore in U.S. waters since 1993 contains an average of about 0.5 ppm mercury (Candler, personal communication 2002).

The most abundant metal in most WBM is barium. Nearly all the barium in drilling mud is from barite (BaSO<sub>4</sub>) added to the mud to increase its density. Clays and clay-rich shales may contain high concentrations of barium. Natural marine sediments and the cuttings themselves also contain barium; barium concentration in sediments tends to be inversely related to sediment grain size. Clean, fine-grained marine sediments may contain more than 1,000 mg/kg barium. Most of the barium in sediments is in barite. Many hydrocarbon seeps in the Gulf of Mexico contain high concentrations of barium, which precipitates rapidly upon mixing with seawater (rich in sulfate) forming barite chimneys (Aharon et al. 2001).

Barite in drilling muds and sediments has a low solubility in seawater (81 µg barite/L or 48 µg Ba/L), because of the high natural concentration of sulfate in the ocean. Because it is insoluble in seawater, it has a low bioavailability and low toxicity to marine organisms.



When present at elevated concentrations, compared to concentrations in clean sediment, drilling mud chromium is derived primarily from chrome- or ferrochrome-lignosulfonates or chromate salts added intentionally to the mud for viscosity control. Barite and bentonite clay also may contain traces of chromium. The chromium in a used drilling mud, even that added as chromate, is in the trivalent, chromic valence state. Trivalent chromium salts have low solubilities and limited mobility in the environment. They usually have a low toxicity to plants and animals. Because of concerns about the environmental impacts of chromium in drilling muds, operators in most offshore areas have replaced chrome lignosulfonates with chrome-free mud thinners. Most modern WBM and SBM contain low concentrations of chromium.

Most of the other metals sometimes detected in drilling muds are present primarily as trace impurities in barite, clay, or the drill cuttings in the formation penetrated by the drill bit. The most abundant metals in barite are barium (not a true metal), lead, zinc, and iron. Lead, zinc, and copper also may enter drilling mud in pipe thread compound (pipe dope) or drill collar dope used to lubricate the threads and promote electrical conduction between pipe sections (Ayers et al. 1980). The dopes contain several percent metallic metal; some of the dope gets into the drilling mud, contaminating it. Various zinc salts may be added intentionally to drilling mud for control of hydrogen sulfide.

The COPCs used for this risk assessment were selected based on the information discussed above and include:

- SBF chemicals (IO, LAO, ester)
- Petroleum hydrocarbons (particularly polycyclic aromatic hydrocarbons [PAH])
- Total organic carbon (TOC)
- Cuttings particles
- Metals (barium, chromium, lead, mercury, and zinc)

#### *16.2.4.2 Sources and Transport Pathways*

Offshore discharge of drilling wastes to Federal waters of the Gulf of Mexico is limited to those drilling muds and cuttings that meet the regulatory requirements of the general NPDES permit. Only WBM and cuttings generated with WBM or SBM are permitted for discharge, if they meet effluent limitations guidelines. Spud muds, WBM containing bentonite clay and (sometimes) barite, and cuttings from the upper interval of a well meet effluent limitations guidelines and are discharged directly to the seafloor. After the riser is installed, cuttings recovered from the solids control equipment on the platform are flushed with seawater into a central discharge pipe (shunt line) that releases the cuttings just above or below the sea surface (Canadian Association of Petroleum Producers 2001). Occasionally, if the platform is in an environmentally sensitive area, the MMS may require that the shunt line extend to near the seafloor. None of the mud and cuttings discharges at the four sites evaluated in this risk assessment were shunted.

WBM or SBM cuttings are discharged continuously during actual drilling, which usually occurs about half the time during drilling of a well. Drill cuttings containing 5% to 10% adsorbed WBM solids usually are discharged to the ocean at a rate of 0.2 to 2 m<sup>3</sup>/hour (53 to 530 gallons/hour) (Neff et al. 1987). SBM cuttings discharged to the Gulf of Mexico during the years of this

investigation usually contained 7% to 15% SBF chemical (Annis 1997). The general NPDES permit for the Western Gulf of Mexico, introduced in February 2002, requires that retention of synthetic base chemical on cuttings not exceed 6.9% (internal olefins) or 9.4% (esters). All drilling in this study occurred before the new permit came into effect, so there probably was an average of about 10% SBF chemical on SBM cuttings discharged at the four sites. Drilling rates often are higher with SBM than with WBM, with a concomitant increase in the rate of SBM cuttings discharge, compared to WBM cuttings discharge, during drilling. However, there are no bulk discharges of drilling muds during drilling with SBM; therefore, total volumes of drilling wastes discharged are much smaller when SBM rather than WBM are used.

There often are periodic bulk discharges of used WBM, particularly when the composition of the WBM system must be changed to address down-hole conditions or at the time of switch-over from a WBM to an SBM during drilling of deep or deviated sections of the well. In addition, when drilling a clay-rich formation, WBM mud viscosity may be controlled by dilution (addition of make-up water) of the return from the shale shaker to maintain an optimum bentonite clay concentration and viscosity. This WBM management strategy requires frequent bulk discharges of drilling mud.

Estimated volumes of drilling muds and cuttings discharged at the four sites are summarized in **Table 16.1**. Total discharges within 500 m of site center ranged from 20,556 bbl during drilling of a single exploratory well at VK 916 to 159,302 bbl during drilling of seven wells at GB 602. The largest drilling discharge at all four sites was bulk WBM, followed by SBM cuttings. As discussed above, WBM was used to drill the upper sections of the wells. In most cases, there was a switch-over to the more expensive SBM systems for drilling the deepest sections of the wells or for sidetracks where the superior technical properties of the SBM are needed.

When WBM and WBM cuttings are discharged to the ocean, the larger particles, representing about 90% of the mass of the mud solids, form a plume that settles quickly to the bottom (or until the plume entrains enough seawater to reach neutral buoyancy) (**Figure 16.2**). About 10% of the mass of the mud solids consisting of fine-grained unflocculated clay-sized particles and a portion of the soluble components of the mud form another plume in the upper water column that drifts with prevailing currents away from the platform and is diluted rapidly in the receiving waters (Ayers et al. 1980; Brandsma et al. 1980; National Research Council 1983). The fine-grained solids in the upper plume settle slowly over a large area of the seafloor. Recent WBM dispersion modeling predicts rapid dilution of WBM and WBM cuttings in the receiving water environment (Nedwed et al. 2004; Smith et al. 2004).

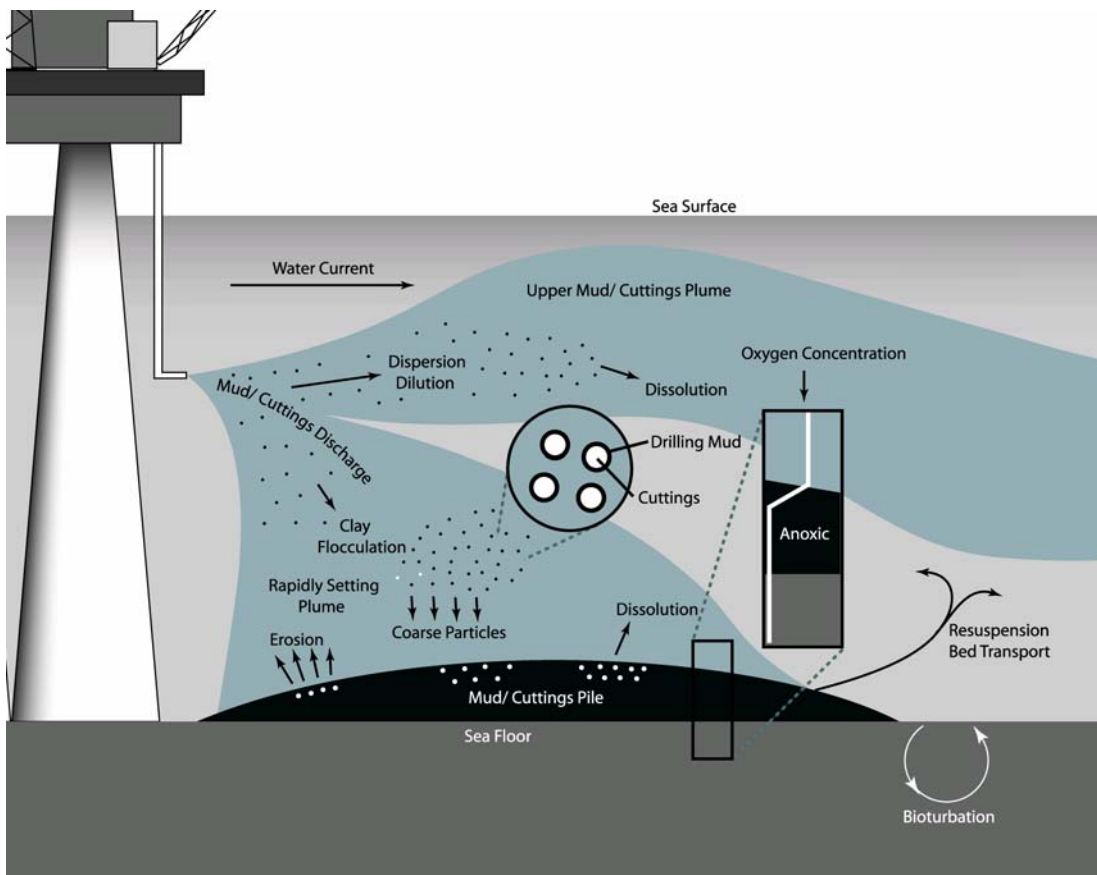


**Figure 16.2.** Dispersion and fates of drilling muds and cuttings following discharge to the ocean.

When discharged to the ocean, SBM cuttings containing more than about 5% adhering SBM solids tend to clump together in discrete masses that settle rapidly to the seafloor (Brandsma 1996; Delvigne 1996). Water cannot penetrate the hydrophobic mass of cuttings, so the cuttings do not disperse efficiently. Ester-based SBM cuttings disperse more readily than cuttings containing a synthetic olefin (Growcock et al. 1994).

Because most SBM cuttings do not disperse effectively in the water column following discharge, they settle rapidly through the water column and accumulate on the seafloor near the discharge site (Neff et al. 2000). Because of the rapid settling of SBM cuttings, water depth has relatively little effect on the depth and areal extent of SBM cuttings accumulations on the bottom (as compared with those of WBM cuttings). SBM cuttings accumulate in a very patchy distribution within a short radial distance of the discharge point.

SBM cuttings accumulations were surveyed near a drilling template at the Pompano II exploratory drilling site in Mississippi Canyon Block 28 (MC 28) in 565 m of water south of the Mississippi River in the northern Gulf of Mexico (Gallaway et al. 1997; Fechhelm et al. 1999). Discharges from the rig included 7,700 bbl of WBM cuttings, 5,150 bbl of SBM cuttings, and an estimated 7,695 bbl of Petrofree LE (an SBF base chemical containing 90% LAO and 10% ester), which was associated with the cuttings. Remotely operated vehicle (ROV) surveys revealed a thin layer of cuttings spread in a patchy distribution on the seafloor near the drilling template.

Maximum cuttings accumulations appeared to be 20 to 25 cm thick in some locations. These larger cuttings accumulations probably were derived from direct drilling returns to the seafloor during initial drilling with spud WBM before the riser was installed. There was no clear gradient of SBM cuttings concentrations with distance in the small radius (<90 m) surveyed.

More recently, a monitoring program was performed near eight WBM and SBM discharge sites in 37 to 556 m of water in the Gulf of Mexico (Continental Shelf Associates, Inc. 2004). There was clear evidence of accumulation of drilling discharge solids in seafloor sediments near all the discharge sites; however, it was not possible to determine the relative proportions of WBM, WBM cuttings, and SBM cuttings in sediments. Most mud and cuttings appeared to be deposited within 100 and 250 m of the discharge site at both continental shelf and continental slope water depths. Thus, most drilling discharge solids accumulate in sediments near the discharge sites; only small amounts are dispersed over a wide area of the seafloor.

#### 16.2.4.3 Receptors of Concern

A study panel of the National Research Council (1983) examined all the information available at that time on the environmental fates and effects of WBM and cuttings discharges to marine waters and concluded:

*“Based on laboratory and field studies to date, most water-based drilling fluids used on the U.S. OCS have low acute and chronic toxicities to marine organisms, (because of) the expected or observed rates of dilution and dispersal of drilling muds in the ocean after discharge. Their effects are restricted primarily to the ocean floor in the immediate vicinity and for a short distance downcurrent from the discharge. The bioaccumulation of metals from drilling fluids appears to be restricted to barium and chromium and is observed to be small in the field.”*

The same generalizations apply to SBM cuttings (Neff et al. 2000; OGP 2003; Melton et al. 2004). As a general rule, effects of drilling mud and cuttings discharges on the benthic environment are related to the total mass of drilling solids discharged and the relative energy of the water column and benthic boundary layer at the discharge site. Near-bottom water currents usually are low at continental slope depths in the Gulf of Mexico. Thus, drilling discharge solids tend to accumulate on the bottom near the discharge and persist there.

A sediment quality triad analysis was performed at three continental shelf sites where WBM and WBM and SBM cuttings had been discharged (Continental Shelf Associates, Inc. 2004). The analysis indicated gradients of decreasing sediment physical and biological disturbance with distance from the discharge site and with time after the last drill cuttings discharge, showing that ecosystem recovery was occurring. The most important direct effect of accumulation of SBM cuttings in near-field sediments was a depletion of oxygen in surficial sediments as a result of microbial activity stimulated by organic enrichment of the sediments. This led to an alteration of macrofaunal community structure. Thus, biological effects of the cuttings accumulations appeared to include microbial, meiofaunal, and macrofaunal communities, and possibly megafaunal communities as well.

Based on the preceding discussion, the receptors of concern for this risk assessment are the near-field benthic and demersal communities at the discharge sites. Water column organisms will not be included because they are at low risk of harm from drilling discharges.

### 16.3 EXPOSURE ASSESSMENT

Several approaches were used to assess exposure of benthic biological communities to physical disturbance and the COPCs from drilling discharges at the four deepwater discharge monitoring sites. Side-scan sonar and chirp sonar subbottom profiling were used to map physical disturbance and cuttings accumulation and distribution on the seafloor. Surface sediment samples and sediment cores were collected in the near-field ( $\leq 500$  m) and far-field ( $\geq 10,000$  m) of each discharge site and analyzed for SBF chemicals, PAH, and TOC to document the distribution and exposure concentrations of organic chemicals associated with drilling discharges. Thirteen metals also were analyzed in the sediment samples. Barium was used as the main tracer of the distribution and relative concentration of drilling mud solids on the seafloor. Several metals may occur in drilling muds and cuttings at concentrations significantly higher than their concentrations in uncontaminated marine sediments. These metals, including arsenic, cadmium, chromium, copper, lead, mercury, nickel, vanadium, and zinc, were analyzed in sediments and tissues of benthic marine animals as an indication of exposure of benthic fauna to excess amounts of metals from drilling discharges. Three other metals were analyzed as an aid to determining the phase associations and possible sources of the metals in sediments and the redox state of the sediments. These metals are aluminum, iron, and manganese. Finally, two species of benthic/demersal megafauna were collected from two sites in July 2001 and analyzed for PAH and 11 metals as an indication of direct exposure to bioavailable forms of organic and metal ingredients of drilling muds and cuttings.

#### 16.3.1 Physical Disturbance of Sediments

##### 16.3.1.1 Anchor Scars

Side-scan sonar surveys and chirp sonar subbottom profiling revealed evidence of anchor scars in the near-field (approximate 3-km radius) at all four sites (see *Chapter 4*). Anchors (usually at least eight) are deployed in a radial pattern around most floating drilling rigs (**Figure 16.1**). The anchor radius depends primarily on water depth. At the water depths of the study sites (1,033 to 1,125 m), anchor radius ranged from 2,377 m to  $>3,000$  m (see *Chapter 3*). Some of the anchor chain between the anchor and the platform rests on or just above the bottom. The anchor chains scour the bottom, producing a radial array of scars on the seafloor. Individual anchor scars ranged in length from about 100 m to more than 3,000 m. Anchor scars from other wells drilled within the block or in adjacent blocks were identified at all four drilling sites. The largest number of anchor scars was at GB 602 (over 80 individual scars, including those associated with wells in adjacent blocks). These linear anchor scars caused a localized disturbance of the soft-bottom seafloor between about 500 and 3,000 m from the site center.

##### 16.3.1.2 Seafloor Equipment

Development of deepwater oil and gas resources requires emplacement of substantial amounts of equipment on the seafloor (Regg et al., 2000; Ward, 2000). This equipment includes the template and wellhead for each well, pipelines and flowlines, umbilical termination modules, etc. The

seafloor equipment causes localized disturbance of the seafloor. If bottom currents and bed transport are high, sediment scour may occur around the seafloor structures. Physical disturbance from seafloor structures is highly localized and probably has minimal impacts on area-wide benthic communities (MMS, 2000a). However, at sites with low sediment accumulation rates and low bottom current speeds, the disturbance of bottom topography by the seafloor structures usually is persistent. Production-related equipment was emplaced on the seafloor at the three development sites (GB 516, GB 602, and MC 292), but not at the exploration site (VK 916).

#### 16.3.1.3 Accumulation of Drilling Muds and Cuttings

The most important physical disturbance of the seafloor from drilling activities, based on areal extent of disturbance and potential for alteration of benthic communities, is accumulation of solids on the seafloor from drilling mud and cuttings discharges. Accumulation of drilling mud and cuttings solids on the seafloor may cause changes in sediment texture and mineralogy, sediment redox depth, and bottom topography. Large accumulations of solids in a small area (primarily when cuttings are shunted to the bottom) may bury benthic fauna. These physical changes to the seafloor may cause changes in benthic community structure and function.

The areal distribution of drilling muds and cuttings on the seafloor in the near-field of the four sites was estimated in *Chapter 4*. Tentative identification of mud and cuttings solids on the seafloor was based on intensity of acoustic signals returned from side-scan sonar and chirp sonar subbottom profiles of mud and cuttings particles, which are denser than surficial sediments. Concentrations of barium and SBF chemical usually were higher in sediments from areas where mud and cuttings accumulations were detected. This observation lends support to the hypothesis that cuttings accumulations were observed in the sonar images.

Zones identified as drilling muds/cuttings were mapped in a small area (0.8 to 2.5 ha) around the site center at three of the four drilling sites (see *Chapter 15, Table 15.4*). The discharges that accumulated in these zones probably were a mixture of spud WBM and cuttings released to the seafloor during initial spudding of the wells before the marine riser was set. These areas also were the sites of bottom equipment installations, such as templates and wellheads, which may have contributed to the local bottom sediment disturbance.

Cuttings, presumably from rig discharges, were tentatively identified over a larger area at each drilling site. The area of cuttings accumulations ranged from 13.4 ha at VK 916, where a single exploration well was drilled, to 108.5 ha at GB 516, a post-development site where two exploration wells had been drilled before the study and five development wells were drilled during the study. The areal extent of mud and cuttings accumulations on the bottom increased as the number of wells drilled before or during the study increased (see *Chapter 15*).

Surficial sediments at the far-field sites were predominantly hemipelagic silts and clays with median grain sizes of 1.6 to 2.4  $\mu\text{m}$  (*Chapter 5*). Mean TOC concentration in far-field sediments ranged from 0.5% to 1.5%. Drill cuttings span a wide range of grain size from fine clays to coarse sands and gravels. Thus, accumulation of cuttings in sediments should result in an increase in mean grain size or the fraction of sandy sediments in the near-field.

Sediment profile imaging (*Chapter 6*) identified a thin layer of sand-sized organic-mineral aggregates overlying a uniform layer of clay sediments in the near-field at GB 516 and VK 916 after drilling. This mineral aggregate layer also was present in near-field sediments at VK 916 at the time of the pre-drilling survey in October-November 2000. Therefore, it is uncertain if these aggregates represent drill cuttings. Surface accumulations of coarse particles in near-field sediments were not reported from sediment profile imaging surveys at GB 602 and MC 292 (*Chapter 7*). All surficial sediments at GB 602 were silt-clay, whereas those at MC 292 were predominantly clay. A few near-field sediments at all four sites contained slightly elevated concentrations of sand. The highest sand concentration (21%) was in a near-field sediment sample from GB 602 (*Chapter 5*). The sediment grain size data provide some evidence of the presence of small amounts of cuttings in near-field sediments at the four sites.

### 16.3.2 Chemical Alteration of Sediments

#### 16.3.2.1 Synthetic Based Fluids

Because SBF base chemicals are well-characterized synthetic mixtures of a small group of organic isomers, they are good tracers of the fate and distribution of the organic phase of SBM cuttings in the marine environment. SBM cuttings discharged offshore in the Gulf of Mexico during this monitoring study probably contained an average of 9% to 12% SBF chemical (Annis 1997). SBF chemicals biodegrade slowly following discharge of SBM cuttings to the ocean (Neff et al. 2000); therefore, concentrations in sediments near a discharge site tend to decrease with time after completion of drilling and cessation of discharges. SBF chemicals in sediments may adversely affect benthic communities by direct toxicity or by organic enrichment and associated development of sediment hypoxia (including production of toxic sulfide and ammonia) caused by microbial degradation of the organic chemicals (Neff et al. 2000; Hartley et al. 2003; Continental Shelf Associates, Inc. 2004).

Far-field sediments from the four sites contained <1.4 to 111 µg/g dry wt (parts per million) SBF chemical (**Table 16.4**). The highest value (for VK 916 FF2) may represent contamination from discharges from wells drilled in an adjacent block (see *Chapter 3*). Most far-field sediments contained 2 to 10 µg/g SBF chemical, which probably represents background concentrations of biogenic and possibly petroleum hydrocarbons that coelute with synthetic olefins in the analytical procedure. Near-field sediments collected in November 2000 from VK 916 contain background concentrations, reflecting the lack of drilling at this site before the November 2000 field survey. Far-field sediments containing more than about 10 µg/g SBF chemical may have received small amounts of SBM cuttings from the drillsites monitored or from other drilling activities in the vicinity of the monitored sites.

SBF chemical concentrations in near-field and discretionary sediment samples ranged from <1.4 mg/kg to more than 136,000 µg/g (13.6%) (**Table 16.4**). These sediment samples were collected at 12 randomly-selected stations and three discretionary stations, selected to maximize the likelihood of detecting drilling discharge solids, within 500 m of site center at each drillsite. The near-field samples were collected from the upper 2 cm of sediment and the discretionary samples were collected from five depth intervals between 0 and 10 cm in sediments to document the vertical distribution of SBF residues.

**Table 16.4.** Concentrations of synthetic based fluid (SBF) chemical in near-field, far-field, and discretionary box core sediments from the four sites monitored in this investigation. Near-field and far-field sediments were from the upper  $\approx$  2 cm; discretionary samples were from different depth intervals between 0 to 2 cm and 8 to 10 cm. Data from *Chapter 9*.

Site	Date	SBF Chemical Concentration Range ( $\mu\text{g/g}$ dry)		
		Near-Field	Discretionary	Far-Field
VK 916	Nov 2000	2.4 – 6.6	---	4.3 – 7.2
	Aug 2002	7.5 – 47,920	159 – 28,138	2.2 – 111 <sup>a</sup>
GB 516	Nov 2000	5.4 – 25,131	---	2.0 – 9.4
	July 2001	56.0 – 29,167	21 – 136,297	3.0 – 7.0
GB 602	July 2001	462 – 13,792	11.0 – 10,572	3.0 – 10.0
MC 292	July 2001	<1.4 – 2,408	9.0 – 714	<1.4 – 28.0

<sup>a</sup> One far-field site may have become contaminated by drilling discharges from an adjacent lease block.

The wide range of SBF chemical concentrations observed in sediments collected within 500 m of the four sites demonstrates the extremely patchy and heterogeneous distribution of SBM cuttings. Highest concentrations generally were located in regions mapped geophysically as cuttings (*Chapter 15*). Highest SBF chemical concentrations were in near-field surface sediments collected at VK 916 in August 2002 shortly after completion of a single exploratory well. Four (of 12) near-field samples contained more than 5,000 mg/kg SBF chemical. The 0 to 2-cm layer of sediment from the three discretionary stations contained more than 10,000  $\mu\text{g/g}$  SBF chemical (range, 10,431 to 28,138  $\mu\text{g/g}$ ). Deeper layers in these discretionary samples contained less than 4,000 mg/kg SBF chemical, and concentration decreased with depth in the sediments. Thus, SBM cuttings were present in near-field sediments as a surface layer. There was no evidence of accumulation of SBM cuttings in far-field sediments at VK 916 (a single high concentration was attributed to discharges from drilling activities in an adjacent lease block).

Near-field sediments at GB 516 and GB 602 contained similar concentration ranges of SBF chemical (**Table 16.4**). The SBF concentration range was smaller at GB 602 than at GB 516, reflecting a more uniform distribution of SBM cuttings in surface sediments at the former site. SBF concentrations in all but one near-field sample from the two sites were higher than in all far-field samples, suggesting that most SBM cuttings deposition was within about 500 m of the discharge location.

The highest concentration of SBF chemical in two of the three discretionary samples from GB 516 was in the 2 to 4-cm depth interval. All three samples in the 0 to 6-cm depth interval in one discretionary sample contained more than 10% SBF chemical, indicating nearly exclusively cuttings solids in the sample. The near-surface, 0 to 2-cm interval contained the highest SBF chemical concentration in the three discretionary samples from GB 602. Drilling had occurred in the near-field at GB 516 between July 1999 and February 2001 (within five months of the July 2001 survey) and at GB 602 between September 1995 and January 2001 (within six months of the July 2001 survey). Thus, the vertical distribution of SBM cuttings in sediments at the two sites was not related to time between completion of drilling and sample collection.



Sediments at MC 292 contained the lowest concentrations of SBF chemical. Only 5 of 12 near-field samples and 2 of 15 discretionary samples contained more than 100 µg/g SBF chemical. This site was the closest of the four sites to the mouth of the Mississippi River (69 km) and had the highest sediment accumulation rate (0.14 cm/year). Five wells had been drilled within 500 m of site center between February and July 1999, more than two years before the survey. Thus, the low SBF chemical concentrations in near-field sediments at MC 292 can be attributed to dilution of cuttings with natural sediments and biodegradation of the SBF chemical. MC 292 also had the lowest volume of SBM discharges (*Chapter 3*).

### 16.3.2.2 Polycyclic Aromatic Hydrocarbons

PAH are composed of two or more fused benzene rings. PAH in the environment are derived primarily from petroleum and from combustion of organic matter (Neff 2002b). Their concentrations were determined in this monitoring program as an indication of possible petroleum contamination of deepwater sediments from drilling discharges.

Modern WBM and SBM rarely contain more than traces of PAH. OBF formulated with diesel fuel or mineral oil may contain PAH. Enhanced mineral oils used to formulate modern OBF contain less than 0.001 weight percent (1 µg/g) total PAH (Jacques et al. 1992). OBF and OBF cuttings, even those prepared with enhanced mineral oil, have never been permitted for discharge to U.S. territorial waters.

Cuttings produced during drilling with WBM or SBM may contain small amounts of petroleum hydrocarbons. The hydrocarbons may come from spotting fluids and lubricants added to the mud, or from the geologic strata being penetrated by the drill. Drilling mud and cuttings from all depths in a well off California contained petroleum hydrocarbons, including PAH (**Table 16.5**). The drilling muds contained higher concentrations of total petroleum hydrocarbons (TPH) and lower concentrations of total and individual PAH than the cuttings at all depths, suggesting that the PAH were derived primarily from the formations being drilled. Cuttings from well intervals through hydrocarbon-bearing formations contain high concentrations of petroleum hydrocarbons and are not permitted for ocean discharge. However, some may be discharged with cuttings from shallower or deeper strata.

**Table 16.5.** Concentrations of hydrocarbons in composite samples of water based mud (WBM) and drill cuttings (in parentheses) from three drilling depths in a well in the Point Arguello Field, California. Concentrations are µg/g dry wt (ppm). From Steinhauer et al. (1994).

Chemical	Surface	Mid-Well	Bottom	Average
Total Petroleum Hydrocarbons <sup>1</sup>	159 (600)	137 (95)	988 (526)	390 (407)
Total PAH <sup>2</sup>	0.87 (2.3)	8.0 (12)	51 (121)	25 (45)
Naphthalenes <sup>3</sup>	0.27 (1.2)	5.4 (8.9)	39 (96)	18 (35)
Fluorenes <sup>3</sup>	ND (ND)	0.38 (0.35)	4.1 (8.2)	2.8
Phenanthrenes <sup>3</sup>	0.34 (0.79)	0.94 (0.64)	4.5 (9.3)	2.8 (3.6)
Dibenzothiophenes <sup>3</sup>	0.03 (ND)	0.71 (0.40)	3.9 (8.1)	1.9 (2.8)

<sup>1</sup> Total resolved + unresolved hydrocarbons.

ND = Not detected.

<sup>2</sup> Total 2- through 5-ringed PAHs plus alkyl homologues.

<sup>3</sup> Includes parent PAH and alkyl homologues.

The source of the high TPH in the cuttings from near the surface is unknown. Total and individual PAH concentrations increased with depth in the well. TPH and PAHs in the cuttings from the bottom of the well closely resembled the crude oil in the reservoir and probably were from the hydrocarbon-bearing formation.

Uncontaminated marine sediments usually contain small amounts of PAH (Neff 2002b). Most of the PAH in offshore marine sediments are from human sources, including petroleum product use and combustion of fossil fuels. Concentrations in sediments tend to decrease with distance from human activities and with increasing water depth. Background concentrations of total PAH in sediments from the continental slope and rise off southern New England are about 0.1 µg/g in surface layers and 0.01 to 0.02 µg/g in the 24 to 35-cm depth interval of sediment cores (Venkatesan et al. 1987). Deep-sea sediments from 2,505 to 5,906 m water depth in the central Pacific Ocean contain 0.0008 to 0.061 µg/g total PAH (sum of 17 analytes) (Ohkouchi et al. 1999). In areas where there is offshore oil production activity or natural oil seeps, sediment PAH concentrations may be much higher. Continental shelf and estuarine sediments off Texas have a background total PAH concentration of about 0.03 µg/g and 0.1 ng/g, respectively (Brooks et al. 1990). Sediments near three platforms in 20 to 150 m of water in the Gulf of Mexico, monitored in the GOOMEX program, contained 0.008 to 1.24 µg/g total PAH (Kennicutt et al. 1996b). Surface sediments from the continental slope of the central and western Gulf of Mexico, including seep areas, sampled during Cruise 1 of the Deepwater Gulf of Mexico Program contained <0.01 to 1.03 µg/g total PAH (Rowe and Kennicutt 2002). Highest concentrations were in lower shelf and upper slope sediments off the Mississippi River and in areas of the upper slope near seeps and brine pools.

Concentrations of total PAH in near-field and far-field sediments from the four sites ranged from 0.012 to 23.84 µg/g dry wt (**Table 16.6**). The highest concentrations were in the surface layer of a discretionary sediment core collected at GB 516. The sediment core containing the highest PAH concentration contained more than 16 µg/g total PAH in the four depth intervals between 0 to 2 cm and 6 to 8 cm, with concentration decreasing slightly with depth in the core. This sediment core also contained high concentrations ( $\geq 10,000$  µg/g) of SBF chemical. The sediments in this core also contained elevated (compared to other sediment samples) concentrations of barium, mercury, lead, and TOC (see *Chapter 8*). The PAH in these samples probably were derived from drilling discharges.

**Table 16.6.** Concentrations of total polycyclic aromatic hydrocarbons (PAH) in near-field, far-field, and discretionary box core sediments from the four sites. Near-field and far-field sediments were from the upper  $\approx 2$  cm; discretionary samples were from different depth intervals between 0 to 2 cm and 8 to 10 cm. Data from *Chapter 9*.

Site	Date	Total PAH Concentration Range (µg/g dry)		
		Near-Field	Discretionary	Far-Field
VK 916	Nov 2000	0.16 – 0.29	---	0.18 – 0.39
	Aug 2002	0.25 – 0.44	0.012 – 2.16	0.18 – 0.40
GB 516	Nov 2000	0.19 – 3.47	---	0.12 – 0.44
	July 2001	0.14 – 0.43	0.043 – 23.84	0.15 – 0.25
GB 602	July 2001	0.13 – 0.55	0.12 – 0.65	0.094 – 0.15
MC 292	July 2001	0.17 – 0.74	0.094 – 0.55	0.21 – 0.75

Most sediment samples from the four sites contained total PAH concentrations higher than background for deepwater sediments. There was no difference in total PAH concentrations in near-field and far-field sediments (**Table 16.6**). Thus, with the exception of the discretionary sediment core from GB 516 discussed above, it is uncertain if the excess PAH came from drilling discharges or other development and production activities.

One of the sediment samples from the discretionary cores at VK 916 contained more than 2 µg/g total PAH. Because no development and production activities occurred at this site, it is possible that the excess PAH in near-field sediments were from drilling discharges. However, two wells were drilled 2.3 km from the site in VK 872 in late 1998, and eight wells were drilled 4.6 to 7.4 km from the site in VK 915 in between January 2001 and June 2002, before the August 2002 field survey (see *Chapter 3*). The sediment PAH and SBF concentrations may have come from these development activities.

### 16.3.2.3 Total Organic Carbon

Mean TOC concentrations in far-field sediments at the four sites ranged from 0.82% to 1.53% (**Table 16.7**) (see *Chapter 8*). Highest concentrations were in sediments from sites nearest the mouth of the Mississippi River (MC 292 and VK 916). These concentrations are typical for fine-grained continental shelf and slope sediments.

**Table 16.7.** Mean ( $\pm$  standard deviation) and range of concentrations of total organic carbon in sediments from the four study sites. Data from *Chapter 8*.

Site	Date	Total Organic Carbon (%)	
		Near-Field	Far-Field
VK 916	Nov 2000	1.54 $\pm$ 0.21 (1.3 – 1.9)	1.44 $\pm$ 0.11 (1.3 – 1.6)
	Aug 2002	2.02 $\pm$ 0.77 (1.4 – 3.4) <sup>a</sup>	1.53 $\pm$ 0.13 (1.3 – 1.7)
GB 516	Nov 2000	1.25 $\pm$ 0.69 (0.8 – 3.3) <sup>b</sup>	0.82 $\pm$ 0.08 (0.7 – 1.0)
	July 2001	1.32 $\pm$ 0.51 (0.8 – 2.9) <sup>b</sup>	1.08 $\pm$ 0.07 (1.0 – 1.3)
GB 602	July 2001	1.44 $\pm$ 0.28 (1.1 – 2.0) <sup>b</sup>	1.12 $\pm$ 0.13 (0.9 – 1.3)
MC 292	July 2001	1.35 $\pm$ 0.12 (1.2 – 1.6)	1.41 $\pm$ 0.08 (1.3 – 1.5)

<sup>a</sup> NF post-expl. >NF pre-expl.; <sup>b</sup> NF > FF.

There was a statistically significant increase in sediment TOC concentrations in near-field sediments between the pre-drilling and post-drilling surveys at VK 916. TOC concentrations were significantly higher in near-field than in far-field sediments at GB 516 and GB 602 (**Table 16.7**). The discretionary sediment core from GB 516 containing high concentrations of SBF chemical and total PAH also contained higher TOC concentrations (6.5% to 8.9% in July 2001) than any of the other sediment samples from the four sites. These results suggest that part of the sediment TOC was associated with drilling discharges.

### 16.3.3 Metals in Sediments

Trefry et al. (*Chapter 8*) measured concentrations of 13 metals in near-field, far-field, and discretionary core sediments collected in November 2000 and August 2002 at VK 916, in November 2000 and July 2001 at GB 516, and in July 2001 at GB 602 and MC 292. The metals include aluminum, arsenic, barium, cadmium, chromium, copper, iron, lead, manganese, mercury, nickel, vanadium, and zinc. Aluminum, iron, and manganese are useful for evaluating the solid phase associations of the other metals. The metal COPCs in this risk assessment, because of their frequent presence at elevated concentrations in drilling muds (**Table 16.3**), are barium, chromium, mercury, lead, and zinc.

#### 16.3.3.1 Barium

Background concentrations of barium in uncontaminated marine sediments increase with decreasing sediment grain size and increasing water depth and range from about 1 to 2,000 mg/kg (**Table 16.3**).

Mean barium concentrations in far-field sediments from the four sites range from 850 mg/kg to 1,480 mg/kg (**Table 16.8**). Barium concentrations in near-field sediments collected in November 2000 at VK 916 are comparable to those in far-field sediments and reflect the lack of drilling operations in the immediate vicinity of the site center previous to the November sampling. These sediment barium concentrations are somewhat higher than expected background concentrations for slope sediments and probably reflect drilling waste inputs from previous drilling operations at nearby sites.

All near-field sediments, except those collected in November 2000 at VK 916, contained significantly higher barium concentrations than far-field sediments collected at the same time (**Table 16.8**). Highest mean concentrations were in near-field sediments collected in July 2001 at GB 516 and GB 602. Barium concentrations were highest in surface layers of sediments from discretionary cores collected at all four drilling sites, and barium concentration decreased with increasing depth below the surface in the cores (*Chapter 8*). This suggests recent deposition of barium, as solid barite, in near-field sediments at all four sites. There is little doubt that the enrichment in barium concentrations in near-field sediments at the four sites was caused by deposition of drilling mud solids from WBM, WBM cuttings, and SBM cuttings discharges. Mean barium enrichments (NF [barium]/FF [barium]) ranged from 12- to 60-fold.

**Table 16.8.** Mean ( $\pm$  standard deviation) and range of concentrations of barium in sediments from the four study sites. Data from *Chapter 8*.

Site	Date	Barium Concentration (mg/kg dry wt)	
		Near-Field	Far-Field
VK 916	Nov 2000	1,090 $\pm$ 160 (800 – 1,290)	870 $\pm$ 170 (700 – 1,180)
	Aug 2002	35,900 $\pm$ 52,600 (1,050 – 171,000) <sup>a</sup>	940 $\pm$ 220 (670 – 1,390)
GB 516	Nov 2000	24,500 $\pm$ 38,300 (3,100 – 135,000)	1280 $\pm$ 340 (760 – 1,970)
	July 2001	59,000 $\pm$ 95,700 (8,600 – 351,000) <sup>b</sup>	1480 $\pm$ 560 (790 – 2,770)
GB 602	July 2001	50,800 $\pm$ 31,900 (16,600 – 116,000) <sup>c</sup>	850 $\pm$ 300 (570 – 1,550)
MC 292	July 2001	9,000 $\pm$ 11,000 (1260 – 39,700) <sup>c</sup>	760 $\pm$ 110 (630 – 920)

<sup>a</sup> NF Aug 2002 > NF Nov 2000; <sup>b</sup> NF July 2001 > Nov 2000 and NF > FF; <sup>c</sup> NF > FF.

### 16.3.3.2 Chromium

Chromium concentrations were similar in near-field and far-field sediments from all four sites (see *Chapter 8*). Concentrations ranged from about 31 mg/kg (near-field at VK 916 and GB 516) to 103 mg/kg (far-field at MC 292). The average concentration of chromium in marine sediments is about 72 mg/kg (Trefry et al. 2002), and concentrations in uncontaminated marine and estuarine sediments range from 50 to 100 mg/kg (Neff 2002b). Thus, there is no evidence that sediments near the discharge sites were contaminated with chromium from drilling discharges.

### 16.3.3.3 Mercury

WBM used offshore in the past sometimes contained elevated (compared to concentrations in clean marine sediments) concentrations of mercury. Much of the mercury in drilling discharges is from drilling mud barite (Neff 2002a). Since the USEPA (1993) placed a limit of 1 mg/kg on mercury in drilling mud barite destined for ocean disposal, offshore operators have been able to reduce mercury concentrations in drilling muds to a mean of about 0.5 mg/kg through use of cleaner grades of barite.

The mean background concentration of mercury in marine sediments is about 0.2 mg/kg (Neff 2002b; also see *Chapter 8*). Sediment samples collected along several transects perpendicular to the shoreline from offshore Corpus Christi, TX, to offshore Panama City, FL, in 210 to 3,140 m of water as part of the Deepwater Program: Northern Gulf of Mexico Continental Slope Habitats and Benthic Ecology Program, contained mercury at concentrations ranging from 0.009 to 0.043 mg/kg; concentrations decreased slightly with distance from shore (Rowe and Kennicutt 2001). Mean mercury concentrations in far-field sediments from the four sites ranged from 0.07 to 0.12 mg/kg (**Table 16.9**), slightly higher than those recorded by Rowe and Kennicutt (2001).

Mercury concentrations were slightly but significantly higher in near-field sediments than in far-field sediments at MC 292 and in near-field sediments from the second than those from the first survey at VK 916 and GB 516 (**Table 16.9**). The differences were small, but do indicate that small amounts of mercury associated with drilling mud barite were accumulating in near-field sediments at some continental slope drilling sites. All mercury concentrations were in the lower part of the range expected for uncontaminated marine sediments.

**Table 16.9.** Mean ( $\pm$  standard deviation) and range of concentrations of mercury in sediments from the four study sites. Data from *Chapter 8*.

Site	Date	Mercury Concentration (mg/kg dry wt)	
		Near-Field	Far-Field
VK 916	Nov 2000	0.071 $\pm$ 0.003 (0.065 – 0.075)	0.071 $\pm$ 0.004 (0.062 – 0.078)
	Aug 2002	0.090 $\pm$ 0.028 (0.071 – 0.15) <sup>a</sup>	0.077 $\pm$ 0.008 (0.064 – 0.087)
GB 516	Nov 2000	0.10 $\pm$ 0.015 (0.079 – 0.13)	0.11 $\pm$ 0.009 (0.092 – 0.12)
	July 2001	0.12 $\pm$ 0.039 (0.088 – 0.24) <sup>b</sup>	0.12 $\pm$ 0.020 (0.095 – 0.15)
GB 602	July 2001	0.10 $\pm$ 0.027 (0.070 – 0.17)	0.098 $\pm$ 0.007 (0.084 – 0.11)
MC 292	July 2001	0.082 $\pm$ 0.012 (0.061 – 0.11) <sup>c</sup>	0.070 $\pm$ 0.006 (0.061 – 0.082)

<sup>a</sup> NF Aug 2002 > NF Nov 2000; <sup>b</sup> NF July 2001 > Nov 2000; <sup>c</sup> NF > FF.

#### 16.3.3.4 Lead

Drilling muds and cuttings often contain elevated concentrations of lead. It is present as an impurity in drilling mud barite and clay, probably as insoluble lead sulfide (galena), and in pipe thread compound used in the joints of drilling pipe (Neff 2002b). Background concentrations of lead in uncontaminated marine sediments usually are in the range of 5 to 30 mg/kg, with a mean background concentration of 19 mg/kg (*Chapter 8*). Most lead concentrations in far-field sediments from the four sites were in the upper part of the range of background concentrations (**Table 16.10**).

**Table 16.10.** Mean ( $\pm$  standard deviation) and range of concentrations of lead in sediments from the four study sites. Data from *Chapter 8*.

Site	Date	Lead Concentration (mg/kg dry wt)	
		Near-Field	Far-Field
VK 916	Nov 2000	30.3 $\pm$ 3.3 (25.0 – 34.8)	28.3 $\pm$ 1.8 (25.3 – 30.9)
	Aug 2002	29.9 $\pm$ 3.5 (26.3 – 36.9)	25.4 $\pm$ 1.4 (22.4 – 27.4)
GB 516	Nov 2000	24.1 $\pm$ 2.5 (18.3 – 28.7)	24.5 $\pm$ 1.6 (20.9 – 27.3)
	July 2001	33.6 $\pm$ 10.3 (21.0 – 60.3)	24.0 $\pm$ 2.0 (20.9 – 26.8)
GB 602	July 2001	41.8 $\pm$ 10.0 (22.1 – 57.0) <sup>a</sup>	21.6 $\pm$ 1.5 (19.5 – 24.1)
MC 292	July 2001	30.1 $\pm$ 5.0 (24.6 – 44.4)	31.4 $\pm$ 1.1 (30.2 – 34.0)

<sup>a</sup> NF > FF.

A few near-field sediment samples from GB 516 and GB 602 contained slightly elevated lead concentrations. The mean lead concentration in near-field sediments from GB 602 was significantly higher than the mean concentration in far-field sediments from the same site. The difference was small but may represent input of lead-contaminated solids from drilling discharges or platform operations (paint chips or sacrificial anodes).

#### 16.3.3.5 Zinc

Zinc concentrations are extremely variable in uncontaminated marine sediments. Most zinc is present in highly insoluble residual forms as part of the mineral lattice of sediment particles or in heavy minerals, such as chromite, ilmenite, and spalerite (zinc sulfide) (Neff 2002b). Zinc concentrations in the sandy sediments of Georges Bank are in the range of 1.2 to 70 mg/kg; they are much higher in fine-grained sediments of Terra Nova Bay, Antarctica, ranging from 75 to 155 mg/kg. Sediments from the coastal zone of Louisiana contain 52 to 133 mg/kg zinc. Reflecting this variability in sediment zinc concentrations, the mean zinc concentrations in far-field sediments from the four sites range from 77.4 to 113 mg/kg (**Table 16.11**).

**Table 16.11.** Mean ( $\pm$  standard deviation) and range of concentrations of zinc in sediments from the four study sites. Data from *Chapter 8*.

Site	Date	Zinc Concentration (mg/kg dry wt)	
		Near-Field	Far-Field
VK 916	Nov 2000	108 $\pm$ 2.0 (106 – 110)	104 $\pm$ 3.0 (99 – 106)
	Aug 2002	106 $\pm$ 13 (88 – 142)	107 $\pm$ 4.0 (101 – 116)
GB 516	Nov 2000	94.4 $\pm$ 14.9 (84.1 – 133)	90.2 $\pm$ 3.3 (83.4 – 95.4)
	July 2001	96.2 $\pm$ 38.3 (63.1 – 213)	86.8 $\pm$ 3.5 (81.5 – 92.6)
GB 602	July 2001	90.3 $\pm$ 8.9 (76.2 – 101) <sup>a</sup>	77.4 $\pm$ 5.2 (71.8 – 89.3)
MC 292	July 2001	120 $\pm$ 58 (50 – 294)	113 $\pm$ 12 (90 – 141)

<sup>a</sup> NF > FF.

The means and range of zinc concentrations in near-field sediments are similar to those in far-field sediments (**Table 16.11**). Highest concentrations are in a few near-field sediment samples from MC 292 and GB 516. The near-field mean sediment zinc concentration was significantly higher than the far-field mean only at GB 602. Thus, there is only limited, weak evidence of zinc contamination of near-field sediments from drilling discharges.

#### 16.3.4 Polycyclic Aromatic Hydrocarbons and Metals in Tissues of Benthic Megafauna

Two species of deep-sea benthic/demersal animals were collected at near-field and far-field sites at MC 292 and GB 602 in July 2001 and analyzed for total PAH and 11 metals. The giant isopod *Bathynomus giganteus* and the red crab *Chaceon quinquegens* were collected in baited traps (*Chapter 2*).

##### 16.3.4.1 Polycyclic Aromatic Hydrocarbons

Concentrations of total PAH in soft tissues of giant isopods and red crabs ranged from 0.039 to 0.18  $\mu\text{g/g}$  dry wt (parts per million) (**Table 16.12**). Concentrations tended to be slightly higher in *Bathynomus* than in *Chaceon*. Concentrations were slightly higher in far-field than in near-field *Bathynomus* at MC 292; the opposite trend was evident at GB 602. Soft tissues of *Chaceon* from near-field and far-field locations at MC 292 and at near-field sites at GB 602 were similar. No samples were available from the far-field at GB 602. Thus, there was no clear evidence of PAH bioaccumulation from drilling discharges, which would have been indicated by substantially higher PAH body burdens in crustaceans from near-field than from far-field sites.

Tissue PAH concentrations in nearly all samples from MC 292 and GB 602 were lower than concentrations in surface near-field and far-field sediment samples collected at the same time as the tissue samples (**Table 16.12**). Thus, biota/sediment accumulation factors were less than 1, indicating limited bioavailability of PAH from site sediments. The PAH in the isopods and crabs probably were derived from sediment ingestion or consumption of benthic infauna that were in equilibrium with local sediments.

**Table 16.12.** Concentrations of total polycyclic aromatic hydrocarbons (PAH) ( $\mu\text{g/g}$  dry wt) in whole soft tissues of giant isopods *Bathynomus giganteus* and red crabs *Chaceon quinquedens* collected in July 2001 from MC 292 and GB 602. PAH concentrations in two composite samples from each site are shown. PAH concentrations in sediments are included for comparison. Data from *Chapter 9*.

Species	MC 292		GB 602	
	Near-Field	Far-Field	Near-Field	Far-Field
<i>Bathynomus giganteus</i>	0.087 – 0.092	0.11 – 0.42	0.13 – 0.16	0.098 – 0.13
<i>Chaceon quinquedens</i>	0.039 – 0.14	0.107 – 0.108	0.095 – 0.18	No Sample
Surface sediment	0.17 – 0.56	0.21 – 0.75	0.13 – 0.55	0.094 – 0.15

#### 16.3.4.2 Metals

The 11 metals analyzed in whole soft tissues of *Bathynomus* and *Chaceon* include arsenic, barium, cadmium, chromium, copper, iron, lead, mercury, nickel, vanadium, and zinc. Three to six replicate composite tissue samples of each species were analyzed for each metal at near-field and far-field sites at MC 292 and GB 602.

Concentrations of most metals were highly variable in the soft tissues of the two species of benthic crustaceans (**Table 16.13**). The coefficient of variation often was 50% or greater. Because of this variability and the small numbers of replicates for each location, significant differences in tissue metals concentrations were difficult to detect.

There were no significant differences between near-field and far-field sites in metals concentrations in giant isopods from MC 292 (**Table 16.13**). However, at GB 602, concentrations of barium, chromium, and lead were significantly higher in near-field than in far-field isopods. Concentrations of cadmium and mercury were significantly higher in soft tissues of isopods from far-field than in those from near-field stations.

Mean barium concentration was about 10-fold higher in tissues of *Bathynomus* from near-field than from far-field sampling sites at GB 602. It is highly likely that the excess barium in the near-field isopods was derived primarily from drilling discharges.

Cadmium and mercury were present at high concentrations in soft tissues of isopods from both near-field and far-field sites at both MC 292 and GB 602. Most of the cadmium and mercury in drilling discharges is associated with drilling mud barite (Neff 2005). Because there was no relationship between concentrations of barium and either cadmium or mercury in the isopods, it is unlikely that the higher than expected concentrations of cadmium and mercury in the crustacean tissues were derived from drilling discharges.

Many non-decapod crustaceans contain high concentrations of cadmium, probably sequestered in insoluble granules in excretory tissues (Neff 2002b). Most crustaceans contain less than 1  $\mu\text{g/g}$  total mercury in soft tissues (Neff 2002b). However, no data are available for *Bathynomus* from other locations. The unusual life habits of this giant deepwater isopod (Barradas-Ortiz et al. 2003) may predispose it to bioaccumulate mercury.



**Table 16.13.** Mean ( $\pm$  standard deviation) concentrations of 11 metals in whole soft tissues of giant isopods *Bathynomus giganteus* and red crabs *Chaceon quinquegens* collected in July 2001 from MC 292 and GB 602. Three to six replicate samples were analyzed for each site. Significant differences between near-field and far-field are shaded and bold. Concentrations are  $\mu\text{g/g}$  dry wt. Data from *Chapter 8*.

Metal	MC 292		GB 602	
	Near-Field	Far-Field	Near-Field	Far-Field
<i>Bathynomus giganteus</i>				
Arsenic	39 $\pm$ 21	28 $\pm$ 23	39 $\pm$ 28	61 $\pm$ 33
Barium	17 $\pm$ 8	16 $\pm$ 15	<b>164 <math>\pm</math> 136<sup>a</sup></b>	<b>15 <math>\pm</math> 9</b>
Cadmium	14 $\pm$ 10	16 $\pm$ 17	<b>7 <math>\pm</math> 4<sup>b</sup></b>	<b>14 <math>\pm</math> 6</b>
Chromium	1.1 $\pm$ 0.8	1.5 $\pm$ 1.3	<b>1.2 <math>\pm</math> 1.2<sup>a</sup></b>	<b>0.43 <math>\pm</math> 0.04</b>
Copper	75 $\pm$ 86	73 $\pm$ 59	51 $\pm$ 50	95 $\pm$ 86
Iron	1,310 $\pm$ 1,220	2,250 $\pm$ 2,530	979 $\pm$ 549	1450 $\pm$ 540
Lead	0.38 $\pm$ 0.27	0.46 $\pm$ 0.38	<b>0.61 <math>\pm</math> 0.39<sup>a</sup></b>	<b>0.26 <math>\pm</math> 0.06</b>
Mercury	3.3 $\pm$ 2.8	4.3 $\pm$ 4.4	<b>3.1 <math>\pm</math> 1.3<sup>b</sup></b>	<b>8.1 <math>\pm</math> 6.8</b>
Nickel	0.9 $\pm$ 0.5	0.9 $\pm$ 0.6	1.3 $\pm$ 0.8	0.55 $\pm$ 0.45
Vanadium	2.8 $\pm$ 1.1	3.0 $\pm$ 1.7	2.8 $\pm$ 1.5	1.7 $\pm$ 1.5
Zinc	264 $\pm$ 183	360 $\pm$ 339	344 $\pm$ 272	327 $\pm$ 94
<i>Chaceon quinquegens</i>				
Arsenic	133 $\pm$ 37	131 $\pm$ 46	<b>65 <math>\pm</math> 25<sup>b</sup></b>	<b>170 <math>\pm</math> 29</b>
Barium	<b>43 <math>\pm</math> 38<sup>a</sup></b>	<b>3.9 <math>\pm</math> 1.8</b>	<b>54 <math>\pm</math> 46<sup>a</sup></b>	<b>11 <math>\pm</math> 7</b>
Cadmium	<b>101 <math>\pm</math> 13<sup>a</sup></b>	<b>2.9 <math>\pm</math> 2.3</b>	<b>2.1 <math>\pm</math> 1.1<sup>b</sup></b>	<b>12 <math>\pm</math> 5</b>
Chromium	<b>2.5 <math>\pm</math> 2.0<sup>a</sup></b>	<b>0.6 <math>\pm</math> 0.4</b>	1.0 $\pm$ 0.6	0.7 $\pm$ 0.2
Copper	248 $\pm$ 73	199 $\pm$ 70	<b>59 <math>\pm</math> 45<sup>b</sup></b>	<b>151 <math>\pm</math> 65</b>
Iron	1,340 $\pm$ 1,100	612 $\pm$ 215	216 $\pm$ 111	254 $\pm$ 81
Lead	0.89 $\pm$ 0.70	0.25 $\pm$ 0.12	0.26 $\pm$ 0.10	0.32 $\pm$ 0.14
Mercury	1.0 $\pm$ 0.4	0.8 $\pm$ 0.4	<b>0.54 <math>\pm</math> 0.14<sup>b</sup></b>	<b>1.5 <math>\pm</math> 0.4</b>
Nickel	14 $\pm$ 4.6	10 $\pm$ 3.2	<b>3.4 <math>\pm</math> 1.6<sup>b</sup></b>	<b>9.2 <math>\pm</math> 2.4</b>
Vanadium	<b>6.0 <math>\pm</math> 4.0<sup>a</sup></b>	<b>2.8 <math>\pm</math> 1.3</b>	<b>1.3 <math>\pm</math> 0.7<sup>b</sup></b>	<b>3.3 <math>\pm</math> 1.0</b>
Zinc	230 $\pm$ 107	226 $\pm$ 27	<b>148 <math>\pm</math> 61<sup>b</sup></b>	<b>261 <math>\pm</math> 31</b>

<sup>a</sup> NF > FF; <sup>b</sup> FF > NF.

The pattern of metal bioaccumulation in red crabs was different from that in giant isopods (**Table 16.13**). Near-field crabs from MC 209 contained significantly higher concentrations of barium, cadmium, chromium, and vanadium than far-field crabs did. Only barium was present at a significantly higher mean concentration in near-field than far-field red crabs at GB 602. However, concentrations of arsenic, cadmium, copper, mercury, nickel, vanadium, and zinc were significantly higher in far-field than in near-field *Chaceon*. As for *Bathynomus*, the higher concentration of barium in crabs from near-field stations is an indication of exposure to drilling discharges containing high concentrations of drilling mud barite. It is probable that much of the excess barium in the soft tissues of the isopods and crabs from near-field sites is present as unassimilated solid barite particles in the gut, digestive gland, and gills (Jenkins et al. 1989).

The high concentrations of several metals in tissues of red crabs from far-field sites at GB 602 may be related to the proximity up-slope of mud mounds and hydrocarbon seeps (Sager et al.

2003) that may be rich sources of metals to bottom waters. The unusually high concentration of cadmium in near-field crabs at MC 292 is unexplained.

### 16.3.5 Summary of Exposure

Several physical and chemical parameters for sediments and benthic megafauna were used to characterize the distribution and relative amounts of drilling discharges (the disturbance or exposure) near four deepwater drilling sites. Evidence of exposure of the benthic environment to drilling discharges was defined as a higher parameter value in near-field than in far-field sediments at a site. The relative magnitude of benthic disturbance or exposure at the four sites was estimated based on the relative areas of seafloor covered by cuttings, as indicated by acoustic surveys, and the relative concentrations of chemicals, particularly SBF chemical and barium, in near-field sediments.

Near-field sediments at all four sites showed evidence of disturbance by or exposure from drilling operations at site center (**Table 16.14**). The ranking of the four sites with respect to increasing area of seafloor covered by cuttings is: VK 916, MC 292, GB 602, and GB 516. This ranking from lowest to highest level of exposure and disturbance is consistent with the data for other indicators of physical disturbance or drilling discharge accumulation on the seafloor, as summarized in **Table 16.14**.

**Table 16.14.** Summary of evidence of physical disturbance to or chemical exposure of the near-field benthic environment at the four study sites. + = evidence of exposure or disturbance; +- = weak or uncertain evidence of exposure; - = no evidence of exposure or disturbance. The area of seafloor with geophysical evidence of cuttings accumulation is summarized.

Parameter	VK 916	GB 516	GB 602	MC 292
Anchor scars	+	+	+	+
Seafloor equipment	-	+	+	+
Cuttings area	13.4 ha	108.5 ha	43.2 ha	25.6 ha
Sediment SBF NF > FF	+	+	+	+
Sediment PAH NF > FF	-	+-	-	-
Sediment TOC NF > FF	+	+	+	-
Sediment Ba NF > FF	+	+	+	+
Sediment Cr NF > FF	-	-	-	-
Sediment Hg NF > FF	+	+	-	+
Sediment Pb NF > FF	-	-	+	-
Sediment Zn NF > FF	-	-	+	-
Tissue PAH NF > FF	NS	NS	-	-
Tissue Ba NF > FF	NS	NS	+	+
Other metals NF > FF	NS	NS	+-	+-

NS = no sample; PAH = polycyclic aromatic hydrocarbon; SBF = synthetic based fluid; TOC = total organic carbon.

Barium concentration can be used as a rough indication of the concentration of total drilling waste solids (WBM, WBM cuttings, and SBM cuttings) in sediments. SBF chemical concentration can be used as a rough indication of the concentration of SBM cuttings solids in sediments. However, neither barium nor SBF chemical concentration is a conservative tracer of drilling discharges. There was a relatively poor correlation in this study and in the earlier study in shallower water (Continental Shelf Associates, Inc. 2004) between barium and SBF chemical concentrations in near-field sediments (see *Chapter 15*). The poor covariance can be attributed to highly variable ratios of relative amounts of WBM/WBM cuttings and SBM cuttings discharged and accumulating in different regions near the different discharge sites. Because WBM and SBM are used sequentially, not concurrently, for drilling, WBM cuttings and SBM cuttings discharges occur at different times under different tidal and residual current regimes, resulting in different distributions of WBM cuttings and SBM cuttings solids on the seafloor. In addition, the total amount of WBM and WBM cuttings discharged per unit depth interval of well drilled is much greater than the amount of SBM cuttings discharged. Thus, the WBM mud and cuttings signal in sediments often swamps the weaker SBF chemical signal.

## 16.4 EFFECTS ASSESSMENT

Several biological parameters were measured in this investigation as indices of biological effects of physical disturbance or chemical contamination of sediments (exposure) from drilling activities. Sediment toxicity tests were performed with near-field and far-field sediments from the two post-development sites, MC 292 and GB 602 (*Chapter 14*). Sediment oxygen concentration was measured in sediments as an index of organic enrichment from microbial biodegradation of organic matter from drilling discharge. Benthic microbial, meiofaunal, macrofaunal, and megafaunal communities were examined by sampling and sediment profile imaging. In most cases, effects were measured as a difference between near-field and far-field biological parameters at each site.

### 16.4.1 Sediment Toxicity

Sediment samples were collected in July 2001 from the two post-development sites, MC 292 and GB 602, for laboratory sediment toxicity tests (*Chapter 14*). The sediment bioassays (10-day exposure to sediments from near-field and far-field stations) were performed with the benthic amphipod *Leptocheirus plumulosus* according to standard USEPA and ASTM protocols. Differences in survival of amphipods in near-field and far-field sediments from each site were used as an indication of biological effects of sediment disturbance or contamination from previous drilling discharges at the site.

For sediments from both MC 292 and GB 602, there was significantly lower mean survival of amphipods in near-field than in far-field sediments (**Table 16.15**). For MC 292 sediments, survival of amphipods in far-field sediments was comparable to that in control sediments, indicating that the animals were healthy and the far-field sediments were non-toxic. In the GB 602 tests, survival of amphipods in control sediments was good; however, survival of controls in the reference toxicant test was poor, suggesting that the amphipods used in the test may not have been healthy.

**Table 16.15.** Survival of amphipods *Leptocheirus plumulosus* in 10-day sediment toxicity tests with 12 replicate sediment samples each from near-field and far-field stations at MC 292 and GB 602. Mean survival was significantly lower in near-field than in far-field sediments at both discharge sites. Data from *Chapter 14*.

Discharge Site	Percent Survival (Mean $\pm$ SD, n = 12)	
	Near-Field	Far-Field
MC 292	76 $\pm$ 21	93 $\pm$ 8
GB 602	17 $\pm$ 18	68 $\pm$ 13

SD = standard deviation.

In summary, near-field sediments from both MC 292 and GB 602 were toxic to benthic amphipods. Far-field sediments from GB 602 also were toxic, but some of this effect could have been due to the poor health of the test animals. The toxicity of near-field sediments may have been caused in part by chemicals from drilling discharges in the sediments.

#### 16.4.2 Sediment Microbial Activity

Biodegradable organic matter often has a greater effect than sediment texture and deposition rate, or in some cases potentially toxic chemicals, on the structure and function of benthic biological communities in accumulations of drilling muds and cuttings on the seafloor (Hartley et al. 2003). Bacteria and fungi indigenous to marine sediments degrade the organic matter and, in the process, may deplete the oxygen in the pore water of near-surface layers of sediment, reduce sediment redox potential, and generate potentially toxic concentrations of sulfide and ammonia (Wang and Chapman 1999; Gray et al. 2002; Wu 2002).

The redox potential (Eh) is a measure of the relative intensity of oxidation or reduction reactions or of the concentration of electrons in solution. The value of Eh (measured in millivolts: mV) reflects the sum of all oxidation/reduction reactions that are occurring in the sediment. Eh values greater than zero indicate oxidizing conditions; those less than zero indicate reducing conditions. The redox potential discontinuity (RPD) is the location in sediment where Eh is zero. Microbes use different inorganic oxidants (electron acceptors) to oxidize organic matter. As the primary oxidant, oxygen (O<sub>2</sub>), is consumed, Eh and oxygen concentration decline; different bacterial consortia then use first denitrification, manganese oxide reduction, iron hydrous oxide reduction, sulphate reduction, and methane formation as energy sources for organic matter oxidation (Van Cappellen and Wang 1995). Additional oxygen is consumed in the sediment column to re-oxidize these alternate electron acceptors by abiotic or microbially-mediated oxidation/reduction reactions. Microbial reduction of nitrate to ammonia begins as Eh falls below about +200 mV; sulfate reduction to sulfide begins at an Eh of about -100 mV. The slope of the vertical dissolved oxygen and Eh gradient in sediment and, therefore, the depth of the RPD and oxygen depletion depend on the oxygen concentration in the overlying water, the permeability of the sediment, and the availability of biodegradable organic matter and reducible inorganic substrates in the sediment (Van Cappellen and Wang 1995).

SBM cuttings and some WBM and WBM cuttings, particularly gel muds containing high concentrations of carbohydrates, contain a large amount of biodegradable organic matter. Most of this organic matter is oxidized more efficiently under aerobic than anaerobic conditions. When

SBM cuttings accumulate on the seafloor, oxygen in the pore water of the cuttings layer is consumed rapidly, resulting in a steep gradient of decreasing oxygen concentration with depth in the sediment (**Figure 16.2**). Sediments contaminated with high concentrations of organic matter from SBM cuttings often become anoxic within about 1 to 2 mm of the surface. This steep gradient of decreasing oxygen concentration with depth in the cuttings pile is caused by a combination of rapid microbial degradation of labile organic matter and the low permeability of the cuttings material, which slows diffusion of oxygen into sediment from the overlying water (Shimmield and Breuer 2000; Shimmield et al. 2000). This process is called organic enrichment and results in substantial changes in sediment physical/chemical properties and in benthic community structure (Pearson and Rosenberg 1978).

As the sediment organic matter concentration increases as a result of SBM cuttings accumulation in surface layers, microbial activity increases and the gradient of declining oxygen concentration with depth in sediment steepens, resulting in a change in benthic community structure. The number of species, faunal abundance, and biomass (the SAB ratio) of the benthic community change in characteristic ways described in the Pearson-Rosenberg model (Nilsson and Rosenberg 2000) along a gradient of decreasing sediment organic matter concentration with distance from a source of sediment organic enrichment. The changes in the benthic community are caused primarily by sediment hypoxia, rather than directly by organic enrichment (Gray et al. 2002). The microbially-mediated increase in hydrogen sulfide and ammonia concentrations in sediments that accompanies sediment hypoxia also may contribute to benthic community alterations (Vismann 1991).

Severely organically enriched sediments may support white mats of the sulfate-oxidizing bacterium *Beggiatoa* spp. They have been observed on the surface of OBF and SBM cuttings piles in the North Sea and Gulf of Mexico (Breuer et al. 1999; Schimmield and Breuer 2000; Continental Shelf Associates, Inc. 2004). These bacterial mats overlie anoxic sulfide-rich marine sediments (Gundersen et al. 1992); *Beggiatoa* bacteria are chemoautotrophs that oxidize sulfide through elemental sulfur to sulfate.

Most of the benthic meiofauna and macroinfauna of continental shelf and slope sediments live in the upper few centimeters of the sediment column, particularly if the sediments are fine-grained (Gray 2002). Most of these benthic fauna utilize the oxygen in the thin surface oxidized layer of sediment. Therefore, the best way to express the critical oxygen concentration for benthic fauna is as the depth-integrated amount of oxygen per unit area of sediment (the oxygen inventory of the sediment) (Trefry et al. 2004). The oxygen inventory is the total amount of oxygen per square centimeter of sediment surface integrated to the depth of the RPD. The Eh gradient in sediments also is a useful indication of the quality of the benthic habitat.

#### 16.4.2.1 *The Oxygen Inventory of Sediments*

Because Eh and dissolved oxygen concentration have a marked effect on speciation, bioavailability, and toxicity of most metals in sediments, these parameters were measured at different depths in sediment samples collected for metals analysis in this study (see *Chapter 8*). Lower oxygen inventory and Eh and shallower RPD depth in near-field than in far-field sediments are circumstantial evidence of organic enrichment of near-field sediments, possibly by accumulation on the bottom of drilling discharges containing biodegradable organic matter.

Mean oxygen inventory in near-field and far-field sediment samples at VK 916 before initiation of exploratory drilling and in far-field sediments after exploratory drilling was  $86 \text{ nM/cm}^2$  (*Chapter 8*). Discretionary and near-field sediments collected after exploratory drilling contained much lower mean oxygen inventories, 11 and  $44 \text{ nM/cm}^2$ , respectively. This is a strong indication of increased oxidative activity in near-field sediments after exploratory drilling, probably caused by microbial oxidation of organic matter in deposited drilling waste solids.

There was a similar pattern of change in oxygen distribution in sediments at GB 516 (*Chapter 8*). Before development drilling began, oxygen inventories in near-field and far-field sediments were similar and high. After development, discretionary and near-field sediments contained much lower oxygen inventories than far-field sediments did. There was a similar distribution, post-development, at GB 602.

Oxygen inventories were low in all sediments at MC 292 after completion of development drilling. This probably was caused by the close proximity to the mouth of the Mississippi River and resulting relatively high sedimentation rate, TOC concentration, and small grain size of sediments at this site.

#### 16.4.2.2 Sediment Eh and RPD Depth

As discussed above, organic enrichment of sediments causes a steeper gradient of declining Eh with depth in sediment, resulting in a shallowing of the RPD depth (the depth in sediment at which Eh is 0 and oxygen is depleted). The range of RPD depth and  $\text{Eh}_{1 \text{ cm}}$  (the Eh at a depth of 1 cm) were lower in near-field than in far-field sediments at all four sites after discharges (**Table 16.16**). These parameters were less variable among replicate samples of far-field sediments than of near-field sediments at each discharge site. The greater variability in near-field sediments may reflect a patchy distribution of drilling discharge solids on the near-field seafloor. RPD depth and  $\text{Eh}_{1 \text{ cm}}$  tended to be lower in discretionary than in near-field sediments, because discretionary samples were collected at near-field sites with the highest likelihood of containing drilling discharge material.

There was a decline in RPD depth and  $\text{Eh}_{1 \text{ cm}}$  in near-field but not far-field sediments between the pre-exploration and post-exploration surveys at VK 916 (**Table 16.16**). There was a much smaller change at near-field stations at GB 516 between the pre-development and post-development surveys. RPD depth and  $\text{Eh}_{1 \text{ cm}}$  were similar in far-field sediments before and after exploratory or development drilling at both sites.

Only post-drilling samples were collected at GB 602 and MC 292. RPD depth and  $\text{Eh}_{1 \text{ cm}}$  of some near-field and discretionary sediment samples were less than values for far-field samples. Some near-field and discretionary sediments from GB 602 and near-field sediments from MC 292 had negative  $\text{Eh}_{1 \text{ cm}}$  values, indicating shallow sediment hypoxia. All these results provide consistent support for the hypothesis that patchy distributions of drilling discharge solids containing biodegradable organic matter in near-field surface sediments at all four sites caused localized sediment hypoxia.

**Table 16.16.** Ranges of redox potential discontinuity (RPD) depths and Eh at 1 cm in sediments from near-field (NF), discretionary (DS), and far-field (FF) zones at the four study sites. Data from *Chapter 8*.

Site	Zone	RPD Depth (cm)		Eh <sub>1 cm</sub> (mV)	
		Min	Max	Max	Min
VK 916 (Nov 2000) Pre-Exploration	NF	1.6	3.5	+675	+328
	FF	2.4	3.1	+614	+135
VK 916 (Aug 2002) Post-Exploration	NF	0.2	3.0	+529	-79
	DS	0.1	0.5	+31	-65
	FF	0.0	3.2	+514	+218
GB 516 (Nov 2000) Pre-Development	NF	0.3	5.7	+664	-163
	FF	3.4	5.8	+692	+406
GB 516 (July 2001) Post-Development	NF	0.2	2.5	+506	-107
	DS	0.1	0.3	+196	-171
	FF	2.7	5.7	+492	+104
GB 602 (July 2001) Post-Development	NF	0.1	2.8	+402	-167
	DS	0.2	1.7	+424	-296
	FF	2.8	>6.1	+462	+225
MC 292 (July 2001) Post-Development	NF	0.2	3.0	+350	-163
	DS	0.8	1.7	+321	+29
	FF	0.2	>3.3	+449	+158

#### 16.4.2.3 Sediment Microbiology

Due to microbial degradation of organic matter from SBM drilling waste solids deposited on the seafloor, one would expect that sediments exhibiting organic enrichment would also have higher microbial metabolism. This possibility was examined by determining concentrations of adenosine triphosphate (ATP) in near-field and far-field sediments from the four sites (see *Chapter 10*). ATP is the main energy-containing cofactor in biochemical pathways in all living aerobic and anaerobic prokaryote and eukaryote organisms. Therefore, ATP concentration is a good index of biological activity in sediments. Much of the biological activity in fine-grained sediments is from microscopic bacteria and protozoa. Therefore, ATP concentration has been adopted as an indication of microbial activity in sediments.

ATP concentrations in near-field and far-field sediments collected during three field surveys at four sites varied widely, from <0.3 to 418.2 ng/g (**Table 16.17**). Mean concentrations were consistently higher in sediments collected in November 2000 (pre-exploration and pre-development) than in near-field and far-field sediments collected in July 2001 or August 2002 (post-drilling). LaRock (*Chapter 10*) interpreted this decline in ATP concentration as evidence of a drilling related biological effect on the benthic environment. However, as observed in *Chapter 15*, the magnitude of apparent effects was similar at near-field and far-field stations and did not vary with concentrations of drilling discharge markers, barium and SBF chemical, in sediments. It is possible that the inter-annual difference reflected a long-term, area-wide change in benthic microbial productivity, or differences in application of the ATP analytical method among batches of samples.

**Table 16.17.** Sediment adenosine triphosphate (ATP) concentrations (ng/g dry wt) in surface sediments collected at 12 near-field and 6 far-field stations at the four study sites. Data from *Chapter 10*.

Site	Zone	Mean ATP ( $\pm$ SD)	ATP Range
VK 916 (Nov 2000) Pre-Exploration	NF	32.1 $\pm$ 9.2	21.9 – 48.3
	FF	36.0 $\pm$ 14.3	19.7 – 61.4
VK 916 (Aug 2002) Post-Exploration	NF	7.9 $\pm$ 13.1	<0.3 – 41.5
	FF	7.1 $\pm$ 17.1	0.9 – 61.1
GB 516 (Nov 2000) Pre-Development	NF	100.4 $\pm$ 130.7	13.1 – 418.2
	FF	43.3 $\pm$ 28.5	14.2 – 102.4
GB 516 (July 2001) Post-Development	NF	4.4 $\pm$ 3.9	0.5 – 11.9
	FF	2.5 $\pm$ 2.1	0.5 – 5.8
GB 602 (July 2001) Post-Development	NF	8.2 $\pm$ 6.6	2.3 – 17.6
	FF	20.1 $\pm$ 61.8	1.1 – 216.3
MC 292 (July 2001) Post-Development	NF	2.8 $\pm$ 1.9	0.9 – 5.5
	FF	7.7 $\pm$ 19.5	0.7 – 66.6

Given uncertainties about temporal differences in sediment ATP concentration, the best approach for examining possible effects of drilling discharges is to compare ATP concentrations between near-field and far-field at each site and sampling time. There were no significant differences in ATP concentrations between near-field and far-field sediments at any of the four sites (see *Chapter 10*). Near-field sediments collected at GB 516 in November 2000 (pre-development) contained a higher mean ATP concentration than far-field sediment samples collected at the same time. This difference can be attributed to two near-field samples containing higher ATP concentrations than any other sediments sampled in this project: 288.3 and 418.2 ng/g dry wt. Similarly, the far-field mean ATP concentration for GB 602 was higher than the near-field mean, because of one sample containing 216.3 ng/g ATP. Thus, there was no real difference in ATP concentrations in near-field and far-field sediments at any site. Apparently, organic enrichment of sediments results in variable responses in the benthic microbial community. An influx of biodegradable organic matter to sediments from drilling wastes would be expected to increase microbial community metabolism and biomass. However, onset of sediment hypoxia or anoxia may reduce total microbial biomass because aerobic metabolism usually far exceeds anaerobic metabolism in oxidized and reduced sediments, respectively.

#### 16.4.2.4 Microbial Mats

There was evidence of enhanced benthic microbial activity in the form of microbial mats at several near-field stations. Microbial mats were observed in sediment profile images at some near-field stations at VK 916, GB 516, and GB 602 (see *Chapters 6 and 7*). Most microbial mats are constructed by oxidation of sulfide to sulfate (white) by sulfide-oxidizing bacteria such as *Beggiatoa* spp. They occur on the surface of reduced marine sediment layers rich in sulfide; they frequently occur on sediments near hydrocarbon vents on the upper slope of the Gulf of Mexico (MacDonald 2002).



### 16.4.3 Meiofaunal and Macroinfaunal Communities

#### 16.4.3.1 Meiofauna

Most meiofauna, except foraminifera, are short-lived, rapidly reproducing invertebrates or the early life stages of larger benthic invertebrates. Meiofaunal communities often respond rapidly to changes in the physical disturbance and chemical contamination of sediments (Coull and Chandler 1992; Carman et al. 1997). They also recover rapidly from acute disturbances.

There was a tendency for meiofaunal density to decline between Cruise 1B and subsequent cruises at VK 916 and GB 516, and to be lower in far-field than in near-field sediments at all four sites (*Chapter 11*) (**Figure 16.3**). At VK 916, mean meiofaunal densities decreased by about an order of magnitude between the pre-drilling (November 2000) and post-drilling (August 2002) cruises. Mean meiofaunal densities were higher at near-field (608 individuals/10 cm<sup>2</sup>) than at far-field (544 individuals/10 cm<sup>2</sup>) stations at the time of the pre-drilling cruise and at near-field (96 individuals/10 cm<sup>2</sup>) than at far-field (19 individuals/10 cm<sup>2</sup>) stations at the time of the post-drilling cruise. The decline between cruises and between near-field and far-field stations was accompanied by a significant increase in the relative abundance of annelids in near-field compared to far-field samples at the time of the post-drilling cruise.

A similar pattern of temporal change in meiofaunal density was observed at GB 516 (**Figure 16.3**). Mean meiofaunal densities decreased between the pre-development cruise (November 2000) and the post-development cruise (July 2001). Meiofaunal density also was lower at far-field (68 individuals/10 cm<sup>2</sup>) than at near-field (122 individuals/cm<sup>2</sup>) stations at the time of the pre-development cruise and at far-field (22 individuals/10 cm<sup>2</sup>) than at near-field (38 individuals/cm<sup>2</sup>) stations at the time of the post-development cruise. There was considerable variability and overlap in meiofaunal densities among all near-field and far-field samples. As at VK 916, annelids were significantly more abundant in near-field than in far-field sediments.

Meiofaunal densities were low and highly variable in near-field and far-field sediments from GB 602 and MC 292 at the time of the single post-development sampling in July 2001 (**Figure 16.3**). Mean densities at GB 602 were 93 individuals/10 cm<sup>2</sup> at near-field stations and 26 individuals/10 cm<sup>2</sup> at far-field stations. Mean densities at MC 292 were 104 individuals/10 cm<sup>2</sup> near-field and 51 individuals/10 cm<sup>2</sup> far-field. Meiofaunal annelids were significantly more abundant in near-field than far-field sediments at MC 292.

Higher total meiofaunal densities in the near-field at all four sites reflected the increased abundance of several groups. The highest densities of annelids, harpacticoid copepods, and nematodes were always seen in the near-field. There were no consistent correlations between abundances of these groups and drilling discharge indicators (e.g., barium and SBF concentrations) within near-field sites (*Chapter 11*).

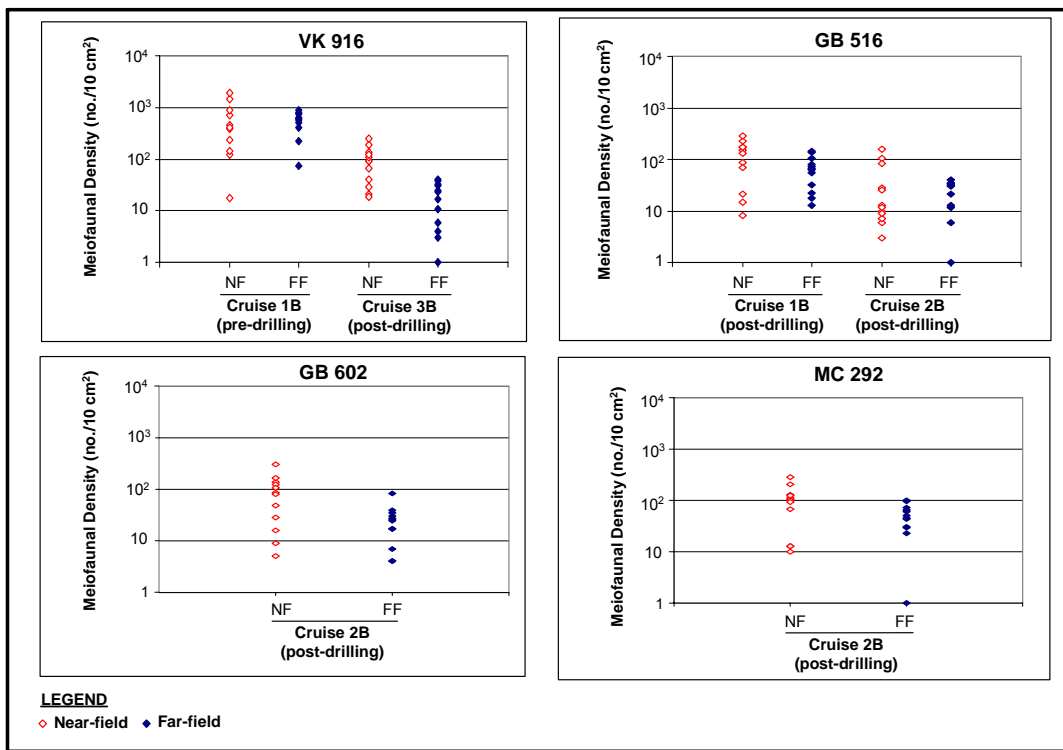


**Figure 16.3.** Total meiofaunal densities in near-field (NF) and far-field (FF) sediments from the four study sites. From *Chapter 11*.

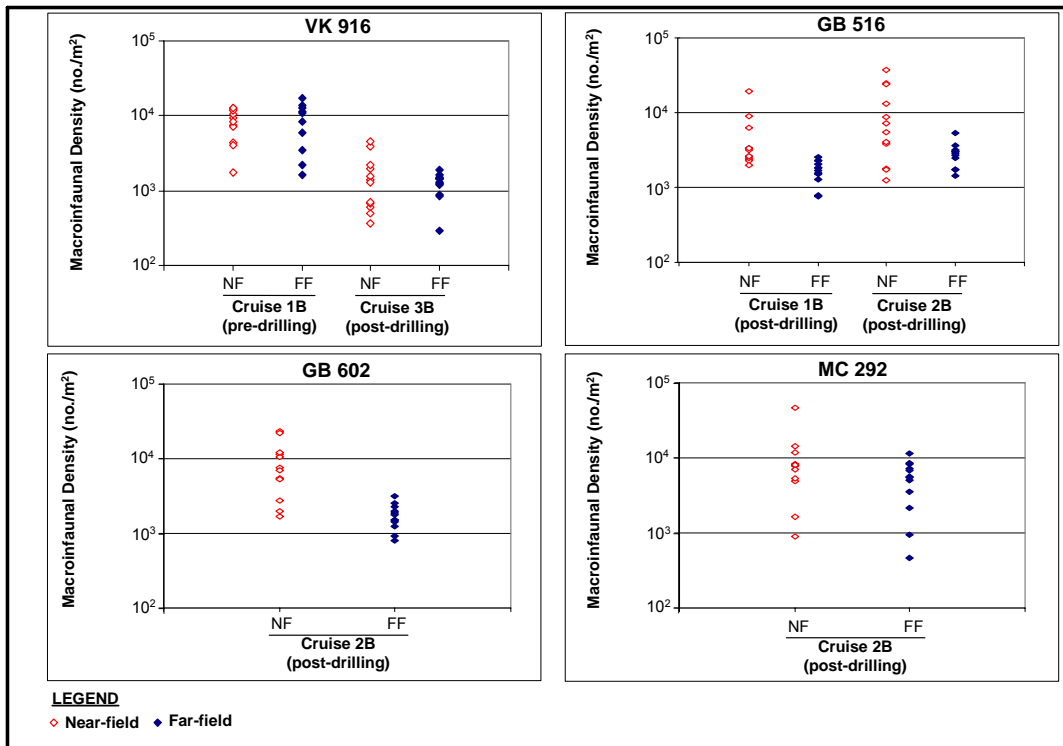


**Figure 16.4.** Total macroinfaunal densities in near-field (NF) and far-field (FF) sediments from the four study sites. From *Chapter 11*.

Benthic community parameters were highly variable at the four sites (**Table 16.18**). The survey in November 2000 at VK 916 occurred before any drilling in the immediate vicinity of the site center. Community parameters were similar for near-field and far-field stations, indicating that the area around the drilling site was fairly uniform before drilling.

All other sampling at VK 916 and the other three sites occurred after some drilling. At all sites, mean macrofaunal density was greater at near-field than at far-field stations (**Table 16.18**). However, mean diversity ( $H'$ ) evenness ( $J'$ ), and richness ( $D$ ) were higher at far-field than at near-field stations. The number of benthic taxa was the same or higher in far-field as in near-field sediments. In many cases, the differences were small and probably not statistically significant. These patterns of benthic community change at near-field sites are consistent with mild organic enrichment of near-field sediments (Gray et al. 2002; Rosenberg et al. 2004).

Most identifications were performed to the family level, decreasing the power of most community parameters to differentiate among sampling sites. However, there was a trend at all sites for highest densities of annelids, gastropods, and bivalve mollusks to be at near-field stations. Amphipods, ostracods, and tanaids tended to be more abundant at far-field than at near-field stations. Some of the taxa that were most abundant in near-field sediments were well-known opportunistic species, such as the annelid *Capitella* spp., characteristic of disturbed, eutrophic sediments. This benthic faunal composition also is consistent with organic enrichment of near-field sediments.

**Table 16.18.** Benthic macrofaunal community parameters for near-field (NF) and far-field (FF) sediments at the four study sites. Data from *Chapter 11*.

Site	Zone	No. Taxa	Density (no/m <sup>2</sup> )	Diversity ( $H'$ )	Evenness ( $J'$ )	Richness ( $D$ )
VK 916 (Nov 2000) Pre-Exploration	NF	14.1±4.3	8517±3672	1.45±0.47	0.53±0.17	1.94±0.64
	FF	14.7±1.9	8751±5319	1.59±0.14	0.60±0.06	2.10±0.19
VK 916 (Aug 2002) Post-Exploration	NF	7.2±3.4	1633±1332	1.10±0.68	0.54±0.27	1.31±0.71
	FF	10.1±2.4	1256±420	1.58±0.31	0.69±0.09	1.89±0.36
GB 516 (Nov 2000) Pre-Development	NF	12.9±2.3	4901±4961	1.22±0.41	0.47±0.13	2.06±0.51
	FF	14.1±1.5	1692±558	1.77±0.15	0.67±0.05	2.58±0.24
GB 516 (July 2001) Post-Development	NF	11.7±3.5	11087±11585	1.42±0.37	0.59±0.13	1.71±0.62
	FF	15.7±2.4	2838±1036	2.00±0.17	0.73±0.05	2.63±0.42
GB 602 (July 2001) Post-Development	NF	9.0±3.0	9251±7109	1.31±0.44	0.61±0.21	1.24±0.48
	FF	13.9±2.8	1743±671	1.92±0.16	0.74±0.07	2.53±0.50
MC 292 (July 2001) Post-Development	NF	13.1±3.1	10327±11780	1.51±0.30	0.59±0.07	1.87±0.44
	FF	13.4±3.9	5448±3261	1.69±0.38	0.69±0.07	2.00±0.58

#### 16.4.3.2 Benthic Community Status

Sediment profile imaging (SPI) was used to characterize benthic community structure along near-field and far-field transects at the four sites (*Chapters 6 and 7*). Two parameters derived from SPI image analysis, infaunal successional stage and organism sediment index (OSI), were estimated from images generated at VK 916 and GB 516 (*Chapter 6*). These parameters were not calculated for SPI images from GB 602 and MC 292 because of the uniformity of the images and

general lack of biogenic activity (*Chapter 7*). However, *Chapter 7* does provide a written summary of benthic biological conditions at these two discharge sites.

Infaunal successional stage is based on observed patterns of recolonization of disturbed shallow-water marine sediments (Rhodes and Germano 1986). Stage I infauna are small and live close to the sediment-water interface. They are pioneers and opportunists in that they do not require a deep layer of oxidized sediment. The burrowing and feeding activity of Stage I fauna, mainly small annelids, deepens the RPD depth, allowing colonization by larger, more aerobic benthic animals, such as amphipods (Stage II). Stage II benthos are transitional species that often are unique to different benthic habitats. The Stage II community at these deepwater, continental slope sites has not been characterized. Stage III animals are large, deep-burrowing, head-down deposit feeders, usually polychaetes and echinoderms, that aerate the sediments to a depth of several centimeters. Stage I through III benthos can co-occur at a site and their presence together often indicates a healthy, diverse benthic community.

The OSI takes into account the depth of the apparent RPD, successional stage, presence or absence of sediment methane bubbles, and the presence or absence of reduced sediments near the sediment-water interface. OSI values can range from +11 (best habitat quality) to -10 (worst habitat quality). OSI values below about +6 often are associated with disturbed benthic habitats. Negative OSI values reflect a highly disturbed benthos.

Most near-field and far-field sediments collected at VK 916 before exploratory drilling were characterized by Stage I-III successional stages and positive OSI values, both indicative of a healthy benthic community (*see Chapter 15, Table 15.6*). There were small patches of sediment with Stage I seres and OSI values between +2 and 6 along both near-field and far-field transects, indicating a patchy distribution of mild sediment disturbance.

The frequency of Stage I or azoic near-field sediments was higher at the time of the post-exploratory drilling in August 2002 at VK 916. Many near-field sediments near the drilling site were azoic or were depauperate of benthic fauna. The surface of some of these sediments contained deposits of black, sulfidic sediment and apparent RPD depth was at the sediment surface, both indicative of severe organic enrichment. OSI values ranged from -7 to +7. The azoic sediments with 0-cm RPD depths had OSI of -4 or lower; sediments with Stage I-III communities had OSI values mostly higher than +5. The post-drilling SPI survey shows that the near-field benthic ecosystem at VK 916 is near or just below the OSI threshold of +6 (disturbed benthic habitat) and 25% of sediment stations had OSI below 0, indicating very poor habitat quality. Most far-field sediments collected in August 2002 from VK 916 contained Stage I-III successional stages.

SPI imagery revealed evidence of a slight improvement in benthic habitat quality at GB 516 between the post-exploration survey (November 2000) and the post-development survey (July 2001). In November 2000, most near-field sediments were either Stage I or azoic. Microbial mats were observed at 29% of near-field stations. More than 35% of near-field sediments had negative values for OSI.

At the time of the post-development survey, about half the sediments were Stage I or azoic. No microbial mats were observed; however, black, sulfidic sediments extended to the sediment surface at 15% of near-field stations. OSI values were negative at 18% of near-field stations. Far-field sediments were mostly healthy before and after development drilling at GB 516.

Although successional stage and OSI were not estimated for GB 602 and MC 292, some comparisons with VK 916 and GB 516 can be made. Post-development conditions in near-field sediments at GB 602 were similar to those in near-field sediments at GB 516 at the time of the post-development survey (*Chapter 7*). There were no Stage III animals at near-field stations; less than half the stations supported Stage I benthic fauna. There also was evidence of microbial mats and sulfidic sediments at the sediment surface. Far-field sediments appeared to be well-oxidized and aerobic. However, benthic fauna were scarce.

Only a few near-field sediments at the other post-development site, MC 292, appeared to be disturbed. More than 80% of near-field sediments contained evidence of benthic fauna, and more than 20% of sediments contained deep-dwelling benthic infauna (Stage III). Sediments appeared well-oxygenated with deep RPD depths. Far-field sediments at MC 292 had biological activity similar to that at near-field sediments. Overall, sediments at MC 292 showed minimal evidence of benthic disturbance.

#### **16.4.4 Demersal/Benthic Megafauna**

Benthic megafaunal abundance and distribution were estimated from bottom photographs taken along near-field and far-field transects at each of the four sites (see *Chapter 12*). Most of the megafauna detected in the photographs were small. Overall, relative abundance of small megafauna was similar along near-field and far-field transects and at the four sites. The average number of megafauna along individual transects at a site ranged from 9.33 animals at MC 292 in July 2001 to 53.6 animals at VK 916 in August 2002 after exploratory drilling. Coelenterates (sea anemones) often were the most abundant megafauna.

The only statistically significant differences in megafaunal abundances at near-field and far-field sites were a higher abundance of fish and a lower abundance of ophiuroids in the near-field. The differences in abundances of these two taxa in the near-field and far-field were greatest at VK 916 (post-exploration) and GB 516 (both post-exploration and post-development). There was little or no difference in megafaunal abundances in the near-field and far-field at GB 602 and MC 292.

#### **16.4.5 Summary of Injury**

Evidence of biological injury to the deepwater benthic ecosystem from drilling discharges was evaluated based on sediment toxicity and various aspects of the structure and function of different components of the benthic community in the near-field and far-field of the four discharge sites. Although pre-drilling and post-drilling surveys were performed at two locations, VK 916 and GB 516, it was difficult to distinguish drilling-related effects from changes attributable to seasonal or interannual changes in environmental conditions on the continental slope. Therefore, biological characteristics of the near-field and far-field benthic environment at each site and each survey were evaluated for evidence of drilling-related biological effects (injury). There were

differences in most biological parameters between near-field and far-field locations at the four sites, or between pre-drilling and post-drilling surveys at VK 916 (**Table 16.19**).

**Table 16.19.** Summary of evidence of biological injury to the near-field benthic environment at the four study sites. + = evidence of biological effects; +- = weak or uncertain evidence of biological effects; – = no evidence of biological effects.

Parameter	VK 916	GB 516	GB 602	MC 292
Sediment toxicity	NS	NS	+	+
Oxygen inventory	+	+	+	+-
Eh and RPD	+	+	+	+
Microbial ATP	–	–	–	–
Microbial mats	+	+	+	–
Meiofauna	+	+	+	+
Macroinfauna	+	+	+	+
Benthic community status	+	+	+	–
Megafauna	+	+	–	–

ATP = adenosine triphosphate; NS = no samples; RPD = redox potential discontinuity.

Sediment toxicity was evaluated at the two post-development sites, MC 292 and GB 602. Near-field sediments at both sites were more toxic than far-field sediments (**Table 16.19**). This toxicity could have been caused by accumulation of toxic drill cuttings ingredients in sediments, or it could be a secondary effect of organic enrichment (sediment hypoxia and increase in sediment sulfide and ammonia).

Changes in sediment Eh, RPD depth, and oxygen inventory in sediments are secondary effects of sediment microbial activity. There was evidence of lower Eh, RPD depth, and smaller oxygen inventory at some near-field than at far-field stations at all four sites (**Table 16.19**). However, it was difficult to detect changes in microbial activity. Nevertheless, the patterns of change in these parameters are consistent with a drilling-discharge-mediated organic enrichment in some near-field sediments. Organic enrichment was patchy, probably reflecting the patchy distribution of drill cuttings solids on the near-field seafloor.

Near-field and far-field meiofaunal and macroinfaunal communities were different at all four sites (**Table 16.19**). Near-field sediments tended to have higher densities of benthic fauna but lower diversity, evenness, and richness than far-field sediments. This is a characteristic feature of mild organic enrichment (Pearson and Rosenberg 1978). Near-field sediments are dominated by a small number of abundant opportunistic species.

There was little evidence of biological effects of drilling discharges on near-field megafaunal communities (**Table 16.19**). Fishes tended to be more abundant and ophiuroids tended to be less abundant in near-field than in far-field sediments. This probably was caused by accumulation of solids on the near-field seafloor.

## 16.5 RISK CHARACTERIZATION

Data on exposure of the species of concern to the chemicals of concern is compared to data on biological effects (injury) in the risk characterization. The relationships between the magnitude of exposure and severity of injury are examined. If the risk assessment is based solely or primarily on field monitoring data, as this one has been, it may be possible to estimate the area of the affected environment exhibiting different levels of risk (or severity) of injury attributable to the chemicals or disturbances of concern.

### 16.5.1 Causes of Sediment Toxicity

Some near-field sediment samples from MC 292 and GB 602 were toxic to benthic amphipods (*Chapter 14*). SBF chemical, PAH, and barium concentrations in sediments were used as quantitative exposure parameters to evaluate possible causes of sediment toxicity. Regression of SBF chemical concentration, PAH concentration, and barium concentration in individual samples of near-field and far-field sediments from GB 602 and MC 292, separately or combined against fraction surviving in each sediment sample, yielded negative slopes: an inverse relationship between concentrations of chemicals in sediment and survival of amphipods in the toxicity test. The correlation coefficients for the regression between sediment barium concentration and fractional survival were  $r^2 = 0.50$  for MC 292 and  $r^2 = 0.57$  for GB 602. For the regression of SBF versus fractional survival, the correlation coefficients were  $r^2 = 0.60$  for MC 292 and  $r^2 = 0.35$  for GB 602. There was no relationship between sediment PAH concentration and survival of benthic amphipods at MC 292, but there was a weak negative relationship for GB 602 ( $r^2 = 0.40$ ).

Barium is a better indicator than SBF chemical of the total drilling solids discharge accumulation on the seafloor, because barium (as barite) is more persistent in sediments than SBF chemical, and barium is derived from WBM and WBM cuttings as well as SBM cuttings. The total mass of WBM-related discharges was nearly 10 times higher than the mass of SBM cuttings discharged at all four sites (**Table 16.1**). These results suggest that chemicals associated with both WBM and SBM waste solids in near-field sediments are contributing to sediment toxicity. The highest concentrations of SBF chemical and barium in sediment associated with significant sediment toxicity ( $\leq 50\%$  survival) are about 1,000 mg/kg and 20,000 mg/kg, respectively. Barite and SBF chemicals have low toxicities to marine animals (Neff et al. 2000), so it is uncertain what drilling waste ingredients actually are causing toxicity.

### 16.5.2 Causes of Organic Enrichment

There was evidence of sediment organic enrichment at all four sites. Organic enrichment was indicated by low Eh and oxygen inventories and shallow RPD depths, as well as the presence of microbial mats on the sediment surface at three sites. Evidence from microbial production was unclear.

Negative Eh and low oxygen inventories (both indicative of a severely disturbed benthic habitat) occurred at stations where barium, SBF chemical, and TOC concentrations were high, indicating that the organic enrichment was being caused all or in major part by accumulation of drilling wastes on the seafloor. WBM cuttings typically have a lower biological oxygen demand than

SBM cuttings (Dow et al. 1990; Neff 2005). SBF chemicals are required by the effluent limitations guidelines in NPDES permits to be biodegradable. Esters are highly biodegradable; IOs and LAOs are somewhat less so (Neff et al. 2000; Melton et al. 2004). There are hydrocarbon seeps in the vicinity of the Garden Banks discharge sites; these could have contributed to organic enrichment of regional sediments. However, this contribution probably would be similar in near-field and far-field sediments. Thus, it is probable that SBF chemicals and other biodegradable organic chemicals in SBM (e.g., emulsifiers) are the major contributors to the enhanced organic enrichment in near-field sediments at the four sites.

### 16.5.3 Changes in Benthic Communities

Meiofaunal and macrofaunal densities and community parameters were different in near-field and far-field sediments after exploratory or development drilling at all four sites. Abundances of several species of benthic fauna tended to be higher in near-field than in far-field sediments, possibly an effect of organic enrichment of near-field sediments.

Statistical correlations were examined between densities of different meiofaunal and macrofaunal groups and the values of several exposure parameters (SBF chemical, barium, TOC, and percent sand) at near-field stations. Most correlations were not significant for meiofaunal groups. There was no consistent relationship between any of the exposure parameter values and the abundance of meiofaunal annelids, harpacticoid copepods, or nematodes. Annelid abundance was positively correlated with sediment barium concentration at GB 516 and MC 292, and with SBF chemical concentration at MC 292, but not at GB 602 and VK 916 (*Chapter 11*). Harpacticoid and nematode densities were negatively correlated with SBF chemical concentration and percent silt at GB 516 and GB 602. These results suggest that the near-field meiofaunal community at some sites was affected by accumulation in sediments of fine-grained material, possibly from drilling discharges.

The abundance of macrofaunal annelids and gastropods in near-field sediments at GB 516, GB 602, and MC 292 was positively correlated with sediment, barium, and/or SBF chemical and TOC concentration. There also was a positive correlation between bivalve mollusk densities and sediment barium concentration at MC 292. Gastropod abundance also was positively correlated with percent sand at GB 516.

In general, near-field sediments supporting elevated densities of macrofaunal annelids had barium concentrations of 10,000  $\mu\text{g/g}$  or higher and SBF chemical concentrations of 1,000  $\mu\text{g/g}$  or higher. Extremely high densities of gastropods in near-field sediments at GB 516 and GB 602 were associated with SBF chemical concentrations of 4,500  $\mu\text{g/g}$  or higher and barium concentrations of 55,000  $\mu\text{g/g}$  or higher.

The abundance of amphipods, ostracods, and aplacophorans in near-field sediments was inversely correlated with one or more of sediment barium, SBF chemical, or TOC concentration, or percent sand, silt, or clay in sediments. Strongest negative correlations were for amphipods and ostracods and barium and SBF chemical concentrations in sediments at GB 516 in November 2000 (before development drilling). These observations suggest that the abundance of annelids, gastropods, and bivalves tends to increase and the abundance of amphipods, ostracods, and aplacophorans



tends to decrease in response to deposition on the sediments of WBM and SBM cuttings solids. This could be a response to organic enrichment or to changes in sediment texture.

#### 16.5.4 Summary

This risk assessment has shown that drilling mud and cuttings ingredients accumulated in a patchy distribution in near-field (<500 m from discharge site) sediments at four exploration or development sites in approximately 1,000 m of water on the continental slope of the Gulf of Mexico. Excess barium and SBF chemical were the best indicators of the presence of drilling wastes in sediments. A few far-field sediment samples also contained excess barium or SBF chemical and may have been contaminated by discharges from the drilling activities monitored during this study or from other nearby exploration and development operations.

The accumulation of drilling wastes in near-field sediments caused a variety of changes in the benthic environment at the sites. It appears that the primary effect of the discharges was organic enrichment of near-field sediments. The influx of biodegradable organic matter to the sediments associated with the discharged solids stimulated microbial metabolism and reduced sediment permeability, causing oxygen depletion and redox changes in surficial sediments. Benthic meiofaunal and macrofaunal communities responded to the reduced oxygen inventories and shallower RPD depths.

The abundance of some species, particularly annelids, increased and the abundance of some other species, particularly amphipods and ostracods, increased in sediments with the greatest organic enrichment. The benthic communities were denser but less diverse in organically-enriched sediments than in far-field, unenriched sediments. These patterns of benthic community change at near-field sites are consistent with mild organic enrichment of near-field sediments (Gray et al. 2002; Rosenberg et al. 2004).

It is possible that organic enrichment contributed to the toxicity of near-field sediments in laboratory toxicity tests, by stimulating production of toxic sulfide and ammonia. The major ingredients of WBM and SBM cuttings have a low toxicity (Neff et al. 2000; Neff 2005). Elevated toxicity in laboratory bioassays was observed in sediments containing more than 10,000 to 20,000  $\mu\text{g/g}$  barium and 1,000  $\mu\text{g/g}$  SBF chemical. These also were the concentrations in near-field sediments associated with increased abundance of annelids. Gastropod abundance was increased markedly in sediments containing more than 55,000  $\mu\text{g/g}$  barium. Thus, sediment toxicity was not caused by barium or SBF chemicals.

Concentrations of 10,000  $\mu\text{g/g}$  barium or 1,000  $\mu\text{g/g}$  SBF chemical in sediments can be used as an indicator of a drill cuttings concentration above which benthic biological community changes can be expected. Sediments with barium or SBF chemical concentrations exceeding this indicator concentration were distributed in a highly patchy fashion in the near-field of the four sites. Even in this relatively small area around a deepwater discharge ( $\approx 78$  ha based on the near-field radius of 500 m), effects on benthic communities are extremely uneven, ranging from unaffected to severely disturbed. The patchy distribution of drilling waste solids and disturbed benthic communities on the near-field seafloor should facilitate ecological recovery as organic matter in the deposited drilling solids is depleted and oxygen penetrates deeper into sediments. The

unaffected substrates can serve as a source of recruits to nearby areas affected by drilling discharges.

The near-field data are primarily from within a 500-m radius around each site. Based on the geophysical surveys, areas mapped as cuttings extended beyond this radius at three of the sites, with the greatest extent (about 1 km) observed at GB 602 and GB 516 (*Chapter 4*). As discussed in *Chapter 15*, areas mapped as cuttings generally had higher barium and SBF concentrations, but the results were not consistent enough to allow for extrapolation of barium and SBF concentrations outside the 500-m radius. One discretionary station at GB 602, located about 1,000 m southwest of the site center (and *not* within the mapped cuttings zone), had a barium concentration of 14,800  $\mu\text{g/g}$  and an SBF concentration of 930  $\mu\text{g/g}$ . These values either exceed (barium) or are just under (SBF) the likely thresholds for biological effects cited above. Barium and SBF concentrations at far-field sites, including those located 2 to 3 km from previous unrelated drilling (*Chapter 3*), were far below these thresholds. The results suggest that biological effects may have occurred in some areas between about 500 and 1,000 m from the development wellsites.

- Aharon, P., D. Van Gent, B. Fu, and L.M. Scott. 2001. Fate and effects of barium and radium-rich fluid emissions from hydrocarbon seeps on the benthic habitats of the Gulf of Mexico offshore Louisiana. OCS Study MMS 2001-004. Report from Louisiana State University, Coastal Marine Institute for the U.S. Dept. of the Interior, Minerals Management Service, Gulf of Mexico OCS Region, New Orleans, LA. 142 pp.
- Anderson, J.B., R.B. Wheeler, and R.R. Schwarzer. 1981. Sedimentology and geochemistry of recent sediments, pp. 59-67. In: B.S. Middleditch (ed.), Environmental Effects of Offshore Oil and Gas Production: The Buccaneer Gas and Oil Field Study. Plenum Press, NY.
- Annis, M.R. 1997. Retention of synthetic-based drilling material on cuttings discharged to the Gulf of Mexico. Report for the American Petroleum Institute (API) *ad hoc* Retention on Cuttings Work Group under the API Production Effluent Guidelines Task Force. American Petroleum Institute, Washington, DC. August 29, 1997. Various pages.
- ASTM. 1999. Method E 1367-99, Standard Guide for Conducting 10-day Static Sediment Toxicity Tests with Marine and Estuarine Amphipods. ASTM, West Conshohocken, PA.
- Atkinson, T., S. Gairns, D.A. Cowan, M.J. Danson, D.W. Hough, D.B. Johnson, P.R. Norris, N. Raven, C. Robinson, R. Robson, and R.J. Sharp. 2000. A microbiological survey of Montserrat Island hydrothermal biotopes. *Extremophiles* 4:305-313.
- Atlas, R.M. 1993. Extraction of DNA from soils and sediments. In: P. Kemp, B. Sherr, E. Sherr, and J. Cole (eds.), Handbook of Methods in Aquatic Microbial Ecology. Lewis Publishers, Boca Raton, FL.
- Avice, J.C. 2000. Phylogeography: The history and formation of species. Harvard University Press, Cambridge, MA. 447 pp.
- Ayers, R.C., Jr., T.C. Sauer, Jr., R.P. Meek, and G. Bowers. 1980. An environmental study to assess the impact of drilling discharges in the Mid-Atlantic. I. Quantity and fate of discharges, pp. 382-416. In: Symposium on Research on Environmental Fate and Effects of Drilling Fluids and Cuttings. American Petroleum Institute, Washington, DC.
- Baker, J.H., W.D. Jobe, C.L. Howard, K.T. Kimball, J. Janousek, and P.R. Chase. 1981. Benthic Biology, Part 6, In: C.A. Bedinger, Jr. (ed.), Ecological Investigations of Petroleum Production Platforms in the Central Gulf of Mexico, Southwest Research Institute, Houston, TX. 209 pp. + app.
- Bancroft, K., E.A. Paul, and W.J. Wiebe. 1976. The extraction and measurement of adenosine triphosphate from marine sediments. *Limnol. Oceanogr.* 21:473-480.
- Barradas-Ortiz, C., P. Briones-Fourzán, and E. Lozano-Álvarez. 2003. Seasonal reproduction and feeding ecology of giant isopods *Bathynomus giganteus* from the continental slope of the Yucatan peninsula. *Deep-Sea Res. I* 50:495-513.
- Baud, R.D., R.H. Peterson, C. Doyle, and G.E. Richardson. 2000. Deepwater Gulf of Mexico: America's emerging frontier. U.S. Dept. of the Interior, Minerals Management Service, Gulf of Mexico OCS Region, New Orleans, LA. OCS Study MMS 2000-022. 89 pp.
- Beaty, B.J., W.C. Black, J.O. Carlson, W.H. Clements, N. DuTeau, E. Harrahy, J. Nuckols, K.E. Olson, and A. Rayms-Keller. 1998. Molecular and genetic ecotoxicologic approaches to aquatic environmental bioreporting. *Env. Health Perspec.* 106:1,395-1,407.
- Belfiore, N.M. and S.L. Anderson. 2001. Effects of contaminants on genetic patterns in aquatic organisms: A review. *Mut. Res.* 489:97-122.

- Bender, M.L., W. Martin, J. Hess, F. Sayles, L. Ball, and C. Lambert. 1987. A whole-core squeezer for interfacial pore water sampling. *Limnol. and Oceanogr.* 32:1,214-1,225.
- Bett, B.J., A. Vanreusel, M. Vincx, T. Soltwedel, O. Pfannkuche, P.J.D. Lamshead, A.J. Gooday, T. Ferrero, and A. Dinet. 1994. Sampler bias in the quantitative study of deep-sea meiobenthos. *Mar. Ecol. Prog. Ser.* 104:197-203.
- Bickham, J.W., S. Sandhu, P.D.N. Hebert, L. Chikhi, and R. Athwal. 2000. Effects of chemical contaminants on genetic diversity in natural populations: Implications for biomonitoring and ecotoxicology. *Mut. Res.* 463:33-51.
- Bjorkman, K.M. and D.M. Karl. 2001. A novel method for the measurement of dissolved adenosine and guanine triphosphate in aquatic habitats: Applications to marine microbial ecology. *J. Microbiol. Methods* 47:159-167.
- Blake, J.A. and J.F. Grassle. 1994. Benthic community structure on the U.S. South Atlantic Slope off the Carolinas: Spatial heterogeneity in a current-dominated system. *Deep-Sea Res. II* 41:835-874.
- Blake, J.A., B. Hecker, J.F. Grassle, N. Maciolek-Blake, B. Brown, M. Curran, B. Dade, S. Freitas, and R.E. Ruff. 1985. Study of biological processes on the U.S. South Atlantic slope and rise. Phase I. Benthic characterization study. Report by Battelle New England Marine Research Laboratory to the U.S. Dept. of the Interior, Minerals Management Service, Washington, DC. OCS Study MMS 85-0097. 2 vol.
- Blake, J.A., B. Hecker, J.F. Grassle, B. Brown, M. Wade, P.D. Boehm, E. Baptiste, B. Hilbig, N. Maciolek, R. Petrecca, R.E. Ruff, V. Starczak, and L. Watling. 1987. Study of biological processes on the U.S. south Atlantic slope and rise, Phase 2. Report to the U.S. Dept. of the Interior, Minerals Management Service, Washington, DC. OCS Study MMS 86-0096. 414 pp. + app.
- Boehm, P., D. Turton, A. Raval, D. Caudle, D. French, N. Rabalais, R. Spies, and J. Johnson. 2001. Deepwater program: Literature review, environmental risks of chemical products used in Gulf of Mexico Deepwater Oil and Gas Operations. Volume I: Technical Report. U.S. Department of the Interior, Minerals Management Service, Gulf of Mexico OCS Region, New Orleans, LA. OCS Study MMS 2001-011. 326 pp.
- Bonsdorff, E., R.J. Diaz, R. Rosenberg, A. Norkko, and G.R. Cutter. 1996. Characterization of soft-bottom benthic habitats of the Åland Islands, northern Baltic Sea. *Mar. Ecol. Prog. Ser.* 142:235-245.
- Boswell, P.G.H. 1961. *Muddy Sediments: Some Geotechnical Studies for Geologists, Engineers, and Soil Scientists.* Heffer, Cambridge, England.
- Bouma, A.H. and H.H. Roberts. 1990. Northern Gulf of Mexico continental slope. *Geo-Marine Letters* 10:177-181.
- Bowen, B.W. and W.S. Grant. 1997. Phylogeography of the sardines (*Sardinops* spp.): Assessing biogeographic models and population histories in temperate upwelling zones. *Evolution* 51:1,601-1,610.
- Brandsma, M.G. 1990. Simulation of benthic accumulations of mud and cuttings discharged from Mobil Oil Corporation well, Manteo Area, Block 467, Cape Hatteras, North Carolina. Volume II, Appendix N-4. In: *Atlantic Outer Continental Shelf: Final environmental report on proposed exploratory drilling offshore North Carolina.* U.S. Department of the Interior, Minerals Management Service, Atlantic OCS Region, Environmental Assessment Section, Herndon, VA.
- Brandsma, M.G. 1996. Computer simulations of oil-based mud cuttings discharges in the North Sea, pp. 25-40. In: *The Physical and Biological Effects of Processed Oily Drill Cuttings (Summary Report).* E&P Forum, London.

- Brandsma, M.G., L.R. Davis, R.C. Ayers, Jr., and T.C. Sauer, Jr. 1980. A computer model to predict the short-term fate of drilling discharges in the marine environment, pp. 588 - 608. In: Volume I. Proceedings of Symposium, Research on Environmental Fate and Effects of Drilling Fluids and Cuttings, January 21-24, 1980, Lake Buena Vista, Florida.
- Breckenridge, R.P. and A.B. Crockett. 1995. Determination of background concentrations of inorganics in soils and sediments at hazardous waste sites. EPA/540/5-95/600. U.S. Environmental Protection Agency, Office of Research and Development, Washington, DC. 32 pp.
- Breuer, E., J.A. Howe, G.B. Shimmield, D.Cummings, and J. Carroll. 1999. Contaminant leaching from drill cuttings piles of the northern and central North Sea: a review. Report to NERC and UKOOA from the Scottish Association for Marine Science, Dunstaffnage Marine Laboratory, Oban, Scotland. 49 pp.
- Brooks, J.M., M.C. Kennicutt II, R.R. Bidigare, and R.A. Fay. 1985. Hydrates, oil seepage, and chemosynthetic ecosystems on the Gulf of Mexico slope. EOS Transactions American Geophysical Union 66:106.
- Brooks, J.M., M.C. Kennicutt II, T.L. Wade, A.D. Hart, G.J. Denoux, and T.J. McDonald. 1989. Hydrocarbon distributions around a shallow water multiwell platform. Env. Sci. Technol. 24(7):1,079-1,085.
- Brooks, J.M., M.C. Kennicutt, T.L. Wade, A.D. Hart, G.J. Denoux, and T.J. McDonald. 1990. Hydrocarbon distributions around a shallow water multiwell platform. Environ. Sci. Technol. 24:1079-1085.
- Burton, R.S. 1998. Intraspecific phylogeography across the point conception biogeographic boundary. Evolution 52:734-745.
- Burton, R.S. and B.- N. Lee. 1994. Nuclear and mitochondrial gene genealogies and allozyme polymorphism across a major phylogeographic break in the copepod *Tigriopus californicus*. Proc. Natl. Acad. Sci. USA 91:5,197-5,201.
- Burton, R.S., M.W. Feldman, and J.W. Curtsinger. 1979. Population genetics of *Tigriopus californicus* (Copepoda: Harpacticoida): I. Population structure along the central California coast. Mar. Ecol. Prog. Ser. 1:29-39.
- Canadian Association of Petroleum Producers. 2001. Technical Report. Offshore Drilling Waste Management Review. Report 2001-0007 from Canadian Association of Petroleum Producers, Halifax, Nova Scotia, Canada. 240 pp.
- Candler, J.E., S. Hoskin, M. Churan, C.W. Lai, and M. Freeman. 1995. Seafloor monitoring for synthetic-based mud discharged in the western Gulf of Mexico, pp. 51-69. In: SPE/EPA Exploration & Production Environment Conference. Houston, TX, 27-29 March 1995. SPE 29694. Society of Petroleum Engineers, Inc., Richardson, TX.
- Carman, K.R., J.W. Fleeger, and S. Pomarico. 1997. Response of a benthic food web to hydrocarbon contamination. Limnol. Oceanogr. 42:561-571.
- Carney, R. (ed.). 1998. Workshop on environmental issues surrounding deepwater oil and gas development. U.S. Dept. of the Interior, Minerals Management Service, Gulf of Mexico OCS Region, New Orleans, LA. OCS Study MMS 98-0022. 62 pp.
- Carney, R.S. 2001. Management applicability of contemporary deep-sea ecology and reevaluation of Gulf of Mexico studies. Final report. U.S. Dept. of the Interior, Minerals Management Service, Gulf of Mexico OCS Region, New Orleans, LA. OCS Study MMS 2001-095. 170 pp.
- Carr, R.S. 1993. Survey of Galveston Bay bottom sediments and benthic communities. Galveston Bay National Estuary Program Rep. GBNEP-30.
- Carr, R.S. and D.C. Chapman. 1992. Comparison of solid-phase and pore-water approaches for assessing the quality of marine and estuarine sediments. Chem. Ecol. 7:19-30.

- Chase, M.R., R.J. Etter, and J.M. Quattro. 1998. Bathymetric patterns of genetic variation in a deep-sea protobranch bivalve, *Deminucula atacellana*. *Mar. Biol.* 131:301-308.
- Chen, Y.N., N. Senesi, and M. Schnitzer. 1977. Information provided on humic substances by E4/E6 ratios. *J. Soil Sci. Soc. Am.* 41:352-358.
- Clarke, K.R. 1993. Non-parametric multivariate analyses of changes in community structure. *Austral. J. Ecol.* 18:117-143.
- Clarke, K.R. and R.N. Gorely. 2001. Primer v5: User Manual/Tutorial PRIMER-E, Plymouth, UK.
- Clement, M., D. Posada, and K.A. Crandall. 2000. TCS: A computer program to estimate gene genealogies. *Mol. Ecol.* 9:1,657-1,659.
- Clesceri, P.R., A.E. Greenberg, and R.R. Trussel. 1989. Standard Methods for the Examination of Water and Wastewater. American Public Health Association.
- Continental Shelf Associates, Inc. 1989. Fate and effects of drilling fluid and cutting discharges in shallow nearshore waters. Report for the American Petroleum Institute.
- Continental Shelf Associates, Inc. 2000. Deepwater Gulf of Mexico environmental and socioeconomic data search and literature synthesis. Volume I, Narrative report. U.S. Dept. of the Interior, Minerals Management Service, Gulf of Mexico OCS Region, New Orleans, LA. OCS Study MMS 2000-049.
- Continental Shelf Associates, Inc. 2004. Final report: Gulf of Mexico synthetic based muds monitoring program. Report for the SBM Research Group, Houston, TX. 3 vol.
- Coull, B.C. and G.T. Chandler. 1992. Meiofauna and pollution: Field, laboratory and mesocosm studies. *Oceanogr. Mar. Biol. Ann. Rev.* 30:191-271
- Cranswick, D. and J. Regg. 1997. Deepwater in the Gulf of Mexico: America's new frontier. U.S. Dept. of the Interior, Minerals Management Service, Gulf of Mexico OCS Region, New Orleans, LA. OCS Study MMS 97-004. 43 pp.
- Creasy, S.S. and A.D. Rogers. 1999. Population genetics of bathyal and abyssal organisms. *Adv. Mar. Biol.* 35:1-151.
- Cunningham, H.W. and R.G. Wetzel. 1978. Fulvic acid interferences on ATP determinations in sediments. *Limnol. Oceanogr.* 23:166-173.
- Dale, N.G. 1974. Bacteria in intertidal sediments: Factors related to their distribution. *Limnol. Oceanogr.* 19:509-518.
- Dalzell, D.J.B. and N. Christofi. 2002. An ATP luminescence method for direct toxicity assessment of pollutants impacting on the activated sewage sludge process. *Water Res.* 36:1,493-1,502.
- Dalzell, D.J.B., S. Alte, E. Aspichueta, A. de La Sota, J. Etxebarria, M. Gutierrez, C.C. Hoffmann, D. Sales, U. Obst, and N. Christofi. 2002. A comparison of five rapid direct toxicity assessment methods to determine toxicity of pollutants to activated sludge. *Chemosphere* 47:534-545.
- DeFlaun, M.F. and L.M. Mayer. 1983. Relationships between bacteria and grain surfaces in intertidal sediments. *Limnol. Oceanogr.* 28:873-881.
- Delvigne, G.A.L. 1996. Laboratory investigations on the fate and physicochemical properties of drill cuttings after discharge into the sea, pp. 16-24. In: *The Physical and Biological Effects of Processed Oily Drill Cuttings (Summary Report)*. E&P Forum, London.
- Deming, J. 1993. <sup>14</sup>C Tracer method for measuring microbial activity in deep-sea sediments. In: P. Kemp, B. Sherr, E. Sherr, and J. Cole (eds.), *Handbook of Methods in Aquatic Microbial Ecology*, Lewis Publishers, Boca Raton, FL.
- Dexter, D.M. 1995. Salinity tolerance of *Cletocamptus deitersi* (Richard 1897) and its presence in the Salton Sea. *Bull. So. Cal. Acad. Sci.* 94:169-171.

- Diaz, R.J. and L.C. Schaffner. 1988. Comparison of sediment landscapes in the Chesapeake Bay as seen by surface and profile imaging, pp. 222-240. In: M.P. Lynch and E.C. Krome (eds.), Understanding the estuary; Advances in Chesapeake Bay research. Chesapeake Res. Consort. Pub. 129, CBP/TRS 24/88.
- Diaz, R.J., G.R. Cutter, and D.C. Rhoads. 1994. The importance of bioturbation to continental slope sediment structure and benthic processes off Cape Hatteras, North Carolina. Deep-Sea Res. Part 2, 41(4-6):719-734.
- Diegel, F.A., J.F. Karlo, D.C. Schuster, R.C. Shoup, and P.R. Tauvers. 1995. Cenozoic structural evolution and tectono-stratigraphic framework of the northern Gulf Coast continental margin, pp. 109-151. In: M.P.A. Jackson, D.G. Roberts, and S. Snelson (eds.), Salt Tectonics: A Global Perspective. AAPG Memoir 65.
- Dow, F.K., J.M. Davies, and D. Raffaelli. 1990. The effects of drilling cuttings on a model marine sediment system. Mar. Environ. Res. 29:103-124.
- Drever, J.I. 1997. The Geochemistry of Natural Waters. Prentice Hall, Upper Saddle River, NJ. 436 pp.
- Dutka, B. J., K.K. Kwan, S.S. Rao, A. Jurkovic, R. Mcinnis, G.A. Palmateer, and B. Hawkins. 1991. The use of bioassay to evaluate river water and sediment quality. Environ. Toxicol. Water Qual. 6:309-327.
- Edmands, S. 2001. Phylogeography of the intertidal copepod *Tigriopus californicus* reveals substantially reduced population differentiation at northern latitudes. Mol. Ecol. 10:1,743-1,750.
- Edzwald, J.K., W.C. Becker, and K.L. Wattier. 1985. Surrogate parameters for monitoring organic matter and THM precursors. J. Am. Water Works Assn. 77:122-132.
- Egeberg, P.K. 2000. ATP as a proxy for bacteria numbers in deep sea sediments, and correlation with geochemical parameters (Site 944). In: C.K. Paull, R. Matsumoto, et al., Proc. ODP, Sci. Results, 164:379-392. Ocean Drilling Program, College Station, TX.
- Etter, R.J., M.A. Rex, M.C. Chase, and J.M. Quattro. 1999. A genetic dimension to deep-sea biodiversity. Deep-Sea Res. I 46:1,095-1,099.
- Ewin, M. and R.A. Davis. 1967. Lebensspuren photographed on the ocean floor, pp. 259-294. In: J.B. Hersey (ed.), Deep-Sea Photography. Baltimore: Johns Hopkins Univ. Press.
- Excoffier, L., P.E. Smouse, and J.M. Quattro. 1992. Analysis of molecular variance inferred from metric distances among DNA haplotypes: Application to human mitochondrial DNA restriction data. Genetics 131:479-491.
- Fauchald, K. 1972. Benthic Polychaetous Annelids from Deep Water off Western Mexico and Adjacent Areas in the Eastern Pacific Ocean. Allan Hancock Monographs in Marine Biology, Number 7. The Allan Hancock Foundation, University of Southern California, Los Angeles, CA.
- Fechhelm, R.G., B.J. Gallaway, and J.M. Farmer. 1999. Deepwater sampling at a synthetic drilling mud discharge site on the outer continental shelf, northern Gulf of Mexico, pp. 509-513. In: 1999 SPE/EPA Exploration and Production Environmental Conference, Austin, TX, 28 February-3 March 1999. SPE 52744. Society of Petroleum Engineers, Richardson, TX.
- Fenchel, T. 1969. The ecology of marine microbenthos. IV. Structure and function of the benthic ecosystem, its chemical and physical factors and microfauna communities with special reference to the ciliated Protozoa. Ophelia 6:1-182.
- Fleeger, J.W., D.W. Foltz, and A. Rocha-Olivares. 2001. How does produced water cause a reduction in the genetic diversity of harpacticoid copepods? Final report. OCS Study MMS 2001-078. U.S. Dept. of the Interior, Minerals Management Service, Gulf of Mexico OCS Region, New Orleans, LA. 35 pp.
- Folk, R.L. 1974. Petrology of sedimentary rocks. Hemphill Publishing Co., Austin, TX. 184 pp.

- Folmer, O., M. Black, W. Hoeh, R. Lutz, and R. Vrijenhoek. 1994. DNA primers for amplification of mitochondrial cytochrome c oxidase subunit I from diverse metazoan invertebrates. *Mol. Mar. Biol. Biotechnol.* 3:294-299.
- France, S.C. and T.D. Kocher. 1996. Geographic and bathymetric patterns of mitochondrial 16S rRNA sequence divergence among deep-sea amphipods, *Eurythenes gryllus*. *Mar. Biol.* 126:633-643.
- French, L.S., E.G. Kazanis, L.C. Labiche, T.M. Montgomery, and G.E. Richardson. 2005. Deepwater Gulf of Mexico 2005: Interim report of 2004 highlights. U.S. Dept. of the Interior, Minerals Management Service, Gulf of Mexico OCS Region, New Orleans, LA. OCS Report MMS 2005-023. 48 pp.
- Froelich, P.N., G.P. Klinkhammer, M.L. Bender, N.A. Luedtke, G.R. Heath, D. Cullen, P. Dauphi, D. Hammond, B. Hartman, and V. Maynard. 1979. Early oxidation of organic matter in pelagic sediments of the eastern equatorial Atlantic: Suboxic diagenesis. *Geochim. Cosmochim. Acta*, 43:1,075-1,090.
- Fugro-McClelland Marine Geosciences, Inc. 1997. Shallow hazards report, Blocks 516 and 602, Garden Banks area, Gulf of Mexico. Report No. 0201-3005. Report for Shell Deepwater Development Inc. 3 volumes.
- Galloway, B. (ed.). 1988. Northern Gulf of Mexico continental slope study, Final report: Year 4. Vol. II: Synthesis report. U.S. Department of the Interior, Minerals Management Service, New Orleans, LA. OCS Study MMS 88-0053.
- Galloway, B.J., R.L. Howard, and G.F. Hubbard. 1988. Observations on the distribution and abundance of the meiofauna of the continental slope of the northern Gulf of Mexico, Chapter 3. In: B.J. Galloway (ed.), Northern Gulf of Mexico continental slope study, Final report: Year 4. Vol. II: Synthesis report. U.S. Department of the Interior, Minerals Management Service, New Orleans, LA. OCS Study MMS 88-0053.
- Galloway, B.J., R.G. Fechhelm, G.F. Hubbard, and S.A. MacLean. 1997. Opportunistic sampling at a synthetic drilling fluid discharge site on the continental slope of the northern Gulf of Mexico: The Pompano development. Report by LGL Ecological Research Associates, Inc. for BP Exploration, Inc., Houston, TX. 36 pp.
- Galloway, B.J., J.G. Cole, and L.R. Martin. 2001. The deep sea Gulf of Mexico: An overview and guide. U.S. Dept. of the Interior, Minerals Management Service, Gulf of Mexico OCS Region, New Orleans, LA. OCS Study MMS 2001-065. 27 pp.
- Galloway, B.J., J.G. Cole, and R.G. Fechhelm. 2003. Selected aspects of the ecology of the continental slope fauna of the Gulf of Mexico: A synopsis of the Northern Gulf of Mexico Continental Slope Study, 1983-1988. U.S. Dept. of the Interior, Minerals Management Service, Gulf of Mexico OCS Region, New Orleans, LA. OCS Study MMS 2003-072. 44 pp.
- Ganz, H.H. and R.S. Burton. 1995. Genetic differentiation and reproductive incompatibility among Baja California populations of the copepod *Tigriopus californicus*. *Mar. Biol.* 123:821-827.
- Gómez, S., J.W. Fleeger, A. Rocha-Olivares, and D.W. Foltz. (in press). Four new species of *Cletocamptus* Schrankewitsch, 1875, closely related to *Cletocamptus deitersi* (Richard, 1897). *J. Nat. Hist.*
- Grassle, J.P. and J.F. Grassle. 1976. Sibling species in the marine pollution indicator *Capitella* (Polychaeta). *Science* 192:567-569.
- Grassle, J.F., H.L. Sanders, R.R. Hessler, G.T. Rowe, and T. MacLellan. 1975. Pattern and zonation: A study of the bathyal megafauna using the research submersible Alvin. *Deep-Sea Res.* 22:643-659.
- Gray, J.S. 2002. Species richness of marine soft sediments. *Mar. Ecol. Prog. Ser.* 244:285-297.
- Gray, J.S., R.S. Wu, and Y.Y. Or. 2002. Effects of hypoxia and organic enrichment on the coastal marine environment. *Marine Ecology Progress Series.* 238:249-279.



- Green, R.H. 1979. Sampling design and statistical methods for environmental biologists. John Wiley & Sons, New York. 257 pp.
- Growcock, F.B., S.L. Andrews, and T.P. Frederick. 1994. Physicochemical properties of synthetic drilling fluids. IADC/SPE 27450. Pages 181-190. In: 1994 IADC/SPE Drilling Conference. Dallas, TX, 15-18 February 1994. International Association of Drilling Contractors/Society of Petroleum Engineers, Inc. (IADC/SPE). Richardson, TX.
- Gundersen, J.K., B.B. Jørgensen, E. Larsen, and H.W. Jannasch. 1992. Mats of giant sulfur bacteria on deep-sea sediments due to fluctuating hydrothermal flow. *Nature London* 360:454-455.
- Hamilton, P. 1990. Deep currents of the Gulf of Mexico. *J. Phys. Oceanogr.* 20:1,087-1,104.
- Hargrave, B.T. 1972. Aerobic decomposition of sediment and detritus as a function of particle surface area and organic content. *Limnol. Oceanogr.* 17:583-596.
- Harpending, H.C., M.A. Batzer, M. Gurven, L.B. Jorde, A.R. Rogers, and S.T. Sherry. 1998. Genetic traces of ancient demography. *Proc. Natl. Acad. Sci. USA* 95:1,961-1,967.
- Harper, D.E., Jr., D.L. Potts, R.R. Salzer, R.J. Case, R.L. Jaschek, and C.M. Walker. 1981. Distribution and abundance of macrobenthic and meiobenthic organisms, pp. 133-177. In: B.S. Middleditch (ed.), *Environmental Effects of Offshore Oil Production. The Buccaneer Gas and Oil Field Study*. Plenum Press, New York, NY. 446 pp.
- Hartley, J., R. Trueman, S. Anderson, J. Neff, K. Fucik, and P. Dando. 2003. *Drill Cuttings Initiative: Food Chain Effects Literature Review*. United Kingdom Offshore Operators Association, Aberdeen, Scotland. 118 pp. + appendices.
- Hartman, O. 1965. Deep-water benthic polychaetous annelids off New England to Bermuda and other North Atlantic areas. *Allan Hancock Foundation Occasional Papers*, 28, pp. 1-378.
- Hebert, P.D.N. and M.M. Luiker. 1996. Genetic effects of contaminant exposure – towards an assessment of impacts on animal populations. *Sci. Tot. Env.* 191:23-58.
- Hecker, B. 1982. Possible benthic fauna and slope instability relationships, pp. 335-347. In: S. Saxov and J.K. Nieuwenhuis (eds.), *Marine Slides and Other Mass Movements*. New York: Plenum Press.
- Hecker, B. 1990. Variation in megafaunal assemblages on the continental slope. *Deep-Sea Res.* 37:37-57.
- Heezen, B.C. and C.D. Hollister. 1971. *The face of the deep*. New York: Oxford Univ. Press. 532 pp.
- Hessler, R.R. and P.A. Jumars. 1974. Abyssal community analysis from replicate box cores in the Central North Pacific. *Deep-Sea Res.* 21:185-209.
- Hicks, G.R.F. and B.C. Coull. 1983. The ecology of marine meiobenthic harpacticoid copepods. *Oceanogr. Mar. Biol. Ann. Rev.* 21:67-175.
- Hinwood, J.B., A.E. Potts, L.R. Denis, J.M. Carey, H. Houridis, R.J. Bell, J.R. Thomson, P. Boudreau, and A.M. Ayling. 1994. Drilling activities, pp. 126-206. In: J.M. Swan, J.M. Neff, and P.C. Young (eds.), *Environmental implications of offshore oil and gas development in Australia. The findings of an independent scientific review*. Australian Petroleum Exploration Association (APEA) and Energy Research and Development Corporation (ERDC). Christopher Beck Books, Queensland, Australia. ISBN 0 908277 17 2.
- Humphries, C.C., Jr. 1978. Salt movement on the continental slope, northern Gulf of Mexico, pp. 69-86. In: A.H. Bouma, G.T. Moore, and J.M. Coleman (eds.), *Framework, facies, and oil-trapping characteristics of the upper continental margin*. American Association of Petroleum Geologists Studies in Geology, No. 7.
- Huys, R. and W. Lee. 1998/99. On the relationship of the Normanellidae and the recognition of Cletopsyllidae grad. Nov. (Copepoda, Harpacticoida). *Zool. Anz.* 237:267-290.

- Hyland, J., D. Hardin, M. Steinhauer, D. Coats, R. Green, and J. Neff. 1994. Environmental impact of offshore oil development on the outer continental shelf and slope off Point Arguello, California. *Mar. Environ. Res.* 37:195-229.
- International Association of Oil & Gas Producers (OGP). 2003. Environmental aspects of the use and disposal of non aqueous drilling fluids associated with offshore oil & gas operations. Report 342 from OGP, London, England. 103 pp.
- Jackson, C.R., J.P. Harper, D. Willoughby, E.E. Roden, and P.F. Churchill. 1997. A simple, efficient method for the separation of humic substances and DNA from environmental samples. *Appl. Environ. Microbiol.* 63:4,993-4,995.
- Jacques, D.F., H.E. Newman, Jr., and W.B. Turnbull. 1992. A comparison of field drilling experience with low-viscosity mineral oil and diesel muds, pp. 341-354. IADC/SPE 23881. In: 1992 IADC/SPE Drilling Conference. New Orleans, Louisiana, February 18-21, 1992. IADC/SPE Drilling Conference. Richardson, TX.
- Jenkins, K.D., S. Howe, B.M. Sanders, and C. Norwood. 1989. Sediment deposition, biological accumulation and subcellular distribution of barium following the drilling of an exploratory well, pp. 587-608. In: F.R. Engelhardt, J.P. Ray, and A.H. Gillam, Eds., *Drilling Wastes*. Elsevier Applied Science, London.
- Jensen, P. 1986. Nematode fauna in the sulphide-rich brine seep and adjacent bottoms of the East Flower Garden, NW Gulf of Mexico. IV. Ecological aspects. *Mar. Biol.* 92:489-503.
- Jumars, P.A. and E.D. Gallagher. 1982. Deep-sea community structure: Three plays on the benthic proscenium. Chapter 10. In: W.G. Ernst and J.G. Morin (eds.), *The Environment of the Deep Sea* Prentice-Hall, Inc., New Jersey.
- Kaiser, M.J. and D.V. Mesyanzhinov. 2005. Study tabulates idle Gulf of Mexico structures. *Oil Gas J.* 103.1:46-49.
- Kang, W.-J., J.H. Trefry, T.A. Nelsen, and H.R. Wanless. 2000. Direct atmospheric inputs versus runoff fluxes of mercury to the lower Everglades and Florida Bay. *Environ. Sci. Tech.* 34:4,058-4,063.
- Karl, D.M. 1986. Determination of the *in situ* microbial biomass, viability, metabolism, and growth. *Bacteria in Nature* 2:85-176.
- Karl, D.M. 1993. Total microbial biomass estimation derived from the measurement of particulate adenosine-5'-triphosphate, pp. 359-368. In: P.F. Kemp, B.F. Sherr, E.B. Sherr, J.J. Cole (eds.), *Handbook of Methods in Aquatic Microbial Ecology*.
- Karl, D.M. and P.L. LaRock. 1976. Adenosine Triphosphate Measurements in Soil and Marine Sediments. *J. Fish. Res. Board Can.* 32:599-607.
- Karl, D.M., P.A. LaRock, J.W. Morse, and W. Sturges. 1976. Adenosine triphosphate in the North Atlantic Ocean and its relationship to the oxygen minimum. *Deep Sea Res.* 23:81-88.
- Kennicutt, M.C., II. 1995. Gulf of Mexico offshore operations monitoring experiment, Phase 1: Sublethal responses to contaminant exposure. OCS Study MMS 95-0045. U.S. Dept. of the Interior, Minerals Management Service, Gulf of Mexico OCS Region, New Orleans, LA. 709 pp.
- Kennicutt, M.C., II, J.M. Brooks, R.R. Bidigare, R.A. Fay, T.L. Wade, and T.J. McDonald. 1985. Vent-type taxa in a hydrocarbon seep region on the Louisiana slope. *Nature* 317:351.
- Kennicutt, M.C., II, R.H. Green, P. Montagna, and P.F. Roscigno. 1996a. Gulf of Mexico Offshore Operations Monitoring Experiment (GOOMEX), Phase I: Sublethal responses to contaminant exposure – Introduction and overview. *Can. J. Fish. Aquat. Sci.* 53:2,540-2,553.
- Kennicutt, M.C., II, P.N. Boothe, T.L. Wade, S.T. Sweet, R. Rezak, F.J. Kelly, J.M. Brooks, B.J. Presley, and D.A. Wiesenburg. 1996b. Geochemical patterns in sediments near offshore production platforms. *Can. J. Fish. Aquat. Sci.* 53:2554-2566.
- Kenny, P. 1993. Ester-based muds show promise for replacing some oil-based muds. *Oil Gas J.* 91:88-91.

- Kidd, R.D. and Q.J. Huggett. 1981. Rock debris on abyssal plains in the NE Atlantic: A comparison of epibenthic sledge hauls and photographic surveys. *Oceanologica Acta* 4:99-104.
- Kilpatrick, S.T. and D.M. Rand. 1995. Conditional hitchhiking of mitochondrial DNA: Frequency shifts of *Drosophila melanogaster* mtDNA variants depend on nuclear genetic background. *Genetics* 141:1,113-1,124.
- Kitchell, J.A. 1979. Deep-sea foraging pathways: An analysis of randomness and resource exploitation. *Paleobiology* 5:107-125.
- Knowlton, N. 1993. Sibling species in the sea. *Ann. Rev. Ecol. Syst.* 24:189-216.
- Knowlton, N. 2000. Molecular genetic analysis of species boundaries in the sea. *Hydrobiologia* 420:73-90.
- Knowlton, N. and L.A. Weigt. 1998. New dates and new rates for divergence across the Isthmus of Panama. *Proc. R. Soc. Lond. B Biol. Sci.* 265:2,257-2,263.
- Knowlton, N., L.A. Weigt, L.A. Solorzano, D.K. Mills, and E. Bermingham. 1993. Divergence in proteins, mitochondrial DNA, and reproductive compatibility across the Isthmus of Panama. *Science* 260:1,629-1,632.
- Koenig, B., G. Holst, R.N. Glud, and M. Kuehl. 2001. Imaging of oxygen distributions at benthic interfaces, pp. 63-71. In: J.Y. Aller, S.A. Woodin, and R.C. Aller (eds.), *Organism-Sediment Interactions*. Belle Baruch Library of Marine Science Number 21, Univ. of South Carolina Press, Columbia, SC. 403 pp.
- Kohl, B. and H.H. Roberts. 1994. Fossil foraminifera from four active mud volcanoes in the Gulf of Mexico. *Geo-Marine Letters* 14:126-134.
- Koster, M. and L.A. Meyer-Reil. 2001. Characterization of carbon and microbial biomass pools in shallow water coastal sediments of the southern Baltic Sea (Nordrugensche Bodden). *Mar. Ecol. Prog. Ser.* 214:25-41.
- Kramer, J.R., H.D. Grundy, and L.G. Hammer. 1980. Occurrence and solubility of trace metals in barite for ocean drilling operations, pp. 789-798. In: *Research on Environmental Fate and Effects of Drilling Fluids and Cuttings, Vol. II*, Courtesy Associates, Washington, DC.
- Kumar, S., K. Tamura, I.B. Jakobsen, and M. Nei. 2001. MEGA2: Molecular Evolutionary Genetics Analysis software, Arizona State University, Tempe, Arizona, USA.
- Llansó, R.L., S. Aasen, and K. Welch. 1998. Marine Sediment Monitoring Program - II. Distribution and Structure of Benthic Communities in Puget Sound, 1989-1993. Washington State Department of Ecology, Olympia, WA. Publication No. 98-328. 114 pp. + appendices.
- Lee, C.C., R.R. Harris, J.D.H. Williams, D.E. Armstrong, and J.K. Syers. 1971. Adenosine triphosphate in lake sediments: 1. Determination, origin and significance. *Soil Sci. Soc. Am. Proc.* 35:82-86.
- Li, W.-H. 1977. Distribution of nucleotide differences between two randomly chosen cistrons in a finite population. *Genetics* 85:331-337.
- Lobel, P.B., S.P. Belkhole, S.E. Jackson, and H.P. Longerich. 1990. Recent taxonomic discoveries concerning the mussel *Mytilus*: Implications for biomonitoring. *Arch. Env. Contam. Tox.* 19:508-512.
- MacDonald, I.R. 1998. Habitat formation of Gulf of Mexico hydrocarbon seeps. *Cah. Biol. Mar.* 39:337-340.
- MacDonald, I.R. (ed.). 2002. Stability and change in Gulf of Mexico chemosynthetic communities. Volume II: Technical Report. Prepared by the Geochemical and Environmental Research Group, Texas A&M University. U.S. Dept. of the Interior, Minerals Management Service, Gulf of Mexico OCS Region, New Orleans, LA. OCS Study MMS 2002-036. 456 pp.

- MacDonald, I.R., J.F. Rilly, II, N.L. Guinasso, Jr., J.M. Brooks, R.S. Carney, W.A. Bryant, and T.J. Bright. 1990. Chemosynthetic mussels at a brine-filled pockman in the northern Gulf of Mexico: *Science* 248:1,096-1,099.
- MacDonald, I.R., W.W. Schroeder, and J.M. Brooks. 1996. Chemosynthetic ecosystem study. Final report prepared by Texas A&M University Geochemical and Environmental Research Group for the U.S. Dept. of the Interior, Minerals Management Service, Gulf of Mexico Region, New Orleans, LA. 360 pp.
- Maciorowski, A.F. 1997. Integration of risk assessment and risk management, pp. 7-9. In: C.G. Ingersoll, T. Dillon, and G.R. Biddinger, Eds., *Ecological Risk Assessment of Contaminated Sediments*. SETAC Press, Pensacola, FL. 390 pp.
- Maier, M.A., I.L. Pepper, and C.P. Gerba. 2000. *Environmental Microbiology*. Academic Press. 585 pp.
- Malin, M.A., L.B. Cahoon, D.C. Parsons, and S.H. Ensign. 2001. Effect of nitrogen and phosphorus loading on plankton in coastal plain blackwater rivers. *J. Freshwat. Ecol.* 16:455-466.
- Martinez-Tabche, L., I.G. Cabrera, L.G. Olivan, M.G. Martinez, and C.G. Faz. 2000. Toxic effects of zinc from trout farm sediments on ATP, protein, and hemoglobin concentrations of *Limnodrilus hoffmeisteri*. *J. Toxicol. Environ. Health-Part A.* 59:575-583.
- Matsunaga, K. and M. Nishimura. 1974. A rapid and sensitive method for determination of submicrogram amounts of ammonia in fresh and sea waters. *Analytica Chim. Acta* 73:204-208.
- McIlroy, W. 1998. Review of BHP's experience into the persistence of drilling fluid pollutants, pp. 121-134. In: *International Workshop on Drilling Fluids Exotoxicology and Biodegradation*. Curtin University, Perth, Western Australia, 8-9 October 1998.
- Melton, H.R., J.P. Smith, H.L. Mairs, R.F. Bernier, E. Garland, A.H. Glickman, F.V. Jones, J.P. Ray, D. Thomas, and J.A. Campbell. 2004. Environmental aspects of the use and disposal of non aqueous drilling fluids associated with offshore oil & gas operations. SPE 86696. Paper presented at the 7<sup>th</sup> SPE International Conference on Health, Safety, and Environment in Oil and Gas Exploration and Production, Calgary, Alberta, Canada. Society of Petroleum Engineers, Richardson, TX. 10 pp.
- Minerals Management Service. 2000a. Gulf of Mexico deepwater operations and activities: Environmental assessment. U.S. Dept. of the Interior, Minerals Management Service, Gulf of Mexico OCS Region, New Orleans, LA. OCS EIS/EA MMS 2000-001. 248 pp.
- Minerals Management Service. 2000b. Proposed use of floating production, storage, and offloading systems on the Gulf of Mexico outer continental shelf, western and central planning areas: Final environmental impact statement. U.S. Dept. of the Interior, Minerals Management Service, Gulf of Mexico OCS Region, New Orleans, LA. OCS EIS/EA MMS 2000-090.
- Minerals Management Service. 2003. Workshop on deepwater environmental studies strategy: A five-year follow-up and planning for the future. U.S. Dept. of the Interior, Minerals Management Service, Gulf of Mexico OCS Region, New Orleans, LA. OCS Study MMS 2003-030.
- Minerals Management Service. 2004a. Moving into deepwater: The challenges of development in the Gulf of Mexico. *MMS Ocean Science* 1(2):4-5. March/April 2004.
- Minerals Management Service. 2004b. Comprehensive strategy for postlease NEPA compliance in deepwater areas of the central and western Gulf of Mexico. <http://www.gomr.mms.gov/homepg/regulate/enviro/strategy/strategy.html>
- Minerals Management Service. 2005. Offshore statistics by water depth. <http://www.gomr.mms.gov/homepg/fastfacts/WaterDepth.wdlist.asp>.
- Montagna, P.A. and D.E. Harper, Jr. 1996. Benthic infaunal long-term response to offshore production platforms in the Gulf of Mexico. *Canadian J. Fish. Aq. Sci.* 53:2,567-2,588.

- Murdoch, M.H. and P.D.N. Hebert. 1994. Mitochondrial DNA diversity of brown bulhead from contaminated and relatively pristine sites in the Great Lakes. *Env. Toxicol. Chem.* 13:1,281-1,289.
- National Research Council. 1983. *Drilling discharges in the marine environment*. National Academy Press, Washington, DC. 180 pp.
- Nedwed, T.J., J.P. Smith, and M.G. Brandsma. 2004. Verification of the OOC mud and produced water discharge model using lab-scale plume behavior experiments. *Environ. Model. Software* 19:655-670.
- Neff, J.M. 1982. Fate and biological effects of oil well drilling fluids in the marine environment: A literature review. Report to U.S. Environmental Protection Agency, Gulf Breeze, FL. Available from NTIS. EPA-600/S3-82-064). 151 pp.
- Neff, J.M. 1987. Biological effects of drilling fluids, drill cuttings and produced waters, pp. 469-538. In: D.F. Boesch and N.N. Rabalais (eds.), *Long-Term Effects of Offshore Oil and Gas Development*. Elsevier Applied Science Publishers, London.
- Neff, J.M. 2002a. Fate and effects of mercury from oil and gas exploration and production operations in the marine environment. Report prepared for the American Petroleum Institute, Washington, DC. 135 pp.
- Neff, J.M. 2002b. *Bioaccumulation in Marine Organisms. Effects of Contaminants from Oil Well Produced Water*. Elsevier Science Publishers, Amsterdam. 452 pp.
- Neff, J.M. 2005. Composition, environmental fates, and biological effect of water based drilling muds and cuttings discharged to the marine environment: A synthesis and annotated bibliography. Report prepared for the Petroleum Environmental Research Forum (PERF). Available from American Petroleum Institute, Washington, DC. 73 pp.
- Neff, J.M., N.N. Rabalais, and D.F. Boesch. 1987. Offshore oil and gas development activities potentially causing long-term environmental effects, pp. 149-174. In: D.F. Boesch and N.N. Rabalais, Eds., *Long Term Effects of Offshore Oil and Gas Development*. Elsevier Applied Science Publishers, London.
- Neff, J.M., M.H. Bothner, N.J. Maciolek, and J.F. Grassle. 1989a. Impacts of exploratory drilling for oil and gas on the benthic environment of Georges Bank. *Mar. Environ. Res.* 27:77-114.
- Neff, J.M., R.E. Hillman, and J.J. Waugh. 1989b. Bioaccumulation of trace metals from drilling mud barite by benthic marine animals, pp. 461-479. In: F.R. Engelhardt, J.P. Ray, and A.H. Gillam (eds.), *Drilling Wastes*. Elsevier Applied Science, New York. 867 pp.
- Neff, J.M., R.J. Breteler, and R.S. Carr. 1989c. Bioaccumulation, food chain transfer, and biological effects of barium and chromium from drilling muds by flounder (*Pseudopleuronectes americanus*) and lobster (*Homarus americanus*), pp. 439-459. In: F.R. Engelhardt, J.P. Ray, and A.H. Gillam (eds.), *Drilling Wastes*. Elsevier Applied Science, New York. 867 pp.
- Neff, J.M., S. McKelvie, and R.C. Ayers, Jr. 2000. Environmental impacts of synthetic based drilling fluids. Prepared by Robert Ayers & Associates, Inc. U.S. Dept. of the Interior, Minerals Management Service, Gulf of Mexico OCS Region, New Orleans, LA. OCS Study MMS 2000-064. 118 pp.
- Neurauter, T.W. and H.H. Roberts. 1992. Seismic and visual observation of seepage-related structures on the continental slope, northern Gulf of Mexico, pp. 355-362. In: *Proceedings 24th Offshore Technology Conference*, Houston, Texas. OTC 6850.
- Nilsson, H.C. and R. Rosenberg. 2000. Succession in marine benthic habitats and fauna in response to oxygen deficiency: Analyzed by sediment profile imaging and by grab samples. *Mar. Ecol. Prog. Ser.* 197:139-194.

- Nowlin, W.D., A.E. Jochens, S.F. DiMarco, R.O. Reid, and M.K. Howard. 2001. Deepwater physical oceanography reanalysis and synthesis of historical data: Synthesis report. U.S. Dept. of the Interior, Minerals Management Service, Gulf of Mexico OCS Region, New Orleans, LA. OCS Study MMS 2001-064. 528 pp.
- Ohkouchi, N., K. Kawamura, and H. Kawahata. 1999. Distributions of three- to seven-ring polynuclear aromatic hydrocarbons on the deep seafloor in the central Pacific. *Environ. Sci. Technol.* 33:3,086-3,090.
- Palmer, M.A. and G. Gust. 1985. Dispersal of meiofauna in a turbulent tidal creek. *J. Mar. Res.* 43:179-210.
- Pearson, T.H. and R. Rosenberg. 1978. Macrobenthic succession in relation to organic enrichment and pollution of the marine environment. *Oceanogr. Mar. Biol. Ann. Rev.* 16: 229-311.
- Pearson, T.H. and S.O. Stanley. 1979. Comparative measurement of the redox potential of marine sediments as a rapid means of assessing the effect of organic pollution. *Mar. Biol.* 53:371-379.
- Pequegnat, W.E., B.J. Gallaway, and L.H. Pequegnat. 1990. Aspects of the ecology of the deep-water fauna of the Gulf of Mexico. *Amer. Zool.* 30:45-64.
- Peterson, C.H., M.C. Kennicutt, R.H. Green, P. Montagna, D.E. Harper, E.N. Powell, and P.F. Roscigno. 1996. Ecological consequences of environmental perturbations associated with offshore hydrocarbon production: A perspective on long-term exposures in the Gulf of Mexico. *Can. J. Fish. Aquat. Sci.* 53:2,637-2,654.
- Phillips, C., J. Evans, W. Hom, and J. Clayton. 1998. Long-term changes in sediment barium inventories associated with drilling-related discharges in the Santa Maria Basin, California, USA. *Environ. Toxicol. Chem.* 17:1,653-1,661.
- Posada, D. and K.A. Crandall. 2001. Intraspecific gene genealogies: Trees grafting into networks. *Trends Ecol. Evol.* 16:37-45.
- Quattro, J.M., M.R. Chase, M.A. Rex, and T.W. Greig. 2001. Extreme mitochondrial DNA divergence within populations of the deep-sea gastropod *Frigidoalvania brychia*. *Mar. Biol.* 139:1,107-1,113.
- Regg, J.B., S. Atkins, B. Hauser, J. Hennessey, B.J. Kruse, J. Lowenhaupt, B. Smith, and A. White. 2000. Deepwater Development: A Reference Document for the Deepwater Environmental Assessment, Gulf of Mexico OCS (1998 through 2007). OCS Report 2000-015. U.S. Dept. of the Interior Minerals Management Service, Gulf of Mexico OCS Region, New Orleans, LA. 94 pp.
- Revsbech, N.P., B.B. Jorgensen, and T.H. Blackburn. 1979. Oxygen in the sea bottom measured with a microelectrode. *Science* 207:1,355-1,356.
- Rhoads, D.C. 1974. Organism sediment relations on the muddy sea floor. *Oceanogr. Mar. Biol. Ann. Rev.* 12:263-300.
- Rhoads, D.C. and S. Cande. 1971. Sediment profile camera for in situ study of organism-sediment relations. *Limnol. Oceanogr.* 16:110-114.
- Rhoads, D.C. and J.D. Germano. 1982. Characterization of organism-sediment relations using sediment profile imaging: An efficient method of remote ecological monitoring of the seafloor (REMOTS system). *Mar. Ecol. Prog. Ser.* 8:115-128.
- Rhoads, D.C. and J.D. Germano. 1986. Interpreting long-term changes in benthic community structure: A new protocol. *Hydrobiologia* 142:291-308.
- Richardson, G.E., L.S. French, R.D. Baud, R.H. Peterson, C.D. Roark, T.M. Montgomery, E.G. Kazanis, G.M. Conner, and M.P. Gravois. 2004. Deepwater Gulf of Mexico 2004: America's expanding frontier. U.S. Dept. of the Interior, Minerals Management Service, New Orleans, LA. OCS Report MMS 2004-021. 150 pp.

- Roberts, H.H. and P. Aharon. 1994. Hydrocarbon-derived carbonate buildups of the northern Gulf of Mexico continental slope: A review of submersible investigations. *Geo-Marine Letters* 14:135-148.
- Robertson, D.E. and R. Carpenter. 1976. Activation analysis, pp. 93-160. In: E.D. Goldberg (ed.), *Strategies for Marine Pollution Monitoring*. Wiley Interscience, New York.
- Rocha-Olivares, A., J.W. Fleeger, and D.W. Foltz. 2001. Decoupling of molecular and morphological evolution in deep lineages of a meiobenthic harpacticoid copepod. *Mol. Biol. Evol.* 18:1,088-1,102.
- Rogers, A.R. 1995. Genetic evidence for a pleistocene population explosion. *Evolution* 49:608-615.
- Rogers, A.R. and H. Harpending. 1992. Population growth makes waves in the distribution of pairwise genetic differences. *Mol. Biol. Evol.* 9:552-569.
- Rosenberg, R., H.C. Nilsson, and R.J. Diaz. 2001. Response of benthic fauna and changing sediment redox profiles over a hypoxic gradient. *Est. Coast. Shelf Sci.* 53:343-350.
- Rosenberg, R., H.C. Nilsson, A. Grémare, and J-M. Amouroux. 2003. Effects of demersal trawling on marine sedimentary habitats analysed by sediment profile imagery. *J. Exp. Mar. Biol. Ecol.* 285-286:465-477.
- Rosenberg, R., M. Blomqvist, H.C. Nilsson, H. Cederwall, and A. Dimming. 2004. Marine quality assessment by use of benthic species-abundance distributions: a proposed new protocol within the European Union Water Framework Directive. *Mar. Pollut. Bull.* 49:728-739.
- Rowan, M.G. 1995. Structural styles and evolution of allochthonous salt, central Louisiana outer shelf and upper slope, pp. 199-228. In: M.P.A. Jackson, D.G. Roberts, S. Snelson (eds.), *Salt tectonics: A global perspective*. AAPG Memoir 65.
- Rowan, M.G., P. Weiner, B. McBride, P. Varnai, Z. Acosta, F. Budhijanto, R. Martinez, A. Navarro, T. Villamil, and J.C. Fidnk. 1995. Interactions between salt tectonics and sedimentation in the Louisiana offshore: Preliminary results, pp. 235-244. In: C. Travis et al. (eds.), *SaH, sediment, and hydrocarbons*. Gulf Coast Section, Society of Economic Paleontologists and Mineralogists Foundation, 16th Annual Research Conference Proceedings.
- Rowe, G.T. 1983. Biomass and production of the deep-sea macrobenthos, pp. 97-121. In: G. Rowe (ed.), *The Sea*, Vol. 8. Wiley, New York.
- Rowe, G.T. and M.C. Kennicutt II. 2001. Deepwater Program: Northern Gulf of Mexico continental slope habitat and benthic ecology. Year 1: Interim report. U.S. Dept. of the Interior, Minerals Management Service, Gulf of Mexico OCS Region, New Orleans, LA. OCS Study MMS 2001-091. 166 pp.
- Rowe, G.T. and M.C. Kennicutt II. 2002. Deepwater Program: Northern Gulf of Mexico continental slope habitat and benthic ecology. Year 2: Interim report. U.S. Dept. of the Interior, Minerals Management Service, Gulf of Mexico OCS Region, New Orleans, LA. OCS Study MMS 2002-063. 158 pp.
- Rowe, G.T. and D. Menzel. 1971. Quantitative benthic samples from the deep Gulf of Mexico with some comments on the measurement of deep-sea biomass. *Bull. Mar. Sci.* 21:556-566.
- Rowe, G.T. and R.J. Menzies. 1969. Zonation of large benthic invertebrates in the deep-sea off the Carolinas. *Deep-Sea Res.* 16:531-537.
- Rowe, G.T., P. Polloni, and S. Horner. 1974. Benthic biomass estimates from the NW Atlantic Ocean and the northern Gulf of Mexico. *Deep-Sea Res.* 21:641-650.
- Sager, W.W., I.R. MacDonald, and R. Hou. 2003. Geophysical signatures of mud mounds at hydrocarbon seeps on the Louisiana continental slope, northern Gulf of Mexico. *Mar. Geol.* 198:97-132.
- Schizas, N.V., G.T. Street, B.C. Coull, G.T. Chandler, and J.M. Quattro. 1997. An efficient DNA extraction method for small metazoans. *Mol. Mar. Biol. Biotechnol.* 6:381-383.

- Schizas, N.V., G.T. Street, B.C. Coull, G.T. Chandler, and J.M. Quattro. 1999. Molecular population structure of the marine benthic copepod *Microarthridion littorale* along the southeastern and Gulf coasts of the USA. *Mar. Biol.* 135:399-405.
- Schizas, N.V., G.T. Chandler, B.C. Coull, S.L. Klosterhaus, and J.M. Quattro. 2001. Differential survival of three mitochondrial lineages of a marine benthic copepod exposed to a pesticide mixture. *Environ. Sci. Technol.* 35:535-539.
- Schizas, N.V., B.C. Coull, G.T. Chandler, and J.M. Quattro. 2002. Sympatry of distinct mitochondrial lineages in a copepod inhabiting estuarine creeks in the southeastern USA. *Mar. Biol.* 140:585-594.
- Schneider, S. and L. Excoffier. 1999. Estimation of past demographic parameters from the distribution of pairwise differences when the mutation rates vary among sites: application to human mitochondrial DNA. *Genetics* 152:1,079-1,089.
- Schneider, S., D. Roessli, and L. Excoffier. 2000. Arlequin ver. 2.000: A software for population genetics data analysis. *Genetics and Biometry Laboratory, University of Geneva, Switzerland.*
- Schropp, S.J., F.G. Lewis, and H.L. Windom. 1990. Interpretation of metal concentrations in estuarine sediments of Florida using aluminum as a reference element. *Estuaries* 13(3):227-235.
- Seilacher, A. 1967. Fossil behavior. *Sci. Am.* 217:72-80.
- Seutin, G., B.N. White, and P.T. Boag. 1991. Preservation of avian blood and tissue samples for DNA analysis. *Can. J. Zool.* 69:82-90.
- Shimmield, G. and E. Breuer. 2000. A geochemical & radiochemical appraisal of offshore drill cuttings as a means of predicting possible environmental impact after site abandonment. Report to NERC and UKOOA from the Scottish Association for Marine Science, Dunstaffnage Marine Laboratory, Oban, Scotland. 22 pp.
- Shimmield, G.B., E. Breuer, D.G. Cummings, O. Peppe and T. Shimmield. 2000. Contaminant leaching from drill cuttings piles of the northern and central North Sea: field results from Beryl "A" cuttings pile. Report UKOOA from the Scottish Association for Marine Science, Dunstaffnage Marine Laboratory, Oban, Scotland. 28 pp.
- Shinn, E.A., B.H. Lidz, and C.D. Reich. 1993. Habitat impacts of offshore drilling: Eastern Gulf of Mexico. U.S. Dept. of the Interior, Minerals Management Service, Gulf of Mexico OCS Region, New Orleans, LA. OCS Study MMS 93-0021. 73 pp.
- Siegel, F.R., J.L. Galasson, J.H. Kravitz, and W.D. Basinger. 2000. The Svalbard western coast: Site of baseline geochemistry and incipient contamination. *Environ. Geol.* 39: 816-822.
- Simpson, E.P., M.R. Gonzales, C.M. Hart, and S.H. Hurlbert. 1998. Salinity and fish effects on Salton Sea microecosystems: Benthos. *Hydrobiologia* 381:153-177.
- Slatkin, M. and R.R. Hudson. 1991. Pairwise comparisons of mitochondrial DNA sequences in stable and exponentially growing populations. *Genetics* 129:555-562.
- Smith, J.P., M.G. Brandsma, and T.J. Nedwed. 2004. Field verification of the Offshore Operators Committee (OOC) mud and produced water discharge model. *Environ. Model. Software* 19:739-749.
- Smouse, P.E. 1998. To tree or not to tree. *Mol. Ecol.* 7:399-412.
- Sokal, R.R. and F.J. Rohlf. 1995. *Biometry*. 3<sup>rd</sup> ed. W.H. Freeman and Company. New York. 887 pp.
- Steinhauer, M., E. Crecelius, and W. Steinhauer. 1994. Temporal and spatial changes in the concentrations of hydrocarbons and trace metals in the vicinity of an offshore oil-production platform. *Mar. Environ. Res.* 37:129-63.
- Street, G.T. and P.A. Montagna. 1996. Loss of genetic diversity in Harpacticoida near offshore platforms. *Mar. Biol.* 126:271-282.



- Street, G.T., G.R. Lotufo, P.A. Montagna, and J.W. Fleeger. 1998. Reduced genetic diversity in a meiobenthic copepod exposed to a xenobiotic. *J. Exp. Mar. Biol. Ecol.* 222:93-111.
- Strickland, J.D.H. and T.R. Parsons. 1972. *A Practical Handbook of Seawater Analysis*. Fish. Res. Board Can. 167. 311 pp.
- Sturges, W., E. Chassignet, and T. Ezer. 2004. Strong mid-depth currents and a deep cyclonic gyre in the Gulf of Mexico: Final report. U.S. Dept. of the Interior, Minerals Management Service, Gulf of Mexico OCS Region, New Orleans, LA. OCS Study MMS 2004-040. 89 pp.
- Sutcliffe, W.H., Jr., and E.A. Orr. 1976. Difficulties with ATP measurements in inshore waters. *Limnol. Oceanogr.* 21:145-149.
- Suter, G.W. II. 1993. *Ecological Risk Assessment*. Lewis Publishers, Boca Raton, FL.
- Suter, G.W. II. 1997. Overview of the ecological risk assessment framework, pp. 1-6. In: C.G. Ingersoll, T. Dillon, and G.R. Biddinger (eds.), *Ecological Risk Assessment of Contaminated Sediments*. SETAC Press, Pensacola, FL. 390 pp.
- Suter, J.R. and H.L. Berryhill, Jr. 1985. Late Quaternary shelf margin deltas, northwest Gulf of Mexico. *American Association of Petroleum Geologists* 69:77-91.
- Takahata, N. 1991. Genealogy of neutral genes and spreading of selected mutations in a geographically structured population. *Genetics* 129:585-595.
- Talbot, C.J. 1993. Spreading of salt structures in the Gulf of Mexico. *Tectonophysics* 228:151-166.
- Terrens, G.W., D. Gwyther, M.J. Keough, and R.D. Tait. 1998. Environmental assessment of synthetic based drilling mud discharges to Bass Strait, Australia, pp. 1-14. In: 1998 SPE International Conference on Health, Safety, and Environment in Oil and Gas Exploration and Development. Caracas, Venezuela, 7-10 June 1998. SPE 46622. Society of Petroleum Engineers, Inc. Richardson, TX.
- Trefry, J.H. and S. Metz. 1984. Selective leaching of trace metals from sediments as a function of pH. *Analytical Chemistry* 56(4):745-749.
- Trefry, J.H. and B.J. Presley. 1976. Heavy metals in sediment from San Antonio Bay and the northwest Gulf of Mexico. *Environ. Geol.* 1:283-294.
- Trefry, J.H. and B.J. Presley. 1982. Manganese fluxes from Mississippi delta sediments, *Geochim. Cosmochim. Acta* 46:1,715-1,726.
- Trefry, J.H. and J.P. Smith. 2003. "Forms of mercury in drilling fluid barite and their fate in the marine environment: A review and synthesis." SPE Paper 80571. Presented at the 2003 SPE/DOE/EPA Exploration and Production Environmental Conference, San Antonio TX, 10-12 March 2003.
- Trefry, J.H., R.P. Trocine, and D.B. Meyer. 1981. Tracing the fate of petroleum drilling fluids in the northwestern Gulf of Mexico. In: *Oceans '81 Conference Proceedings*.
- Trefry, J.H., R.P. Trocine, M.L. McElvaine, and R.D. Rember. 2002. Concentrations of total mercury and methylmercury in sediment adjacent to offshore drilling sites in the Gulf of Mexico. Report to the Synthetic Based Muds (SBM) Research Group, American Petroleum Institute, Washington, DC and Minerals Management Service, New Orleans, LA. 46 pp.
- Trefry, J.H., R.P. Trocine, M. McElvaine, R. Rember, and L. Hawkins. 2003. Concentrations of total and methylmercury in sediment adjacent to oil platforms in the Gulf of Mexico. SPE Paper 80569. Presented at the SPE/DOE/EPA Exploration and Production Environmental Conference, San Antonio, TX, 10-12 March 2003.
- Trefry, J.H., R.P. Trocine, R.D. Rember, and M.L. McElvaine. 2004. Metals and redox chemistry in sediments, Chapter 9. In: *Gulf of Mexico Synthetic Based Muds Monitoring Program: Final Report*. Report prepared by Continental Shelf Associates, Inc. for the SBM Research Group, Houston, TX. 3 vol.

- Tsai, Y.-L. and P. Rochelle. 2001. Extraction of nucleic acids from environmental samples. In: P.A. Rochelle (ed.), *Environmental Molecular Microbiology: Protocols and Applications*. Horizon Scientific Press, Wymondham, UK.
- U.S. Environmental Protection Agency. 1991. Methods for the determination of metals in environmental samples. EPA/600/4-91/010. USEPA Office of Research & Development, Cincinnati, OH.
- U.S. Environmental Protection Agency. 1992. Framework for ecological risk assessment. EPA/630/R-92/001. Risk Assessment Forum, U.S. Environmental Protection Agency, Washington, DC.
- U.S. Environmental Protection Agency. 1993. Oil and gas extraction point source category, offshore subcategory; effluent limitations guidelines and new source performance standards. *Federal Register* 58(41), March 4, 1993, pp. 12,454-12,512.
- U.S. Environmental Protection Agency. 1994. Methods for Assessing the Toxicity of Sediment-Associated Contaminants with Estuarine and Marine Amphipods. EPA 600/R-94/025. June 1994. U.S. Environmental Protection Agency, Office of Research and Development, Washington, DC.
- U.S. Environmental Protection Agency. 1998. Final guidelines for ecological risk assessment. EPA 630-R-95-002F. U.S. Environmental Protection Agency, Risk Assessment Forum, Washington, DC.
- U.S. Environmental Protection Agency. 2001a. Methods for Assessing the Chronic Toxicity of Marine and Estuarine Sediment-Associated Contaminants with the Amphipod *Leptocheirus plumulosus* – First Edition. EPA/600/R-01/020. Washington, DC.
- U.S. Environmental Protection Agency. 2001b. 40 CFR Parts 9 and 435 [FRL-6929-8] RIN 2040-AD14 Effluent Limitations Guidelines and New Source Performance Standards for the Oil and Gas Extraction Point Source Category; OMB Approval Under the Paperwork Reduction Act: Technical Amendment; Final Rule. January 22, 2001. *Federal Register* 66(14):6,850-6,919.
- Valente, R.M., D.C. Rhoads, J.D. Germano, and V.J. Cabelli. 1992. Mapping of benthic enrichment patterns in Narragansett Bay, Rhode Island. *Estuaries* 15:1-17.
- Van Cappellen, P. and Y. Wang. 1995. Metal cycling in surface sediments: modeling the interplay of transport and reaction, pp. 21-64. In: H.E. Allen (ed.), *Metal Contaminated Aquatic Sediments*. Ann Arbor Press, Chelsea, MI.
- van Lancker, M. and L.C. Gheysens. 1986. A comparison of four frequently used assays for quantitative determination of DNA. *Analytical Letters* 19:615-623.
- Vendeville, B.C. and M.P.A. Jackson. 1993. Rates of extension and deposition determine whether growth faults or salt diapers form, pp. 263-268. In: J.M. Armentrout, R. Bloch, H.C. Olson, and B.F. Perkins (eds.), *Rates of geologic processes*. Gulf Coast Section, Society of Economic Paleontologists and Mineralogists Foundation, 14th Annual Research Conference Proceedings.
- Venkatesan, M.I., E. Ruth, S. Steinberg, and I.R. Kaplan. 1987. Organic geochemistry of sediments from the continental margin off southern New England, U.S.A. Part II. Lipids. *Mar. Chem.* 21:267-299.
- Viles, C. and R.J. Diaz. 1991. Bencore, an image analysis system for measuring sediment profile camera slides. School of Marine Science, Virginia Institute of Marine Science, College of William and Mary, Gloucester Pt., VA. 13 pp.
- Vismann, B. 1991. Sulfide tolerance: Physiological mechanisms and ecological implications. *Ophelia* 34:1-27.
- Wakefield, W.W., III and A. Genin. 1987. The use of a Canadian (perspective) grid in deep-sea photography. *Deep-Sea Res.* 34:469-478.
- Walk, Haydel & Associates, Inc. 1989. Water-based drilling fluids and cuttings disposal study update. Report for the Offshore Operators Committee.

- Walsh, P.S., D.A. Metzger, and R. Higuchi. 1991. Chelex 100 as a medium for simple extraction of DNA for PCR-based typing from forensic material. *Biotechniques* 4:506-513.
- Wang, F. and P.M. Chapman. 1999. Biological implications of sulfide in sediment—a review focusing on sediment toxicity. *Environ. Toxicol. and Chem.* 18(11):2,526-2,532.
- Ward, E.G. 2000. Deepwater technology, Chapter 2. In: Continental Shelf Associates, Inc. Deepwater Gulf of Mexico environmental and socioeconomic data search and literature synthesis. Volume 1: Narrative report. U.S. Dept. of the Interior, Minerals Management Service, Gulf of Mexico OCS Region, New Orleans, LA. OCS Study MMS 2000-049.
- Weimer, P., P. Varnai, Z.M. Acosta, F.M. Budhijanto, R.E. Martinez, A.F. Navarro, M.G. Rowan, B.C. McBride, and T. Villamil. 1994. Sequence stratigraphy of Neogene turbidite systems, northern Green Canyon and Ewing Bank, northern Gulf of Mexico, pp. 383-396. In: Gulf Coast Section Society of Economic Paleontologists and Mineralogists 15th Annual Research Conference Proceedings.
- Wheatcroft, R.A., C.R. Smith, and P.A. Jumars. 1988. Dynamics of surficial trace assemblages in the deep-sea. *Deep-Sea Res.* 36:71-91.
- Wu, R.S.S. 2002. Hypoxia: from molecular responses to ecosystem responses. *Mar. Poll. Bull.* 45:35-45.
- Yamamoto, N. and G. Lopez. 1985. Bacterial abundance in relation to surface area and organic content of marine sediments. *J. Exp. Mar. Biol. Ecol.* 90:209-220.
- Yim, M.W. and N.F.Y. Tam. 1999. Effects of wastewater-borne heavy metals on mangrove plants and soil microbial activities. *Mar. Poll. Bull.* 39:179-186.
- Yingst, J.Y. and D.C. Rhoads. 1985. The structure of soft bottom communities in the vicinity of the Texas Flower Garden Banks, Gulf of Mexico. *Est. Coast. Shelf Sci.* 20:569-592.
- Zajac, R.N. 2001. Organism-sediment relations at multiple spatial scales: Implications for community structure and successional dynamics, pp. 119-139. In: J.Y. Aller, S.A. Woodin, and R.C. Aller (eds.), *Organism-Sediment Interactions*. Belle Baruch Library of Marine Science Number 21, Univ. of South Carolina Press, Columbia, SC. 403 pp.
- Zar, J.H. 1999. *Biostatistical Analysis*. 4th ed. Prentice Hall, Upper Saddle River, NJ.



### The Department of the Interior Mission

As the Nation's principal conservation agency, the Department of the Interior has responsibility for most of our nationally owned public lands and natural resources. This includes fostering sound use of our land and water resources; protecting our fish, wildlife, and biological diversity; preserving the environmental and cultural values of our national parks and historical places; and providing for the enjoyment of life through outdoor recreation. The Department assesses our energy and mineral resources and works to ensure that their development is in the best interests of all our people by encouraging stewardship and citizen participation in their care. The Department also has a major responsibility for American Indian reservation communities and for people who live in island territories under U.S. administration.



### The Minerals Management Service Mission

As a bureau of the Department of the Interior, the Minerals Management Service's (MMS) primary responsibilities are to manage the mineral resources located on the Nation's Outer Continental Shelf (OCS), collect revenue from the Federal OCS and onshore Federal and Indian lands, and distribute those revenues.

Moreover, in working to meet its responsibilities, the **Offshore Minerals Management Program** administers the OCS competitive leasing program and oversees the safe and environmentally sound exploration and production of our Nation's offshore natural gas, oil and other mineral resources. The MMS **Minerals Revenue Management** meets its responsibilities by ensuring the efficient, timely and accurate collection and disbursement of revenue from mineral leasing and production due to Indian tribes and allottees, States and the U.S. Treasury.

The MMS strives to fulfill its responsibilities through the general guiding principles of: (1) being responsive to the public's concerns and interests by maintaining a dialogue with all potentially affected parties and (2) carrying out its programs with an emphasis on working to enhance the quality of life for all Americans by lending MMS assistance and expertise to economic development and environmental protection.